AFWAL-TR-83-4154

AD-A140 701

CONFERENCE ON AEROSPACE TRANSPARENT MATERIALS AND ENCLOSURES

S. A. Morolo
Materials Engineering Branch
Systems Support Division

December 1983

Conference Report for Period 11-14 July 1983

Approved for Public Release; Distribution Unlimited

DTIC
ELECTE
MAR 14 1984
S
E

MATERIALS LABORATORY
AIR FORCE WRIGHT AERONAUTICAL LABORATORIES
AIR FORCE SYSTEMS COMMAND
WRIGHT-PATTERSON AIR FORCE BASE, OHIO 45433

DTIC FILE COPY

84 03 13 026

NOTICE

When Government drawings, specifications, or other data are used for any purpose other than in connection with a definitely related Government procurement operation, the United States Government thereby incurs no responsibility nor any obligation whatsoever; and the fact that the government may have formulated, furnished, or in any way supplied the said drawings, specifications, or other data, is not to be regarded by implication or otherwise as in any manner licensing the holder or any other person or corporation, or conveying any rights or permission to manufacture use, or sell any patented invention that may in any way be related thereto.

This report has been reviewed by the Office of Public Affairs (ASD/PA) and is releasable to the National Technical Information Service (NTIS). At NTIS, it will be available to the general public, including foreign nations.

This technical report has been reviewed and is approved for publication.

MR. SAMUEL A. MAROLO,
Materials Engineer
Materials Behavior and
Evaluation

THEODORE J. REINHART, Chief
Materials Engineering Branch
Systems Support Division
Materials Laboratory

FOR THE COMMANDER:

MR. WARREN JOHNSON, Chief
Systems Support Division
Materials Laboratory

If your address has changed, if you wish to be removed from our mailing list, or if the addressee is no longer employed by your organization please notify AFWAL/MLSE, W-PAFB, OH 45433 to help us maintain a current mailing list

Copies of this report should not be returned unless return is required by security considerations, contractual obligations, or notice on a specific document.

COMPONENT PART NOTICE

THIS PAPER IS A COMPONENT PART OF THE FOLLOWING COMPILATION REPORT:

(TITLE): Conference on Aerospace Transparent Materials and Enclosures Held at Scottsdale, Arizona on 11-14 July 1983.

(SOURCE): Dayton Univ., OH

TO ORDER THE COMPLETE COMPILATION REPORT USE AD-A140 701.

THE COMPONENT PART IS PROVIDED HERE TO ALLOW USERS ACCESS TO INDIVIDUALLY AUTHORED SECTIONS OF PROCEEDINGS, ANNALS, SYMPOSIA, ETC. HOWEVER, THE COMPONENT SHOULD BE CONSIDERED WITHIN THE CONTEXT OF THE OVERALL COMPILATION REPORT AND NOT AS A STAND-ALONE TECHNICAL REPORT.

THE FOLLOWING COMPONENT PART NUMBERS COMPRISE THE COMPILATION REPORT:

AD#:	TITLE:
P003 184	Pyrotechnic Clear Path Egress System for the T-38 Trainer Aircraft
P003 185	Battle Damage Repair of Birdstrike Resistant Laminated Transparencies
P003 186	Windshield Weight Reduction through the Use of High Strength Glass and Polyurethane Interlayers
P003 187	New Aircraft Windshield Applications Using Ion Exchange Glass
P003 188	A New and Unique Conductive Element for Aircraft Transparencies
P003 189	T-38 Student Windshield Bird Proofing Efforts Utilizing Metal and Composite Materials for Aft Arch Reinforcement
P003 190	Development of Lightweight Commercial Aircraft Windshields with New High Strength Glasses
P003 191	Transparency Technology Needs for Military Aircraft
P003 192	Testing Polycarbonate for Utilization in the Production of Transparent Enclosures
P003 193	Degradation of the Bird Impact Resistance of Polycarbonate
P003 194	The Effect of Accelerated Ultra Violet Weathering on the Rain Erosion Resistance of Coated Aircraft Transparencies
P003 195	Service-Life Induced Failure of Bird Impact Resistant Windshields
P003 196	Some Crazing Experiments on 'As-Cast' Acrylic to MIL-P-8184
P003 197	The Effects of Moisture on Fracture Toughness and Thermal Relaxation of Stretched Acrylic Plastics
P003 198	Comparison of Bullet Resistance of New and Aged Polycarbonate
P003 199	New High Performance Windshield/Canopy Materials
P003 200	An Industry Test Program for Interlayer Equivalency

This document has been approved for public release and sale; its distribution is unlimited.

COMPONENT PART NOTICE (CON'T)

AD#:		TITLE:
	P003 201	Fluroepoxy and Fluroacrylic Transparencies
	P003 202	Polycrystalline MgA1204 Spinel for High Performance Windows
	P003 203	An Improved Acrylic Sheet Material with Enhanced Craze
	P003 204	Protective Liner Materials for Transparent Plastics
	P003 205	Heat Resistant Copolyester-Carbonate Transparent Plastics
	P003 206	Specialty Coatings for Increased Service Life of Acrylic Aircraft Transparencies. Part 2
	P003 207	In-Flight Measurement of Pressure Distribution Over T-38 Student Canopy
	P003 208	Swedish Air Force Maintenance Programme for Aged Transparent Enclosures for Jet Trainer and Jet Fighter Aircraft
	P003 209	Measurement of Residual Strains and Stresses in Transparent Products
	P003 210	Aritificial Ageing of Transparent Aerospace Materials
	P003 211	The Need for Application of Dynamic Mechanical Analysis in the Evaluation of Interlayer Materials
	P003 212	Simulation of Exposure of Aircraft Transparencies to Flight Line Environment
	P003 213	Aircraft Transparency Testing
	P003 214	Civil Aircraft Windscreen Damage Due to Birdstrikes
	P003 215	USAF Aircraft Windshield/Canopy Bird Strikes
	P003 216	Increasing Birdstrike Rates and Improved Birdstrike Analysis of the Royal Netherlands Air Force
	P003 217	Investigations Concerning Improvements of the SAAB 37 Windshield Birdstrike Resistance
	P003 218	Bird Impact Evaluation of F/RF-4 Transparency System
	P003 219	Alternate T-38 Transparency Development
	P003 220	A Triangulation Technique for Obtaining Deflections of Aircraft Transparencies During Bird Impact Testing
	P003 221	Visual Effects of F-16 Canopy/HUD (Head Up Display) Integration
	P003 222	Optical Effects of F-16 Canopy and HUD (Head Up Display) Integration
	P003 223	Visual Perception through Windscreens: Effects of Minor Occlusions and Haze on Operator Performance
	P003 224	The Reduction of Life-Cycle Costs through Continuing Acrylic Maintenance
	P003 225	The Certification of Polycarbonate Transparencies - An Appeal for Reasonable Requirements
	P003 226	Lufthansa German Airlines Experience with Cabin and Cockpit Windows of Boeing 707, 727, 737, 747, Douglas DC10 and Airbus A300
	P003 227	The Wiper Abrasion and Rain Erosion Resistance of Tra Transparent Materials and Coatings for Aircraft Glazing
	P003 228	Windshield Problems on UK Operated Transport Sized Jet Aircraft 1976 to 1982

COMPONENT PART NOTICE (CON'T)

AD#:	P003 229	TITLE: Validation of the MAGNA (Materially and Geometrically Nonlinear Analysis) Computer Program for Nonlinear Finite Element Analysis of Aircraft Transparency Bird Impact
	P003 230	MAGNA (Materially and Geometrically Nonlinear Analysis) Computer Simulation of Bird Impact on the F-15 Aircraft Canopy
	P003 231	Simulation of T-38 Aircraft Student Canopy Response to Cockpit Pressure and Thermal Loads Using MAGNA (Materially and Geometrically Nonlinear Analysis)
	P003 232	Parametric Studies of the T-38 Student Windshield Using the Finite Element of Code MAGNA (Materially and Geometrically Nonlinear Analysis)
	P003 233	Current Problems and Progress in Transparency Impact Analysis
	P003 234	Nastran Analysis of Nuclear Effects on Helicopter Transparencies
	P003 235	Theoretical Evaluation of the Structural Performance of Swedish Fighter Aircraft Windshield Subjected to Impact
	P003 236	Status of New Aerothermodynamic Analysis Tool for High-Temperature Resistant Transparencies

Accession For	
NTIS GRA&I	☑
DTIC TAB	☐
Unannounced	☐
Justification	
By	
Distribution/	
Availability Codes	
Dist	Avail and/or Special
A-1	

UNCLASSIFIED

SECURITY CLASSIFICATION OF THIS PAGE (When Data Entered)

REPORT DOCUMENTATION PAGE		READ INSTRUCTIONS BEFORE COMPLETING FORM
1. REPORT NUMBER AFWAL-TR-83-4154	2. GOVT ACCESSION NO. AD-A140 701	3. RECIPIENT'S CATALOG NUMBER
4. TITLE (and Subtitle) CONFERENCE ON AEROSPACE TRANSPARENT MATERIALS AND ENCLOSURES		5. TYPE OF REPORT & PERIOD COVERED Conference Report 11 - 14 July 1983 6. PERFORMING ORG. REPORT NUMBER
7. AUTHOR(s) Compiled by Samuel A. Marolo		8. CONTRACT OR GRANT NUMBER(s) F33615-80-C-3401
9. PERFORMING ORGANIZATION NAME AND ADDRESS AFML/AFFDL Wright-Patterson Air Force Base, Ohio 45433		10. PROGRAM ELEMENT, PROJECT, TASK AREA & WORK UNIT NUMBERS PROJ 1926
11. CONTROLLING OFFICE NAME AND ADDRESS Materials Laboratory (AFWAL/MLSE) Air Force Wright Aeronautical Laboratories, AFSC Wright-Patterson AFB, Ohio 45433		12. REPORT DATE December 1983 13. NUMBER OF PAGES
14. MONITORING AGENCY NAME & ADDRESS (if different from Controlling Office)		15. SECURITY CLASS. (of this report) UNCLASSIFIED 15a. DECLASSIFICATION/DOWNGRADING SCHEDULE

16. DISTRIBUTION STATEMENT (of this Report)

Approved for public release; distribution unlimited.

17. DISTRIBUTION STATEMENT (of the abstract entered in Block 20, if different from Report)

18. SUPPLEMENTARY NOTES

19. KEY WORDS (Continue on reverse side if necessary and identify by block number)

Polycarbonate, Acrylic, Interlayers, Windshields, Canopies, Interlayers, Coating, Transparent Materials, Environmental Resistance, Optical Requirements, Compurated Design, Design Criteria, Cost of Ownership Reduction

20. ABSTRACT (Continue on reverse side if necessary and identify by block number)

The purpose of this report is to make available the technical papers presented at the Fourteenth Conference on Aerospace Transparent Materials and Enclosures. fifty three technical papers are presented in seven sessions that address transparent material for enclosures, coatings for transparencies; transparency design; bird impact resistance; human factor and optics; operational problems; design criteria on transparent plastics, glasses, and elastomers;

DD FORM 1 JAN 73 1473 EDITION OF 1 NOV 65 IS OBSOLETE

UNCLASSIFIED

SECURITY CLASSIFICATION OF THIS PAGE (When Data Entered)

aircraft-structural integration of windshields and conopies; compurated design; testing techniques; and cost of ownership reduction. The papers contained herein have been reproduced directly from the original manuscripts.

PREFACE

This report was prepared by the Materials Engineering branch under Project 1926, "Aircraft Windshield Development," Project. It was administered under the the direction of the Materials Laboratory, Air Force Wright Aeronautical Laboratories, Air Force Systems Command. Mr. S. A. Marolo (AFWAL/MLSE) served as Project Engineer.

The technical papers contained in this report were presented at the Materials Laboratory/Flight Dynamics Laboratory Conference on "Aerospace Transparent Materials and Enclosures", which was held at The Registry Resort, Scottsdale, Arizona on 11-14 July 1983.

Gratitude and appreciation are expressed to Mr. Ralph J. Speelman, AFWAL/FIEA, Mrs. Karen K. Pettus and Mrs. Jennie L. Long, University of Dayton, for the outstanding job accomplished as Technical Chairman, Conference Coordinator, and Conference Secretary, respectively. Gratitude is also expressed to Mr. George P. Peterson, Director, Materials laboratory, and Mr. James Mattice, Acting Director, Flight Dynamics Laboratory, for their support of the conference and their expressed support of this technical area. Gratitude is also expressed to Mr. George Peterson for his introductory remarks at the Conference.

The report was submitted by the author on 2 December 1983.

Publication of this report does not constitute Air Force approval of the findings or conclusions presented. It is published only for the exchange and stimulation of ideas.

Accession For
NTIS GRA&I ☒
DTIC TAB ☐
Unannounced ☐
Justification
By
Distribution/
Availability Codes
Dist | Avail and/or Special
A-1

DTIC COPY INSPECTED 2

TABLE OF CONTENTS

SESSION I: EMERGING SYSTEM CAPABILITIES (PART I)	Page No.
PYROTECHNIC CLEAR PATH EGRESS SYSTEM FOR THE T-38 TRAINER AIRCRAFT S. Phillips, Space Ordinance Systems	2
BATTLE DAMAGE REPAIR OF BIRDSTRIKE RESISTANT LAMINATED TRANSPARENCIES 2 Lt. D. A. Crocker, Flight Dynamics Laboratory	25
WINDSHIELD WEIGHT REDUCTION THROUGH THE USE OF HIGH STRENGTH GLASS AND POLYURETHANE INTERLAYERS J. H. Lawrence, Jr., Douglas Aircraft Company	46
NEW AIRCRAFT WINDSHIELD APPLICATIONS USING ION EXCHANGE GLASS W. W. Hornsey and W. F. Rothe, PPG Industries Inc.	57
SESSION I: EMERGING SYSTEM CAPABILITIES (PART II)	
A NEW AND UNIQUE CONDUCTIVE ELEMENT FOR AIRCRAFT TRANSPARENCIES D. M. Trebes and J. B. Olson, Sierracin/Sylmar	72
T-38 STUDENT WINDSHIELD BIRD PROOFING EFFORTS UTILIZING METAL AND COMPOSITE MATERIALS FOR AFT ARCH REINFORCEMENT J. M. Schlueter, PPG Industries, Inc.	108
DEVELOPMENT OF LIGHTWEIGHT COMMERCIAL AIRCRAFT WINDSHIELDS WITH NEW HIGH STRENGTH GLASSES W. E. Gourley and H. E. Littell, PPG Industries, Inc.	134
TRANSPARENCY TECHNOLOGY NEEDS FOR MILITARY AIRCRAFT R. H. Walker, Flight Dynamics Laboratory	158
SESSION II: UNDERSTANDING CURRENT MATERIALS (PART I)	
TESTING POLYCARBONATE FOR UTILIZATION IN THE PRODUCTION OF TRANSPARENT ENCLOSURES A. J. Bonje and J. Irion, Texstar Plastics	174
DEGRADATION OF THE BIRD IMPACT RESISTANCE OF POLYCARBONATE J. B. R. Heath and R. W. Gould, National Research Council of Canada	183
SOURCES OF ENVIRONMENTAL INFORMATION FOR USE IN TRANSPARENCY SYSTEM DESIGN AND TESTS Capt. N. E. Buss and Lt. J. K. Hayward, Flight Dynamics Laboratory (Paper Not Furnished)	212

THE EFFECT OF ACCELERATED ULTRA VIOLET WEATHERING ON THE RAIN EROSION RESISTANCE OF COATED AIRCRAFT TRANSPARENCIES 213
C. J. Hurley, University of Dayton and G. F. Schmitt, Materials Laboratory

SESSION II: UNDERSTANDING CURRENT MATERIALS (PART II)

SERVICE-LIFE INDUCED FAILURE OF BIRD IMPACT RESISTANT WINDSHIELDS 238
P. J. Burchell and R. H. Stacewicz, Department of Defense Support

SOME CRAZING EXPERIMENTS ON "AS-CAST" ACRYLIC TO MIL-P-8184 260
K. B. Armstrong, British Airways

THE EFFECTS OF MOISTURE ON FRACTURE TOUGHNESS AND THERMAL RELAXATION OF STRETCHED ACRYLIC PLASTICS 275
J. Tirosh, Technion-Israel Institute of Technology and S. A. Sutton, Digital Technology, Inc., and P. W. Mast, R. W. Thomas, and I. Wolock, Naval Research Laboratory

COMPARISON OF BULLET RESISTANCE OF NEW AND AGED POLY-CARBONATE 296
J. B. R. Heath, R. W. Gould, and E. B. Stimson, National Research Council of Canada

SESSION III: NEW MATERIALS (PART I)

NEW HIGH PERFORMANCE WINDSHIELD/CANOPY MATERIALS 339
B. T. DeBona, Allied Chemical Corporation

AN INDUSTRY TEST PROGRAM FOR INTERLAYER EQUIVALENCY 382
P. H. Bain, Boeing Commercial Airplane Company

FLUROEPOXY AND FLUROACRYLIC TRANSPARENCIES 407
J. R. Griffith, Naval Research Laboratory

POLYCRYSTALLINE $M_gAl_2O_4$ SPINEL FOR HIGH PERFORMANCE WINDOWS 415
D. W. Roy, Coors Porcelain Company

SESSION III: NEW MATERIALS (PART II)

AN IMPROVED ACRYLIC SHEET MATERIAL WITH ENHANCED CRAZE RESISTANCE 428
M. V. Moncur and W. F. Fisher, Swedlow Incorporated

PROTECTIVE LINER MATERIALS FOR TRANSPARENT PLASTICS 451
J. E. Mahaffey and T. G. Rukavina, PPG Industries, Inc.

HEAT RESISTANT COPOLYESTER-CARBONATE TRANSPARENT PLASTICS 469
T. J. Reinhart, Materials Laboratory

SPECIALTY COATINGS FOR INCREASED SERVICE LIFE OF ACRYLIC AIRCRAFT TRANSPARENCIES - PART II
W. C. Harbison, Swedlow, Inc.

SESSION IV: TESTING - CAPABILITIES AND LIMITATIONS (PART I)

IN-FLIGHT MEASUREMENT OF PRESSURE DISTRIBUTION OVER T-38 STUDENT CANOPY
W. R. Pinnell, Flight Dynamics Laboratory

SWEDISH AIR FORCE MAINTENANCE PROGRAMME FOR AGED TRANSPARENT ENCLOSURES FOR JET TRAINER AND JET FIGHTER AIRCRAFT
R. Forss, Defence Material Administration

MEASUREMENT OF RESIDUAL STRAINS AND STRESSES IN TRANSPARENT PRODUCTS
A. S. Redner and T. W. Corby, Jr., Vishay Intertechnology, Inc.

SESSION IV: TESTING - CAPABILITIES AND LIMITATIONS (PART II)

ARTIFICIAL AGEING OF TRANSPARENT AEROSPACE MATERIALS
A. Davis, Ministry of Defense

THE NEED FOR APPLICATION OF DYNAMIC MECHANICAL ANALYSIS IN THE EVALUATION OF INTERLAYER MATERIALS
A. Jayarajan, Boeing Commercial Aircraft Company

SIMULATION OF EXPOSURE OF AIRCRAFT TRANSPARENCIES TO FLIGHT LINE ENVIRONMENT
A. Piekutowski, University of Dayton

AIRCRAFT TRANSPARENCY TESTING
M. E. Kelly, Flight Dynamics Laboratory

SESSION V: BIRDSTRIKES - PROBLEM DEFINITION AND REDUCTION (PART I)

CIVIL AIRCRAFT WINDSCREEN DAMAGE DUE TO BIRDSTRIKES
J. Thorpe, Civil Aviation Authority

USAF AIRCRAFT WINDSHIELD/CANOPY BIRD STRIKES
Capt. R. C. Kull, Air Force Engineering and Services Center

INCREASING BIRDSTRIKE RATES AND IMPROVED BIRDSTRIKE ANALYSIS OF THE ROYAL NETHERLANDS AIR FORCE
L. S. Buurman, Royal Netherlands Air Force

SESSION V: BIRDSTRIKES - PROBLEM DEFINITION AND REDUCTION (PART II)

INVESTIGATIONS CONCERNING IMPROVEMENTS OF THE SAAB 37 WINDSHIELD BIRDSTRIKE RESISTANCE 717
B. P. Fonden and K. I. Persson, Saab-Scandia

BIRD IMPACT EVALUATION OF F/RF-4 TRANSPARENCY SYSTEM 730
G. T. Stenger, University of Dayton and Lt. R. Simmons, Flight Dynamics Laboratory

ALTERNATE T-38 TRANSPARENCY DEVELOPMENT 756
B. S. West and K. I. Clayton, University of Dayton, and Capt W. W. Saeger, Jr., Flight Dynamics Laboratory

A TRIANGULATION TECHNIQUE FOR OBTAINING DEFLECTIONS OF AIRCRAFT TRANSPARENCIES DURING BIRD IMPACT TESTING 776
W. R. Pinnell and 2 Lt. D. A. Crocker, Flight Dynamics Laboratory

SESSION VI: UNDERSTANDING CURRENT SYSTEM (PART I)

VISUAL EFFECTS OF F-16 CANOPY/HUD INTEGRATION 792
Lt. Col. L. V. Genco, Air Force Aerospace Medical Research Laboratory

OPTICAL EFFECTS OF F-16 CANOPY AND HUD INTEGRATION 808
H. L. Task, Air Force Aerospace Medical Research Laboratory

VISUAL PERCEPTION THROUGH WINDSCREENS: EFFECTS OF MINOR OCCLUSIONS AND HAZE ON OPERATOR PERFORMANCE 825
W. N. Kama, Air Force Aerospace Medical Research Laboratory

THE REDUCTION OF LIFE-CYCLE COSTS THROUGH CONTINUING ACRYLIC MAINTENANCE 845
R. J. Stillman and H. A. Wilson, Micro-Surface Finishing Products, Inc.

SESSION VI: UNDERSTANDING CURRENT SYSTEM (PART II)

THE CERTIFICATION OF POLYCARBONATE TRANSPARENCIES - AN APPEAL FOR REASONABLE REQUIREMENTS 859
B. G. Hinds, Sierracin/Sylmer

LUFTHANSA GERMAN AIRLINES EXPERIENCE WITH CABIN AND COCKPIT WINDOWS OF BOEING 707, 727, 737, 747, DOUGLAS DC10 AND AIRBUS A300 874
K. W. Ewald, Lufthanse German Airlines

THE WIPER ABRASION AND RAIN EROSION RESISTANCE OF TRANSPARENT MATERIALS AND COATINGS FOR AIRCRAFT GLAZING 892
N. S. Corney, Royal Aircraft Establishment and R. J. King, National Physical Laboratory

WINDSHIELD PROBLEMS ON UK OPERATED TRANSPORT SIZED JET AIRCRAFT 1976 to 1982 910
J. Thorpe, Civil Aviation Authority

SESSION VII: COMPUTER AIDED STRUCTURAL ANALYSIS (PART I)

VALIDATION OF THE MAGMA COMPUTER PROGRAM FOR NONLINEAR FINITE ELEMENT ANALYSIS OF AIRCRAFT TRANSPARENCY BIRD IMPACT 921
R. E. McCarty and 2 Lt. J. L. Hart, Flight Dynamics Laboratory

MAGNA COMPUTER SIMULATION OF BIRD IMPACT ON THE TF-15 AIRCRAFT CANOPY 973
R. E. McCarty, Flight Dynamics Laboratory

SIMULATION OF T-38 AIRCRAFT STUDENT CANOPY RESPONSE TO COCKPIT PRESSURE AND THERMAL LOADS USING MAGNA 1009
R. E. McCarty and R. A. Smith, Flight Dynamics Laboratory

PARAMETRIC STUDIES OF THE T-38 STUDENT WINDSHIELD USING THE FINITE ELEMENT OF CODE MAGNA 1040
R. NASH, University of Dayton

SESSION VII: COMPUTER AIDED STRUCTURAL ANALYSIS (PART II)

CURRENT PROBLEMS AND PROGRESS IN TRANSPARENCY IMPACT ANALYSIS 1057
R. A. Brockman, University of Dayton

NASTRAN ANALYSIS OF NUCLEAR EFFECTS ON HELICOPTER TRANSPARENCIES 1083
P. T. Lin and J. S. Jorgenson, Goodyear Aerospace Corporation

THEORETICAL EVALUATION OF THE STRUCTURAL PERFORMANCE OF SWEDISH FIGHTER AIRCRAFT WINDSHIELD SUBJECTED TO IMPACT 1096
L. A. Samuelson, F. Nilsson, and L. Sornas, Stockholm, Sweden

STATUS OF NEW AEROTHERMODYNAMIC ANALYSIS TOOL FOR HIGH-TEMPERATURE RESISTANT TRANSPARENCIES 1132
M. O. Varner, Sverdrup Technology, Inc. and C. A. Babish, III, Flight Dynamics Laboratory

SESSION I

EMERGING SYSTEMS CAPABILITIES (PART I)

Chairman: D. S. Riddle
Grumman Aerospace Corp
Bethpage, New York

Co-Chairman: J. H. Lawrence, Jr.
Douglas Aircraft Company
Long Beach, California

AD-P003 184

PYROTECHNIC CLEAR PATH EGRESS SYSTEM FOR THE T-38 TRAINER AIRCRAFT

S. Phillips, Space Ordinance Systems

PYROTECHNIC CLEAR PATH EGRESS SYSTEM (PCPES)

FOR THE

T-38 TRAINER AIRCRAFT

BY

STAN PHILLIPS

SPACE ORDNANCE SYSTEMS
CANYON COUNTRY, CA

ABSTRACT

Training for low altitude flying has resulted in the need to upgrade windshield and forward canopy structures to eliminate bird impact related injuries. The existing canopy and structure provides little protection against impact of a four pound bird at 400 knots. The primary T-38 egress system using ballistic gas for canopy jettison is compatible with the bird resistant canopy requirement. However, the backup modes are incompatible. In these modes the seat/man ejects through the canopy for in-flight egress, with ground egress achieved by piercing the canopy with a weighted blade. This incompatibility has created the need for a safe, reliable pyrotechnic backup system for incorporation with the thicker, stronger bird resistant canopy.

DESCRIPTION OF EXISTING T-38 CREW EGRESS SYSTEM

The existing T-38 system is shown schematically on Figure 1. Function and modes of operation are described below.

IN-FLIGHT EGRESS

- PRIMARY MODE
  - Pilot actuates seat handle initiators
    - Canopy is jettisoned
    - Shoulder harness inertia reel actuated
    - 0.3 second time delay initiator actuated
      - CKU-7 catapult initiated
        - Seat/man ejection

- BACKUP MODE
  - Pilot actuates seat handle initiators
    - Canopy fails to jettison
    - Shoulder harness inertia reel actuated
    - 0.3 second time delay initiator actuated
      - CKU-7 catapult initiated
        - Seat mounted blade pierces canopy
        - Seat/man ejected through canopy

GROUND EGRESS

- PRIMARY MODE
  - Pilot actuates cockpit T-Handle initiator
    - Canopy is jettisoned
  - Ground Crew actuates external D-Handle Initiators
    - Canopy is jettisoned

- BACKUP MODE
  - Pilot breaks through canopy using hand held weighted blade
  - Ground crew breaks through canopy using bladed tool

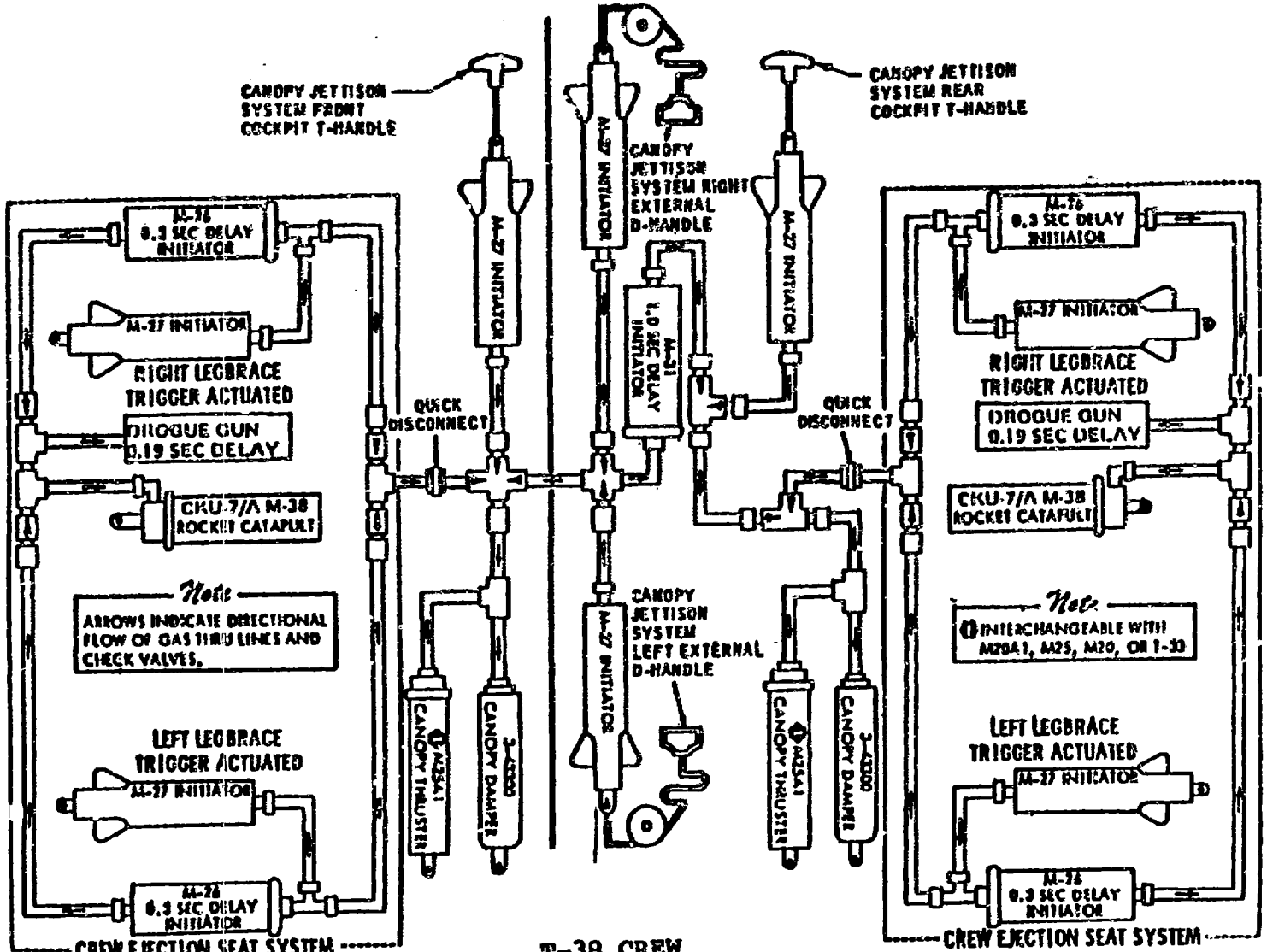

T-38 CREW ESCAPE SYSTEM SCHEMATIC

FIGURE 1

PCPES REQUIREMENTS

Listed below are the design criteria for the T-38 backup pyrotechnic clear path egress system (PCPES):

- o Clear out egress path for air crew member
- o Must be functional after bird strike
- o No degradation of primary ejection system
- o Maximum reliability
- o Consideration of injury to air and ground crews
- o Minimize T-38 modifications
- o Compatibility with T-38 airframe and systems
- o No scheduled maintenance
- o Minimum function time
- o Pyrotechnic output shall not cause injury, fire or explosive hazard in fuel spill environment.

The T-38 application requires three basic functions which must be integrated to provide the overall system parameter of clearing the canopy out of the egress path. These functions are:

- o System initiation
- o Canopy severance
- o Clearing the ejection or escape path

Two system concepts were selected for the detail design phase from all candidate concepts using a quantitative evaluation and ranking order process. The final design shall be selected using a similar process at the completion of the detail design phase of the program.

DESCRIPTION OF INPUT STIMULUS TO THE "PCPES"

The existing T-38 Crew Escape System (primary system) inputs are utilized for initiation of the backup "PCPES". The "PCPES" modes and their respective crew actuation points are described below:

In Flight Ejection - Initiated by actuating the two seat handle initiators. This initiates the primary system and "PCPES".

Ground Egress, Aircrew Initiated - Initiated by pulling the cockpit mounted T-Handle initiator. This initates the primary canopy jettison system and the "PCPES" system.

Ground Egress, Ground Crew Initiated - Initiated by pulling the external D-Handle lanyards on each side of the aircraft. This initiates the Primary Canopy Jettison System and the "PCPES" system.

By using the primary system input points to initiate the "PCPES", the time consuming pilot decision making process for backup system actuation is totally eliminated.

For in-flight egress, the "PCPES" receives input stimulus from the 0.3 second time delay initiator within the T-38 primary system. Figure 2 illustrates the takeoff location for gas at

the rocket catapult input port. A high pressure pneumatic "Y" fitting and flexible line are provided to supply ballistic gas to the "PCPES" initiator.

A study was conducted to determine if the primary ballistic gas system would be degraded by adding the free volume necessary to actuate the "PCPES". The analysis verifies that the primary system will not be degraded and that there is in fact a substantial safety margin with the additional free volume.

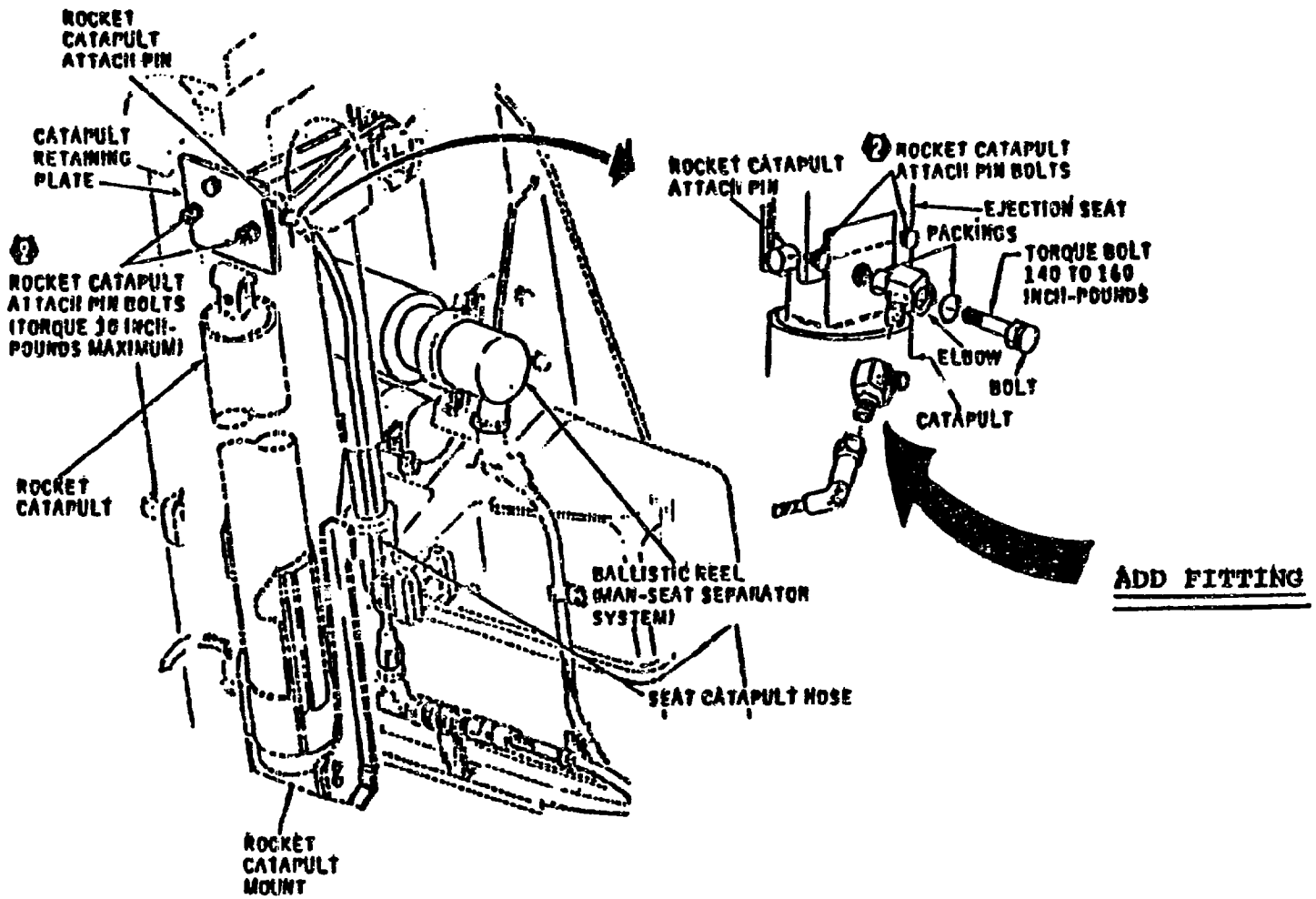

FIGURE 2

TAKEOFF LOCATION FOR BALLISTIC GAS

INITIATION CONCEPT NO. 1

SINGLE INITIATOR WITH CABLE ACTUATED GROUND EGRESS

This concept is shown on Figure 3 and consists of the following components:

- o "Y" fitting (installed in CKU-7 rocket catapult)
- o Flexible high pressure gas line
- o Initiator
- o Control cable (pilot input - ground egress)
- o Control cables (2) (ground crew input - ground egress)

The initiator is mounted to the rear canopy former. The flexible high pressure gas line and flexible ground egress control cables allow the canopy to open and close.

The iniiator is shown on Figure 4 and incorporates the following features:

- o Converts primary system ballistic gas to a detonation stimulus for the canopy mounted detonating cord in the in-flight egress mode
- o Dual gas inputs assure in-flight redundancy
- o Dual cable inputs assure ground egress redundancy
- o Crossover detonation path to assure dual output for the ground and in-flight egress modes

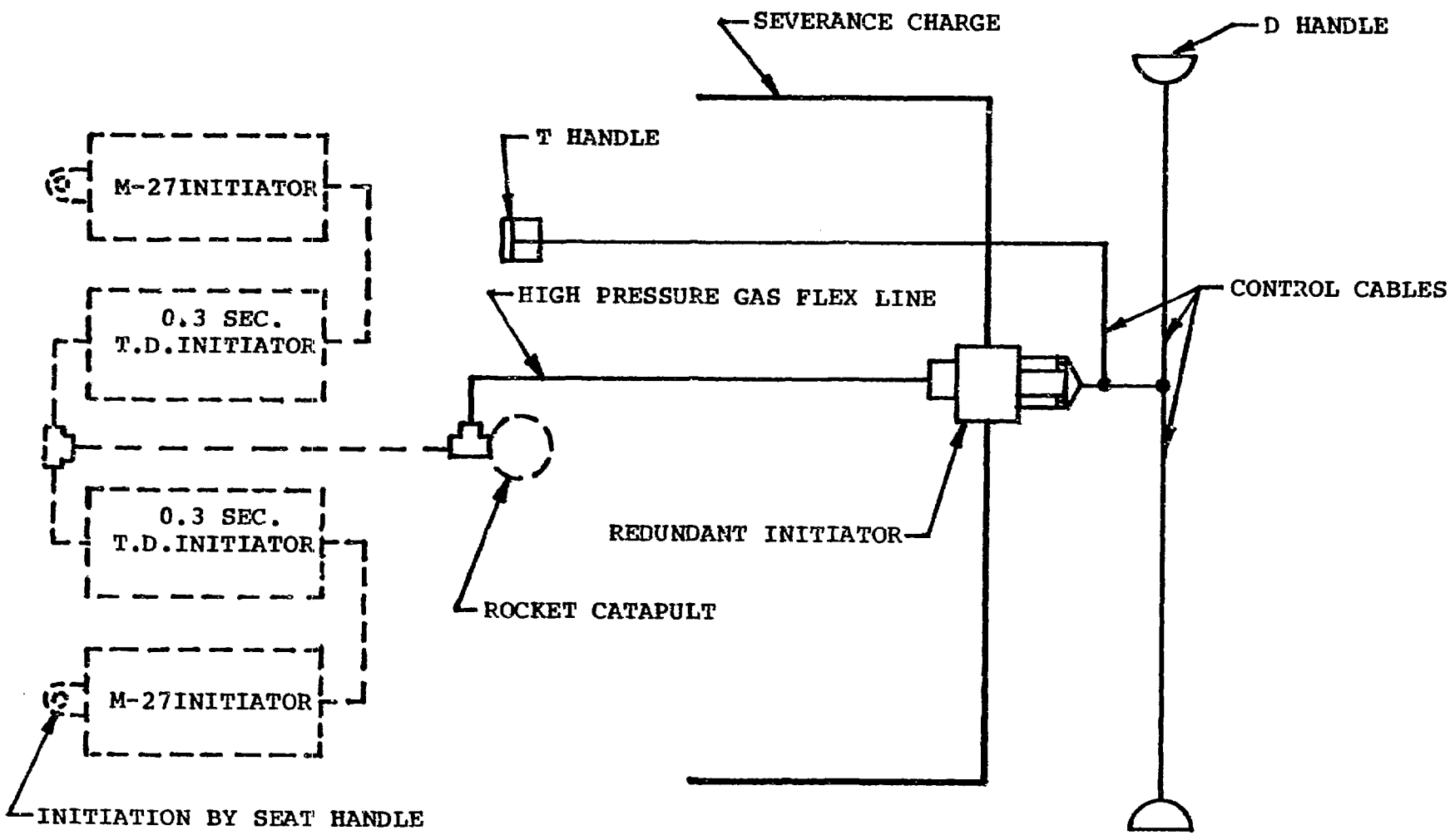

FIGURE 3

INITIATION CONCEPT NUMBER 1

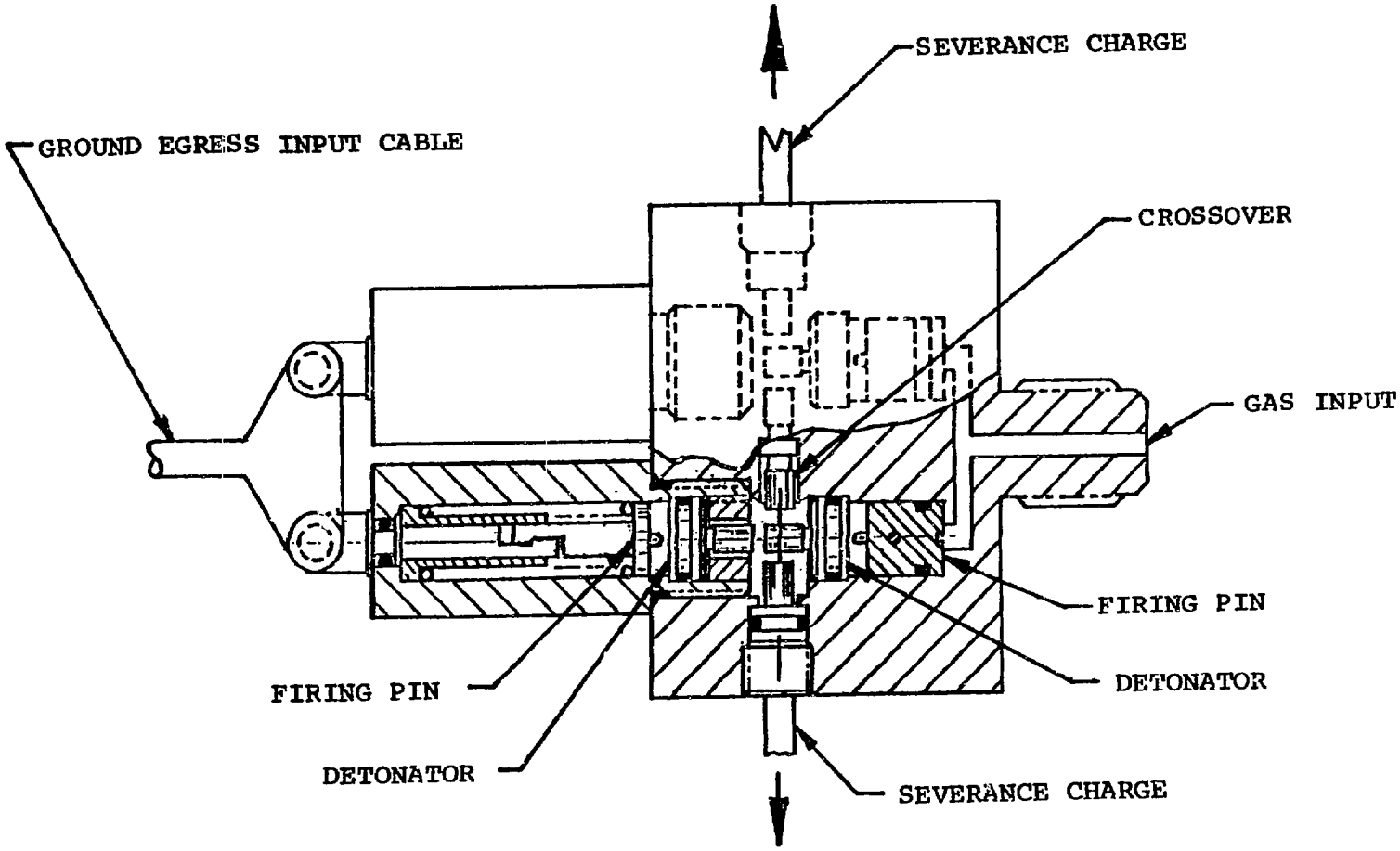

FIGURE 4

REDUNDANT INITIATOR-GAS AND CABLE ACTUATED

INITIATION CONCEPT NO. 2

DUAL INITIATORS WITH CABLE ACTUATED GROUND EGRESS

This concept is shown schematically on Figure 5. This design consists of the following components:

- o "Y" fitting (installed in the CKU-7catapult)
- o Flexible high pressure gas line
- o Tee fitting and gas line (routes gas to both initiators)
- o Initiators (2) - See Figure 6
- o SMDC crossover
- o Control cable (pilot input, ground egress)
- o Control cables (2) (ground crew input, ground egress)

Initiators, tee fitting, gas line and SMDC crossover are mounted to the rear canopy former. The flexible gas line and flexible ground egress control cables allow unrestricted opening and closing of the canopy.

The initiators, tee fitting, gas line and SMDC crossover combine to incorporate the following features:

- o Convert primary system ballistic gas to a detonation stimulus for the canopy mounted detonating cord in the in-flight egress mode
- o Dual gas inputs to assure in-flight redundancy
- o Crossover detonation path to assure dual output for the ground and in-flight egress modes
- o Dual cable inputs assure ground egress redundancy

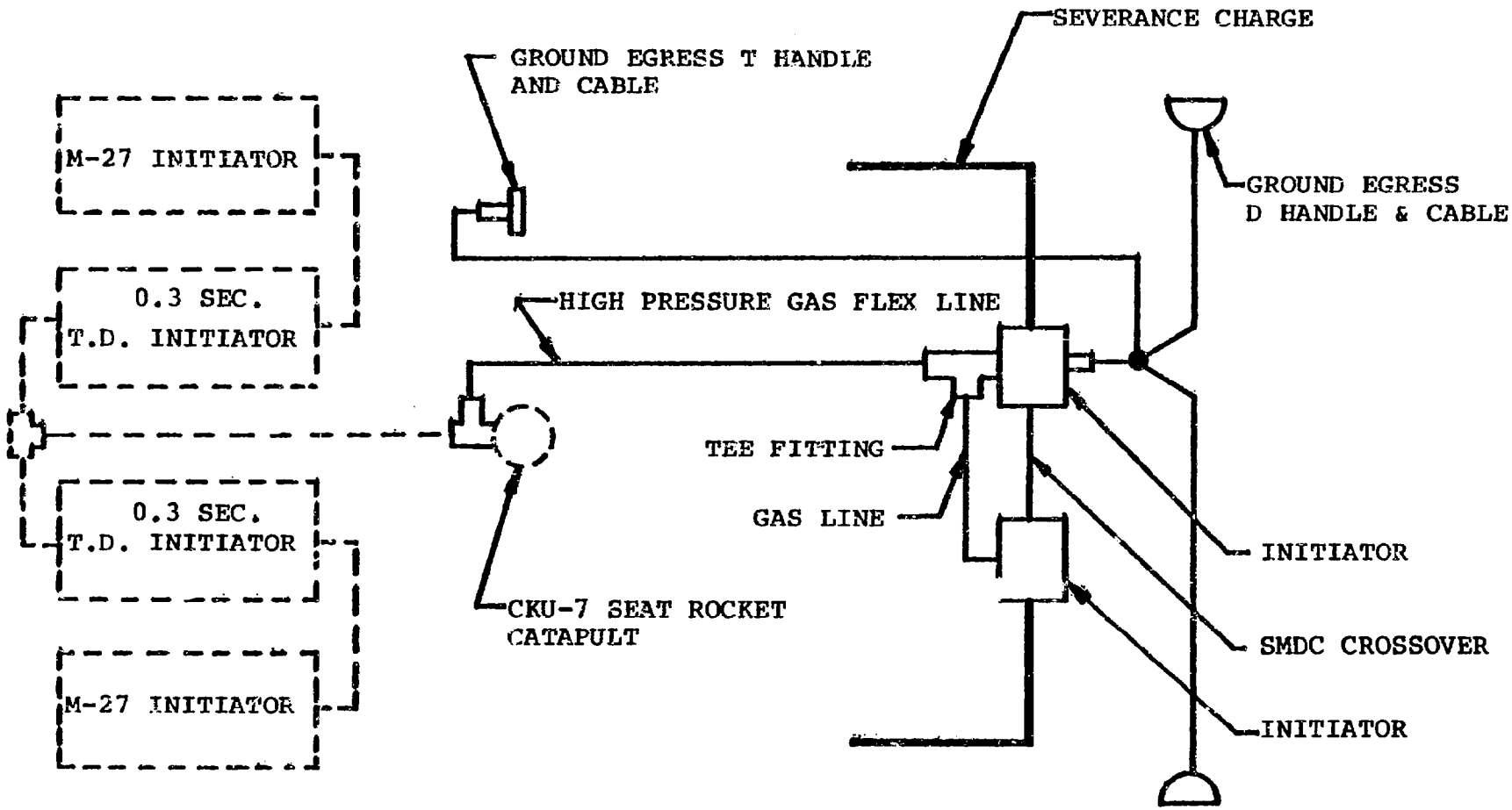

FIGURE 5

INITIATION CONCEPT NUMBER 2

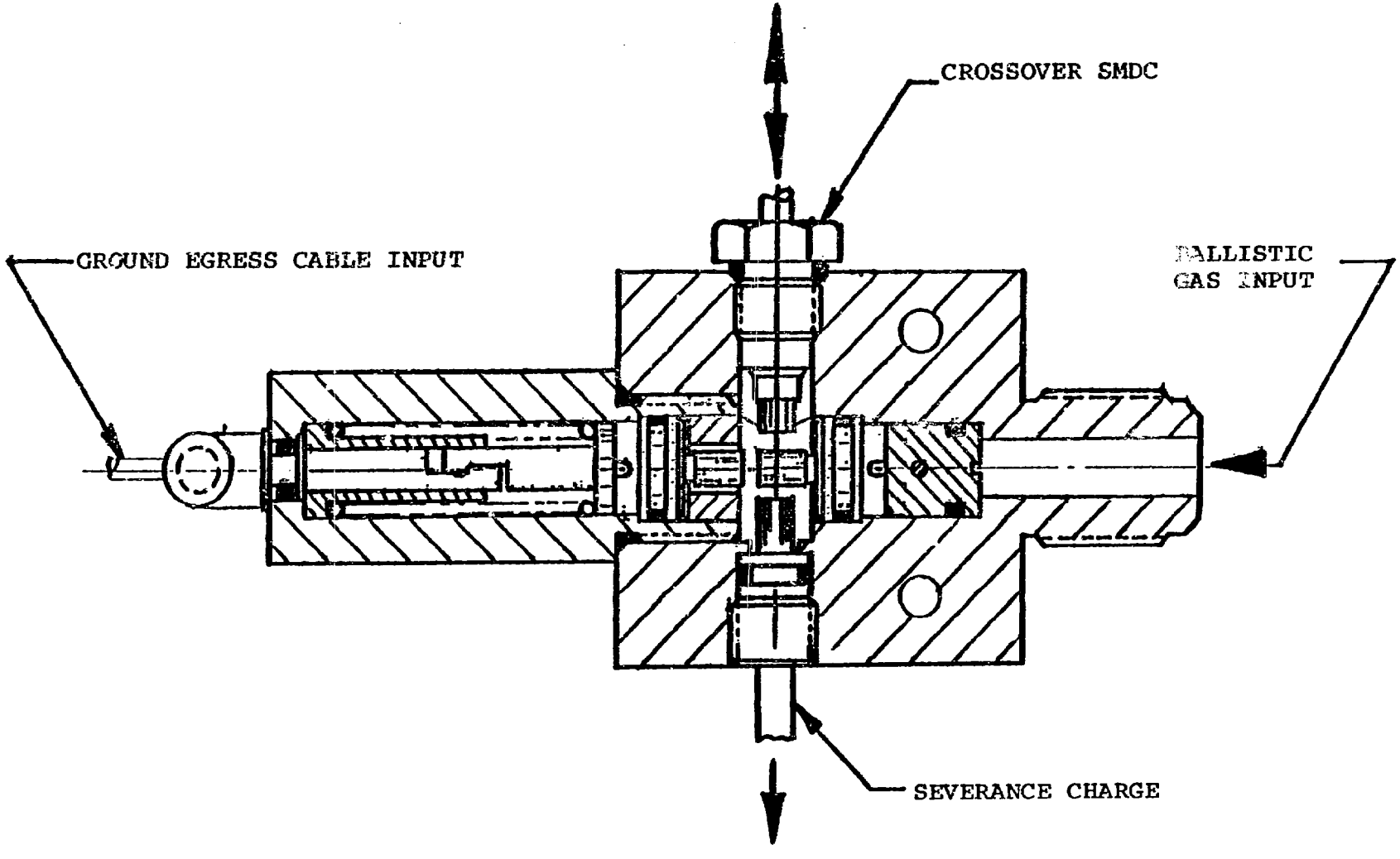

FIGURE 6

GAS & CABLE ACTUATED INITIATOR

CANOPY REMOVAL CONCEPT NO. 1

Side and Rear FLSC Severance with Seat Mounted Pusher

This design is shown on Figure 7. Flexible linear shaped charge (FLSC) is used to cut the forward former, side edge attach plates and the rear of the transparency except for the hinge section. A seat mounted pushing structure is utilized to push the canopy up and out of the ejection path. At the rear of the canopy a central hinge sectin is left uncut and intact with the canopy frame. This section provides a hinge point which controls the severed canopy as it is pushed up & out of the ejection path by the seat mounted pushing structure.

The concept utilizes surface mounted FLSC wherein a high strength retainer is utilized, as shown on Figure 8. Use of the retainer protects the student pilot from residual splatter. The FLSC cutting process is depicted on Figure 9.

This concept has the advantage that no structure or transparency cutting is accomplished directly in front of the student pilot. Further, any spalled debris will be directed outward away from the student pilot. This precludes the possiblity of injury as a result of debris and splatter.

Vision will be unaffected with this concept since all hardware will be mounted below the canopy structure.

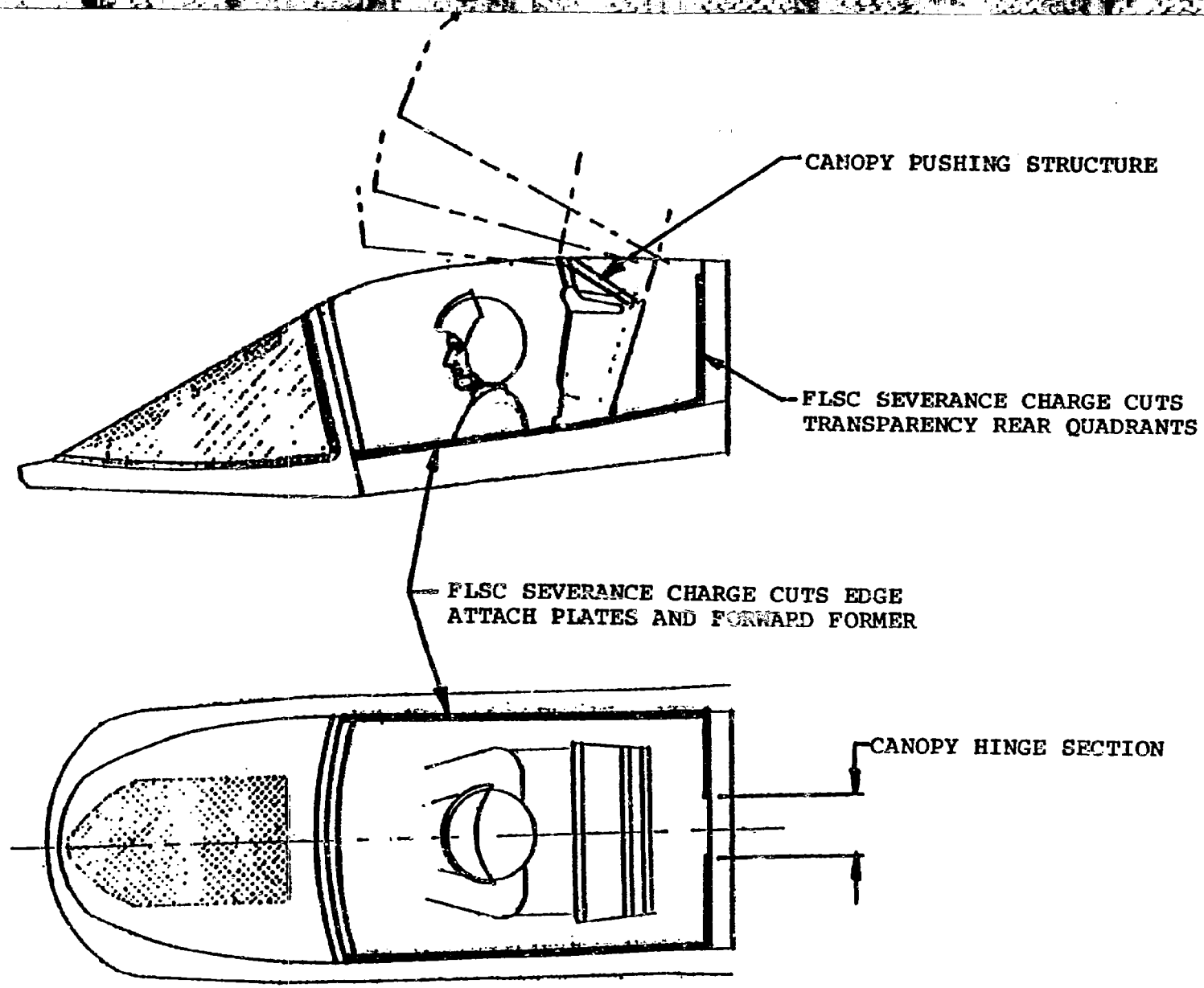

FIGURE 7

CANOPY REMOVAL CONCEPT NUMBER 1

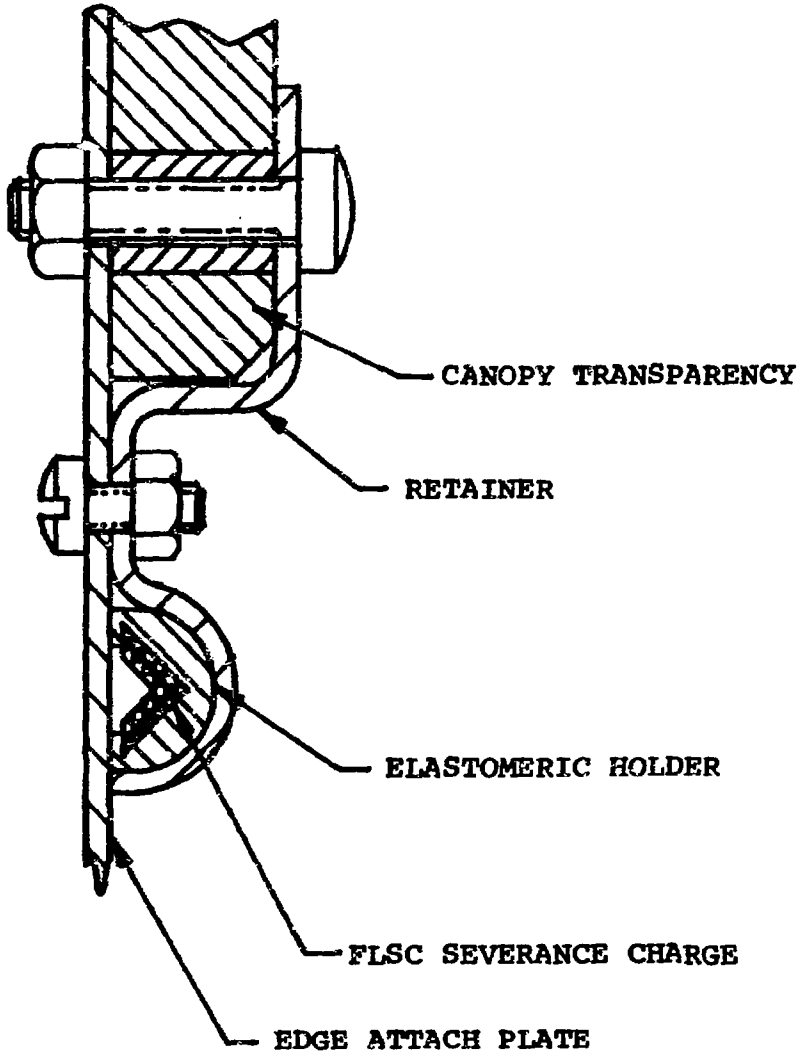

FIGURE 8

FLSC RETENTION TECHNIQUE

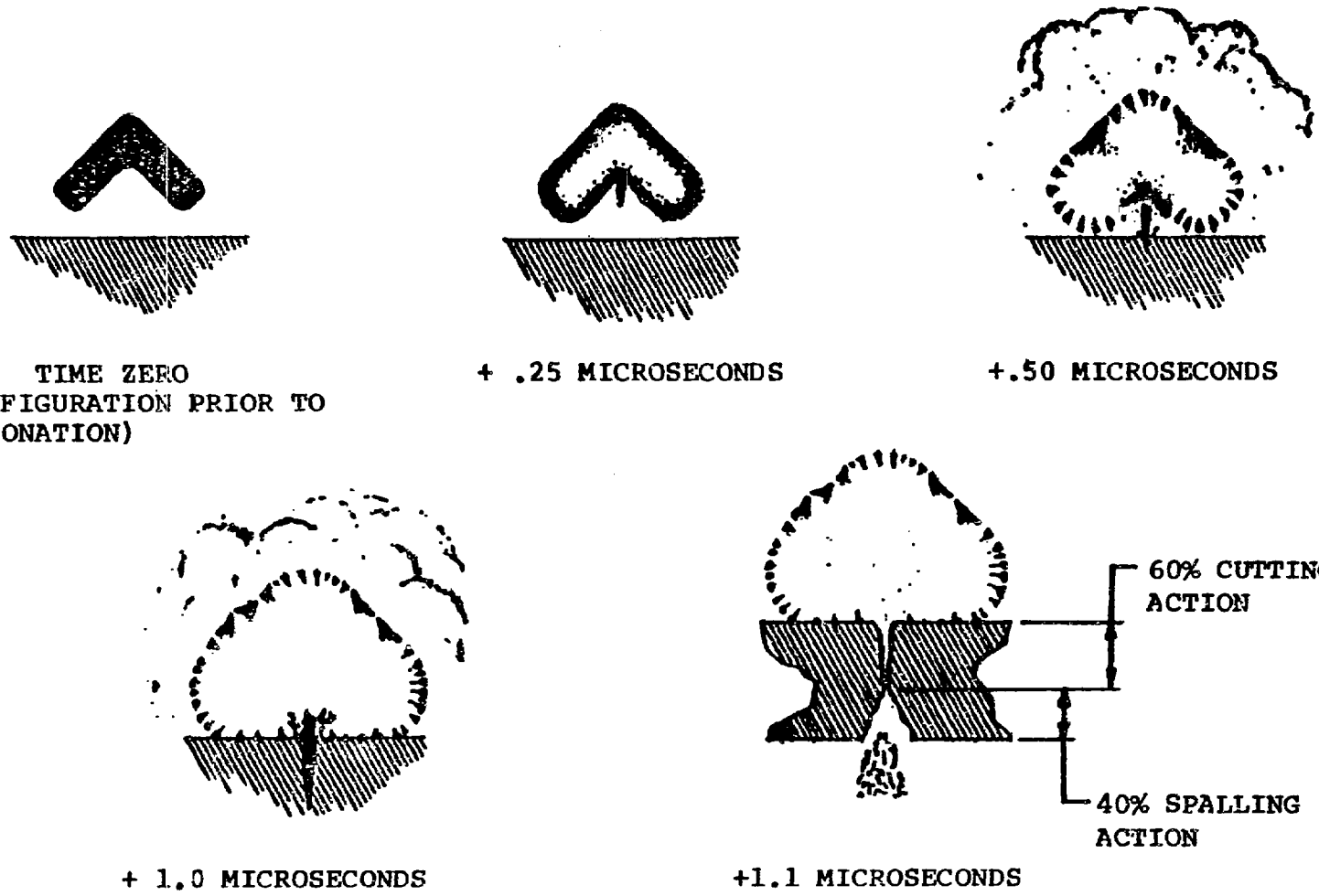

FIGURE 9

FLSC CUTTING PROCESS

CANOPY REMOVAL CONCEPT NO. 2

Side and Rear Severance Using Edge Imbedded MDF With Seat Mounted Pusher

The design is shown on Figure 10. The concept severs the sides and rear arch of the transparency except for the hinge section. The forward former is cut on each side at the sill level. The seat mounted pushing structure is used to push the transparency up and out of the ejection path.

Edge imbedded MDF is utilized to sever the sides and rear of the trasparency in the manner shown on Figure 11. Installation for this technique is shown on Figure 11. The MDF will terminate in the forward retainer blocks. Charge retaining blocks are mounted at the foot of the forward former on each side of the canopy. This block houses the former cutting charge and will provide splatter shield capability. With this concept no structure or transparency cutting is accomplished directly in front of the student pilot. Further, all spalled debris will be directed outward away from the student pilot. This precludes the possibility of injury as a result of debris and splatter.

Pilot vision will be unaffected with this concept since all hardware will be mounted below the canopy structure.

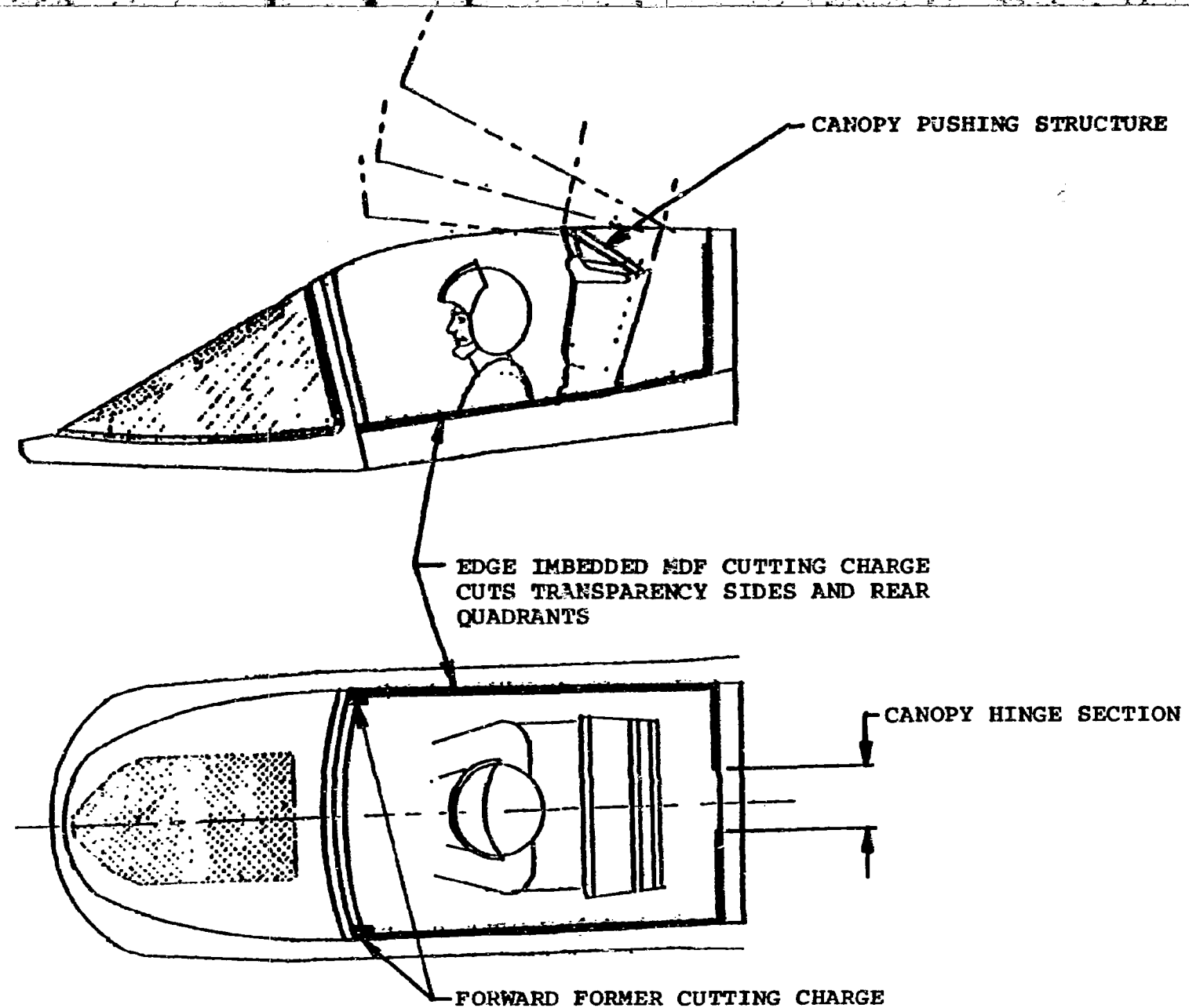

FIGURE 10

CANOPY REMOVAL CONCEPT NUMBER 2

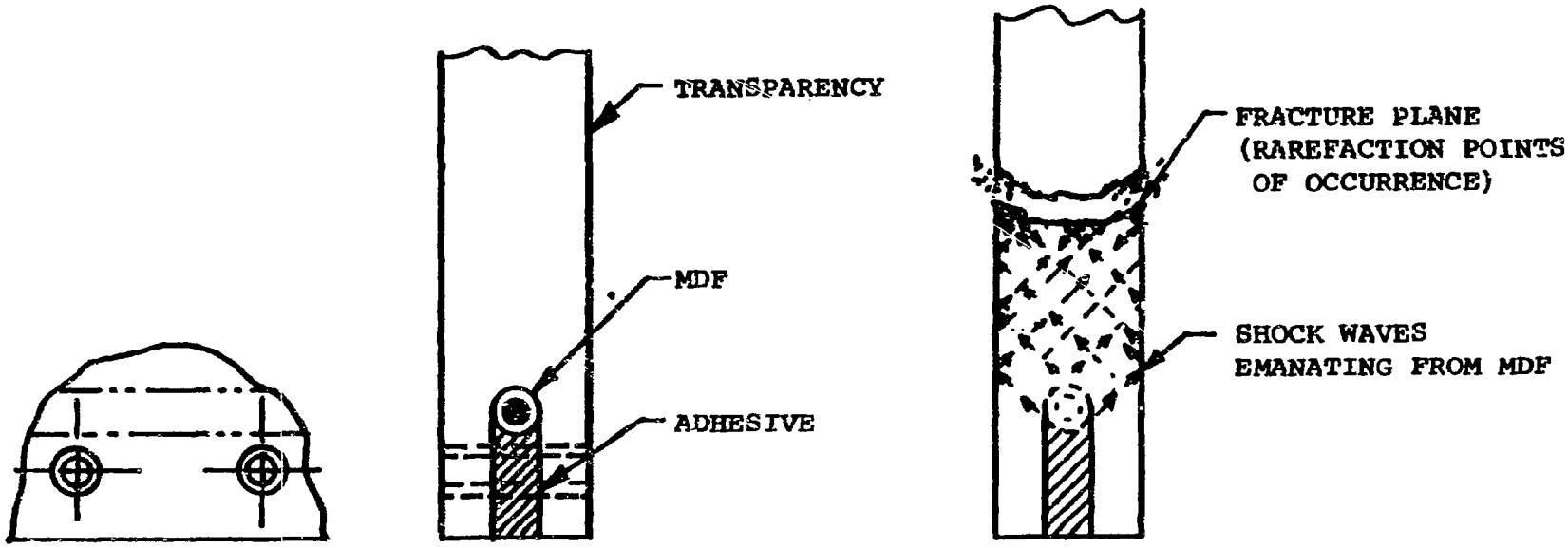

FIGURE 11

EDGE IMBEDDED MDF

FUNCTION TIME

The fastest possible function time for canopy severance can be realized by using the gas to detonation output initiator combined with the detonating cord or the linear shaped charge. No other canopy removal technique approaches the rapidity of the selected concepts.

Given below is the anticipated function time for the "PCPES" system. The data was gathered from qualification and lot acceptance testing of similar components.

COMPONENT	$\bar{x}$ Seconds	$\bar{x} + 3\sigma$ Seconds	$\bar{x} - 3\sigma$ Seconds	σ Seconds
Initiator	.02780	.03016	.02544	.00078
Detonating Cord*	.00046	.00047	.00044	.000034
Total System	.02826	.03063	.02588	.000814

* = Data shown is for a length of 10 feet of detonating cord and a known detonation velocity of

$\bar{x}$ = 6620 meters per second (21,721 feet per second)

WEIGHT OF PCPES

The maximum total system weight is calculated to be 9.0 pounds.

AD-P003 185

BATTLE DAMAGE REPAIR OF BIRDSTRIKE RESISTANT LAMINATED TRANSPARENCIES

2 Lt. D. A. Crocker,
Flight Dynamics Laboratory

ABSTRACT

BATTLE DAMAGE REPAIR OF BIRDSTRIKE RESISTANT LAMINATED TRANSPARENCIES

2Lt Dale A. Crocker
Flight Dynamics Laboratory
Wright-Patterson AFB, Ohio 45433

Aircraft battle damage repair is a growing area of concern in today's Air Force. Methods of quickly repairing battle damaged aircraft in the field are currently being developed to provide increased sortie generation rates in a wartime environment.

A battle damage repair program for bird impact resistant laminated transparencies is currently underway. This program is designed to evaluate experimental battle damage repair techniques for bird impact resistant laminated transparencies. Representative laminated transparencies have been ballistically damaged to simulate various anticipated threats. The experimental battle damage repair procedures have been applied to the damaged transparencies. The final portion of this program will consist of pressure and thermal fatigue testing of the repaired transparencies to determine the structural integrity of the repairs.

The results of this program will be used to define additional development efforts and to determine the applicability of the repair techniques to other aircraft transparency systems.

INTRODUCTION

In a wartime environment, one of the major problems the Air Force will have to deal with is the repair of aircraft that have been damaged in combat. Aircraft will sustain damage from various threats including: air-to-air, air-to-ground, and ground-to-air threats. In order to achieve the maximum sortie generation rates, methods are needed to quickly repair battle damaged aircraft. Aircraft Battle Damage Repair (ABDR) techniques are currently being developed for many aircraft subsystems including transparencies.

Until the start of this program, there was little or no work being done to develop ABDR techniques for transparencies that would repair the transparency to a condition where the aircraft cockpit could be pressurized. Currently, damaged transparencies are repaired by bolting a sheet of aluminum over the damaged area. This technique is sufficient to keep the windblast out of the cockpit for a ferry flight, but would not be an effective repair for an aircraft making another combat mission. The philosophy of ABDR is not to fix the aircraft to "as good as new" condition, but to fix it so it can fly one more mission; therefore, simplicity and speed are major factors in the selection of ABDR techniques. To be effective, ABDR techniques must also make use of tools and materials that are readily available at an Air Force Base.[1]

This paper covers the progress of an initial effort to evaluate experimental ABDR techniques for bird impact resistant laminated transparencies. This program will determine the structural integrity of ballistically damaged transparencies to which the experimental repair procedures have been applied. The results of this initial program will be used to define additional development work which must be done to define ABDR techniques for all laminated plastic transparencies.

BALLISTIC DAMAGING

The first portion of this program consisted of ballistically damaging the transparencies using projectiles that represent Soviet threats. The damage was accomplished at the Air Force Flight Dynamics Laboratory's Aircraft Survivability Research Facility (ASRF) at Wright-Patterson Air Force Base, Ohio. To make the damage as realistic as possible, a recovered aircraft crew escape module was used to hold the transparencies during the damaging. The ASRF's Mobile Threat System, capable of launching a wide variety of projectiles, was used to fire all projectiles. The set-up of the module and Mobile Threat System is shown in Figure 1.

The projectiles used in this program included Armor Piercing Incendiaries (API), High Explosive Incendiaries (HEI), and fragments. The API's and the HEI's all represent either ground-to-air, air-to-air or air-to-ground threats. The fragments represent fragments from the detonation of a surface-to-air missile.

The Mobile Threat System was positioned 50 feet from the module. All projectiles (with the exception of the fragment) were down-loaded to simulate a stand-off distance of 2000 feet. The fragment was launched at a velocity to simulate a SAM detonation.

The first transparency was designated as a test transparency to determine what the typical amount of damage from three different threats would be. The first test shot was an API. The resulting damage consisted of a hole through the transparency with cracks in the outer acrylic ply radiating outward from the hole. An area of delamination, approximately 8 inches in diameter and charred from the incendiary material, occurred between two of the plies of the transparency. The second API test shot resulted in the same type of damage as the previous shot, but with a larger hole and more frequent and longer cracks. The area of delamination of this shot was actually slightly smaller than that on the first shot and was not charred by the incendiary. The fact that the delamination was not charred could have been due to a malfunction in the round.

The final API test shot was fired into the open left-hand side of the module and through a piece of plexiglass positioned approximately 3 feet from the inner surface of the right-hand windshield. This was done to simulate a projectile entering the module through one windshield and exiting through the opposite windshield. The round started tumbling when it penetrated the plexiglass and passed through the transparency sideways, making an oblong hole in the part. As with the previous shots, there was delamination and cracking of the outer acrylic ply. The cracking was more severe due to the bullet exiting instead of entering through the acrylic. The incendiary material was burned out by the time the round entered the transparency; thus, there was no charring in the delaminated area.

Twelve more transparencies were damaged with the various threats. The damage caused by all API's was similar to that of the test shots. A transparency showing the representative damage due to each of these rounds is shown in Figures 2 through 4. The damage resulting from a fragment, shown in Figure 5, was much less severe than that in any other shot. It resulted in a small hole through the transparency, with cracking of the outer ply in a 2 inch diameter circular area. The point detonating HEI resulted in severe damage, as shown in Figure 6. The transparency was delaminated over approximately half of its area, and a piece of the transparency, approximately 25 square inches, was blown out of the part. None of the repair techniques being evaluated were able to be used to repair this damage.

REPAIR TECHNIQUES

Once the transparencies were damaged, one structural repair specialist was brought in from each of the five operational USAF Combat Logistics Support Squadrons (CLSS) to perform the repairs. Each transparency was repaired using one of the techniques shown in Figures 7, 9, and 11. A number of different adhesives were used to determine which had quicker curing time and which made better pressure seals.

Repair Technique A, shown in Figure 7, consists of a polycarbonate patch on both sides of the transparency with a roughly fitted circular plug in the hole. For this program, the plugs were fabricated from old transparencies. The hole caused by the projectile must be enlarged to rid the transparency of the most damaged area and to create a clean circular hole for the plug to fit. The patch and plug are sealed and then secured with aluminum bolts placed at one inch intervals around the periphery of the patch. Five transparencies were repaired using this technique. The size of the enlarged circular hole

was varied from 2 to 4 inches in diameter, and one transparency was repaired using the technique with the plug omitted. Figure 8 shows this repair technique applied to a transparency.

Two transparencies were repaired using Repair Technique B, shown in Figure 9. This technique consists of simply gluing a cellulose acetate sheet to the outboard surface of the transparency. The only preparation required for this repair is to clean and degrease the surface, and smooth out the damaged portion so there are no pieces of polycarbonate or acrylic interfering with the patch. The cellulose acetate patch should cover the hole caused by the projectile and extend approximately two inches outside the most extensively damaged areas. For the windshields repaired with this technique, patches approximately six inches in diameter were used. Two different adhesives were used for this technique (one transparency being repaired with one of the different adhesives). Both adhesives were quick drying and dried clear. Future pressure and thermal fatigue testing will determine which adhesive is better for the application. Figure 10 shows this repair technique applied to a transparency.

Two transparencies were repaired using Repair Technique C, shown in Figure 11. The idea behind this technique is to incorporate the plug concept used in Technique A and the simplicity of the cellulose acetate sheet used in Technique B. The plug used in this technique is tapered rather than straight, with the diameter of the taper being larger at the inner surface of the transparency and smaller at the outer surface; therefore, the damaged area of the transparency must be cut to a circular hole and tapered. A tapered plug must be fabricated to fit the tapered hole. The plug is then glued into the hole and a cellulose acetate sheet is glued to the inner surface of the transparency. The cellulose acetate sheet is glued to the inner surface rather than the outer surface to do away with any adverse aerodynamic heating effects caused by a protruding patch. If any portion of the plug protrudes past the outer surface of the transparency, it can be ground away to a flush condition. Figure 12 shows this repair technique applied to a transparency.

The last transparency was repaired using Repair Technique C, with the exception that the cellulose acetate patch was omitted. A tapered plug was fabricated for the tapered hole and glued in place. Figure 13 shows the finished repair on the transparency.

FATIGUE TESTING

The final phase of this program, which has not been initiated yet, is to fatigue test the repair transparencies to determine their structural integrity. Fatigue testing will be conducted at the Air Force Flight Dynamics Laboratory Structures Test Facility at Wright-Patterson AFB, using the transparency static test fixtures (Figure 14). When this phase is started, the repaired transparencies will first be pressure tested at ambient temperatures to assure that the repairs can hold up to the pressures. Once the ambient tests are completed, the transparencies will go through pressure and thermal fatigue test cycles. Pressure and thermal fatigue testing subjects the test article to both the pressure and temperature conditions simultaneously. The pressure and temperature profiles will be the same as used to qualify the initial bird resistant laminated transparencies. The fatigue cycling results will be used

to determine the structural integrity of the repaired transparencies for an additional one hundred (100) flight hours.

DISCUSSION

The small amount of damage resulting from all projectiles except the HEI is very encouraging. It does appear to be possible to repair transparencies damaged by these projectiles to a condition where they can hold cockpit pressurization; however, further ballistic testing will have to be performed to determine the effects of the projectile entering the transparency at different angles. Future ballistic testing should also include damaging the transparency while it is in a pressurized module and/or in a moving airstream. The Flight Dynamics Laboratory's ASRF has the capability of ballistically damaging parts in an airflow of up to 550 knots. It will be interesting to see if these conditions have any added effects on the amount of damage created by each projectile.

Another factor that must be addressed in future testing is the adequacy of the pressure and thermal profiles used in this program. Since it is desired to determine the structural integrity of the repaired transparencies for fifty additional combat missions, it will be necessary to determine the actual pressure and thermal conditions each aircraft will see in a combat situation. Each combat aircraft will experience unique pressure and thermal conditions for their given flight mission. Using actual pressure and thermal profiles will lead to much more realistic test results.

This follow-on program will also determine the applicability of the repair techniques to use on other aircraft transparency systems. The high curvature of some transparencies could prove to be a problem when applying these repair techniques. Future programs will have to use these highly curved transparencies as test articles to determine the extent of this problem. It might be found to be necessary to develop and test more repair techniques than those already considered. Future programs will also include newly developed repair techniques to try to come up with the quickest, most structurally sound repair possible.

The eventual objective of the aircraft transparency battle damage repair program will be to publish a handbook that defines battle damage repair techniques for all transparencies. It will identify the tools and materials needed and the procedures for applying the repair to the transparency.

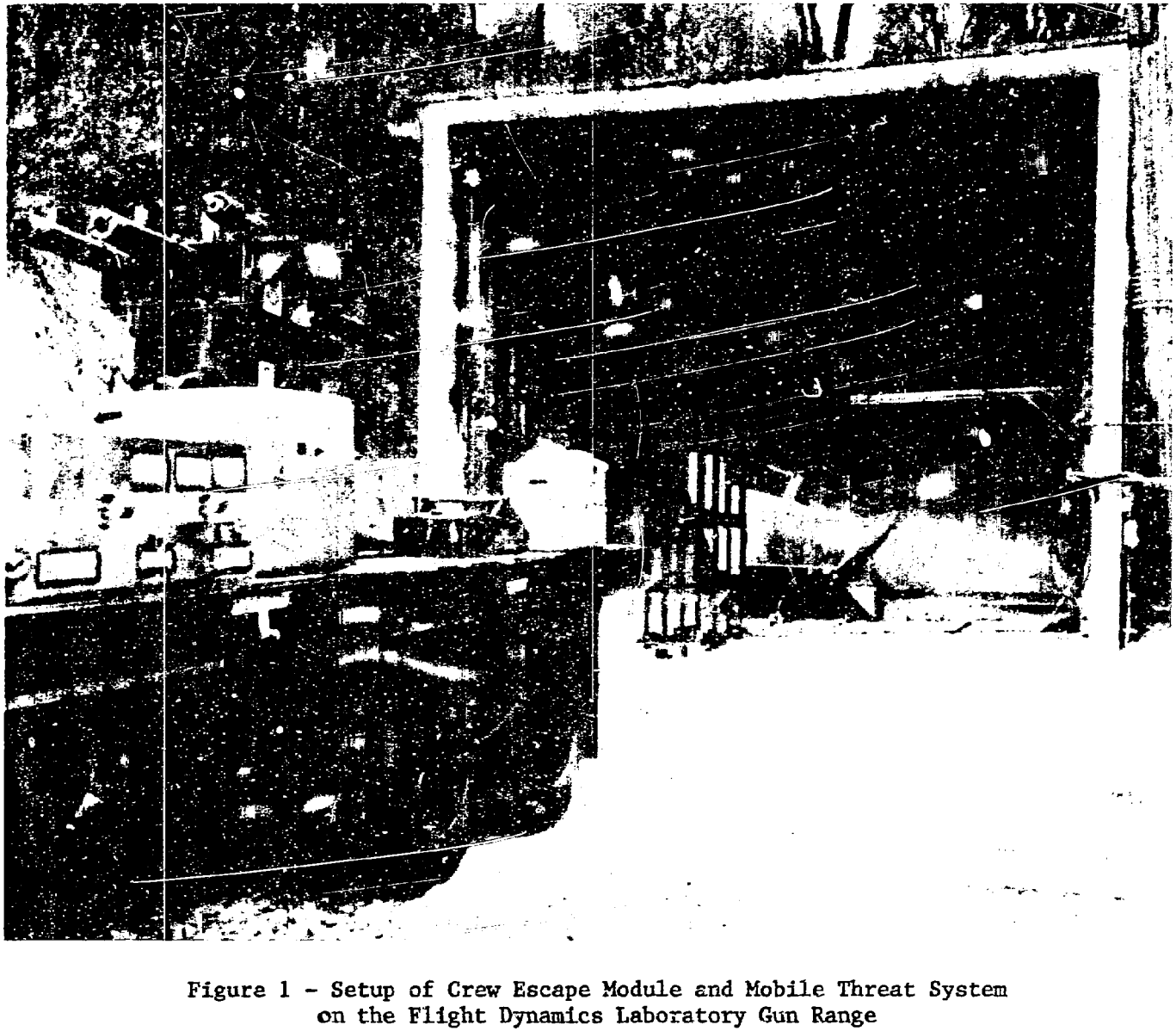

Figure 1 - Setup of Crew Escape Module and Mobile Threat System on the Flight Dynamics Laboratory Gun Range

Figure 2 - Typical Damage Resulting from Smallest Armor Piercing Incendiary

Figure 3 - Typical Damage Resulting from Largest Armor Piercing Incendiary

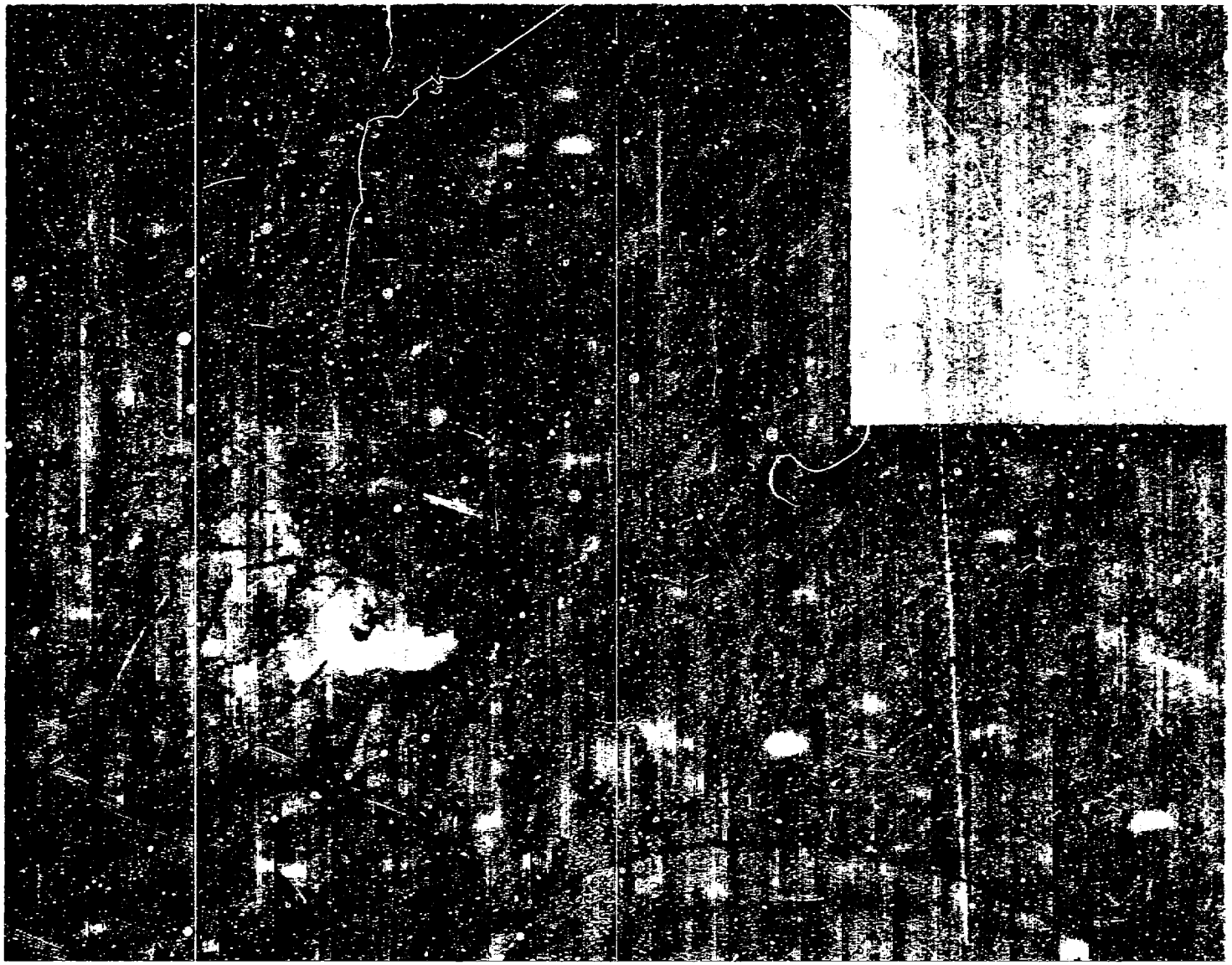

Figure 4 - Typical Damage Resulting from Tumbling Armor Piercing Incendiary

Figure 5 - Typical Damage Resulting from a Simulated Surface-to-Air Missile Fragment

Figure 6 - Damage Resulting from a High Explosive Incendiary

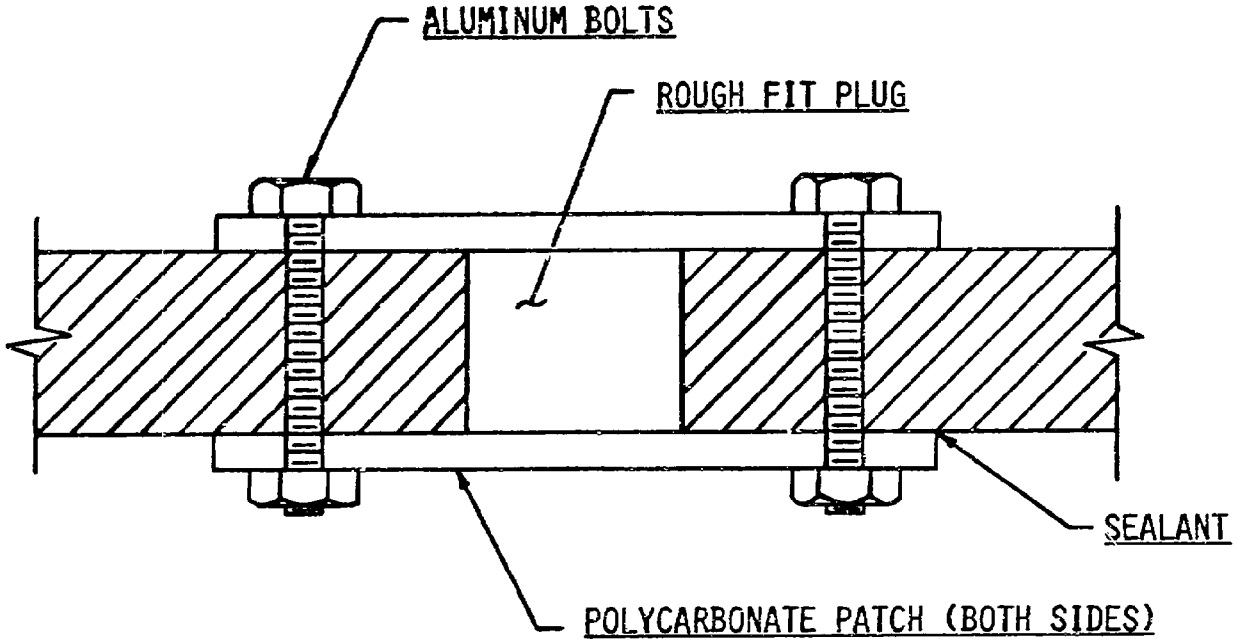

FIGURE 7 - REPAIR TECHNIQUE A

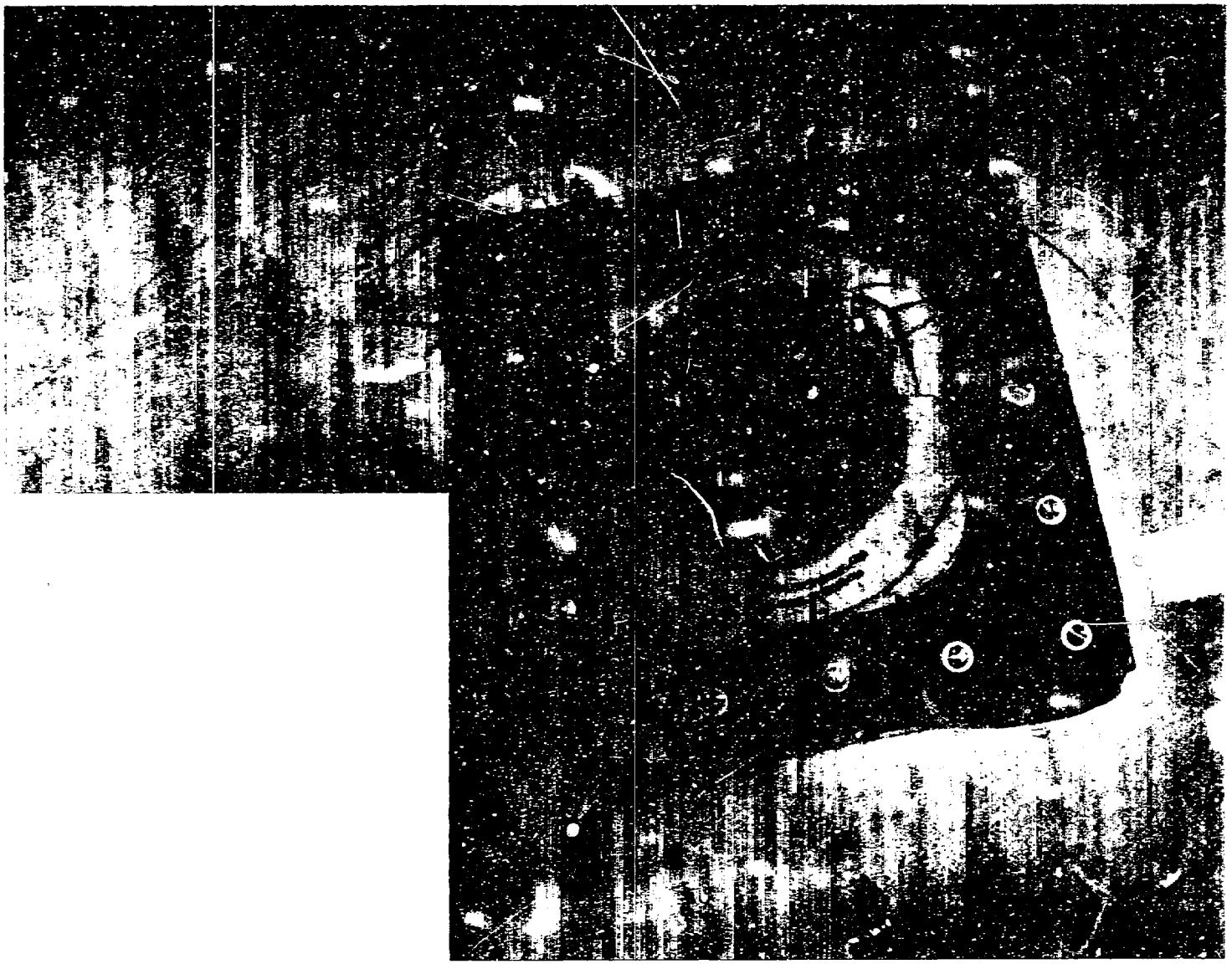

Figure 8 - Repair Technique A Applied to a Transparency

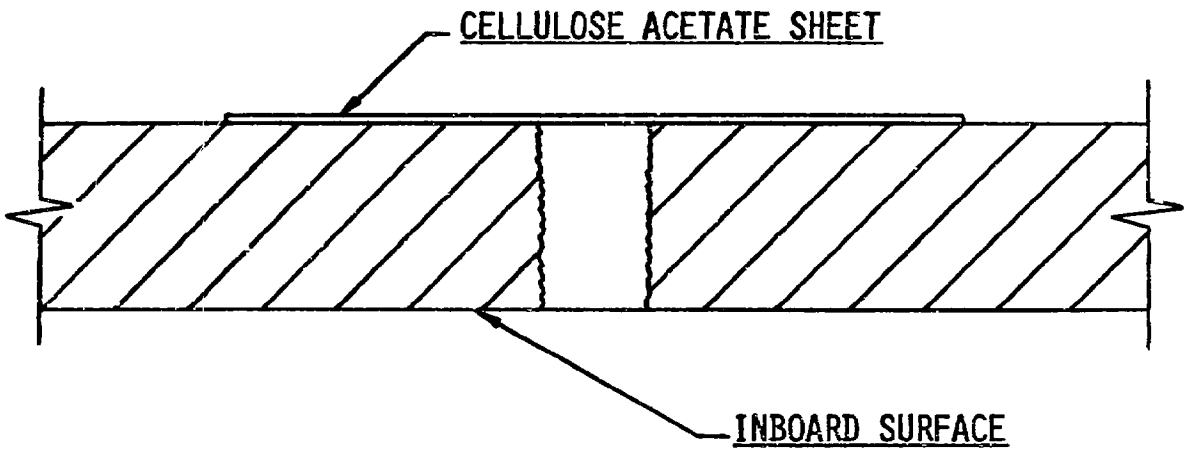

FIGURE 9 - REPAIR TECHNIQUE B

Figure 10 - Repair Technique B Applied to a Transparency

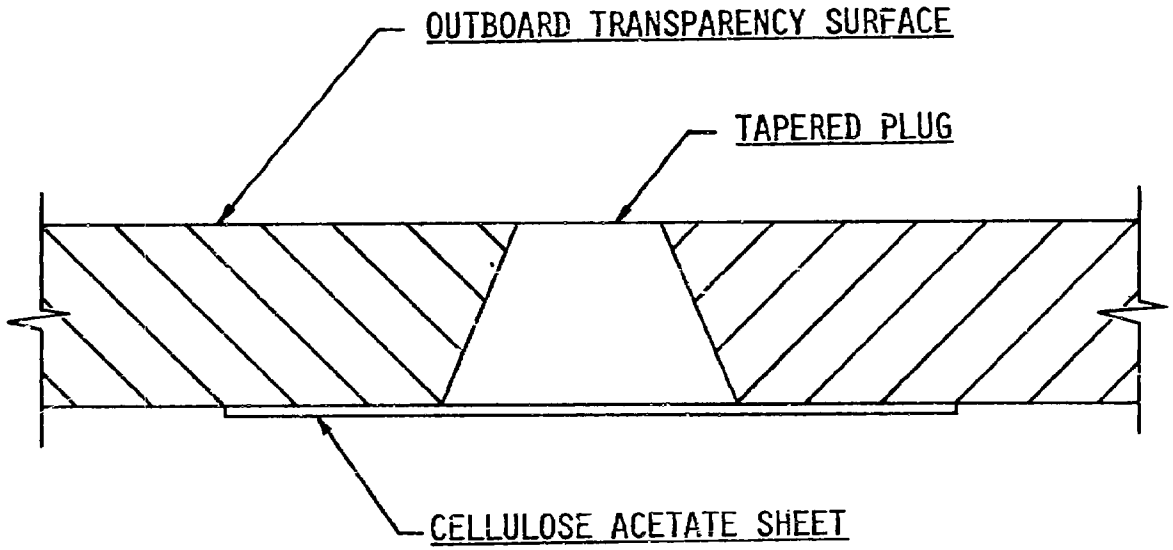

FIGURE 11 - REPAIR TECHNIQUE C

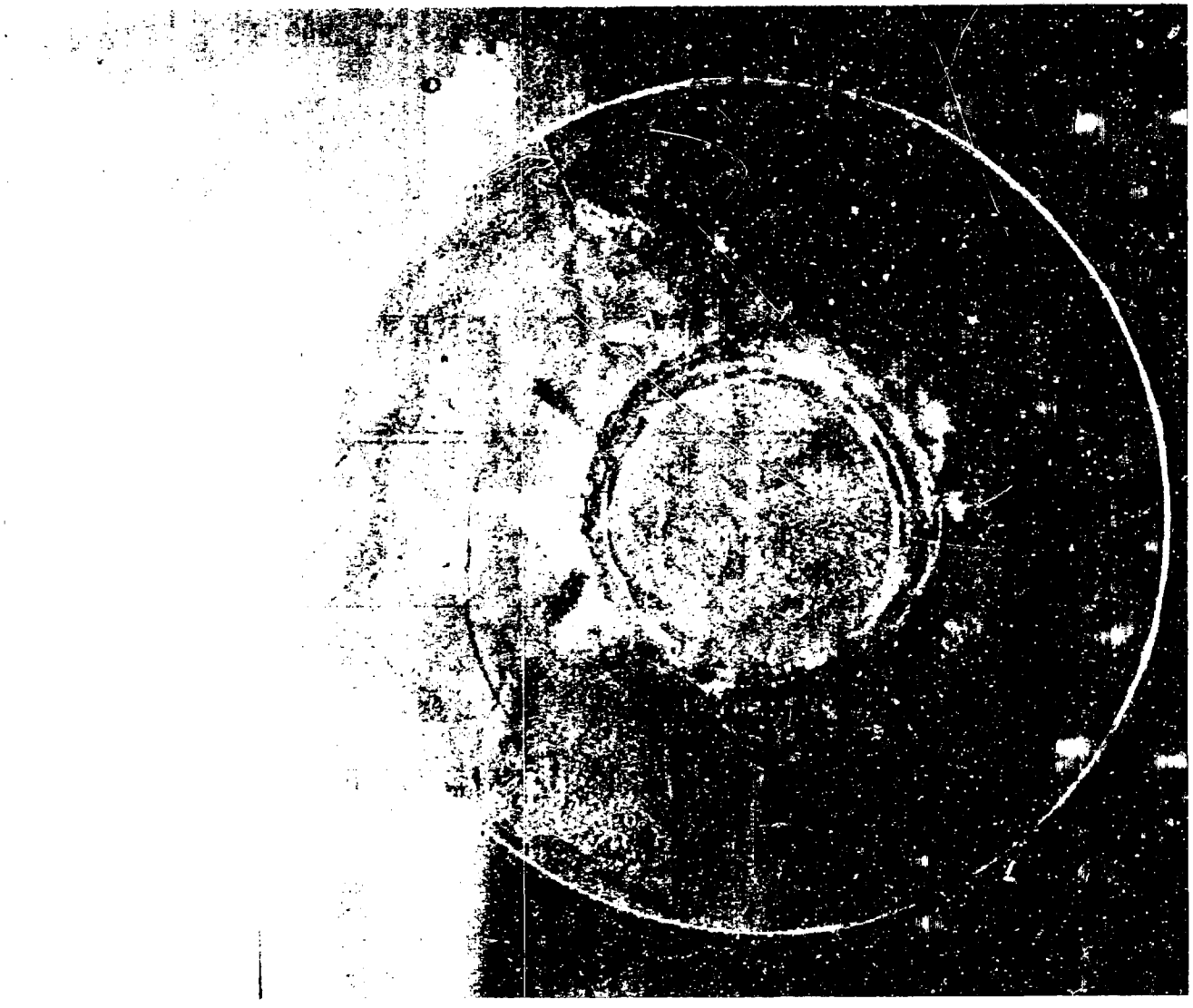

Figure 12 - Repair Technique C Applied to a Transparency

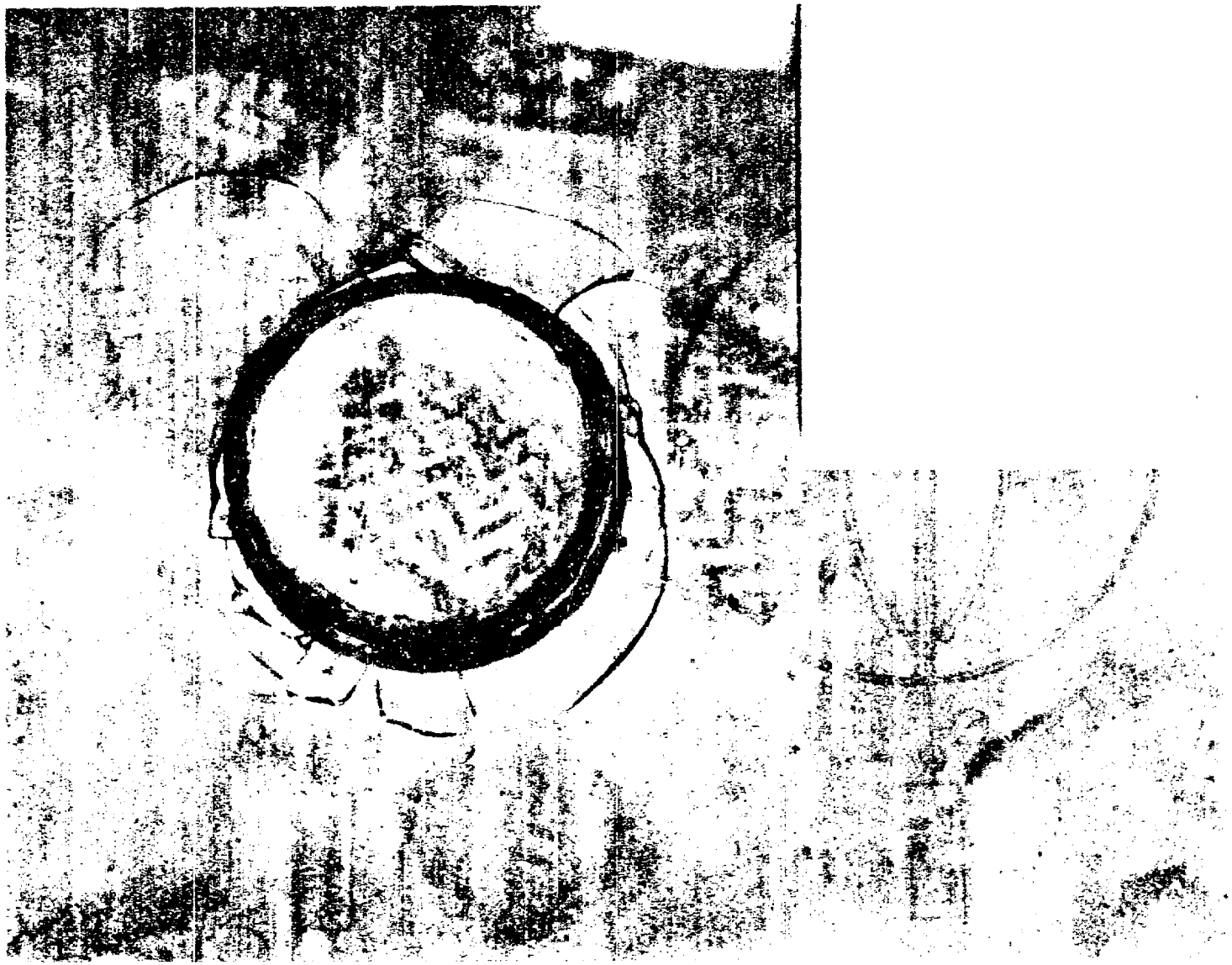

Figure 13 - Repair Technique C
(With Cellulose Acetate Sheet Omitted) Applied to a Transparency

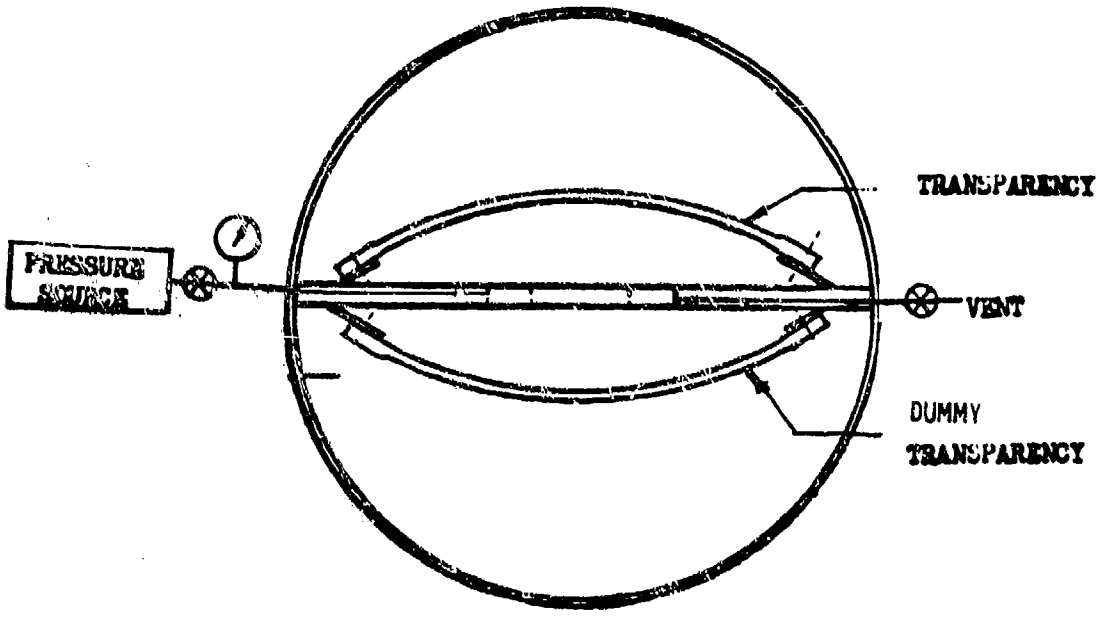

TYPICAL SECTION VIEW SHOWING SETUP
FOR INTERNAL PRESSURIZATION

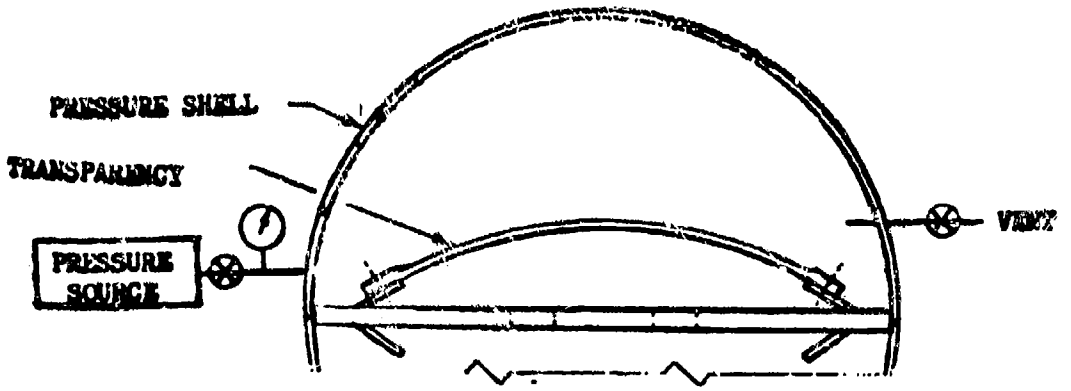

TYPICAL SECTION VIEW SHOWING SETUP
FOR EXTERNAL PRESSURIZATION

Figure 14 - Schematic of Transparency Static Test Fixtures

REFERENCES

1. Technical Manual General - Aircraft Battle Damage Repair, USAF, T.O. 1-1H-39, 15 March 1980.

AD-P003 186

WINDSHIELD WEIGHT REDUCTION THROUGH THE USE OF HIGH STRENGTH GLASS AND POLYURETHANE INTERLAYERS

J. H. Lawrence, Jr.,
Douglas Aircraft Company

WINDSHIELD WEIGHT REDUCTION THROUGH USE OF HIGH-STRENGTH GLASS AND POLYURETHANE INTERLAYERS

by
James H. Lawrence, Jr.
Douglas Aircraft Company
McDonnell Douglas Corporation
Long Beach, California

ABSTRACT

Polyurethane interlayers were developed during the 1970s and are a potential replacement material for the polyvinyl butyral interlayer, specified in MIL-G-25871, for laminated glass. In addition to the interlayer, higher strength glass has become available through the advancement of manufacturing techniques for thermally tempering glass that appears to be an improvement over thermally tempered glass, specified in MIL-G-25667.

Through minor modifications, current laminated glass windshields could be redesigned to utilize these new materials. Potentially, the resultant effect could be a weight reduction or an improvement for aircraft cold dispatch capabilities.

To fully quality a redesigned windshield for commercial aircraft, testing and analysis is required to meet FAA requirements for bird impact, fail-safe, environmental (anti-ice and defog), and optical qualities.

To utilize these new materials, full-size windshield specimens interchangeable with the DC-10/KC-10 were tested successfully to the FAR 25 requirements. The weight difference between the production windshields versus the lighter weight windshields was 17.5 pounds nominal.

INTRODUCTION

Commercial transport aircraft windshields must meet various Federal Aviation Administration (FAA) requirements. When laminated glass windshields are used to meet these requirements, they are generally manufactured in accordance with MIL-G-25871 specification. The glass is usually semitempered or fully tempered, and the laminating interlayer is limited to 20 percent 3GH plasticizer.

Shown in Figure 1 is the DC-10 windshield configuration designed in 1968. The design was based on a study of the then available historic data regarding crew compartment windshield designs. This design was intended to withstand bird impact with cold dispatch capabilities, have ease of maintenance for removal/replacement, and have a service life of at least 10,000 hours.

As the windshield was bird-impact tested under cold environmental extremes, these design commitments were met: the bird bounced, the windshield could be replaced by two men in less than 2 hours, and the service life eventually became in excess of 5 years.

Utilizing new materials of the 1970s, shown in Figure 2, a 33-percent-thinner polyurethane is substituted for the polyvinyl butyral, 16-percent-thinner high-strength glass is substituted for the MIL-G-25667 fully tempered glass core pane, and fiberglass was substituted for the outer aluminum insert. The purpose of substituting the fiberglass was to minimize the amount of cold thermal environment normally transmitted by the aluminum insert. Full-size specimens were obtained from each of two vendors for the testing described in subsequent paragraphs.

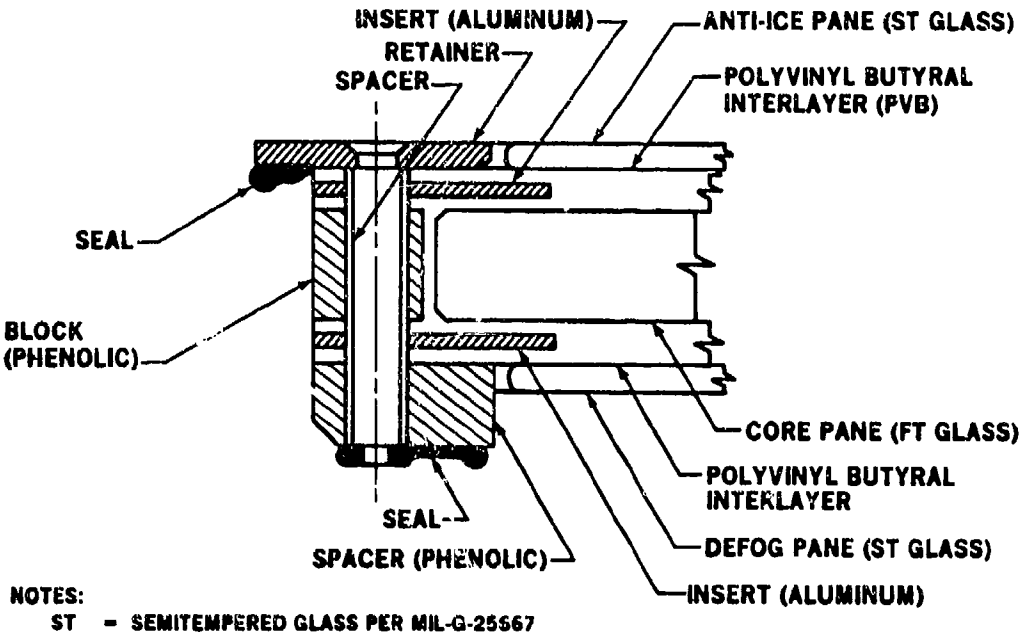

NOTES:
- ST = SEMITEMPERED GLASS PER MIL-G-25667
- FT = FULLY TEMPERED GLASS PER MIL-G-25667
- PVB = POLYVINYL BUTYRAL PER MIL-G-25871
- CONDUCTIVE COATINGS ON DEFOG AND ANTI-ICE PANE SURFACES

FIGURE 1. PRODUCTION WINDSHIELD CONFIGURATIONS

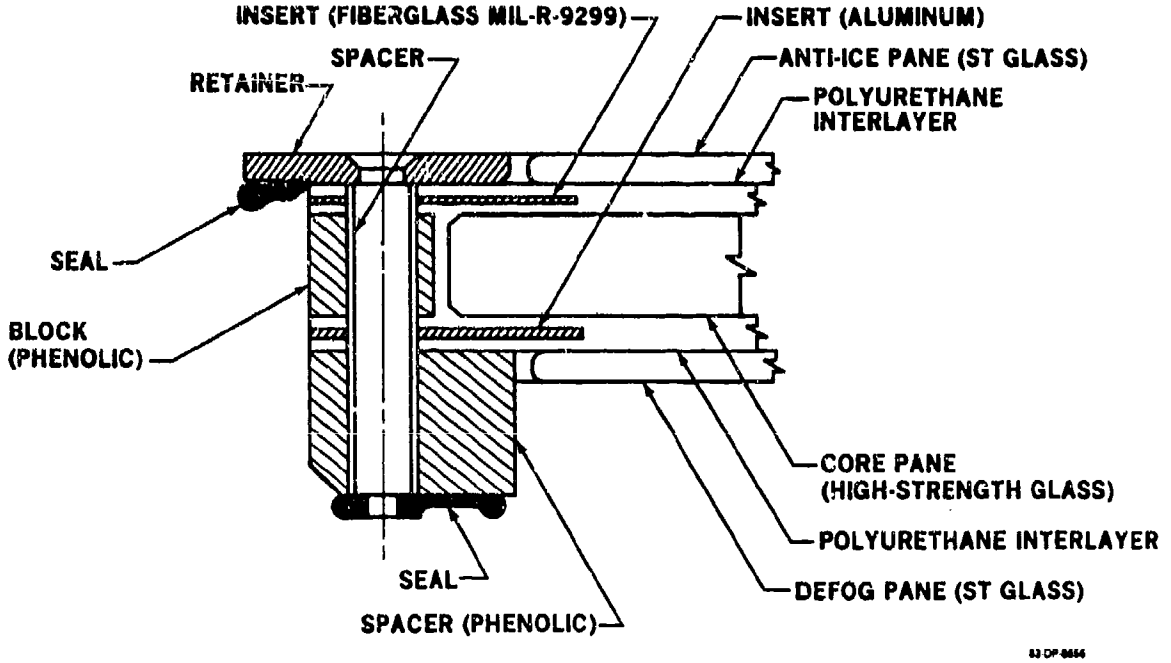

FIGURE 2. LIGHTWEIGHT WINDSHIELD SPECIMEN CONFIGURATION

BIRD IMPACT TESTING

The FAA requirements specify that the windshield must resist the impact of a four-pound bird at V_C of the aircraft at sea level under extreme temperature conditions. Prior to the introduction of the DC-10, windshields were tested on both a fixture representative of the aircraft support structure and on a full production DC-10 nose. Test results were comparable between those two test series.

The recent bird impact tests were conducted on a similar fixture at the National Research Council (NRC) in Ottawa, Canada. The facilities and equipment at NRC conform to the ASTM method F330-79 titled "Standard Method for Bird Impact Testing of Aerospace Transparent Enclosures."

A sufficient number of test conditions were defined to meet the FAA requirements, and additional requirements were specified that would give the airlines cold dispatch capabilities when either the anti-ice or defog panes were cracked. To show such windshield impact resistance, the shot locations selected were the windshield geometric center and aft upper corner. The impact at the center location would demonstrate the maximum deflection and the aft upper corner shots would demonstrate the maximum stress.

The following test conditions were established to meet the requirements, including those marked with an asterisk* which indicates that a minimum for FAA structural integrity had to be accomplished.

1. Windshield Center Shots

   *A. Electrical Systems Operating

   B. Electrical System Inoperative – Elevated Temperatures (Defog and anti-ice plies cracked)

   C. Electrical System Inoperative – Cold Temperatures (Defog and anti-ice plies cracked)

   *D. Electrical System Inoperative – Cold Temperatures (Defog and anti-ice plies inoperative – test if Condition C is not complied with)

2. Windshield Aft Upper Corner Shots

   *A. Electrical System Inoperative – Cold Temperatures (Anti-ice and defog systems off)

   B. Electrical System Inoperative – Cold Temperatures (Anti-ice and defog plies cracked)

   C. Electrical System Inoperative – Hot Temperatures (Anti-ice system may be off and/or glass plies may be cracked)

   *D. Electrical System Operating (Anti-ice and defog system on – test if Condition C above is not complied with)

These temperature conditions are compatible with the thermal extremes for normal operation of the DC-10/KC-10 aircraft, as dictated by MIL-STD-210. These temperatures also exceed the temperatures established by the FAA (formerly CAA) as the criteria for bird impact capabilities of currently used MIL-G-25871 materials.[1]

[1] Kangas, Pell and Pigman, George L., Impact Characteristics of Aircraft Windshields Incorporating Polyvinyl Butyral Plastic Interlayer, Technical Development Report No. 105, CAA Technical Development and Evaluation Center, Indianapolis, Indiana, March 1950.

FAIL-SAFE TESTING

The primary purpose of this series of tests was to determine the structural integrity of proposed lightweight windshields, with one or more detail glass components having failed when subjected to the combined effects of normal aircraft pressurization and extreme thermal conditions.

The secondary purpose of this series of tests was to establish deflection characteristics and determine the effect on the installation when subjected to normal, proof, and ultimate pressures under extreme thermal conditions.

The windshield is attached to the aircraft supporting structure through the interlayer and windshield edge structural components. The glass components transmit load through the bonding strength between the glass and the interlayers. It should be noted that these glass components are not mechanically attached to the aircraft structure.

Historically, polyvinyl butyral (per MIL-G-25871) has been used as the interlayer material for glass laminated windshields. For the parts used in these tests, the polyurethane interlayer and high-strength glass were incorporated. Compared to previous FAA certification windshield fail-safe tests, the performance of the polyurethane interlayer proved to be better than the prior polyvinyl butyral. In the temperature range of −65°F through +120°F the polyurethane was less susceptible to change; the elongation characteristics and the tear resistance seemed superior.

Due to the irregular shape of a transparency, as dictated by the specific shape of the aircraft in which it is installed, accepted industry practice is to test full-size transparency specimens on specially designed fixtures.

For these fail-safe tests, full-size specimens were mounted on a support frame representative of the aircraft, which was attached to an aluminum adapter plate. The adapter plate was mounted to a pressure fixture or box that was fabricated from steel. This pressure fixture was mounted on rollers so that it could be rolled into an environmental chamber. Contained in the pressure fixture were heaters with high-velocity fans to move air uniformly. Cooling of the air inside the fixture, to represent cockpit cabin, was done with refrigeration by an external compressor. Dry nitrogen was used as the pressurization medium to prevent moisture freezing problems at low temperatures. As a safety precaution, "pop-off" valves were incorporated into the system, as well as an electrically "normally open" exhaust solenoid for pressure relief in the event of a plant electrical failure while the tests were in progress.

To simulate external flight environments, the chamber used had temperature capabilities from −100°F to +200°F and had high-velocity airflow to represent aerodynamic airflow, but it was not used.

The electrical systems contained in the transparency specimens were operated and temperatures were controlled by monitoring the embedded sensing elements to maintain the required interlayer temperatures. Thermocouples were located on each side of the test specimens.

Deflections were taken at specified locations utilizing deflection transducers. These transducers had excellent linear readability and temperature range compatibility.

The entire sequence of tests was controlled by a computer. The whole test chamber, environmental chamber, fixture, and all of the data and control elements were fed through and operated by the computer. Pressurization was controlled by the same computer using a pressure transducer and solenoid valve system.

The test specimen internal sensing elements were closely computer monitored for resistance and for temperature conversions to meet the requirements and to determine the "off" and "on" cycling time of the electrical systems, thus maintaining required internal test-specimen steady-state conditions.

Pressurization tests performed on proposed DC-10 lightweight windshields subjected to extreme thermal conditions demonstrated the structural ability to perform under any conditions conceivable and met the fail-safe requirements of FAR 25, paragraph 25.775(d).

Two specimens were utilized in this series of tests. Various glass components of each specimen were failed to demonstrate the capability to perform under the FAA fail-safe requirements. The testing sequence and specimen conditions are identified in the following list:

1. Deflection Characteristics Testing (Undamaged Specimens)
2. Anti-ice and Defog Plies Cracked
3. Anti-ice, Core and Defog Plies Cracked
4. Core Ply Cracked
5. Anti-ice and Core Plies Cracked
6. Anti-ice, Core and Defog Plies Cracked

There was no evidence that the specimens could not perform structurally for long periods of time under the extreme pressure at altitude and thermal requirements required by FAR 25, paragraph 25.775(d).

It was further concluded that the laminating material described as polyurethane interlayer demonstrated superior performance to withstand the extreme conditions regardless of the glass component failed. This interlayer, because of its ability to perform more consistently under all temperature regimes, has greater elongation capabilities, has higher tear strength, and is a better laminating material than the currently-used polyvinyl butyral (per MIL-G-25871) for glass components. This superiority was demonstrated with only 66 percent as much polyurethane interlayer as the previously-used polyvinyl butyral.

The important features of the test results are presented. The tests are listed in chronological order with the headings describing the condition of the test specimen.

1. Deflection Characteristics Testing (Undamaged Specimen) — The purpose of these tests was to determine the maximum deflections at the centroid of a lightweight windshield subjected to normal, proof, or ultimate pressure for each of the thermal conditions.

It must be noted that the edge attachments are free to rotate under expansion/contraction caused by thermal conditions and under pressure loads. As a consequence, under cold thermal extremes, deflectometers will indicate a negative amount of deflection inward and under pressure will indicate a positive amount of deflection outward. Under the combined effects of thermal and pressure conditions, the stiffness of the interlayer material limits the amount of positive deflection depending upon the temperatures.

This test series represents a total of 15 hours of almost continuous testing under normal, proof, and ultimate pressure in conjunction with steady-state temperature conditions with extreme cold, hot, and room temperatures, while the anti-ice and defog electrical systems were operating.

The results of this testing were compared to the original DC-10 certification tests, and they were found to be comparable.

By virtue of the fact that the polyurethane is a stiffer material under the higher temperature regimes, it was shown that it requires only 66 percent as much polyurethane interlayer as polyvinyl butyral to perform the same operational functions.

2. Characteristics of Lightweight Windshields with Anti-Ice and Defog Plies Cracked – These tests were performed to determine the structural integrity of the lightweight windshield core ply under normal operating pressure and extreme thermal conditions as the anti-ice and defog plies are cracked.

In the design of glass laminated windshields, the core ply is considered to be the main load-carrying member. A goal of this test program was to determine the extent that the anti-ice and defog plies contribute to the stiffness and load-carrying capability of the total assembly.

In an attempt to obtain the maximum amount of information, the specimen was pressurized to normal operating conditions at room temperature; the pressure was maintained through the remaining temperature regimes.

It appeared that the difference between uncracked face plies and cracked plies was insignificant. There was minimal change in deflection through the temperature range which showed the consistency of the polyurethane interlayers reaction to loads in a constant manner.

The results of this testing indicated that with the two face plies cracked, the lightweight windshield satisfactorily performed under fail-safe conditions and met the requirements of FAR 25, paragraph 25.775(d).

3. Characteristics of Lightweight Windshields with All Glass Components Failed – The purpose of this series of tests was to determine the capability of the polyurethane interlayer material to withstand normal operating pressure, with all three glass components cracked, when exposed to extreme thermal conditions.

The core ply of the specimen previously tested was cracked.

The specimen was cooled down until it was in a cold steady-state condition (exterior −65°F temperature). Normal pressure was applied and held for 2 hours. The maximum deflection was 1-1/2 inches.

Heat was then applied for a period of 3 hours until the temperatures on the outside interlayer were as though the anti-ice electrical system were operative, and in the inner interlayer as though the defog electrical system were operative.

A normal operating pressure was applied and maintained for 2 hours. The specimen bowed out approximately 5-3/4 inches and maintained pressure.

This test result was compared to the original DC-10 certification testing on a production windshield similar to that shown in Figure 1. The original tests showed that under extreme hot temperatures the deflection or bow outward exceeded 12 inches. When the polyvinyl butyral is cold, the material is stiff and brittle; thus, the deflection is low, but when the material is heated to over 100°F the tensile properties decrease and the tear strength is very small.

It was thus shown that the polyurethane interlayer had a tensile strength and tear resistance great enough to withstand normal pressure at least 2 hours under extreme thermal conditions.

It was also shown that with all glass plies cracked in a windshield the polyurethane interlayer satisfactorily performed under fail-safe conditions and met the requirements of FAR 25, paragraph 25.775(d). Further, in the event all three glass plies were failed in-flight, the polyurethane interlayer would allow the pilot sufficient time to make a flight descent, reduce pressure, or both without causing discomfort to the passengers.

4. Characteristics of Lightweight Windshields with Core Ply Cracked — The purpose of this series of tests was to determine the capability of the lightweight windshield to withstand normal operating pressure with only the main load-carrying member (core ply) failed when subjected to extreme thermal conditions.

For this test series, consideration must be given to the construction of the laminated assembly. As noted, the core ply is clamped at the edges by the interlayers, the outer retainer, inserts, supporting structure, as well as being bonded to the interlayers. The defog ply, which is bonded to the interlayer, is not clamped at the edges but under pressure it pushes against the interlayer, insert, and core ply. The anti-ice ply, which is also bonded to the interlayer, is not clamped at the edges. So when pressure and thermal conditions are applied, if the bond strength of the interlayer to the glass is exceeded, the two tend to delaminate.

Since the core ply is laminated between the interlayers, it was expected that when cracked the glass cubes of the core ply would lock together under pressure.

The specimen over a period of 2 hours was cooled down to a cold steady-state condition for cold temperatures. The specimen was then pressurized and held in excess of 8 hours except for short intervals when equipment was adjusted. During this 8-hour period, tests were conducted through the required temperature ranges to include hot temperatures as though both the anti-ice and defog electrical system were operating.

This testing indicated that the anti-ice and defog plies contributed to a degree toward the structural stiffness of the assembly. Little change was observed during the cold conditions when the interlayer was stiff. However, when the temperatures were increased and the interlayer became heated, it appeared to stretch or elongate, and after 8 hours the deflections had increased to 0.390 inch. It was believed that the bond strength of the interlayer to the anti-ice and defog glass plies prevented any greater deflection.

Previously, with only the anti-ice and defog plies cracked but with the core ply as the main load-carrying member intact, the rate of elongation was negligible but for this test the elongation rate seemed to be almost twice as great.

These tests did, however, demonstrate that with only the main load-carrying member failed, the laminated assembly satisfactorily performed under fail-safe conditions and met the requirements of FAR 25, paragraph 25.775(d).

It must be concluded that the success of these tests was due mostly to the capability of the polyurethane interlayer to maintain its bond strength to the anti-ice ply and withstand the normal operating pressures under all temperature extremes. In the event of such a failure during flight, it has been shown that lightweight windshield meets the fail-safe requirements and the pilot does not have to change his flight objectives.

5. Characteristics of Lightweight Windshields with Core and Anti-ice Plies Failed — The purpose of these tests was to determine the capability of the lightweight windshield to withstand normal operating pressure with both the main load-carrying member (core ply) and the anti-ice ply cracked when tested to extreme thermal conditions.

The extent of the defog ply's structural integrity for sustaining pressure loads was demonstrated.

These tests were a continuation of the prior 8-hour test series. The pressure was reduced and the anti-ice ply was then cracked.

The testing sequence was in a cool down phase when the anti-ice ply was cracked. Within 20 minutes, after the normal pressure was resumed, the temperatures reached cold steady-state conditions as required. The maximum deflection obtained was 1.09 inches for the cold phase after 80 minutes under normal pressure. The test was shut down and allowed overnight to return to room temperature.

The next morning the test was resumed at normal pressure under room temperature conditions and held 120 minutes, at which time the maximum deflection was estimated to be 1-1/4 inches. The specimen was then subjected to increased temperatures to reach required high temperatures that would represent conditions as though both the anti-ice and defog electrical systems had been operating. The transition required 71 minutes to reach steady-state hot conditions. At the moment the required temperature were reached, the defog ply cracked and immediately the deflection increased from 1-1/4 inches to approximately 6.65 inches.

The first specimen completely cracked and bowed outboard approximately 5.75 inches; the second specimen completely cracked and bowed outboard approximately 6.65 inches under normal pressure. It was believed the two specimens were equivalent since the first specimen was subjected to only 4 hours of pressure with all three plies failed, while the second specimen was subjected to almost 14 hours of pressure after the core ply was failed. Yet, it was apparent that the anti-ice and defog plies did sustain load-carrying capabilities during the 14 hours and the polyurethane slowly elongated only at the hot temperatures.

From these tests it was again shown that the polyurethane interlayer had a tensile strength and tear resistance great enough to sustain normal pressure under extreme thermal regimes.

Once again, it was shown that a windshield with all three glass components failed would satisfactorily perform under fail-safe conditions providing the windshield had been laminated with the polyurethane interlayer. It was demonstrated, therefore, that the fail-safe requirements of FAR 25, paragraph 25.775(d) had been met.

6. Characteristics of Lightweight Windshield to Sustain Design Ultimate (1.5 times proof) Pressure Conditions with All Glass Plies Failed — This test was performed to determine the capability of the polyurethane interlayer material, the laminating medium of the lightweight windshields, to withstand design ultimate pressures when all three glass plies are failed.

The test specimen was thermally conditioned so that the resultant temperatures would represent the conditions of the anti-ice and defog electrical systems in operation.

Under temperature extremes, ultimate pressure was applied and held for 5 minutes. Gradually, the interlayer ballooned outward a maximum of 24 inches and maintained the pressure during the 5 minutes.

Previously, the two test specimens had demonstrated that at these elevated temperatures they were capable of maintaining normal pressure over long periods of time with a maximum outward bow of 6.65 inches.

Even though the conditions for this test would never occur in service, it was believed the high temperatures and the ultimate pressures would be the most severe conditions that could be imposed on a windshield. This test demonstrated the superior capability of the polyurethane interlayer to perform under the most adverse conditions. Comparatively, when similar fail-safe tests were performed on production-type windshields laminated with polyvinyl butyral, the maximum pressure they could withstand before complete failure with all glass plies intentionally cracked was less than proof pressure.

Without question, the polyurethane interlayer demonstrated its capability to withstand fail-safe requirements with all three glass plies cracked in a laminated windshield and to comply with FAR 25, paragraph 25.775(d).

OPTICAL EVALUATION

In an endeavor to evaluate these new materials and any effects the manufacturing processes for laminating these new materials would have on the optical quality, each test specimen was examined by the use of standard methods.

Optical quality considerations such as haze, orange peel, light transmission, deviation and distortion were assessed.

Inspection of the specimens showed no increase in haze properties of the polyurethane versus prior polyvinyl butyral interlayer. Neither was there any evidence of orange peel effects that have on occasion been prevalent in polyvinyl butyral interlayer windshields. Light transmission readings were taken of each specimen, and it was found that for this application it was possible that there could be a 2-percent reduction in light transmission compared to production windshield minimum values. The difference, should it occur, was considered to be insignificant.

Doubly exposed photographs, taken of a grid board before and after a specimen was in-place, were obtained for each specimen. It was found that the photographs were comparable to similar photographs of production windshields. These photographs, when properly interpreted, indicate the degree of angular deviation or distortion that might be prevalent in a laminated transparency.

When these photographs were compared to similar photographs of production windshields, no significant difference was noted.

Subsequently, specimens were compared to randomly selected production windshields by looking through the windshields at distant objects. It was concluded that the optical clarity of the polyurethane interlayer parts was better than that of prior production parts.

ENVIRONMENTAL REQUIREMENTS

As noted in Figures 1 and 2, the outer pane has an electrically conductive coating that, when energized, prevents the formation of ice on the windshield exterior surface. Likewise as noted in Figures 1 and 2, the inner pane has an electrically conductive coating that, when energized, removes fogging from the windshield surface next to the cockpit.

Since thermal studies were previously performed for the DC-10 configuration to determine the electrical power requirements and control temperatures in accordance with FAA specifications of FAR 25.773(a)1 and 25.773(b)1(ii), a thermal assessment had to be made of the new configuration.

Under operating conditions with the defog system on and anti-ice system off, more power is required to keep the defog surface clear. In general, with the thinner cross section, the new configuration shown in Figure 2 will heat up at a faster rate but the power requirements between the two configurations remain the same.

RESULTS

Specimens from one supplier have completed all of the FAA-required certification tests and are qualified for future production usage. Similar specimens from the second supplier have met 70 percent of the required bird-impact testing, and the remaining tests will be completed soon.

SERVICE EVALUATION

Six windshields have been obtained from the qualified supplier for service evaluation by DC-10 airline operators. The service evaluations indicate that their expected service life and reliability will be at least equivalent to those of current production windshields. After a year of service experience, it is anticipated that decisions can be made to use the lighter weight windshields on the DC-10/KC-10, the MD-100, and possibly the C-17 airplanes.

AD-P003 187

NEW AIRCRAFT WINDSHIELD APPLICATIONS USING ION EXCHANGE GLASS

W. W. Hornsey and W. F. Rothe,
PPG Industries Inc.

INDUSTRIES

NEW AIRCRAFT WINDSHIELD APPLICATIONS USING ION EXCHANGE GLASS

By

W. W. Hornsey and W. F. Rothe
PPG Industries, Inc.

INTRODUCTION

PPG has been involved in a continuing program to develop lighter weight, bird-resistant aircraft transparencies. This effort has been intensified in recent years due to higher fuel costs. In the pursuit of weight reduction, the effect on long-term reliability must always be considered. This is especially true in today's world of ever increasing maintenance costs. It is generally accepted that a laminated glass transparency is the most reliable product available. Its major disadvantage was the thickness and corresponding weight required to meet the bird impact and pressurization requirements.

PPG Industries has recently increased its inventory and thickness availability of Herculite II glass. Due to its superior Modulus of Elasticity and Modulus of Rupture, Herculite II glass in a transparency allows a significant reduction in the glass thickness required to meet the structural requirements, thereby reducing the weight of the transparency.

Since the bird impact requirement normally dictates the necessary glass thickness, PPG has embarked on an extensive bird-impact test program to determine the full potential of Herculite II glass. Past bird impact study results have been evaluated on a pass/fail criteria where a close grouping of several passes and failures on a cross section at a particular velocity are necessary to establish its true capability. To get a clearer idea of the actual bird impact resistance, the test samples were instrumented with strain gages and impacted at increasing speeds while strains were recorded using a high speed oscilloscope. This method offers several advantages:

1. more accurate prediction of failure velocity
2. more accurate prediction of the effect of angle change or interlayer temperature
3. reduced number of samples required to evaluate a particular design

TEST DESCRIPTIONS

The primary goal of the test program was to develop stress versus velocity curves for each of seven cross sections. To minimize the effect of other variables, the samples were 26 inches square with radius corners and were fabricated with outboard glass thickness and interlayer thicknesses held constant while the internal and inboard glass ply thicknesses were varied. Each sample was instrumented with a minimum of one 2-element rosette strain gage on the inboard glass surface opposite the impact point. Prior testing had confirmed that the maximum stress would always be at the inboard surface of the inner glass ply on two structural ply laminates. Some samples had additional element gages above and below the impact point to determine the peak stress location. To determine the effect of test frame stiffness, curves were developed at a 37° angle to the bird path in two different test frames which are shown in Figures 2 and 3.

To determine the effect of elevated temperatures, two cross sections were heated to an outboard surface temperature of 135°F and held until the inboard surface temperature had risen to 90°F. Heating was accomplished with an insulated heating blanket over the outboard surface which was removed just prior to impact. The test article was allowed to stabilize at room temperature between impacts.

All impacts were made at room temperature with four pound birds unless otherwise noted. A minimum of three impacts was made at each test condition to develop the stress versus velocity curve. All impacts were at the center of the sample.

TEST RESULTS

Figures 4 through 10 show the resulting data from the seven cross sections tested. The plots of stress versus bird velocity suggest a linear relationship for all of the parameters investigated. The general discussion of the test results for each of the parameters is as follows:

1. Effect of glass thickness

Figures 4 through 10 show that failure will occur at a stress of approximately 60000 PSI. This is to be expected since the unabraded Modulus of Rupture of Herculite II has been experimentally determined to be an average of 62000 PSI. To summarize the test results, the total Herculite II thickness is plotted versus the velocity where a stress of 60000 PSI would have resulted in the rigid and less rigid test frame and is shown in Figure 11. For comparison, the bird impact data on "Ten-Twenty" and thermally toughened glass which was published by M. J. Mott[1] of Hawker Siddeley Aviation Ltd. is also shown. This data indicates that

[1] M. J. Mott, "Experimental Investigation Into the Bird Impact Resistance of Flat Windscreen Panels with Clamped Edges," p. 347, Conference on Transparent Aircraft Enclosures, AFML-TR-73-126, Compiled by R. E. Wittman, June, 1973.

Herculite II in the less rigid frame has approximately 48% greater bird impact resistance than "Ten-Twenty" glass and 90% greater than thermally toughened glass. In the rigid fixture, Herculite II has approximately 79% greater bird impact resistance than thermally toughened glass and 38% greater than "Ten-Twenty" glass.

2. Effect of frame stiffness

Figures 5 through 10 show comparative plots for each cross section in the rigid and less rigid test frames (Figures 2 and 3). In all cases, the stresses were higher in the rigid frame for a particular velocity. The frame stiffness appeared to have a greater influence on the thinner cross sections.

3. Effect of elevated temperatures

Figures 6 and 10 show the comparative stresses in the rigid test frame at elevated temperature. (135°F outboard and 90°F inboard) Figure 6 suggests a 15% higher stress at elevated temperature while the thicker cross section in Figure 10 indicates a 22% higher stress.

4. Effect of impact angle

Table 1 shows the stresses recorded on a windshield sample consisting of two plies of .12 Herculite II laminated with .18 PVB interlayer during 150 kt impacts with two pound birds at different angles of the windshield's surface to the bird path. When the relationship between the recorded stress and the sine of the impact angle was quantified statistically the resulting correlation coefficient was significant at a greater than 90% confidence level.

TABLE I

Average of windshield surface to bird path path (degrees)	Peak stress at 150 kt impact (PSI)
30 °	25195
37	36100
45	46598
60	58372

5. Effect of strain gage location

The samples that had additional strain gages above and below the impact point confirmed that the peak stress was under the impact point on the inboard surface.

CONCLUSIONS

The greater Modulus of Elasticity and Modulus of Rupture of Herculite II glass will allow the design of significantly lighter aircraft transparencies while maintaining the long service life and low maintenance requirements long associated with glass.

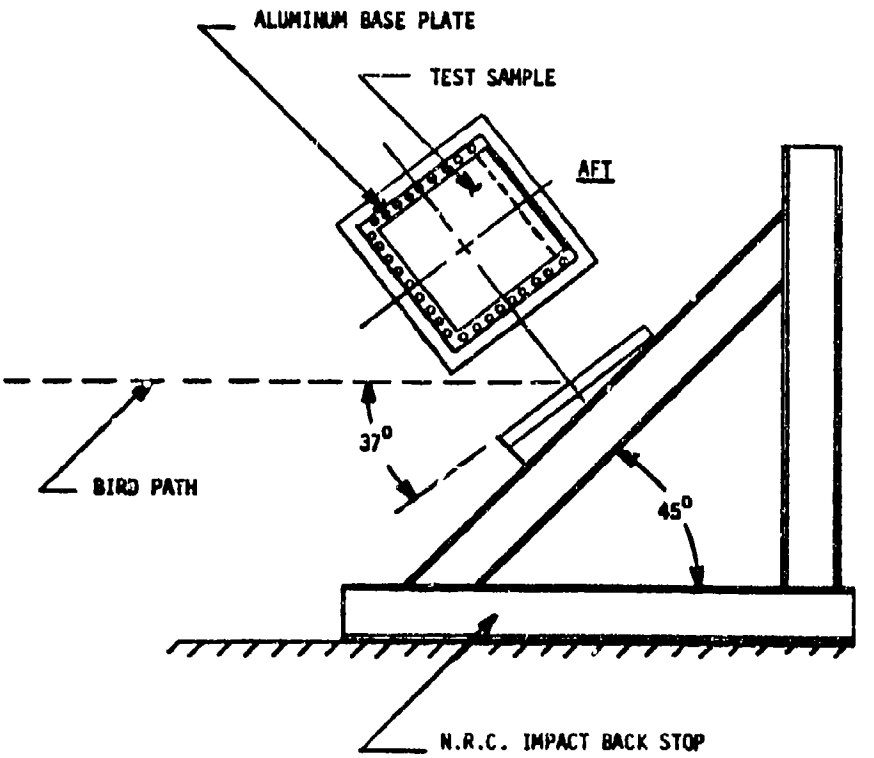

TEST SET UP

FIGURE 1

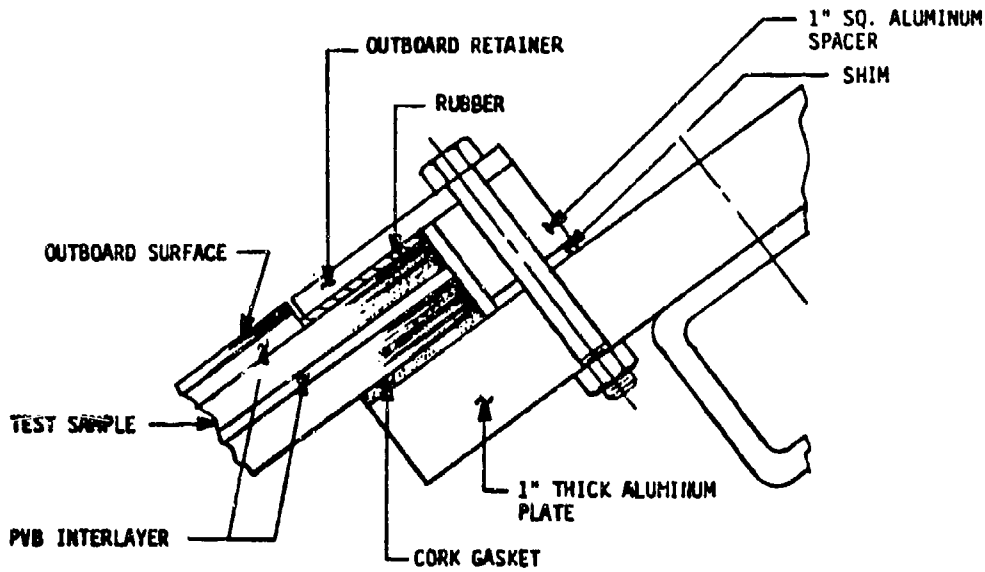

RIGID TEST FRAME
FIGURE 2

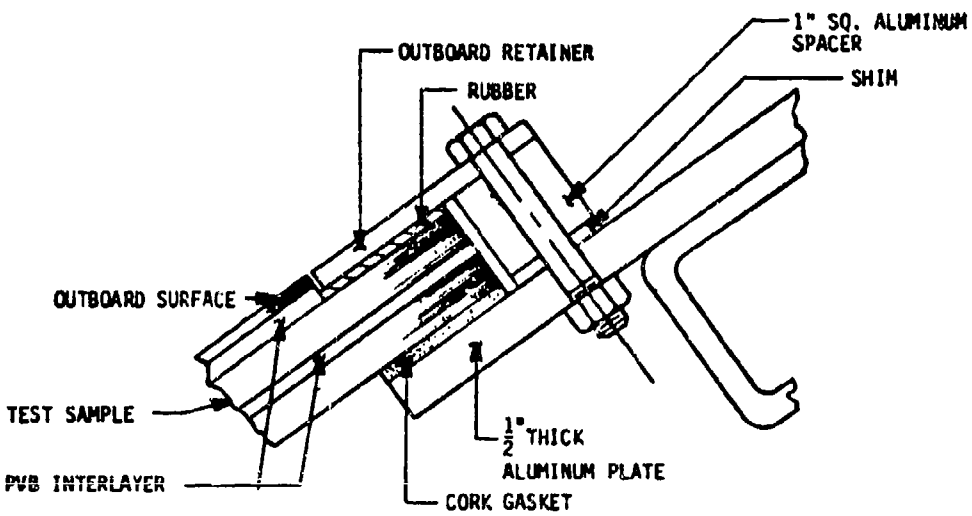

LESS RIGID TEST FRAME
FIGURE 3

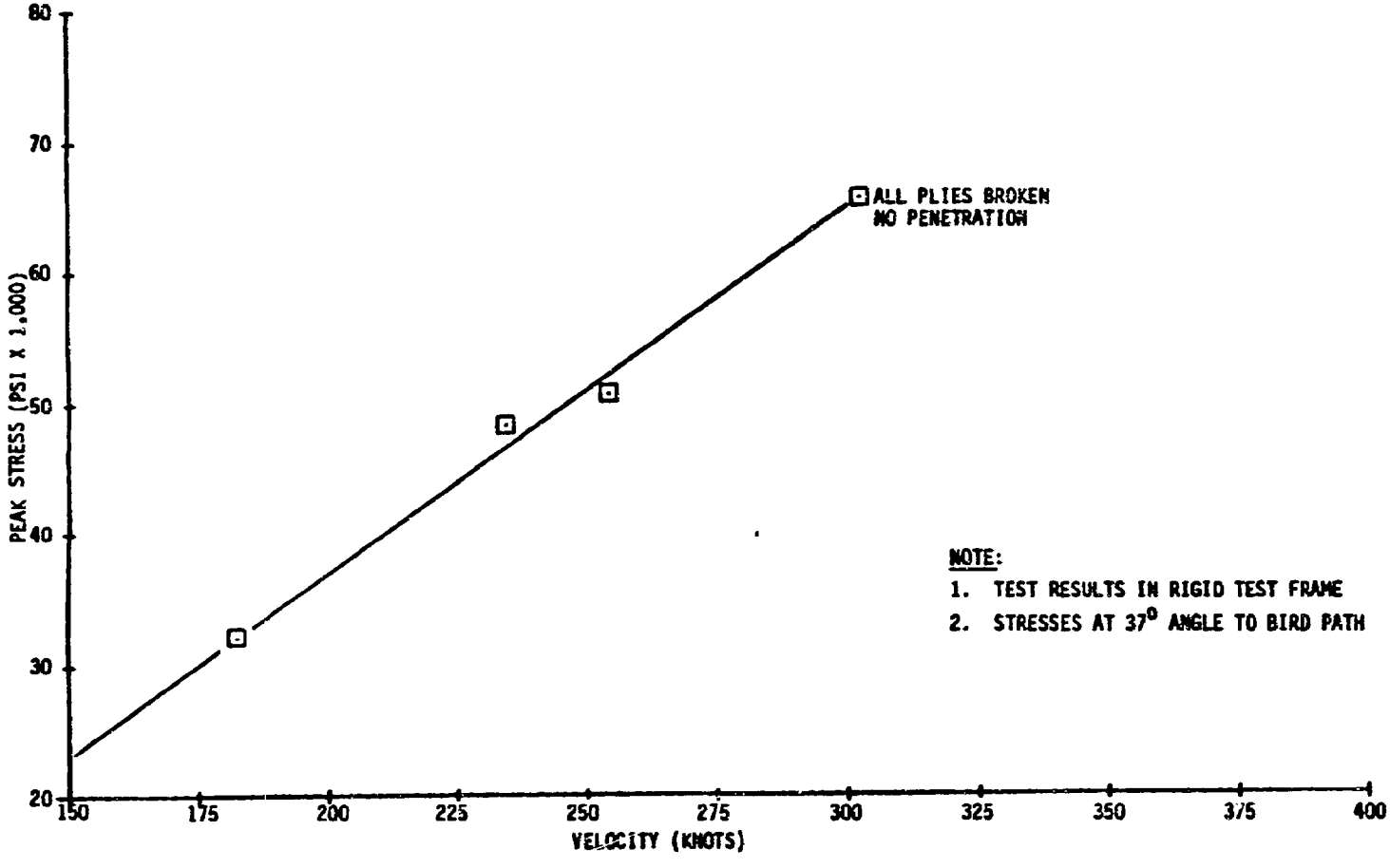

FIGURE 4 — .50 TOTAL HERCULITE II THICKNESS

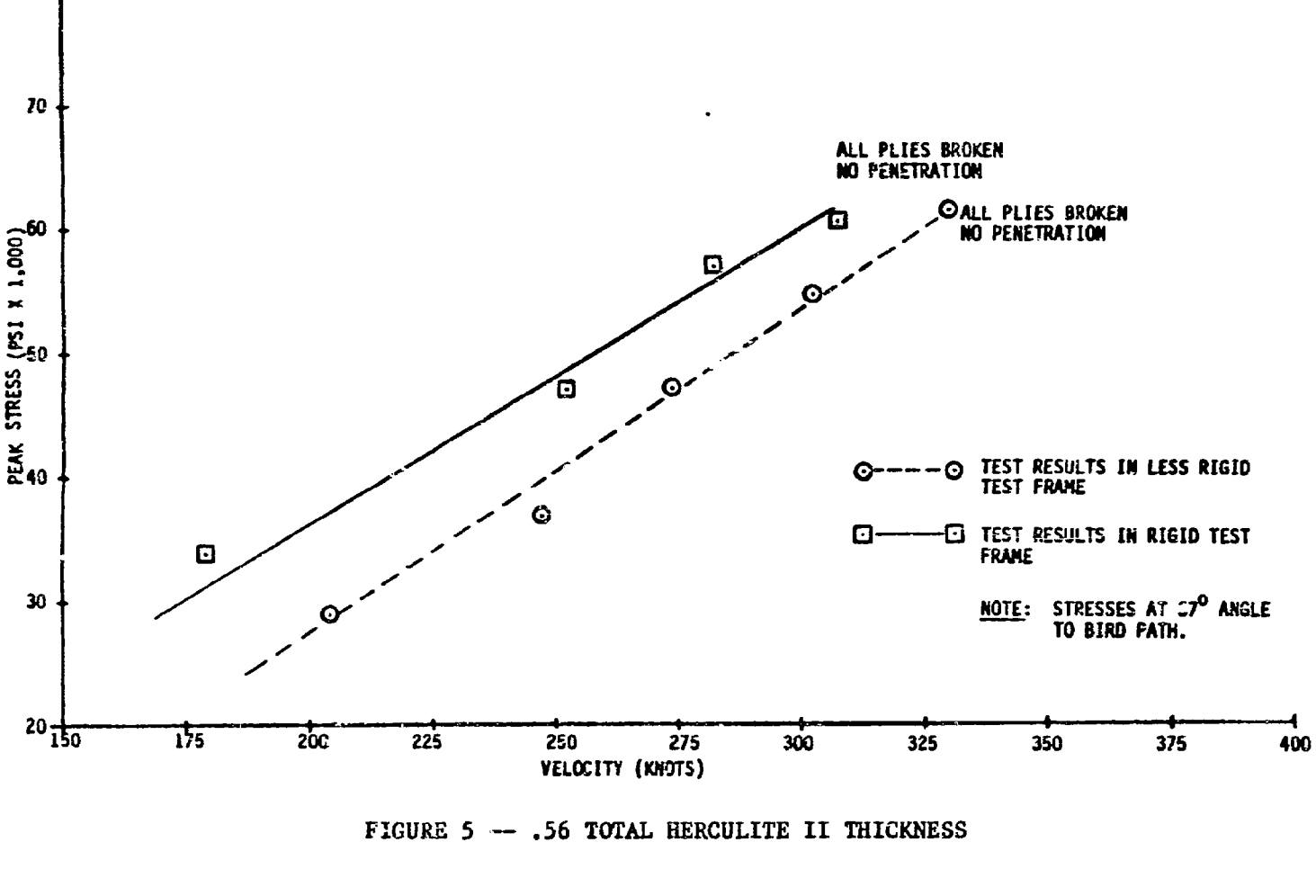

FIGURE 5 — .56 TOTAL HERCULITE II THICKNESS

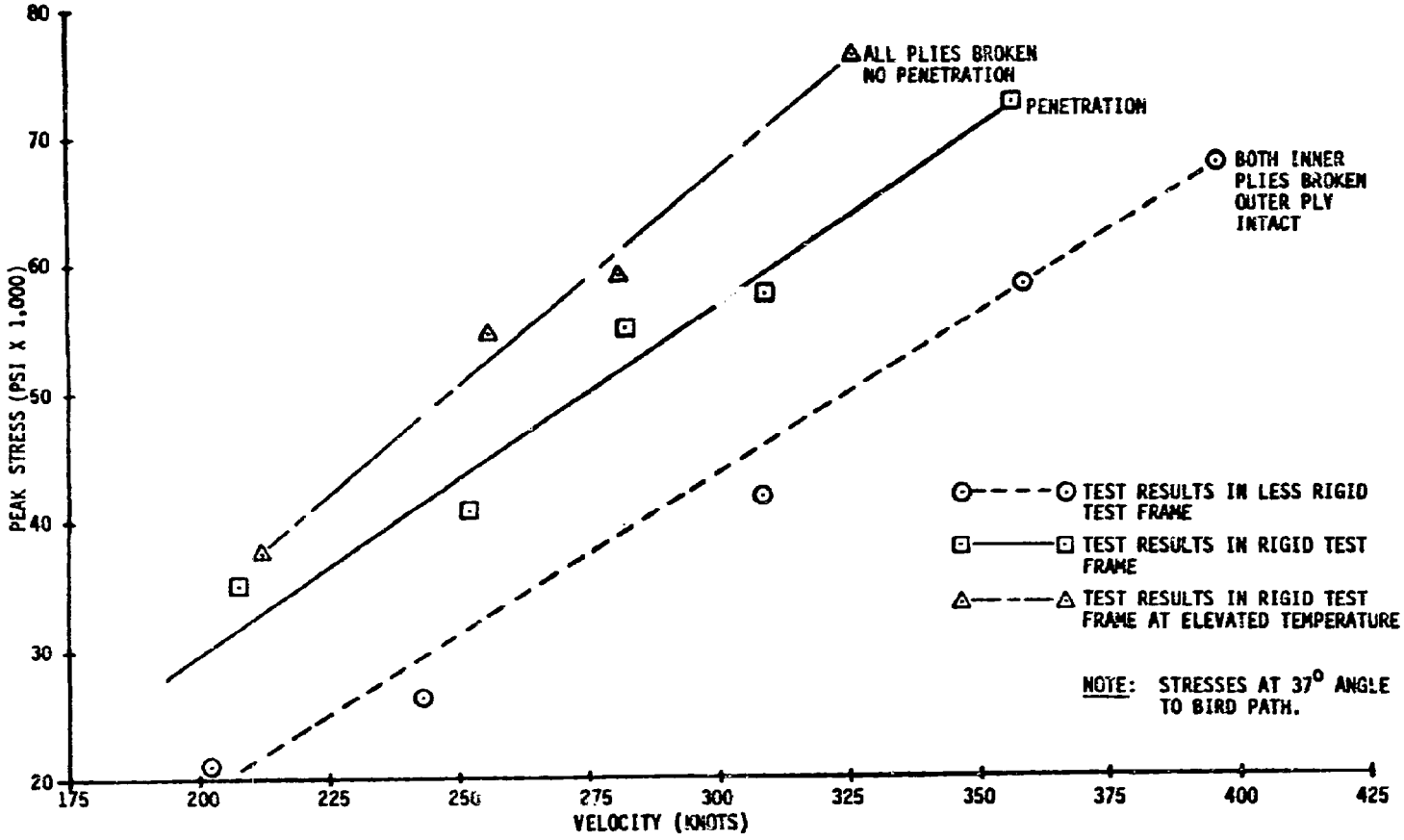

FIGURE 6 -- .625 TOTAL HERCULITE II THICKNESS

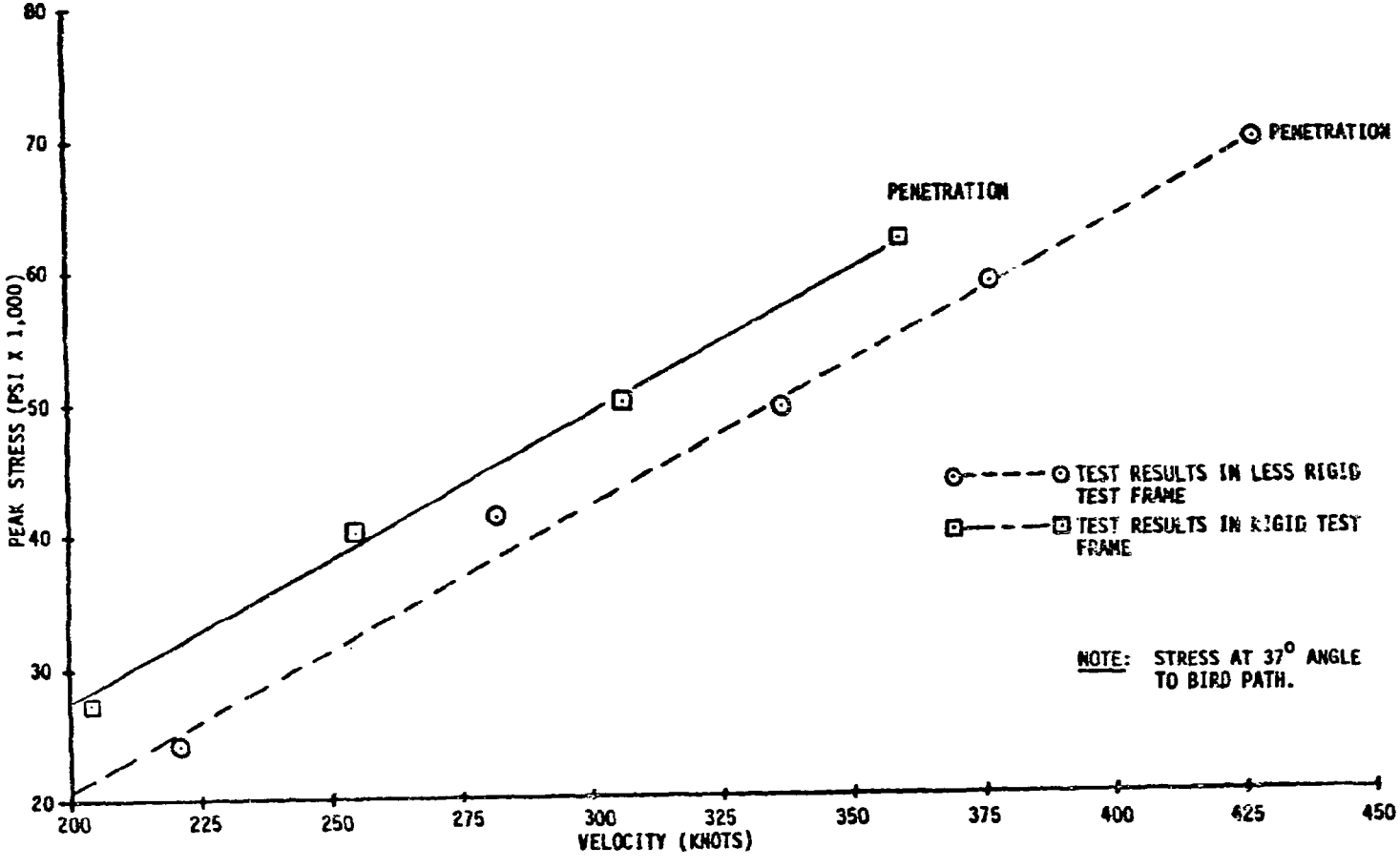

FIGURE 7 -- .69 TOTAL HERCULITE II THICKNESS

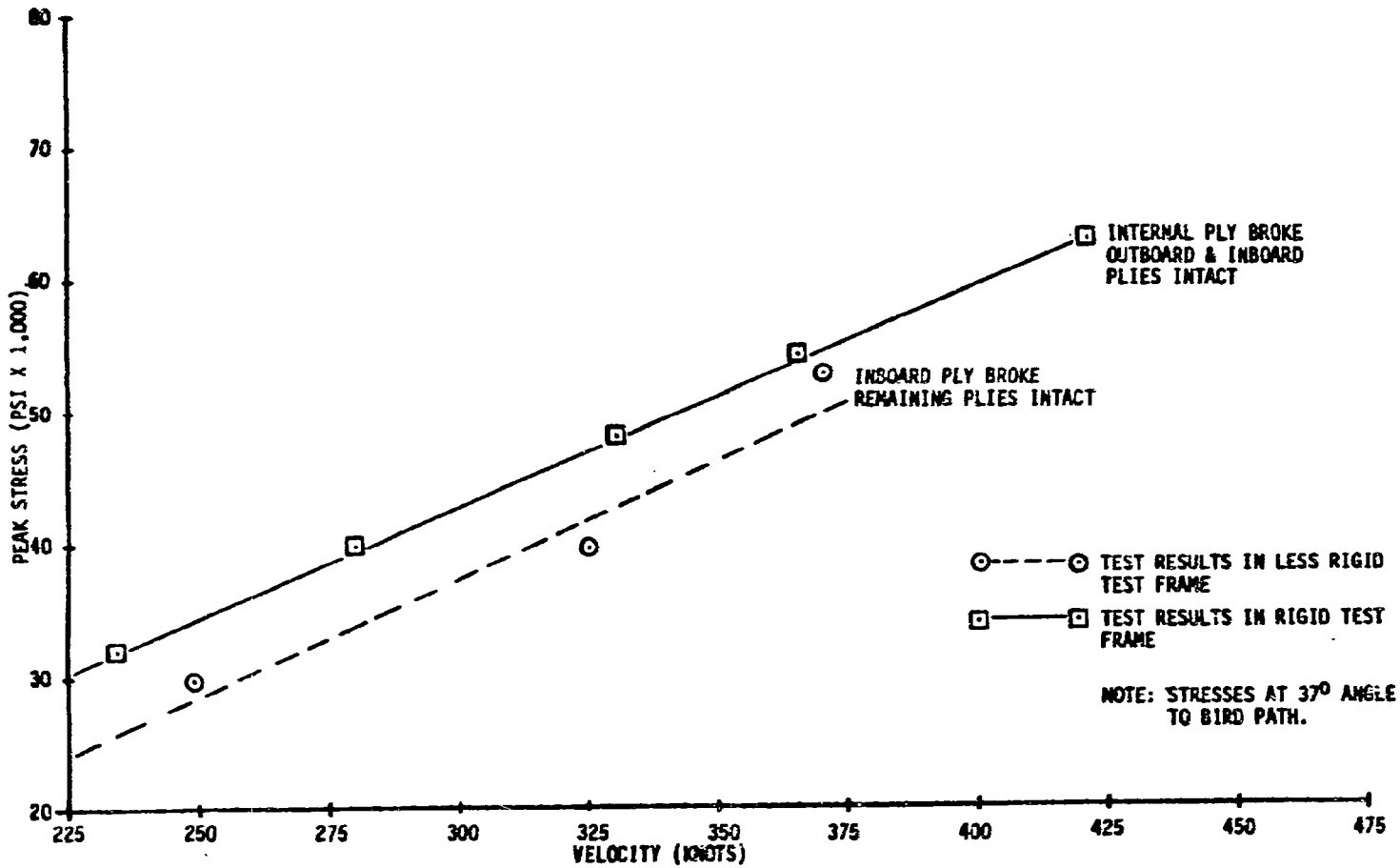

FIGURE 8 — .75 TOTAL HERCULITE II THICKNESS

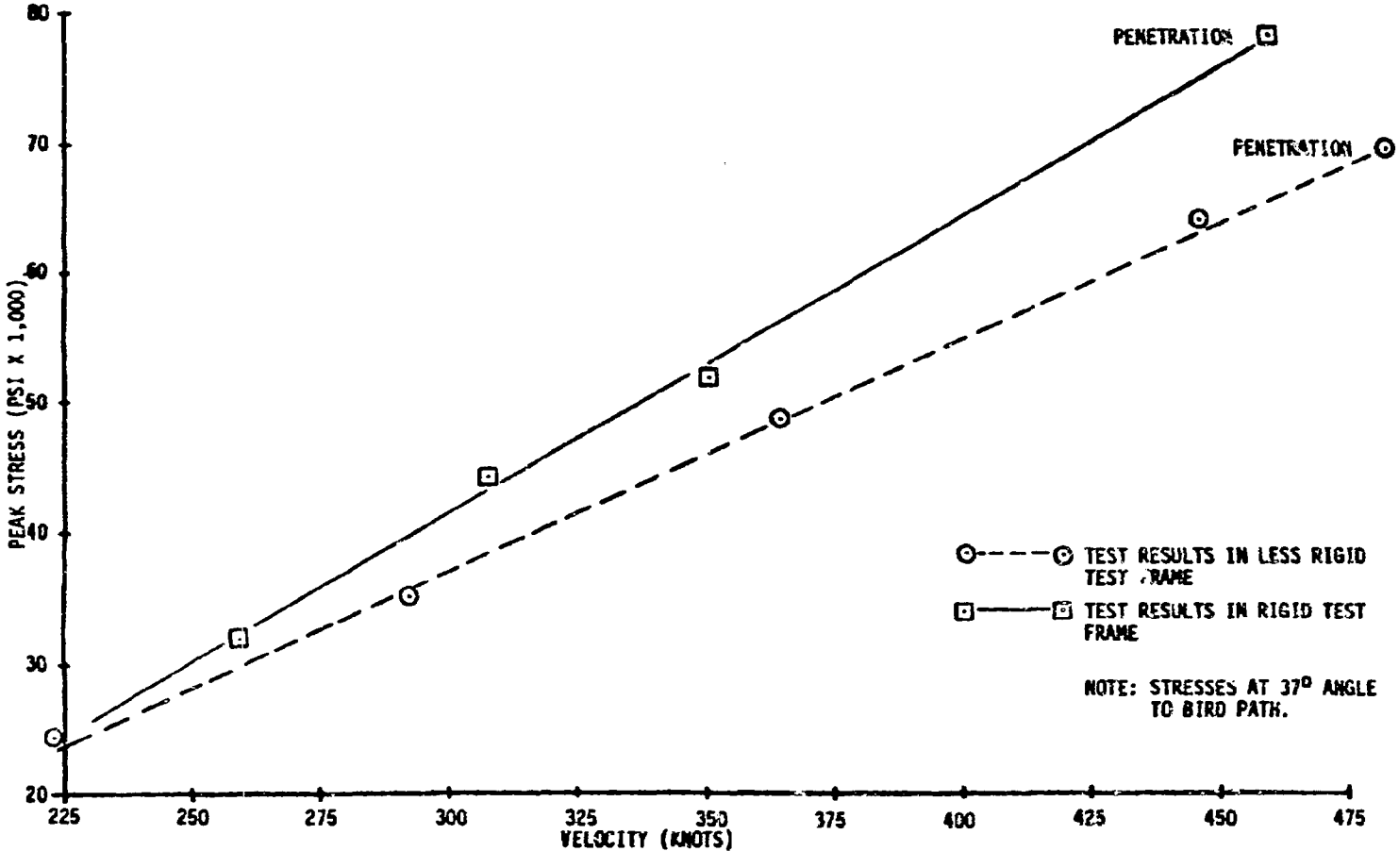

FIGURE 9 -- .81 TOTAL HERCULITE II THICKNESS

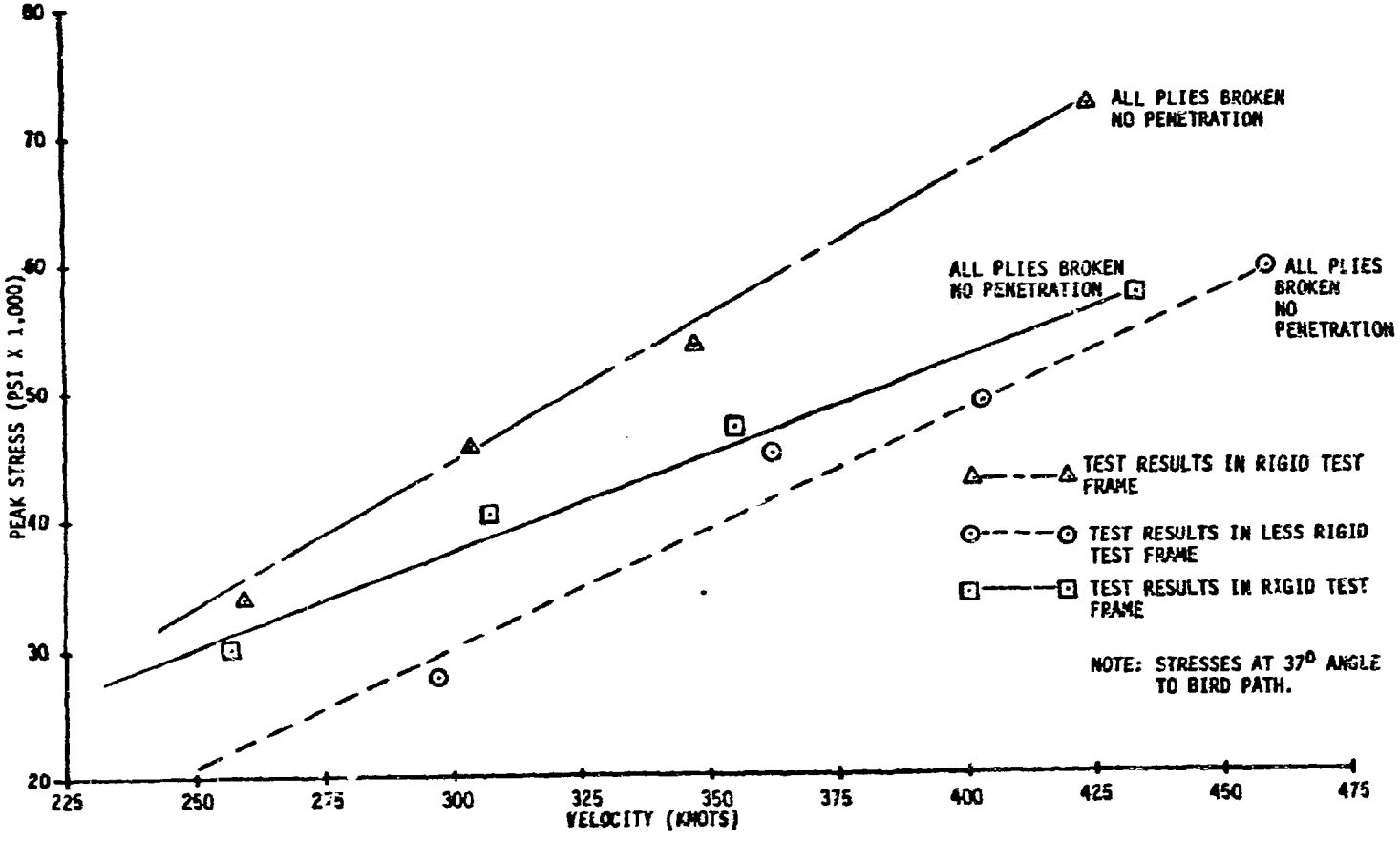

FIGURE 10 — .875 TOTAL HERCULITE II THICKNESS

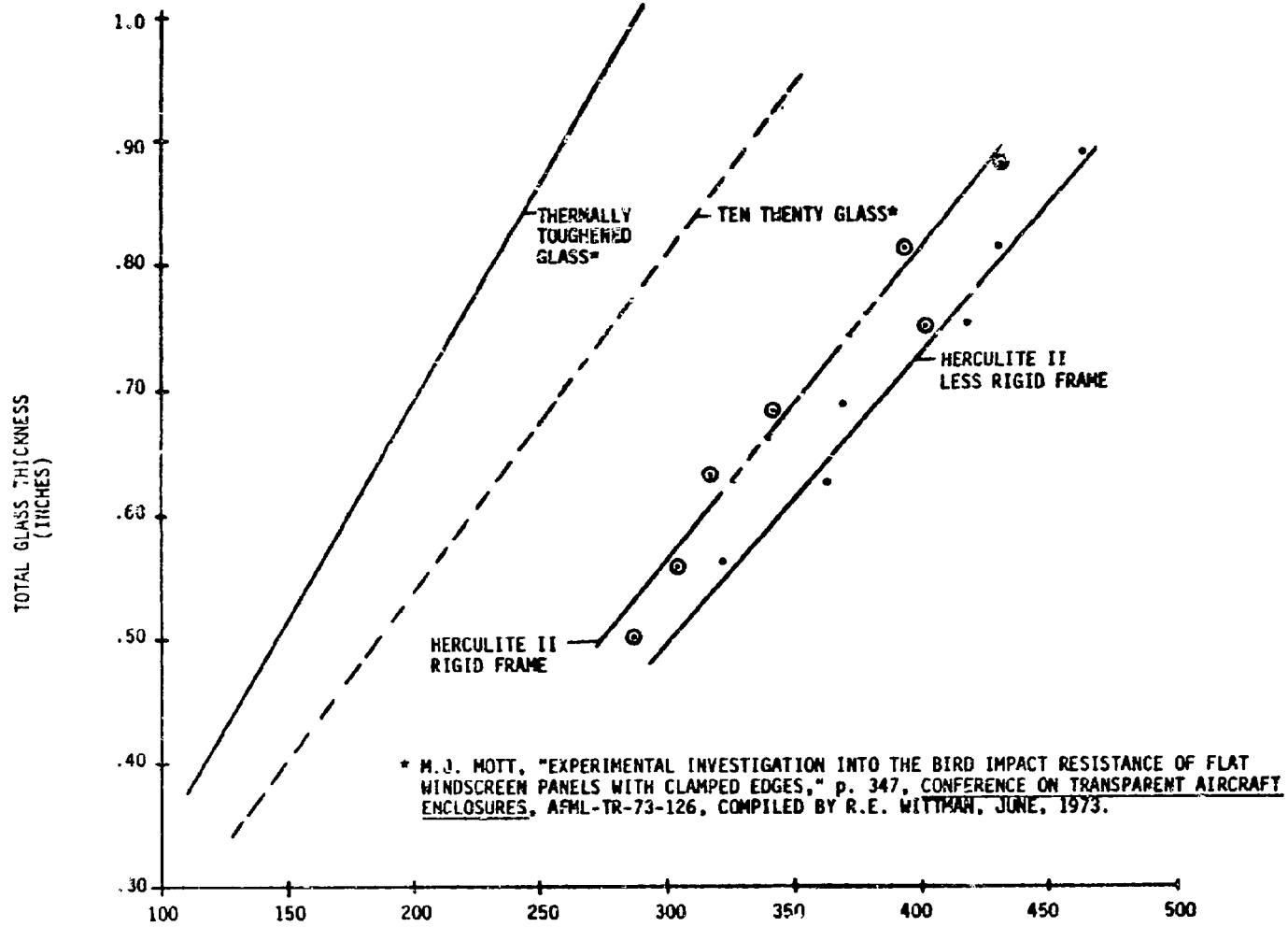

* M.J. MOTT, "EXPERIMENTAL INVESTIGATION INTO THE BIRD IMPACT RESISTANCE OF FLAT WINDSCREEN PANELS WITH CLAMPED EDGES," p. 347, CONFERENCE ON TRANSPARENT AIRCRAFT ENCLOSURES, AFML-TR-73-126, COMPILED BY R.E. WITTMAN, JUNE, 1973.

FIGURE 11

SESSION I

EMERGING SYSTEMS CAPABILITIES (PART II)

Chairman: J. H. Lawrence, Jr.
Douglas Aircraft Company
Long Beach, California

Co-Chairman: D. S. Riddle
Grumman Aerospace Corp
Bethpage, New York

AD-P003 188

A NEW AND UNIQUE CONDUCTIVE ELEMENT FOR AIRCRAFT TRANSPARENCIES

D. M. Trebes and J. B. Olson,
Sierracin/Sylmar

A NEW AND UNIQUE ELEMENT FOR AIRCRAFT TRANSPARENCIES

Jan B. Olson*

Dave M. Trebes**

Sierracin/Sylmar

ABSTRACT

A significant breakthrough in transparent conductive elements has been achieved by extending and modifying sophisticated microcircuitry technology to the scale and materials used in aircraft windshields. The resultant conductive element possesses more potential for versatility than any contemporary transparent element type.

Like conventional "wiggle-wire" elements, this new element is comprised of myriad thin filaments which are too small to be individually visible from normal distances. Based on a photolithographic technology and lacking mechanical constraints, however, this unique element produces infinitely more design flexibility than the conventional wire elements. Design parameters such as wave form, pitch, amplitude, filament width and spacing can be varied at will, even on the run; i.e., within a given filament. The technique lends itself to computerization, and general programs have been developed to provide design solutions in minutes. The flexibility of this technology will allow more difficult areas to be heated more uniformly than presently.

Advantages over existing elements include:

1. ability to heat more difficult shapes uniformly,
2. control over wave-form to eliminate "star-burst" diffraction annoyance in "wiggle-wire" elements,
3. better mechanical stabilization and thermal coupling to rigid plies raises power density limitations due to blurring phenomenon inherent in wire elements buried in thermoplastic interlayers, and
4. ideal for EMP application directly to rigid plies.

* Vice President - Engineering
** Manager, Advanced Technology
Sierracin/Sylmar
Division of The Sierracin Corporation
12780 San Fernando Road
Sylmar, California 91342
© Sierracin Corporation, 1983

A NEW AND UNIQUE CONDUCTIVE ELEMENT FOR AIRCRAFT TRANSPARENCIES

INTRODUCTION

In 1980, Sierracin/Sylmar embarked on an ambitious program to develop a superior low-voltage transparent conductive element. This effort was undertaken to provide ourselves with a totally complete aircraft transparency capability, as this was the only significant gap that remained after acquisition of the all-glass product line from Libbey-Owens-Ford in 1979.

Direct operation on low-voltage supplies (e.g. 28-VDC) precludes use of continuous film conductive coatings, and forces reliance on filamentary-type elements. Traditionally, this need has been served by almost invisibly fine wires, "marcelled" for mechanical and optical reasons, and embedded in an internal thermoplastic layer, usually the interlayer. These elements, often referred to as "wiggle wires", represent technology that is over 20 years old and are known to have technical and operational drawbacks. With a few notable (and usually unsatisfactory) exceptions, their use has been relegated to smaller, non-airliner-type aircraft where the necessary concessions are acceptable.

An intial study showed that the major deficiencies were theoretically surmountable through the adaptation of more modern technology from another industry; namely, photolithographic processing used at the leading edge of micro-circuitry technology. In micro-circuitry, however, all processes and equipment are geared to fractional-inch sizes on flat substrates, whereas aircraft windshields are two orders of magnitude larger and often curved.

What at first appeared to be a simple process of upscaling to our size requirements turned out to be a monumental undertaking for a company the size of Sierracin. We found it necessary to accomplish significant technical breakthroughs and state-of-the-art extensions in diverse and unfamiliar technical disciplines. The resulting technology, with the tradename Sierragrid™, does provide the sought-after improvements, and is the first significant technical advance in aircraft windshield heater elements in over fifteen years.

As of this writing, the technology is in the process of transition from full-scale laboratory prototyping to contractual production and qualification testing, and will appear on two new aircraft models in 1983. This paper provides a detailed description of the element, including microscopic detail with emphasis on how certain unique physical characteristics relate to the sought-after improvements. Additionally, this paper provides design guidelines and performance projections as currently known or predicted at this admittedly early stage.

DISCUSSION

Windshields for aircraft designed to the requirements of FAR 25 must be equipped with a means to preclude ice accretion and/or fogging which would impair or limit visibility. In addition to these FAR 25 planes, many others are equipped with some type of windshield anti-icing system as an option to be used in the event they are caught in severe weather.

There are two commonly used anti-icing systems; hot engine-bleed air and electrically-generated heat. Bleed air has several drawbacks and is not often used, and electrically generated windshield anti-ice/de-fog systems are clearly the preferred solution.

To generate heat electrically, a voltage potential is impressed across a transparent resistive element in the windshield, and current flow between bus bars at opposing ends of the element generates the heat to keep the windshield free of fog and/or ice.

Sierracin employs all of the commonly used continuous conductive film transparent elements, which include:

Gold - vacuum deposited coating pioneered by Sierracin for use in plastic windows, Sierracote™ 3 and 303 can also be used on glass. These elements generally operate on moderate voltages which are readily available on larger aircraft (e.g., 115/200 VAC).

Tin Oxide - the venerable pyrolytic coating can be used on glass plies only, and requires high voltages (generally 200 - 400 V).

Indium Tin Oxide (ITO) - a newer sputtered coating, currently used only on glass, which combines the durability of tin oxide with the advantageous voltage range of gold, and has optical properties superior to either.

The continuous conductive films have limitations. The resistivity of these films generally requires a voltage source upwards of 115 volts to meet power requirements and still maintain high light transmission. To provide this, the aircraft must provide A.C. power. This is not a problem on larger aircraft which normally generate AC power at voltages which suit gold and ITO, and which can be elevated to suit tin oxide with step-up transformers.

On lighter aircraft, however, only direct current power (usually 28 VDC) is available, and use of film elements is dependent on adding both expensive inverters and heavy step-up transformers. The advantages of film elements are such that several 28V aircraft pay the cost and weight penalties to employ them. More often, though, a non-film element is used, consisting of myriad fine marcelled wires, often referred to as the "wiggle-wire" element. The low resistance of these wires in parallel is such that they can be made to operate directly on low available voltages.

In 1980, Sierracin decided to expand its heater element capability to make it all inclusive and the broadest in the industry, by adding this low voltage capability. It was quickly determined that it was not possible to do so with continuous coatings at acceptable light transmissions, and the filamentary-type element appeared to be the only solution.

The most obvious prospect, of course, was simply to obtain wiggle-wire machines and produce this conventional element. However, an investigation of the "wiggle-wire" element revealed several limitations and fairly widespread dissatisfaction with this type of element by many aircraft companies and users.

These complaints include:

"fuzziness" (also referred to as "venetian-blind" effect) - optical distortion when powered due to severe, local thermal gradients around wires. This imposes power density limitations which can prevent attainment of full anti-ice or de-fog protection. This is particularly restrictive in all-plastic transparencies due to thermal insulation effect.

"starburst" - organized diffraction of point sources of light in which orderly repetition of relatively straight-sided "wave form" (due to mechanical constraints) creates a "smear", "flair" or "starburst" effect. This can be particularly objectionable with rows of landing lights in which the flairs overlap, thus confusing the pattern, not to mention the crew.

manufacturability constraints - available equipment laboriously deposits a single wire, inch-by-inch, and there is over one-half mile of wire in a typical element! The economic impact is significant in that both the initial investment in multiple machines required to support a product line is high, and the production cost is also relatively high. Design flexibility is also constrained by the inability to change effective resistivity (a function of wire diameter, and pitch, amplitude and spacing of "wave" form) often or at will within a run of wire. Thus, heat distribution can vary in quite a gross, step-wise fashion on heated area shapes other than rectangular, or where power density gradation is desired.

After much consideration, Sierracin elected to attempt to improve on this state-of-art in low voltage elements by seeking other filamentary solutions where wave-form and design flexibility were not so constrained by the fabrication process, and which would approach the more favorable heat transfer characteristics of coatings.

After surveying, and in many cases experimenting with alternate approaches, we seized on the photolithographic/chemical processing approach. In this approach, "wave form" characteristics are created in the artwork with virtually unlimited flexibility, and process-time is theoretically greatly improved.

This basic technique is used for large scale heater elements such as for rotor blade and intake anti-icing by companies such as our sister division, Sierracin /Thermal Systems. These elements do not require transparency, however, and are dimensionally very gross relative to the fineness of 1 mil or less required in windshields to maintain individual filament "invisibility". On the other hand, the micro-electronics industry had refined this technology to the point that, at the leading edge of their state-of-art, sub-mil line widths are possible. Unfortunately, the sophisticated equipment used is scaled to very small chip size, wherein .25 inch square is usual, and 2.0 inch square is considered very large. Aircraft windshield elements are one or two orders of magnitude larger, with 20 - 30 inch dimensions characteristic.

It turned out that reconciling these two extremes of scale was a monumental (translated slow and expensive) task. The resultant process appears to have achieved the targeted improvements, and the element called Sierragrid™ will be introduced into service in the near future. Sierragrid's characteristics will be explored in some detail in the remainder of this paper, but the unique process which is proprietary and on which patents are pending, will not be discussed beyond the aspects essential to understanding its nature and usage.

SIERRAGRID SYSTEM AND PROCESS

Sierragrid is a network of solid filamentary conductors. The conductors are flat or ribbon shaped rather than circular in cross section as are wire conductor systems. The cross sectional configuration and the fact that they are bonded to the substrate on a flat surface offer significant advantages over circular cross section wire systems as will be detailed later.

The Sierragrid conductors have the general shape shown in Figure 1. They are applied directly to the glass or plastic substrate using modern micro-electronic chip technology concepts.

Sierragrid is produced by a photolighographic process. For those readers unfamiliar with the process, the major steps are oulined below:

1. A pattern, called a master, is generated either by numerical (CAD) means or by digitizing pictorial artwork.

2. A photomask of the pattern is produced. This photomask, analogous to a "negative" in conventional photography, is used to "print" the pattern on the substrate (the faceply in the case of an aircraft windshield). It may in fact be negative or positive with respect to the end product.

3. A conductive metal "layer" is applied over the area that will ultimately have the desired Sierragrid pattern.

4. The conductive material is coated with a photoresist material, which may be negative or positive-acting.

5. The photomask is laid on the photoresist material and the package is subjected to radiation to "expose" the photoresist through the pattern in the photomask.

6. The photoresist material is chemically "developed", leaving the desired pattern on the substrate.

7. The substrate is then placed in an etchant and the unwanted material is removed leaving the printed pattern.

This really seems simple enough, and if windshield heated areas were the size of electronic chips, there would have been no problem and only a minor development activity. With existing technology, however, there was no way to obtain full-size photomasks with the state-of-art detail required to produce an "invisible" element. Various laser pattern generators and plotters were evaluated, with the conclusion being that, as sophisticated and extensive as the micro-electronic industry is, there was no available process or equipment to produce photomasks to our size and resolution requirements.

DEVELOPMENTAL ACTIVITY

Typical aircraft windshields require a heater element size which represents the largest printed circuit board with sub-mil width conductors ever produced. Even for the semi-conductor industry, large photomask with sub-mil feature capability does not exist, and the establishment of this capability accounted for a large part of our development activity.

Sierracin Corporation has nine separate divisions. Each of these is a leader in its respective technologies, and we can call upon their technical expertise for a synergistic approach to problem solving. One of our Divisions is Sierracin/EOI (Electro-Optical Imaging). They specialize in state-of-art imaging production through use of both advanced optical and electronic technologies. Sierracin/EOI has the modern sophisticated equipment and instrumentation required to meet any needs in the imaging business. For our photomask, we used their Varian E_eBes-40A raster scan mask generation system.

The E-beam apparatus is capable of beams as small as .25 micron (0.0000098 inches), and this will yield reticles having features as small as one micron. This equipment is not capable of producing full-sized masks, however, so a program to upscale from this size was pursued to successful conclusion.

The line width is variable with the E-beam device, of course, and this is one of the beneficial aspects of the photo-imaging process. The line (conductor) width, and therefore resistance, can be varied "on the run" according to electrical/thermal needs - a capability which does not exist in the "wiggle-wire" approach.

Sierracin/EOI has full digitizing and computer aided design (CAD) capability. Design requirements are established and Sierragrid configuration parameters are calculated at the Sylmar facility. This data is then transcribed into plotting format and the photomask is subsequently produced.

The photomask is the tool by which the pattern is dictated and "printed" onto the substrate. Once the photomask is generated, copies are inexpensive and perfectly reproducible. All resistance requirements, with the exception of filament thickness, are accounted for in the pattern design. This extremely versatile system can be tailored to any configuration, with the only significant impact of a difficult design being in the non-recurring "art work" cost.

Another case of inter-divisional synergism affected the downstream development and etching process. Sierracin/Thermal Systems Division is a leader in the field of non-transparent heater elements and flexible circuits using the etched-foil approach, but to much larger conductor dimensions than required by the need for "invisibility". Their expertise and equipment provided many valuable "stepping-stones" to our ultimate success, however, and their contribution as well as that of Sierracin/EOI is hereby gratefully acknowledged.

The history of this program abounds with examples of extrapolating the state-of-art in various unfamiliar fields in order to achieve our ultimate success, but it would be too revealing of proprietary details to describe them here. Suffice it to say that a great deal of original work and technology advancement was necessary in order to achieve Sierragrid.

CHARACTERISTICS OF SIERRAGRID

Sierragrid is the only fundamentally new conductive system to become available in the past 15 years, and the advantageous features described below will be of interest to both designers and users.

Optical Considerations

Optical characteristics (namely, unobtrusiveness in both the passive or powered state) are naturally among the foremost considerations in a transparent heater element. We listed the known objections to the currently available heater systems and then set about to develop a new system that would address each of these objectives. We have spent considerable time looking at the grid board and natural scenes through Sierragrid parts. The filaments have a projected cross section of less than one mil and the color is a non-distracting neutral gray as viewed from the aircraft interior side. These characteristics add up to the fact that in an unpowered condition or normal viewing situation, they present no viewing restriction and even are superior to conventional wires. In addition to these obvious visual considerations, however, there are two less obvious characteristics that account for most of the concerns about wire systems.

Diffraction

A frequent complaint is that point light sources, and landing lights in particular, turn into a confusing blur when viewed through wire heaters. Pilots have lived with this because there has been no acceptable alternative in aircraft having only low voltage available, and on which the cost, weight and/or space penalties of inverter/transformers are unacceptable. The diffraction phenomenon causing this was analyzed, and it was realized that the mechanical constraints of the wire "wiggling" machine were aggravating this phenomenon. It was also appreciated that the design flexibility of the photolithographic approach could be employed to minimize this effect.

Diffraction is the breaking up of a ray of light into dark and light bands or into the colors of the spectrum by the interference of one part of a beam with another when the ray is deflected at the edge of an opaque object, or when it passes through a narrow slit. This is the basic problem. A diffraction grating occurs when the slit effect is repeated by a set of close, equidistant and parallel lines. This is generally the case with mechanically laid wires; they are close, equidistant and parallel, and have relatively straight runs connecting bent segments (Ref. Figure 6).

We went through various attempts to circumvent these laws of physics. With regard to "close", we really could do nothing because our heat transfer calculations resulted in spacing limitations somewhat similar to those for wires. We found, however, that small changes to "equidistant" and

"parallel" yielded remarkable improvements to observed diffraction patterns. Interestingly, one early attempt to maximize thermal uniformity without regard to diffraction by using a heated semi-hexagon shape grossly aggravated the starburst effect. This element was the ultimate in "close, equidistant and parallel", and provided an early clue to our ultimate solution. A set of diffraction photos was taken using the set up shown in Figure 2.

Figure 3 shows a point source of light as seen through the camera lens. The hexagonal pattern shown in Figure 4 was evaluated for diffraction pattern. We certainly verified the classical effects as is evidenced by the pattern shown in Figure 5 where the results of six parallel facets are seen. Figure 6 shows an approximate 1.5 mil diameter wire system pattern. Note that the "runs" between bends are much straighter than the bends themselves. Figure 7 shows the point source of light when viewed through this psuedo-sinewave pattern. The diffraction pattern star-bursts are aggravated as they are viewed at installed angle. Figure 8 shows the sine-wave systems viewed at 45°. These starburst patterns are a source of the crew coaplaint.

Now the good news! We are currently using two Sierragrid patterns which have dramatically improved diffraction patterns. Both are based on connected semi-circular wave forms which have no predominant "facet", and therefore do not organize the diffraction into "streaks". Properly done, this "wave form" results only in a halo around the point source of light, thus removing any ambiguity as to location.

Figure 9 shows the recent computer-generated pattern. This orderly pattern optimizes the thermal uniformity by controlling the inter-filament spacing to small values. There are periodic interconnects between conductors to ensure electrical continuity around a "break" in the event that a conductor sustains local damage. Figure 10 shows the point source of light viewed through a windshield incorporating this pattern at 90°. Figure 11 shows the same windshield viewed at 45°

Figure 12 shows a photo of our "pseudo-random" pattern. This was an attempt to further disorganize the diffraction grating by purposefully avoiding element coherence, at some expense to thermal optimization. Figure 13 and 14 show this pattern at 90° and 45°, respectively, while observing the same point source of light. Any slight additional benefits are not considered sufficient to justify this approach, however, and it probably will not be pursued except in cases where diffraction optimization is the dominant technical requirement.

Fuzziness

A similar set of photos depicting the dramatic difference in powered optics is not available. It is definitely achieved, but this phenomena is harder to capture on still film, and is best seen using a moving point source of light at great distance. This is evidenced by a recent program

using a conventional wire heater in an all-plastic cockpit side window. It is understood that these parts passed all required photographic and grid board requirements, but were unsatisfactory in service as discovered late in the program in night flights.

When conventional wires are powered, there is a definite fuzziness observed as the wires heat and the index of refraction of the the interlayer is affected by high thermal gradients created around each wire. In photos, this could easily be interpreted as out-of-focus. Anyone who has seen it and is bothered by it needs no photographic proof.

Sierragrid, with its ribbon-like cross-sectional configuration, has no significant optical distortion in a glass laminate even when powered to eight watts per square inch; twice the typical anti-ice power density. This amazing capability is due to the unique filament design and its location. The heated conductor is bonded to the faceply with a contact area tremendously larger than the point contact of a circular heater element cross section. Heat generated in the Sierragrid filament is conducted more directly into the faceply due to the "flat face" contact area. The "rectangular" cross section is favorably oriented with its major dimensions in the plane of the window and its minor dimensions in the direction of heat flow, thus approaching this favorable aspect of film-type elements.

Accordingly, calculations confirm that Sierragrid filaments on a glass faceply operate with much lower filament-to-space thermal gradient or "ripple" under normal operating conditions than round wires in a laminate interlayer. This means that the Sierragrid filaments can operate at a lower temperature to achieve a minimum required temperature in the ply to be heated. The difference is not as pronounced for plastic parts using a vinyl interlayer because the thermal conductivity of vinyl and stretched acrylic are more similar, but will nonetheless raise the "fuzziness" distortion threshold power density due to the greater stability of the rigid plastic ply to which Sierragrid is intimately in contact, and the reduced interlayer contact in the inter-filamentary transparent spaces.

Design Versatility

Conventional continuous films used for anti ce or de-fog applications have certain geometrical limitations. They cannot heat into corners or generally be used with a great variation in bus-bar spacing because the useful resistivity range is exceeded on either the high or low end. "Wiggle-wire" elements are more adaptable to irregular (non-rectangular) shapes, but cannot be graded smoothly to avoid large step-wise power density variations. The Sierragrid System, with its unique ability to vary conductor size, spacing and shape, as well as electrical circuitry, can be tailored to overcome these problems. This provides the designer with greater flexibility than ever before. In fact, if a design problem does exist with Sierragrid, it is that attractive alternatives exist in almost bewildering profusion, and knowing when to quit (the point of diminishing return) and how best to optimize

among them presents an appealing challenge to the designer. This type of problem obviously lends itself to computerization, and we have made significant strides in that direction.

Computerized Design Program

The windshields shown in Figure 15 shows greatly varying bus-bar spacing, but the area as shown can be uniformly heated by varying the element size from 0.0005 inches to 0.001 inches and, where required, running multiple conductor passes in series to obtain the required "resistivity". All of this is designed on a computer program developed expressly for this heater system.

The program basically uses the following sequence to construct a heater element design.

1. It will find the minimum possible number of areas of uniform electrical, hence filament parameter, characteristics. Such an area is called a column. The number of columns will depend on the slope of each bus-bar and/or the rate at which the separation between bus bars changes with respect to a coordinate along an axis perpendicular to the direction of the filaments, as shown in Figure 15. If the bus bars are parallel and of equal length, then only one column is required. When an adjacent incremental area has electrical property requirements differing by a pre-established limit (we usually use one percent maximum), a new column with its revised properties is established.

2. It will decide whether the required heated area can be heated with or without the need of sectioning the bus-bars to create series connection, taking into account all possibilities of filament parameters. If the computer program "decides" to section the bus-bars to add resistance (length), it will indicate where and how many sections are needed to eliminate all resistivity limitations, and will calculate the voltage drop of each series section.

3. After the first steps are completed, the program will take the voltage and average distance between bus-bars for each column and calculate the optional combinations of filament properties that will meet the resistivity requirement for that column. The filament design parameters are its width, number of passes if in series (which must be a positive odd integer and the number of filaments.
While "wave form" parameters such as pitch relative to amplitude, spacing, and wave shape itself could be independently varied to control "resisitivity", a fixed relationship among these features (namely, connected circular segments at 2.3 radius spacing) has been selected based on optical considerations as was explained in the preceding section, and for thermal uniformity optimization.

After all possible solutions to this column's resistivity are found, the program will calculate the required amplitude, width of column, percentage of area covered by filaments in that column, and the percent error caused by not using all possible combinations of properties available. As can be seen, the possible solutions to the required resistivity could differ in amplitude, width, area covered by filament and whether the error is negative or positive. The designer can choose among all possible solutions and set limits to a column instead of the computer doing so.

In addition to this procedure, the program can be executed several times for different filament thicknesses, which would determine the overall optimal design.

The computer program contains other selectable limits and features, including:

(1) only solutions that do not cover over 10% of the column area in order limit light transmission loss,

(2) only admit a greater percentage of area covered if there is no solution under 10% area covered that comes within 5% of the required resistivity.

(3) the ability to select the maximum column width by two approaches:

a) it will insert a step of certain acceptable size in the bus bar to equalize the potential across a column as seen in Figure 16, or

b) it will allow the power density to vary within a column on a non-stepped, sloped bus bar, and the program will choose the maximum column width possible to stay within the selected thermal uniformity tolerance.

Electrical Considerations

Sierragrid was developed primarily for low voltage applications, inasmuch as Sierracin's Sierracote 303 gold, Electropane® tin-oxide and Sierracote 404 indium tin-oxide coatings essentially meet all other needs. Sierragrid parts with a resistivity requirement down to 0.26 ohms per square are now being produced for qualification testing on 28V applications. This is contrasted with representative light transmission-imposed minimum sheet resistivities of about 8 ohms/square for gold, 30 for tin oxide and 2 for indium tin oxide.

Sierragrid's usefulness is not limited to low voltage, however. Unusual power density, bus bar spacing and/or heated area shape requirements might preclude available film-type elements and favor Sierragrid even though the available voltage is high enough for films. Sierragrid elements can provide these higher resistivities with equal ease.

Sierragrid offers advantages of both film and wiggle-wire systems. Film coat-coatings cannot be graded to heat acute or obtuse corner regions because the two-dimensional conductivity in these systems would overheat obtuse corners, and fail to heat acute corners. Therefore, film element heated area patterns should ideally intersect bus bars at right angles. Sierragrid patterns, on the other hand, can be designed to intersect the bus bars at any desired angle, and, because current flow can be confined to filaments or groups of filaments, heat will be uniformly generated in these non-right angle corners. This provides a real advantage over film elements.

Maintaining the area covered by filaments below ten percent of total, the theoretical range of resistivities for the Sierragrid thicknesses and widths available is 0.10 to 1000 ohms/square, an amazing four decades and a key contributor to the versatility claimed for this system.

Even though Sierragrid is not a two-dimensional conductor like film, it can be thought of as having a one-dimensional "sheet" resistivity within a column of like filaments, and the conventional film equation used for preliminary electrical analysis, can be used as follows:

$$r = \frac{E^2}{pl^2}$$

where: r = "sheet" resistivity (actually "ohms/square" in the direction of the filament axes only).

p = power density (watts/unit area).

l = bus bar spacing (length unit).

E = potential (volts).

The following examples result from considering some typical design cases:

1. For a typical anti-icing power density of 4.5 watts per square inch, the range of bus bar spacing for common voltages are:

   a. 41.7 to .417 inches for a 28 volt system,
   b. 171 to 1.7 inches for a 115 volt system, and
   c. 298 to 3.0 inches for a 200 volt system.

2. For a typical defogging power density of .70 watts per square inch, the range of bus bar spacing for common voltages are:

   a. 106 to 1 inch for a 28-volt system

   b 435 to 4.3 inches for a 115 volt system, and

   c. 756 to 7.6 inches for a 200 volt system.

It is obvious from these figures and an understanding of Sierragrid's shape accommodation versatility, that almost any conceivable windshield could be very effectively heated with this system. In many cases, thermal uniformity and area coverage would be far better with Sierragrid than with any other system.

Thermal Considerations

The thermal uniformity of Sierragrid elements is process sensitive and subject to variation, not unlike film type elements. Uniformities comparable to film elements are acheivable, but insufficient data is available at this time to establish nominal production tolerances. As with any tolerance, if tighter tolerances than those nominally resulting from the process are required, there will be a direct relationship between required accuracy and cost.

The fact that Sierragrid on glass will operate 20°F or so cooler than a comparable wire element will allow higher over-all or local power densities without jeopardizing the interlayer or plastic plies. This, in turn, means that this element will be more tolerant of thermal non-uniformities, either self-induced or due to aerodynamic variations over the windshield surface.

EMP Protection Possibilities

Sierragrid also offers excellent prospects for providing an improved approach to transparent EMP (electro-magnetic pulse) shielding. Conventional approaches include incorporation of rather coarse screen or etched-foil meshes into the laminated transparencies. The foil approach is preferred to avoid the double thickness and poor contact at the wire intersections which occur in woven screens. Both of these approaches lack design flexibility, resulting in very coarse (and visible) rectilinear patterns which will introduce a significant diffraction effect -- in this case a four-pointed, or cross-shaped starburst. Being free-standing and delicate, they are also prone to sustaining damage in handling and, due to the interlayer flow which occurs during pressure-laminating.

Sierragrid offers certain distinct advantages in this usage, as follows:

1. It is "printed" directly on the structural material, and can be used on monolithical designs or, if laminated, will not be prone to damage during lamination.

2. Finer element designs are possible, so that the presence of this mesh is less obtrusive, or even totally unobvious to the naked eye if desired for any security reasons.

3. Curved "wave form" can be used to minimize, if not eliminate, the diffraction starburst problem.

4. As with the free-standing etched foil approach, thickness will be uniform and continuity at filament intersections is assured.

Sierragrid coupons have been subjected to EMP testing, and while the test and results are classified, the feedback has been encouraging. Interest in Sierragrid is very enthusiastic and widespread in this rapidly expanding field of application.

Light Transmission

By regulating the Sierragrid pattern, the light transmission loss due to the conductor system can be greatly controlled. As mentioned above, we set an upper limit of 10% for the area covered, but most configuration solutions have five or six percent of the area covered by filaments. Measurements of completed assemblies with a fail-safe polycarbonate mainply and an inner acrylic abrasion shield yield light transmissions in the 72 plus percent range.

Adhesion

With only five to ten percent of the substrate covered by conductors, over 90% of the substrate ply is exposed. As a result, the preponderance of interlayer bond to the faceply is direct to the substrate rather than carried through the element as with films. Thus the interlayer encapsulates the individual heater filaments, thereby enhancing the integrity of the already excellent filament-to-substrate bond.

The Sierragrid system has another advantage over continuous films in that, in the event a filament does become disrupted and broken, a castrophic failure to the heater does not occur. With the film conductive systems, delaminated or scratched areas can lead to serious hot spots and, in the extreme, propagate to cause total heater failure. Sierragrid has a system of cross-connects that provides alternate paths around discontinuities. These paths are sized and spaced to preclude local over-heating. (Reference Figures 9 and 12).

TESTING

Standard structural integrity verification tests have been conducted on Sierragrid coupons. Very good values for peel, shear and bond tensile tests have been obtained. Bond tensile and shear tests were conducted at room temperature and 160°F. The Sierragrid elements occupy only between 5 and 10% of the substrate surface area, therefore the evaluations were mostly verifying the interlayer bond to the substrate. When failure occurred, the interlayer material separated from the substrate leaving the elements adhered -- the preferred failure mode.

The real proof of the system is in pressure-temperature cyclic testing. With our Sierragrid system being intended for a variety of aircraft and service conditions, a generalized test sequence was developed. The sequence requires static tests for one hour at 125°F and -65°F before beginning the cyclic testing. Cyclic testing consists of pressure deflection to a specified value and return to zero in two minutes. The Sierragrid system is active while pressure cycles are being repeated at room ambient, -25°F, +125°F and -65°F temperatures.

Preliminary cyclic testing has been completed with an instrumented coupon as shown in Figure 17. These tests have verified the filament integrity as indicated in coupon tests. The complete cyclic testing program as described above is being conducted at the time of this writing. Laboratory verification of various respresentative cross-sections is expected to be complete by the end of the third quarter 1983.

A similar coupon to that shown in Figure 17 was laminated in a bullet-resistant ground vehicle cross-section. The panel was designed to operate uncontrolled at 0.6 watts/in.^{2}. A test is in progress at the time of writing with the panel operating around-the-clock for 65 days at 0.8 watts/in.^{2}. No change in resistance of Sierragrid has been obs rved even though this watt density yields an operating temperature of approximately 170°F!

SUMMARY

Sierragrid offers a unique combination of the benefits of both film and "wigglewire" types of transparent conductive elements, without possessing any of the limiting features of either. To wit, Sierragrid approaches the desirable optical and thermodynamic characteristics of film elements, while offering versatility and control to provide a wide range of "resistivities", thermal uniformity and coverage of irregular shapes that surpasses the capability of wire elements. Specifically, Sierragrid's advantages over conventional wire-type elements include:

1. Minimization of diffraction patterns from point sources of light.

2. Uniform heating of extremely irregular shapes and gradient power densities (fade-outs) possible, with little impact on manufacturing cost.

3. Clear, non-distorted viewing while operating to, or even well beyond, normal anti-icing power densities.

4. Better heat transfer path which lowers operating temperatures or increases allowable power densities.

5. Superior design flexibility including essentially unlimited control over, and repeatability of, filament "wave form", width, spacing, amplitude, cross-connects and intricate segmented or stepped bus bar configurations.

If Sierragrid lives up to expectations regarding manufacturability and serviceability, it can be expected that it will be the element of choice for new designs that heretofore would have used conventional wire, or in some cases, even film type elements. Sierragrid may replace either wire- or film-type elements on certain existing applications where less than optimum characteristics have been grudgingly tolerated. Moreover, Sierragrid's unique capabilities may provide solutions to design problems which could not be solved satisfactorily with either of these conventional technologies, thus expanding the role of transparent conductive elements.

Copyright 1985, Sierracin® Corporation

The information contained in this document is thought to be reliable, but the Sierracin Corporation expressly disclaims all responsibility for loss or damage caused by or resulting from the use of the information herein contained. The information is given on the express condition that the user assumes all risk.

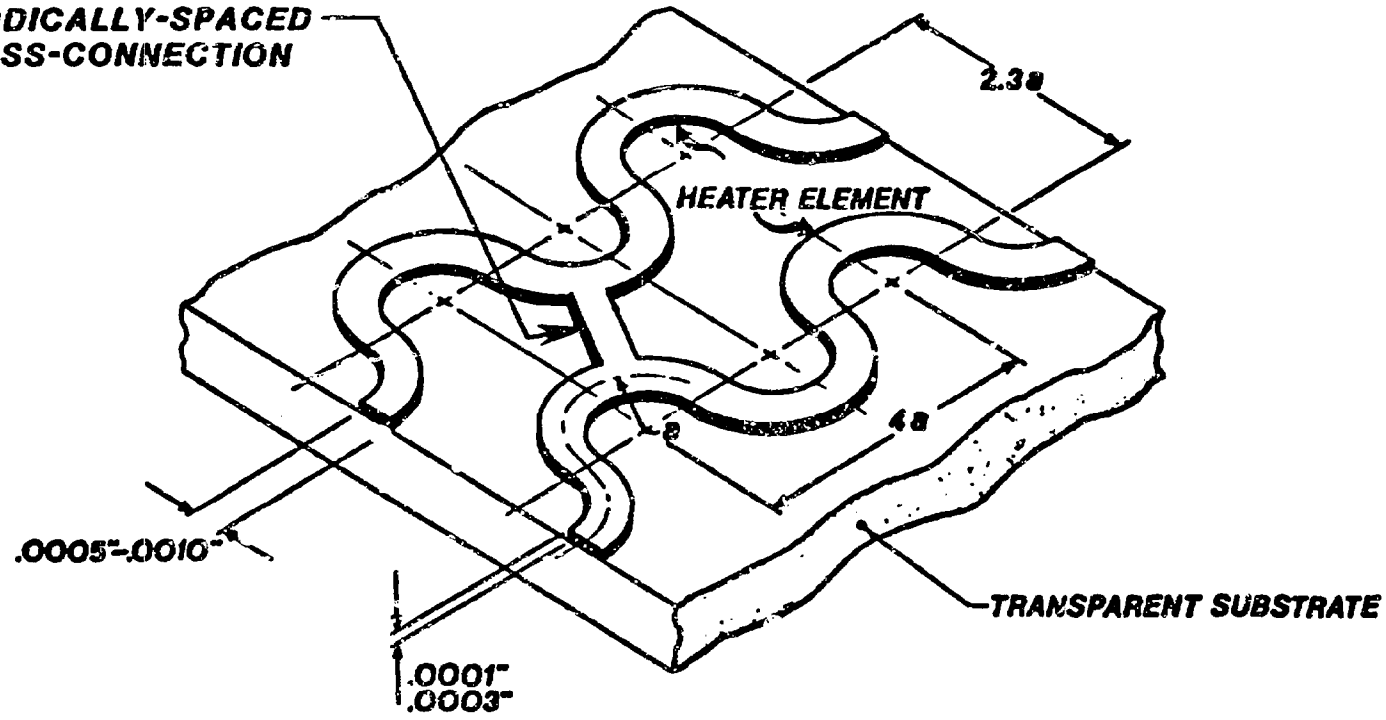

FIGURE 1
SIERRAGRID CONFIGURATION

Sierracin

FIGURE 2
PHOTOGRAPHING POINT SOURCE OF LIGHT FOR DIFFRACTION EVALUATION

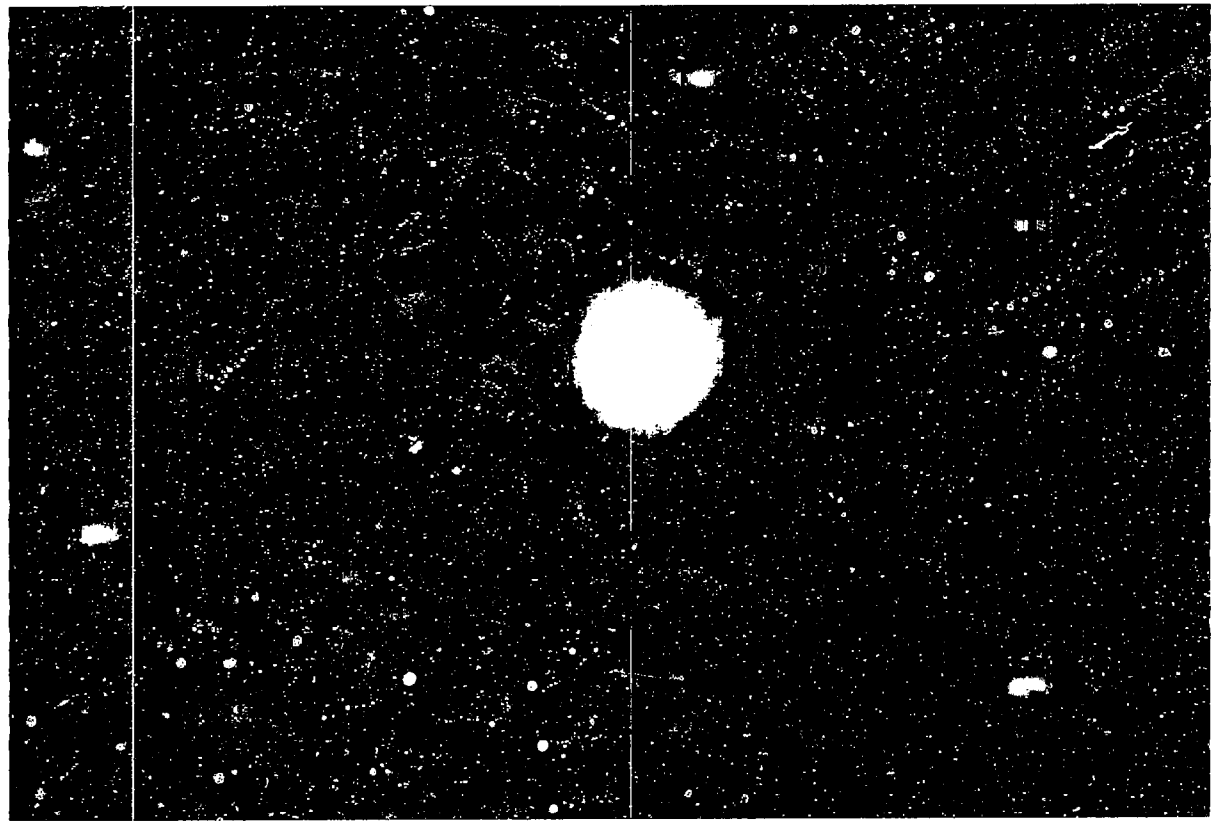

FIGURE 3
POINT SOURCE OF LIGHT
AS SEEN BY A CAMERA LENS

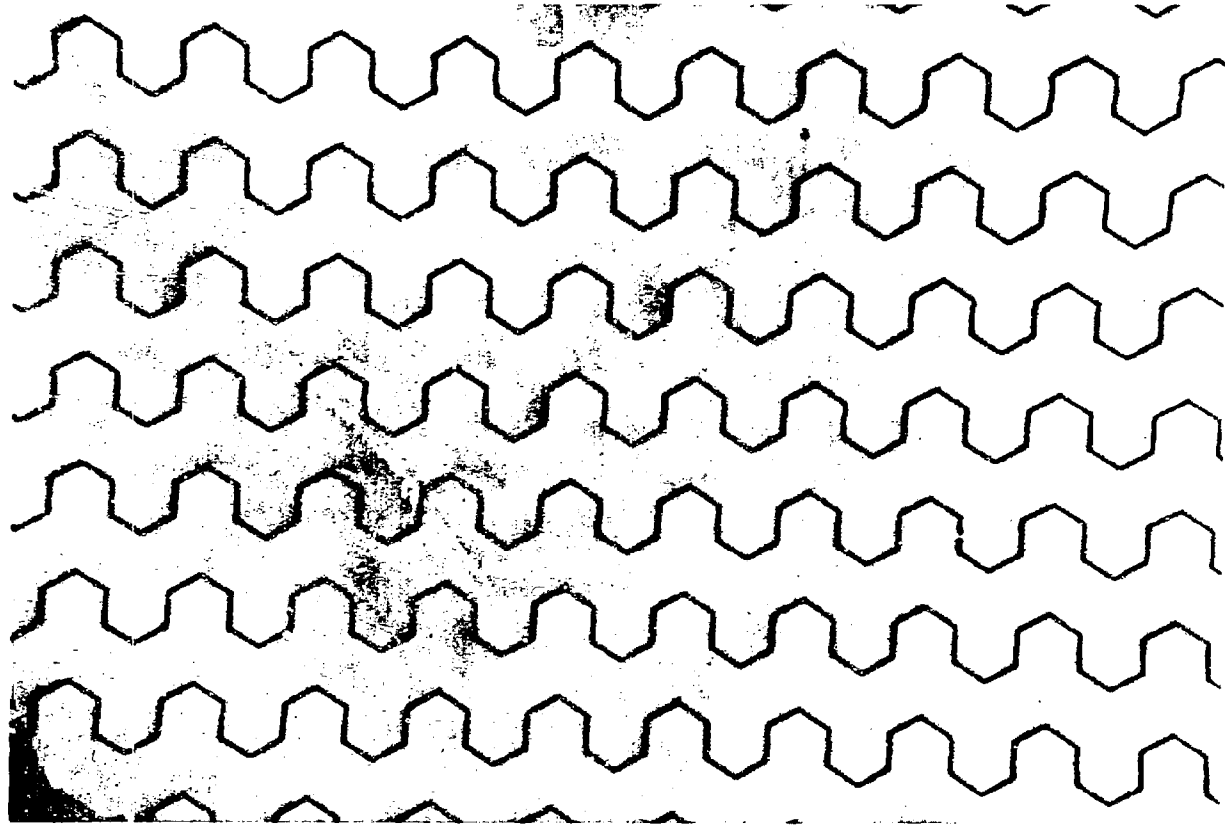

FIGURE 4
SEMI-HEXAGON ELEMENT

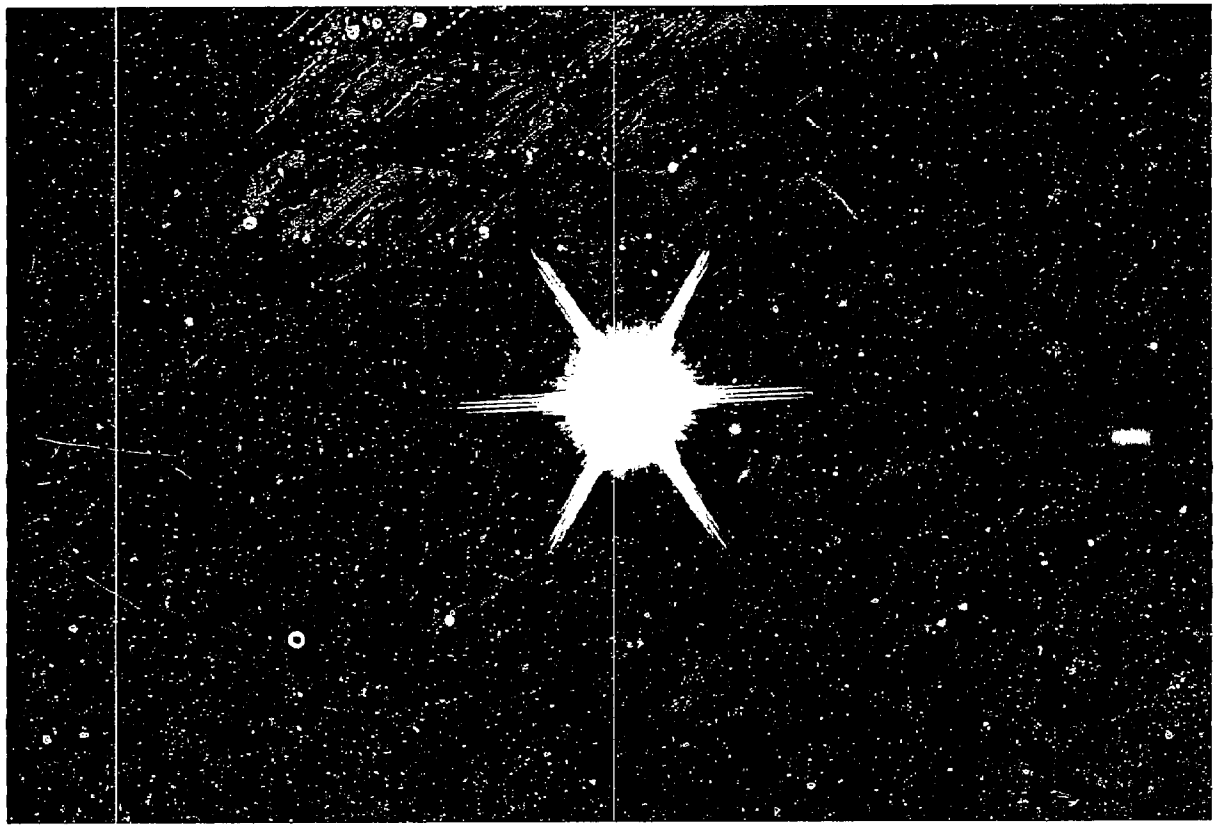

FIGURE 5
DIFFRACTION PATTERN FROM
SEMI-HEXAGON LINE ELEMENT

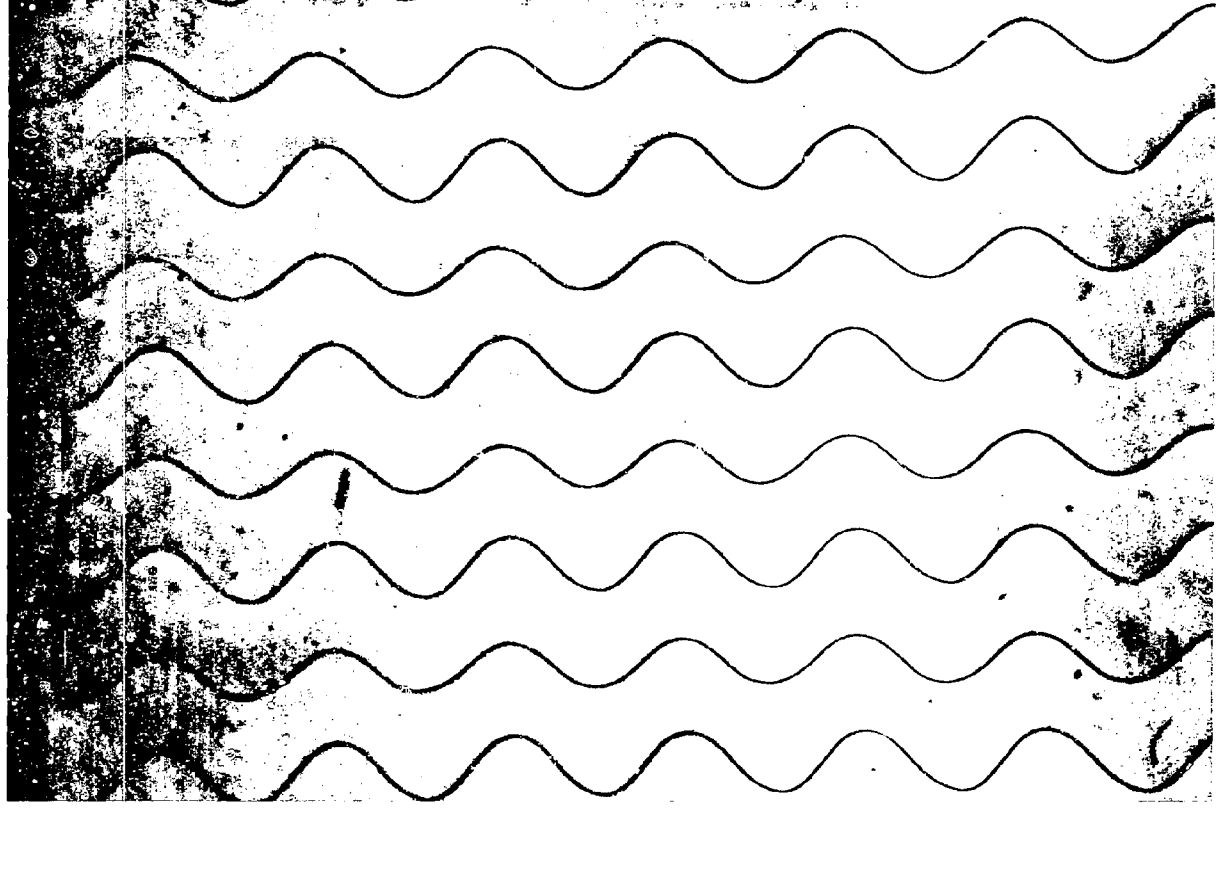

FIGURE 6
TYPICAL PATTERN OF MACHINE "LAID" WIGGLE WIRE ELEMENT

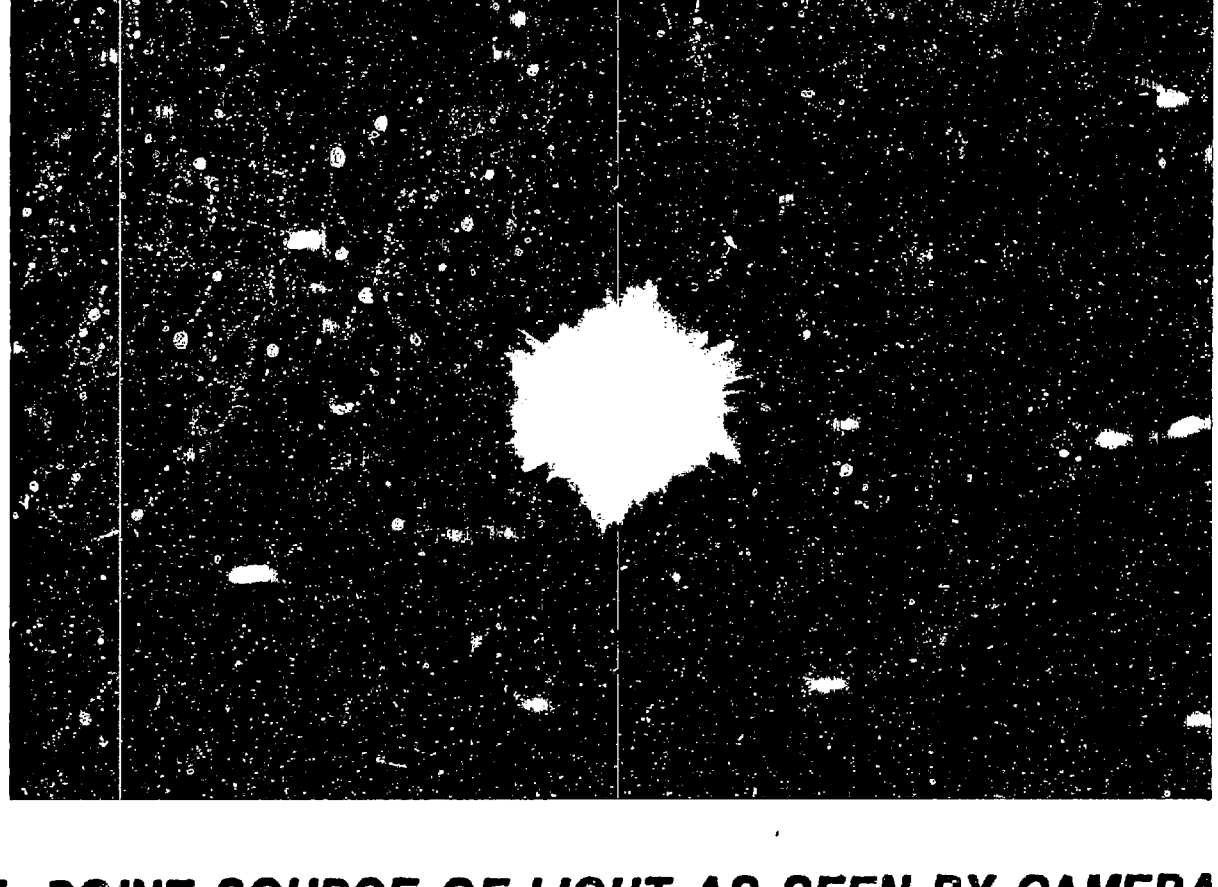

FIGURE 7 POINT SOURCE OF LIGHT AS SEEN BY CAMERA LENS THROUGH A WINDSHIELD WITH "WIGGLE" WIRE HEATER (VIEWED AT 90°)

FIGURE 8 POINT SOURCE OF LIGHT AS SEEN BY CAMERA LENS THROUGH A WINDSHIELD WITH "WIGGLE" WIRE HEATER (VIEWED AT 45°)

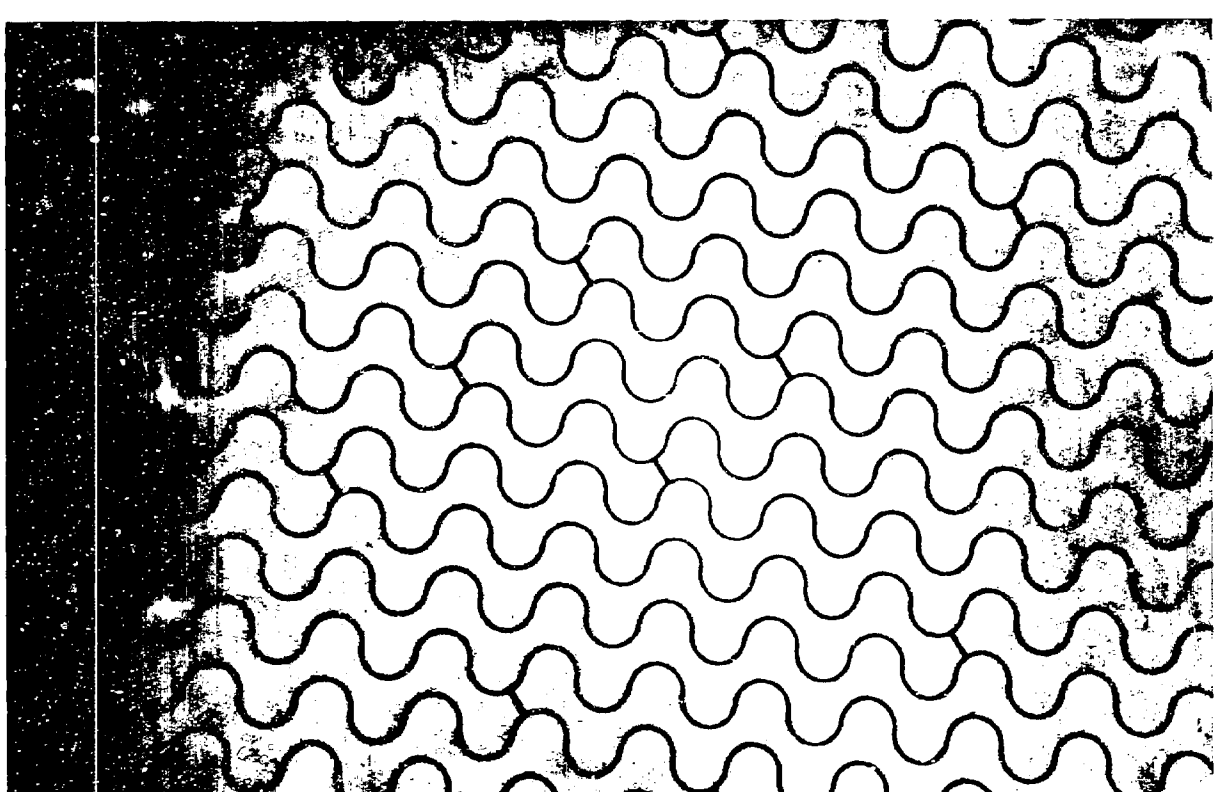

FIGURE 9
SIERRAGRID COMPUTER GENERATED ELEMENT

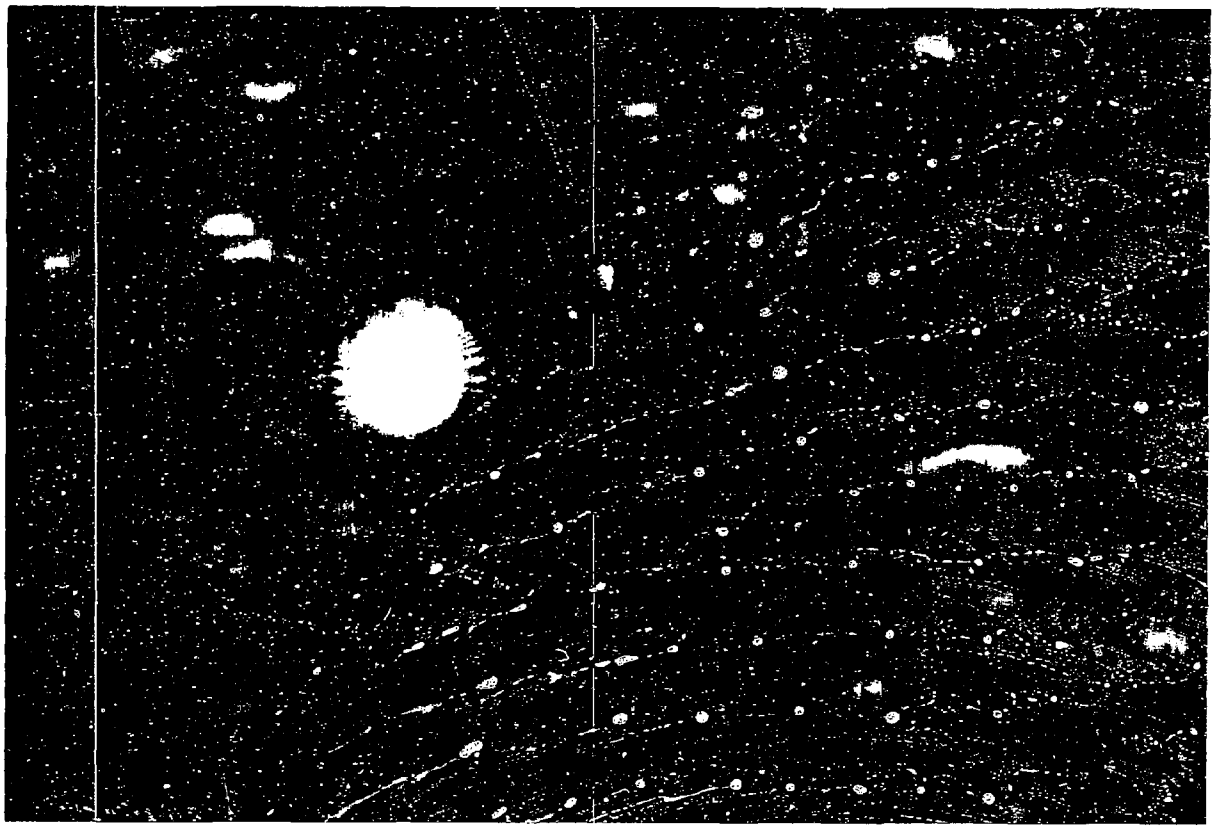

FIGURE 10 POINT SOURCE OF LIGHT AS SEEN BY CAMERA LENS THROUGH THE SIERRAGRID C A D PATTERN (VIEWED AT 90°)

FIGURE 11 POINT SOURCE OF LIGHT AS SEEN BYCAMERA LENS THROUGH THE SIERRAGRID C A D PATTERN (VIEWED AT 45°)

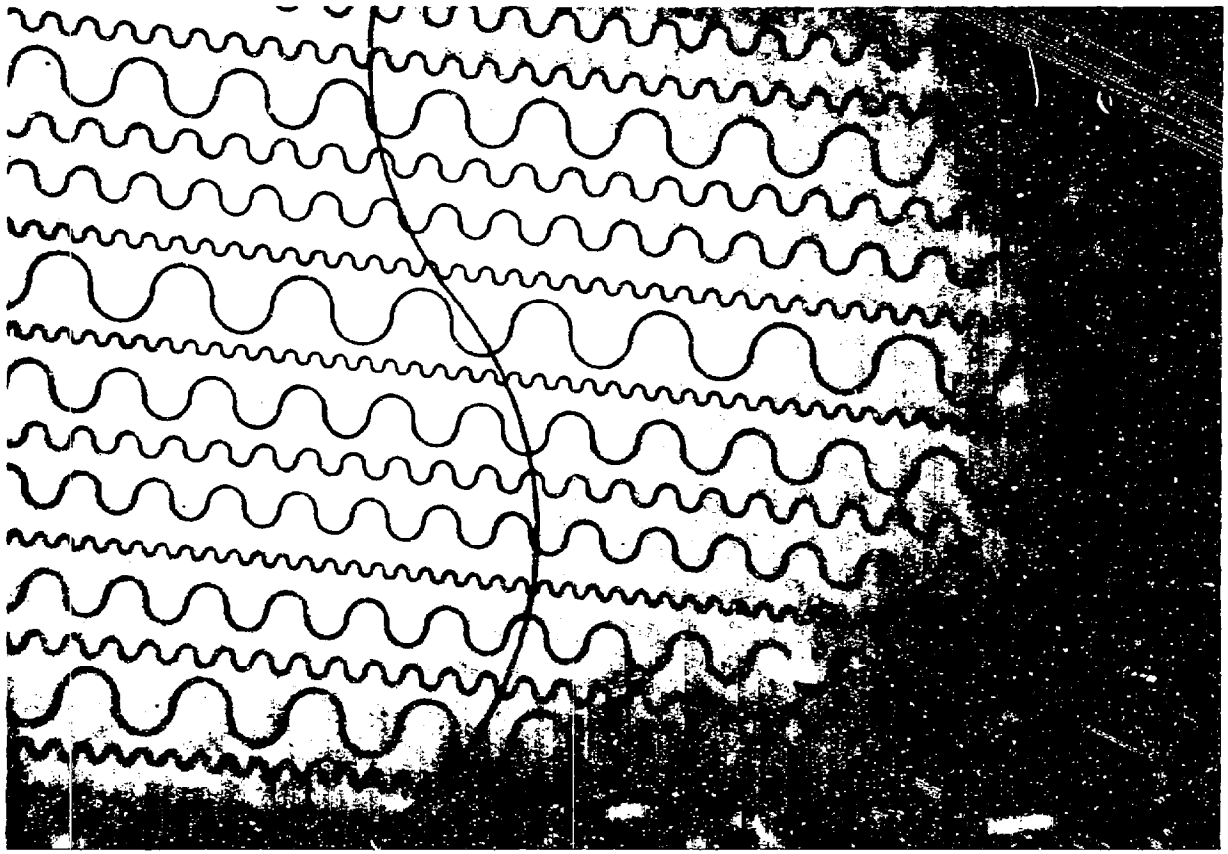

FIGURE 12
SIERRAGRID HEATER USING
PSEUDO-RANDOM LINE CONFIGURATION

FIGURE 13
POINT SOURCE OF LIGHT AS SEEN BY CAMERA LENS THROUGH PSEUDO-RANDOM LINE CONFIGURATION (VIEWED AT 90^{O})

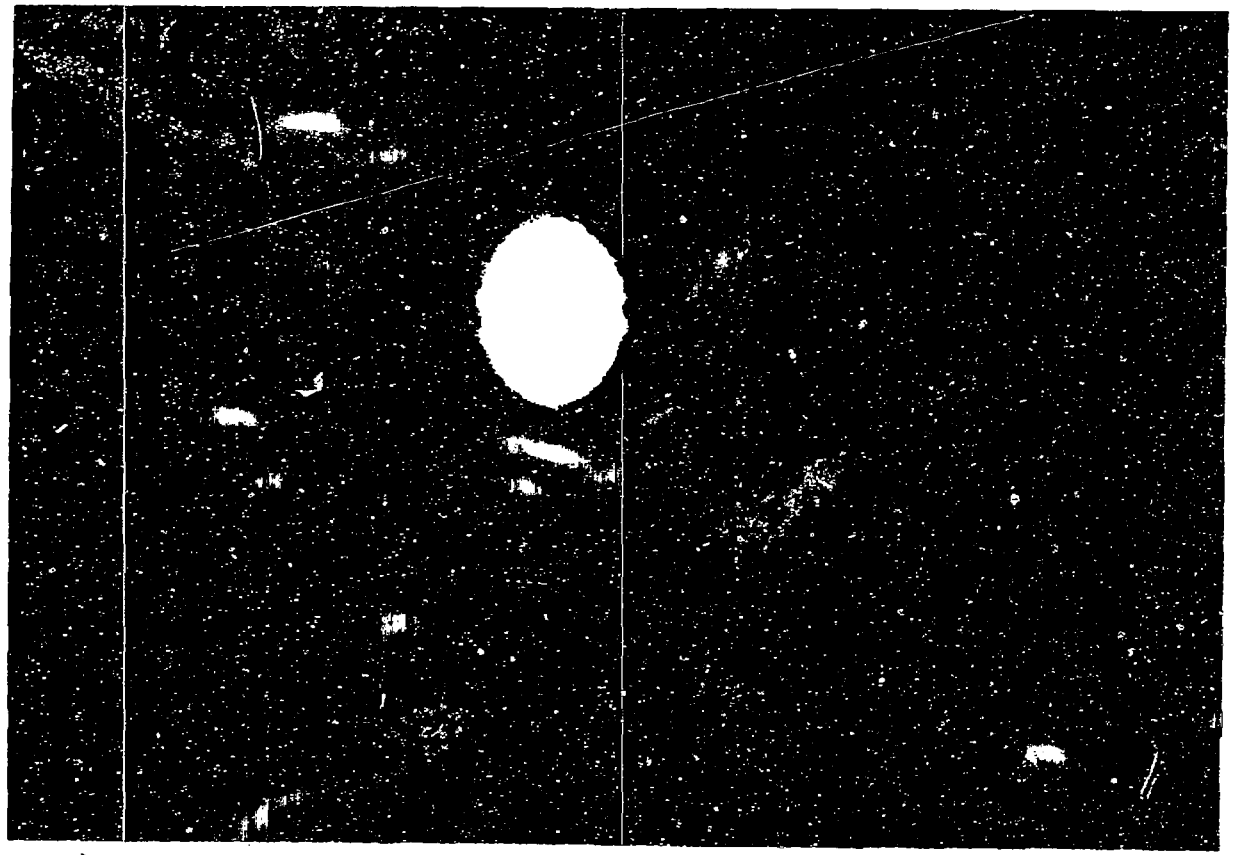

FIGURE 14
POINT SOURCE OF LIGHT AS SEEN BY CAMERA LENS THROUGH PSEUDO-RANDOM LINE CONFIGURATION (VIEWED AT 45°)

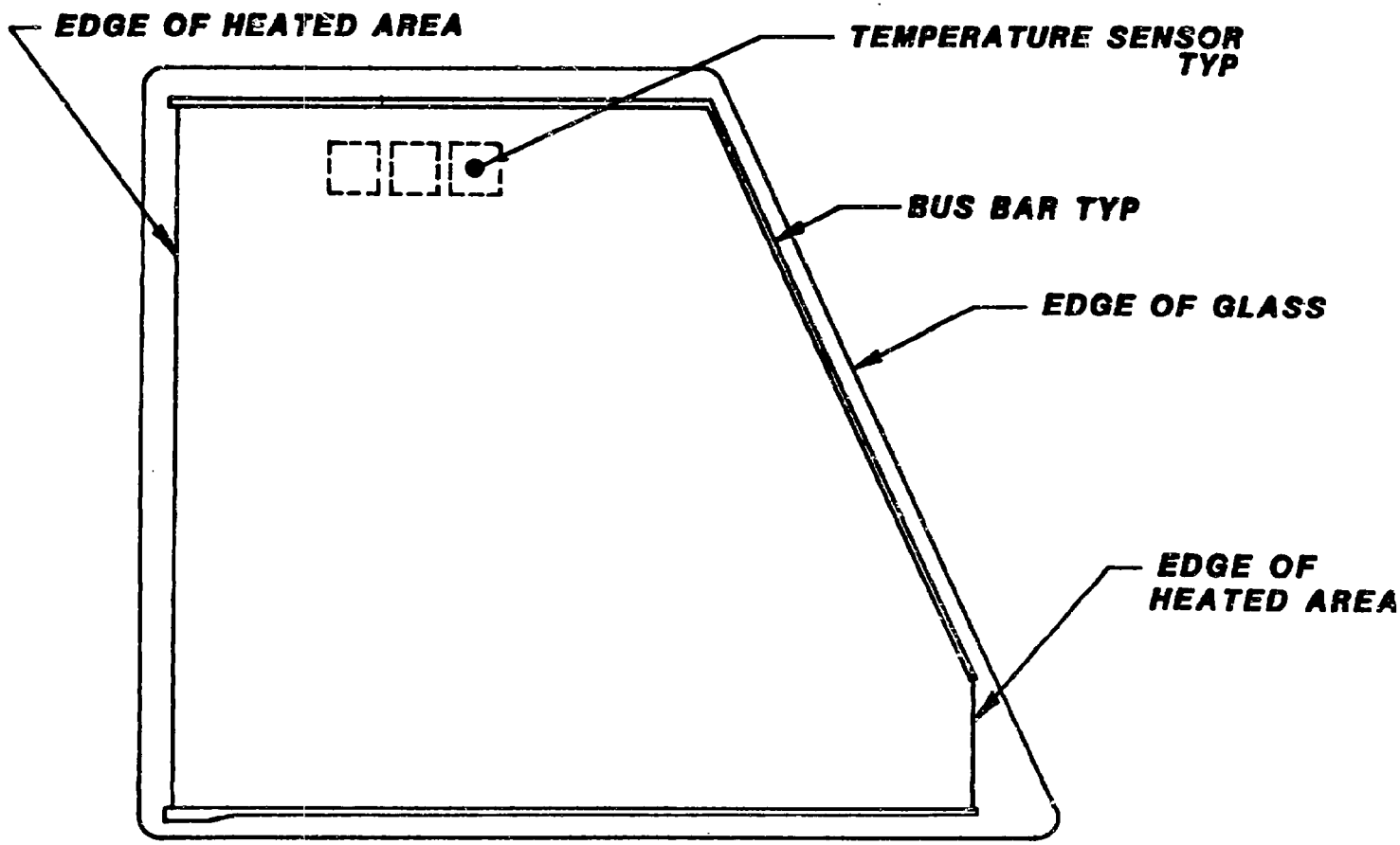

FIGURE 15
TYPICAL WINDSHIELD FLAT PATTERN UNIFORMLY HEATED BY SIERRAGRID

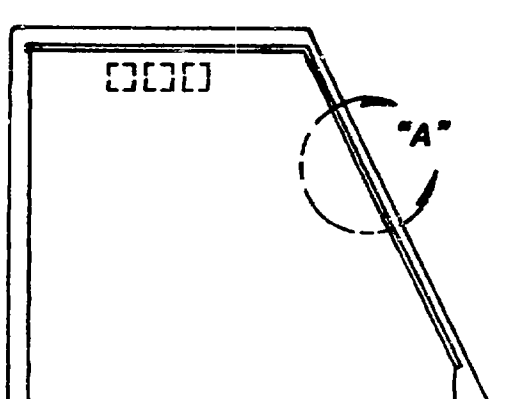

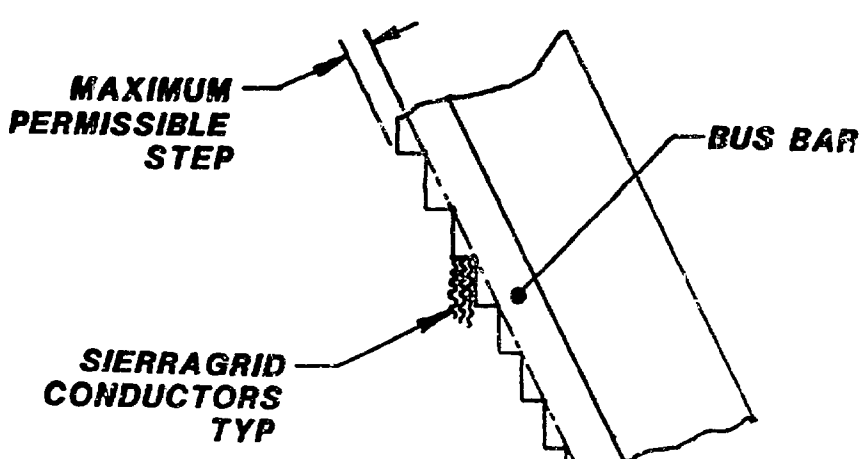

a) EQUAL LENGTH FILAMENTS IN EACH COLUMN. WIDTH LIMITED BY ACCEPTABLE STEP WIDTH

b) UNEQUAL LENGTH FILAMENTS - COLUMN WIDTH LIMITED BY ACCEPTABLE THERMAL NON-UNIFORMITY

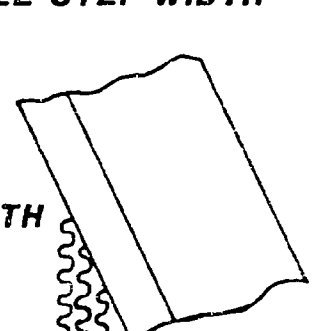

FIGURE 16
BUS BAR CONFIGURATION

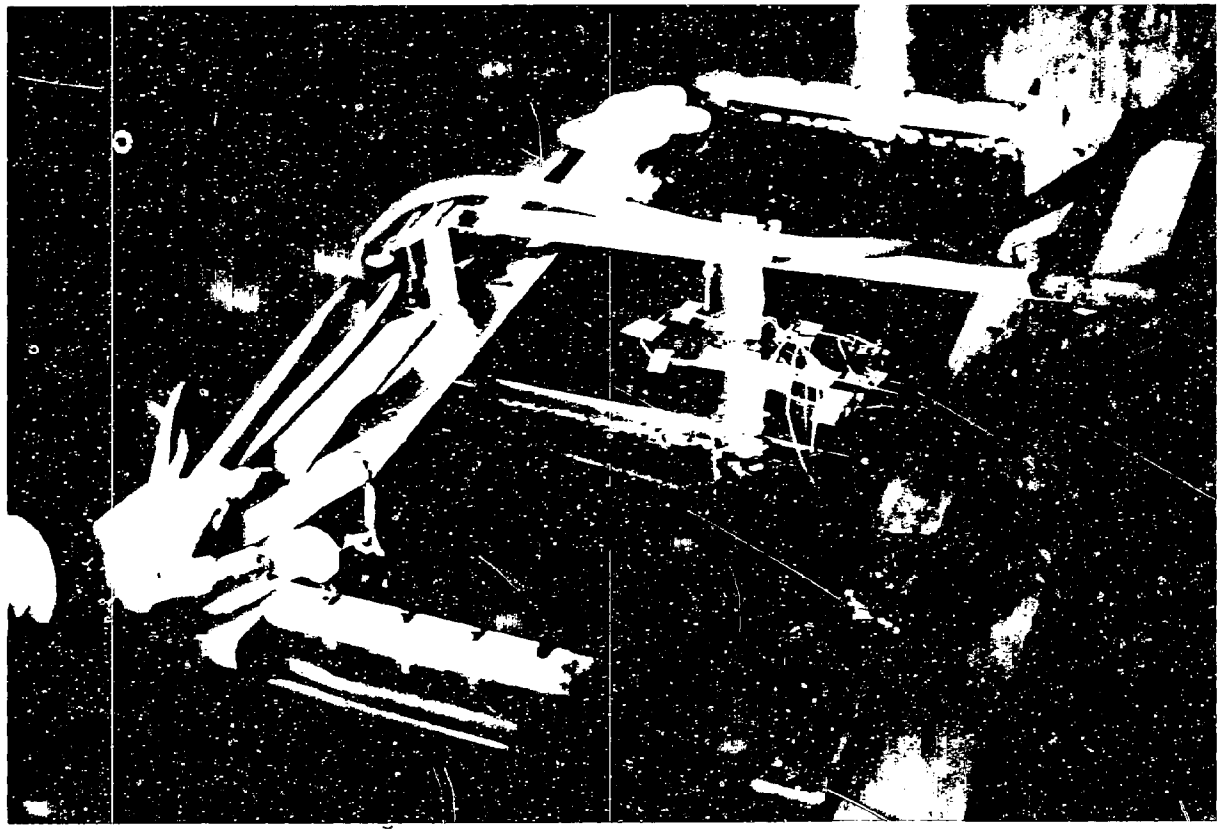

FIGURE 17
INSTRUMENTED SIERRAGRID TEST COUPON

AD-P003 189

T-38 STUDENT WINDSHIELD BIRD PROOFING EFFORTS UTILIZING METAL AND COMPOSITE MATERIALS FOR AFT ARCH REINFORCEMENT

J. M. Schlueter, PPG Industries, Inc.

T-38 STUDENT WINDSHIELD BIRDPROOFING EFFORTS

UTILIZING METAL & COMPOSITE MATERIALS

FOR AFT ARCH REINFORCEMENT

TRANSPARENCY CONFERENCE PRESENTATION

SCOTTSDALE, ARIZONA

JULY 11, 1983

JOHN M. SCHLUETER
T-38 PROGRAM COORDINATOR
PPG INDUSTRIES

ROBERT PINNELL
AFWAL/FIEA
WRIGHT PATTERSON AIR FORCE BASE

GREGORY J. STENGER
UNIVERSITY OF DAYTON
RESEARCH INSTITUTE

T-38 STUDENT WINDSHIELD BIRDPROOFING EFFORTS UTILIZING METAL & COMPOSITE MATERIALS FOR AFT ARCH REINFORCEMENT

This paper provides a review of the T-38 arch reinforcement as it relates to the T-38 Birdproofing Program.

Due to the increase in low level training missions in the T-38 Aircraft, there exists a need for an improved transparency system capable of withstanding a four (4) pound bird impact at 400 knots.

The existing student windshield frame shown in Figure 1 is made of cast magnesium alloy (AS9LC-T6) and is neither strong enough nor stiff enough to support a windshield or canopy during the bird impact event. The development of a reinforcement for the rear arch is a key step in the development of a bird resistant transparency system for the T-38. As a result, three methods of reinforcing the frame are under consideration: (1) a three piece metal casting, (2) a continuous composite, (3) a continuous machined or stretched formed high strength metal reinforcement.

The testing consisted of mounting the transparency and reinforcement to the T-38 frame, which was then bolted to a test frame, as shown in Figure 2. This test frame system was used in order to facilitate high speed photography for general visual analysis and deflection analysis utilizing the triangulation method which will be discussed in another presentation.

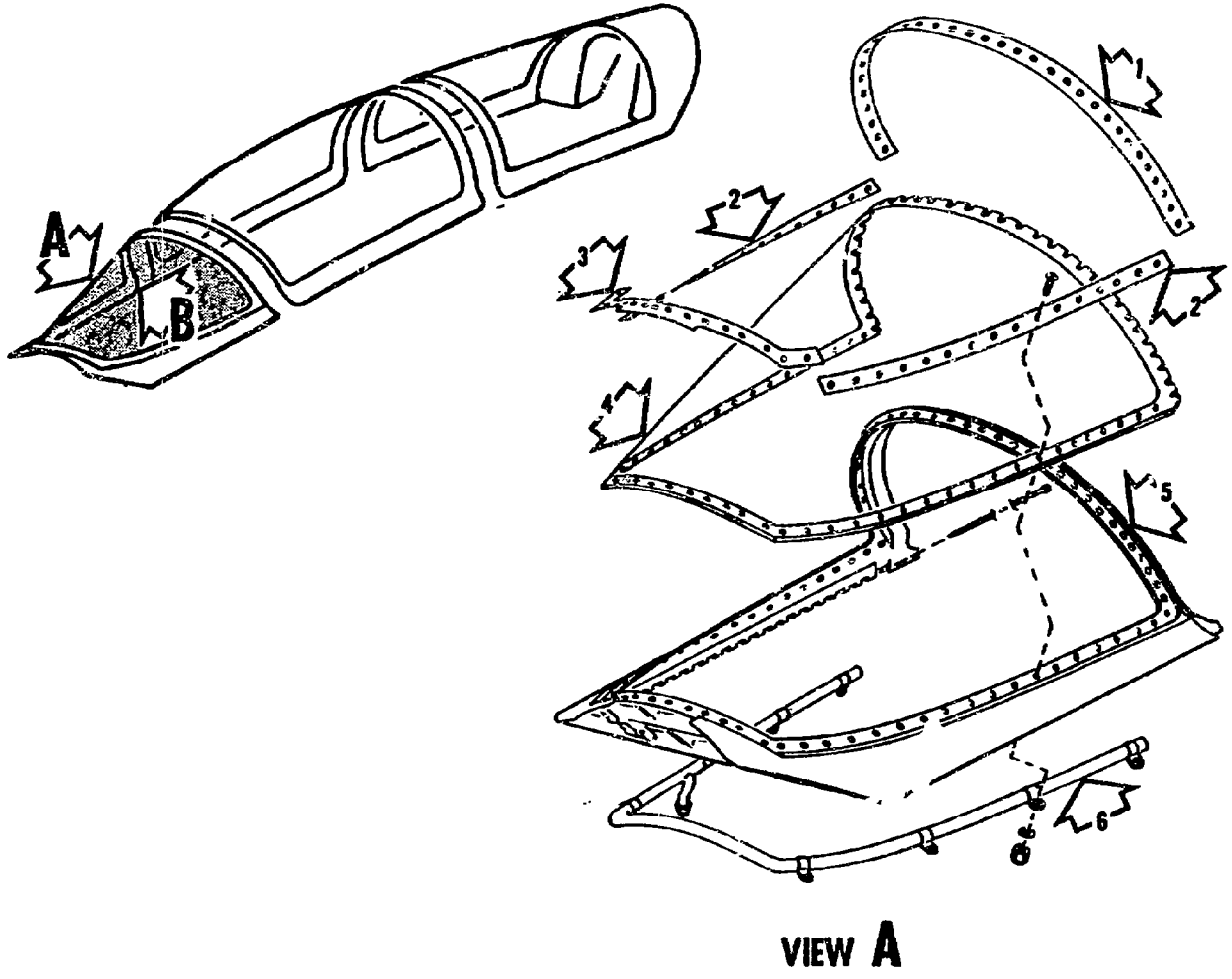

T-38 STUDENT WINDSHIELD FRAME

FIGURE 1

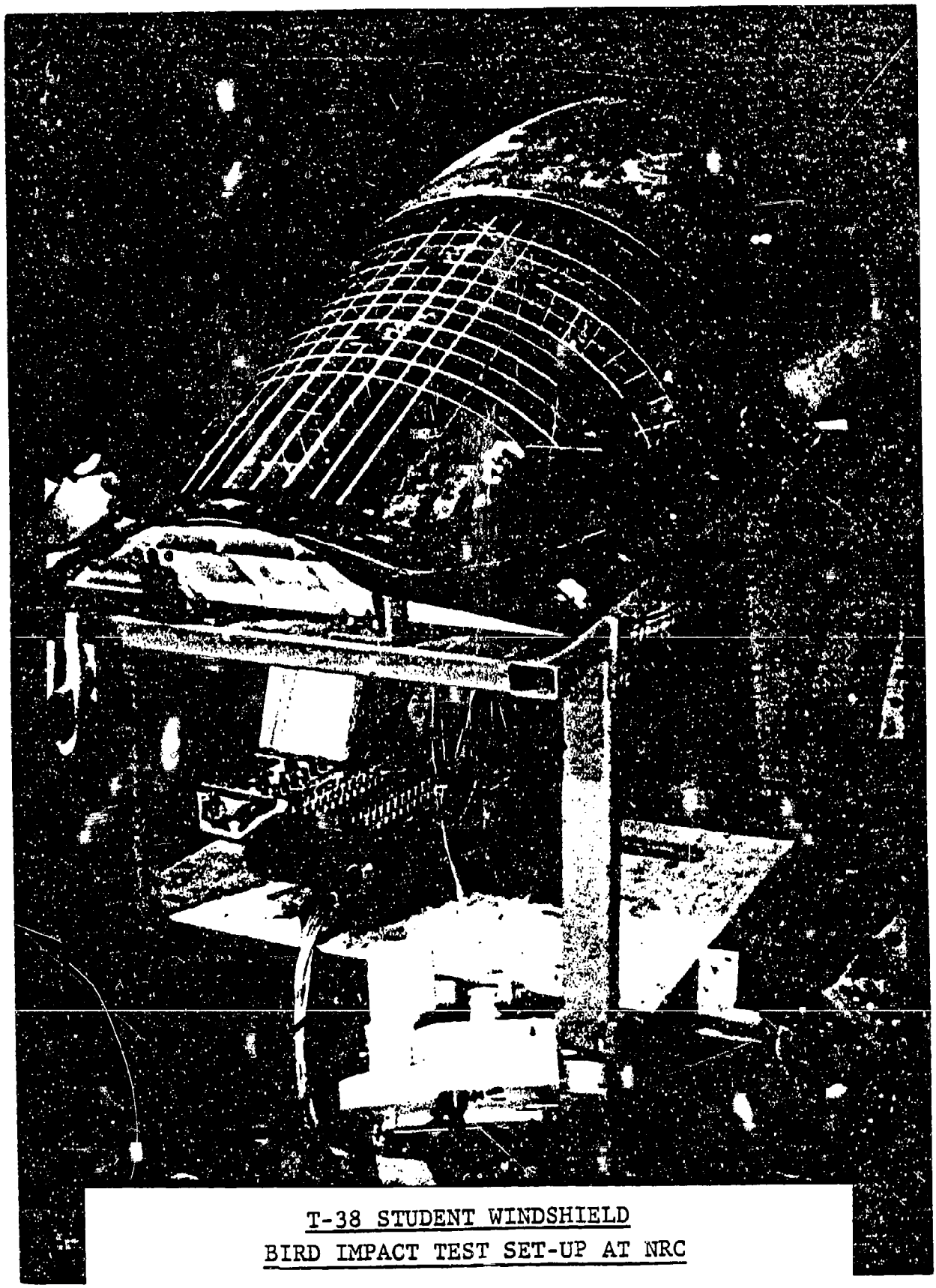

T-38 STUDENT WINDSHIELD
BIRD IMPACT TEST SET-UP AT NRC

FIGURE 2

T-38 STUDENT WINDSHIELD BIRDPROOFING EFFORTS UTILIZING METAL & COMPOSITE MATERIALS FOR AFT ARCH REINFORCEMENT

Impact locations 2 (aft arch) and 3 (sill) as shown in Figure 3 were the areas that were tested, with the greatest emphasis being placed on the aft arch impact point. Also shown in Figure 3 are the pass/fail impact resistances of the unreinforced 0.6 inch stretched acrylic transparencies currently in flight use.

In order to have some low speed as well as high speed strain and deflection measurements of the reinforced transparency system, impacts with four pound birds at 200 knots and progressively higher speeds were made. The data collected will be used for comparison of one system to another, and for correlation with "MAGNA", a computer program currently being developed to predict bird impact responses.

The initial testing was done on a three piece nickel chromium cast arch add-on, as shown in Figure 4, with a 0.6 inch monolithic polycarbonate transparency. The three piece casting method was selected because it was relatively inexpensive on a production basis, and the three pieces would allow for better fit to the uncontrolled inner surface of the T-38 magnesium arch than a single piece.

At a 200 knot (Shot 1948) impact of the aft arch, there was no apparent damage to the transparency system other than one broken bolt near the aft arch centerline.

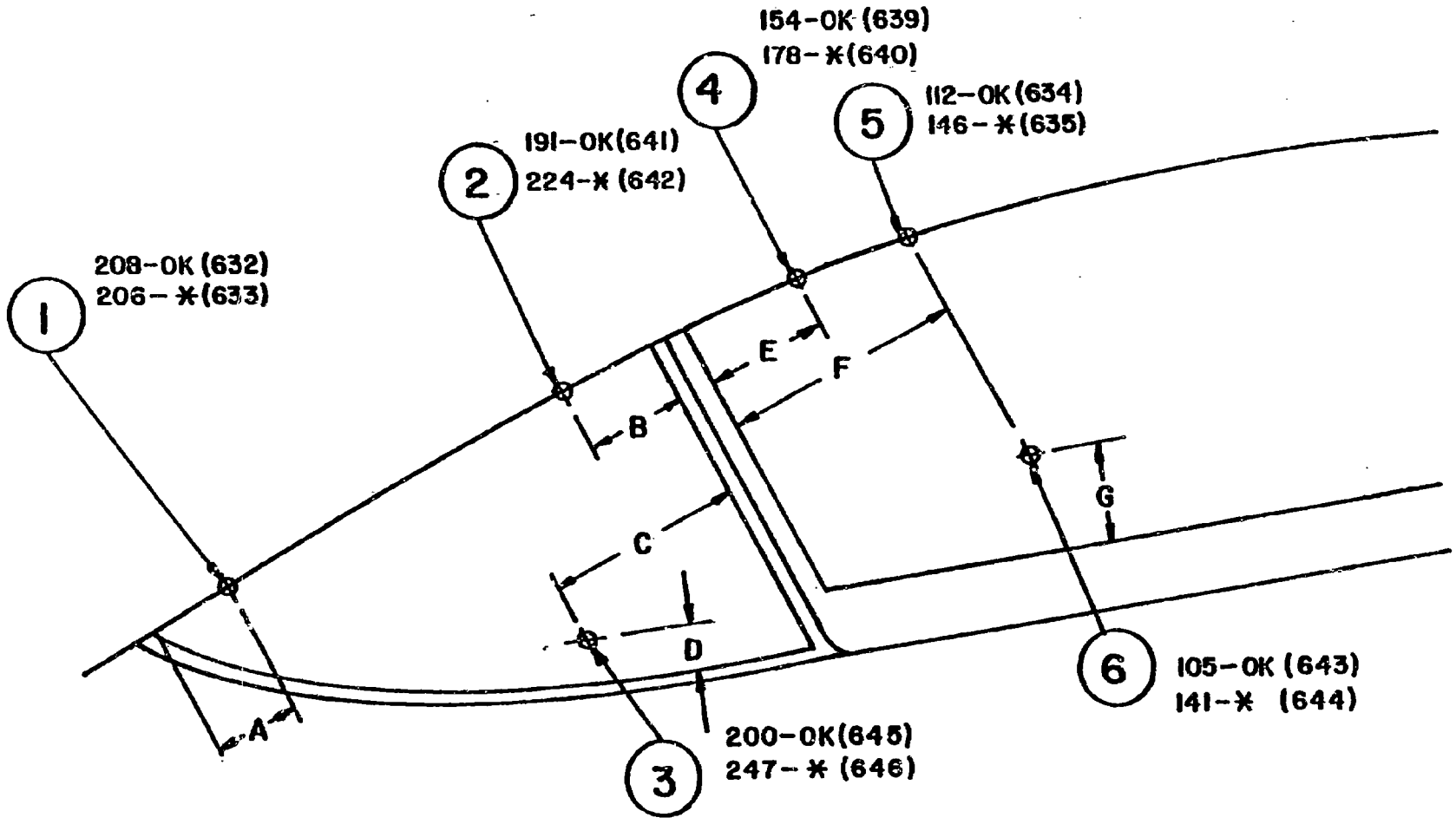

* FAILURE

NOTES:

(1) IMPACT POINTS 1, 2, 4, AND 5 ON FUSELAGE CENTERLINE

(2) ALL DIMENSIONS IN INCHES, AS MEASURED ALONG TRANSPARENCY SURFACES.

A-6.125
B-6.25
C-9.875
D-3.00
E-7.00
F-12.55
G-6.00

BIRD IMPACT LOCATIONS
AND PASS/FAIL IMPACT RESISTANCES
OF THE UNREINFORCED 0.6 INCH STRETCHED ACRYLIC
TRANSPARENCIES CURRENTLY IN FLIGHT USE

FIGURE 3

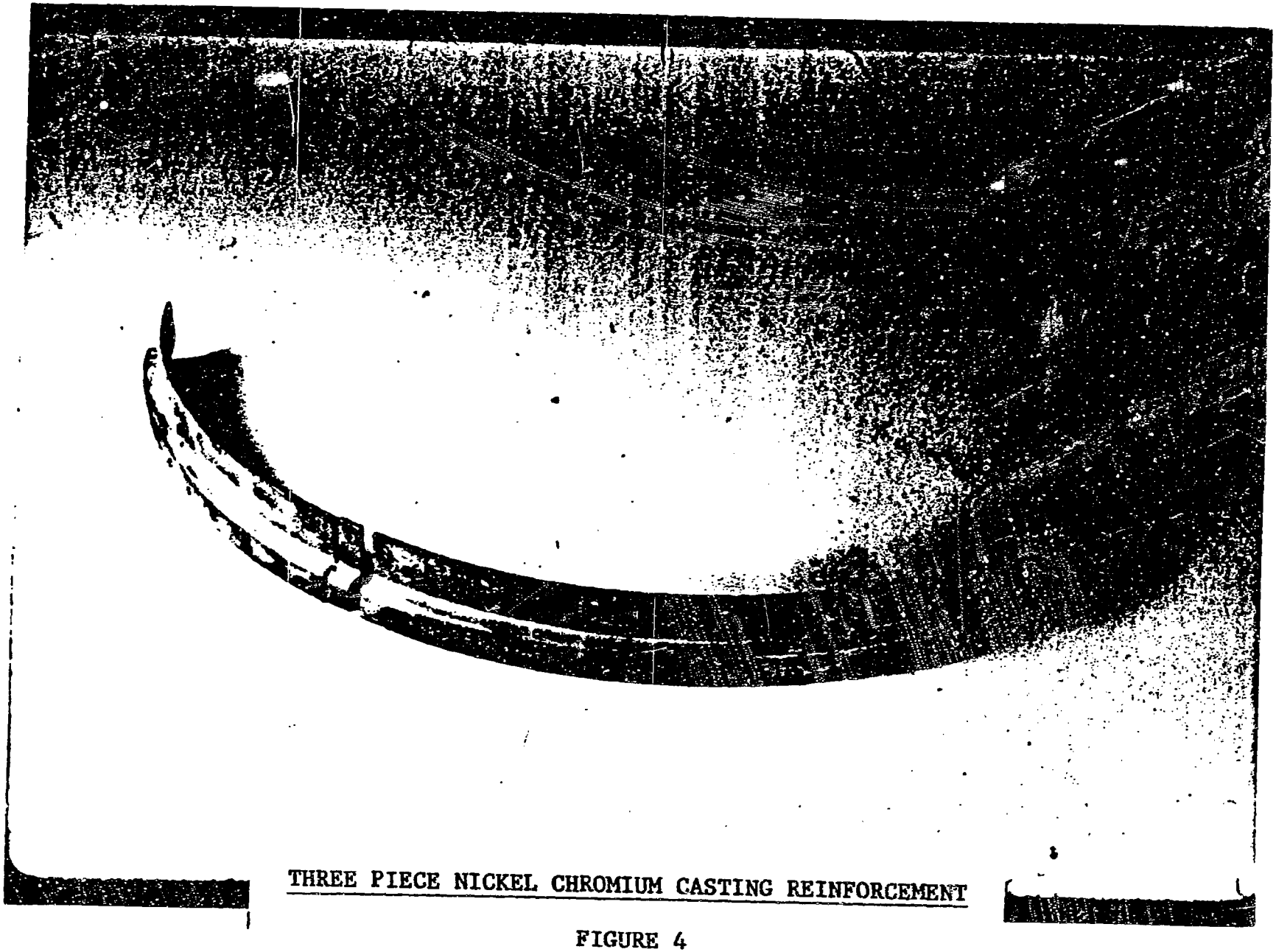

THREE PIECE NICKEL CHROMIUM CASTING REINFORCEMENT

FIGURE 4

At a 250 knot (Shot 1949) impact on the same transparency system, the bird was deflected but there was appreciable damage. Sixteen of the 3/16 inch retainer bolts failed in tension; there was a permanent deformation of the aft arch. Along the centerline, the windshield aft arch was 3/4 inch lower than the canopy. Half way between the centerline and the sill the aft arch bulged out 1/4 inch from the canopy.

No additional aft arch shots were made on this transparency system; however, it was used for four additional sill shots, two on the right sill and two on the left sill. Figure 5 is a view of the aft arch showing the damage that occurred after all six impacts.

On a right sill impact at 250 knots, there was no apparent damage to the transparency system.

On a second right sill impact at 400 knots (Shot 1951) the transparency remained intact but the magnesium frame broke at the end of the right cast reinforcement section. This free end then rotated in and broke free an 8 inch segment of the magnesium and reinforcement. The final break in the 610 casting was in a slag contaminated gusset.

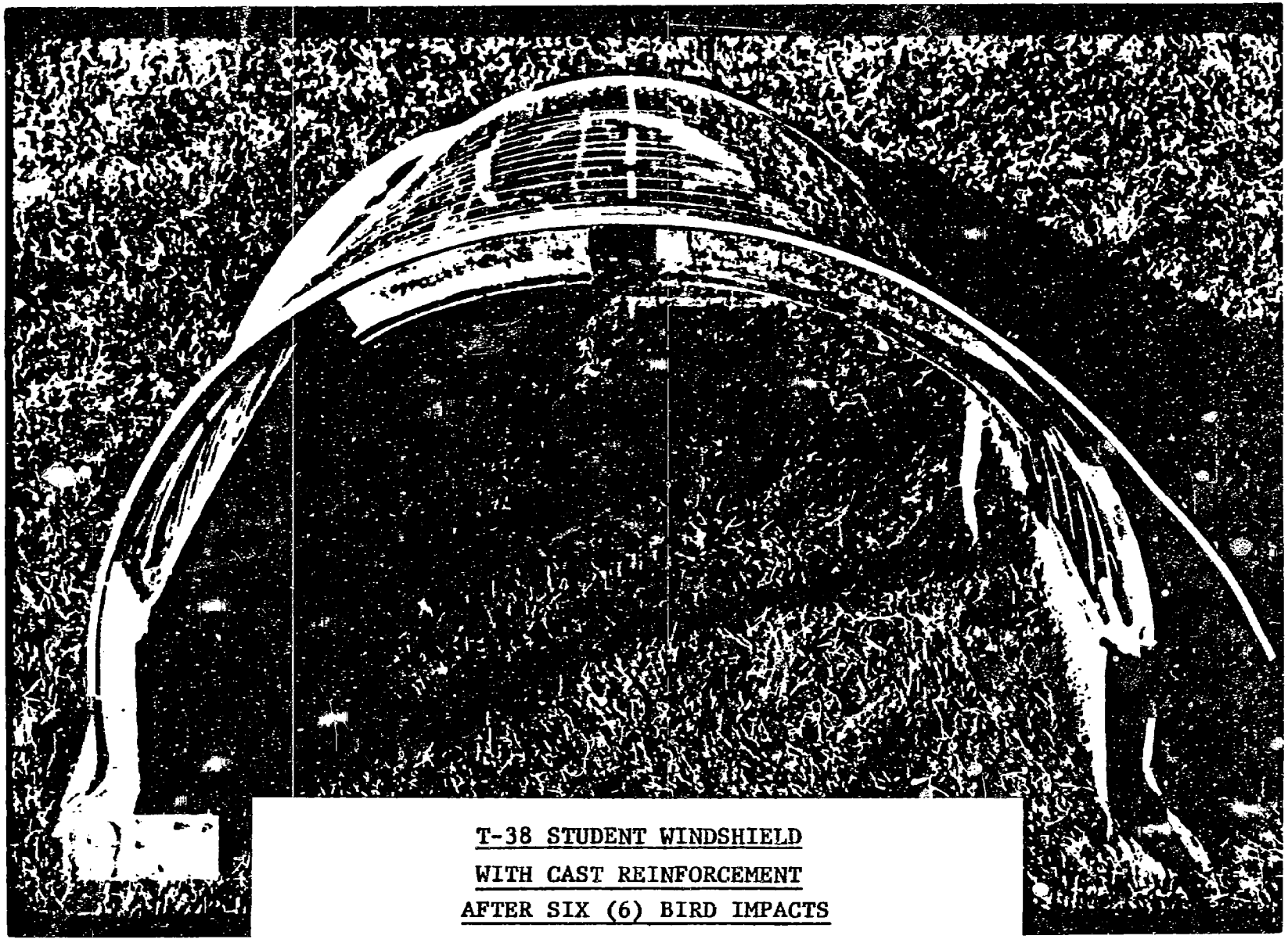

T-38 STUDENT WINDSHIELD
WITH CAST REINFORCEMENT
AFTER SIX (6) BIRD IMPACTS

FIGURE 5

Without replacing the missing right hand section, sill shots were made on the left hand side of the transparency. The first shot on this side was at 300 knots (Shot 1952) with no apparent additional damage.

The last shot on this transparency system was at 400 knots (Shot 1953) on the left sill, and the results were very similar to the 400 knot right sill shot. The transparency remained intact and the magnesium frame broke at a point where the left cast reinforcement section ended. This free end then rotated in and broke free a 12 inch segment of the magnesium and reinforcement. The final break in the 610 casting occurred at the lap joint between reinforcement sections. Figure 6A summarizes the impacts on the casting reinforced transparency system.

From this sequence of bird impact tests, it was learned that the reinforcement should be continuous, down to the sill and extended forward along the sill in order to provide the maximum support.

Two concepts were next considered as alternative solutions for frame reinforcements, a composite and continuous metal reinforcement. The University Of Dayton Research Institute was subcontracted to design and fabricate two composite reinforcements, while PPG designed a continuous metal reinforcement.

T-38 STUDENT WINDSHIELD

BIRD IMPACT TESTING

6.A. SUMMARY OF FOUR POUND BIRD IMPACTS ON CASTING REINFORCED TRANSPARENCY SYSTEM

OCTOBER, 1982

.600 MONOLITHIC POLYCARBONATE
3 PIECE CAST 610 STAINLESS STEEL REINFORCEMENT

200 KT. CTR.SHOT
250 KT. CTR.SHOT
250 KT. R/SILL
*400 KT. R/SILL
300 KT. L/SILL
*400 KT. L/SILL

*FRAME FAILURE

6.B. SUMMARY OF FOUR POUND BIRD IMPACTS ON COMPOSITE REINFORCED TRANSPARENCY SYSTEM

MAY, 1983

.600 MONOLITHIC POLYCARBONATE,
LINER & COATING, COMPOSITE REINFORCEMENT

200 KT. CTR.SHOT
**250 KT. CTR.SHOT
***300 KT. CTR.SHOT

**COMPOSITE CAME APART
***TRANSPARENCY FAILED AT AFT ARCH

FIGURE 6

Kevlar Epoxy was chosen as the composite material because of its strength, weight, and toughness. The centerline cross section of the design is shown in Figure 7 and is composed of twenty plies of woven fabric sandwiched between fifteen plies of unidirectional tape. The cross section does change from the centerline to the sill and this is shown in Figures 8 and 9. There is also a section of composite projecting forward along the sill, as shown in Figure 10, in an effort to hold the frame system together if sill corner cracking should occur.

The unidirectional pre-impregnated tape that was used had a low resin content. As a result, after curing, there was some delamination of the unidirectional tape; there was also additional delamination and some fraying of the tape when it was drilled, as shown in Figure 11. These flaws were not seen in the woven portion of the laminate.

As a result of a 200 knot (Shot 2106) aft arch bird impact, there was delamination of the unidirectional tape on the rear flange of the arch along the center and right side as shown in Figures 12 and 13. The measured 1-1/2 inch maximum deflection as determined by the triangulation method at the impact point on the transparency, was about equal to the

[0] denotes unidirectional tape
[0/90] denotes fabric
[±45] denotes fabric

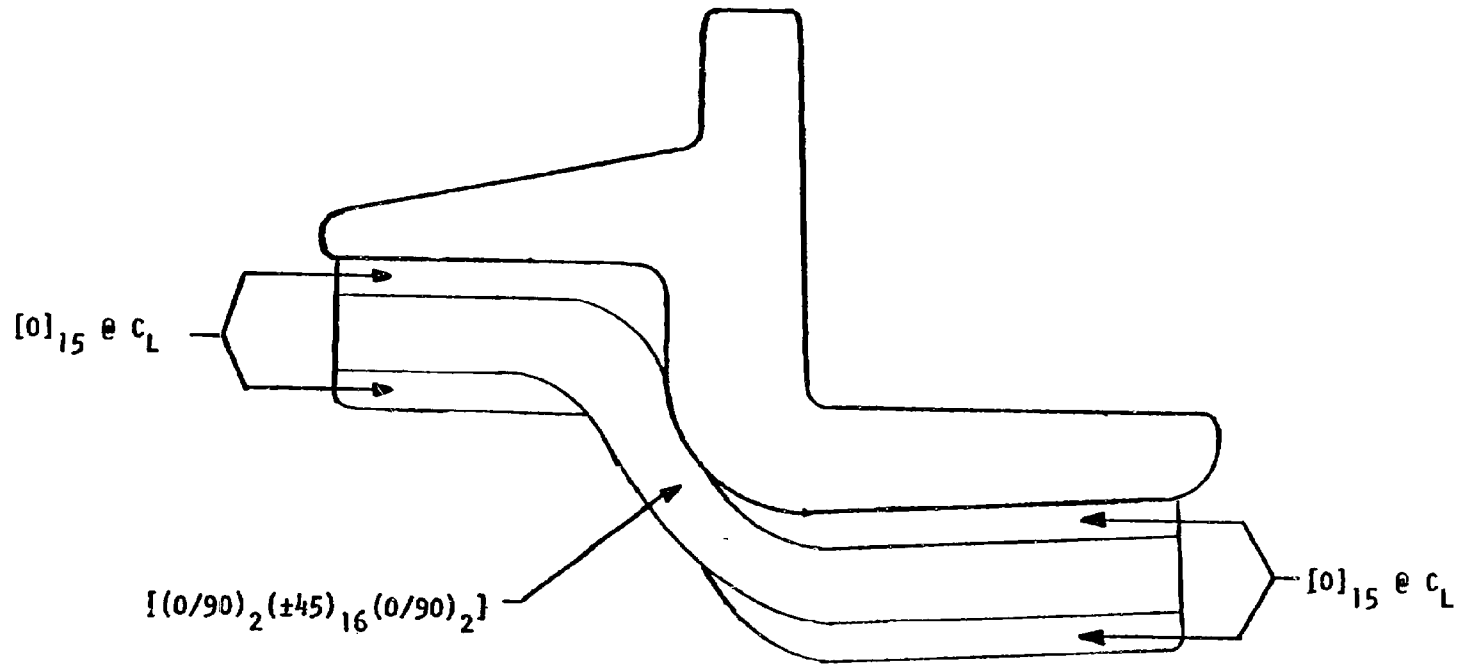

CENTERLINE CROSS SECTION
OF THE COMPOSITE DESIGN
AND T-38 STUDENT WINDSHIELD FRAME

FIGURE 7

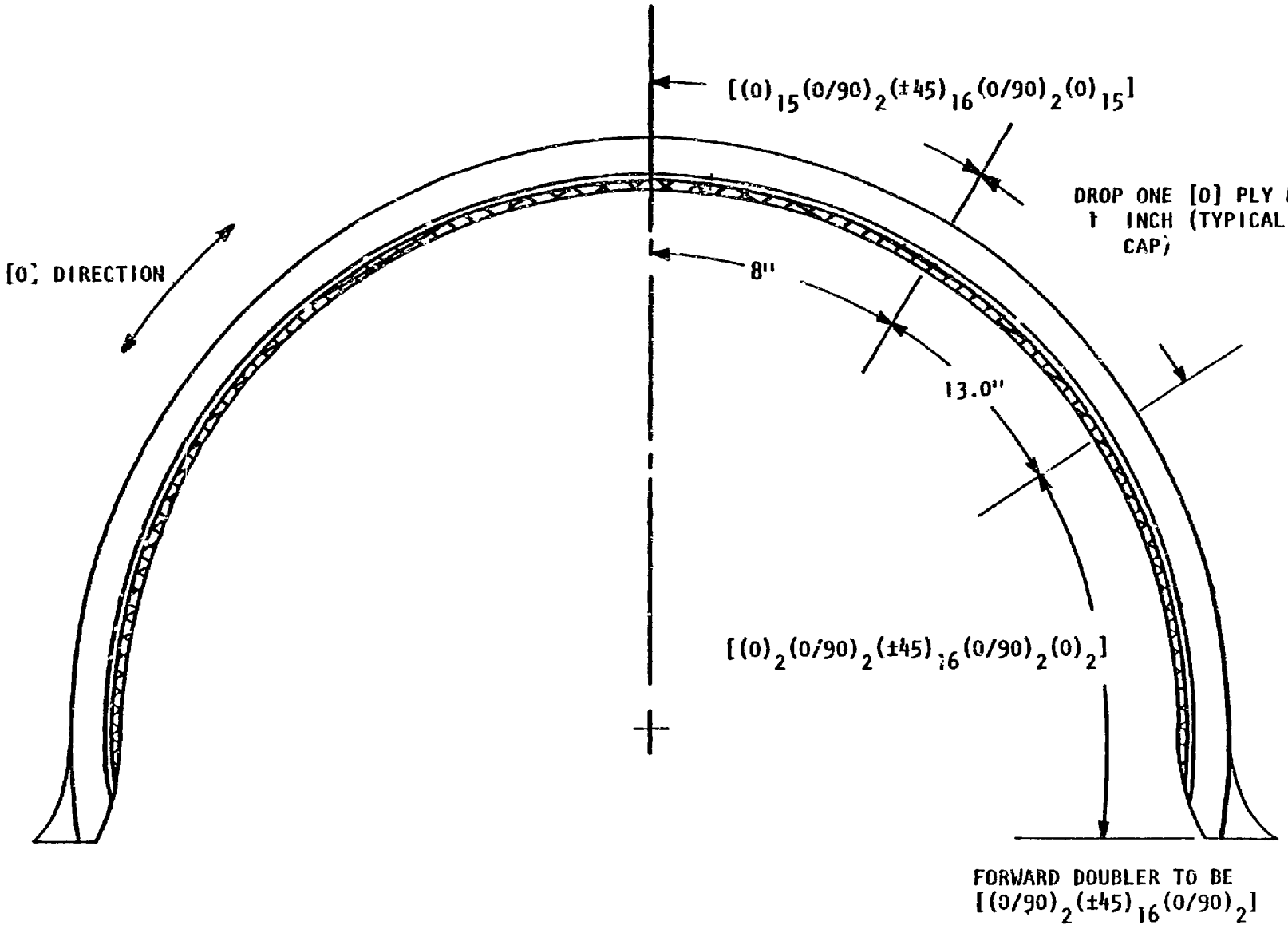

COMPOSITE DRAWING
SHOWING CHANGING CROSS SECTION

FIGURE 8

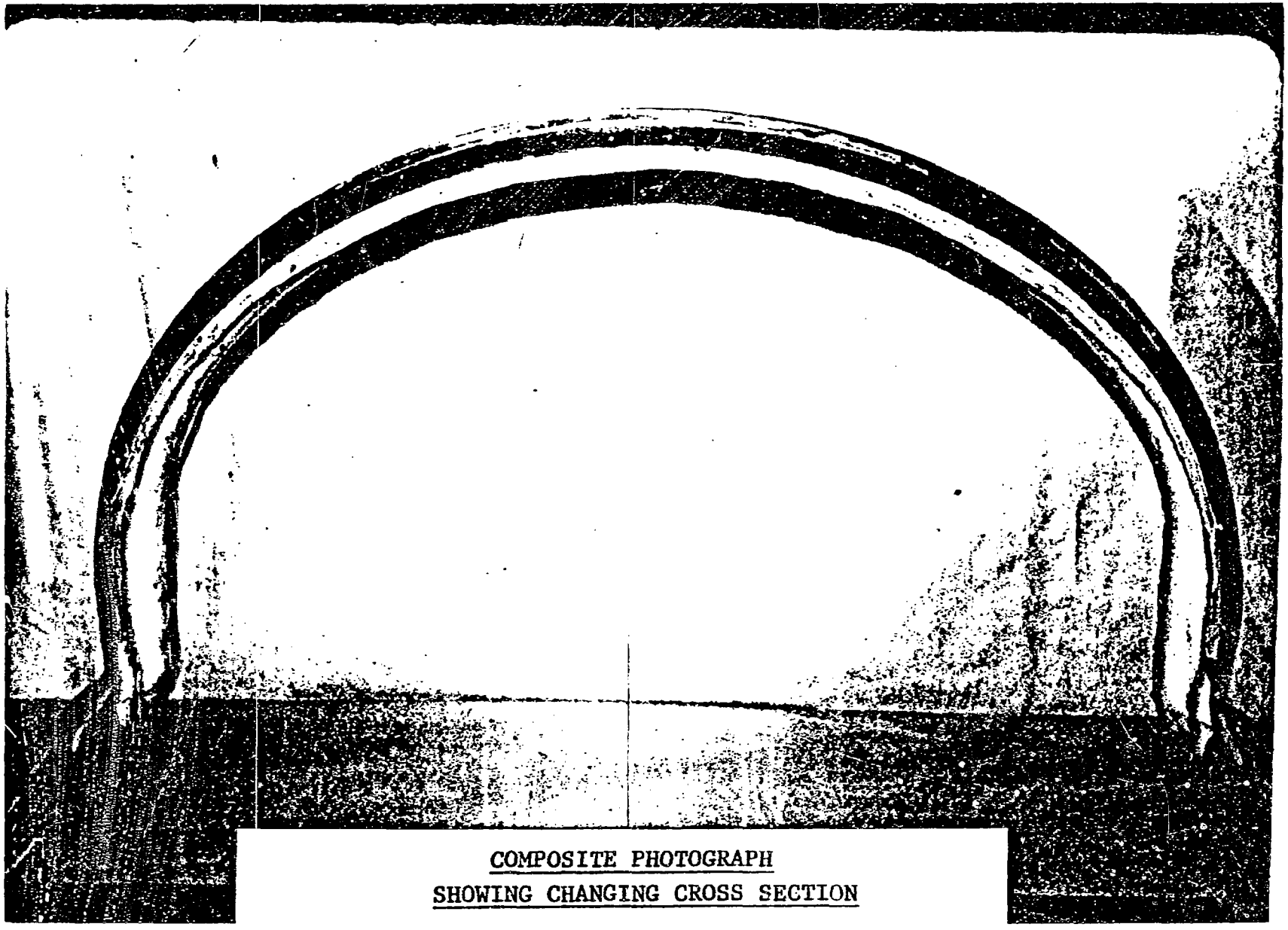

COMPOSITE PHOTOGRAPH
SHOWING CHANGING CROSS SECTION

FIGURE 9

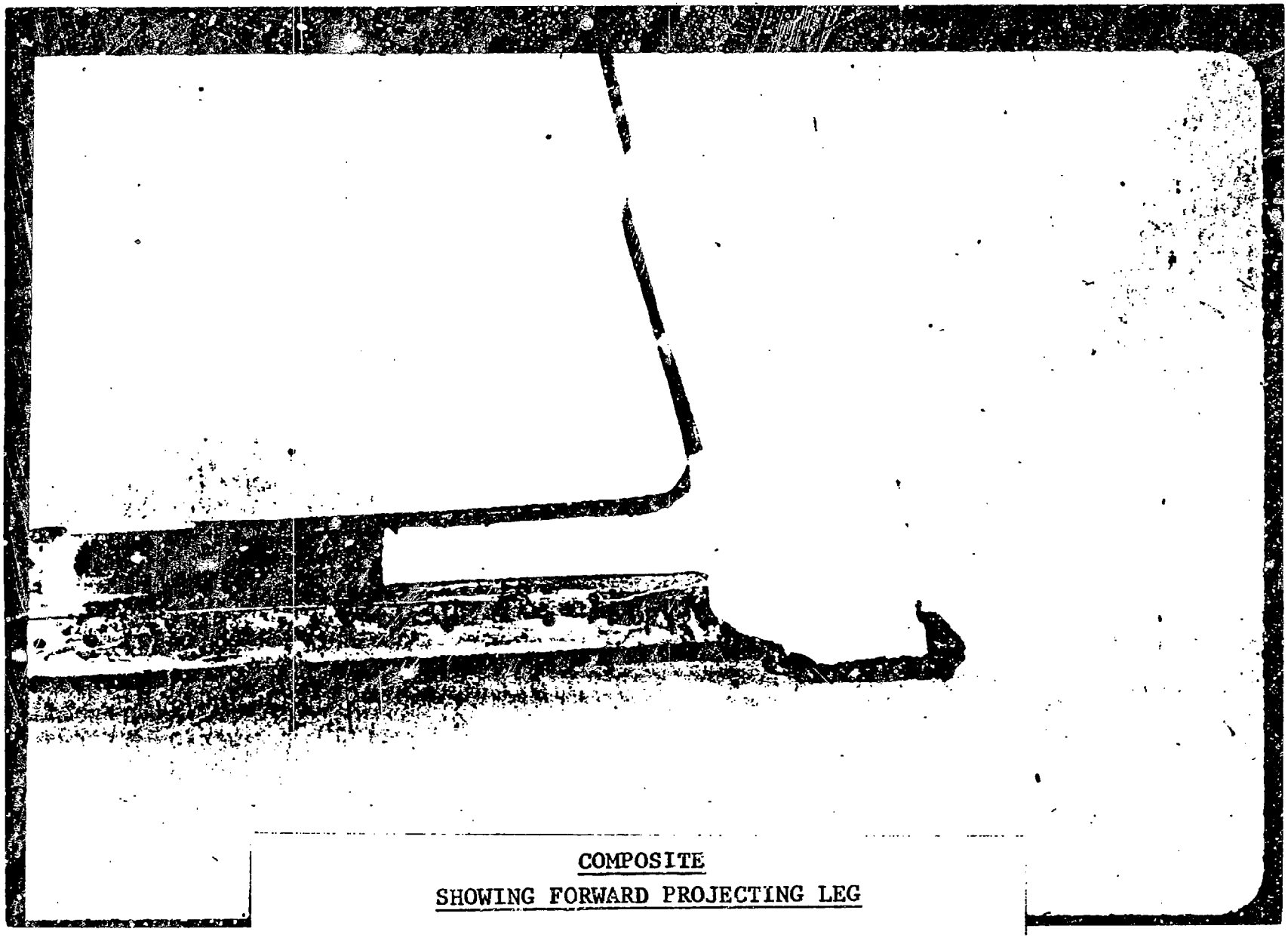

COMPOSITE

SHOWING FORWARD PROJECTING LEG

FIGURE 10

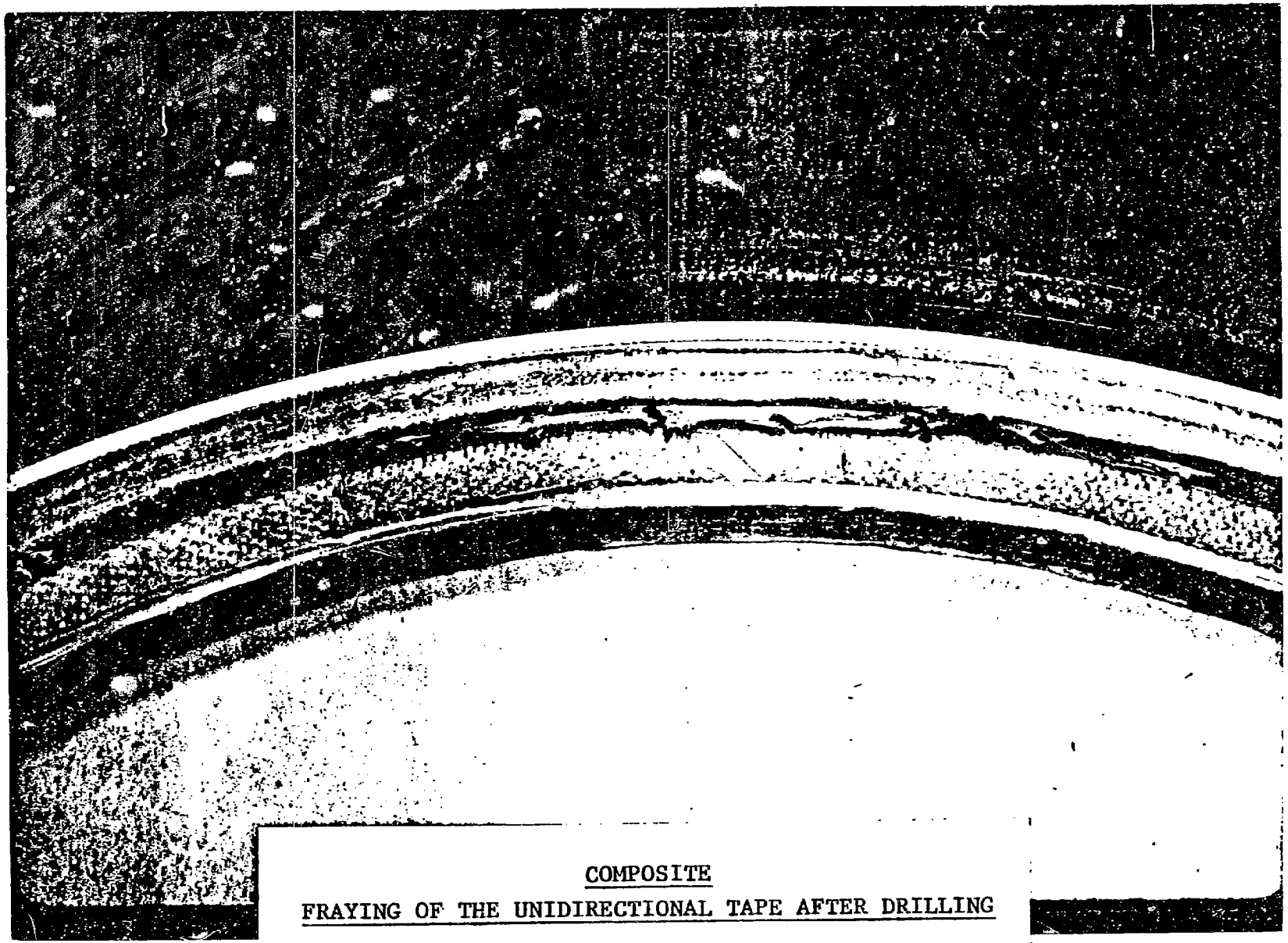

COMPOSITE

FRAYING OF THE UNIDIRECTIONAL TAPE AFTER DRILLING

FIGURE 11

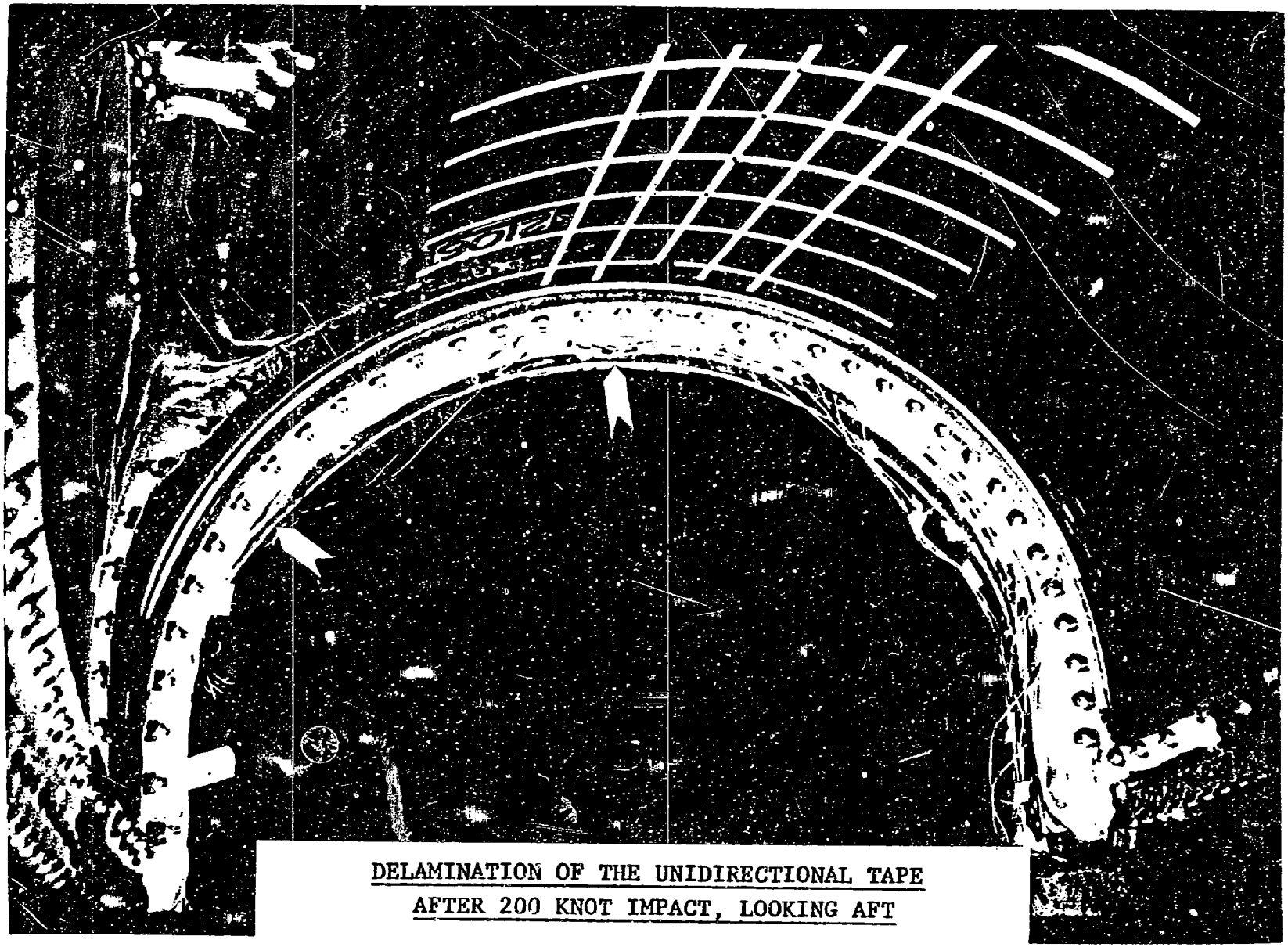

DELAMINATION OF THE UNIDIRECTIONAL TAPE
AFTER 200 KNOT IMPACT, LOOKING AFT

FIGURE 12

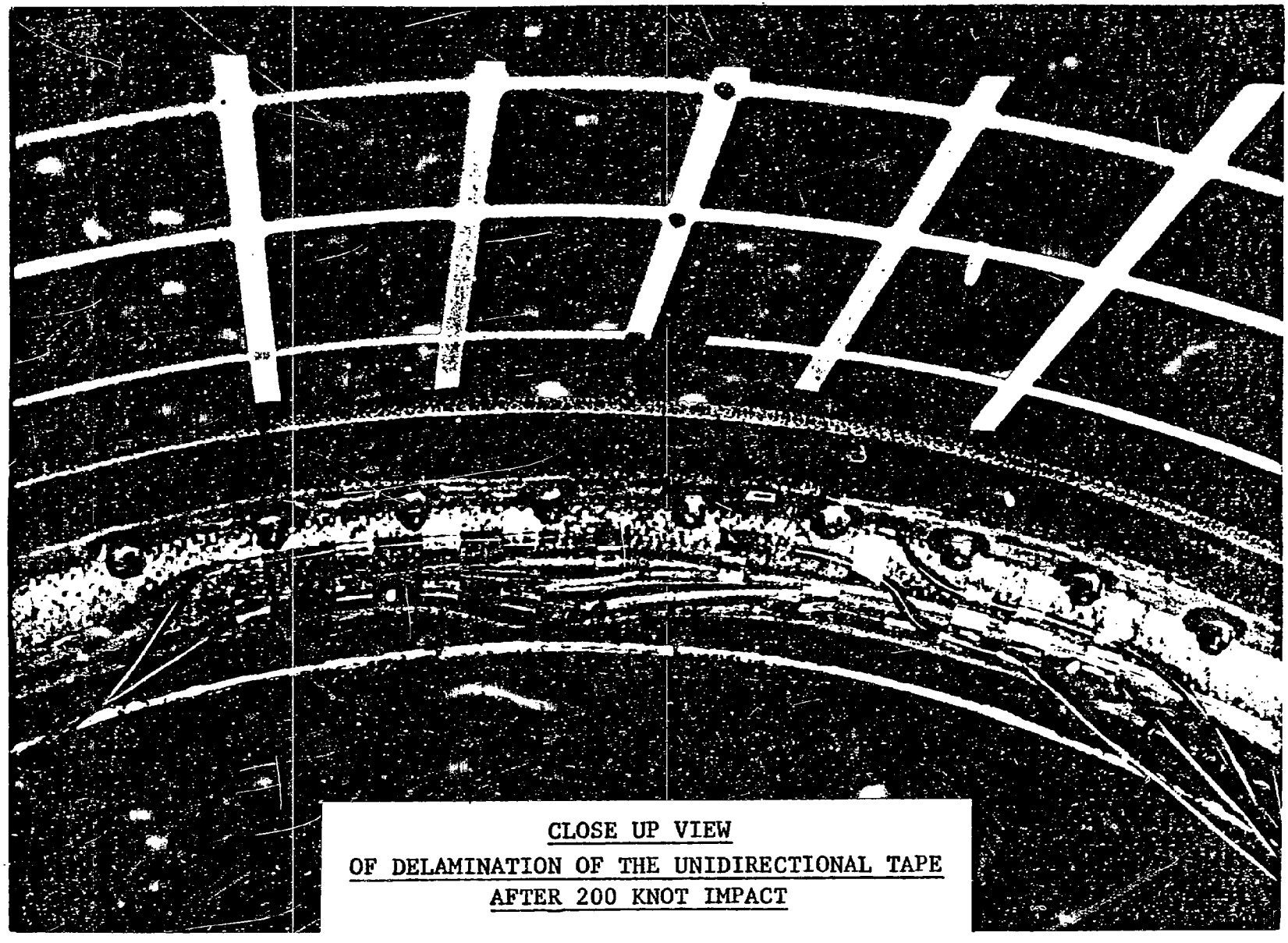

CLOSE UP VIEW
OF DELAMINATION OF THE UNIDIRECTIONAL TAPE
AFTER 200 KNOT IMPACT

FIGURE 13

deflection measured for the 200 knot impact on the casting reinforced transparency. The composite reinforced aft arch deflected a maximum of 0.8 inches.

At a 250 knot (Shot 2107) aft arch bird impact, there was further delamination of the unidirectional tape on the rear arch flange, rendering it non functional on the next shot. There was no other apparent damage to the system. However, the magnesium frame was hidden from view and the canopy was not removed between tests to enable a close inspection of the magnesium frame.

At a 300 knot (Shot 2108) aft arch bird impact, the transparency failed. The failure origin was a half moon shaped flaw on the inside surface of the polycarbonate located .375 inch forward of the frame mounting ledge, 1.5 inches to the right of the centerline. The unidirectional tape on the rear flange of the arch separated completely. The woven portion of the Kevlar reinforcement showed localized delamination beneath the large crack in the magnesium to the left of center, as shown in Figures 14 and 15. Figure 6B summarizes the impacts on the composite reinforced transparency system.

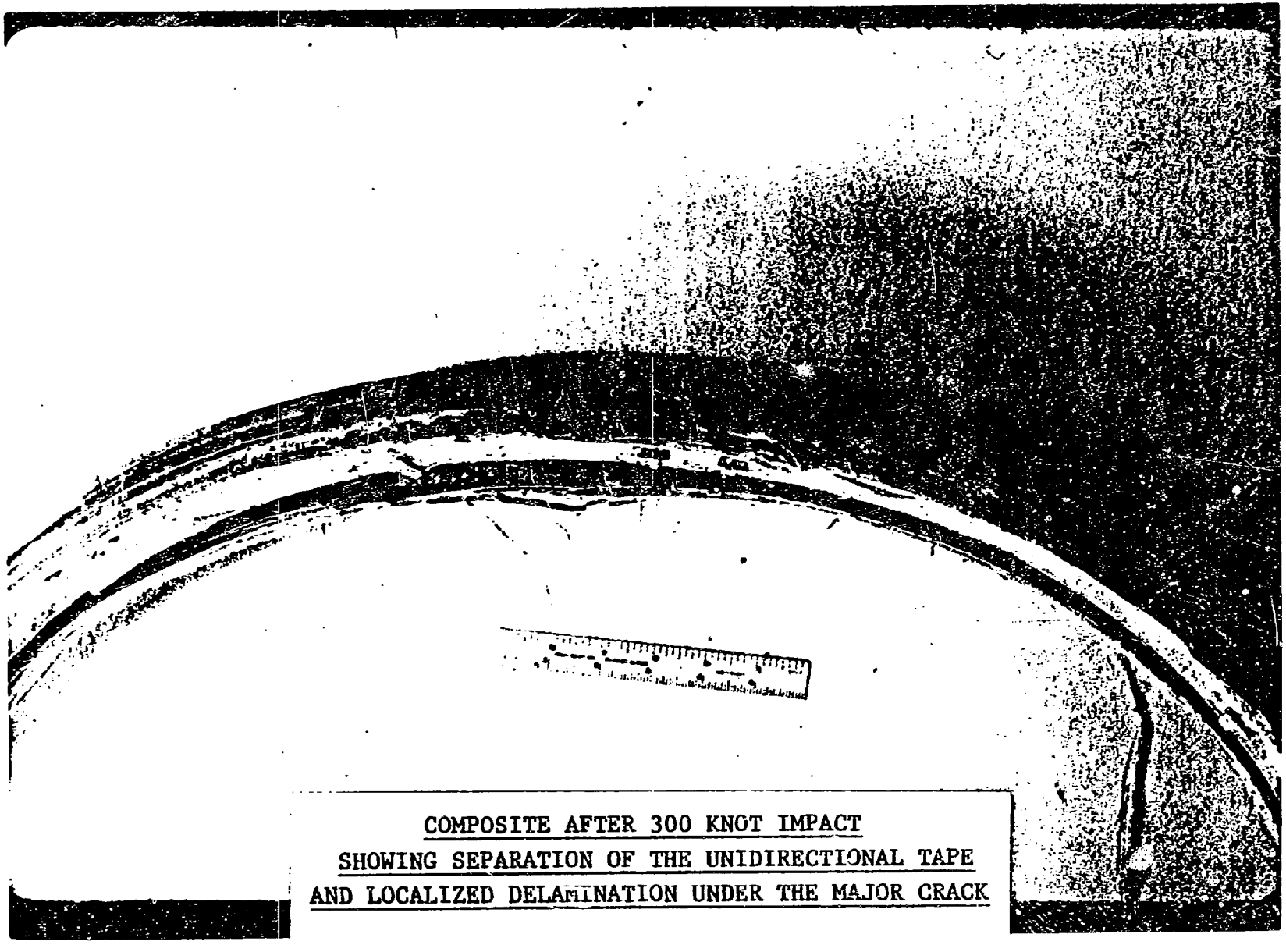

COMPOSITE AFTER 300 KNOT IMPACT
SHOWING SEPARATION OF THE UNIDIRECTIONAL TAPE
AND LOCALIZED DELAMINATION UNDER THE MAJOR CRACK

FIGURE 14

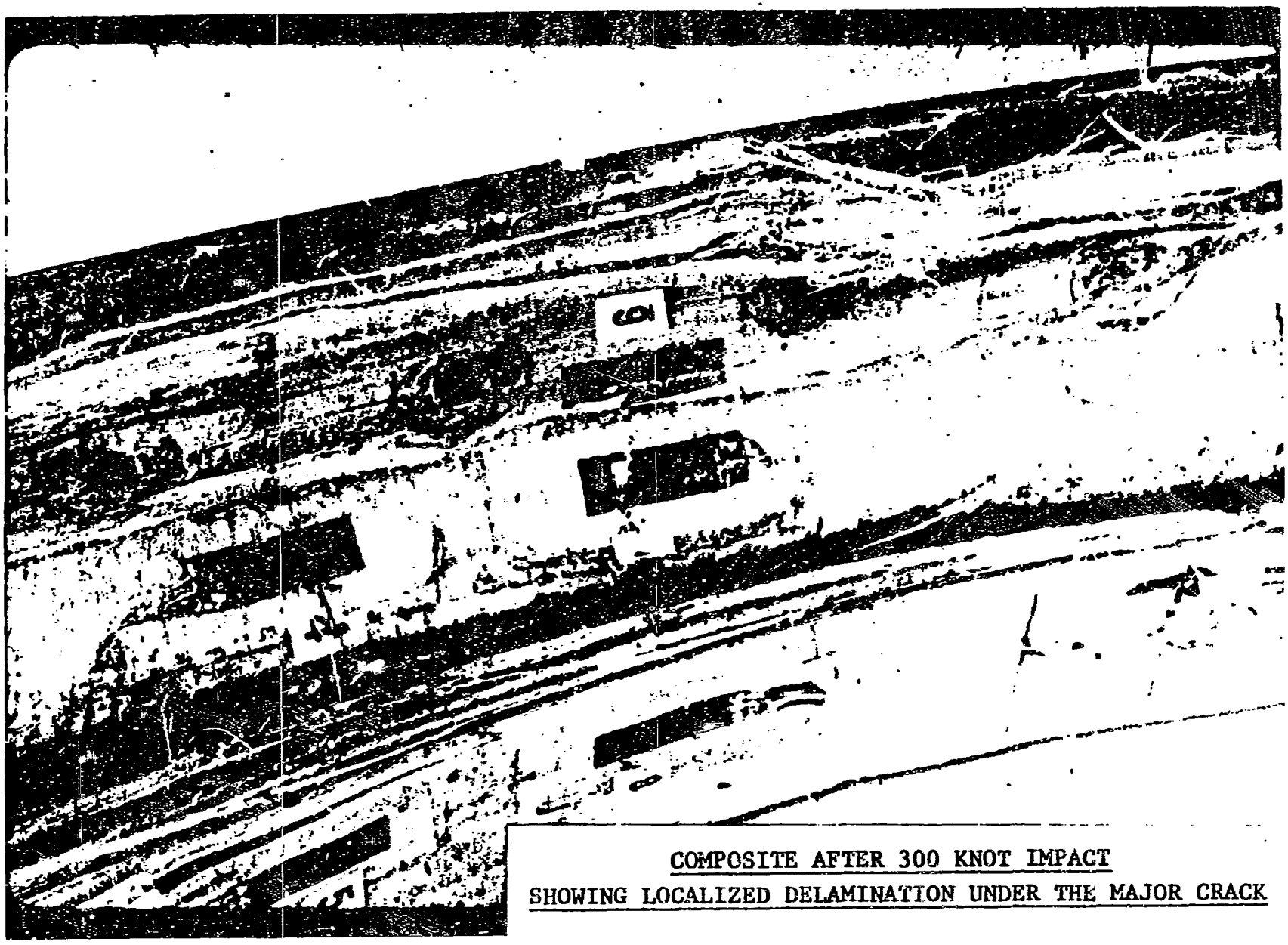

COMPOSITE AFTER 300 KNOT IMPACT
SHOWING LOCALIZED DELAMINATION UNDER THE MAJOR CRACK

FIGURE 15

The magnesium frame had a total of seven crackes in it, spaced somewhat symmetrically around the aft arch as shown in Figure 16, including a crack in the corner of each sill. The largest crack in the magnesium was 1.5 inches to the left side of the centerline.

From the composite arch reinforcement efforts it has been determined that:

- The stiffness of the composite configuration was inadequate based on the 0.8 inch arch deflection at 200 knots.
- Delamination of the unidirectional tape compromised the stiffness of the reinforcement.

Recommendations for future composite reinforcements include the following:

- Materials with higher resin content should be used.
- The outer most plies should be woven, as opposed to unidirectional tape, in order to facilitate drilling.
- Stiffness should be increased by using a hybrid design, which incorporates higher modulus fibers.

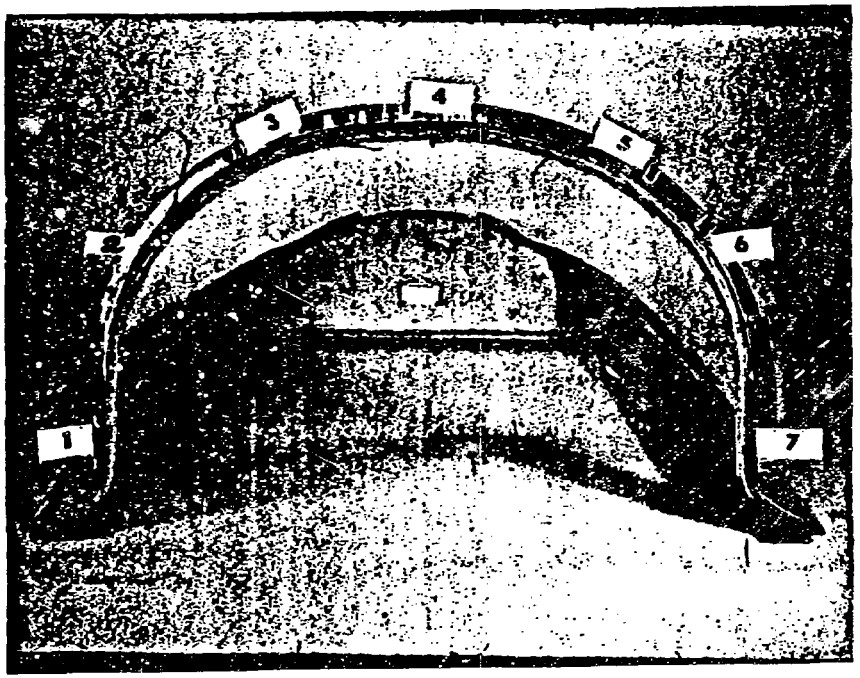

T-38 STUDENT WINDSHIELD FRAME
WITH COMPOSITE REINFORCEMENT, SHOWING THE FRAME CRACKS
POST 300 KNOT BIRD IMPACT

FIGURE 16

T-38 STUDENT WINDSHIELD BIRDPROOFING EFFORTS UTILIZING METAL & COMPOSITE MATERIALS FOR AFT ARCH REINFORCEMENT

Future efforts in the development of an aft arch reinforcement include:

- The fabrication of a metal aft arch reinforcement.
- Development of a hybrid composite reinforcement.

AD-P003 190

DEVELOPMENT OF LIGHTWEIGHT COMMERCIAL AIRCRAFT WINDSHIELDS WITH NEW HIGH STRENGTH GLASSES

W. E. Gourley and H. E. Littell,
PPG Industries, Inc.

Development of Lightweight Commercial Aircraft Windshields With New High Strength Glasses

W. E. Gourley and H. E. Littell, Jr.
PPG Industries, Inc.
Glass Research Center
Pittsburgh, PA

Abstract

Laminated glass has provided durable service as the main structural component in forward-facing commercial aircraft windshields. However, weight considerations and more stringent performance requirements have forced the transparency designer to employ advanced glass technology in developing windshields for new generation aircraft.

The Boeing 757/767 No. 1 windshield is one example. In addition to a requirement for less weight than previous designs, the transparency has to provide enhanced bird impact protection resulting in no spall from the inboard surface. Initial tests on "standard" designs showed that regular thermally tempered glass would not meet the conflicting weight/spall requirements and that designs with high strength glass would be required. Work with Lucas-Aerospace-Siddeley Aviation in the mid 1970's had shown that two glasses could provide bird impact protection with less weight than standard thermally tempered glass, and these became candidates for inclusion in new windshield cross sections.

Concurrently, finite element analysis using ADINA and MSC/NASTRAN provided guidelines for the ply arrangements in possible designs. This work showed that relatively thick core plies would minimize dynamic tensile stresses during impact. Since such plies could be tempered to higher surface compressions than thinner glass, they were ideal for the application.

To evaluate the effect of increased surface compression on failure resistance, it was necessary to test instrumented windshields and measure surface stress versus velocity for different designs. A resulting test program included 164 bird impacts against 28 full-size, flat windshields incorporating different interlayers and glass plies of varying thicknesses at varying locations and temperature conditions. This paper presents the results of the program in the form of stress-velocity curves and pass-fail results for different designs. It also shows the evolution of a design which features a thick high strength thermally tempered core for load carrying and a thin chemically strengthened inboard ply to enhance fail-safe yet survive the stresses which occur during impact.

The thick/thin high strength glass windshield met all bird impact qualification tests at Boeing and subsequent thermal-pressure certification. This design concept was also employed for lighter weight retrofit applications for other commercial aircraft windshields.

Laminated glass has provided durable service as the main structural component in forward facing commercial aircraft windshields for many years. Recently weight reduction demands and more stringent performance requirements have forced the transparency designer to employ advanced glass technology in developing windshields for new generation aircraft. No longer were pass/fail bird tests enough in design work; designing an optimum cross section to meet the current specifications entailed the use of dynamic strain measurements from strain gaged bird impact test parts combined with finite element analyses for the proper placement of new, high strength glass plies within the laminate. The emergence of low cost, high speed computers provided the designer with the finite element modeling tool, just when the need to model the bird impact event was greatest.

The Boeing 757/767 No. 1 windshield is one example of a design expected to do more with less weight. In the past, most FAR 25 windshields were required to prevent penetration during bird impact but could produce non-injurious spall from a cracked glass ply. Boeing specified for the 757/767 that no spall whatsoever was to be ejected during 360 KT bird strikes at various locations and temperature conditions. With the further restriction that only state-of-the-art materials could be used, the inboard glass ply of a minimum weight windshield could therefore not fail during bird impact.

The difficulty of this restriction was borne out by PPG Industries during exploratory bird impact testing. Designs with various cross sections which were actually heavier than the target weight survived 4 lb bird impacts at 360 KT without penetration, but always developed spall from the fractured inboard surface. Figure 1 shows two acceptable lighter weight designs from a 360 KT penetration standpoint which began to develop glass breakage and spall at about 360 KT.

The exploratory parts were made using standard air tempered glass. However, work in the mid 1970's showed that high strength glasses would provide superior protection. Following the work reported by M. J. Mott, PPG Industries provided specimens incorporating HERCULITE® II chemically strengthened glass to Hawker Siddeley for test. Subsequently, PPG borrowed a Hawker Siddeley test frame for additional bird strikes against panels with main plies of a new high strength thermally strengthened glass. A combined plot of new work on previous curves appears in Figure 2. The results showed that the proprietary high strength glasses would provide higher penetration speed for given weight or equivalent protection with less weight than other available materials.

PPG also evaluated 26" x 26" flat bolted edge panels of the design shown in Figure 3. Again, the high strength was superior to standard tempered glass. With the windshields installed at 45° sweepback, the standard core parts exhibited a penetration limit of 485 KT while the high strength thermal tempered glass had a limit of 590 KT.

In order to assess the use of high strength glass for a no-failure situation, it was apparent that failure stress would have to be known as a function of velocity. Therefore, a bird impact test program evolved which

FIGURE I

PRELIMINARY TEST WINDSHIELD CROSS SECTIONS

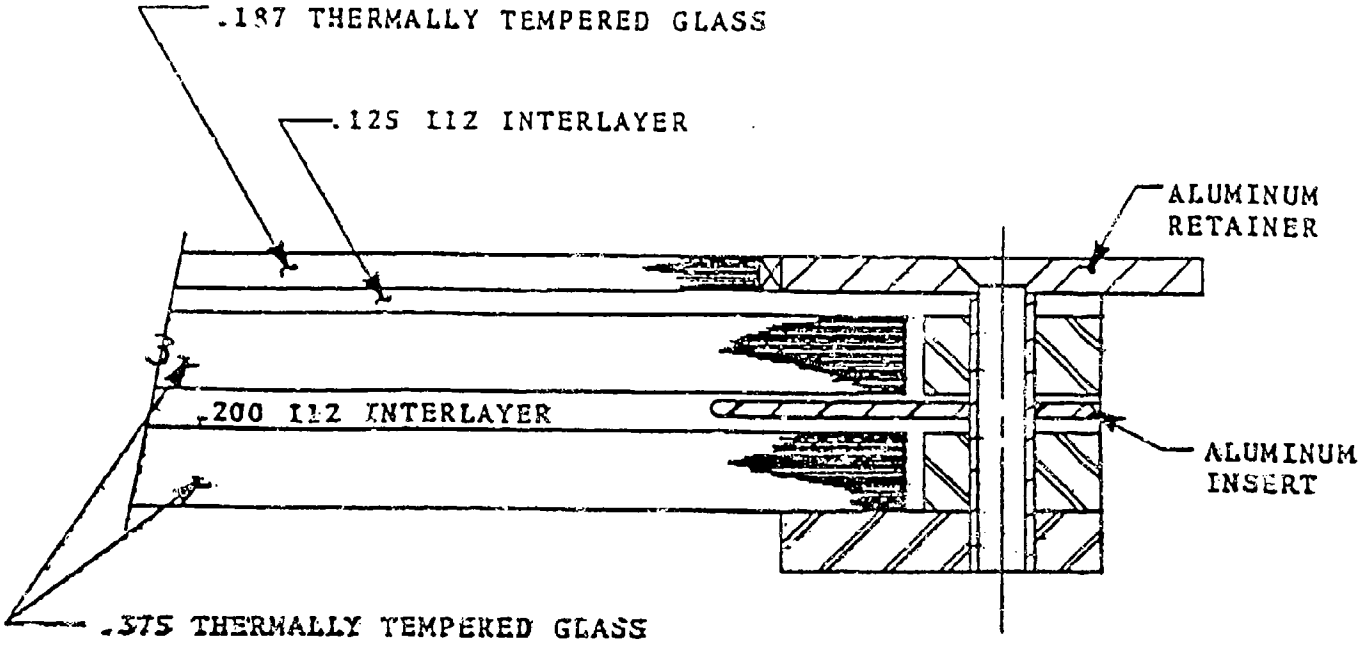

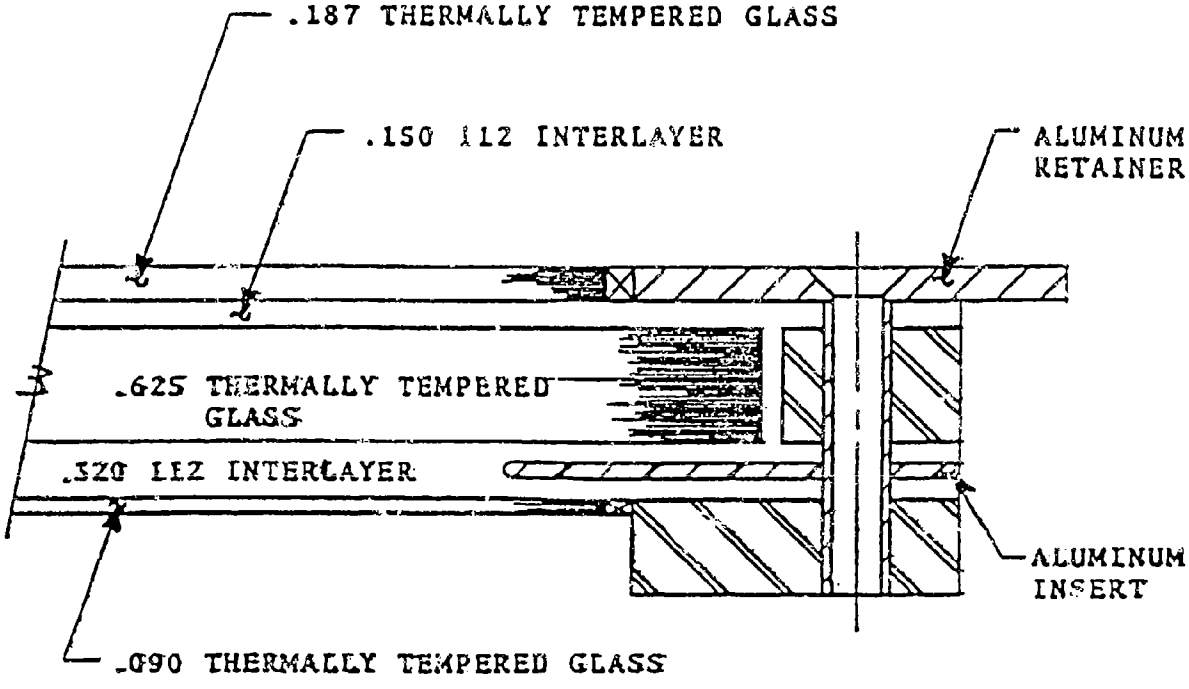

FIGURE 2

HIGH STRENGTH GLASS
BIRD IMPACT PENETRATION DATA

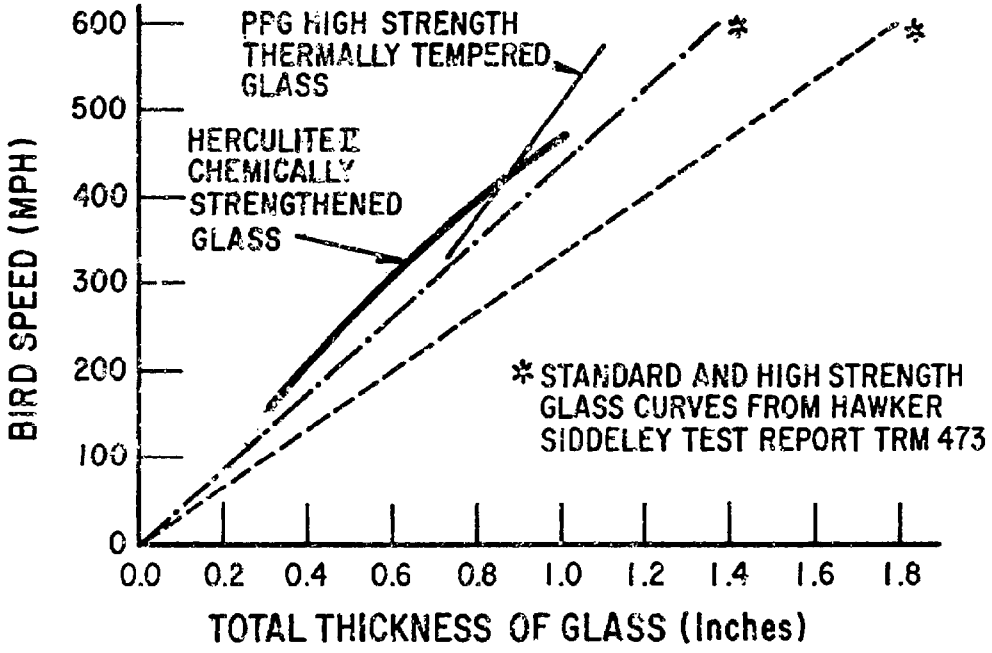

FIGURE 3 - 26" X 26" BIRD IMPACT PANELS WITH BOLTED EDGES

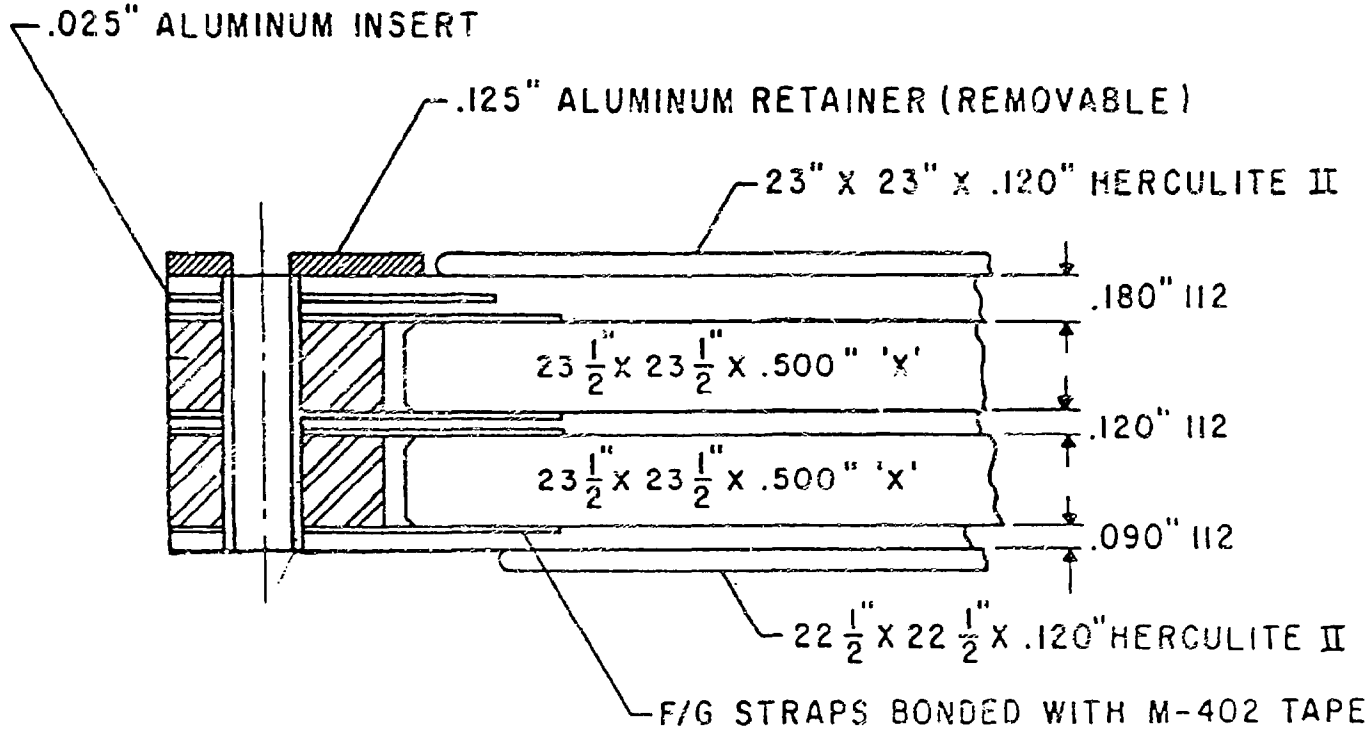

NOTE:

'X' = STD. LEVEL AIR QUENCHED GLASS OR HIGH STRENGTH GLASS

would both evaluate specific design protection limits and their stress-velocity relationships at lower energy levels. The effort involved 182 bird impacts against 42 windshields at the National Research Council of Canada's Flight Impact Simulator. The concurrent design support involved finite element analysis at PPG's Glass Research Center.

Finite element analyses helped in design selection by permitting comparisons of maximum stresses in each ply of different cross sections. Linear, dynamic models were run using MSC/NASTRAN, Solution 31,6 Direct Transient Analysis and NISA. Such models were appropriate for these relatively thick, flat "bounce the bird" type designs where maximum deflection was approximately half the thickness. Figure 4 shows a typical 26" x 26" square, five ply model. One eighth of the part was modeled to take advantage of symmetry. Figures 5 and 6 show stress contours in the inboard glass ply and core glass ply, respectively, in a typical modeled cross section. As these stress results compared well with strain gage generated data they could be used as an indication of how strong each glass ply needed be to survive the given impact. The advantage of time required per run and cost per model made finite element analysis increasingly important as a design tool in the total program. Many more cross sections could be screened using this tool. Overall, modeling showed thick core ply designs to be preferable with the cross section shown in Figure 7 using high strength glass plies being the selected lightweight, high performance candidate.

Not only are there bird impact requirements on aircraft windshields but also various pressure load demands. The ADINA finite element program was used primarily on uniform pressure load analyses. The only really interesting pressure load analysis is the fail-safe condition where two glass plies are assumed to be broken. The nonlinear capability of ADINA came into use in this case.

While Boeing 757/767 windshield tooling was unavailable early in the program, it was known that the shape was similar to that of the McDonnell Douglas DC-10 No. 1 windshield. With Douglas' permission, a DC-10 test frame was employed in the early tests using DC-10 shaped test parts. This procedure was continued until Boeing 757/767 windshield tooling became available. Figure 8 shows a typical test article installed on the 3/4" thick back plate aluminum test frame with 1-1/2" periphery aluminum spacer which was clamped to the National Research Council base structure. The transparencies were positioned in the Boeing 757/767 orientation with the center beam edge at a 45° vertical sweepback and the surface rotated 33° back from a plane normal to the bird line of attack. Tests used either the deice film or a heating blanket as a heat source for hot gradient tests.

Most of the test parts were instrumented with strain gages on interior and inward-facing external surfaces for dynamic impact area strain measurements. Biaxial gages were employed throughout the program. As many as eight 2100 Series Vishay Conditioners and strain amplifiers were used in the testing and a CEC oscillograph was used for recording the results. Calibration of the amplifiers was performed prior to each test. Figure 9 pictures the instrumentation system.

FIGURE 4

FIVE PLY ONE-EIGHTH FINITE ELEMENT MODEL DEFORMED SHAPE CENTER OF PLATE IS AT LOWER LEFT

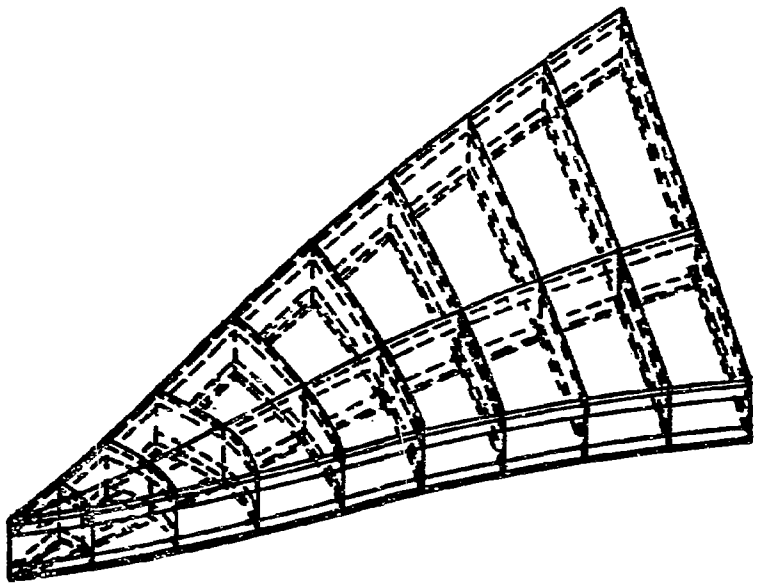

360 KNOTS – 45° ANGLE – 4 LB. BIRD – (26 IN. x 26 IN.) x (.150G/.270I/ .625G/.270I/.100G) PLOT NO. 1 TIME STEP 448 0.00447999 SEC
DEFORMED STRUCTURE

FIGURE 5

INBOARD PLY STRESS CONTOURS

CENTER OF PLATE IS AT LOWER LEFT

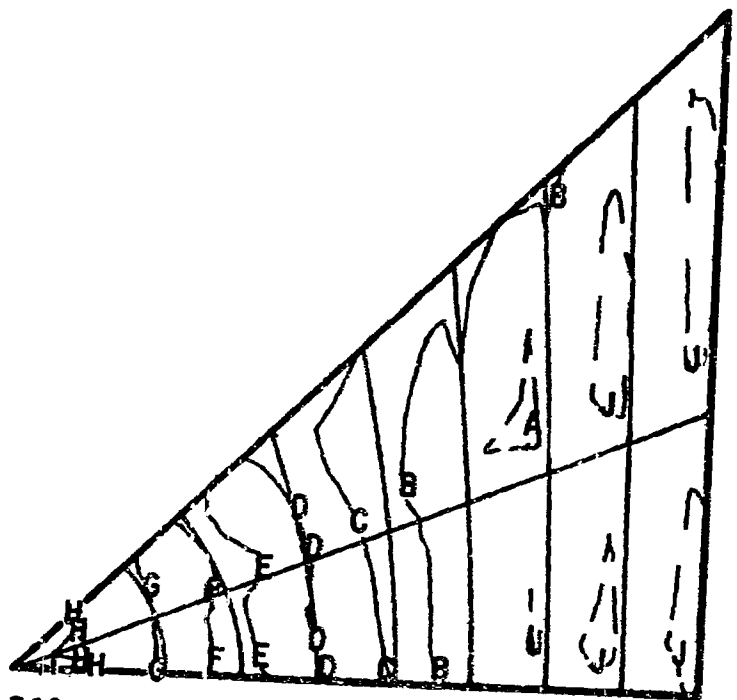

LEGEND

A = -1.225E+2
B = +8.238E+2
C = +1.770E+3
D = +2.716E+3
E = +3.663E+3
F = +4.609E+3
G = +5.555E+3
H = +6.502E+3
I = +7.448E+3
J = 0.000E 0

360 KNOTS-45°ANGLE-4 LB. BIRD-(26 IN. x 26 IN.) x (.150G/.270I/.625G/.270I/.100G) PLOT NO.2 TIME STEP 448 0.00447999 SEC
S3 CONTOURS

FIGURE 6

CORE PLY STRESS CONTOURS
CENTER OF PLATE IS AT LOWER LEFT

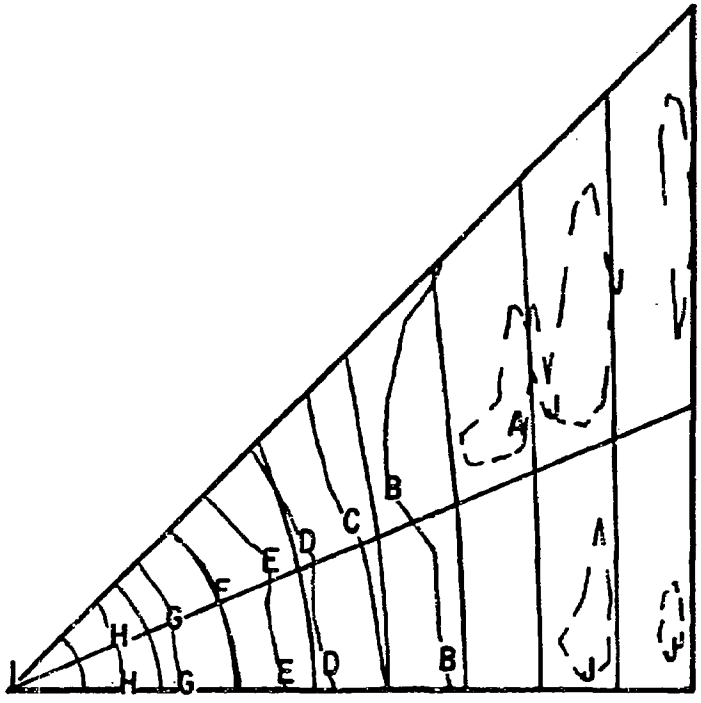

LEGEND

A = -6.527E+2
B = +4.288E+3
C = +9.229E+3
D = +1.417E+4
E = +1.911E+4
F = +2.405E+4
G = +2.899E+4
H = +3.393E+4
I = +3.887E+4
J = +0.000E+0

360 KNOTS – 45°ANGLE – 4 LB. BIRD – (26 IN. x 26 IN.) x (.150G/.270I/ .625G/.270I/.100G) PLOT NO.3 TIME STEP 448 0.00447999 SEC S3 CONTOURS

FIGURE 7

FINITE ELEMENT MODEL RECOMMENDED CROSS SECTION

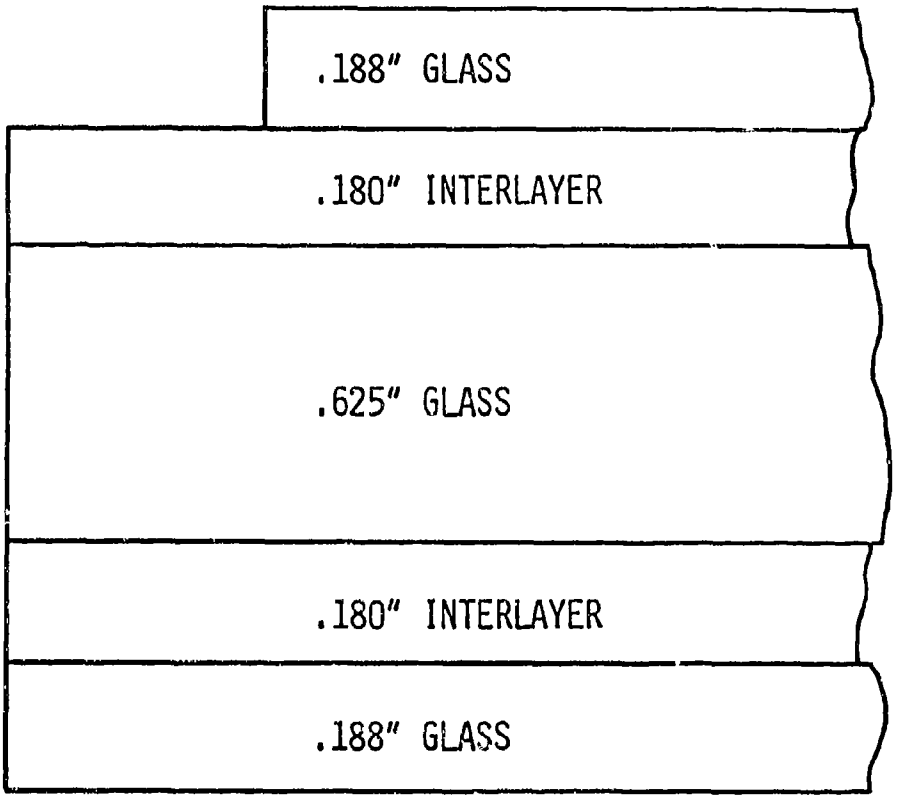

FIGURE 8. WINDSHIELD TEST SETUP AT N.R.C.

FIGURE 9

INSTRUMENTATION FOR BIRD IMPACT STRAIN GAGE STUDY

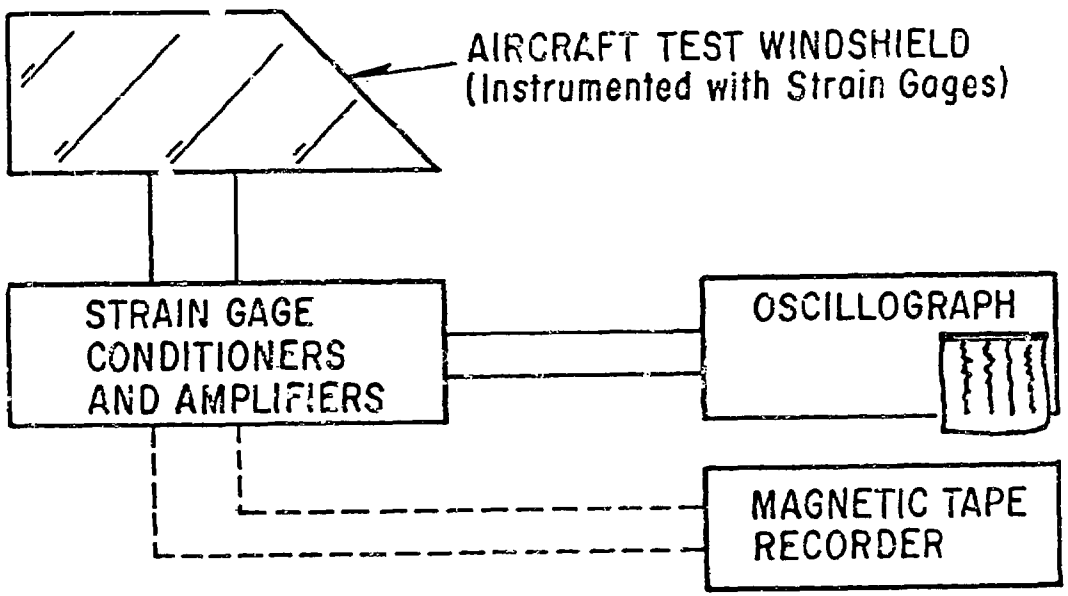

Instrumentation was an important factor in the development program since it allowed generation of load distribution and stress-speed curves for different cross sections at different temperatures. The initial stress-velocity work used windshields with two nominal .400" core plies and 21 parts 3GH plasticized PVB interlayers for baseline evaluation of the effect of temperature on stress. Figure 10 shows the results of center impacts at room temperature and under hot gradient conditions. Extrapolation of the room temperature curve to 360 KT indicated that only about 27,000 psi would occur on the inboard surface, which would be survivable for even standard strengtn glass. However, a stress of approximately 48,000 psi could be expected for the 130°F outboard surface to 100°F inboard surface gradient. As a result, the hot gradient condition became the basis for all nominal 360 KT pass/fail tests for the two-core design.

The importance of knowing the stress obtained in each glass ply is seen from considering the formula

$$TPS = (K)\ (BS) + SC \qquad (1)$$

where TPS is total performance strength
BS is basic strength
SC is surface compression
and K is a function of area and time.

Knowing these values one can predict whether a glass processed by each tempering technique will survive the known stress.

Figure 11 shows the results of all of the failure limit tests for windshields with two nominal .400" cores. This group included some transparencies with PPG 112 interlayer. All of the parts suffered inboard ply breakage with spall at speeds above 359 KT. One of the windshields with high strength thermal tempered glass was undamaged at 358 KT but then had the inboard fail at 369 KT. The resulting failure limit was considered too close to the requirement to recommend the two core design for qualification.

Figure 12 shows comparisons of analytical and experimental strain gage results on one representative cross section. With confidence obtained from comparisons like this one additional analytical simulations were made. Finite element analysis indicated the advantage of a single relatively thick core for reducing stress in certain glass plies. In addition, a higher surface compression could be imparted on a relatively thick ply. These advantages were offset by potential fail-safe problems due to one interlayer and the danger of exposing the high strength core to damage. The thick/thin ply combination which demonstrated its capability in the exploratory work, overcame the single thick ply shortcomings but introduced the problem of strengthening thin glass. Thermal processes were unable to produce the necessary level, but chemical strengthening via ion exchange did have potential. Therefore, a design with a .625" high strength thermally tempered core and nominal .100" HERCULITE II chemically strengthened inboard ply was introduced into the test program.

FIGURE 10 - MAXIMUM IMPACT AREA I/B GLASS STRESS

NOTE: CENTER IMPACTS ON DC-10 SHAPE WINDSHIELDS OF NOM .188 GLASS - .120 INT - NOM .400 GLASS - .200 INT - NOM .400 GLASS

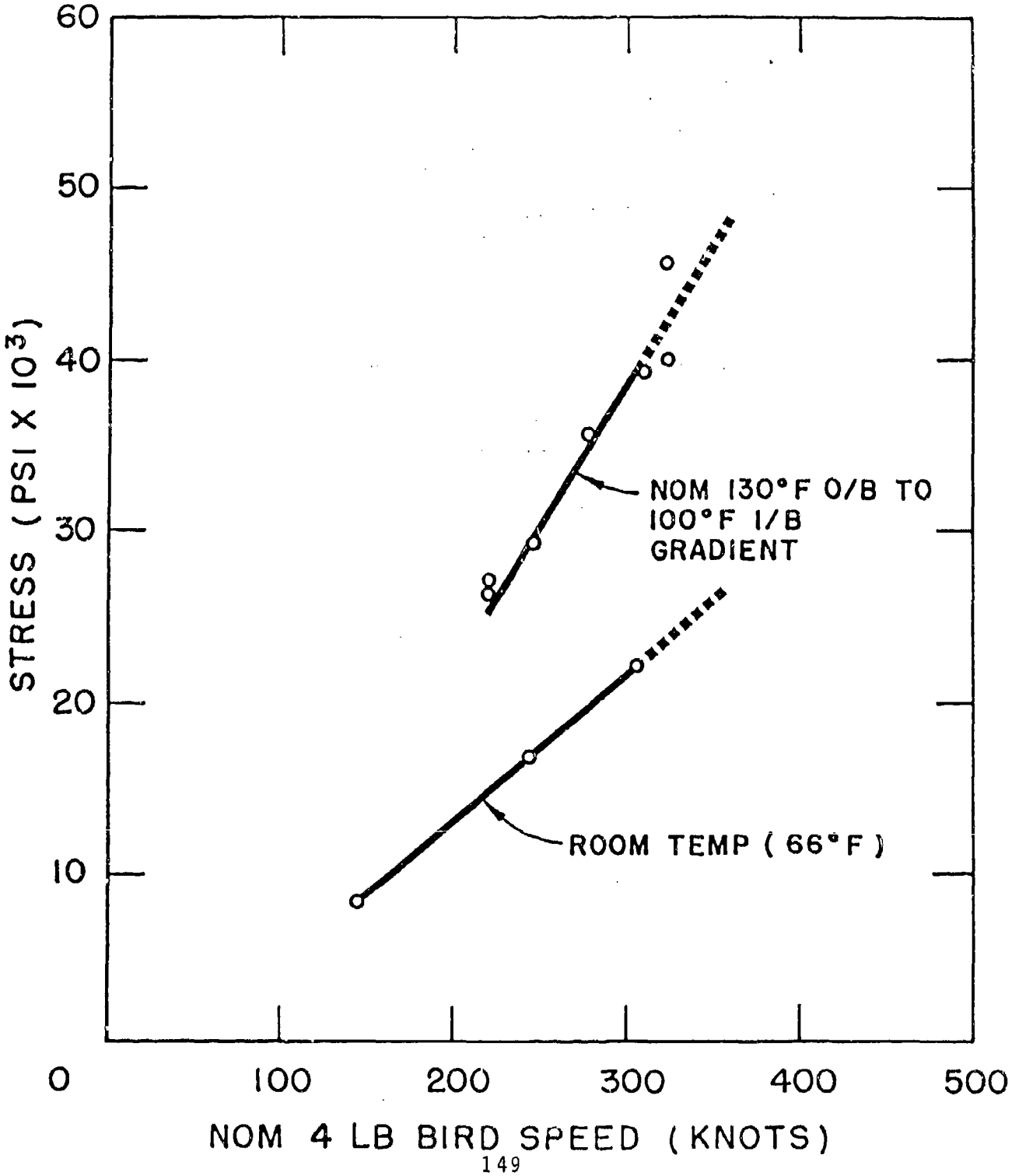

FIGURE 11

BIRD IMPACT SUMMARY – TWO CORE PLY CANDIDATES

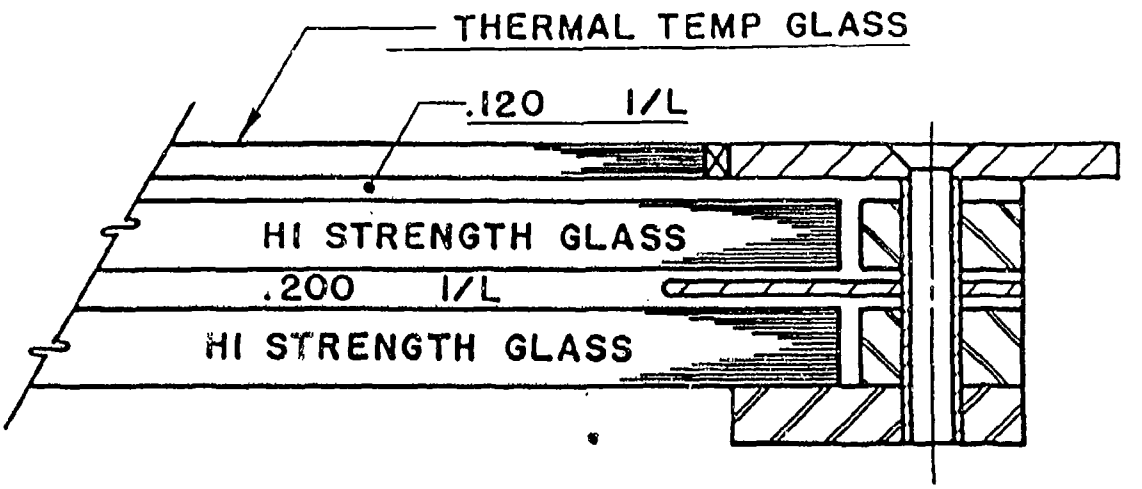

(ALL TEST UNDER "HOT" 130°F O/B - 100°F I/B GRADIENT)

O/B GLASS	I/L	CORES	LOCATION	RESULTS
.188	112	.400"S-L*	CENTER	OK TO 325 KT; ALL PLIES FRACTURED AT 359 KT
.150	PVB	.400"S-L*	CENTER	OK TO 358 KT; ALL PLIES FRACTURED AT 369 KT
.188	112	.375"C-T**	CENTER	OK TO 331 KT; ALL PLIES FRACTURED AT 361 KT
.188	PVB	.375"C-T**	CENTER	OK TO 332 KT
.188	PVB	.375"C-T**	CORNER	OK TO 272 KT; ALL PLIES FRACTURED AT 361 KT

*THERMALLY TEMPERED SODA-LIME GLASS

**EXPERIMENTAL CHEMICALLY STRENGTHENED GLASS

FIGURE 12

MSC/NASTRAN - NISA - EXPERIMENT COMPARISON
BIRD IMPACT ANALYSIS - 360 KN - 4-LB BIRD - 45° ANGLE
100°F INBOARD - 130°F OUTBOARD
ONE CORE PLY
.150" GLASS/.180" PPG 112/.625" GLASS/.180" PPG 112/.100" GLASS
OUTBOARD CORE INBOARD

	MSC/NASTRAN	NISA	EXPERIMENT
PRINCIPAL STRESSES			
CORE PLY	57,200 PSI	55,700 PSI	63,000 PSI
INBOARD PLY	22,100 PSI	22,700 PSI	26,000 PSI
MAXIMUM DISPLACEMENT	.71"	.62"	.68"
TIME OF MAXIMUM DISPLACEMENT	2.7 MILLISECOND	2.6 MILLISECOND	
COMPUTER TIME CPU MINUTES	270	246	

The stress-velocity curve for the thick/thin windshields appears in Figure 13. This plot contains the hot gradient and room temperature curves for the core and an overall reference curve for the HERCULITE II inboard ply. The results indicated that high temperature gradient tests were critical for the .625" core, although stresses would not be significantly different from those on the inboard surface of a windshield with two nominal .400" plies. The hot gradient also produced higher core ply stress than ambient, so it was picked for conditioning pass/fail impacts to determine the thick/thin design's ability to meet the 360 KT no fracture capability.

The results of pass/fail tests on thick core windshields with HERCULITE II inboard plies appear, with an edge section, in Figure 14. It shows the first examples of no breakage at speeds consistently above the 360 KT requirement. These results demonstrated a general increase in glass fracture threshold with increasing core strength.

In addition to its superior performance in the bird impact tests, the .625"/.125" design exhibited several other advantages over the .400"/.400" combination.

1. Areal density was about 9% less.
2. Two inserts could be used.
3. The inboard ply could be heated for defog.
4. A chemically strengthened inboard face and buried core would minimize distortion.
5. Surfaces of the main load carrying ply would be protected from scratches.

As a result, the cross section of .150" semi-tempered glass - .625" high strength thermally tempered glass - .125" HERCULITE II chemically tempered glass was recommended to Boeing as the PPG lightweight candidate. It was accepted with only a change to a .188 outer ply for improved hail resistance.

Even though the glass ply configuration was fixed, testing continued to evaluate the effects of interlayer and test conditions on performance. For example, Figure 13 shows the inboard surface stress predominates at 66°F, so impacts were made under -30°F outboard surface to +30°F inboard surface temperature gradient. Under such conditions, windshields with PVB inboard interlayers exhibited HERCULITE II ply breakage below the 360 KT requirement and at stresses below those predicted to cause failure. Attention to parting material on the inboard glass to prevent the PVB from pulling chips overcame premature inboard ply failures but initiated core ply failures close to the 360 KT speed. Analysis of failed windshields and review of high speed motion pictures showed that the PVB inboard of the parting medium was now pulling chips out of the core during the impact event.

The low temperature gradient failures necessitated a switch to PPG 112 interlayer, which has demonstrated excellent cold chip resistance. Use of 112 also meant that stresses were relatively unaffected by temperature compared to PVB. With the change, Boeing 757/767 windshields with the cross section shown in Figure 15 survived impacts at 360 KT and above in various locations (center, top aft, top center) and under temperatures from hot

FIGURE 13 – MAXIMUM .625 CORE PLY STRESS

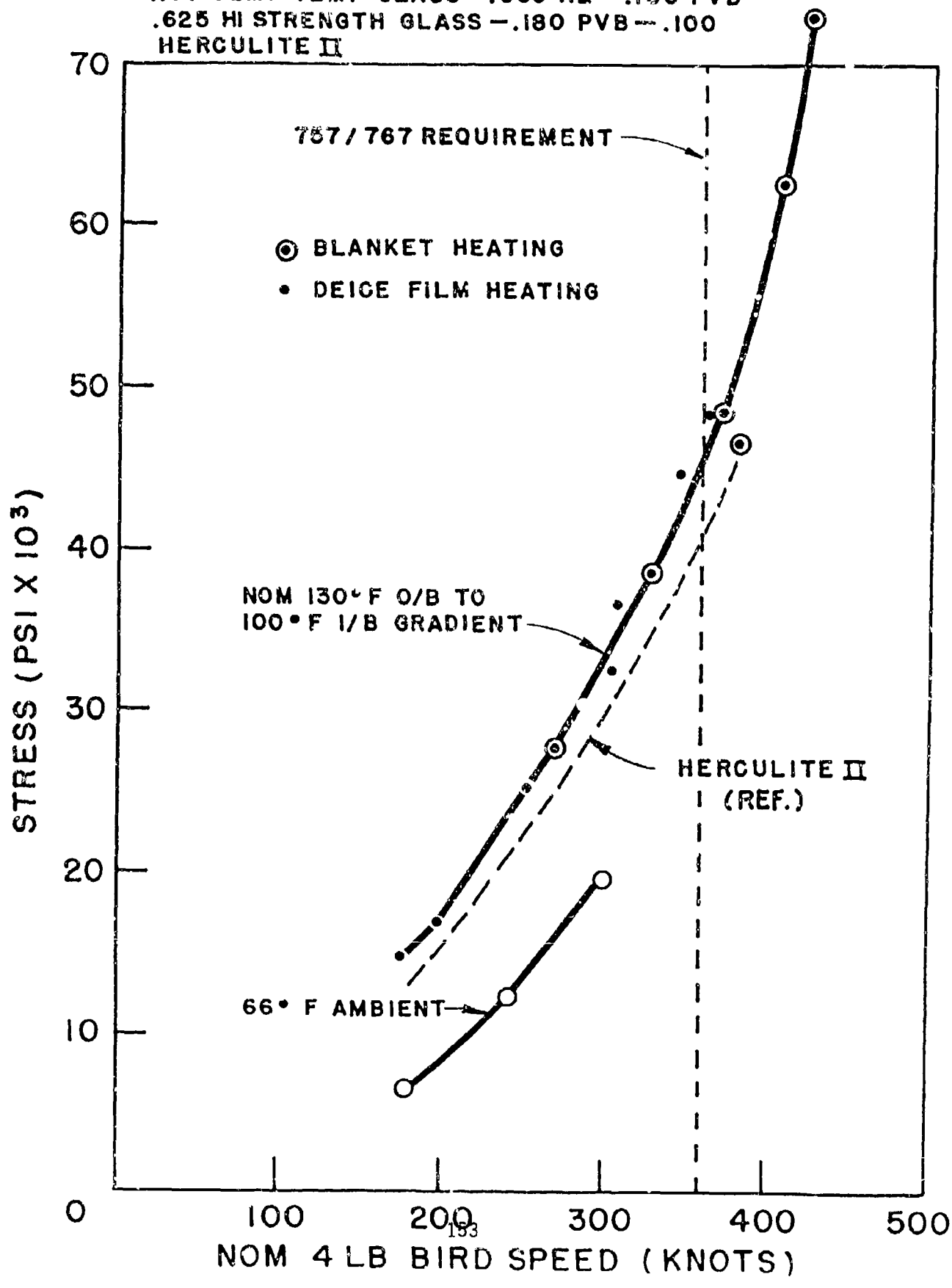

FIGURE 14

BIRD IMPACT SUMMARY - SINGLE CORE CANDIDATES

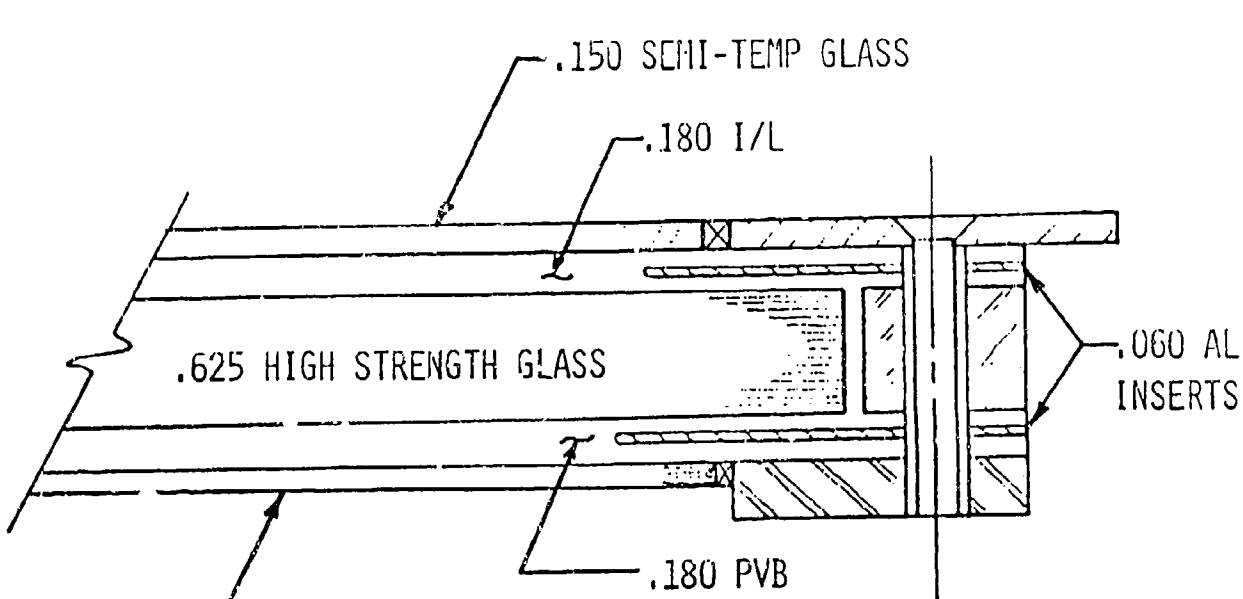

(ALL TEST UNDER "HOT" 130°F O/B - 100°F I/B GRADIENT)

CORE	O/B I/L	LOCATION	RESULTS
MIN.STRENGTH	.180 PVB	CENTER	OK TO 360 KT O/B FRACTURED - 357 KT OK AT 380 KT ALL FRACTURED - 379 KT
MED.STRENGTH	.030" 112+ .150" PVB	CENTER	O/B FRACTURED - 381 KT ALL FRACTURED - 400 KT
MAX.STRENGTH	.030" 112+ .150" PVB	CENTER	OK AT 365 KT O/B FRACTURED 381 KT OK AT 403 AND 421 KT
MAX.STRENGTH	.030" 112+ .150" PVB	CORNER	OK AT 358 AND 385 KT

FIGURE 15

BOEING 757/767 NO. 1 WINDSHIELD RECOMMENDED QUALIFICATION DESIGN

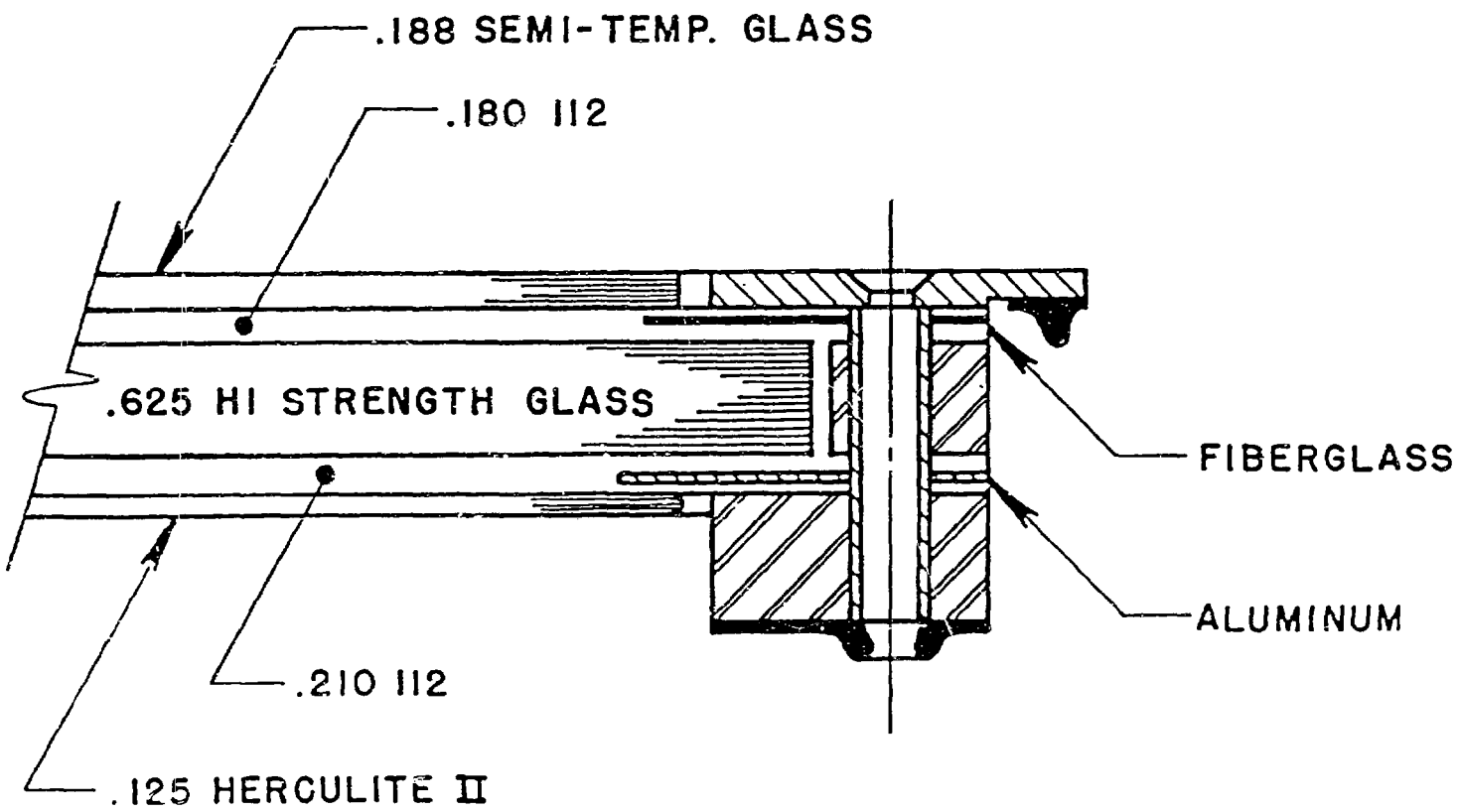

gradient to cold gradient. This configuration was also used for the qualification windshields fabricated for testing at Boeing.

The final demonstration of the Figure 15 cross section occurred during bird impact qualification. The testing, conducted at Boeing's Tulalip, WA, test site, employed a Boeing 767 cab section with relatively stiff airframe mounting members. Seven shots on four windshields produced the results summarized in the following table:

Bird Impact Qualification Summary

Location	Average Surface Temperatures	Bird Speed	Results
Center	129°F to 101°F	365 KT	No penetration. Core and inboard plies OK.
Center	-36°F to 34°F	367 KT	No penetration and all plies OK.
Mid-Top Edge	133°F to 100°F	365 KT	No penetration and all plies OK.
Mid-Top Edge	-34°F to 35°F	376 KT	No penetration. Core and inboard plies OK.
Top Aft Corner	-35°F to 36°F	360 KT	No penetration. Core and inboard plies OK.
Center Post Edge	-36°F to 33°F	368 KT	No penetration. Inboard ply OK.

In addition to preventing penetration and surviving all shots with no breakage of the inboard ply, the qualification transparencies afforded an opportunity to compare stresses obtained during test shots in a frame with those encountered in the actual aircraft. The cold top aft corner qualification shot produced impact area stresses of 47,100 psi and 19,900 psi in the core and inboard plies, respectively. A test shot at equivalent temperatures and location and 367 KT bird speed generated 42,700 psi and 23,800 psi. The similarity of these values reinforce our opinion that dynamic stress/strain measurement is invaluable in developing optimized glass transparencies where both failure stress and weight are critical.

The immediate net result of this program was a lightweight windshield that satisfied all impact qualification requirements including the difficult weight reduction/no spall dilemma. The need for high strength glass for new, lightweight windshield applications was amply demonstrated. Combined use of finite element analysis and dynamic stress/strain measurement helped make achievement of the overall goal manageable. Continuation of these methods on additional windshield applications has proved to be valuable by building a comprehensive data base, building confidence in modeling, and achieving designs that met performance requirements economically.

References

ADINA, Klaus-Jürgen Bathe, Editor, Acoustics and Vibration Laboratory, Department of Mechanical Engineering, Massachusetts Institute of Technology, Cambridge, Massachusetts 02139.

Mahaffey, J. E., "Heat Resistant Sheet Interlayer," p. 660, Conference on Aerospace Transparent Materials and Enclosures, AFML-TR-76-54, April 1976.

Mott, M. J., "Experimental Investigation into the Bird Impact Resistance of Flat Windscreen Panels with Clamped Edges," pp. 345-371, Conference on Transparent Aircraft Enclosures, AFML-TR-73-126, June 1973.

MSC/NASTRAN, The Macneal Schwendler Corporation, 7442 North Figueroa Street, Los Angeles, California 90041

NISA, Engineering Mechanics Research Corporation, P.O. Box 696, Troy, Michigan 48099

AD-P003 191

TRANSPARENCY TECHNOLOGY NEEDS FOR MILITARY AIRCRAFT

R. H. Walker, Flight Dynamics Laboratory

Transparency Technology Needs for Military Aircraft

R. Harley Walker
Flight Dynamics Laboratory
Air Force Wright Aeronautical Laboratories
Wright-Patterson AFB, Ohio

Abstract

Military operations have indicated in many varied and different instances how aircraft transparent enclosure system technology lags the airplane in scientific development and engineering. In some cases maximum performance of current operational aircraft is limited because of the inability of the windshield or canopy to operate under the structural or thermal loads imposed. To eliminate transparent enclosure deficiencies the needed capabilities must be identified and transparency technology advancement investigations must be conducted to fill the technology voids. This paper attempts to identify transparent enclosure technology needs and separates the needs by technology areas such as design, testing, system, etc. As there are numerous technology needs identified, some condensing and/or combining of specific needs is necessary; although as many needs as possible are discussed in sufficient detail to provide the reader a clear understanding of the problem area and what technology is needed to fill a particular void. It is expected that the entire transparency technical community can find within this description of needed technologies, areas of work which fall within their individual interest and capabilities as a company or government agency and to which they may address some future effort, thus helping to solve the many problems facing transparency systems of the future.

Introduction

There is very little if anything at all glamorous about a piece of glass or plastic on an airplane to keep out the wind, and its not too surprising to find that transparency technology was taken for granted for several years. Not until the loss of aircraft and crews due to birdstrike during high speed low altitude flight reached serious proportions in the early 1970's did the Air Force take positive action. The formation of the Improved Windshield Protection Advanced Development Project Office (ADPO) and later the Subsystems Development Group were steps taken in a positive direction to solve many of these system and technology problems with USAF aircraft transparent enclosures. There were serious deficiencies and gaps in the technology base due to long term neglect. Since the mid to late 70's much progress has been made, particularly in improving certain transparency systems with much of the credit due to the Improved Windshield Protection ADPO. However, in the technology arena many of the gaps still remain.

At times we may have improved our system's performance but not really understood how or why. One may argue that's OK as long as it works and there is some truth to that; however, by not understanding the "hows" and "whys" it is impossible to apply engineering logic to the next system having the same or similar problem. The same fix does not always work for two different systems. This is to be expected in R&D.

In discussing some of the technology needs in the transparency area, three areas have been chosen in which to clarify the needs. These areas are Design needs, Testing needs and System needs. Design needs are a category in which the technology gap if filled would have the greatest impact in that portion of the transparency development (i.e. early in the development stage). Testing needs are those technologies which fall into a category identified with proving the transparency design capable of performing the task for which it was designed. System needs are those which apply to a category of needs which give the overall transparency system increased capability or improved performance from a total system standpoint.

The following technology needs described in this paper will be presented in one of these three areas; Design, Testing or System needs.

Design Needs

Edgemember (Figure 1)

Need: Edgemember design criteria.

Edge failure has been determined to be one of the critical factors contributing to aircraft transparency deficiencies. Increased operating costs have prompted effort to utilize advanced technology for the design of transparent enclosure systems. However, the technology for attaching the transparency to the aircraft is for the most part from the past (i.e., the way its been done for many years). Significant cost savings would be achieved by developing advanced methods of attaching a transparency system to the aircraft. A wide variety of methods and concepts are used in transparency

designs; standardization is lacking. Common edge problems result in cracks, crazing, delamination and stress concentration.

We know edge loads are affected by:

- shape of the transparency
- transparency stiffness
- bolt stiffness
- support structure stiffness
- hole clearance
- load path
- temperature

We need to develop standardized edge designs, design criteria, and analytical techniques that will promote the production of cost effective windshield and canopy systems for military aircraft by maximizing reliability and minimizing weight and maintainability.

Consistent Material Properties (Figure 2)

Need: Quality control of the raw material.

A major problem associated with the fabrication of polycarbonate parts is related to the quality control of the raw material. There is often a wide enough variation of properties to necessitate definition of processing and forming temperatures on a lot-to-lot basis. This usually means a significant cost increase on delivered parts.

Some users have observed lot-to-lot variations of melt index to vary by a factor of two. The melt index affects the forming temperature and this variation can require a change in the forming temperature of 15-20°F.

Mean molecular weight of the resins to be used in formation of a sheet of polycarbonate is a specified quantity, but the actual affect of molecular weight on forming properties and performance is not well understood.

Current practice of polycarbonate users is to assign their own inspector at the mill to accept or reject individual lots. Suppliers have been cooperative in this procedure. There is a need for research efforts which determine the effects of property variation on formability and processing methods.

A need exists to accurately define material mechanical properties, to establish acceptable criteria for material allowables and to define variable relationships and parameter ranges of interest for transparency related problems and material behavior.

New Materials (Figure 3)

Need: Improved transparent materials, specifically high temperature capability.

Future Air Force tactical aircraft, with supersonic persistence capabilities, will operate at speeds where aerodynamic heating will significantly affect the design and performance characteristics of their transparent windshield and canopy systems. These transparency systems must not only withstand the temperatures of high speed flight, but they must also react flight pressure and bird impact loads; provide a large field-of-view with good optics (sometimes at low viewing angles) that can be integrated with advanced Heads Up Display devices; resist surface abrasion; protect against a variety of combat threats including nuclear burst effects, lasers, chemicals and radar detection; allow for crew ingress, egress, and escape; be equipped to remove rain, ice and condensation; be low in cost, weight, drag, observables, and aerodynamic noise; and be easily replaceable and maintainable.

Current tactical aircraft incorporate transparency systems that are lightweight, strong, and functional, and that provide a large field-of-view. However, they are fabricated using plastics and this limits their use to very short times at the maximum Mach number of the aircraft.

Current aircraft that operate at sustained supersonic speeds use relatively small, and flat or single curvature, glass panels to withstand the high temperatures encountered by the transparency systems. This approach yields transparency systems which are heavy and which severly restrict vision.

Emerging system performance requirements for tolerance of the birdstrike hazard at increased speed while also integrating radar cross section reduction, laser hardening, increased thermal tolerance and increased chemical tolerance indicate that advancements in materials and material usage technologies are needed. Today's materials are being used near their practical limits. For example, optical distortion of F-15 acrylic transparencies occurred due to overheat during high speed flight, and thermal/moisture induced crazing of outer plies of F-111 acrylic faced polycarbonate transparencies occurred due to the questional environment in Australia.

Strain Measuring Technique (Figure 4)

Need: A method for accurately measuring the strain experienced by full scale monolithic and laminated aircraft transparencies undergoing dynamic impact testing.

Dynamic impact testing of plastic transparent materials is a conventional and standard method used for evaluating aircraft windshield, canopy and window designs. Until recently this type of design evaluation, usually on full scale parts, has been the only method available; however, analysis methods have evolved which now permit fairly accurate prediction of the impact resistance of plastics to high speed impacts. One way to validate these analysis methods is to compare calculated strains to experimentally measured strains acquired during full scale bird impact testing. Conventional strain gauges and standard bonding techniques have proven to be less than satisfactory when used to instrument full scale aircraft transparencies for bird strike testing. Development of a method for economically and accurately measuring the strains experienced by monolithic and laminated aircraft transparencies undergoing dynamic impact testing is needed.

Testing Needs

Test Methodology and Evaluation Criteria (Figure 5)

Need: A validated test methodology and evaluation criteria for evaluating the durability of high performance aircraft transparencies.

No laboratory test method, combined with simulated environmental conditioning used to date provides a valid correlation with in-service operational experience. The reason is that none of the available test techniques realistically and/or cumulatively simulate (duplicate) the forming, installation, storage, transport, in-flight, flight line, maintenance and environmental aging conditions witnessed by todays real world transparencies.

A realistic, cost effective test methodology for evaluating the durability of high performance aircraft transparencies through the use of simulated in-service environments is needed to eliminate the problem of redesign and field retrofit when problems start showing up after the transparency is in the field. Tests would be required to evaluate three material configurations, i.e., monolithic stretched acrylic, coated monolithic, polycarbonate and acrylic faced/polycarbonate laminate. Durability testing should be accomplished during the preproduction phase of transparency development with emphasis placed on early coupon articles. Test/exposure methods should be developed to thoroughly evaluate the failure mechanisms of delamination, coating loss, impact resistance degradation, surface abrasion crazing and bolt hole cracking/crazing.

Full Scale, Coupon and Subscale Relationships (Figure 6)

Need: Relationships established between full scale, coupon and subscale specimens of aircraft transparencies.

Currently, there are no relationships established between coupons, subscale and full scale transparency testing. Practice has been to perform some of the initial design tests using coupons primarily because they are easier and less expensive to work with. However, very little of the fracture data or environmental data or other type of data acquired on the coupons is used to totally justify a full scale design. Similar testing must be done on the full scale item before confidence is gained on the merits of the transparency configuration.

If for a given material make-up, i.e. monolithic stretched acrylic, coupon or subscale tests are conducted, the behavior of the design in its full scale configuration should be known as a result of established relationships. To establish these types of relationships much testing on coupons, subscale and full scale designs is needed. Initially these relationships may be very broad but show applicability. As additional data is acquired more refined relationships may come into being. Once available these relationships may allow more work to be done in the coupon or subscale size, thus reducing the costs associated with large amounts of full scale testing.

Structural Durability of Aged Transparencies (Figure 7)

Need: Method to determine structural durability of aged transparencies prior to failure.

A need exists for us to be able to tell if birdstrike resistance is retained in windshields and canopies after some period of service in the field. Actually, we would like to be able to assess the structural durability without removal of the transparency from the aircraft and, of course, without having to damage the transparency. Some method for non-destructive testing in the field is what is needed. Perhaps if sufficient information is known about a group of transparencies then testing of one (destructive) with application of similarity to the others is the best we can expect to ever attain. However, there may be some photographic techniques which could be developed that would provide knowledge of the transparency's residual stress or weak areas even though no potential problems are obvious to the naked eye.

System Needs

Variable Thickness Transparency (Figure 8)

Need: Ability to manufacture transparencies which have controlled variable thickness.

Thicknesses of present day transparencies are generally specified by structural capabilities in a selected area of the transparency. Other areas within the same unit are therefore commonly thicker than necessary, thus the part carries extra weight. A transparency with controlled variable thickness could eliminate this weight penalty. In addition to weight savings, bird impact, pressurization effects, escape techniques or critical optical needs may also be improved with controlled thickness transparencies.

Historically, aircraft transparencies have been manufactured from flat plastic sheets of uniform thickness which are thermoplastically formed to specific shapes. Where compound curvature is required, present day forming techniques generally create thickness variations due to the non-uniform material elongations dictated by the specific geometrics involved. The crown region is the area of deepest draw, and therefore it is where the most thinning occurs. Fundamental processes to control the thickness at any point on the transparency have not yet been developed.

Thin-out does not generally occur on those designs where no compound curvature is generated. Cylindrical or conical shapes can usually be wrap formed from a flat sheet of stretched acrylic without thin-out (i.e., cylindrical or conical shapes can be formed to uniform thickness.) Two examples of these are the single degree curvature designs for the F-15 windshield (cone) and the F-105 canopy (cylinder).

Combat Hardened Transparency (Figure 9)

Need: A hardened transparency design which will defeat combat threats such as

ballistic fragments, lasers, and directed high energy beams, and which provides reduced radar cross section.

Technology to improve aircraft crew station transparency flight hazard tolerance in a combat environment should be developed. Hazard reduction technologies include ballistic fragments; lasers; nuclear EMP, flash and thermal effects; radar detection; and chemical and biological. In addition to these combat hazards we must retain resistance to hazards such as birdstrikes, lightening, ice, hail, rain and aerodynamic heating. To produce an effective transparency system these hazard reduction technologies must be integrated into a transparency system which is acceptable to the aircraft operators from a optical standpoint and to the aircraft owners from a durability and cost of ownership standpoint. To date efforts at such integration have been essentially limited to the birdstrike hazard.

An effort is needed to define one or more highly probable combinations of these hazards and demonstrate the ability to integrate the required technologies into an affordable/usable/survivable transparency system.

Birdproof/Fracturable Transparency (Figure 10)

Need: A transparency which is hardened to impacts external to the cockpit but easily fractured by impacts to the interior of the cockpit transparency.

While much progress has been made toward bird proofing our military aircraft's windshields and canopies there are still several aircraft which are vulnerable to birdstrikes and which need improved bird impact resistant transparencies. In most cases providing a harder or tougher transparency only has positive benefits, however, in a few cases, as structurally improved transparency presents problems because it is now harder to fracture, for instance if one attempts to retain through-the-canopy ejection. Really what is needed is a transparency which is difficult to fracture from impacts on the external surface but ruptures easily from impact to the internal surface.

Thinning of the transparency may be an alternative but one must be careful that the thinning can be tolerated under high speed birdstrikes.

Battle Damage Repair (Figure 11)

Need: Methods and techniques developed for assessing the magnitude of battle damage and for making the necessary repair to permit the aircraft's return to flight ready status.

Increased sortie generation rates is a goal for the wartime environment. Methods of quickly repairing battle damaged aircraft in the field are needed to provide increased sortie rates. The transparency is one subsystem for which battle damage repair techniques should be developed to be consistent with efforts directed at repair techniques for other aircraft subsystems and structures. Repair techniques must be developed after which pressure and fatigue testing should be conducted to determine the expected service life of

the repaired part. Some effort is underway in this area and hopefully repair techniques can be shown to be feasible and practical for the transparency subsystem.

Conclusions

The technology needs discussed in this paper are by no means all inclusive. They are however those that are felt to be most needed at this time. The time has come when we must all pitch in and strive to find the answers to the technology voids. Too many of our most recent transparency systems have had to undergo redesign and retrofit. This is an extremely expensive way to go about getting systems in the field that are good performers and have the durability needed for acceptable life cycle costs.

By pointing out some of the technology needs, I hope to stimulate the transparency technical community to continue thinking about these problems areas and perhaps initiate some programs to try and find solutions.

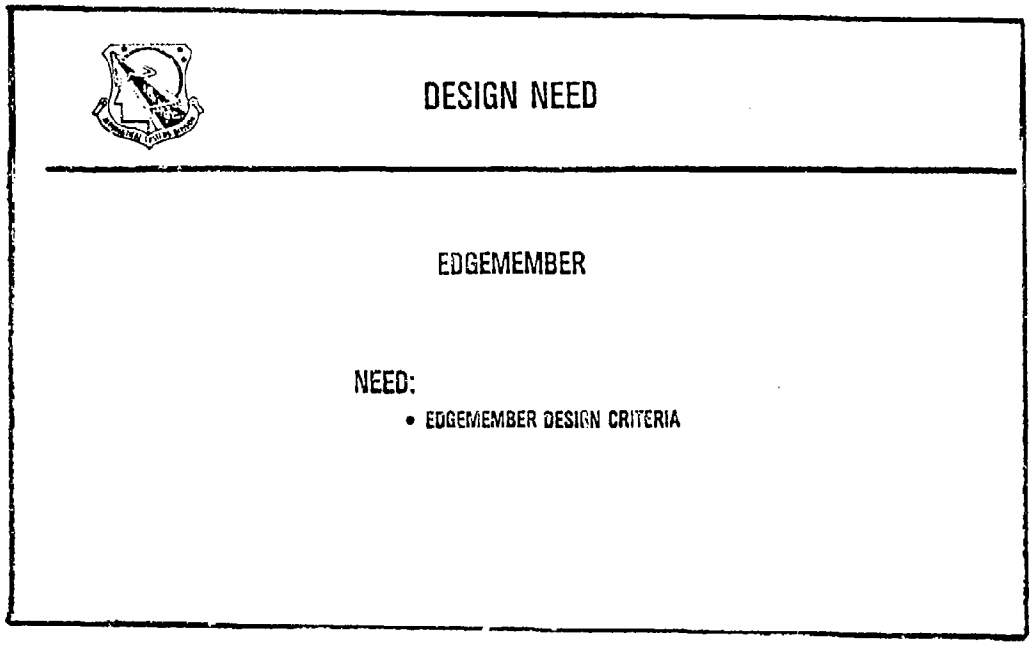

FIGURE 1

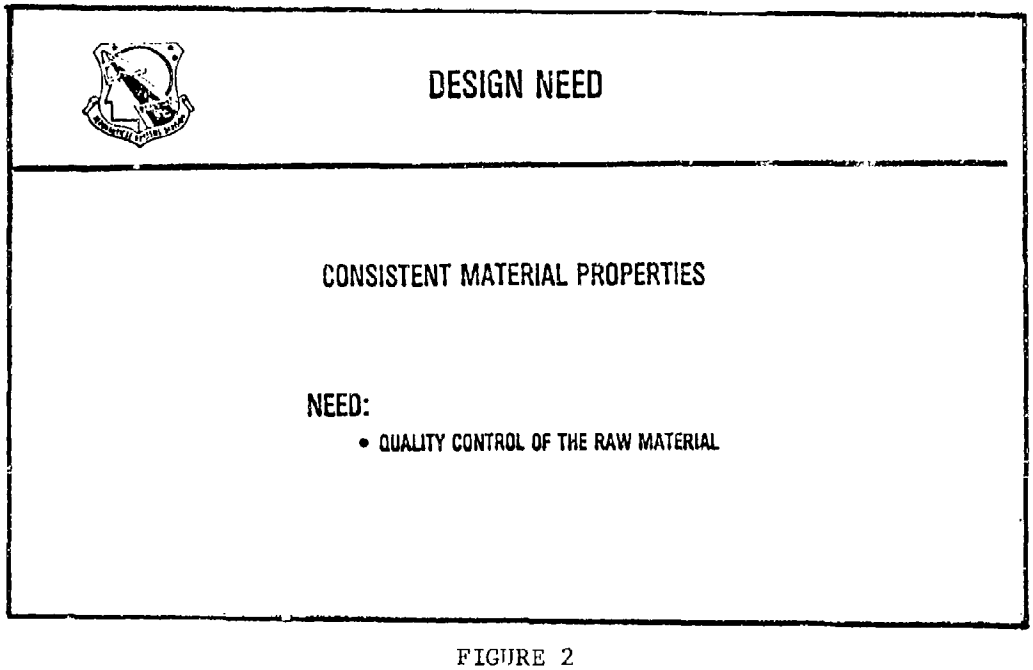

FIGURE 2

DESIGN NEED

NEW MATERIALS

NEED:

- IMPROVED TRANSPARENT MATERIALS, SPECIFICALLY HIGH TEMPERATURE CAPABILITY

FIGURE 3

DESIGN NEED

STRAIN MEASURING TECHNIQUE

NEED:

- A METHOD FOR ACCURATELY MEASURING THE STRAIN EXPERIENCED BY FULL SCALE MONOLITHIC AND LAMINATED AIRCRAFT TRANSPARENCIES UNDERGOING DYNAMIC IMPACT TESTING

FIGURE 4

TESTING NEEDS

TEST METHODOLOGY AND EVALUATION CRITERIA

NEED:

- A VALIDATED TEST METHODOLOGY AND EVALUATION CRITERIA FOR EVALUATING THE DURABILITY OF HIGH PERFORMANCE AIRCRAFT TRANSPARENCIES

FIGURE 5

TESTING NEEDS

FULL SCALE, COUPON AND SUBSCALE RELATIONSHIPS

NEEDS:

- RELATIONSHIPS ESTABLISHED BETWEEN FULL SCALE, COUPON AND SUBSCALE SPECIMENS OF AIRCRAFT TRANSPARENCIES

FIGURE 6

TESTING NEEDS

STRUCTURAL DURABILITY OF AGED TRANSPARENCIES

NEED:

- A METHOD TO DETERMINE STRUCTURAL DURABILITY OF AGED TRANSPARENCIES PRIOR TO FAILURE

FIGURE 7

SYSTEM NEEDS

VARIABLE THICKNESS TRANSPARENCY

NEED:

- ABILITY TO MANUFACTURE TRANSPARENCIES WHICH HAVE CONTROLLED VARIABLE THICKNESS

FIGURE 8

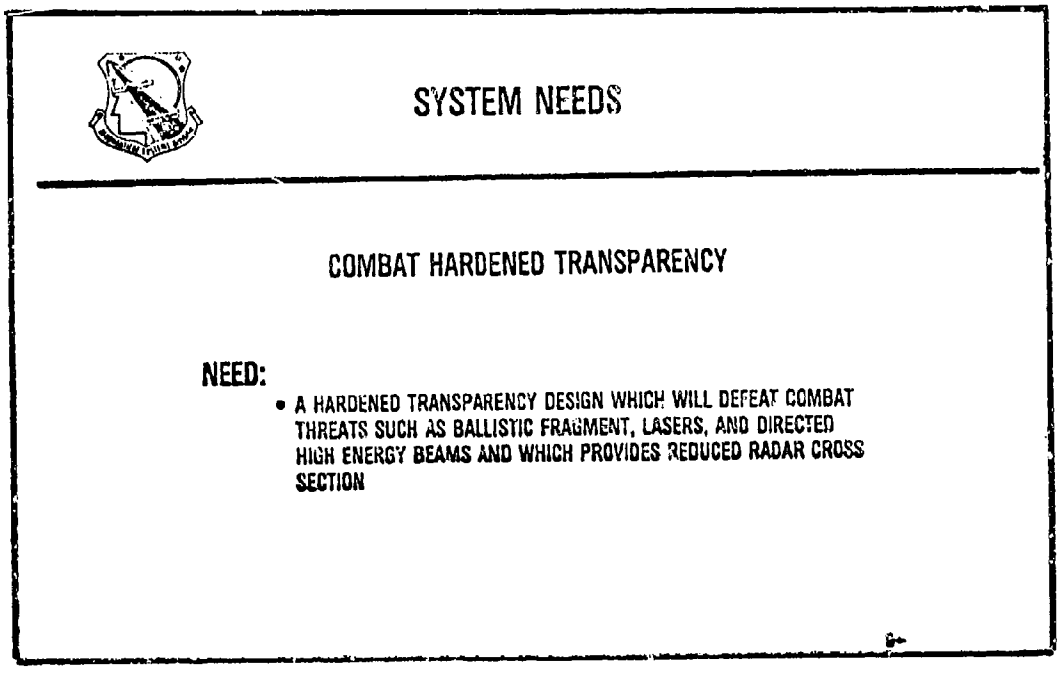

FIGURE 9

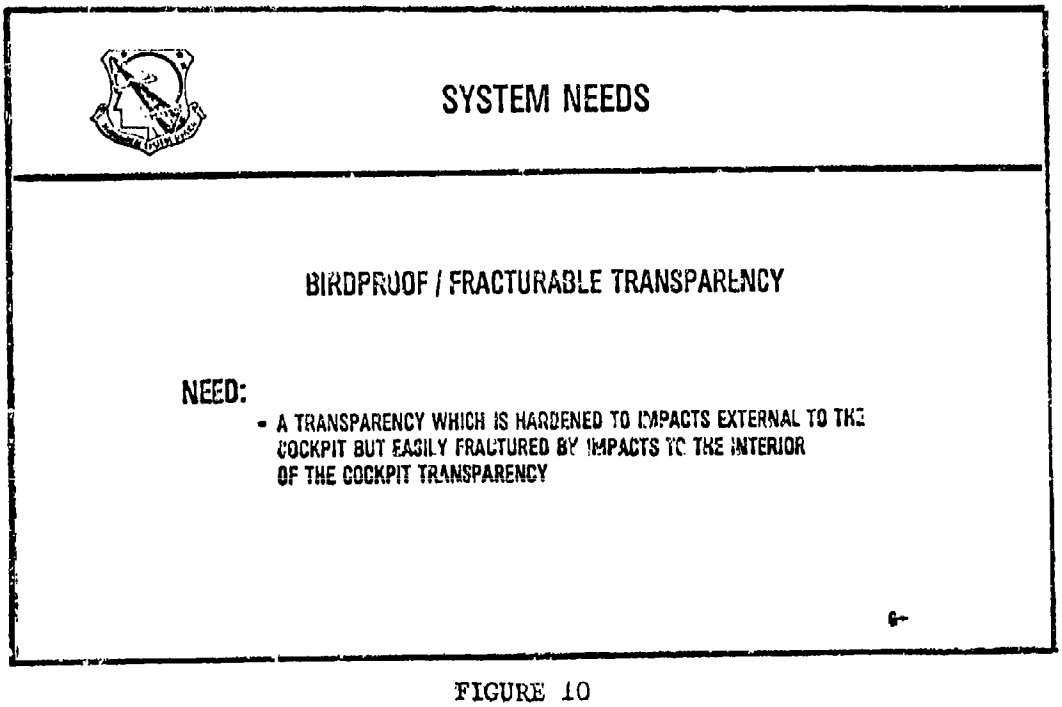

FIGURE 10

SYSTEM NEEDS

BATTLE DAMAGE REPAIR

NEED:

- METHODS AND TECHNIQUES DEVELOPED FOR ASSURING MAGNITUDE OF BATTLE DAMAGE AND FOR MAKING THE NECESSARY REPAIR TO PERMIT THE AIRCRAFT'S RETURN TO FLIGHT READY STATUS

FIGURE 11

SESSION II

UNDERSTANDING CURRENT MATERIALS (PART I)

Chairman: T. J. Reinhart
Materials Laboratory
Wright-Patterson Air
Force Base, Ohio

AD-P003 192

TESTING POLYCARBONATE FOR UTILIZATION IN THE PRODUCTION OF TRANSPARENT ENCLOSURES

A. J. Bonje and J. Irion, Texstar Plastics

TESTING POLYCARBONATE FOR UTILIZATION IN THE PRODUCTION OF TRANSPARENT ENCLOSURES

Alfred J. Bunje - Technical Consultant
Co-author Jim Irion - V.P. Operations
Texstar Plastics
Grand Prairie, Texas

Abstract

The development of aircraft with high performance capabilities has led to the utilization of new transparent plastic materials in the manufacture of transparent enclosures. The performance requirements include increased temperature requirements, increased impact resistance to bird strikes, and decreased fragmentation spalling from ballistic impact. This paper looks at the polycarbonate now being utilized in the fabrication of high performance aircraft enclosures. Polycarbonate is now being utilized both in a monolithic form and in conjunction with traditional enclosure materials; such as acrylic, and glass.

It is the intent of this paper to look at the testing and evaluation of polycarbonate prior to processing into acceptable enclosure hardware. The present procurement specifications such as Mil-P-83310 or L-P-393 are inadequate in addressing materials properties that are critical in the processing and fabrication of acceptable hardware. Since material properties can determine acceptable hardware and therefore the yield from any given lot of material, this can dramatically effect the price of finished goods. In addition, these material properties can ultimately impact the quality and life of the finished enclosures.

Traditionally, polymeric materials have been procured by certain physical tests, that is tensile strength, Izod impact, modulus, etc., to determine material acceptability. These are necessary attributes to determine design criteria and performance goals but do little to determine processing ability, optical quality, and downstream use life.

It is the intent of this paper to discuss some of the tests being utilized to date and to also address a need for additional evaluation methods. We shall look at "snow" development during processing, black spots both benign and malignant and contaminants that outgas. Why the difference from lot to lot in processing characteristics, for example a difference in forming temperatures up to 15°F has been experienced from lot to lot. How can this attribute be predetermined prior to production or can specifications be written to control the polycarbonate material.

Introduction

The development of aircraft with high performance capabilities has led to the utilization of new transparent plastic materials in the manufacture of transparent enclosures. The performance requirements include increased temperature requirements, increased impact resistance to bird strikes, and decreased fragmentation spalling from ballistic impact. This paper looks at the polycarbonate now being utilized in the fabrication of high performance aircraft enclosures. Polycarbonate is now being utilized both in a monolithic form and in conjunction with traditional enclosure materials; such as acrylic and glass.

Discussion

Traditionally, polymeric materials have been procured by certain physical tests, that is tensile strength, Izod impact, modulus, etc., to determine material acceptability. These are necessary attributes to determine design criteria and performance goals but do little to determine processing ability, optical quality, and downstream use life. Polycarbonate is presently procured to specifications such as Mil-P-83310 and L-P-393 which addresses certain optical and physical requirements. It is interesting to note that in Mil-P-83310 out of a 16 page specification, 4 pages or 25% of the specification is devoted to packaging. But nowhere is basic polymeric data defined. We would define basic polymeric data as intrinsic viscosity, molecular weight, molecular weight distribution, melt flow and glass transition temperature. In addition to the basic polymeric data of the polycarbonate, one other variable must be considered. That is, the effect of the various additives introduced into the polymer by the material supplier. These additives, either singularly or in conjunction with each other, affect the processability of the polycarbonate and can influence the physical characteristics of the finished hardware.

In addition to the basic characteristics of polycarbonate resin, there are other factors that need to be addressed. These are contaminates, and resin anomalies, or "critters" present in the extruded sheet but not always apparent until the polycarbonate sheet is exposed to various processing conditions. In some cases, the material must be processed and formed into the final configuration, to highlight resin problems.

We shall address these as two seperate areas of concern. One, the basic resin system, and two, contaminates in the as extruded sheet as received. We should understand at the outset, the intent of this paper is to better understand the polymeric materials that we are asked to convert into usable hardware at a reasonable cost; when sometimes less than 50% of the material received ends up as acceptable transparencies or windscreens. Better and additional methods of material evaluation are needed.

At present, there are two primary sources of supply for optical grade polycarbonate resin to convert into extruded sheet. General Electric Company with their Lexan resins and Mobay with Merlon resins. General Electric converts their own resin into Lexan sheet and Mobay furnishes resin to Rohm & Haas for conversion into Rohm & Haas Tuffak Sheet. Both General Electric and Mobay consider their methods of processing the resin to be proprietary and it is not our intent to abridge their process know how. However, it is our desire, and that of our industry, to receive a uniform product that will respond to processing in the same way from lot to lot. When the glass transition temperature can vary as much as 15°F from one lot to another and the forming temperatures must be held within ±3°F to control the optical quality, each new lot becomes an adventure to determine process perimeters. It is an attempt to determine, prior to processing, how a given lot will behave that we will address this paper. Polycarbonate resin is available in a variety of molecular weights. Blends of different molecular weights create the term "average molecular weight". These resins are normally referred to as low, medium and high viscosity materials when used as injection molding resins. The low viscosity materials are utilized in molding intricate parts with thin wall sections, where material flow is critical and impact resistance is not important. High viscosity resins are used to injection mold thick walled parts that have high impact requirements along with better temperature attributes. This background is needed to better understand the basic polycarbonate resins we are dealing with. The sheet currently being used is made from what was originally referred to as a medium viscosity resin and now, at least by G.E., is referred to as high viscosity resin. Generally, these resins are made up of various molecular weight materials and this is referred to as "weight average molecular weight", ($\bar{M}w$) the molecular weight distribution is designated as the "number average molecular weight" ($\bar{M}n$).

The viscosity of the material has a relationship to the molecular weight which in turn appears to have a relationship to the forming characteristics and to a great degree the performance characteristics of the final product. To determine this attribute, an extrusion plastometer can be utilized to determine the melt flow rate. The melt flow rate is inversely proportional to molecular weight. The melt flow rate of a particular lot of resin can be determined by the ASTM-D-1238 test. By means of this test at least some understanding of a particular lots forming behavior can be determined. Over 50 lots of sheet material have been tested for the melt flow characteristics both as received and after exposure to temperature of 250°F for periods of 24, 48, and 72 hours. See Table I. Note the differences from lot to lot and also the changes as a reuslt of temperature exposure. We have also tested material after all processing cycles and again, some lots showed very little change and others a significant change.

The melt flow test doesn't always give us the entire picture of how the material will act. For example, Lot 11 and Lot 17 have similar melt flow characteristics but would not form at the same temperature, nor would the material move in the same way. That is, one lot required not only

I.D. #	Ave. Melt Flow initial as received.	Ave. Melt Flow 24 hours @ 250°F	Ave. Melt Flow 48 hours @ 250°F	Ave. Melt Flow 72 hours @ 250°F	% Chg.
1	6.30	5.58		7.55	19.8
2	7.26	7.48		8.84	21.8
3	6.37	7.27		8.56	34.2
4	5.32		5.52	5.65	6.6
5	5.31		5.48	5.68	7.0
6	7.19		7.36	7.88	9.6
7	7.11		7.32	7.79	9.6
8	6.15	7.19		7.84	27.5
9	5.89			7.82	32.8
10	6.44	6.41	7.08	7.14	10.9
11	4.44		4.66	4.88	9.9
12	4.86	5.23	5.63	5.80	19.3
13	6.21	6.17	7.49	7.46	20.1
14	5.89	6.26	7.06	7.05	19.7
15	5.41	5.65	5.82	6.06	12.0
16	5.04		4.96	4.74	-6.0
17	4.01	4.10	4.15	4.16	3.7
18	4.12	4.12	4.23	4.27	3.6
19	4.78	5.00	4.96	5.01	4.8
20	5.03	5.08	5.15	5.40	7.4
21	6.10	5.21	5.32	5.41	-11.3
22	5.31	5.54	5.64	5.68	7.0
23	4.41	4.89	5.32	5.01	13.8
24	6.00	6.20	6.40	6.60	10.0

Average Melt Flow Data
Extruded Polycarbonate Sheet

Table I

higher temperatures but higher forming pressures. In further evaluations of the resin it was found that the molecular weight distribution was different. This test was done by Gel Permeation Chromatography or G.P.C. By means of this test. the $\overline{M}w/\overline{M}s$ ratio can be determined and preliminary indications are that this ratio plays some part in the material behavior. Since G.P.C. tests require a skilled operator and are time consuming and costly to run, this attribute has not been actively pursued. However, we do feel this is an area that needs a better understanding along with the effect of the various additives. For example, why did Lot 24 go from an average melt flow of 6.2 to an average of 9.7, a 56% change, after processing into a 3/4 inch thick sheet? Something changed and changed dramatically. What effect will time and impact have on this particular lot? We have found, for example, in forming sheets made from two different lots with a spread in melt flow values, the forming characteristics are completely different and in some cases we were never able to make an acceptable part.

The other end of the material spectrum is the problem of anomalies and "critters" appearing in the material when processing. Some are present and visible in the received sheet. These do not affect the final optical quality unless concentrated in numbers or on the surface causing an aberation when the material is stretched. These are generally black specks (degraded or burned polycarbonate) from the pelleting and sheet extrusion process. Values have been established for the size and number of black specks per square foot that would be acceptable. This is indigneous to all extruded polymers. The problems arise when new optical defects show up during the processing of the material into transparent hardware. It is necessary to understand that various chemicals are added to the polycarbonates resin to enable the material to be processed and also utilized in the outdoor environment. These include such materials as heat stabilizers, antioxidents, and UV-stabilizers. These are highly proprietary with the resin producers as to the types of additive, percentage added, and how they are introduced into the polymer! The point we must be aware of, is that these additives are all contaminates in the polymer. We suspect that these play a part in some of the "critters" that show up as a result of processing. They can take the form of "snow" as in Lots 21 and 22. An agglomeration of additive can result in outgassing during the final forming operation, or develop into an objectionable optical condition.

The snow problem becomes apparent only after thermal exposure such as drying or forming. This condition is very apparent when the sheet is edge lighted. The entire cross section of the sheet is filled with fine particles or "snow". Looking at the sheet, this "snow" condition is not apparent but against a strong light such as that encountered when landing into the sun, would make the problem very apparent. It was determined this snow condition would only show up after the sheet had picked up approximately .2% moisture and then heated. It should be noted all polycarbonate will reach this level of moisture a few weeks after extrusion. Now tests are being done on all lots for this attribute by

introducing moisture into the sheet and then exposing the sheets to 250°F temperature for 24 hours. The sheet is then edge lighted and visually observed for this type of defect.

Another type of defect that had a devastating effect on the optical quality was "critters" that would pucker the surface during the forming operation as the material was stretched. The eventual culprit turned out to be rubber particles from the rubber rolls used in the pelleting operation. Tiny flakes and pieces of rubber came off the rolls and were picked up in the pellets. These specks would then be incapsulated in the sheet during the extrusion operation. This defect could be tested for by forming a dome out of the extruded sheet and visually observing the surface.

There are any number of "critters" that show up during the processing that are not visible in the sheet prior to the forming operation. These usually appear as bubbles or as outgassing around a foreign material in the sheet. If internal, and within acceptable size limits, they are ignored. However, these defects are a source for the rejection of a number of formed parts. They are normally random and unlike the "snow" are not uniform throughout the sheet. The dome forming test will expose this type of defect if a great number are present.

One other anomaly that shows up consistantly in some degree or another is "warbles", or an area of short shakiness. We have had two lots of polycarbonate sheet where this was so pervasive the material could not be used. This condition would only manifest itself after the part was formed. We were never able to predetermine this condition in the extruded sheet or in a fusion bonded blank prior to forming. We have yet to come up with a satisfactory explanation for this condition. Since the area is clear we attempted to utilize polarized light with a compensator to evaluate the amount of birefringence in the warble areas and adjacent to it. There was a significant birefringence in the area of the warble, but to understand the significance of what we saw and what it meant involved a technology beyond our capability at the time. We should note that we have counted up to 27 fringes in extruded sheet, as received, but this did not track into the fusion bonded blank. The world of polarized light, multiple order compensator's, stress patterns and birefringence borders on the black art and belongs in the realm of the polymer physicist, of which there are few about. However, there are indications the warbles could result from inhomogeneous material, that is, molecular weight differences in local areas, or a lack of certain stabilizers in the melt during pelleting and subsequent extrusion. In the study by C. L. Walters of Bendix[1], he shows the variation in shrinkage due to difference in melt flow and $\bar{M}w/\bar{M}n$ ratio. For example, we had one lot of polycarbonate sheet that had an average melt flow of 6.2 and after 72 hours of 250°F temperature the average was 6.4, not a significant change. However, when the 3/4 fusion bonded coupon was tested, that had seen temperature above the glass transition point, the melt flow average was 9.3, a dramatic change. The explanation was that the stabilizers percentage was wrong or missing.

Following this reasoning; if there was poor blending of one of the stabilizers, then indeed there could be a change in the way the material cools and shrinks in a localized area causing the warble when viewed against a grid.

We have attempted to present some ideas and thoughts in an endeavor to stimulate our customers to help us better understand the polycarbonate material we are presently working with. We as fabricators don't have the large staffs to devote to evaluating the material we are asked to use. The producer of the polycarbonate is going to furnish what we ask for and no more.

If material anomalies show up, we have no source to presently go to that can give unbiased assistance in evaluating the material. The material supplier may have met the requirements (Mil-Spec) but the fabricator may not be able to produce a quality part with the material. In some cases, the material supplier will make adjustments and give assistance, but there is no way at present to determine the cause of the anomalies except by in-house research which is costly and time consuming. If we could receive material that is consistant and uniform, a better product could be produced for less cost. We have attempted to show that some preliminary tests can be utilized to help predict how the material will process, but there is much to do yet to establish not only a meaningful procurement specification but a better understanding of the polymer itself.

REFERENCES

1. Walter, C. L., Polycarbonate Material Study for Precision Injection Molding of Polycarbonate, Materials Engineering Dept. 814-2, Bendix, Kansas City Division, P.D.O. 6984213, June 15, 1971.

2. LeGrand, D. G., "Crazing, Yielding and Facture of Polymers. I.The Ductile/Brittle Transition of Polycarbonate", G.E. Research & Development Center, Schenectady, New York, Journal of Applied Polymer Science, Vol. 13, pp. 2129-2147, 1969.

3. Brodway, G. S., Plastics Engineering Consultant, "Preventing Fatigue and Environmental Stress Cracking", Lawrenceville, Georgia, Plastics Design Forum, May/June, 1983.

AD-P003 193

DEGRADATION OF THE BIRD IMPACT RESISTANCE OF POLYCARBONATE

J. B. R. Heath and R. W. Gould,
National Research Council of Canada

DEGRADATION OF THE BIRD IMPACT RESISTANCE OF POLYCARBONATE

J.B.R. Heath and R.W. Gould
National Aeronautical Establishment
National Research Council of Canada
Ottawa, Canada, K1A 0R6

ABSTRACT

This paper describes a program, comparing the bird impact resistance of new as-extruded polycarbonate with polycarbonate that has undergone natural aging, artificial heat aging, fabrication heat treatments, and fabrication heat treatments with subsequent artificial heat aging.

The two pound bird impacts were carried out on flat 24 inch by 24 inch monolithic specimens mounted 45° to the horizontal. A rigid test frame incorporating a "clamped" specimen edge design was utilized.

Bird impacts on the modified material resulted in a significant decrease of penetration velocity, with a corresponding change from a ductile to a brittle type failure mode.

1.0 INTRODUCTION

Recent published information on the design and development of aircraft transparencies reveals that the majority of new generation transparencies are fabricated with polycarbonate as the main structural material. Because of its high ductility, and hence exceptional bird impact resistance, polycarbonate has become the transparency designer's first choice when a birdproof, lightweight part is required for a high performance military aircraft. Laminated polycarbonate transparencies are now capable of withstanding, without penetration or major transparency damage, a four pound bird impact at speeds in excess of 500 knots. These results are obtainable mainly because of the energy absorbed through transparency deflections during impact.

The sensitivity of polycarbonate to solvent and stress crazing, heat aging, fabrication heat treatments, and natural and artificial weathering has been well documented (Ref.1). All of the work has been carried out utilizing standard type (ASTM) test procedures. Very little work, if any, has taken place in which actual bird impacts were used to investigate the change in impact resistance of polycarbonate due to natural aging or other factors.

By a fortunate combination of circumstances, the Flight Impact Simulator Group of NAE/NRCC, found itself in a position to investigate the effect of natural aging on the bird impact resistance of polycarbonate. A number of monolithic panels which had been in storage for up to seven years were available. These panels were left over from a previous research project (Ref.2), during which they had been subjected to bird impacts. The velocities, however, were sufficiently low, that visible damage, if any, was limited to localized deformation or tearing around the bolt holes.

Storage conditions would be expected to produce natural aging, as opposed to weathering, with degradation due to ultra-violet exposure minimized.

As work progressed on the naturally aged material, the program was expanded to include artificially heat aged material. This was carried out to establish a relationship between the bird impact resistance of the artificially aged and naturally aged material.

Published data (Ref.3) indicated that the bird impact resistance of polycarbonate that undergoes normal fabrication heat treatments, including drying, press-polishing and forming cycles, was lower than that of the as-extruded material. Verification of these results as well as the artificial aging of the processed material before bird impacting was also carried out.

The impact tests resulted in substantially lower penetration velocities of the modified material compared to the new as-extruded material. The ductility normally associated with polycarbonate was almost non-existent with the modified material. Based on these results, it was decided to carry out Izod impact tests on samples taken from the penetrated panels.

2.0 PROGRAM

The objective of the test program was to obtain meaningful bird impact data on polycarbonate macerial whose impact properties might have been altered through natural aging, artificial aging, and fabrication heat treatments. The program was carried out in two parts. The first part was the actual bird impacting of selected polycarbonate panels having a documented history. The second part of the program was a study to ascertain a correlation between the bird impact data from part one and the Izod impact property of the material.

3.0 BIRD IMPACT TESTS

The bird impacts were carried out at the NRCC/NAE Flight Impact Simulator Facility, as detailed in Ref. 4, utilizing the 10 inch bore compressed air powered cannon to propel packaged real bird carcasses to the test specimens. The birds had been killed and immediately frozen for storage some weeks prior to use. The carcasses were allowed to thaw at room temperature for at least 24 hours before being packaged, weighed and placed into the gun breech. The carcasses were selected so the total package weight, including bag packaging, was two pounds ±two ounces.

The velocity of the package was timed, just prior to impact, with two independently operating optoelectronic timing systems. The accuracy of each of the systems is considered to be within 0.5%. The mean velocity of the two systems was recorded as the velocity of the package.

To position the test article for impact, a surveyor's transit was first aligned to the gun barrel axis and then the test article was positioned so that the impact point (geometric centre of the test specimen) coincided with the transit line. The transit line was also used to set the longitudinal

axis of the test article parallel to the gun barrel axis. The aligned test article was then secured to the tie-down plates on the target site floor. The test article is shown in Fig. 1.

3.1 Test Specimen Set-up

The polycarbonate test specimen, 24 inches by 24 inches, was "clamped" to a one inch thick aluminum mounting plate at 45° to the horizontal. The mounting plate had outside dimensions of 28 inches by 30 inches with inside dimensions of 19 inches by 19 inches. The inside edges were radiused to prevent shearing of the specimen during impact. The mounting plate was bolted to two, four inch by four inch box beams, which were then clamped to the support sturcture. The test specimen set-up is shown in Fig. 2.

The method for clamping polycarbonate specimens was developed in earlier work (Ref. 2) and under bird impact loading prevented failures from originating at the bolt holes or specimen edges. Fig. 3 compares a typical bolted edge restraint to the "clamped" method used for these tests.

All impacts were carried out under ambient room temperature and humidity conditions.

3.2 Polycarbonate Test Specimens

3.2.1 New Material As-Extruded

The new as-extruded polycarbonate was commercial grade "Lexan" (General Electric), purchased locally. The material was assumed to have an age of less than 6 months based on information from the supplier.

3.2.2 Naturally Aged Material

The naturally aged panels consisted of 0.125 inch and 0.250 inch thick panels that had been tested in 1973 and subsequently stored in a closed cabinet. Impact damage to the panels was limited and consisted of yielding about the original bolt holes. The edge of the panel with the most damage was always installed at the bottom of the mounting plate. No panel with any permanent deformation near the impact point was utilized in these tests.

During storage, the panels could have been subjected to temperature extremes of 40°F to 100°F, and humidity would have ranged from a high of 100% to a low of 10%.

Some material that had been in inventory at the suppliers for a minimum of 18 months was also obtained. It was assumed that temperature and humidity conditions during storage would have been less severe than with the older material.

3.2.3 Artificially (Heat) Aged Material

New as-extruded (see 3.2.1) material was first cut into 24 inch by 24 inch panels and then aged at 260±5°F for 100 hours in an air circulating oven. A copper-constantan thermocouple connected to a digital indicator and a strip chart recorder monitored the temperature of the oven during aging. Some of the panels that were used in the as-extruded series and in the heat aged series were selected from the same parent sheet. Impacting of the as-extruded material verified that the parent sheet material behaved in a normal ductile manner under bird impact loading.

3.2.4 As-Extruded New Material, Dried, Polish and Forming Heat Treatments

The conditioning of this material was carried out in the same manner as in 3.2.3 except for the following temperatures and times, which are typical of fabrication heat treatments for formed transparencies.

Drying	:	18 hours at 265±5°F
Polish Heat	:	2 hours at 305±5°F
Forming Heat	:	2 hours at 305±5°F

During the polish and forming heat cycles the panels were clamped between two ¼ inch thick aluminum plates to prevent warping. Between each heat cycle the panel was allowed to cool to room temperature.

3.2.5 As-Extruded New Material, Dried, Polish and Forming Heat Treatments and Artificial (Heat) Aging

The conditioning of this material was the same as in 3.2.4 with an additional heat aging cycle as in 3.2.3 (100 hours at 260±5°F).

4.0 MECHANICAL PROPERTIES

Because the amount of material available for mechanical testing was limited and the published literature (Ref. 1) indicated that there was no significant change in tensile properties of aged polycarbonate, it was decided to only carry out Izod impact tests on the material. Since polycarbonate is known to be extremely notch-sensitive during impact, an attempt was made to carry out the Izod impact tests utilizing un-notched specimens.

4.1 Impact Tests

The un-notched impact tests were carried out on an Avery-Denison 6709 Charpy and Izod Impact Testing Machine.

Preliminary Izod impact testing was carried out with specimens obtained from new as-extruded, artificially heat aged, and naturally aged (seven years) material.

5.0 RESULTS

5.1 Bird Impact Tests

The results of the bird impacts are contained in Tables 1 to 6.

It should be noted that after two impacts on the 7 year old 0.125 inch thick material, (Table 3), there was no sign of material degradation due to loss of ductility (see Fig. 4). This result was not unexpected since other investigators have found that the material undergoes a ductile to brittle transition at a thickness between 0.140 and 0.180 inch (Ref. 5). Consequently further testing of 0.125 inch thick material was discontinued.

The results of the impacts of the 0.250 inch thick panels are summarized in Table 7. The effect of natural aging and various heat cycles are shown in Figs. 5 and 6. Typical impact results are shown in Figs. 7 to 13.

The radical change in failure mode with aging should be noted. New material exhibits high ductility, large deformations and a limited amount of fracturing as shown in Fig. 7. In contrast, most of the aged material shatters on impact into a large number of fragments with little or no evidence of ductility as shown in Figs. 8 and 9.

5.2 Un-notched Izod Impact Tests

Only a limited number of tests were carried out as it was observed that even specimens from the seven year naturally aged material showed no signs of brittle failure as a result of the Izod impact test. Since the material used for the Izod impact test (naturally aged) was obtained from fragments of a panel that had failed in a brittle manner during bird impact, one surmises that the material is extremely rate sensitive. This result would render standard material properties tests of polycarbonate questionable when bird impact is considered.

6.0 CONCLUSIONS

6.1 Bird Impact Resistance

6.1.1 Naturally Aged Polycarbonate

The results show that the bird impact resistance of 0.250 inch thick monolithic polycarbonate is 10% lower than new as-extruded material after only two years of storage under ambient room conditions. Polycarbonate transparencies stored under these conditions should be suspect if they were initially designed to be bird impact resistant.

6.1.2 Heat Treated Polycarbonate

The bird impact resistance of 0.250 inch thick monolithic polycarbonate that undergoes the normal fabrication heat treatments (drying,

polishing and forming) is reduced by as much as 11% as compared to the new as-extruded material. Obviously, if these fabrication heat treatments can be minimized the exceptional bird impact resistance of polycarbonate can be retained.

6.1.3 New Material, Artificially Heat Aged

The results from these bird impacts indicate that artificial heat aging of the polycarbonate at 260°F for 100 hours is equivalent to natural aging (i.e. storage) of somewhere between five and six years. These results should be of interest to studies of the relationship between natural and artificial aging.

It is worth noting, that if the results from material conditioned under 3.2.4 and 3.2.5 were plotted on Fig. 6 at the 0 year point and the 5½ year point respectively and the points were joined by a curve, the resulting curve indicates that the impact resistance of 4 year old material with normal fabrication heat treatments would be 25% less than new as-extruded material.

6.2 Mechanical Properties

Most published information on the mechanical properties of aged polycarbonate does not indicate a dramatic change in the material properties. The published (Ref. 1) un-notched Izod impact results are inconsistent to say the least. The failure to initiate brittle type failures in the aged polycarbonate samples by the Izod impact method indicates that the material is impact rate sensitive.

A method should be developed by which Izod type tests can be carried out at impact velocities approaching 1000 ft/sec.

The relationship between meaningful mechanical properties and bird impact resistance is still an area that merits further study.

REFERENCES

1. Design Criteria, Transparent Polycarbonate Plastic Sheet, Richard S. Hassard, Goodyear Aerospace Corp. Tech. Report AFML-TR-117 Aug. 1972.

2. Study of Bird Impacts on Monolithic Aircraft Windshields, A.J. Bosik, J.B.R. Heath and R.W. Gould, NRCC, Laboratory Technical Report LTR-ST-998, April 1978.

3. Bird Strike Capabilities of Transparent Aircraft Windshield Materials, Goodyear Aerospace Corp. Technical Report AFML-TR-74-324, Dec. 1974 and Part II Oct. 1975.

4. Capabilities of the NAE/NRCC Flight Impact Simulator; A.J. Bosik, J.B.R. Heath, M.R. Gleeson, NRC Laboratory Technical Report LTR-ST-701, April 1974.

5. Environmental Data and Machining Techniques of Polycarbonates G.E. Husman and R.J. Kuhbander, Conference on Transparent Aircraft Enclosures, Las Vegas, February 1973, sponsored by Air Force Materials Laboratory, Air Force Systems Command, Wright-Patterson Air Force Base.

TABLE 1: POLYCARBONATE NEW MATERIAL

TEST	PANEL THICK-NESS IN	MATERIAL HISTORY					IMPACT VELOCITY FT/SEC	RESULTS
		ESTIMATED AGE	HEAT TREATMENT (HOURS)					
			DRY CYCLE @ 265°F	POLISH CYCLE @ 305°F	FORMING CYCLE @ 305°F	AGING CYCLE @ 265°F		
8	.250	NEW MATERIAL	—	—	—	—	779	PENETRATION; NORMAL YIELDING BEFORE FAILURE ALONG TOP BOLT HOLES.
9	.250	NEW MATERIAL	—	—	—	—	735	PENETRATION; MATERIAL FAILURE. NORMAL YIELDING BEFORE FAILURE.
10	.250	NEW MATERIAL	—	—	—	—	692	NO PENETRATION; LARGE PANEL DEFORMATION NORMAL YIELDING 3 5/8in. DEEP POCKET ABOVE IMPACT POINT.

TABLE 2 POLYCARBONATE 7 YEAR OLD MATERIAL

TEST NO	PANEL THICK-NESS IN	PREVIOUS PANEL HISTORY, PANEL ANGLE 45°, AMBIENT, EDGE DESIGN Fig. 3(a)					PRESENT TEST CONDITIONS, 21b BIRD, 45° PANEL ANGLE, AMBIENT, EDGE DESIGN Fig. 3(b)		
		DATE OF TEST	PACK WT (lbs)	PENETR-ATION VELOCITY ft/sec (Ref. 2)	IMPACT VELOCITY ft/sec	RESULTS	PENETRATION VELOCITY AS-EXTRUDED MATERIAL ft/sec	IMPACT VELOCITY ft/sec	RESULTS
1	.250	5-73	4	434	420	NO PANEL DEFORMATION SLIGHT PULLING IN UPPER BOLT HOLES	714	575	PENETRATION; 80% OF PANEL DESTROYED, LIMITED SIGNS OF YIELDING BEFORE BRITTLE TYPE FAILURE
2	.250.	6-73	2	523	503	AS IN TEST 1	714	401	NO PENETRATION; SLIGHT YIELDING ALONG TOP EDGE, SMALL DEFORMATION ABOVE IMPACT POINT, 1/8 IN. DEEP POCKET
3	SAME	PANEL	AS	TEST	2		714	451	NO PENETRATION; DEFORMATION ABOVE IMPACT POINT 1/4 IN. DEEP POCKET
4	SAME AND 3	PANEL PANEL ROTATED	AS	IN TESTS 2 180° (TOP TO BOTTOM)			714	483	NO PENETRATION; DEFORMATION ABOVE IMPACT POINT 1-1/4 IN. DEEP POCKET, SOME PULLING IN TOP BOLT HOLES
5	.250	5-73	4	434	447	PANEL PENETR-ATED ALONG TOP BOLT HOLES	714	542	PENETRATION; 25% OF PANEL DESTROYED, NO SIGNS OF YIELDING BEFORE BRITTLE TYPE FAILURE, FRACTURE DOES NOT INITIATE FROM PREVIOUS DAMAGED AREA

cont'd.

TABLE 2 CONT'D

TEST NO	PANEL THICK-NESS IN	PREVIOUS PANEL HISTORY, PANEL ANGLE 45°, AMBIENT EDGE DESIGN Fig. 3(a)					PRESENT TEST CONDITIONS, 21b BIRD, 45° PANEL ANGLE, AMBIENT, EDGE DESIGN Fig. 3(b)		
		DATE OF TEST	PACK WT (lbs)	PENETR-ATION VELOCITY ft/sec (Ref. 2)	IMPACT VELOCITY ft/sec	RESULTS	PENETRATION VELOCITY AS-EXTRUDED MATERIAL ft/sec	IMPACT VELOCITY ft/sec	RESULTS
6	.250	6-73	2	523	464	NO PANEL DEFORMATION SLIGHT PULL-ING IN BOLT HOLES	714	509	NO PENETRATION, PANEL DEFOR-MATION ABOVE IMPACT POINT 1-1/4 IN. DEEP POCKET, SOME PULLING IN BOLT HOLES
19	.250	6-73	NO DOCUMENTED HISTORY			PANEL PENET-RATED ALONG TOP BOLT HOLES	714	544	NO PENETRATION; PANEL DEFOR-MATION ABOVE IMPACT POINT 1-1/2 IN. DEEP POCKET, PULLING IN TOP BOLT HOLES, FRACTURE OCCURRED IN PANEL WHEN UNCLAMPING FROM FRAME

TABLE 3 POLYCARBONATE 7 YEAR OLD MATERIAL

TEST NO	PANEL THICK-NESS IN	PREVIOUS PANEL HISTORY, PANEL ANGLE 45°, AMBIENT, EDGE DESIGN Fig. 3(a)					PRESENT TEST CONDITIONS, 21b BIRD, 45° PANEL ANGLE, AMBIENT, EDGE DESIGN Fig. 3(b)		
		DATE OF TEST	PACK WT (lbs)	PENETR-ATION VELOCITY ft/sec (Ref.2)	IMPACT VELOCITY ft/sec	RESULTS	PENETRATION VELOCITY AS-EXTRUDED MATERIAL ft/sec	IMPACT VELOCITY ft/sec	RESULTS
1	.125	6-73	2	390	373	NO PANEL DE-FORMATION SLIGHT PULL-ING IN UPPER BOLT HOLES	500	397	NO PENETRATION; PANEL DEFORMATION ABOVE IMPACT POINT 1-7/8 IN. DEEP POCKET
2	.125	6-73	1	469	432	AS IN TEST 1	500	449	NO PENETRATION; DEFORMATION ABOVE IMPACT POINT 2-3/4 IN. DEEP POCKET

TABLE 4 POLYCARBONATE 5 YEAR OLD MATERIAL

TEST NO	PANEL THICK-NESS IN	PREVIOUS PANEL HISTORY, PANEL ANGLE 45°, AMBIENT, EDGE DESIGN Fig. 3(a)					PRESENT TEST CONDITIONS, 21b BIRD, 45° PANEL ANGLE, AMBIENT, EDGE DESIGN Fig. 3(b)		
		DATE OF TEST	PACK WT (lbs)	PENETR-ATION VELOCITY ft/sec (Ref.2)	IMPACT VELOCITY ft/sec	RESULTS	PENETRATION VELOCITY AS-EXTRUDED MATERIAL ft/sec	IMPACT VELOCITY ft/sec	RESULTS
7	.250	5-75	1	690	469	NO PANEL DAMAGE	714	585	PENETRATION; 80% OF PANEL DESTROYED. SIGNS OF SIGN-IFICANT YIELDING ALONG TOP EDGE AND ABOVE IMPACT POINT, BRITTLE TYPE FAILURE ONE LARGE PIECE APPROX. 1 ft^2, 90% OF PIECES FOUND IN FRONT OF TEST STAND
11	.250	6-75	1 1 1	690 690 690	510 518 554	NO PANEL DAMAGE	714	598	NO PENETRATION; PANEL DEFOR-MATION ABOVE IMPACT POINT 1-5/8 IN. DEEP POCKET YIELDING ALONG 4 SIDES THROUGH BOLT HOLES, INCREASING PENETRATION VELOCITY

TABLE 5 POLYCARBONATE 2 YEAR OLD MATERIAL

TEST	PANEL THICK-NESS IN	MATERIAL HISTORY					IMPACT VELOCITY ft/sec	RESULTS
		ESTIMATED AGE	HEAT TREATMENT (HOURS)					
			DRY CYCLE @ 265°F	POLISH CYCLE @ 305°F	FORMING CYCLE @ 305°F	AGING CYCLE @ 265°F		
20	.250	2 yrs.	——	——	——	——	658	PENETRATION; YIELDING BEFORE FAILURE - DUCTILE TYPE
21	.250	2 yrs.	——	——	——	——	588	NO PENETRATION; PANEL DEFORMATION 1-1/2 IN. DEEP POCKET ABOVE IMPACT POINT
22	.250	2 yrs.	——	——	——	——	634	NO PENETRATION; PANEL DEFORMATION 2 IN. DEEP POCKET ABOVE IMPACT POINT

TABLE 6: POLYCARBONATE NEW MATERIAL - HEAT TREATED

TEST	PANEL THICK-NESS IN	MATERIAL HISTORY					IMPACT VELOCITY FT/SEC	RESULTS
		ESTIMATED AGE	HEAT TREATMENT (HOURS)					
			DRY CYCLE @ 265°F	POLISH CYCLE @ 305°F	FORMING CYCLE @ 305°F	AGING CYCLE @ 265°F		
12	.250	NEW MATERIAL				100	557	PENETRATION; 40% OF PANEL DESTROYED. YIELDING ALONG TOP EDGE AND 1¼ in. DEEP POCKET ABOVE IMPACT POINT. BRITTLE TYPE FAILURE.
13	.250	NEW MATERIAL				100	525	NO PENETRATION ; YIELDING ALONG TOP EDGE. NO PANEL DEFORMATION ABOVE IMPACT POINT NORMALLY PRODUCED.
14	.250	NEW MATERIAL				100	563	NO PENETRATION; PANEL DEFORMATION ABOVE IMPACT POINT ¾ in. DEEP POCKET ¼ in. LONG FRACTURE ON BACK SURFACE AT MAXIMUM POINT OF DEFORMATION.
16	.250	NEW MATERIAL	18	2	2		639	NO PENETRATION; PANEL DEFORMATION 2 in. DEEP POCKET ABOVE IMPACT POINT.
17	.250	NEW MATERIAL	18	2	2		685	PENETRATION ; SHEARED ALONG TOP EDGE. PANEL YIELDING BEFORE DUCTILE TYPE FAILURE.

(Cont'd.)

TABLE 6 (continued) - POLYCARBONATE NEW MATERIAL - HEAT TREATED

TEST	PANEL THICKNESS IN	MATERIAL HISTORY					IMPACT VELOCITY FT/SEC	RESULTS
		ESTIMATED AGE	HEAT TREATMENT (HOURS)					
			DRY CYCLE @ 265°F	POLISH CYCLE @ 305°F	FORMING CYCLE @ 305°F	AGING CYCLE @ 265°F		
18	.250	NEW MATERIAL	18	2	2		638	PENETRATION, MATERIAL FAILURE. PANEL YIELDING BEFORE DUCTILE TYPE FAILURE.
23	.250	NEW MATERIAL	18	2	2	100	504	NO PENETRATION ; PANEL DEFORMATION YIELDING ALONG TOP AND SIDE EDGES. NO POCKETING
24	.250	NEW MATERIAL	18	2	2	100	525	PENETRATION; 80% OF PANEL DESTROYED. SLIGHT YIELDING BEFORE FAILURE. BRITTLE TYPE VERY SMALL PIECES.

TABLE 7

SUMMARY OF RESULTS

.250 tk. Polycarbonate, Panel 45° to Horiztonal, Clamped Edge, Ambient Conditions, 2lb Bird Package Impacts.

Panel History	Penetration Velocity ft/sec	% Decrease From New As-Extruded Panels	Failure Mode (Brittle) (Ductile)
As-Extruded New Material	714±22		Duct.
As-Extruded 7 Year Old	526±17	26	Brit.
As-Extruded 5 Year Old	<585	>18	Brit.
As-Extruded 2 Year Old	646±12	10	Duct.
As-Extruded New Material Artificially Aged	560±5	22	Brit.
As-Extruded New Material, Dried, Polish Heat, Forming Heat	638±1	11	Duct.
As-Extruded New Material, Dried, Polish Heat, Forming Heat, Artificially Aged	515±10	28	Brit.

FIG. 1 TEST ARTICLE

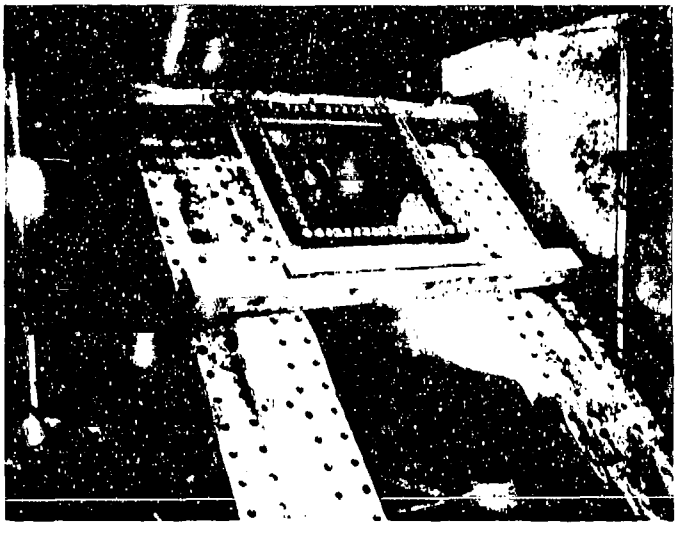

FIG. 2 TEST SPECIMEN SET-UP

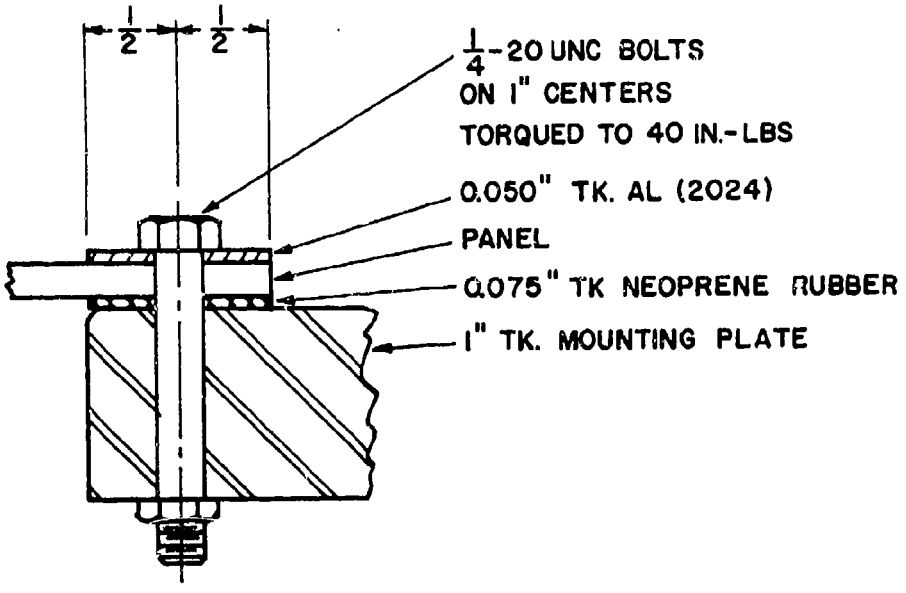

FIG. 3(a) BOLTED METHOD

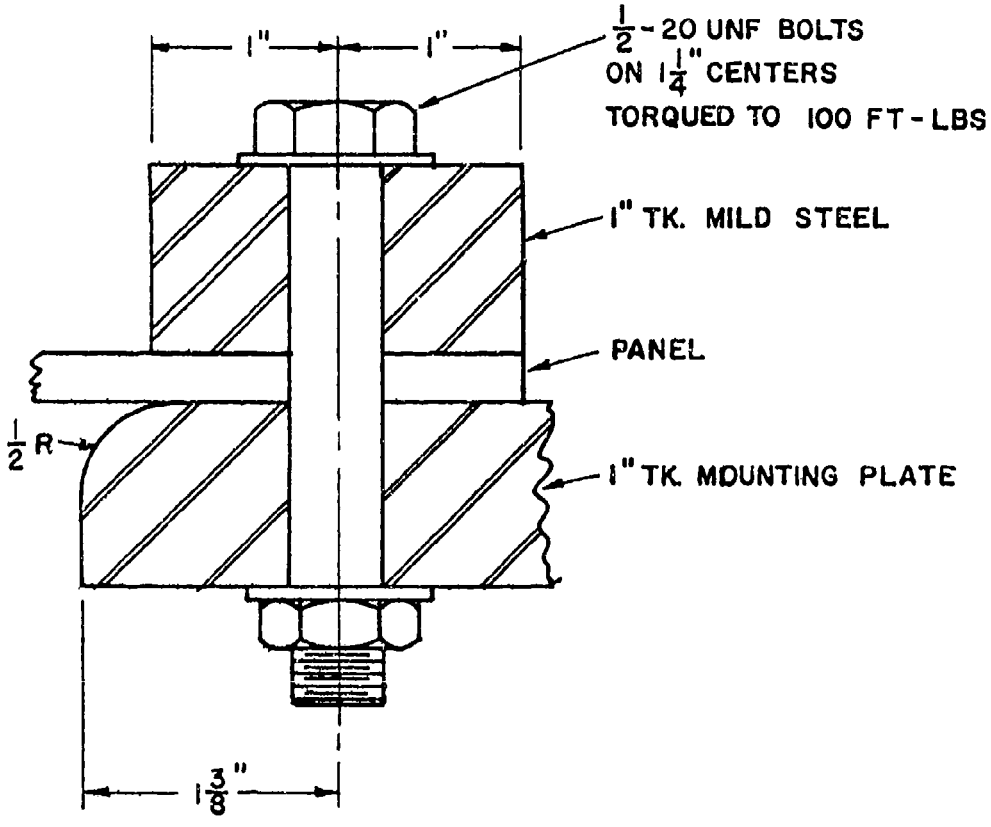

FIG. 3(b) "CLAMPED" METHOD

(a) VIEW OF OUTBOARD SURFACE

(b) VIEW OF INBOARD SURFACE

FIG. 4 0.125 IN. TK. POLYCARBONATE
7 YEARS OLD - TYPICAL FAILURE

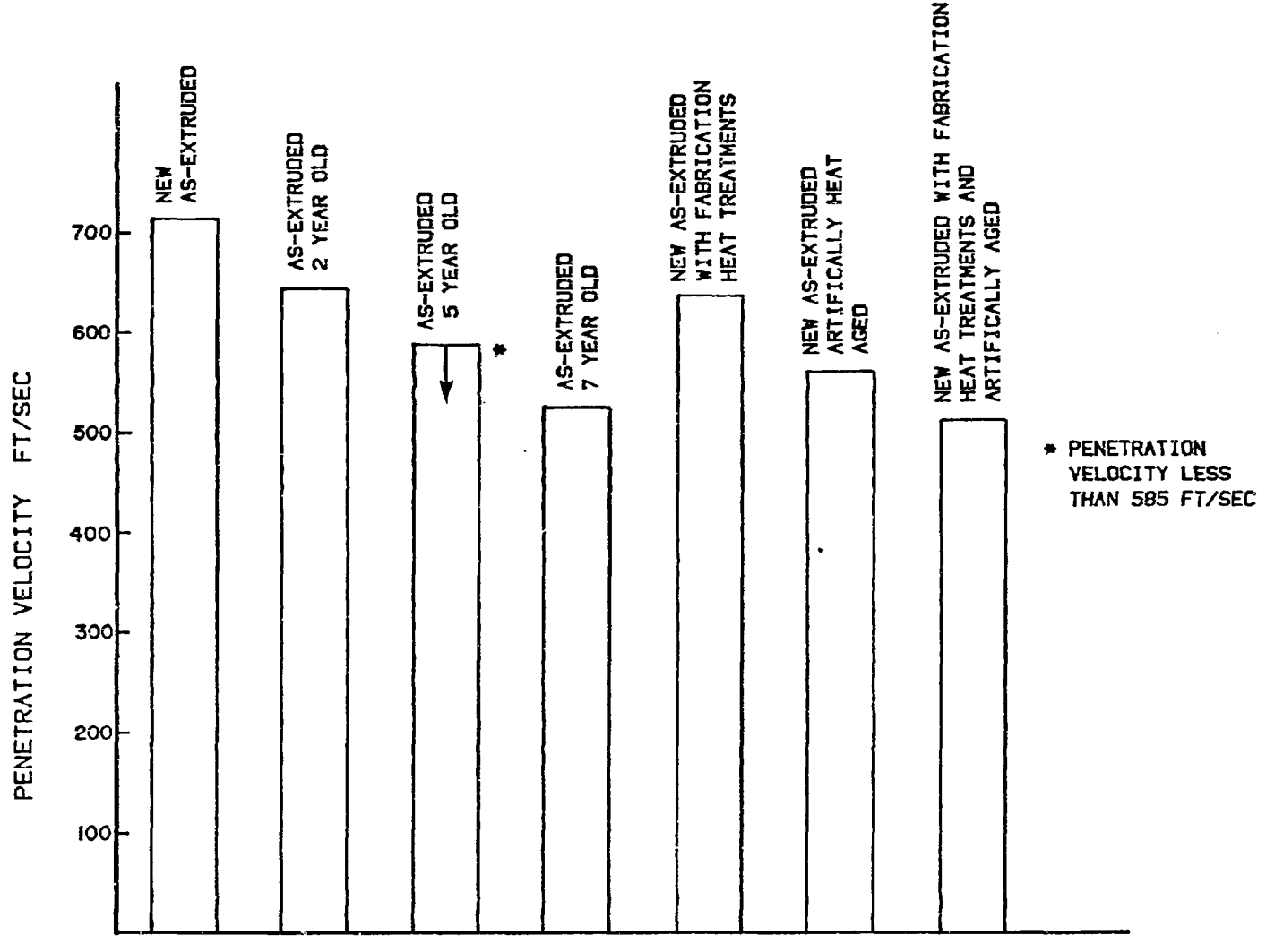

FIG. 5 EFFECT OF MATERIAL HISTORY ON PENETRATION VELOCITY OF POLYCARBONATE

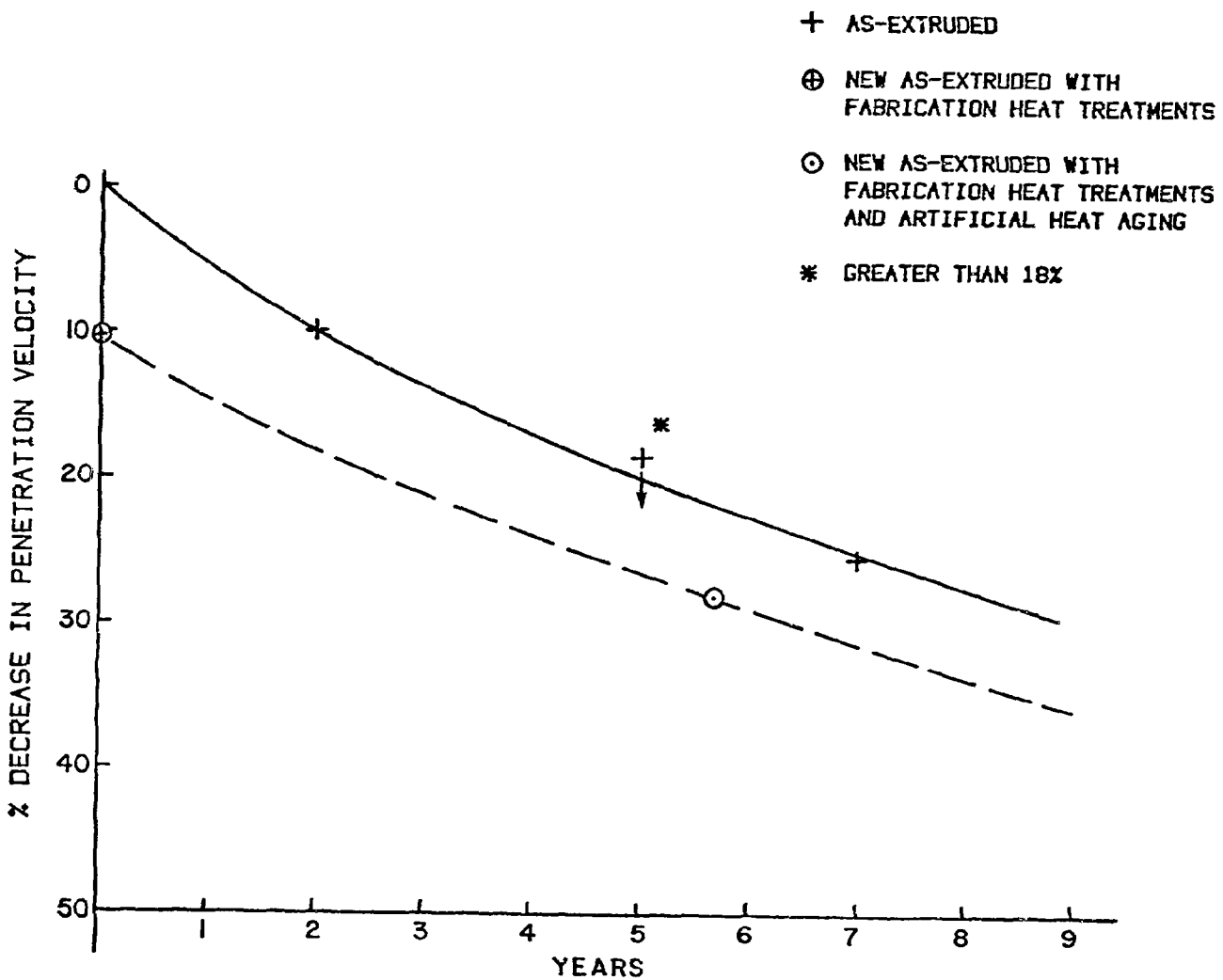

FIG. 6 EFFECT ON PENETRATION VELOCITY OF NATURAL AGING OF POLYCARBONATE (RELATED TO NEW AS-EXTRUDED MATERIAL)

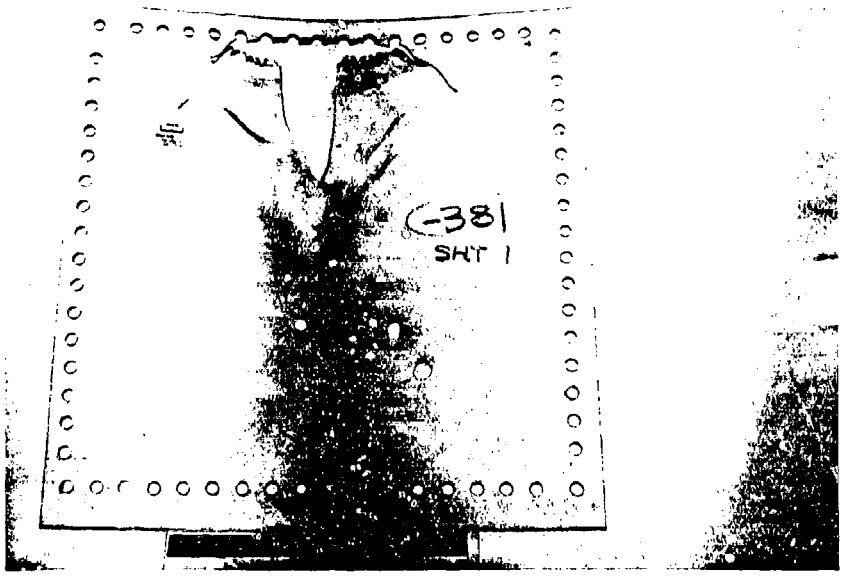

(a) TEST 8 FAILURE INDICATES INSUFFICIENT CLAMPING

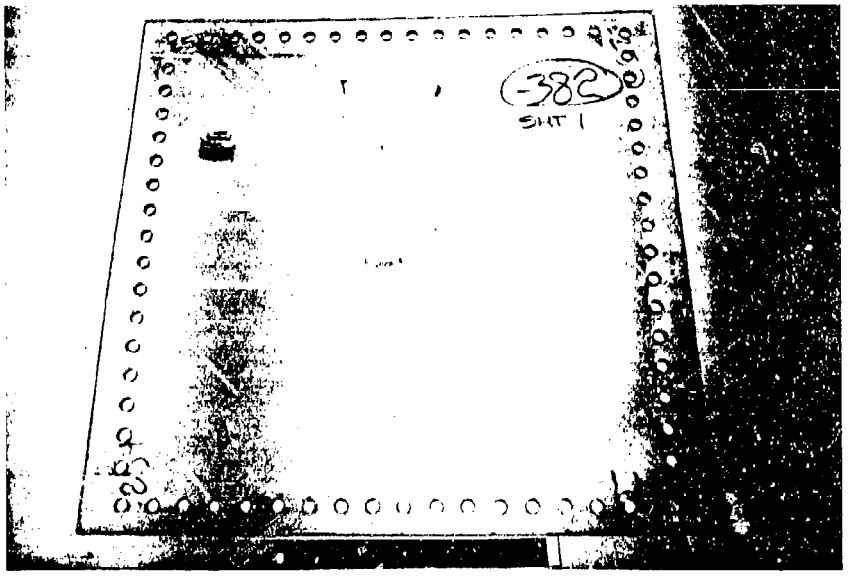

(b) TEST 9 MATERIAL FAILURE, NO EDGE EFFECT

FIG. 7 0.250 IN. TK. POLYCARBONATE NEW MATERIAL - TYPICAL FAILURE

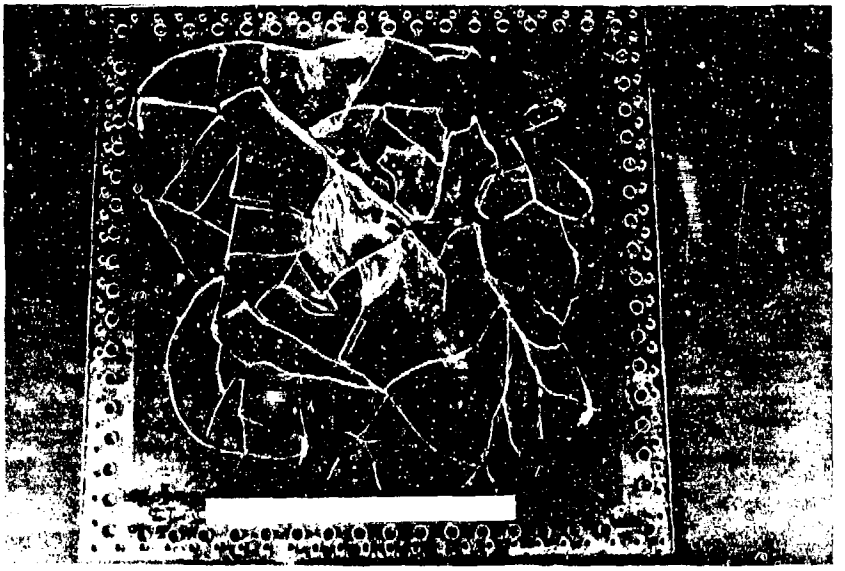

(a) TEST 1 (RECONSTRUCTED FRAGMENTS)

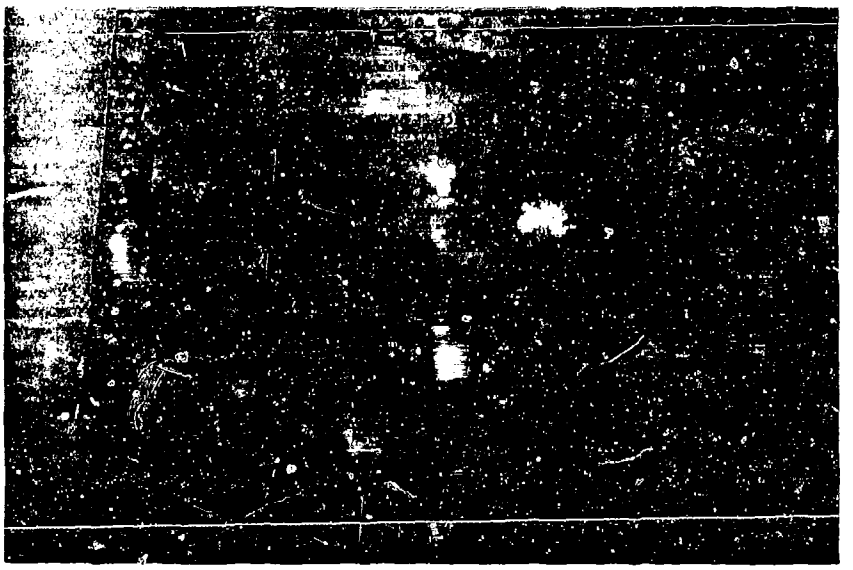

(b) TEST 1

FIG. 8 0.250 IN. TK. POLYCARBONATE
7 YEARS OLD - TYPICAL FAILURE

(a) TEST 7 (RECONSTRUCTED FRAGMENTS)

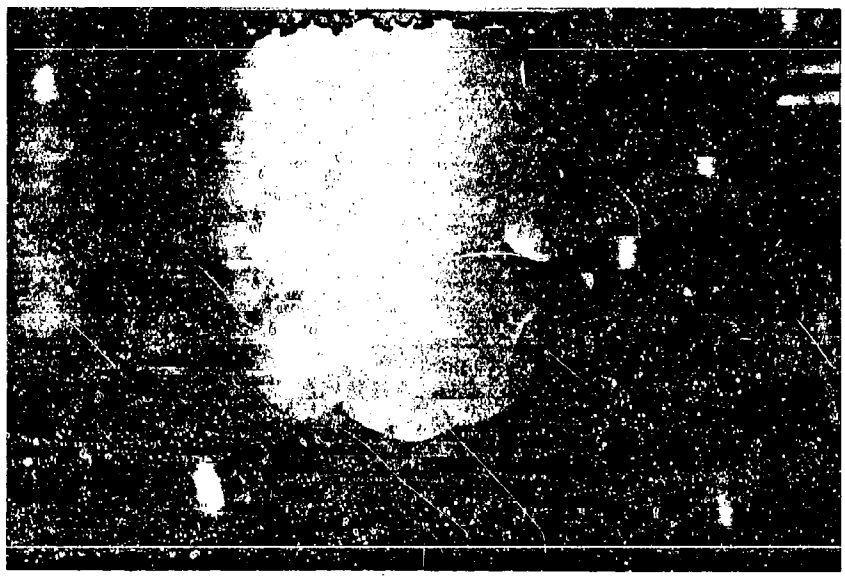

(b) TEST 7

FIG. 9 0.250 IN. TK. POLYCARBONATE
5 YEARS OLD - TYPICAL FAILURE

(a) TEST 20 OUTBOARD SURFACE

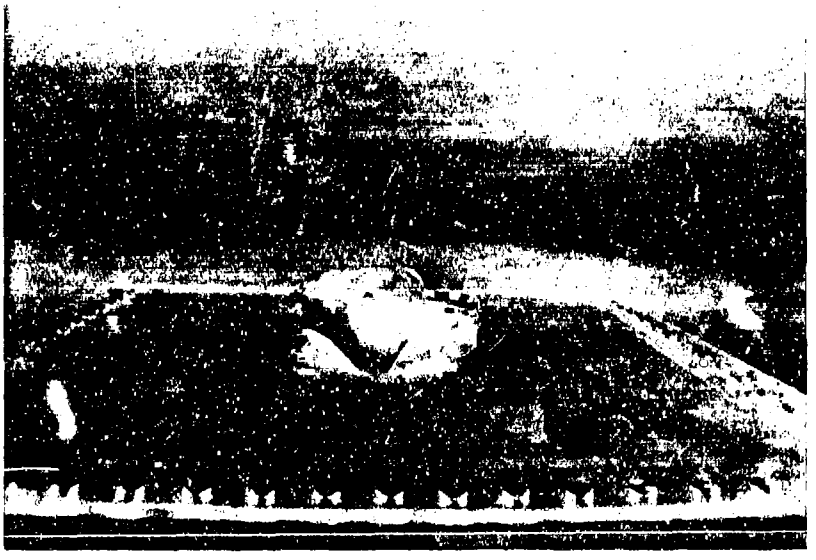

(b) TEST 20 VIEW ALONG OUTBOARD SURFACE

FIG. 10 0.250 IN. TK. POLYCARBONATE
2 YEARS OLD - TYPICAL FAILURE

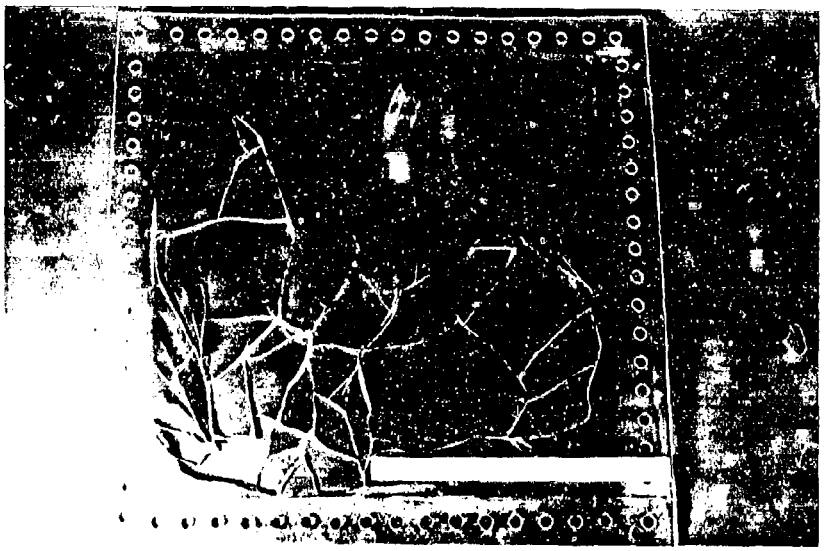

(a) TEST 12 (RECONSTRUCTED FRAGMENTS)

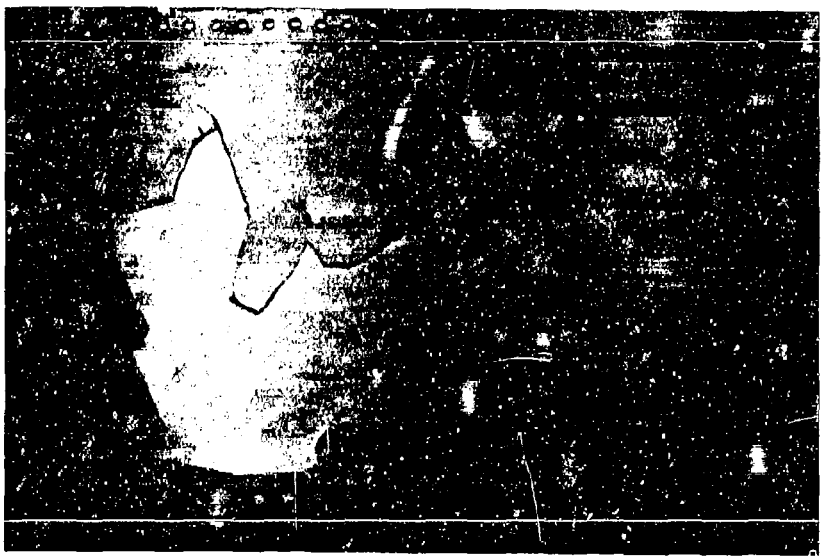

(b) TEST 12

FIG. 11 0.250 IN. TK. POLYCARBONATE
NEW MATERIAL - HEAT AGED
TYPICAL FAILURE

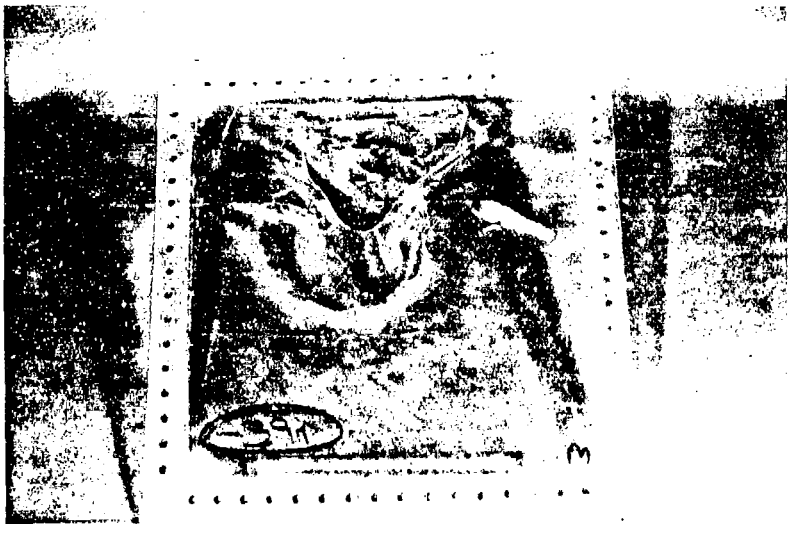

(a) TEST 18 OUTBOARD SURFACE

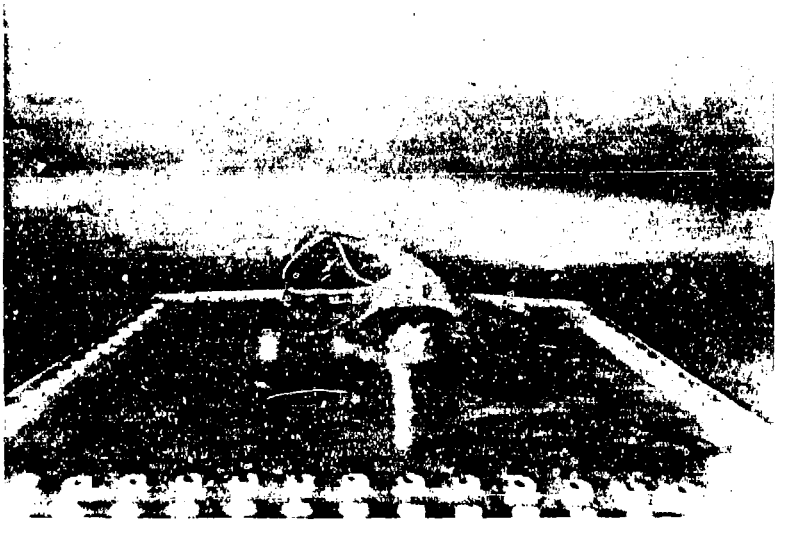

(b) TEST 18 VIEW ALONG INBOARD SURFACE

FIG. 12 0.250 IN. TK. POLYCARBONATE, NEW MATERIAL - HEAT TREATED (DRY, POLISH, FORM) TYPICAL FAILURE

(a) TEST 24 (RECONSTRUCTED FRAGMENTS)

(b) TEST 24

FIG. 13 0.250 IN. TK. POLYCARBONATE, NEW MATERIAL - ARTIFICALLY AGED - HEAT TREATED (DRY, POLISH, FORM) - TYPICAL FAILURE

SOURCES OF ENVIRONMENTAL INFORMATION FOR USE IN TRANSPARENCY SYSTEM DESIGN AND TESTS

Capt. N. E. Buss and Lt. J. K. Hayward,
Flight Dynamics Laboratory

(PAPER NOT FURNISHED)

AD-P003 194

THE EFFECT OF ACCELERATED ULTRA VIOLET WEATHERING ON THE RAIN EROSION RESISTANCE OF COATED AIRCRAFT TRANSPARENCIES

C. J. Hurley, University of Dayton and
G. F. Schmitt, Materials Laboratory

The Effects of Accelerated Ultra Violet Weathering On The Rain Erosion Resistance of Coated Aircraft Transparencies

by

Charles J. Hurley
University of Dayton Research Institute

George F. Schmitt
Air Force Wright Aeronautical Laboratories
Materials Laboratory

ABSTRACT

A number of high performance aircraft are utilizing polycarbonate transparencies as the structural ply. This usage is dictated by the need to provide a transparency which can survive high speed impact energies. The effects of accelerated ultra violet weathering on the rain erosion resistance of coated aircraft transparencies were investigated. Three proprietary coatings on monolithic polycarbonate transparency material were examined. The coated polycarbonate materials were exposed to one and three years of accelerated ultra violet exposure. The specimens were then exposed at a 30° impact angle to a simulated one inch/hour rainfall at 500 mph in the AFWAL Mach 1.2 Rain Erosion Test Apparatus. Percent coating removal as a function of rainfield exposure was determined.

Kinetic behavior of coating removal was similar for Vendor P and Vendor A materials before and after accelerated UV weathering. An S-curve type of behavior was exhibited with incubation periods ranging from 2 to 5 minutes for Vendor P and Vendor A coatings, respectively. Increased rainfield exposure duration, beyond the so-defined incubation period, resulted in substantial increases in coating removal. Coating removal in the Vendor B material was essentially nil, being independent of rainfield exposure time as well as UV radiation exposure effects. Exposure of Vendor P material to the desert sunshine EMMA test resulted in a mode of coating removal very similar to the Vendor P materials exposed to accelerated UV weathering in the laboratory. Vendor P material exhibited damage to the polycarbonate substrate after these tests after 3 years of simulated UV weathering.

Accelerated UV weathering exposure did not directly affect the coatings' behavior under rainfield exposure conditions but did have an indirect effect on the adhesion of the coatings to the polycarbonate substrate materials. SEM techniques are the most effective in assessing the role of mechanistic processes in rain erosion phenomena.

INTRODUCTION

The impact resistance of polycarbonate material is influenced by such parameters as thickness, temperature, configuration, surface finish, aging and environmental exposure. Coated monolithic polycarbonate transparencies, as well as laminated acrylic/polycarbonate plies, are being considered for current and potential future windshield and canopy applications. Investigation of the rain erosion behavior of transparent plastics, specifically polysulfone and uncoated polycarbonate, has been conducted by the Air Force Wright Aeronautical Laboratories (AFWAL) Materials Laboratory and reported in Reference 1. Although numerous proprietary coatings for polycarbonate have been evaluated in the AFWAL Materials Laboratory rotating arm apparatus over the past seven years, this represents the first systematic study of the influence of environmental exposures on the erosive behavior of those transparent coatings. The purpose of this study was to determine the effects of accelerated ultra violet weathering on the relative rain erosion resistance and the damage mechanisms involved with different types of coated monolithic polycarbonate transparency materials. The materials were evaluated before and after simulated environmental exposure.

EXPERIMENTAL PROCEDURE

1. Materials

All materials for evaluation were supplied by the U.S. Air Force. The materials were furnished in flat sheet form and processed to be representative of material used in aircraft transparencies. The three vendors supplying coated monolithic polycarbonate material are identified as Vendor P, Vendor A, and Vendor B. The base material for each vendor consisted of nominal 0.75 inch thickness. Three different coatings were utilized: Vendor P material was supplied with the Texstar C-254-1C coating, Vendor A had its own specific coating, and, similarly, Vendor B had its own specific coating. All specimens were first cut from the parent material sheet by band sawing. Cutting temperature was controlled during milling through the use of cooling air. Great care was taken to ensure that the coated surfaces to be tested were not damaged or adversely affected by fabrication. The test specimens used for rain erosion evaluations required a reduction in thickness and two beveled edges as shown in Figure 1. The coated surface to be exposed to rain erosion was always protected during milling. After milling the backface was polished to a level which would allow visual inspection before and after rain erosion exposure. Further descriptions of test specimen fabrication and conditioning can be found in Reference 2.

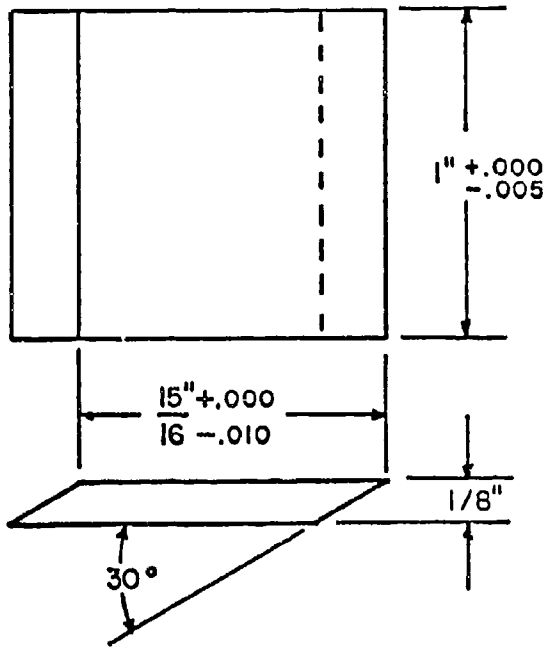

Figure 1. Rain Erosion Test Specimen for 30° Impact Angle.

2. Simulated UV Exposures

Accelerated UV Laboratory Conditioning -- The UV radiation environmental conditioning of the test specimens was implemented in two stages: the as-received baseline materials which had not been exposed to UV and the baseline materials that had been subjected to accelerated laboratory UV exposure for one and three years. All UV conditioning was performed using a Sunlighter IV accelerated sunlight tester, manufactured by the Test-Lab Apparatus Co., Amherst, NH. Basically, this apparatus consists of four sunlamp bulbs mounted over a rotating turntable. The tester acceleration ratio over natural sunlight is based on a cabinet temperature of 131-140°F. The energy level in the range where nearly all UV degradation occurs, supplied by the General Electric RS-4 sunlamp bulbs in the tester, varies from a wavelength of 290 nm at an intensity of 1300 W/sq. meter to 360 nm at 30,000 W/sq. meter. The wavelength of maximum sensitivity for polycarbonates is 295 nm. Specimens were mounted on a screen to avoid contact with the non-reflective turntable.

One sunlamp bulb is mounted directly over the center portion of the turntable, and three additional bulbs are mounted over the outboard portion of the turntable. Consequently, two areas with different exposure accelerations are produced on the turntable, an inner circle with a diameter of approximately 6 in. and the remaining outer ring of diameter 17.5 in. For

the inner circle the acceleration ratio is approximately exposure for 8 h which is equivalent to one year of natural sunlight according to the manufacturers. The inner circle was used for all UV exposure of the rain erosion test specimens. For the purposes of this report, the data will indicate no accelerated UV weathering, one year of UV accelerated weathering and three years of UV accelerated weathering.

Accelerated Outdoor Sunshine Conditioning -- Accelerated outdoor weathering of simulated three year exposure was accomplished by utilizing the equatorial mount with mirrors for acceleration (EMMA) machine at the Desert Sunshine Exposure Test Laboratory near Phoenix, Arizona. It is estimated that 40 days of exposure on the EMMA machine is approximately equivalent to one year of exposure to natural weathering at 45°S. The specimens receive about eight times as much radiation as those exposed on a follow-the-sun rack during equal periods of time. Each simulated year was based on an exposure rate of 164,250 langleys.

3. Apparatus

The AFWAL Mach 1.2 rain erosion test apparatus consists of a double-arm blade 8 ft in diameter. It is designed to produce high tip velocities with negative lift and a low drag coefficient. Mated test specimens are mounted at each leading edge tip section of the double rotating arm. The test specimens can be subjected to variable speeds of 0-900 mile/hr. The double arm is mounted horizontally on a vertical drive shaft (Figure 2). Simulated rainfall is produced by four curved manifold quadrants. Each manifold quadrant has 24 equally spaced capillaries. Raindrop size and drop rate are controlled by the capillary orifice diameter and the head pressure of the water supply. The manifold quadrants are mounted above the tips of the double rotating arm. Raindrops from the simulation apparatus impact the test specimens throughout their entire annular path. Rain droplets are 2.0 mm in diameter and are generated at a rate to give simulated rainfall of 1 inch/hour. The apparatus is fully described in Reference 3.

4. Rain Erosion Tests

For the purposes of this study, matched specimens of the coated monolithic polycarbonate materials were inserted into the leading edge tip sections of the double rotating arm at a 30° angle of incidence to the rain droplet impact. All rainfield exposure testing was conducted at 500 miles per hour in a calibrated simulated rainfall of 1 inch/hour. The durations of the tests were 1, 2, 5, 10, and 15 minutes.

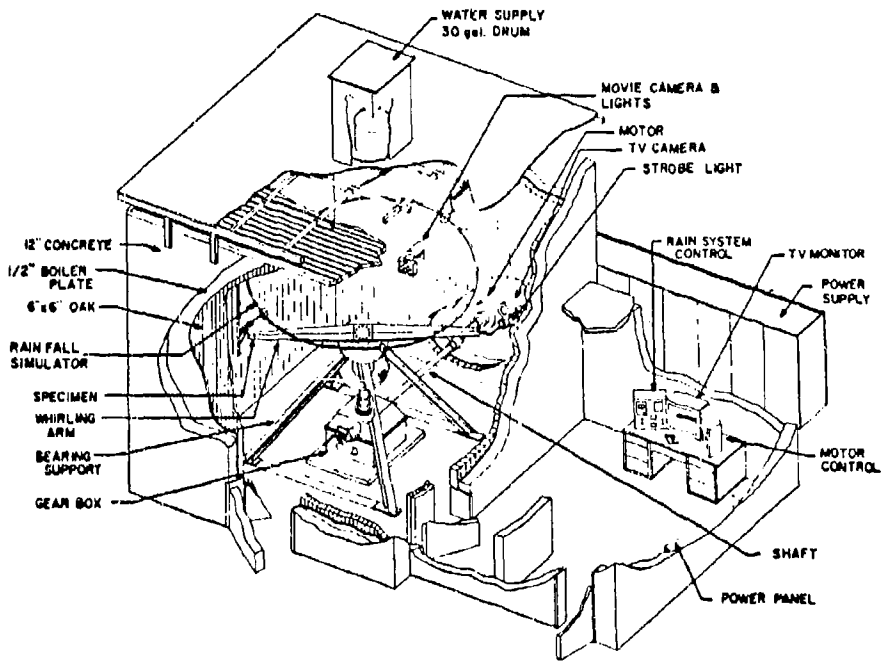

Figure 2. Mach 1.2 Rain Erosion Test Apparatus.

5. Visual Observations

All specimens were examined after rainfield exposure with an illuminated magnifier and the surface condition was recorded. Comments included scratches, pitting, and percentage coating removal.

6. Surface Characterization

The surface of the exposed specimens were examined directly by scanning electron microscopy (SEM) together with an x-ray unit. Specimens were vapor shadowed with a heavy metal or carbon to provide contrast.

RESULTS

The primary effects of the rainfield exposure were examined, namely the rain erosion kinetics (percent coating removal as a function of accelerated UV exposure and duration of rainfield exposure) and the surface morphology of the coated transparencies after the rainfield exposure. Reference 4 describes the in-house effort conducted.

1. Vendor P Observations

Visual observations of the effect of rainfield exposure duration on the Vendor P unexposed and exposed to accelerated UV conditioning is shown graphically in Figure 3. An incubation period followed by a progressive increase in coating removal was observed as a function of rainfield exposure duration. The Vendor P specimens (one year and three year accelerated exposure) exhibited a decrease in the erosion incubation period and an increase in percent coating removal as a function of increasing accelerated UV exposure with a decrease in rainfield exposure time. Exposure of the Vendor P specimens (no UV exposure) to rain erosion test conditions resulted in coating surface damage as determined by SEM examination. Short term exposure led to the formation of localized defects in the coating surface up to 10 microns in diameter as shown in Figure 4. Further exposure to the rainfield led to the development of pits up to 30 microns in diameter at the localized damage sites and subsequently to localized coating removal as shown in Figure 5. Continued exposure resulted in substantial coating removal without the introduction of damage in the monolithic polycarbonate substrates as shown in Figure 6.

Short term exposure to rainfield conditions of the Vendor P material (one year UV exposure) resulted in increased damage and coating removal as shown in Figure 7. Additional exposure time

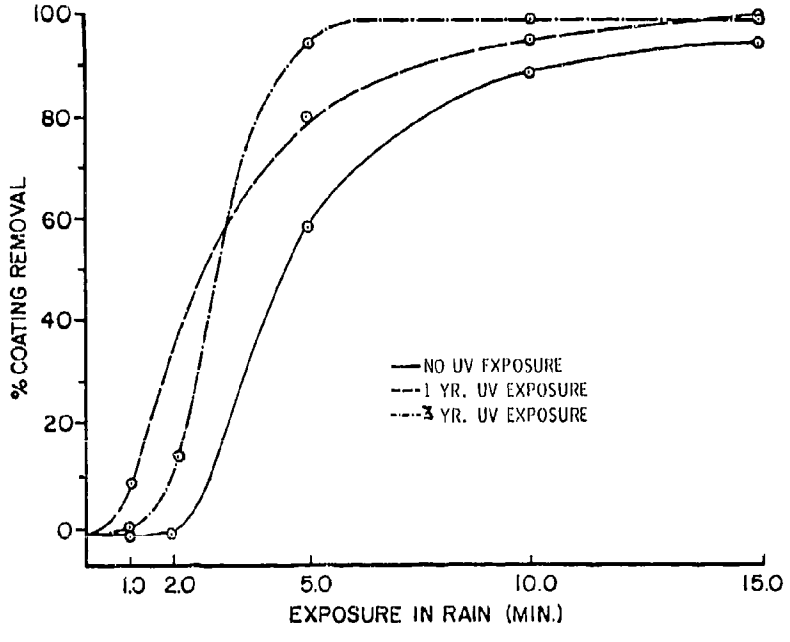

Figure 3. Percent Coating Removal vs. Time in Rain for Vendor P.

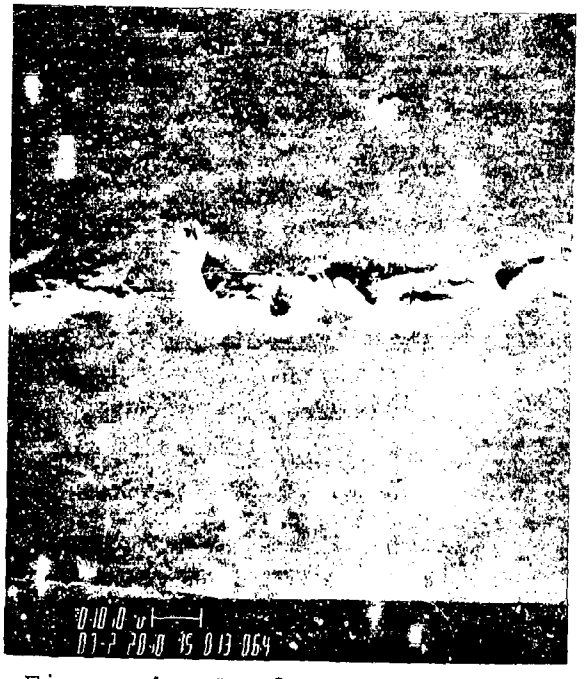

Figure 4. Vendor P (no UV exposure) 1 min rain exposure.

Figure 5. Vendor P (no UV exposure) 2 min rain exposure.

Figure 6. Vendor P (no UV exposure) 15 min rain exposure.

Figure 7. Vendor P (1 yr UV exposure) 2 min rain exposure.

resulted in progressive coating removal and formation of localized craters about 10 microns in diameter in the monolithic polycarbonate substrate as shown in Figures 8 and 9. Typical surface damage of the Vendor P (three year UV exposure) exposed to rainfield conditions is shown in Figure 10. Coating damage and removal after 1 minute of rainfield exposure is clearly shown. Increased exposure time to rainfield conditions revealed coating damage and removal associated with damage to the polycarbonate substrate. This is demonstrated in Figures 11 and 12.

2. Vendor A Observations

Visual observation of the effect of rainfield exposure on Vendor A materials unexposed and exposed to accelerated UV conditioning is shown graphically in Figure 13. An incubation period followed by a progressive increase in coating removal was observed for Vendor A materials as a function of rainfield exposure duration. The Vendor A specimens (one year and three year accelerated UV conditioning) demonstrated no decrease in the erosion incubation period but exhibited a marked increase in percent coating removal as a function of UV weathering with increasing rainfield exposure duration. The typical mode of surface coating damage engendered by rain erosion processes for a Vendor A specimen (no UV exposure) with short term rainfield exposures is shown in Figure 14 as determined by SEM examination. Initial coating damage was characterized by isolated and localized events of eroded or removed coating material in the range of 30-50 microns. Further exposure of the test specimens to rainfield conditions resulted in progressive coating removal associated with crack formation, but without the introduction of cratering damage into the polycarbonate substrate as shown in Figure 15. The mode of surface damage obtained in a Vendor A specimen (one year UV exposure) after a rainfield exposure of 5 minutes is shown in Figure 16. The damage is characterized by coating removal associated with coating separation and crack formation. Furthermore, noticeable strain-like lines were detected in the coating as indicated in Figure 17. This may be indicative of some phase (compositional or structural) changes within the substrate or coating. Vendor A specimens (three year UV exposure) subjected to rainfield exposure underwent surface damage as shown in Figure 18. Coating material was removed and the formation of elongated channels 1-10 microns in width together with craters or pits up to 20 microns in diameter was detected in the polycarbonate substrate surface as shown in Figure 19. These specimens were exposed to the rainfield for 10 minutes. The elongated channel-like lines appeared in groups aligned in various directions to each other. However, within the individual group, these channels tended to be parallel with one another. The formation of such surface morphology suggests that the material may have undergone phase (compositional or structural) changes as a result of UV exposure and subsequent rainfield exposure.

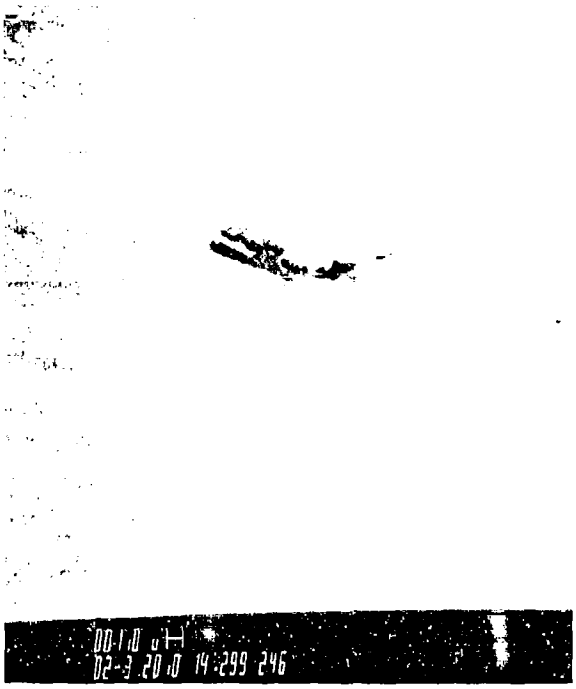

Figure 8. Vendor P (1 yr UV exposure) 10 min rain exposure.

Figure 9. Vendor P (1 yr UV exposure) 15 min rain exposure.

Figure 10. Vendor P (3 yr UV exposure) 1 min rain exposure.

Figure 11. Vendor P (3 yr UV exposure) 2 min rain exposure.

Figure 12. Vendor P (3 yr UV exposure) 10 min rain exposure.

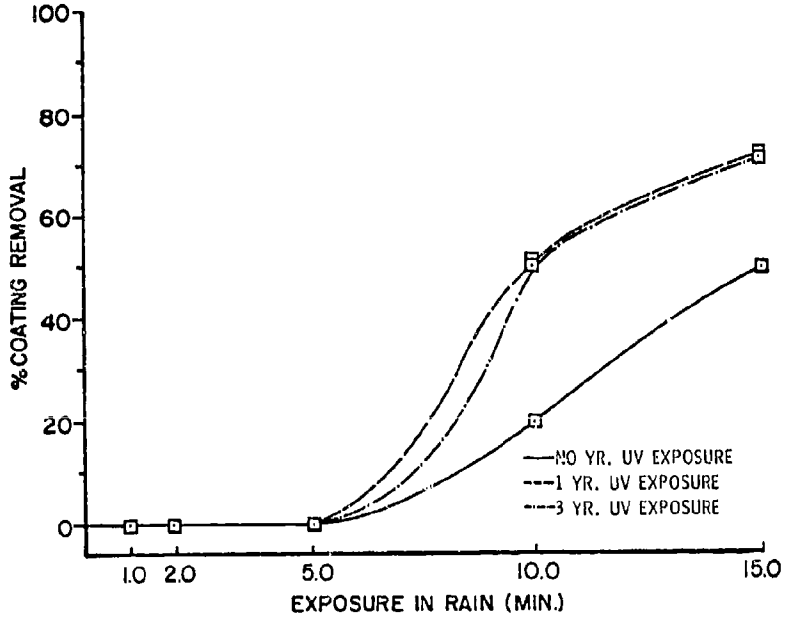

Figure 13. Percent Coating Removal vs. Time in Rain for Vendor A.

Figure 14. Vendor A (no UV exposure) 2 min rain exposure.

Figure 15. Vendor A (no UV exposure) 10 min rain exposure.

Figure 16. Vendor A (1 yr UV exposure) 5 min rain exposure.

Figure 17. Vendor A (1 yr UV exposure) 5 min rain exposure.

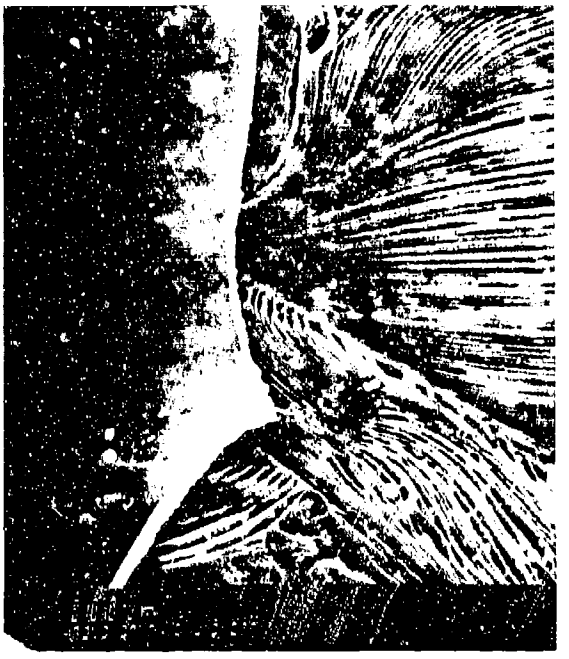

Figure 18. Vendor A (3 yr UV exposure) 10 min rain exposure.

Figure 19. Vendor A (3 yr UV exposure) 10 min rain exposure.

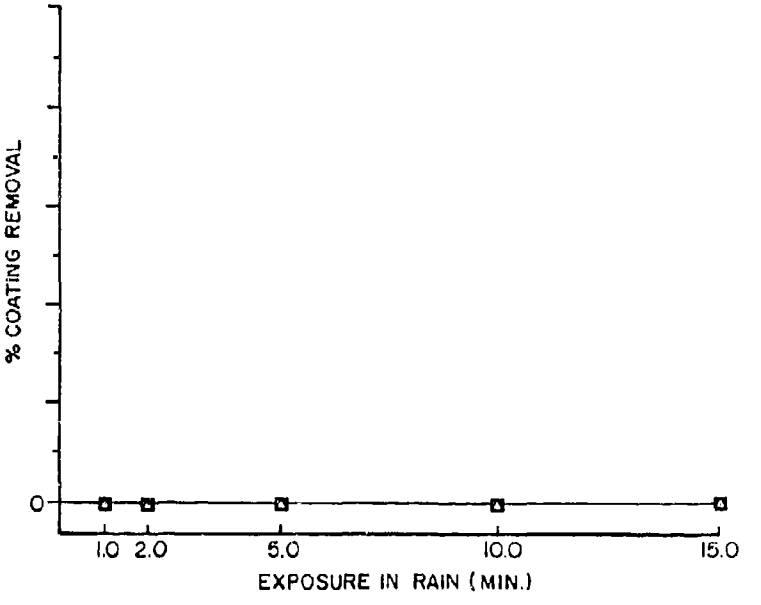

Figure 20. Percent Coating Removal vs. Time in Rain for Vendor B.

3. Vendor B Observations

The Vendor B material exhibited no visually observable percentage of coating removal with increasing rainfield exposure time as depicted in Figure 20, but did show surface pitting after 15 minutes of rainfield exposure. Surface morphology of the Vendor B test specimens (no UV exposure) subjected to rainfield exposure ranging from 2 to 15 minutes resulted in localized erosion sites up to 20 microns in diameter as shown in Figures 21 and 22. These erosion sites were characterized by the formation of craters or pits engendering one another as well as microcracks in the coating. Furthermore, in only a few of the erosion sites was the coating completely removed from the substrate. Overall no substantial coating removal was detected.

The Vendor B test specimens (one year UV exposure) exposed to rainfield conditions are shown in Figures 23 and 24. Localized sites characterized by coating removal were observed after 1 and 10 minutes of rainfield exposure. These localized sites were approximately 100 microns in diameter. No substantial amount of coating removal was detected in these specimens.

Test specimens of Vendor B material (three year UV exposure) subjected to rainfield exposure are shown in Figures 25 and 26.

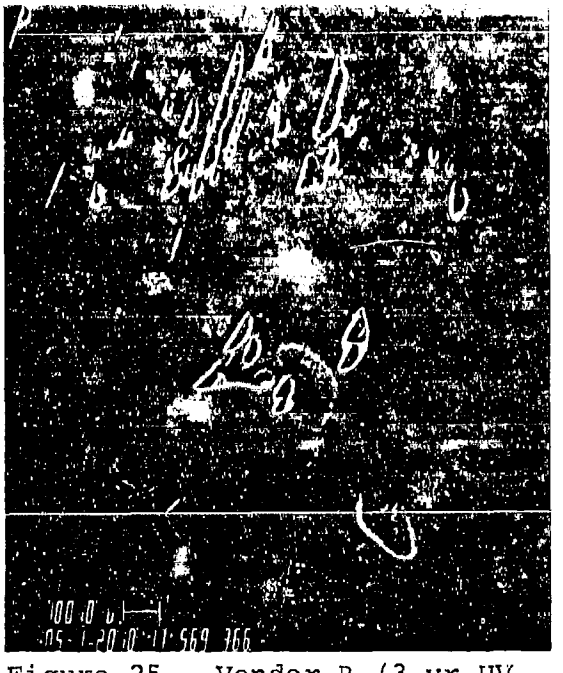

Figure 25. Vendor B (3 yr UV exposure) 1 min rain exposure.

Figure 26. Vendor B (3 yr UV exposure) 10 min rain exposure.

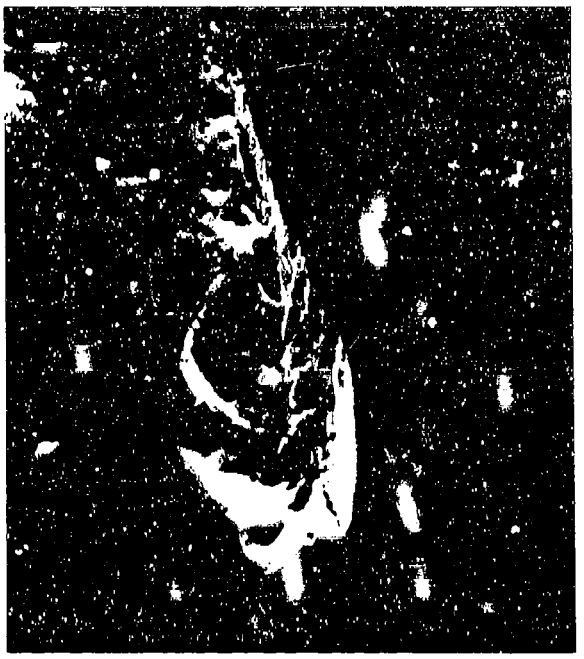

Figure 21. Vendor B (no UV exposure) 2 min rain exposure.

Figure 22. Vendor B (no UV exposure) 15 min rain exposure.

Figure 23. Vendor B (1 yr UV exposure) 1 min rain exposure.

Figure 24. Vendor B (1 yr UV exposure) 10 min rain exposure.

These observations were characterized by the presence of localized sites of eroded coating material and coating removal ranging up to 200 microns in diameter. These figures are for rainfield exposures of 1 minute and 10 minutes, respectively.

DISCUSSION

1. Effects of Accelerated UV Exposure

Accelerated UV exposure effects on the subsequent rain erosion behavior of the Vendor P, A, and B materials were evaluated as a function of the kinetic behavior of coating removal and surface characterization as obtained by SEM observations. Exposure of the Vendor P materials to accelerated UV weathering resulted in a reduction in the erosion incubation period from 2 to 0.5 minutes with a significant increase in the rate of coating removal. The erosion incubation period of the Vendor A materials was not affected by accelerated UV weathering exposure; however, the coating removal rate did substantially increase with UV exposure as shown. Furthermore, exposure to accelerated UV weathering apparently caused the introduction of damage into the polycarbonate substrates of Vendor P and Vendor A materials. These observations are depicted in Figures 8, 9, 11, 12, and 19. Polycarbonate is known to be sensitive to UV radiation, especially in the presence of moisture as reported in References 2, 5, and 6. Consequently, the resultant reduction in adhesion of the coatings to the polycarbonate substrates at their interface led to the decrease in incubation time as well as an increase in the rate of coating removal in the Vendor P and Vendor A materials.

Since the polycarbonate substrates were apparently affected by accelerated UV weathering, it is suggested that the Vendor P and Vendor A coatings were transparent in the UV wavelength region. By contrast, in the Vendor B material essentially no coating removal was visually observed and there was no apparent damage to the polycarbonate substrate. These observations suggest that Vendor P and Vendor A coatings did not apparently contain the necessary type and amount of UV absorbers. The Vendor B coating may have contained sufficient amounts of UV absorbers which apparently prevented damage to the polycarbonate substrate and consequently prevented delamination and coating removal. Accelerated UV weathering did not substantially affect the coating properties in so far as their rain erosion properties are concerned. In all three cases, the coatings were subject to rain erosion damage prior to accelerated UV weathering. Similar rain erosion damage occurred after exposure to accelerated UV weathering. These observations support the hypothesis that accelerated UV weathering did not directly affect the coatings' behavior under rainfield exposure conditions but rather had an

indirect effect through the reduction of adhesion to the polycarbonate substrate as discussed above.

2. Effects of Desert Sunshine Exposure

Exposure of the Vendor P material to the desert sunshine EMMA test for the equivalent of three years and thereafter to rainfield exposure conditions resulted in coating removal as shown in Figure 27. Damage was also evident in the polycarbonate substrate as shown in Figure 28. The mode of coating removal was very similar to that of the Vendor P specimens exposed to accelerated UV weathering in the laboratory. Furthermore, the mode of damage introduced in the polycarbonate substrate was associated with the formation of craters together with microcracks, as was the case for the Vendor P materials irradiated with UV radiation in the laboratory. Based on these findings, it is possible to deduce a good correlation between the rain erosion behavior of the Vendor P specimens UV irradiated in the laboratory and the Vendor P desert sunshine exposures.

3. Rain Erosion Kinetics

The behaviors of three types of coated monolithic polycarbonate materials under rainfield exposure conditions before and after exposure to accelerated UV weathering were investigated and evaluated. The effects of accelerated UV weathering and exposure time under rainfield conditions were characterized by specific damage categories of coating erosion, coating removal, and substrate erosion.

A comparison of the rain erosion kinetics were characterized by the amount of coating removal from the coated monolithic polycarbonate materials under rainfield exposure conditions as shown in Figures 29, 30, and 31. Kinetic behavior of coating removal was similar for Vendor P and Vendor A materials before and after UV weathering. An S-curve type of behavior was exhibited with incubation periods ranging from 2 minutes to 5 minutes for Vendor P coatings and Vendor A coatings, respectively. The longer incubation period of the Vendor A coating may be attributed to better adhesion to the polycarbonate substrate. Increased rainfield exposure durations beyond the so-defined incubation period, resulted in substantial increases in coating removal reaching a saturation level of nearly 100% removal for the Vendor P coating. The Vendor A coating exhibited a lower rate of coating removal after the incubation period and began to level off at values of 60%-70% coating removal after 15 minutes of rainfield exposure. The increased rate of gross coating removal is probably associated with the critical impact energy on the coatings surface needed initially to reduce the adhesive forces at the coating substrate interface.

Figure 27. Vendor P (3 yr EMMA exposure) 1 min rain exposure.

Figure 28. Vendor P (3 yr EMMA exposure) 1 min rain exposure.

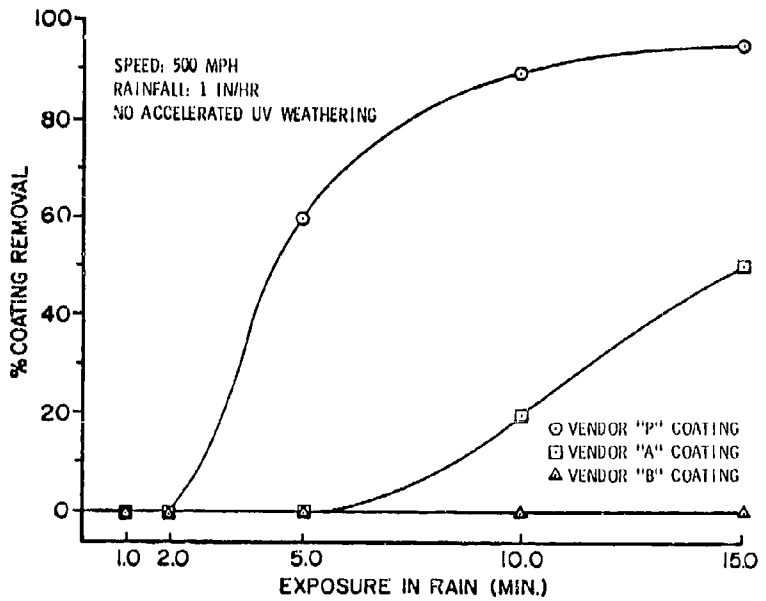

Figure 29. Percent Coating Removal vs. Time in Rain at 500 mph.

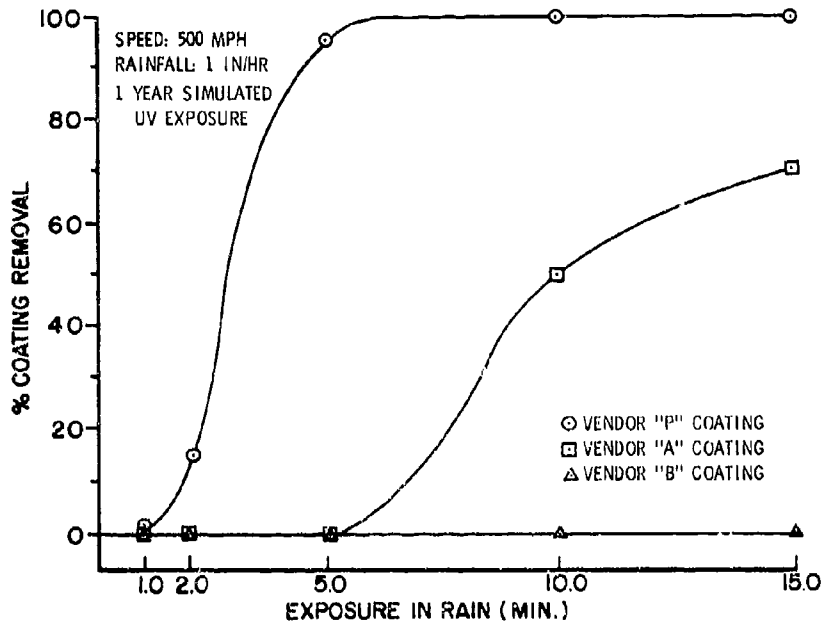

Figure 30. Percent Coating Removal vs. Time in Rain at 500 mph.

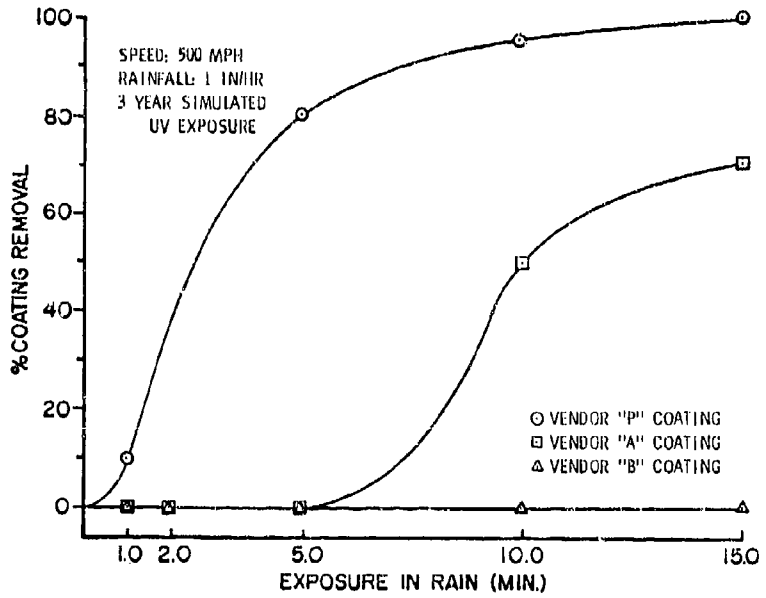

Figure 31. Percent Coating Removal vs. Time in Rain at 500 mph.

The Vendor A coating compared with the Vendor P coating appears to have higher ductility. This may be deduced by comparing Figure 16 (where coating foldback was possible because of high coating ductility) with Figure 9 (where coating brittleness is demonstrated by the formation of sharp boundaries and cracks in the zones of removed coating). Vendor A coating could absorb more rain droplet impact energy and remain adhered to the polycarbonate substrate, resulting in a longer incubation period as well as a decreased coating removal rate.

Coating removal in the Vendor B material was nearly 0%, being independent of rainfield exposure time as well as UV radiation exposure effects. The lack of substantial coating removal may be associated with the existence of high adhesion forces between the coating and substrate interface. This may be deduced from Figures 21 and 23, where the coating itself was eroded prior to delamination from the substrate surface.

4. Rain Erosion Initiation

The initiation process was associated with the incubation time. The erosion process at the initiation stage was characterized by localized erosion events which resulted in isolated craters or pits 10-30 microns in size. These localized events consisted of material removal from the coating as well as localized coating separation from the polycarbonate substrate. With continued rainfield exposure, these local isolated events merged with each other. Further exposure of the test specimens, beyond the incubation period, resulted in rain erosion damage in the polycarbonate substrate material. Substrate damage occurred in the UV irradiated test specimens of the Vendor P and A substrates but not in the Vendor B substrates. The initiation stage of rain erosion damage was characterized by the formation of localized craters or pits, up to 10 microns in diameter, with associated microcracks.

5. Rain Erosion Propagation

The propagation stage of the rain erosion process, affecting the surface coatings, occurred through the joining of the local damage events. Continuation of the damage "growth" process of the local events resulted in coating removal from large areas a few hundred micrometers in size and subsequently from the entire area of the test specimen exposed to rainfield conditions. Coating removal through the propagation stage correlated with the high rate of coating removal as shown in the S-type, kinetic curves. Whenever the propagation stage of uniting local erosion events stopped, no general erosion damage, i.e., coating removal, occurred and the coating surface remained fundamentally undamaged as observed in the Vendor B materials. The observation that no advanced propagation stage occurred in the Vendor B material was also reflected in the kinetic curves, as the amount of

coating material removal was essentially insignificant. The erosion propagation mode in the polycarbonate substrate could be characterized in several forms. One form suggests the combination of initially formed craters or pits, after growth to 30 microns in size, to form an elongated channel. Another form suggests the joining of minute isolated events (1 micron in size) to form a continuous stream of parallel channels. Further investigation should be considered in order to provide more data to evaluate and support the actual mode of rain erosion damage in the polycarbonate substrate.

6. Conclusions

Visual examinations of the Vendor P, A, and B specimens after rainfield exposure indicated the following.

(1) The Vendor P coating (no UV exposure) exhibited the earliest initiation of coating removal due to rainfield exposure. Increasing duration of accelerated UV exposure caused a progressive reduction in the initiation period of coating removal and increased the rate of coating removal as a function of rainfield exposure time.

(2) The Vendor A coating (no UV exposure) exhibited a longer period of coating removal initiation. An increase in the duration of accelerated UV exposure resulted in an increased coating removal as a function of rainfield exposure time but no increase in the initiation period.

(3) The Vendor B coating (no UV exposure) exhibited surface pitting but no observable coating removal after 15 minutes of rainfield exposure. An increase in the duration of accelerated UV exposure resulted in no observable coating removal as a function of rainfield exposure time.

SEM observations of the Vendor P, A, and B specimens after rainfield exposure indicated the following.

(1) Rainfield exposure of the Vendor P specimens (no UV exposure) led initially to localized surface defects in the coating, then to pit formation and localized coating removal followed by substantial coating removal without the introduction of damage in the polycarbonate substrate. Exposure to rainfield conditions of the accelerated UV exposure test specimens resulted in increased coating damage and coating removal as well as localized cratering in the polycarbonate substrate.

(2) Short-term rainfield exposure of the Vendor A material (no UV exposure) resulted in isolated and localized areas of coating removal. Further rainfield exposure resulted in progressive coating removal and crack formation without cratering damage to the polycarbonate substrate. Vendor A material (one

year UV exposure) exhibited increased coating removal and crack formation as a function of rainfield exposure duration, as well as coating separation and noticeable stream-like lines. The stream-like lines may be indicative of some phase change in the coating or substrate. The rates of surface damage and coating removal were the same for the one year and three year accelerated UV exposure Vendor A specimens. In addition, craters or pits as well as formation of elongated channels were detected in the specimens with three year accelerated UV exposure.

(3) The Vendor B coating (no UV exposure) resulted in localized erosion sites characterized by the formation of craters and associated microcracks under rainfield exposure conditions. No substantial coating removal was detected. One year and three year accelerated UV exposure test specimens exhibited localized sites of eroded coating material and removal. Again, no substantial amount of coating was removed.

(4) The kinetic behavior of coating removal was similar for Vendor P and Vendor A materials before and after accelerated UV exposure. A longer erosion incubation period for Vendor A coating is attributed to better adhesion to the polycarbonate substrate. The fact that there was no substantial coating removal on the Vendor B material could be associated with high adhesion forces between the coating and substrate interface.

Exposure of the Vendor P specimens to accelerated UV weathering reduced the erosion incubation period. The incubation period of erosion of the Vendor A specimens was not affected by accelerated UV weathering exposure. However, the rate of coating removal did increase with UV exposure. Also, accelerated UV weathering exposure introduced cratering and pitting into the polycarbonate substrates of Vendor P and Vendor A. The Vendor B specimens with accelerated UV weathering exposure resulted in no substantial coating removal as well as no apparent damage to the polycarbonate substrate.

Vendor P and A specimens may not have contained the necessary type and amount of UV absorber to prevent substrate damage and coating removal. Vendor B specimens may have contained sufficient amounts of UV absorbers or the coating itself may have been sufficiently resistant to incident UV light to prevent apparent substrate damage and delamination and coating removal.

Accelerated UV weathering exposure did not directly affect the coatings' behavior under rainfield exposure conditions but did have an indirect effect on the adhesion of the coatings to the polycarbonate substrates.

There is a good data correlation between the Vendor P coatings exposed to accelerated UV weathering exposure in the laboratory and those exposed to the desert sunshine EMMA test. The

mode of coating removal and mode of damage to the polycarbonate substrate were similar.

Visual observations of coating damage and coating removal are an effective means of making relative comparisons between materials. However, visual observations are limited in their ability to determine erosion mechanisms in coated transparent materials.

SEM techniques are most effective in assessing the role of mechanistic processes in rain erosion phenomena. These techniques can detect incubation and initiation stages, erosion characteristics, i.e., pitting, cratering and microcracking, and adhesion characteristics of coated materials.

Vendor B materials were the most resistant to erosion processes regardless of their pretest environmental exposures and duration of rainfield exposure conditions.

REFERENCES

1. G. F. Schmitt, Jr., Rain droplet erosion mechanisms in transparent plastic materials. In A. A. Fyall and R. B. King (eds.), Proc. 4th Int. Conf. Rain Erosion and Associated Phenomena, Meersburg, May 8-10, 1974, Royal Aircraft Establishment, Farnborough, 1974.

2. K. I. Clayton, J. F. Millholland, and G. J. Stenger, Experimental evaluation of polycarbonate canopy material, AFWAL-TR-81-4020, April 1981 (Air Force Wright Aeronautical Laboratories, Wright-Patterson Air Force Base, OH).

3. C. J. Hurley and G. F. Schmitt, Jr., Development and calibration of a Mach 1.2 rain erosion test apparatus, AFML-TR-70-240, October 1970 (Air Force Materials Laboratory, Wright-Patterson Air Force Base, OH).

4. C. J. Hurley, J. Zahavi, and G. F. Schmitt, Jr., Rain erosion evaluation and analysis of selected coated monolithic polycarbonate transparency materials, AFWAL-TR-82-4029, April 1982 (Air Force Wright Aeronautical Laboratories, Wright-Patterson Air Force Base, OH).

5. A. Davis and J. H. Golden, Macromol. Sci. C 3 (1969) 49.

6. R. S. Yamasaki and A. Blaga, Mater. Constr. 10 (1977) 197.

SESSION II

UNDERSTANDING CURRENT MATERIALS (PART II)

Chairman: T. J. Reinhart
Materials Laboratory
Wright-Patterson Air
Force Base, Ohio

AD-P003 195

SERVICE-LIFE INDUCED FAILURE OF BIRD IMPACT RESISTANT WINDSHIELDS

P. J. Burchell and R. H. Stacewicz,
Department of Defense Support

SERVICE-LIFE INDUCED FAILURE OF

BIRD IMPACT RESISTANT WINDSHEILDS

P.J. Burchill and R.H. Stacewicz
Materials Research Laboratories, Defence Science and
Technology Organisation, Department of Defence
Melbourne 3032, Australia

ABSTRACT

Bird-impact resistant transparencies (BIRT), which are laminates of modified poly(methylmethacrylate), polycarbonate and a rubbery interlayer, have been fitted to all Royal Australian Air Force F111C aircraft. However their service-life has often been severely limited by factors other than bird-impact, and in one instance was as little as 30 flying hours for an alternate design bird-impact resistant transparency (ADBIRT) windshield. Unserviceability has arisen due to cracks, crazes, delamination, optical distortions or scratches; the most critical are cracks and crazes. All failed first generation windshields (BIRT) examined showed crazing of the inner acrylic layer, while 60% of them had serious crazing of the outer acrylic layer, and in 35% this layer was cracked. With ADBIRT windshields all failures examined were crazed, while some were cracked or showed delamination.

The shapes of the crazes seen on these windshields show that the stresses involved in their formation and growth are complex. Aside from flight, such stresses may arise from the influence of the environment on the properties of the acrylic polymer used in these windshields. This acrylic readily absorbs water and swells which will result in tensile stresses being produced when desorption occurs, so lowering the external loads the acrylic layer can withstand. The effect may be so large that crazing can appear to occur at zero critical stress. These stresses due to swelling have been studied as a possible cause of rapid failure of F111C windshields in Australia. In addition once crazes are formed they may propagate at loads much lower than those required for initiation. Consequently, the effects of cleaning methods, rain removal system, aerodynamic heating, climate, and even the design may have led to the short service lives of these windscreens.

INTRODUCTION

The windshield of an F111 aircraft may be considered as being a quarter segment of a truncated cone of 5° half angle [1], with base radius of 89 cm (35 in) and a height of 122 cm (48 in), and was originally a glass laminate. Since 1978 these aircraft in Australia (F111C) have been fitted with bird-impact resistant transparencies (BIRT) which are plastic laminates having plies of polycarbonate and an acrylic polymer with interlayers of a soft rubber. The forces on the windshield are carried by the polycarbonate layers which are protected from the environment by the acrylic layers. During this time they have suffered only one serious impact with a bird, and this only resulted in a badly cracked windshield. However almost all the first generation transparencies, BIRT, (Figure 1) have now been replaced by the newer ADBIRT which has fewer plies (Figure 2) and even some of these have had to be replaced. The reasons for declaring a windshield defective are poor optical properties or loss of mechanical integrity, and in all cases the defects appear in the acrylic layers or at the acrylic-interlayer boundary.

The severity of conditions during use and the maintenance procedures appear to be the causes of the defects. During flight, the windshields may be overheated from either aerodynamic effects or from the rain removal system which is a high temperature air jet [2]. In addition, the climate promotes significant changes in the dimensions of the acrylic layers due to absorption of water. The defects are described in this paper and have been discussed in terms of these service conditions and their effects on the mechanical properties of the acrylic layers.

DISCUSSION

Service-Induced Defects

The defects which render a windshield unserviceable are cracking, crazing, delamination and distortion. Seventeen defective BIRT windshields have been examined to obtain some estimate of the frequency with which these failure modes occur. All windshields showed crazing of the inner 0.08 in (2 mm) thick acrylic ply (Figure 1), while only ten outer plies were crazed; all crazing occurs at the exposed face. Six of these windshields were cracked, the cracks occurring in the outer acrylic ply and always transverse to the long axis. Bad delamination was found in one windshield, and all windshields showed some evidence of this defect located on the edges between the outer acrylic and the first interlayer. Only cracked or crazed windshields, but not all, showed evidence of heat damage from the rain removal system, however none had been rejected due to the distortion caused by this system alone. Figure 3 shows a BIRT windshield with cracks and distortions, the same windshield was crazed but only on the inner ply. The service lives of these transparencies was generally less than 500 flying hours, and so less than half the expected 4 year usage was achieved.

Four ADBIRT windshields have been examined; in all cases the acrylic ply (Figure 2) was crazed, and on one it was also cracked. Heat damage, which was sufficient to cause local distortion of the structure, could be seen on three of these windshields, and in one it was so severe that it caused delamination. These second generation windshields had failed more rapidly than the first generation system, and in one instance failure occurred after only 30 flying hours when the transparency was rejected due to intense crazing.

The much thinner external acrylic ply in the ADBIRT system renders it more susceptible to heat damage by the rain removal system. None of the BIRT system had suffered delamination by overheating. The rain removal system is a hot air jet having a maximum temperature of 200°C [2], and continuous use for as long a 20 minutes in heavy rain has been reported. This temperature greatly exceeds the recommended maximum continuous use temperature for acrylic of 80-90°C [3]. Moreover, permanent distortion can be easily produced in this material when it is bent at 80°C for only half an hour at a maximum outer fibre stress of 13.8 MPa (2000 psi) then cooled to room temperature.

1. Cracking

The cracked BIRT windshields show little or no crazing of the outer ply, and besides the main crack other small cracks are seen which do not penetrate through the thickness. These cracks are always transverse to the long axis of the windshield. The initiation points for the main cracks are not at the edges but towards centre. Figure 4 shows this point for one of the cracks shown in the previous figure. This part of the fracture surface which shows very rough bands suggests intermittent growth during the early stages of cracking and similar features are seen in the small cracks. Figure 5 gives the appearance of a small crack when viewed in the plane of propagation and appears to show crack branching [4]. These features probably result from very high transient loads or long time intervals between periods of slow growth. When continuous growth occurs during the later stages of fracture the surface features are very similar to those described by Berry [5]. Their orientation through the thickness of the acrylic ply suggests failure by bending.

2. Crazing

The crazes seen in the internal acrylic ply of BIRT windshields are always aligned with the long axis. Their lengths are about 1 mm and the distribution is uniform over most of the windshield. The outer acrylic ply of both types of windshields may have crazes that are either oriented randomly or with a high longitudinal component. Their distribution is less uniform and they are much shorter, typically less than 0.2 mm. These crazes are very numerous with densities as high as 36 per mm^2. This difference in appearance indicates that conditions for the initiation and growth of crazes in the inner and outer acrylic plies are not similar.

A necessary requirement for formation of crazes is a dilational stress [6],and their orientation is at right angles to the major principal tensile stress. Longitudinal alignment of the crazes in the inner acrylic layer of BIRT windshields show that this stress is in the hoop direction. Such stress may have been applied during installation when the radius of curvature is increased, or during pressurization of the crew module. Random orientation will arise from a uniform biaxial stress, or by a change in direction of the major principal stress during growth, or even by initiation and growth events occurring more than once. The shapes of the crazes (Figure 6) seen in a crazed ADBIRT indicate all of these possibilities.

The internal structure of these crazes (ADBIRT) was revealed by the fracture parallel to their growth plane, and the banded appearance (Figure 7) suggests intermittent growth. However sectioning at right angles (Figure 8) indicates the crazes are micro-cracks, and a scanning electron micrograph of the surface (Figure 9) confirms they are open at the surface. Thus the appearance in Figure 7 could also be due to the craze having become a crack at the surface. This failure then might have been a single event in the life of the windshield rather than a type of fatigue process.

3. Delamination and Distortion

Windshield deficiencies due to delamination and distortion were not investigated any further than the observations given in the first part of this discussion.

Studies on the Crazing of Plexiglas-55

Since crazing was the most common failure mode of these windshields, a study of the properties of the acrylic used in their construction has been carried out, taking into account likely environmental parameters they would experience. All of these windshields were manufactured by PPG Industries, and contained Plexiglas-55 from Rohm and Haas [7]. This acrylic was used in the study, however, the results in general are applicable to those modified acrylic sheets conforming to MIL-P-8184B manufactured by the other two registered suppliers.

Crazing in plastics occurs at tensile loads less than the yield stress, and has been thoroughly reviewed by Kambour [8], and by Rabinowitz and Beardmore [9]. The minimum load required or its associated strain are known as critical values, however they are by no means material constants. Many factors may influence the values, for example, temperature, time, fluids fatigue, orientation and platicization, and although studies of these have been reported it is not easy to determine the likely cause of crazing in service. Besides the weather, other variables that need to be considered are service stress, environment, and maintenance procedures. In assessing some of these, the standard crazing test in the military specification MIL-P-8184B has been adopted with variations: loads other than 13.8MPa (2000 psi) and test bars kept moist with the test fluid for the whole period (30 minutes) of the experiment [10].

Water is readily absorbed by acrylic polymers with an increase in volume yet its influence on their craze resistance has only recently been studied [11]. The stress to craze Plexiglas-55 at 25°C using isopropanol falls with increasing water content of the plastic (Figure 10). The effect is not due to plasticization by water but due to a tensile stress at the surface as a result of a non-uniform distribution of the water. During the test the surface of the test-piece dries out, but because of the constraint imposed by the core this surface cannot shrink so a uniform biaxial tensile stress is produced. This stress can be so large that an external load does not have to be applied when the specimen is treated with isopropanol, and the crazes produced are completely random in their orientation. This situation occurs when the Plexiglas has a water content of about 2.35% or 62% of the maximum content at saturation. It can be shown that the stress developed by this desorption does not depend on the actual water distribution provided it is symmetrical about the centre, or if the sheet is constrained from bending but not in changes of shape [12]. This latter requirement is true of the acrylic plies in the windshields, and this design will maximize the stress at the surface due to this effect. All of the failed windshields had been cleaned with a 1:1 isopropanol-water mixture, (V/V).

Although water absorption is undoubtedly a major factor in the reduction of the critical stress for crazing, several failures seem to have occurred too rapidly. In one instance, an ADBIRT was severely crazed after only 30 flying hours, or less than 2 months service. The calculated time [13] required for dry acrylic on an ADBIRT to reach 2.35% water content with absorption only occurring through the exposed face is 35 days when the face is maintained in 100% RH conditions at 25°C. The equivalent time for the outerply of a BIRT is 140 days. Figure 11 shows calculated absorption curves for the outer plies of both styles of windshield using a value for the diffusion coefficient of 1×10^{-8} cm^2 sec^{-1} [14]. In addition, assuming that water absorption obeys Henry's Law then for a content of 2.35% to be achieved the windshields would have to be exposed to relative humidities in excess of 62% RH. However at higher temperatures, the water content necessary to cause solvent crazing, without having to apply a load, would be less than this critical value of 2.35%.

The prevailing climate at Amberley (27°38'S; 152°43'E; elevation 25 metres) where the Australian F111C aircraft are based is warm and humid [15]. This climate is summarized in Figure 12 which depicts the fraction of a year for which the humidity or temperature is less than a selected value. Water contents of 2.35% should be attainable since humidities in excess of 60% occur for most of the year.

Conditions are available for water absorption to occur at elevated temperatures either from aerodynamic heating or from use of the rain removal system. To investigate these conditions Plexiglas-55 test pieces were immersed in water at different temperatures before performing the crazing test. The time of immersion was selected so that the water contents of all the pieces were similar and less than 0.2%. The specimens were loaded at room temperature (25°C) and ispropanol was used as the crazing fluid. For

immersion temperatures of 80° and higher the hot water pre-treatment is catastrophic. Despite the absolute water content being low, the acrylic crazes without having to apply any load. The test data are summarized in Table 1.

When water at temperatures greater than 80°C is being absorbed by the Plexiglas, the compressive stress, which usually occurs in the surface due to absorption, is not produced. This arises from the ability of water to plasticize the polymer sufficiently at these temperatures for the material to deform easily. Thus on cooling to room temperature the surface layer will be saturated with water but at low stress. Desorption of the water at room temperature now creates a tensile stress in the surface even though the total water content of the material is small. These facts are summarized in diagrammatic form in Figure 13 showing how the stress at the surface for the experiments described varies with water content for absorption and desorption at different temperatures. The diagram assumes that changes in dimension with water content are linear, that Hooke's Law is obeyed and that the change in modulus with water content is not significant.

The experiments described show that the acrylic can be crazed at very low appled stresses by isopropanol after pre-treatments which closely simulate the service conditions of the material. The windshields may also come into contact with many different liquids. Table II gives some data on the measured minimum stress to craze Plexiglas-55 by various fluids some of which may be found around an aircraft. These measurements, though, are only of the stress required to initiate a craze, once a craze is formed growth can occur at much lower stress. Recent measurements on crazing with 1:1 isopropanol/water mixtures show that the craze will grow at a stress of 13.8 MPa (2000 psi) which is less than half that required for initiation.

Conclusion

Failure of windshields in service appears to be due to the variety of ways in which tensile stresses can arise. Humidity, temperature and the design of the windshield all contribute to produce conditions whereby these stresses may develop, and the situation can be exacerbated by various fluids. For these reasons use of isopropanol/water mixtures to clean transparencies has been stopped, and only water with or without a non-ionic surfactant is now allowed. In addition, pilots and navigators have been directed to minimize their use of the rain removal system; however, their theatre of operation still demands occasional prolonged use of this system.

REFERENCES

1. Saito, T.T., Taboada, J. and Altschuler, B.B., Conference on Aerospace Transport Materials and Enclosures, R.E. Wittman (Ed.), p. 640, Dec. 78, AFFDL-TR-78-168.

2. Liggitt, F.R. and Fagan, R.T., "Study means of assuring that rain removal system operation will not damage optical characteristics of the polycarbonate windshield", Final Engineering Report, Nov. 1977, FZA-12-116, General Dynamics (Fort Worth Division).

3. Rohm and Haas, Plexiglas Sheet Physical Properties, Plexiglas Design and Fabrication Data, PL-229n.

4. Broek, D., Elementary Engineering Fracture Mechanics, Noordhoff International Publishing, The Netherlands, 1974.

5. Berry, J.P., "Fracture of Polymeric Glasses", in Fracture - An Advanced Treatise, Vol. VII, H. Liebowitz (Ed.), Academic Press, 1972.

6. Sternstein, S.S. and Ongchin, L., Polymer Preprints 10(2), 1117, 1969.

7. Private Communication, PPG Industries, Inc., Huntsville, Alabama, 1982.

8. Kambour, R.P., J. Polym. Sci. Macromol. Rev., 7, 1-154, 1973.

9. Rabinowitz, S. and Beardmore, P., CRC Critical Reviews in Macromolecular Science 1, 1-45 (1972).

10. Private Communication, Dept. of the Navy, Naval Air Engineering Centre, Lakehurst, N.J., 1982.

11. Burchill, P.J. and Stacewicz, R.H., J. Mater. Sci. Lett. 1, 448-450, 1982.

12. Parkus, H., Thermoelasticity, Springer-Verlag, New York, 1976.

13. Crank, J., The Mathematics of Diffusion, Clarendon Press, 1956.

14. Burchill, P.J., Unpublished data.

15. Murrell, B.T. and McRae, J.A., Climatic Conditions at Air Force Bases in Australia, Oct. 1980, MRL-R-787.

TABLE 1

Minimum Stress to Craze Plexiglas-55 with Isopropanol at 25°C after Brief Immersion in Water[#].

Immersion Temperature °C	Stress MPa
25	25
50	22
60	16
70	14
80	0
100	0

[#] Water absorbed during immersion less than 0.2% w/w.

TABLE 2

Minimum Stresses to Craze Plexiglas-55 at 25°C by Various Liquids

Test Fluid	Plexiglas-55 Dry	Plexiglas-55 Saturated with Water
Water	79 MPa	32 MPa
Water/Isopropanol 1:1	42	4
Isopropanol	25	0
Iso-Octane	59	26
Lubricating Oil (a)	58	22
Cleaning Fluid (b)	50	23
Degreasing Detergent (c)	50	14
Plastic Polish (d)	>66	34

(a) Turbine Engine Lubricating Oil, Jet Oil II, MIL-L-23699B

(b) Turco Jet Clean B, Def. Aust. 5570.

(c) Detergent Emulsion, Def. Aust. 5157.

(d) Plastic Polish Acrylic Conditioner, MIL-C-18767A.

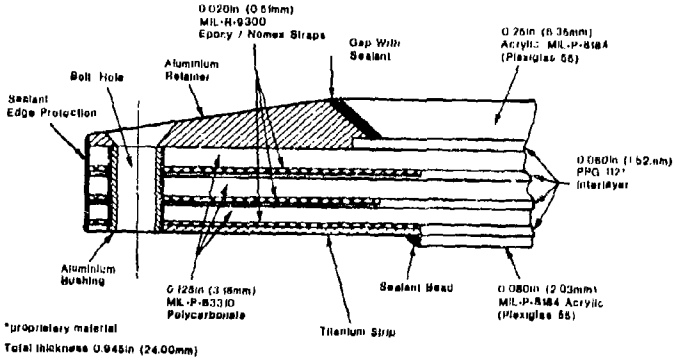

FIGURE 1 - Cross Section of BIRT windshield at the aft arch.

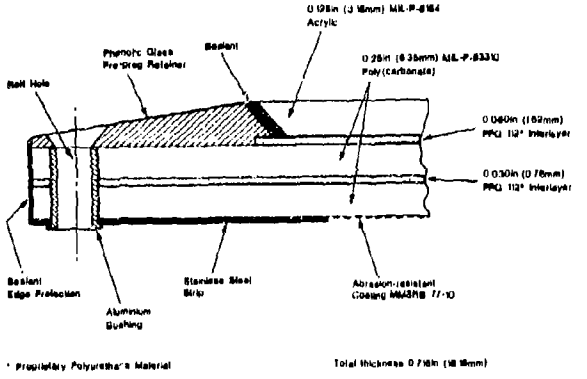

FIGURE 2 - Cross section of ADBIRT windshield at the aft arch.

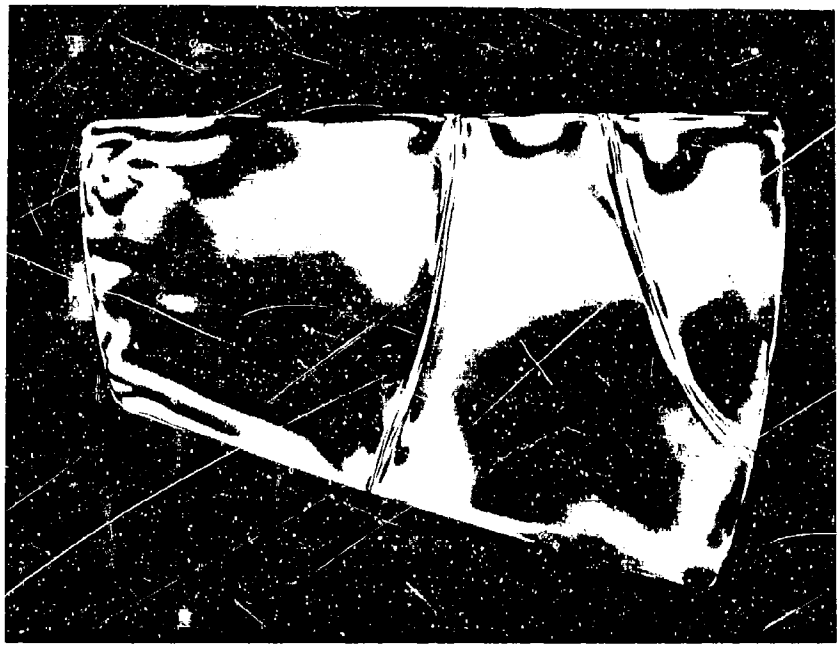

FIGURE 3 - Cracked BIRT windshield showing distortions at the forward arc (L.H.S.) due to heat damage seen using polarized light.

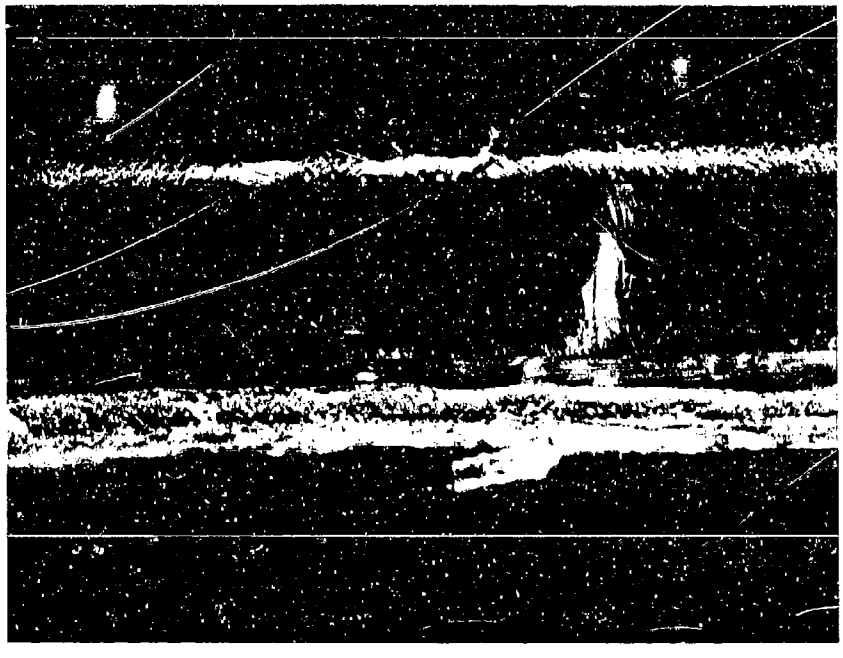

FIGURE 4 - Initiation zone for one of the cracks shown in Figure 3.

FIGURE 5 - Small crack viewed along the plane of propagation, actual length 4 mm.

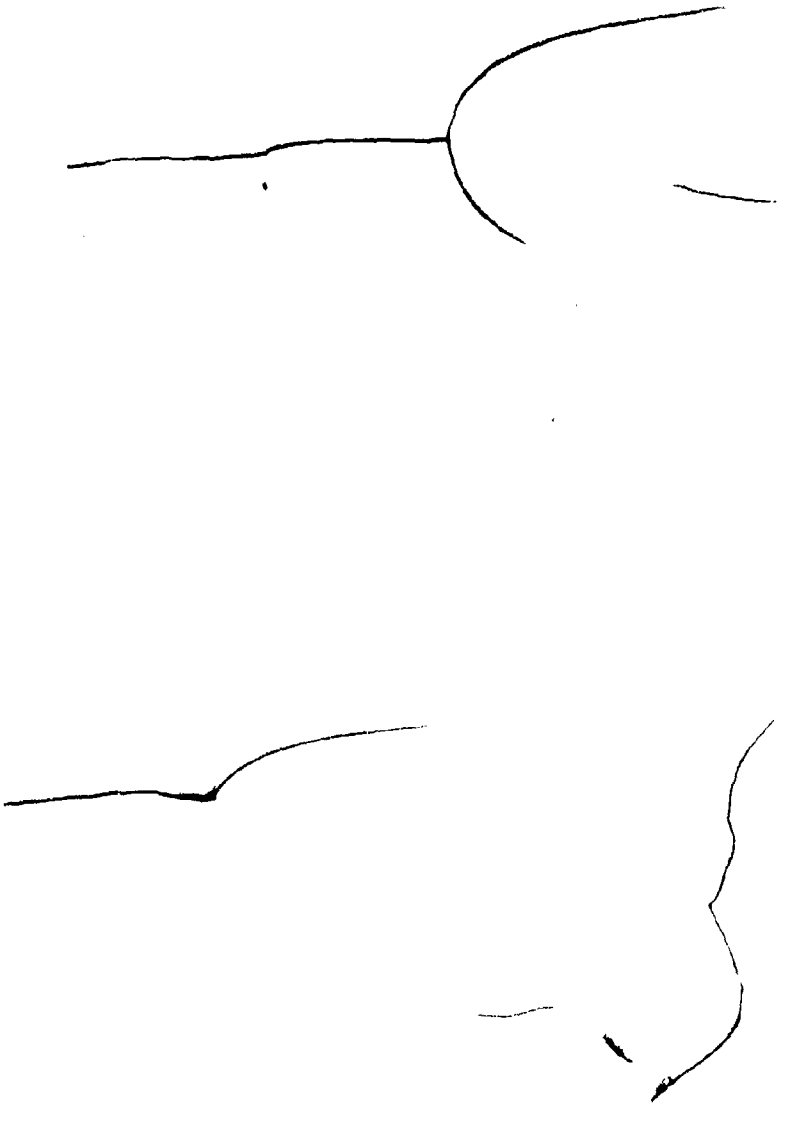

FIGURE 6 - Craze shapes seen on an ADBIRT windshield.

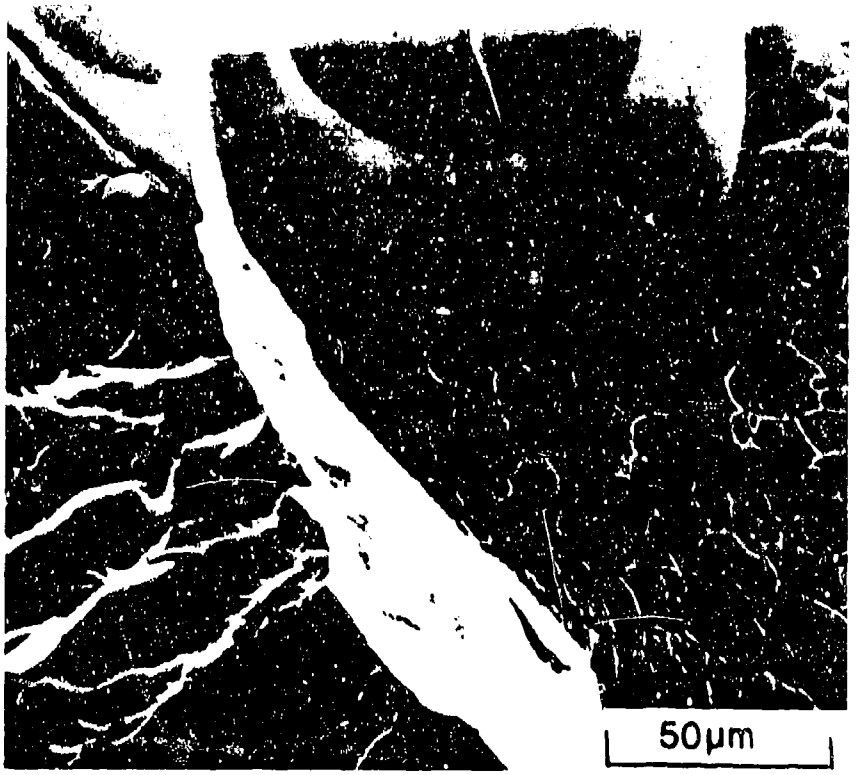

FIGURE 7 - Internal structure of these crazes - acrylic layer broken parallel to growth plane.

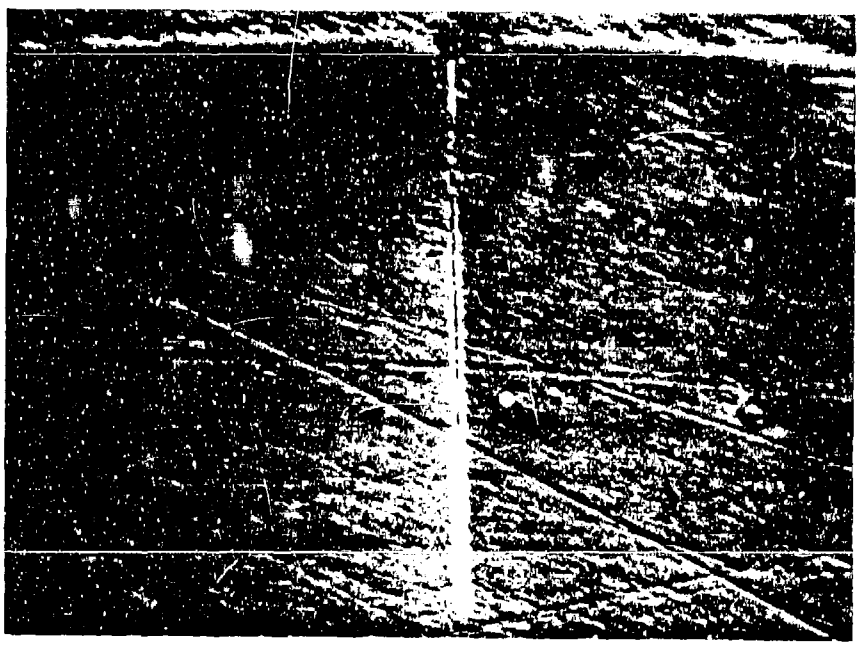

FIGURE 8 - Internal structure of these crazes - acrylic layer sectioned perpendicular to growth plane.

FIGURE 9 - Surface appearance of these crazes.

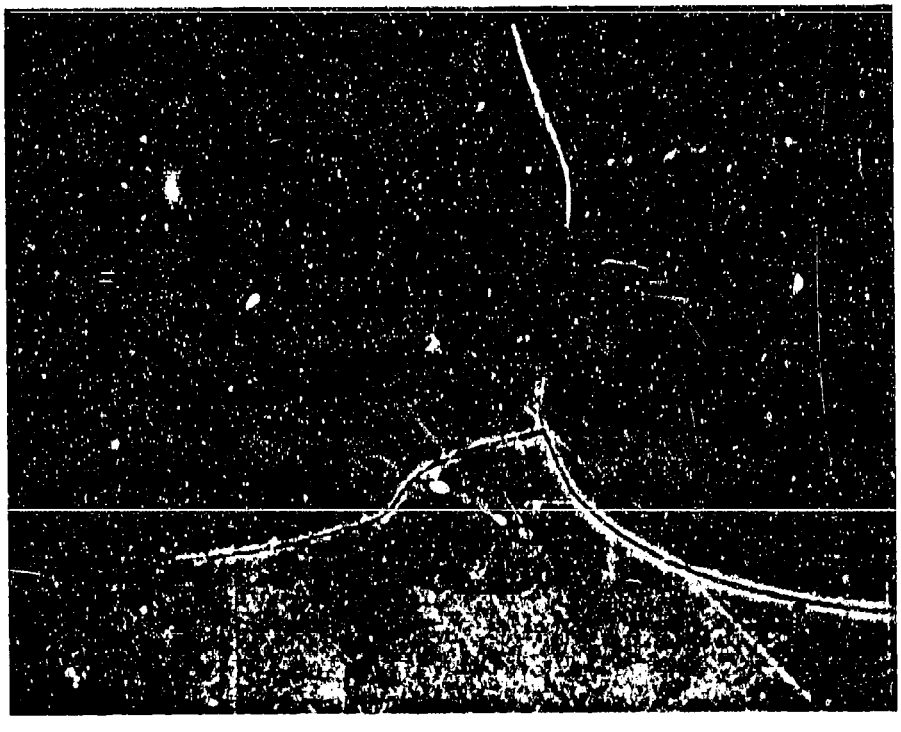

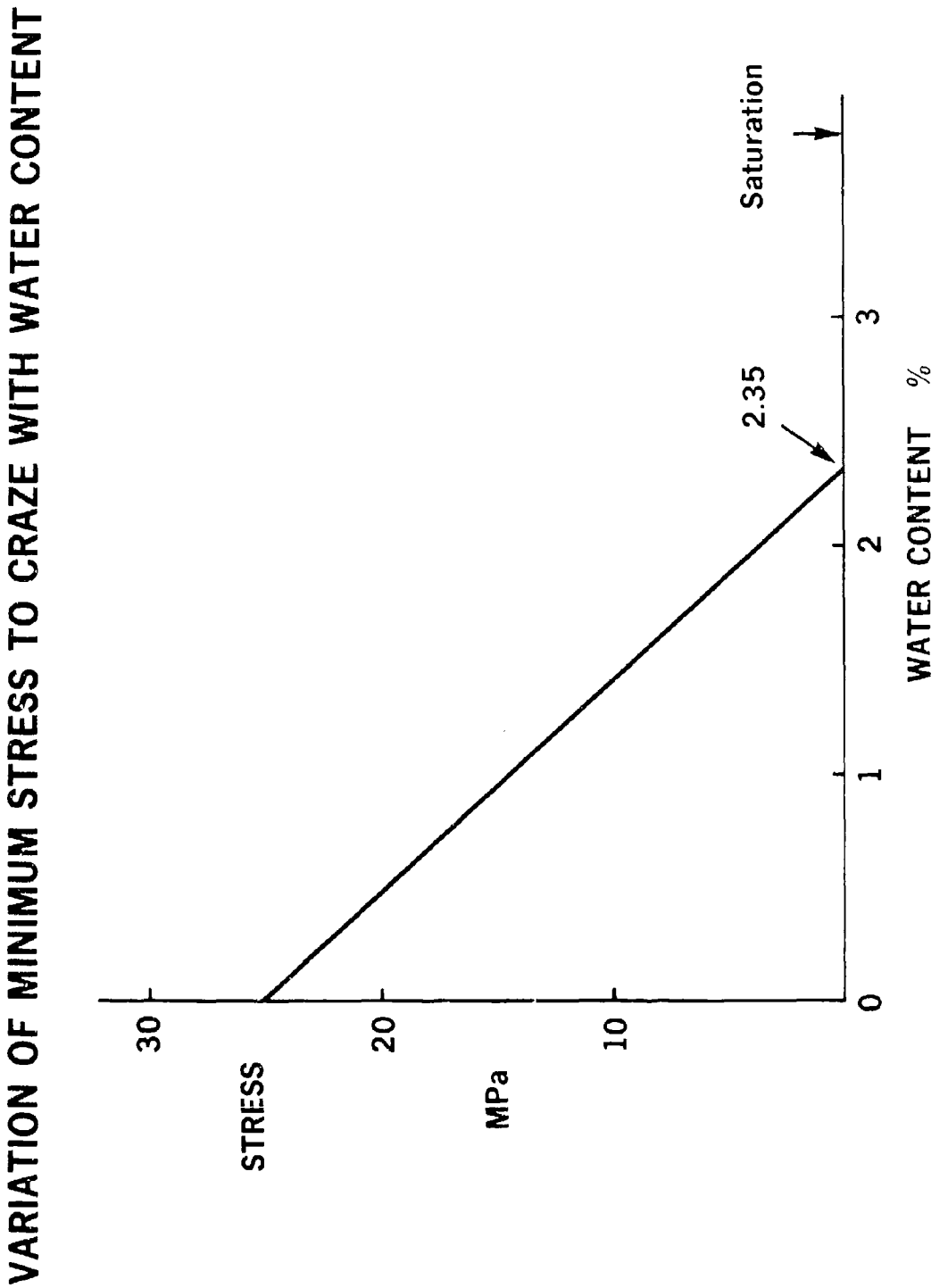

FIGURE 10 - Effect of water content of the Plexiglas-55 on the minimum stress to craze this material using isopropanol.

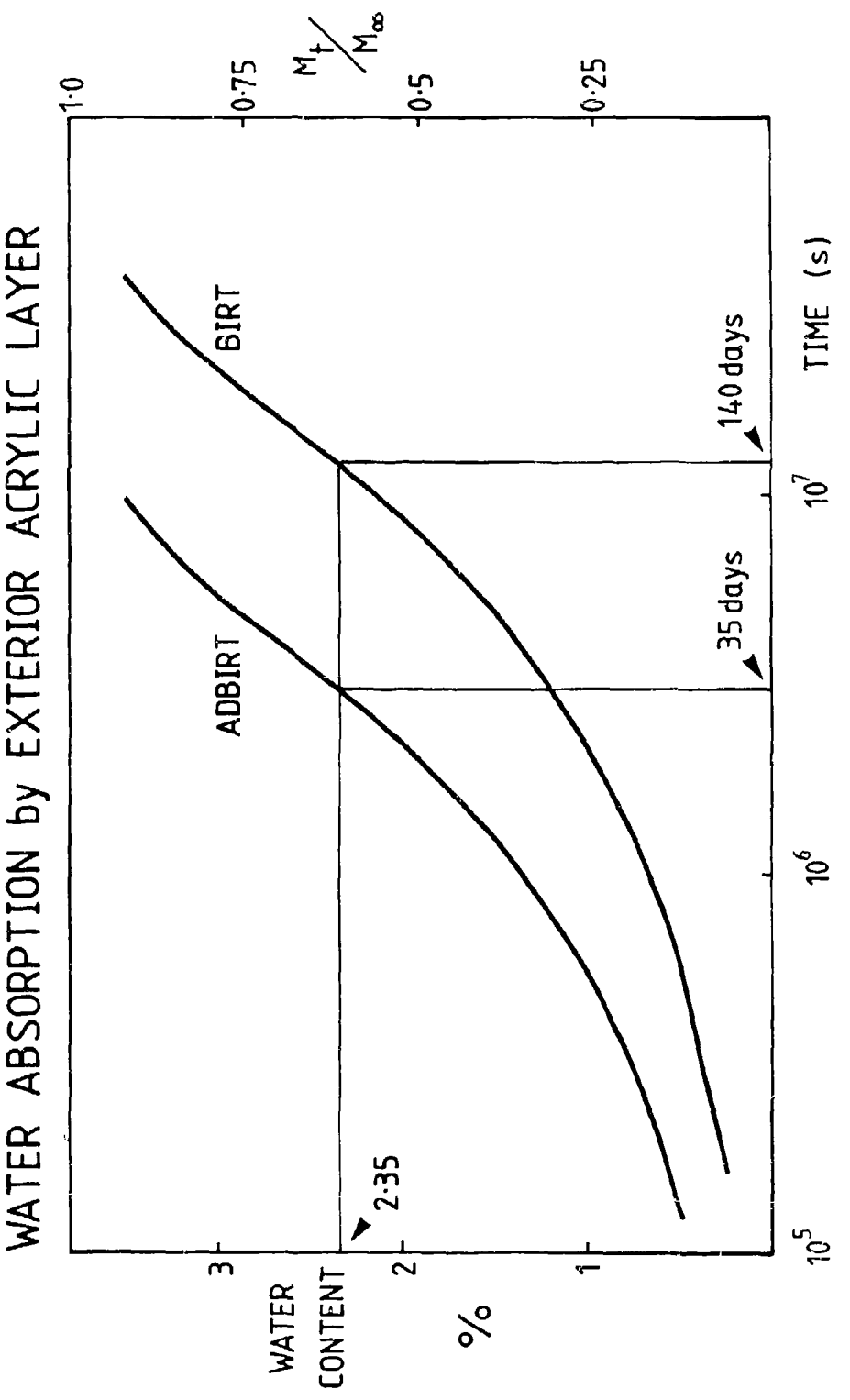

FIGURE 11 - Rate at which water is absorbed by the external acrylic layers of BIRT and ADBIRT windshields, (Mt/Mα is the mass absorbed at time t over the mass absorbed at infinite time).

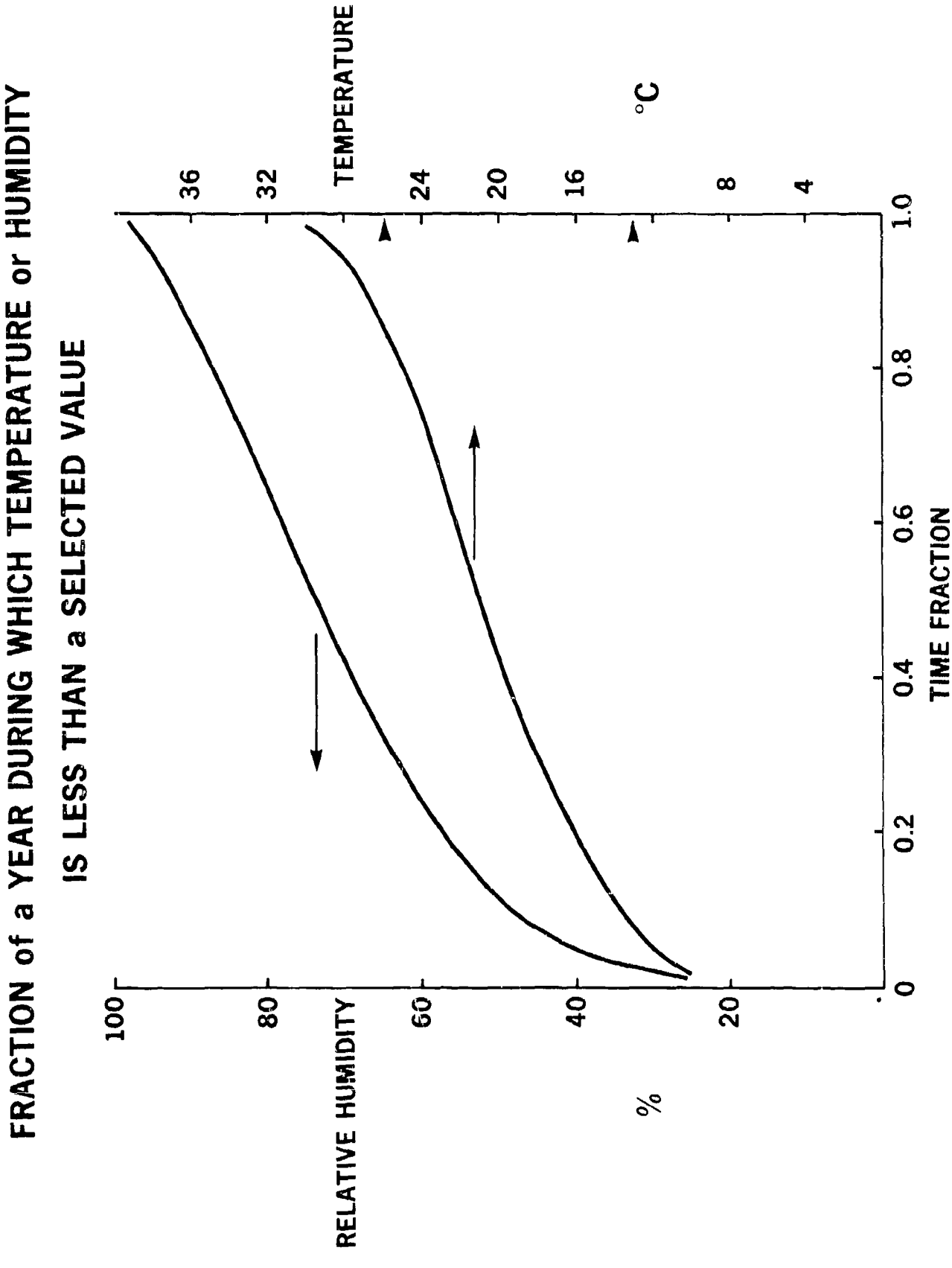

FIGURE 12 - Climate at Amberley : fraction of a year for which the temperature or humidity are less than a selected value. Arrows on the temperature scale mark the average annual maximum and minimum temperatures.

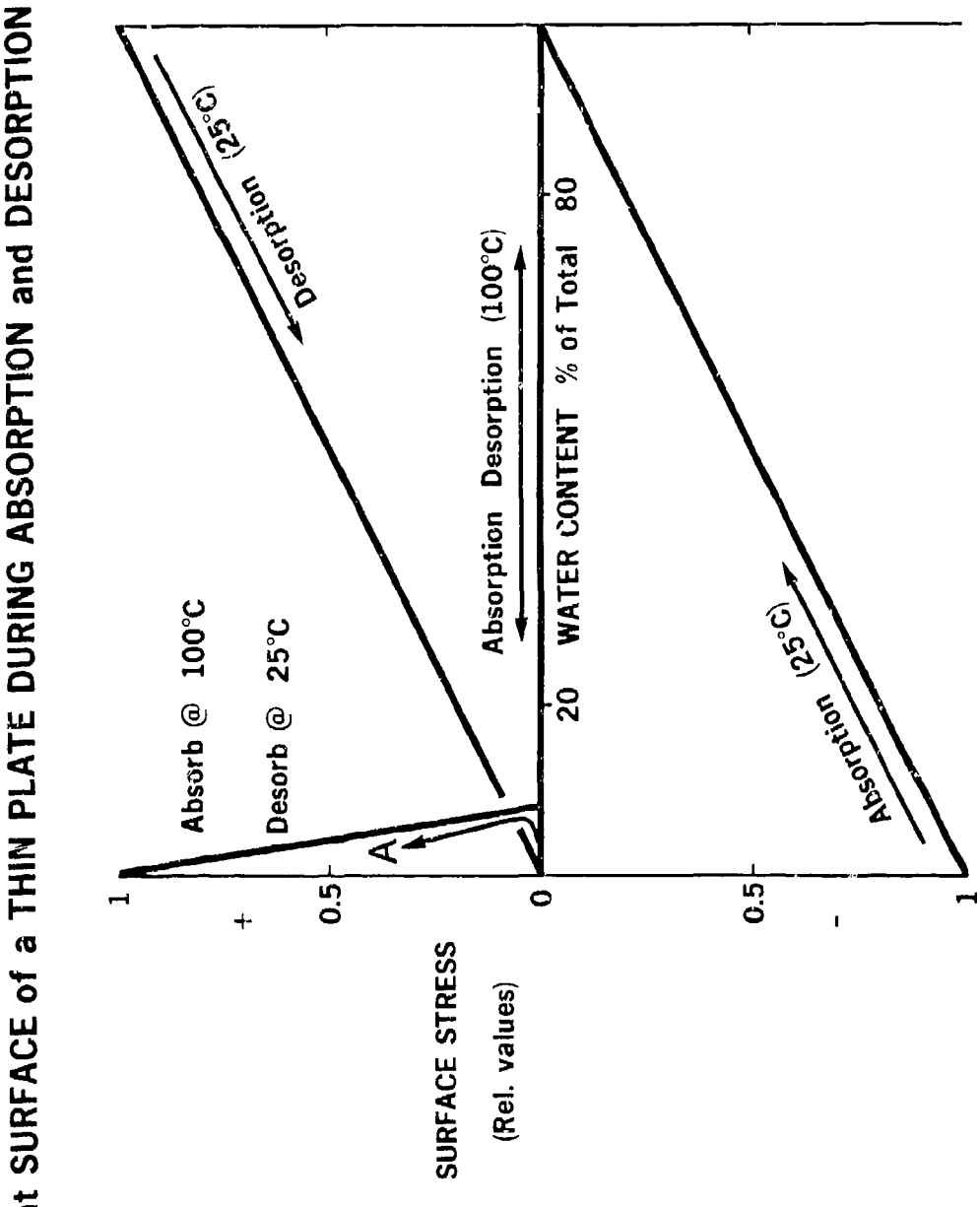

FIGURE 13 - Relative stresses at the surface of a thin plate during absorption and desorption of water at 25° and 100°C. A, this arrow indicates how the stress varies due to absorption at 100°C followed by desorption at 25°C.

FIGURE CAPTIONS

1. Cross Section of BIRT windshield at the aft arch.

2. Cross section of ADBIRT windshield at the aft arch.

3. Cracked BIRT windshield showing distortions at the forward arc (L.H.S.) due to heat damage seen using polarized light.

4. Initiation zone for one of the cracks shown in Figure 3.

5. Small crack viewed along the plane of propagation, actual length 4 mm.

6. Craze shapes seen on an ADBIRT windshield.

7. Internal structure of these crazes - acrylic layer broken parallel to growth plane.

8. Internal structure of these crazes - acrylic layer sectioned perpendicular to growth plane.

9. Surface appearance of these crazes.

10. Effect of water content of the Plexiglas-55 on the minimum stress to craze this material using isopropanol.

11. Rate at which water is absorbed by the external acrylic layers of BIRT and ADBIRT windshields, (M_t/M_α is the mass absorbed at time t over the mass absorbed at infinite t me).

12. Climate at Amberley : fraction of a year for which the temperature or humidity are less than a selected value. Arrows on the temperature scale mark the average annual maximum and minimum temperatures.

13. Relative stresses at the surface of a thin plate during absorption and desorption of water at 25° and 100°C A, this arrow indicates how the stress varies due to absorption at 100°C followed by desorption at 25°C.

AD-P003 196

SOME CRAZING EXPERIMENTS ON "AS-CAST" ACRYLIC TO MIL-P-8184

K. B. Armstrong, British Airways

SOME CRAZING EXPERIMENTS ON "AS-CAST" ACRYLIC TO MIL-P-8184

K. B. ARMSTRONG

BRITISH AIRWAYS

ABSTRACT

This short paper describes the findings of three separate experiments carried out to provide information for airline use.

The first set of experiments was done to provide threshold crazing stress data on "As-cast" acrylic to MIL-P-8184 using a variety of fluids likely to be found in an airline environment.

The second set of experiments was done to study the effect of water soluble cutting oils on acrylic. The oils were for potential use as corrosion inhibitors on a machine for sanding acrylics.

The third and smallest experiment was to study the effect of de-icing fluid (propylene glycol) on cast acrylic following the discovery of de-icing fluid between the inner and outer panes on Trident passenger windows.

The results of these experiments led to the measurement of a crazing stress for water and also cast doubt upon using threshold crazing stresses after 30 minutes testing. It would appear that some fluids do not reach their threshold in 30 minutes and need to be tested for a longer time.

INTRODUCTION

This paper consists of three quite separate parts limited by the common concern with materials that craze acrylics and the use of MIL-P-8184 acrylic for all the tests.

The first series of tests are listed in Table 1 and give the threshold crazing stress values obtained for a number of fluids likely to contact aircraft windows. Testing was to European Standard EN 2155 Part 19, Cantilever Beam Test; but using higher stress levels. The values given were obtained after the standard test period of 30 minutes.

The second series of tests was conducted in the same way but for a different purpose. In this case the objective was to assess the effect of four water-soluble cutting oils for use with a sanding machine for the removal of crazing from acrylic windows. The oils were to be used as rust inhibitors and it was necessary to check whether they would damage the acrylic material being sanded. In the course of this work a crazing stress for water was obtained.

The third experiment also used the cantilever beam test to measure the threshold crazing stress of propylene glycol. Testing was carried out because during the particularly cold winter of 1981/82, Trident aircraft had been found with up to 2 inches of fluid lying between the inner and outer panes of some passenger cabin windows. Infra-red spectroscopy revealed that the fluid was propylene glycol, which is regularly used as a de-icing fluid. The fluid had been present for some time when it was discovered and so testing was continued for several hours rather than the usual 30 minutes. It was found that the threshold crazing stress was very dependent on the time under stress before measurement of the distance along the beam that crazing had progressed.

DISCUSSION

A study of Table 1 is interesting, in particular the discovery that water alone has a crazing stress of about 9,000 psi in the standard test. It would appear to be the safest cleaning material of those tested. However, several other fluids or vapours cannot be completely avoided. Kerosene fumes, de-icing fluids and aircraft cleaners are used

...../Continued.

universally but the sooner they are washed off with water the better. Some de-icing fluids are not as safe as Propylene Glycol.

Of the two cleaners tested, admittedly at 100% concentration and not the usage dilution with water, "Ceebee" 280 would seem to be the safest. The Ardrox material contains small quantities of chemicals known to be damaging in themselves. As a result of these tests Ambersil Cleaner was banned for use as a window cleaning material.

These tests also showed that the threshold crazing stress method of comparing fluids is not as clear cut a method as it might be. For example, stabilised 1,1,1 Trichloroethane sold as "Genklene" and under other trade names had a threshold crazing stress somewhere in the range 3,600 psi to 4,900 psi on two samples. The specimen with the higher value failed in 20 mins, the lower one had not fractured in the 30 minute period of the test. However, MEK caused crazing to spread rapidly down the beam, gave a threshold crazing stress of 1,200 psi, but did not cause fracture in 30 minutes. A further test gave a value as low as 600 psi.

Chemicals such as de-icing fluids or cleaners would need to be tested more thoroughly over longer periods of time. The standard 30 minute test would not seem to be adequate to assess likely long term damage for all materials. It does appear adequate for the more severe solvents.

The second series of tests is illustrated by Fig.1 which shows the time to fracture in the cantilever beam test of various concentrations of Castrol Syntilo 3 in water. Four oils were tested, Table 2, and all appeared safe enough for use at the recommended dilution. Syntilo 3 was selected for further investigation after the initial trial because odd effects were found. All four oils were tested at 6,000 psi and no crazing was caused.

The same specimens were then tested again at the recommended working dilution of 1.25% oil in water. Two of the oils caused crazing and two did not. Tests were then carried out on new specimens at the working dilution of oil and no crazing occurred. To check these results a further test using 100% oil was done; this time for one hour and no crazing occurred. A re-test of this specimen using oil at the working dilution also caused crazing, Table 2. This led to the view that this particular oil might be damaging at some mix ratio of oil and water between 100% and 1.25%.

...../Continued.

To ensure that results were obtained the stress was raised to 9,000 psi maximum and tests were carried out at oil concentrations of 100%, 90%, 70%, 50%, 40%, 35%, 30%, 25%, 20%, 10%, 1.25% and finally NIL % oil, i.e. pure water. Under these conditions many test pieces fractured and effort was then concentrated on time to fracture versus % oil, Fig.1, instead of threshold crazing stress. If a specimen did not last 30 minutes then a threshold crazing stress could not be obtained for the same time for each specimen.

Fig.1 shows clearly that in this case the most damaging fluid is the water, not the oil. This was a very unexpected result. After getting a fracture at 1.25% oil, two tests were carried out with water alone and at 9,000 psi crazing could be seen to form and fracture occurred in 1 minute. No fracture occurred in one hour with a new specimen and no water or oil. Some crazing but no fracture occurred in 95 minutes with 100% oil. At high enough stress levels water alone can cause crazing. Inspection of the specimens, crazed by water alone, was made a few days after testing when any "permanent" set that might have occurred had relaxed. No crazing could be seen. This would suggest that crazing can exist without being visible to the naked eye. It would further suggest that crazing as a result of normal service may begin before it can be seen and that when polishing aircraft windows the amount of material removed should be a little greater than the depth of visible crazing.

The various mixes of Syntilo 3 and water were kept in glass bottles with Polythene "Snap-on" tops. A number of the polythene tops fractured. This suggests a solubility parameter for Syntilo 3 close to polythene. From this it may be concluded that no polythene or similar tubing should be used with this fluid if any significant stress level is involved.

The final experiment was a standard cantilever beam test using Propylene Glycol. Over enthusiastic application of de-icing fluid to Trident aircraft during the cold winter of 1981/82 resulted in considerable amounts of fluid being trapped between the inner and outer passenger window panes. Because this fluid was trapped for several days in some cases these tests were continued beyond 30 minutes. Fig.2B, a logarithmic plot shows that for Propylene Glycol the stress below which crazing does not occur goes on getting lower with time. At the time of completing this report a true threshold for Propylene Glycol had not been reached at 168 hours. The curve

..../Continued

has since levelled off at 207 hours. (Test 2). The lower data (Test 1) was obtained using Kilfrost ABC (basically propyleneglycol with additives) obtained from between the window panes of a Trident aircraft. Crazing due to creep in a normal atmosphere follows this logarithmic law as does much other data for plastics.

A limited amount of further testing was done to see if other fluids showed a logarithmic reduction in threshold crazing stress with time. The fluids tested all showed that a 30 minute test was apparently sufficient to indicate a threshold - Fig.2A. Only Propylene Glycol, showed the continuously downward trend. Other similar fluids might behave in the same way. Eau de Cologne was tested because it was observed that it was used to remove flies and for window cleaning when nothing else was available. Fortunately, it appears to be one of the safer fluids.

Although Eau de Cologne caused crazing when applied to a tissue that kept the surface wet, under test at 6,000 psi a more practical test caused no crazing. In the second test Eau de Cologne was used to soak a tissue and the specimen was wetted for 30 minutes before test but without stress.

The fluid was wiped off with a rag before the load was applied. In this case a stress of 6,000 psi did not cause any crazing in 30 minutes.

A P.V.C. aerosol called "Vycoat" ACA60 advertised as a tough, flexible P.V.C. coating for sealing, encapsulating and waterproofing, was also tested. When applied to a test piece loaded to 6,000 psi it caused immediate crazing and its curve was so close to Methanol that it could not be separately plotted. The solvents in this material are said to be a blend of Acetone, MEK, Toluene and possibly Xylene. However, another test piece was given 5 spray coats of "Vycoat" in quick succession and allowed to dry at room temperature for 24 hours. This specimen was loaded to 6,000 psi for 23 hours and no crazing could be found.

These results suggest that more long term testing could be useful and that only extremely powerful solvents are likely to cause damage when used as cleaners and then wiped off. Practical experience provides some confirmation in that B747 No.2 and No.3 windows suffered very early fracture when fitted by Airlines and sealed with PR1422, which contains MEK, and then flown immediately. Windows sealed on the production line, where the MEK had time to evaporate, did not suffer this problem. The only fluid repeatedly and unavoidably applied is water so a long time test keeping the specimen wet as far as

..../Continued.

possible was run. The tissue usually dried overnight.

Previous data showed that in a tensile creep test a stress of 2,000 psi caused crazing after about 6,000 hours in air. It was thought that the time would be greatly reduced at 6,000 psi although the beam is a flexure test and not a tensile test. At the time of completing this paper to meet the time schedule the water crazing test had run 215 hours without any crazing indicating that water is even safer than pure turpentine, the next safest fluid of those tested. It is intended to continue this test to at least 1,000 hours to see if crazing due to water can occur at 6,000 psi.

CONCLUSIONS

1/ From the third series of tests it would seem that threshold crazing tests do not necessarily provide an accurate comparison of fluids in terms of damage likely to be caused and that fluids expected to be in contact with windows such as aircraft cleaners and de-icing fluids should be tested for longer periods of time.

2/ Water alone can cause crazing at high stress levels and long term tests using water might reveal a lower threshold crazing stress.

3/ There is a suggestion that for some fluids the threshold crazing stress reduces with time of test following a logarithmic law unique to each fluid. This would also suggest more long term tests for fluids used in contact with acrylics.

4/ Eau de Cologne and the solvent in "Vycoat" did not cause crazing when allowed to dry out before testing.

5/ Some fluids are more dangerous than they appear and can cause fracture above a particular critical stress although the threshold crazing stress they produce in the standard test is well above that of apparently more dangerous materials. Fluids tested that behaved in this way were stabilised 1, 1, 1 Trichloroethane and Turpentine. It would be useful to obtain a stress to cause fracture in 30 minutes for each fluid to compare with the threshold crazing stress obtained after 30 minutes.

..../Continued.

6/ In seeking threshold crazing stress the tissue was only kept wet at and beyond the point of crazing to avoid fracture at the maximum stress point. It was very clear from this that keeping the tissue wet all the time is important. Areas kept wet were more crazed at a lower stress than the maximum stress are left dry.

These results would suggest that when solvent crazing is found on acrylic windows the solvent used must have been a very powerful one. A test programme is needed to find those aircraft fluids able to cause crazing even when applied for a short time and then wiped off. This should reduce the number of offending materials considerably.

NOTE: Work carried out, since this Paper was completed, because of a crazing epidemic on B747 cockpit windows, has only found one fluid so far that meets the above requirement apart from paint stripper. Lockheed Automobile Brake Fluid Universal Series 329S does have this effect after being wiped off. It contains Polyalkylene Glycol Ethers.

TABLE I

CRAZING TESTS ON AS-CAST ACRYLIC TO MIL-P-8184

Threshold crazing stresses for the following fluids are given in Table 1 below.

Test Method - Cantilever Beam to European Standard EN2155 Part 19 using higher stresses. All tests for 30 mins.

TEST FLUID	THRESHOLD CRAZING STRESS	REMARKS
Ardrox 6025 4.5% IPA 2.5% Butyl Oxytol	4,900 psi	Aircraft Cleaning Fluid. Usage concentration 10% in water. Tested at 100% Ardrox.
"Ceebee" 280 Cleaner	No Craze at 6,000 psi	Aircraft Cleaning Fluid. Alkaline cleaner used at 20% in water. Tested at 100% concentration.
Industrial White Spirit	6,000 psi	Sometimes mixed with Aircraft cleaners.
Ambersil Cleaner	4,750 psi	Carpet Cleaner
Propylene Glycol	4,500 psi	De-icing Fluid

Table to be Continued....

TABLE 1 CONTINUED

Lockheed Commercial Auto Brake Fluid	3,000 psi	
Kerosene	4,750 psi	
MEK	1,300 psi 1,200 psi Repeat Test 600 psi	Crazed to about .05" depth; penetration to final depth in about 1 minute.
"Genklene" Stabilised 1, 1, 1 Trichlorcethane	4,900 psi	Fractured in 20 minutes.
	3,600 psi	Not fractured in 30 minutes.
Skydrol 7,000	5,600 psi	Hydraulic Fluid
Eau de Cologne	4,300 psi	
Methanol	2,100 psi	

TABLE 2

		Column 1	Column 2	Column 3
SPEC. NO.	TEST FLUID	THRESHOLD CRAZING THRESHOLD CRAZING STRESS 100% CONC	THRESHOLD CRAZING STRESS AT WORKING DILUTION OF 1.25% OIL USING SAME SPECIMENS AS COL.1	STRESS AT WORKING DILUTION OF 1.25% OIL USING NEW SPECIMENS
1	CASTROL SYNTILO 3	NO CRAZE AT 6,000 psi	CRAZED AT 6,000 psi	
4	MOBILE EXU66/286	NO CRAZE AT 6,000 psi	NO CRAZE AT 6,000 psi	
7	MOBILE SOLVAC 68	NO CRAZE AT 6,000 psi	NO CRAZE AT 6,000 psi	
10	MOBILE EU66/274	NO CRAZE AT 6,000 psi	CRAZED AT 6,000 psi	
5	CASTROL SYNTILO 3	-	-	NO CRAZE AT 6,000 psi

Table to be continued....

TABLE 2 CONTINUED

6	CASTROL SYNTILO 3	NO CRAZE AT 6,000 psi TESTED FOR 1 HOUR	CRAZED AT 6,000 psi	-
	WATER	CRAZED AT 9,000 psi	-	-
	WATER	CRAZED AT 9,000 psi	-	-
	NONE	NO CRAZE AT 9,000 psi AFTER 1 HOUR	-	-
	CASTROL SYNTILO 3	CRAZED AT 9,000 psi NO FRACTURE AFTER 95 MINS		

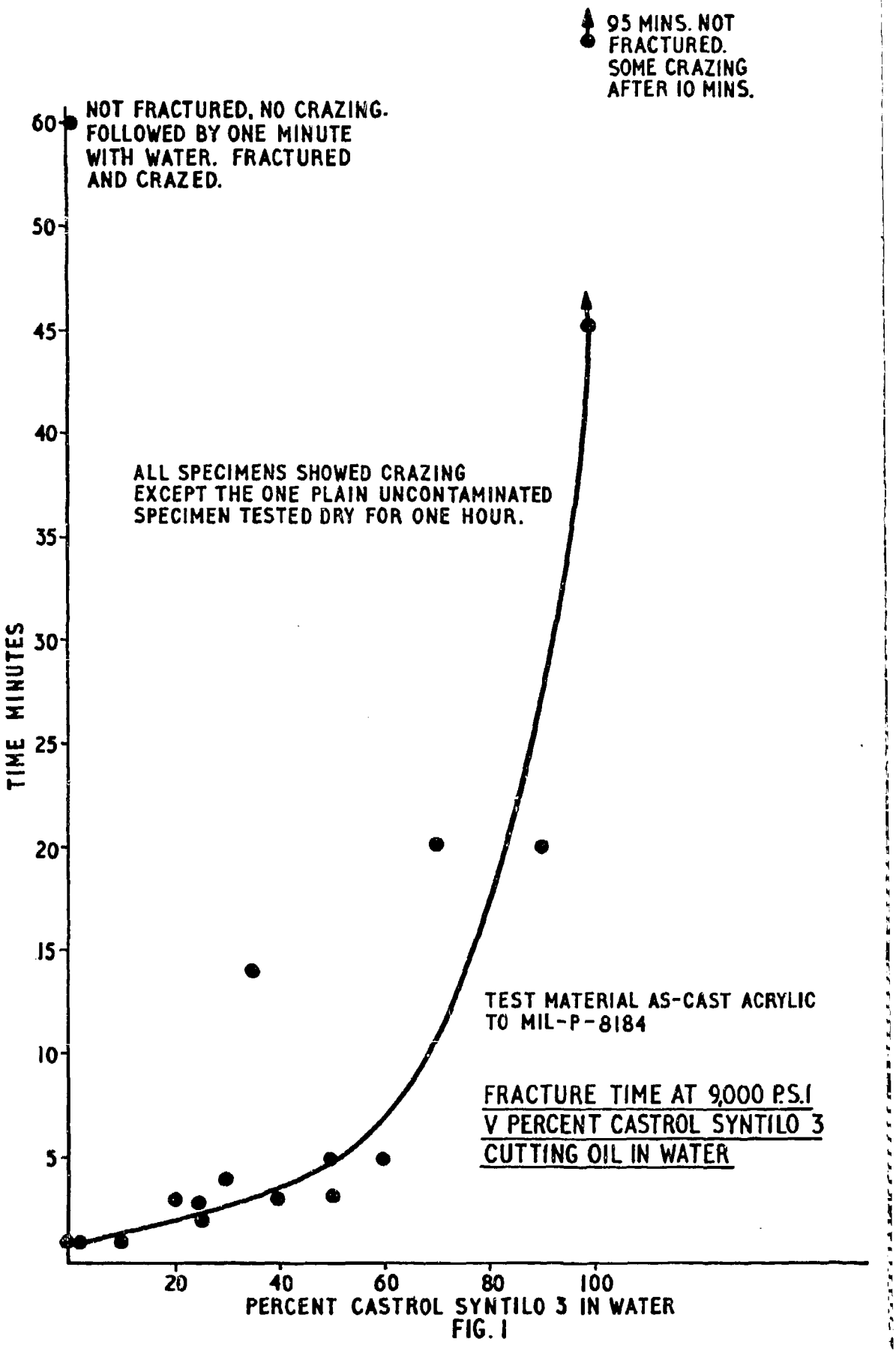
95 MINS. NOT FRACTURED. SOME CRAZING AFTER 10 MINS.
NOT FRACTURED, NO CRAZING. FOLLOWED BY ONE MINUTE WITH WATER. FRACTURED AND CRAZED.
ALL SPECIMENS SHOWED CRAZING EXCEPT THE ONE PLAIN UNCONTAMINATED SPECIMEN TESTED DRY FOR ONE HOUR.
TIME MINUTES
60
50
45
40
35
30
25
20
15
10
5
TEST MATERIAL AS-CAST ACRYLIC TO MIL-P-8184
FRACTURE TIME AT 9,000 P.S.I
V PERCENT CASTROL SYNTILO 3 CUTTING OIL IN WATER
20
40
60
80
100
PERCENT CASTROL SYNTILO 3 IN WATER
FIG. 1

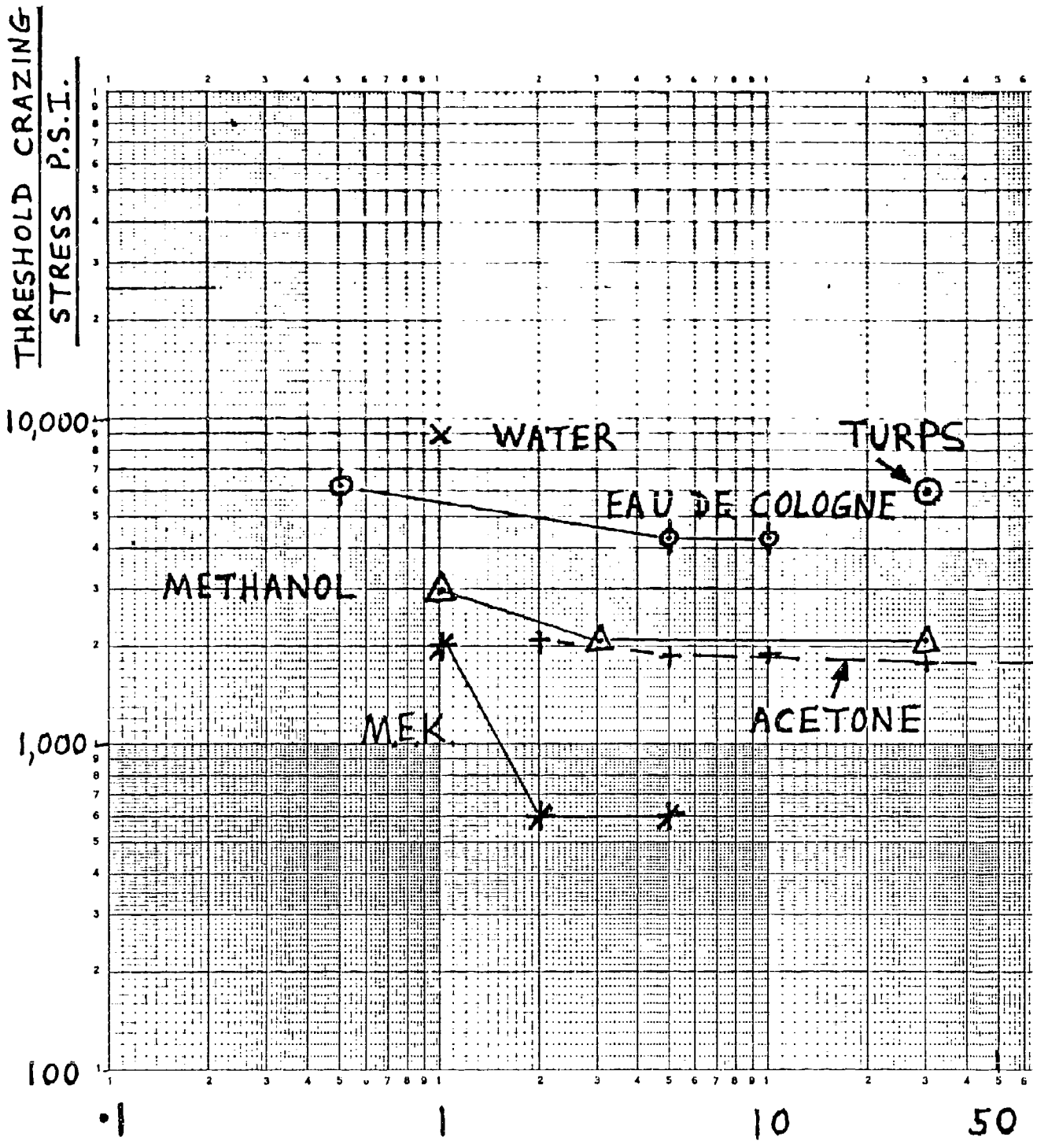
THRESHOLD CRAZING STRESS P.S.I.
10,000
1,000
100
WATER
TURPS
EAU DE COLOGNE
METHANOL
M.E.K.
ACETONE
·1
1
10
50
TIME (MINUTES)

FIG: 2A

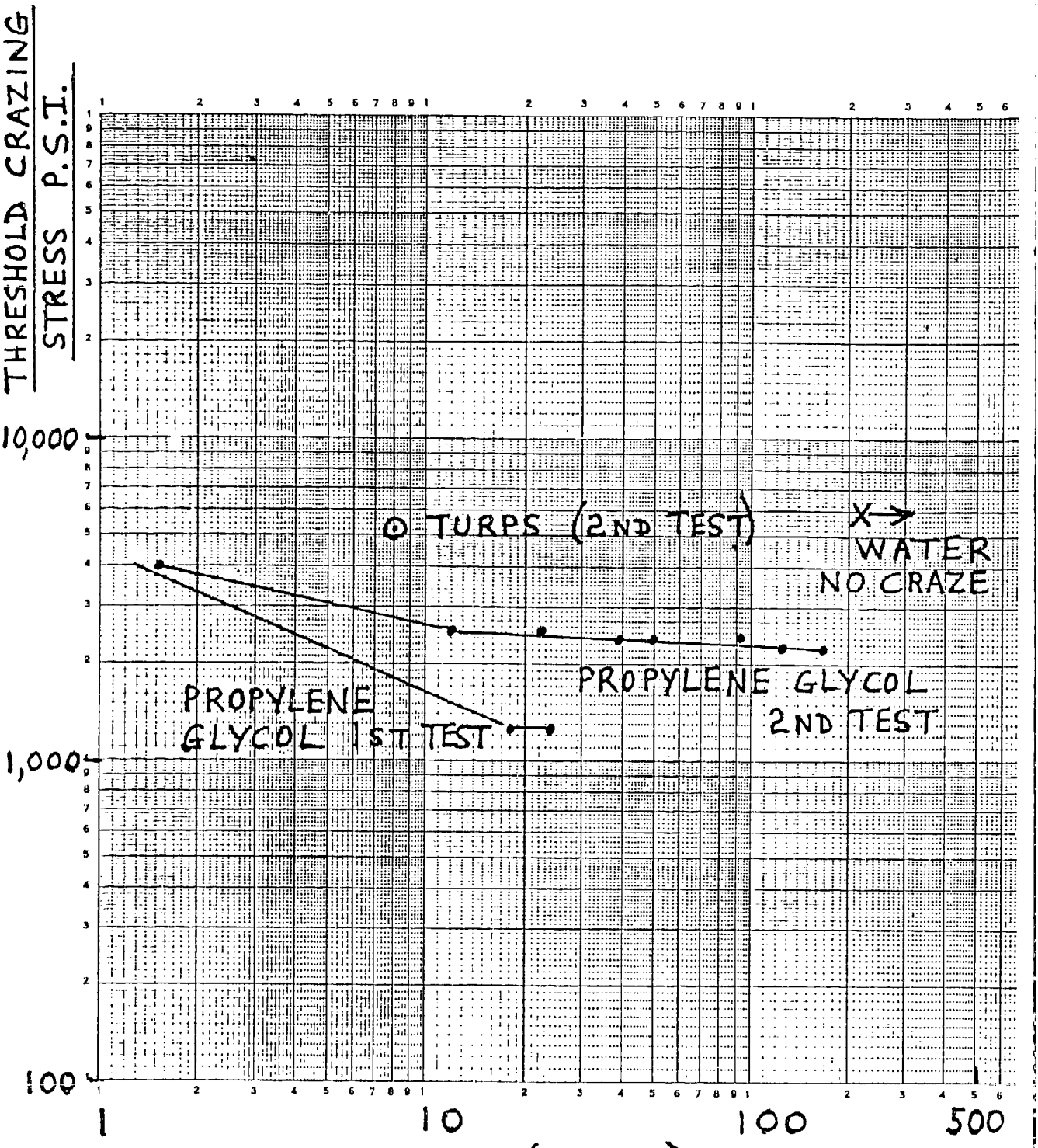
THRESHOLD CRAZING
STRESS P.S.I.
10,000
1,000
100
1
10
100
500
TIME (HOURS)
⊙ TURPS (2ND TEST)
X → WATER
NO CRAZE
PROPYLENE GLYCOL
2ND TEST
PROPYLENE
GLYCOL 1ST TEST

FIG: 2B

AD-P003 197

THE EFFECTS OF MOISTURE ON FRACTURE TOUGHNESS AND THERMAL RELAXATION OF STRETCHED ACRYLIC PLASTICS

J. Tirosh, Technion-Israel Institute of Technology and S. A. Sutton, Digital Technology, Inc., and P. W. Mast, R. W. Thomas, and I. Wolock, Naval Research Laboratory

THE EFFECT OF MOISTURE ON FRACTURE TOUGHNESS AND THERMAL RELAXATION OF STRETCHED ACRYLIC PLASTIC

J. Tirosh*, P. W. Mast, G. Nash, S. A. Sutton**
R. W. Thomas, I. Wolock

Naval Research Laboratory
Washington, DC 20375

Abstract

Studies were conducted to determine the effects of absorbed moisture on the thermal relaxation behavior and fracture toughness of stretched acrylic plastic. The thermal relaxation behavior was characterized by measuring shrinkback at elevated temperatures in accordance with Military Specification MIL-P-25690. The results indicate that the thermal relaxation behavior is affected significantly by the amount of absorbed moisture. Test results can be obtained on the same material that meet or do not meet the requirements of that specification, depending on the moisture content of the test specimens.

Fracture toughness tests were conducted over a range of loading rates and for different moisture contents, using the compact tension specimen. The material with a high moisture content had a higher fracture toughness (K_{Ic}) than dry material at lower rates of loading. At high loading rates, moisture content did not affect fracture toughness. Thus, if a specification stipulates a high loading rate for the fracture toughness test, control of moisture content is not necessary.

Data previously obtained on polycarbonate plastic indicates that this material has a higher fracture toughness than stretched acrylic for lower moisture contents. However, at high moisture contents, there is little difference between the two materials for the thicknesses and loading rates studied.

---

*Visiting Scientist, on leave from the Technion-Israel Institute of Technology, Haifa, Israel

**Current Address: Digital Technology Inc., Champaign, IL

INTRODUCTION

Stretched acrylic (polymethyl methacrylate) plastic was first used in aircraft glazing somewhat over 20 years ago. A military specification was adopted at that time, based on the use of modified acrylic sheet for stretching (Reference 1). Little attention was paid to the effects of absorbed moisture on the results obtained in the specified tests. It was apparently assumed that the specimens would be at ambient conditions prior to testing.

Approximately five years ago, it was reported that tests conducted at the Royal Aircraft Establishment in England indicated that absorbed moisture affected the thermal relaxation behavior of stretched acrylic. Tests were conducted using differential scanning calorimetry and thermomechanical analysis and showed that the temperature for the onset of thermal relaxation decreased with increasing water content. These and related results were subsequently published (References 2, 3, 4,). One question that remained was how did absorbed moisture affect the results obtained in the thermal relaxation test in MIL-P-25690A. A second question was how did absorbed moisture affect the fracture toughness of the stretched acrylic, a key property of this material.

The current investigation was undertaken to answer these two questions.

EXPERIMENTAL AND PROCEDURE

Materials

The stretched acrylic plastic was purchased from one of the fabricators in 1/4-inch (6.4 mm) and 1/2-inch (13 mm) thicknesses. The material conformed to MIL-P-25690A.

Test Specimens

The thermal relaxation specimens conformed to MIL-P-25690A. The specimens were 3-inches (76 mm) square. A 2-inch (51 mm) diameter circle was scribed on each specimen and the change in diameter measured as a result of each heating cycle.

A 2 x 2-inch compact tension specimen (Figure 1) was used for the fracture toughness tests. The specimens were machined and notched but not precracked before exposure to the various environmental conditions.

Conditioning

Some of the specimens were dried to constant weight in a vacuum oven at 160°F (71°C) for 15 weeks prior to testing. A second set of specimens was stored in a chamber maintained at 160°F (71°C) and 95% relative humidity for 5 weeks, using a saturated lead nitrate solution. A third set of specimens was stored in the laboratory at ambient conditions (approximately 72°F (23°C) and 50% relative humidity).

Test Procedure

Thermal relaxation: The specimens were placed in a circulating air oven at 230°F (110°C) for 24 hours and the diameter of the scribed circles measured to determine the shrinkback that had taken place. The specimens were then placed in an oven at 293°F (145°C) for 24 hours and the shrinkback measured again.

Fracture toughness: The test procedure followed the ASTM recommendation for plane-strain fracture toughness testing of metal (E399-74), and is described further in Reference 5. The loading rates, expressed as $\dot{K}$, (where K is the plane strain stress intensity factor) were 100, 400, 4000 and 20,000 psi$\sqrt{\text{in}}$/sec. The approximate times to failure for these loading conditions were 20, 5, 0.5 and 0.1 second.

TEST RESULTS

Thermal Relaxation Tests

The results are presented in Table 1 and in Figure 2. The MIL-P-25690A requirements are a maximum shrinkback of 10% at 230°F and a minimum shrinkback of 40% at 293°F. The data indicates that the thermal relaxation behavior at 293°F is affected significantly by the moisture content. Thus a less heat resistant material that would not meet the requirement of 10% shrinkback if tested at ambient conditions might meet the requirement if tested dry. The effect appears to be greater for 1/2-inch thick material than for 1/4-inch thick material.

The shrinkback at 293°F, which represents complete recovery of the material to its unstretched condition, is strictly a function of the degree of stretch of the material. This was not influenced by moisture content, as would be expected.

The results indicate that any test method or specification that involves partial thermal relaxation of stretched acrylic plastic should contain a requirement for control of moisture content.

There are other questions that have been raised regarding the MIL-P-25690A test method for thermal relaxation. This includes the variability of the results obtained at 230°F due to small deviations from the nominal exposure temperature. This effect was not investigated in this study.

Fracture Toughness Tests

The results obtained are presented in Figurs 3-7. In Figure 3, the dry material (0% moisture) exhibits a slight reduction in K_{Ic} with increased loading rate. The 1/4-inch thick material appears to exhibit a slightly lower toughness than the 1/2-inch thick material.

In Figure 4, the materials conditioned under ambient conditions and containing approximately 1.1% moisture exhibit toughness behavior similar to that for the dry material. In Figure 5, the material containing approxi-

mately 4% moisture exhibits a much greater loading rate sensitivity than the two previous materials. At the lower loading rates, the toughness is higher than that exhibited by the materials with lower moisture contents. However, the toughness decreases rapidly with increasing loading rate, and at the higher rates, it is similar to that exhibited by the previous materials.

The results obtained for all three moisture contents are summarized in Figures 6 and 7. Data on stretched acrylic previously reported by Sutton (Reference 5) was obtained for ambient material only and at lower loading rates. There was a slight overlap of testing rate and for these conditions the data are consistent.

During the conditioning of the test specimens at 160°F and 95% relative humidity, "delamination" cracks parallel to the specimen faces were observed to form in some of the 1/2-inch thick specimens. The cracks formed usually after the fourth week of exposure in both thermal relaxation and compact tension specimens. Figure 8 is an edgewise view of a compact tension specimen showing the cracks parallel to the faces. Figure 9 shows the extent of delamination viewed from a specimen face. The cracks originate at the free surfaces - i.e., the edges, the notches and the loading holes. This phenomenon has been observed and reported previously - for example, in Reference 6. It is usually associated with the absorption of water, followed by desorption. It is probably also related to the relatively low resistance of stretched acrylic to crack propagation parallel to the plane of stretching (Reference 7).

Fracture toughness tests were conducted on some of the delaminated specimens. The results are shown in Figure 5. The limited tests seem to indicate a slightly higher toughness for these specimens compared to standard material.

The fracture toughness data obtained for the stretched acrylic was compared to that previously reported for polycarbonate plastic (Reference 8), also for different moisture contents and loading rates. Under similar environments, the moisture content of the polycarbonate is approximately one-tenth that of the stretched acrylic. At ambient conditions, it contains approximately 0.1% moisture, and when saturated, it contains approximately 0.4% moisture. The toughness data is presented in Figures 10 to 12. For the dry and the ambient materials, the fracture toughness of the polycarbonate was significantly higher than that of the stretched acrylic for the thicknesses and loading rates investigated. However, a high moisture content reduced the toughness of the polycarbonate and increased the toughness of the acrylic. As a result, there was little difference in the toughness of the two materials for these latter conditions.

SUMMARY

1. The thermal relaxation behavior of stretched acrylic plastic is affected significantly by absorbed moisuture. The moisture reduces the thermal resistance and increases the tendency for the stretched plastic to relax at a given temperature. It is possible for the same material to meet or not meet the requirements of a specification, such as MIL-P-25690, depending on

the moisture content of the test specimens. Therefore a thermal relaxation test should specify the allowable moisture content of the test specimens.

2. Absorbed moisture also affects the fracture toughness of stretched acrylic, for higher moisture contents. There was no significant difference in the behavior of dry material (0% moisture) and material conditioned in the laboratory atmosphere (1% moisture content). However, material containing 3% to 4% moisture exhibited a higher fracture toughness than the dry or ambient materials at lower rates of loading. At high loading rates, there was no effect of moisture content. Thus if a specification for stretched acrylic plastic stipulates a high loading rate for the fracture toughness test, control of moisture content is not necessary.

There was little difference in the fracture toughness of the two thicknesses tested - 1/4-inch (6.4 mm) and 1/2-inch (13 mm).

3. Some of the stretched acrylic specimens developed in-plane cracks during the conditioning at 160°F (71°C) and 95% relative humidity.

4. When tested in the dry condition or as conditioned in the laboratory, the fracture toughness of the stretched acrylic was less than that previously reported for polycarbonate plastic. However, very high moisture contents decreases the fracture toughness of polycarbonate and increases the toughness of stretched acrylic. As a result, when both materials are tested wet, there is little difference in the fracture toughness for the thicknesses and loading rates studied.

TABLE 1.

THERMAL RELAXATION OF STRETCHED ACRYLIC[a]

Specimen Thickness In (mm)	Moisture Content %	Shrinkback 24 Hours at 230°F (110°C) %	Shrinkback 24 Hours at 293°F (145°C) %
0.25 (6.4)	0[b]	0.9	41.1
	1.1 (Ambient)	2.0	41.0
	3.9[c]	35.0	41.1
0.50 (13)	0[b]	1.2	40.2
	1.1 (Ambient)	6.0	39.5
	3.4[c]	35.0	40.5

[a]Tests were conducted in accordance with MIL-P-25690A

[b]Dried to equilibrium weight for 15 weeks in a vacuum oven at 160°F (71°C)

[c]Exposed to moisture for 5 weeks at 160°F (71°C) and 95% relative humidity to equilibrium weight

REFERENCES

1. Military Specification MIL-P-25690; Plastic, Sheets and Parts, Modified Acrylic Base, Monolithic, Crack Propagation Resistant

2. Barton, J. M., "Effect of Absorbed Water on the Thermal Relaxation of Biaxially Stretched Crosslinked Poly (methyl methacrylate)", Polymer, Vol. 20 (1979), pp. 1018-1024

3. Worsdall, R. L., "Problems Associated with the Quality Assurance of Stretched Acrylic Sheet", Proceedings of the Conference on Aerospace Transparencies, The Society of British Aerospace Companies Ltd., London (1980), pp. 371-397

4. Mason, A. J., "The Effects of Absorbed Moisture Upon the Physical Properties of Stretched Acrylic Materials", Proceedings of the Conference on Aerospace Transparencies, The Society of British Aerospace Companies Ltd., London (1980), pp. 399-416

5. Sutton, S. A., "Fracture Toughness of Stretched Acrylic Plastic", J. Testing and Evaluation, Vol. 6, No. 6, (1978), pp. 356-363

6. Wolock, I., Mulville, D. A., and Thomas, R. W., "Study of Failed TA-4 Aircraft Canopies", Proceedings of the Conference on Transparent Aircraft Enclosures, Las Vegas, 1973 (AFML-TR-73-126), pp. 617-640

7. Broutman, L. J. and McGarry, F. J., "Fracture Surface Work Measurements on Glassy Polymers by a Cleavage Technique. II. Effects of Crosslinking and Preorientation", J. Applied Polymer Science, Vol. 9 (1965), pp. 609-619

8. Sutton, S. A., Tirosh, J., Thomas, R. W., Mast, P. W., and Wolock, I., "The Effect of Loading Rate, Temperature and Moisture on the Fracture Toughness of Polycarbonate", Proceedings of the 27th National SAMPE Symposium, San Diego, (1982), pp. 1003-1021

FIGURES

1. Compact Tension Specimen (2 x 2 inches)

2. Effect of Absorbed Moisture on Thermal Relaxation of Stretched Acrylic Plastic at 230°F (110°C)

3. Effect of Loading Rate on Fracture Toughness of Stretched Acrylic Plastic in Dry Condition

4. Effect of Loading Rate on Fracture Toughness of Stretched Acrylic Plastic in Ambient Condition

5. Effect of Loading Rate on Fracture Toughness of Stretched Acrylic Plastic in Wet Condition

6. Effect of Loading Rate on Fracture Toughness of Stretched Acrylic Plastic for Various Conditions

7. Effect of Loading Rate on Fracture Toughness of Stretched Acrylic Plastic for Various Conditions

8. Edge View of Compact Tension Specimen Showing In-Plane Cracks

9. Top View of Compact Tension Specimen Showing In-Plane Cracks

10. Comparison of Fracture Toughness of Polycarbonate and Stretched Acrylic in Dry Condition

11. Comparison of Fracture Toughness of Polycarbonate and Stretched Acrylic in Ambient Condition

12. Comparison of Fracture Toughness of Polycarbonate and Stretched Acrylic in Wet Condition

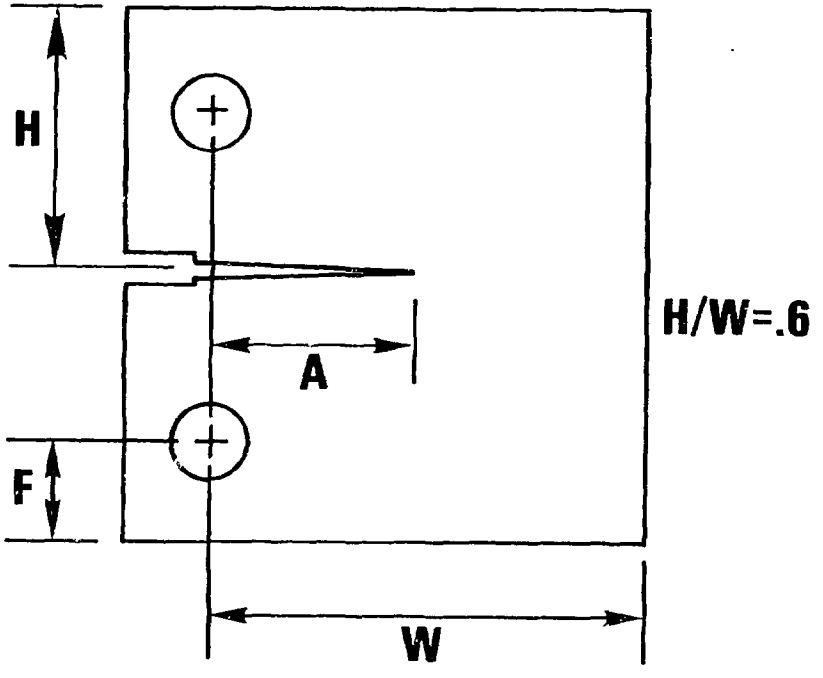

Figure 1 - Compact Tension Specimen (2 x 2 inches)

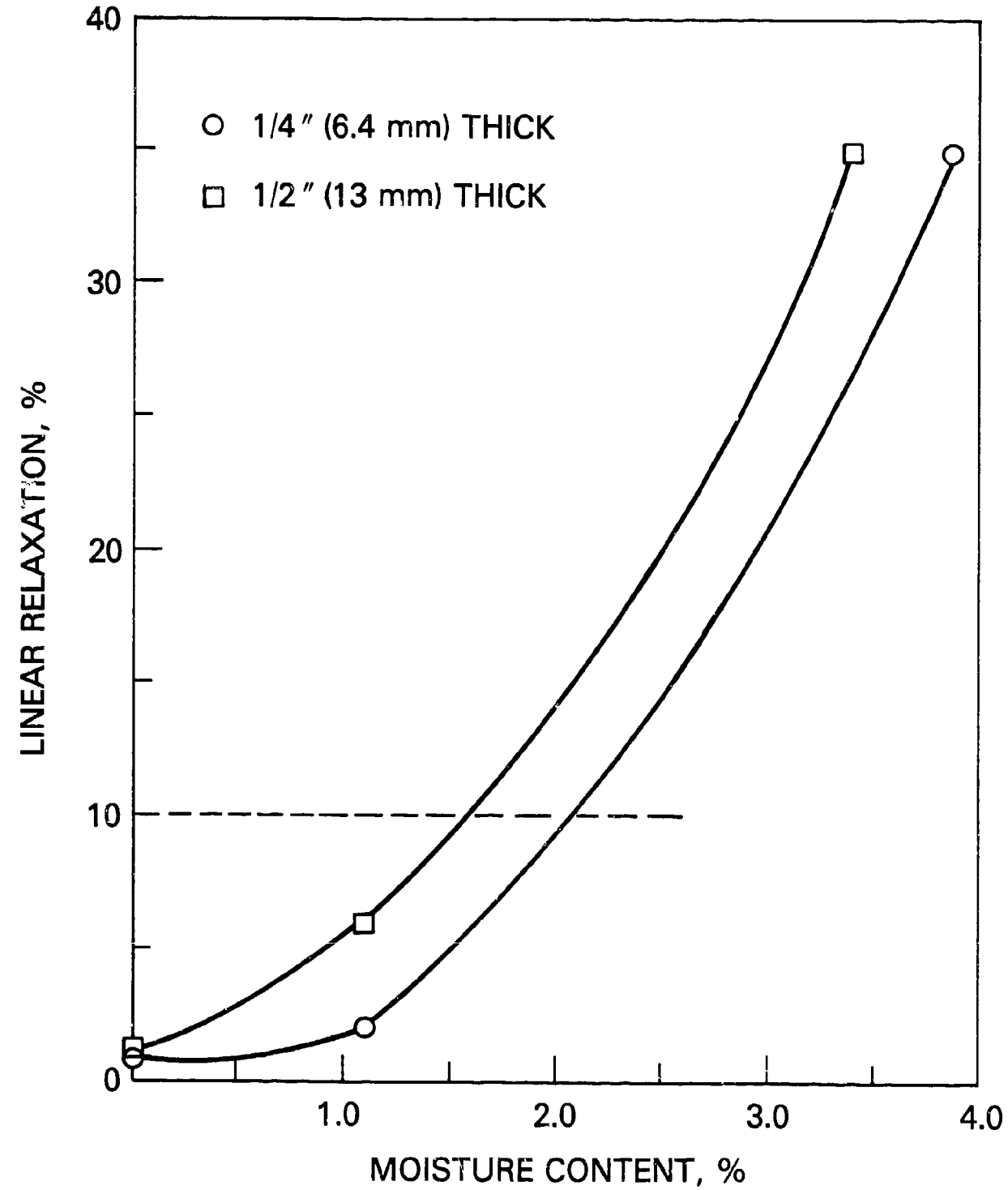

2. Effect of Absorbed Moisture on Thermal Relaxation of Stretched Acrylic Plastic at 230°F (110°C)

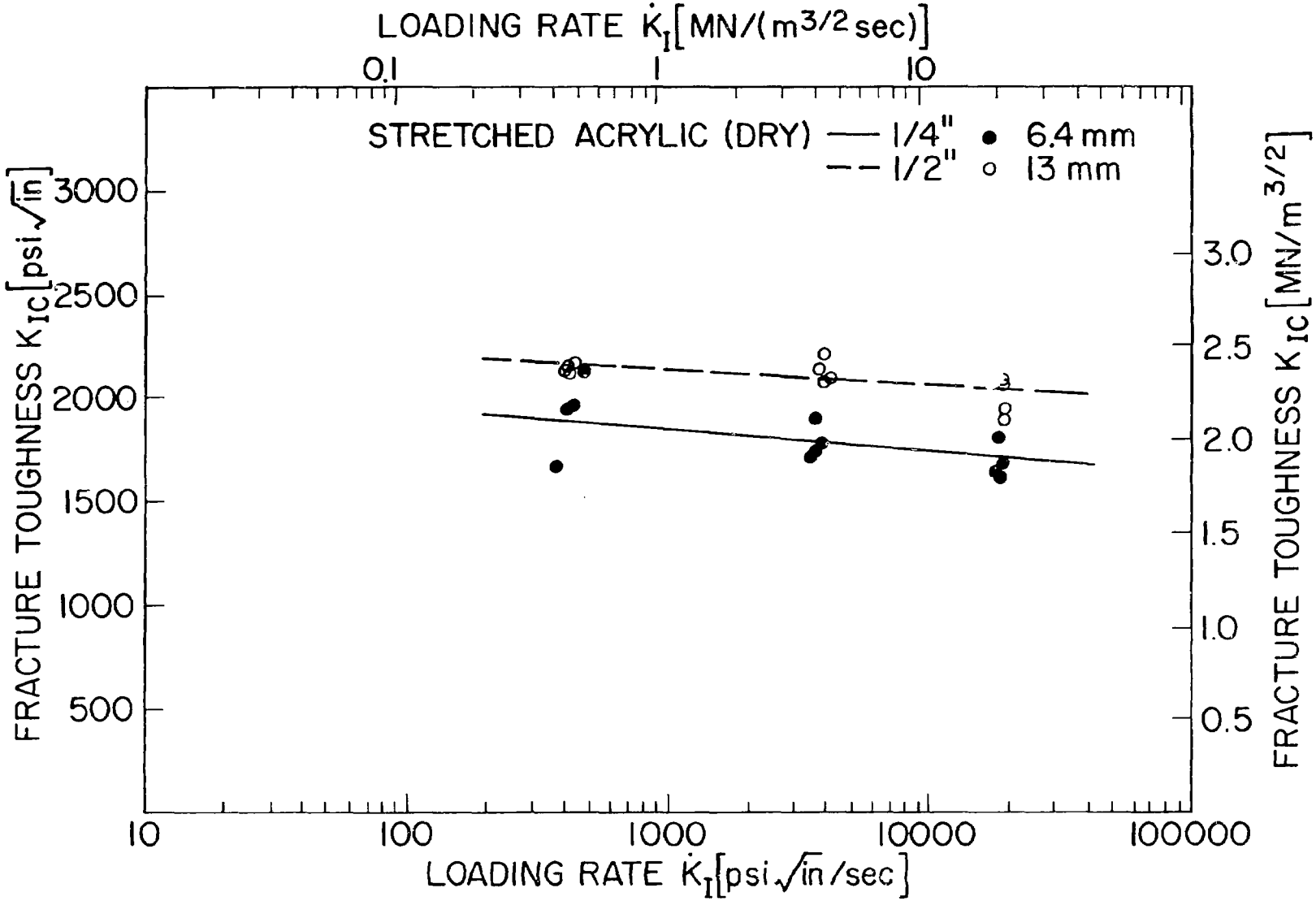

3. Effect of Loading Rate on Fracture Toughness of Stretched Acrylic Plastic in Dry Condition

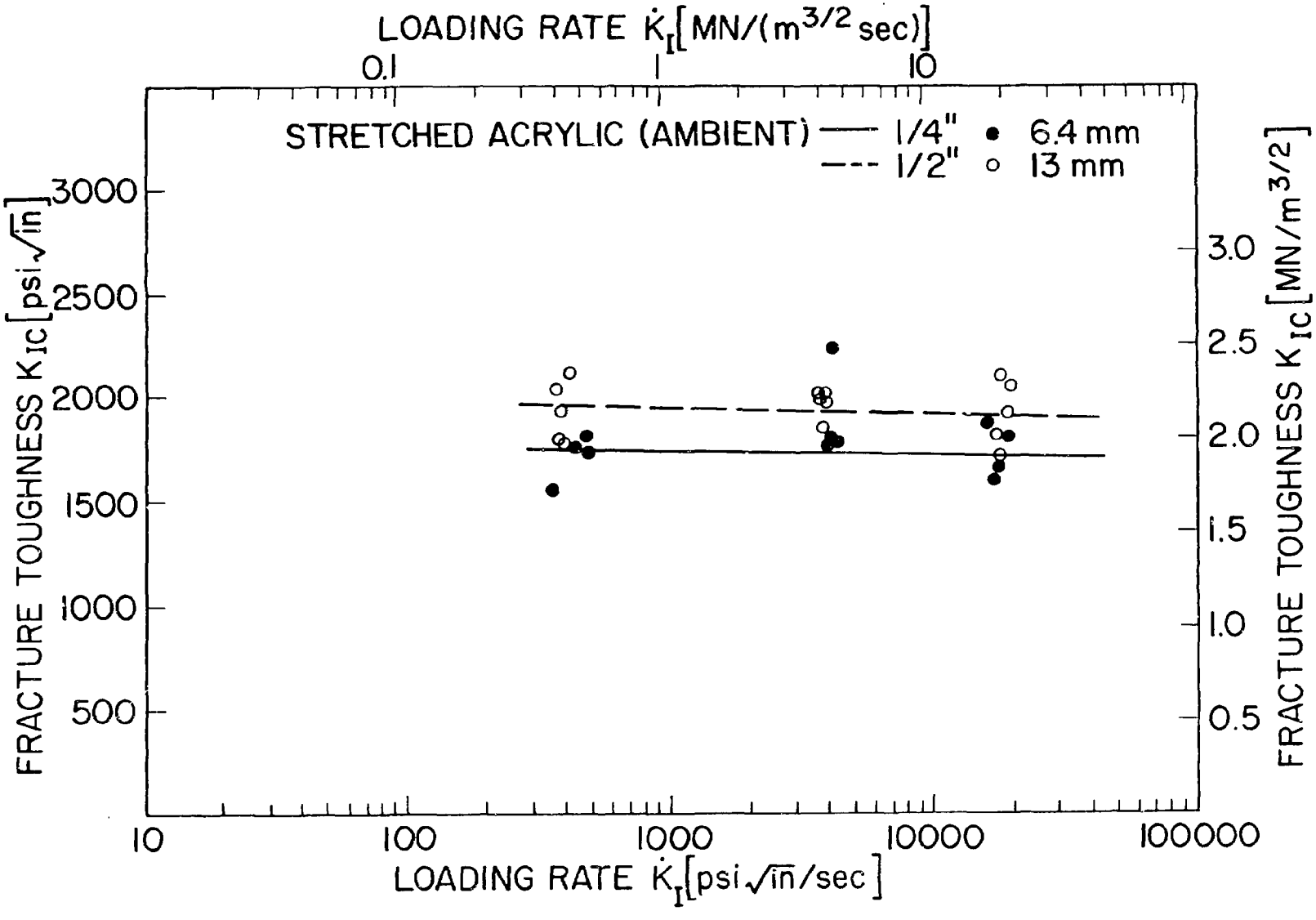

4. Effect of Loading Rate on Fracture Toughness of Stretched Acrylic Plastic in Ambient Condition

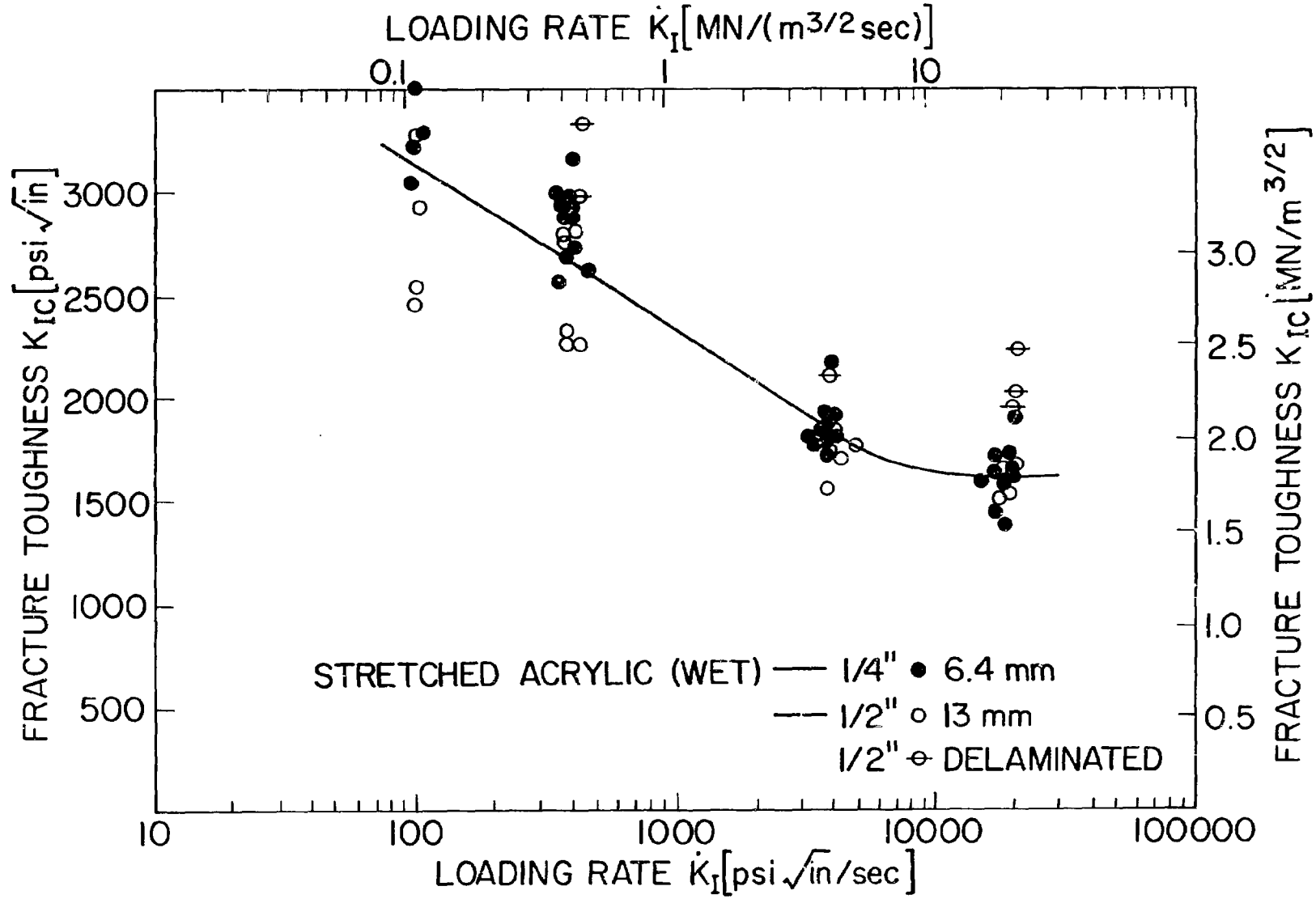

5. Effect of Loading Rate on Fracture Toughness of Stretched Acrylic Plastic in Wet Condition

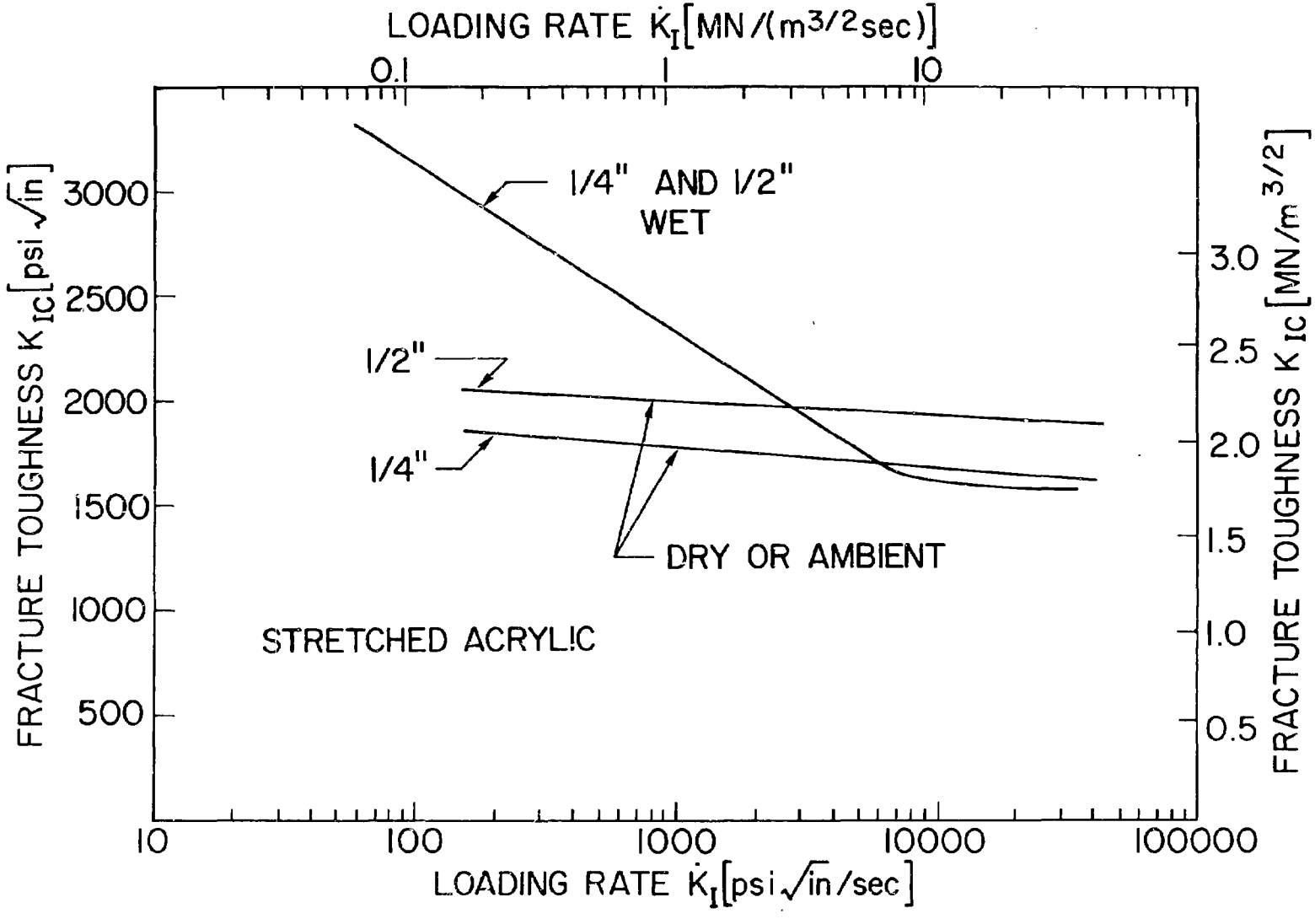

6. Effect of Loading Rate on Fracture Toughness of Stretched Acrylic Plastic for Various Conditions

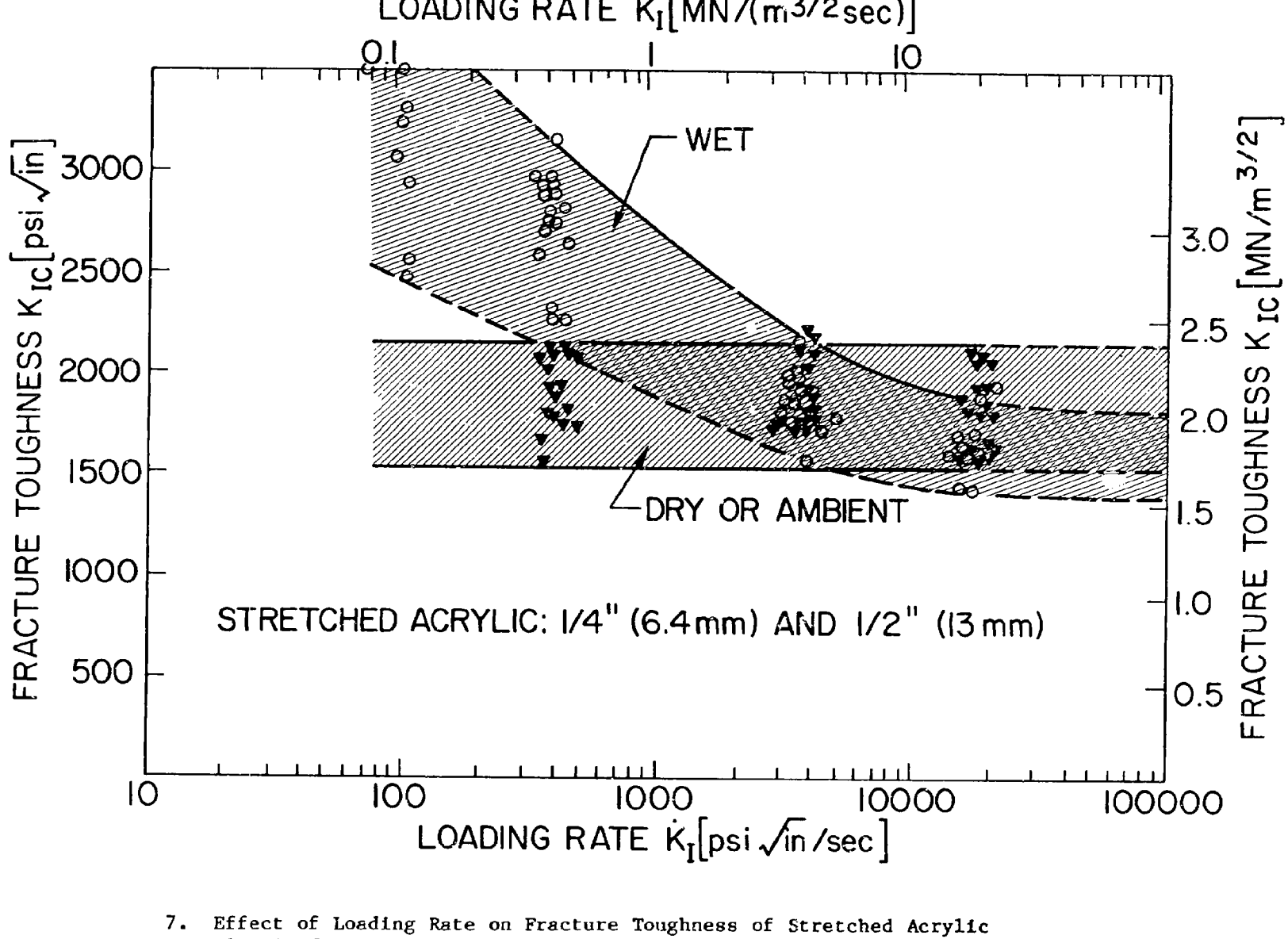

7. Effect of Loading Rate on Fracture Toughness of Stretched Acrylic Plastic for Various Conditions

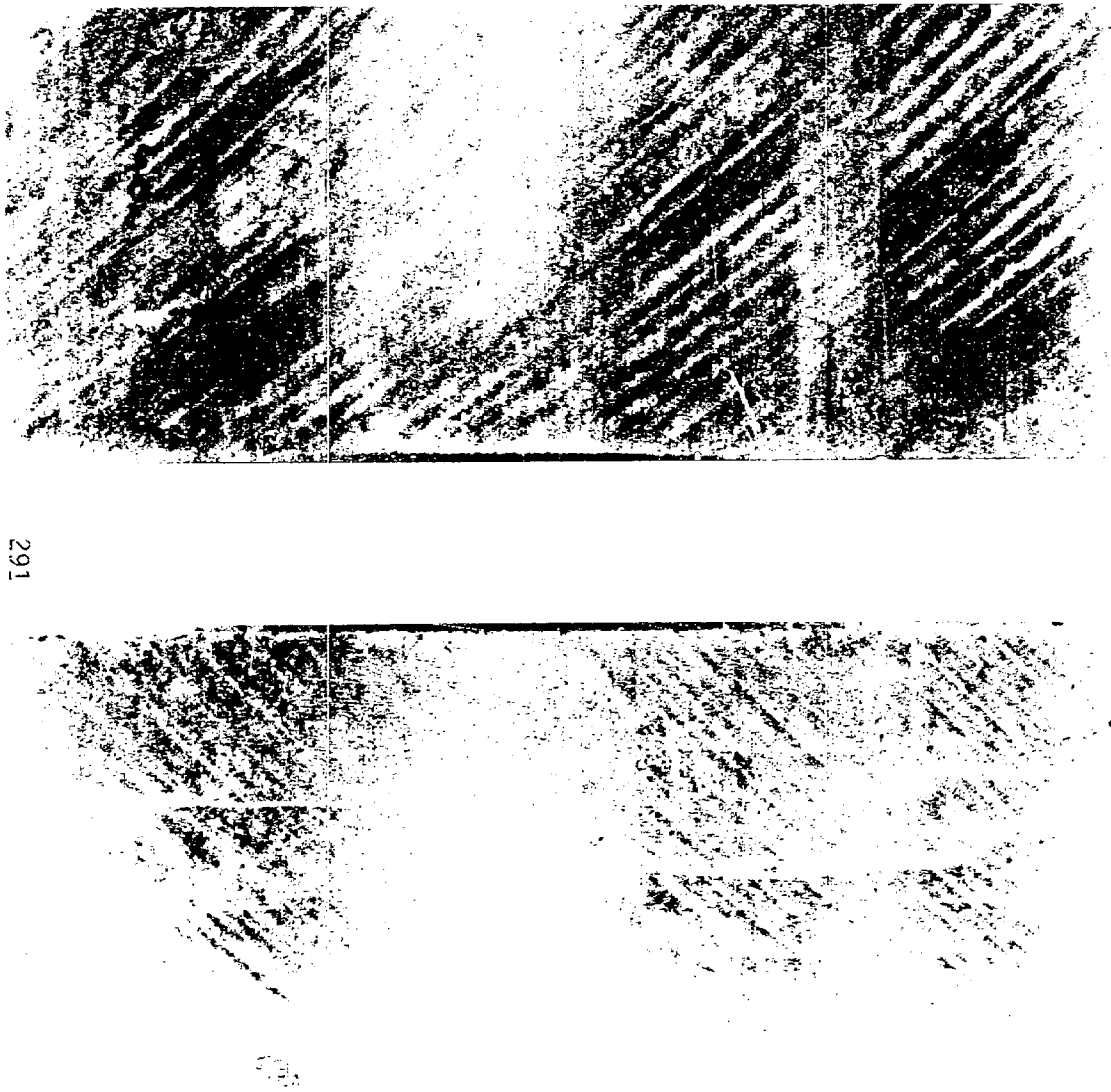

8. Edge View of Compact Tension Specimen Showing In-Plane Cracks

9. Top View of Compact Tension Specimen Showing In-Plane Cracks

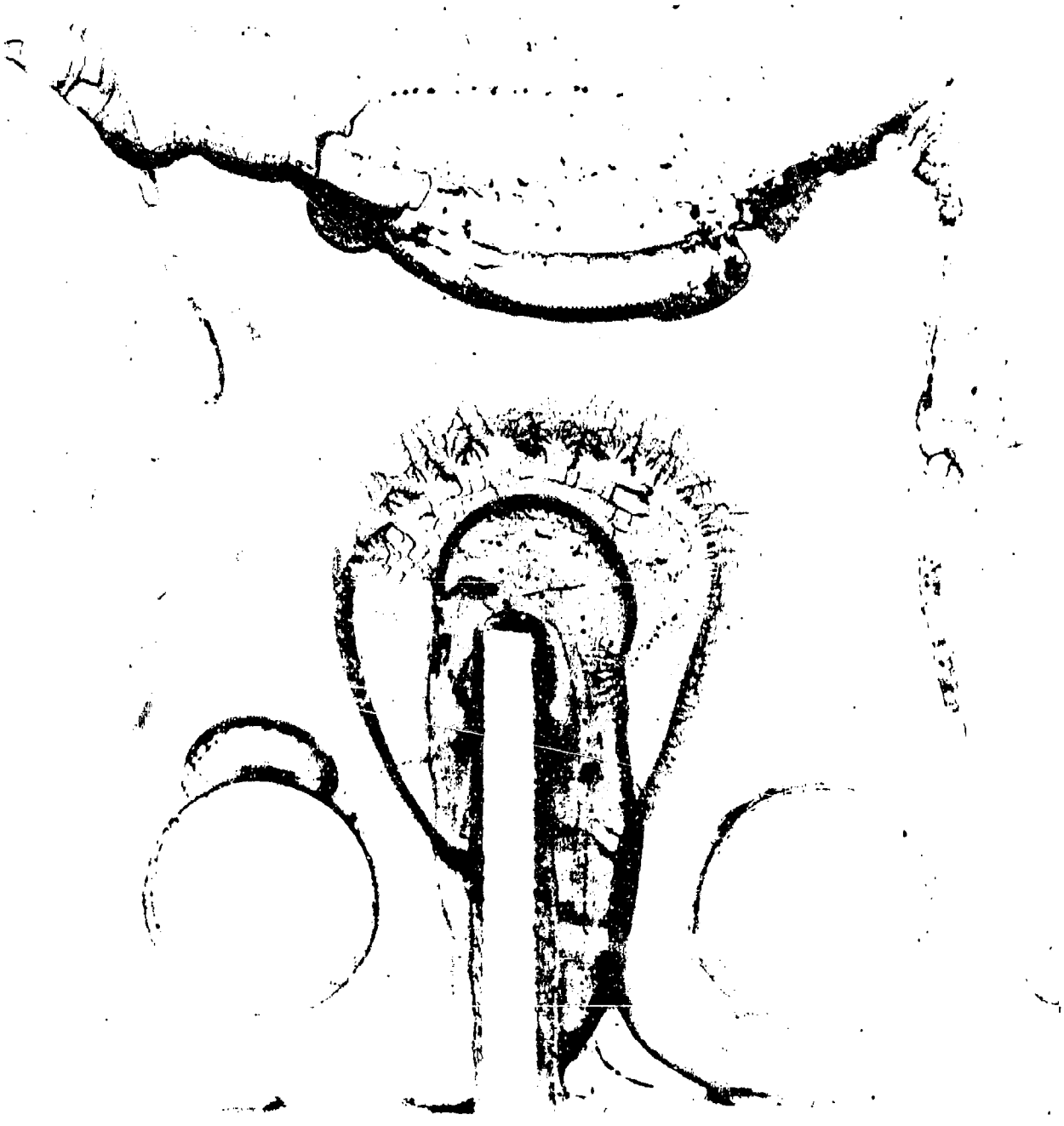

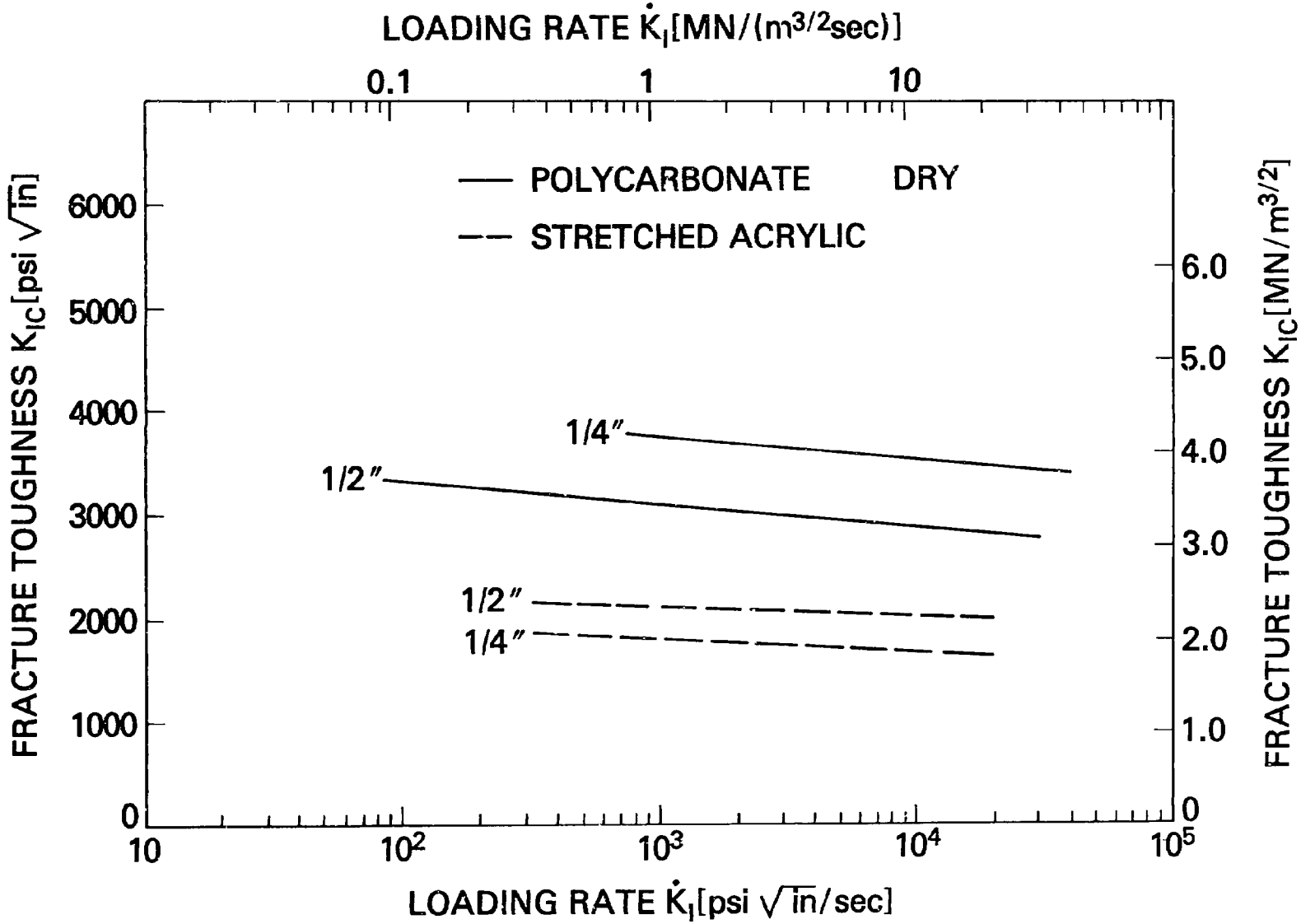

10. Comparison of Fracture Toughness of Polycarbonate and Stretched Acrylic in Dry Condition

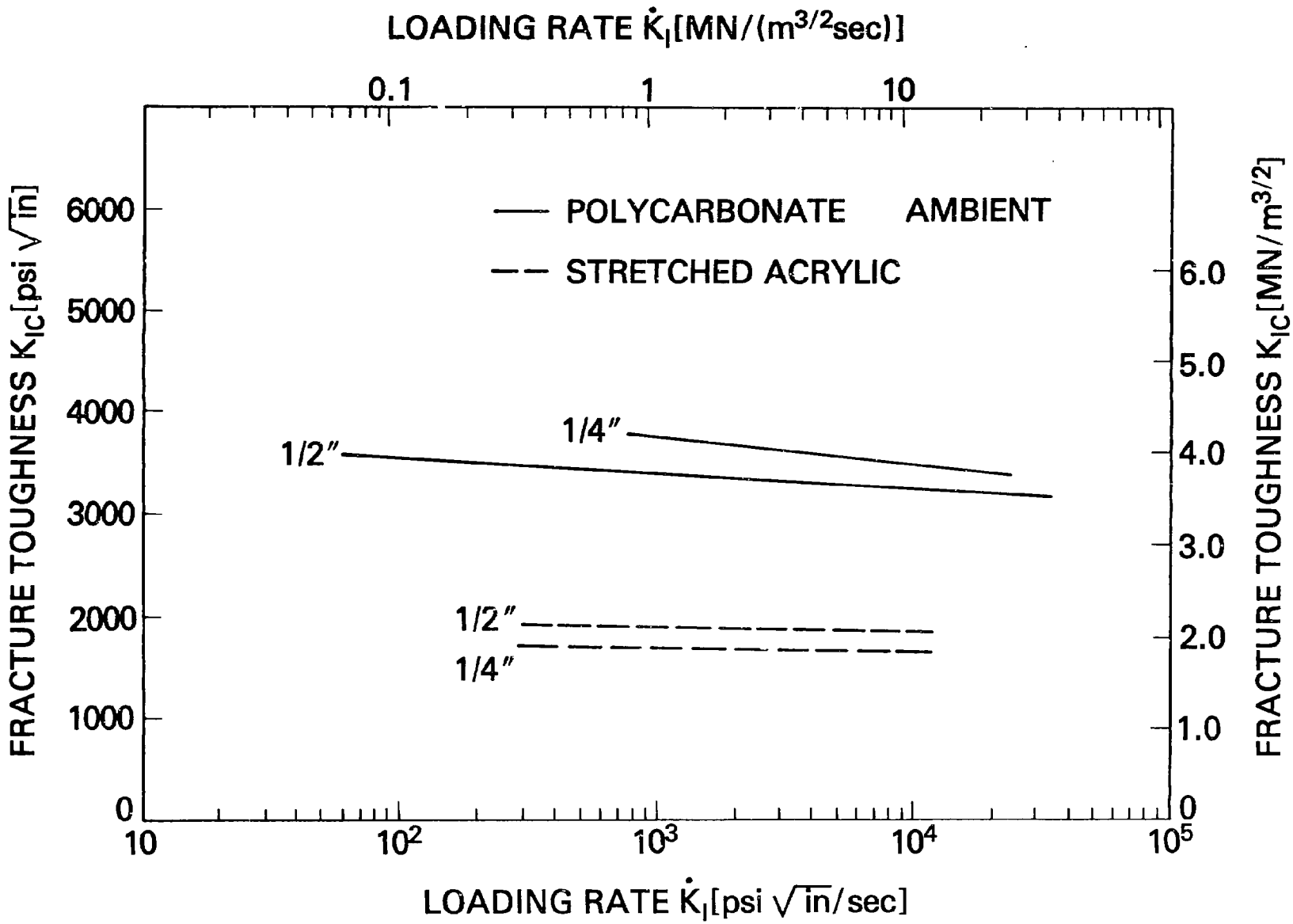

11. Comparison of Fracture Toughness of Polycarbonate and Stretched Acrylic in Ambient Condition

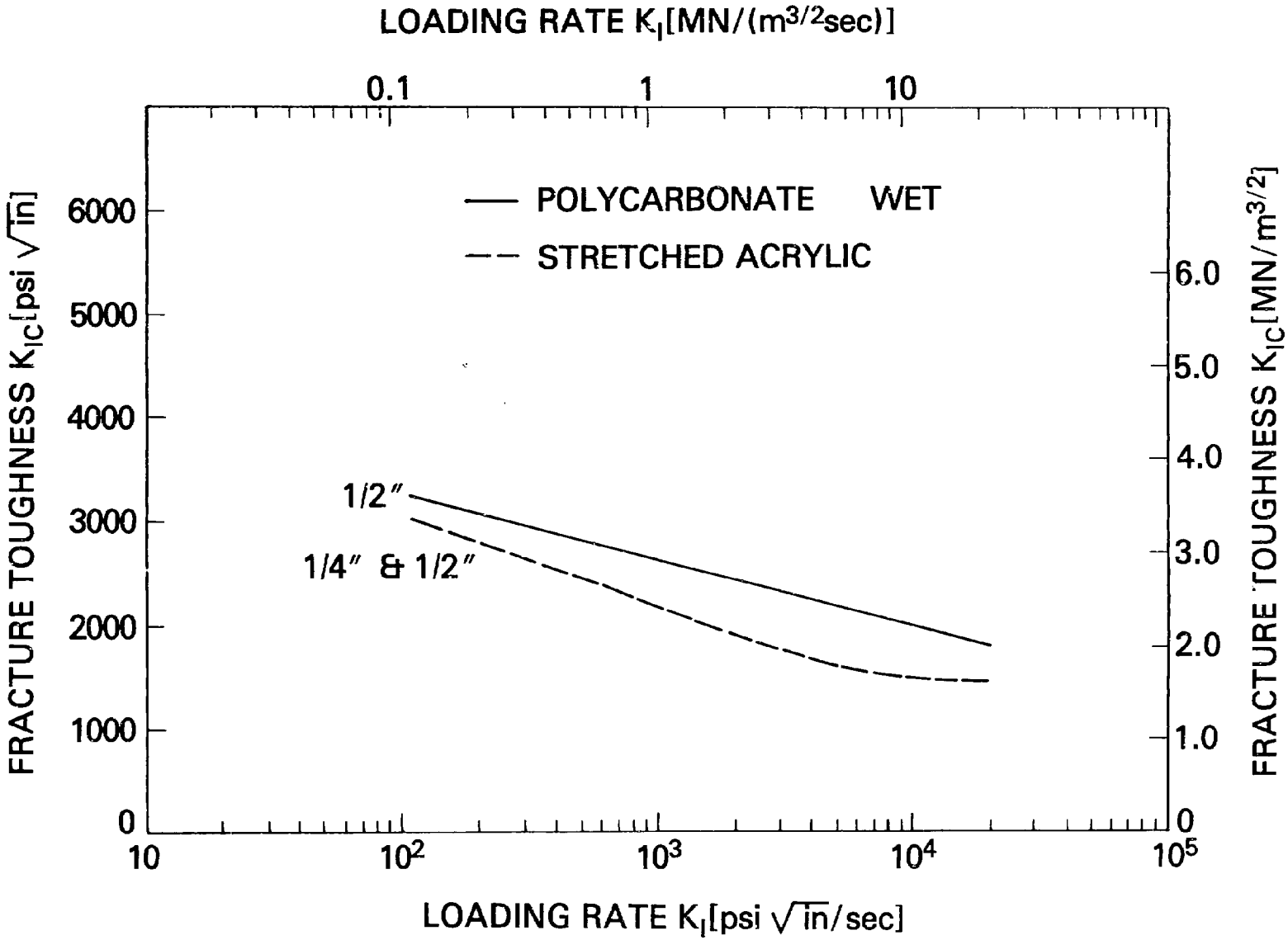

12. Comparison of Fracture Toughness of Polycarbonate and Stretched Acrylic in Wet Condition

AD-P003 198

COMPARISON OF BULLET RESISTANCE OF NEW AND AGED POLY-CARBONATE

J. B. R. Heath, R. W. Gould, and
E. B. Stimson, National Research
Council of Canada

COMPARISON OF BULLET RESISTANCE OF NEW AND AGED POLYCARBONATE

J.B.R. Heath, R.W. Gould, E.B. Stimson

National Aeronautical Establishment
National Research Council of Canada
Ottawa, Canada, K1A OR6

ABSTRACT

The effects of aging on the ballistic characteristics of monolithic polycarbonate were studied.

The program was carried out in two parts. Part I compared the decrease in bullet velocity after penetration of new to aged polycarbonate panels, and Part II compared the behaviour of new to aged panels where penetration does not occur.

No appreciable difference was noted in residual bullet velocity between those bullets which penetrated the different panels. In assessing bullet resistance through non-penetration, no significant change was observed due to age degradation of the polycarbonate.

It was noted however, that both the artificially aged and naturally aged specimens behaved somewhat unpredictably and both showed signs of being susceptible to the initiation of fractures upon bullet impact.

1.0 INTRODUCTION

In the aerospace industry, polycarbonate, either monolithic or laminated, is one of the designers' primary choices when a light-weight high performance transparent material is required. Due to inherent characteristics, transparencies can now withstand the impact of a four pound bird at speeds in excess of 500 knots. Polycarbonate is currently used extensively when designing impact resistant glazings for use in locations susceptible to armed violence such as banks, airports and embassies.

A study carried out at the NRCC/NAE Flight Impact Simulator Facility (Ref. 1) showed a decrease in the bird impact resistance of naturally aged and artificially heat aged polycarbonate. It was on the basis of this work that a joint program to assess the bullet resistance of aged polycarbonate was set up between the Flight Impact Simulator Group and the Public Safety Project Office, NRCC, Ottawa.

The design of the experimental program took account of the fact that double or multiple panels are frequently used in security glazings. When impacted by bullets, the outer panel of the glazing may be penetrated, and in fact a single panel of polycarbonate of $\frac{1}{4}$ inch thickness can be penetrated by bullets from common types of hand guns. However, the bullet loses energy in the process and may be slowed down to the point where it can be arrested by

the second panel. It therefore seemed important to examine the effect of aging on the behaviour of polycarbonate panels both in the case where impact results in penetration and in the case where it does not. The program was therefore divided into two parts.

Part I was to determine any change in bullet velocity and deviation from line of fire after penetration of single polycarbonate panels. Both artificially and naturally aged material was employed for these tests as well as panels of recently manufactured material for comparative purposes.

Part II was to provide an assessment of the degree of ballistic resistance of the various polycarbonate panels without complete penetration of a two-panel set-up.

In both parts, the effect of multiple impacts was investigated.

2.0 TEST APPARATUS

A schematic of the test set-up is shown in Figure 1, and a brief description of each of the components is given in the following sections.

2.1 FIREARMS AND SUPPORT

For initial calibration tests a Smith & Wesson Model 19-2, .357 Magnum revolver with a 2.5 inch barrel was used. Ammunition was .38 Special, 158 grain semi-wadcutter + P, manufactured by Winchester-Western.

Part I of the program employed a Dan Wesson Model 15, .357 Magnum revolver which could be fitted with barrels of various lengths. A two inch barrel was used for this part of the program. Ammunition was .357 Magnum, 158 grain semi-wadcutter, manufactured by Winchester-Western. This developed an average bullet velocity at impact of 1063 ft/sec with a corresponding kinetic energy of 397 ft.lb.

Part II was carried out with the same revolver equipped with a six inch barrel and using .38 Special, 158 grain semi-wadcutter, + P ammunition manufactured by Winchester-Western. In this case the average bullet velocity at impact was 987 ft/sec with a corresponding kinetic energy of 337 ft.lb.

The revolver was held in a Ransom Gun Rest which was clamped to a rigid steel frame. Discharge of the firearm was carried out manually by a triggering linkage, integral with the Ransom Rest. Figure 2 shows the set-up.

2.2 VELOCITY MEASUREMENT

Two methods were used to measure initial bullet velocity. One utilized a chronograph system manufactured by Oehler Research, incorporating a Model 30 Chronotach, with two Model 55 Photoelectric triggering screens set six feet apart. Redundancy of initial velocity was supplied by an aluminum foil screen system, comprising two screens seven feet apart. A single screen of this system was constructed of two foil sheets separated by a tissue paper insulator. This

assembly was taped to the front of a cardboard panel mounted on a plywood support. D.C. Voltage was applied to the foil sheets, and as a bullet passed through the screen, contact was made between the two sheets. An electrical pulse was thus generated which triggered a timer counter. Bullet velocity was then calculated from the measured time interval between the start and stop screens. Figure 3 shows the light screens and foil screens for initial velocity measurements.

Residual velocity for Part I of the program was determined with a second aluminum foil screen system. The screens set seven feet apart are shown in Figure 4.

2.3 PANEL SUPPORT FIXTURE

For Part I, the test panels were set in one of two aluminum fixtures, depending on panel size. The fixtures are shown in Figures 5 and 6.

For Part II the same aluminum fixtures were used, but the two panels were separated by a one inch thick spacer, as shown in Figures 5 and 6. Rubber gaskets were used behind each panel after Test 13, in order to minimize fixture inside edge effects.

The aluminum fixtures were clamped to support structure as shown in Figure 7.

2.4 TEST PANELS

For all the tests 0.25 inch thick polycarbonate was used. The overall dimensions of the panels were either 12 inches by 12 inches or 8 inches by 8 inches depending on the amount of material available. Material history is detailed in the following sections.

2.4.1 NEW POLYCARBONATE

All the panels were cut from a single sheet and assumed to have an age of less than six months based on information from the supplier.

2.4.2 NATURALLY AGED POLYCARBONATE

The naturally aged polycarbonate was obtained from panels that had been used during bird impact tests carried out in 1973, and subsequently stored in a closed cabinet. During storage, the panels could have been subjected to temperature extremes of 40°F to 100°F and humidity could have ranged from 10% to 100%.

Some material that had been on inventory at a local supplier for approximately two years, and on hand at the facility for another year, was also available.

2.4.3 ARTIFICIALLY HEAT AGED

New as-extruded material was conditioned at 260±5°F for either 100 hours or 196 hours in an air circulating oven. A copper constantan thermocouple connected to a digital indicator and strip chart recorder monitored the temperature during the heat aging. This procedure was previously established and reported in Ref. 1.

3.0 METHOD

3.1 CALIBRATION

Prior to testing, calibration shots were carried out, measuring bullet velocities with two foil screen systems as located in Figure 1. These were to determine typical bullet velocity loss over the distance between the two systems.

A Smith & Wesson .357 Magnum with a 2.5 inch barrel was used for the calibration shots. Ammunition was .38 Special, 158 grain, semi-wadcutter +P.

3.2 GENERAL - PART I and PART II

Before commencing a test series, a cardboard panel was placed on the first light screen, and one at the bullet trap (Fig. 1). Preliminary shots were taken with the firearm mounted in the gun rest, and adjustments made to the gun rest for the desired line of fire. Once this alignment was completed a laser was mounted on a tripod stand in front of the first light screen, (Fig. 8), and adjusted until the beam passed through the center of the bullet holes in the two cardboard panels. The test panel fixture was then positioned so that the laser beam impinged on the desired target point, and the fixture clamped to the support structure (Fig. 7). The aluminum foil velocity screens were also positioned in this manner.

After impact, the laser beam was again positioned to pass through the bullet holes in the foil screens, and the hole in the target panel (Fig. 9). The panel fixture and foil screens were repositioned, for a second impact, using the laser beam as a reference. This procedure was repeated as required.

Impact locations for the first three test shots on a panel were as follows:

- 12 x 12 panels - three equidistant points on the circumference of a six inch diameter circle.
- 8 x 8 panels - three equidistant points on the circumference of a four inch diameter circle.

Impact locations in excess of the initial three were chosen in accordance with panel integrity.

All tests were carried out under ambient room conditions.

A bullet trap (Fig. 10) was positioned down-range.

3.2.1 PART I

The object of Part I of the program was to compare the residual velocity of a bullet after penetration of new to aged polycarbonate panels. Change in velocity was calculated using the results from the two velocity measuring systems, described in paragraph 2.2.

It was decided at this time to also obtain a measure of bullet deviation from line of fire after penetration. Bullet deviation was obtained by aligning a laser beam through the bullet holes in the initial velocity measuring foil screens, and the hole in the test panel. The panel was then removed, and the point at which the laser beam impinged on the deviation screen at the bullet trap (Fig. 1 and 10) was taken as the true line of fire. The position of the resulting bullet hole on the deviation screen was measured relative to the laser point and the deviation recorded as Y inches vertically up or down, and X inches horizontally left or right.

3.2.2 PART II

The object of Part II was to determine any loss in the bullet resistance of a two-panel polycarbonate set-up due to degradation of the material. The test set-up is shown in Figure 1. Considerable experimentation was required in order to arrive at a combination of handgun calibre, barrel length and ammunition loading which would provide, with new material, bullet penetration of the first panel yet non-penetration of the second.

During testing, the panels were visually checked after each impact and any damage noted and recorded before a subsequent test shot was carried out.

When testing was completed, an attempt was made to ascertain if there was any change in material behaviour of the various panels that actually arrested the bullet. One method considered was to compare the crater depth to the initial bullet velocity. Use of a depth micrometer proved ineffective, due to panel deformation within two inches of the bullet crater.

An alternative method whereby the volume of the crater was compared to the initial velocity of the impacting bullet was then tried. Several unsuccessful methods of measuring the crater volume were attempted before a workable procedure was developed. One unsuccessful procedure was to measure fluid volume with various low viscosity fluids that were dropped into the crater using a hypodermic syringe. Difficulties were encountered due to surface tension effects, static induced capilliary action and indeterminable crater circumferential boundaries. This method was thus discarded.

It was decided that a male casting of the crater could be taken, weighed and converted to volume.

A flat steel washer 7/8 inches ID., when placed on the surface of the panel and centered about the crater, established the circumferential limits of the sample.

Casting material was introduced until the crater was filled and the material overflowed the top surface of the washer. This excess material allowed for any shrinkage experienced during the curing/cooling of the casting. The flat top surface of the washer provided the reference plane to which the casting was trimmed. Silicone rubber and two-part epoxy glue were discarded due to excessive cure times and the possibility of voids. Modeler's clay or Plasticene was not easily released from the crater.

After rejecting several types of material it was found that paraffin wax could be utilized. Molten wax was deposited around the periphery of the washer, centered about the crater, to locate it during the trimming process (Figs. 11 and 12). The crater was then filled to a level above the top surface of the washer. Once the wax had completely solidified the excess was trimmed off flush with the top surface of the washer (Figs. 13 and 14). The panel was inverted and tapped to release the casting (Fig. 15), the washer removed and the wax casting weighed (Fig. 16). This measurement, minus the value for the weight of wax required to fill the hole of the washer, was converted to an equivalent volume. (The density of the paraffin wax was taken to be 0.925 gms/cc.).

4.0 RESULTS

4.1 CALIBRATION

The results of the calibration shots, measuring the change in bullet velocity over the test set-up distance, are summarized in Table 1. The results showed that the velocity change was insignificant for the purposes of the program and was not considered further.

4.2 PART I

The data from Part I are summarized in Table 2. As can be seen from the $\Delta V/V$ results there was no significant change between the different polycarbonate panels of various histories. There was however, some indication that the eight year old naturally aged material was susceptible to fracturing after an initial impact. (See tests 13, 14, 15, 16 and 21). Figures 17 to 20 show the panels from Part I.

Bullet deviation, after penetration, is plotted in Figure 21, and as can be seen from the scatter, seems to be independent of material history.

4.3 PART II

The results of Part II are summarized in Table 3, and Figure 22 shows a plot of crater volume versus initial bullet velocity. It should be noted that bullet penetration of panel 2 did not occur in any of the tests. Figure 23 shows typical impact damage in sections taken through panels 1 and 2. The following sections detail the results of the various tests.

4.3.1 NEW MATERIAL 12 x 12 PANELS

Results of Tests 4 to 9 inclusive show that the new material can withstand closely spaced (2-5/8 inches apart) multiple impacts without any serious damage to either panel 1 or panel 2.

4.3.2 NEW MATERIAL 8 x 8 PANELS

Results of tests 26 to 31 inclusive showed that the outer panel can withstand four impacts approximately 1½ inches apart, but on the fifth, fractures began to initiate from previous damage. Eventually after six impacts the outer panel suffered major damage rendering the set-up non resistant to additional impacts. Figure 24 shows panel 1 after the fifth and sixth impacts. The results from Tests 32 to 35 and Tests 36 to 39 showed fracturing of the outer panel occurring on the third impact with spacing approximately 2-3/4 inches (Figs. 25 and 26). It would be unlikely that an additional impact without bullet penetration of both panels could be carried out.

It is interesting to note that the 12 x 12 panels can withstand at least six impacts without any panel fracturing, while with the 8 x 8 panels, fracturing occurred on the fifth impact in one case and on only the third impact in two cases.

4.3.3 NATURALLY AGED (3 YEARS) 12 X 12 PANELS

A total of six impacts (Tests 17 to 22 inclusive) with a minimum spacing of 2¼ inches was carried out on this material without any sign of fractures initiating from existing holes.

4.3.4 NATURALLY AGED (8 YEARS) 12 X 12 PANELS

Because of the limited supply of material only one test set-up was assessed.

The first impact, Test 50, caused major damage to panel 2, as shown in Figure 27. Obviously the set-up would not withstand a second impact without bullet penetration of both panels.

4.3.5 NATURALLY AGED (8 YEARS) 8 X 8 PANELS

In tests 23 to 25, with impact spacing similar to that on new material 8 x 8 panels, fracturing occurred in the naturally aged (8 year) material on the second impact, with major damage occurring on the third as shown in Figures 28 and 29. As a result of the damage from the third impact, a fourth would obviously result in bullet penetration of both panels. The aged panels suffered major damage on the third impact compared to the new material, where major damage occurred on the fourth impact in two cases and on the sixth in one case.

4.3.6 ARTIFICIALLY HEAT AGED (100 HOURS) 12 X 12 PANELS

The results of the impacts carried out on these panels were very inconsistent. New material that had been heat aged six months prior to the ballistic tests suffered major damage after just one or two impacts. In Test 3 a large section of panel 2 separated as a result of the single impact. The damage is shown in Figure 30. Fracturing occurred in panel 1 (Test 14, 15 and 16) on the second impact and major damage occurred on the third (Test 16) as shown in Figure 3.

Material that was heat aged days prior to testing showed no signs of damage after a total of six impacts with spacing as close as $2\frac{1}{2}$ inches (Tests 40 to 45).

4.3.7 ARTIFICIALLY HEAT AGED (196 HOURS) 12 X 12 PANELS

There were no signs of fracturing of this material after four closely spaced impacts (Tests 46 to 49). Spacing was approximately three inches.

5.0 DISCUSSION OF RESULTS

5.1 PART I

In the tests carried out on the 12 x 12 panels there was no indication of any difference in either bullet residual velocity or deviation from line of flight after penetration due to material degradation. Fractures occurred in the 8 x 8 panels assessed, on the second impact with the naturally aged material, but as was discovered in Part II, this might be as a result of panel size rather than material degradation.

5.2 PART II

5.2.1 PANEL SIZE

Results of multiple impacts carried out on 8 x 8 panels (Tests 26 to 39) showed that with new material fractures initiated from previous damage on the fifth impact in one case and on the third impact in two cases. On the 12 x 12 panels (Tests 4 to 9) no fracturing occurred after six closely spaced impacts. There seems to be a relationship between initiation of fractures and panel size. Because of the velocity of the bullet impact, these results are puzzling and additional testing is suggested.

5.2.2 NATURALLY AGED MATERIAL

Tests on three year old material indicated no material degradation.

The single impact on the eight year old material (12 x 12 panels) was quite interesting as the test set-up would not withstand a second impact without penetration of both panels.

Unfortunately, it is difficult to draw any firm conclusion on the basis of a single test, but the result is certainly noteworthy.

Signs of material degradation occurred with the 8 year old 8 x 8 panels (Tests 23, 24 and 25). Fracturing of the outer panel resulted on the second impact, while with the new material 8 x 8 panels the outer panel did not fracture until the third impact in two cases and on the fifth impact in one case.

Obviously more work should be undertaken with naturally aged material, preferably with 12 x 12 panels to minimize possible panel size effects.

5.2.3 ARTIFICIALLY AGED MATERIAL

The results from the tests carried out on this material were inconsistent. Material that had been heat aged six months prior to ballistic testing showed degradation as major damage occurred to test panels on only the first or second impact (Tests 14, 15 and 16). However, material that had been heat aged days prior to testing showed no signs of degradation (Tests 40 to 49). This material should be tested at some future date to see if degradation continues after the heat aging process.

5.2.4 PLOT OF CRATER VOLUME VRS. INITIAL BULLET VELOCITY

Figure 22 further supports some points discussed in the previous parts. It is quite evident that material behaviour, particularly yielding on impact, had changed as a result of both artificial heat aging, and natural aging. Also, quite evident is the difference in behaviour between the artificially heat aged (100 hours) material that had been processed some six months before testing and the material processed days before.

It is interesting to note that there is a significant difference in crater volume between new material 12 x 12 panels and the 8 x 8 panels, remembering that all the panels were cut from the same sheet. These results again support a panel size effect occurring with the polycarbonate.

A portion of the scatter of the various curves can probably be attributed to the fact that the initial bullet velocity does not relate directly to the velocity of the bullet impacting the second panel. Since the bullet penetrates the first panel the residual impact velocity (relative to initial velocity) can vary somewhat. In addition the shape of the bullet, orientation and deviation also might add to the scatter shown on the curves.

REFERENCES

(1) "Degradation of the Bird Impact Resistance of Polycarbonate" J.B.R. Heath and R.W. Gould, National Research Council of Canada, National Aeronautical Establishment, Laboratory Technical Report LTR-ST-1326, January 1982.

TABLE 1

RESULTS OF CALIBRATION SHOTS
(Average Velocity Change in 10 Feet)

TEST NO.	INITIAL VEL. ft/sec.	FINAL VEL. ft/sec.	CHANGE IN VEL. ft/sec.
1	833	821	12
2	815	803	12
3	807	799	08
4	817	806	11
5	805	796	09
6	814	803	11
7	777	767	10
8	821	812	09
9	826	816	10
			MEAN 10.2
			STD. DEV. 1.4

TABLE 2

TEST No.	PANEL HISTORY	PANEL SIZE (in.)	INITIAL VEL. V_1 ft/sec.	FINAL VEL. V_2 ft/sec.	$\Delta V = V_1 - V_2$ ft/sec.	$\frac{\Delta V}{V_1}$	DEFLECTION - Inches U (Up), D (Down) L (Left), R (Right)	RESULTS
7	New	12 x 12	1066	781	285	0.27	0.13U, 2.25L.	
8	Same	Panel	1071	797	274	0.26	0.38U, 1.19L.	
10	"	"	1083	817	266	0.25	0.13D, 0	
2	N - 3*	12 x 12	1112	839	273	0.25	0.75D, 0.19R.	
3	Same	Panel	1043	735	308	0.30	0.75D, 1.13R.	
5	"	"	1033	733	300	0.29	1.13U, 0.75L.	
13	N - 8	8 x 8	1002	688	314	0.31	0.5U, 1.88L.	
14	Same	Panel	1116	854	262	0.24	0.69D, 0.19L.	Fracture from panel edge to hole test 13 almost to hole test 14
15	N - 8	8 x 8	1044	764	280	0.27	1.13D, 1.13R.	Fracture from test 15 hole. Fracture through all holes.
16	Same	Panel	1069	791	278	0.26	1.13D, 1.88L.	
21	"	"	1081	796	285	0.26	0.69D, 2.38L.	
11	A.A.**	12 x 12	1056	751	305	0.29	1.19U, 1.88L.	
19	Same	Panel	1082	773	309	0.29	1.69U, 1.88L.	
20	"	"	1021	695	326	0.32	2.0D. Z.44R.	

* Naturally Aged - X years

** Artificially Heat Aged - 100 hrs.

TABLE 3

TEST	PANEL HISTORY	PANEL SIZE (in.)	INITIAL VEL. ft/sec.	PANEL 1	PANEL 2	VOLUME of CRATER PANEL 2 (cc)	COMMENTS
4	New	12x12	1000	Pen	No Pen	.380	All shots within 6 in., dia.,
5	Same	Panel	976	"	"	.320	circle shots 4 and 9 spaced
6	"	"	993	"	"	.376	2-5/8 apart. No signs of
7	"	"	1004	"	"	.383	fracturing.
8	"	"	997	"	"	.339	
9	"	"	962	"	"	.275	
26	New	8x8	981	Pen	No Pen	.267	All shots within 4 in.,
27	Same	Panel	1003	"	"	.274	dia., circle.
28	"	"	995	"	"	.306	
29	"	"	968	"	"	.190	
30	"	"	991	"	"		Crack from test 26 to bottom L.H. corner crack from test 27 intersecting 1st crack - Test
31	"	"	980	"	"		31 at intersection of cracks, piece broke out of P_1 resulting in 1 in., dia., hole.

Table 3 cont.

TABLE 3 cont. (a)

TEST No.	PANEL HISTORY	PANEL SIZE (in.)	INITIAL VEL. ft/sec.	PANEL 1	PANEL 2	VOLUME of CRATER PANEL 2 (in.)	COMMENTS
32	New	8x8	986	Pen	No Pen	.299	All shots within 4 inch dia.,
33	Same	Panel	991	"	"	.290	circle. Crack from Test
34	"	"	989	"	"		32, 1½ in., crack from 33
35	"	"	991	"	"		4 in. Extensive Panel 1 damage.
36	New	8x8	982	Pen	No Pen	.283	All shots within 4 in. dia.
37	Same	Panel	1000	"	"	.374	circle. Crack from test
38	"	"	973	"	"		36, 1¼ in. Extensive
39	"	"	971	"	"		Panel 1 damage.
17	N-3*	12x12	1001	"	"	.243	All shots within 6 in. dia.
18	Same	Panel	995	"	"	.235	circle.
19	"	"	998	"	"	.277	
20	"	"	1016	"	"	.330	
21	"	"	1000	"	"	.248	
22	"	"	991	"	"	.201	No panel fracturing

TABLE 3 cont. (b)

TEST No.	PANEL HISTORY	PANEL SIZE (in.)	INITIAL VEL. ft/sec.	PANEL 1	PANEL 2	VOLUME of CRATER PANEL 2 (in.)	COMMENTS
23	N-8	8x8	974	Pen	No Pen	.209	All shots witnin 4 in. dia. cracking from test 23 large piece (7x3) separated from panel 1.
24	Same	Panel	1001	"	"		
25	"	"	974	"	"		
50	N-8	12x12	973	Pen	Pen		Large piece (4 in. dia.) separated from panel 2 major cracking occurred.
03	AA, 100 hrs. + 6 mos.	12x12	972	Pen	Pen		Major cracking in panel 2 large piece (3 x 4 x 5) separated from panel.
10	AA, 100 hrs. + 6 mos.	12x12	989	Pen	No Pen	.204	All shots within 6 in. dia.
11	Same	Panel	993	"	"	.207	
12	"	"	999	"	"	.207	Cracking along edge of panel 2, - 6 in. long.
13	"	"	995	"	"		Continuation of cracking due to edge of support frame.

TABLE 3 cont. (c)

TEST No.	PANEL HISTORY	PANEL SIZE (in.)	INITIAL VEL. ft/sec.	PANEL 1	PANEL 2	VOLUME of CRATER PANEL 2 (in.)	COMMENTS
14	AA, 100 hrs + 6 mos.	12x12	1000	Pen	No Pen	.189	All shots within 6 in. , dia., major crack along top edge major damage to panel 1, large piece 5 x 1½ separated from top cor.
15	Same	Panel	996	"	"		
16	"	"	994	"	"		
40	AA, 100 hrs	12 x 12	992	Pen	No Pen	.294	All shots within 6 in. dia.
41	Same	Panel	999	"	"	.326	
42	"	"	968	"	"	.195	
43	"	"	973	"	"	.246	
44	"	"	949	"	"	.128	
45	"	"	949	"	"	.126	
46	AA 196 hrs	12 x 12	961	Pen	No Pen	.156	All shots within 6 in. dia.
47	Same	Panel	982	"	"	.186	
48	"	"	1013	"	"	.350	
49	"	"	1000	"	"	.265	

* Naturally aged 3 years.
** Artificially heat aged.

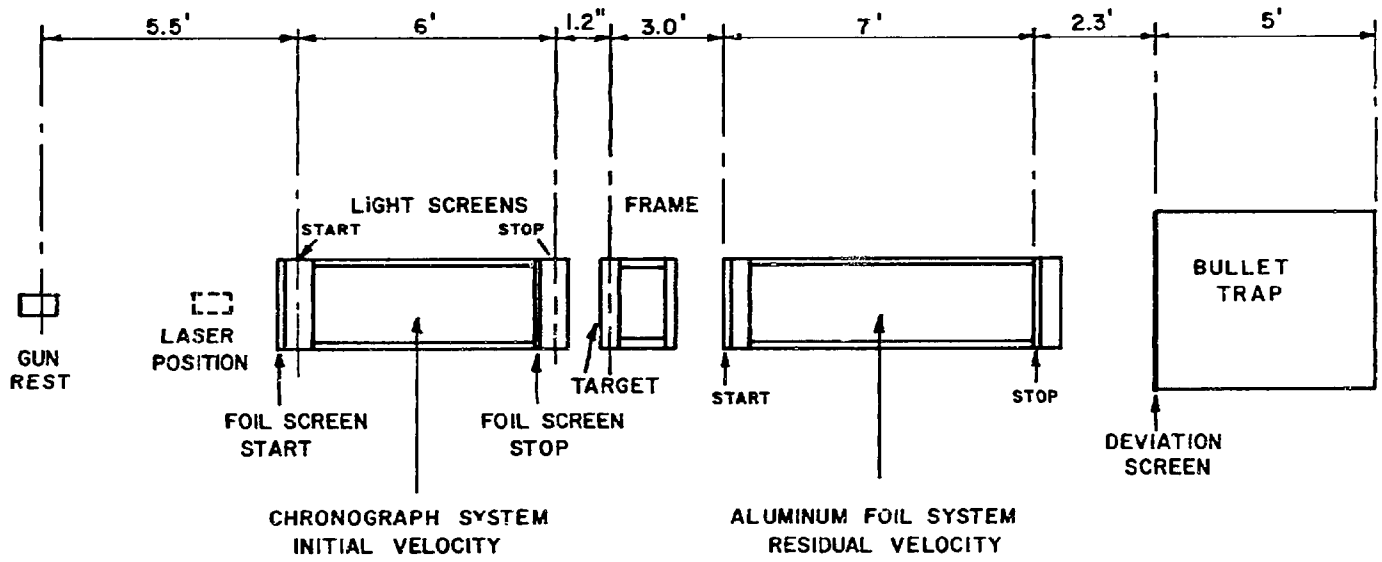

* CALIBRATION - NO TARGET
PART I - AS ABOVE
PART II - RESIDUAL VELOCITY SYSTEM REMOVED

FIG. 1 SCHEMATIC OF SET-UP *

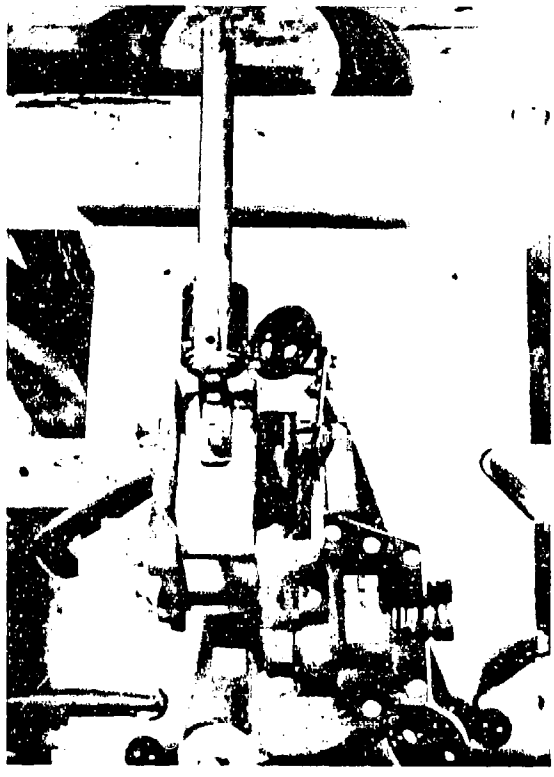

TOP VIEW

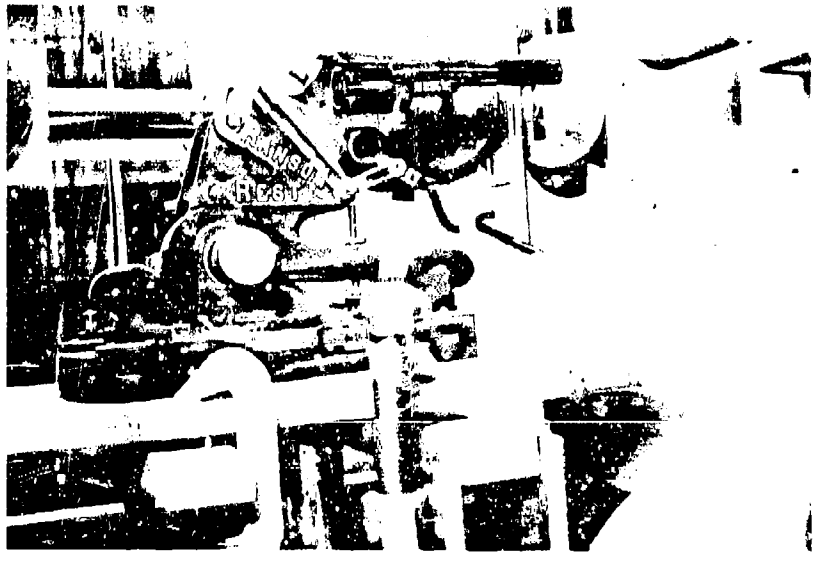

SIDE VIEW

FIG. 2 GUN REST SET-UP

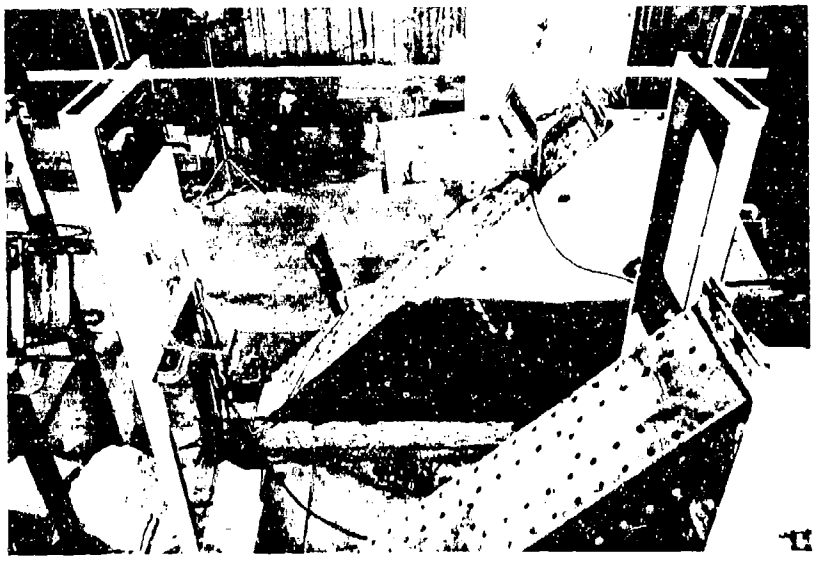

FIG. 3 FOIL SCREENS MOUNTED ON LIGHT SCREEN FRAMES - INITIAL VELOCITY MEASUREMENT

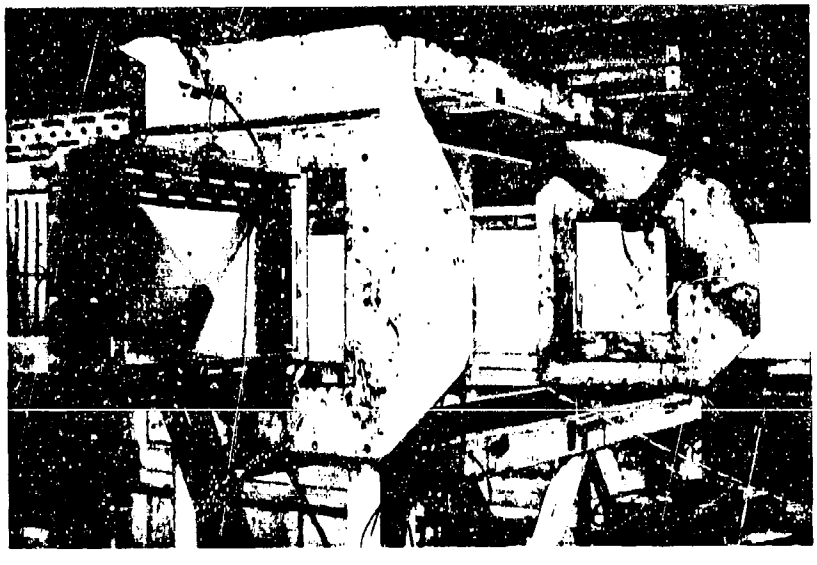

FIG. 4 FOIL SCREENS ON 7FT. FRAME - RESIDUAL VELOCITY MEASUREMENT

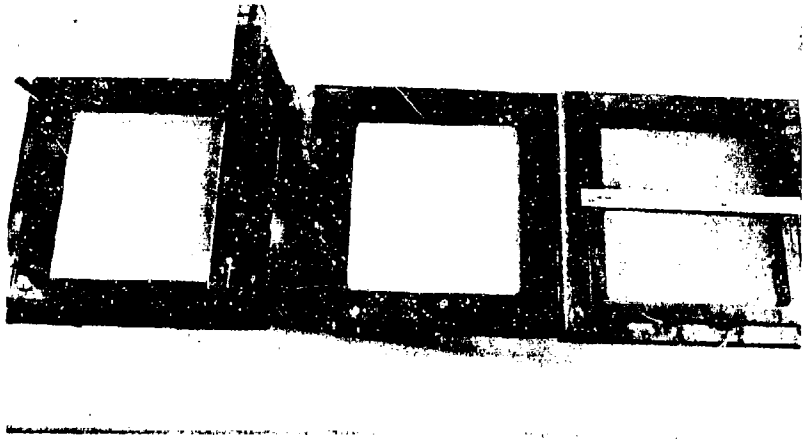

(a) COMPONENTS

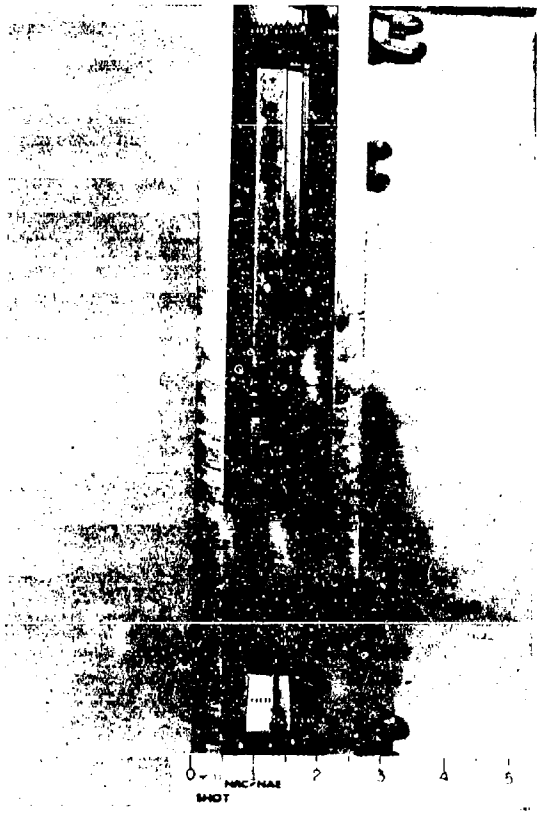

(b) SIDE VIEW
(PART II SET-UP)

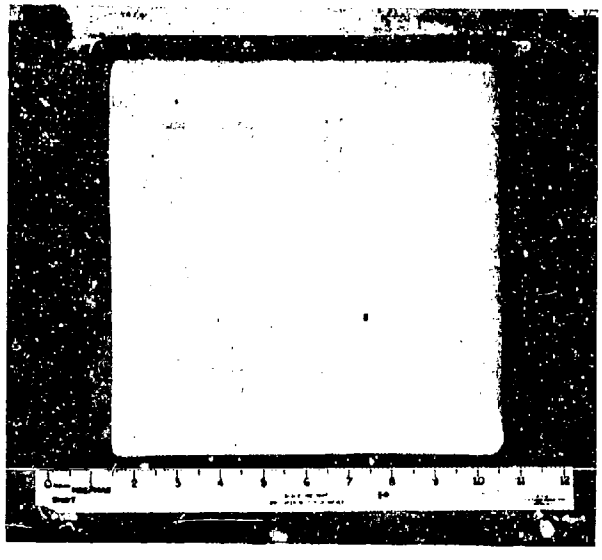

(c) FRONT VIEW

FIG. 5 TEST FIXTURE - 12" x 12" PANEL

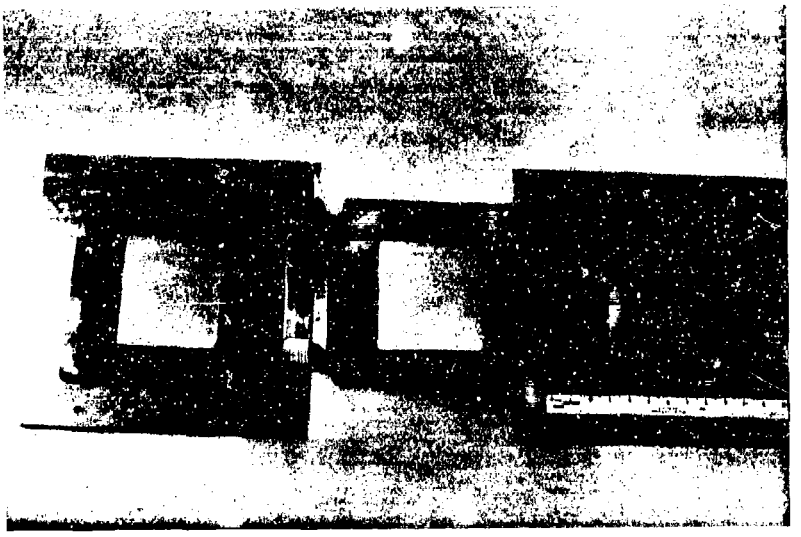

(a) COMPONENTS

(b) SIDE VIEW
(PART II SET-UP)

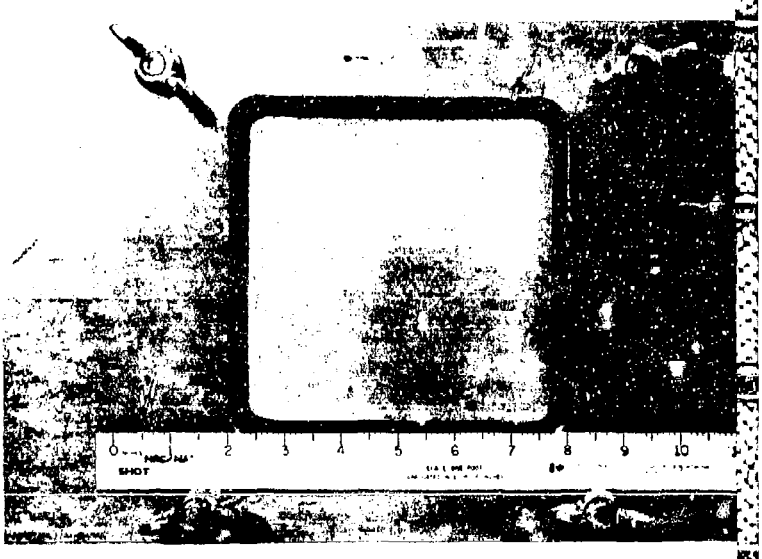

(c) FRONT VIEW

FIG. 6 TEST FIXTURE - 8" x 8" PANEL

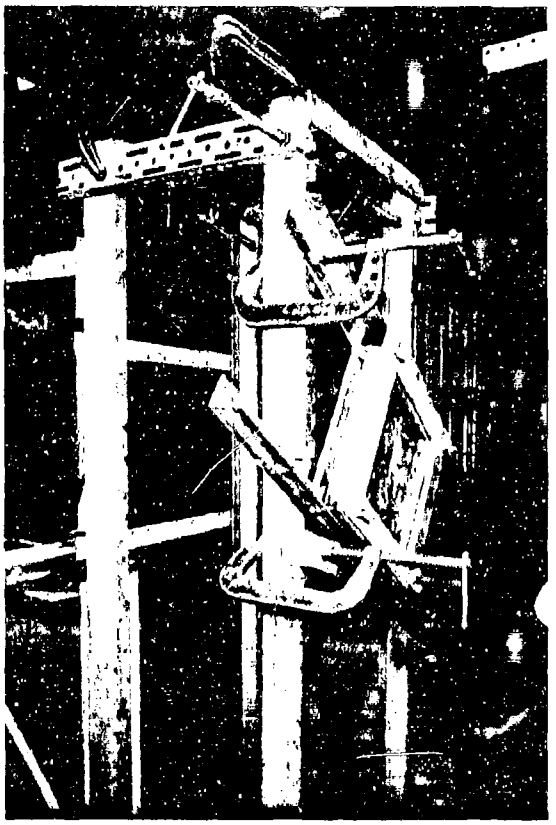

FIG. 7 TEST FIXTURE CLAMPED TO SUPPORT STRUCTURE

FIG. 8 LASER MOUNTED ON TRIPOD

(a) LASER BEAM PROJECTED THROUGH
BULLET HOLES IN INITIAL VELOCITY SCREENS

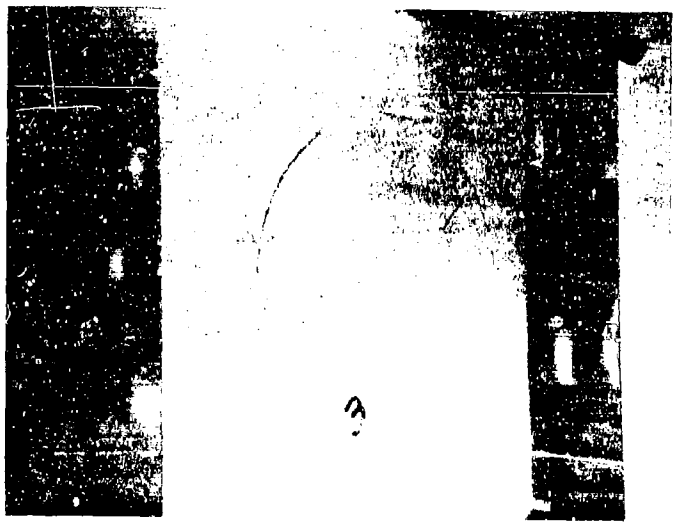

(b) LASER BEAM PROJECTED THROUGH
BULLET HOLE IN TEST PANEL

FIG. 9 ALIGNMENT OF SCREENS AND TEST FIXTURE

FIG. 10 BULLET TRAP

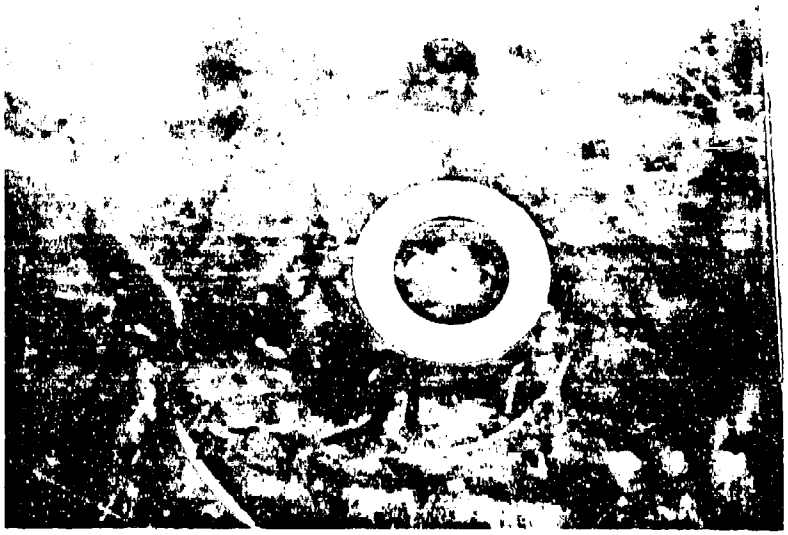

FIG. 11 FLAT STEEL WASHER CENTERED ABOUT CRATER

FIG. 12 PARAFFIN WAX DEPOSITED INTO CRATER AND TO LOCATE WASHER

FIG. 13 PARAFFIN WAX TRIMMED FLUSH

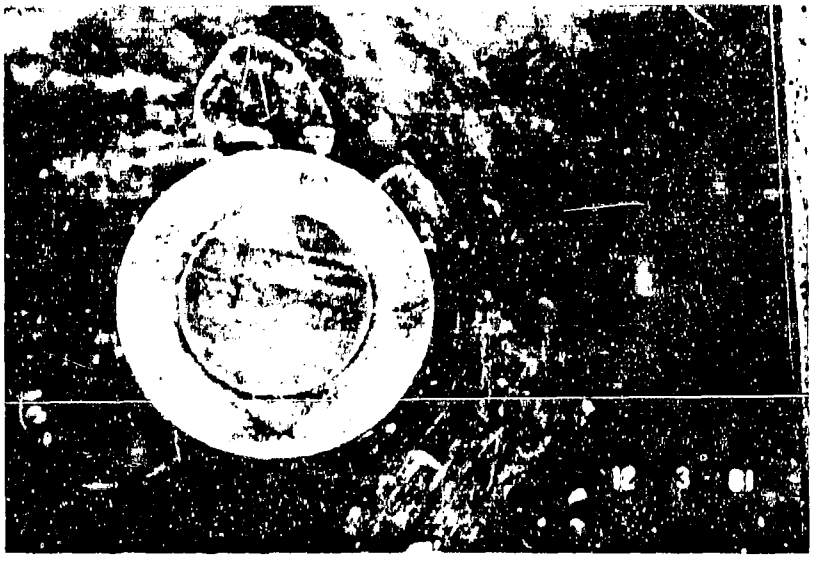

FIG. 14 WAX LOCATING DEPOSITS REMOVED

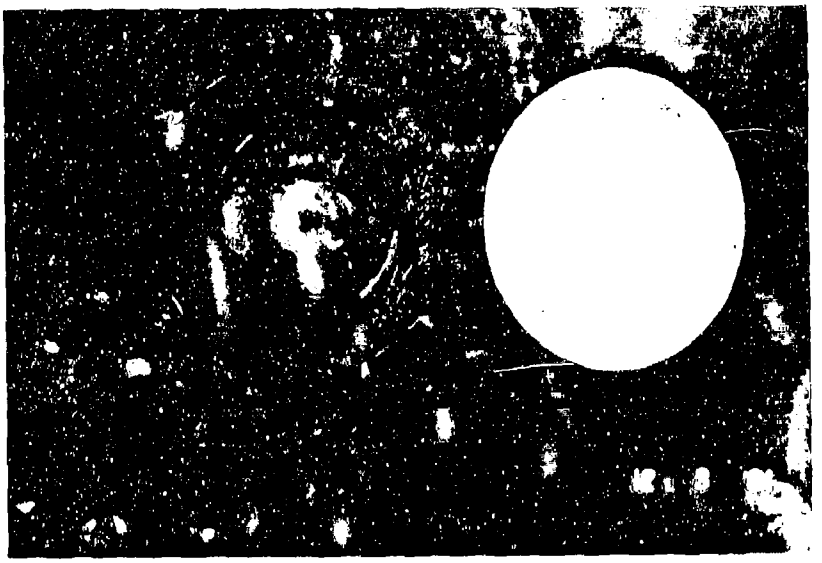

FIG. 15 WAX CASTING REMOVED

FIG. 16 EXAMPLES OF WAX CASTINGS. STEEL WASHER REMOVED. READY FOR WEIGHING

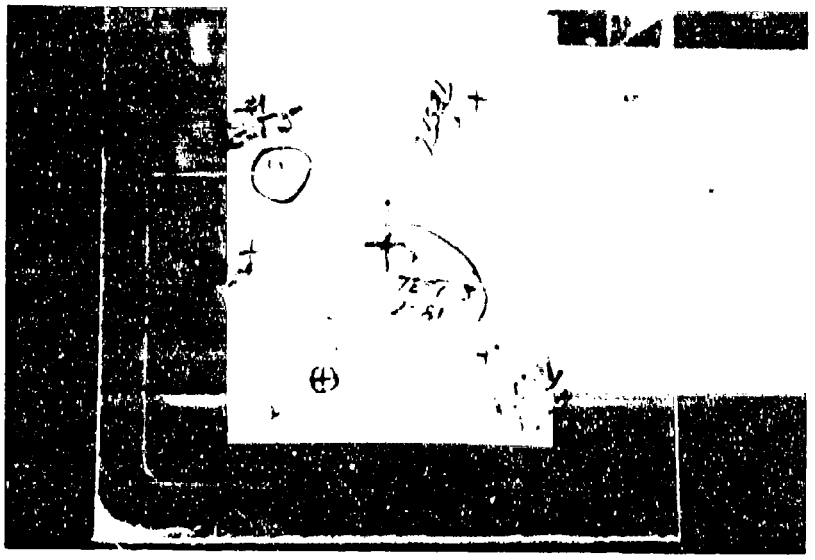

FIG. 17 TESTS 1 TO 6
PART I

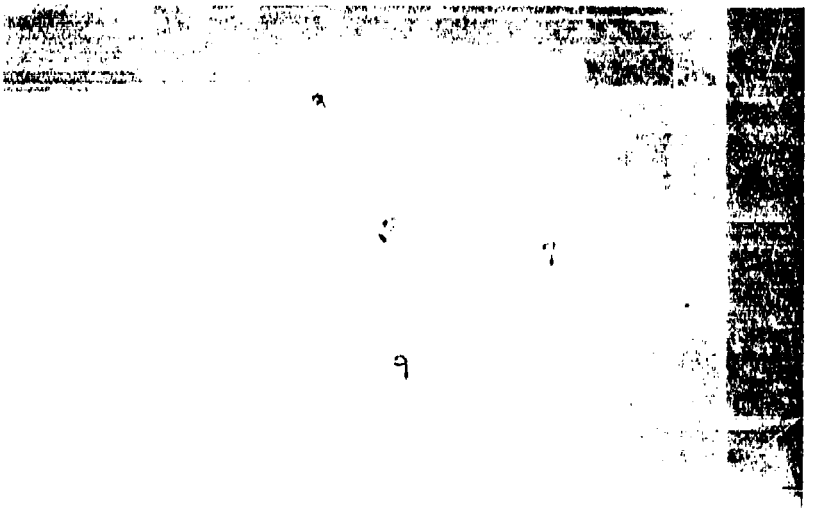

FIG. 18 TESTS 7 TO 10
PART I

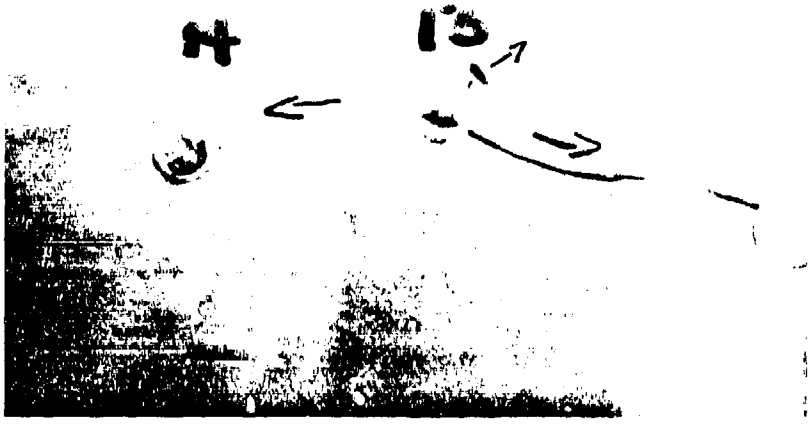

FIG. 19 TESTS 13 AND 14
PART I

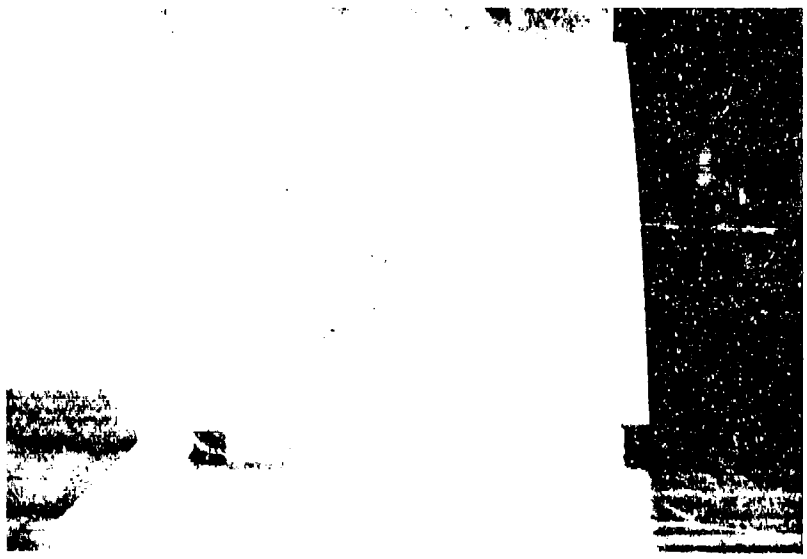

(a) TESTS 15 AND 16

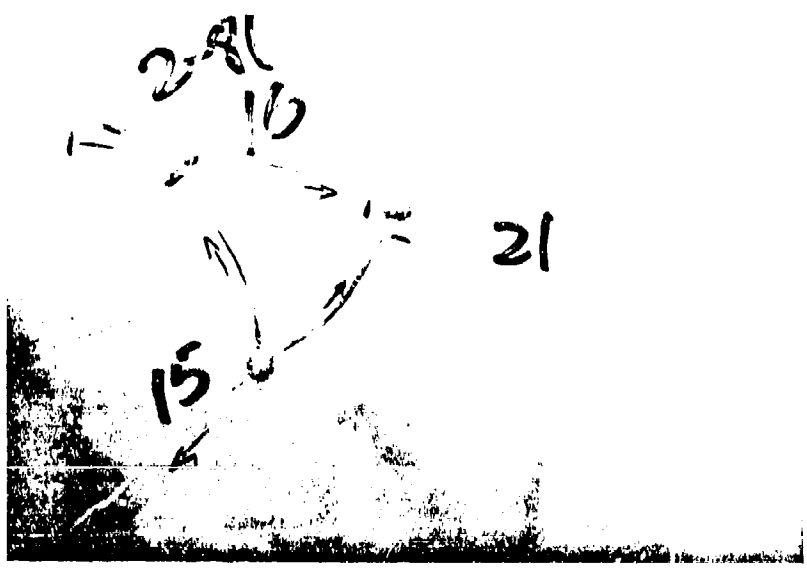

(b) TESTS 15, 16 AND 21

FIG. 20 PART I

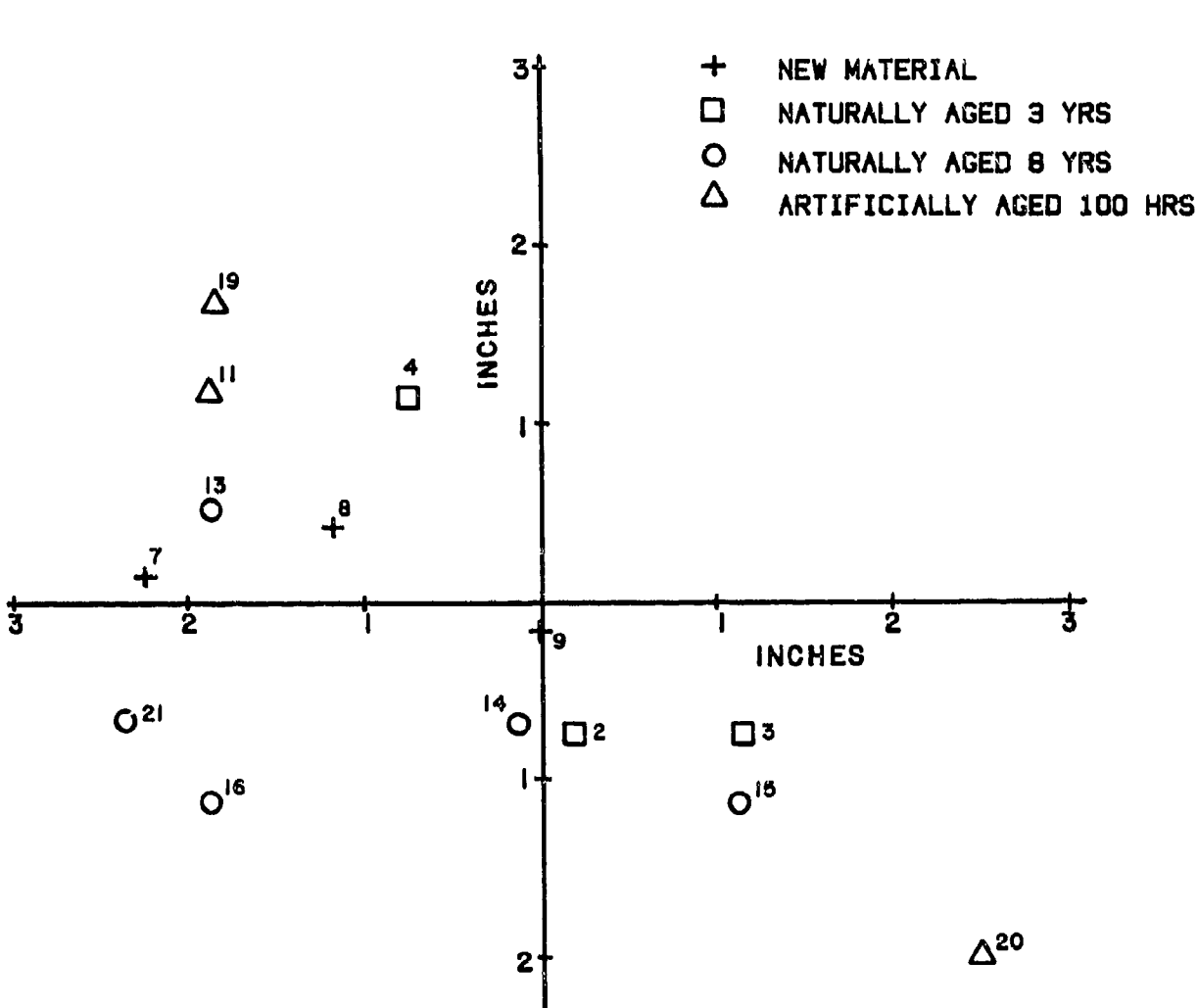

FIG. 21 BULLET POSITIONS ON DEVIATION SCREEN AFTER PANEL PENETRATION

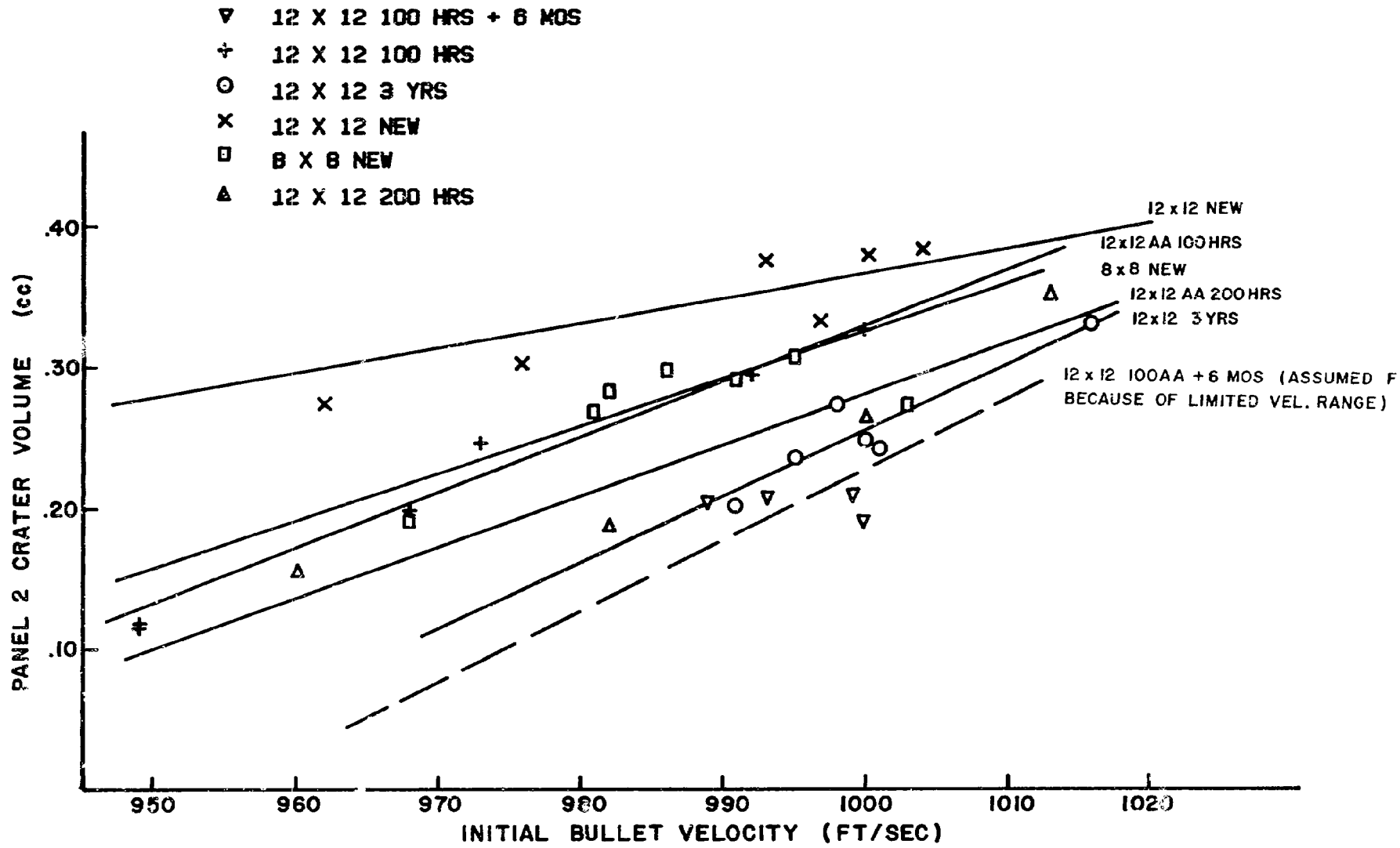
12 X 12 100 HRS + 6 MOS
12 X 12 100 HRS
12 X 12 3 YRS
12 X 12 NEW
8 X 8 NEW
12 X 12 200 HRS
12 x 12 NEW
12x12 AA 100 HRS
8x8 NEW
12x12 AA 200 HRS
12x12 3 YRS
12 x 12 100AA + 6 MOS (ASSUMED FIT BECAUSE OF LIMITED VEL. RANGE)
PANEL 2 CRATER VOLUME (cc)
.40
.30
.20
.10
950
960
970
980
990
1000
1010
1020
INITIAL BULLET VELOCITY (FT/SEC)

FIG. 22

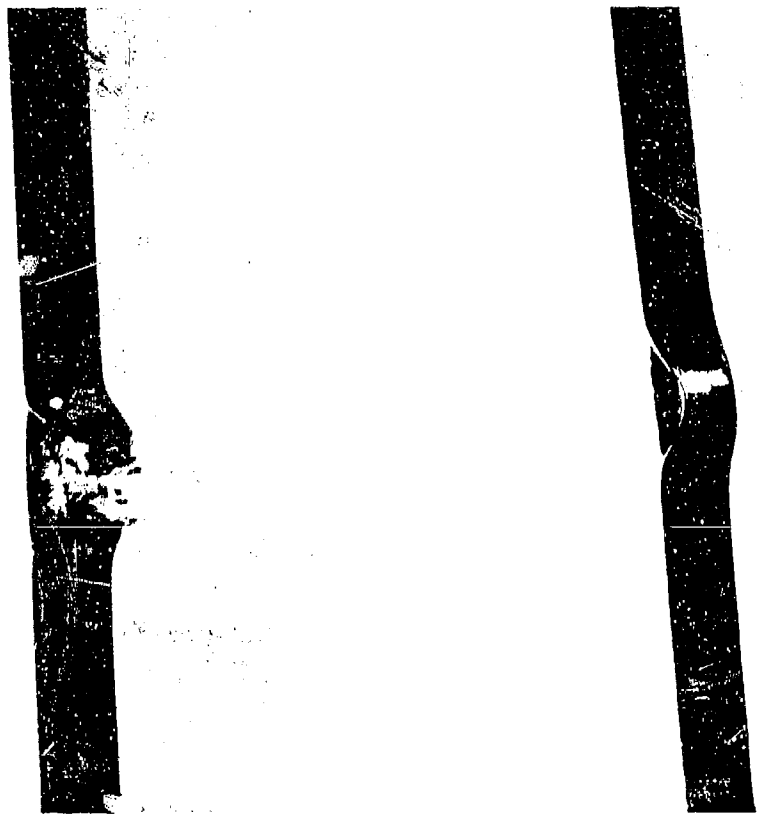

P1 P2

FIG. 23 TYPICAL IMPACT DAMAGE - PART II

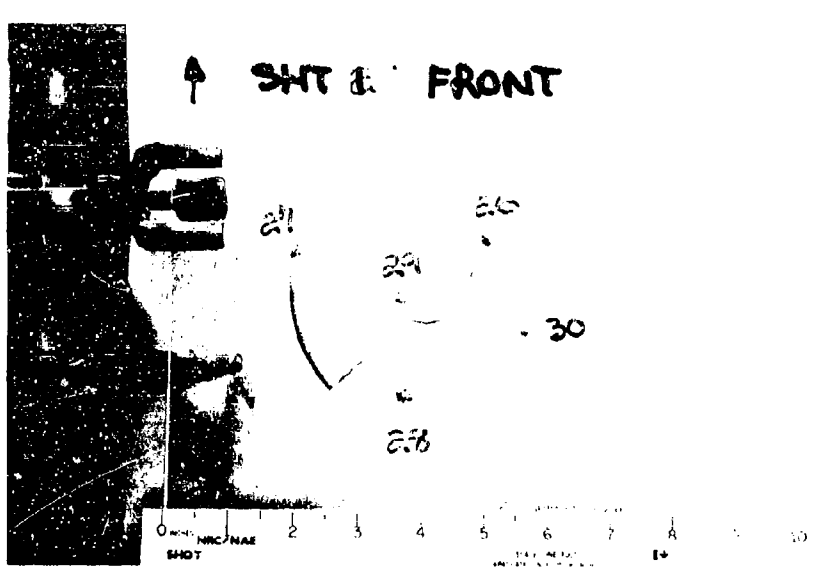

(a) DAMAGE AS A RESULT OF TEST 30

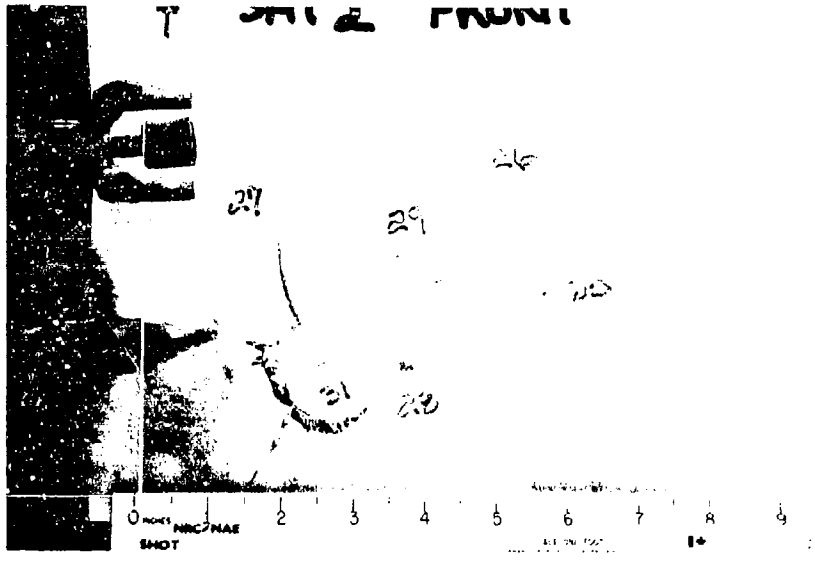

(b) DAMAGE AS A RESULT OF TEST 31

FIG. 24 TESTS 26 TO 31 - PANEL P1 - PART II

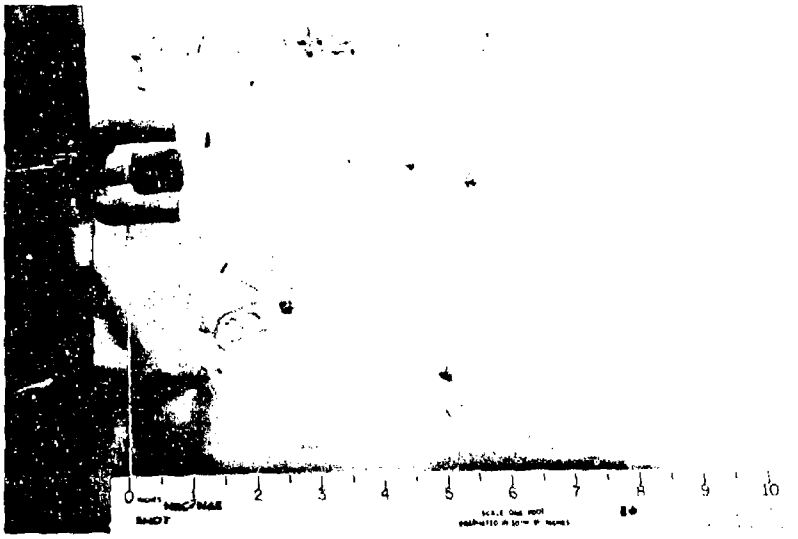

(a) DAMAGE AS A RESULT OF TEST 34

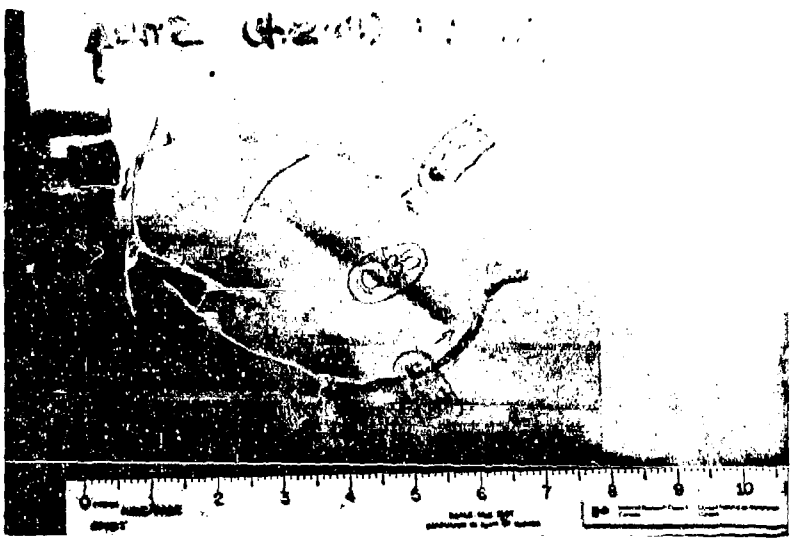

(b) DAMAGE AS A RESULT OF TEST 35

FIG. 25 TESTS 32 TO 35 - PANEL P1 - PART II

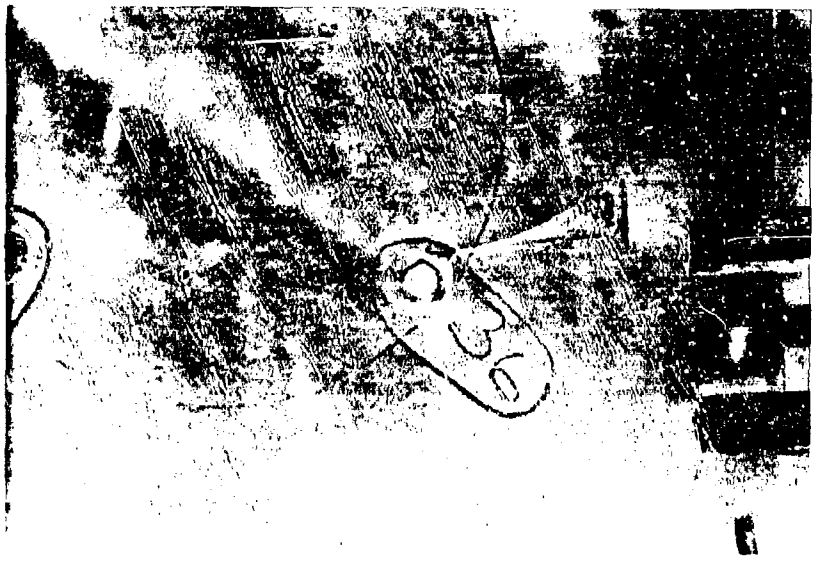

(a) DAMAGE AS A RESULT OF TEST 38

(b) DAMAGE AS A RESULT OF TEST 39

FIG. 26 TESTS 36 TO 39 - PANEL P1 - PART II

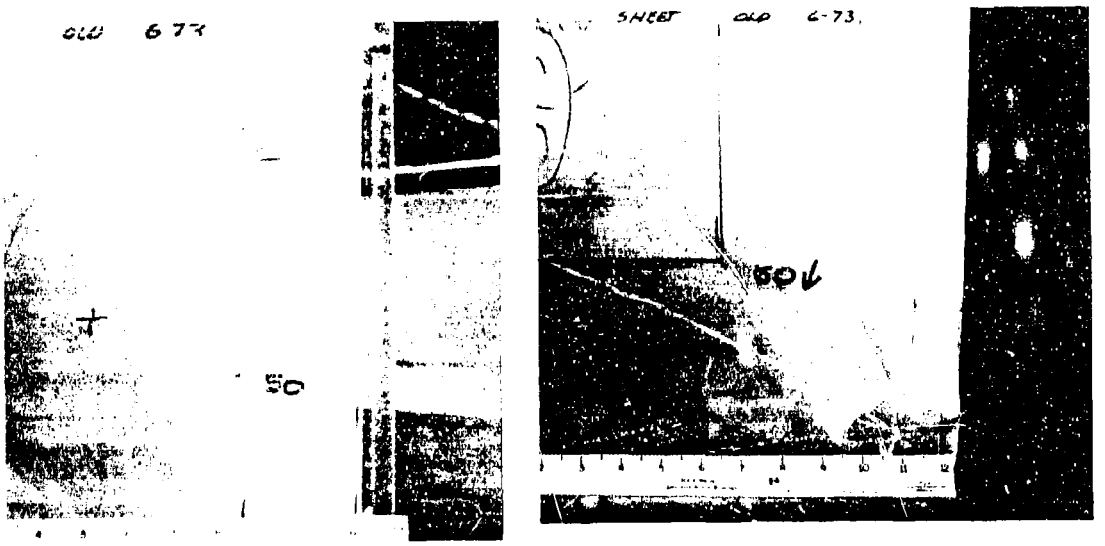

(a) P1 P2

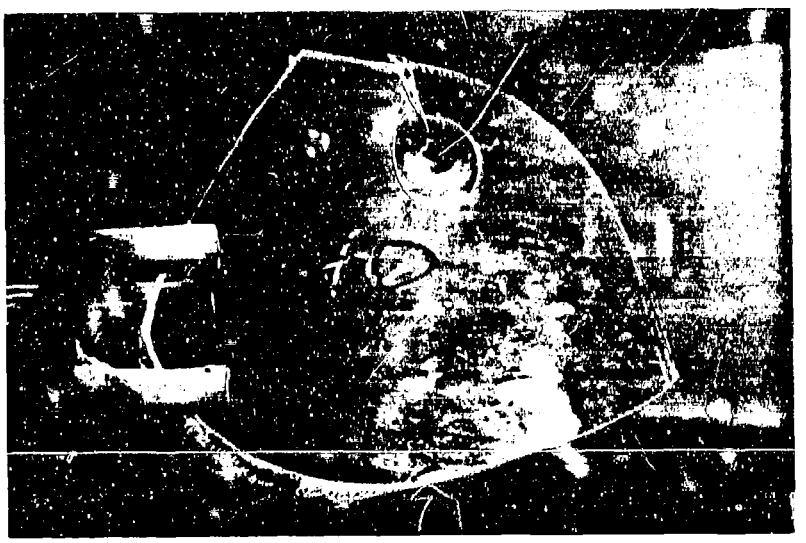

(b) PIECE SEPARATED FROM P2

FIG. 27 TEST 50 - PART II

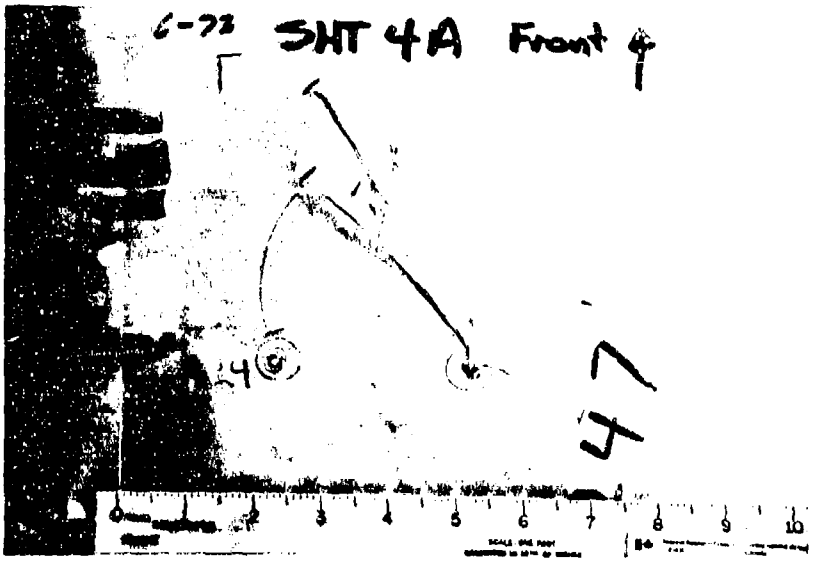

(a) DAMAGE AS A RESULT OF TEST 24

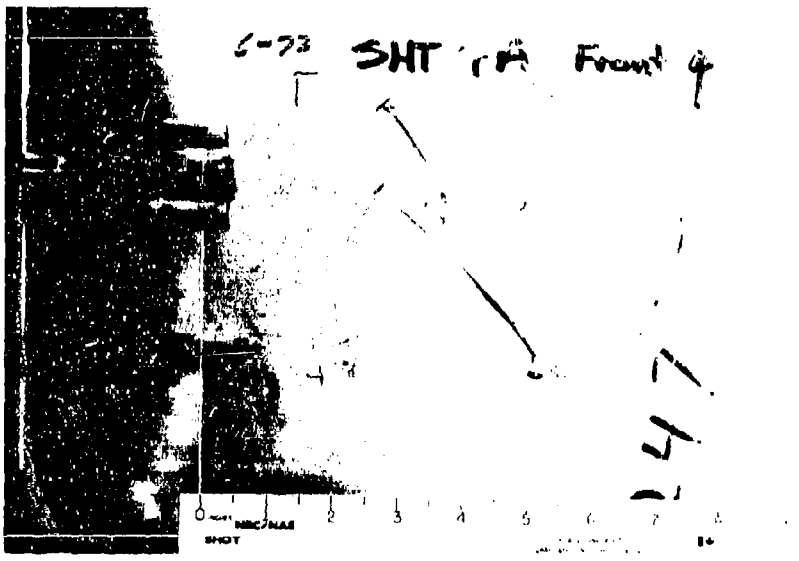

(b) DAMAGE AS A RESULT OF TEST 25

FIG. 28 TESTS 23 TO 25 - PANEL P1 - PART II

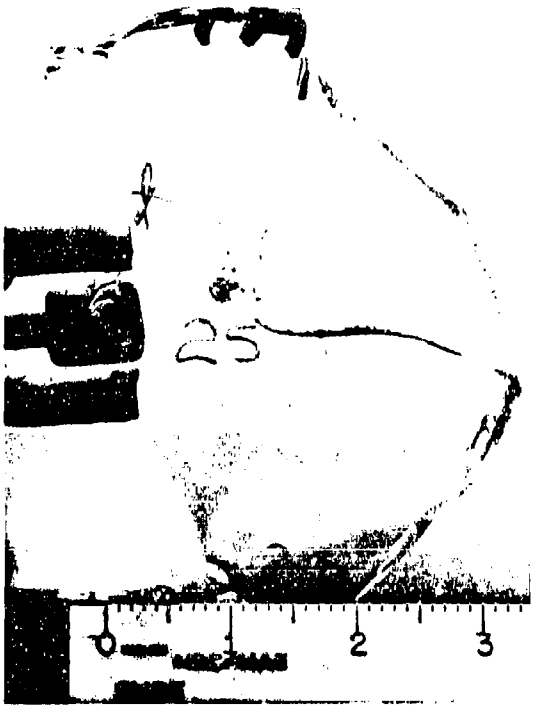

FIG. 29 PIECE SEPARATED FROM P1
TEST 25 - PART II

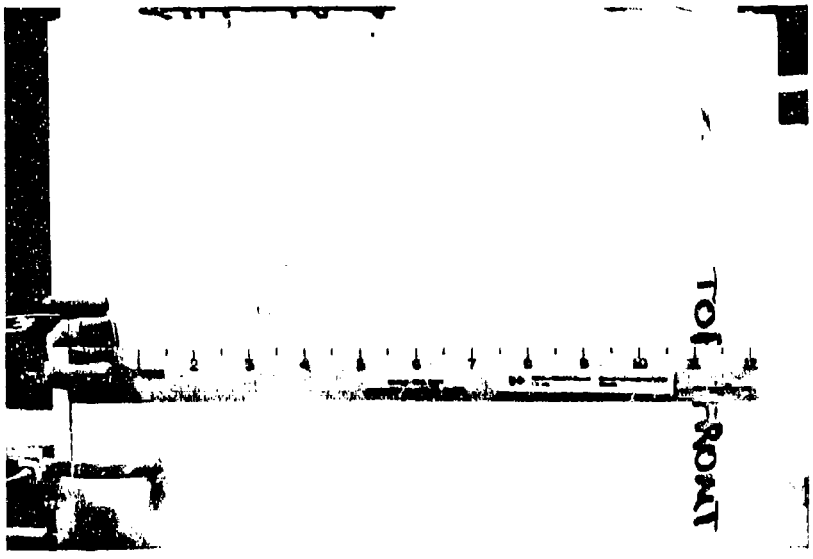

(a) PANEL P1

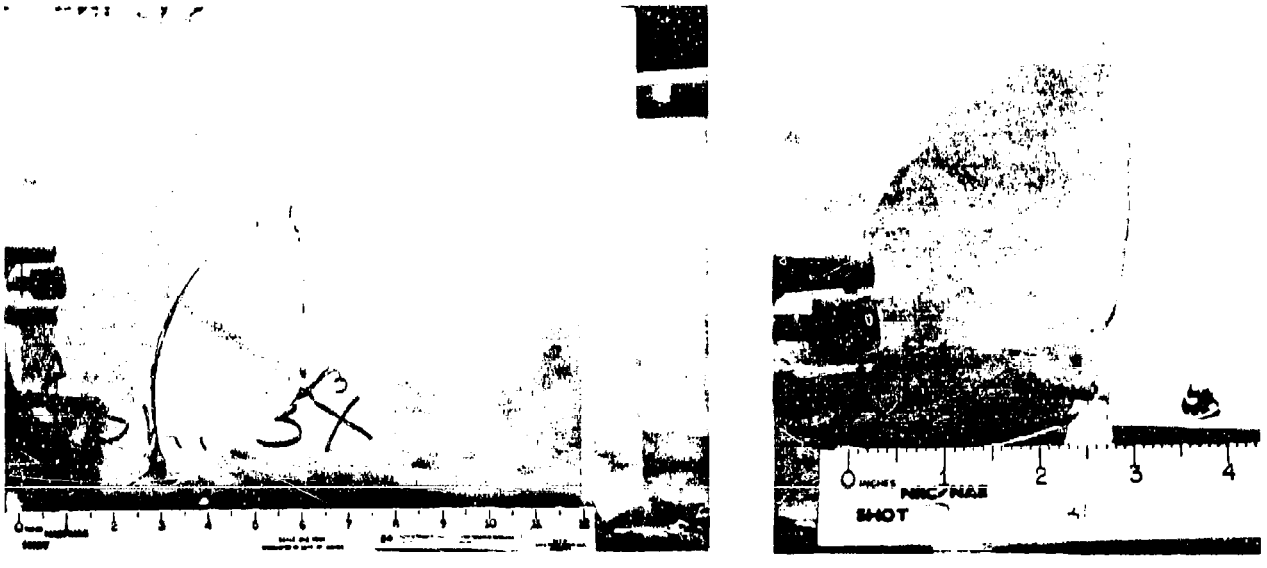

(b) DAMAGE, PANEL P2

FIG. 30 TEST 3 - PART II

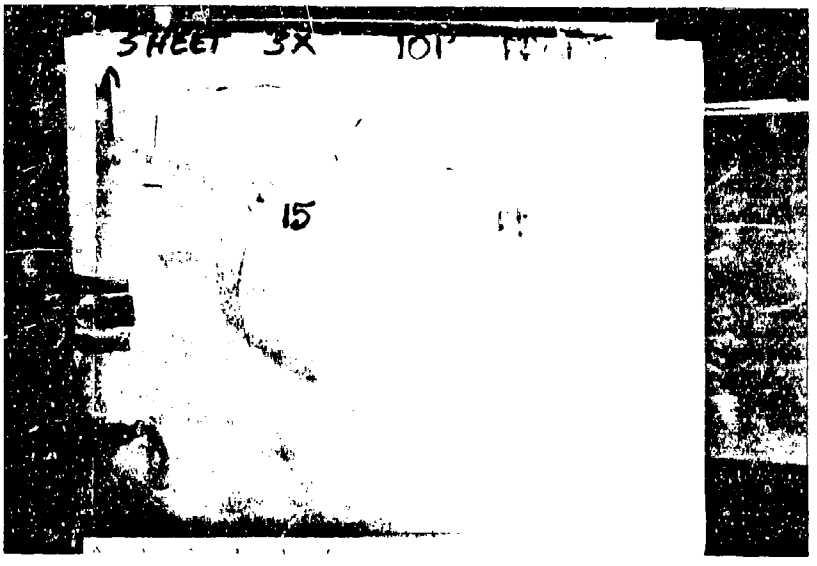

(a) DAMAGE AS A RESULT OF TEST 15

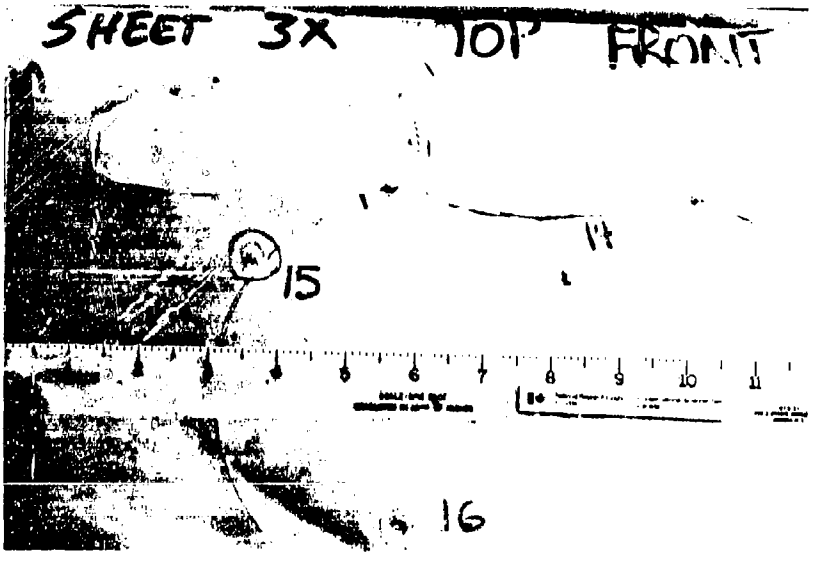

(b) DAMAGE AS A RESULT OF TEST 16

FIG. 31 TESTS 14 TO 16 - PANEL P1 - PART II

SESSION II

NEW MATERIALS (PART I)

Chairman: E. J. Morrisey
Materials Laboratory
Wright-Patterson Air
Force Base, Ohio

Co-Chairman: I. Wolock
Naval Research
Laboratory
Washington, D. C.

AD-P003 199

NEW HIGH PERFORMANCE WINDSHIELD/CANOPY MATERIALS

B. T. DeBona, Allied Chemical Corporation

New High Performance Windshield/Canopy Materials

B. T. DeBona
D. C. Prevorsek

Corporate Technology
Allied Corporation
Morristown, NJ 07960

Abstract

This paper covers a three year program to develop new, thermally stable, transparent plastics for use in high performance aircraft windshields and/or canopies. Forty-seven new materials were prepared during this period, each with a glass transition temperature exceeding those of currently used acrylic and polycarbonate plastics, and possessing varying degrees of transparency, color and impact strength. Substitution of thermally stable, aromatic diols and diacids by appropriate techniques for bisphenol-A in modified preparatory procedures for polycarbonates and polyesters has resulted in more thermally stable materials. Depending upon the reactants involved, new polyesters, polycarbonates, polyester-carbonates, copolyesters and copolyester-carbonates were prepared. Concepts governing the choice of monomers and their effects on final polymer properties is presented along with a brief discussion on the importance of molecular chain entanglement in the glassy state.

Materials based upon tetramethyl dicumyl bisphenol (coded AF-TP-2) have glass transition temperatures (Tg) ranging from 190° to 228°C (374°F to 442°F); light transmittance is generally over 80%; however, haze is rather high, the yellowness index is high, and the impact strength (notched Izod) is between 1.0 to 3.0 ft-lb per inch of notch. Materials based upon combinations of tetramethyl dicumyl bisphenol, bisphenol-A, terephthaloyl chloride and phosgene also possess desirable properties.

Polyester-carbonates based on phenolphthalein (coded AF-TP-10, 11 and 12) show outstanding thermal and mechanical properties. These transparent materials have Tg's ranging from 200°-234°C, notched Izod impact strengths of 3 to 8 ft-lb/in, and yellowness indices as low as 9. For AF-TP-10, 11 and 12, comprehensive evaluations were conducted including long-term environmental aging. These three materials show exceptionally good resistance to thermal embrittlement.

A novel surface hardening agent was evaluated with these materials. One surface hardened material survived the Rain Erosion Test without damage for 105 minutes at 500 mph.

BACKGROUND

During the last decade, there has been an increasing need for improved materials of construction for advanced aircraft that operate at supersonic speeds. One materials area in which improvements continue to be needed is the transparencies of windshield-canopy assemblies. Several requirements for these transparencies are thermal stability, resistance to bird impact, abrasion resistance, optical clarity, and minimum maintenance. While glass transparencies have adequate thermal resistance properties, various problems exist such as the weight of finished part, brittleness and the difficulty of making contoured parts.

Properties such as low density, impact strength and optical clarity have been relatively easily achieved with several synthetic plastics. However, the existing plastics which meet requirements of transparency and impact strength do not have sufficient heat resistance for windshield-canopy applications in advanced aircraft. Two noteworthy examples are acrylics and biphenol-A polycarbonate. In the case of acrylics the service limit is about 250°F (121°C). With polycarbonate dimensional stability can be maintained up to about 300°F (149°C) for short periods of time. Since the windshield - canopy structures of advanced aircraft can reach temperatures as high as 450°F (232°C), the need for a more thermally resistant plastic having the required optical clarity, impact resistance, abrasion resistance and processability is clearly evident.

During the past several years Allied Corporation has been involved in an extensive program aimed at the development of a family of novel engineering thermoplastics having higher heat distortion temperatures than conventional polycarbonates. The primary member of this series is a polyester-carbonate copolymer which has a heat distortion temperature of about 350°F (177°C), good optical properties, high impact resistance and is processable with conventional equipment.

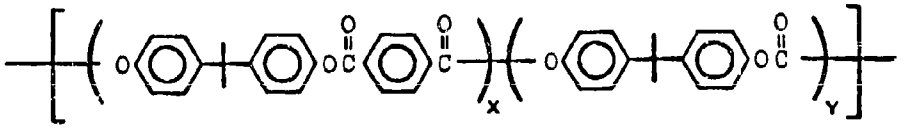

Reference Polyester-carbonate

Unlike bisphenol-A polycarbonate this material does not undergo thermal embrittlement which is a serious problem for any application requiring the retention of impact strength after heating cycles. This polyester-carbonate comes very

close to meeting the major target objectives for advanced aircraft transparencies. The only shortcoming of the material is a heat distortion temperature below 200°C.

The main objective of this research program was the development of analogs of the polyester-carbonate which embody all of the general physical properties listed below* and in particular an increase in the heat distortion temperature of about 50 to 100°F (25 to 50°C). The technical approach employed to arrive at suitable materials involved primarily a selective structural redesign of the monomeric components comprising the basic polyester-carbonate.

* - Clear, colorless, totally amorphous
- Melt processability
- Abrasion resistance
- Thermal stability, high Tg (~ 200°C or higher)
- Excellent mechanical properties, high impact strength
- Impact strength retention after environmental exposure

TECHNICAL DISCUSSION AND RESULTS

Since the reference polyester-carbonate possessed most of the characteristics required for high performance transparencies, the primary thrust of this research was directed toward the synthesis of structural analogs having Tg's of at least 200°C. Figure 1 shows the idealized repeat unit for the reference polymer along with that for commercial polycarbonate. From an examination of these structures it can be seen that in effect the Tg of polycarbonate was raised ~ 25°C by replacing 50% of the carbonate linkages with terephthalate ester linkages. With regard to most other physical and mechanical properties the two materials are similar. Within this approach the reference polymer could be further modified by employing structural variations in the diol component (bisphenol-A) as well as the diacid components (terephthalic and carbonic acids).

In order to provide a sound scientific and systematic basis for the synthetic work, certain criteria were established governing the molecular design of the monomeric components and their effects on the final polymers.

1. Expected Tg
2. Effects on chain entanglement density (mechanical properties)
3. Environmental stability (thermal, chemical, uv-visible radiation)
4. Effects on crystallinity (optical properties).

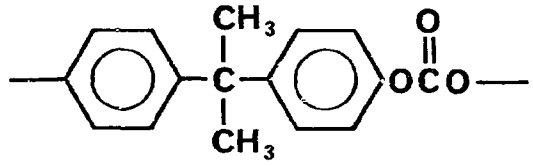

BPA POLYCARBONATE, Tg = 150°C

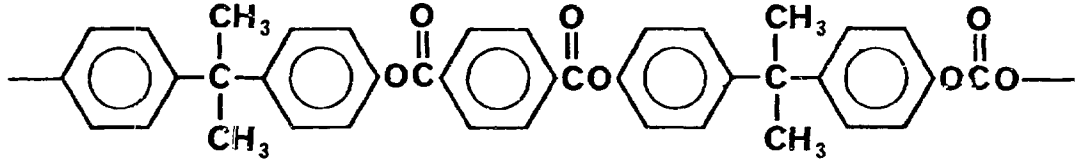

REFERENCE POLYESTER-CARBONATE, Tg = 180°C

FIGURE 1 POLYCARBONATE AND REFERENCE POLYESTER-CARBONATE

For many polymer structures Tg can be roughly calculated using the empirical methods described by Van Krevelen which involve functional group contributions to Tg[1]. In this study these estimates were of value in narrowing the very large number of dicl and diacid structures which could meet the remaining three criteria.

During the development of the reference polyester-carbonate, we postulated that the unique characteristics of bisphenol-A polycarbonate (PC), i.e., its high impact resistance and toughness below Tg must be attributed to the geometry of the bisphenol-A group. On the basis of a comprehensive review of polymer properties and molecular structure, we postulated that the spatial arrangement of the phenylene groups prevents close packing of the polymer coil, which in turn leads to a high degree of chain entanglement as indicated by viscoelastic measurements. We have further speculated that high entanglement also indicates a high degree of chain interpenetration.

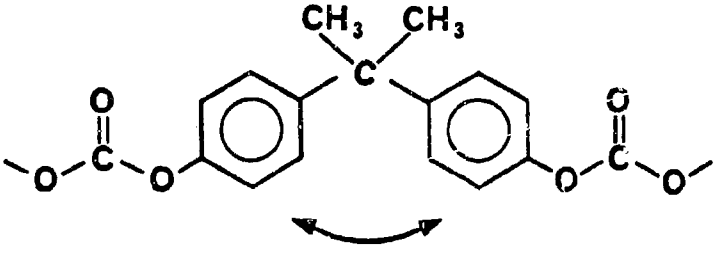

We then rationalized that in systems where all other factors except chain interpenetration remain constant, increases in chain entanglement and chain interpenetration should have a positive effect on many mechanical properties such as yield stress and yield strain, dimensional stability under load, impact resistance, etc. This latter assumption was recently verified by the results of M. Hoffman.[2]

Our interpretation of polycarbonate behavior differs considerably from the interpretation proposed in the published literature which attributes high impact strength and ductility below T_g primarily to secondary motions involving the carbonate linkage. Since relatively strong transitions associated with these relaxations appear at about -40°C, it was assumed that PC remains ductile and impact resistant as long as these motions remain activated.

In our judgment, the carbonate group is relatively unimportant in impact resistance but essential for the control of T_g and crystallinity, especially with polyester-carbonates derived from bisphenol-A and terephthalic acid. With this system, the polycarbonate moiety is required to render the polymer melt processable and amorphous.

Using the polycarbonate molecule, we can define the structural variables which affect the mechanical and thermal properties of high T_g polymers. These are illustrated in Figure 2.

For our purposes, the primary concerns were the effect of:

1. Stiff segment length "L"
2. Characteristics of chain redirecting group
3. Groups affecting packing and free volume
4. Main chain angle "δ" and its bending force constant
5. Side groups
6. Chain interaction (hydrogen bonding, polar groups, etc.)

The effects of an increase in stiff segment length was to some extent established with the reference polyester-carbonate. This effect is illustrated in Figure 3. The results showed that with all other parameters essentially unchanged, the increase in stiff segment length leads to an increase in chain entanglement, improvements in impact resistance and resistance to embrittlement at low temperatures and on thermal aging. Since this modification involves an increase in T_g, there is a limitation in the length of "L" because melt processability is required. Nevertheless, the studies with the reference polyester-carbonate clearly demonstrated the improvements resulting from increases in "L" above the value in polycarbonate. Furthermore, it was shown that the reduction of carbonate linkages by a factor of two had little detrimental effect on such mechanical properties as ductility and impact resistance.

Using the concepts developed for the properties of bisphenol-A polycarbonate and the polyester-carbonate, the molecular design of suitable candidates (i.e., higher T_g) for high performance windshield/canopy materials can be met with the following criteria:

1. Chain interaction similar to BPA polycarbonate and the reference polymer.

2. Stiff segment length "L" greater than that of BPA polycarbonate but in the same range as that for the reference polymer.

3. Absence of carbonate moieties or at least sufficient reduction to maintain T_g.

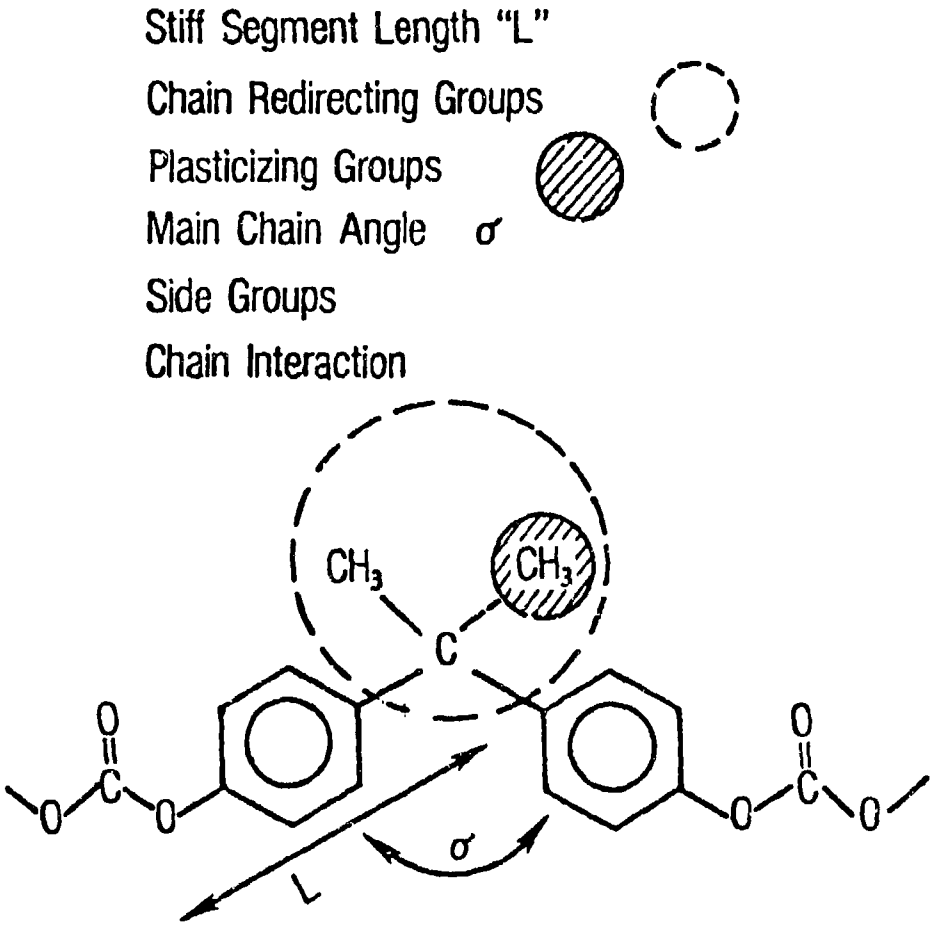

FIGURE 2 STRUCTURAL VARIABLES AFFECTING PROPERTIES OF HIGH Tg POLYMERS

BPA POLYCARBONATE

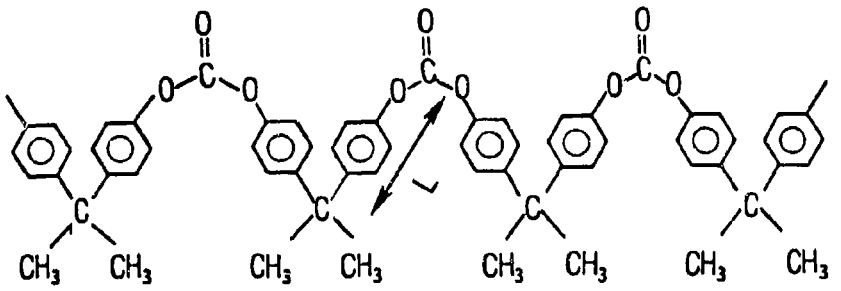

REFERENCE POLYESTER-CARBONATE

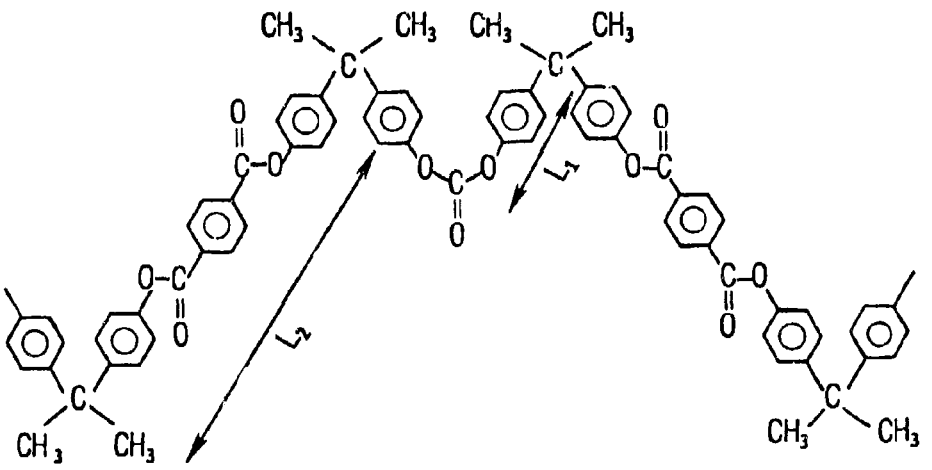

FIGURE 3 STRUCTURES OF POLYCARBONATE AND POLYESTER-CARBONATE: COMPARISON OF STIFF SEGMENT LENGTH.

The remaining criteria of environmental stability and low crystallinity for the polymers placed further restrictions on the structural variations possible within the scope of the program. Such factors as thermal stability, moisture sensitivity, color and opacity (crystallinity) effectively ruled out many monomeric structures which otherwise might have met T_g and mechanical property requirements in the appropriate polymers.

The starting point of our synthesis effort was the preparation of polyesters derived from tetra-substituted bisphenols. Our primary focus was on such monomers in which the ring positions ortho to the hydroxyl groups were substituted with moderately bulky substituents ($-CH_3$). Such substitution is known to result in attenuation of the inherent flexibility of the carbonate or ester linkages which in general is manifested by an increase in the glass transition temperature, T_g, of the substituted vs. unsubstituted polymer. In addition, the proximity of alkyl substituents ortho to the carbonate or ester linkage provides a steric "shielding" which effectively enhances the overall hydrolytic stability of the polymer, especially polycarbonates.

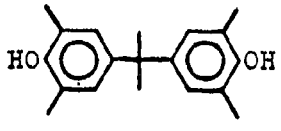

TMBA

Although the above approach was expected to raise the T_g above 200°C and provide greater hydrolytic stability, two important difficulties were anticipated as a direct result of the steric bulk of the substituents. The first was the difficulty in attaining high molecular weight polymer in solution polycondensations, the second and more important was the adverse effect on mechanical properties.

In the case of polyesters derived, for example, from unsubstituted aromatic and aliphatic acid chlorides, solution polycondensation in the presence of tertiary amine catalysts was sufficient for attainment of high molecular weight. In contrast, polycarbonates had to be prepared by activating the

hindered hydroxyl groups enough to overcome the steric boundary. This was conveniently accomplished by converting the hydroxyls to phenoxide anion in what is essentially a two-stage interfacial polycondensation. The procedures were also extended to allow for preparation of polyester-carbonate copolymers (acid chloride and phosgene) by a two stage one pot process. By utilization of these techniques, the entire range of copolymer composition was easily obtainable in which the monomer ratios in the final polymer were the same as the monomer feed ratios.

A preliminary investigation of this approach provided necessary information with respect to T_g and mechanical property changes. The likelihood that suitable additional structural modifications along with the basic approach could suffice to raise T_g without compromising mechanical properties was also assessed.

Initial experimental work was conducted on the preparation and preliminary screening of polymers derived from 0,0,0',0'-tetramethylbisphenol-A (TMBA). Although all polymers prepared from this monomer were unacceptable in terms of mechanical properties (i.e., brittle), new polymerization chemistry was developed which was directly applicable to structural analogs of TMBA.

Table 1 - POLYMERS OF TETRAMETHYLBISPHENOL-A (TMBA)

Designation	Type	η sp/C*	T_g (°C)	TGA (°C)	Ductility
AF-TP-1	Oxalate	4.0	153	> 350	---
AF-TP-1A	TPA Ester[a]	1.9	253	> 400	Brittle
AF-TP-1B	Carbonate	0.87	195	> 400	Brittle
AF-TP-1B-1	Carbonate	1.23	200	> 400	Brittle
AF-TP-1C	TPA-Carbonate[b]	1.43	223	> 400	Somewhat Brittle

* C = 0.5, phenol-TCE, 25°C
a = Terephthalate Homopolymer
b = 1:1 Copolymer

In order to further identify some molecular-structural factors responsible for the poor elongation properties of AF-TP-1C an investigation of some related polymers based on ortho-substituted dicymyl bisphenols was initiated.

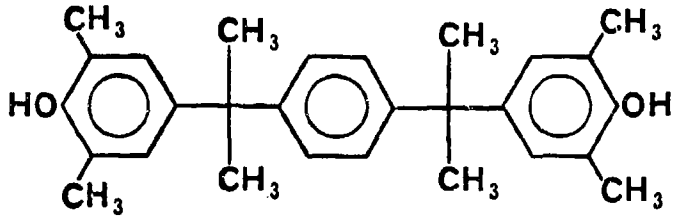

(TMDCB)

Tetramethyl dicumyl bisphenol (TMDCB) is essentially a structural modification of TMBA. The reason for this choice was two-fold. Reduction of the inherent flexibility of the carbonate or ester linkages by ortho-substitution while desirably raising the T_g of polycarbonates and polyestercarbonates was also recognized as a factor which seriously lowers the ducility. Thus, a beneficial modification would be one in which a number of carbonate or ester linkages is replaced with a unit which is known to keep the T_g within the necessary range without sacrifice in mechanical properties. There was ample evidence to indicate that the dicumyl bisphenol structure would meet these requirements, since mechanical properties, as well as T_g of the corresponding polycarbonate are quite similar to those of bisphenol-A polycarbonate.

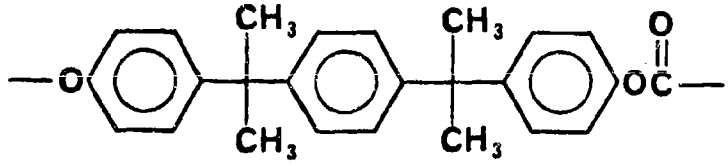

(DCB Polycarbonate)

By examining the effects on mechanical properties of ortho substitution in polymers derived from dicumyl bisphenols, a qualitative assessment of the importance of carbonate or ester flexibility vs that of structural modification between the phenolic rings would be possible.

The TMDCB was synthesized by starting with p-diisopropyl benzene as presented in the following scheme:

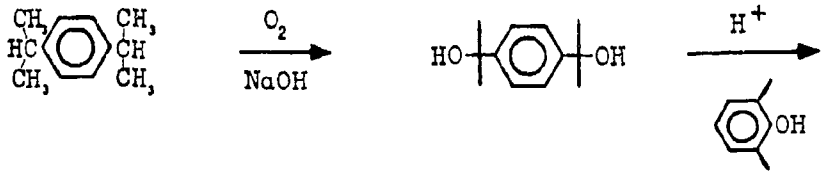

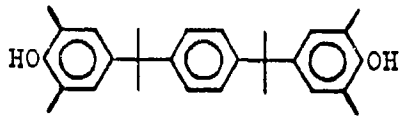

The reaction was conducted in two steps with purification of the intermediate p-diisopropyl benzene - α, α' -diol by recrystallization. The yield of highly pure TMDCB monomer after two recrystallizations averaged over many runs was 50% based on starting diol.

The preparation of polyester-carbonates from TMDCB is outlined in the scheme in Figure 4.

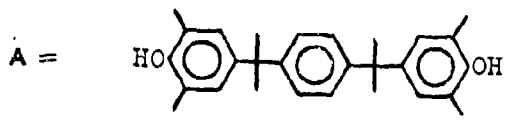

STAGE I

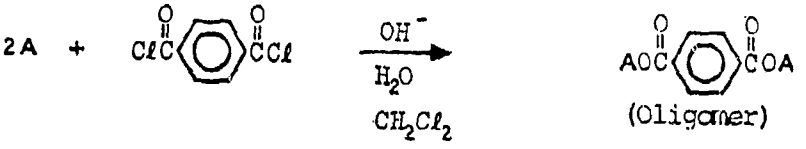

STAGE II

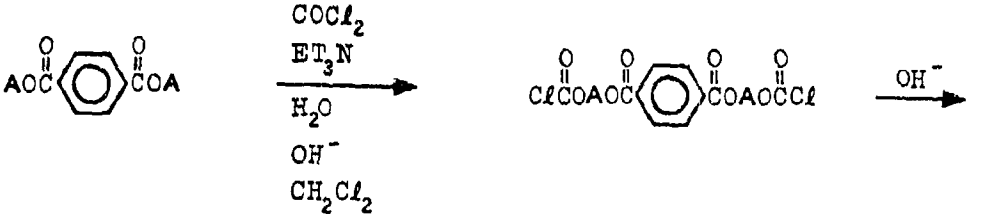

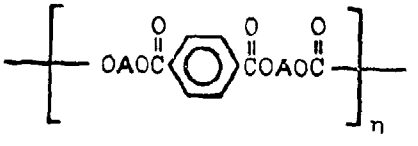

(AF-TP-2)

FIGURE 4 TWO STAGE INTERFACIAL PROCESS FOR AF-TP-2 SERIES

The first stage of the process involved the preparation of low molecular weight hydroxyl terminated oligomer by the interfacial technique, followed by addition of phosgene to form chloroformate terminated oligomers which then undergo polycondensation to the final product. The above equation for the two-stage scheme shows the "idealized" alternating copolyestercarbonate resulting from a 2:1 ratio feed of TMDCB:TPC. However, the actual situation is somewhat more complicated. Under the conditions of complete reaction and with the assumption of a most probable distribution, a 2:1 feed ratio of monomers should give rise to a distribution of oligomers of the type $(AB)_nA$; where, on a number average basis, $n = 0$ accounts for 50% of the molecules (i.e., pure A) and $n = 1,2,3,4...$accounts for the remaining $(AB)_nA$ oligomers.[3] It has been demonstrated that this analysis very accurately describes the situation encountered in the reaction of bisphenol-A with TPC at 2:1 ratio in a solution process. In this case, the weight contribution of oligomers for which n is beyond 5 is insignificant.[4]. Thus, polymers prepared by this technique are more accurately represented by the following structure.

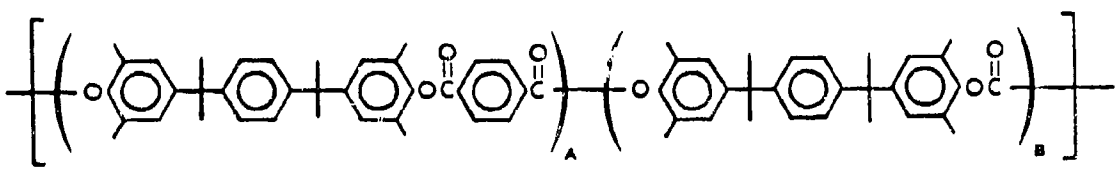

Suitable techniques were developed to control the final molecular weights in the interfacial polycondensation stage as well as capping of unstable chloroformate end groups. The polyester-carbonate resulting from TMDCB with a 1:1 molar ratio of terephthalate to carbonate was designated as AF-TP-2. Depending upon molecular weight this polymer has a T_g of 200-210°C. Compression molding evaluations showed that the initially colorless and clear material (cast films) became yellow and cloudy at molding temperatures of ~ 300°C. This problem was related primarily to polymer purity and was resolved by forming the Stage I oligomer by a homogeneous solution process. The oligomer was not isolated but was purified by washing the solution followed by interfacial polycondensation. Polymer prepared by this improved method essentially remained clear and colorless after thermoforming. A summary of important physical and mechanical properties is displayed in Table 2.

TABLE 2

SUMMARY PROPERTIES OF TMDCB
POLYESTER CARBONATE (AF-TP-2)

$\bar{M}w$	82,000
nsp/c (dl/g)	1.15
Tg (°C)	210
HDT (°C)[a]	190
TGA (°C)[b]	385 (Air) 400 (Argon)
% Transmittance (T)	83
% Haze (H)	9
Yellowness Index (YI)	17
Izod Impact (ft-lb/in)	1.2 notched 22 Unnotched
UE (%)	63
Tensile Strength (psi)	9100
Hydrolysis Resistance	Excellent
Solvent Resistance[c]	Poor
Short Term Environmental Aging (200 hr Thermal, Humidity, UV Radiation)	Poor

a. 264 psi

b. 10°C/min

c. Cantilever beam stress cracking with isopropanol, jet fuel and Skydrol hydraulic fluid.

The main deficiencies of AF-TP-2 are the rather low notched Izod impact strength, poor solvent resistance and poor environmental aging characteristics in comparison to the reference polyester-carbonate.

In view of the above deficiencies, a series of copolyester carbonates was prepared in which only part of the bisphenol-A was replaced with TMDCB. These polymers were prepared by the improved combination solution - interfacial technique employed for AF-TP-2. A range of diol composition from 40 to 90 mol% TMDCB/BPA + TMDCB was investigated. The T_g values for these copolymers ranged from 191°C for 40 mol% TMDCB to 210°C for 90 mol%. The terephthalate/carbonate ratio was held at 1:1. Considering the Tg values and BPA content the composition containing 60 mol% TMDCB (AF-TP-6) appeared best for more complete characterization.

AF-TP-6 samples were characterized in a manner identical to AF-TP-2. Only marginal improvements in impact strength, solvent resistance and environmental aging characteristics were realized. For example, the best notched Izod value obtained for compression molded specimens was 2.0 ft-lbs/in.

The same principles used for structural variations governing the selection of the diol components were also employed for the diacid components. With this approach it was possible in principle to optimize stiff segment length, chain interactions, T_g and degree of molecular chain entanglement for polyesters derived from various diacids and bisphenol-A. However, the scope of this effort was to a great extent limited by the difficulty in synthesizing many of the appropriate diacid structures in the amounts and purity required for a meaningful evaluation.

The most promising results were obtained with the polyester composed of bisphenol-A and 4,4'-benzophenone dicarboxylic acid (BDA). The structure which is displayed in Figure 5 bears a structural similiarity to the reference polyester-carbonate as well as a similiarity in the average stiff segment length and entanglement density. The material is entirely amorphous and has a limiting T_g of ~ 210°C.

Although the monomer synthesis was cumbersome and not amenable to scale-up, enough material was prepared to permit a reasonable evaluation of polymer properties. The most direct procedure was the oxidation of 4,4'-dimethyl-benzophenone to the diacid with chrominum trioxide in acetic acid.

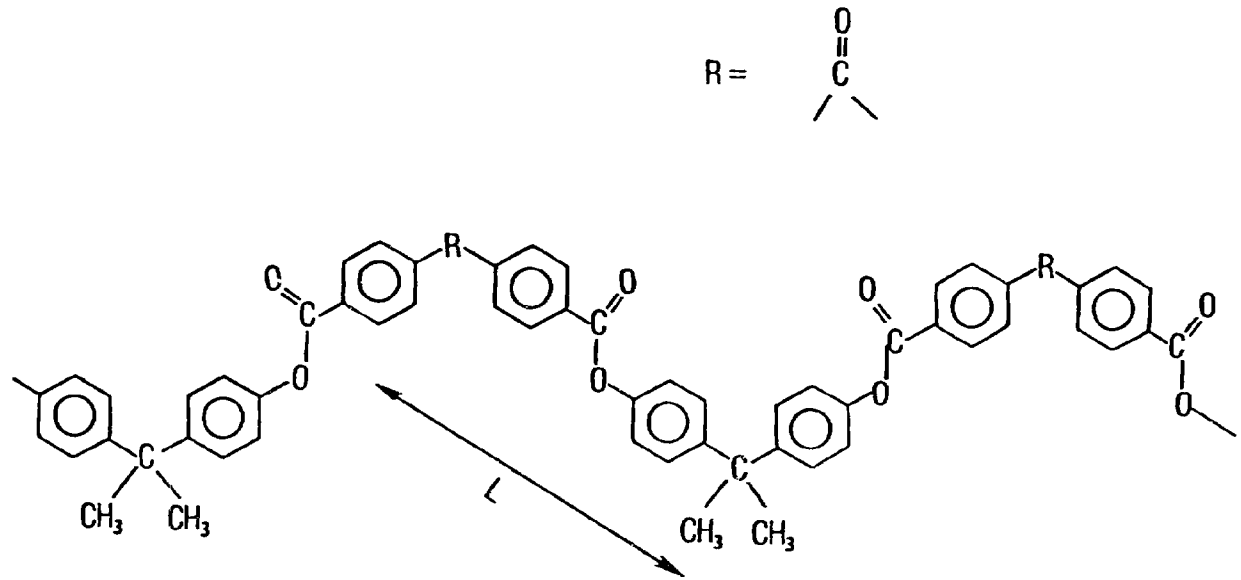

FIGURE 5 POLYESTER OF BPA AND 4,4'-BENZOPHENONE DICARBOXYLIC ACID

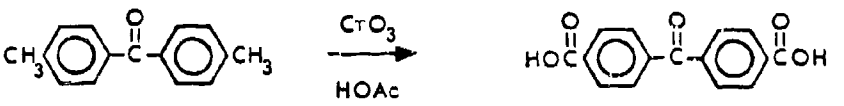

After several purification steps involving the diamonium salt, the free diacid was converted to the diacid chloride required for low temperature polycondensation with bisphenol-A (BPA).

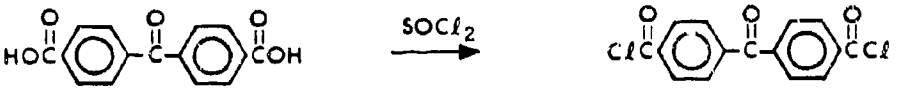

For the preparation of the polyester derived from BPA and 4,4'-BDAC (AF-TP-9) both solution and interfacial polymerization techniques were studied in order that the most effective method could be chosen for obtaining material of sufficiently high molecular weight and purity. In small scale experiments solution techniques (inert solvent and pyridine acid acceptor) gave materials of only moderate molecular weight at best. The highest solution viscosity for preparations conducted in homogeneous solution was obtained with chloroform as a reaction solvent. Preparations conducted in dichloromethane gave somewhat lower values of solution viscosity, but in either case the molecular weights were judged to be too low for mechanical property studies. On the other hand, with interfacial techniques in the presence of benzyl triethyl ammonium chloride, acceptably higher molecular weights were achieved especially with chloroform as a polymer phase solvent. Some typical results for small scale experiments are presented in Table 3.

Table 3

POLYMERS DERIVED FROM BPA & 4,4'-BDAC (AF-TP-9)

Entry	Process[a]	Reaction Solvent	$\eta_{sp/C}$ (dl/g)[b]	T_g (°C)
1	Solution	CH_2Cl_2	0.39	180
2	Solution	CH_2Cl_2	0.41	180
3	Solution	CH_2Cl_2	0.42	180
4	Solution	$CHCl_3$	0.56	200
5	Solution	$CHCl_3$	0.58	200
6	Interfacial	CH_2Cl_2	0.81	210
7	Interfacial	$CHCl_3$	1.21	210

a. 1:1 mole ratio BPA: 4,4'-BDAC in all cases
b. C = 0.5 in phenol/TCE at 25°C

The mechanical and thermal properties of AF-TP-9 are exceptionally good as can be seen from the summary data in Table 4. These properties were obtained from compression molded specimens of polymers prepared interfacially and having a minimum $\eta_{sp/C}$ value of 0.8 dl/g. Unfortunately, the optical characteristics (color) of molded specimens was always poor in spite of numerous attempts to exhaustively purify both the monomer and polymers. Even in the best cases yellowness index values below 60 could not be obtained. Furthermore, while solvent cast films were initially colorless, exposure to natural sunlight for relatively short periods resulted in development of an intense yellow-green color. Presumably, a ketone activated photo-Fries rearrangement of the arylate ester occurs to give a structure which has absorbance bands extending into the visible region of the spectrum.

Table 4

SELECTED PROPERTIES OF AF-TP-9

Tensile Elongation (UE)	15.5%
Ultimate Tensile Strength	10,600 psi
Tensile Modulus	288,000 psi
Notched IZOD Impact	~ 5 ft-lb/in
Heat Distortion Temperature	190°C @ 264 psi
T_g	210°C

Up to this point, our theoretical predictions regarding the effects of structural modification on the properties of high T_g aromatic polyesters have agreed remarkably well with experimental results. For example, the effect of increasing the stiff segment length, L, was established to a convincing extent with the reference polyestercarbonate and benzophenone polyester (AF-TP-9). Results obtained independently from this contract showed that an increase in the stiff segment length leads to an increase in molecular chain entanglement. At the same time it was determined that a high degree of chain entanglement in the glassy state is an important factor leading to improvements in impact resistance, resistance to embrittlement at low temperatures and on thermal aging, abrasion resistance and solvent resistance. Thus, the two desirable and fundamental effects of increasing "L" are an increase in T_g and molecular chain entanglement. However, there are distinct limitations to the actual length of "L" in these polymer systems, because eventually a point is reached at which some undesirable properties of stiff segments begin to predominate. The first is a T_g so high that the melt processing temperature approaches the decomposition point of the polymer.

THIS PAGE INTENTIONALLY LEFT BLANK

The second is the potential for cyrstallization of long rigid sequences which would seriously compromise optical properties. For this research program we reached the optimum length for "L" with respect to bisphenol-A polycarbonate as shown in Figure 6. It should be noted that this figure also includes the stiff segment of polymers derived from tetramethyldicumylbisphenol (TMDCB), and that this segment was purposely chosen to be of about the same length and relative concentration as that of the reference polyester-carbonate. However, TMDCB polymers were designed primarily to examine the effect of an entirely different structural modification - viz the restriction of mobility of the carbonate and ester group. Unfortunately, for polyarylates there exists only one practical approach which leads to a decrease in this mobility and hence, the desired increase in T_g. This approach which involves the introduction of bulky substituents ortho to the ester or carbonate linkages was examined in great detail with various polymers derived from TMDCB. In all cases, these polymers showed the expected increases in T_g over their unsubstituted counterparts. However, at the desired level of increase in T_g the mechanical properties (i.e., impact strength) were in all cases adversely effected.

Another major structural factor which can be considered for "bisphenol" type polyarylates involves mobility of the two phenyl rings relative to the central carbon atom. In Figure 7 this motion is illustrated as a bending moment for the bisphenol-A residue. Any increase in the size of the substituent groups bonded to the central carbon atom decreases this bending moment and in general would be reflected in an increase in T_g when present in the polymer backbone. From theoretical considerations, as well as experimental data, the size of the substituents required in order to significantly raise the T_g is so large that undesirable perturbation of chain interpenetration (entanglement and free volume) result. The most serious effect of such perturbtions is an intolerable loss in many desirable mechanical properties. Again from theoretical considerations, it follows that even with large substituents, sufficient unoccupied space exists between them to accommodate bending motions of the phenyl rings and perhaps more important the σ bonds between the central carbon and the substituents are themselves capable of considerable "bending". The most effective way to circumvent these problems is to immobilize the σ bonds to the substituents by introducing a rigid ring structure at the central carbon while simultaneously reducing the relative size of the overall substituents to a minimum. However, there are several other requirements which must be met among which are chemical inertness and thermal stability. In addition, the phenyl groups should have the same average geometry

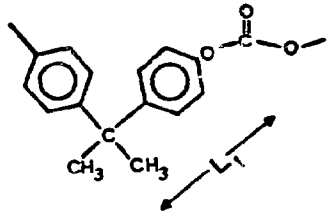

POLYCARBONATE

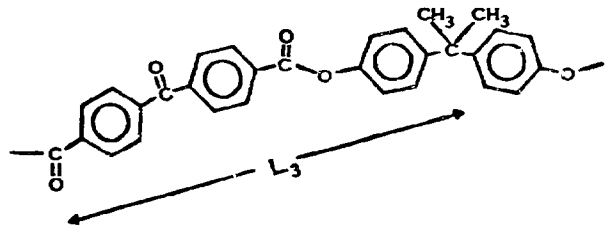

AF-TP-9

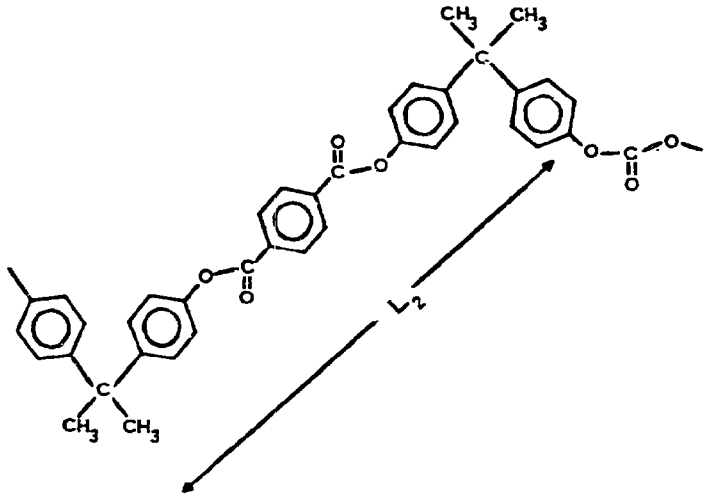

REF. PEC

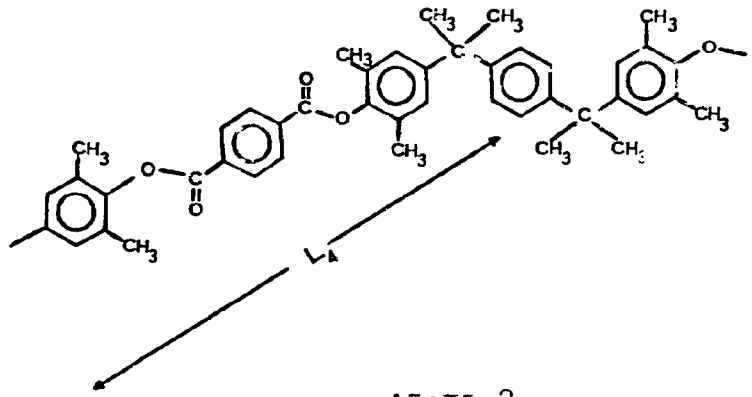

AF-TP-2

$L_2 \cong L_3 \cong L_4 > L_1$

FIGURE 6 STIFF SEGMENT LENGTHS

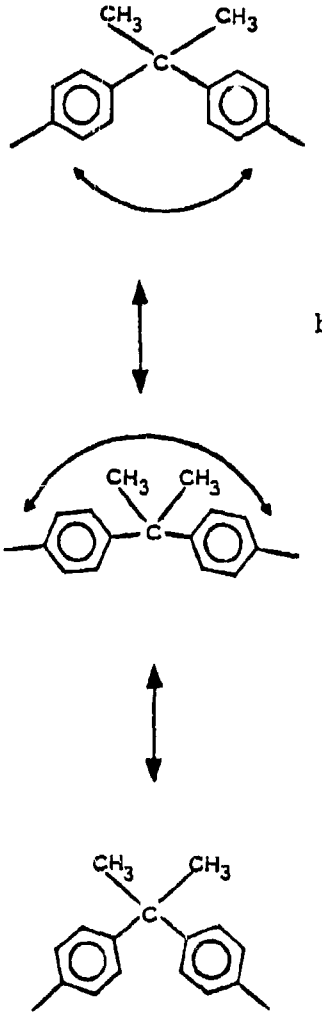

FIGURE 7 MOBILITY OF ISOPROPYLIDENE LINKAGE OF BISPHENOL-A

as in bisphenol-A, and the monomer structure should have enough spatial dissymmetry to preclude any tendency of the resultant polymers to crystallize.

One desirable structure which follows from this analysis is the family of para-linked 1,1-diphenylcyclopentanes.

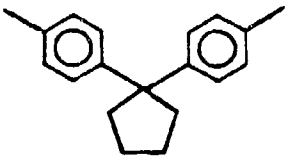

p - Linked 1,1 - Diphenylcyclopentane

Although the above structure in itself does not provide for a sufficient increase in T_g, it is the basis for several derivatives which meet all the necessary criteria.

The phenolphthalein molecule can be considered as a derivative of the above diphenylcyclopentane.

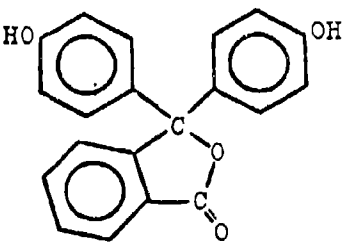

Phenolphthalein

Until relatively recently the use of phenolphthalein in polymer chemistry has been largely overlooked because of the tendency to associate instability of the lactone ring and color forming properties to the material in its monomeric form. Phenolphthalein undergoes several equilibria governed reactions which involve salt formation and opening of the lactone ring. A quinoid intermediate is responsible for the intense red color in alkaline media. However, this intermediate cannot form in the absence of free hydroxyl groups on the phenolphthalein molecule. Thus, there is no possibility of color formation in polyesters derived from phenolphthalein.

Over the past 20 years there has been a considerable number of reports in the literature concerning the preparation of phenolphthalein polyesters and polycarbonates. Most notable in this field is the work of Morgan[5] and Howe in the United States and Korshak and his co-workers in the Soviet Union. Since information on the mechanical properties of these polymers is generally lacking, it must be inferred that these properties are inferior to conventional thermoplastics. This conclusion is not surprising in view of the fact that the available literature is composed mainly of general polymer synthesis studies in which no attention was directed to careful consideration of the many structural and theoretical factors controlling the mechanical properties of high T_g polymers.

In the final phase of our exploratory research, we further applied the principles developed in the design of the reference polyester-carbonate combined with the new findings obtained here. The phenolphthalein based polyester-carbonates represent the embodiment of most of these principles among which are molecular chain entanglement, stiff segment length and reduction in mobility of the phenylene rings. In a sense, this new class of polyester-carbonates represents a "breakthrough" in that there exists no other single polymer system which possesses the overall properties of the new high T_g materials.

- Tg of 200-235°C
- Excellent mechanical properties
- Impact strength and strength retention
- Surface hardness
- Good optical properties
- Good solvent resistance
- Chemically inert
- Melt processability

The exploratory phase of this work was structured to provide answers to two important questions regarding the nature of phenolphthalein derived polyester-carbonates. The first was the level of phenolphthalein residues required to achieve the desired T_g, and the second, the effect that these residues have on certain critically sensitive properties such as notched Izod impact strength. In order to simplify the experimental approach, the overall composition of the polyester-carbonates was restricted to the ratio phenolphthalein + bisphenol-A: terephthalate: carbonate = 2:1:1. With this composition the stiff segment length was held reasonably close to that of the

reference polyester-carbonate. The ratio of phenolphthalein to bisphenol-A was the variable providing a controlled change in phenyl group mobility and hence T_g. By the nature of the polycondensation reaction the effects of sequence lengths and sequence length distributions could be qualitatively assessed depending upon at which point during the reaction the phenolphthalein was added.

Synthesis of these polyester-carbonates was accomplished by a solution polycondensation which involved essentially two distinct steps. In the first step a mixed polyester oligomer was formed from a mixture of the aromatic diols [bisphenol-A (BPA) and phenolphthalein (PHTH)] and terephthaloyl chloride. The reaction was conducted in the presence of pyridine which functions as both catalyst and acid acceptor and dichloromethane which serves as an inert solvent. The reaction was homogeneous and the stoichiometry was controlled so that the oligomers had an average chain length of approximately 2-5 and were phenolic hydroxyl terminated. This reaction can be generalized by the following simplified scheme, where A, B & C represent bisphenol-A, phenolphthalein and terephthaloyl chloride, respectively.

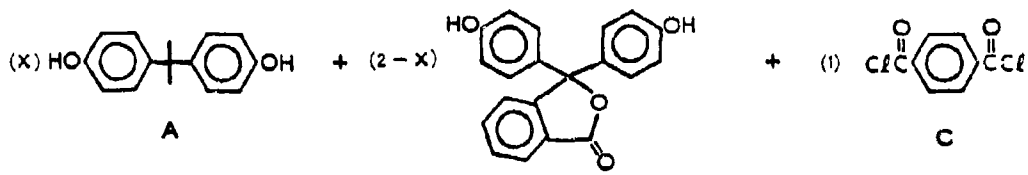

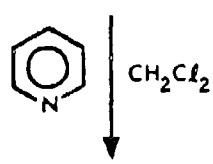

$(AC)_n(BC)_mA$

$(AC)_n(BC)_mB$

Under the conditions of complete reaction and with the assumption of a most probable distribution, a 2:1 feed ratio of total diols to acid chloride gives rise to a range of

mixed oligomers where, on a number average basis n = 0 and m = 0 account for about 50% of the molecules. In other words, in such a system about one-half of the total diol (A+B) remains unreacted. The esterified diol comprises the mixed oligomers as well as the two homo-oligomers, $(AC)_nA$ and $(BC)_mB$. This analysis was shown to accurately describe the oligomer stage of the reference-polyester carbonate and has been treated in general terms by Flory.

In the second step the hydroxyl terminated oligomers and remaining free diols are polymerized with phosgene to give the final copolyester-carbonates. This reaction is illustrated below for one specie of mixed oligomer. However, it should be appreciated that, in reality, the situation is much more complicated, since many different oligomer species are present.

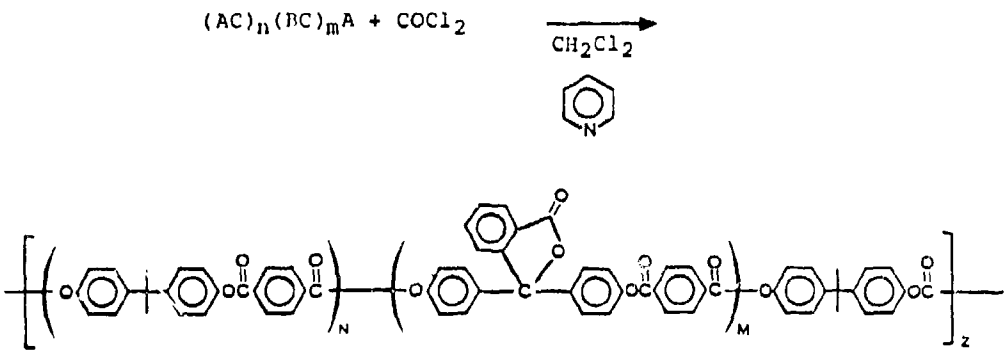

The resulting copolyester-carbonates are essentially random with relatively short terephthalate ester blocks interconnected by short polycarbonate sequences. In all cases, the reaction chemistry led to complete incorporation of monomers so that the final monomer residue ratios corresponded within experimental error to the feed ratios employed. The two-step synthesis was conducted in one reaction vessel without isolation or purification of the oligomer.

In order to assess the effect of copolymer composition and molecular weight on properties, copolymers were prepared containing varying amounts of phenolphthalein residues and having different solution viscosities. Initially the greatest emphasis was placed on copolymer composition, since at intermediate values of solution viscosity overall properties begin to level off. Some practical limits were applied to values of viscosity in that the evaluation was confined to those polymers having η sp/C in the range of 0.6 to 2.5 dl/g. The lower limit was chosen by analogy with the reference polyester-carbonate as the point at which significant drop off in Tg and mechanical properties occurs. The upper limit relates to the point at which the melt viscosity becomes high enough to impart difficulty in melt processing.

Table 5 shows results which illustrate the effects of copolymer composition and molecular weight on T_g.

These results show that with respect to the reference polyester-carbonate only relatively small amounts of phenolphthalein are required to raise the T_g of the copolymers to well within the target range. This effect is in sharp contrast to the behavior observed for copolyester-carbonates of approximately the same molecular weight based on BPA and TMDCB. For example, while a 60% mole% replacement of BPA by TMDCB is required for a T_g of 200°C in AF-TP-6, only 15% mole of phenolphthalein is required for the same T_g value in AF-TP-10.

From this comparison it can be concluded that the phenyl-phenyl ring mobility in the diol components has a much more pronounced effect on T_g than the carbonate or ester group flexibility at equivalent "concentrations" within copolyester-carbonate chains. Since the relatively low levels of phenolphthalein modification result in less perturbation of the reference polyester-carbonate structure, it was postulated that the overall desirable mechanical properties of the reference material would be maintained, albeit at a higher T_g. That this prediction is the case was exemplified in a detailed evaluation of properties of the phenolphthalein based materials. Furthermore, several properties of these materials are enhanced over those of the reference polymer.

A summary of the most important initial (as molded) properties of the phenolphthalein based copolyester-carbonates is shown in Table 6 along with suitable reference materials. Note that Izod impact values are reported for 3/16" thick specimens rather than the more usual 1/8". For increasing

TABLE 5

DESIGNATION	RATIO PHT/PHT + BPA[a] IN MONOMER FEED	RATIO PHT/BPA IN COPOLYMER IR	NMR	AVG	η sp/C[b] (dl/g)	T_g[c] (°C)
AF-TP-10	.15	.17	.15	.16	0.72	200
AF-TP-10-1	.15	.14	.15	.145	1.27	208
AF-TP-10-2	.15	.15	.15	.15	0.72	202
AF-TP-11	.20	.21	.20	.205	0.65	195
AF-TP-11-1	.20	.19	.22	.205	0.70	205
AF-TP-11-2	.20	.19	.19	.19	1.83	212
AF-TP-11-3	.20	.21	.25	.23	2.47	219
AF-TP-12	.30	.26	.32	.29	2.01	234
AF-TP-12-1	.30	.29	.31	.30	0.79	220

a. Mole fraction, PHT = phenolphthalein, BPA = bisphenol-A
b. C = 0.5 in phenol-TCE at 25°C
c. by DSC at 10°C/min in Argon

TABLE 6

INITIAL PROPERTIES OF PHENOLPHTHALEIN BASED COPOLYESTER-CARBONATES

MATERIAL[a]	$\bar{M}w$	η sp/c[b]	Tg (°C)	HDT (°C)[c]	TGA (°C)[d]	%T	%R	Y.I
AF-TP-10	22400	0.72	202	190	400	84	13	10
AF-TP-11	28600	0.88	204	194	395	81	15.8	11.6
AF-TP-12	25000	0.79	220	210	390	81	6.2	12.4
REFERENCE PEC	28000	0.70	182	170	400	88	2	2
POLYCARBONATE	-	0.65	150	140	400	89	1-2	2

MATERIAL	Izod Impact[e]	UE %	UTS (psi)	Modulus (psi)	Rockwell Hardness
AF-TP-10	5.0	50	9300	270000	M80
AF-TP-11	4.0	60	10000	285000	M87
AF-TP-12	3.0	40	9900	300000	M87
REFERENCE PEC	5-8	70	9600	270000	M71
POLYCARBONATE	3-4	120	9600	297000	M70-71

a. 10,11,12 correspond to 15,20 and 30 mole % PHTH/BPA + PHTH in copolymer
b. dl/g, c = 0.5% in phenol-TCE at 25°C
c. ASTM-D648, 264 psi
d. 10°C/min in Air
e. ASTM-D256, 3/16" thick, ft-lb/in

thicknesses between 1/8" and at least 1/4" the impact strength for AF-TP-10,11,12 and the reference PEC shows no thickness sensitivity, whereas BPA polycarboante impact values range from ~ 13 down to 2 ft-lb/in.

In Table 7 the solvent resistance characteristics of these polymers are shown.

Long term exposure tests were conducted on the phenolphthalein based copolyester-carbonates to assess the effects of temperature, humidity and uv - visible radiation primarily on the mechanical properties of molded specimens. These effects on other properties such as optical, solvent resistance and abrasion resistance were not studied quantitatively. All specimens were evaluated without stabilizers, plasticizers or other additives.

Recent studies have shown that the mechanical properties of BPA polycarbonate change considerably after thermal aging at temperatures between 70°C and T_g. This undesirable phenomenon, which is termed "thermal embrittlement", manifests itself primarily by a significant drop in impact resistance. Although the general phenomenon has been studied for numerous polymers, the results for polycarbonate by Broutman and Krishnakumar[6] are most notable. Their work strikingly shows an abrupt drop in the notched IZOD impact strength from ~ 18 ft-lbs/in to $\leq$ 2 ft-lb/in which occurs at progressively shorter times as the temperature of the experiment is increased. Thus, at 120°C embrittlement is complete in less than one hour, whereas at 70°C the time required is about 170 hours. In addition, for polycarbonate the drop in IZOD strength is so extraordinarily sudden that it is difficult to observe any intermediate values between 18 and 2 ft-lb/in.

Recent analyses of the general phenomenon have shown that it results from a decrease in free volume and a shift in relaxation times to longer times, both of which are related to increases in polymer density. From the comprehensive analysis of Struick[7] it must be concluded that these changes occur with all polymers regardless of their chemical composition and that they cannot be avoided. However, from our concepts of molecular entanglement in the glassy state, it was postulated that while the embrittlement process may never be entirely eliminated, its rate may be slowed considerably.

TABLE 7

SOLVENT STRESS CRAZING

Polymer	Stress Cracking (psi)[a] at 25°C				
	IPA[b]	Skydrol[c]	JP-4[d]	JP-8[d]	Jet Reference Fluid[d]
AF-TP-10	14000	4000	13600	14900	5900
AF-TP-11	13000	4000	12300	>13000	5500
AF-TP-12	14000	4000	12000	>14000	5000
REFERENCE PEC	10000	3400	6800	9300	2500
POLYCARBONATE	5300	200	4300	6300	500

a. Cantilever beam test
b. IPA = isopropyl alcohol
c. Aviation hydraulic fluid
d. Jet fuels and reference fluid kindly supplied by USAF, WPAFB, Ohio

It has been demonstrated that this is the case for the reference polyester-carbonate and the phenolphthalein based materials covered in this program, both of which possess much higher levels of chain entanglement than polycarbonate. The results are shown graphically in Figures 8, 9 and 10. It should be noted that the temperature of the experiment is defined by the T_g value of the individual polymers, where T aging = T_g-30°C. This relationship was chosen to provide a reference point relative to the standard condition reported for polycarbonate (120°C). The high temperatures also provide for an accelerated test.

Within the time span of the heat aging test, the AF-TP-11 and AF-TP-12 samples show no tendency to embrittle. The reference polyester-carbonate does show measurable loss in impact strength, but there is no abrupt embrittlement phenomenon as observed with BPA polycarbonate. The fact that the changes in impact strength are related to some physical phenomenon such as embrittlement rather than, for example, polymer degradation was clearly demonstrated by comparison of solution viscosities before the test and at the longest aging time. In no cases did the viscosity decrease by more than 10% of the initial value.

Tensile data for long term thermal exposure (in air) on AF-TP-11 and AF-TP-12 specimens is displayed in Table 8. In spite of the very high test temperature the performance is excellent. AF-TP-11 samples perform best with almost 50% retention of initial UE. None of the samples showed any tendency to embrittle or severely discolor after 1000 hours. Comparison of solution viscosities before heating and after 1000 hours demonstrates the high degree of thermal stability of these materials. The same test was also conducted at 150°C. In this case, results were similar except that retention of UE was generally higher, as expected.

Likewise, results for long term thermal-humidity exposure are displayed in Table 9. In this case some of the property losses can be explained as a result of a reduction in molecular weight. This is especially evident in AF-TP-12 where the $\eta sp/C$ value at 500 hrs. is below the critical threshold for good mechanical properties.

Finally, the results for long term uv-visible radiation exposure are shown in Table 10. The behavior of the materials in this case is similar to thermal aging. Although the greatest effect of uv radiation was expected to be on the color of the materials, only minor discoloration was observed in the case of AF-TP-11. Most likely, discoloration could not be accurately observed for these because of the rather high initial YI values and specimen thickness.

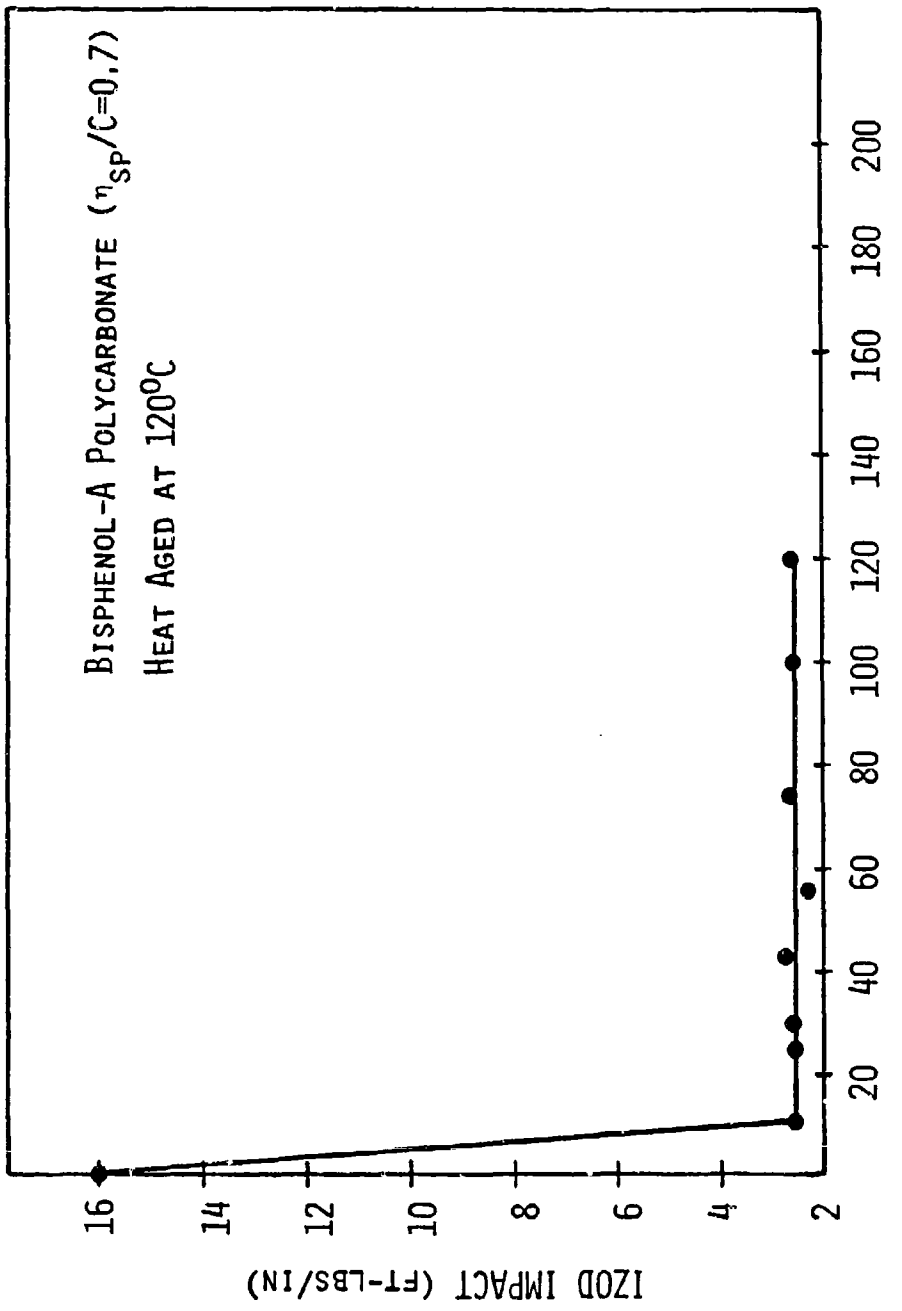

FIGURE 8 EFFECT OF THERMAL AGING ON IMPACT RESISTANCE FOR BISPHENOL-A POLYCARBONATE

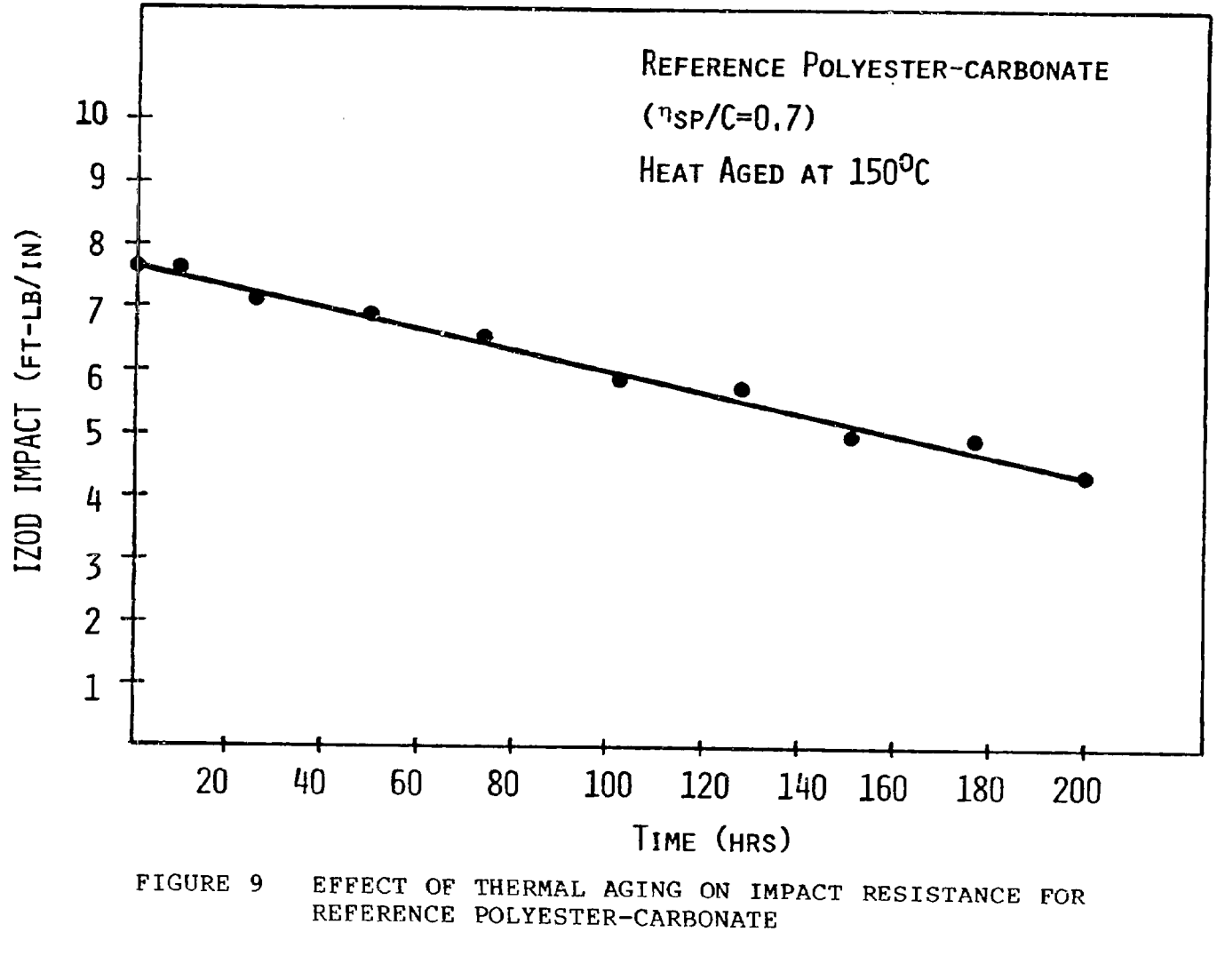

FIGURE 9 EFFECT OF THERMAL AGING ON IMPACT RESISTANCE FOR REFERENCE POLYESTER-CARBONATE

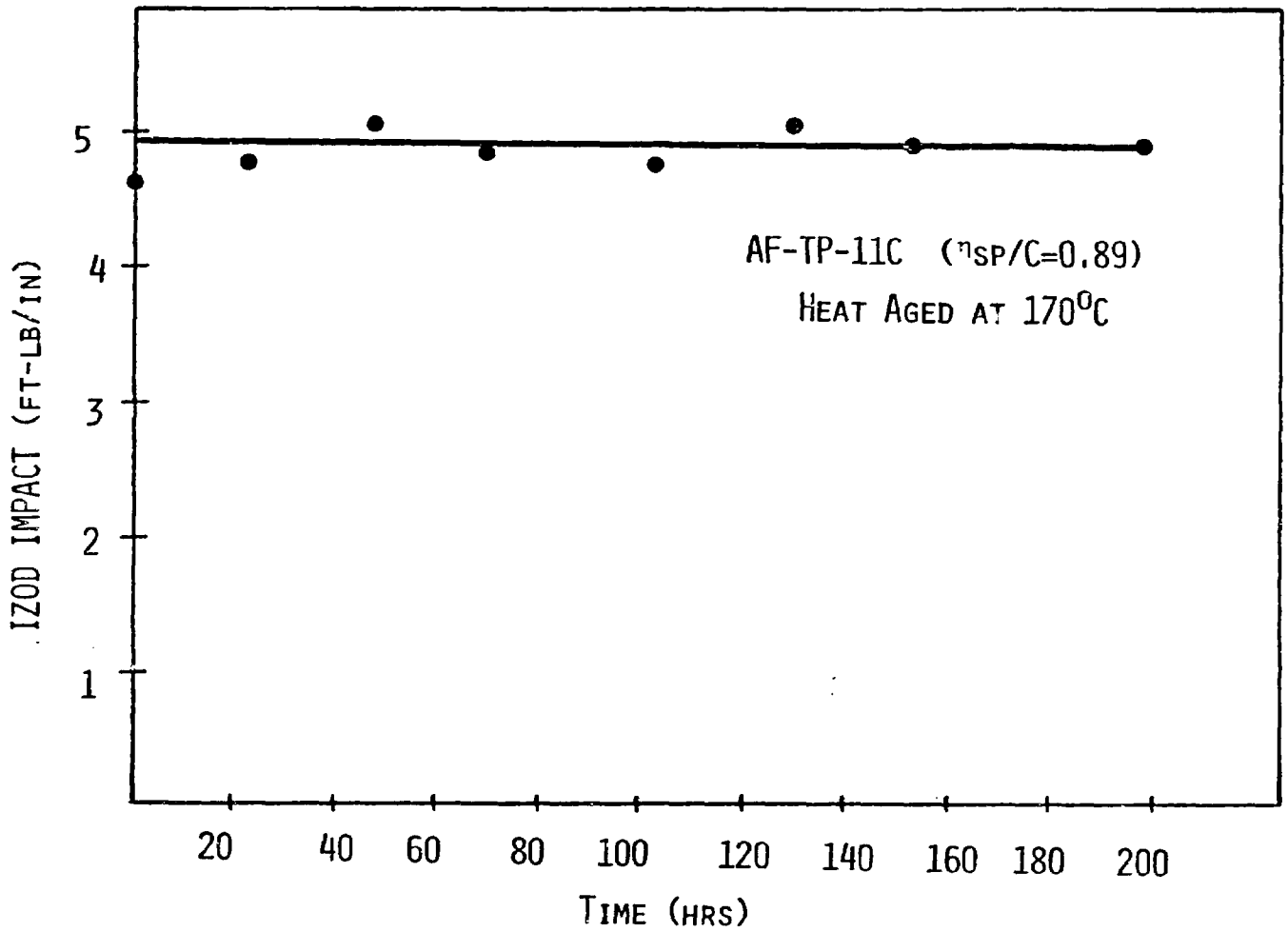

FIGURE 10 EFFECT OF THERMAL AGING ON IMPACT RESISTANCE FOR AF-TP-11C

TABLE 8

LONG TERM THERMAL EXPOSURE

Tensile Properties after Exposure at 180°C (356°F)

Polymer	Time (Hrs)	YE (%)	YS (psi)	UE (%)	UTS (psi)	TM (psi x 10^3)	ηsp/C (dl/g)
AF-TP-11D-1	0 (Control)	21	10300	85	10620	268	0.89
	200	18.6	10530	60	9840	294	
	500	18.8	10560	50	9730	292	0.84
	750	18.6	10580	48	9740	288	
	1000	17.8	10560	40	9760	297	0.80
AF-TP-11D-2	0 (Control)	21.1	9640	75	9930	287	1.15
	200	19.6	10000	50	9440	274	
	500	19.3	10040	30	9540	281	1.09
	750	18.7	10100	35	9290	259	
	1000	18.7	10300	30	9400	269	1.01
AF-TP-12	0 (Control)	19.4	10620	44	10020	294	0.70
	200	19.2	11030	44	10230	294	
	500	-	-	13	9740	297	0.66
	750	-	-	10	8570	289	
	1000	-	-	12	9300	298	0.64

TABLE 9

LONG TERM THERMAL-HUMIDITY EXPOSURE

Tensile Properties after Exposure at 71°C & 95% RH

Polymer	Time (Hrs)	YE (%)	YS (psi)	UE (%)	UTS (psi)	TM (psi x 10^3)	ηsp/C (dl/g)
AF-TP-11D-1	0 (Control)	21	10330	85	10620	268	0.89
	200	18.8	9510	50	8990	287	
	500	18.8	9840	70	9770	298	0.78
	750	18.3	9840	40	9190	287	
	1000	18.5	9830	40	9280	297	0.73
AF-TP-11D-2	0 (Control)	21.1	9640	75	9930	287	1.15
	200	19.5	9500	50	9220	277	
	500	-	-	18	8900	290	0.92
	750	18.3	9420	18	8430	277	
	1000	-	-	14	8620	287	0.85
AF-TP-12	0 (Control)	19.4	10620	44	10020	294	0.70
	200	19.1	10400	25	9510	300	
	500	Broke before yield		8	7080	305	0.58
	750	Broke before yield		8	6940	293	
	1000	Broke before yield		7	6530	301	0.58
		REFERENCE POLYMERS					
Polyester Carbonate	0 (Control)	17.5	8570	90	9410	259	0.73
	200	14	7780	Broke at Yield		257	
	500	12.5	7800	Broke at Yield		272	0.73
	750	14.7	8230	Broke at Yield		268	
	1000	15.9	8370	Broke at Yield		260	0.71
Poly-Carbonate	0 (Control)	13.4	8900	125	10300	282	0.66
	200	11	8130	Broke at Yield		297	
	500	11	8440	Broke at Yield		309	0.65
	750	10.9	8580	Broke at Yield		300	
	1000	10.6	8580	Broke at Yield		311	0.63

TABLE 10

LONG TERM UV-VISIBLE RADIATION EXPOSURE

Tensile Properties after Exposure at (380nm) at 45°C

Polymer	Time (Hrs)	YE (%)	YS (psi)	UE (%)	UTS (psi)	TM (psi x 10^3)	ηsp/C (dl/g)
AF-TP-11D-1	0 (Control)	21	10300	85	10620	268	0.89
	200	19.3	9710	40	9040	281	
	500	18.9	10100	25(?)	9300	293	0.92
	750	19.2	10190	60	9300	280	
	1000	18.6	9510	-	-	253	0.74
AF-TP-11D-2	0 (Control)	21.1	9640	75	9930	287	1.15
	200	19.6	9530	50	9060	281	
	500	19.3	10000	65	9530	291	1.26
	750	19.6	10000	60	9630	282	
	1000	19.4	9860	39	9220	262	0.98
AF-TP-12	0 (Control)	19.4	10620	44	10020	294	0.70
	200	-	-	10.5	8110	295	
	500	18.1	10600	14	8890	310	0.75
	750	19.8	11000	31.2	10100	299	
	1000	18.1	9880	19.2	8450	254	0.66
			REFERENCE POLYMERS				
Polyester Carbonate	0 (Control)	17.5	8570	90	9410	259	0.73
	200	13.2	8060	Broke at Yield		263	
	500	15.2	7960	Broke at Yield		-	0.72
	750	16.4	8730	Broke at Yield		262	
	1000	13.8	7500	Broke at Yield		233	0.68
Poly-Carbonate	0 (Control)	13.4	8900	125	10300	282	0.66
	200	11.8	8680	25	6090	291	
	500	14	9220	Broke at Yield		-	0.62
	750	11.9	8910	Broke at Yield		291	
	1000	11.9	8520	Broke at Yield		260	0.56

CONCLUSIONS

Of the forty-seven polymer compositions prepared and characterized in the course of this study, two clearly meet most of the target objectives defined for thermal resistance (T_g and TGA), mechanical properties, long-term environmental aging and optical characteristics. These are the materials designated AF-TP-11 and AF-TP-12 which represent a new class of melt processable thermoplastics derived from bisphenol-A, phenolphthalein, terephthalic acid and phosgene. This class of polymers is economically attractive, since the monomers are of relatively low cost and the polymerization process is simple. In addition, many of the polymer properties can be adjusted over a substantial range by simply varying the ratio of bisphenol-A to phenolphthalein. Of particular importance is the lack of thermal embrittlement (i.e., retention of Izod impact strength and tensile properties after long-term thermal exposure) and the superior solvent and abrasion resistance inherent in this class of thermoplastics. These polymers are also easily melt processed by conventional methods such as compression and injection molding, as well as sheet extrusion.

At the present state of development the primary shortcomings of these materials are the haze and color values for molded samples. Although some selected preparations of AF-TP-10, 11 & 12 showed quite acceptable optical properties, consistent results were not yet achieved. Based on our experience with other experimental polymers, we believe that these deficiencies can readily be eliminated. Of even greater importance may be the effect of selected color and heat stabilizing additives. Unfortunately, studies in this area could not be made under this contract. However, by analogy with conventional optical quality thermoplastic technology, significant improvement in optical properties can be expected by proper selection and blending of additives with the base polymer.

Two other classes of new polymers which were prepared under this contract initially showed promise as acceptable candidates. These are polyester-carbonates derived from 0,0,0',0'-tetramethyldicumylbisphenol (AF-TP-2, 6) and the polyester of BPA and 4,4'-benzophenone-dicarboxylic acid (AF-TP-9). As the research evolved into the more advanced testing stages, major deficiencies were found. For example, the mechanical properties of the AF-TP-2 and 6 series were inferior to those of the AF-TP-10, 11 and 12 series, and in some cases, fell short of the target values. The AF-TP-9 series showed development of considerable color during

molding which could be only marginally improved by exhaustive and costly monomer (diacid) purification. In addition preparation of the intermediate diacid chloride is costly and not readily adaptable to scale up for the quantities required in this program.

Experimental

Complete details on experimental techniques, synthesis, characterization and testing can be obtained from Technical Report AFWAL- TR-81-4178, Materials Laboratory, Air Force Wright Aeronautical Laboratories.

Acknowledgments

This work was sponsored by the Materials Laboratory (AFWAL/MLBC), AFSC, Wright-Patterson AFB, Ohio, under Contract No. F33615-78-C-5077 (October 1978 - October 1981).

We gratefully acknowledge the support and technical assistance of:

T. J. Reinhart, Jr. W. H. Gloor E. Arvay (dec)	AFWAL
C. Hurley	Univ. of Dayton
G. J. Schmitt W. K. Stemple Chemical Physics Dept.	Allied Corporation

REFERENCES

1. Van Krevelen, D. W., "Properties of Polymers, Correlations with Chemical Structure", Elsevier Publishing Company, New York, 1972, p. 109.

2. Hoffman, M., Pr. Polymer J., 6, 243 (1974).

3. Flory, P. J., "Principles of Polymer Chemistry", Cornell University Press, New York, 1953, p. 319.

4. Prevorsek, D. C., DeBona, B. T., Kesten, Y., J. Poly. Sci., Polymer Chemistry Ed., Vol. 18, 75-90 (1980)

5. Morgan, P. W., "Condensation Polymers by Interfacial and Solution Methods", Interscience Publishers, New York, 1965, p. 360.

6. Broutman, L. J., Krishnakumar, S. K., Polymer Engineering and Science, 16, 74 (1976)

7. Struik, L.C.E., "Physical Aging in Amorphous Polymers and Other Materials", Elsevier Publishing Company, Amsterdam, 1978.

AD-P003 200

AN INDUSTRY TEST PROGRAM FOR INTERLAYER EQUIVALENCY

P. H. Bain, Boeing Commercial Airplane Company

AN INDUSTRY TEST PROGRAM FOR INTERLAYER EQUIVALENCY

Peter H. Bain

Boeing Commercial Airplane Company

ABSTRACT

After the announcement in 1980 that Monsanto will have to discontinue production of their interlayer "Saflex PT" due to the non availability of 3GH plasticizer, an Industry team, under the auspices of the Aerospace Industries Association (AIA), was formed to identify and obtain approval for a replacement interlayer.

A test program was derived to examine the physical, mechanical and operational characteristics of candidate replacement materials and compare them to those of the current PVB/3GH. Typical production batches of material were procurred and the test program was completed by an Industry cooperative effort. The program demonstrated a high degree of equivalency and finally resulted in FAA approval of an interlayer as a general direct replacement for all existing designs of glass windshields utilizing PVB/3GH interlayer in either a bird bouncing or bird bagging mode. It is believed that this is the first time a windshield material has received FAA approval without the usual expensive certification program normally required for each design.

An additional benefit derived is a wealth of baseline data pertinent to the new interlayer which will be useful for future comparisons with newly developed interlayers as they may become available.

Although the laboratory testing demonstrated a high degree of equivalence in the physical and mechanical characteristics required for safety of flight, service durability cannot be interpolated from the results. A flight evaluation program involving some forty windshield units has been initiated and will be on-going for two more years to ascertain the operational stability of the interlayer.

AN INDUSTRY TEST PROGRAM FOR INTERLAYER QUALIFICATION

Introduction

At the 1980 Transparencies Conference it was confirmed that, due to the relatively small demand, Union Carbide was about to phase out the production of their Flexol 3GH plasticizer; without this plasticizer, Monsanto would have to terminate the production of its PVB Interlayer known as Saflex® PT. This interlayer has been the basic material for some thirty years and is currently used in nearly all subsonic aircraft which have windows and windshields fabricated from laminated glass.

In anticipation of the termination of their current interlayer, Monsanto had, at that time, completed initial development of a replacement interlayer and PPG had performed a limited amount of laboratory testing on this material. Monsanto considered the alternate interlayer to be a viable candidate for the Saflex® PT replacement and, thus, have offered it to the aerospace industry on that basis. The interlayer is planned to be commercially available at the same point in time as the exhaustion of the current stocks of 3GH vinyl. However, Industry and FAA approval of this material would be required before it could be used in commercial aviation.

Subsequently, a meeting was held in the Los Angeles area to examine the problem and identify a means to its solution. Representatives from all the major airframe and transparency companies in the U.S., Canada and Europe were invited to attend, in addition to others from the chemical industry, the United States Air Force and Navy. The problem overview described the reasons and events leading up to the termination of the current supply of 3GH plasticizer and to the identification of alternative candidates. Various proposals were addressed in order to effect a solution to the problem; these are summarized in Figure 1.

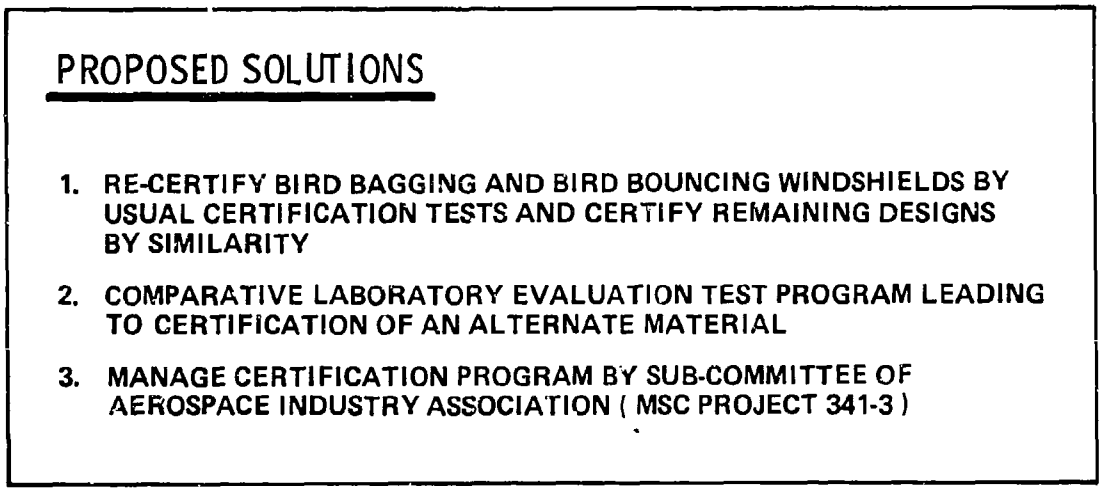

Figure 1 - Solutions Proposed

A discussion of requirements for certification identified two possible variations. The first was to recertify a series of differently designed windshields by the usual methods of bird impact, pressure and fail-safe loading, along with additional operational characteristics, and then attempt to obtain certification by similarity for the remaining designs not actually tested. The second alternative was to compare the characteristics of the candidate replacement vinyl with those of the existing 3GH vinyl. The second alternative would be less expensive, but the total certification plan would need to be agreed upon by the FAA before any start was made.

A first cut at a test plan was proposed at the meeting. The plan was broken down into several phases addressing the physical, chemical and mechanical characteristics of the vinyl sheet, and the properties of the vinyl when laminated to glass both with and without electrically conductive coatings. Also included were optical, thermal and low velocity impact tests.

The meeting concluded with the formation of a Technical Committee which was to finalize the test program to reflect the requirements of both the users and the FAA. In order to provide the proper legal authority for a liaison of competitor companies in such a venture, the Technical Committee requested an affiliation with the Aerospace Industries Association (AIA). This affiliation was granted and the program was identified as Project 341-3; it is administered by the Materials and Structures Committee (MSC) of the AIA.

Test Program Definition

After several meetings of the Technical Committee the test program (shown in Figure 2) was finalized. It consisted of several phases, each of which evaluated specific characteristics. Broadly, the test program was divided into two parts - one examining the vinyl sheet and the other evaluating the vinyl laminated between typical substrates.

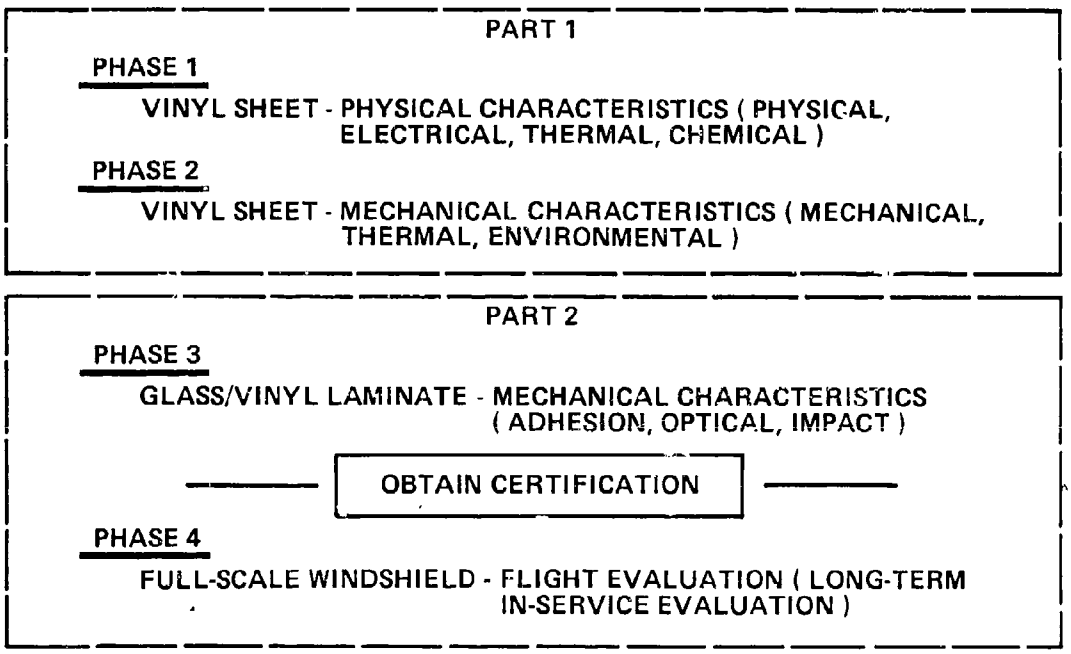

Figure 2 - Evaluation Test Program

The vinyl sheet tests were subdivided into two phases identified as Physical Characteristics and Mechanical Characteristics. Phase 1 comprised a series of tests to determine baseline physical, thermal, electrical and chemical characteristics; Phase 2 examined ultimate stress, elongation, tear strength and stiffness of the sheet vinyl.

The second stage utilizing vinyl laminates was also divided into two parts designated Phase 3 and Phase 4. Phase 3 examined the adhesive/cohesive properties of the laminate, the reaction to low and high speed impact and optical properties (all after a variety of thermal and environmental exposures). Test specimens for this phase were to be procurred from all current U.S. and European suppliers of aerospace glass laminates.

Finally, Phase 4 consisted of a flight evaluation of full size windshield components in airline service. No amount of laboratory testing can accurately predict the performance of an interlayer in "real world" service, so a flight-service evaluation is necessary during which a number of units are closely observed for the first year or two.

Test Program Activity

The total proposal was outlined to the FAA before commencement of the test program to ensure that it satisfied their certification requirements; only after their concurrence was the program initiated. The program was conducted within the previously defined phases of vinyl sheet tests, laminate tests and (after certification) flight-service evaluation.

The roles of the participating companies are shown in Figure 3. Program direction and progress was reviewed at technical committee meetings (at approximately quarterly intervals) while the overall effort was continuously coordinated by Boeing. Two vinyls were identified as candidates to replace the discontinued 3GH vinyl. For the test program, they were identified as Monsanto AG2 and Sekisui 3GH. Monsanto AG2 was considered the mainstream candidate with Sekisui 3GH as an alternate.

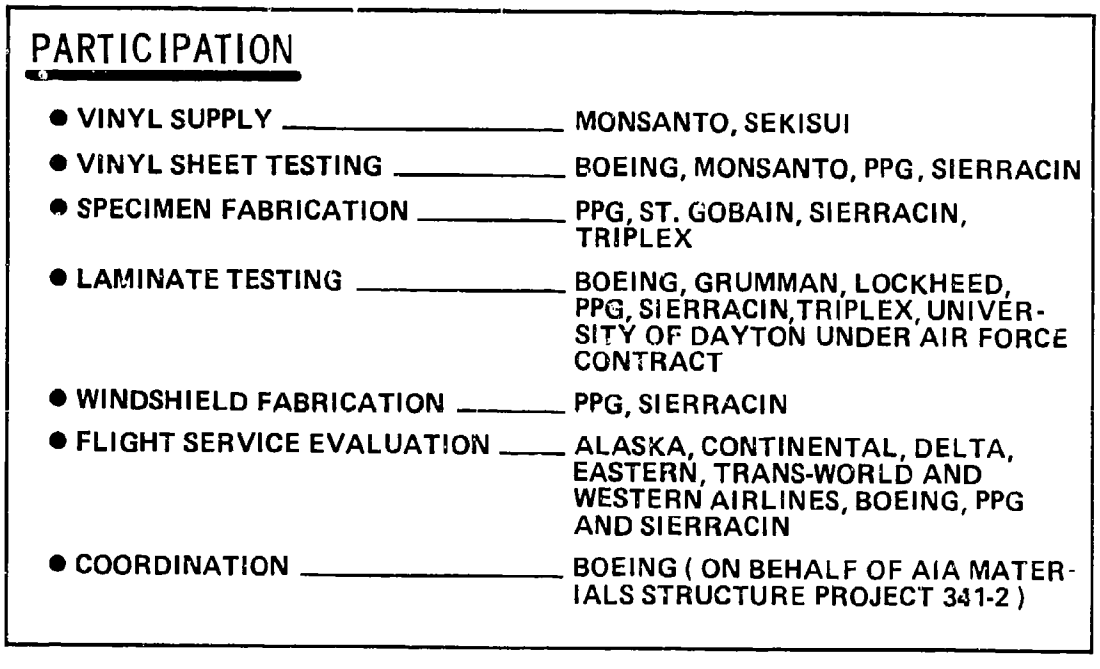

Figure 3 - Interlayer Test Program Participation

Sheet Vinyl Tests

All the sheet vinyl tests were performed on specimens from each of three separate production batches of the current Monsanto 3GH vinyl and, also, from three similar batches of Monsanto AG2 vinyl. Different production batches were required to ascertain any inter-batch variations and to select the median batch for further downstream laminate testing.

Physical Characteristics - Vinyl Sheet

Tests conducted in Phase 1 to determine physical characteristics (and their results) are shown in Figure 4. All these tests, except threshold bubbling, were completed by Monsanto. The threshold bubbling test was conducted on a 12-inch square laminate, but, as it was considered a materials characteristic test, it was included in this phase. PPG fabricated the specimens and conducted the tests. After controlling the moisture content of the vinyl before laminating, no bubbling was experienced up to a temperature of 310°F in either material. As the AG2 vinyl was formulated to simulate 3GH vinyl it was no surprise to see such close similarity between the two materials in all these tests.

		COMPARATIVE PERFORMANCE $\frac{\text{AG2 VINYL}}{\text{3GH VINYL}} \times 100 = \%$
P1	SPECIFIC GRAVITY	99.08
P2	SPECIFIC HEAT	101.88
P3	THERMAL CONDUCTIVITY	102.75
P4	THERMAL EXPANSION	101.00
P5	REFRACTIVE INDEX	100.06
P6	SOLUBILITY	100.60
P7	CHEMICAL STABILITY	99.03
P8	TOXICITY	100.00
P9	ELECTRICAL RESISTANCE	94.22
P10	CHEMICAL CHARACTARIZATION	*
P11	THRESHOLD BUBBLING **	100.00
P12	GLASS TRANSITION TEMPERATURE	100.80
	AVERAGE OF ALL DATA	99.95

* No Numerical Comparison Possible
** Laminate Test

Figure 4 - Physical Characteristics, Vinyl Sheet

Mechanical Characteristics - Vinyl Sheet

Ultimate Tensile Strength

Mechanical tests included ultimate tensile strength, tear strength and thermally-induced stiffness change.

The ultimate tensile test was run at 20.0 in/min and, as can be seen in Figure 5, produced quite different stress-strain curves for each temperature tested. The

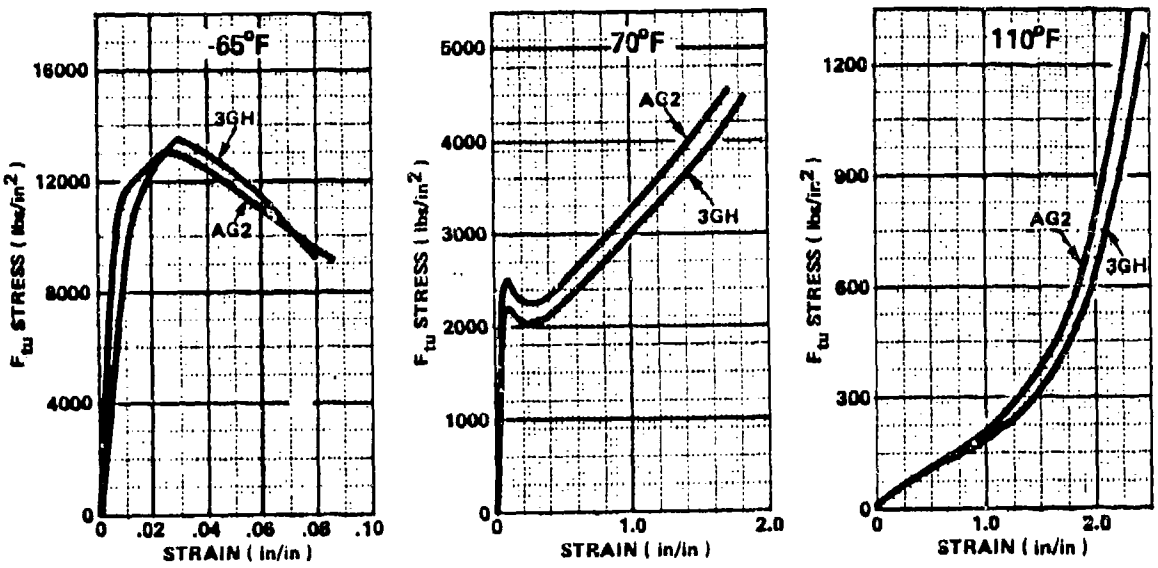

Figure 5 - Mechanical Characteristics, Tensile Stress/Strain, 3GH vs AG2

curves graphically illustrate the changing stiffness characteristics of the vinyl at various temperatures, although it can be seen that the two vinyls are remarkably similar. Data is the average of 15 test specimens for each temperature. Figure 6 shows the average energy absorbed by the material under test. These curves were produced by statistically reducing the stress-strain data to maximums and minimums and then integrating those results to define the energy absorbed (per cubic inch) by the vinyl during stretching vs axial load.

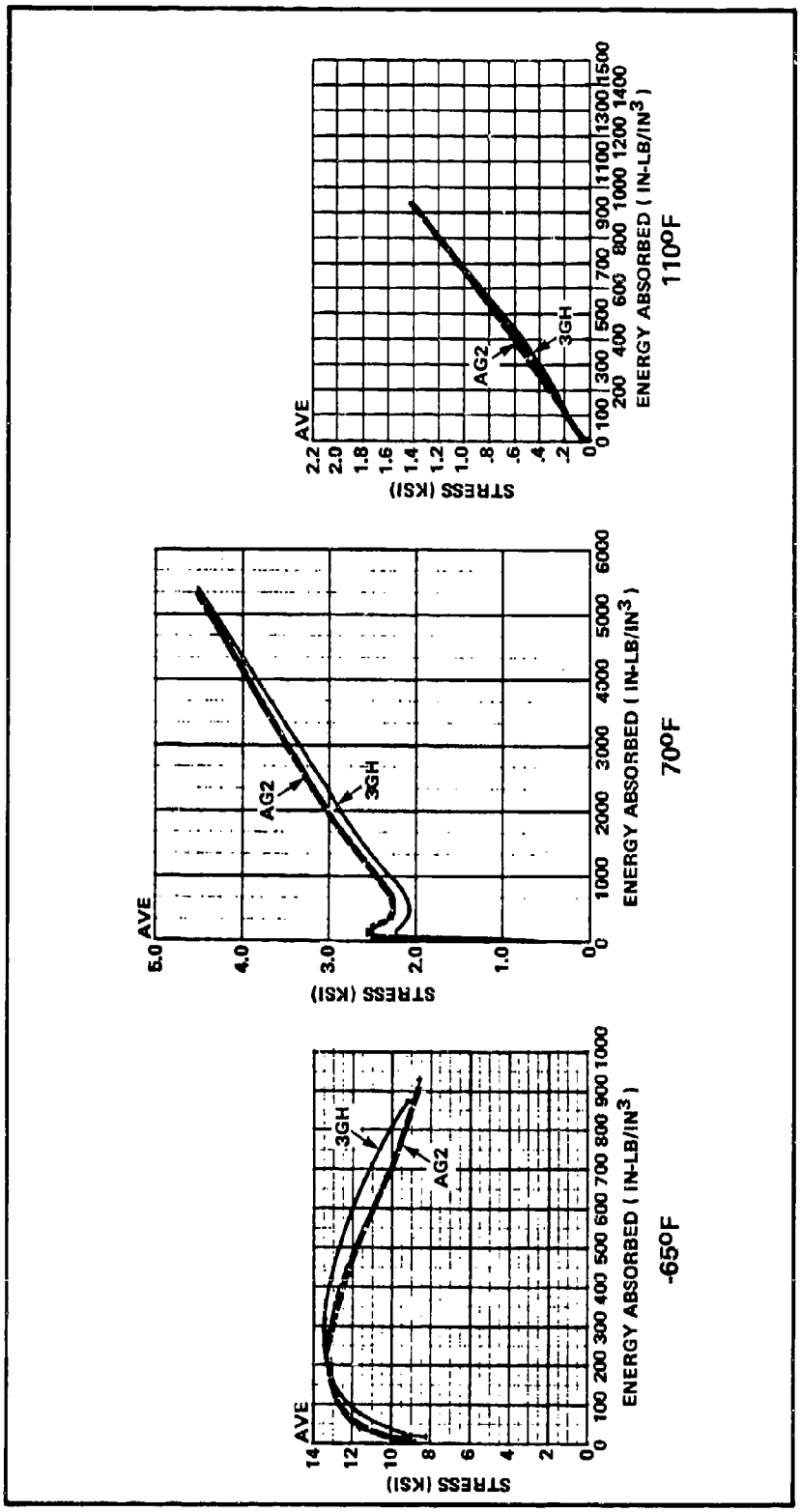

Figure 6 - Mechanical Characteristics, Stress Energy, 3GH vs AG2

Tear Strength

The standard ASTM D.1004 Tear Test was used with specimens of .025 thick vinyl. Head speed was 2.0 in/min and the data shown in Figure 7 is the average of a total of 30 specimens for each temperature tested. It is well illustrated that the AG2 produced consistently higher test results at all temperatures than the original 3GH vinyl.

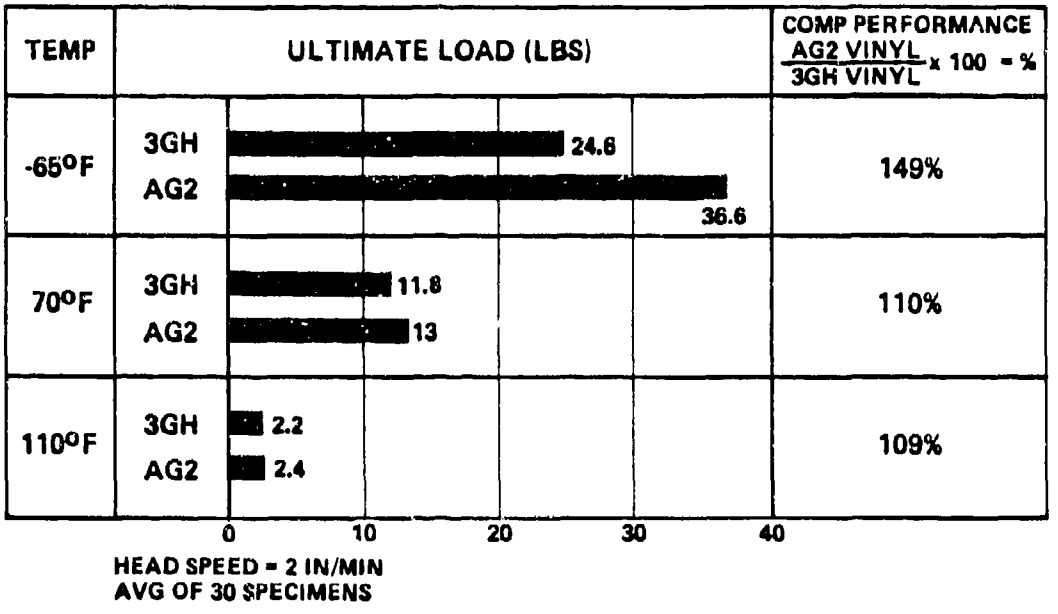

Figure 7 - Tear Strength

Stiffness

The simple method of measuring the deflection of a PVB/Aluminum laminated beam under a standard load and after controlled thermal soak was used to compare the changing stiffness of AG2 and 3GH vinyl and comparative results are shown in Figure 8. Variations of stiffness at temperature are almost identical and exhibit characteristic stiffening at about 50°F.

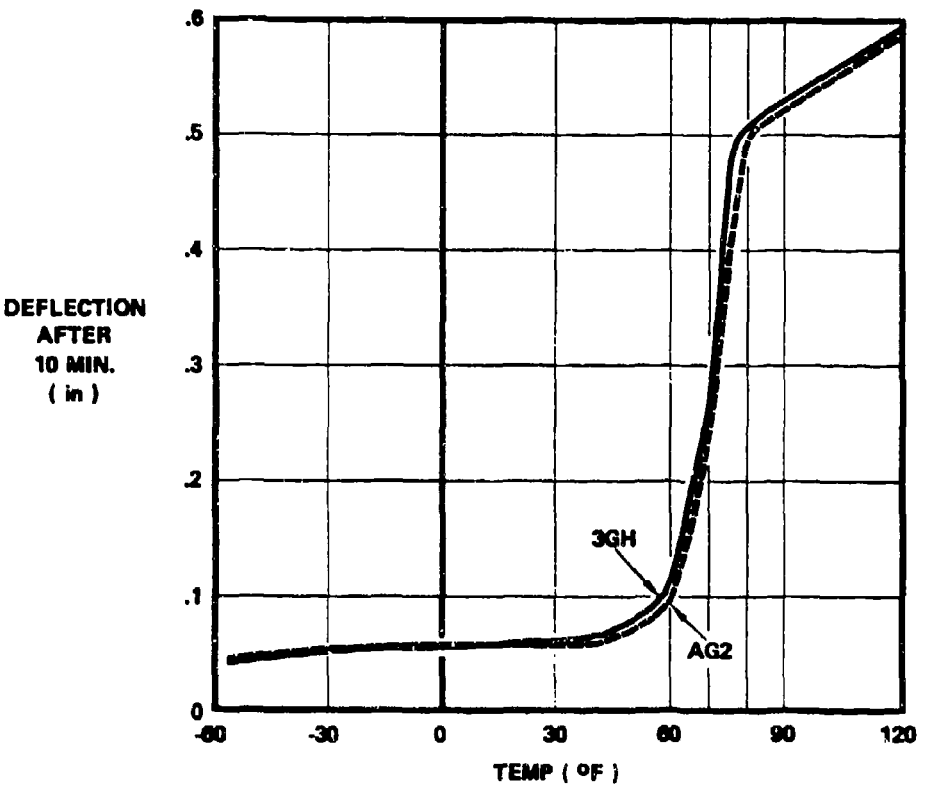

Figure 8 - Mechanical Characteristics, Vinyl Stiffness

The AIA Technical Committee found such close correlation of data from the sheet vinyl tests that FAA approval of the vinyl for limited certification was requested without the necessity of the laminate tests. The request was denied, so a median batch of vinyl was identified and laminated specimens were procurred from the participating suppliers for the Phase 3 laminate tests.

Vinyl Laminate Test

This phase is outlined in Figure 9 and consisted of the examination of ultimate shear and flatwise tensile adhesion, edge insert adhesion, optical performance and low/high speed impacts, all under a range of thermal and adverse environmental conditions Tests were performed in laboratories at Boeing, Lockheed, Grumman and the Universit, of Dayton.

	TEST ENVIRONMENT AND TEMPERATURE								
	AMBIENT					U/V		100% RH	
	-65	-30	0	70	110	70	110	70	110
SHEAR ADHESION			√	√	√	√		√	
SHEAR CREEP					√		√		
FLATWISE TENSILE ADHESION			√	√	√	√		√	
EDGE INSERT ADHESION	√			√	√			√	
IMPACT NON-SCATTERABILITY				√					
LUMINOUS TRANSMITTANCE / HAZE				√		√			
THERMAL TOLERANCE	√	√	√	√	√				
THERMAL SHOCK	√	√	√	√	√				
HIGH VELOCITY IMPACT		√			√				

Figure 9 - Laminate Tests

Adhesion Tests

Shear adhesion tests were done at Boeing and examined standard five-ply, 2-inch square laminated specimens supplied by PPG, Sierracin, St. Gobain of France and Triplex of England. Some specimens embodied EC coatings used by the different suppliers and others were bare glass. The test set up is shown diagramatically in Figure 10. Testing was performed at an Instron head speed of .05 in/min and the

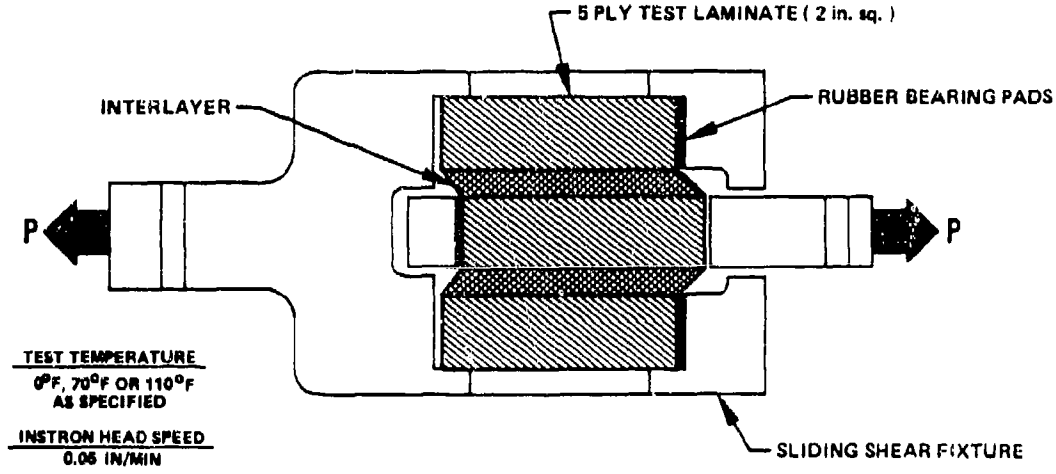

Figure 10 - Ultimate Shear Test

temperature was controlled at 0°F, 70°F and 110°F. Some specimens underwent U/V or 100% RH exposure prior to testing. Individual data for each company's specimens is considered proprietary so the data presented in Figure 11 is a comparison of the averages of all the 3GH and AG2 specimens in each temperature or environmental group. At the lower temperatures, most failures were due to glass shattering caused by the increased interlayer stiffness; at 110°F nearly all failures were due to delamination.

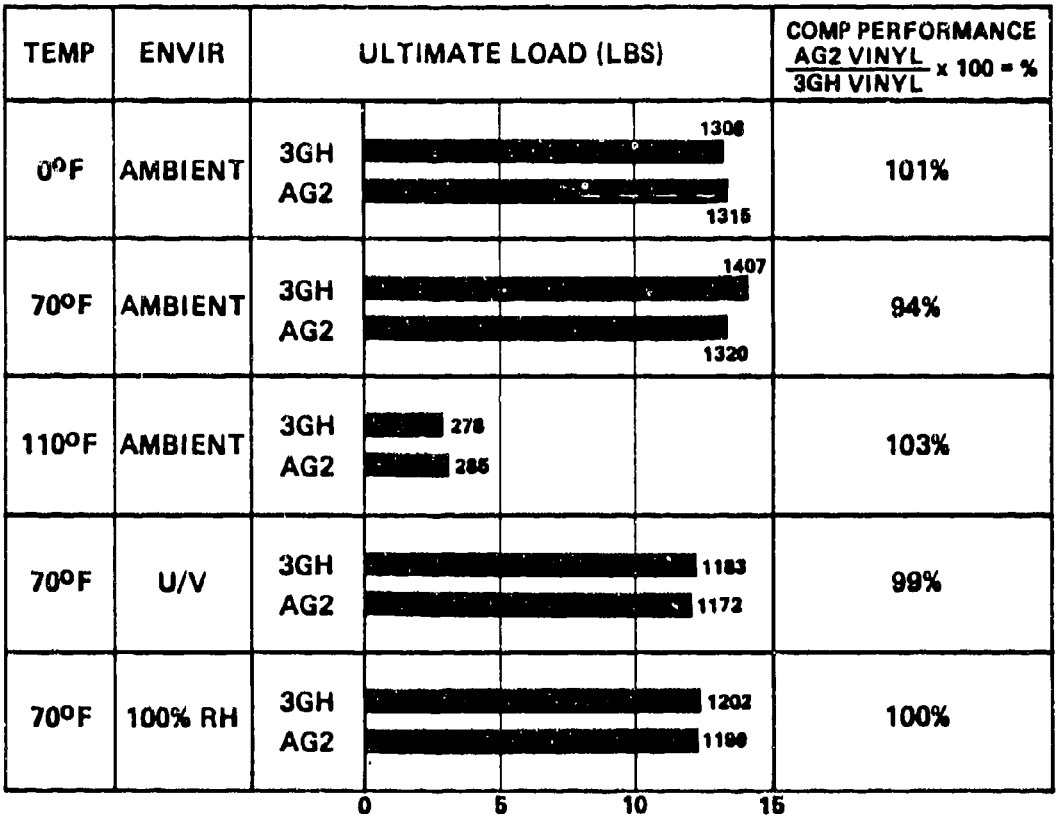

Figure 11 - Ultimate Shear Adhesion Performance

Flatwise tensile adhesion testing was also completed by Boeing using 2-inch square three-ply laminated specimens bonded to tensile blocks, as shown in Figure 12. Specimens were again supplied by the same four suppliers, both with and without EC coatings. Instron head speed, temperature and environmental conditioning were all similar to those used for the shear adhesion testing.

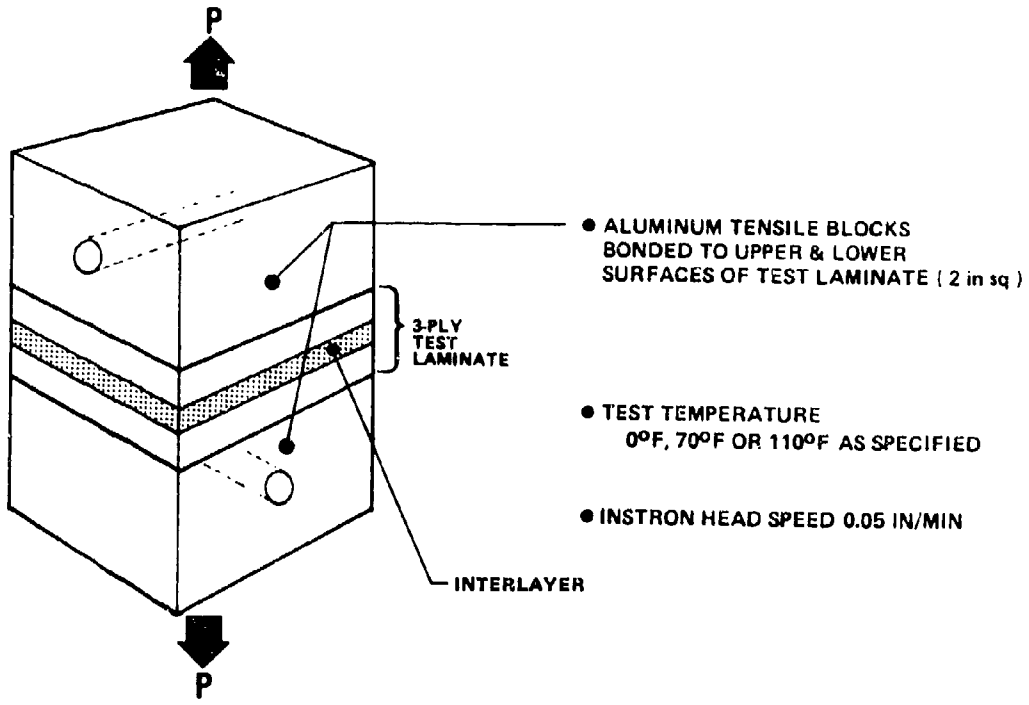

Figure 12 - Flatwise Tensile Adhesion Test Configuration

Averages of all the 3GH and AG2 specimens are compared in Figure 13 and, as with the shear test results, there is very close correlation of data.

Comparative testing was performed on the adhesion of both vinyls to various metallic substrates (used in windshields) using both the flatwise tensile method and an edge-insert adhesion test method. The flatwise tensile adhesion method was identical to that used for glass, but the specimens had plies of bare aluminum, clad aluminum or stainless steel substituted for the glass plies. Comparative results were very similar but it is interesting to note that average loads to failure were approximately 50% greater than the glass specimens.

TEMP	ENVIR	ULTIMATE LOAD (LBS)		COMP PERFORMANCE $\frac{\text{AG2 VINYL}}{\text{3GH VINYL}} \times 100 = \%$
0°F	AMBIENT	3GH	1198	94%
		AG2	1124	
70°F	AMBIENT	3GH	935	89%
		AG2	827	
110°F	AMBIENT	3GH	328	96%
		AG2	313	
70°F	U/V	3GH	1060	91%
		AG2	968	
70°F	100% RH	3GH	640	97%
		AG2	621	

0 5 10 15

Figure 13 - Flatwise Tensile Adhesion Test Performance

Edge-insert adhesion testing was performed at Lockheed Georgia Company. Figure 14 shows the details of the specimen and the test method. Testing was

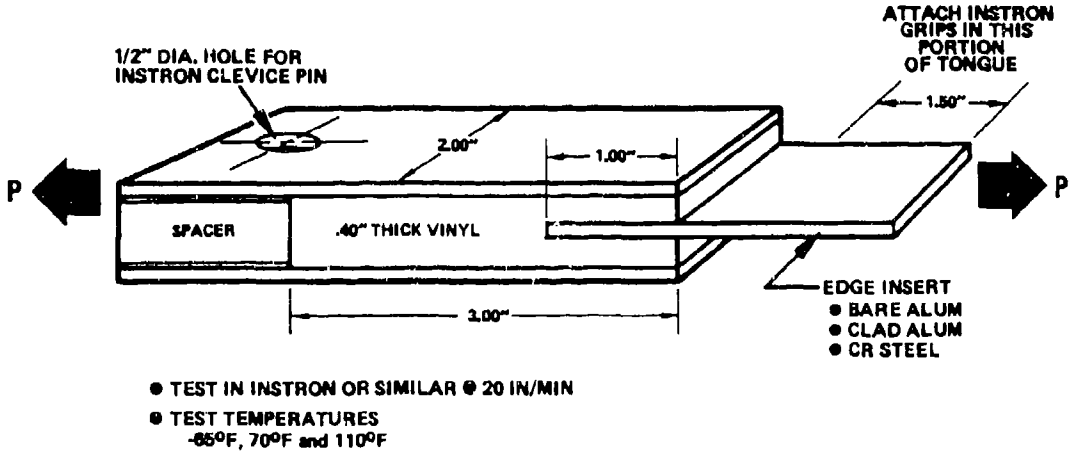

Figure 14 - Edge Insert Adhesion Test Configuration

completed at -65°F, 70°F and 110°F, and some specimens were pre-conditioned by exposure to 100% RH. The specimen simulates the edge-insert usually fitted to "bird-bagging" windshields and the test determines the comparative strength of the two vinyls for this type of bonded-in edge support. As can be seen in Figure 15, the data obtained from this test was extremely consistant and very similar for the two vinyls. Except for three or four instances, the failure mode was always adhesive failure at the insert, even at the test temperature of -65°F.

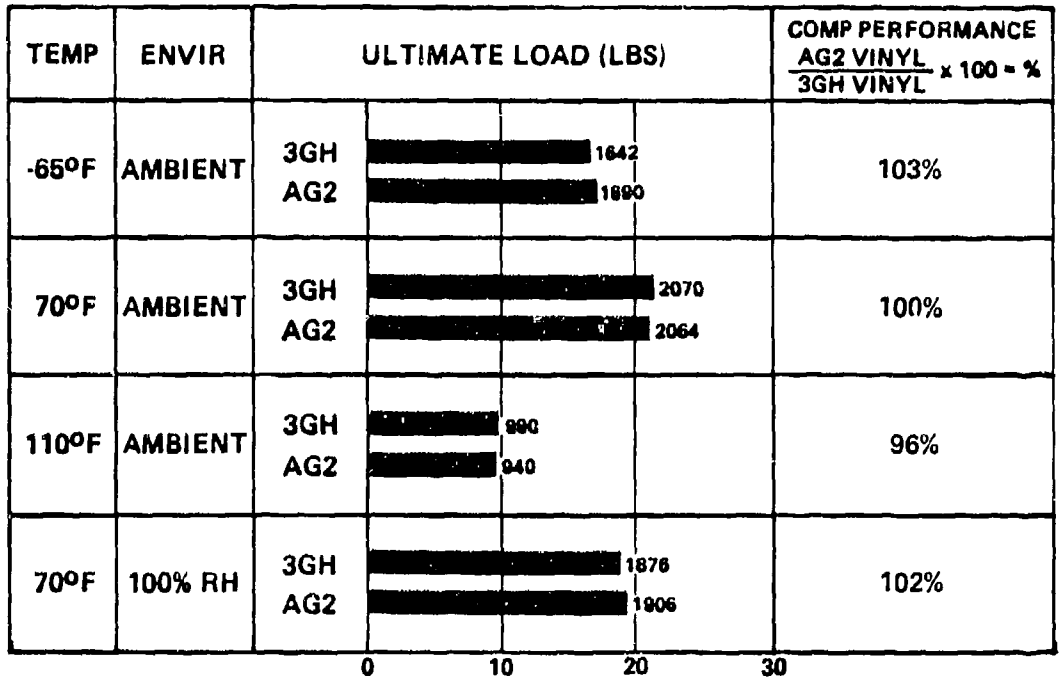

Figure 15 - Edge Insert Adhesion Test Performance

Impact Non-Scatterability

The standard Mil-G-25871 Impact Test was performed by Grumman Aerospace on simple 12-inch square, uncoated, glass laminates supplied by St. Gobain. The test set up is shown diagramatically in Figure 16. The falling ball must break the glass plies but without causing delamination greater than 0.25 inch diameter beneath the point of impact. The results of this test, shown in Figure 17, indicate two marginal results with 3GH vinyl, whereas the AG2 vinyl fully met the test requirements.

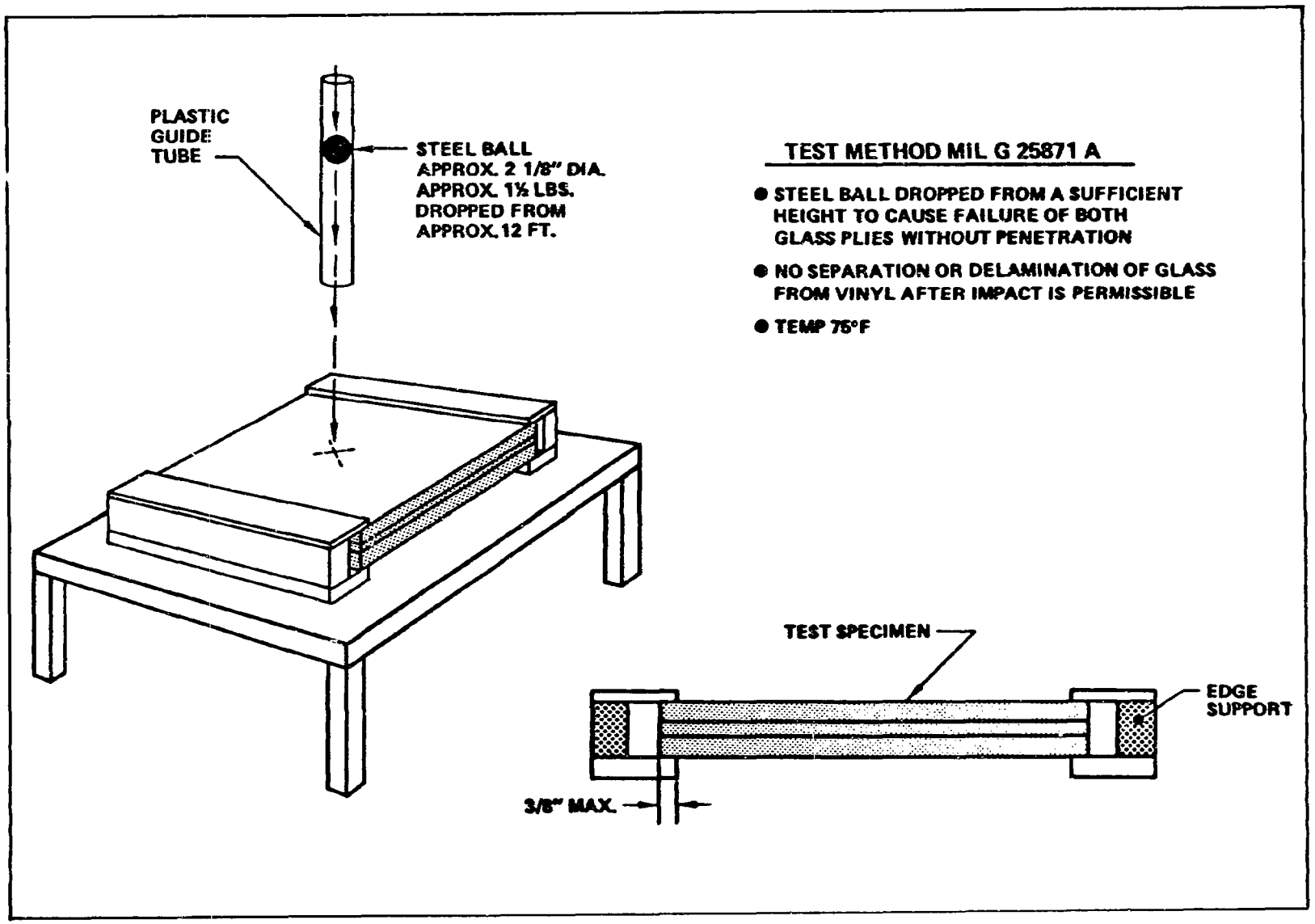

Figure 16 - Impact Non-Scatterability Test Configuration

TEST NO.	VINYL	TEST RESULT				REMARKS	
		PLY FAILURE		DELAMINATION			
		FRONT	REAR	FRONT	REAR		
1	3GH	YES	YES	NO	1/2" DIA.	MARGINAL RESULT	
2	3GH	YES	YES	NO	NO	PASS	
3	3GH	NO	YES	NO	NO	NO FAILURE OF FACE PLY	MARGINAL RESULT
		YES	ALREADY FAILED	NO	3/16" DIA.	2ND DROP TO FAIL FACE PLY CAUSED DELAM ON FAILED REAR PLY	
4	3GH	NO	YES	NO	NO	NO FAILURE OF FACE PLY	PASS
		YES	ALREADY FAILED	NO	NO	2ND DROP TO FAIL FACE PLY	
5	AG2	YES	YES	NO	NO	PASS	
6	AG2	YES	YES	NO	NO	PASS	
7	AG2	YES	YES	NO	NO	PASS	

TEST TO MIL G-25871A

Figure 17 - Impact Non-Scatterability Test Data

Optical and Thermal

Standard luminous transmittance before and after U/V exposure, in addition to thermal effects and thermal shock tests, were conducted on test specimens and full size windshields by PPG and Sierracin. All units passed the test successfully. Sierracin also conducted the ball drop impact test on a full size windshield and a pressure fail-safe test on a windshield (with all glass plies intentionally broken, at a pressure of 10.8 psi for six hours). Figure 18 and 19 show photographs of these tests.

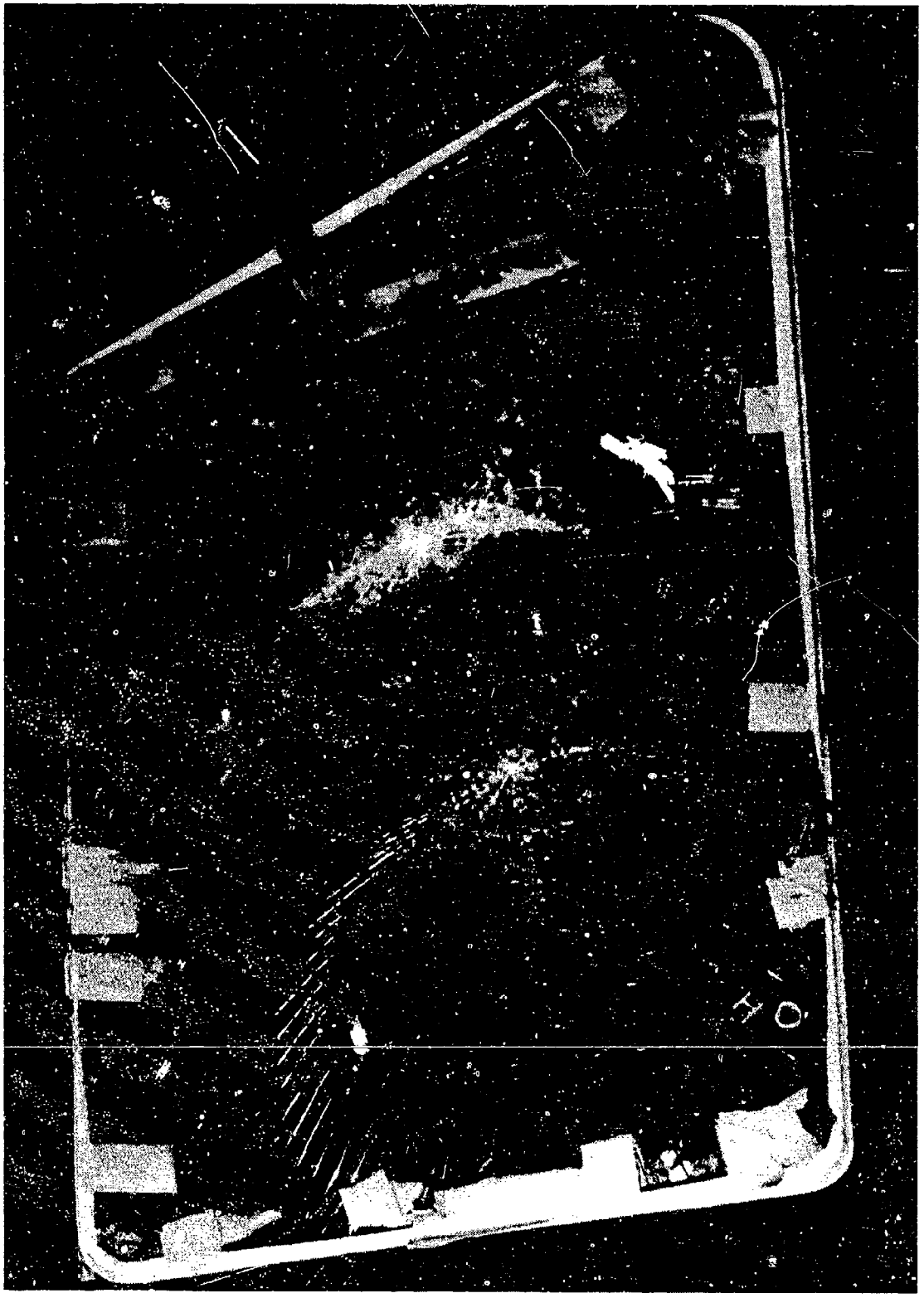

Figure 18 - Windshield Ball Drop Test

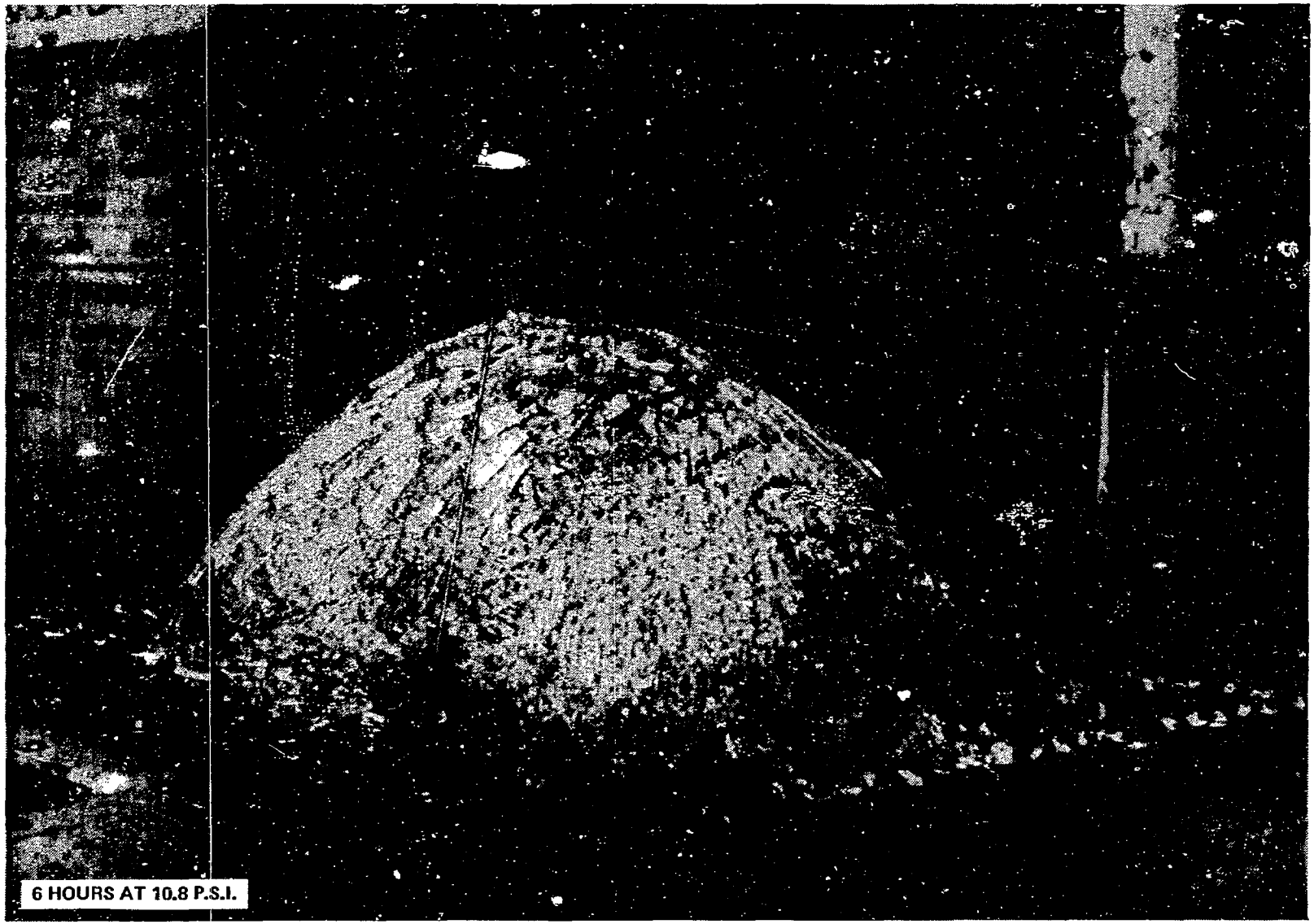

Figure 19 - Windshield Failsafe Pressure Test

High Speed Impact

The final laboratory test was a series of high-speed impacts on a test window of bird-bagging design. Testing was performed at the University of Dayton, with funding provided by the Air Force. As these were purely comparative tests of the response of two vinyls under high-speed impact, there was no specific projectile size or velocity requirements. The 'plastic bird' developed by the Dayton Impact Physics Laboratory was selected for simplicity and the 1.5-lb seagull size projectile was used with the 3.5-inch bore bird gun (shown in Figure 20) throughout the test. The test specimen is shown in Figure 21. It consists of a 24.0-inch by 18.0-inch simple laminate. Glass plies are each 3/16" tempered glass and the .30-inch thick vinyl interlayer is retained with an aluminum edge insert. The test specimen was bolted into a heavy test fixture, shown in Figure 22.

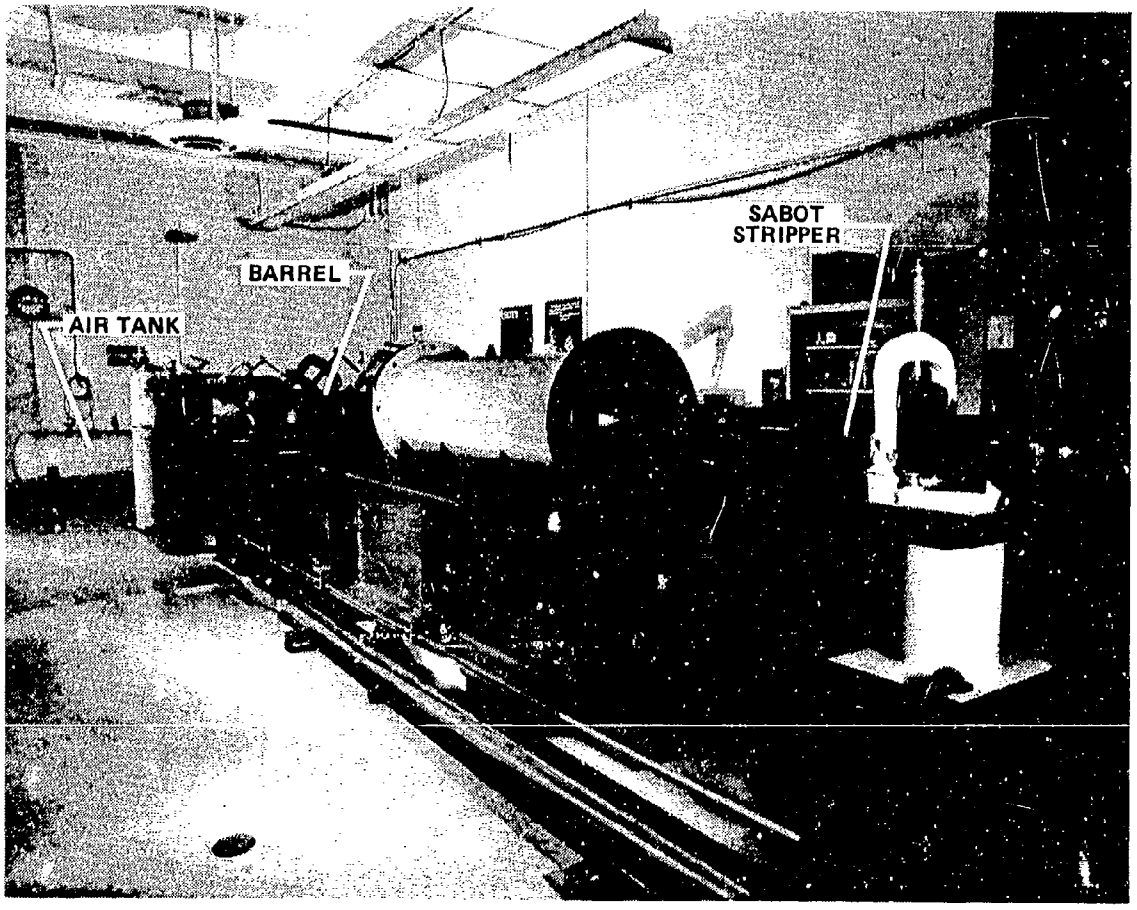

Figure 20 - 3.5 in. Bore Bird Gun

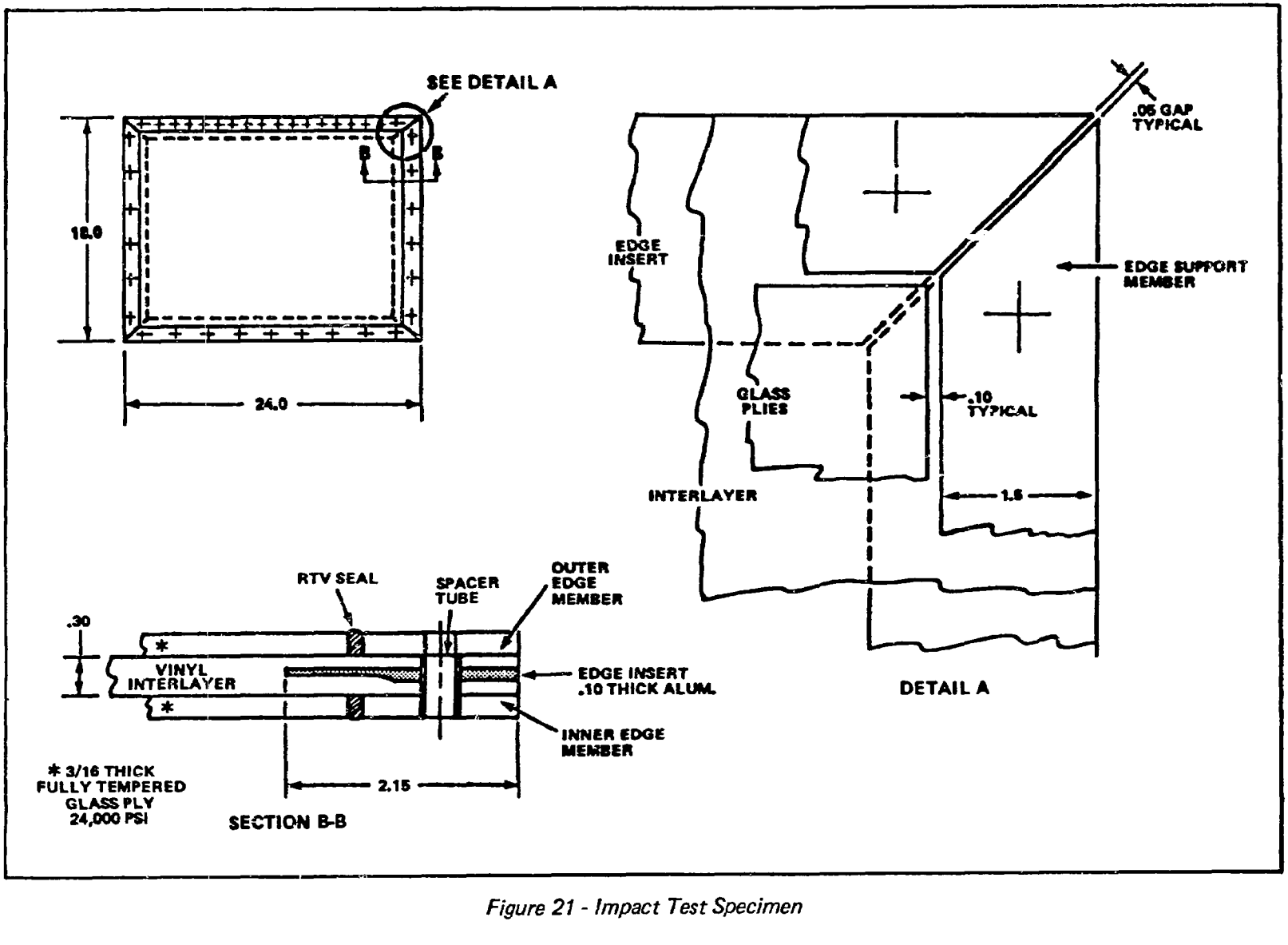

Figure 21 - Impact Test Specimen

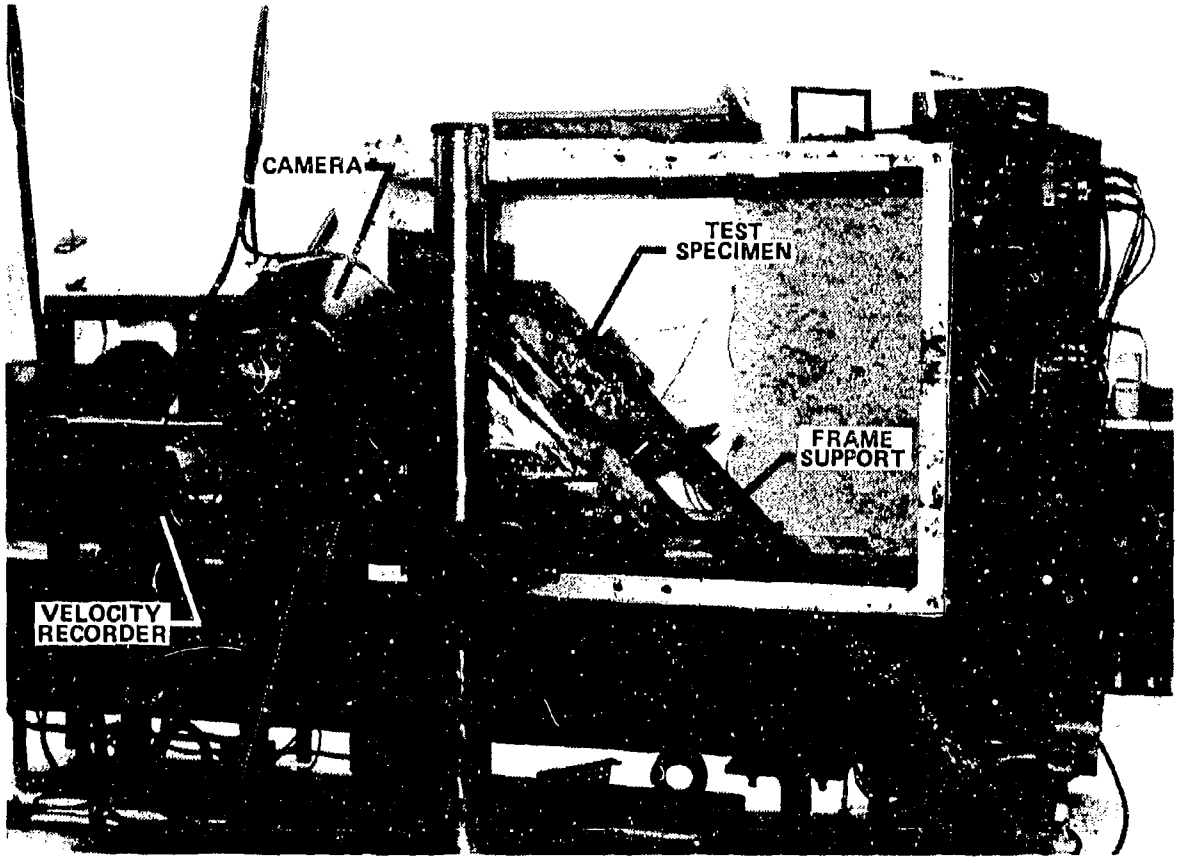

Figure 22 - Test Specimen in Fixture

It was originally intended to photograph the vinyl deflection at impact but this was found to be impractical due to spall fragments; as a result, a comparison was made of the penetration velocities of the respective vinyls. This entailed slowly increasing the impact velocity until penetration of the 3GH vinyl occurred, then impacting the AG2 at the same velocity. The results are shown in Figures 23 and 24; it can be seen that the AG2 did, in fact, perform somewhat better than the 3GH. Testing was done with window temperatures of 110°F and -30°F, which were the extreme temperatures expected in flight with an operating or non-operating heating system. At both temperatures, the AG2 vinyl performed a little better than 3GH.

SHOT NO.	TEMP	TARGET VELOCITY		ACTUAL F.P.S.	VINYL TYPE	RESULT	REMARKS
		KNOTS	F.P.S.				
1	110°F	412	696	697	EXP **	PASS *	1ST SHOT AT 350+15% KNOTS CAMERA MALFUNCTION
2		412	696	694	3GH	PASS *	REPEAT AT 350+15% KNOTS PHOTOGRAPHY POOR
3		350	591	593	3GH	PASS *	1ST SHOT AT 350 KNOTS FOR COMPARATIVE PHOTOS PHOTOGRAPHS OBSCURED
4		350	591	592	3GH	PASS *	2ND SHOT AT 350 KNOTS PHOTOS OBSCURED
5		350	591	598	3GH	PASS *	3RD SHOT AT 350 KNOTS PHOTOS OBSCURED
6		350	591	600	3GH	PASS *	4TH SHOT AT 350 KNOTS PHOTOS OBSCURED
7		480	810	787	3GH	PENETRATION 3x1½ TEAR	1ST SHOT TO OBTAIN PENETRATION VELOCITY (Pv) LOWEST FAILURE VELOCITY FOR 3GH
8		439	742	742	3GH	PASS *	1ST SHOT TO BRACKET Pv
9		454	767	765	3GH	PASS *	2ND SHOT TO BRACKET Pv HIGHEST PASS VELOCITY FOR 3GH
10		466	787	794	AG2	PASS *	1ST AG2 SHOT HIGHEST PASS VELOCITY FOR AG2
11	110°F	466	787	770	EXP **	PASS *	1ST EXP ** SHOT FOR COMPARISON HIGHEST PASS VELOCITY FOR EXP **

* PASS INDICATES NO TEARING OR FAILURE OF VINYL
** ADDITIONAL EXPERIMENTAL INTERLAYER NOT RELATED TO 3GH/AG2 VINYL COMPARISON

Figure 23a - High Velocity Impact Test, Elevated Temperature

SHOT NO.	TEMP	TARGET VELOCITY		ACTUAL F.P.S.	VINYL TYPE	RESULT	REMARKS
		KNOTS	F.P.S.				
1	-30°F	250	422	485	3GH	Complete Penetration	1ST COLD SHOT
2		165	280	279	3GH	Pass *	NO VISUAL DAMAGE
3		200	338	343	3GH	Pass *	PANEL FROM #2 SHOT - 2ND IMPACT NO VISUAL DAMAGE
4		225	380	375	3GH	Pass *	PANEL FROM #2 SHOT - 3RD IMPACT NO VISUAL DAMAGE
5		246	415	405	3GH	Pass *	Panel from #2 shot - 4th Impact No Visual Damage Highest Pass Velocity for 3GH
6		260	440	451	3GH	Complete Pentration	RE-USE PANEL FORM #2 SHOT FAILURE
7		252	425	419	3GH	Diagonal Tear	PANEL FAILURE LOWEST FAILURE VELOCITY FOR 3GH
8		249	413	413	AG2	Pass *	NO VISUAL DAMAGE HIGHEST PASS VELOCITY FOR AG2
9		249	413	283	Exp **	Pass *	GUN MALFUNCTION LOW VELOCITY NO DAMAGE
10		249	413	406	Exp **	Pass *	NO INITIAL DAMAGE GLASS CRACKED ON WARM-UP HIGHEST PASS VELOCITY FOR EXP.
11	-30°F	255	430	430	AG2	Complete Pentration	PANEL FAILURE LOWEST FAILURE VELOCITY FOR AG2

* Pass indicates no tearing or failure of vinyl

** Additional Experimental Interlayer not related to 3GH/AG2 vinyl comparison

Figure 23b - High Velocity Impact Test, Low Temperature

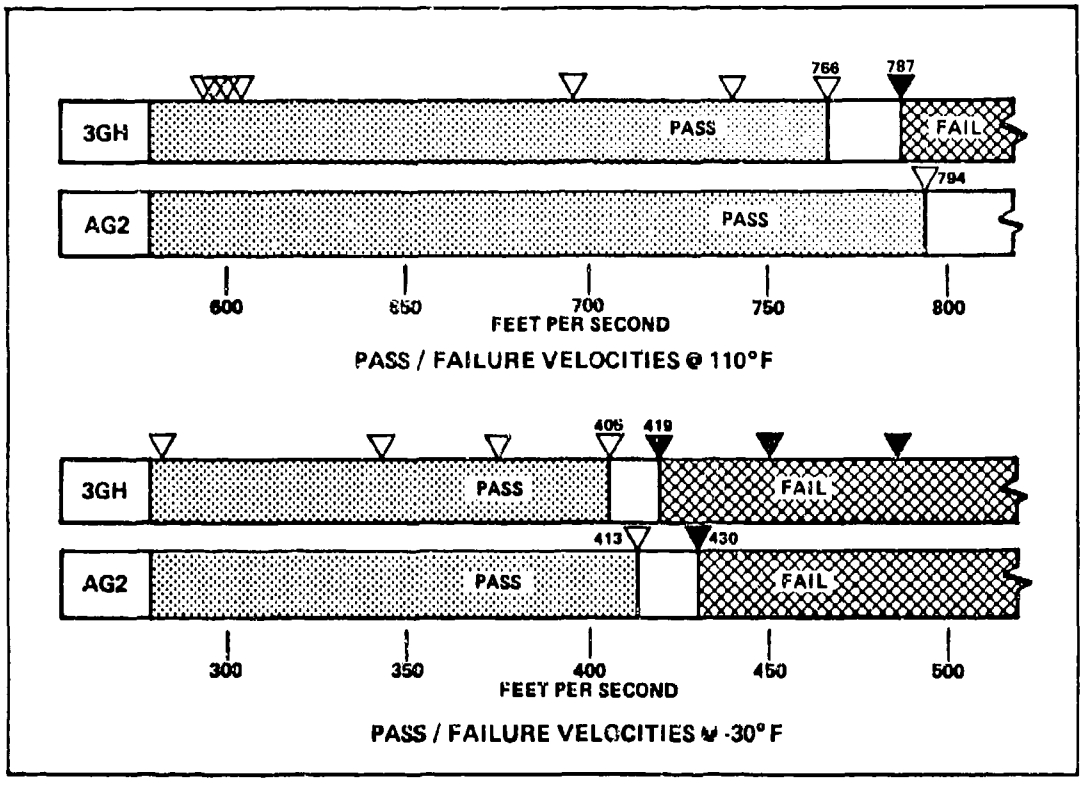

Figure 24 - High Velocity Impact Test Performance

▽ PASSING* IMPACT TEST SHOT VELOCITY

▼ FAILING IMPACT TEST SHOT VELOCITY

* PASS INDICATES NO TEARING OR RUPTURE OF INTERLAYER

Flight-Service Evaluation

The data reviewed here was presented to the FAA in greater detail. In December 1982, the FAA agreed that the AG2 vinyl could be used as an alternative to the current 3GH vinyl. But, as in any development program, the real test is under real-life service conditions, so a flight evaluation program was initiated. A total of forty front windshields for the (B727 and 737) with AG2 interlayer were built by PPG and Sierracin. Installation in commercial airplanes began in February, this year. Six airlines (Alaska, Continental, Delta, Eastern, TWA, Western) are cooperating in the flight evaluation and at this time there are about 20 units installed and flying. It is too early to draw any conclusions as to the AG2 service performance, but they are being very carefully monitored to ensure that not only is AG2 vinyl a structurally sound and safe alternate but that it is also reliable under the extreme flight environments encountered in-service.

AD-P003 201

FLUROEPOXY AND FLUROACRYLIC TRANSPARENCIES

J. R. Griffith, Naval Research Laboratory

FLUOROEPOXY AND FLUOROACRYLIC TRANSPARENCIES

James R. Griffith
Naval Research Laboratory

ABSTRACT

Heavily fluorinated epoxy resins and acrylic polymers which have been synthesized and developed at NRL during the last fifteen years are transparent, nearly colorless plastics of low refractive index which seem to be prime candidates for aerospace transparency applications.

The presence of 50% or more fluorocarbon in these classes of well-known polymers impart some properties which are uncommon and may be of special benefit in selected instances. For example, a helicopter with a fluoropolymer canopy could be expected to have better visibility in a rain storm than one with a conventional type because the unusual hydrophobicity of the fluorinated material would prevent wetting and consequent shimmering on the surfaces. Also, the refractive indices of the fluoropolymers are quite low compared to those of the common materials and this should result in less optical distortion of transmitted light.

At the present time, substantial sums of money are being committed to the effort to make commercial materials of the NRL fluoropolymers. It is expected that during the next three years these products will move from the laboratory into pilot plant production and be available in quantities sufficient for testing in stretch experiments, bird impact, erosion, etc., of interest to the transparency community.

INTRODUCTION

The few fluoropolymers which are commercially available are often regarded as top-of-the-line materials possessing superb and unusual properties. Generally they are not regarded as structural materials nor do they have the optical clarity that is required for an aircraft transparency application. The conventional acrylics are, of course, widely useful in transparencies, and the introduction of substantial quantities of fluorocarbon into acrylic polymers produces hybrids that possess useful properties of both classes, including the excellent clarity and optical properties associated with common acrylics. Epoxy plastics are thermoset materials which are normally yellow in color. Some of their properties, such as high heat distortion temperatures, could be useful in transparencies if the other properties were suitable. On the other hand, the fluoroepoxies can be produced in colorless forms which rival the acrylics in optical quality.

This paper is intended to introduce the fluoroepoxy and fluoroacrylic polymers to the transparency community. It is admittedly short on the type of data that the community will ultimately need, but such data can be quickly generated when enough interest is aroused to prompt commercial production of the necessary monomers.

COMPOSITION

The chemistry of the fluoroepoxy and fluoroacrylic polymers has been developed at the Naval Research Laboratory during the last fifteen years and has been reported elsewhere (References 1, 2, 3, 4). In essence, the conventional molecular structures have been loaded with fluorocarbon groups in such a way that the convenient common properties were not compromised. The following examples compare the NRL "C" series epoxy resins with the conventional diglycidyl ether of Bisphenol-A, which is the most common commercial epoxy:

FLUOROEPOXY RESINS OF THE NRL "C" SERIES

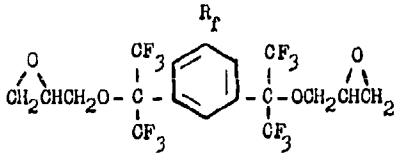

$R_f = CF_3CF_2CF_2-$ for C-3 resin

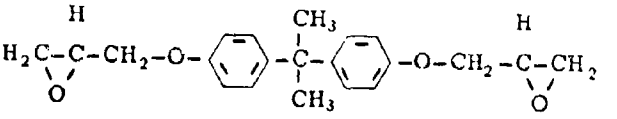

Diglycidyl Ether of Bisphenol-A

The common features of all these structures of importance include the two epoxy groups composing glycidyl ether functions and the aromatic nucleus which affords strength and rigidity to the final polymer. The pure fluoro-epoxy resins are generally syrups at room temperature which are easily poured into molds for casting.

FLUOROACRYLIC RESINS

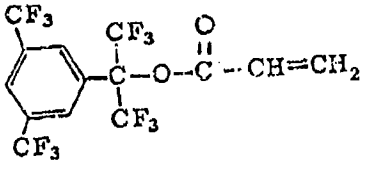

Linear fluoroacrylic monomer

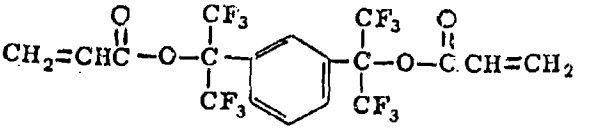

Crosslinked fluoroacrylic monomer

The fluoroacrylics are divided into two principal series of polymers, the monomers of which are illustrated. The linear type produces thermoplastic polymers upon suitable reaction, and this type should be capable of processing in much the same manner as conventional transparency acrylics. For example, the linear polymers should be "stretchable" like the more common materials. The crosslinked type is capable of producing more rigid plastics with higher glass transition temperatures than the linear types. In situations calling for resistance to relatively high levels of aerodynamic heating, the crosslinked variety should be superior. The optical qualities of the fluoroacrylic polymers of either type are superb, since they are colorless plastics of high transmission capability in the visible region of the spectrum.

CURING

Several types of curing agent systems are available for the fluoroepoxies. Similar to the conventional resins, they are curable by polyamines and organic anhydrides. However, the fluoro resins are not compatible with most of the common curing agents and special types have been evolved.

Of particular interest among the polyamine types are certain silicone amines of the following general formula:

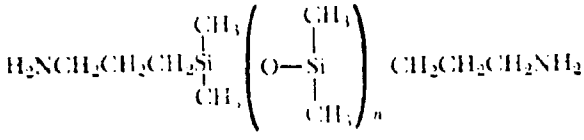

When "n" is 1, the plastic produced upon cure of a fluoroepoxy is relatively rigid, and as "n" increases, the plastics become increasingly flexible until an elastomeric composition is attained. For transparency purposes, the shortest structure is probably most desirable. Fluoroepoxy castings made with this system normally have a slight color which is in evidence as light is transmitted through an inch or more thickness.

The fluoroanhydride curing agents are illustrated by the following example:

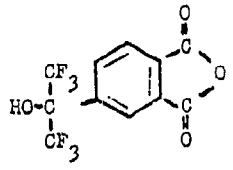

This material produces a colorless solution when dissolved in a fluoroepoxy resin, and if care is taken, the cured plastic is nearly as colorless as a fluoroacrylic. This result is somewhat dependent upon the catalyst employed. The common tertiary amine catalysts generate some color whereas quarternary ammonium salts allow colorless products.

DISCUSSION

At the very least, the fluoroepoxy and fluoroacrylic polymers afford new classes of highly transparent plastics which are clearly applicable to the enclosure use. They can be produced in a wide variety of forms with respect to such properties as rigidity, heat distortion temperature, impact resistance, etc. What do they offer which is special relative to the conventional acrylics or polycarbonate? The following is an attempt to answer this question.

Organic materials which contain much fluorocarbon are among the most water-repelling substances known. One result of this property is that the surface of a fluorocarbon causes water to retract into droplets very quickly, and a consequence of this is that the visibility through such a windshield when an aircraft is in a rain storm is much better than it is when a layer of water is allowed to shimmer as a sheet upon the outer surface. This was demonstrated by a major aircraft manufacturer several years ago by the application of coatings to windshields (5). Unlike a coating which may erode and lose adhesion with time, a fluoropolymer transparency retains the water repelling property throughout its bulk.

This particular property may be exceptionally valuable for helicopters since they fly relatively low, in the rain zone. Secondly, fluoroorganic materials have a lower refractive index than comparable non-fluorinated analogs. Methyl methacrylate monomer, for example, has a refractive index of approximately 1.41, while several fluoroacrylic monomers are in the 1.37 vicinity. Comparable levels should be shown by the polymers, and this should translate into canopies with less optical distortion of transmitted images when the fluoromaterials are used.

The extremely low water absorption of the fluoropolymers combined with a high resistance to degradation by light, and a lack of nutritional value to microorganisms, indicates that natural degrading elements of the environment should have relatively small effect upon fluoropolymer transparencies. And indeed, such is often the case with respect to other types of applications for fluoropolymers. Thus, when the service life of an aircraft transparency is limited by cracking, hazing, blistering, etc. as a result of exposure to the environment, a fluoropolymer material should last substantially longer than a conventional material.

Since the crosslink density of a fluoroepoxy plastic can be easily varied at will, it should be relatively easy to design a transparency from this type of polymer with higher glass transition temperatures than are afforded by stretched acrylic or polycarbonate. Such would also be the case with conventional epoxies were it not for a pronounced tendency for these plastics to become colored during processing or in service. Alternatively, the fluoroepoxies could be used as adhesives for multilayered transparencies composed of combinations of fluoropolymers and the conventional types.

FUTURE ACTIVITY

Patents covering the basic materials of the fluoroepoxy and fluoroacrylic polymers are owned by the U. S. government as represented by the Secretary of the Navy. Because of the risk and expense involved in the commercial exploitation of such patents, there has been a "chicken-and-egg" problem involved in the establishment of commercial supplies of the basic monomers, and to date only research quantities have been available. Because of valuable and unique properties that have been discovered for these polymers in applications other than transparencies, we believe that they have an excellent possibility of becoming available materials in the near future. If so, or if they remain research items for the time being, the community interested in transparencies should explore the technical possibilities that these new classes of polymers offer.

REFERENCES

1. Griffith, J. R., O'Rear, J. G. and Reines, S. A., "Fluorinated Epoxy Resins", CHEMTECH, 311 (May 1972).

2. Hunston, D. L., Griffith, J. R. and Bowers, R. C., "Fluoro Epoxies: Surface Properties and Applications", Ind. Eng. Chem Prod. Res. Dev., 17, No. 1, 10 (1978).

3. Griffith, J. G. and O'Rear, J. R., "The Synthesis of Fluorinated Acrylics Via Fluoro Tertiary Alcohols", Biomedical and Dental Applications of Polymers, Plenum Publishing Corp., New York (1981).

4. Griffith, J. R., "Epoxy Resins Containing Fluorine", CHEMTECH, 290 (May 1982).

5. Mallenieks, O. J., "Transparent Rain-repellant Polymer Coatings", Modern Plastics, 48, 68 (Feb 1973).

Figure 1. Light transmission through 1/8-inch thick disc of fluoroacrylic plastic.

AD-P003 202

POLYCRYSTALLINE $M_gAl_2O_4$ SPINEL FOR HIGH PERFORMANCE WINDOWS

D. W. Roy, Coors Porcelain Company

Polycrystalline $MgAl_2O_4$ Spinel for High Performance Windows

Donald W. Roy, James L. Hastert

Coors Porcelain Company
600 Ninth Street, Golden, Colorado, 80401

Introduction

The performance requirements of many electro-optical (EO) systems now in the planning stages have window and dome material requirements that are not adequately satisfied by existing materials. Plastics and glasses which are inexpensive have limitations in respect to thermal stability and resistance to particle impact at high velocity. Hot-pressed magnesium fluoride which has been widely used in the intermediate IR region does not transmit well in the visible spectrum, and does not have good thermal shock or rain erosion properties. Single crystal aluminum oxide (sapphire) which is transparent from the UV to the intermediate infrared range is optically anisotropic and is very expensive to fabricate in significant window sizes or dome configurations. Thus there is a need for optical materials which are highly transparent at wavelengths from the ultraviolet to the infrared, hard enough to resist high speed rain erosion, strong enough to resist mechanically or thermally induced fracturing and are inexpensive to fabricate.

Magnesium aluminate spinel ($MgAl_2O_4$) possesses an unusual combination of optical, dielectric, physical and mechanical properties that make it an attractive candidate for windows on EO systems that are moving at very high speeds, and is cost effective when compared with sapphire.

Spinel is cubic and optically isotropic; thus polycrystalline shapes may be fabricated without the severe scattering problems inherent in noncubic materials. In the microwave region the isotropy of spinel prevents localized absorption and heating that occurs in noncubic materials because of differing grain boundary orientation and anisotropic dielectric loss index. Spinel undergoes no polymorphic transformations and is thus free of problems due to thermally induced phase changes.

Typical physical and mechanical properties

The physical and mechanical properties of spinel are summarized in Table 1. Spinel is exceptionally strong and hard for an optical material, has good thermal shock resistance, moderate thermal expansion coefficient, and is dimensionally and mechanically stable at temperatures up to 1250°C. The polycrystalline structure results in blunting and redirecting of cracks at grain boundaries; thus offering greater toughness than spinel single crystals. The high strength and hardness make it feasible to use thinner windows than is necessary with lower strength, softer materials. The reduced wall thickness results in lower thermal stresses and improved optical performance. The homogeneity, isotropy and very low dielectric loss index, along with the thermomechanical properties, result in an exceptionally stable electromagnetic window.

Transmission. Using the relationship $T = \frac{2n}{n^2+1}$

where n is the refractive index as listed in Table 2 the total theoretical transmission of an uncoated window is calculated to be 86.5 percent at 0.4 microns and 87.8 percent at 4.0 microns. In Figure 1 the typical transmission for an uncoated 0.1 inch thick window is shown from 0.20 to 6.0 microns.

The transmission of polycrystalline spinel is compared with single crystal Al_2O_3 (sapphire) in Figure 2. Note that primarily because of scattering losses from residual microporosity in polycrystalline spinel the transmission of sapphire is better at shorter wavelengths; however, there is a crossover at 4.5 microns beyond which the transmission of spinel exceeds that of sapphire.

Antireflection. Antireflection (AR) coatings can be applied to spinel to maximize the transparency in a selected spectral band. As shown in Figure 3 the transmission can be increased to 92 percent by coating one surface. By coating both surfaces the transmission can be increased to at least 95 percent over a narrow waveband.

Absorption and emissivity. The specular transmittance of spinel and sapphire (0° orientation) has recently been measured at temperatures as high as 1400°C in two thicknesses (0.1 and 0.2 inches)[1]. The transmittance data was then used to calculate the material absorption coefficient and emittance. The absorption coefficient β was found from:

$$\beta = \frac{-\ln (T_2/T_1)}{t_2 - t_1}$$

β = absorption coefficient

T_i = transmittance

t_i = window thickness

The calculated absorption coefficient at 4.5 and 5.0 microns is summarized for both spinel and sapphire at several temperatures in Table 3.

The emittance was then determined by:

$$\varepsilon = \frac{(1-\rho)\quad 1 - e^{-\beta t}}{1 - \rho e^{-\beta t}}$$

ε = emittance

ρ = single surface reflectivity

t = window thickness

Table 4 is a summary of the calculated emissivity at 4.5 and 5.0 microns at several temperatures. The data for both spinel and sapphire is again included for comparison for a 0.1 inch thickness.

Scatter. The total integrated forward scatter (TIS) has also been measured on 0.1 inch thick windows in the visible as well as at 3.39 microns in the infrared. A detailed description of the measurement technique is contained in a paper by Archibald and Bennett.[2] The system makes use of a krypton laser beam, typically 1-2 mm. in diameter, and two coblentz spheres. The results are the ratio of the total scatter from the two surfaces and the bulk material (not corrected for reflection losses at the surfaces) measured relative to the incident beam intensity. The values reported are averages of 37 points on the surface taken in concentric circles; the radial increment was 0.10 inch and the maximum radius was 0.30 inches. The data for seven samples which have been evaluated is summarized in Table 5.

Surface quality. The surface roughness of a polished disc was measured with a Talystep profilometer using a diamond stylus with a one micron radius and a two mg. load.[3] This loading was not sufficient to make a permanent mark on the sample. A roughness calculated from 17,000 surface height data points was 17.7A° rms which is equivalent to a good polish on an optical glass.

Thermal and Mechanical Properties

Material selections for EO windows are limited not only by the optical and dielectric properties, but also by the ability of the materials to withstand severe thermo-mechanical environments. Properties of particular importance include strength, toughness, thermal shock resistance, and erosion resistance. Young's elastic modulus and the shear modulus are plotted for polycrystalline spinel in Figure 4.[4] The fracture toughness was measured at Pennsylvania State University using the controlled flaw technique.[5] The data, at temperatures to 1400°C, is summarized in Figure 5. No relationship between grain size and fracture toughness was observed for the four grain sizes which were examined. The room temperature fracture toughness of MgF_2 is also noted for comparison.[6] In Table 6 the hardness of spinel is compared with some other common optical materials. Because of the high hardness, spinel is very resistant to rain and abrasive particle erosion when compared with MgF_2 and silica glasses. Adler[7] and Hackworth[8] have independently made tests on both spinel and MgF_2; however there have not yet been sufficient tests to firmly establish damage threshold levels. It appears, based on the data in the references cited, that spinel is thirty to fifty percent more resistant to rain erosion than is MgF_2. The increase in haze resulting from blasting with ten pounds of abrasive grit is summarized for spinel, acrylics and glass in Table 5.[9]

Metallizing

Spinel can be metallized using traditional molybdenum/manganese systems fired in the range of 1300°C.

Fabrication and Cost

During recent years, the availability of high purity starting materials and the use of rate controlled hot-press technology has resulted not only in improved

optical quality but also higher yields and lower manufacturing costs. Further, as optical finishers have gained experience, the cost for grinding and polishing has been reduced dramatically.

Flat round discs as large as five and one-half inches in diameter and 0.2 inches thick can be reproducibly fabricated. Hemispherical domes with a three and one-half inch diameter base have been made, as have hollow cones which are five inches tall. Development activities are in progress for the extension of both shape and size capability.

We can now offer 2.8 inch diameter hemispherical domes in quantities of 10 for approximately $1,200. In quantities of 5,000 the price is projected to be between $300 and $400.

References

1. Arendt, J. W., personal communication 2/17/83, "Results of the High Temperature Transmission Testing of Sapphire and Spinel", conducted by General Electric of Philadelphia.
2. Archibald, P. G., Bennett, H. E., "Scattering from Infrared Missile Domes", NWC, China Lake, CA.
3. Bennett, J. M., personal communication of January 25, 1979, NWC, China Lake, CA.
4. Stewart, R. L., "Fracture of Magnesium Aluminate Spinel", a thesis in Ceramic Science, The Pennsylvania State University, May, 1981, pp. 104.
5. Ibid. pp. 105.
6. Adler, W. F., "Development of Design Data for Rain Impact Damage in Infrared Transmitting Materials," Effects Technology, Inc., 5383 Hollister Ave., Santa Barbara, CA., 93111.
7. Adler, W. F., "Investigation of Liquid Drop Impacts on Ceramics", CR-82-1075, Office of Naval Research, Contract N00014-76-C-0744 NR032-565.
8. Hackworth, J. V., "Exploratory Development of Erosion Resistant Infrared Windows and Radomes", Contract No. F33615-80-C-5150, AFWAL/MLPO.
9. Sand Erosion Tests made at Coors Porcelain Company, 1972.

TABLE 1. Typical Physical Properties of Hot-Pressed $MgAl_2O_4$ Spinel

Property	Units	Test	Value
Specific Gravity (Density)	g/cc	ASTM C20	3.58
Melting Point	°C	-	2135
Hardness, Knoop (see comparison chart)	GPa	ASTM E18 200-g load	1300
Surface finish, polished	Microinch AA	Profilometer	1
Flexural Strength: (min. 10 piece mean)	psi	ASTM F417	25,000
4-point bending 800°C			20,000
Room Temperature to 1000°C			
Tensile Strength	psi	ACMA Test #4	16,000
Compression	psi	ASTM C773	390,000
Modulus of Elasticity	10^6psi static	ASTM C623	39
Shear Modulus	10^6psi dynamic	ASTM C623	15.89
Bulk Modulus	10^6psi dynamic	ASTM C623	27.93
Poisson's Ratio	-	-	0.2608
Coefficient of Linear Thermal Expansion	10^{-6}/°C	ASTM C372	
25 - 200°C			5.6
25 - 500°C			7.3
25 - 1000°C			7.9
Thermal Conductivity	(g-cal/(sec)(cm^2)(°C/cm)	ASTM C408	
100°C			0.0357
1200°C			0.0130
Specific Heat	g-cal/g/°C	ASTM C351	
20°C			0.200
1040°C			0.214
Dielectric Constant	10^3Hz	ASTM D150	8.2
	10^6Hz	ASTM D2520	8.2
	9.3×10^9	ASTM D2520	8.3
Dissipation-Factor	10^3Hz	ASTM D150	3.0×10^{-5}
	10^6Hz	ASTM D2520	2.0×10^{-5}
	9.3×10^9Hz	ASTM D2520	1.0×10^{-5}
Loss Index	10^3Hz	2.5×10^{-4}	
	10^6Hz	2.0×10^{-4}	
	9.3×10^9Hz	1.0×10^{-4}	

TABLE 2. Index of Refraction vs. Wavelength in Microns

Microns	Refractive Index	
0.4047	1.736	
0.5461	1.719	Established accuracy
1.0140	1.703	$\pm$ 1 x 10^3
1.0000	1.704	
2.0000	1.702	
3.0000	1.698	
4.0000	1.685	
5.0000	1.659	
6.0000	1.558	

TABLE 3. Absorption Coefficient at 4.5 and 5.0 Microns

Temperature (°C)	Absorption at 4.5 microns		Absorption at 5.0 microns	
	spinel	sapphire	spinel	sapphire
30	0.323	0.221	0.678	0.887
200	0.376	0.323	0.909	1.25
400	0.500	0.531	1.32	1.87
600	0.651	0.777	1.82	2.66
800	0.863	1.10	2.54	3.70
1000	1.14	1.58	3.42	4.95
1200	1.46	2.05	4.67	6.63
1400	1.95	2.71	7.00	8.83

TABLE 4. Emissivity at 4.5 and 5.0 Microns

Temperature (°C)	Emissivity at 4.5 microns		Emissivity at 5.0 microns	
	spinel	sapphire	spinel	sapphire
30	0.078	0.051	0.157	0.199
200	0.091	0.074	0.203	0.268
400	0.118	0.119	0.280	0.370
600	0.151	0.168	0.361	0.477
800	0.194	0.229	0.461	0.587
1000	0.247	0.311	0.559	0.686
1200	0.303	0.381	0.664	0.777
1400	0.381	0.468	0.788	0.848

TABLE 5. Resistance to Damage by Sand Erosion

Material	Percent Haze	
	Before Sandblast	After Sandblast*
Spinel	6.5	8.3
Acrylic No. 1	1.3	79
Acrylic No. 2	1.3	74
Glass	1.9	82

*Ten pounds tabular alumina

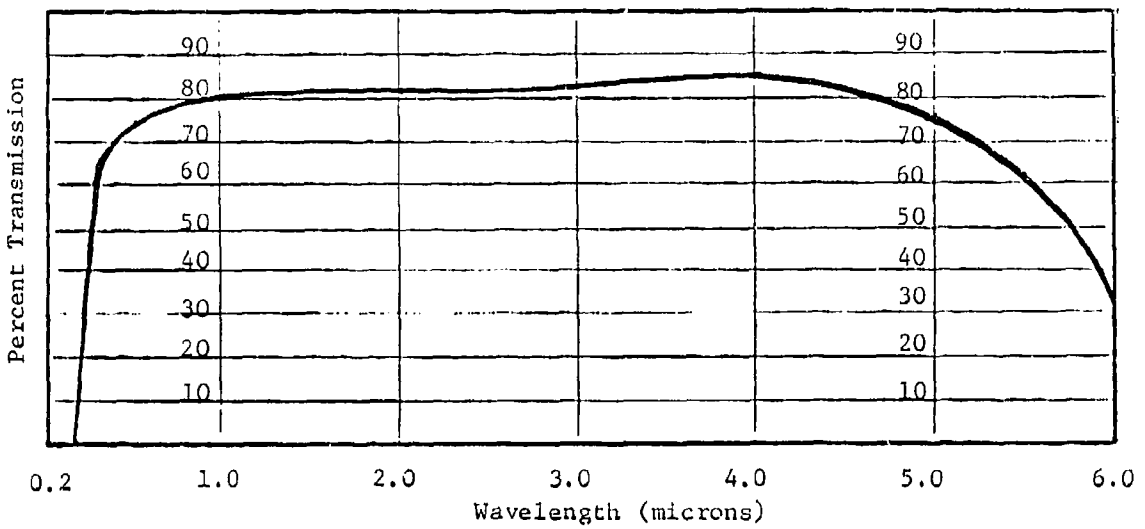

FIGURE 1. Specular Transmission, Uncoated, 0.1" Thick, Not Corrected for Reflection Losses

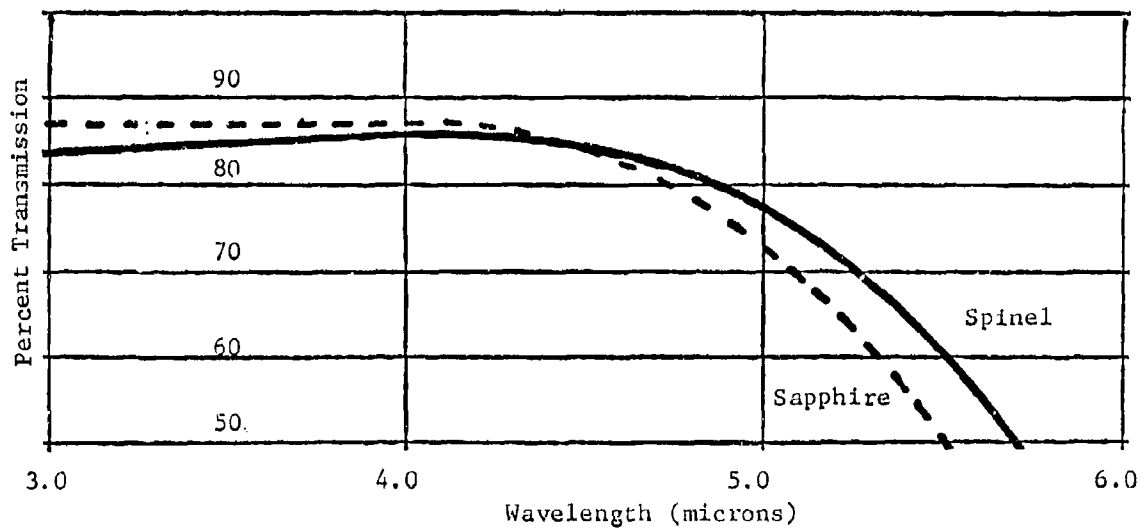

FIGURE 2. Transmission of Spinel vs. Sapphire, 0.1" Thick

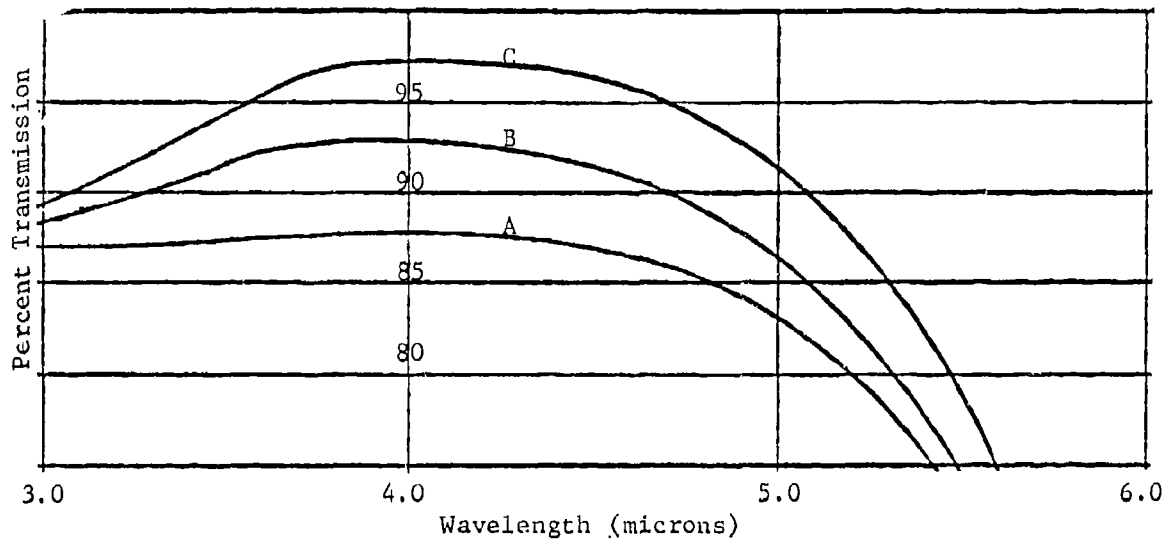

FIGURE 3. Percent Transmission; A-uncoated, B-one surface coated, C-two surfaces coated, window thickness 0.040"

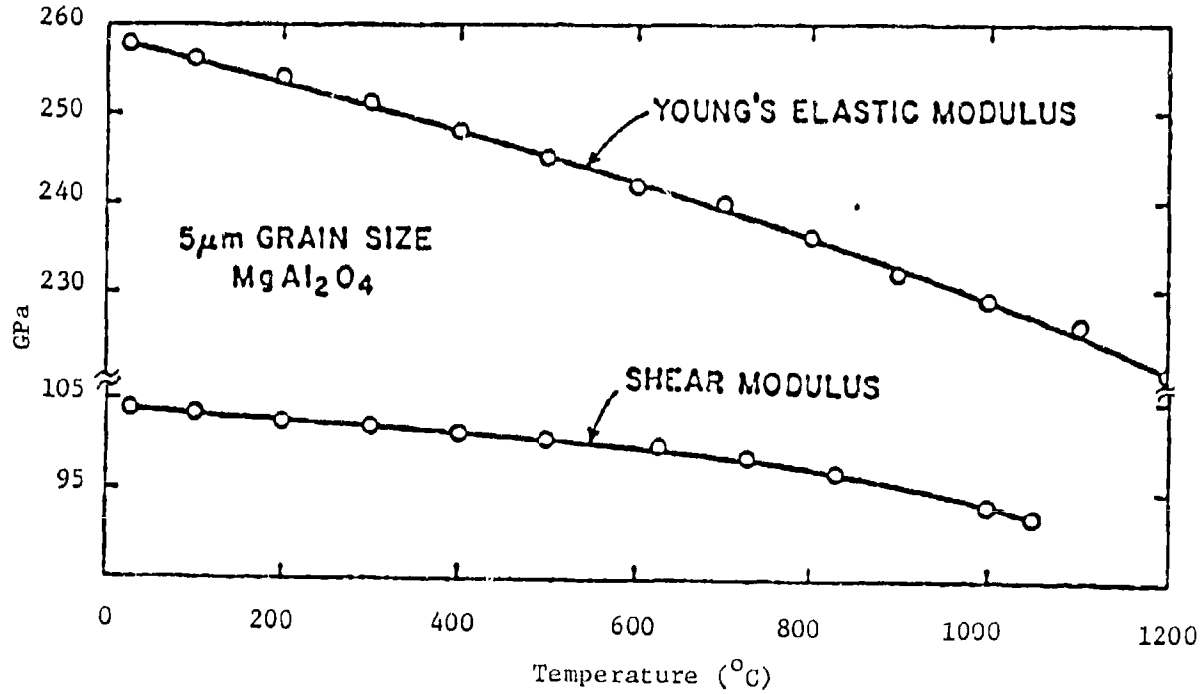

FIGURE 4. Variation of Young's Elastic Modulus and Shear Modulus with Temperature

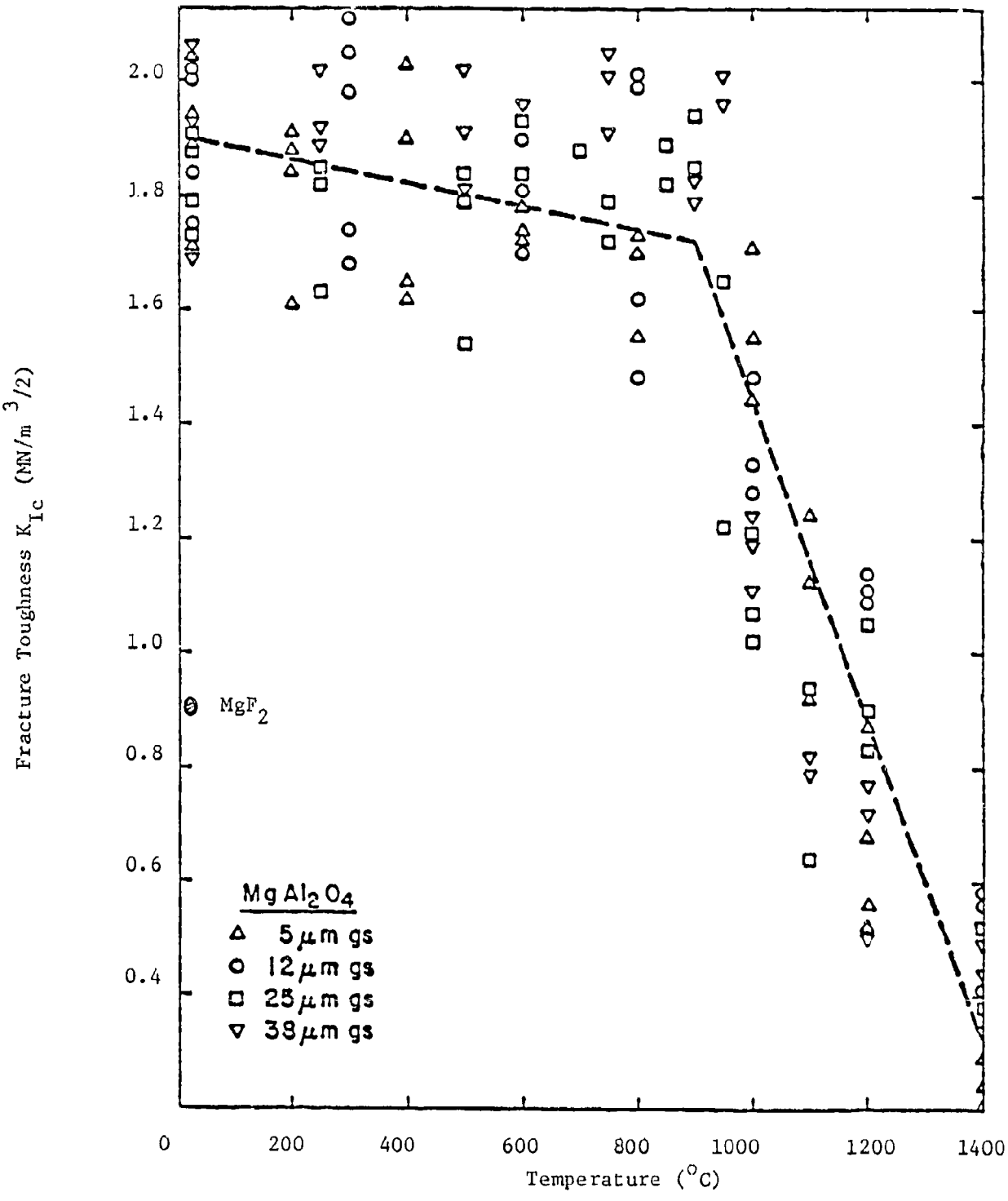

FIGURE 5. Variation in Fracture Toughness with Grain Size and Temperature

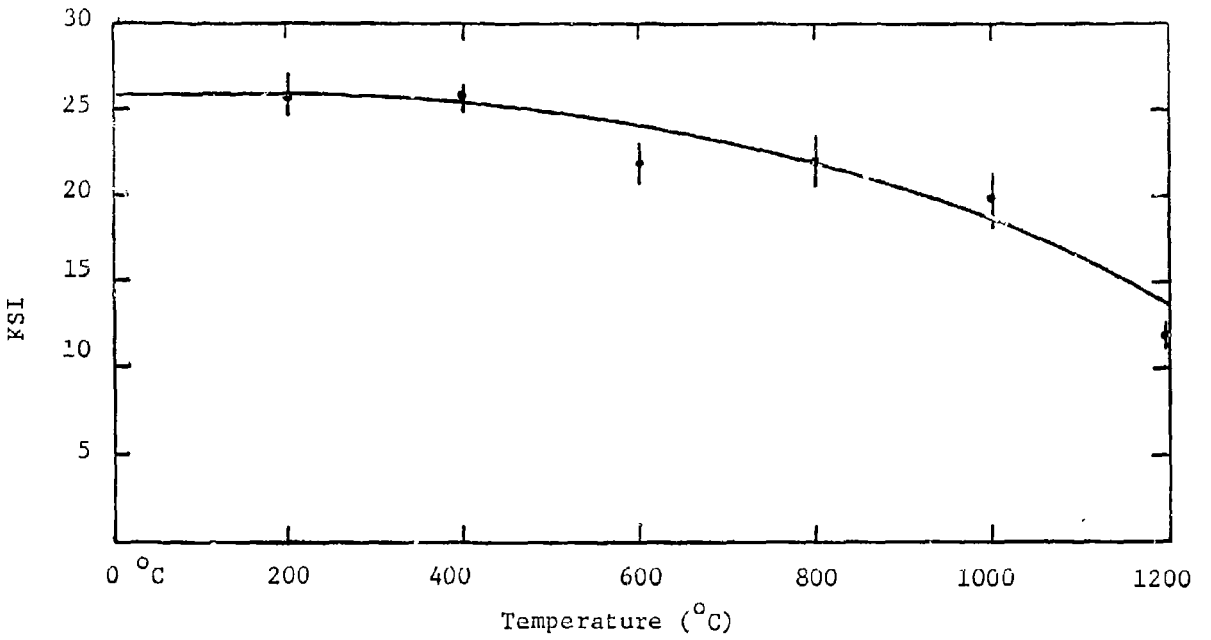

FIGURE 6. Flexural Strength vs. Temperature, in 4-Point Bending

SESSION III

NEW MATERIALS (PART II)

Chairman: I. Wolock
Naval Research Laboratory
Washington, D. C.

Co-Chairman: E. J. Morrisey
Materials Laboratory
Wright-Patterson
Air Force Base, Ohio

AD-P003 203

AN IMPROVED ACRYLIC SHEET MATERIAL WITH ENHANCED CRAZE RESISTANCE

M. V. Moncur and W. F. Fisher,
Swedlow Incorporated

AN IMPROVED ACRYLIC SHEET MATERIAL WITH ENHANCED CRAZE RESISTANCE

M. V. Moncur, W.F. Fischer
SWEDLOW, Inc.

ABSTRACT

Crazing of the exterior surface in monolithic and laminated acrylic aircraft transparencies is one of the major causes of replacement. Water absorption and desorption processes are believed to play a major role in generation of this type of defect by reducing the inherent craze resistance of the acrylic material and by increasing surface stress levels.

MIL-P-8184 acrylic sheet is susceptible to water-induced crazing because of its relatively high moisture uptake rate. MIL-P-5425 acrylic sheet has lower moisture absorption properties but also has lower inherent craze resistance, so it is also susceptible to field crazing.

This paper describes a new acrylic material developed by Swedlow, Inc., Acrivue 351, which has been designed to provide improved resistance to water-induced crazing when compared to current acrylic materials. Acrivue 351 combines the high inherent craze resistance of MIL-P-8184 acrylic plastic with the low moisture uptake characteristic of MIL-P-5425. Stretching of Acrivue 351 further enhances its inherent craze resistance.

Results of lab craze studies are presented, comparing as-cast Acrivue 351 to MIL-P-8184 and MIL-P-5425 acrylic materials. Standard solvent stress crazing tests were used to determine craze resistance of these materials as a function of water content. The crazing stress advantage of Acrivue 351 over the other cast acrylic materials increases upon exposure to moisture. Other properties of Acrivue 351 are very similar to MIL-P-8184 acrylic sheet.

A similar study comparing crazing behavior of stretched Acrivue 351 to MIL-P-25690 acrylic is described. Acrivue 351-S has much higher inherent crazing stress than conventional stretched acrylic with a variety of solvents, and again the difference increases upon moisture exposure. Stretched Acrivue 351 has lower crack propagation resistance than MIL-P-25690 acrylic sheet.

Potential aircraft applications of both as-cast and stretched Acrivue 351 will be discussed. F-111 transparencies incorporating Acrivue 351 as the outer ply have recently been manufactured for the Air Force and are now in a flight testing program.

INTRODUCTION

Development of crazing in acrylic aircraft transparencies after long flight exposure is a fairly common occurrence. It is observed in both monolithic stretched acrylic parts and in laminated structures containing an as-cast or stretched acrylic outer ply. Occasionally, crazing occurs after a relatively short time in service, which leads to premature replacement of the transparency.

Modified acrylic plastic meeting MIL-P-8184 in the as-cast state and MIL-P-25690 after stretching is used almost exclusively for aircraft applications. Use of unmodified MIL-P-5425 acrylic sheet in the U.S. is limited to the as-cast outer ply in laminated transparencies. The modified grade has superior craze resistance, which is further enhanced by stretching.

Previous studies have shown that modified acrylic has a relatively high moisture uptake rate and high equilibrium water content compared to unmodified acrylic sheet, and that absorbed water reduces craze resistance. Water absorption and desorption processes are believed to play a major role in formation of crazes in transparencies under use conditions[1-4].

Mason[1] reported saturation water contents of 2-4 percent for different samples of stretched acrylic, and showed that crazing stress in contact with isopropanol drops to very low levels at saturation. In a similar study, Burchill and Stacewicz[2,3] reported that no external stress is required to craze saturated stretched acrylic samples exposed to isopropanol. Armstrong[4] reported threshold crazing stress drops 1000 psi for each 1 percent of absorbed water. Water content reportedly reaches about 1.5 percent in acrylic transparencies in use.

Other acrylic properties are also adversely affected by absorbed water. The most serious is relaxation temperature of stretched acrylic, which is depressed by absorbed moisture [1,4-6]. Water content of about 1 percent or less is required to meet the MIL-P-25690 thermal relaxation requirement[1]. Relaxation temperatures of dry versus water-saturated acrylic materials can differ by as much as 20°C[1,6].

These problems related to the moisture uptake characteristics of modified acrylic sheet suggest that an improved material is needed. Such a material would ideally have low water absorption characteristics, like unmodified MIL-P-5425 acrylic sheet, with other physical, thermal and craze resistance properties equivalent to MIL-P-8184 material in the dry as-cast state, and equivalent to MIL-P-25690 material after stretching. Swedlow has been working towards this goal for several years. The new acrylic material described in this paper, Acrivue 351, is a result of this development work and partially satisfies the need for an improved modified acrylic material for aircraft applications.

ACRIVUE 351

Acrivue 351 is a cast, crosslinked acrylic material with inherent low water uptake characteristics. Other properties are similar to conventional MIL-P-8184 acrylic material, and are described in more detail below.

Acrivue 351 responds to stretching differently than MIL-P-8184 acrylic sheet, and properties of stretched sheet are quite different than those of MIL-P-25690 acrylic sheet. As a result, Acrivue 351-S is not considered a general replacement for current stretched acrylic plastic, but has advantages for many applications. Properties of the stretched material are also described in more detail below.

AS-CAST ACRIVUE 351 PROPERTIES

Water Uptake Characteristics

The rates of water absorption of Acrivue 351, MIL-P-5425 and conventional MIL-P-8184 materials* were compared under immersion conditions. Specimens (0.125 x 1 x 3 inch) were initially conditioned at 250°F for 4 hours followed by 150°F for 48 hours in an air oven to obtain "dry" weights. Conditioned samples were then immersed in water at 120°F and weight gain was monitored.

Results plotted in Figure 1 show moisture uptake rates of Acrivue 351 and MIL-P-5425 acrylic plastic are virtually equivalent, while MIL-P-8184 absorbs water at a significantly higher rate. Similar relative water uptake rates were measured on a second set of samples immersed at room temperature, and a third set conditioned at 100% relative humidity.

Craze Resistance

The effect of absorbed water on craze resistance was evaluated using the standard MIL-P-8184 solvent crazing test. Craze bars (0.125 x 1 x 7 inch) were dried as described above prior to starting the test. Specimens were then immersed in water at 120°F, and removed at various intervals for testing. Removed specimens were equilibrated at room temperature in sealed polyethylene bags, then wiped off and tested under standard conditions. A series of weights was used to cover a range of applied stress levels to determine threshold crazing stress (lowest applied stress at which crazing is observed).

* The MIL-P-5425 material used was Acrivue 320, and the MIL-P-8184 material was Acrivue 350. Our tests have shown that the corresponding Rohm and Haas materials, Plexiglas II and Plexiglas 55, are essentially equivalent.

Figure 2 shows threshold crazing stress of Acrivue 351 versus MIL-P-8184 and MIL-P-5425 materials as a function of immersion time, using isopropanol as a crazing agent. While MIL-P-8184 acrylic and Acrivue 351 have approximately equal craze resistance when dry, Acrivue 351 maintains much higher levels after exposure as a result of its low water uptake rate. MIL-P-5425 acrylic has relative low craze resistance when dry but shows better retention of initial levels after exposure than MIL-P-8184 acrylic. The MIL-P-5425 grade has much lower craze resistance than Acrivue 351 under all exposure conditions.

Figure 3 shows data from the same study, with crazing stress plotted as a function of water content. Acrivue 351 shows higher craze resistance than MIL-P-8184 sheet even under these normalized conditions in which the effect of absorption rate is eliminated.

Similar studies were carried out using lacquer thinner and other solvents as crazing agents. Results paralleled those just described.

Chemical Resistance

Threshold crazing stress was also determined using a series of chemicals which are reportedly used for aircraft maintenance[7]. Results are given in Table 1. These tests were run as described above for isopropanol.

Acrivue 351 shows good resistance to most of the solvents and chemicals tested. In many cases, crazing stress is lower for Acrivue 351 than for MIL-P-8184 acrylic material in the dry state, especially with non-polar and chlorinated solvents. However, in all cases, crazing stress of Acrivue 351 is higher than MIL-P-5425 acrylic sheet. Since MIL-P-5425 is used in several laminated transparencies without apparent problems with chemical resistance, these results do not suggest any chemical crazing problems should be expected. In fact, after equilibration with water in use, Acrivue 351 should have better craze resistance versus most of these solvents than MIL-P-8184 material.

Physical Properties

Table 2 gives physical properties of Acrivue 351 compared to minimum MIL-P-8184 requirements. All properties except for flammability surpass the requirements and are very similar to current MIL-P-8184 grades. Flame spread of Acrivue 351 is about 10 percent above the maximum allowed under MIL-P-8184, but is lower than the maximum allowed under MIL-P-5425. This requirement was written around existing grades, and so is somewhat arbitrary. Slightly higher flame spread should not cause any problems in aircraft applications.

STRETCHED ACRIVUE 351-S PROPERTIES

Effect of Stretching on Physical Properties

Full-sized Acrivue 351 sheets were stretched from 20 to 50 percent under similar conditions to those used to produce MIL-P-25690 sheet. Key physical properties were then evaluated versus conventional stretched acrylic using tests called out in the specification. A property comparison is shown in Table 3.

Craze resistance of Acrivue 351 increases dramatically upon stretching. Crazing stress of Acrivue 351-S at only 30 percent stretch is equivalent to MIL-P-25690 sheet at 70 percent stretch. At a stretch ratio of 50 percent, Acrivue 351 is extremely resistant to crazing: Applied stress levels of 8000 to 10,000 psi are required to craze Acrivue 351-550 with isopropanol. This is more than twice the threshold crazing stress of conventional MIL-P-25690 material.

Crack propagation resistance (K-factor) values for the two types of stretched acrylic materials also show contrasting dependence on stretch ratio. The K-factor of Acrivue 351 increases gradually on stretching and reaches about half the level of MIL-P-25690 material at 30-50 percent stretch. Laboratory studies have shown that K-factor of Acrivue 351-S does not increase further if stretch ratio is increased to 70 percent.

Craze Resistance

Water uptake rates and dependence of craze resistance on water content were evaluated for a 50 percent stretched sample of Acrivue 351 and MIL-P-25690 sheet. Specimens (0.125 x 1 x 3 inch) were preconditioned in an air oven at 215°F for 2 hours followed by 150°F for 48 hours, then immersed in water at 120°F. Weight gain versus immersion time is plotted in Figure 4.

Moisture uptake characteristics of the two stretched samples were comparable to the corresponding as-cast materials: The rate for Acrivue 351-S was significantly lower than for MIL-P-25690 material.

Standard 70 percent stretched MIL-P-25690 craze specimens (0.125 x 1 x 7 inch) and specimens of 30 and 50 percent stretched Acrivue 351-S were oven dried and then conditioned in water under the same conditions as the weight gain specimens. Crazing stress was determined at various intervals using the technique described for as-cast material.

Threshold crazing stress of the three materials is plotted versus time immersed in Figure 5. Acrivue 351-S samples showed very high initial crazing stress values as mentioned above plus much better retention of craze resistance after immersion. At the maximum exposure time of 10 days, Acrivue 351-S50, Acrivue 351-S30 and MIL-P-25690 acrylic materials had threshold crazing stress values of 5300, 3000 and 200 psi respectively.

Data from the same study is presented differently in Figure 6, in which threshold crazing stress is plotted versus total water absorbed. This data shows that even when uptake rate differences are eliminated, craze resistance of Acrivue 351-S is superior to MIL-P-25690 sheet.

A similar study was carried out using lacquer thinner as the crazing agent rather than isopropanol. Results paralleled those just described.

Chemical Resistance

Craze resistance of dry samples of Acrivue 351-S30, Acrivue 351-S50 and MIL-P-25690 acrylic sheet was evaluated with the same series of aircraft chemicals and solvents used with the as-cast materials. The standard MIL-P-25690 craze test procedure was again used. Results are given in Table 4.

Acrivue 351-S shows remarkable resistance to these chemicals. At the maximum stress level used, 8500 psi, crazing of Acrivue 351-S50 was observed with only two solvents.

Thermal Relaxation Properties

The MIL-P-25690 surface shrinkback test was used to evaluate thermal relaxation properties of Acrivue S-351 stretched 30 and 50 percent. Standard pre-dried samples were exposed for 24 hours at a series of temperatures including those called out in the specification, 230 and 293°F. Results are shown in Figure 7.

These results cannot be compared directly to properties of MIL-P-25690 material because stretch ratios are different. However, thermal relaxation properties of Acrivue 351-S are qualitatively similar to those of conventional stretched acrylic. At 220°F, neither material experienced any significant shrinkback. At 230°F, surface shrinkback percentage is low; both Acrivue 351-S samples easily met the specification requirement of less than 10 percent relaxation. Reversion at 293°F is primarily a function of stretch ratio, so comparison of materials is not meaningful. As mentioned above, absorbed water reduces reversion temperatures significantly. Because of its inherently lower water uptake rate, Acrivue 351-S will show less depression of reversion temperature on exposure than conventional stretched acrylic. Studies are underway to confirm this.

DISCUSSION

Crazing in Aircraft Transparencies

Crazes can form when applied tensile stress exceeds a critical level. This critical crazing stress is an inherent property of the material. However, like most polymer property parameters, the crazing phenomenon displays visco-

elastic characteristics. Thus, critical crazing stress is dependent both on time and temperature. The stress at which crazing will occur decreases with increasing temperature and with decreasing strain rate (increasing time).

A number of factors may be identified which either increase applied stress in a transparency or reduce critical crazing stress of the material. These factors may be considered possible causes of crazing in the field.

Factors which could increase the applied stress at the surface of a transparency are:

1. The thermal gradient through the material created by various flight conditions.

2. Residual stresses introduced by manufacturing processes.

3. Pressurization of the transparency.

4. Residual mounting stresses.

5. Stresses introduced by optically refinishing the surface.

6. A water concentration gradient near the acrylic surface caused by desorption of absorbed water.

Factors which could decrease the inherent critical crazing stress of the material are:

1. Polymer chain scission processes caused by UV, oxidative or chemical degradation.

2. Plasticization effects caused by absorbtion of water or an organic solvent.

Water Crazing Mechanism

Absorbed water is believed to play an important role in formation of crazes in acrylic aircraft transparencies. Water may act in two ways to induce or accelerate crazing. One effect is to lower the critical stress at which crazing can occur by plasticization. This effect is comparable to increasing temperature.

The other effect is more subtle, but perhaps more important. It relates to the absorbed moisture gradient-induced stresses, caused by the volumetric differences between "wet" and "dry" acrylic material. A high surface tensile stress situation is believed to develop when the surface, at a high moisture content, is rapidly dried.

The flight environment experienced by a transparency would seem to compound this water egress-induced crazing through thermally-induced stresses. Consider an aircraft which has been exposed to high humidity for an extended period of time. It is now subjected to a high speed, low altitude flight. In a high speed flight, the outer surface is raised to high tempertures, which results in rapid water loss from the surface. The surface won't craze at this time because it's under expansive compression. The core of the outer ply also warms up and expands during this time. When the aircraft decelerates and climbs to high altitude, the surface skin cools rapidly while the underlying material stays warm. The cold and dry outer surface now wants to contract but is constrained by the warm and wet underlying material. The result is substantial tensile stress and potential for craze development.

Expected Performance of Acrivue 351

The low water uptake characteristics of Acrivue 351 should result in reduced tendency to craze in the field based on both of the above mechanisms involving water. Water is a less effective plasticizer with Acrivue 351 than with MIL-P-8184 acrylic material, as shown by lab results described above. Surface stress induced by rapid drying should be lower for Acrivue 351 because equilibrium water content is lower.

Applications for As-Cast Acrivue 351

Target applications for as-cast Acrivue 351 include:

1. Outer protective shields in laminated transparencies.

   Aircraft employing this type of design include the F-111,F-14, F-16, T-37 and A-10. The outer as-cast acrylic ply protects underlying material from environmental degradation in the case of polycarbonate, or from heat in the case of stretched acrylic. These thin plies are prone to surface crazing, so a more craze resistant material should significantly improve product life.

2. The outer ply in laminated cabin windows.

   Laminated fail-safe designs are being evaluated to replace the current air gap construction. Good craze resistance is one of the most important requirements of the outer ply material, so Acrivue 351 should be the best choice if an as-cast material proves to have adequate crack propagation resistance.

3. As-cast canopies.

   In aircraft where monolithic as-cast acrylic is now used for the canopy due to pilot ejection considerations, Acrivue 351 offers

some potential advantages. Higher craze resistance should increase product life and might allow weight savings by using thinner material for a given design stress. Also, since crack propagation resistance of Acrivue 351 increases more gradually than MIL-P-8184 when the as-cast materials are oriented during forming, ejection through the canopy should be less difficult.

Applications for Stretched Acrylic 351

Current target applications for Acrivue 351-S include:

1. Outer ply protective shields in laminated transparencies.

   In cases where surface temperatures in flight are low enough that stretched acrylic can be used, Acrivue 351-S may be preferred over the as-cast grade because of its superior craze resistance.

2. The outer ply in either laminated or air-gap cabin windows.

   Acrivue 351-S is also being evaluated in the new laminated cabin window design mentioned above. Advantages over as-cast Acrivue 351 are better craze resistance and crack propagation resistance, although manufacturing cost would be higher.

   In the air-gap cabin window design, Acrivue 351-S would offer better craze resistance compared to MIL-P-25690 acrylic now used. Crack propagation resistance is lower, but might be adequate for this application, since stretched acrylic is used primarily for craze resistance. Testing of Acrivue 351-S under explosive decompression conditions will be required to evaluate its suitability.

3. The outer ply in laminated, fail-safe cockpit enclosures.

   Such a structure would have a MIL-P-25690 inner ply capable of carrying the load if the outer ply were to fracture, an interlayer, and an Acrivue 351-S outer ply having higher craze resistance but lower crack propagation resistance than the inner ply.

Flight Testing of Acrivue 351

While the laboratory studies described in this paper predict improved resistance to environmental crazing, this must be confirmed by actual flight testing of transparencies incorporating Acrivue 351. The first such test has just started on the F-111 aircraft.

F-111 transparencies have experienced severe crazing of the outer acrylic ply recently. As a result, the U.S. Air Force has funded a test program to evaluate as-cast Acrivue 351 as the outer ply of this polycarbonate-based laminate. Manufacture of test parts was completed in March, 1983, and actual flight exposure should begin soon.

CONCLUSIONS

Acrivue 351 is a new acrylic material with improved craze resistance compared to all current as-cast acrylic grades used in aircraft transparencies. Properties of as-cast Acrivue 351, other than craze resistance and moisture uptake, are virtually the same as MIL-P-8184 material. Therefore, Acrivue 351 is an improved-performance acrylic material for all as-cast applications.

Stretched Acrivue 351 has much higher inherent craze resistance and lower water uptake characteristics than MIL-P-25690 material. Crack propagation resistance is lower but should be adequate for most applications. Other potential advantages of Acrivue 351-S are higher allowable in-plane shear stress and better dimensional stability in humid environments. Therefore, Acrivue 351-S should offer superior performance in many aircraft applications in which conventional stretched acrylic sheet is now used.

REFERENCES

1. A.J. Mason, Proceedings of the Society of British Aerospace Companies Conference on Aerospace Transparencies, London, 1980, p. 399.

2. P.J. Burchill and R.H. Stacewicz, TTCP-PTP-4 Workshop "Life Enhancement of Military Systems through Advanced Materials Technology", Melbourne, March 17, 1982.

3. P.J. Burchill and R.H. Stacewicz, submitted for publication, J. Mater. Sci. Lett.

4. K.B. Armstrong, Proceedings of the Society of British Aerospace Companies Conference on Aerospace Transparencies, London, 1980, p. 459.

5. R.L. Worsdall, Proceedings of the Society of British Aerospace Companies Conference on Aerospace Transparencies, London, 1980, p. 371.

6. J.M. Barton, "The Effect of Absorbed Water on the Thermal Relaxation of Stretched Acrylic Polymer Transparency Materials", 1980.

7. "Survey of Development, Testing and In-Service Durability of F-15, F-16 and F-111 Transparencies", AFWAL-TR-81-3151.

TABLE 1. Chemical Resistance of As-Cast Acrylic Sheet

	Threshold Crazing Stress, psi		
SOLVENT	MIL-P-5425 Sheet	Acrivue 351	MIL-P-8184 Sheet
Mild Soap & Water	>8500	>8500	>8500
Phosphoric Acid Cleaner	5000	5800	7700
Alodine Spray	>8500	>8500	>8500
Rain Repellent Fluid	2200	3300	3100
JP-4 Jet Fuel	4900	6300	8400
De-Ice Fluid	>8500	>8500	7100
Bug & Tar Remover	7800	7800	>8500
Naptha	5900	3500	3200
Turco T-5975A Airplane Wash	5000	5800	8400
Turco Air-Tec #19 Airplane Wash	7900	>8500	>8500
Hoechst Airplane Wash	>8500	>8500	>8500
Kilfrost Airplane Wash	8000	>8500	>8500
Benzene	1500	2300	3800
Xylene	2100	3300	5300
Acetone	1100	1300	1900
Carbon Tetrachloride	3200	2900	6900
Toluene	1500	3100	3900
Kerosene	3300	3800	5000
IPA	2000	3500	3200

TABLE 2. Physical Properties of As-Cast Acrivue 351

Property	Minimum Requirements, MIL-P-8184 B Specification	Acrivue 351 (0.125 inch)
Tensile Strength, psi	9000, Min.	10,700
Tensile Elongation, %	2, Min.	6
Heat Deflection Temp., °F	209, Min.	225
Stress to Craze, PSI:		
Lacquer Thinner	2000, Min.	2,800
Isopropanol	2000, Min.	3,800
Original Luminous Transmittance, %	91, Min.	92
Original Haze, %	3.0, Max.	0.5
Haze After Weathering, %	4.0, Max.	0.5
UV Transmittance, %	5.0, Max.	0.44
Water Absorption, %	0.4, Max.	0.15
Thermal Expansion, in/°C	0.00010, Max.	0.00007
Index of Refraction	1.48 to 1.50	1.49
Thermal Stability	Pass	Pass
Thermoformability	Pass	Pass
Specific Gravity	1.18 to 1.20	1.19
Internal Strain, % Dimensional Change	1.0, Max.	0.19
Flammability, in/min.	1.15, max	1.38

TABLE 3. Properties Of Stretched Acrylic Sheet

	MIL-P-25690 Sheet[a]	Acrivue 351-S	Acrivue 351-S	Acrivue 351-S	Acrivue 351-S
Percent Stretch[b]	70	20	30	40	50
Crazing Stress(psi) IPA	4000	3500	5500	5900	>8000
LT	2800	2400	3300	3900	5500
K-Factor	3000	950	1200	1500	1700
Tensile Strength(psi)	11,500	11,600	11,700	11,900	11,600
Tensile Modulus(Kpsi)	450	450	450	450	450
Tensile Elongation(%)	15	9	15	15	15

a. Typical properties for Acrivue 350S

b. Cast thickness = 0.25 inch for all Acrivue 351 samples.

TABLE 4. Chemical Resistance of Stretched Acrylic Sheet

	Threshold Crazing Stress, psi		
	MIL-P-25690 Sheet	Acrivue 30% 351-S	Acrivue 50% 351-S
Soap and Water	>8500	>8500	>8500
Phosphoric Acid Cleaner	>8500	8300	>8500
Alodine Spray	>8500	>8500	>8500
Rain Repellent Fluid	5500	5600	>8500
Jet Fuel	>8500	>8500	>8500
De-Ice Fluid	>8500	>8500	>8500
Naptha	5200	>8500	>8500
Airplane Washes:			
Turco T-5975A	>8500	>8500	>8500
Turco Air Tec No.19	>8500	>8500	>8500
Hoechst	>8500	>8500	>8500
Kilfrost	>8500	>8500	>8500
Benzene	6500	3900	8000
Xylene	>8500	5400	>8500
Acetone	3100	2200	3700
CCl_4	>8500	>8500	>8500
Toluene	5800	4500	>8500
Kerosene	>8500	8200	>8500
IPA	5200	4500	>8500

FIGURE 1. WATER UPTAKE OF AS-CAST ACRYLIC SHEET

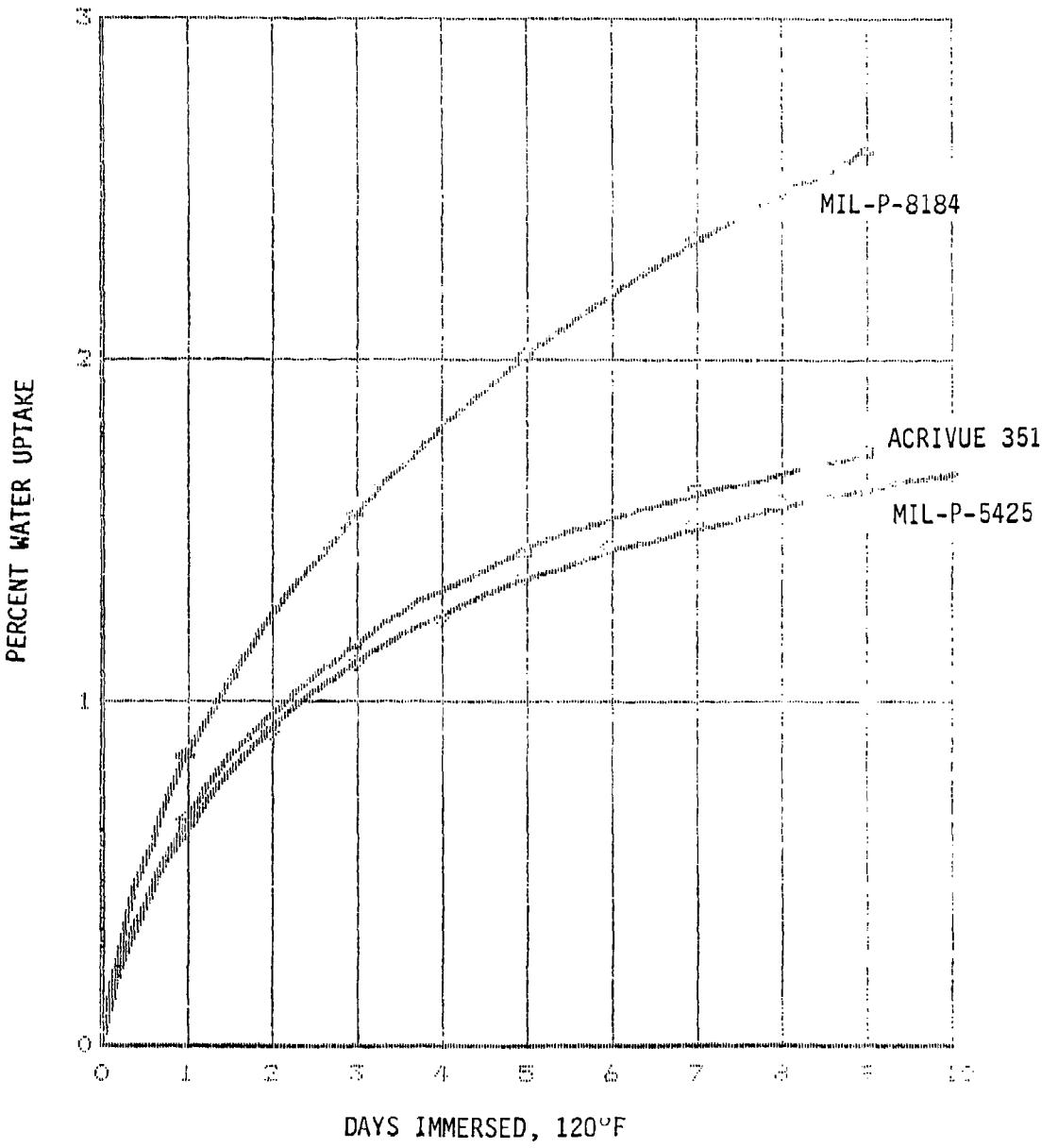

FIGURE 2. IPA STRESS CRAZE RESISTANCE vs.DAY IMMERSED, AS-CAST ACRYLIC SHEET

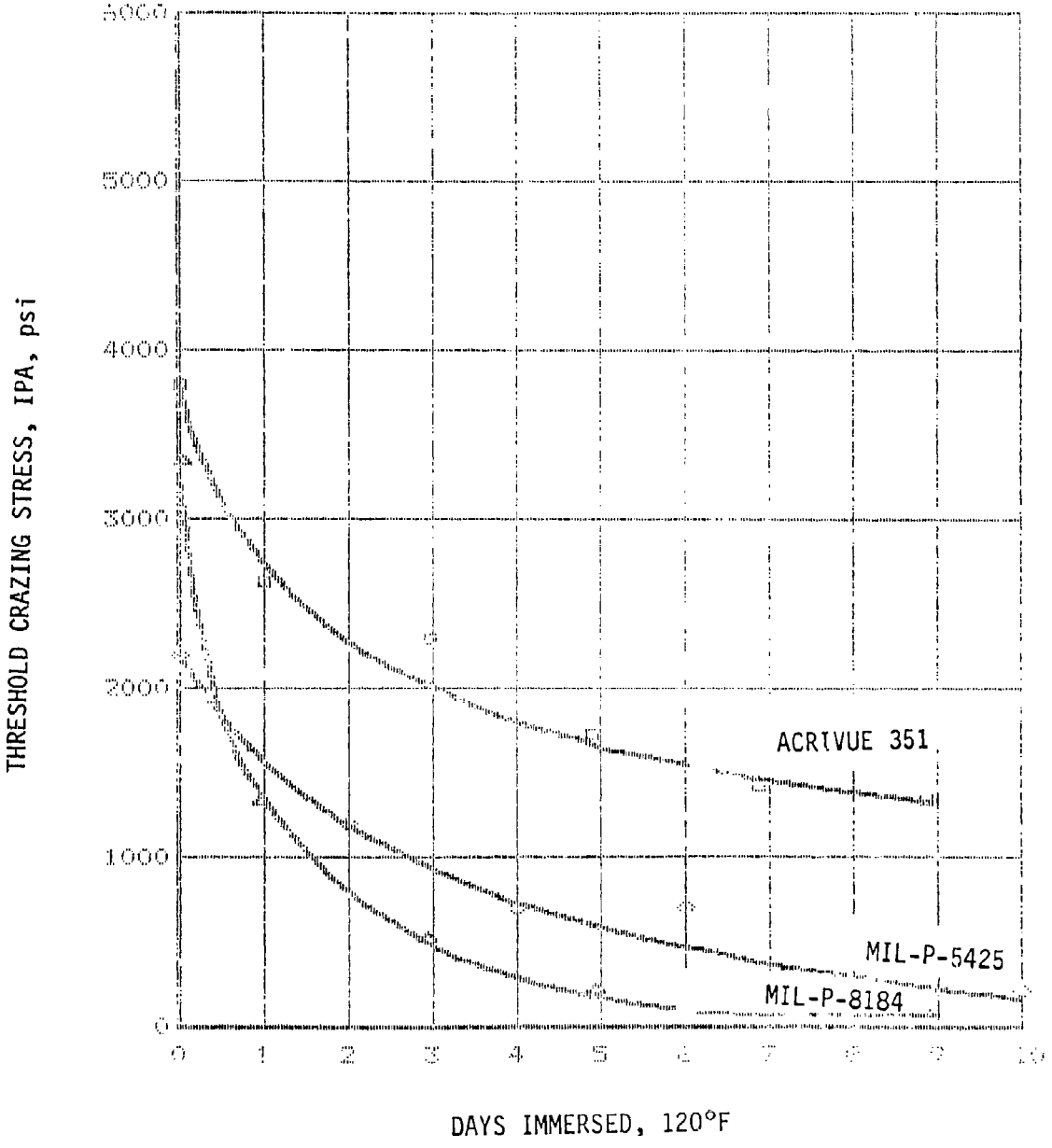

FIGURE 3. IPA CRAZE RESISTANCE VS. PERCENT WATER ABSORBED, AS-CAST ACRYLIC SHEET

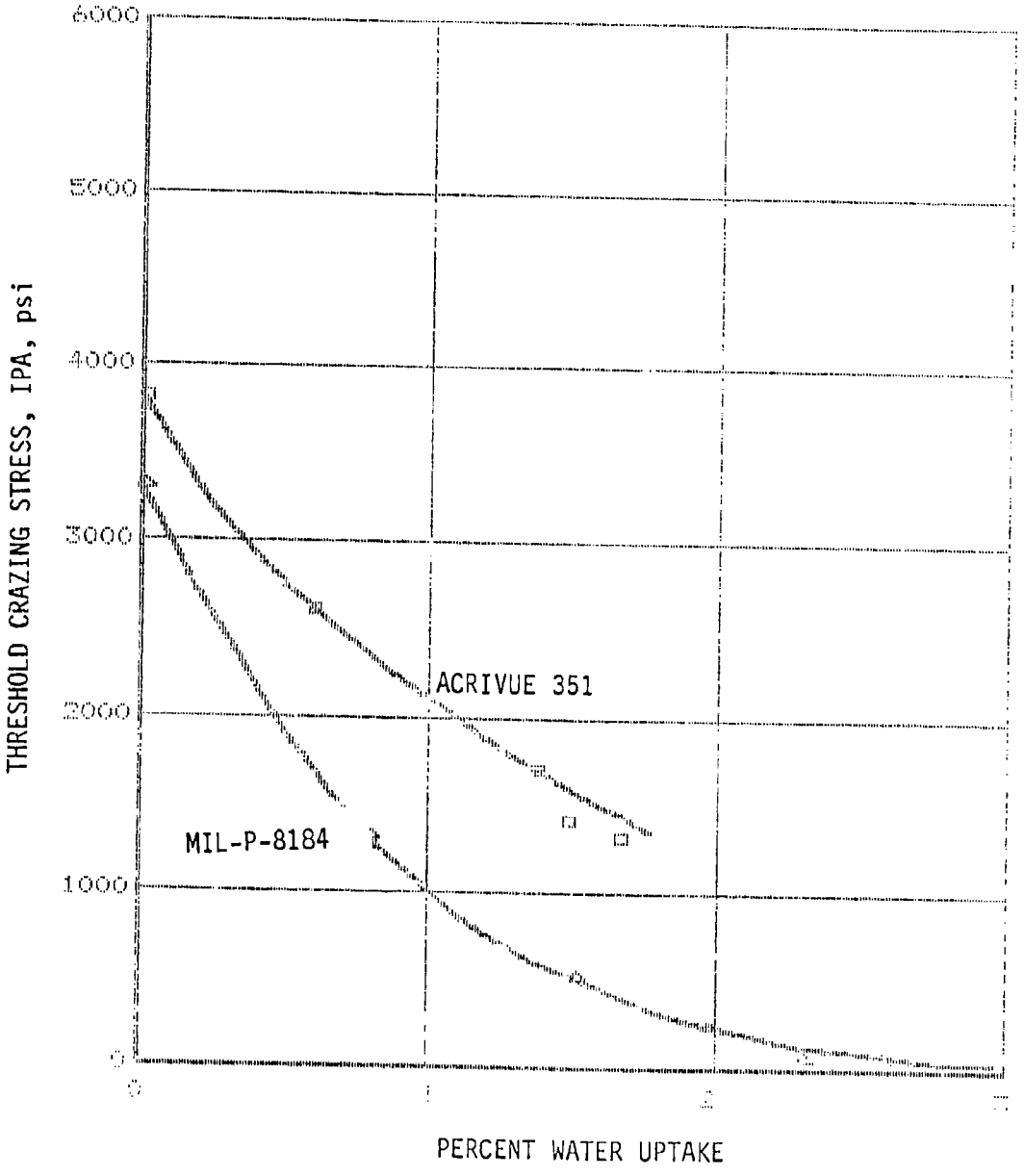

FIGURE 4. WATER UPTAKE OF STRETCHED ACRYLIC SHEET

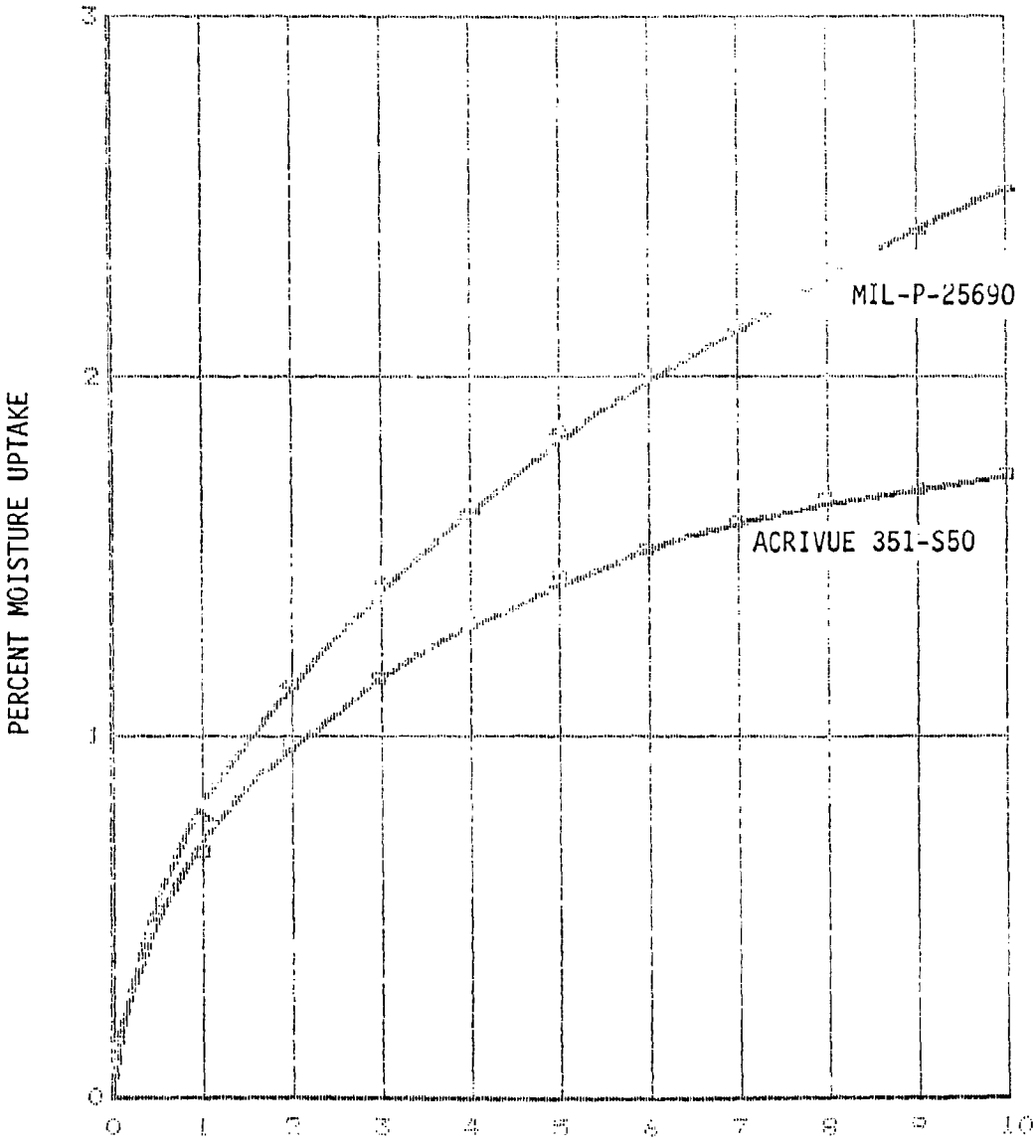

FIGURE 5. IPA CRAZE RESISTANCE vs.DAYS IMMERSED, STRETCHED ACRYLIC SHEET

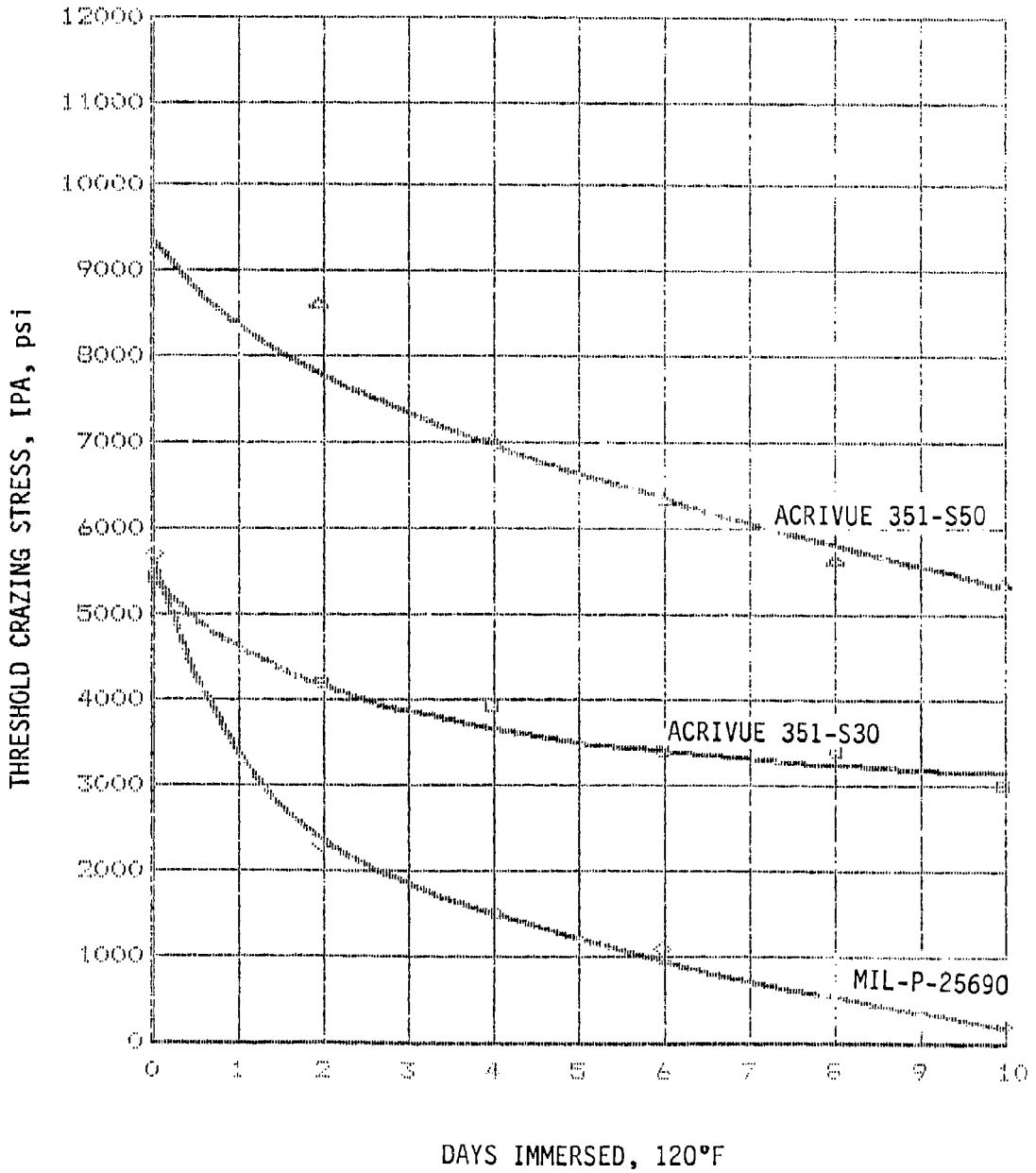

FIGURE 6. IPA CRAZE RESISTANCE vs. PERCENT MOISTURE, STRETCHED ACRYLIC SHEET

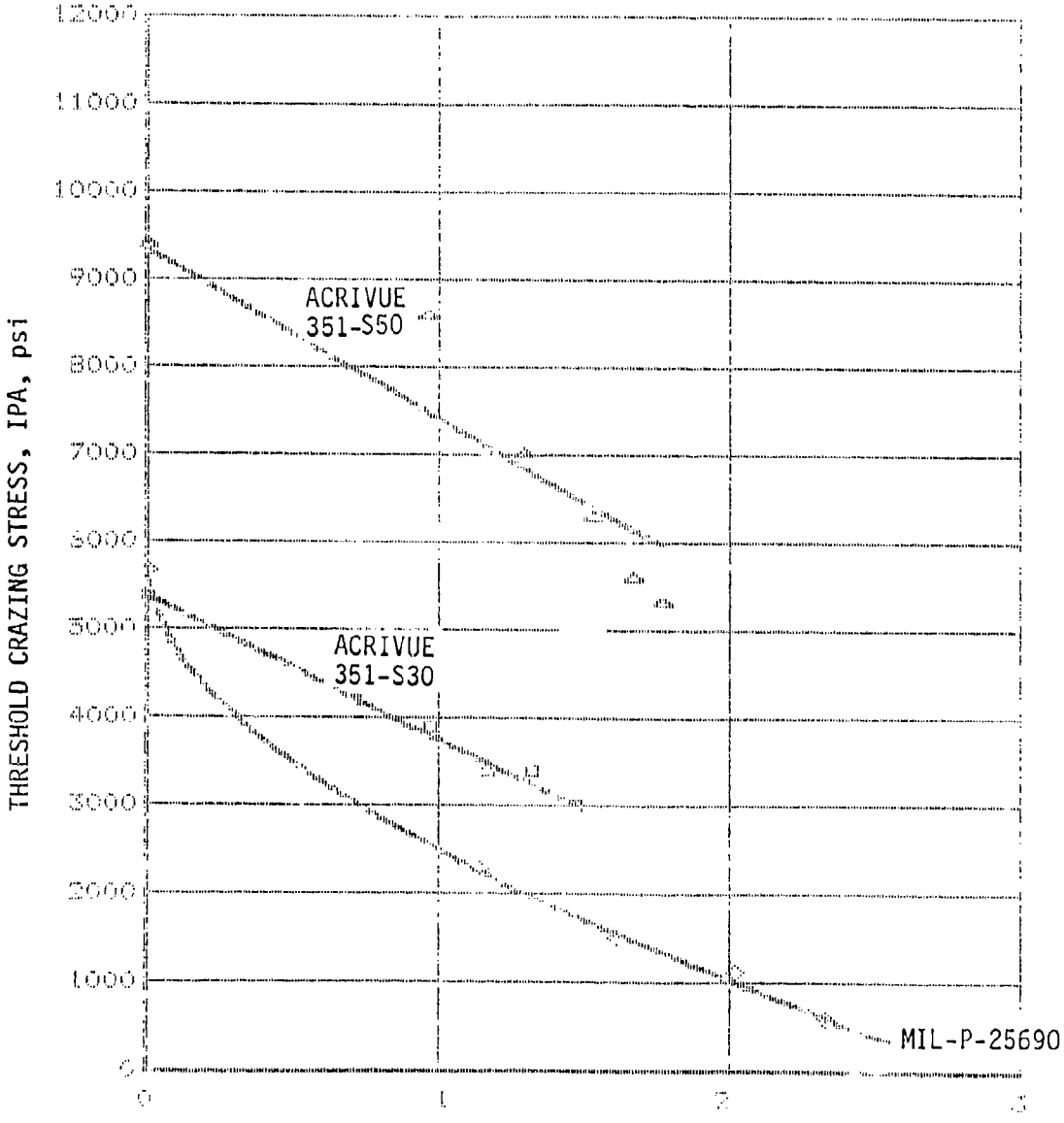

FIGURE 7. PERCENT SURFACE SHRINKBACK vs. TEMPERATURE

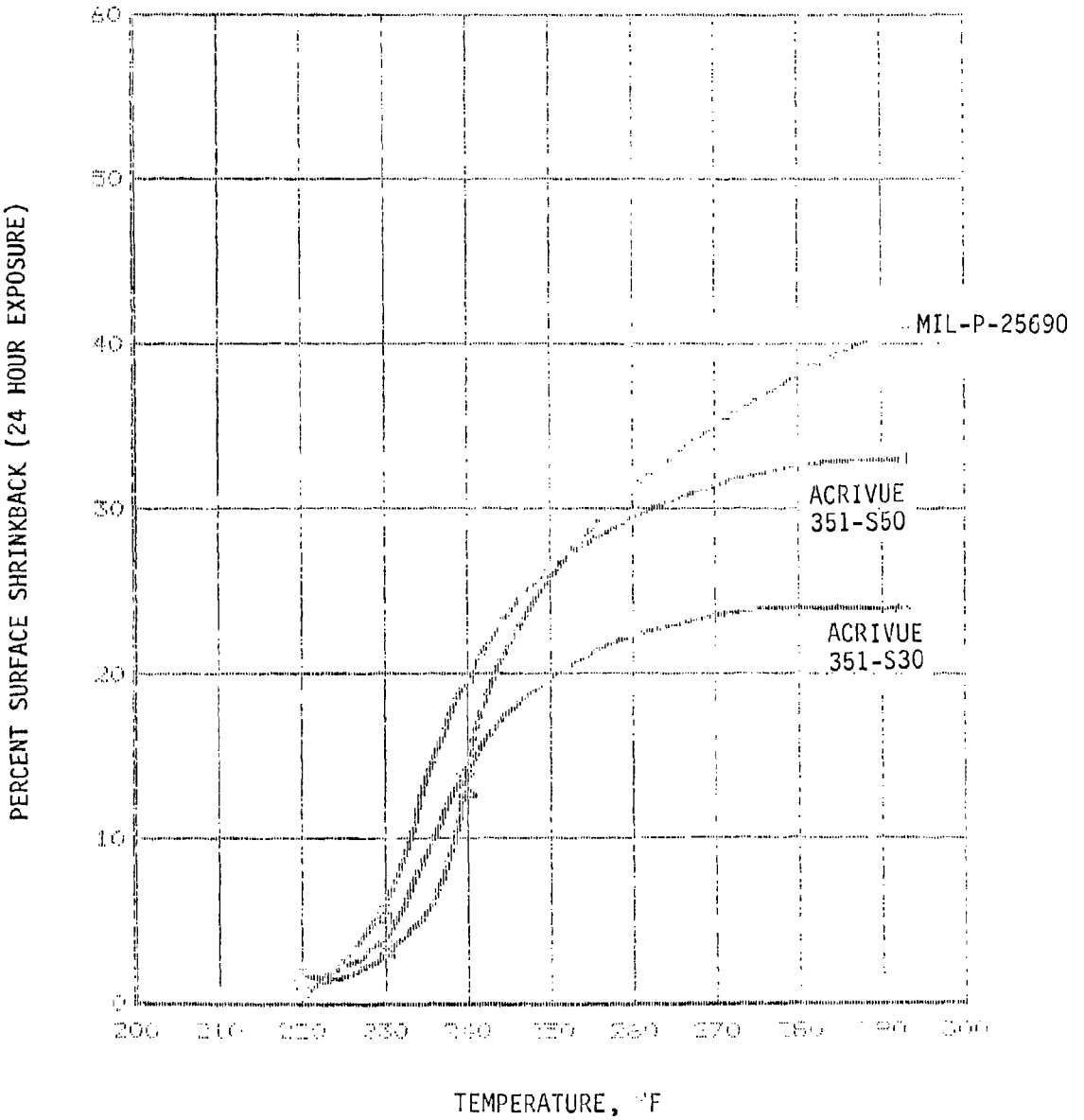

AD-P003 204

PROTECTIVE LINER MATERIALS FOR TRANSPARENT PLASTICS

J. E. Mahaffey and T. G. Rukavina,
PPG Industries, Inc.

Protective Liner Materials For Transparent Plastics

J. E. Mahaffey and T. G. Rukavina
PPG Industries, Inc.
Glass Research Center
Pittsburgh, PA

Abstract

Parasitic plies such as acrylic used to protect polycarbonate from the environment in aircraft transparencies add undesirable weight and are subject to crazing. Thin coatings also have serious drawbacks. They cannot adequately protect the substrate from ultraviolet radiation nor can they protect the substrate from impingement type damage. PPG Industries has recently developed a family of elastomeric liner materials specifically formulated to provide complete isolation of the substrate to which it is applied. The thickness of the liner is 30 mils and bonds directly to the substrate. Besides providing a much greater degree of substrate protection than thin coatings, liner-faced transparencies, as compared to acrylic-faced transparencies, offer superior abrasion-resistance, reduced weight, and are completely resistant to crazing.

This paper describes two specific liner materials. The first was designed to withstand the relatively severe environments encountered on the exterior surface of an aircraft transparency. The second was developed for use on the inboard surface where environmental considerations are not as demanding. Comprehensive testing and evaluation of these liners have been performed by PPG over the past two years. Environmental-resistance testing has included humidity exposure, ultraviolet radiation, chemical resistance, rain erosion resistance, accelerated and natural weathering, and abrasion resistance. The results of these tests have been very encouraging and the liners are currently being tested on full-scale transparencies. In addition, the outboard liner has been flight-tested for over a year with excellent results. The complete testing program for these liners, including field service performance, will be reviewed.

Taber Abraser (ASTM D-1044)

The Taber Abraser test is a well known ASTM abrasion test which has been in use for several years. This test consists of two abrasive wheels, to which a predetermined load is applied, which rest on the specimen surface. The specimen is fixed to a rotating table. As the specimen is rotated the abrasive wheels abrade the surface of the specimen in a circular pattern.

Abrasion Test Results

The results of the abrasion tests are given in Figures 1 and 2, and Table 1. The abrasion resistance of acrylic, stretched acrylic, and polycarbonate are also given for comparison purposes. These data show that the abrasion resistance of both the 5300 and 6300 liners is significantly superior to the acrylics and polycarbonate by all three abrasion tests used.

Humidity Exposure

Cyclic humidity tests were performed on the liner materials on polycarbonate substrate in accordance with MIL-STD-810C, Method 507, Procedure I. This is a 10-day cyclic humidity test where the temperature varies between ambient and 65°C and the humidity between 85% and 95%. After exposure the specimens were inspected for any evidence of degradation, adhesion loss, and change in light transmission or haze. The specimens were then tested for abrasion resistance using 300 cycles on the Bayer abrader to determine if the humidity exposure affected durability.

The results of the cyclic humidity tests are listed in Table 2. After exposure there was no evidence of deterioration, loss of adhesion, and no significant change in optical properties. Abrasion resistance after exposure was not changed compared to unexposed material indicating durability was not degraded due to humidity.

Ultraviolet Radiation Exposure

Accelerated weathering tests were performed on the liner materials using a carbon arc Weather-Ometer with intermittent water spray. The exposure was performed with the liner surface facing the light source and an exposure period of 1000 hours. After exposure the specimens were subjected to 300 cycles on the Bayer abrader. The results of the ultraviolet radiation exposure are listed in Table 3. At the conclusion of the test there was no evidence of liner degradation or adhesion loss, and virtually no change in light transmission or haze. After abrasion, the haze increase was comparable to unexposed material indicating no change in abrasion resistance due to the exposure.

Chemical Resistance

Stress Craze Resistance

Stress craze resistance of the 5300 liner on polycarbonate substrate was conducted in accordance with Federal Test Method Std. 406, Method 6053.

Introduction

Polycarbonate is in many ways an attractive alternative to glass in designing aircraft transparencies. The desirable characteristics of polycarbonate that make it useful as an engineering plastic are its outstanding impact strength, good hydrolytic and oxidative stability, and light weight. Undesirable characteristics include the tendency to craze or crack under stress, particularly when exposed to the environment or chemical solvents, the susceptibility to surface degradation induced by ultraviolet light, and poor abrasion resistance. Thus, the successful utilization of polycarbonate in aircraft transparency designs is dependent on the degree of the surface protection provided for the plastic. Thin coatings and laminated acrylic plies are currently the most popular mediums used to protect polycarbonate surfaces. Thin coatings do not adequately protect the substrate from ultraviolet radiation or impingement type damage. Acrylic facing plies add parasitic weight and can stress craze. This paper presents the results of extensive accelerated testing and some field testing of what we think are currently the best overall surface protective materials yet developed for polycarbonate. The new materials are referred to in this paper as 5300 and 6300 liners. The 5300 liner can be used on inboard and outboard surfaces whereas the 6300 liner was developed primarily for inboard surfaces. Both liners are applied in 20-30 mil thicknesses directly to the polycarbonate surface.

Abrasion Resistance

No single abrasion test is considered adequate to provide an accurate assessment of the abrasion resistance of transparent plastics used in aircraft transparencies because of the different types of abrasion actually encountered in service. For this reason three different types of abrasion tests were performed on the liner materials. Two of the tests are basically rubbing type abrasion tests and the third an impingement type test.

Bayer Abrasion (ASTM F-735)

This test was developed by Bayer AG, West Germany and has been adopted by ASTM as a standard abrasion test method for abrasion resistance of transparent plastics used in aircraft transparencies. The test consists essentially of quartz silica sand which is oscillated over the test specimen surface. The severity of abrasion is controlled by the number of oscillating cycles with 300 cycles being considered a relatively severe test for transparent plastics. Increase in haze is used as the criteria for measuring the severity of abrasion.

Salt Abrader

The salt abrader was developed by PPG several years ago as an impingement type test to simulate ice crystal erosion encountered on aircraft windshields when flying through certain types of clouds. The test consists of impacting the surface to be tested with salt crystals of specified size at a high velocity. The test is currently being developed by ASTM Subcommitte F7.08 as test method standard.

This is the standard cantilever beam stress craze test used for transparent plastics. The tests were performed using a variety of fluids normally encountered by aircraft transparencies, and are listed in Table 4. At the conclusion of the tests there was no crazing, cracking or other evidence of chemical attack on the liner or polycarbonate substrate.

Sled Abrasion Tests

Since the 5300 and 6300 liners are relatively thick compared to coatings, the cantilever beam stress craze test is not considered entirely adequate for chemical resistance. For this reason the PPG sled abrasion test was used to provide additional chemical resistance data. This test, illustrated in Figure 3, consists of a felt pad under a 1-1/2 psi load which is drawn back and forth over the specimen surface for 500 cycles using 400 mesh alundum abrasive. The test can be conducted dry with the abrasive only or wet with a variety of solvents. The effect of the sled abrasion is determined by a subjective evaluation of the degree of scuffing of the substrate surface on a scale of 0 to 100 in which 0 indicates no effect and 100 indicates that the surface is virtually destroyed. This test is considered to be relatively severe. The 5300 and 6300 liners were tested and using acetone, heptane, isopropyl alcohol, and a mixture of alcohol and water. The results of the sled abrasion tests are listed in Table 5 along with data for acrylic and polycarbonate. The data show that the two liner materials significantly improve the chemical resistance of acrylic and polycarbonate.

Rain Erosion

Rain erosion tests were performed on the 5300 liner on both acrylic and polycarbonate substrates by the Air Force Materials Laboratory using the rotating arm test facility. This equipment consists of an eight foot double arm propeller blade mounted horizontally and capable of variable tip speeds of up to 600 MPH. Water droplets of controlled size are inserted at the blade tips. The rain erosion tests were performed at a 30° angle of impact in a simulate one inch per hour rainfall, at velocities of 345 MPH to 600 MPH. Specimens were tested with no environmental conditioning and after 1000 hours exposure in a Weather-Ometer with intermittent water spray. The 5300 coating performed very well in these tests. There was no damage or loss of adhesion of the liner after three hours exposure to one inch per hour rain at a speed of 345 MPH on both acrylic and polycarbonate substrates. At speeds of 500 and 600 MPH slight surface pitting and localized delamination was encountered but there was no loss of the liner in any of the tests at the higher velocities. There was also no change in performance after 1000 hours Weather-Ometer exposure.

Impact Resistance

Certain coatings and cladding materials for polycarbonate can have an adverse effect on the impact strength of the material. The effect of the 5300 liner on the impact strength of polycarbonate was determined using the PPG air cannon impact test. The test consists essentially of impacting a 150 gram missile on a 12" x 12" specimen at speeds of up to 350 MPH. This

test has been used successfully by PPG Industries for several years as a screening test for the impact resistance of materials. Several 1/4" x 12" x 12" panels of uncoated polycarbonate and 5300 lined polycarbonate were prepared for these tests. All test panels were impacted at a constant velocity of 330 MPH with the 150 gram missile. The temperature of the test panels was decreased in increments until penetration was incurred. The results are summarized in Table 6. The results show that the temperature where penetration occurs is the same for both 5300 lined polycarbonate and uncoated polycarbonate indicating the liner has no effect on the impact resistance of the polycarbonate.

Ultraviolet Light Protection

The surface of polycarbonate can be degraded by ultraviolet light and is particularly sensitive to wavelengths between 280-290nm. Chain scission occurs at these wavelengths resulting in low molecular weight products which can cause surface embrittlement and loss of impact strength. PPG's liners will screen out virtually 100% UV light below 390nm. The UV transmittance spectrum is shown in Figure 3.

Accelerated Sunshine Exposure

Specimens of the 5300 lined polycarbonate were exposed at the DSET Laboratories, Inc., Arizona facility using the DSET EMMAQUA® equipment. This device consisted of a series of flat mirrors so positioned to reflect the solar energy on the test sample and incorporates a mechanism to follow the sun during daylight hours. The samples are sprayed with water eight minutes out of each hour to simulate a humid environment. By concentrating the solar energy in this manner the equivalent of five years exposure in Florida (800,000 Langleys) can be obtained in approximately six months. After this exposure there was no evidence of liner degradation or loss of adhesion except for slight water spotting. Haze due to water spotting after exposure was 7.3%. The water spotting can be easily removed by buffing similar to removing light scratches from acrylic surfaces.

Natural Weathering

Accelerated environmental conditioning tests are valuable tools in evaluating materials such as the liner materials described in this paper. It is difficult, however, to correlate accelerated environmental exposure data to the actual environments the material will be exposed to in service. For this reason PPG utilizes natural weathering to complement accelerated conditioning tests even though longer time periods are required to obtain meaningful data. Test panels of the 5300 and 6300 liners on polycarbonate substrates are currently being exposed at the PPG Ft. Lauderdale, Florida weathering test facility. Test panels are exposed on test racks at angles of 45° facing south. The 6300 liner is exposed in a closed cell construction, simulating an inboard liner application. The 5300 liner is exposed directly to the solar radiation. To date the test panels have been exposed for 12 months with no evidence of degradation of either liner. These exposure tests are continuing.

Field Tests

Two F-111 canopies with the 5300 outboard liner on the outer acrylic surface have been flight tested for over a year. Air Force personnel commented that the canopies showed no signs of surface degradation and that cleaning sleeks could not be observed. Two additional F-111 canopies and two F-111 windshields have been fabricated and are currently awaiting installation in Australia, where severe crazing of outer acrylic surfaces is occurring in both windshields and canopies.

T-39 landing light covers utilizing the 5300 outboard liner bonded directly to the outboard polycarbonate surface have been fabricated and will be installed in the near future. PPG has flight test data on coated T-39 landing light covers for comparison.

PPG has proposed a liner-faced T-38 forward facing windshield design and is currently involved in prototype work on this design.

Weight Savings

A substantial weight savings, approximately 1 lb/ft^2, can be had using the 5300 liner on transparcencies that utilize laminated acrylic plies to isolate polycarbonate from the environment. For example, replacing the outboard acrylic facing ply and the interlayer used to bond the acrylic to the polycarbonate on the F-111 windshield with a .030" thick 5300 liner, would result in a weight savings of 10 lbs.

Conclusions

PPG has developed a new material that overcomes the deficiencies of existing protective systems for polycarbonate aircraft transparencies. Extensive accelerated testing and over one year of flight evaluation has shown the 5300 liner to be superior to thin coatings and laminated acrylic plies. The liner is now ready for extensive flight evaluation on existing transparencies and new designs.

TABLE I

TABER ABRASER TESTS RESULTS*

SUBSTRATE	HAZE INCREASE (%)
5300/POLYCARBONATE	3.8
6300/POLYCARBONATE	0
PLEXIGLAS 55	19.8
STRETCHED ACRYLIC	29.5
POLYCARBONATE	36.4

*100 CYCLES PER ASTM D-1044

TABLE 2
RESULTS OF CYCLIC HUMIDITY EXPOSURE

MATERIAL	INITIAL OPTICAL		AFTER CYCLIC HUMIDITY		HAZE INCREASE AFTER HUMIDITY AND ABRASION (%)
	L.T. (%)	HAZE (%)	L.T.(%)	HAZE (%)	
5300	83.5	1.2	83.4	1.1	4.4
6300	83.8	1.2	86.6	1.3	0.3

TABLE 3
RESULTS OF WEATHEROMETER EXPOSURE (1000 HOURS)

MATERIAL	ORIGINAL OPTICAL		AFTER U.V. EXPOSURE		HAZE INCREASE AFTER U.V. AND ABRASION (%)
	L.T. (%)	HAZE (%)	L.T. (%)	HAZE (%)	
5300	83.5	1.2	84.1	1.2	6.0
6300	83.6	1.2	84.2	1.1	0.9

TABLE 4

SOLVENTS USED IN CRAZE RESISTANCE TESTS

JET FUEL (JP-4)
ISOPROPYL ALCOHOL
ETHYLENE GLYCOL
LUBRICATION OIL (MIL-L-7808)
GREASE (MIL-G-23827)
HYDRAULIC FLUID (MIL-H-5606)
AIRPLANE WASH (MIL-C-25769)
BUG REMOVAL FLUID (P-6009)
WINDSHIELD CLEANER (MIL-C-18767)

TABLE 5
RESULTS OF SLED ABRADER TESTS

MATERIAL	DRY	ABRASION RATINGS WITH CHEMICALS			ISOPROPYL ALCOHOL AND WATER (50/50)
		ACETONE	HEPTANE	ISOPROPYL ALCOHOL	
5300	70	4	50	30	30
6300	15	10	20	15	10
ACRYLIC	70	80	70	70	60
POLYCARBONATE	80	100	70	70	60

TABLE 6
SUMMARY OF AIR CANNON IMPACT TESTS

TEST PANEL DESCRIPTION	TEST TEMPERATURE (°F)	RESULTS
UNCOATED POLYCARBONATE	-20	NO PENETRATION
UNCOATED POLYCARBONATE	-30	PENETRATION
5300 LINED POLYCARBONATE	-17	NO PENETRATION
5300 LINED POLYCARBONATE	-30	PENETRATION

FIGURE 1
BAYER ABRADER TEST RESULTS–
UNCOATED PLASTIC

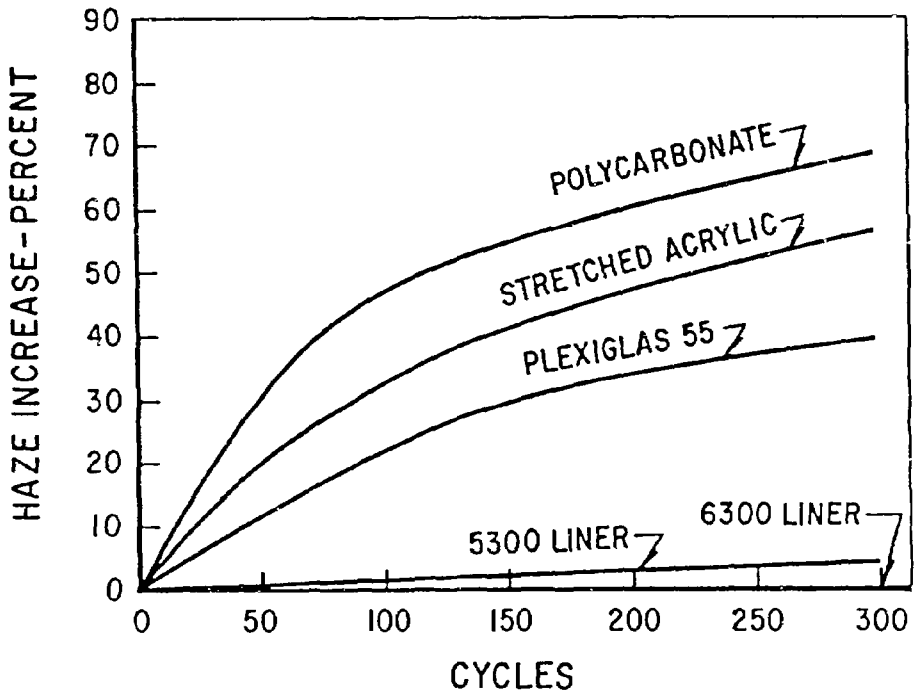

FIGURE 2
PPG SALT ABRADER TEST RESULTS-
UNCOATED PLASTIC

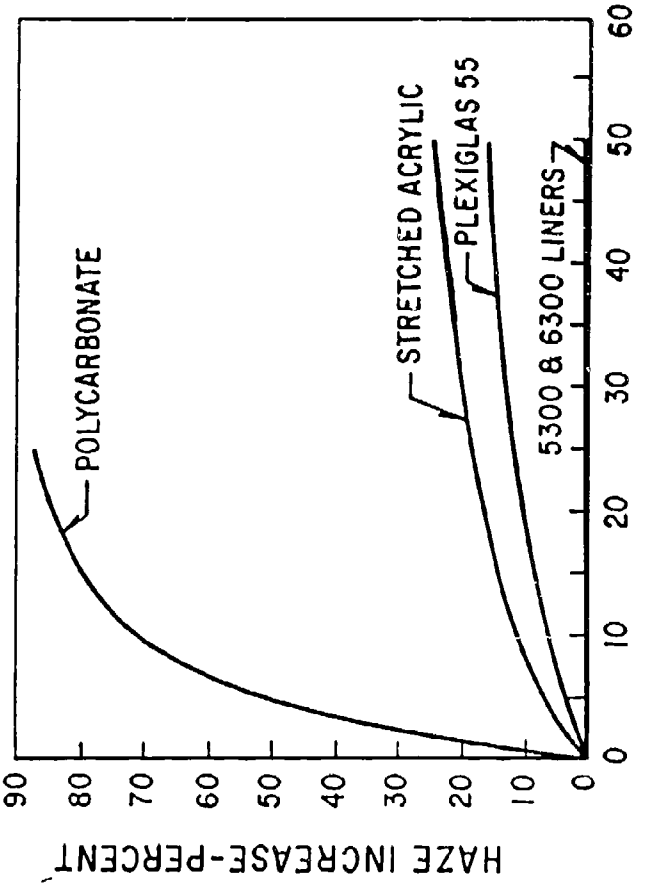

FIGURE 3

MODIFIED SLED ABRADER

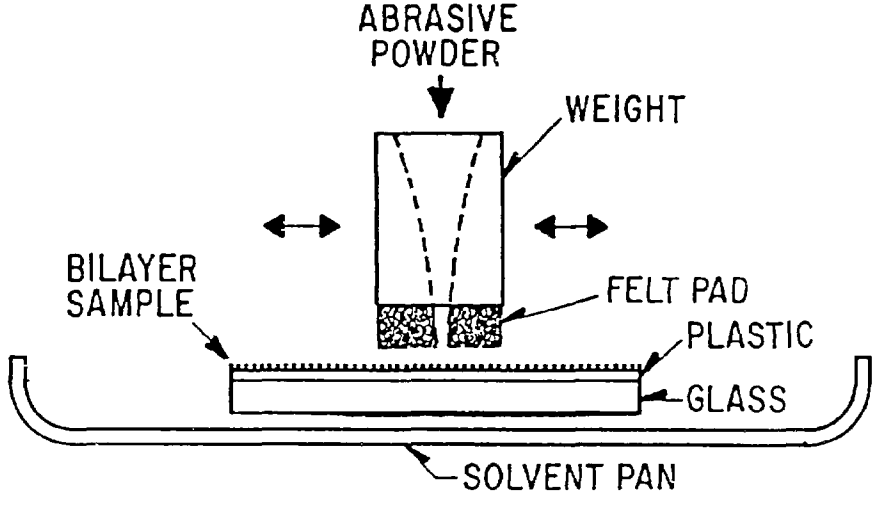

FIGURE 4

UV TRANSMITTANCE SPECTRUM 5300 LINER

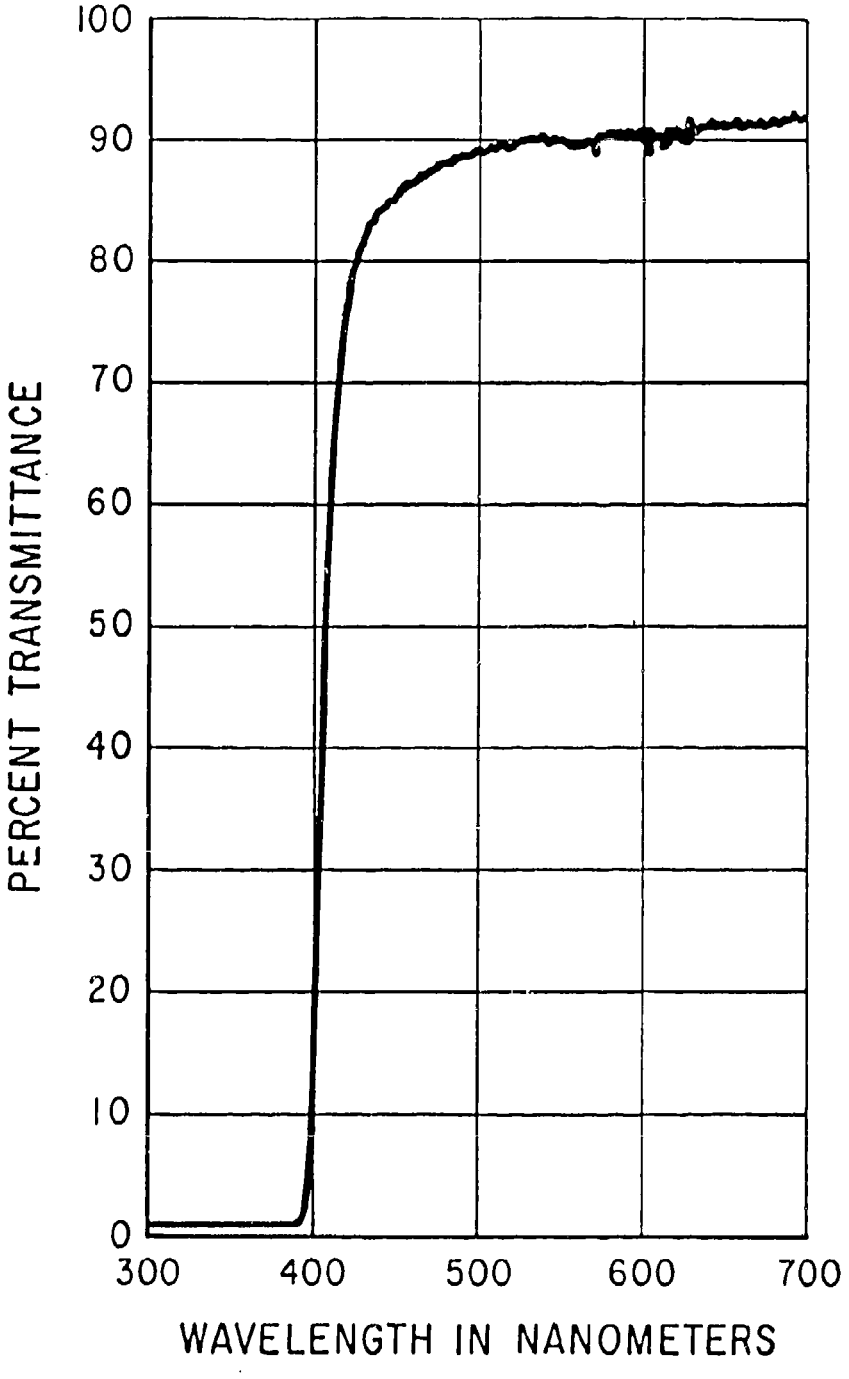

AD-P003 205

HEAT RESISTANT COPOLYESTER-CARBONATE TRANSPARENT PLASTICS

T. J. Reinhart, Materials Laboratory

HEAT RESISTANT COPOLYESTER-CARBONATE TRANSPARENT PLASTICS

BY

Theodore J. Reinhart
Chief, Materials Engineering Branch
Systems Support Division
Materials Laboratory
Air Force Wright Aeronautical Laboratories
Wright-Patterson AFB, Ohio

ABSTRACT

Air Force service experience with state-of-the-art transparent plastics has demonstrated the need for improved materials. A project was started to evaluate research samples of copolyester-carbonate (PEC) plastics received from the Allied Corporation as a result of a research and development contract funded by the Materials Laboratory of the Air Force Wright Aeronautical Laboratories. Mechanical, physical and chemical properties of the PEC materials were evaluated in order to assess the potential of the material for use in aircraft transparencies. It was found that the PEC materials possess several advantages over the state-of-the-art polycarbonate plastics and that the materials showed promise for use in high performance transparencies.

INTRODUCTION

Service experience with state-of-the-art transparent materials (acrylics and polycarbonate) has demonstrated the need for materials improvements. Bird strike requirements on many of our aircraft have necessitated the construction of complex multilayer transparencies using combinations of acrylic, polycarbonate and elastomeric inner layers to meet the system needs. While very successful these new transparencies are costly and must be made via exacting manufacturing procedures in order to meet the needed optical characteristics.

Advanced systems, that is, aircraft having temperature resistance requirements in excess of todays' vehicles are continually plagued, in the design phases by the limitations of existing transparent materials. Designers must resort to heavy systems which incorporate glass or to complex installation which involve multiple layers with spacing for cooling of the structural members.

This situation has prompted the Materials Laboratory to seek through research and development contracts transparent materials having performance capabilities significantly increased over existing state-of-the-art materials.

It should be recognized that the challenges in this research and development area are extreme and the chemical approaches very limited.

BACKGROUND

There is no single transparent plastic that combines all of the mechanical physical and chemical attributes needed to perform as an aircraft windscreen or canopy material.

The transparent acrylic materials possess excellent clarity, ultraviolet resistance and surface hardness required for many windscreen and canopy applications and indeed have proven their worth by many years of excellent service in demanding applications. The acrylics, however, lack the toughness and crack propagation resistance where applications require resistance to bird impact. Also the temperature limitations of the acrylics will preclude their use as the main structural member in windscreen applications on future high performance aircraft. The polycarbonate materials possess excellent clarity and high toughness for transparency applications involving bird impact resistance. They are, however, deficient in several areas which complicate their use in service as transparencies for aircraft. They are relatively soft and their surface finish (smoothness) can easily be marred or damaged by abrasion from dust, ice crystals, improper cleaning or inadvertent contact such as by tools or clipboards, etc. This situation prompted the development of a variety of protective coatings for polycarbonates, mostly proprietary, to prevent this surface abrasion phenomena from taking place. Air Force experience with such coatings has been less than satisfactory and the required abrasion protection for polycarbonate materials is obtained via the use of an outer ply of either glass or acrylic plastic. Another deficiency of polycarbonate materials is their sensitivity to certain combinations of stress and chemical environments. Improperly drilled holes,

poor fit up upon installation, and contact with moisture vapor (humidity) and various chemical substances such as certain plasticizers, solvents and lubricants can cause stress cracks to form which can cause the polycarbonate material to lose its high toughness characteristics unless proper design procedures have been followed. It is believed that this chemical-stress cracking tendency of the polycarbonates can be minimized by the proper protection (insulation) of the material from the environment as well as proper fit up and installating procedures. Nevertheless the Air Force has experienced significant and serious problems caused by inattention to this limitation of the polycarbonates.

Over the last 10 years the Materials Laboratory has pursued through contract research and development investigations into potential new and improved transparent plastics for use in high performance transparency applications.

The primary topic of this presentation is the research and development work conducted by the Allied Corporation under contract to the Composites, Adhesives and Fiberous Materials Branch of the Materials Laboratory. The contract number was F33615-78-C-5077 and the principal investigators were Drs. Tom DeBona and Dusan Prevorsek.

Since the chemical aspects of this research were the topic of a previous paper by Dr. DeBona this discussion will concentrate on an evaluation of research materials received from the Allied Corporation under the contract and evaluated at the University of Dayton Research Institute. Special appreciation is due to Mr. Sam Marolo of AFWAL/MLSE and to Mr. Dee Pike of the University of Dayton Research Institute for the planning and performance of the work required to test the research materials.

DISCUSSION

A test program was planned and initiated to evaluate transparent polyester-carbonate materials received from the Allied Corporation under the previously referenced research contract. In addition to this polyester-carbonate materials, SL-2000 polycarbonate was also tested to provide comparative data. Table A lists all of the tests that were conducted.

It should be pointed out that only 18 pressed sheets (pressed not extruded) were available for testing. This drastically limited the testing and number of specimen replicates that could be utilized. The physical and chemical properties of the PEC are listed in Table B. Standard ASTM test procedures were utilized throughout the program wherever possible. Most of the panels furnished were 6" x 6" x 0.125" in dimensions. All were formed by compression molding. Since these were research samples optical properties such as transmission and haze were not representative of clean production materials.

Tensile tests of polycarbonate (PEC) and SL-2000 polycarbonate were conducted in accordance with ASTM-D638. Tables 1 and 2 present the tensile data.

The QUV accelerated weathering tests were completed with exposure times equivalent to one year.

Flexure tests of PEC were run in accordance with ASTM-D790, Method II. Table 3 presents the flexure data.

Hardness tests on PEC and SL-2000 were completed using Rockwell M and Barcol Hardness testers. Table 4 presents the hardness data.

Table 5 presents the specific gravity of PEC.

The data for coefficient of thermal expansion over the temperature range from 72°F (22°C) to 300°F (149°C) of PEC are presented in Table 6 and were obtained in accordance with ASTM-D696.

Heat Distortion Temperature Deflection tests were run on three replicates of PEC in accordance with ASTM-D648 and their result are presented in Tables 7, 8, and 9.

Water absorption measurements were conducted over a six week period in accordance with ASTM-D570.

Table 10 presents the weight gain data, while Figure 1 illustrates the data graphically.

Polyester-carbonate material was tested as received for optical properties and SL-2000 polycarbonate was also tested on a limited basis to provide comparative data. Optical properties of the PEC material were also measured after QUV exposure (ASTM-D1499) and after Bayer abrasion. The optical properties were measured in accordance with ASTM method D1003. All of these optical data are presented in Tables 11 through 15.

Index refraction of PEC was measured. A reference fluid of index 1.4640 was used for all determinations. These results are presented in Table 16 and were obtained in accordance with ASTM-D542.

Stress crazing tests were run on PEC material and the results are reported in Table 17. We were unable to make these specimens 7" long because the panels received were only 6" x 6". Therefore, the samples were only 6" long. The load was adjusted to produce an outer fiber stress of 3,000 psi as follows:

$$\frac{w \times t^2 \times 3000}{18} = \text{Pounds Load}$$

w = width
t = thickness

This testing was in accordance with ANSI/ASTM-F484-77.

The PEC materials were chosen as the subject of this research and development primarily because of their indicated superior chemical resistance and heat resistance compared to the state-of-the-art polycarbonates. It can be seen by a comparison of Tables 1 and 2 that the elongation to break of the SL-2000 materials starts out quite high at 50% +, however, after quite moderate heat aging the breaking elongation is about 12%. The PEC materials

which do not have anti oxidant or ultraviolet protective additives started out quite low in elongation but the breaking elongation was relatively unaffected by the various exposure to which it was subjected.

Hardness testing was conducted using both the Barcol and the Rockwell M instrument. While the PEC materials demonstrated increased hardness over the SL-2000 material it is not known if the PEC materials can be polished using mechanical techniques that are effective on the acrylics. The hardness values obtained are in Table 4. Heat distortion values are shown in Table 7, 8 and 9. Several of the PEC materials displayed HDT values in the 180°C (355°F) temperature range. This is a distinct increase over SL-2000 material which has HDT's in the 143°C (290°F) range. The most impressive property of the PEC materials is their ability to withstand continued elevated temperatures without loss in properties without the assistance of anti oxidant or UV absorbers. Tables 10 through 17 provide the remainder of the data obtained from the research samples. All of the data obtained in our study corroborated the data obtained by the Allied Corporation in their research program.

Figure 1 is a plot of the water pick up of the PEC materials

SUMMARY

Several different PEC materials were received from the Allied Corporation as a result of their contract research and development work for the Materials Laboratory. While the limited amount of materials prevented the conduction of a comprehensive evaluation, preliminary data on several versions of PEC materials was obtained. This data revealed that the PEC materials are quite promising in several areas and do possess certain advantages over the SL-2000 materials. The PEC materials are inherently resistant to heat and exposures to 200°F and 350°F had little impact upon the tensile strength and tensile elongation. The PEC materials have HDT's about 50°F or more above the SL-2000 materials. These particular PEC materials were not formulated with anti oxidants or UV screens or absorbers. Work will have to be done to find suitable additions for the PEC materials. The chemical-stress cracking tolerance levels of the PEC materials is well above that of the SL-2000 material. More work is needed to optimize the elongation characteristics of the PEC materials and not compromise too much on the HDT.

REFERENCES

1. AFWAL-TR-81-4178, "High Temperature Windshield/Canopy Materials Development"

2. University of Dayton Memorandum, 9 May 1983, "Polyester Carbonate Transparent Material"

TABLE A

TESTS TO BE CONDUCTED FOR TRANSPARENT
POLYESTER-CARBONATE PROGRAM

Test Type	Applicable ASTM Specification	Test Conditions	Replicates	Material
Tension	D638	R.T.	5	PEC
		R.T. after QUV exposure	5	PEC
		R.T. after 72 hrs. @ 200°F (93°C)	5	PEC
		R.T. after 72 hrs. @ 350°F (177°C)	5	PEC
		R.T.	5	SL 2000
		R.T. after QUV exposure	5	SL 2000
		R.T. after 72 hrs. @ 200°F (93°C)	5	SL 2000
Flexure	D790	R.T.	5	PEC
Specific Gravity	D792	R.T.	3	PEC
Coeff. Therm. Exp.	D696	R.T.-300°F (149°C)	2	PEC
Heat Distortion Temp.	D648	---	3	PEC
Water Absorption	D570	Immersion at R.T.	3	PEC
Hardness	---	Rockwell M	18	PEC
			6	PEC
Haze & Transmittance	D1003	As-Received	18	PEC
		After 1 equiv. yr. QUV exposure	5	PEC
		After Bayer abrasion (50-300 cycles)	5	PEC
		As-Received	6	SL 2000
		After 1 equiv. yr. QUV exposure	5	SL 2000
Index of Refraction	D542	As-Received	18	PEC
Stress-Crazing	F484	R.T., 3000 psi, isopropanol	5	PEC

TABLE B

VARIOUS PROPERTIES OF TRANSPARENT
POLYESTER-CARBONATE

Property	Average Value (±stnd.dev.)	No. of Specimens	Remarks
Specific Gravity	1.22 (±0)	3	
Rockwell M Hardness	101.0 (±0.5)	18	
Heat Distortion Temperature	325°F (±33°F)	3	All specimens broke.
Coefficient of Thermal Expan.	3.50×10^{-5}/°F 3.43×10^{-5}/°F	2 2	Longitudinal Transverse
Index of Refraction	1.4627 (±0.0006)	18	
Stress Crazing	All specimens passed	5	

TABLE 1

TENSILE PROPERTIES OF POLYESTER CARBONATE
TRANSPARENT MATERIAL

Specimen Number	Condition of Test	Pre-Test Conditioning	Tensile Str. @ Yield (10^3 psi)	Elongation @ Yield (%)	Tensile Str. @ Break (10^3 psi)	Elongation @ Break (%)	Modulus (10^6psi)
2-3-1	R.T.	None	10.00	9.25	10.00	9.25	0.280
3-3-1	R.T.	None	10.42	10.50	10.42	10.50	0.29
4-3-1	R.T.	None	10.38	8.75	9.02	14.13	0.29
5-3-1	R.T.	None	10.19	8.75	9.80	9.25	0.32
6-3-1	R.T.	None	10.38	8.88	9.11	15.75	0.29
Avg.			10.27	9.23	9.67	11.78	0.29
Std.Dev.			0.18	0.74	0.60	2.99	0.01
1-1-1	R.T.	72 hrs. @	10.25	5.5	10.25	5.5	0.25
1-2-1	R.T.	200°F (93°C)	10.31	5.75	9.99	6.75	0.26
1-3-1	R.T.	↓	10.38	8.75	9.77	11.25	0.24
7-1-1	R.T.		10.49	8.5	9.81	10.63	0.24
8-1-1	R.T.		9.74	5.75	9.74	5.75	0.29
Avg.			10.23	6.85	9.91	7.98	0.26
Std.Dev.			0.29	1.63	0.21	2.75	0.02
2-1-1	R.T.	72 hrs. @	11.06	8.0	8.48	15.75	0.22
3-1-1	R.T.	350°F (177°C)	11.16	8.5	9.48	14.0	0.22
4-1-1	R.T.	↓	11.08	7.5	10.68	8.25	0.22
5-1-1	R.T.		6.31	2.5	6.31	2.5	0.28
6-1-1	R.T.		10.90	9.0	9.92	11.0	0.22
Avg.			10.10	7.1	8.97	10.3	0.23
Std.Dev.			2.12	2.63	1.69	5.22	0.03

TABLE 1 (Concluded)

TENSILE PROPERTIES OF POLYESTER CARBONATE TRANSPARENT MATERIAL

Specimen Number	Condition of Test	Pre-Test Conditioning	Tensile Str. @ Yield (10^3 psi)	Elongation @ Yield (%)	Tensile Str. @ Break (10^3 psi)	Elongation @ Break (%)	Modulus (10^6psi)
9-1-1	R.T.	1 equiv. yr.	10.27	8.13	9.54	9.13	0.29
9-2-1	R.T.	@ QUV	10.21	8.25	9.58	9.75	0.25
9-3-1	R.T.	↓	10.12	7.63	9.96	8.25	0.28
9-4-1	R.T.		9.91	7.38	9.81	7.63	0.29
9-5-1	R.T.		10.01	8.0	9.88	8.25	0.26
Avg.			10.10	7.88	9.75	8.60	0.27
Std.Dev.			0.15	0.36	0.19	0.84	0.02
2-2-1	200°F(93°C)	None	7.34	5.5	2.82	14.25	0.21
3-2-1	200°F(93°C)	None	7.30	7.0	5.40	12.0	0.17
4-2-1	200°F(93°C)	None	7.43	6.75	3.83	14.5	0.20
5-2-1	200°F(93°C)	None	7.45	6.5	4.23	13.5	0.20
6-2-1	200°F(93°C)	None	7.38	7.0	4.80	19.5	0.18
Avg.			7.38	6.55	4.21	14.75	0.19
Std.Dev.			0.06	0.62	0.98	2.83	0.01

TABLE 2

TENSILE PROPERTIES OF SL2000 POLYCARBONATE
TRANSPARENT MATERIAL

Specimen Number	Condition of Test	Pre-Test Conditioning	Tensile Str. @ Yield (10^3 psi)	Elongation @ Yield (%)	Tensile Str. @ Break (10^3 psi)	Elongation @ Break (%)	Modulus (10^6 psi)
6	R.T.	None	9.41	5.25	0.78	49.5	0.34
9	R.T.	None	9.44	5.5	8.32	50.0+	0.31
12	R.T.	None	9.18	5.5	6.99	21.0	0.29
15	R.T.	None	9.46	5.5	8.75	50.0+	0.35
18	R.T.	None	9.43	5.5	8.26	50.0+	0.32
Avg.			9.38	5.5	8.03	44.1	0.32
Std.Dev.			0.11	0.1	0.67	12.3	0.02
7	R.T.	72 hrs. @	9.80	6.0	6.95	10.8	0.24
11	R.T.	200°F (93°C)	9.78	5.3	7.02	11.3	0.31
14	R.T.		9.75	6.0	5.45	12.5	0.23
17	R.T.		9.80	5.5	1.65	12.0	0.30
20	R.T.	↓	9.86	5.5	3.67	14.0	0.31
Avg.			9.80	5.7	4.95	12.1	0.28
Std.Dev.			0.41	0.3	2.30	1.2	0.04

TABLE 2 (Concluded)

TENSILE PROPERTIES OF SL2000 POLYCARBONATE
TRANSPARENT MATERIAL

Specimen Number	Condition of Test	Pre-Test Conditioning	Tensile Str. @ Yield (10^3 psi)	Elongation @ Yield (%)	Tensile Str. @ Break (10^3 psi)	Elongation @ Break (%)	Modulus (10^6 psi)
1	R.T.	1 equiv.	9.27	6.0	6.77	16.5	0.28
2	R.T.	yr. @ QUV	9.36	5.5	6.76	9.5	0.32
3	R.T.		9.36	6.0	6.71	18.0	0.29
4	R.T.		9.43	5.5	6.67	19.0	0.32
5	R.T.		9.30	5.3	6.62	16.0	0.30
Avg.			9.34	5.7	6.70	15.8	0.30
Std.Dev.			0.06	0.3	0.06	3.7	0.02
8	200°F(93°C)	None	5.53	4.0	5.68	50.0+	0.22
10	200°F(93°C)	None	5.36	4.0	5.12	50.0+	0.19
13	200°F(93°C)	None	5.61	4.5	5.45	50.0+	0.20
16	200°F(93°C)	None	5.72	4.0	5.76	50.0+	0.22
19	200°F(93°C)	None	5.65	4.0	5.39	50.0+	0.26
Avg.			5.57	4.1	5.48	50.0+	0.22
Std.Dev.			0.14	0.2	0.25	0.0	0.03

TABLE 3

FLEXURE PROPERTIES OF POLYESTER CARBONATE TRANSPARENT MATERIAL

Specimen Number	Condition of Test	Ultimate Strength (10^3psi)	Modulus of Elasticity (10^6psi)
2	R.T.	8.89	0.328
3	R.T.	8.38	0.334
4	R.T.	8.39	0.328
5	R.T.	8.63	0.334
6	R.T.	8.26	0.333
Avg.		8.51	0.331
Std. Dev.		0.25	0.003

TABLE 4

HARDNESS OF PEC AND SL2000
TRANSPARENT PLASTICS

Polyester Carbonate (PEC)				SL2000			
Spec. No.	Barcol	Spec. No.	Rockwell M	Spec. No.	Barcol	Spec. No.	Rockwell M
1	13.5	1	101.5	21	11.0	21	81.0
2	14.0	2	100.5	22	11.0	22	81.5
3	13.0	3	101.0	23	12.0	23	82.0
4	12.0	4	100.5	24	11.0	24	81.0
5	12.0	5	100.0	25	10.0	25	81.0
6	14.0	6	101.0	26	10.0	26	82.0
7	14.0	7	101.0				
8	14.0	8	101.0				
9	14.0	9	100.5				
10	12.0	10	101.0				
11	13.0	11	101.0				
12	14.0	12	101.0				
13	14.0	13	101.5				
14	13.0	14	101.0				
15	14.0	15	102.0				
16	12.0	16	101.5				
17	11.5	17	100.5				
18	13.0	18	101.0				
Avg. Std.Dev.	13.17 (±0.9)		101.0 (±0.5)		10.8 (±0.8)		81.4 (±0.5)

TABLE 5

SPECIFIC GRAVITY OF PEC

Specimen Number	Specific Gravity
2	1.22
4	1.22
6	1.22
Avg. Std. Dev.	1.22 ±0.0

TABLE 6

THERMAL EXPANSION OF POLYESTER
CARBONATE TRANSPARENT MATERIAL

Sample Orientation and Number	Coefficient of Thermal Expansion ($10^{-5}°F^{-1}$)
Transverse #1	3.39
Transverse #2	3.47
Avg.	3.43
Longitudinal #1	3.57
Longitudinal #2	3.43
Avg.	3.50

TABLE 7

HEAT DISTORTION OF POLYESTER CARBONATE

Specimen Number	Time in Minutes	Temperature °C	(°F)	Deflection (inches)
4-1-6	Load no Heat 0-5	24	(75.2)	0.0000
	5	30	(86.0)	0.0000
	10	42	(107.6)	
	15	50	(122.0)	
	20	60	(140.0)	
	25	70	(158.0)	
	30	80	(176 0)	
	35	89	(192.2)	
	40	95	(203.0)	
	45	102	(215.6)	
	50	109	(228.2)	
	55	116	(240.8)	
	60	123	(253.4)	
	65	129	(264.2)	
	70	136	(276.8)	
	75	144	(291.2)	
	80	155	(311.0)	
	85	165	(329.0)	0.0000
	90	173	(343.4)	0.0015
failed @	93	179	(354.2)	0.0100

0.0100" Deflection @ 179°C (354°F) in 93 minutes (specimen broke).
Stress 264 PSI

TABLE 8

HEAT DISTORTION OF POLYESTER CARBONATE

Specimen Number	Time in Minutes	Temperature °C	(°F)	Deflection (inches)
3-1-6	Load no Heat 0-5	24	(75.2)	0.0000
	5	30	(86.0)	0.0000
	10	42	(107.6)	
	15	50	(122.0)	
	20	60	(140.0)	
	25	70	(158.0)	
	30	80	(176.0)	
	35	89	(192.2)	
	40	95	(203.0)	
	45	102	(215.6)	
	50	109	(228.2)	0.0000
	55	116	(240.8)	0.0001
	60	123	(253.4)	
	65	129	(264.2)	
	70	136	(276.8)	
	75	144	(291.2)	
	80	155	(311.0)	0.0001
	85	165	(329.0)	0.0002
failed @ 86		166	(330.8)	0.0100

0.0100" Deflection @ 166°C (330.8°F) in 86 minutes (Specimen broke). Stress 264 PSI.

TABLE 9

HEAT DISTORTION OF POLYESTER CARBONATE

Specimen Number	Time in Minutes	Temperature °C	(°F)	Deflection (inches)
2-1-6	Load no Heat 0-5	24	(75.2)	0.0000
	5	30	(86.0)	
	10	42	(107.6)	
	15	50	(122.0)	
	20	60	(140.0)	
	25	70	(158.0)	
	30	80	(176.0)	
	35	89	(192.2)	
	40	95	(203.0)	
	45	102	(215.6)	
	50	109	(278.2)	0.0000
	55	116	(240.8)	0.0001
	60	123	(253.4)	
	65	129	(264.2)	
	70	136	(276.8)	0.0001
failed @ 74		143	(289.4)	0.0100

0.0100" Deflection @ 143°C (289.4°F) in 74 minutes (Specimen broke). Stress 264 PSI.

TABLE 10

WATER ABSORPTION OF POLYESTER CARBONATE
TRANSPARENT MATERIALS

Specimen Number		Initial Wt.	24 Hours	One Week	Two Weeks	Four Weeks	Six Weeks
2	Weight(gms)	6.6009	6.6178	6.6356	6.6389	6.6408	6.6424
	Wt.Gain(%)		0.2560	0.5257	0.5751	0.6045	0.6287
	Wt.Gain(gms)		0.0169	0.0347	0.0380	0.0399	0.0415
3	Weight(gms)	6.5227	6.5394	6.5565	6.5603	6.5617	6.5630
	Wt.Gain(%)		0.2560	0.5182	0.5765	0.5979	0.6178
	Wt.Gain(gms)		0.0167	0.0338	0.0376	0.0390	0.0403
4	Weight(gms)	6.5283	6.5450	6.5636	6.5661	6.5674	6.5688
	Wt.Gain(%)		0.2558	0.5407	0.5790	0.5989	0.6204
	Wt.Gain(gms)		0.0167	0.0353	0.0378	0.0391	0.0405
Avg. Wt. Gain (%)			0.2559	0.5282	0.5771	0.6004	0.6223
Std. Dev. (%)			±0.0001	±0.0115	±0.0017	±0.0036	±0.0057

TABLE 11

OPTICAL PROPERTIES OF HAZE STANDARDS

Material	Test Condition	Average Results (±Std. Dev.)		
		% Direct Transmittance	% Diffuse Transmittance	% Haze
1% Nominal	Before and after each set of sample tests. Total of 6 times.	90.0(5.5)	0.88(0.05)	0.95(0.08)
13% Nominal		80.4(1.2)	12.9(0.4)	16.02(0.40)
23% Nominal		73.1(2.6)	18.4(0.6)	24.22(1.24)
33% Nominal		71.0(1.1)	26.1(0.4)	36.71(0.26)

TABLE 12

OPTICAL PROPERTIES OF AS-RECEIVED
POLYESTER CARBONATE TRANSPARENT MATERIAL

Panel Specimen	% Direct Transmittance	% Diffuse Transmittance	% Haze
1	81.00	14.80	18.27
2	80.20	18.60	23.19
3	77.30	13.50	17.46
4	78.10	15.00	19.21
5	77.80	18.10	23.27
6	80.85	3.45	4.27
7	80.45	13.20	16.40
8	78.85	11.80	14.97
9	80.40	14.75	18.35
10	79.80	12.20	15.29
11	79.45	15.25	19.19
12	79.50	15.85	19.94
13	77.90	20.75	26.64
14	80.40	15.00	18.66
15	81.25	4.15	5.11
16	77.60	13.35	17.20
17	80.30	13.25	16.50
18	78.50	14.90	18.98
Avg.	79.39	13.77	17.38
Std. Dev.	± 1.25	± 4.27	± 5.46

TABLE 13

OPTICAL PROPERTIES OF POLYESTER CARBONATE
TRANSPARENT MATERIAL AFTER QUV EXPOSURE

Panel Specimen	% Direct Transmittance	% Diffuse Transmittance	% Haze[1]
12	76.65	15.45	20.16
1	77.70	17.20	22.14
14	78.55	14.90	18.97
18	76.65	16.20	21.14
11	75.50	17.50	23.18
Avg.	77.01	16.25	21.12
Std.Dev.	± 1.16	± 1.11	± 1.65

[1]Exposure times were for 1 yr. equivalent.

TABLE 14

OPTICAL PROPERTIES OF POLYESTER CARBONATE
AFTER BAYER ABRASION

Sample	Cycles[1]	% Transmitted		% Haze
		Diffuse	Luminous	
2	0	18.60	80.20	23.19
	50	21.85	74.40	29.37
	100	24.10	73.40	32.83
	150	26.80	76.15	35.19
	300	29.20	78.00	37.44
3	0	13.50	77.30	17.46
	50	17.70	74.00	23.92
	100	18.00	74.05	24.31
	150	20.55	76.55	26.85
	300	22.90	78.25	29.27
4	0	15.00	78.10	19.21
	50	16.85	74.95	22.48
	100	17.85	74.10	24.09
	150	23.45	75.65	31.00
	300	24.85	77.90	31.90
5	0	18.10	77.80	23.27
	50	19.45	73.85	26.34
	100	21.50	73.35	29.31
	150	23.65	76.00	31.12
	300	27.80	78.50	35.41
6	0	3.45	80.25	4.27
	50	5.70	77.50	7.35
	100	9.35	76.90	12.16
	150	10.70	80.35	13.32
	300	14.45	81.60	17.71
Averages and Standard Dev.	0	13.73±6.13	78.73±1.39	17.48±7.80
	50	16.31±6.23	74.94±1.49	21.89±8.54
	100	18.16±5.57	74.36±1.46	24.54±7.83
	150	21.03±6.18	76.94±1.93	27.50±8.46
	300	23.78±5.92	78.85±1.55	30.35±7.73

[1]Number of cycles represents number of cycles that abrasive medium (Quartz-Silica) slid back and forth over sample surface; thus, one cycle represents two strokes.

TABLE 15

OPTICAL PROPERTIES OF LEXAN
SL2000 POLYCARBONATE

Panel	% Direct Transmittance	% Diffuse Transmittance	% Haze
24	85.95	16.50	19.20
25	85.95	13.00	15.13
26	86.50	12.00	13.87
23	85.65	21.00	24.52
22	85.65	19.50	22.77
21	85.85	13.00	15.14
Avg.	85.93	15.83	18.44
Std. Dev.	± 0.31	± 3.78	± 4.45

TABLE 16

INDEX OF REFRACTION OF POLYESTER CARBONATE
TRANSPARENT MATERIAL

Specimen Number	Index of Refraction
1	1.4629
2	1.4617
3	1.4618
4	1.4619
5	1.4617
6	1.4616
7	1.4631
8	1.4631
9	1.4630
10	1.4630
11	1.4630
12	1.4631
13	1.4628
14	1.4630
15	1.4632
16	1.4633
17	1.4630
18	1.4631
Average	1.4627
Std. Dev.	±0.0006

TABLE 17

STRESS CRAZING BEHAVIOR OF
POLYESTER CARBONATE

Specimen Number	Stress (psi)	Load (lbs)	Test Fluid	Test Condition	Test Results
2	3000	2.47	Isopropanol	R.T.	Passed
6	3000	2.32	Isopropanol	R.T.	Passed
4	4000	3.24	Isopropanol	R.T.	Passed
5	4000	3.44	Isopropanol	R.T.	Passed
3	5000	3.86	Isopropanol	R.T.	Passed

TABLE 23

OPTICAL PROPERTIES OF PEC AND SL 2000
TRANSPARENT PLASTICS

Material	Test Condition	Avg. Result (±Std. Dev.) % Direct Transmittance	% Diffuse Transmittance	% Haze
Haze Standards				
1% Nominal	Before and after each set of sample tests	90.0 (5.5)	0.88 (0.05)	0.95 (0.08)
13% Nominal		80.4 (1.2)	12.9 (0.4)	16.02(0.40)
23% Nominal		73.1 (2.6)	18.4 (0.6)	24.22(1.24)
33% Nominal		71.0 (1.1)	26.1 (0.4)	36.71(0.26)
PEC	As-received	79.4 (1.3)	13.8 (4.3)	17.4 (5.5)
	After 1 yr. QUV	77.0 (1.2)	16.3 (1.1)	21.1 (1.6)
SL 2000	As-received	85.9 (0.3)	15.8 (3.8)	18.4 (4.5)

TABLE 24

OPTICAL PROPERTIES OF PEC TRANSPARENT PLASTICS AFTER BAYER ABRASION

Sample	Cycles[1]	% Transmittance		% Haze
		Diffuse	Luminous	
2	0	18.60	80.20	23.19
	50	21.85	74.40	29.37
	100	24.10	73.40	32.83
	150	26.80	76.15	35.19
	300	29.20	78.00	37.44
3	0	13.50	77.30	17.46
	50	17.70	74.00	23.92
	100	18.00	74.05	24.31
	150	20.55	76.55	26.85
	300	22.90	78.25	29.27
4	0	15.00	78.10	19.21
	50	16.85	74.95	22.48
	100	17.85	74.10	24.09
	150	23.45	75.65	31.00
	300	24.85	77.90	31.90
5	0	18.10	77.80	23.27
	50	19.45	73.85	26.34
	100	21.50	73.35	29.31
	150	23.65	76.00	31.12
	300	27.80	78.50	35.41
6	0	3.45	80.25	4.27
	50	5.70	77.50	7.35
	100	9.35	76.90	12.16
	150	10.70	80.35	13.32
	300	14.45	81.60	17.71
Avg.[2]	0	13.73 ± 6.13	78.73 ± 1.39	17.48 ± 7.80
	50	16.31 ± 6.23	74.94 ± 1.49	21.89 ± 8.54
	100	18.16 ± 5.57	74.36 ± 1.46	24.54 ± 7.83
	150	21.03 ± 6.18	76.94 ± 1.93	27.50 ± 8.46
	300	23.84 ± 5.80	78.85 ± 1.55	30.35 ± 7.73

[1]Number of cycles represents number of cycles that abrasive medium (quartz-silica) slid back and forth over sample surface. Thus, one cycle represents two strokes.

[2]Plus/minus values behind averages represent standard deviations.

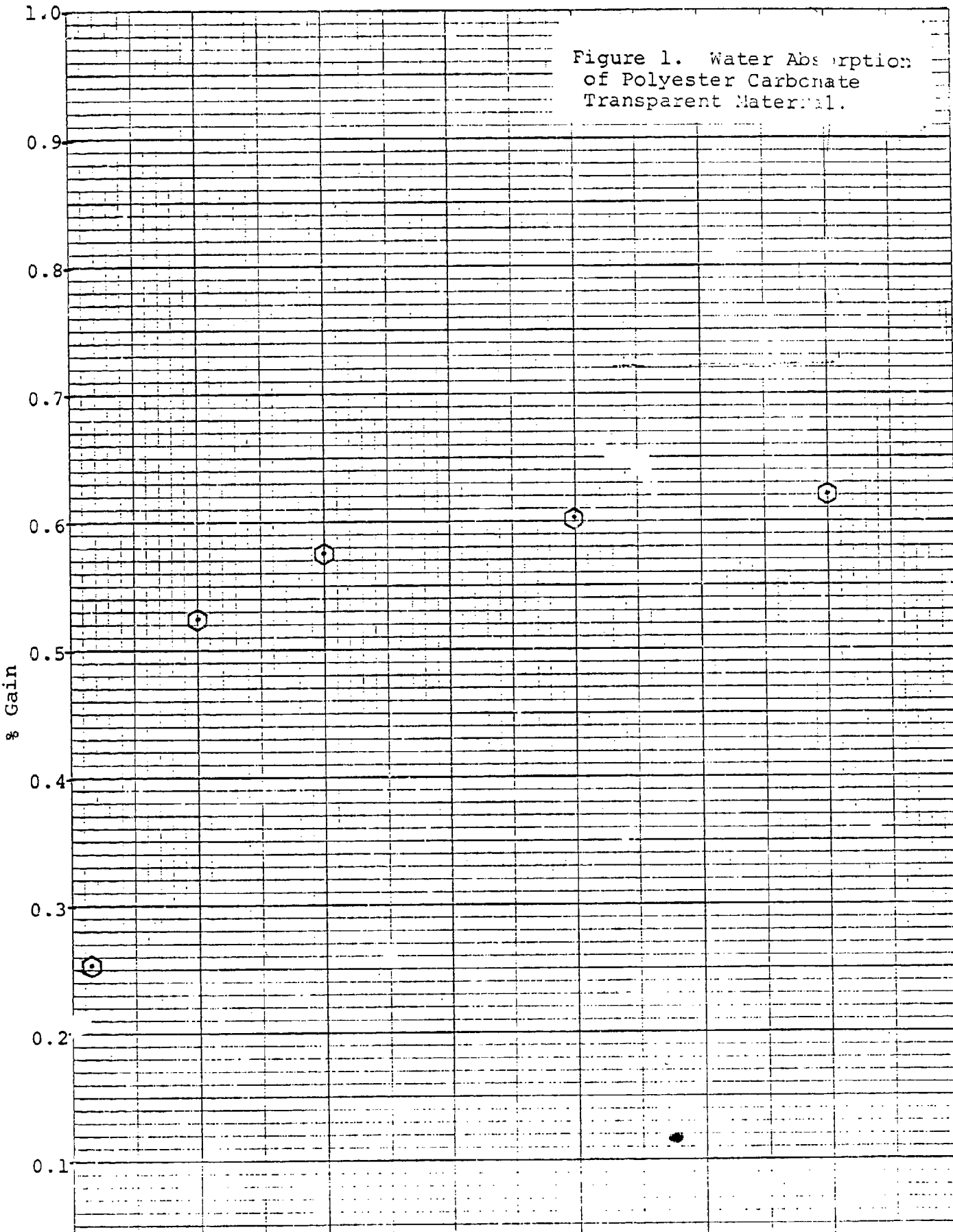

Figure 1. Water Absorption of Polyester Carbonate Transparent Material.

AD-P003 206

SPECIALTY COATINGS FOR INCREASED SERVICE LIFE OF ACRYLIC AIRCRAFT TRANSPARENCIES - PART II

W. C. Harbison, Swedlow, Inc.

SPECIALTY COATINGS FOR INCREASED SERVICE LIFE OF ACRYLIC AIRCRAFT TRANSPARENCIES - Part II

W.C. Harbison
SWEDLOW, Inc.

ABSTRACT

As a follow up to our paper delivered at the last conference in September, 1980, an update on the continued development and field testing experience of Swedlow protective coatings for acrylic transparencies is described.

In the ground transportation industry, Swedlow's abrasion resistant coatings on acrylic windows have now provided up to eight years serviceability against the harsh environments of people abuse and automated cleaning procedures. The superior performance of the Swedlow coatings over that of all other commercially available coatings has been confirmed by many independent facilities. General Motors Corp., for example, has recently approved only two coatings, Swedlow's SS-6590 and SS-6712, for use on the formed acrylic sunroofs for their 1984 Corvette. This represents the first significant entry for plastics into automotive transparencies in this country.

In aircraft applications, the SS-6590 and SS-6712 coatings are undergoing extensive laboratory and flight testing. Coated as-cast acrylic windshields have demonstrated excellent abrasion and chemical resistance in non-pressurized general purpose and agricultural spray aircraft. On stretched acrylic material, the coatings conform to CAR 3.27(a) and 3.396(a) pressurization testing and have successfully achieved over 5000 flight hours on cabin windows in a TWA operated 727 aircraft.

In addition to abrasion resistant coatings, Swedlow has developed a patented, edge sealing coating which greatly retards the development of in-plane edge fractures in stretched acrylic transparencies. A primary cause for premature fracturing of stretch oriented acrylic material is differential tensile stress across the edge of the transparency arising from an absorbed moisture gradient. SS-6704 moisture barrier coating retards the transport of water through the edges and reduces stresses in the in-plane direction. Accelerated laboratory testing and actual flight testing confirm the effectiveness of SS-6704.

INTRODUCTION

In Part I of our studies on specialty coatings, which was presented at the transparency conference in September, 1980, Swedlow's experience with abrasion resistant coatings applied to acrylic and polycarbonate was described. Durability of these coated compositions in accelerated laboratory tests and in ground transportation and architectural installations was reviewed. The excellent serviceability of coated acrylic, in particular Swedlow's Acrivue A, was documented in these applications. The demonstrated poor weathering qualities of coated and uncoated polycarbonate was coupled with a failure mechanism theory.

Here in Part II, the performance of Swedlow's SS-6590 abrasion resistant coating on as-cast and stretched acrylic aircraft transparencies is further examined. The development of two additional, unique coatings to increase the service life of acrylic windows is also discussed. SS-6712 is a new generation "hard" coating offering improved abrasion resistance over all other commercially available coatings. SS-6704 is a special moisture vapor barrier coating offering dramatic reduction in the occurrence of in-plane fracture of stretched acrylic windows due to moisture ingress and egress. Both the SS-6704 and SS-6712 compositions have been patented.

DISCUSSION

SS-6590 - Proven Field Performance

(1) Non-Aircraft Application Experience

In 1975, Swedlow Inc. introduced the first commercial abrasion resistant coated acrylic sheet products using a silica filled polysiloxane coating (Table 1). This chemical class of coating remains unsurpassed in abrasion resistance performance (Table 2).

The Swedlow Inc. SS-6590 coating was applied to both as-cast acrylic sheet (Acrivue A) and stretched acrylic sheet (Acrivue SA). These materials were used extensively in ground transportation glazing, where repeated physical and chemical abuse was experienced from passengers, outdoor elements, and daily auomated brush washings. The superior durability and life cycle cost of the coated acrylic sheet over coated polycarbonate sheet in this environment became readily apparent. Major transportation systems, such as the Long Island Railroad, specified the exclusive use of Acrivue coated acrylic sheet.

After 8 years field service, the combination of a highly serviceable SS-6590 silicone coating on polymethyl methacrylate, with weatherability unchallenged among polymers, has provided outstanding performance. The coated polycarbonate compositions

suffered from relatively rapid UV degradation and hydrolysis under comparable exposure conditions. Figure 1 provides comparative results after laboratory accelerated exposure testing. These results agree with field experience.

2. Aircraft Application Experience

With coating durability proven in architectural and ground transportation glazing, Swedlow Inc. embarked on a test program to establish the flight performance of SS-6590. Many windshields on unpressurized general aviation and private aircraft were coated and monitored. As anticipated, flight experience has been excellent. The dramatic decrease in surface erosion and scratching of the windshields provided by SS-6590 became apparent within several months. This protection has remained evident after two years. Testing of these articles is continuing.

Several coated windshields were installed in agricultural spray aircraft, where chemical and insect damage are a major problem. After three spraying seasons (440 flight hours) only minor changes in the physical properties of the coating were observed (Table 3). It is noted that conventional, uncoated windshields are often nearly translucent after comparable exposure in this environment and must be replaced.

In pressurized aircraft applications, one key concern was coating elongation. The strain allowable to craze SS-6590 at ambient temperature ranges from 1.2 to 1.5 percent. The expected strain on the outer surface of a pressurized aircraft is commonly around 0.6 percent, taking into account the combined effects of pressurization, thermal and moisture expansion. Based upon a mechanical analysis there appears therefore to be a safety margin for the use of SS-6590 in pressurized aircraft applications. A monolithic stretched acrylic window, ~ 15 x 22 x 0.250", with SS-6590 on the outer surface, was evaluated on a pressurized general aviation aircraft. The window was pressurized through 30,000 cycles to demonstrate fatigue strength in accordance with CAR 3.270(a). Loading during this cyclic test was 6.5 psi. Following completion of the cyclic test, an ultimate pressure test at 11.4 psi was conducted to demonstrate compliance with CAR 3.197(c). The load determinations are detailed in Table 4. The coated window successfully passed the test, and no deterioration of the coating was observed. A photograph of this window after testing is provided in Figure 2.

Six stretched acrylic cabin windows were installed in a TWA operated 727 aircraft (#4312). Four of these windows were coated on the outer surface with SS-6590; two of the windows were uncoated controls. After 5426 flight hours and 3054 pressurization cycles, the windows were carefully inspected. The four SS-6590 coated windows displayed no deterioration. The two uncoated

windows exhibited minor scratching and surface erosion. Two of the windows (Figures 3 and 4) were removed at this time. The remaining four windows (3 coated, 1 uncoated) are continuing flight exposure.

Another key concern in aircraft applications, of course, is impact resistance. Based upon the development of a family of abrasion resistant coated, ballistics resistant security compositions (Figures 5,6 and 7), Swedlow Inc. has developed the critical technology necessary to minimize the potential embrittling effects of a hard coating on the tension side of a transparency under impact. With this knowledge, Swedlow Inc. has qualified AR coated B-1 and F-111 windshields to the specified bird strike requirements.

A number of additional flight tests with SS-6590 coated acrylic cabin windows and helicopter windshields have been initiated. The preliminary results are very encouraging and we plan to follow the progress of these articles closely.

SS-6712 - A Significant Improvement in Abrasion Resistance

SS-6712[1] is a new generation, filled polysiloxane coating which provides significantly improved abrasion resistance over SS-6590 and all other commercially available transparent coatings. Figure 8 provides the results of Taber abrasion testing conducted by U.S.Testing Co.. A comparison of steel wool resistance is provided in Figure 9.

In addition to superior abrasion resistance, the SS-6712 coating also demonstrates excellent chemical resistance (Table 5) and accelerated exposure stability. No deterioration of SS-6712 on acrylic sheet was observed within 5000 hrs. in a Xenon Arc weatherometer (ASTM G-26-70) or two years, 45°S outdoor weathering in Garden Grove, CA.

Confirmation of the improved performance offered by SS-6712 has been obtained from Dow Corning and General Motors. After extensive testing of nearly all commercially available transparent coatings, the Chevrolet Engineering Division has approved only two coatings, SS-6590 and SS-6712, for use on the formed acrylic sunroof for their 1984 Corvette. This represents the first significant entry for plastics into automotive transparencies in this country. Swedlow Inc. is currently in production of this article (Figure 10).

A number of aircraft transparencies coated with SS-6712 are also undergoing or will shortly begin flight testing. Included are various helicopter windshields (AH-1S, OH-58A, Bell XV15) and several cabin windows in 727 and 747 aircraft.

(1) US Patent 4,390,373

SS-6704 - A Way to Reduce In-Plane Fracturing of Stretched Acrylic

Premature failure of stretched acrylic transparencies has occurred due to "in-plane fracturing". These fractures normally begin as crazes in the peripheral edge surface of the window and propagate inward after a period of use. The fractures are usually oriented in the plane of the transparencies, due to the anisotropic nature of the multi-axially oriented material (Table 6). Fracturing may occur due to physical abuse or improper mounting; however, we suspect that moisture is the primary culprit. This is supported by the fact that in-plane fractures tend to occur much sooner in stretched acrylic transparencies which are exposed to high humidity environments.

We propose that moisture is absorbed and desorbed rapidly through the peripheral edge of the transparency, and that the volume of the transparency varies in accordance with its moisture content. When moisture is being absorbed into the transparency, a gradient is created with higher moisture content near the transparency's perihery. Thus the transparency's volume would be greater at its periphery and the edge surface would be in compression. When moisture is being desorbed, a gradient is created with higher moisture near the central portion of the transparency. In this case, the transparency's volume would be greatest near its center and its peripheral edge would be in tension. High internal stress at the edge surface is the exact strain which multi-axially oriented material is least able to withstand. (Figure 11)

As a consequence of these moisture gradient induced tensile stresses at the edge, the acrylic material relieves energy by initially forming crazes. These crazes further localize the stresses and subsequently generate into cracks. Because the tensile strength properties are weakest perpendicular to the direction of orientation, the fractures tend to stay in the plane of the window.

To overcome this problem, a moisture vapor barrier coating (SS-6704) was developed by Swedlow to reduce the transmission rate of water both into and out of the acrylic edge. SS-6704 possesses a water permeation rate considerably lower than acrylic sheet and the common window installation edge sealants (Table 7). By restricting the development of the moisture egress gradient, the potential tensile stresses are reduced and the crazing which leads to in-plane fracture can be greatly curtailed. The physical properties of SS-6704 are detailed in Table 8.

Extensive laboratory testing support these theories. Accelerated cyclic water immersion and high humidity tests with untreated cabin windows will induce catastropic in-plane fracture. Cabin windows coated about the peripheral edge with SS-6704 and exposed to these cyclic conditions exhibit no in-plane fracture (Figures 12,13, and 14).

In another comparison, stretched acrylic panels were equilibrated at 100% relative humidity/120°F for 13 days and then allowed to stand at 50% relative humidity/70°F. The samples with no (SS-6704) edge coating crazed and developed deep in-plane fractures within one day. The samples edge coated only with SS-6704 required more than 30 days to develop fine craze and did not display the stressed in-plane fracture after 45 days.

Stretched acrylic cabin windows with the SS-6704 edge coating[2] have now been in service for over 5000 hours on a Boeing 727 aircraft, with excellent results to date. The uncoated cabin windows exposed to the same flight conditions exhibit some fine edge crazing but no in-plane fracturing. This test is continuing and a similar comparative study has been initited in a 747 aircraft.

CONCLUSIONS

1. SS-6590 coated acrylic sheet provides outstanding resistance to abrasion and chemical attack based upon up to 8 years of service in architectual and ground transportation glazing installations.

2. SS-6590 coated acrylic windshields demonstrate high durability on unpressurized, general aviation and agricultural spray aircraft over several years flight exposure.

3. The SS-6590 coating appears to provide sufficient elongation to withstand cyclic pressurization loading based upon actual flight history.

4. Bullet resistant security compositions and bird strike resistant aircraft transparencies coated with Swedlow Inc.'s abrasion resistant coatings demonstrate high resistance to failure upon required impact.

5. The superior abrasion resistance of Swedlow's new SS-6712 coating was confirmed by several independent test facilities. Both the SS-6590 and SS-6712 coatings were selected over all other commercially available coatings for use on the 1984 Corvette sunroof by General Motors.

6. SS-6712 coated acrylic surpasses two years 45°S outdoor exposure in California and is now experiencing flight exposure on both pressurized and non-pressurized aircraft.

(2) (US Patent 4,377,611)

7. SS-6704 water vapor barrier edge coating dramatically reduces the occurrence of in-plane fracturing of stretched acrylic material under cyclic, moist environmental exposure conditions. Confirmation of this performance under actual flight conditions is being established.

8. In the near future, Swedlow Inc. plans to conduct flight testing of SS-6590, SS-6712, and SS-6704 coatings on acrylic commercial airline cockpit windows and fighter aircraft windshields.

TABLE 1

Market Introduction of AR Coated, Transparent Sheet

	Product	Producer	Year of Introduction	Coating Composition
(1)	AR Coated Acrylic Sheet			
	Abcite*	duPont	1970	Organo-silicate
	Lucite AR*	duPont	1974	Organo-silicate
	Acrivue A	Swedlow Inc.	1975	Silica-filled polysiloxane
	Acrivue SA	Swedlow Inc.	1975	Silica-filled polysiloxane
	Lucite SAR	duPont	1978	Silica-filled polysiloxane
(2)	AR Coated Polycarbonate Sheet			
	Lexan MR-4000	General Electric	1967	Melamine polyester
	Lexan MR-5000	General Electric	1976	Silica-filled polysiloxane
	Margard	General Electric	1979	Silica-filled polysiloxane
	Rowlex*	Rowland Industries	1975	Polysiloxane
	Tuffak CM	Rohm & Haas	1977	Polyurethane
	Tuffak CM-2	Rohm and Haas	1978	Silica-filled polysiloxane

*no longer commercially available

TABLE 2

Comparative Abrasion Resistance Performance

	Composition	Producer	Taber Abrasion Resistance[1] Δ Haze After 100 Cycles	500 Cycles	1000 Cycles
1.	Float Glass	-	1	2	3
2.	Acrylic Sheet				
	Uncoated	duPont, Polycast, PPG, Rohm & Haas, Swedlow, Inc.	32-38	-	-
	Acrivue A, SA	Swedlow Inc.	1	6	8
	Lucite AR	duPont	6	25	45
	Lucite SAR	duPont	2	7	10
3.	Polycarbonate Sheet				
	Uncoated	General Electric, Rohm & Haas	38-50	-	-
	Lexan MR-4000	General Electric	6	28	-
	Lexan MR-5000	General Electric	3	7	-
	Margard	General Electric	3	8	-
	Tuffak CM	Rohm & Haas	5	30	56
	Tuffak CM-2	Rohm & Haas	4	25	-

[1] ASTMD-1044, CS-10F wheels, 500 gm. load

TABLE 3

Performance of SS-6590 Coated Cessna AG-180 Windshield After 3 Spray Seasons

	Initial Witness Plate	Returned Windshield 440 Flight Hrs.
Light Transmittance, %	94.3	93.6
Haze	0.2	2.1
Coating Adhesion, %	100	100
Taber Abrasion Resistance[1]		
Δ Haze after 100 cycles	1.9	1.8
500 cycles	6.7	7.8

[1] ASTMD-1044, CS-10F wheels, 500 gm. load

TABLE 4

Load Determination for Pressure Testing

The fuselage was pressure cycle tested 30,000 cycles to demonstrate fatigue strength in accordance with CAR 3.270(a). Repeated service loads are defined as follows:

Normal operating pressure differential	=	5.5 psi
Relief valve	=	5.65 ± .05 psi
External aerodynamic pressure	=	0.5 psi
Flight load increment (+1. 0 g ballast)	=	0.5 psi
Fatigue cycle pressure:		
Normal operating + external aero + flight increment	=	6.5 psi

A 1.0 g fuselage loading, corresponding to approximately a 9474 lb. loading at 137.0 inches, was maintained during cycling. This loading was applied with ballast.

Following completion of the cyclic test series and the required fuselage static tests, an ultimate pressure test was conducted to demonstrate compliance with CAR 3.396(a).

The required ultimate pressure differential, as specified in CAR 3.197(c) is:

Ult. Pressure = (5.65 + 0.05) (1.33) (1.5) = 11.4 psi

TABLE 5

Chemical Resistance of Uncoated and Coated Acrylic

Chemical	Uncoated Acrylic Sheet*	SS-6590 Coated Acrylic Sheet*	SS-6712 Coated Acrylic Sheet*
Benzene	A	NA	NA
Toluene	A	NA	NA
Xylene	A	NA	NA
Methylene chloride	A	NA	NA
Chloroform	A	NA	NA
Trichloroethylene	A	NA	NA
Acetone	A	NA	NA
Methyl ethyl ketone	A	NA	NA
Ethyl acetate	A	NA	NA
Butylamine	A	NA	NA
Methanol	NA	NA	NA
Ethanol	NA	NA	NA
Isopropanol	NA	NA	NA
Acetic acid	A	NA	NA
Sulfuric acid(40%)	A	NA	NA
Ethylene glycol	NA	NA	NA
Motor oil	NA	NA	NA
Gasoline	NA	NA	NA
Diesel fuel	NA	NA	NA

*Acrivue S-310 (unannealed MIL-P-5425 acrylic sheet)

A = attacked NA = no attack

Each test performed by vigorously rubbing the surface of the material for 20 seconds with a cloth saturated with the chemical, followed by drying with a clean cloth.

TABLE 6

Properties of MIL-P-25690 Stretched Acrylic vs. Orientation Direction

Stretch Orientation Direction	Fracture Propagation Resistance K Value($lbs/in^{3/2}$)	Tensile Strength (lbs/in^2)
Perpendicular	3700	11,000
Parallel (in plane)	440	4,000

TABLE 7

Water Vapor Permeation Rates of Polymers*

Polymer	Water Vapor Permeation Rate ($Kg.cm/Km^2 \cdot day$) at 38°C- 100% RH
Polyvinylidene chloride**	8
Polytetrafluoroethylene, Teflon	10
Chlorinated polyether, Penton	20
Polyvinylidene fluoride, Kynar	39
Polyethylene	20-60
Polyvinyl chloride	90-120
Butyl rubber	80
Polyethylene terephthalate	80-160
Neoprene	200
Nitrile elastomers	200-240
Polymethyl methacrylate	470
Polycarbonate	550
Silicone	1970
Polyurethane	4800
Cellulosic	14,000

* Kirk-Othmer - Encyclopedia of Chemical Technology, Volume 3, Third Edition, 1978, pg. 480-502, John Wiley and Sons.

** SS-6704 is a polyvinylidene chloride based resin formulation.

TABLE 8

Typical Properties of SS-6704 Film

Property	Value	Test Method
Tensile Strength	1640 psi	ASTM D-882
Tensile Elongation	250%	ASTM D-882
Tensile Modulus	1152 psi	ASTM D-882
Tear Strength	260 lbs/in	ASTM D-1004
T_g	20°C	ASTM D-3418
Adhesion to Acrylic Sheet	100%	Crosshatch/tape (3M-600) pull procedure

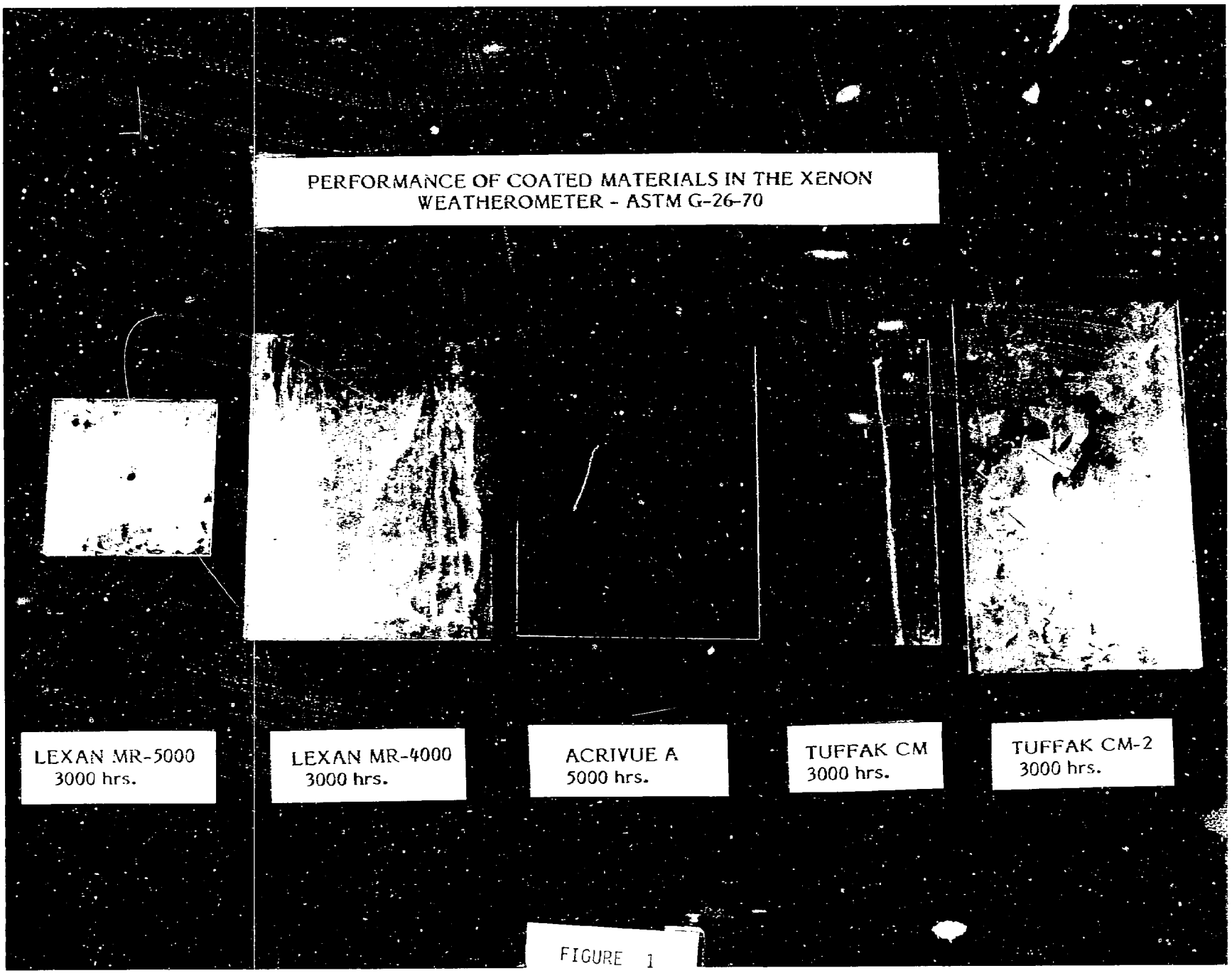
PERFORMANCE OF COATED MATERIALS IN THE XENON WEATHEROMETER - ASTM G-26-70
LEXAN MR-5000
3000 hrs.
LEXAN MR-4000
3000 hrs.
ACRIVUE A
5000 hrs.
TUFFAK CM
3000 hrs.
TUFFAK CM-2
3000 hrs.

FIGURE 1

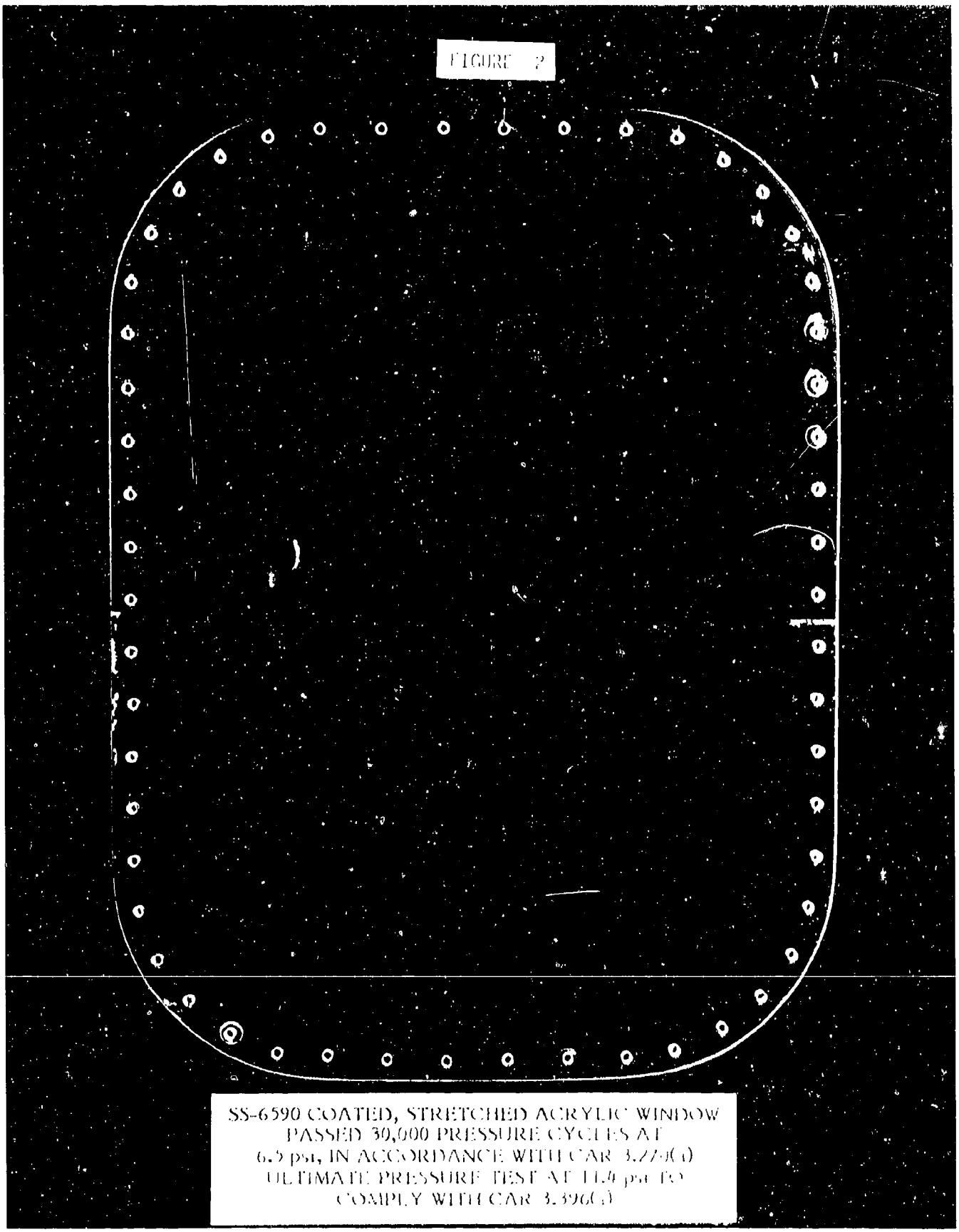

SS-6590 COATED, STRETCHED ACRYLIC WINDOW
PASSED 30,000 PRESSURE CYCLES AT
6.5 psi, IN ACCORDANCE WITH CAR 3.270(d)
ULTIMATE PRESSURE TEST AT 11.4 psi TO
COMPLY WITH CAR 3.396(a)

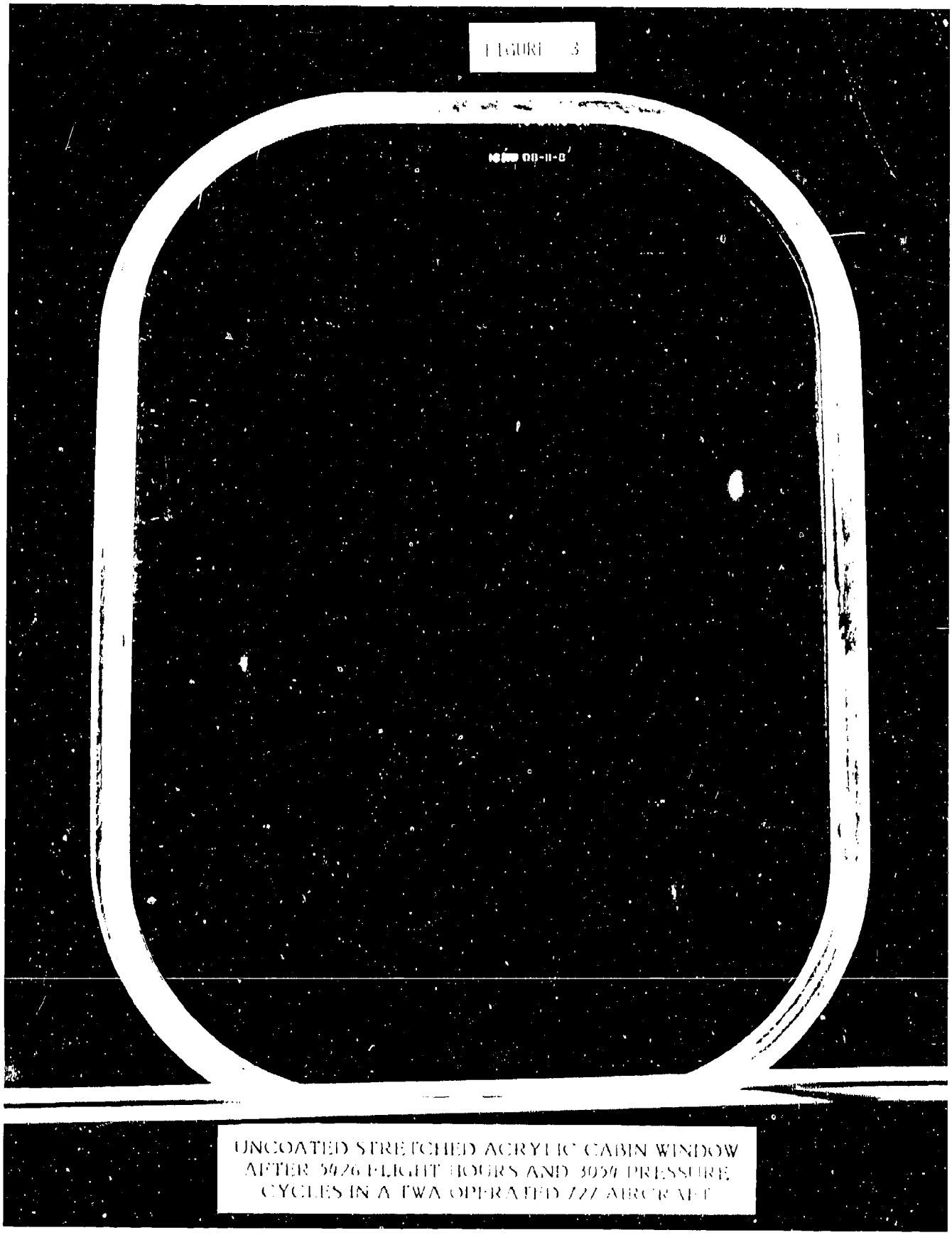

UNCOATED STRETCHED ACRYLIC CABIN WINDOW AFTER 5926 FLIGHT HOURS AND 3054 PRESSURE CYCLES IN A TWA OPERATED 727 AIRCRAFT

FIGURE 4

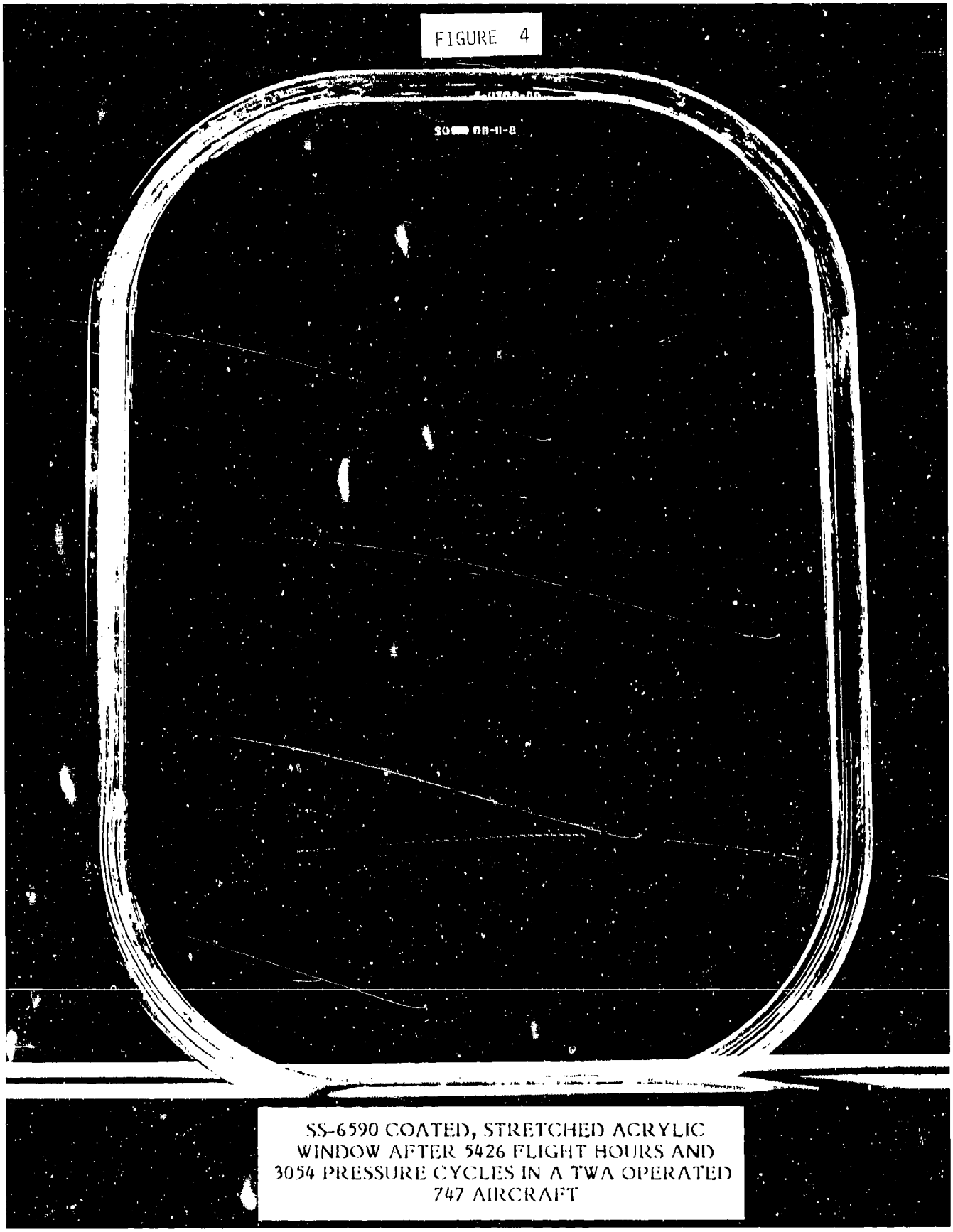

SS-6590 COATED, STRETCHED ACRYLIC WINDOW AFTER 5426 FLIGHT HOURS AND 3054 PRESSURE CYCLES IN A TWA OPERATED 747 AIRCRAFT

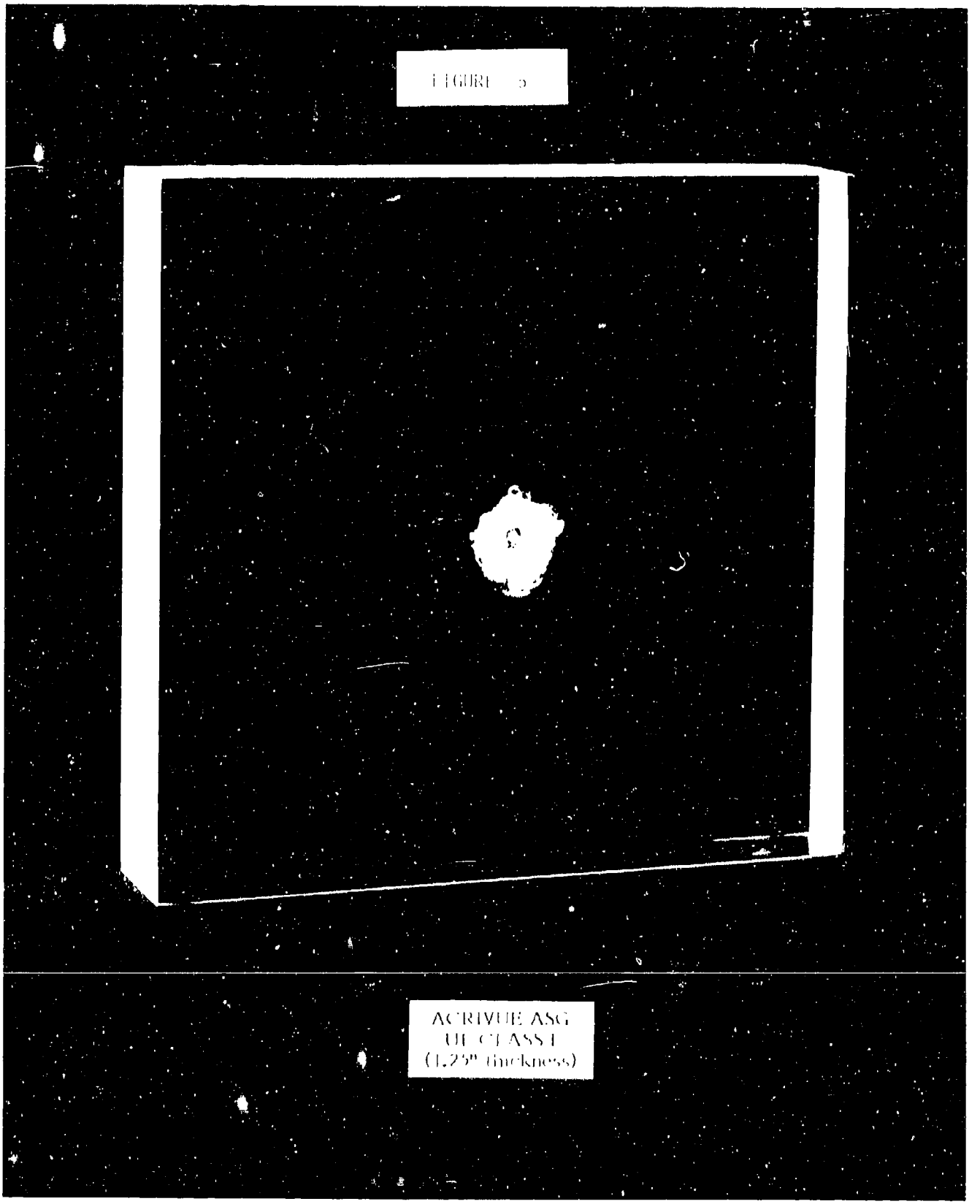
FIGURE 5
ACRIVUE ASG
UE CLASS I
(1.25" thickness)

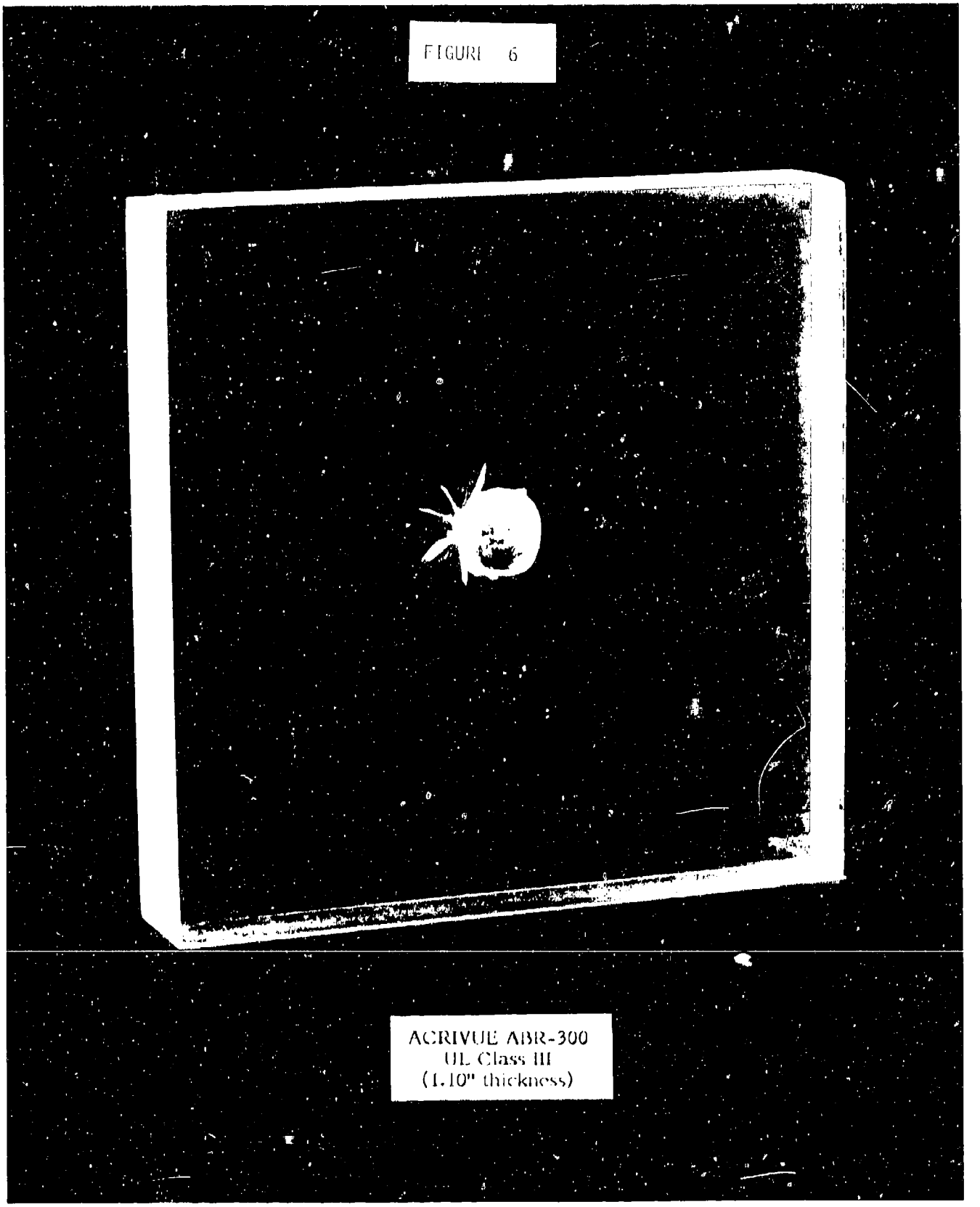
FIGURE 6
ACRIVUE ABR-300
UL Class III
(1.10" thickness)

FIGURE 7

ACRIVUE ABR-300L
DESIGNED TO DEFEAT HIGH VELOCITY
FRAGMENT PROJECTILES

FIGURE 8

TABER ABRASION RESISTANCE OF COATED MATERIALS
ASTMD-1044, CS-10F wheels, 500gm. loading, (Results determined by U.S. Testing Co.)

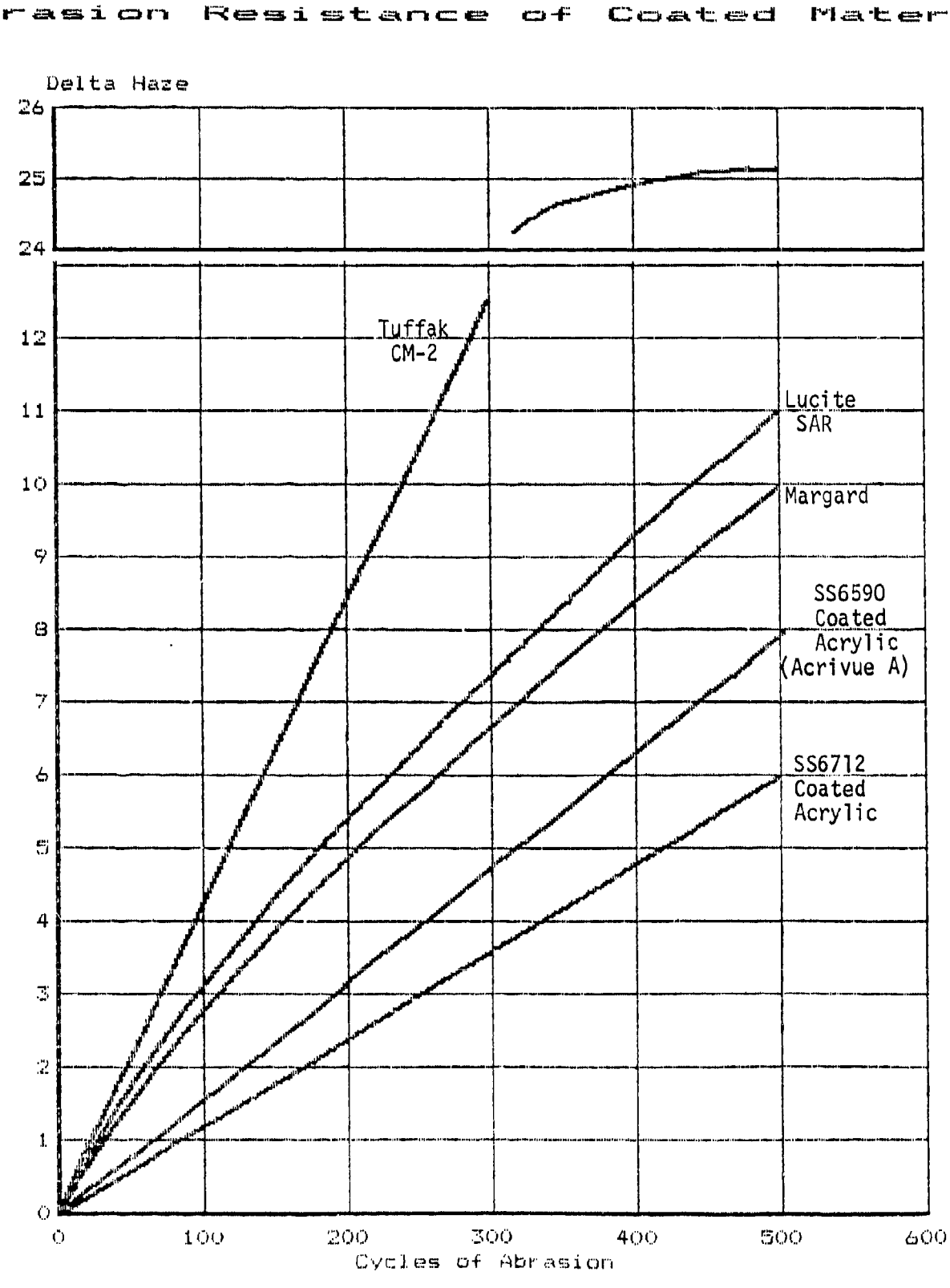

FIGURE 9

DEGREE OF SCRATCHING vs. RUBBING WITH STEEL WOOL

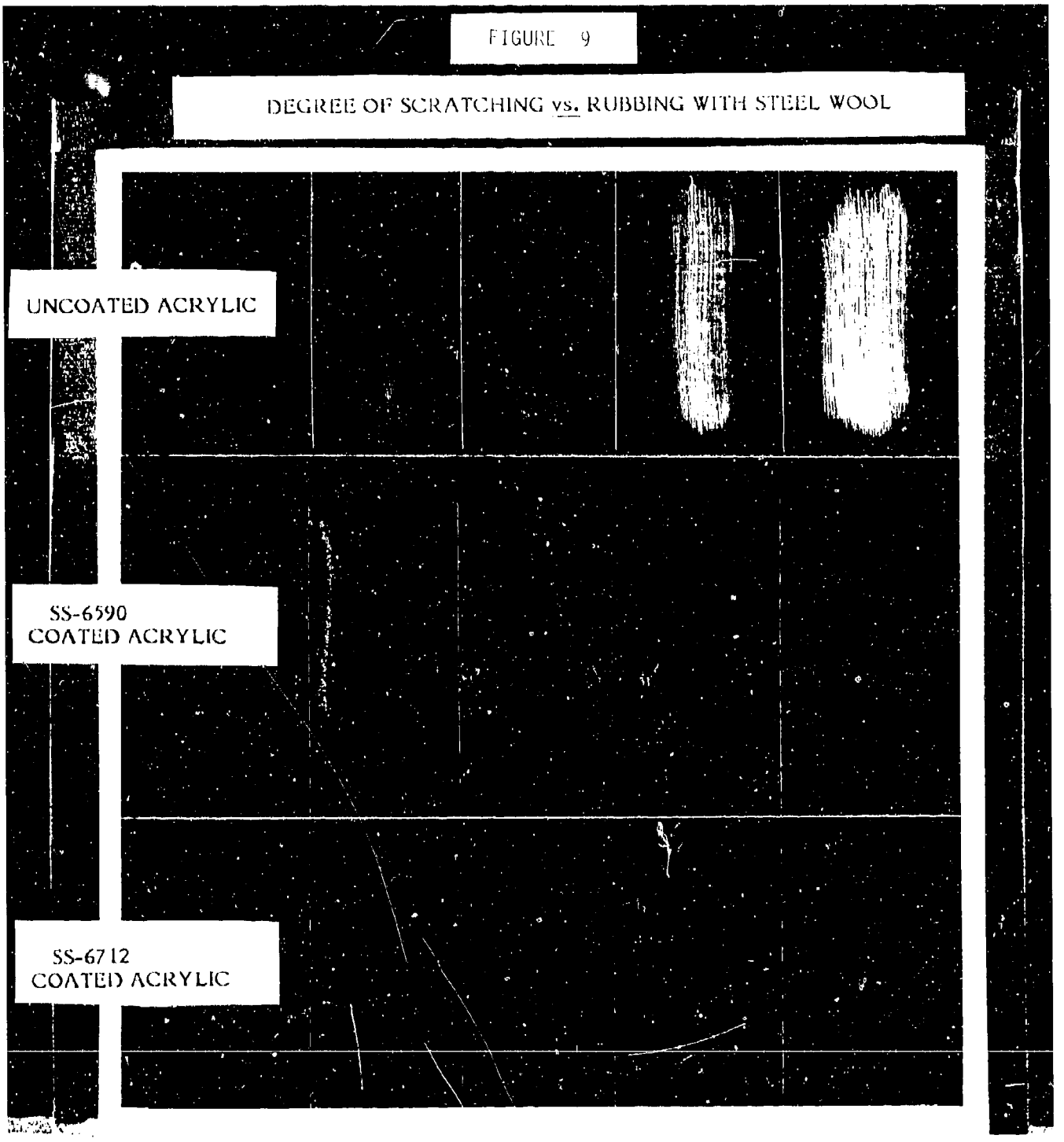

Grade 0000 (extra fine) | Grade 00 (fine) | Grade 1 (medium) | Grade 3 (coarse)

FIGURE 10

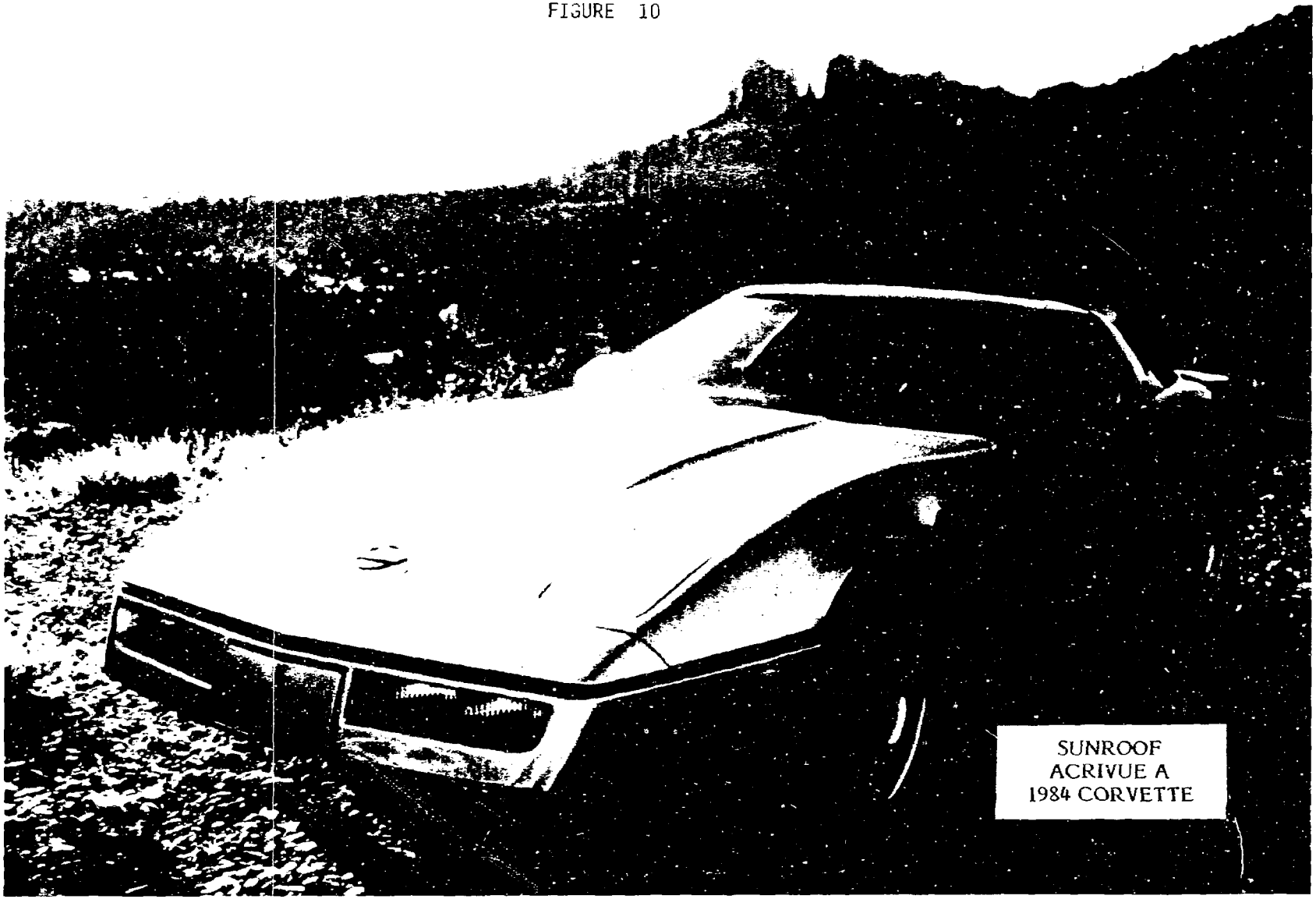

FIGURE 11

STRESS DIFFERENTIAL IN STRETCHED ACRYLIC INDUCED BY MOISTURE ABSORPTION/DESORPTION

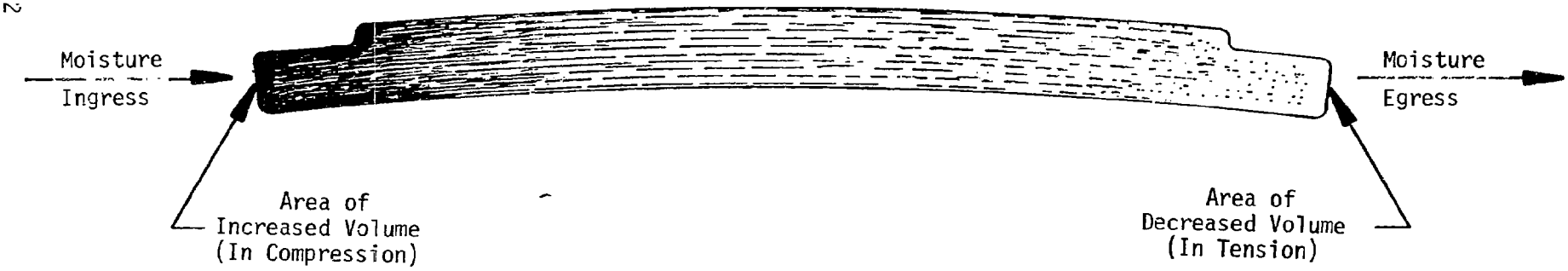

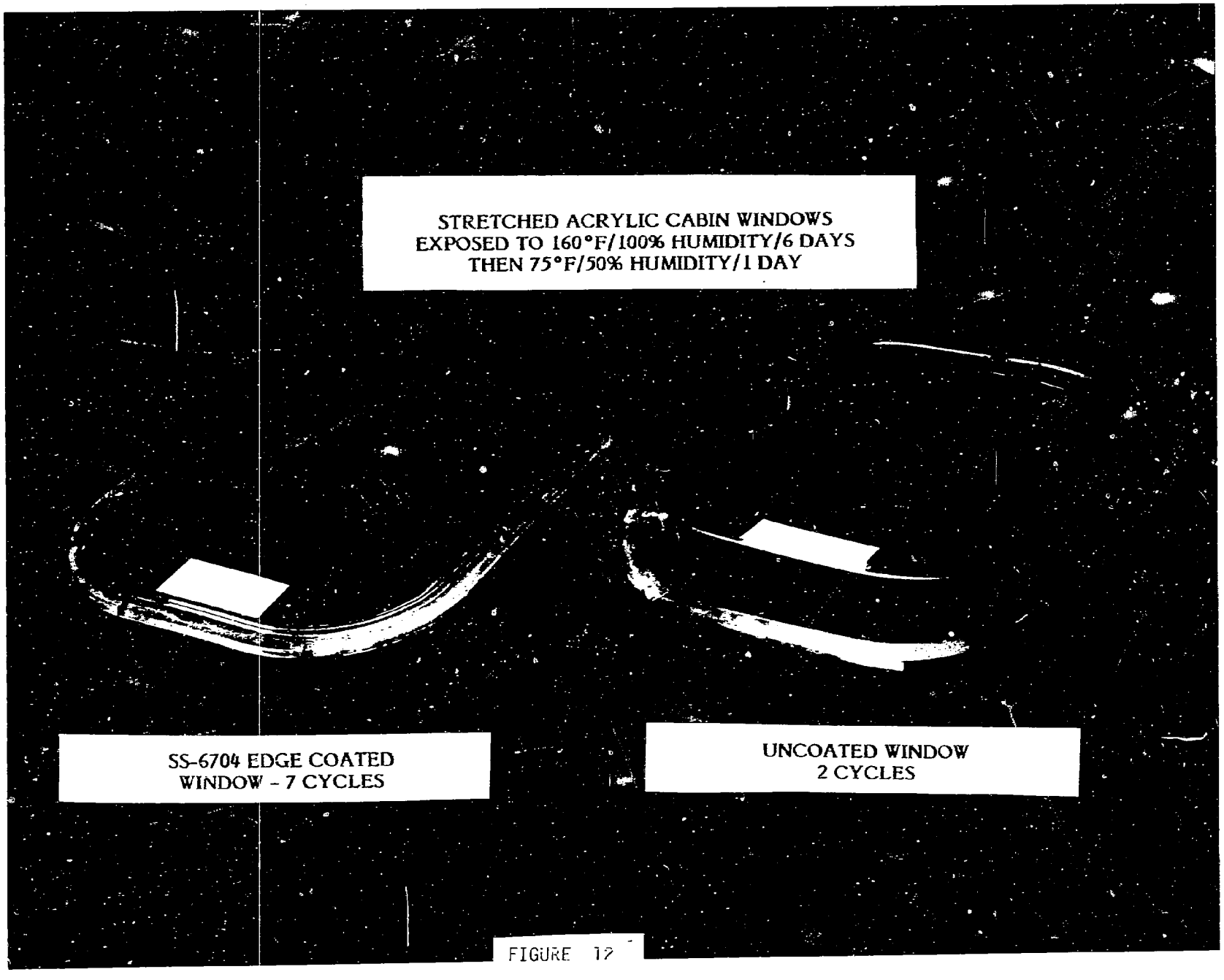
STRETCHED ACRYLIC CABIN WINDOWS
EXPOSED TO 160°F/100% HUMIDITY/6 DAYS
THEN 75°F/50% HUMIDITY/1 DAY
SS-6704 EDGE COATED
WINDOW - 7 CYCLES
UNCOATED WINDOW
2 CYCLES

FIGURE 12

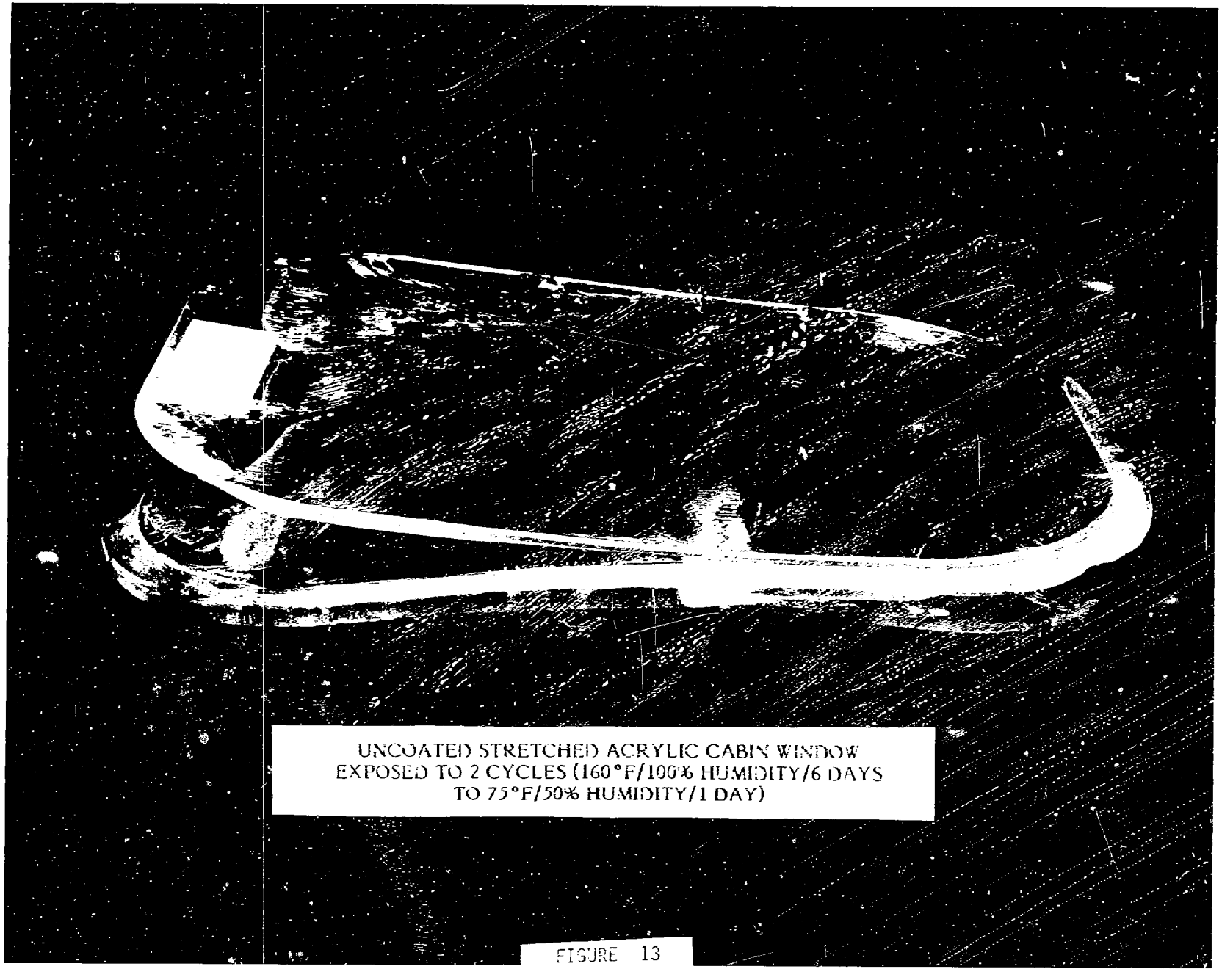

UNCOATED STRETCHED ACRYLIC CABIN WINDOW
EXPOSED TO 2 CYCLES (160°F/100% HUMIDITY/6 DAYS
TO 75°F/50% HUMIDITY/1 DAY)

FIGURE 13

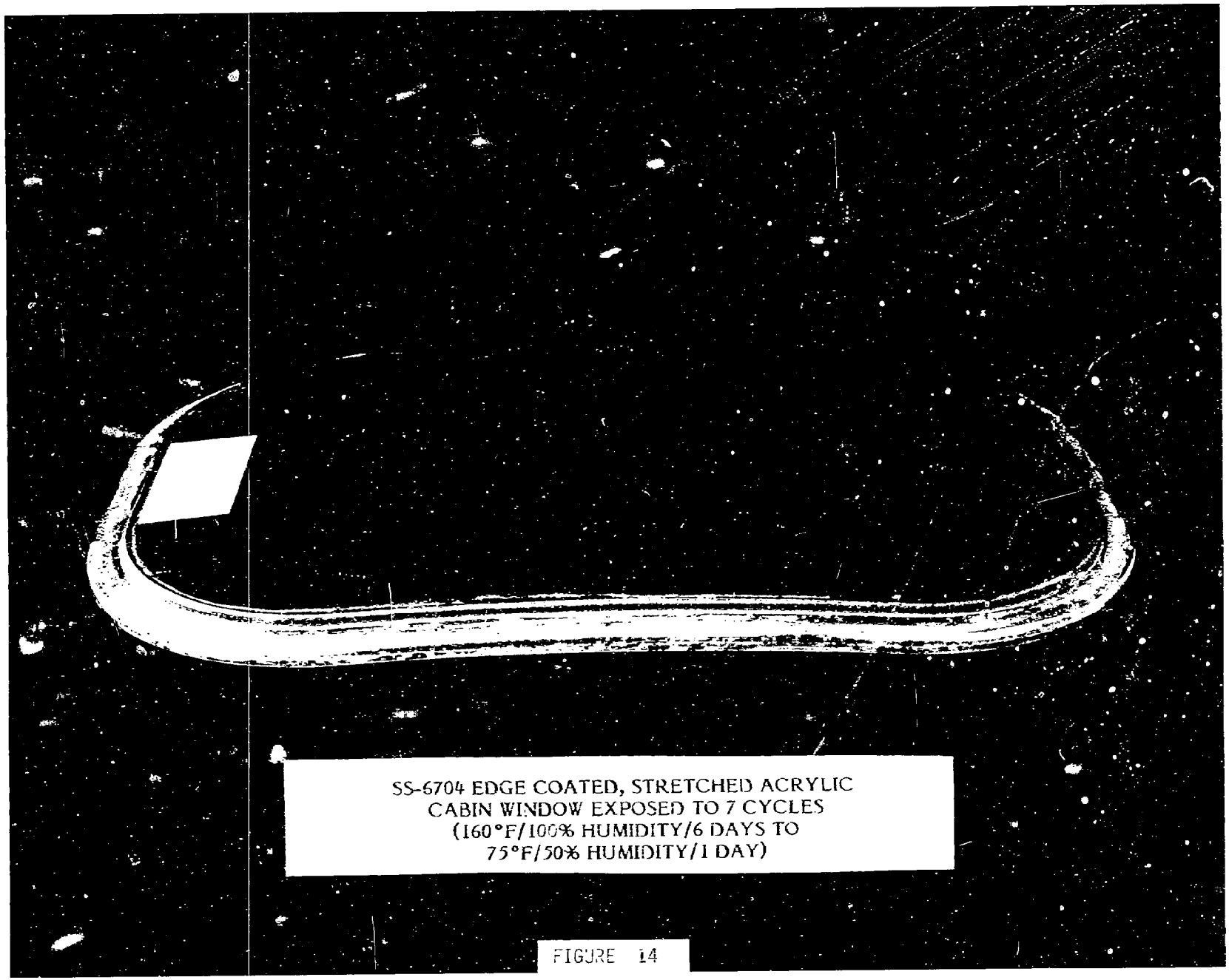

SS-6704 EDGE COATED, STRETCHED ACRYLIC
CABIN WINDOW EXPOSED TO 7 CYCLES
(160°F/100% HUMIDITY/6 DAYS TO
75°F/50% HUMIDITY/1 DAY)

FIGURE 14

SESSION IV

TESTING - CAPABILITIES AND LIMITATIONS (PART I)

Chairman: J. W. Kozmata
Douglas Aircraft Company
Long Beach, California

Co-Chairman: R. H. Walker
Flight Dynamics Laboratory
Wright-Patterson
Air Force Base, Ohio

AD-P003 207

IN-FLIGHT MEASUREMENT OF PRESSURE DISTRIBUTION OVER T-38 STUDENT CANOPY

W. R. Pinnell,
Flight Dynamics Laboratory

IN-FLIGHT MEASUREMENT OF PRESSURE DISTRIBUTION

OVER T-38 STUDENT CANOPY

a paper prepared by

William R. Pinnell
Air Force Wright Aeronautical Laboratories
AFWAL/FIER
Wright-Patterson Air Force Base, Ohio 45433

for presentation at the

Conference on Aerospace Transparent Materials and Enclosures
11-14 July 1983
Phoenix, Arizona

ABSTRACT

As part of a current in-house effort supporting the development of bird impact resistant transparencies for T-38 aircraft, a system for measuring aerodynamic pressure distribution over a T-38 student canopy has been developed. Static pressures were measured at 103 positions on the canopy of an aircraft in flight. Flight conditions included speeds in the range from 50 (taxi) to 500 knots, 5 degree side slip, and stalled flight. The paper includes a description of the in-flight recording system, the utilization of a microcomputer and software for data reduction and analysis, and test results.

This concept of testing and measurement is believed to be unique and to have potential application to other transparency testing including measurement of in-flight loads and temperatures.

In-Flight Measurement of Pressure Distribution Over T-38 Student Canopy

BACKGROUND

The US Air Force Wright Aeronautical Laboratories, Flight Dynamics Laboratory is currently sponsoring an effort to develop bird impact resistant transparencies for T-38 aircraft. The objective of this effort is to develop transparencies which will resist 400 knot impacts with birds weighing up to 4 pounds to the extent that the flight crew could recover the aircraft subsequent to the impact. Of the four transparencies which make up the T-38 set, only one, the student (forward) canopy has been included in the effort reported here.

The student canopy forms the outer fuselage mold line from the aft arch of the forward windshield to the forward arch of the instructor canopy . Figure 1 depicts the T-38 transparency arrangement. The frontal area presented by the student canopy is seen in Figure 2.

Currently, T-38 aircraft fly with stretched acrylic student canopies .23 inches thick. This transparency offers very little bird impact resistance. An example case occurred 6 May 1983 at Sheppard AFB when a 2½ pound hawk impacted a T-38 student canopy at about 280 knots (the bird carcass and the aircraft were subsequently recovered) . The student canopy failed in this incident as indicated in Figure 3.

The thin acrylic canopy currently on the T-38 does, however, allow the student pilot to eject through the canopy in cases where the canopy jettisoning system fails to remove the canopy. Additionally, the pilot can effect emergency ground egress by manually chopping through the acrylic material using a tool provided in the cockpit. A requirement for replacement anopies imposed by T-38 using commands is to preserve the capability to eject the pilot from the aircraft in cases where the canopy cannot be removed. Transparent materials with toughness required to defeat 400 knot impacts with four pound birds can also be expected to offer significant resistance to the ejection seat and pilot's body. For this reason it is anticipated that some system for removing that portion of the transparency in the path of the ejection seat and the pilot's body will have to be included in the design of replacement canopies.

Effecting emergency escape with a canopy in place on other aircraft has generally included cutting or breaking the canopy into segments. These techniques lead to the strong possibility of severe injury to the escaping pilot caused by canopy sections or shards impacting the pilot's body or critical equipment (parachute, breathing apparatus, face shield, etc). Development efforts for thru-the-canopy ejection capability for A-7 and TA-7 aircraft were complicated by these problems and pointed to the desirability of a knowledge of canopy external pressure distribution.

When considering transparency removal techniques, particularly those which include cutting or partial cutting of the transparent panel into

FIGURE 1 T-38 TRANSPARENCY ARRANGEMENT

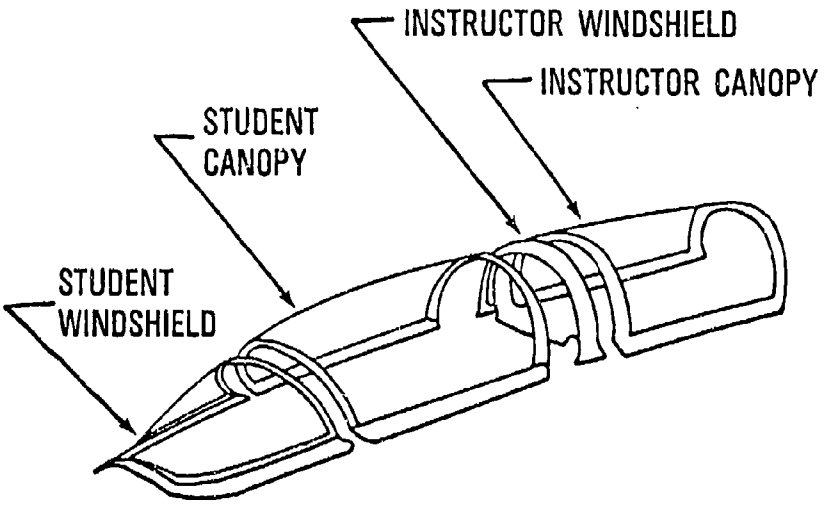

FIGURE 2 STUDENT CANOPY PROJECTED FRONTAL AREA

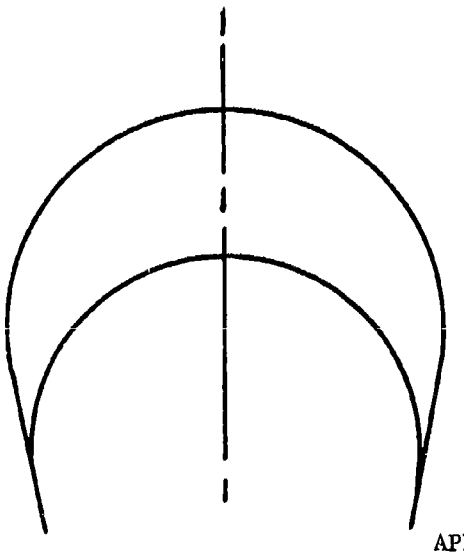

FIGURE 3

BIRD IMPACTED T-38

STUDENT CANOPY

(AND BIRD)

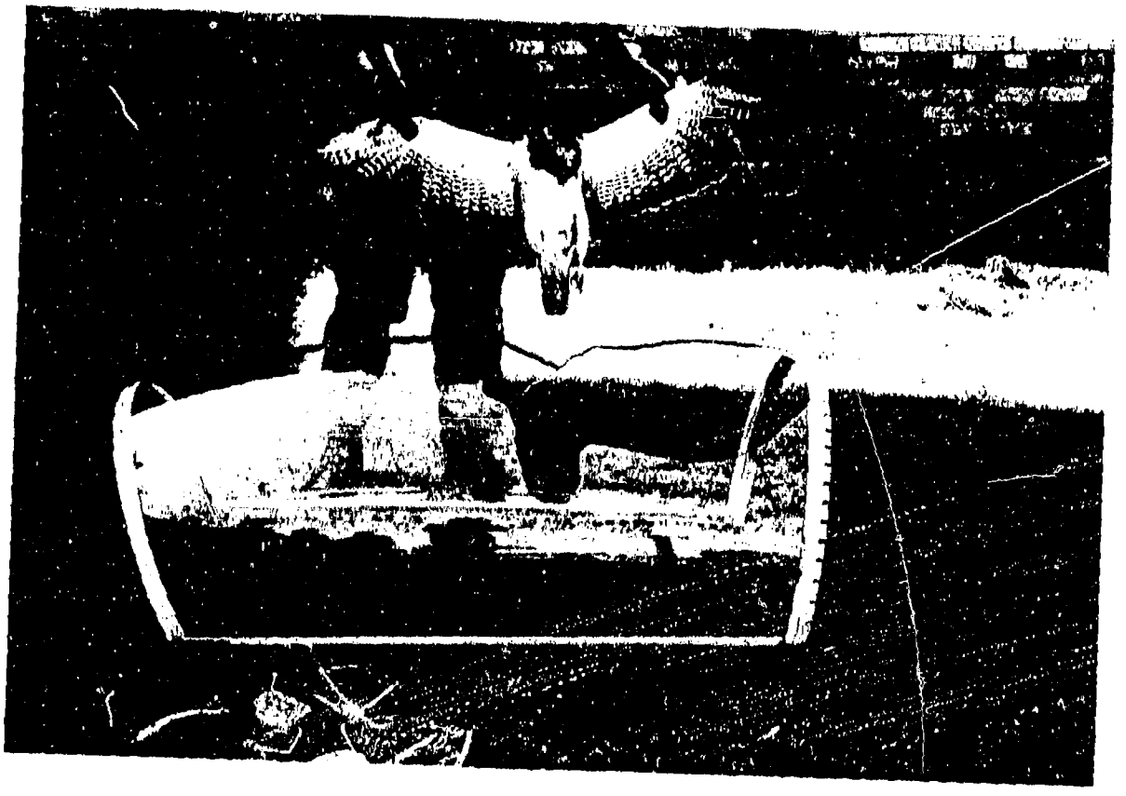

2½ LB BIRD

280 KIAS

SHEPPARD AFB MAY 1983

sections, a knowledge of the pressure loading and distribution of this loading over the canopy is necessary. Loading on the canopy is the combination of pressure on the inside surface or cabin pressure, and the aerodynamic pressures on the external surface. The cabin pressure can be assumed to be evenly distributed over the canopy inside surface while the external pressure and the distribution of this pressure is dependent upon flight conditions and aircraft attitude. The purpose of the effort reported in this paper is to measure the magnitude and distribution of the external pressures over the T-38 student canopy surface over a range of flight conditions representative of the aircraft escape system operational envelope.

APPROACH

In order to obtain directly applicable data economically, external pressures were continuously recorded on-board a T-38 aircraft as the aircraft was flown at various flight conditions in accordance with a pre-determined test plan. One hundred and three static pressure ports were formed by drilling holes normal to the canopy surface. An on-board recording system was designed and fabricated specifically for this purpose. The recording system was located inside the survival kit which normally contains emergency survival gear which is ejected with the ejection seat and pilot. One sixteenth inch diameter vinyl tubing was used to connect each pressure port to a scanning valve within the survival kit container. Recorded data on a magnetic tape was read into a ground based microcomputer subsequent to each flight. Data were automatically processed by the portable microcomputer on the flight line to indicate data quality prior to the next flight. The microcomputer further processed measured data producing static pressure at each canopy port for time periods during which the aircraft was flown at desired flight conditions. Cabin pressure was also monitored by the recording system and the microcomputer program had options for output of differential pressure, pressure coefficient, and plots of these parameters over the canopy surface. Figure 4 is a schematic representation of the data measuring and processing system.

A specially prepared student canopy incorporating 103 static pressure ports was installed on a T-38 aircraft currently operated by SA ALC/MM. The normal survival kit was replaced in this aircraft with the data recording system housed in a survival kit container. Vinyl tubing was arranged into two bundles leading upward from the aft corners of the survival kit container to the canopy frame sills where each bundle was clamped. From this clamp, tubing was routed to individual pressure ports and secured to the canopy inside surface with clear tape. Routing of tubing was selected to minimize obstructions to the vision of the aircrew. Installation of the modified canopy is shown in Figure 5.

In the interest of economy the on-board system was designed for minimal aircraft modification and in the interest of flying safety, the system was designed to permit retention of the full (2 pilots) aircrew.

DATA RECORDING SYSTEM

Pressure tubing leading from 103 canopy ports was connected to three

FIGURE 4

DATA MEASURING AND PROCESSING SCHEMATIC

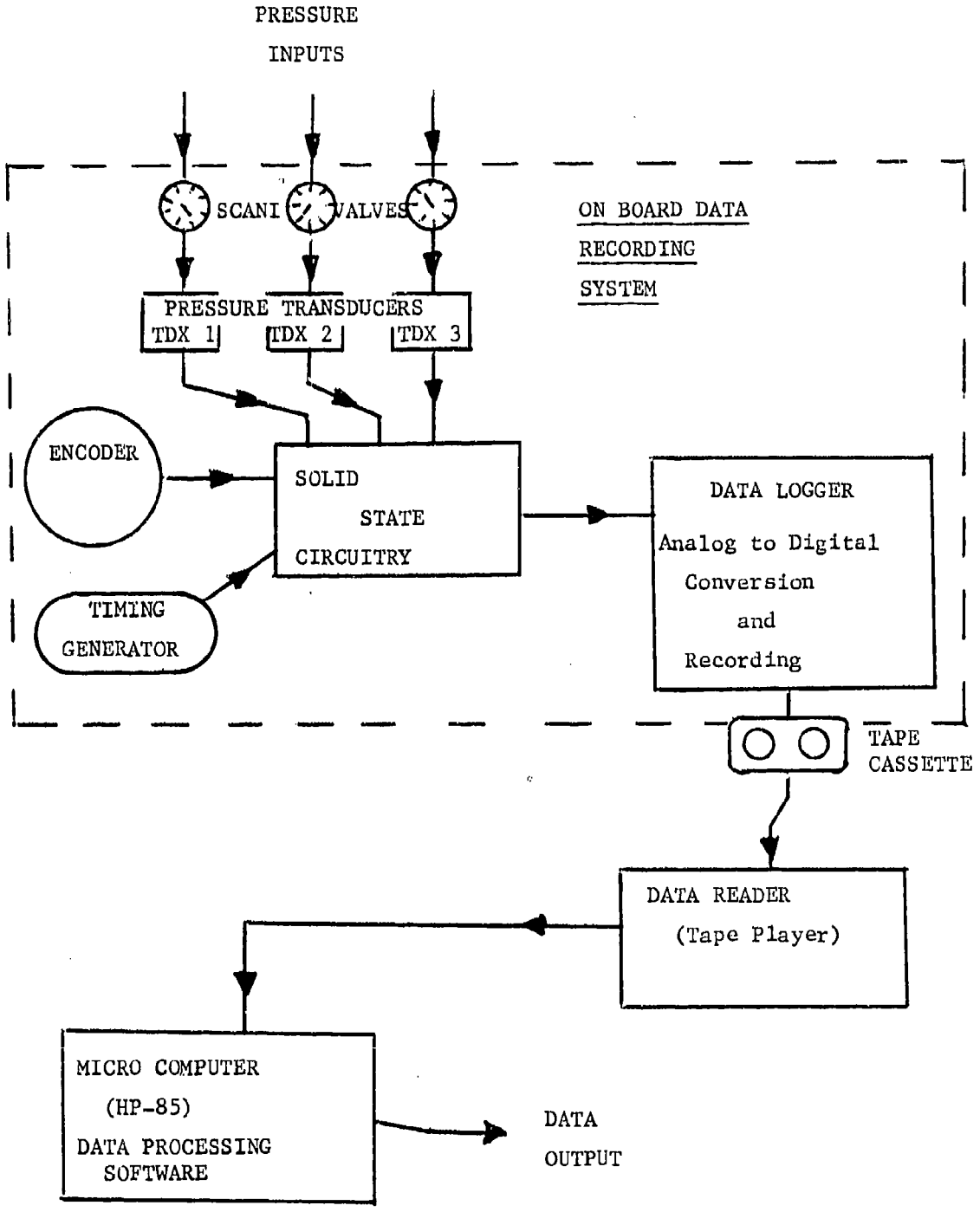

FIGURE 5

T-38 STUDENT CANOPY
FOR MEASUREMENT OF
IN FLIGHT PRESSURE DISTRIBUTION

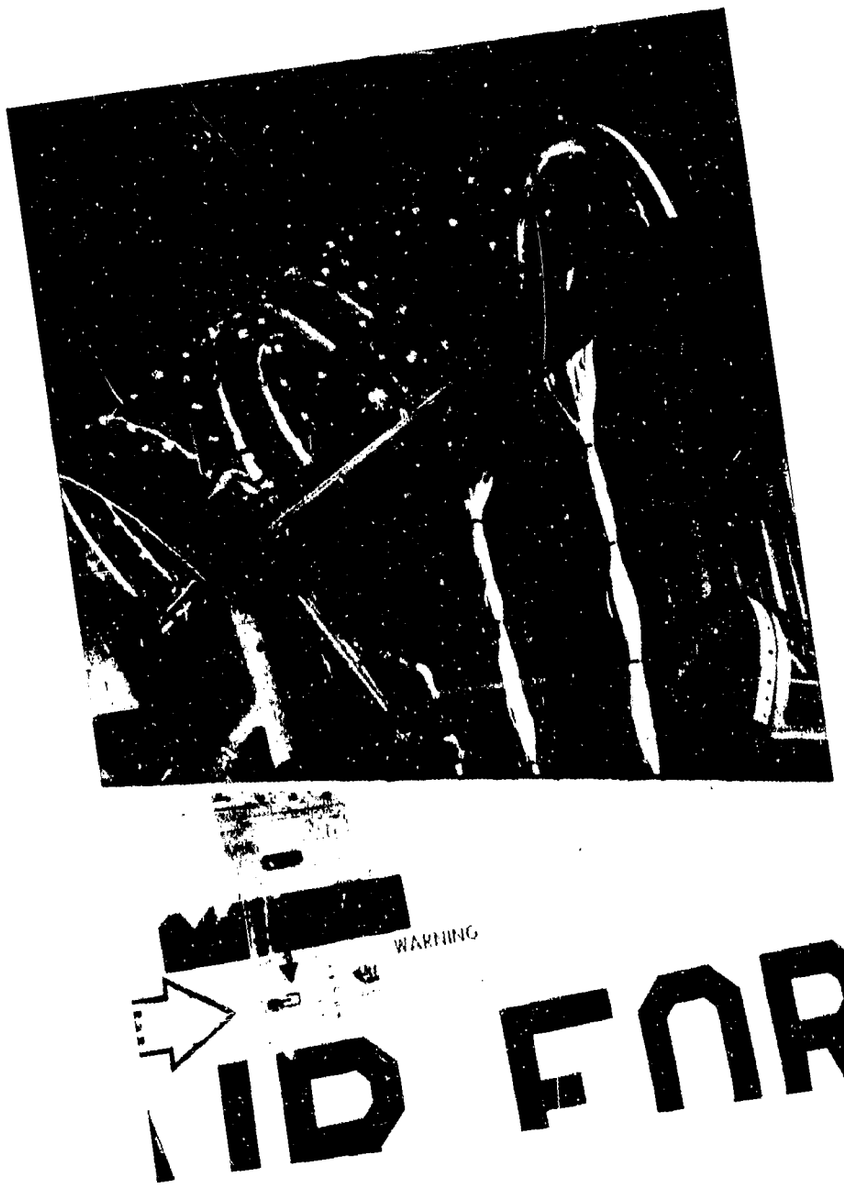

scanning valves (Reference 1) which sequentially connect these tubes to pressure transducers. Analog output from the pressure transducers was fed into solid state circuity which generated a serial data format including order and sequencing of data samples, and time from an initial start signal. This formulated data was input into a miniature data logger (Reference 2) which converted the multiplexed analog data to digital data which was recorded on magnetic tape (Refer to Figure 4).

The recording system was powered by the aircraft 28 volt DC system. When the aircraft engines were not running, power originated from a ground power unit normally utilized with T-38 aircraft. The recording system included voltage regulation circuits.

The elapsed time for the data recording cycle to repeat was approximately 30 seconds. To evaluate possible changes in data in the 30 second recording period, three pressure ports were manifolded to three scanning valve ports so that the selected pressure would be sampled near the beginning, middle, and end of the data recording cycle. This technique can be used to derive a time dependent correction function which could be applied to the data from all pressure ports in accordance with the order in which data was recorded.

Tape cassettes were taken from the on board system after each flight. A data reader programmed for the data logger format was used to read the data from tapes. Output from the data reader was input into a microcomputer and processed to produce pressure data utilizing software prepared to account for transducer calibration, pressure port manifolding, and transducer pressure reference values.

A time schedule of flight conditions was recorded by one of the aircraft pilots in the form of manual notes and on a voice recorder. This schedule was synchronized with the recorded data utilizing time data recorded in each recording period.

TEST PROGRAM

A test plan was generated which provided for successive increases in test condition severity and programmed fuel consumption to yield the maximum number of test conditions per aircraft flight. Test conditions for which data were measured are indicated in Table 1.

Preflight activities included balancing of pressure transducer circuits, recording system mechanical checks, tape cassette installation, establishing the on-board pressure reference, recording of calibration data and, synchronization of recording system time and aircraft clocks. After the time synchronization activity, the recording system ran continuously throughout the flight and until after deplaning of the aircrew. The recording system preflight activities utilized ground power which was switched to aircraft power after the aircraft engines were started. Ground power was applied to the aircraft system after each flight before engine shut-down so that the recording system could run continuously until post flight calibrations and time synchronization were achieved.

When the aircraft attained the scheduled flight conditions, the aft seat pilot actuated a momentary switch which effected an indication in the recorded data. The aft seat pilot noted flight conditions and the time of switch actuation on a manually written card and on a voice recorder. The flight conditions were then maintained by the front seat pilot for a minimum of 45 seconds. The aft pilot then recorded the end of the test interval and flight conditions were adjusted to the next scheduled test point.

DATA PROCESSING

Output from pressure transducers and the recording system timing circuit recorded on-board was read from a tape cassette and automatically input into the ground based microcomputer where the data processing was accomplished.

Figure 6 shows the schematic arrangement of the pressure measuring devices. The recording system/reader yielded digital values for each scanning value tube. Previously generated calibration functions for the pressure transducers were used to calculate pressures across pressure transducers as follows:

$$\text{Pressure (psi)} = \frac{\text{Digital Value} - 2054}{206} \qquad \text{(EQN 1)}$$

Since the reference side of each pressure transducer was left open to the cockpit (cabin pressure R2), and since the pressure in the on-board reference bottle R1 (see Figure 6) was known, the cabin pressure was obtained using the following relationship:

$$R2 = R1 - \frac{(\text{Average Digital Values Ref Bottle Tubes}) - 2054}{206} \qquad \text{(EQN 2)}$$

For a typical pressure port, then, the external pressure P(I) (I from 1 to 103 identifying a specific canopy pressure port) is found using

$$P(I) = \frac{A(I) - 2054}{206} + R2 \qquad \text{(EQN 3)}$$

where A(I) is the digital value recorded by the system for a specific pressure port. When ports were manifolded to more than one scanning valve tube, A(I) represented the average of digital values recorded for this port. If manifolded scanning tube digital values indicated a significant change during the recording period, all A(I) values could be adjusted using a linear time function derived from the three manifolded values.

Equations 1, 2, and 3 reflect the algebraic sign convention indicated in Figure 6. The differential pressure across the canopy transparency thickness is then

$$\text{Differential Pressure at Port I} = P(I) - R2 \qquad \text{(EQN 4)}$$

FIGURE 6 PRESSURE MEASURING ARRANGEMENT

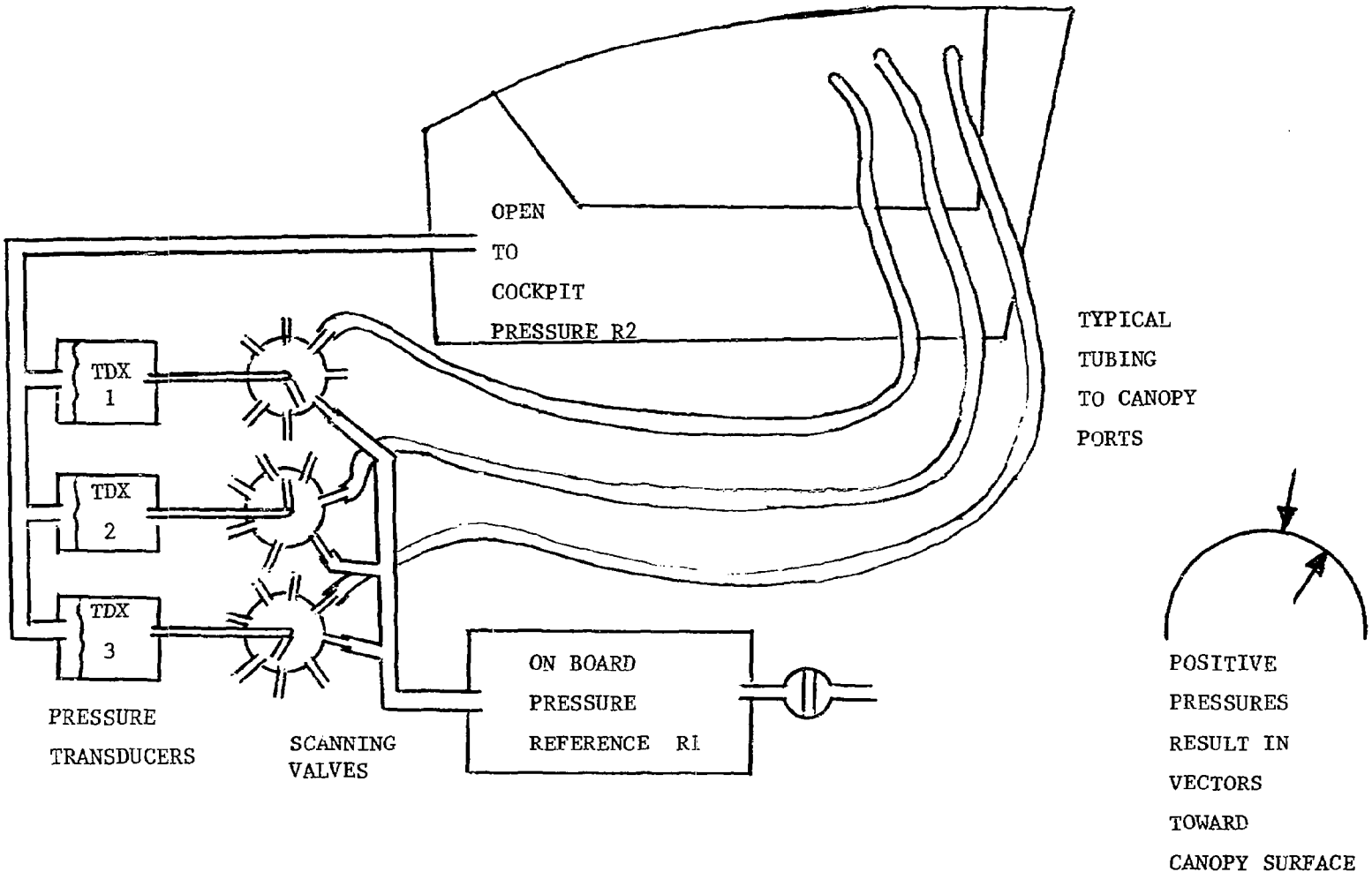

If pressure coefficient is defined as

$$CP = \text{Pressure Coefficient} = \frac{\text{Local Static Pressure} - \text{Free Stream Static Pressure}}{.7\ (\text{Free Stream Static Pressure})(\text{Mach No Squared})}$$

then

$$C_P = \frac{P(I) - P}{.7 \times P \times M^2} \qquad \text{(EQN 5)}$$

Where P is free stream static pressure based on standard conditions and altitude and M is Mach number based on flight velocity and standard day conditions for the test altitude.

RESULTS

For flight conditions included in Table 1, the external pressure at each of 103 static ports in the outside canopy surface was measured. Data representative of test results are included in this paper. A more thorough treatment of the test results and a complete collection of the data will be included in a forthcoming technical report. Figure 7 is a flattened representation of the canopy showing pressure port locations. Data are presented for the pressure ports in lists, plots along longitudinal lines (centerline and angles from the centerline) and lateral or cross-wise plots (parallel to the canted forward edge and at fuselage stations). Pressure data included in this paper are absolute pressure values in psi. Pressure in the cockpit (cabin pressure), flight conditions, and ground level barometric pressure and temperature are also reported.

Flight conditions were obtained as follows:

Altitude - (Ft MSL) as read by pilots from the aircraft altimeter.

Indicated Airspeed - (Knots) as read by pilots from cockpit airspeed indicators. Readings varied from nominal test values by as much as 5 knots.

Mach Number - Calculated values based on nominal test plan indicated airspeeds and standard day conditions at nominal test altitudes.

Free Stream Static Pressure - (psia) Calculated values based on nominal test plan altitudes and standard day conditions.

Atmospheric conditions (barometric pressure and temperature) on the ground at time of takeoff were recorded. Values were obtained from Kelly AFB weather and were always recorded within one hour of any flight recording period. It should be noted that flights 07 through 11 were conducted in a controlled airspace located approximately 100 miles from Kelly AFB.

FIGURE 7 FLAT REPRESENTATION OF T-38 STUDENT CANOPY SHOWING PRESSURE PORT LOCATIONS

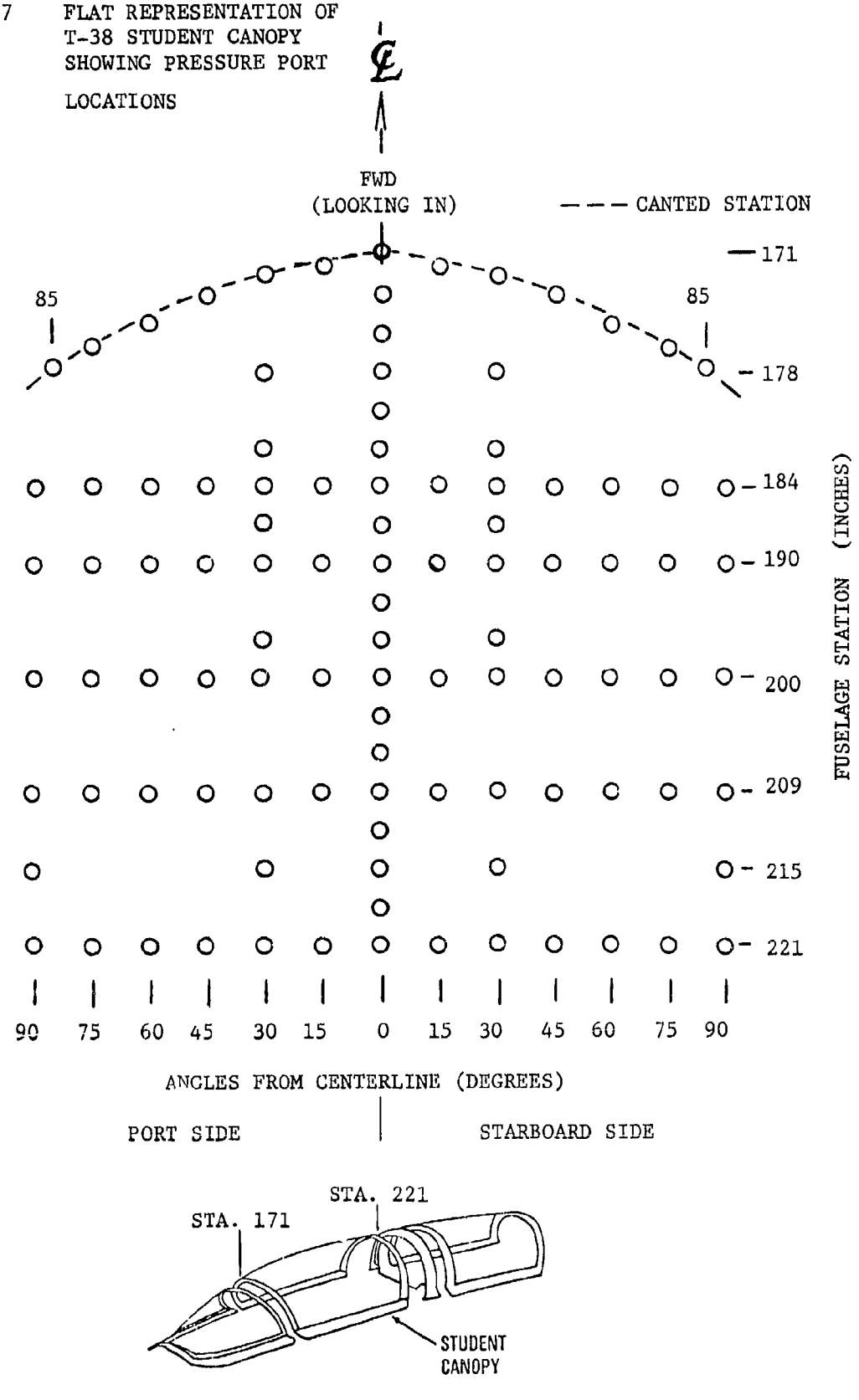

Figure 8 includes several plots which show the effects of Mach number on pressure distribution along the canopy centerline while the aircraft attitude was held straight and level. Lists of data for 300, 400, and 500 knots airspeeds are included in Tables 2, 3, and 4. From these lists, distributions of pressures over the entire canopy can be observed. Figures 9, 10 and 11 include transverse plots across the canopy at indicated fuselage stations. The canted forward station is parallel to the extreme forward edge of the canopy with the centerline point located at fuselage station 171. The outboard points for the canted station are 85 degrees (in a plane normal to the aircraft longitudinal axis) from the canopy surface centerline and at fuselage station 177.5. The remaining plots are along the exterior canopy surface in planes normal to the aircraft axis at specified fuselage stations.

Comparison of data measured during normal flight and data for flight with full left rudder deflection consistantly indicated slightly lower external pressures on the forward port side (left) corner area of the canopy and slightly higher external pressures on the starboard (right) forward corner area. The assymetry due to side slipped flight was not in excess of the sensitivity of the measuring system (i.e. .1 psi). The side slip angle was estimated by the aft cockpit pilot observing a cord attached to the outside surface of the aft (instructor canopy). Angles obtained were estimated to be five to seven degrees (nominal value was 5 degrees).

Figure 12 includes plots which represent pressure levels and distributions associated with sustained stalled flight. The stalled flight condition was obtained by reducing power and airspeed until a stalled condition was reached. Aircraft heading was maintained and altitude diminished at a sink rate of approximately 6,000 ft per minute. The stall was initiated at an altitude of 26,000 ft and an airspeed of 163 knots. Airspeed decreased to 135 knots within 20 seconds and varied between 135 and 150 knots for the remainder of the one minute recording period. Data were recorded between altitudes of 26,000 and 20,000 feet. Decreasing altitude during the recording period had the effect of increasing free stream static pressure which effects the magnitude of measured external pressures. The plotted values of Figure 12 have been corrected for this variation by generating time functions for specific ports which were manifolded to permit three measurements of the pressure at these ports at the beginning, middle and end of the recording period.

Distributions of external pressure values over the canopy surface are reported. These values must be combined with pressure values on the inside (cabin pressure) when using the data to establish pressure loading for the canopy or parts of the canopy. Determination of pressure coefficient (EQN 5) requires assumption of an atmosphere model from which free stream static pressure and Mach number can be estimated. Values for free stream static pressure and Mach number included in the data are based on an ARDC model atmosphere on a standard day. No measurements of free stream static pressure or Mach number were made. Ground level temperature and pressure could be utilized to estimate deviations from the standard day assumptions. Figure 13 is the distribution of pressure coefficient along the canopy centerline for a velocity of 400 knots at 25000 ft altitude (same condition as Figure 8D).

FIGURE 8 EXTERNAL PRESSURE DISTRIBUTION ALONG CENTERLINE OF T-38 STUDENT CANOPY
25,000 ft MSL, 0° SIDE SLIP, FREESTREAM STATIC PRESSURE 5.4 psia

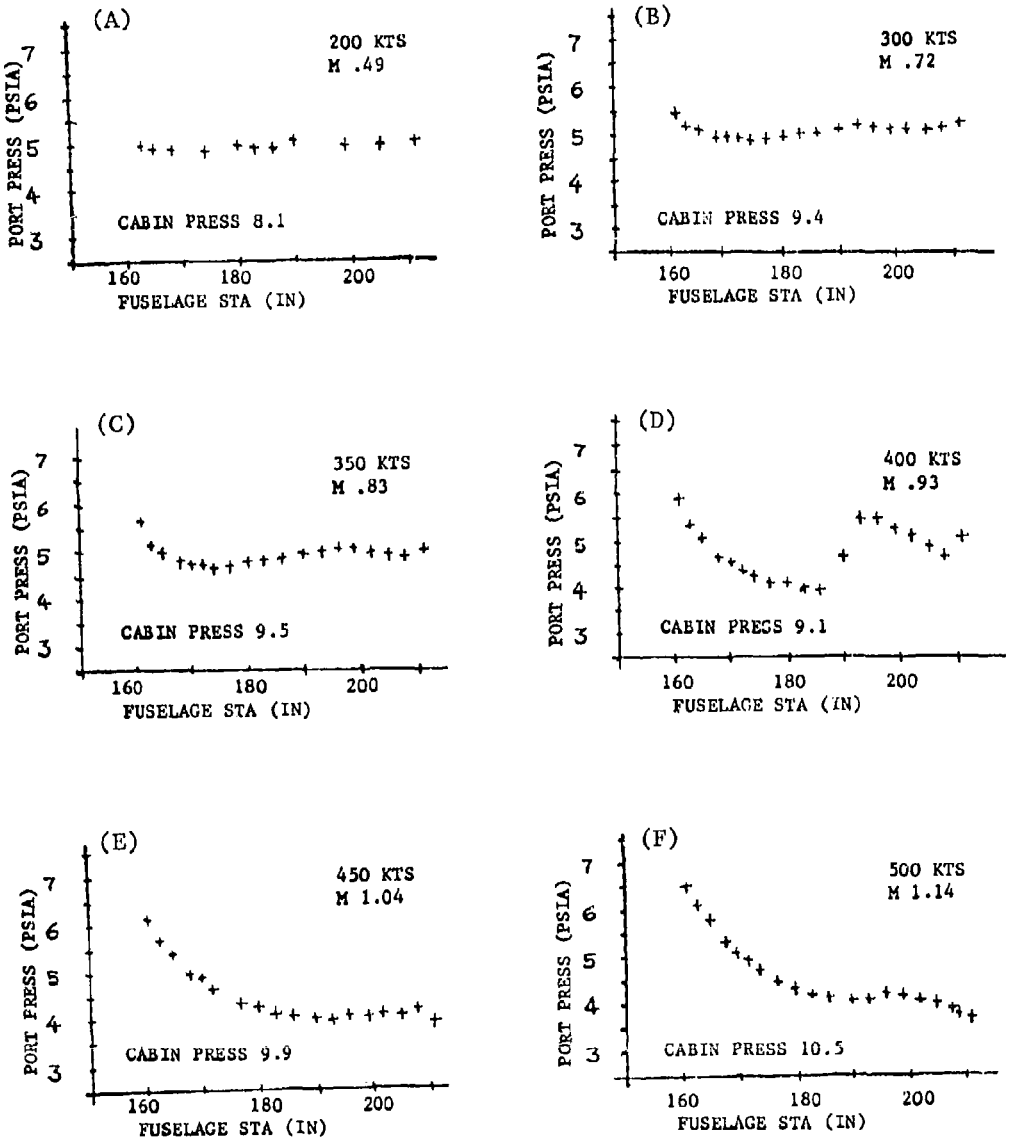

FIGURE 9 LATERAL EXTERNAL PRESSURE DISTRIBUTION ON T-38 STUDENT CANOPY AT VARIOUS FUSELAGE STATIONS
25,000 ft MSL, 300 KIAS, MACH .72

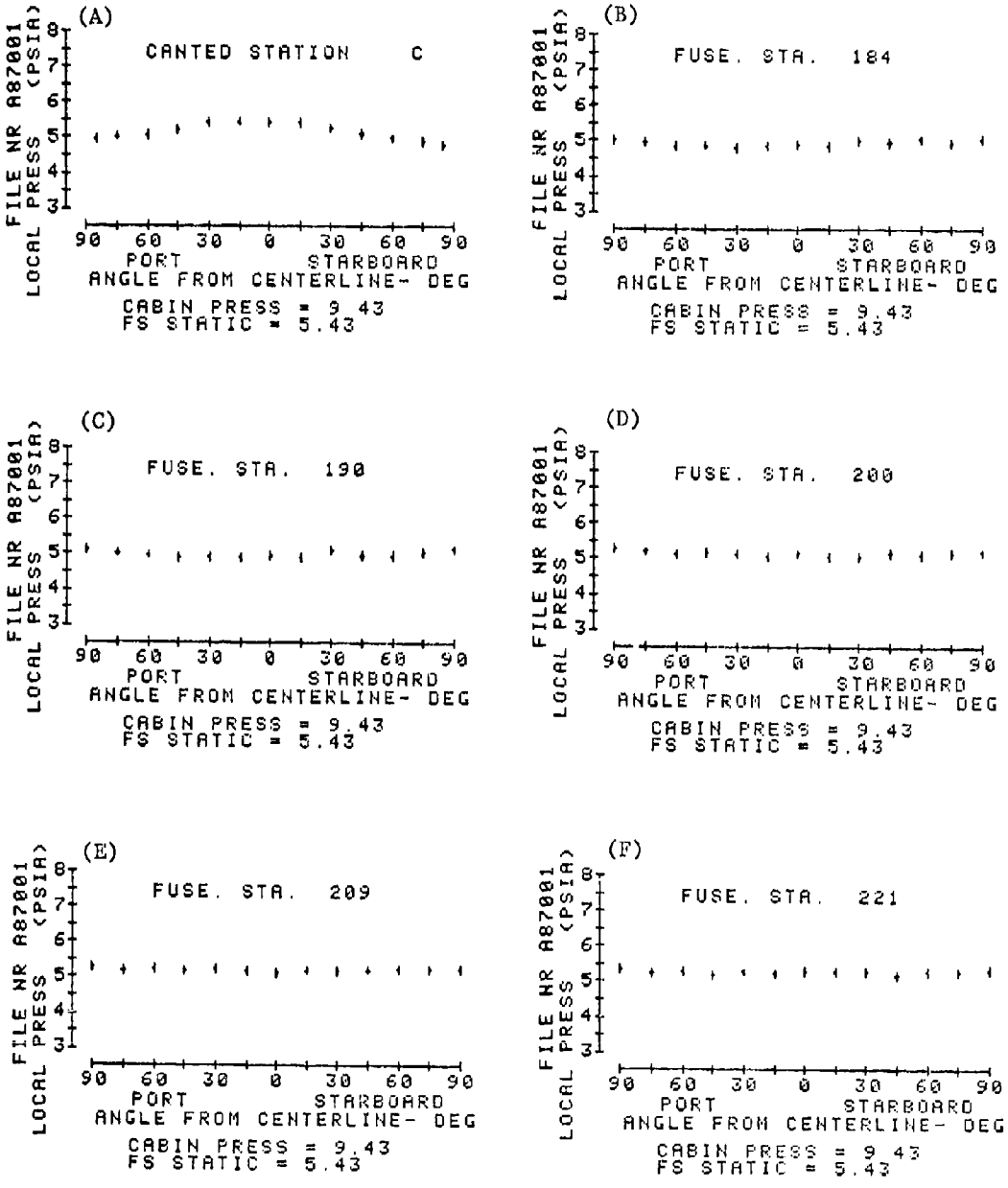

FIGURE 10 LATERAL EXTERNAL PRESSURE DISTRIBUTION ON T-38 STUDENT CANOPY AT VARIOUS FUSELAGE STATIONS
25,000 ft MSL, 400 KIAS, MACH .93

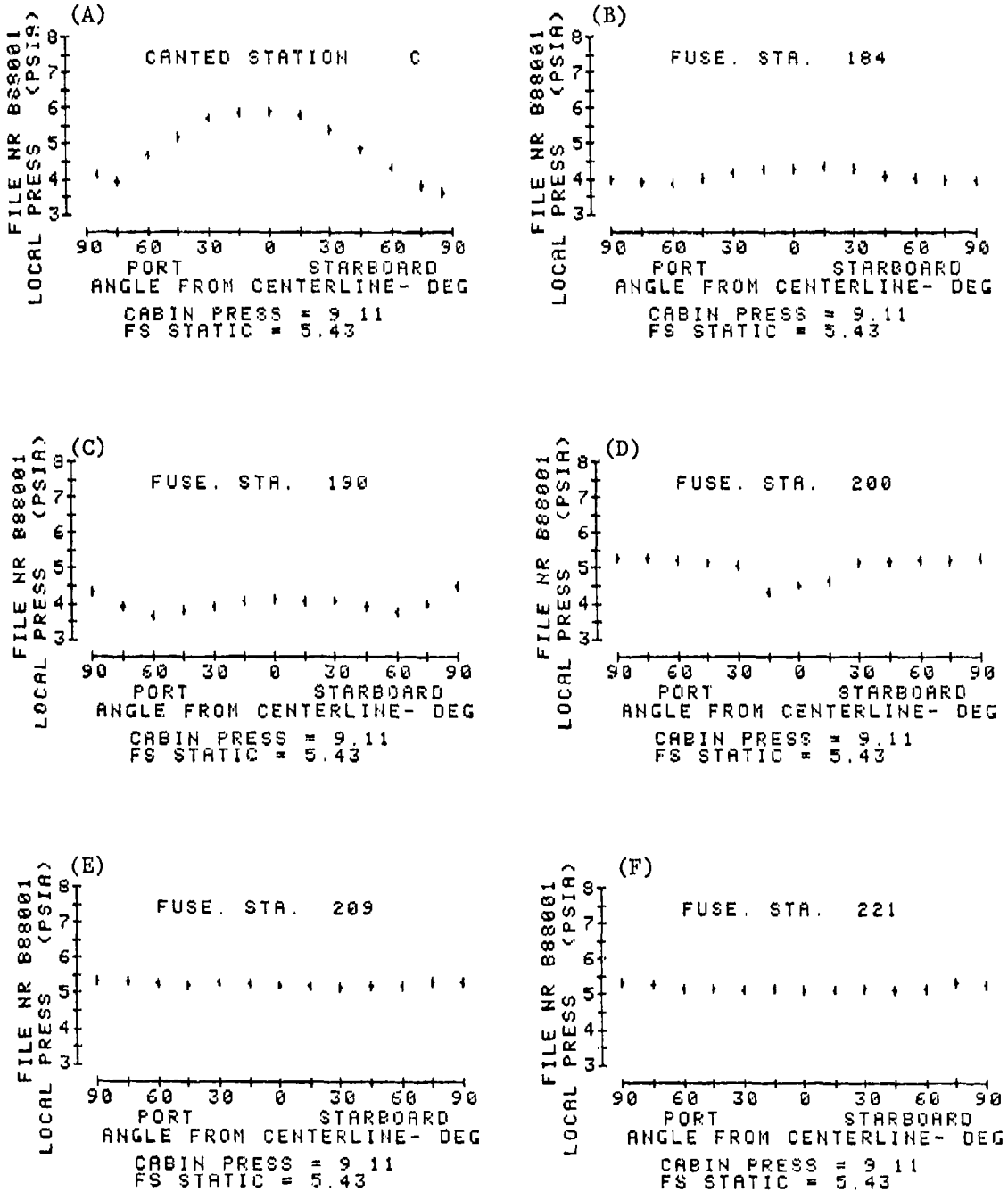

FIGURE 11 LATERAL EXTERNAL PRESSURE DISTRIBUTION ON T-38 STUDENT CANOPY AT VARIOUS FUSELAGE STATIONS
25,000 ft MSL, 500 KIAS, MACH = 1.14

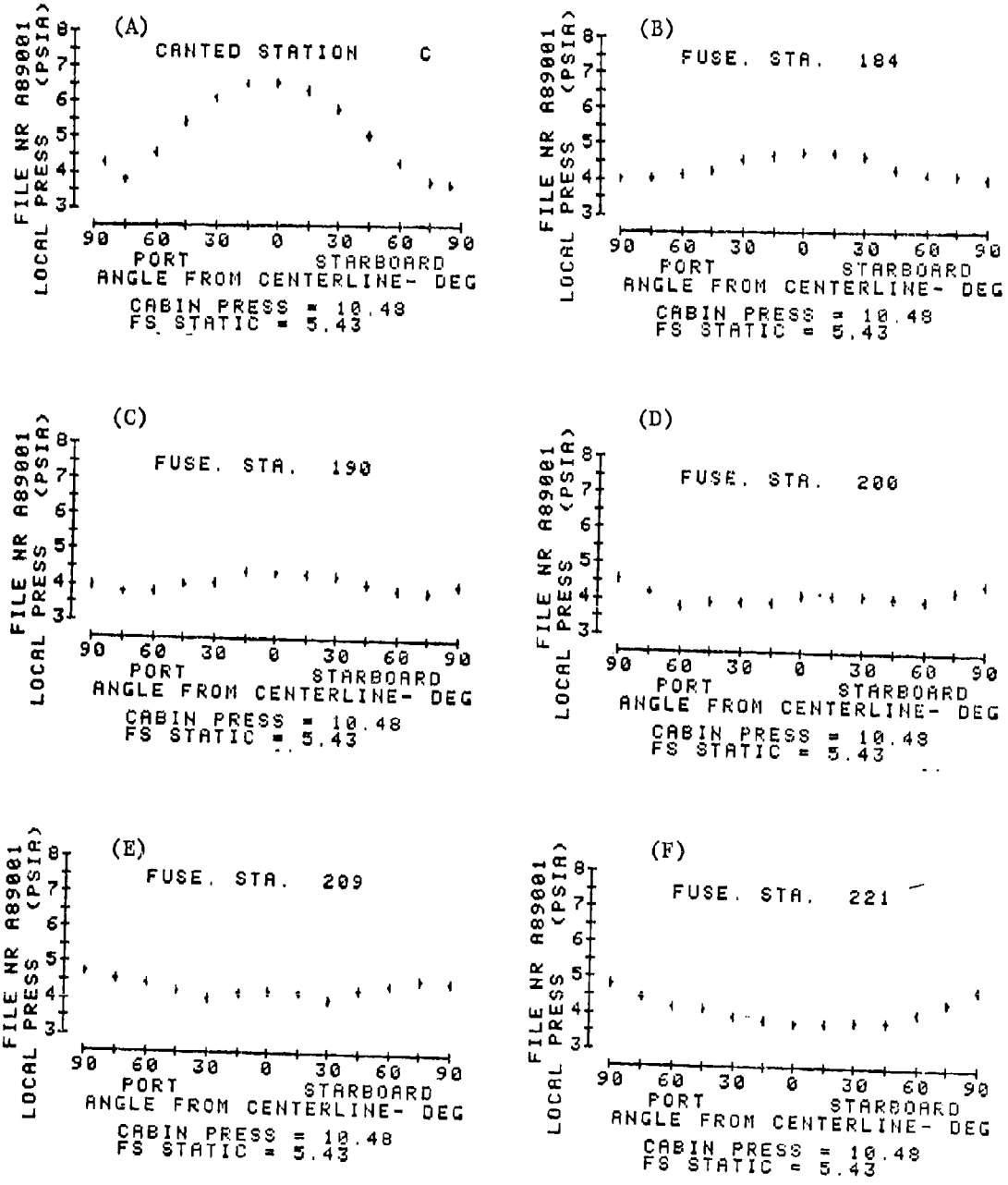

FIGURE 12 LONGITUDINAL AND LATERAL DISTRIBUTION OF EXTERNAL PRESSURES OVER T-38 STUDENT CANOPY IN STALLED FLIGHT
STALL INITIATED AT 26,000 ft MSL and 163 KIAS (M = .24)
600 ft/min SINK RATE - 34 SECOND DATA MEASURING PERIOD.

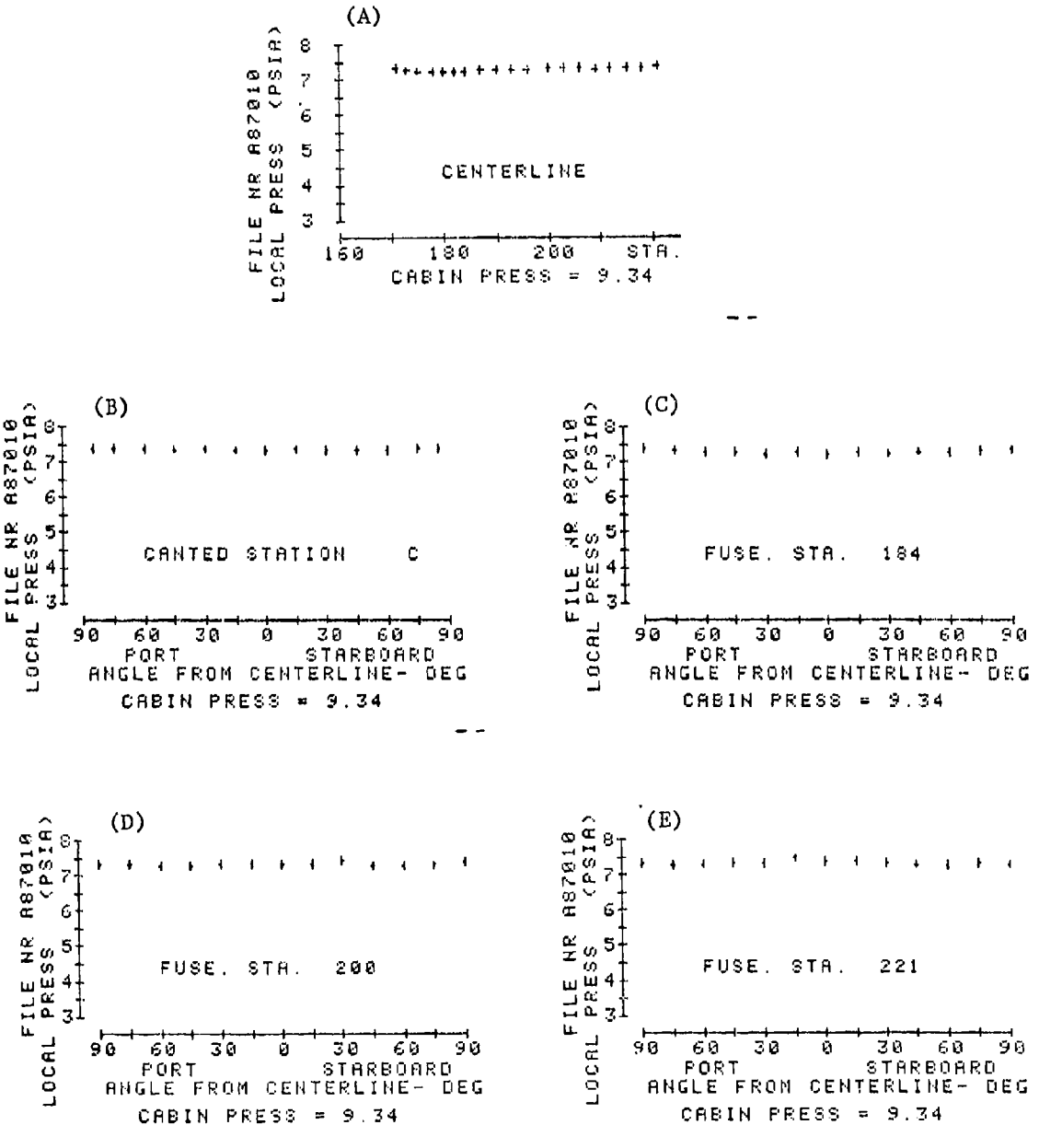

FIGURE 13 DISTRIBUTION OF PRESSURE COEFFICIENT ALONG CENTERLINE OF T-38 STUDENT CANOPY
400 KTS, 25,000 ft, M = .93

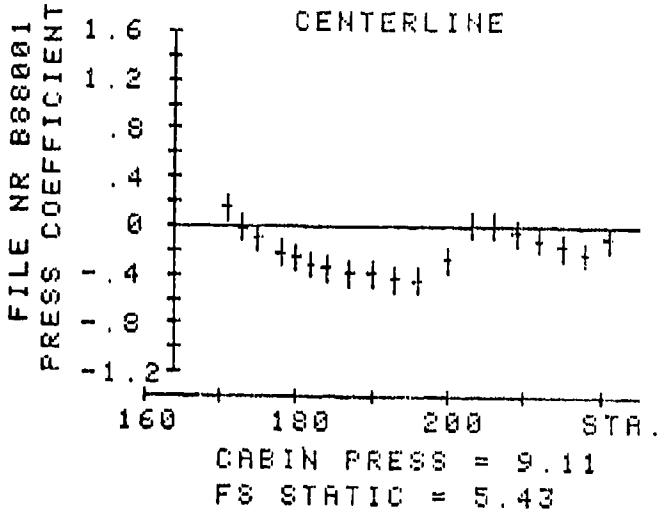

CONCLUSIONS BASED ON RESULTS

Straight and Level Flight - At lower velocities (Mach numbers less than .6) both longitudinal and lateral distributions of pressure are relatively constant. Although magnitudes at lower altitudes were higher, Figure 8A is representative of the constant distribution seen at other altitudes and low velocities. Lateral distributions when Mach numbers are less than .6 were also observed as constant (no data presented in this paper). Figures 8B through 8F illustrate effects of higher Mach numbers on external pressure distributions. Figures 8B and 8C indicate regions of higher pressure at the forward central area of the canopy and evidence of a compression/expansion in the vicinity of fuselage station 190-200. This condition is maximized in Figure 8D which shows a pressure distribution which suggests that sonic velocity has been reached on the canopy surface. At the next two higher velocities, the sonic condition has apparently moved off the canopy (Figures 8E and 8F). The effect of Mach number on lateral distribution of external pressure can be seen in Figures 9, 10 and 11 where relatively constant distributions are seen for Mach .72, and the sonic disturbance can be seen when free stream Mach number is .93 (Figure 10). When the free stream Mach number is supersonic (Figure 11) some definite lateral distributions develop, particularly at the canopy ends, Figures 11A, 11B and 11F.

Yawed Attitude Flight - For the side slip angles possible with the test aircraft (determined by rudder effectiviness and by rudder deflection limit) assymetries in pressure distribution were small relative to the .1 psi sensitivity of the data measurement and reduction techniques.

Stalled Flight - Distribution of pressure over the student canopy was observed (Figure 12) to be nearly uniform in both longitudinal and lateral directions during stalled flight. Changes in pressure magnitude which could be expected as altitude decreased were accounted for by applying time functions reflecting manifolded pressure ports.

RECOMMENDATIONS

It is recommended that the pressure distribution data measured under this effort be utilized in the following T-38 transparency improvement applications:

Design of systems for non-jettisoned canopy emergency escape - Specifically the design of patterns for and the extent of pyrotechnic cutting of bird impact resistant canopy material to effect a clear path for pilot and ejection seat could use these data as input.

Design of transparent panel edge attachments - Pressure distribution data should be used in the definition of loading at canopy edges which must be overcome by edge attachment structure.

Design of canopy jettisoning and retention hardware - It is anticipated that bird resistant transparencies for the

canopy will result in increases in canopy weight and will dictate analysis and possible redesign of the canopy jettisoning hardware. Pressure distribution data should be included in describing canopy loading.

Analytical tools - Computer codes for predicting stresses and possible stress concentrations in the canopy transparency prior to bird impacts should use pressure distribution data as input.

The approach used to gather the pressure distribution data should be utilized to obtain other data relative to aircraft transparencies including in flight measurement of stresses and temperatures in transparencies and frames.

REFERENCES

1. J Model Scanivalve Catalog and Manual, June 1980 available from Scanivalve, Inc. P. O. Box 20005, 10222 San Diego Mission Road, San Diego, CA 92120

2. Model LPS-16 Cassette Data Logger and LPR-16 Reader Instruction Manuals Document No. 58-12140-1, March 1980. Datel Intersil Systems, Inc. 11 Cabot Boulevard, Mansfield, MA 02048

TABLE 1

Flight Conditions For Which T-38 Student Canopy Pressure Distribution Data were Measured

TEST COND. NR	AIRSPEED (KNOTS)	MACH NR	ALTITUDE (FT. MSL)	SIDE SLIP ANGLE (DEG)	REMARKS
T1	50	.08	675	0	TAXI
T2	100	.15	675	0	TAXI
1	180	.28	2500	0	
2	200	.31	2250	0	
3	250	.41	5000	0	
4	300	.49	5000	0	
51	200	.36	10000	0	
52	200	.36	10000	5	
54	200	.40	15000	0	
55	200	.40	15000	5L	
57	200	.44	20000	0	
58	200	.44	20000	5L	
510	200	.49	25000	0	

Table 1 - Continued

TEST COND. NR	AIRSPEED (KNOTS)	MACH NR	ALTITUDE (FT. MSL)	SIDE SLIP ANGLE (DEG)	REMARKS
511	200	.49	25000	5L	
513	160	.41	26000	0	Initiate Stall Conditions
71	300	.72	25000	0	
72	300	.72	25000	5L	
73	300	.65	20000	0	
74	300	.65	20000	5L	
75	300	.59	15000	0	
76	300	.59	15000	5L	
77	300	.54	10000	0	
78	300	.54	10000	5L	
710	163	.41	26000	STALL	Initiate Stall Conditions
81	350	.83	25000	0	
82	350	.75	20000	0	
83	350	.75	20000	5L	
84	350	.69	15000	0	
85	350	.69	15000	5L	
86	350	.63	10000	0	
87	350	.63	10000	5R	
89	350	.58	5000	0	
91	400	.93	25000	0	
92	400	.85	20000	0	
93	400	.78	15000	0	
94	400	.72	10000	0	
95	400	.72	10000	5L	
97	400	.66	5000	0	
101	450	1.04	25000	0	
102	450	.95	20000	0	
103	450	.87	15000	0	
104	450	.80	10000	0	
105	450	.80	10000	5L	
107	450	.74	5000	0	
111	500	1.14	25000	0	
112	500	1.05	20000	0	
113	500	.96	15000	0	
114	500	.89	10000	0	
115	500	.82	5000	0	
116	200	.44	20000	0	Repeat NR 57

NOTE: L - Left yaw
R - Right yaw

TABLE 2

EXTERNAL PRESSURE DISTRIBUTION ON T-38 STUDENT CANOPY

STRAIGHT AND LEVEL FLIGHT

AIRSPEED (KIAS)..... 300
ALTITUDE (FT)..... 25000
MACH NUMBER..... .72
O.A. TEMP (DEG F).... 59
BARO PRESS (PSIA)..... 14.49
COCKPIT PRESS (PSIA). 9.43
(STD DAY)
FS STATIC P (PSIA)... 5.43
ATTITUDE CODE..... 1

CANOPY PORT	EXTERNAL PRESSURE (PSIA)	LOCATION - SIDE AND ANGLE FROM CENTERLINE
1	5.448	
2	5.278	
3	5.099	
4	5.075	
5	4.851	
6	4.939	
7	4.905	
8	4.885	
9	4.953	
10	4.992	C.L.
11	5.036	
12	5.152	
13	5.152	
14	5.152	
15	5.12	
16	5.041	
17	5.157	
18	5.016	
19	5.264	
20	5.463	
21	4.851	
22	4.924	
23	5.6	P 15
24	5.156	
25	5.215	
26	5.453	
27	4.822	
28	4.801	
29	4.827	
30	4.982	
31	4.929	P 30
32	4.968	
33	5.128	
34	5.23	
35	5.303	
36	5.259	
37	5.235	
38	4.888	
39	4.929	
40	5.167	P 45
41	5.157	
42	5.172	
43	5.055	
44	4.876	
45	4.992	P 60
46	5.143	
47	5.225	
48	5.283	
49	5.099	
50	4.948	
51	5.045	P 75
52	5.206	
53	5.196	
54	5.211	
55	4.978	
56	5.026	
57	5.133	
58	5.264	P 90
59	5.288	
60	5.371	
61	5.342	
62	5.419	
63	4.885	
64	4.934	
65	5.089	S 15
66	5.201	
67	5.274	
68	5.298	
69	4.958	
70	4.934	
71	5.021	
72	5.011	
73	5.133	S 30
74	5.026	
75	5.055	
76	5.186	
77	5.206	
78	5.288	
79	5.138	
80	4.982	
81	4.978	
82	5.174	S 45
83	5.201	
84	5.172	
85	4 997	
86	5.05	
87	4.958	S 60
88	5.143	
89	5.211	
90	5.288	
91	4.929	
92	4.973	
93	5.084	S 75
94	5.172	
95	5.244	
96	5.283	
97	4.793	
98	5.094	
99	5.152	
100	5.296	S 90
101	5 249	
102	5.259	
103	5.351	

LIST COMPLETE

TABLE 3

EXTERNAL PRESSURE DISTRIBUTION ON T-38 STUDENT CANOPY

STRAIGHT AND LEVEL FLIGHT

AIRSPEED (KIAS)..... 400
ALTITUDE (FT)..... 25000
MACH NUMBER..... .93
C.L. TEMP (DEG F).... 71
BARO PRESS (PSIA).... 14.39
COCKPIT PRESS (PSIA). 9.11
(STD DAY)
FS STATIC P (PSIA)... 5.43
ATTITUDE CODE..... 1

CANOPY PORT	EXTERNAL PRESSURE (PSIA)	LOCATION - SIDE AND ANGLE FROM CENTERLINE
1	5.922	
2	5.388	
3	5.101	
4	4.713	
5	4.587	
6	4.397	
7	4.299	
8	4.15	
9	4.14	
10	3.997	C.L.
11	3.983	
12	4.523	
13	5.451	
14	5.456	
15	5.257	
16	5.077	
17	4.897	
18	4.689	
19	5.111	
20	5.854	
21	4.295	
22	4.067	
23	4.324	P 15
24	5.261	
25	5.184	
26	5.727	
27	4.509	
28	4.266	
29	4.179	
30	4.023	
31	3.936	P 30
32	3.795	
33	5.091	
34	5.31	
35	4.994	
36	5.13	
37	5.181	
38	4.021	
39	3.8	
40	5.152	P 45
41	5.237	
42	5.162	
43	4.679	
44	3.849	
45	3.65	P 60
46	5.213	
47	5.276	
48	5.164	
49	4.504	
50	3.936	
51	3.917	P 75
52	5.281	
53	5.354	
54	5.276	
55	4.125	
56	3.965	
57	4.344	
58	5.261	P 90
59	5.354	
60	5.29	
61	5.344	
62	5.81	
63	4.358	
64	4.082	
65	4.635	S 15
66	5.208	
67	5.15	
68	5.407	
69	4.65	
70	4.373	
71	4.281	
72	4.091	
73	4.101	S 30
74	3.926	
75	5.164	
76	5.159	
77	4.878	
78	5.189	
79	4.841	
80	4.075	
81	3.941	
82	5.193	S 45
83	5.223	
84	5.108	
85	4.31	
86	4.014	
87	3.781	S 60
88	5.227	
89	5.227	
90	5.184	
91	3.82	
92	3.96	
93	3.999	S 75
94	5.237	
95	5.349	
96	5.315	
97	3.621	
98	3.994	
99	4.519	
100	5.266	S 90
101	5.32	
102	5.261	
103	5.261	

LIST COMPLETE

TABLE 4

EXTERNAL PRESSURE DISTRIBUTION ON T-38 STUDENT CANOPY

STRAIGHT AND LEVEL FLIGHT

AIRSPEED (KIAS)..... 500
ALTITUDE (FT)..... 25000
MACH NUMBER..... 1.14
G.L. TEMP (DEG F).... 74
BARO PRESS (PSIA).... 14.4
COCKPIT PRESS (PSIA). 10.48
(STD DAY)
FS STATIC P (PSIA)... 5.43
ATTITUDE CODE..... 1

CANOPY PORT	EXTERNAL PRESSURE (PSIA)	LOCATION - SIDE AND ANGLE FROM CENTERLINE
1	6.539	
2	6.131	
3	5.822	
4	5.359	
5	5.136	
6	4.966	
7	4.758	
8	4.505	
9	4.369	
10	4.253	C.L.
11	4.16	
12	4.117	
13	4.112	
14	4.243	
15	4.215	
16	4.088	
17	4.034	
18	3.913	
19	3.743	
20	6.51	
21	4.67	
22	4.389	
23	3.927	P 15
24	4.199	
25	3.825	
26	6.097	
27	5.054	
28	4.622	
29	4.534	
30	4.364	
31	4.097	P 30
32	3.952	
33	3.923	
34	4.02	
35	4.311	
36	3.927	
37	5.442	
38	4.243	
39	4.049	
40	3.918	P 45
41	4.243	
42	4.129	
43	4.549	
44	4.136	
45	3.811	P 60
46	3.806	
47	4.427	
48	4.175	
49	4.384	
50	4.02	
51	3.791	P 75
52	4.209	
53	4.558	
54	4.457	
55	4.306	
56	4	
57	3.986	
58	4.539	P 90
59	4.733	
60	4.709	
61	4.801	
62	6.325	
63	4.777	
64	4.33	
65	4.146	S 15
66	4.214	
67	3.782	
68	5.821	
69	5.243	
70	4.811	
71	4.66	
72	4.389	
73	4.272	S 30
74	4.112	
75	4.136	
76	4.029	
77	4.267	
78	3.83	
79	5.073	
80	4.289	
81	4.068	
82	4.059	S 45
83	4.272	
84	3.808	
85	4.272	
86	4.156	
87	3.913	S 60
88	4.024	
89	4.432	
90	4.097	
91	3.777	
92	4.112	
93	3.869	S 75
94	4.296	
95	4.607	
96	4.413	
97	3.685	
98	4.029	
99	4.058	
100	4.51	S 90
101	4.558	
102	4.699	
103	4.777	

LIST COMPLETE

AD-P003 208

SWEDISH AIR FORCE MAINTENANCE PROGRAMME FOR AGED TRANSPARENT ENCLOSURES FOR JET TRAINER AND JET FIGHTER AIRCRAFT

R. Forss, Defence Material Administration

SWEDISH AIR FORCE MAINTENANCE PROGRAMME FOR AGED TRANSPARENT ENCLOSURES FOR JET TRAINER AND JET FIGHTER AIRCRAFT

Wing Commander Rutger Forss
Defence Material Administration (FMV)
Air Material Department
Flight Safety Unit (FMV:Flygsäk)
Stockholm, SWEDEN

ABSTRACT

In February 1977 the canopy of a Swedish Air For jet trainer was shattered during a routine flight. The investigation involving FMV, SAAB-SCANIA and FFV Maintenance triggered a chain of activities concerning questions about the structural reliability of acrylic enclosures 10-15 years old or more, and questions about different types of edge attachement defects, and methods for the detection of hidden edge defects.

The Acrylics Defect Prism Inspection Method was re-invented and further developed, making it possible to detect defects such as cracks, delaminations and bond separations within the otherwise concealed regions of the edge attachments of windshields and canopies. The prism inspection of the inner sides of the transparency edges is done from the outside of the enclosure.

Today the aged windshields and canopies of the SAAB-SCANIA 35 Draken and the canopies of the SAAB-SCANIA 105 trainer are periodically inspected and the defects are traced. The SAAB-SCANIA 37 Viggen enclosures are due for a similar inspection programme.

The criteria for repair or retrofit of transparencies with edge defects are dictated by the type, size and location of the defect for each type of enclosure.

A special resin injection method for the repair of bond separations has been developed by FFV Maintenance and is now beeing utilized for canopy repairs.

On the flight line, a special cleaning kit must be used exclusively. Reconditioning of scratced or pitted transparency surfaces is made by specialists from FFV Maintenance.

All these efforts aim for an improved flight safety.

INTRODUCTION

Flight safety work is involved in most activities in aviation; the maintenance of windshields and canopies is of utmost importance for the safety of the crew and the aircraft.

There are a number of jet trainer and jet fighters in active service still flying with the original transparencies fitted. This has been made possible because of careful maintenance, aimed at maintaining good optical qualitiy in the transparencies that are 10-15 years old and even more. The Swedish Air Force philosophy has been to replace aircraft transparencies only if optical or structural deficiencies have become irreparable. The aging effects known in transparencies have mainly been crazing, various types of erosion damage and discoloration. During the last 5-6 years considerable knowledge has been gained about the aging damage that affects the structural strength of the transparensies inside the earlier inaccessible regions of the transparency edge attachments.

HISTORY

In the early spring of 1977 an incident occurred that started a chain of activities centered on the aging effects on aircraft transparencies and consequently on maintenance aspects of old transparencies.

The canopy of a SAAB-SCANIA 105 trainer (SK 60) was shattered at 16.500 feet altitude, 325 knots indicated airspeed, during a routine aerobatic training flight. The navigator received minor bruises on his forehead, the fan jet engines were damaged by acrylic fragments but a safe landing was made at home base.

The SAAB-SCANIA 105, since its introduction in the Swedish Ais Force in 1965, had never before experienced a canopy failure and there were no deficiencies known in that type of canopy design. The investigation of the incident could not explain the canopy failure. But about one year later cracks were found in the aft corners of the canopy transparency of another aircraft and the technical investigation that followed became the starting point for many activities leading to a better understanding about what goes on in aircraft transparencies during their service lives. Figure 1.

The Acrylics Defect Prism Inspection Method was re-invented and developed. During the development period it appeared that the same basic idea had been tried at SAAB-SCANIA several years earlier but it had never been developed into a routine inspection method.

Prism inspections revealed cracks of various dimensions in a number of canopies. Now there was a better base to operate from for studies, for tests in laboratories and full scale testing. The obvious aim was to determine the cause of the cracks, their propagation speed and critical dimensions of cracks in different regions of the transparency.

Among the parameters studied were:

- Cabin pressure cycling
- Vibrations during gun firing
- Vibrations from engine fan and compressor
- Torsional stress in fuselage/canopy during taxi turns
- Chemical attack by cleaning agents
- Chemical attack by the weather seal components

Cabin pressure fatigue tests were made; known and defined cracks showed no significant propagation after a simulated flight time of over 4000 hours. The cracks were photographed via an inspection prism at intervals during the test period.

Taxi test were made; strain gauges fitted to the transparency edges indicated very low stress levels during turns.

The cause of the canopy faulure in 1977 was never determined and no more canopy failures have occurred after that incident. One lesson learned, however, was the fact that cracks do develop and propagate in the hidden regions of aircraft transparency edges and that these cracks can be detected and traced by simple means.

THE PRISM INSPECTION METHOD

The index of refraction of acrylics (1.5) will allow visual inspection of the inner regions of a transparency edge to a depth approximately equal to the thickness of the transparency. Figure 2.1.

An ideal transparency edge design for visual inspections is shown in figure 2.2 but it will not be favoured by the transparency manufacturers and the aerodymamics experts.

Instead, visual inspection of most types and shapes of transparency edges can be made by using a simple prism, made of acrylics, and glycerin as an optical contact fluid. The $30^{\circ}/60^{\circ}/90^{\circ}$ lay-out seems to be a good compromise. An acrylic prism will not harm the transparency surface and it will not break in pieces if it drops to the ground. Glycerin is harmless to the acrylic material and its viscosity simplifies the inspection work on a sloping transparency surface. Glycerin and acrylics have just about the same index of refraction. Water can be used, of course, but is not recommended. Figure 2.3.

The inner wall of the transparency edge will be observed directly through the prism. The outer wall is observed as a reflected image because of the fact that the inner wall, outside of the edge attachment, will act as a mirror.

A prism inspection should be made in a low ambient light environment, if possible. A narrow light beam from a penlight directed through the inspection is suitable means of illumination. Still better, in many applications, is the use of a penlight plus a "half-cylinder prism" attached to the penlight. Figure 4.
A gauge prism like the one demonstrated in figure 3 can be used for estimating lengths an depths of cracks inside and outside edge attachments in some cases.

TRANSPARENCY DEFECTS AND MAINTENANCE MEASURES

SAAB-SCANIA 105 Trainer

The windshield is made of 14 mm single curvature stretched acrylics. The aircraft type entered service in the mid-sixties and the windshield transparency has endured a long service life without anystructural problems. Most erosion defects have been cured by sanding and polishing.

The canopy is made of 8 mm as cast acrylic material.The edges are bonded to nylon laminate, the attachment bolts pass through the laminate below the transparency edge.

The transparency edges now have been periodically inspected with the prism method for more than four years. The prism inspections will be made at 125 flight hour intervals on canopies with known cracks, earlier it was done more often.Canopies without known cracks will be inspected at 250 hour intervals.During these years the propagation of known cracks as well as the appearance of new ones has been kept on record for each individual canopy.

Special attention is given to the regions above the canopy locks, at the lower corners of the canopy.Cracks mainly perpendicular to the edge may not exceed a depth of 1 mm or a length of 15 mm. All cracks parallel to the edge or at an angle to the edge of 45° or less will be given special attention.Most cracks in the canopy transparency are found on the outer wall of the transparency, below the edge of the nylon laminate.Figure 6,figure 7.

It is now understood that these cracks have originated from chemical attack by the neoprene sealant that has penetrated the primer layer that was supposed to protect the acrylic material. The sealant used nowadays is a thiokol rubber product.

During prism inspections bond separations between the transparency edges and the nylon laminate have been discovered. These defects are considered a more serious hazard to the structural strength of the edge attachment than most of the cracks that can be detected. For example, in the regions marked A in figure 6,a bond separation between the outer wall of the transparency and the laminate is not allowed to exceed 1 cm^2 in area. Large separation pocket(or cavities) may not be closer to each other than 30 mm. The added areas of bond separations in each area marked A may not exceed 10 percent of the bonded area.

The limit figures for cracks and bond separations are the results of strength calculations and laboratory tests.

The bond separations are probably the results of the manufactoring procedures used in the mid-sixties. TENSOL 3 resin has been used for the bond and still is used because of its shear strength properties.

Nowadays bond separations can be repaired; a special resin injection method has been developed and will be described later in this paper.

SAAB-SCANIA 35 Draken

The J 35F Draken fighter, the last version built, entered service in 1967 and was at that time fitted with a monolithic windshield transparency made of double curvature as cast acrylics like the ones on the 35C Trainer and the 35D fighter that are still in service. Later in the series, around 1969, the stretched acrylic windshield transparency was introduced.

The as cast transparencies have endured the elements and time quite well. Erosion damage at the front edge, cracks in a bonded acrylic trim strip on the inside of the edges and discoloration have been the major deficiences. Transparencies made of as cast acrylics now are beeing replaced by stretched acrylic transparencies.

On the Draken the windshield transparency is attached to the airframe by the use of a slip-joint attachment system, there are no bonded laminate strips along the edges.

Aging defects inthe stretched acrylic transparencies, thickness 18mm, mainly have been erosion at the front edge and delaminations in the side edges.Most delaminations are relatively easy to detect with an inspection prism and a penlight with a "half"-cylinder" prism preferably. The depth of delamination cracks is comparably difficult to assess. The delamination is not permitted to propagate above the top edge of the edge attachment.

The conditions for delaminations now have been reduced by the retrofit of a cork strip supporting the edge of the transparency, replacing the previous rubber strip that could absorb moisture.

The Draken canopy is made of as cast acrylics, thickness 14 mm. The edges are reinforced by nylon laminate, bonded to the transparency edges by TENSOL 3 resin. The transparency is attached to the frame by bolts going through the laminate,below the edge of the acrylic material.

In the canopy, no cracks may exist in the regions above the canopy locks, the regions marked C in figure 8.1. Between the canopy lock regions, cracks parallel to the edge may not exceed 3 mm in depth.Figure 8.3. Cracks in the front and aft arch edges, perpendicular to the edges, may not exceed 5 mm in length or 3 mm in depth. Figure 8.2.

All detected defects are kept on record. Canopies with known cracks will be inspected at 100 hour intervals,those without known cracks at 200 hour intervals.

During prism inspections bond separations have been detected between the as cast acrylic edge and the nylon laminate. The maximum local shear loads will be located to the canopy lock regions. In the outer bond layer, bond separations may not exceed 1 cm^2 in area, the added areas of the bond separations may not exceed 10 percent of the total bonded area, marked C in figure 8.1.

Draken canopies with bond separation defects will be repaired by the use of the resin injection method.

SAAB-SCANIA 37 Viggen.

The Viggen entered service in 1972. This aircraft has a single curvature windshield made of 23 mm stretced acrylics. The canopy is made of 10 mm stretched acrylics.

The windshield transparency is attached along the sides by a bolt and bushing system, the bolts go through the acrylic material. The front and aft edges are attached to the frame by tension straps over the arhes.

The canopy transparency edge has a nylon laminate reinforcement and is attached to the canopy frame by bolts going through the acrylic material.

The risk of delamination defects will be minimized by the introduction of a seal along the edges of the transparencies.

At present the inspection programme for the Viggen transparencies is not fully outlined.

During prism inspections, special attention will be paid to the regions surrounding the canopy locks, marked A in figure 9. In these areas no cracks will be permitted to propagate from the attachment bolt holes.

By looking sideways, from both sides of each hole, it will be possible to detect all possible cracks from the bolt holes with the possible exception of microcracks on the lower side of the holes.

A RESIN INJECTION METHOD FOR THE REPAIR OF BOND SEPARATIONS

This method has been developed and tested by FFV Maintenance, an aviation industry beeing a corporate member of the Group of the State Industrial Department.All repair work using this method is done by FFV Maintenance specialists exclusively.

The canopy is removed from the aircraft; the retainer strip is removed from canopy frame before the actual repair work begins.

By using a fixture attached to the transparency by a suction cup,a 1.5 mm drill is guided during drilling until the point of the drill reaches the bond separation pocket or cavity. The progress of the drill through the laminate is checked via an inspection prism attached to the transparency by another fixture using suction cups, this one belonging to the FFV Maintenance Prism Inspection Set. Figure 10.1.

Two holes or more are drilled through the laminate . The guide for the drilling operation then is replaced by the resin injector. Figure 10.2.

Then a polyurethane resin,dyed in a blue colour, is injected into the separation cavity until all trapped air has been evacuated through the ventilation hole or holes drilled. This part of of the operation also is carefully checked via the inspection prism. This special resin is said to be able to penetrate extremely narrow gaps in the separations. Figure 10.2.

The shear strength criteria for the original bond are met.

TRANSPARENCY MAINTENANCE AT THE AIR BASE

The aging processes for the precious aircraft transparencies are , of course, day-to-day as well as year-to-year proceedings.

The aging of the acrylics goes on on the outer surface of the transparency as well as in the attachment edges.By proper cleaning methods and careful polishing much can be done to preserve the original perfect optical qualities of a recently fitted new transparency.

The Swedish Air Force had to lose two Draken fighters and one young pilot, in a mock dogfight climbing into the sun, before it was realized that a good old chamois leather rag, used for transparency cleaning, was a contributing factor working against flight safety. This happened in 1969.

Since 1970 special cleaning sets are used at the air bases for the daily cleaning of windshields and canopies. Chamois leather, the perfect collector of sand and metal particles is banned, rags of fabric or cloth materials are banned. For transparency cleaning purposes only paper towels of a selected quality may be used and thrown away after use. The mechanics are encouraged to be wasteful with the towels, an unusual recommendation in the military world. But this recommendation will lead to the result that very few hard particles will get the chance to carve their little signatures in the shining surface of the transparency.

Generous amounts of water should be used during the rinsing part of the operation , before washing and after washing. Only the recommended mild soap-based washing agent may be used.

For polishing,only one recommended type of polish may be used.

There are ways of holding down the aging pace of aircraft transparencies on a day-to-day basis in every single parking area on every single air base.

Minor scratches and erosion defects in the peripheral regions of windshield transparencies can be repaired by technical personnel at the air bases, special training is required. More severe defects must be repaired by service teams from FFV Maintenance.

DISCUSSION

In the Swedish Air Force acrylic transparencies 10-15 years old or more are still in service. This has been made possible due to careful maintenance planning and through the efforts of ambitious technicians at the air bases plus positive assistance from the Swedish aviation industry.

During the last five years much knowledge has been gained about hidden aging defects in the edge attachment regions of windshields and canopies. These defects can be critical for the structural strength of the enclosures, but we now have means for keeping their propagation under control. Periodic inspections, criteria for the location of defects and their permitted sizes now are tools routinely used in daily life in the Swedish Air Force.

A new repair method for as cast acrylic canopies with bond separations is now in use, making it possible to restore the structural strength of the canopies at considerable cost savings.

The philosophy of replacing the aircraft transparencies,only if optical or structural deficiencies have become irreparable, still holds.We feel that we can still keep our aged aircraft transparencies in service because the now running maintenance programme will contribute to keep the flight safety level high or even higher than yesterday.

We now have a markedly raised level of knowledge about how to look for trouble,where to look for it and how to treat it.

At the same time we are aware of the fact that the aging of acrylic windshield transparencies will affect the bird impact resistance of windshields; these are effects that only can be evaluated by fullscale testing. These effects might lead to measures in the future.

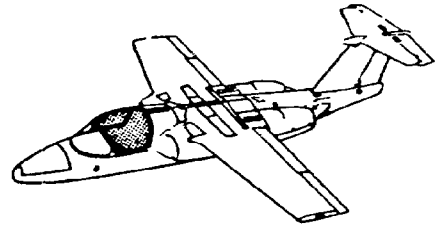

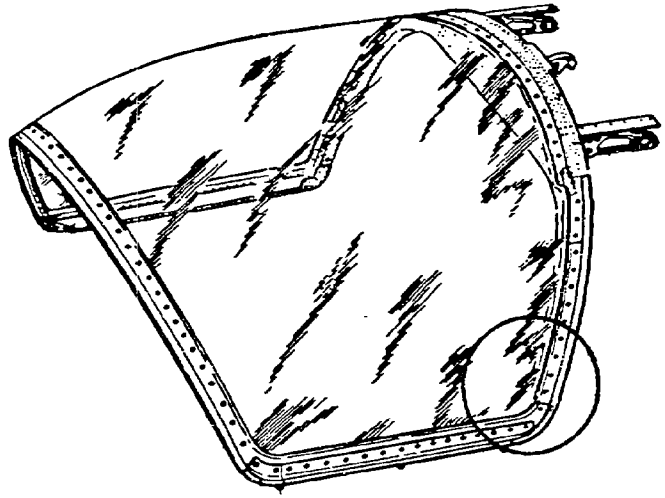

Figure 1.
SAAB-SCANIA 105. Cracks in the canopy transparency edge.The weather seal,fairing and laminate are removed.

The principle of the inspection prism .

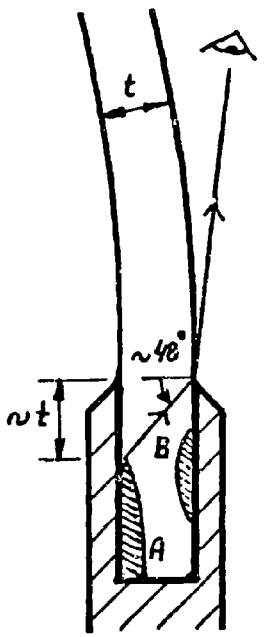

Figure 2.1.
Maximum inspection depth without a prism. The cracks A and B are not visible.

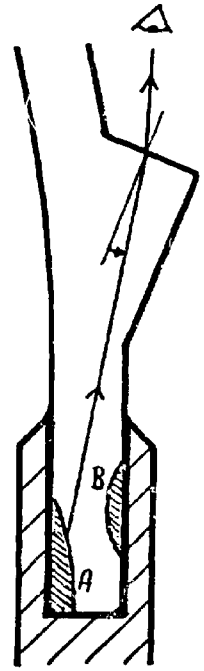

Figure 2.2.
An ideal transparency edge design for crack inspections.

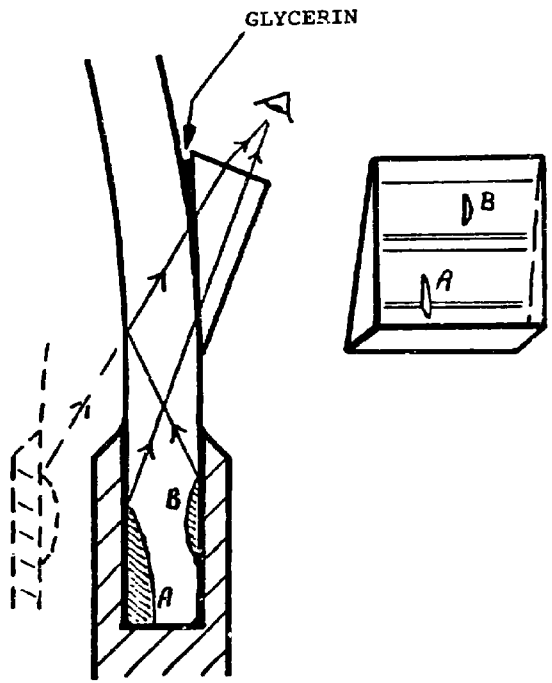

Figure 2.3.
With an inspection prism in the proper place, the cracks A and B can be seen at the same time in many cases.

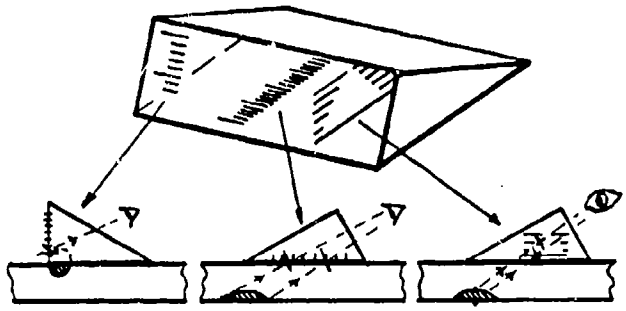

Figure 3.
Gauge prism

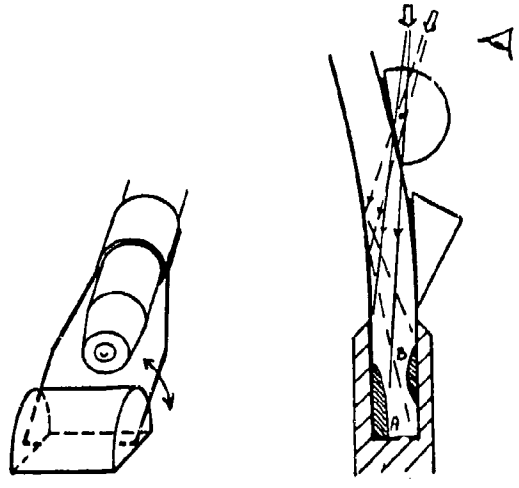

Figure 4.
Penlight with a "half-cylinder prism"

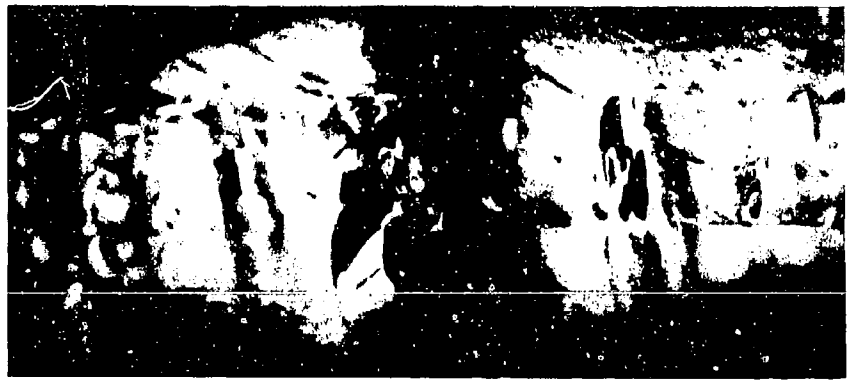

Figure 5.
Well illuminated cracks in a Draken canopy transparency

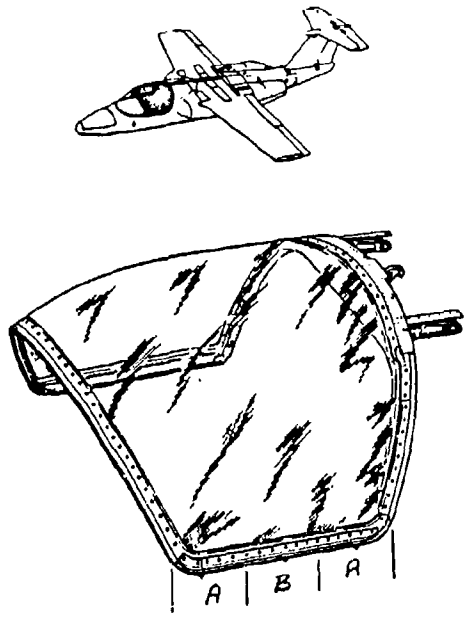

Figure 6.

SAAB-SCANIA 105. Canopy. 8mm as cast acrylics.

Some types of defects and measures:

Cracks located along the edge attachment top may not exceed the depth 1 mm or the length 15 mm. A crack making an angle of less than 45° to the edge will need special attention.

A canopy is replaced when these limits are exceeded.

Bond separations in edge attachments. The highest shear loads will be found in the regions marked A where smaller bond separation defects are permitted than in region B.

Repairs are possible with the resin injection method.

Figure 7.
Prism photo. Cracks approx. 2-5 mm deep in aft corner.

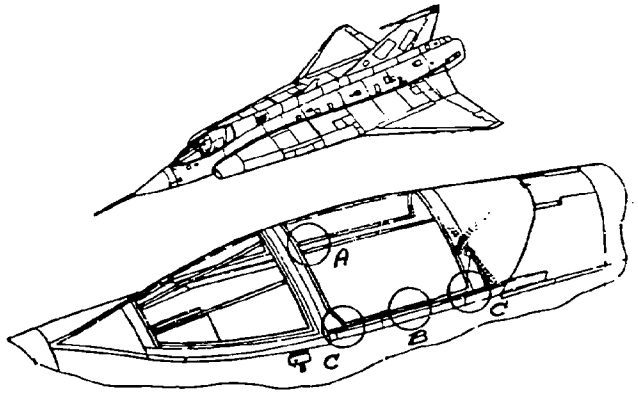

Figure 8.1
SAAB-SCANIA J 35F Draken. Windshield: 18 mm stretched acrylics; canopy: 14 mm as cast acrylics.

Some typical aging defects in the canopy:

Figure 8.2. Reference to region A in figure 8.1. Prism photo. Small erosion pits and cracks at the top of the canopy's front arch, at the reinforcement edge. Normally repairable.(The photo here shown is inverted).

Figure 8.3. Reference to region B in figure 8.1. A cut-out section of the horisontal edge attachment of a canopy.The deepest crack parallel to the edge is approx. 7-8mm, max depth is 3 mm. No cracs are permitted in the regions of the canopy locks. Region C.

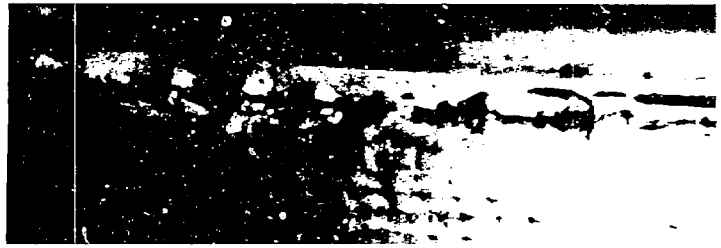

Figure 8.2

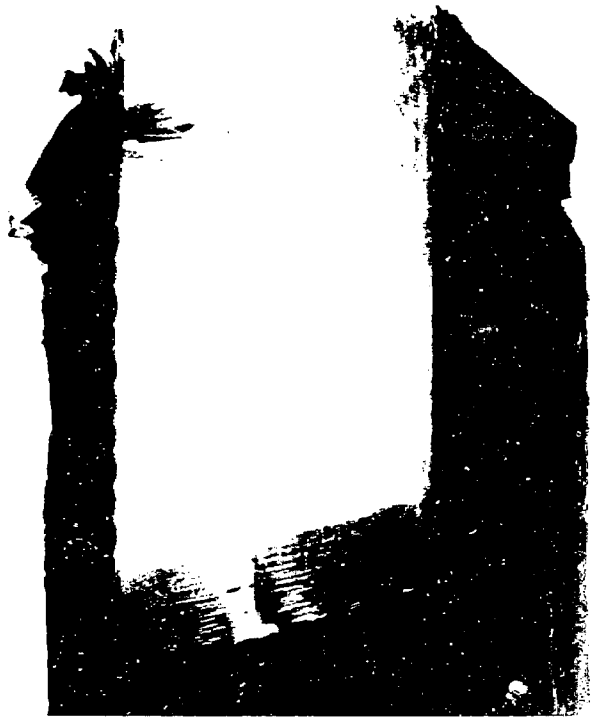

Figure 8.3

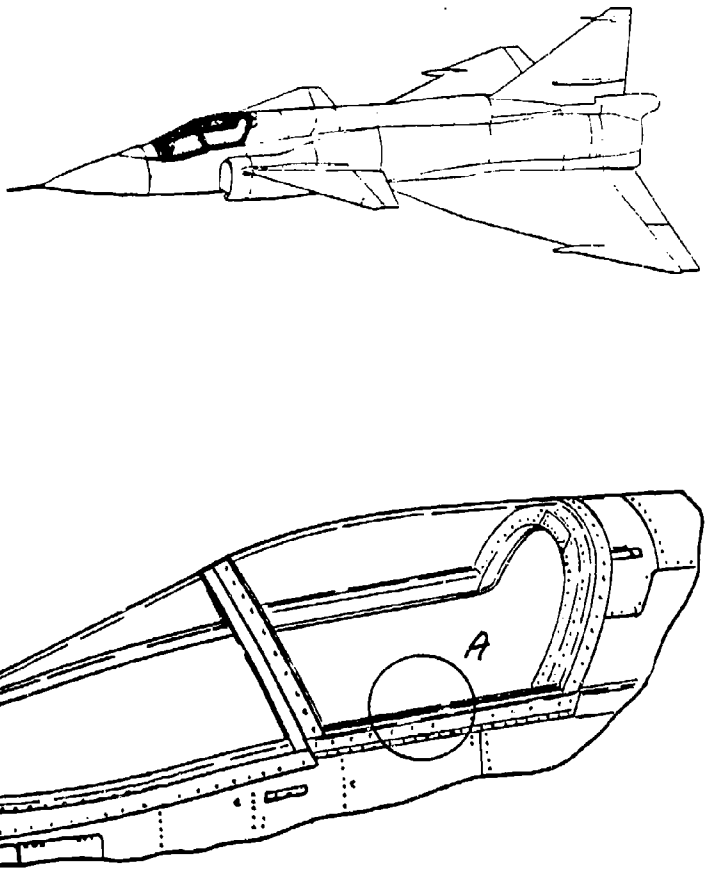

Figure 9.
SAAB-SCANIA 37 Viggen. Windshield: 23 mm stretched acrylics; canopy: 10 mm stretched acrylics.

The risk of delamination will be minimized by the introduction of a seal along the edges of the transparencies.

During prism inspections, special attention will be paid to the regions (A) surrounding the canopy locks where no cracks will be permitted to propagate from the attachment bolt holes.

Figure 10.1
The resin injection method.Drilling of holes.

1.5 mm holes are drilled for resin injection and air ventilation.Via an inspection prism the drilling operation can be checked. The drill is guided by a fixture attached to the transparency by a suction cup.

Figure 10.2
The resin injection method. Resin injection.

The resin is dyed in a blue colour. The injection procedure is checked via the prism so that there will be no air bubbles trapped in the narrow cavity and so that the resin will fill the cavity completely.

All photos in this paper are supplied by courtesy of FFV Maintenance.

AD-P003 209

MEASUREMENT OF RESIDUAL STRAINS AND STRESSES IN TRANSPARENT PRODUCTS

A. S. Redner and T. W. Corby, Jr., Vishay Intertechnology, Inc.

MEASUREMENT OF RESIDUAL STRAINS AND STRESSES IN TRANSPARENT MATERIALS

BY:

A. S. Redner and T. W. Corby
Measurements Group, Inc.
Raleigh, NC

INTRODUCTION:

Residual stresses introduced during the manufacturing process have a well known and important influence on the structural integrity and material performance. In some instances, residual stresses or strains are introduced intentionally to enhance the life or performance of the product. This approach is used with both metallic and nonmetallic materials. Typical examples include:

Shot-Peening - Creating a compressive surface stress enhancing the fatigue life of the structure.

Auto-Frettage - Creating a compressive stress in a region subjected to tensile service stress.

Glass-Tempering - Heat treating, or a chemical process designed to produce a compressive surface stress thus preventing chipping or surface damage when tensile stresses are introduced in service.

"Orientation" of Polymer - Straining in manufacturing to enhance the mechanical properties of materials.

Undesired residual stresses usually appear as a result of manufacturing process, such as welding, casting, molding, or machining. It is not unusual to encounter structural failures directly traceable to the presence of such undesired residual stresses.

Clearly, the presence of the "desired", or absence of the "undesired", residual stress influences the quality of a product. Therefore, measuring residual stresses must be considered an important part of product quality assurance programs. Since manufacturing processes are usually a direct source of residual stress, measuring these stresses not only concerns the design engineer, but also the material and process specialists.

Residual stress measurement is considerably more complex than measuring load-induced stresses. Sensors typically used to measure stress introduced by external forces such as strain gages, photoelastic coatings, and brittle lacquers, are not directly applicable since once bonded or deposited on the sur-

face, they ignore the already present internal strains. In order to measure the internal residual stress using these methods, the equilibrium must be redistributed by sectioning, layer removal, or hole drilling. Only the hole-drilling strain gage method is considered as "semi-destructive", and it is used extensively in quality assurance testing programs. In many applications, the small shallow hole that is introduced in the part or structure can be eliminated in the final machining process, leaving a useful part.

Nondestructive measurements of internal residual stresses can be accomplished using the x-ray diffraction technique, and, in the case of transparent and translucent materials, photoelasticity. Both of these techniques are limited in their applicability. The x-ray technique is confined to the surface layer, requires highly accurate goniometer alignment, and careful time-consuming point-per-point data acquisition. The photoelastic method on the other hand, is a relatively simple technique yielding "full-field" images of the stress. However, it is limited to light-transmitting materials.

GLASS INSPECTION PROCEDURES:

The glass industry is perhaps the oldest user of the photoelastic inspection process. In some instances, inspection is dedicated to measuring the casting stresses, or to verify the efficiency of an annealing process. A typical example of the procedures used for this purpose is ASTM Standard Test Methods[1] C 148, "Polariscopic Examination of Glass Containers", (originally issued in 1939), and F 218, "Standard Method for Measuring Residual Stresses in Cylindrical Glass to Metal Seals", (originally issued in 1950). Both methods have been frequently upgraded, and the title of F 218 has been changed to, "Standard Method for Analyzing Stress in Glass". These methods describe typical photoelastic measuring setup techniques using the Senarmont compensation method for measuring fractional fringe orders. A full-wave retardation plate (also called "tint plate") is used to enhance the sensitivity when a low order of birefringence is evaluated using color-matching. In order to calculate the residual stresses from the measured birefringence, the calibration procedure, as described in ASTM Standard Test Method, C 770, is used to yield the stress-optical constant. To account for the integrating effect, empirical equations are shown in recent revisions of the above mentioned methods. The polariscope setup used in this method is shown in Figure 1. Here the polarizer and analyzer must be placed at 45° to the direction of principal stresses. If α is the rotation angle of the analyzer necessary to produce a dark fringe at a point, the measured retardation is $\delta = \frac{\alpha\lambda}{\pi}$.

Measuring internal stresses in tempered glass is considerably more difficult since, (a) the integrated value through the thickness is typically zero, and (b) the steepness of the stress gradient near the surface requires special care. The Engineering Standards Manual[2] published by the Glass Tempering Association, describes a method of observing photoelastic fringes along the edges of tempered glass. It suggests fringe order values that are indicative of "full tempered" or "heat strengthened" conditions, for a typical thickness of glass. A more complex method to measure the surface stress is based on

[1]ASTM Standard Test Methods are available from AMERICAN SOCIETY FOR TESTING AND MATERIALS, 1916 Race Street, Philadelphia, Pennsylvania 19103.

[2]Engineering Standards Manual is available from Glass Tempering Assoc., Topeka, Kansas, 66611.

measuring the absolute changes of refractive index.

The photoelastic sensitivity of various types of glass range between 2.4 to 3.6 Brewsters (stress optical constant between 900 to 1300 psi/in/fringe). The sensitivity of a specific type of glass can usually be obtained from the manufacturer or through calibration.

PLASTIC MATERIALS:

Measurement of residual strains and birefringence in transparent or translucent plastics can be easily accomplished using a compensator, as described in the recently developed ASTM Standard Test Method D 4093-82. The polariscope setup is shown in Figure 2 illustrating the "normal" and "oblique" path of light.

The residual strains ε_x and ε_y are related to the retardation measured in normal incidence δ and in the oblique path δ_o

$$\varepsilon_x - \varepsilon_y = \frac{\delta}{tk} \quad \text{(general)}$$

$$\text{and} \quad \varepsilon_x = \frac{\delta}{tk\ (1 + \nu)} \quad \text{(for uniaxially strained material)}$$

Since in plastic forming operation the Poisson's ratio $\nu = 0.5$, the following relation can be derived for biaxially strained material:

$$\varepsilon_x = \frac{1}{1.5\ tk_R \sin^2\theta} [0.5\ \delta_{ox} \cos\theta_x - \delta(\cos^2\theta_x - 0.5)]$$

$$\varepsilon_y = \frac{1}{1.5\ tk_R \sin^2\theta_x} [0.5\ \delta_{ox} \cos\theta_x - \delta(1 - 0.5\ \cos^2\theta_x)]$$

Where ε_x and ε_y are the principal strains
t is the thickness of examined item
δ_{ox} and δ are the measured retardations
θ is the angle of the light path as shown in Figure 2
k_R is the coefficient relating the observed birefringence to residual strains.

The angle θ is set usually at 30^o, and the above equation is reduced to:

$$\varepsilon_x = \frac{1}{tk} (1.15\ \delta_{ox} - .67\delta)$$

$$\varepsilon_y = \frac{1}{tk} (1.15\ \delta_{ox} - 1.67\delta)$$

The correlation between orientation strains and birefringence was discovered by Ambronn [1][3] in 1898. Results of research on this topic were reported by McNally and Sheppard [4], Spence [6], Stein and Tobolsky [7], Stein [8 & 9], Wilkes [10], Doyle [2], and Matsumoto et al [3], to cite just a few. Each study provides several additional references.

---

[3]Numbers in brackets designate References at end of paper.

In view of the large number of parameters, the correlation between applied stress, strain, time, temperature, crystallinity and birefringence cannot be put into a simple expression, and indeed, no simple formula or relation was suggested in the references quoted above. An analysis limited to residual (or permanent) strains only is simpler, since the consideration of time, rate, etc., can be eliminated.

Unlike glass, which is capable of retaining residual stresses for a significant period of time, plastic materials usually exhibit stress-relaxation. If internal stresses develop during the manufacturing process as a result of restraints imposed by the mold, temperature gradients during solidification, nonuniform shrinkage, etc., these stresses will frequently vanish, and only permanent residual strains will remain with molecular chains "frozen" in the deformed condition. In such a simplified (but not unusual) situation of a near-total stress relaxation, the birefringence observed in amorphous polymers is mostly related to the permanent or frozen-in strain imposed in the manufacturing process.

A qualitative illustration of this effect is shown in Figure 3. The first photograph (1a) shows a pattern of photoelastic fringes in a molded polystyrene lid. Photograph (1b) shows the same item cut to relieve residual stresses. It can be easily seen that the photoelastic pattern remains unchanged since only the negligibly small elastic stresses are relieved. Photograph (1c) shows an identical item after annealing. The lid was heated slightly above its softening point allowing elastic recovery of its molecular chains thus relieving the "permanent" or "frozen-in" strains. Also, the optical anisotropy vanishes showing an essentially strain-free and birefringence-free state.

The photoelastic coefficient k relating birefringence to stress-induced deformation is known for many transparent materials, and can be easily established using calibration methods described in Reference [11].

To establish the strain-optic coefficient k_R relating residual strain to the observed birefringence, the residual strains must be relieved and measured. Measurement of the "orientation release stress" and "orientation release strain" is described in ASTM Standard Test Methods D 1204, D 1504, and D 2838. Although these methods were developed to evaluate the dimensional changes of plastic film and sheets, the concept of measuring the "orientation release stress" or "orientation release strain" can be related to the measured birefringence, and either stress or strain optical coefficients can be determined.

Measurement of the "orientation release stress" requires special tooling to measure forces exerted during shrinkage. This method is not sufficiently flexible or accurate to justify its general use since in its present form (D 1504 and D 2838) it can only deal with uniaxial tensile stress and relatively large residual strains. The measurement of the "orientation release strain", described in ASTM Standard Test Method D 1204 is relatively simple, and was used to calibrate the strain-optical constant needed to relate residual strains to birefringence.

CALIBRATION METHOD FOR STRAIN-OPTICAL CONSTANT k_R

Calibration of the strain-optical constant k_R was carried out using the following procedure:

a. Specimen Selection and Preparation - Flat specimens exhibiting uniform birefringence were cut from commercially available stock sheets. While theoretically any thickness can be used, it was observed in practice that very thin sheets tend to warp or curl, and a practical thickness range appears to be 0.25 to 10 mm (.010 to .375 inch). Specimen dimensions influence the precision of strain measurement, and it appears that 100 x 100 mm (4 x 4 in.) yields good results. Small specimens could be used when large strains are measured or when it is difficult to locate a large region exhibiting uniform birefringence. The specimen should be cut with its edges along the direction of principal strains as established by isoclinic observation.

b. Measurements of Birefringence - The retardation δ was measured prior to annealing in normal incidence δ_n, and in two oblique planes δ_{ox} and δ_{oy}, using rotation about the X and Y axes (see Figure 2).

c. Strain Relieving Process - The optimum strain-relieving temperature depends on the material and should be established by trial and error. A specimen placed in the oven is observed as the temperature slowly increases. When the proper strain-relieving temperature is reached, the birefringence decreases rapidly as deformation occurs. The specimen should be adequately supported, but unrestrained and allowed to expand or contract freely until the birefringence vanishes. Plate glass dusted with talcum powder provides good support. The specimen is cooled down slowly in order to avoid the introduction of thermal stress. After completion, the birefringence is essentially zero.

d. Measuring Strain - The change in length ΔL in the X and Y directions is defined as the difference in length before and after the annealing process.

Using a large micrometer, or a traveling microscope, one can measure L_x and L_y within 0.02 mm (.001 in). Exerting proper care, it is possible to assess the strains ε_x and ε_y to 0.1% or better, depending upon the initial size of the specimen. Since the measured strains are usually in excess of 2%, this procedure provides a satisfactory resolution.

Using the above procedure, several materials were evaluated and their permanent strain-optical sensitivities determined using the standard relation:

$$k_R = \frac{n_x - n_y}{\varepsilon_x - \varepsilon_y} = \frac{\delta_n}{t(\varepsilon_x - \varepsilon_y)}$$

where n_x and n_y are the indexes of refraction, and t is the measured thickness before the annealing process. When biaxially strained samples were evaluated, oblique incidence measurements were needed to evaluate k_R. The results of calibration performed on a large variety of material is shown in Table I.

It should be noted that when a biaxial strain field is investigated, or when a biaxially oriented specimen is used for calibration purposes, the oblique light path must be employed since δ measured in normal incidence could be small or zero. In this case, the relation used for calibration is:

$$k_R = \frac{\delta_{ox} + \delta_{oy}}{3t(\varepsilon_x + \varepsilon_y)} \frac{\cos\theta}{\sin^2\theta}$$

where δ_{ox} and δ_{oy} are retardations measured in the oblique path in the OX and OY planes. The Oblique Incidence Method is described in reference 5.

CONCLUSIONS:

Measurement of birefringence is a straight forward process that can be accomplished on any transparent or partly transparent material by using methods described in presently existing standards. Present methods permit observation and inspection of large non-flat objects by using either transmission or reflection photoelastic techniques. The method is applicable to a large variety of polymers, as shown in Table I. In some partly crystalline polymers, the birefringence is observed even in a totally strain-relieved condition, and special care must be exerted to avoid misinterpretation. Using material constants from Table I (or by obtaining via the calibration process described above), one can calculate residual strains from the measured birefringence, and thus obtain valuable information revealing the quality or safety margin of the tested part.

REFERENCES

[1] Ber. Sachs.Akad. Wiss. Math Physik Klasse (1898), 1-31

[2] Doyle, J. F. "An Interpretation of Photoelastic/Plastic Data." Experimental Mechanics, 20, No. 2, (1980), 65-67.

[3] Matsumoto, K., J. F. Fellers, and J. L. White. "Uniaxial and Biaxial Orientation Development and Mechanical Properties of Polystyrene Films." Journal of Applied Polymer Science, 20, (1981), 85-96.

[4] McNally, J. G. and S. E. Sheppard. "Double Refraction in Cellulose Acetate and Nitrate Films." Journal of Physical Chemistry, 34 (1930).

[5] Redner, S. "New Oblique-incidence Method for Direct Photoelastic Measurements of Principal Strains." Experimental Mechanics, 3, No. 3, (1963), 67-72.

[6] Spence, J. "Optical Anisotropy and the Structure of Cellulosic Sheet Materials." Kodak Research Lab Communication, No. 700 (1938).

[7] Stein, R. S. and A. V. Tobolsky. "An Investigation of the Relativity Between Polymer Structure and Mechanical Properties." Textile Research Journal, 18, No. 4, (1948), 201-223 and 302-314.

[8] Stein, R. S. "Measurements of Birefringence of Biaxially Oriented Films." Journal of Polymer Science, 24, (1957), 383-386.

[9] Stein, R. S. "Optical Studies of Stress-induced Crystallization of Polymers." Polymer Engineering and Science, 16, No. 3, (1976).

[10] Wilkes, G. L. "The Measurement of Molecular Orientation of Polymeric Solids." Advances in Polymeric Sciences, (1971), 91-136.

[11] Zandman, F., S. Redner, J. W. Dally. Photoelastic Coatings. Monograph No. 3, (1977), Society for Experimental Stress Analysis and Iowa State University.

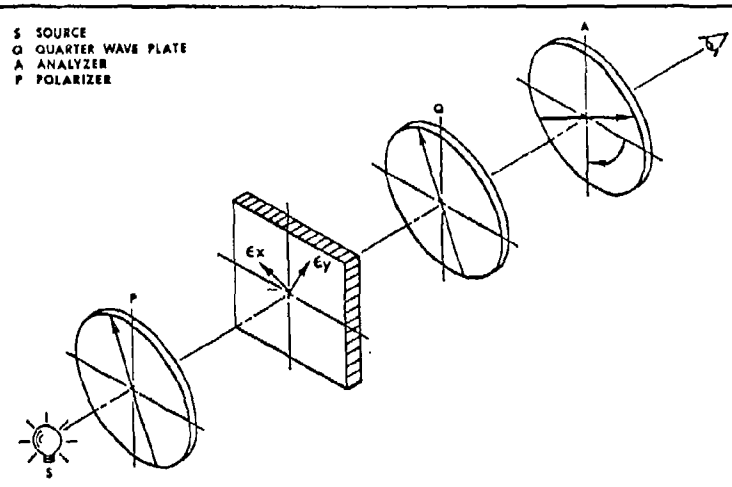

FIGURE 1

Polariscope Setup for Measurements of Small Birefringence in Glass.

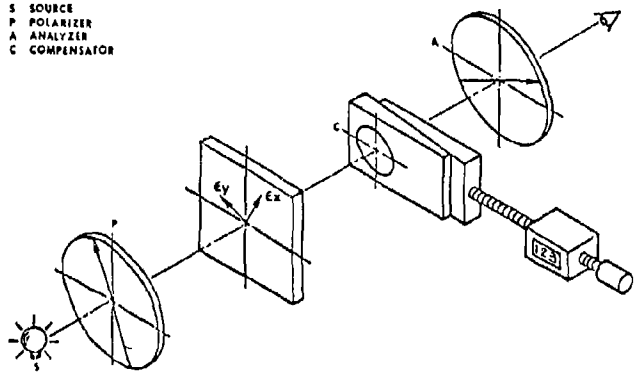

NORMAL INCIDENCE MEASUREMENT OF δ

FIGURE 2

Setup for Measurement of Birefringence in Plastic Materials.

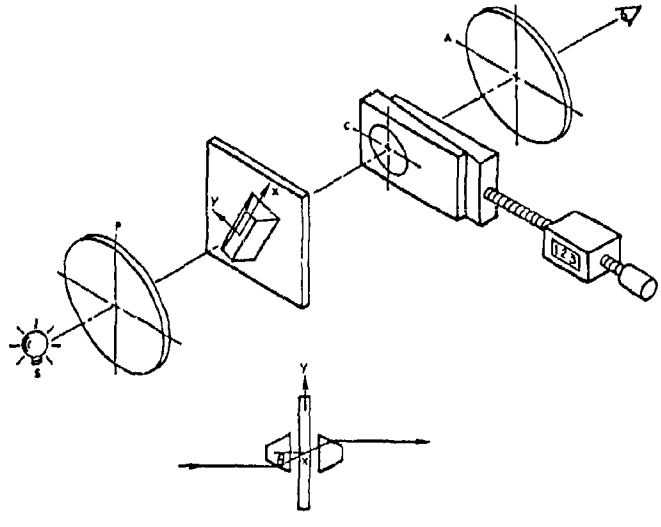

OBLIQUE INCIDENCE MEASUREMENT OF δ_{ox}

Photo 1a) Residual Strains in a Molded Polystyrene Lid.

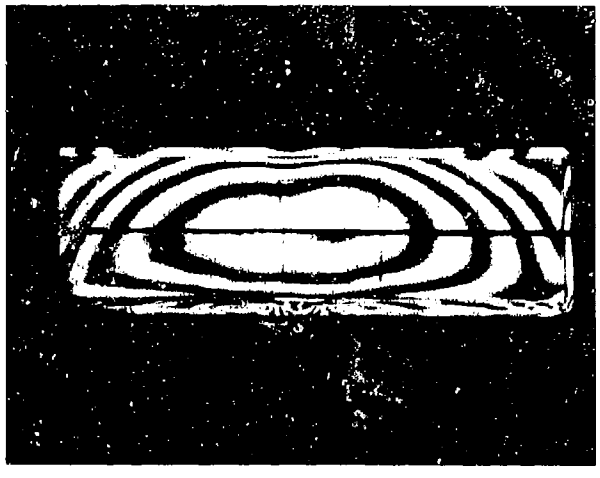

Photo 1b) After Cutting.

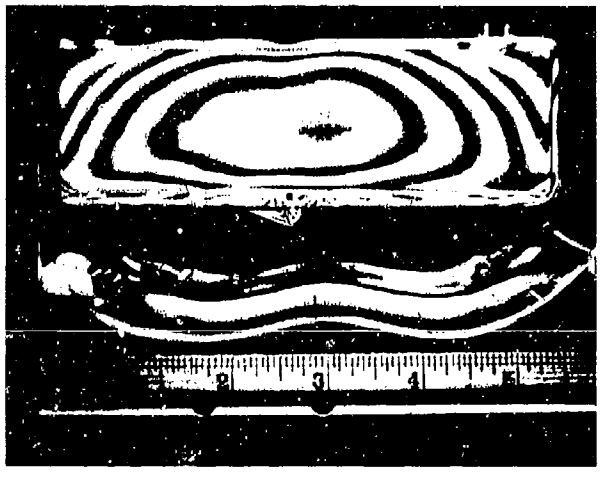

Photo 1c) After Annealing.

FIGURE 3 - RESIDUAL STRAINS IN A MOLDED POLYSTYRENE LID.

TABLE I

MATERIAL	STRAIN RELIEVING TEMPERATURE, °C	RELEASED STRAIN-OPTICAL CONSTANT $k_R \times 10^3$
Polyetherimide	220°	26
Amine Cured Cast Epoxy Resin	100°	28
PETG	100°	17
Polycarbonate (extruded)	160°	16
Polystyrene (Injection Molded)	120°	0.8
Acrylic	120°	0.5

SESSION IV

TESTING - CAPABILITIES AND LIMITATIONS (PART II)

Chairman: R. H. Walker
Flight Dynamics Laboratory
Wright-Patterson
Air Force Base, Ohio

Co-Chairman: J. W. Kozmata
Douglas Aircraft Company
Long Beach, California

AD-P003 210

ARTIFICIAL AGEING OF TRANSPARENT AEROSPACE MATERIALS

A. Davis, Ministry of Defense

Artificial Ageing of Transparent Aerospace Materials

A Davis

Ministry of Defence

Propellants, Explosives and Rocket Motor Establishment

Waltham Abbey
Essex
UK

Abstract

The AECMA working party which is drawing up a standard for the artificial weathering of aircraft transparencies has through a collaborative experimental programme shown the importance of measuring the output of ultraviolet radiation of the various lamps used in weathering chambers.

A simple method of monitoring radiation below 320 nm, based on the use of polysulphone film, is described. The manufacture and properties of the film are presented along with details of its use.

Variability in the output of a Xenon-arc source as a result of lamp and filter ageing is demonstrated and data on the ultraviolet intensity of different types of lamp are compared with measurements made outdoors at Dhahran, Innisfail and London.

INTRODUCTION

Solar ultraviolet radiation can cause chemical breakdown of many synthetic polymers and therefore it is important that the resistance of polymeric materials used in the construction of aircraft transparencies to this wavelength region is assessed.

In this context artificial ultra-violet sources are widely employed to assess the weathering capability of polymeric materials primarily because they can reduce the time required for evaluation. Another reason advanced for their use is that, with their controllable environment, weathering devices can provide a quality control test for materials. Certainly weathering machines present a much less variable environment than that found outdoors but the literature indicates that it would be erroneous to assume that the output of artificial ultraviolet sources can be considered constant.[1-3]

The value of ultraviolet sources as a means of assessing materials would be increased if their output could be readily measured for this would allow different exposure periods before the same lamp to be related. It would also permit the comparison of data obtained with different types of lamps to be put on a more sound basis. A factor which has limited progress in this area has been the lack of a simple means of monitoring the output of lamps particularly in the important UV region. Methods based on chemical actinometry have been successfully employed.[4][5] They have the advantage of requiring little capital outlay and of providing absolute measurements, however they are time consuming and require a high degree of technical skill.

The attraction of instrumental techniques are obvious; ideally they can provide continuous information and they should require little attention. However they are generally expensive and in practice their high level of sophistication calls for significant attention to their maintenance and calibration and to date there is no such instrument in common use.

At the Propellants Explosives and Rocket Motor Establishment, through our interest in the weathering of materials, we have developed a simple method of monitoring ultraviolet radiation based on the use of polysulphone film.[6]

This paper describes the properties of polysulphone film as a monitor of ultraviolet radiation and demonstrates how it has been used to compare the output of ultraviolet lamps and to measure the levels of solar radiation at a number of sites throughout the world.

Experimental

The UV monitoring technique referred to in this paper is based on the polysulphone manufactured by Union Carbide. Polysulphone film is prepared by casting a 10% chloroform solution on glass. A spreader with a 0.5 mm gap is used to give a film 40 microns thick. After removal from the glass the film is dried at 60°C in a vacuum oven overnight and stored in the dark before use.

Polysulphone film is only sensitive to wavelengths below 320 nm[6] (figure 1). When exposed to such radiation the UV absorption spectrum of the film increases and this increase, in particular the change in optical density at 330 nm (ΔA_{330}) as measured on a conventional UV spectrometer gives a measure of the incident radiation dose. The original A_{330} should be in the range of 0.155 to 0.175 and after exposure, to maximise the accuracy of the estimation ΔA_{330} should be less than 0.300.

The ΔA_{330} resulting from exposure of polysulphone film to a UV source can be expressed in terms of an equivalent dose of 305 nm monochromatic radiation and the resulting ΔA_{330} for polysulphone film is detailed in Table 1.[7]

By comparing ΔA_{330} for films irradiated at -4°C and 53°C it has been shown that temperature has no significant effect on the response of polysulphone. A dark reaction after exposure has been noted. This can amount to an increase in ΔA_{330} of around 4% over 24 hours and 5% over a week.

Table 1 Conversion of OD_{330} of Polysulphone Film to equivalent Dose of 305 nm Radiation, whm^{-2}

ΔOD_{330}	.01	.02	.03	.04	.05	.06	.07	.08	.09	.10	.11	.12	.13	.14	.15	.16
.000	.04	.09	.14	.19	.25	.32	.38	.45	.53	.60	.68	.76	.84	.92	1.0	1.09
.002	.05	.10	.15	.205	.265	.33	.395	.465	.54	.62	.70	.78	.86	94	1.02	1.10
.004	.06	.11	.16	.22	.28	.345	.41	.48	.555	.63	.715	.79	.87	.96	1.04	1.12
.006	.07	.12	.17	.23	.29	.355	.42	.50	.57	.65	.73	.81	.89	.97	1.05	1.14
.008	.08	.13	.18	.24	.31	.37	.43	.51	.59	.67	.55	.83	.91	.98	1.07	1.16

	.18	.18	.19	.20	.21	.22	.23	.24	.25	.26	.27	.28	.29	.30	.31	.32
.000	1.18	1.27	1.38	1.49	1.62	1.75	1.88	2.03	2.17	2.30	2.46	2.63	2.78	2.97	3.20	3.47
.002	1.19	1.29	1.4	1.51	1.65	1.77	1.90	2.06	2.20	2.34	2.49	2.65	2.82	3.02	3.25	3.53
.004	1.21	1.305	1.42	1.535	1.67	1.80	1.93	2.09	2.22	2.37	2.52	2.69	2.86	3.07	3.30	3.6
.006	1.23	1.33	1.44	1.56	1.70	1.83	1.96	2.12	2.25	2.40	2.56	2.72	2.895	3.11	3.35	3.67
.008	1.25	1.35	1.465	1.585	1.72	1.86	1.99	2.14	2.28	2.44	2.59	2.75	2.94	3.15	3.41	3.74

Results

The reproducibility of the polysulphone monitoring technique is indicated in Table 2 which shows ten simultaneous measurements.

Table 2 Reproducibility of Polysulphone Monitor

Film	ΔA_{330} Before exposure	ΔA_{330} After exposure*	ΔA_{330}	Dose† whm^{-2} of 305 nm
1	.170	.465	.295	2.88
2	.169	.459	.290	2.78
3	.166	.461	.295	2.87
4	.170	.459	.289	2.75
5	.168	.455	.287	2.74
6	.170	.461	.291	2.80
7	.171	.461	.290	2.78
8	.172	.460	.288	2.75
9	.169	.453	.284	2.69
10	.175	.474	.299	2.95

*30 minutes exposure

†obtainable from Table 1

Artificial Weathering Devices

The various weathering chambers examined, in particular their radiation sources are described below.

Carbon-arc Devices

The fugitometer has as its source a 1600W carbon-arc which is surrounded by a drum 500 mm in diameter equipped with a rack for holding test specimens. The carbon-arc is enclosed in a clear borosilicate glass cylinder and is mounted with its axis vertical and in the centre of the drum. The carbons are renewed daily and one hour is usually set aside for their replacement and for cleaning the glass cylinder.

A variation on this instrument which has the source off-set from the centre of a larger (2.1 m diameter) rotating drum was also included in the comparison (Marr).

Xenon-arc Devices

The Xenotest 150, 450 and 1200 arc weathering chambers developed by Original Hanau Quarylampen GMBH which have a Xenon-arc light source. Other manufacturers, offer similar instruments.

The light source of the Xenotest 150 is an air cooled high pressure 1500W Xenon burner. In this study six infra-red filters and one UV window (UG11) were employed.

The 4500W Xenon burner in the Xenotest 450 was also operated with six infra-red filters and one UV window (UG11).

The Xenotest 1200 has three 4500W Xenon burners one of which is replaced in sequence every 500 hours ie a lamp is used for a total of 1500 hours. A complex filter arrangement has been designed to reduce the infra-red intensity and the transmissivity in the UV region. In this study although most measurements were made with the UV filter; a few observations were made without the UV filter.

Fluorescent Lamp Devices

The Climatest is a development of the device first introduced by workers at The American Cyanamid Co. It has a radiation source consisting of 32 fluorescent lamps arranged vertically in pairs on the circumference of a drum around which specimens rotate at a distance of 40 mm from the lamps.

The spectral energy distribution depends on the choice of lamps; the lamps used in this study are described in the results section.

The Q-U-V is one of a number of weathering devices in which specimens under test are subject to UV exposure followed by periods of exposure to a hot humid environment. The UV source usually consists of 8 fluorescent tubes (FS-40) which have wavelength range of 280 to 450 nm with max at 313 nm.

In each weathering device measurements were made at positions normally occupied by specimens on test. To eliminate reflection films were exposed against a matt black background. By a process of trial and error a suitable exposure period was found for each weathering device which gave a A_{330} within the range covered by Table 1. For example for the Fugitometer exposures ranged from one to four days whereas with the Xenotest 1200 films were exposed for only five minutes when the machine was operated with the UV filter.

The Xenotest 1200 can be taken as representative of the current state of Xenon arc devices. It is instructive therefore to examine how its output of ultraviolet radiation varies with time. In this experiment starting with a completely new system ie new lamps, new filter etc the Xenotest 1200 was run with a UV filter which removes most of the radiation below 300 nm (figure 2). Up to about 1000 hours the UV level is constant but thereafter there is a gradual drop in output. This occurred even although after every 500 hours one of the lamps were sequentially replaced by a new lamp. Replacing a lamp increased the UV output but the effect varied. The output was also increased when the outer surface of the filters were washed with acid as recommended by the manufacturer (Table 3).

Table 3 Effect of Lamp Change and Filter Cleaning on UV Output of Xenotest 1200

Lamp Change				Filter Clean			
	Intensity (wm^{-2} 305 nm)				Intensity (wm^{-2} 305 nm)		
Hours	Before Change	After Change	% Increase	Hours	Before Cleaning	After Cleaning	% Increase
1504	4.44	4.5	1	1300	4.50	4.68	4
2004	3.6	3.6	0				
2516	3.18	3.78	19	2840	3.18	3.54	11
3000	3.66	3.84	5				
3498	3.54	4.08	15	3260	3.18		17

It is seen from table 3 that the combination of lamp changes and filter cleaning causes the output of the Xenotest 1200 to fluctuate in a periodic fashion. It is apparent that failure to replace or to wash the filters could reduce the output significantly.

Comparison of UV Sources

Table 4 compare the output below 320 nm of the artificial weathering devices examined.

Table 4. Comparison of UV Output of Artificial Sources

Weathering device	Intensity (Wm^{-2})
Fluorescent lamps	
Climatest (a) White and Black	13.3
(b) 05 Actinic	4.5
Q-U-V	18
Xenon-arc	
Xenotest 1200 (with uv/filter)	3.6
Xenotest 1200 (no uv/filter)	21.0
Xenotest 1200 (window glass)	0.2
Xenotest 450*	1.0
Xenotest 150*	2.3
Carbon-arc	
Fugitometer	0.02
Marr	0.01
Outdoors	
Vertical sun, clear sky conditions	4.2

*Age of lamps, 1000 h.

The devices with fluorescent lamps gave the highest UV levels. Dose levels of the order of .07 whm^{-2} min^{-1} have been measured outdoors with polysulphone when the sun overhead and clear sky conditions. The Q-U-V source is thus about 5 times more intense than global solar radiation below 320 nm.

The UV output of the Xenotest 1200 is very similar to the limiting outdoor value. Run without filters, as is suggested by the manufacturers for the evaluation of surface coatings, the UV intensity of the Xenotest 1200 is increased by a factor of 3.8.

Berger[9] has concluded from tests over a number of years on a wide variety of polymers that to produce the same change in properties the exposure times of the Xenotest 1200, 150 and 450 are in the ratio 1:2:3.0-3.5.

That is, the effective light intensities are in the ratio 3.5:1.75-1.15-1.0. This is very similar to the ratio of UV below 320 nm for these instruments shown in Table 11 and indicates the importance of this region of the spectrum in determining the breakdown of polymers.

The carbon-arc sources have outputs well below that which is found outdoors below 320 nm and therefore it must be considered unsuitable for the assessment of materials for aircraft transparencies.

The value of solar radiation intensity given in Table 4 refers to clear sky conditions when the sun is overhead. To get some estimate of the acceleration afforded by the artificial weathering devices considered data on the average daily dose of ultraviolet radiation at representative sites would be more appropriate. Figure 3 shows the average daily dose of solar ultraviolet radiation for each month at a temperate site, London (10), a dry tropical site, Dhahran on the Persian Gulf coast of Saudi Arabia (11) and at wet tropical site, Innisfail in Queensland, Australia (10). The expected seasonal variation in ultraviolet radiation dose with elevation of the sun is evident.

Figure 3 also shows the relative severity of the ultraviolet environment in Dhahran, particularly at the summer peak. The average daily dose there is more than double that received in the summer in London and one third greater than the summer dose experienced at Innisfail.

One consequence of the difference in latitude of the three sites is revealed on consideration of the ratio of the mid-summer average daily dose to that experienced at mid-winter for each site. In Dhahran ($26^{o}16'N$) at mid-summer the average daily ultraviolet radiation is about four times that received in mid-winter. In London ($51^{o}30'N$) there is approximately a thirty-fold increase between winter and summer, while at Innisfail ($17^{o}30'S$) the increase on going from winter to summer is about two-fold.

From figure 3 it can be estimated that the average daily dose of ultraviolet radiation over the year at Innisfail, Dhahran and London is 12, 12 and 3 whm^{-2} respectively. Comparison of these values with the dates of table (multiplied by 24 to give dosage in whm^{-2}) allows acceleration factors to be estimated. For example the Xenotest 1200 run with the UV filter gives an average acceleration factor of seven for Innisfail and Dhahran and 29 for London.

The AECMA Group, C7/SC2, has been directed to produce a standard for the artificial weathering of transparent aerospace materials. A working party composed of representatives from France (10) Germany (11) Italy (12) Spain (13) Sweden (14) and the UK (15) who are active in the field of artificial ageing was formed to help draw up this standard.

For the past two years the working party has been comparing the performance of weathering chambers they employ and trying to normalise the ageing data produced. This is being done by measuring at one laboratory (Rohm) the visual and optical properties of 4 test materials (3 polyacrylates and a polycarbonate) after various periods of exposure in a weathering chamber in each of the six participating countries (3 Xenotest 1200s and Xenotest 450, a Xenotest 150 and a fluorescent lamp chamber). The conditions within each chamber, namely air temperature, black panel temperature, relative humidity, radiation intensity and where applicable water spray cycle have been monitored.

The changes in optical properties as a result of exposure in the different chambers showed poor agreement when compared on a time scale. However when property change was plotted against ultraviolet radiation dose good agreement was observed. (There was a factor of about 5 between the lamp with the lowest and the lamp with the highest ultraviolet intensity).

We feel the agreement between the different weathering chambers can be improved and a second programme of exposures has been started where the effect of differences in ambient conditions other than ultraviolet environment will be investigated.

In addition to these artificial ageing programmes the same 4 test materials are being exposed outdoors at Huelva (Spain) and Innisfail (Australia). It is encouraging to note that the changes observed in these materials after a year's exposure when considered on an ultraviolet radiation scale are consistent with the changes observed produced by artificial ageing.

(C) Controller, Her Majesty's Stationery Office London 1983

References

1 N Z Searle, P Giesecke, R Kinmouth and R C Hirt, Appl. Optics 3, 923, 1964

2 E Capron and J R Crowder, JOCCA 58, 9, 1975

3 T Laus Plast. and Rub: Mats and Applications 2, 77, 1977

4 G S Forbes and L J Heidt, J. Amer. Chem Soc 56, 2363, 1934

5 C G Hatchard and C A Parker, Proc. Roy. Soc. A235, 518, 1956

6 A Davis, G H W Deane and B L Diffey, Nature 261, 169, 1976

7 A Davis and D Gardiner, Pol. Degn and Stab. 4, 145, 1982

8 J Hennig and H H Horn, Kunst, 68, 494, 1978

9 K Berger Popular Plast. 23, 19, 1978

10 M Kuras Aerospatiale

11 Dr Lehmann Rohm

12 M Tocci Aeritalia

13 M. Ruis Murillo Inta

14 M. Ossiansson Saab-Scania

15 Dr Davis MOD

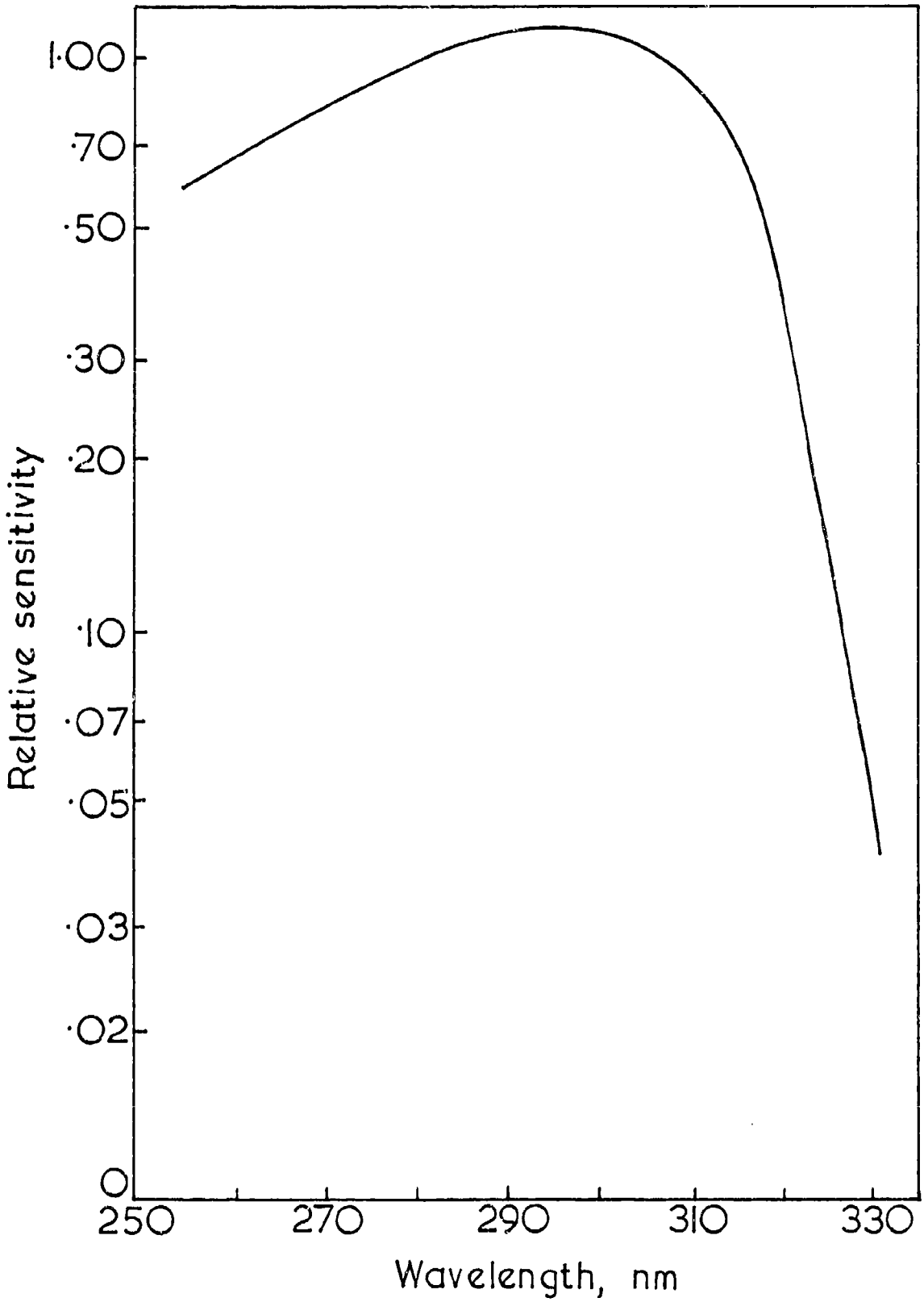

Figure 1 Spectral sensitivity of polysulphone film

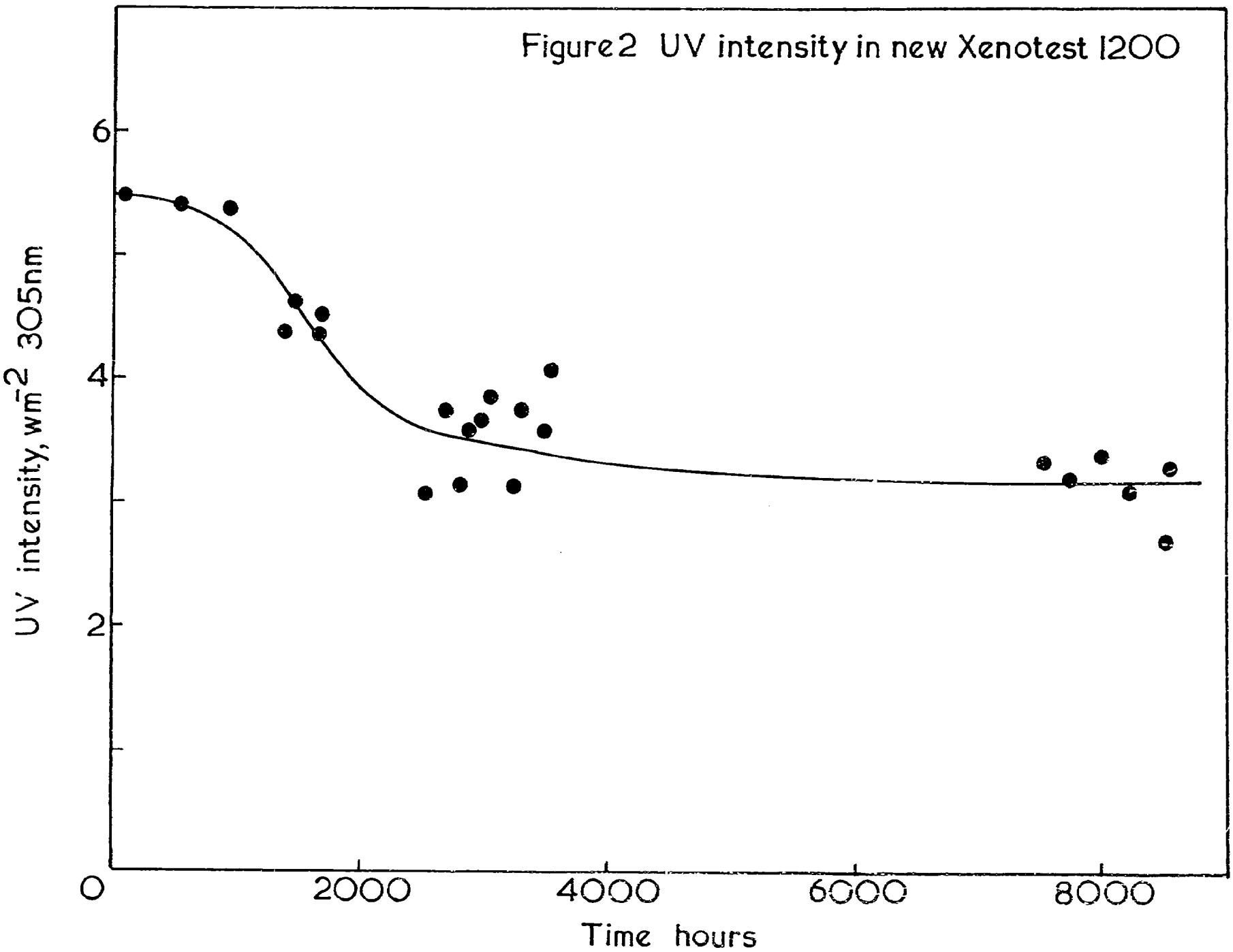
Figure2 UV intensity in new Xenotest 1200
UV intensity, wm⁻² 305nm
595
6
4
2
0
2000
4000
6000
8000
Time hours

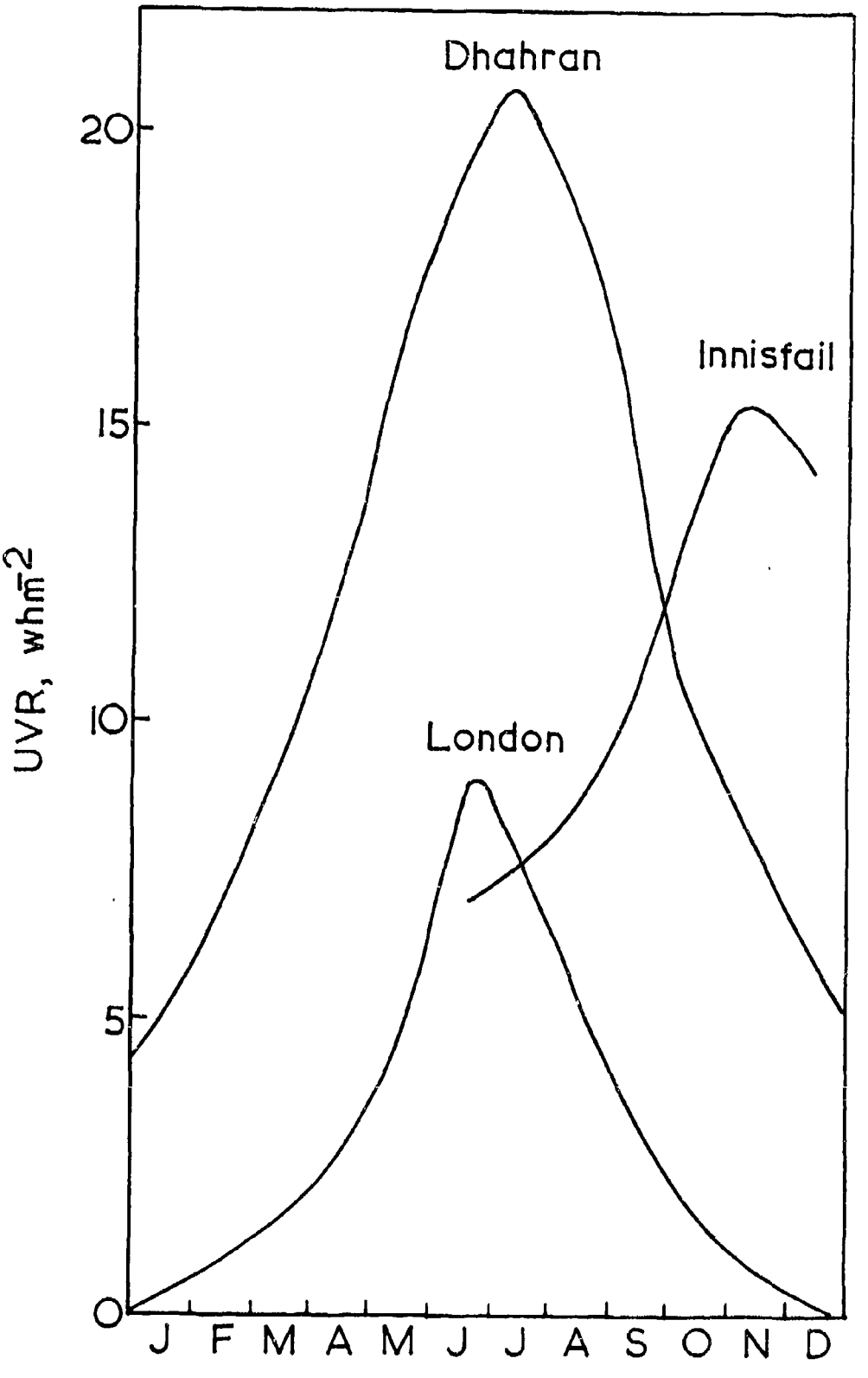

Fig3 Average daily UV at three sites

AD-P003 211

THE NEED FOR APPLICATION OF DYNAMIC MECHANICAL ANALYSIS IN THE EVALUATION OF INTERLAYER MATERIALS

A. Jayarajan, Boeing Commercial Aircraft

THE NEED FOR APPLICATION OF DYNAMIC MECHANICAL ANALYSIS IN THE EVALUATION OF INTERLAYER MATERIALS

A. JAYARAJAN
BOEING MATERIALS TECHNOLOGY
P.O. BOX 3707, M.S. 73-43
SEATTLE, WASHINGTON 98124

ABSTRACT

Interlayer materials like Polyvinyl Butyral (PVB), Silicone and Urethane are viscoelastic in their mechanical behavior. Mechanical properties of a viscoelastic material are not only dependent on temperature, but also highly dependent on frequency or strain rate. Dynamic mechanical analysis provides an effective experimental tool to measure the viscoelastic properties over a wide range of temperatures and in the time range of a few seconds up to 10^{-5} seconds. It is especially suitable for studying the viscoelastic nature of interlayer materials since the temperature and strain rate conditions for windshield design and service are within the measurement and analytical capabilities of DMA.

For illustration of the above facts, the viscoelastic properties of PVB-3GH and PVB-AG2 interlayers have been studied using DMA. Compression modulus and tan δ curves at 4°C increments from 30 to 70°C, in the frequency range of 0.1 Hz to 100 Hz have been measured. Master curves for complex modulus and tan δ with respect to frequency at the reference temperature of 39°C have been obtained by applying the time-temperature superposition principle to the above data. G', G" and tan δ vs. temperature characteristics have been measured for the same materials ranging from -100 to 140°C.

LIST OF FIGURES

Figure	
1	Schematic of One Type of Dynamic Mechanical Test
2	PVB/AG2, Complex Modulus vs Frequency
3	PVB/AG2, Tan δ vs Frequency
4	PVB/3GH, Complex Modulus vs Frequency
5	PVB/3GH, Tan δ vs Frequency
6	PVB/AG2, G', G" vs Temperatures Below Tg
7	PVB/AG2, Tan δ vs Temperatures Below Tg
8	PVB/AG2, G', G" vs Temperatures Above Tg
9	PVB/AG2, Tan δ vs Temperatures Above Tg
10	PVB/3GH, G', G" vs Temperatures Below Tg
11	PVB/3GH, Tan δ vs Temperatures Below Tg
12	PVB/3GH, G', G" vs Temperatures Above Tg
13	PVB/3GH, Tan δ vs Temperatures Above Tg

LIST OF TABLES

Table	
1	Damping Characteristics Comparison for PVB/AG2 and PVB/3GH Interlayers

INTRODUCTION

Interlayers in windshields perform important functions under conditions of large variations in temperature and strain rate. For commercial aircraft windshield application, this temperature range is approximately from -65°F to 130°F and the strain rate range is from a low of 0.01 in./min (.00017 in./in./sec) to a high of 12000 in./in./min (200 in./in.sec)[1]. In the case of low strain-rate loading and high temperature environment, the interlayer must transfer loads without excessive deformation or permanent set, which depend on good elastic properties. Under high strain rate conditions and low temperature environment, good plastic properties interlayers are needed to absorb shock loads like a bird impact.

The mechanical properties of interlayers under these varied but important conditions can be measured more easily and reliably using Dynamic Mechanical Analysis (DMA).

DMA

DMA tests measure the response of a material to a sinusoidal or other periodic stress. Since the stress and strain are generally not in phase, two quantities can be determined - a modulus and a phase angle or a damping term. There are many types of dynamic mechanical test instruments. One type is schematically illustrated in Figure 1. The general types of dynamic mechanical instruments are free vibrations, resonance forced vibrations, non-resonance forced vibrations, and wave and pulse propagation instruments.

Although any one instrument has a limited frequency range, the different types of apparatus are capable of covering the range from a fraction of a cycle per second up to millions of cycles per second or a time range of a few seconds up to 10^{-5} seconds. Whenever the frequency range on any one instrument is not adequate for the application, a master curve covering a wider frequency scale can be generated by conducting the experiments at different temperatures using the available frequency range of the instrument. This is possible to do since most polymers especially interlayers lend themselves for the application of time temperature superposition principle.

The master curves for median batches of PVB-3GH (99081) and PVB/AG2 (57150) are illustrated in Figures 2-5. These plots at the reference temperature shown yield the required data in the strain rate range of interest for the application to windshields.

Schematic of One Type of Dynamic Mechanical Test

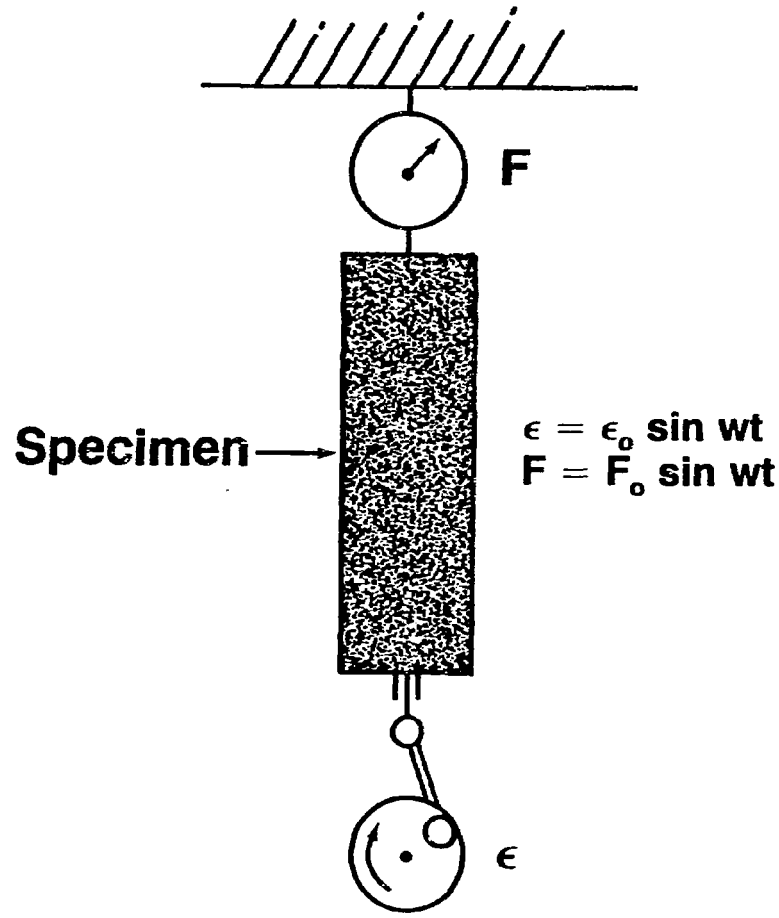

Figure 1

PVB/AG2 Complex Modulus Versus Frequency

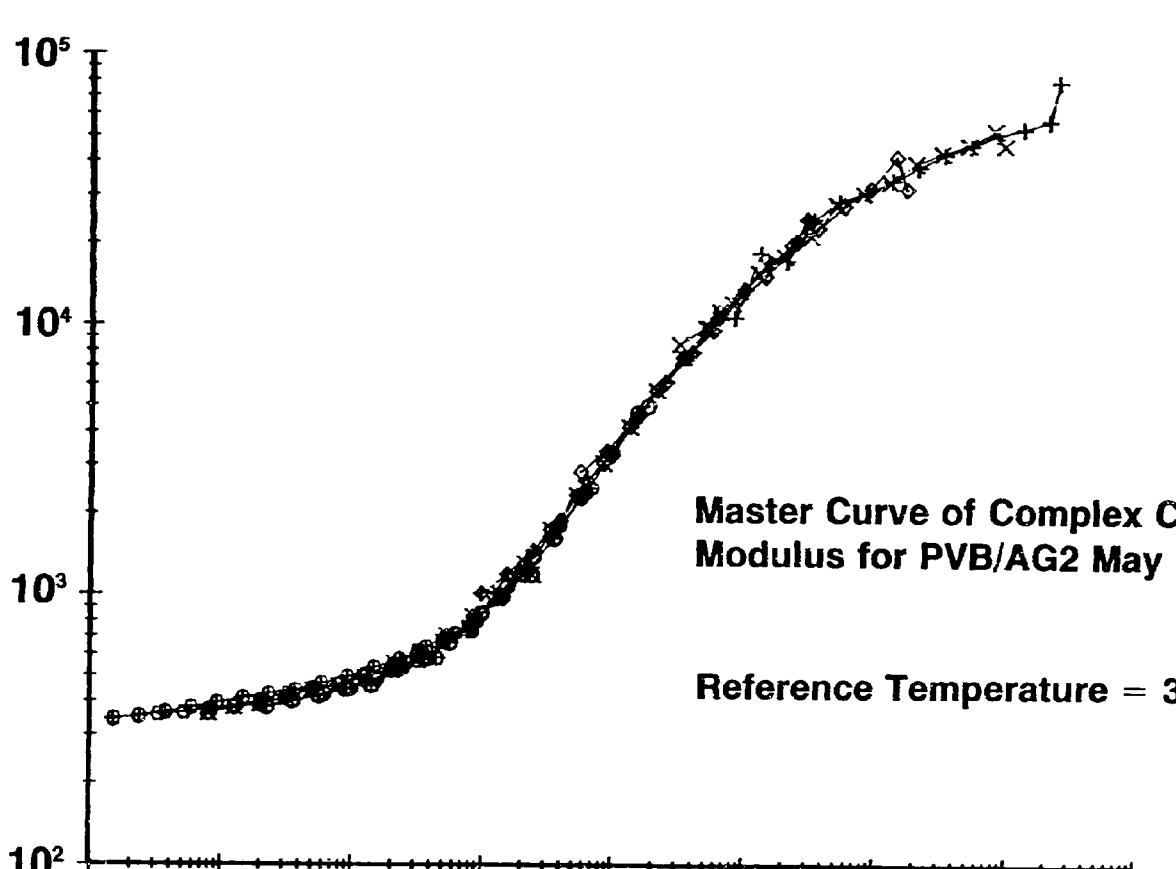

Master Curve of Complex Compression Modulus for PVB/AG2 May 17, 1983.

Reference Temperature = 39.6 deg C

Figure 2

602

PVB/AG2 Tan δ Versus Frequency

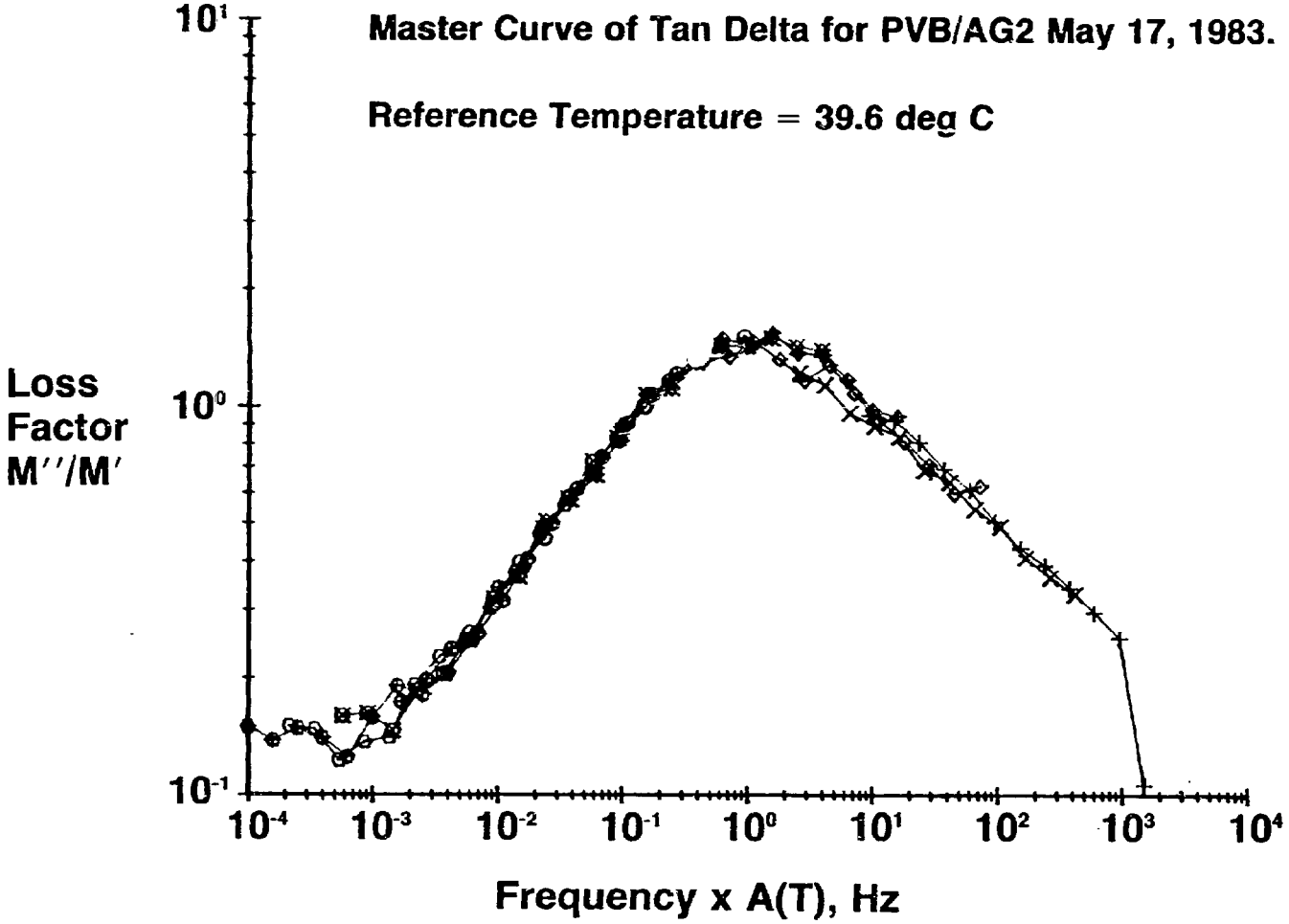

Figure 3

PVB/3GH Complex Modulus Versus Frequency

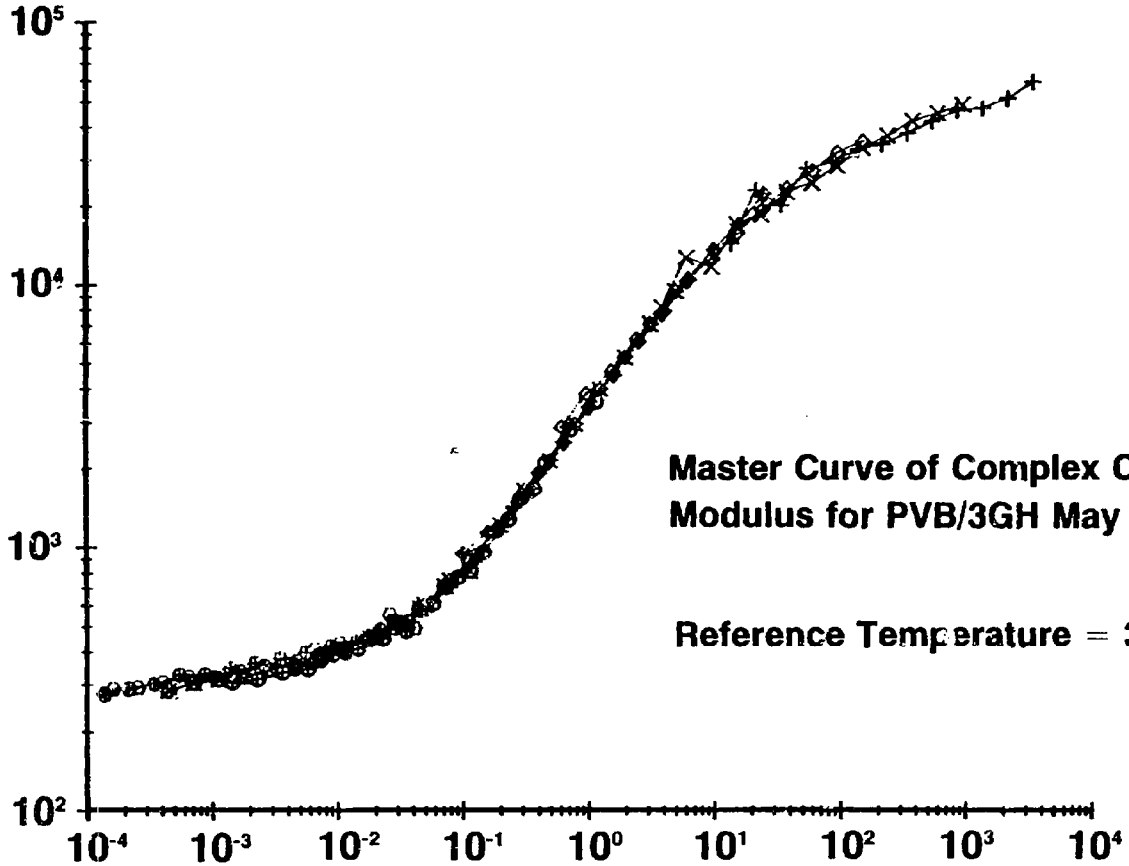

Figure 4

PVB/3GH Tan δ Versus Frequency

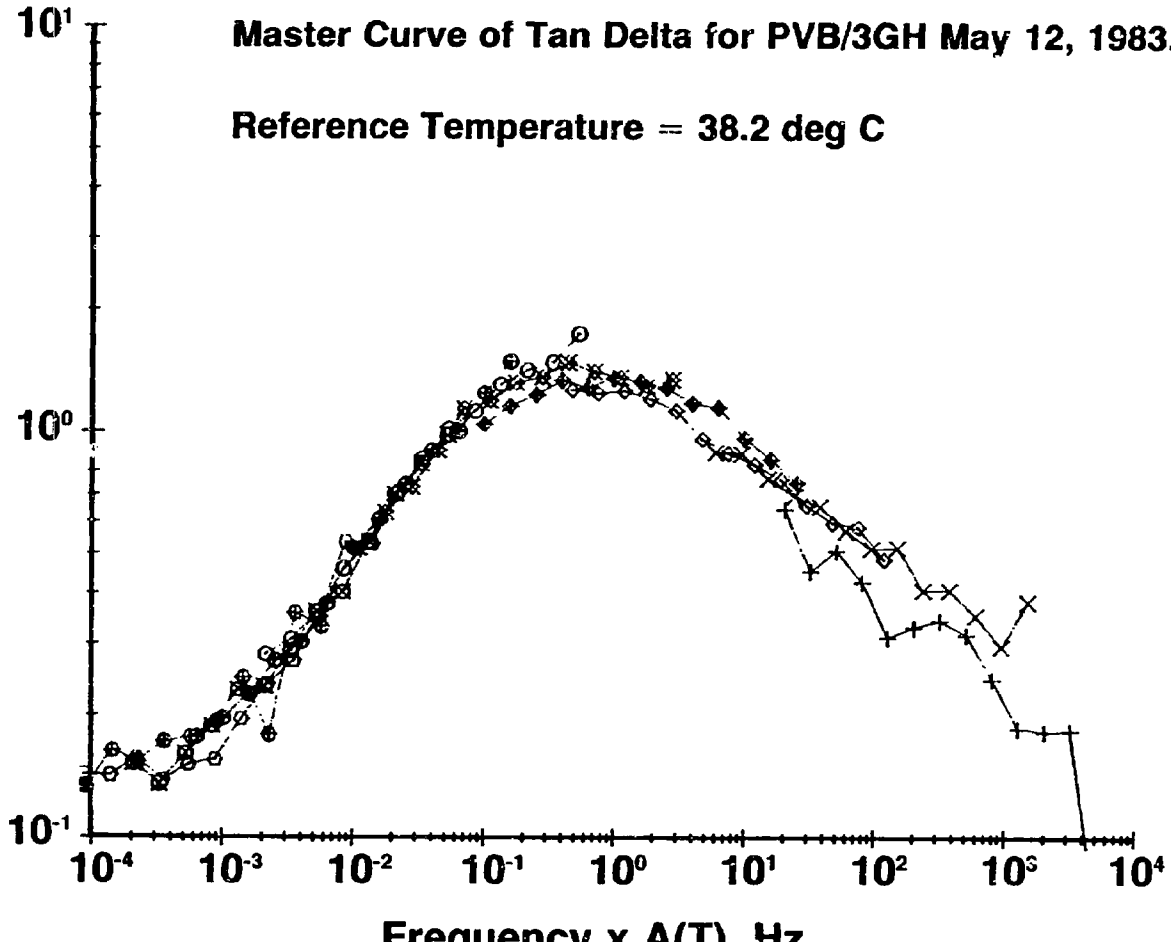

Figure 5

Discussion of DMA Data on PVB Interlayers

[2]Dynamic mechanical results are generally given in terms of complex moduli or compliances. The notation will be illustrated in terms of shear modulus G, but exactly analogous notation holds for Young's modulus E. The complex moduli are defined by:

$$G^* = G' + i\,G'' \tag{1}$$

where G^* is the complex shear modulus, G' is the real part of the modulus and $i = \sqrt{-1}$. G'' is called the loss modulus and is a damping or energy dissipation term. The angle which reflects the time lag between the applied stress and strain is δ and it is defined by a ratio called the dissipation factor.

$$\tan\delta = G''/G' \tag{2}$$

The '$\tan\delta$' is a damping term and is a measure of the ratio of energy dissipated as heat to the maximum energy stored in the material during one cycle of oscillation. For small to medium damping, G' is the same as the shear modulus measured by other methods at comparable time scales. The loss factor G'' is directly proportional to the heat H dissipated per cycle as given by,

$$H = \pi G''\,\gamma_o \tag{3}$$

where γ_o is the maximum value of the shear strain during a cycle.

Figures 6, 7, 8 and 9 show G', G'' and tan vs. temperature plots for PVB/AG2 interlayer. Figures 10, 11, 12 and 13 show the same plots for PVB/3GH interlayer.

The dynamic modulus or the modulus measured by any other technique is one of the most basic of all mechanical properties and its importance in any structural application is well known. Damping is often the most sensitive indicator of all kinds of molecular motions which are going on in a material even in the solid state. These motions are of great practical importance in determining the mechanical behavior of polymers. The absolute value of the damping and the temperature and frequency at which damping peaks occur will be of considerable interest in the selection and comparison of interlayer materials. Many other mechanical properties are intimately related to damping; these include toughness and impact strength and fatigue life.

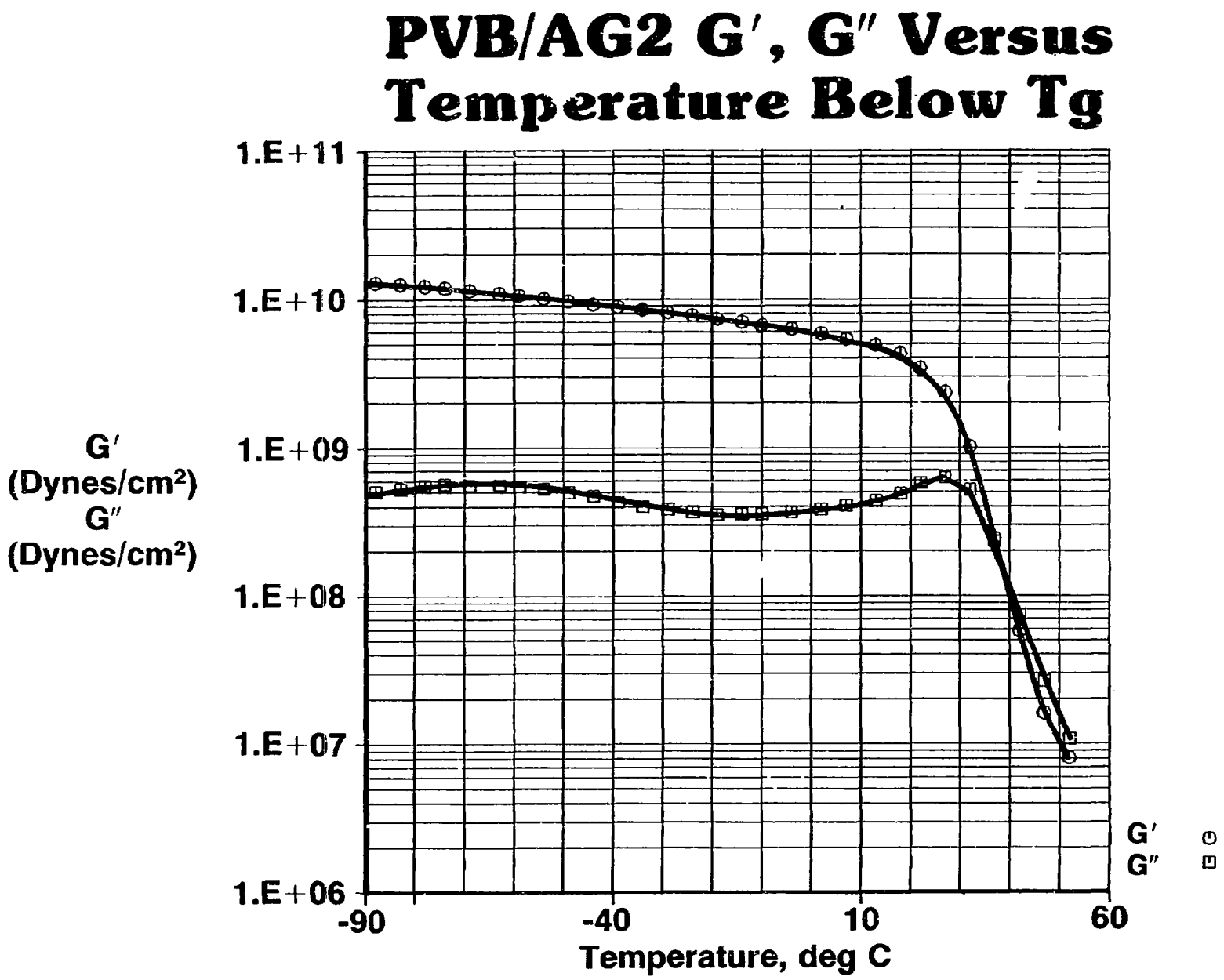
PVB/AG2 G′, G″ Versus Temperature Below Tg
1.E+11
1.E+10
1.E+09
1.E+08
1.E+07
1.E+06
G′ (Dynes/cm²)
G″ (Dynes/cm²)
-90
-40
10
60
Temperature, deg C
G′
G″

Figure 6

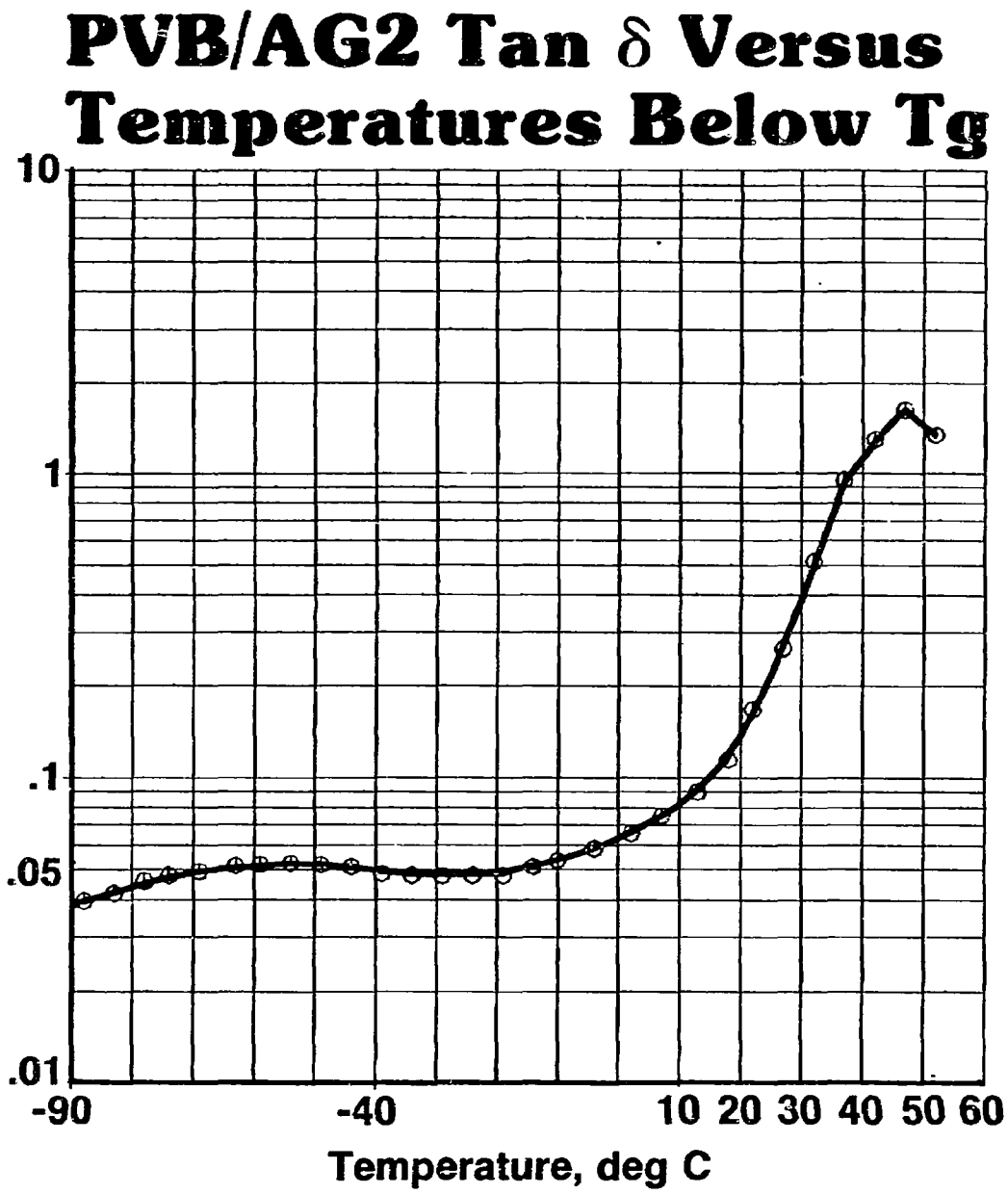
PVB/AG2 Tan δ Versus Temperatures Below Tg
Tandel
10
1
.1
.05
.01
-90
-40
10 20 30 40 50 60
Temperature, deg C

Figure 7

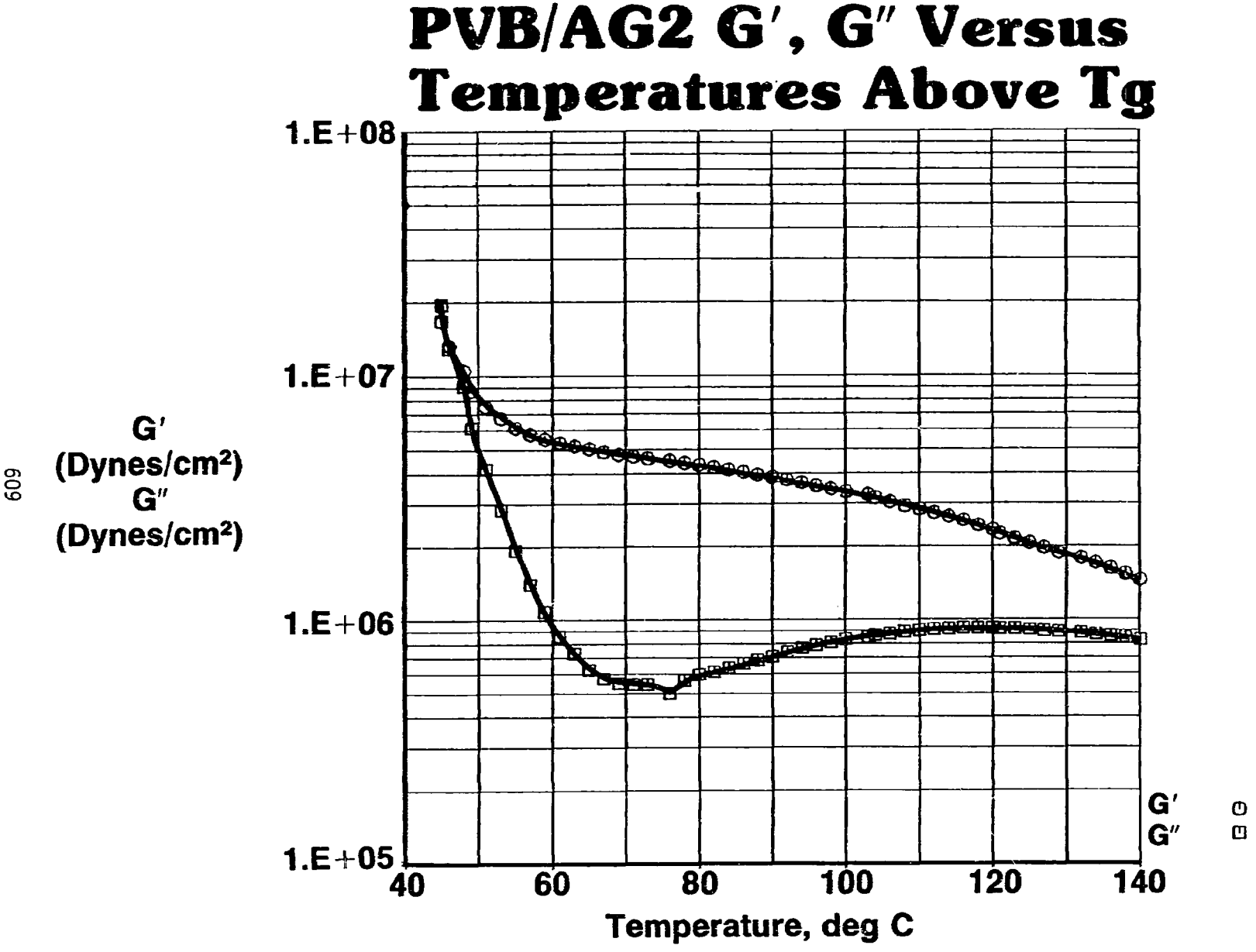
PVB/AG2 G′, G″ Versus Temperatures Above Tg
1.E+08
1.E+07
1.E+06
1.E+05
G′ (Dynes/cm²)
G″ (Dynes/cm²)
40
60
80
100
120
140
Temperature, deg C
G′
G″

Figure 8

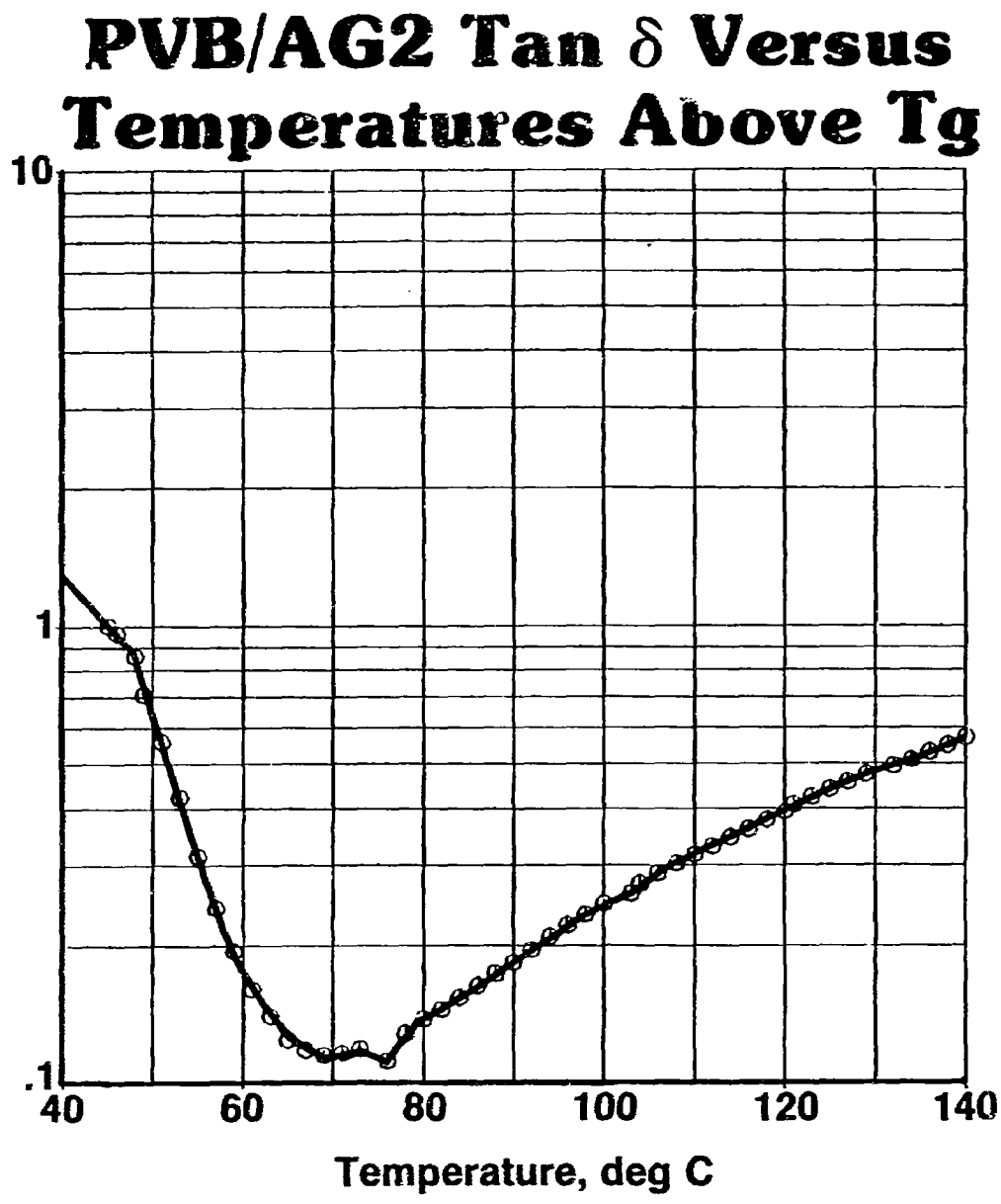
PVB/AG2 Tan δ Versus Temperatures Above Tg
Tandel
10
1
.1
40
60
80
100
120
140
Temperature, deg C

Figure 9

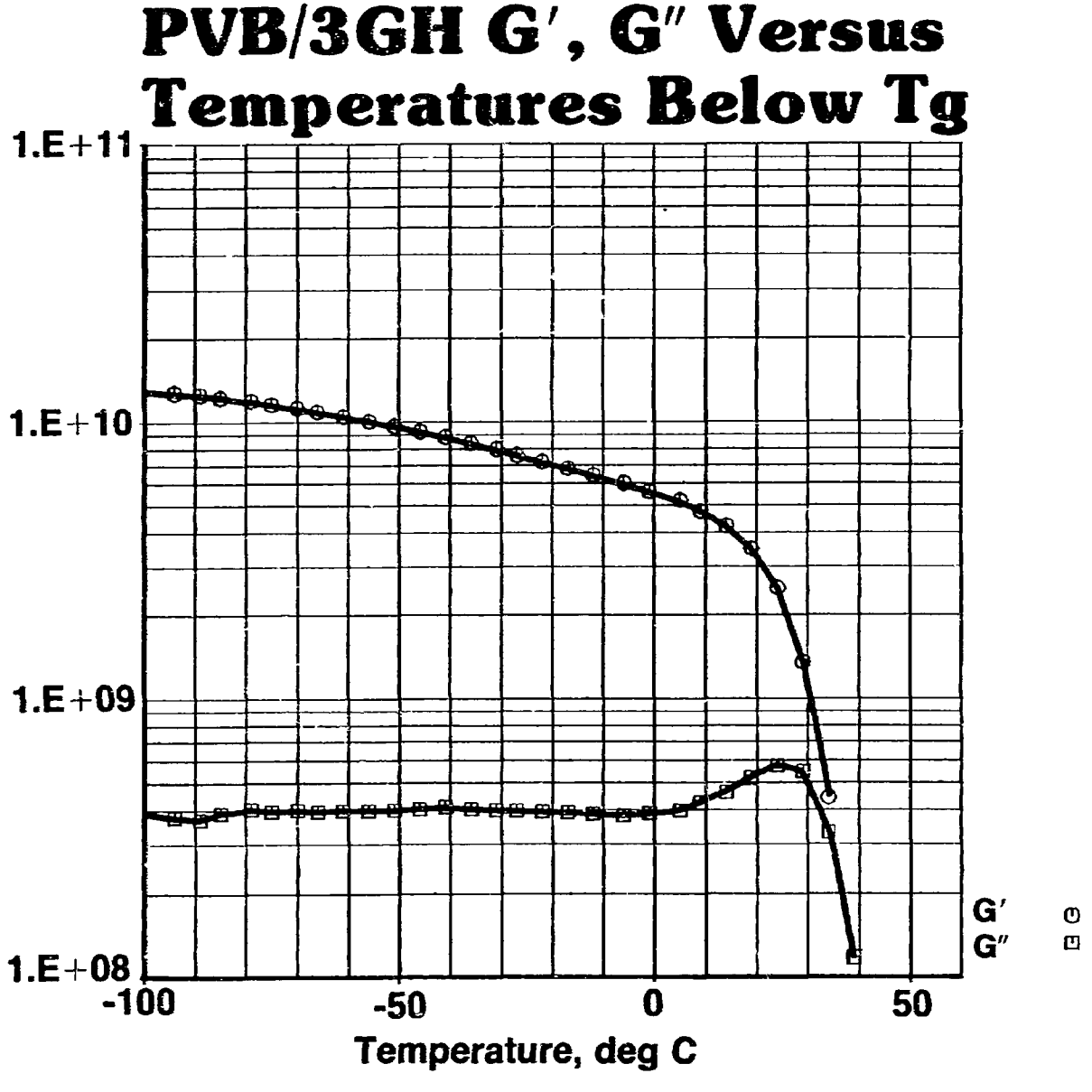
PVB/3GH G′, G″ Versus Temperatures Below Tg
1.E+11
1.E+10
1.E+09
1.E+08
G′ (Dynes/cm²)
G″ (Dynes/cm²)
-100
-50
0
50
Temperature, deg C
G′
G″

Figure 10

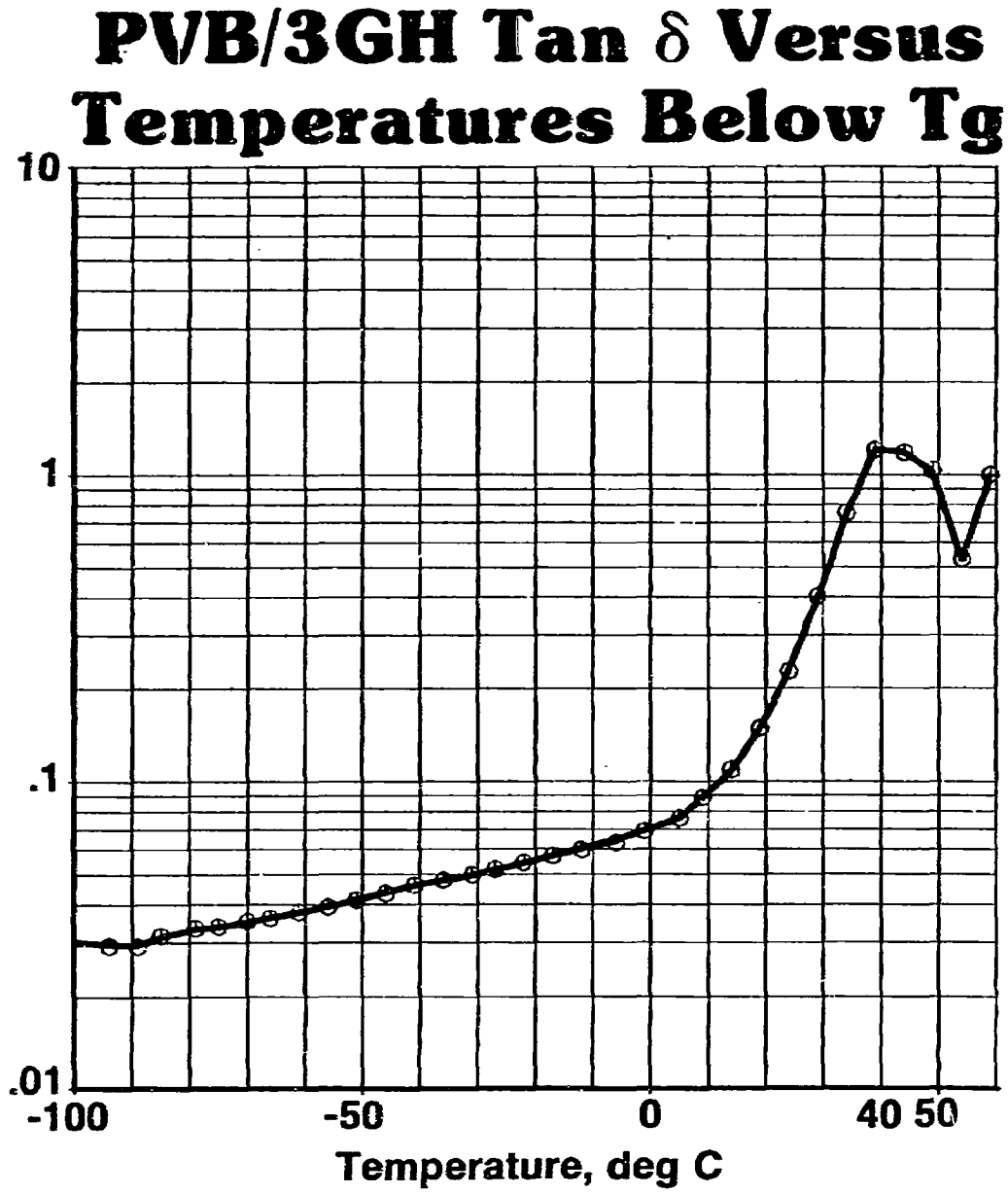
PVB/3GH Tan δ Versus Temperatures Below Tg
Tandel
10
1
.1
.01
-100
-50
0
40 50
Temperature, deg C

Figure 11

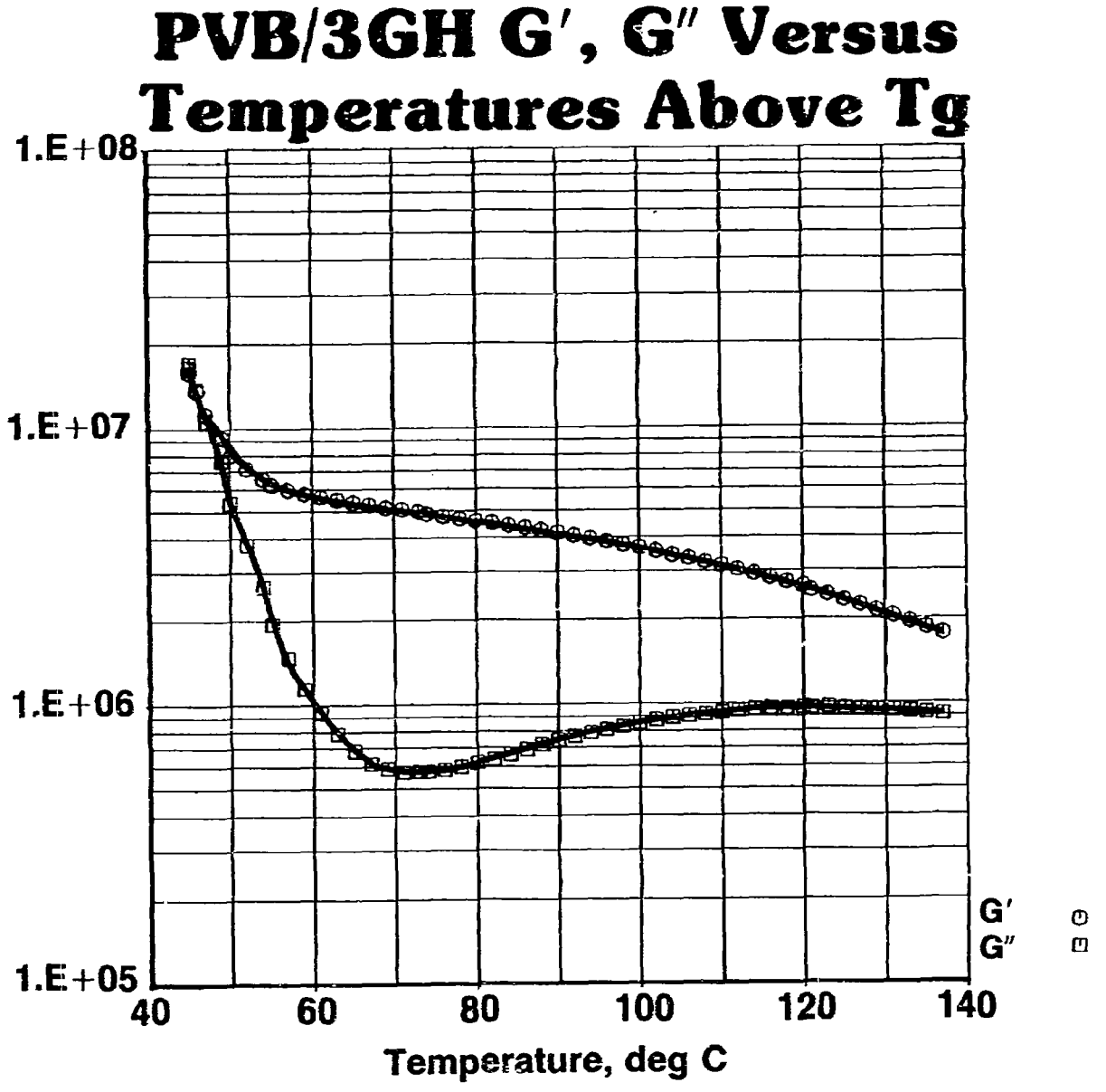
PVB/3GH G′, G″ Versus Temperatures Above Tg
1.E+08
1.E+07
1.E+06
1.E+05
G′ (Dynes/cm²)
G″ (Dynes/cm²)
40
60
80
100
120
140
Temperature, deg C
G′
G″

Figure 12

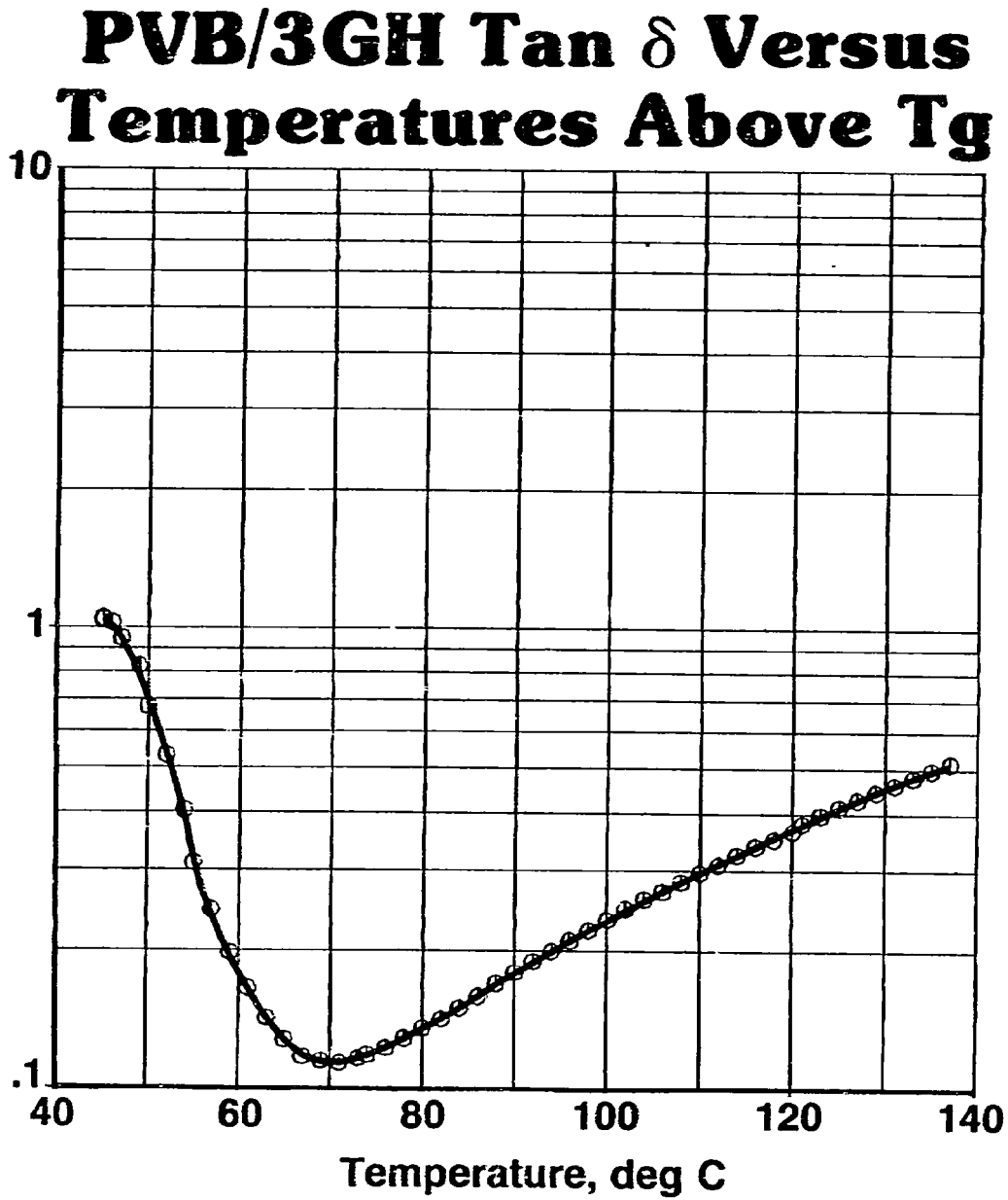
PVB/3GH Tan δ Versus Temperatures Above Tg
Tandel
10
1
.1
40
60
80
100
120
140
Temperature, deg C

Figure 13

Dynamic Mechanical Analysis Equations

$$G^* = G' + \sqrt{-1}\, G'' \quad \ldots . 1$$

$$\text{Tan } \delta = G''/G' \quad \ldots \ldots \ldots . 2$$

$$H = \pi\, G''\, \gamma_0 \quad \ldots \ldots . 3$$

Where

G^* = Complex Modulus

G' = Storage Modulus

G'' = Loss Modulus

δ = Angle Which Reflects the Time Lag Between the Applied Stress and Strain

$\text{Tan } \delta$ = Loss or Dissipation Factor

γ_o = Maximum Shear Strain During a Cycle

H = The Heat Dissipated per Cycle

Figure 14

Frequency is expressed using the units of Hertz (1 Hz = 1 cycle/sec.). Time period of a cycle is the inverse of the frequency value.

Table 1 summarizes the damping characteristics for PVB/AG2 and PVB/3GH interlayers. A major damping peak for 3GH plasticized vinyl occurs at a lower temperature and strain rate than AG2 vinyl, but the peak values of tan are slightly smaller.

The secondary damping peak for AG2 vinyl at colder temperatures is an attractive feature of this interlayer. AG2 vinyl has better impact resistance than 3GH vinyl at colder temperatures.

CONCLUSION

DMA offers an important test method to study mechanical behavior of interlayer materials in the temperature and strain rate ranges of interest for windshield applications. This analysis can also aid in material formulation and quality control.

The author is grateful to Mr. Ken Tanino of Boeing Materials Technology for conducting the necessary DMA experiments and producing all the plots included in this paper.

Damping Characteristics of PVB/AG2 and PVB/3GH Interlayers

Material		Tan δ Versus Temperature		Tan δ Versus Frequency	
		Temperature of Damping Peak (°C)	Absolute Value	Frequency of Peak (Hz)	Absolute Value
57150 PVB/AG2	a)	47	1.63	1.9	1.5
	b)	-54°C	0.0525	–	–
99081 PVB/3GH	a)	39	1.2	0.4	1.4
	b)	Nil	Nil	–	–

Table 1

REFERENCES

1. Greene, F. E., "Testing for Mechanical Properties of Monolithic and Laminated Polycarbonate Materials," AFFDL-TR-77-96, Part 1, Oct. 1978.

2. Nielsen, L. E., "Mechanical Properties of Polymers and Composites, Vol. 1," Marcel Dikker, Inc., New York, 1974.

AD-P003 212

SIMULATION OF EXPOSURE OF AIRCRAFT TRANSPARENCIES TO FLIGHT LINE ENVIRONMENT

A. Piekutowski, University of Dayton

SIMULATION OF EXPOSURE OF AIRCRAFT TRANSPARENCIES TO FLIGHT LINE ENVIRONMENT

Andrew J. Piekutowski
University of Dayton Research Institute

Abstract

During the major portion of their lifetime, aircraft transparencies are subjected to the flight line environment. Processes initiated or aggravated by exposure to the elements usually reduce the useful life of the transparency. A procedure for developing an accelerated flight line environment test is presented.

Determination of the acceleration rate of weathering simulated in the test cycle is based on the definition of a so-called worst case day for exposure to ultraviolet radiation. In the continental United States, this day would occur near the summer solstice at a number of locations in the southern states. Consideration of yearly variations in the terrestrial ultraviolet spectrum was used to define a worst case day and determine the number of worst case days which would be equivalent to a year of normal exposure at Phoenix, Arizona. Acceleration rate for the simulated flight line environment test was determined by dividing the total dosage of ultraviolet radiation produced by a "constant" laboratory source in the test environment by the total amount of ultraviolet radiation which would have been absorbed during a "year" of worst case days.

In the combined flight and flight line environment test facility, the test article was exposed to ultraviolet radiation produced by fluorescent sunlamps and black lights. A year of normal exposure to ultraviolet radiation was simulated in two months of testing. The flight line environment test cycle which is presented also incorporated runway thermal and moisture effects in the test cycle, although not at accelerated rates.

Introduction

While in the flight line environment, aircraft transparencies are exposed to agents which tend to reduce their useful life. Accidental or prolonged contact with fuels, oils, or other chemicals, for example, can produce a sudden change in the useful life of a transparency. Exposure to sunlight, rain, dew, dust, temperature changes, etc., result in a more subtle and gradual degradation of transparency optical and material properties. In general, several years of exposure to these natural elements (weathering) is required before transparency performance is determined to be unacceptable. For the purposes of evaluating new transparency designs or

materials and/or acceptance testing of production articles, an accelerated test facility for the effects of weathering was constructed. The method used to determine an acceleration rate for the simulated exposure tests represents one of several approaches which were considered; however, it was determined to be appropriate for the transparency materials which would be evaluated.

Determination of the acceleration rate of the weathering exposure simulated in the test facility will remain an area of controversy since acceptance of certain assumptions and compromises was required. The basic concept involved in the formulation of an acceleration rate is the definition of a worst case day. Realistically, this day would occur near the summer solstice at a location in Florida or Arizona or some other nearby area of the southwestern United States.

Considerations of the daily and yearly variation in the amount and spectral content of solar radiation which reaches the earth's surface were used to determine the number of worst case days equivalent to a year of natural exposure. Since the sources in the test facility produced radiation at levels which significantly exceeded those in natural radiation, a relatively short exposure time was required to produce the equivalent of one worst-case-day exposure. Thus, a year of natural exposure can be simulated by merely exposing the test article to the appropriate number of worst case days. Test acceleration rate can then be determined in a straightforward manner.

Discussion

The manner in which solar radiation effects are to be duplicated and/or accelerated in a test facility dominates design concept considerations. A variety of solar simulators and test equipment have been designed and are available commercially. Light sources used in these simulators are generally designed to faithfully duplicate the solar spectrum which reaches the earth's surface. These sources, carbon arc, short-arc xenon, and long-arc xenon, etc., are very costly and, at best, provide little or no capability for accelerated tests.

Review of the literature (References 1,2,3) indicates that only the quanta of light in the ultraviolet region of the solar spectrum have sufficient energy to initiate degradation of polycarbonates and most polymeric materials. Moderately priced fluorescent sunlamps and black lights which produce an abundance of ultraviolet radiation in the range of wavelengths which promote degradation of these materials are available. The level of ultraviolet radiation produced by these sources is such that a test facility using these lamps will permit test times that are reasonably accelerated. Use of fluorescent

lamps, however, will permit the transparency to be exposed only to the ultraviolet portion of the solar spectrum with only insignificant amounts of visible and infrared radiation present in the test facility environment.

Solar spectral irradiation varies with path length through the earth's atmosphere to the earth's surface. This path length is called the Optical Air Mass or simply Air Mass. Representative levels and spectral content of solar radiation for two air masses are given in Figure 1.

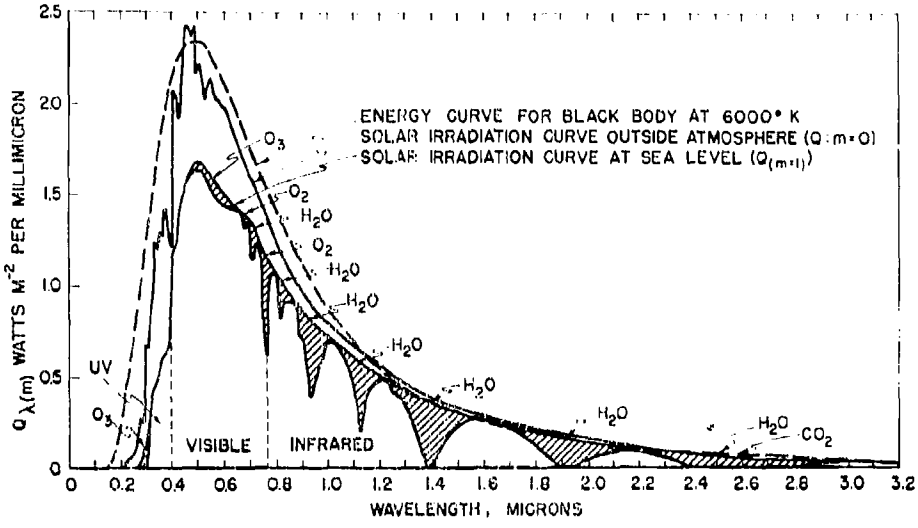

Figure 1. Spectral Energy Curves Related to the Sun (Taken from Reference 4).

In this figure, note the significant difference in the total amount (area under the curve) and the spectral characteristics of the ultraviolet portion of the spectrum, i.e., wavelengths shorter than 0.4 microns or 400 nm. As the Optical Air Mass numbers increase, i.e., path lengths greater than m = 1, corresponding reductions in the total amount of ultraviolet and other wavelengths of radiation occur.

On or near the summer solstice, the shortest wavelengths of ultraviolet radiation in the solar spectrum reach the earth's surface. In addition, the total amount of radiation which reaches the earth is greatest for this day. As the annual cycle approaches or recedes from this day, the total daily dosage of irradiation decreases and the shorter wavelengths of ultraviolet radiation begin to be absorbed in the earth's atmosphere as the path length through the atmosphere lengthens. In winter, and for a portion of spring and fall, the wavelength which polycarbonate is most sensitive to, 295 nm, is not present in the spectrum. In addition, the total amount of ultraviolet

radiation present in the winter is considerably less than is present in the summer, and in terms of potential to degrade polycarbonate, may be of little significance. Development of the worst-case-day concept must consider and account for the daily and yearly variation in the terrestrial ultraviolet spectrum.

Data presented in Figure 2 represent average daily solar irradiation for a number of locations in the United States. Casual examination of this figure will provide the reader an indication for various locations in the contiguous 48 states. Further work will concentrate on a location like Phoenix, AZ (site No. 9); however, the procedure outlined could be applied to the determination of worst-case-day values for other locations.

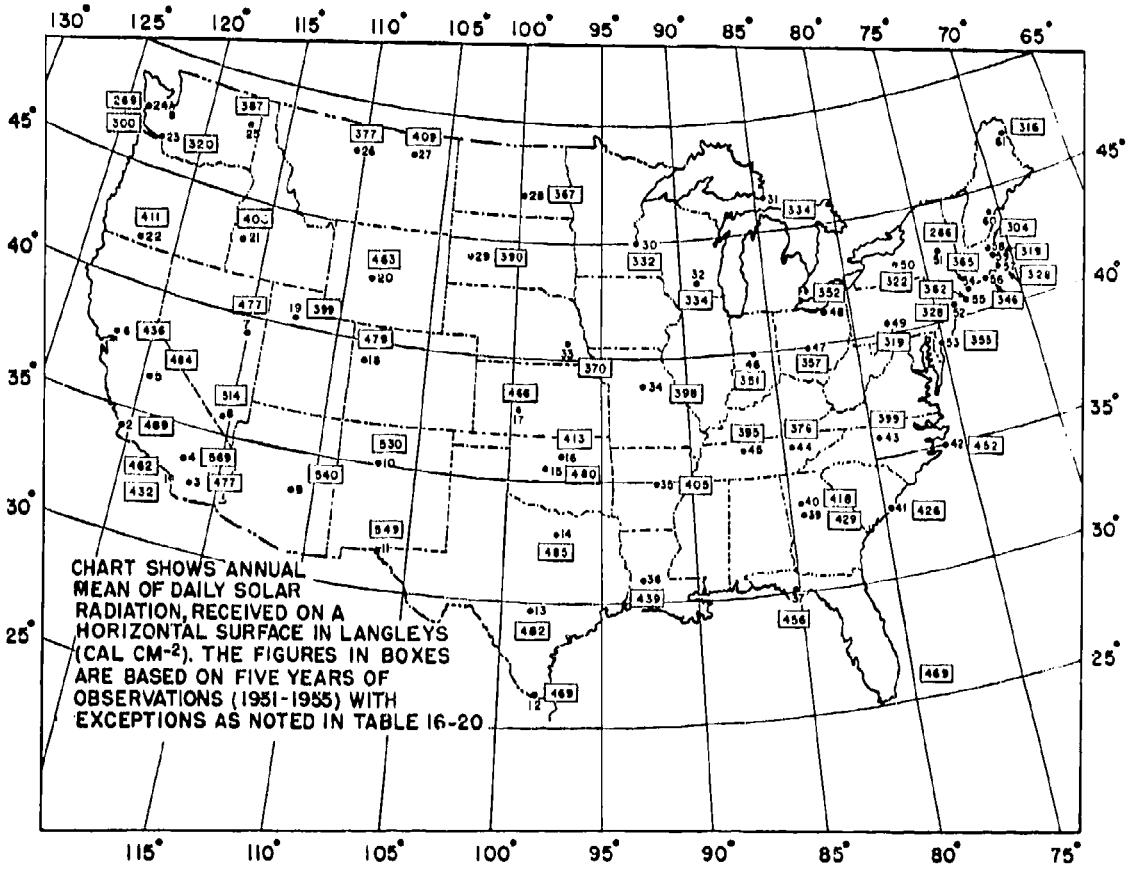

Figure 2. Average Daily Solar Irradiation, Direct and Diffuse, in the United States (Taken from Reference 4).

Facility Design

Before describing the process leading to formulation of specific facility design values, some comments regarding units

and the conversion of units used to describe solar radiation are appropriate.

Two types of units are used in the remainder of this discussion: (1) those associated with the total amount of energy received per unit area and (2) those associated with spectral intensity of the radiation or the amount of energy radiated per wavelength. Normal units for total radiation are: (1) Langley's/unit of time, (2) watts/m^2, and (3) BTU/hr-ft^2. Normal units for spectral intensity are: (1) watts/m^2/μ and (2) BTU/hr-ft^2/μ. Because of the relatively small values which are associated with ultraviolet radiation, the following units will be adopted for use in further discussions and calculations: (1) total energy - μWatts/cm^2 and (2) spectral intensity - μWatts/cm^2/nm.

Conversion factors for units of total radiation are as follows:

1 Langley/day = 3.69 BTU/hr-ft^2
= 11.638 watt/m^2
= 0.0011638 watt/cm^2
= 1163.8 μW/cm^2

1 BTU/hr-ft^2 = 3.154 watt/m^2
= 0.0003154 watt/cm^2
= 315.4 μW/cm^2

Conversion of units for spectral intensity are as follows:

1 watt/m^2/μ = 0.001 watts/m^2/nm
= 0.1 μW/cm^2/nm

1 BTU/hr-ft^2/μ = 315.4 μW/cm^2/μ
= 0.3154 μW/cm^2/nm

Figure 3 presents, in graphical form, the yearly variation in mean daily solar radiation for Phoenix, Arizona. Maximum and minimum values are shown on the figure. The value for the worst case day, 780 langleys per day, represents the total (direct and diffuse) radiation received. Threlkeld (Reference 5) indicates that diffuse radiation, which can constitute 10 to 12 percent of the total radiation, results from scattering of direct solar radiation by atmospheric constituents and that diffuse solar radiation is typically of rather short wavelengths. Ultraviolet radiation certainly falls in this category. Whenever possible, values used for further calculations will be for total radiation. However, certain data are available only for direct radiation; these data will be used in the calculations without attempting to compensate for the missing diffuse radiation.

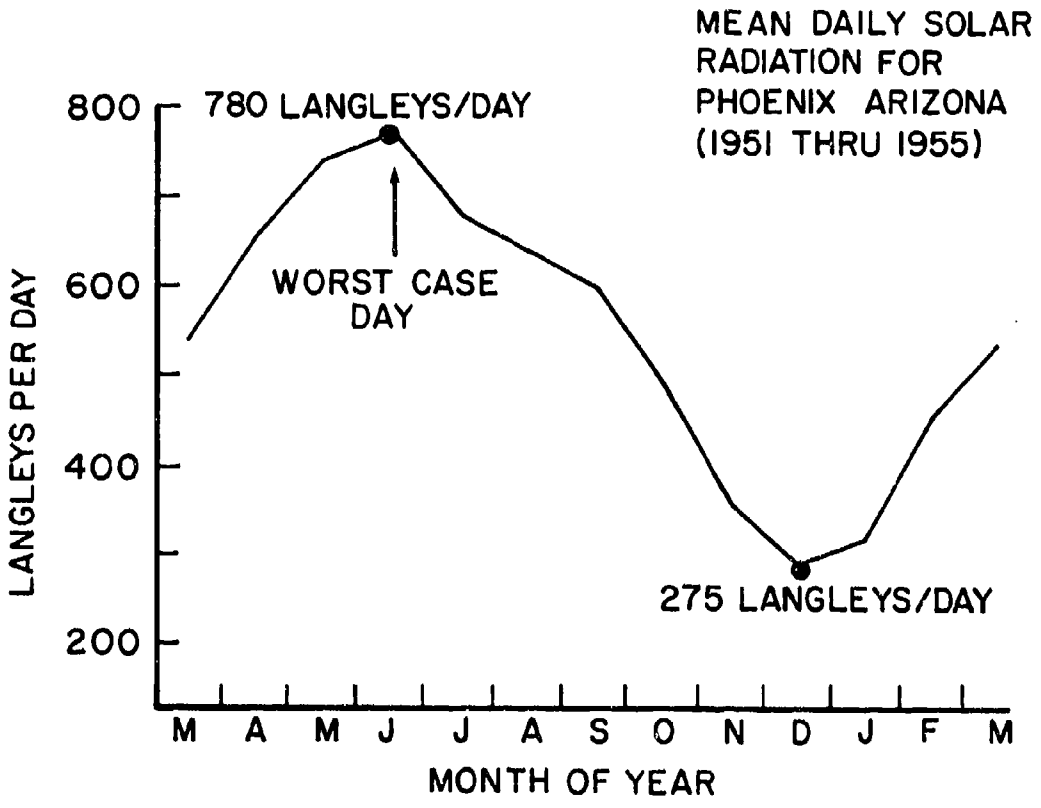

Figure 3. Annual Variation in Mean Daily Radiation for Phoenix, Arizona. (Adapted from Data Presented in Reference 4.)

Since simulation of weathering is concerned primarily with the amount of ultraviolet radiation which reaches the transparency, the amount of ultraviolet radiation which is present for the worst case day must be determined. Direct solar radiation data, as a function of ranges of wavelengths for various air masses, are presented in Table 1. The percentage of ultraviolet radiation (290 to 400 nm) in the spectrum for each air mass is given at the bottom of the table.

Using the worst-case-day value for total radiation (from Figure 3) and assuming the Air Mass on the worst case day to be 2, the total ultraviolet radiation reaching the earth's surface at Phoenix on the worst case day is:

780 langleys/day x 0.0268 = 20.9 langleys/day or 24,328 $\mu W/cm^2$.

Definition of the worst case day will be complete when length of the day, in hours, and the "radiation rate" have been determined. Data presented in Figure 4 illustrates the daily variation in solar radiation on both solstices for a latitude similar to that of Phoenix. Since the earth is

nearest the sun (perigee) at the winter solstice, the peak value of solar radiation on that day is greater than the peak value for the summer solstice. However, the spectral content and total radiation (area under curve) are considerably different for each of these days. At solar noon of the summer solstice, the irradiation rate from Figure 4 is 285 BTU/hr-ft^2. The ultraviolet portion of this radiation is:

$$285 \text{ BTU/hr-ft}^2 \times 315.4 \frac{\mu\text{W/cm}^2}{\text{BTU/hr-ft}^2} \times 0.0268 = 2409 \ \mu\text{W/cm}^2$$

A source radiating at this rate would have to operate for 10.1 hours to produce the 24,328 μW/cm^2 of total UV radiation which reaches Phoenix on the worst case day. For convenience, the worst case day will now be defined as that day on which 24,330 μW/cm^2 of UV radiation reaches the test article. This radiation is produced by a source which emits radiation at the rate of 2,433 μW/cm^2 for a period of 10 hours.

In order to determine the number of worst case dyas in a year, it is assumed that the daily dosage of UV radiation varies in a sinusoidal fashion over the period of a year. It is further assumed that the maximum and minimum values of UV radiation occur at the summer and winter solstices, respectively. From Figure 3, the total daily solar radiation at the winter solstice is 275 langleys/day. It is assumed that the UV portion of this total radiation is that which is present in the solar spectrum for an Air Mass of 3. Total UV radiation for Phoenix at the winter solstice is:

$$275 \text{ langleys/day} \times 1163.8 \frac{\mu\text{W/cm}^2}{\text{langleys/day}} \times 0.0165 = 5280 \ \mu\text{W/cm}^2$$

The values for maximum and minimum daily UV dosages are shown in Figure 5. The total UV radiation received in a year is the area under the curve. Since the average daily radiation is simply the average of the maximum and minimum values or 14,805 μW/cm^2, the total yearly radiation is 14,805 μW/cm^2 x 365 or 5,403,825 μW/cm^2. This value assumes that each day of the year is clear. Realistically, a certain number of days are cloudy or have large amounts of dust in the air. Consequently, the total yearly radiation will be reduced by 15 percent to compensate for those days when UV radiation does not reach the earth because of clouds, dust, or other atmospheric contaminants. The total yearly UV radiation used in further calculation thus becomes 4,593,325 μW/cm^2. The number of worst case days in a year is found by dividing this value by the worst-case day UV radiation dosage.

$$\frac{4,593,325 \ \mu\text{W/cm}^2}{24,330 \ \mu\text{W/cm}^2} = 188.8 \text{ (days/year)}$$

Table 1. Irradiation Normal to Sun's Rays at Sea Level in Watts/m^2 Calculated for Different Air Masses.

Bandwidth, nm	Air Mass 0	1	2	3	4	5
290 - 400	94.6	40.1	19.8	10.0	5.4	2.7
400 - 700	540.0	419.7	327.8	258.6	205.8	163.7
700 - 1100	365.4	309.2	267.5	233.4	205.1	181.5
1100 - 1500	162.5	95.3	70.7	57.0	48.1	40.7
1500 - 1900	72.8	50.8	45.1	41.0	38.0	35.2
1900 - ∞	86.8	12.8	9.2	7.5	6.5	5.8
Total	1322.1	927.9	739.8	607.5	508.9	429.6
%UV	7.16	4.32	2.68	1.65	1.06	0.62

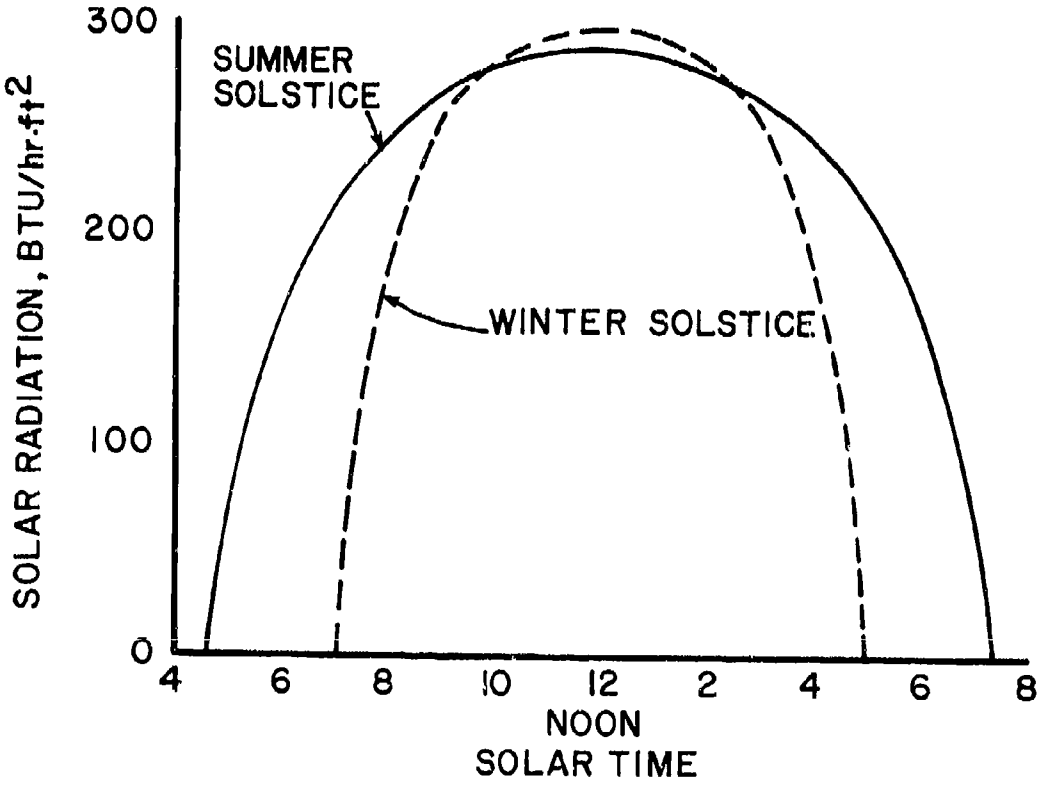

Figure 4. Variation in Direct Solar Radiation for a Location at 33°N Latitude (Adapted from Data Presented in Reference 5).

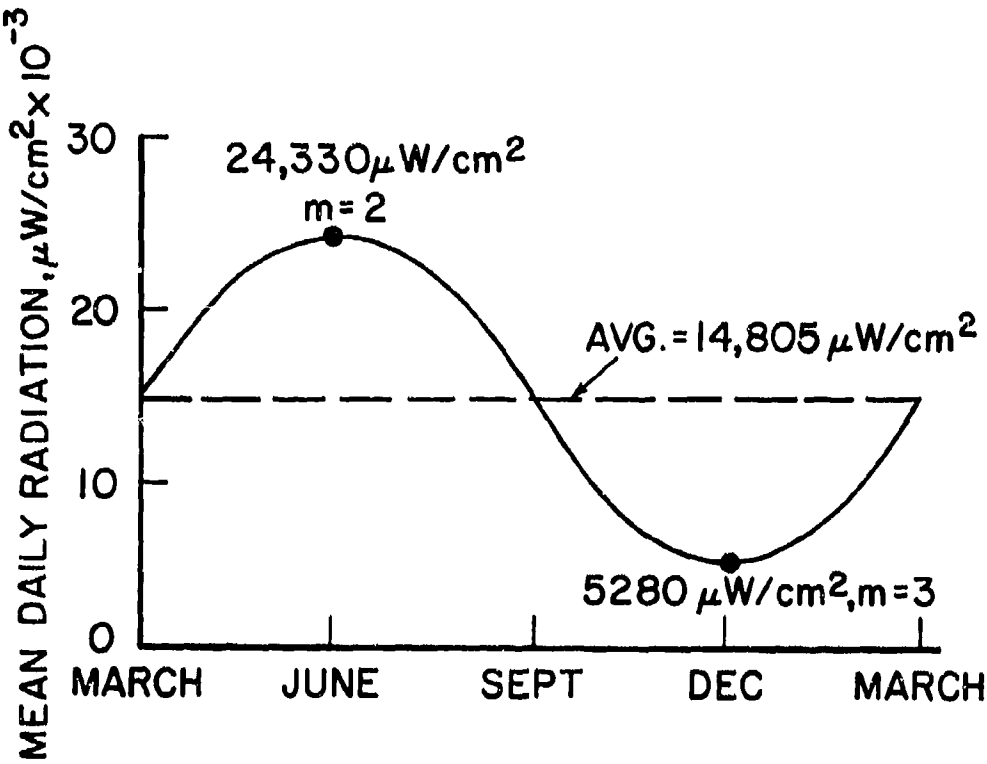

Figure 5. Assumed Annual Variation in Ultraviolet Radiation for Phoenix, Arizona.

For simplicity, 190 worst case days will be equivalent to a year of natural exposure.

An examination of the radiation characteristics of the flourescent ultraviolet sources selected for use in the facility must be made before determination of the acceleration rate of a test can be made. Spectral radiation data for the two sources, FS40 Sunlamps and F40BL Black Lights, were obtained from the manufacturer (Reference 6). These data are presented as two of the curves in Figure 6. Other curves shown in the figure are for (1) natural sunlight, (2) the combined intensity of radiation for the sunlamps and black lights, and (3) "acceleration", i.e., intensity of combined lamps divided by the intensity of sunlight. This acceleration rate varies considerably as a function of wavelength. In addition, the spectral output of both lamps is considerably different than natural sunlight. Determination of an acceleration rate in a facility using a 50:50 mix of these flourescent lamps as radiation sources can be determined, however, by considering the mechanism which causes polycarbonate and other polymeric materials to degrade. Basically, polymeric materials degrade as a result of undesirable reactions that occur within the material after a quanta of ultraviolet light breaks the stable polymer chain. If

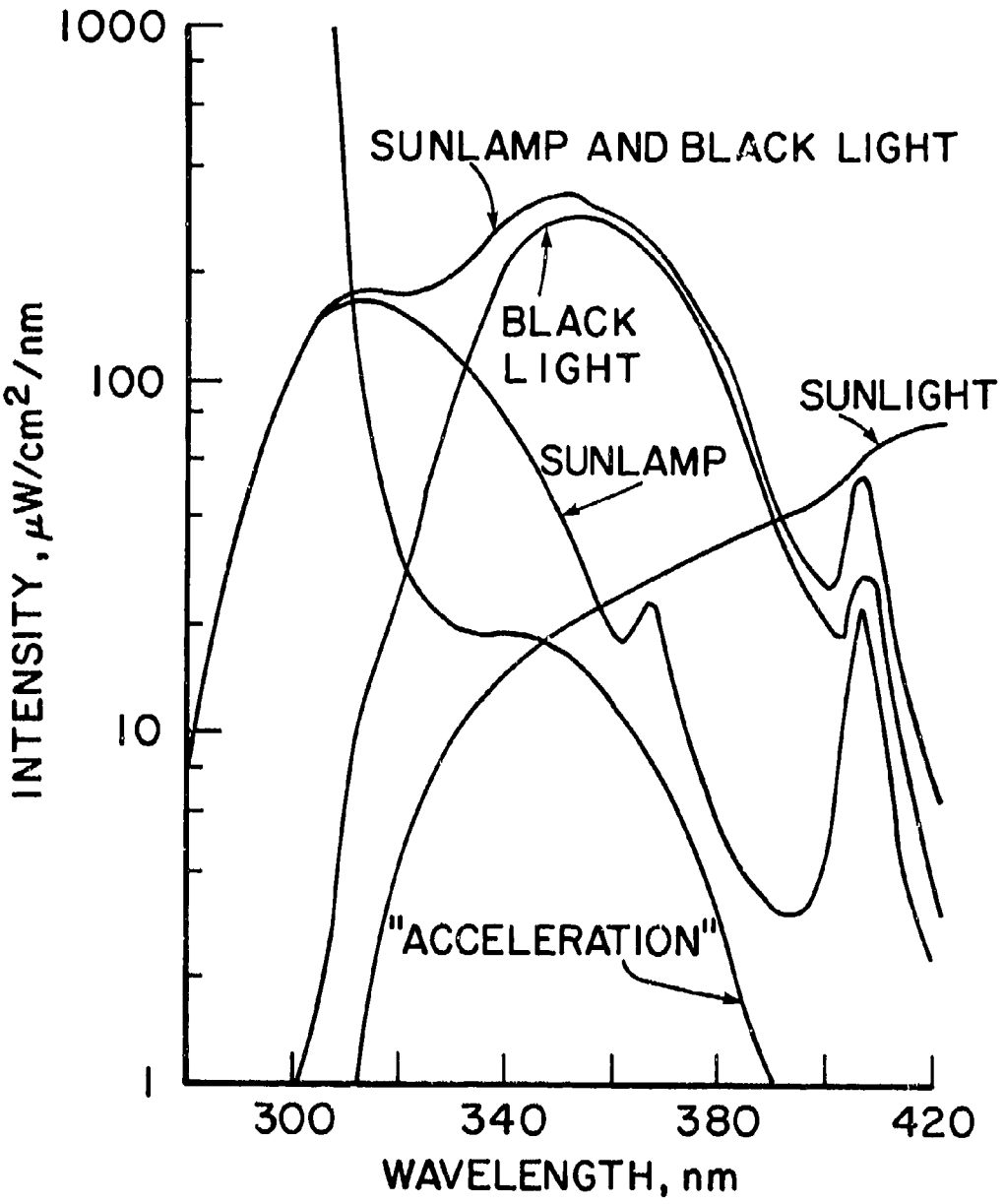

Figure 6. Comparison of Ultraviolet Sources by Radiation Intensity.

degradation is a function of the number of collisions, then an acceleration rate based on comparisons of total radiation can be determined. This method of determining acceleration rate should be reasonable since the bulk of radiation produced by the flourescent tubes is in the range of 300 to 370 nm, a range of sensitivity to most polymeric materials.

Using data supplied by the manufacturer, the hourly total radiation supplied by the combined lamps for wavelengths ranging from 280 nm to 400 nm was determined to be 19,414 $\mu W/cm^2$. The number of hours in the test facility required to produce the equivalent of a year of exposure can now be determined as,

$$\frac{4,593,325\ \mu W/cm^2\ \text{(per year)}}{19,414\ \mu W/cm^2\ \text{(per hour)}} = 236.6\ \text{hours}$$

Using lamp manufacturer's data for the normal decrease in output of UV radiation during the life of the lamps, it was determined that a total of 905 hours of UV exposure in the test facility would be required to simulate 3 years of natural exposure at Phoenix.

Data and values just determined were incorporated in a recommended runway thermal environment profile, supplied by the Air Force sponsor, to provide the accelerated test cycle shown in Figure 7. Since the Runway Environment Tests were one part of a two part test cycle, the maximum amount of time which was permitted for the Runway Environment tests was 12 hours. Additionally, the effects of moisture on the outer surface of the transparency were to be simulated in as realistic a manner as possible. In order to make this portion of the Runway Environment Test more indicative of the natural environment, the moisture (dew) should remain in contact with the transparency for an extended period of time. Consequently, the concept of a "lumped" test-cycle-day was adopted.

Procedures used to develop a "lumped" test-cycle-day follow. Since 905 hours of UV exposure are required to simulate 3 years of natural exposure and 1 year of natural exposure is equivalent to 190 worst case days, 1.6 hours of UV exposure in the facility will be required to simulate 1 day of natural exposure. From Figure 4, 14.3 hours of natural sunshine exist for the worst case day. The length of an accelerated day (including nighttime) is determined as:

$$\frac{1.6\ \text{hrs}}{T\ \text{hrs}} = \frac{14.3\ \text{hrs}}{24\ \text{hrs}}$$

or T = 2.68 hrs. If the lamps are to operate for 7 hours of the test cycle, 7 hrs divided by 1.6 hrs/day or 4.38 days of natural exposure will be simulated. The overall length of the "lumped" test-cycle-day then becomes 4.38 days/cycle x 2.68 hrs/day or 11.7 hrs/cycle. During the UV exposure, cabin temperature and test facility ambient temperature are varied as shown. Moisture effects were simulated by allowing moisture (introduced as water vapor to the facility environment) to condense on the cooling transparency surface. In this way, the effects of dew formation

and its prolonged contact with the transparency during the nighttime hours were duplicated.

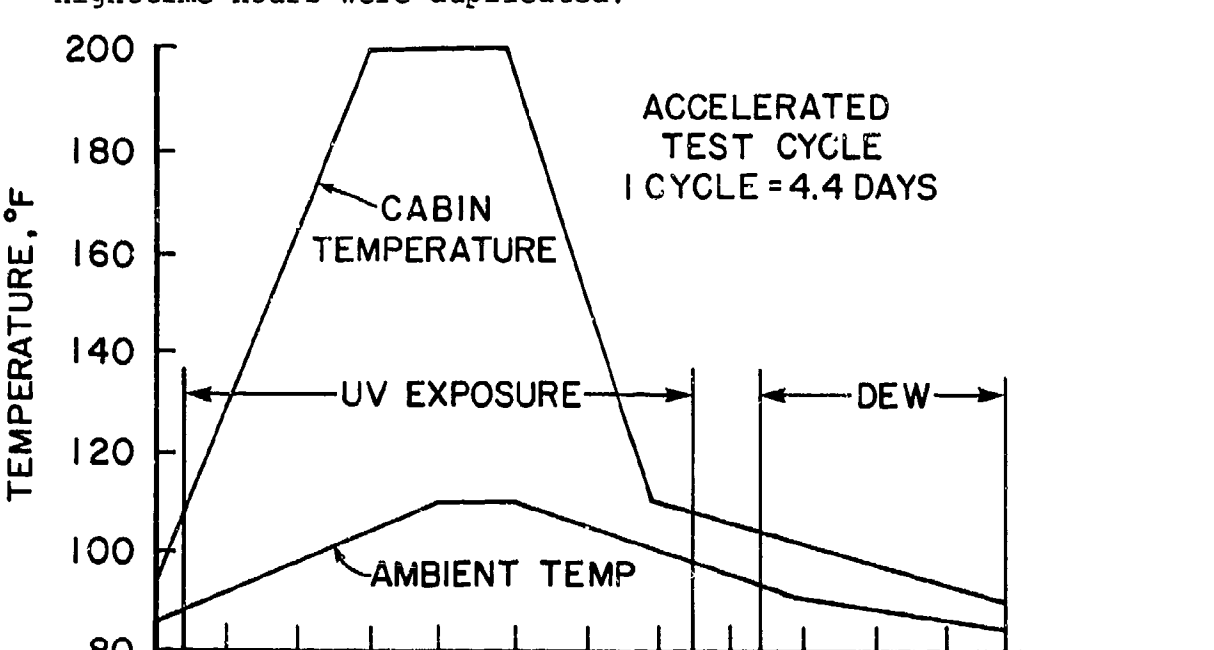

Figure 7. Accelerated Runway Environment Test Cycle.

Facility Description

The Runway Environment Test Facility is an insulated sheet metal enclosure which contains the fluorescent lamps, heating and ventilating equipment, and a small container used to heat water to produce water vapor for dew formation. The enclosure and its support structure are rolled into the test area from one side of the table-top fixture holding the test article. To meet space and operational limitations, the chamber was split in half, lengthwise, and hinged at the top. During installation, the back half of the chamber is opened as shown in Figure 8. When properly located above the test article, the rear half is hinged down and the entire enclosure is lowered slightly, until it rests on the test article support fixture.

Spacing of the flourescent lamps above the transparency surface was nominally 2 inches. A mill finish aluminum reflector was placed behind the lamps. The relationship of reflector-lamp-transparency is the same used by the lamp manufacturer during measurements to determine the spectral intensity of radiation produced by the lamps. A total of 36 lamps (18 sunlamps and 18 black lights) were positioned in an alternating fashion in the enclosure. As shown in Figure 9, the lamps have

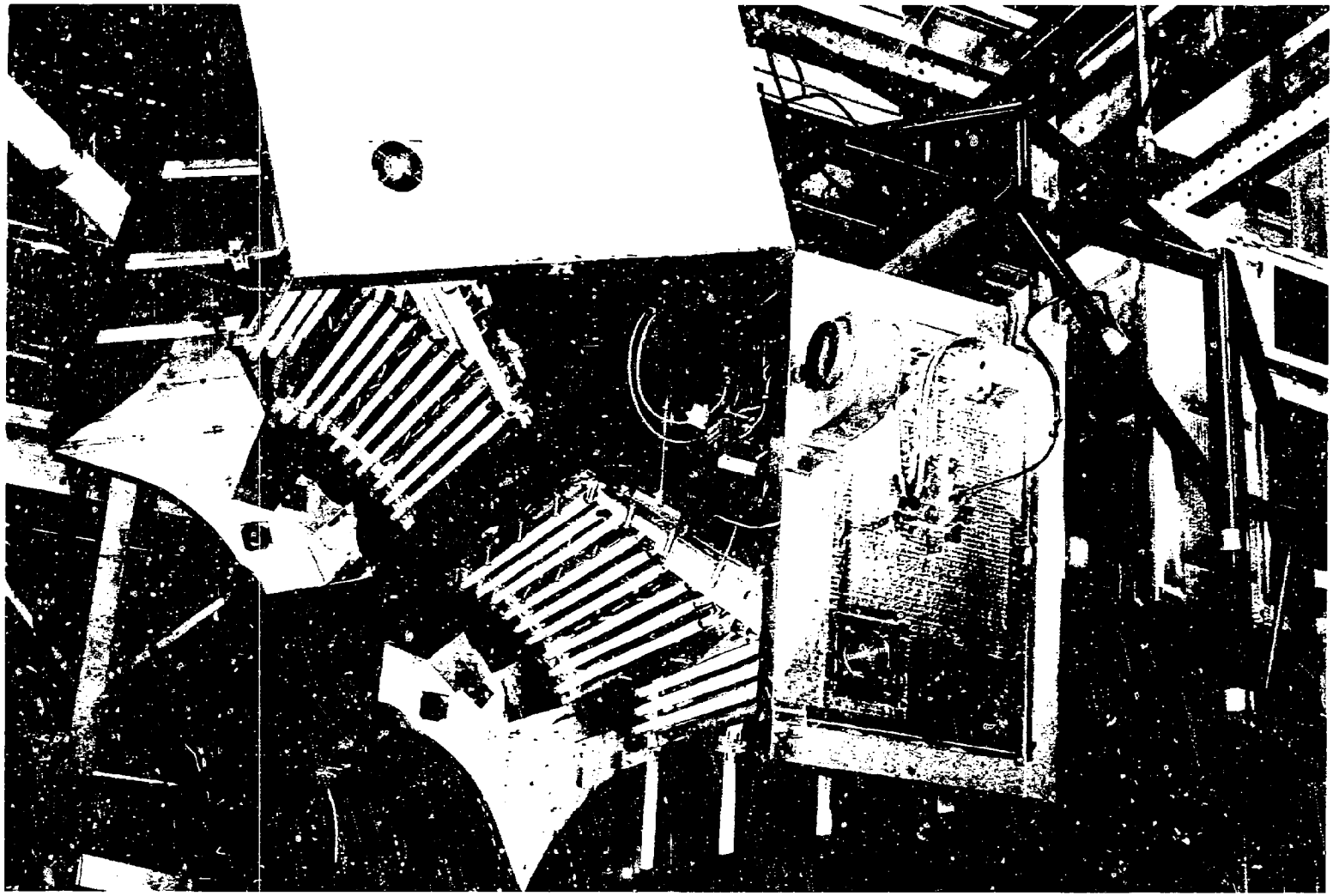

Figure 8. External View of Runway Environment Test Facility.

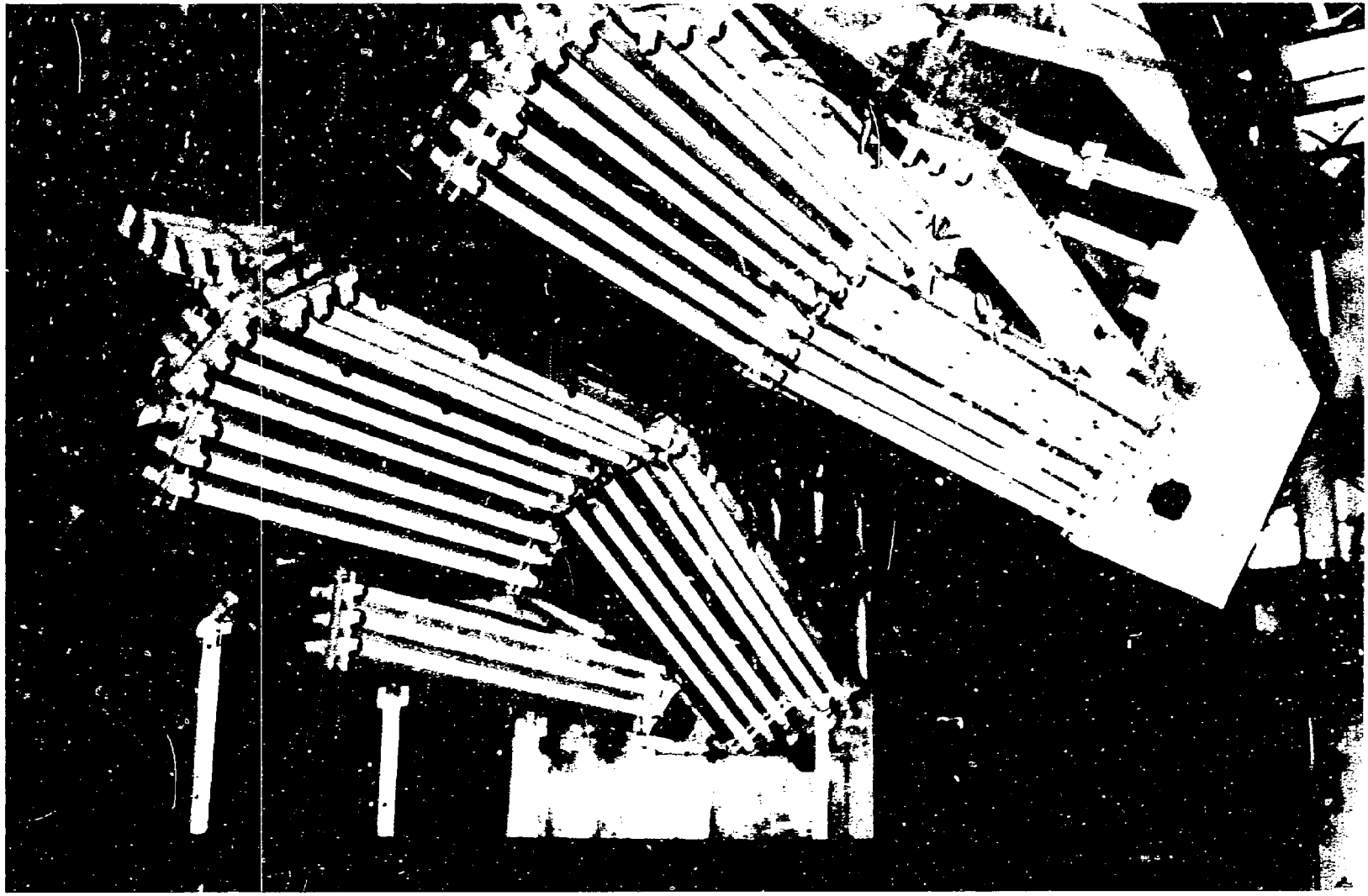

Figure 9. Internal View of Runway Environment Test Facility Showing Flourescent Lamps.

been configured for use in evaluating F-16A transparencies. A fixed schedule for rotation of lamp positions and lamp ends is followed to attempt to expose the transparency to a uniform dosage and spectral content of ultraviolet radiation.

References

1. Swasey, C.C., "Ultraviolet Stabilizers," In Modern Plastics Encyclopedia, McGraw-Hill, New York, NY, p. 221-224, (1979-80).

2. Hirt, R.C., Searle, N.Z., and Schmitt, R.G., "Ultraviolet Degradation of Plastics in the Use of Protective Ultraviolet Absorbers," SPE Trans., pg. 21-25, January (1961).

3. Grossman, G.W., "Correlation of Laboratory to Natural Weathering," Journal of Coatings Technology, Vol. 49, No. 633, pg. 45-54, (1977).

4. Gast, P.R., "Thermal Radiation," In Handbook of Geophysics for Air Force Designers, Chapter 16, Section 3, Air Force Cambridge Research Center, Cambridge, MA, pg. 16-14 to 16-31, (1957).

5. Threlkeld, J.L., Thermal Environmental Engineering, Prentice-Hall, Englewood Cliffs, N.J., (1970).

6. Lally, W.J., Personal Communication, (1981).

AD-P003 213

AIRCRAFT TRANSPARENCY TESTING Methodology

M. E. Kelly, Flight Dynamics Laboratory

Aircraft Transparency Testing Methodology

Malcolm E. Kelley
Flight Dynamics Laboratory
Air Force Wright Aeronautical Laboratories
Wright-Patterson AFB, Ohio

Abstract

Accurately predicting in-service durability of aircraft transparencies is beyond the present state-of-the-art. There are, however, approaches to testing and evaluating candidate designs and materials that may provide more useful test results than some of the more commonly used test methods. A testing methodology has been derived that uses a logical combination of exposure conditions and test methods to evaluate the durability of plastic aircraft transparency materials. While most testing naturally involves coupons, durability testing of full scale transparencies is also recommended. A large, complex facility has been constructed which can impose combinations of temperatures, pressure differentials, and exposure conditions that represent both the in-flight and flight line environments. This paper describes the tests and exposures recommended in the methodology, plus describes the preliminary conclusions and lessons learned from using the full scale testing equipment.

INTRODUCTION

Flight vehicle transparent enclosures are a high cost item in the US Air Force. Unexpected deterioration or catastrophic failure of transparencies after being in service has necessitated expensive programs to redesign, retest, and retrofit new transparencies of the affected aircraft. Types of visually detectable deterioration have included crazing, delamination and coating loss. On other occasions transparencies have had to be redesigned because of changing aircraft mission environment. In most cases it has been extremely difficult to accurately predict the durability of a transparency design in a service environment. The unexpected failures can be attributed in part to inadequacies in the state-of-the-art for identifying all the important aspects of the in-service environment, testing the effects of these aspects in the laboratory, and translating laboratory results into reliable predictions of in-service durability.

DISCUSSION

It is difficult to develop transparencies for modern fighter aircraft. The Air Force wants to have transparencies with superior optical properties, good bird impact resistance, minimum weight, and low cost, yet have good durability when subjected to the complex mix of both flight and ground environmental exposures.

An important phase in the transparency design development process is determining the type and severity of environmental exposures the transparency will encounter. Test requirements can then be levied that assess the transparency's capability and durability using reasonable and applicable criteria. There are significant problems that can arise if the testing criteria imposes conditions (temperatures, pressures, etc) that cannot be attained by the operational aircraft. Such testing could eliminate possibly successful designs from consideration, and a design that did pass the imposed testing requirements might have to sacrifice other desirable features (optics, weight, etc) to meet the unreasonable requirement. However, the reverse situation of either having no requirements or inadequate requirements for some important aspect could be a more serious flaw. Transparencies designed without sufficient imposed requirements would prove to have deficiencies that would cause poor durability, reduced aircraft capability, or might even contribute to aircrew injuries or aircraft losses.

Typically, a transparency vendor is required to provide a canopy or windshield to fill a specifically sized hole in the aircraft. Requirements are usually determined in terms of size, weight, optical properties, emergency crew escape, bird impact resistance, and the ability to withstand specified extremes of temperature and pressure. Coupon tests are usually required to indicate resistance of the materials to specific exposures, such as UV radiation, cleaning abrasion, chemical craze resistance, temperature extremes and changes, and moisture. Also, various impact and interlayer adhesion strength tests are often required. The time available for designing and testing the transparency system is another factor to be considered. Some possible designs are discarded due to the time necessary for developing new forming techniques and equipment.

The optical, temperature, pressure, and bird impact tests on the full scale article give strong assurances that the transparency will survive the in-flight environment and will be safe to fly. However, these tests do not indicate long term durability. Passing the individual coupon tests cannot be considered a guarantee that the full scale transparency will have acceptable durability when it encounters combined exposure factors.

The Flight Dynamics Laboratory has been doing both in-house and contract work in the aircraft transparency testing area, seeking to identify what are important environmental conditions to represent, good tests to use, and appropriate ways of formulating a testing and evaluation program. Comments were solicited from aircrew members, maintenance personnel, transparency and other members of the technical community. This has lead to the development of a suggested aircraft testing methodology (Ref 1 and 2) that could be used in evaluating the durability of new plastic aircraft transparency designs, to include stretched acrylic, coated monolithic polycarbonate, and acrylic/polycarbonate laminates. The methodology identifies test methods that yield meaningful information and also identifies tests that are not recommended. The testing methodology provides guidance on how to select the tests and combinations of tests most suited to a specific program.

The methodology was derived using existing information in the literature plus inputs from those who use, maintain, build, or test aircraft transparencies. The methodology was designed to be cost-effective, realizing testing is not cheap and that time is usually limited. Standard test methods and environmental exposure equipment and conditions are used as much as possible. More importantly, the tests and exposure conditions have real world significance, so that a low score on a specific test can be understood in terms of reduced durability or limiting operational capability.

Tables 1, 2 and 3 summarize the suggested durability testing methodology for each of the three types of plastic aircraft transparency. Basically, the methodology calls for subjecting coupons to artificial weathering, then performing specific durability tests or measurements, to include craze resistance, haze, impact strength, thermal shock, abrasion resistance, coating durability (for coated polycarbonate), and interlayer delamination resistance (for laminated materials). Artificial weathering coupons before they undergo specific tests better represents the real world conditions in the laboratory testing program.

The total dosages for the various exposures were selected to approximate the quantity an aircraft transparency would encounter in its operational environment. The intensity level of the exposure condition is reasonably close to the intensity level of the operational environment, with increased repetition and duration being used to accelerate the exposure rather than increased intensity. The exception is the UV radiation dosage rate in the QUV tester. The general consensus seems to be that the higher dosage rate in the tester does not introduce any significant effects for these plastic materials, although this has not been experimentally proven for all the materials of interest.

TABLE 1

DURABILITY EVALUATION OF HIGH PERFORMANCE USAF TRANSPARENCY SYSTEMS.
MONOLITHIC STRETCHED ACRYLIC* SUMMARY

TEST PARAMETER	TEST METHOD	ENVIRONMENTAL CONDITION	SIMULATION	ACCEPTANCE CRITERIA
Surface/Chemical Craze	1"x7" beam per MIL-P-25690A, Para.4.6.7; ASTM F 484-77 or equiv.; or 1"x15" incremental stress beam per Sect. 4.1; isopropyl alcohol & ethylene glycol; f=2000 psi	Accelerated weathering	Q.U.V., 120°F, 7 hr. UV/5 hr. condensation cycles; 264 hrs. = 1 equiv. yr.	No crazing after 3 equiv. yrs. of exposure/test.
Haze-Transmittance	F406, Method 3022, or equivalent			After 3 equiv. yrs. of exposure/test, haze < 4% and luminous transmittance to be within 2% of unexposed value.
Impact: (a) Coupon	Falling weight plate or beam per ASTM F736-81 or Sect. 4.2 (high rate MTS beam test)	Baseline (unexposed) and accelerated weathering		After 3 equiv. yrs. of exposure/test, threshold-of-failure energy to be within 15% of unexposed value.
(b) Subscale	12"x12" plates, free edge, air cannon tested using 1" dia. steel sphere			After 3 equiv. yrs. of exposure/test, threshold-of-failure energy to be within 15% of unexposed value.
Thermal Shock	In accordance with ASTM F520-77, plus rapid drying in partial vacuum	accelerated weathering	Refer to ASTM F520-77	After 3 equiv. yrs. of exposure/test, no loss of coating cracking, spalling, loss of transparency, or other visible deterioration.
Abrasion Resistance (a) In-flight	3" sq. samples per Sect. 4.3; following QUV and abrasion, measure haze with a std. hazemeter	Accelerated weathering plus salt blast abrasion	(264 hrs. acc. weathering followed by 8 cycles of salt blast) x 1 = 1 equiv. yr, x 2 = 2 equiv. yr, x 3 = 3 equiv. yr.	After exposure/test, haze < 4% after 1 equiv. yr, haze < 5% after 2 equiv. yr, haze < 6% after 3 equiv. yr.
(b) Flightline	4"x4" test samples subjected to 50 normal cleanings at 33 hr. intervals	accelerated weathering	QUV, 120°F, 7 hr. UV/5 hr. condensation cycles; 264 hr. = 1 equiv. yr.	After 3 equiv. yrs. of exposure/test, no visible damage and haze < 4%.
Edge Attachment	Flex. beams, approx. 3"x15", simulating design cross-section and edge fixity, per Sect. 4.4; 3- or 4-point loaded at high rate (2000 in/min)	Unexposed	Critical combined load condition during bird impact and/or in-flight	Successful edge designs will exceed design ultimate load without failure.
Pressure/Temperature/Durability	Full-scale transparency installed in airframe support structure; Bldg. 65 Test Facility at WPAFB	Simulated temp. and press. mission profiles combined with critical ground environment, incorporating realistic rates to evaluate thermal shock.		Successfully withstand 2000 simulated flight hours and 3 equiv. yrs. of flightline exposure/test.
Birdstrike	Full-scale transparency installed in airframe support structure; AEDC test per ASTM F330-79.	Unexposed; following flight/flightline testing in Bldg. 65 facility; and from in-service at yearly intervals	In-flight birdstrike.	Pass impact of 4 lb. bird at specified velocity.

*MIL-SPEC Qualified

TABLE 2

DURABILITY EVALUATION OF HIGH PERFORMANCE USAF TRANSPARENCY SYSTEMS
COATED MONOLITHIC POLYCARBONATE* SUMMARY

TEST PARAMETER	TEST METHOD	ENVIRONMENTAL CONDITION	SIMULATION	ACCEPTANCE CRITERIA
Surface/Chemical Craze	1"x7" beam per MIL-P-83310, Para. 4.5.5.2, ASTM F484-77 or equiv.; or 1"x15" incremental stress beam per Sect. 4.1; isopropyl alcohol & ethylene glycol; f=2000 psi.	Accelerated weathering	QUV, 120°F, 7 hr. UV/5 hr. condensation cycles; 264 hrs. = 1 equiv. yr.	No crazing after 3 equiv. yrs. of exposure/test
Haze/Transmittance	FTM 406, Method 3022, or equivalent			After 3 equiv. yrs. of exposure/test, haze < 4% and luminous transmittance to be within 2% of unexposed value.
Coating Adhesion	Rain impingement at 500 mph in a 1-inch/hr. rainfall on rotating arm apparatus at WPAFB.	Accelerated weathering plus stress	QUV, 120°F, 7 hr. UV/5 hr. condensation cycle, 264 hr.=1 equiv. yr. in combination with an outer fiber stress of 1000 psi.	After 3 equiv. yrs. of exposure and 5 min. test, no substantial amount of coating removal, measured by S.E.M. exam.
Coating Embrittlement (Impact)	Falling weight beams per ASTM 735-81 or Sect. 4.2 (high rate MTS beam test).	Baseline (unexposed) and accelerated weathering plus stress	QUV, 120°F, 7 hr. UV/5 hr. condensation cycles; 264 hrs. = 1 equiv. yr.	After 3 equiv. yrs. of exposure/test, threshold-of-failure energy to be within 15% of unexposed value.
Thermal Shock	In accordance with ASTM F520-77, plus rapid drying in partial vacuum	Accelerated weathering	Refer to ASTM F520-77	After 3 equiv. yrs. of exposure/test, loss of coating, cracking, spalling, loss of transparency, or other visible deterioration.
Abrasion Resistance (a) In-Flight	3" sq. samples per Sect. 4.3; following QUV and abrasion, measure haze with a std. hazemeter.	Accelerated weathering plus salt blast abrasion	(264 hrs. acc. weathering followed by 8 cycles of salt blast) x 1 = 1 equiv. yr, x 2 = 2 equiv. yr, x 3 = 3 equiv. yr.	After exposure/test, haze < 4% after 1 equiv. yr, haze < 5% after 2 equiv. yr. haze < 6% after 3 equiv. yr.
(b) Flightline	4"x4" test samples subjected to 50 normal cleanings at 33 hour intervals	Accelerated weathering	QUV, 120°F, 7 hr. UV/5 hr. condensation cycles; 264 hr. = 1 equiv. yr.	After 3 equiv. yrs. of exposure/test, no visible damage and haze < 4%.
Edge Attachment	Flex. beams, approx. 3"x15", simulating design cross-section and edge fixity, per Sect. 4.4; 3- or 4-point loaded at high rate (2000 in/min)	Unexposed	Critical combined load condition during bird impact and/or in-flight	Successful edge designs will exceed design ultimate load without failure.
Impact (Subscale)	12" sq. plates, free edge, air cannon tested using 1" dia. steel sphere	Baseline (unexposed) and accelerated weathering	QUV, 120°F, 7 hr. UV/5 hr. condensation cycles; 264 hr. = 1 equiv. yr.	After 3 equiv. yrs. of exposure/test, thresold-of-failure energy to be within 15% of unexposed value.
Pressure/Temperature/Durability	Full-scale transparency installed in airframe support structure, Bldg. 65 Test Facility at WPAFB	Simulated temp. and press. mission profiles combined with critical ground environment incorporating realistic rates to evaluate thermal shock		Successfully withstand 2000 simulated flight hours and 3 equiv. yrs. of flightline exposure/test.
Birdstrike	Full-scale transparency installed in airframe support structure; ASDC test per ASTM F330-79.	Unexposed; following flight/flightline testing in Bldg. 65 Facility; and from in-service at yearly intervals.	In-flight birdstrike	Pass impact of 4 lb. bird at specified velocity.

*MIL-SPEC Qualified

TABLE 3

DURABILITY EVALUATION OF HIGH PERFORMANCE USAF TRANSPARENCY SYSTEMS
ACRYLIC FACED/POLYCARBONATE LAMINATE* SUMMARY

TEST PARAMETER	TEST METHOD	ENVIRONMENTAL CONDITION	SIMULATION	ACCEPTANCE CRITERIA
Surface/Chemical Craze	1"x7" beam per MIL-P-5184E, Para. 4.5.5, ASTM F484-77 or equiv.; or 1"x15" incremental stress beam per Sect. 4.1; isopropyl alcohol; f=2000 psi	Accelerated weathering	QUV, 120°F, 7 hr. UV/5 hr. condensation cycles; 264 hrs. = 1 equiv. yr.	No crazing after 3 equiv. yrs. of exposure/test
Haze/Transmittance	FTM 406, Method 3022, or equivalent			After 3 equiv. yrs. of exposure/test, haze < 4% and luminous transmittance to be within 2% of unexposed value.
Interlaminar Bond Integrity (Delamination)				
(a) Flatwise Tension	Use ASTM D952 or F521-77 as guideline; urethane interlayer sa; be undercut to 1 sq. in. in test area per Sect. 4.7			After 3 equiv. yrs. of exposure/test, interlayer flatwise tensile stress shall exceed design ultimate without failure.
(b) Torsional Shear	Use ASTM D229 as guideline; lock inner portion to load cell, applying torque to outside of specimen as per Sect. 4.8			After 3 equiv. yrs. of exposure/test, interlayer shear stress shall exceed design ultimate without failure.
(c) Wedge Peel	Use ASTM D3762-79 as guideline; insert and hold wedge into machined slot in interlayer of 1"x10" specimen per Sect. 4.9			After 3 equiv. yrs. of exposure/tests, no measurable delamination length for 100 hrs. after insertion of wedge.
Impact (a) Coupon	Falling weight beams per ASTM F736-81 or Sect. 4.2 (high rate MTS beam test)	Baseline (unexposed) and accelerated weathering plus stress	QUV, 120°F, 7 hr. UV/5 hr. condensation cycles, 264 hrs. = 1 equiv. yr. in combination with an outer fiber stress of 1000 psi.	After 3 equiv. yrs. of exposure/tests, structural ply threshold-of-failure to be within 15% of unexposed value.
(b) Subscale	12" sq. plates, free edge, air cannon tested using 1" dia. steel sphere	Baseline (unexposed) and accelerated weathering	QUV, 120°F, 7 hr. UV/5 hr. condensation cycles; 264 hr. = 1 equiv. yr.	After 3 equiv. yrs of exposure/test, structural ply threshold-of-failure to be within 15% of unexposed value.
Thermal Shock	In accordance with ASTM F520-77, plus rapid drying in partial vacuum	Accelerated weathering	Refer to ASTM F520-77	After 3 equiv. yrs. of exposure/test, no loss of coating, cracking, spalling, loss of transparency, or other visible deterioration.
Abrasion Resistance				
(a) In-flight	3" sq. samples per Sect. 4.3; following QUV and abrasion, measure haze with a std. hazemeter	Accelerated weathering plus salt blast abrasion	(264 hrs. acc. weathering followed by 8 cycles of salt blast) x 1 = 1 equiv. yr, x 2 = 2 equiv. yr, x 3 = 3 equiv. yr.	After exposure/test, haze < 4% after 1 equiv. yr, haze < 5% after 2 equiv. yr., haze < 6% after 3 equiv. yr.
(b) Flightline	4"x4" test samples subjected to 50 normal cleanings at 33 hr. intervals	Accelerated weathering	QUV, 120°F, 7 hr. UV/5 hr. condensation cycles; 264 hr. = 1 equiv. yr.	After 3 equiv. yrs. of exposure/test, no visible damage and haze < 4%.
Edge Attachment	Flex. beams, approx. 3"x15", simulating design cross-section and edge fixity, per Sect. 4.4; 3- or 4-point loaded at high rate (2000 in/min)	Unexposed	Critical combined load condition during bird impact and/or in-flight	Successful edge designs will exceed design ultimate load without failure.
Pressure/Temperature/Durability	Full-scale transparency installed in airframe support structure; Bldg. 65 Test Facility at WPAFB	Simulated temp. and press. mission profiles combined with critical ground environment, incorporating realistic rates to evaluate thermal shock		Successfully withstand 2000 simulated flight hours and 3 equiv. yrs. of flightline exposure/test.
Birdstrike	Full-scale transparency installed in airframe support structure; AEDC test per ASTM F330-79	Unexposed; following flight/flightline testing in Bldg. 65 facility and from in-service at yearly intervals	In-flight birdstrike	Pass impact of 4 lb. bird at specified velocity.

*MIL-SPEC Qualified

CRAZE RESISTANCE

The chemical craze resistance test uses a stressed beam for all three types of transparency. Either the standard type test can be used that has the 2000 PSI outer fiber stress, or a slightly more informative version of the test can be used. The version developed by UDRI uses a longer beam and a higher stress at the fulcrum, and recording the time to craze at different points on the beam. Since the outer fiber stress is a function of the distance from the fulcrum, this provides the time to craze at different stress levels (to include 2000 PSI), not just at the 2000 PSI value as with the standard test.

HAZE AND TRANSMITTANCE

Haze and luminous transmittance measurements are made using generally accepted procedures and equipment. This measures some of the changes in optical properties caused by QUV exposures.

Impact strength is measured with a falling weight impact test, a high rate MTS beam test, or an air cannon test.

FALLING WEIGHT

The falling weight test is much less expensive to run than the MTS beam, and most or all of the vendors have some sort of falling weight tester. However, if the average strength is desired, a necessary but usually unstated assumption is that the coupons being tested all have approximately the same impact strength. If significant data scatter occurs, the falling weight tester can be used to determine how many coupons met or exceeded a specific strength value. In the methodology a 15% strength reduction after exposure was selected as an acceptable figure.

MTS BEAM

The MTS beam tests are considerably more expensive per coupon than the falling weight tests, but provide more informative results. Data can be recorded, then played back as a plot of load versus displacement for each test specimen. The actual strength (energy to failure) of each coupon can be determined.

AIR CANNON

The air cannon test is also expensive to run, but is still much cheaper than impacting full scale transparencies. The primary advantage is in the loading rate, which can approximate bird impact rates. Some materials, to include polycarbonate, become brittle due to environmental exposure. This change first become apparent at the high loading rates, with no significant change at the lower rates. Air cannon tests can also provide information that might prove helpful in selecting initial bird strike test velocities and interpreting the results, making the bird impact testing program more cost effective.

THERMAL SHOCK

The thermal shock tests for each of the three types of transparency are based on the standard ASTM test method, ASTM F520-77, which includes artificial weathering as part of the standard test method. This artificial weathering is similar to the artificial weathering with QUV called for with the other tests in the methodology. The standard test method is used in preference to using the same QUV artificial weathering so that all the past testing can be directly comparable with future thermal shock test results. The only suggested change from the standard test method is the addition of partial vacuum. This is representative of reduced atmospheric pressure in flight and should produce rapid drying of the surface. This effect may be an important contributor to the crazing process.

ABRASION RESISTANCE

A transparency should have good abrasion resistance for both in-flight and flight line environments. The material characteristics that make a substance especially resistive to the rubbing type abrasion of the flight line (i.e., hard surface) are not necessarily the same as the characteristics needed for the impact type abrasion of the in-flight environment (i.e., tough and flexible surface). Resistance to both types of abrasion is needed for for both acrylic (monolithic or outer ply of a laminate) and coated polycarbonate surfaces. Acrylic has an advantage in that when the surface becomes too abraded (indicated by increased haze) the optical characteristics can be partially restored by removing some of the outer surface (grinding, polishing, buffing, etc), thereby improving the optical qualities to an acceptable level. Coated polycarbonate, however, must retain its coating, so the thin coating must be able to endure both types of abrasion.

EDGE ATTACHMENT

The edge attachment design can make or break an overall transparency design. A transparency with an optimized edge attachment design can better handle high loading rate events, such as bird impacts. To evaluate candidate edge designs, screening tests are run using high loading rates on coupons with the appropriate cross-section edge attachment, and edge fixity at high loading rates. Use of the high performance, electrohydraulic closed-loop test equipment is suggested. The information on edge response, fracture, and energy absorption can indicate the better design versions which could then be adopted for use in the full scale canopy.

RAIN EROSION

Rain encountered in flight is another exposure condition that transparencies must endure. Acrylic, either as a monolithic transparency or as the face ply for a laminate does not seem to be susceptible to damage from rain at reasonable velocities. Consequently, the rain erosion coupon tests do not seem to be cost effective for these designs. However, coated polycarbonate can be significantly affected. The rain erosion test can differentiate between coatings that would and would not have reasonable in-service durability. A suitable rain erosion exposure fixture sould be

used, which can control the rain drop size, rate, speed and angle of impact. The effects of the water drop impacts on the coupons should be assessed with a scanning electron microscope (or other appropriate equipment).

INTERLAMINAR BOND STRENGTH

For laminates, one significant problem is delamination. The strength, flexibility and adhesive properties of the interlayer are important factors in preventing this problem. Three tests are suggested for evaluating a laminate: flatwise tension, torsional shear, and wedge peel. Coupons with suitable edge sealing are subjected to accelerated weathering, then machined to the testing geometry and tested. Passing the three tests would indicate the interlayer should be able to resist the stresses that produce delamination and the edge sealing material was effective.

Once a candidate design has successfully passed coupon tests it can then undergo the final full scale testing prior to being placed into actual service. Some testing should continue into later years to spot adverse trends before they become serious operational problems. Two types of full scale tests are called for in the methodology: bird impact tests and full scale pressure/temperature/durability tests.

BIRD STRIKE

Bird impact tests should be performed using the appropriate ASTM standard test method (ASTM F330-79). These tests would provide the necessary initial assurances that the aircraft transparency would be safe to fly. After the aircraft have been in service for a time, one service aged transparency should be bird impact tested annually to determine if the service environmental exposures are causing significant impact strength losses. One of the oldest transparencies should be selected, preferably one that has been removed from service due to gradual degradation. Yearly testing of aged monolithic stretched acrylic is not as important. One study found significant strength losses starting to appear in monolithic sketched acrylic windshields and canopies did not start until the 14 to 18 year range (Ref 3). There are, however, indications that significant impact strength losses occur much sooner with laminates and monolithic polycarbonate materials. Some bird impact tests on service aged laminated transparencies have produced failures at speeds considerably less than the speeds that unexposed transparencies had passed during the initial acceptance testing. Some coupons of monolithic polycarbonate, after exposure in the EMMA fixtures in Arizona, showed retention of impact strength for about 3 years worth of equivalent UV exposure followed by rapid loss of strength with additional exposure time (Ref 6). Interpreting these coupon results is difficult. It has not been determined what the effects of the higher EMMA dosage rates are on polycarbonate and if the dosage rate would produce invalid or misleading results. The results do suggest it would be prudent to check for possible in-service strength losses through periodic bird strike tests. Detecting such a strength loss problem with a bird impact test would provide time for devising and implementing cost-effective corrective measures.

FULL SCALE DURABILITY

The last full scale test would assess the full scale transparency's durability when exposed to simulated in-flight and flight line environments. In many instances there would be insufficient testing time available, and procurement decisions would be made before the full scale durability test results were completed. In these cases, the testing would yield information that could indicate a possible durability problem before it had serious operational impact. This would provide more time for design changes (or developing new designs) that could be more durable.

The testing methodology is a good approach to follow in testing new aircraft transparency designs for durability. The coupon tests that have been included should cost no more to run than coupon tests that have been required in many previous transparency qualification programs. In addition, the results should be more informative. The methodology was derived using ground rules that testing costs, time available for testing, and the value of generated test information were all important factors. However, when a particular testing program comes along where the relative importance of these factors is quite different, then it is appropriate to consider using a modified version of the testing methodology. If, for instance, there are several good transparency candidates for a new aircraft and there is plenty of time before a transparency selection decision is needed, it would probably be beneficial to run additional tests and test combinations. If, on the other hand, there is an urgent operational need for a new aircraft transparency (for a new aircraft or perhaps to replace an existing design that has proven unsafe to use) and there is only one candidate design, it would be appropriate to change the emphasis and sequence of the testing program. If the need is indeed urgent, the testing program should initially determine the transparency will withstand bird impact and the in-flight temperatures, pressures, and change rates without sudden failure before the transparency system is purchased. Durability testing should continue so that if durability was inadquate, work could start promptly on design changes or new designs.

Whether a specific testing program uses the methodology exactly as written, or with added tests is not too important. What is significant is for the methodology to be the starting point for as many different evaluation programs as possible. The methodology's strong and weak points will become evident through its use. Results from different programs can be compared. The methodology will continually evolve as more information is accumulated. The correlation between specific laboratory test results and in-service durability of the transparency design will be better understood.

The remaining portion of this paper will discuss the full scale durability test of the laminated F-16A canopy that was conducted at Wright-Patterson AFB. There have been some very interesting results and worthwhile lessons learned to date with this facility.

The transparency testing facility is fairly large and complex. The equipment can subject a full scale transparency to various temperatures, pressures, and change rates that represent the in-flight environment.

The flight line environment is represented with various temperatures, cleaners, moisture, and UV radiation.

The computer control and data recording and analysis systems have more than enough capability, with the primary data analysis capability depending upon the main computers for the building. Backup systems using smaller computers can "fly" the missions and record the data for later analysis when the main computers are down. There are numerous sensors that indicate temperatures and pressures outside and inside the test specimen, plus indicators of system performance such as temperatures at various locations, valve positions, blower motor status, etc.

The system has more capability for attaining high temperatures, low temperatures, rapid temperature changes, and for data recording than is needed for the present F-16 canopy testing. This additional capability resulted from the way the equipment evolved, with the system design process being driven by the need to have enough capability to satisfy testing requirements (with those testing requirements initially being unrealistically severe, especially with rapid temperature change rates down to very low temperatures), and to use items and equipment that were readily available or already on hand to the maximum extent possible.

The test fixture can accurately duplicate the canopy temperatures which are expected to be encountered inflight. It is a prototype fixture, constructed to demonstrate the feasibility of this transparency testing approach.

It is important to have a good understanding of the actual environment the transparency will encounter in conducting representative tests. The most difficult portion of the in-service environment to accurately predict is representative flight profiles. When the F-16A laminated canopy durability test plan was developed there was no published usage data on which to base the flight profiles. However, the F-16A aircraft structure was designed to perform specific flight profiles (Table 4)(Ref 4). These profiles include speeds, altitudes, engine power settings, times at each condition and rates of speed and altitude changes. From this information it was possible to calculate the temperatures the canopy exterior surface would experience throughout the flight profile. The temperatures were calculated using standard, hot, and cold atmospheres. Since cockpit pressurization is a function of altitude, the pressure differential (cockpit vs exterior ambient pressure) was easily determined. The result of these calculations was 36 combat and peacetime mission profiles (12 missions in three atmosphere conditions) expressed as exterior canopy surface temperatures and cockpit/exterior pressure differential versus time. A paper on the temperature calculation process was given recently by AFWAL/FIBE personnel (Ref 5). These profiles were programmed into the control computer. The computer then tracked these missions. The "mix" for the flight profiles was to use 80% with the standard atmosphere conditions and 10% each with the hot and cold atmospheres The temperature profiles shown at the back of this paper are taken from the FIBE paper.

In addition to simulating the flight portion of the transparency environment, some of the more important aspects of the flight line environment

TABLE 4

16PS007B Structural Design Criteria

PROJECTED F-16 MISSION USAGE

MISSION NUMBER	TYPE OF MISSION	% USAGE
1.	TRANSITION	5
2.	INSTRUMENT/NAV/REFUELING	10
3.	AIR COMBAT MANEUVERS/TACTICS	20
4.	AIR-TO-AIR GUNNERY	10
5.	AIR-TO-GROUND WPN DELIVERY	10
6.	FIGHTER SWEEP	10
7.	ESCORT	10
8.	AIR DEFENSE/INTERCEPT	5
9.	CLOSE AIR SUPPORT	5
10.	INTERDICTION	5
11.	FERRY	5
12.	FUNCTIONAL CHECK FLIGHT	5

Missions 1-5 are training and 6-10 are combat. Combat missions could be either actual or simulated.

were also included. The test plan calls for exposing the canopy to the equivalent ultraviolet (UV) radiation exposure of 3 years in Arizona. The UV is provided by 2 kinds of bulbs (alternating between Westinghouse FS40 sunlamps (code 26473-9) and F40BL blacklamps (code 31439-3)) which are turned on during the hottest portion of the temperature exposure profile. The profile (Figure 1) represents a hot and humid environment, and has a cockpit air temperature that climbs to a maximum of 200°F. Calculations indicate a parked F-16A can have the cockpit air temperature approach 200°F in some hot, sunny locations. The outside air temperature reached a maximum value of 110°F.

Water is sprayed onto the canopy during the cool down portion of the exposure profile, representing a late afternoon shower. The moisture is allowed to remain on the canopy for the rest of the exposure profile.

The test plan also called for cleaning the canopy at frequent intervals. Different portions of the canopy were cleaned with different cleaning chemicals and combinations of cleaners. The cleaning solutions used were plain water and each of the solutions listed in the appropriate F-16A technical orders. The F-16 technical orders had not been updated to add cleaners for acrylic faced laminated designs. The plastic polish and rain repellent used by F-111 units were added to the test plan for use on the laminated canopy. The chemicals used and the usage pattern on the canopy are shown in Figure 2. By using the chemicals alone and in combination with each other, it is possible to understand the significance of test results should crazing become a failure mode. For example, if only the sections of the canopy where one cleaner was used had crazing, further coupon tests should be run and consideration should be given to deleting that item from the technical orders as an approved cleaning solution.

The canopy is cleaned before and after each flight line exposure run, plus whenever convenient at the beginning or end of a work day. All cleanings were recorded in the test log.

The testing approach was to run each profile until a very good match was obtained to the desired exposure profile. This accurate run was filed away as a reference. The data system measured and stored the temperature and pressure readings for each sensor outside and inside the canopy. The test plan called for having the computer system compare each run with the reference run. Temperatures or pressures that differed from the reference by more than some tolerance (±10°) would be noted, and only those times and sensors that exceeded the tolerance would be printed out. The data for each sensor would be retained on tape and the complete data printouts could be obtained if needed.

The flight profiles were run as planned. There were some problems with the ground exposure equipment, so for the first 153 hours of total exposure run time there were only 30.5 hours of the ground environment (about ½ the amount desired). The canopy was cleaned 9 times during this period. Some crazing of the outer acrylic ply was observed after 116 hours of in-flight exposure. An 11 hour flight line exposure was run with no further crazing in the canopy. Six in-flight profiles were then run. Two of these profiles did

FLIGHT LINE ENVIRONMENT TEST CYCLE

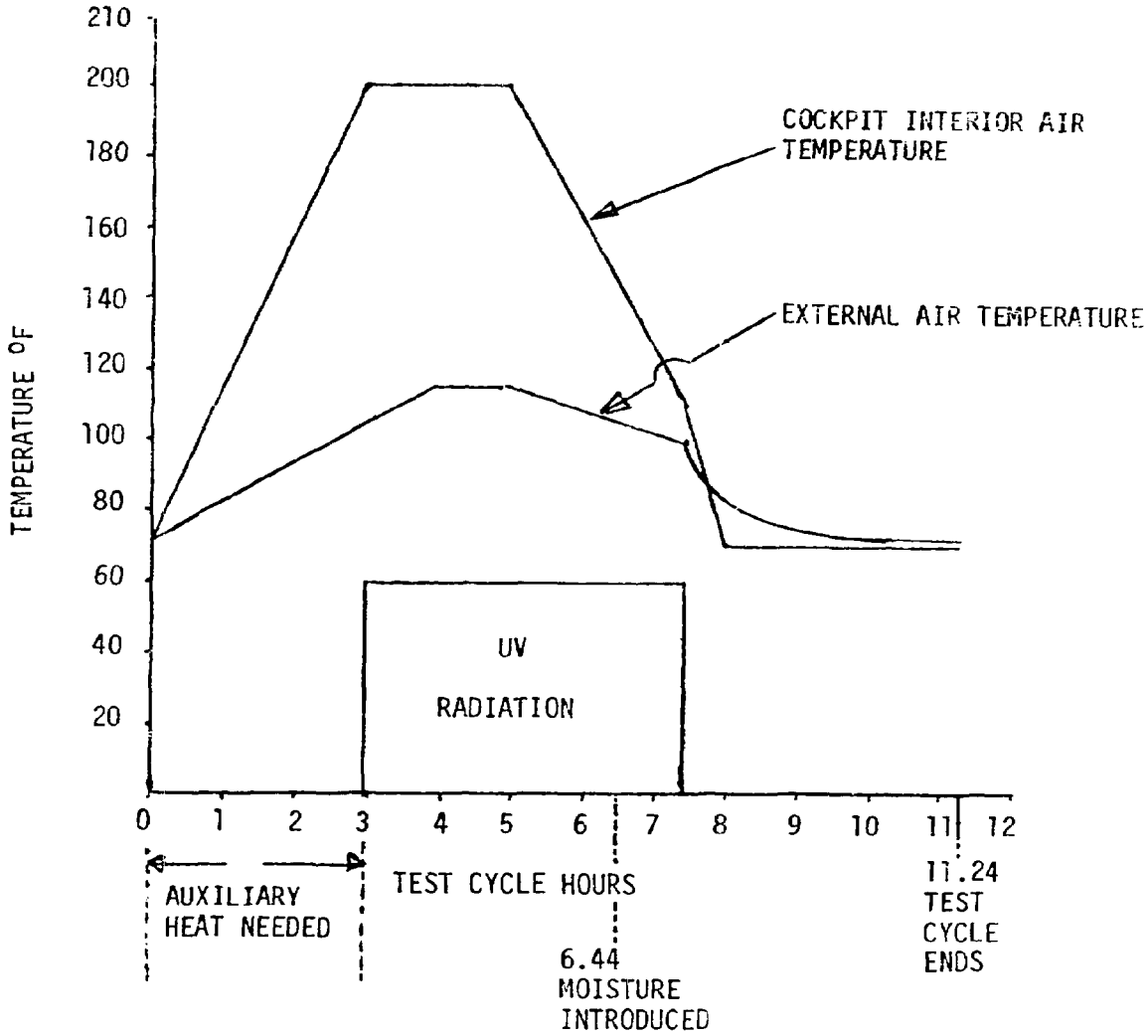

Figure 1

F-16 CANOPY AND COUPON TESTING

EXPOSURES	CANOPY SECTIONS							
	1	2	3	4	5	6	7	8
IN-FLIGHT TEMPS	X	X	X	X	X	X	X	X
GROUND TEMPS	X	X	X	X	X	X	X	X
U.V. RADIATION	X	X	X	X	X	X	X	X
MOISTURE	X	X	X	X	X	X	X	X
CLEANING CHEMICALS AND SOLUTIONS:								
NONE	X							
AMMONIA, IPA AND WATER		X				X	X	X
WATER AND IPA			X			X	X	X
SOAP AND WATER (DOVE SOAP USED)				X		X	X	X
WINDEX					X	X	X	X
POLISH (NOVUS 2)							X	X
RAIN REPELLENT (NOVUS 1)								X

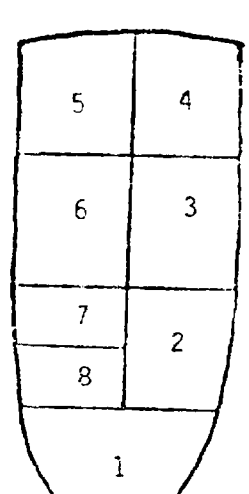

Figure 2

not have very stressful temperature changes. These were followed by four repeats of the Functional Check Flight (FCF). The FCF features a high temperature (representing Mach 2 flight) followed by a rapidly decreasing temperature (representing subsonic flight at 50,000 feet). When the canopy was examined, the outer acrylic face ply was found to have failed, with cracks running over the entire canopy.

This massive cracking failure was rather puzzling. There have been a few reported cases of cracked outer plies on some operational F-16s (with at least some of them being caused by impacts), but nothing as spectacular as our failure. If the aircraft were flying the mission profiles we were using, we would expect similar results. The pilots who fly the FCF missions were contacted on how they actually flew those FCF missions. The pilots stated the FCF mission profile as given in the Structural Design Criteria document were not flown. Speeds over Mach 1.5 were rarely attempted, and even if they should try and attain Mach 2.0, it would not be followed by flight at 50,000 feet. Actual usage data from flight recorders eventually became available and verified what the pilots had said. This pattern held true for all the peacetime mission profiles, with the aircraft being flown both lower and slower than the profiles we used in our testing (Table 5).

The Functional Check Flight was not the only profile that had temperatures representing Mach 2 flight. Some of the combat flight profiles repeatedly also had these high temperatures. Other mission profiles had cold temperatures considerably lower than the FCF. The temperature change rates for both heating and cooling were also no more severe than other missions. The thermal stresses involved in having a cold exterior acrylic face ply on a laminate where the other plies were still warm, combined with whatever stresses had been induced by previous exposures was apparently enough to initiate and propagate extensive cracking.

Further tests were run to better assess the cause and significance of this cracking event. These included additional FCF missions and special high exterior temperature soak profiles. These additional exposures produced very little additional cracking, but the existing cracks opened noticeably. This suggested the cracking had effectively relieved the stresses in the outer ply, with additional shrinkback of the acrylic ply causing the cracks to widen. After these additional exposures, the canopy was subjected to the same pressurization tests that were used to initially flight certify the design. There were no noticeable effects from the pressure tests, demonstrating the canopy was still structurally sound.

NEW DEVELOPMENTS

There are, of course, new and improved products being developed all the time. One recent achievement by Texstar is singled out for discussion. Texstar has developed a process which takes F-16 canopies that have failed in service, restores the coating, and returns them to the inventory. This has the potential of significantly reducing life cycle costs of coated polycarbonate canopies by extending their useful life. The solving of this one problem may make it possible for other problems to appear. Specifically, the presently correct belief that undamaged monolithic polycarbonate retains

TABLE 5

F-16 DESIGN GUIDE MISSIONS VS ACTUAL USAGE DATA

TYPE OF MISSION	MAX SPEED DESIGN GUIDE	MAX SPEED USAGE DATA		
		HILL AFB	MACDILL AFB	NELLIS AFB
AIR COMBAT MANEUVERS (ACM)	MACH 1.6	1.3-1.5	1.1-1.3	1.5-1.7
AIR DEFENCE/ INTERCEPT (AD/I)	MACH 2.0	1.5-1.7	1.0-1.1	.9-1.0
FUNCTIONAL CHECK FLIGHT (FCF)	MACH 2.0	1.5-1.7	1.5-1.7	1.7-2.0

structural strength for the life of the F-16 canopy will have to be reexamined.

Several conclusions were drawn about both this testing approach and the laminated F-16A canopy.

1. The high temperatures of Mach 2.0 flight and the low temperature of subsonic flight above 50,000 feet in the test profiles are not presently experienced by operational F-16A aircraft.

2. It is important to use exposure conditions and temperature extremes that are representative of the actual usage if peacetime durability is to be evaluated.

3. The canopy had survived all the combat mission profiles before the FCF was run, indicating that the canopy can survive these missions if they are flown.

4. There is no operational requirement to perform the FCF mission profile as given in the General Dynamics design documents, nor is there an equivalent combat profile.

5. If the sequence of hot, then cold temperatures is the cause of the cracking failure (the most popular theory) this would not occur with the operational aircraft.

6. This cracking susceptability probably would not have been detectable with any test using coupons. Although testing of full scale transparencies is much more costly and time consuming than coupon tests there are some potential problems that cannot be identified when only coupons are used.

7. The cracking event is a durability problem, not a safety of flight problem. The canopy retained structural strength and even in the severely cracked condition there would be sufficient visual clarity to operate and land the aircraft.

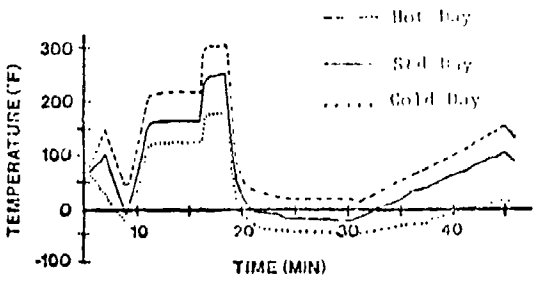

The Influence of the Atmospheric Model on Surface Temperature Prediction

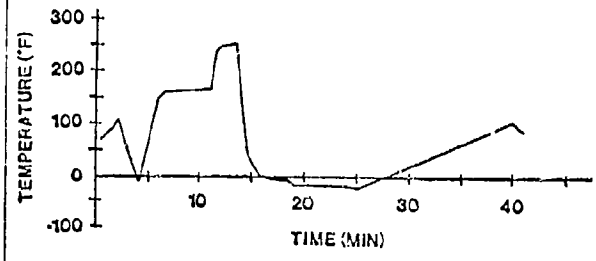

Exterior Surface Temperature History for the Air Defense/ Intercept Mission

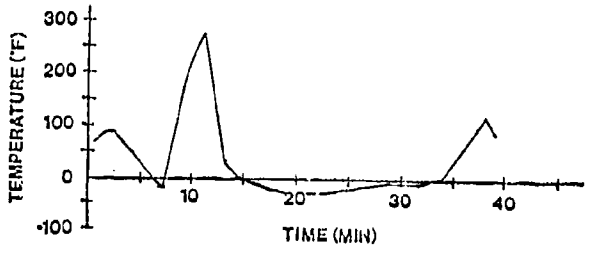

Exterior Surface Temperature History for the Functional Check Flight Mission

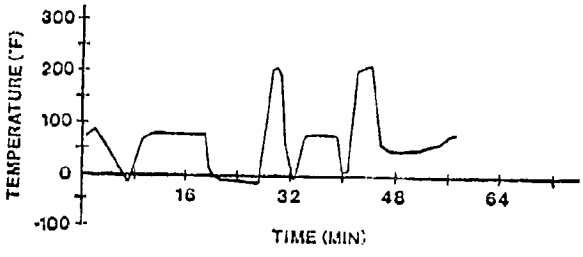

Exterior Surface Temperature History for the Air Combat Maneuvers Mission

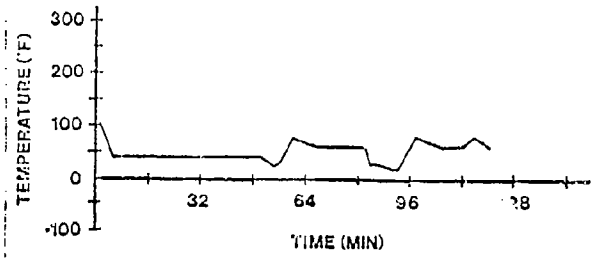

Exterior Surface Temperature History for the Instrument/Navigation/ Air Refueling Mission

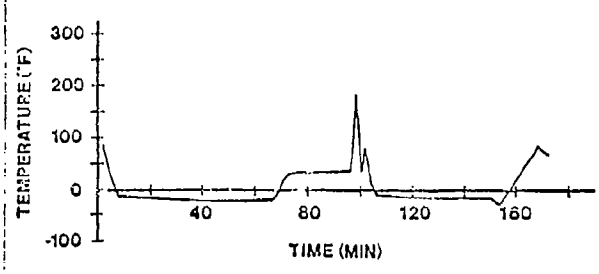

Exterior Surface Temperature History for the Fighter Sweep Mission

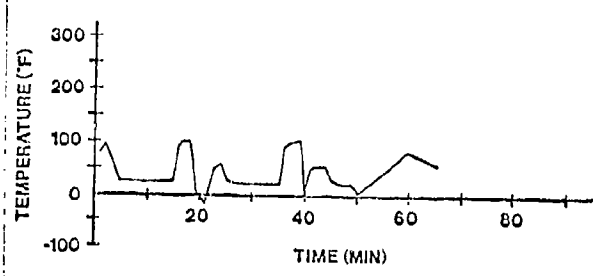

Exterior Surface Temperature History for the Air/Air Gunnery Mission

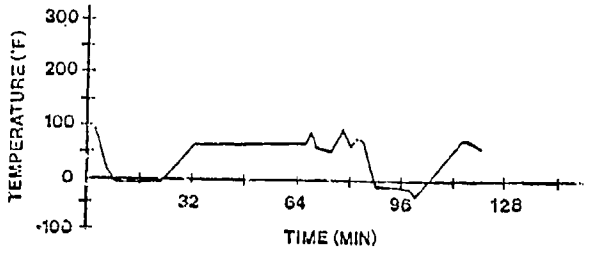

Exterior Surface Temperature History for the Close Air Support Mission

REFERENCES

1. Clayton, Kenneth I.; West, Blaine S., Aircraft Transparency Testing Methodology and Evaluation Criteria, Part I - Test Methods and Information Analysis, AFWAL-TR-83-3045, Part I, Flight Dynamics Laboratory, AFWAL/FIER, Wright-Patterson AFB, Ohio 45433, April 1983.

2. Clayton, Kenneth I.; West, Blaine S., Aircraft Transparency Testing Methodology and Evaluation Criteria, Part II - Methodology Development for Improved Durability, AFWAL-TR-83-3045, Part II, Flight Dynamics Laboratory, AFWAL/FIER, Wright-Patterson AFB, Ohio 45433, April 1983.

3. Ursell, C. R., Investigation of the Effect of Age on the Structural Integrity of F-5 Canopies, Southwest Research Institute, 6220 Culebra Road, San Antonio, Texas 78284. Report prepared for San Antonio Air Logistics Command, Kelly AFB, Texas 78241, 24 June 1981.

4. Structural Design Criteria, General Dynamics, 16PS007B, 15 March 1976.

5. Paul, Donald B.; Clay, Christopher L., "Thermal Fatigue Spectra Generation for the F-16 Canopy," Flight Dynamics Laboratory, AFWAL/FIBE, Wright-Patterson AFB, Ohio 45433. Paper presented at 24th AIAA/ASME/ASCE/AHS Structures, Structural Dynamics and Materials Conference, Lake Tahoe, Nevada, held May 1983.

6. Clayton, Kenneth I.; Milholland, John F.; Stenger, Gregory J., Experimental Evaluation of F-16 Polycarbonate Canopy Material, AFWAL-TR-81-4020, Materials Laboratory, Air Force Wright Aeronautical Laboratories, Wright-Patterson Air Force Base, Ohio 45433, April 1981.

SESSION V

BIRDSTRIKES - PROBLEM DEFINITION AND REDUCTION (PART I)

Chairman: W. Bussard
Flight Dynamics Laboratory
Wright-Patterson
Air Force Base, Ohio

Co-Chairman: J. Thorpe
Civil Aviation Authority
Surrey, England

PREVIOUS PAGE
IS BLANK

AD-P003 214

CIVIL AIRCRAFT WINDSCREEN DAMAGE DUE TO BIRDSTRIKES

J. Thorpe, Civil Aviation Authority

CIVIL AIRCRAFT WINDSHIELD DAMAGE DUE TO BIRDSTRIKES

by John Thorpe - UK Civil Aviation Authority
Safety Data & Analysis Unit

ABSTRACT

Brief details are presented of all known cases world wide of penetration of civil aircraft windshields. The information is divided into:

(a) transport aircraft (piston engined aircraft are excluded),

(b) twin engined general aviation aeroplanes,

(c) single engined aeroplanes, and

(d) helicopters.

Windshield design requirement crieria are summarised.

Examination of the data shows that penetration of transport aircraft windshields is extremely rare and damage to the outer pane is very rare (in Europe one per 1.5 million flying hours). There would appear to be little justification for a change in the current 1.8 Kg (4 lb) bird design requirement.

There have been three fatal windshield penetrations on twin engined general aviation aircraft and six cases of injury. Many of the birds were large. The trend towards single pilot operations carrying a significant number of passengers (up to 22) may suggest a need for windshield design requirements, even though the rate of penetration is not high.

Windshield penetrations on single engined aeroplanes are kept to a small number, probably because, with their modest speed there is more time for birds to take avoiding action. There is some evidence that birds of prey will attack small aircraft.

There have been few cases of helicopter windshield penetrations, the modest speed and generally loud rotor noise providing birds with adequate time to get out of the way. In newer designs the trend towards increased speed and quieter rotors may justify the need to provide design requirements for their large transparency areas.

1 Introduction

World wide data on windshield damage due to birdstrikes has been examined and presented in brief tabulated form in four groups:

(a) Transport aircraft (excluding piston engined aircraft as they are of older design built prior to any design requirements)

(b) Twin engined general aviation aeroplanes

(c) Single engined aeroplanes

(d) Helicopters

The information has been collected from as many sources as possible including Bird Strike Committee Europe, ICAO and the FAA. It is obviously not complete but is thought to give a representative guide to the extent of the problem.

2 Design Requirements

(a) A design requirement that aeroplanes over 5700 Kg (12,500 lb) shall be able to withstand windshield impact with a 1.8 Kg (4 lb) bird at V_C (normal operational speed) at sea level (or at speeds likely to be used up to 8000 ft), has been applicable for many years to aeroplanes constructed to UK or United States regulations. Additionally, in the UK aeroplanes between 2730 Kg (6000 lb) and 5700 Kg (12,500 lb) are required to be able to withstand impact with a 0.91 Kg (2 lb) bird at speeds appropriate to climb or approach. In the UK there are also similar requirements for helicopters above and below 5700 Kg. There is also a UK requirement for agricultural aeroplanes of a 0.91 Kg (2 lb) bird at speeds used in agricultural operations.

3 Operational Information

In order to provide appropriate advice to pilots a UK Aeronautical Information Circular (85/1978) "Effect of Temperature on the Resistance of Glass Laminated Windscreens to Bird Impact" was issued in October 1978 to remind pilots, amongst other factors, that correct and timely operation of windshield heat is necessary to maintain bird resistance capability. It is not known if similar advice has been issued in other countries.

4 Discussion of Bird Strike Data

(a) Transport Aircraft (Table 2)

(i) The brief details of incidents involving penetration of the windshield or of crew injury show that there have only been a few cases. There appears to be only one (possible) case on a jet transport aircraft of total penetration of all layers. Even if, unknown to the author, there have been more cases they have not resulted in fatalities or accidents. This record is associated with some 12 million flying hours per annum in recent years, excluding USSR. (Ref 1).

(ii) A rather more accurate assessment can be made from data reported world-wide by European Airlines (1972 to 1980) and involving mostly jet aeroplanes. It shows that in 39 million hours there were 1639 birdstrikes on the windshield, resulting in 26 cases of damage but none of penetration. (Ref 2). The damage rate is thus one per 1.5 million flying hours - rare indeed. Only one of these incidents was known to involve a bird heavier than 4 lbs.

(iii) Earlier fears about the danger of striking high flying birds have not been substantiated. A UK registered B727 flying at 295 kts IAS at 20,000 ft over the UK struck a bird, shattering the windshield outer layer. In another case a Belgian B707 struck a bird while at 33,000 ft over the Sahara, (leaving a blood and feather smear on the windshield), but without damage. In neither was the bird species, hence weight known, nor why the birds were flying so high.

(iv) From the available data it seems that the current design and construction standards are coping with the situation on civil transport aeroplanes.

(b) Twin Engined General Aviation Aeroplanes (Table 3)

(i) In this group there have been five fatal accidents due to birdstrikes, of which three were a result of windshield penetrations on Mitsubishi MU2J, Lear 23 and Cessna 402. There have been six cases of injury following windshield penetration. In several of the incidents the birds were heavier than 1.8 Kg (4 lb), and in all of them they were heavier (possibly much heavier) than 300 gm. The hours flown per annum by such aircraft are very considerable, probably of the order of 8 million per annum. (Ref 1).

(ii) Aircraft in this class spend more of their time at the lower altitudes where birds are prevalent (92% of strikes are below 2500 ft -(Ref 3). The increased risk is offset by the lower flying speed which allows birds a better opportunity to avoid the aircraft, particularly during take-off and landing.

However, there is a growing use of turboprop "commuter" aircraft which are gradually being permitted to carry more and more passengers (up to 22), and which can be flown by a single pilot. Consequently, consideration should be given to the need for wider application of windshield design requirements for aircraft between 2730 Kg and 5700 Kg. It is possible that some aircraft already have this capability although it has not been required.

(c) Single engined aeroplanes (Table 4)

(i) In this group, for which the information may not be so comprehensive, there is only one known fatal accident (and one possible) due to windshield penetration, but there have been 14 cases of injury (and 6 fatal accidents due to all birdstrike causes). The low speed of most of these aircraft and the partial protection afforded by the propeller reduce the likelihood of windshield penetration and pilot incapacitation.

(ii) There is some evidence that large birds of prey will attack smaller aircraft. A Swiss ornithologist believes this may be connected with the birds' mating display. Interestingly, UK data contains few cases of birdstrikes on agricultural aircraft, but several cases where accidents have resulted from attempts to avoid birds.

(iii) It appears that on the Piper PA28/Cessna 150 class of aircraft, a 270 gm bird will penetrate the windshield at quite a modest speed, 70 kts or so. Although sixteen of the 29 cases involve Cessna aircraft, 52% of single engined aircraft in the US are Cessnas, (Ref 4) the world figure probably being very similar. There is thus no difference in penetration rate.

(iv) The annual hours flown by single engined aircraft are currently in the order of 30 million worldwide. The windshield penetration rate is thus low and the fatal accident rate very low; there may be little justification for any design requirement in this area,

perhaps with the exception of designs where loss of the windshield would seriously affect controllability or airflow over the wing.

(d) Helicopters (Table 5)

The generally slow speeds and noisy approach of most helicopters, which mostly fly at low altitude, provide birds with ample opportunity to get out of the way. European data from a recent four year period shows a strike rate on any part of large helicopters of one per 10,000 hours, compared with transport aeroplanes 4.5 per 10,000 hours (Ref 2). However, current helicopter development is mainly aimed at higher cruising speeds and much quieter rotors and it is likely that there will be an increase in bird strikes on helicopters. It may be that military statistics are now showing this trend. The Bell Jet Ranger and Sikorsky S61 cruise at around 120 kts, but the recent Agusta A109 cruises at 150 kts and the Sikorsky S76 at 145 kts. There is believed to have been only one (possible) fatal helicopter accident and only one case of injury due to birdstrikes. Both of these were the result of windshield penetration. It appears that for comparatively slow and noisy helicopters there may be little need for windshield requirements, but consideration should be given to implementation of requirements on higher speed and quieter designs, especially those with vulnerably large areas of transparency.

5 Conclusions

(a) There have been very few cases of transport aircraft windshields being penetrated by birds of any size. Furthermore, the low rate of damage (one per 1.5 million hours) may indicate that the 1.8 Kg (4 lb) design requirement is adequate.

(b) For twin engined general aviation aircraft windshield penetration is the dominant reason for fatal accidents due to birdstrikes. This could indicate a need for wider application of design requirements, particularly on single pilot "commuter" aircraft with a significant number of passengers.

(c) The windshields of single engined aircraft can be penetrated by birds of around 250 gm (½ lb) at speeds as low as 70 kts. Nevertheless, the numbers of fatal accidents and injuries are low bearing in mind the very considerable hours flown per annum by these aircraft.

(d) The slower and noisier helicopters appear to experience bird-strikes very rarely (about a quarter the rate of similar aeroplanes). The situation may change with the trend to higher speed and quieter helicopters. The large transparency area may justify the application of design criteria.

Table 1 - DESIGN REQUIREMENTS

Aircraft		European (JAR)	UK (BCAR)	US (FAR)
Aeroplanes	Maximum weight greater than 5700 Kg (12,500 lb)	1.8 Kg (4 lb) V_C at sea level or 0.85 V_C at 8000 ft whichever is the more critical	as European	1.8 Kg (4 lb) V_C at sea level
	Maximum weight 2730 Kg (6000 lb) to 5700 Kg (12,500 lb)	Not finalised	0.91 Kg (2 lb) speeds appropriate to climb after T/O and during approach	Nil
	Below 2730 Kg (6000 lb)	Nil	Nil	Nil
Rotorcraft	Maximum weight greater than 5700 Kg (12,500 lb)	Not yet implemented	1.8 Kg (4 lb) at maximum TAS used up to 8000 ft	Nil
	Maximum weight greater than 2730 Kg (6000 lb) and less than 5700 Kg (12,500 lb)	Not yet implemented	0.91 Kg (2 lb) at maximum TAS used up to 8000 ft	Nil
	Below 2730 Kg (6000 lb)	Nil	Nil	Nil
Agricultural	Any weight	Not finalised	0.91 Kg (2 lb) speeds used in agricultural operation	Nil

Table 2 - JET AND TURBOPROP TRANSPORT AEROPLANE WINDSHIELD DAMAGE

Date	Aircraft	Location	Phase	Injury	Bird	Weight	Remarks
-.2.76	Fokker F28	Oron, Nigeria	-	Co-pilot cut	Vulture	Up to 5 Kg	Believed windshield penetrated
-.-.76	Antonov 24	Guinee,Africa	-	Co-pilot cut	-	-	Windshield penetrated
15.3.78	VC10	Nairobi, Kenya	T/O	Co-pilot cut	Marabou Stork	4 Kg	Outer panel crazed
-.-.-.	Fokker F27	- ,Africa	Cruise	Co-pilot's arm cut. Cabin attendant face and eye injury	Vulture	9 Kg	Windshield penetrated. Speed 200 kts
29.3.81	Boeing 727	JFK, USA	Climb	Co-pilot cut	Goose	Up to 4.5Kg	Outer panel crazed

Table 3 - TWIN ENGINED GENERAL AVIATION AEROPLANES, WINDSHIELD PENETRATIONS

Date	Aircraft	Location	Phase	Injury	Bird	Weight	Remarks
17.11.68	Beech 95	Hamilton, USA	-	-	Goose	Up to 4.5Kg	Broken windshield, force landed
16.4.72	Mitsubishi MU2J	Atlantic City, USA	Climb	3 killed	Geese	Up to 4.5Kg	Windshield penetrated, one or both pilots incapacitated. Uncontrolled descent into sea
1.9.72	Beech 99	- USA	-	-	Buzzard	-	RH windshield shattered at 2500 ft, 140 kts
1.10.72	Cessna 402	- -	-	-	Coopers Hawk	-	Windshield broken, 160 kts 5000 ft
15.11.72	Piper PA23	-	-	-	-	-	LH windshield shattered
10.8.74	Piper PA23	Wakunai, Australia	-	-	Brown Hawk	-	Windshield broken. 155 kts at 1000 ft
9.11.74	Beech 18	Minneapolis, USA	-	Pilot injured	Duck	300 g to 1.5 Kg	Pilot cut, glass in eye. 125 kts at 1400 ft at night
14.11.74	Cessna 310	-	-	-	-	-	Windshield broken, 160 kts at 1500 ft
8.2.78	Piper PA31 Navajo	Nr Edinburgh, UK	Descent	Nil	Herring Gull	1.1 Kg	At 2,700 ft, 180 kts struck RH windshield, which disintegrated and Captain's cracked. Roof buckled and split at top where bird hit. Weather 4/8 at 1500 ft

Table 3 - TWIN ENGINED GENERAL AVIATION AEROPLANES - continued

Date	Aircraft	Location	Phase	Injury	Bird	Weight	Remarks
7.3.78	Piper PA31 Navajo	Sacramento, California,USA	-	2 Minor injuries	Ducks	300 g-1.5 Kg	Two ducks broke through windshield injuring pilot and pax. Emergency landing at night
4.4.78	Shcrt SC7 Skyvan	Philadelphia USA	Cruise	Nil	-	-	Windshield destroyed by bird while in level flight at 3,500 ft
-.9.78	Cessna 402	Honolulu,Hawaii	Cruise	-	Frigate Bird	1 to 1.6 Kg	Cruising at 1000 ft over water, windshield shattered and some flight instruments destroyed
28.9.78	Cessna 310R	Majir, Kenya	Landing	2 passengers seriously injured	Vulture	Up to 5Kg	Windshield shattered
5.4.79	Beech 99	Lafeyette, USA	Descent	1 minor injury	Ducks	300 g - 1.5 Kg	Collided with flock of ducks,co-pilot's windshield broken, co-pilot hospitalised. A/C was at 2000 ft
20.5.80	Mitsubishi MU2G	Teterboro, USA	Climb	-	-	-	Windshield penetrated, and one engine shutdown
26.9.80	Beech 76 Duchess	Rome,Georgia,USA	Cruise	-	Hawks	-	Windshield penetrated in cruise
18.10.80	Partenavia P68	St Gatien,France	Approach	Nil	Black-headed Gull	300 g	Windshield penetrated, no injuries

Table 3 - TWIN ENGINED GENERAL AVIATION AEROPLANES - continued

Date	Aircraft	Location	Phase	Injury	Bird	Weight	Remarks
17.12.80	Piper 600 Aerostar	Nr Baton Rouge USA	Cruise	1 injury	Ducks	300 g - 1.5 Kg	Ducks holed windshield, pilot made emergency landing. Pilot required stitches in chest
-.-.80	Cessna 310	Great Rockford USA	Approach	1 minor injury	Ducks	300 g - 1.5 Kg	Windshield penetrated
7.4.81	Lear 23	Nr Cincinnati USA	Climb	1 killed	Loon	4.5 Kg	At 4000 ft bird penetrated RH windshield killing co-pilot. Pilot's arm badly cut. Eng 2 shutdown due to ingestion of windshield debris. Emergency landing
6.8.81	Cessna 402	Nr Musiara,Kenya	Cruise	1 killed	Marabou Stork	7 Kg	Bird penetrated windshield killing pilot. Aircraft crashed
7.3.83	Partenavia P68	Ipswich, UK	T/O	Nil	Lapwing	270 g	Bird cracked windshield, T/O abandoned. Speed 60 kts

Table 4 - SINGLE ENGINED AIRCRAFT, WINDSHIELD PENETRATION

Date	Aircraft	Location	Phase	Injury	Bird	Weight	Remarks
12.3.70	C150	Opalocke,USA	T/O	-	Gulls	300 g - 1.8 Kg	Student first solo. Screen shattered. Attempted forced landing substantial damage
2.7.71	C180	British Columbia Canada	Cruise	3 killed	Bald Eagle	5 Kg	Windshield destroyed. Aircraft crashed
28.4.72	C172	-	Cruise	-	-	-	Most of windshield broken out. Impact at 3000 ft, 150 kts.
29.5.72	Piper PA32	-	Cruise	-	Gull	300 - 1.8 Kg	Screen demolished at 140 kts, 5000 ft
22.10.72	C175	-	Cruise	-	Buzzard	-	Screen broken out, compass damaged
14.8.73	C206	Nr Nairobi,Kenya	Approach	2 injured	Griffon Vulture	5.4 Kg	Bird dived and shattered screen. Pilot's face cut right eye blinded and jaw dislocated, upsetting sense of balance. Force landed in 'bush'
12.9.73	C182	Nr Nairobi,Kenya	Cruise	2 injured	White Backed Vulture	5.5 Kg	At 7300 ft and 140 mph pilot turned to avoid bird ahead and above. Bird dived on A/C shattering shield, injuring pilot and passenger. A/C needed full power to hold 90 mph. Severe damage

Table 4 - SINGLE ENGINED AIRCRAFT - continued

Date	Aircraft	Location	Phase	Injury	Bird	Weight	Remarks
10.6.74	C210	-	Cruise	-	-	-	Shattered windshield, 8000 ft, 170 kts
21.6.75	Beech 23	- , Sweden	-	-	-	-	Screen holed at 250 ft
27.11.75	MS880 Rallye	-, France	-	1 injury	Black Headed Gull	300 g	Pilot seriously wounded. 100 ft 70 kts
26.1.76	C150	Bath,Carolina, USA	Cruise	2 injuries	Hawk	-	Windshield destroyed. Pilot made forced landing causing substantial damage
6.11.76	C172	Windsor,Ontario, Canada	-	1 injury	Duck	300 g - 1.5 Kg	-
10.2.77	Piper PA28	Nottingham,UK	Climb	1 injury	Lapwing	270 g	Facial cuts
14.4.77	C150	Atlanta, USA	-	2 injuries	Hawk	-	Both pilots injured
29.8.77	Victa Air-tourer	Glamorgan,UK	Climb	Nil	Pigeon	450 g	Windshield holed at 300 ft, 70 kts
23.11.77	C182	Nr Libreville, Gabon	Cruise	1 injury	Sea eagle	3 Kg	At 1000 ft, pilot's face and arm injured
10.1.78	C172	Sacremento,USA	Climb	2 injuries	Goose	up to 4.5 Kg	Climbing through 3000 ft, pilot and passenger cut
29.3.78	Piper PA28	Tweed Haven, Connecticut,USA	Approach	Nil	Gull	300 g - 1.8 Kg	At 2000 ft, bird passed through side of windshield

Table 4 - SINGLE ENGINED AIRCRAFT - continued

Date	Aircraft	Location	Phase	Injury	Bird	Weight	Remarks
22.4.78	Gulfstream AA5	Stonesville,Ohio, USA	-	1 injury	Hawk	-	At night at 2500 ft bird passed through windshield injuring passenger
27.10.78	Piper PA32	-	Cruise	1 injury	-	-	At 6000 ft at night RH windshield shattered, passengers face and hands cut
15.4.79	Gulstream AA5	Kentland,USA	Approach	Nil	Goose	Up to 4.5 Kg	Windshield shattered
-	Piper PA28	Nr Menindee, Australia	-	-	Pelican	9 to 13 Kg	At 1000 ft pilot saw birds ahead, one dived, hitting top of windshield. Trim control jammed
23.2.80	C152	Stockton, USA	Approach	1 injury	Hawk	-	Windshield and pilot's nose broken
28.3.80	C172	Nr Vancouver, Canada	-	2 injuries	Duck	300 g to 1.5 Kg	Facial injuries to pilot and passenger
7.5.80	C172	Nr Monterey,USA	Cruise	-	-	-	Several birds caused 1' x 2' hole in windshield
21.10.80	Gulstream AA5	Laurens, USA	-	-	-	-	Windshield broken
26.10.80	Beech 33	Des Moines,USA	Climb	-	Ducks	300 g to 1.5 Kg	Windshield and aerials broken
31.12.80	Piper PA28	Amarillo, USA	Approach	-	-	-	LH windshield holed

Table 4 - SINGLE ENGINED AIRCRAFT - continued

Date	Aircraft	Location	Phase	Injury	Bird	Weight	Remarks
18.7.81	C152	Nr Lerwick, UK	Descent	1 minor injury	Gull	300 g to 1.8 Kg	At 1000 ft, 90 kts windshield holed. Pilot's nose cut

Table 5 - HELICOPTER WINDSHIELD PENETRATIONS

Date	Aircraft	Location	Phase	Injury	Bird	Weight	Remarks
5.4.74	Bell 47	- , USA	-	-	Gull	300 g to 1.6 Kg	Windshield shattered
9.2.78	Bell 206	Lake Arthur, Louisiania,USA	-	-	Duck	300 g to 1.5 Kg	Approaching coast at 300 ft penetrated lower right hand bubble
24.2.78	Bell 206	Newark, USA	-	Pilot injured	-	-	At 500 ft at night struck bird,breaking windshield and cutting pilot's face and arms. Speed 100 kts
16.6.78	Hughes 300	Washington State, USA	Approach	3 minor	Small	-	At 1100 ft small birds shattered a windshield panel
-.-.-	Turbine helicopter	USA	-	-	Swallow	15 g	In cruise at 150 kts, screen holed
-.-.-	Hughes 500	San Francisco, USA	-	-	Duck	300 g to 1.5 Kg	Lower LH chin bubble shattered by duck which was still flying around inside cockpit. Collective jammed by pieces of plexiglass
12.7.80	Bell 206	USA	-	-	Turkey Buzzard	3 Kg	During powerline patrol LH screen shattered. Airspeed 60-70 mph
15.7.80	Bell 206	Indiana,USA	Cruise	-	Buzzard	-	Broke LH screen

Table 5 - HELICOPTER WINDSHIELD PENETRATIONS - continued

Date	Aircraft	Location	Phase	Injury	Bird	Weight	Remarks
2.3.81	Bell 206	Vancouver State, Canada	-	4 killed	Raven	1.3 Kg	Helicopter went missing during low altitude sheep count, not found till June. Believed windshield shattered and pilot disabled
23.7.81	Aerospatiale SA316	-	En-route	Nil	Swift	40 g	Holed windshield
27.7.81	Aerospatiale SA341	-	En-route	Nil	Swift	40 g	Holed windshield
22.10.81	Aerospatiale SA341	-	En-route	Nil	-	-	Penetration of windshield

REFERENCES

1 ICAO Civil Aviation Statistics of the World 1981 Doc 9180/7

2 Bird Strike Committee Europe Working Papers published in Proceedings of 1977, 1978, 1979, 1981 and 1982 meetings

3 CAA Paper 77008 "Analysis of Bird Strikes reported by European Airlines 1972-1975"

4 Aviation Accident Statistical Summary - General Aviation 1976 (RIS-FS-8020-21)

AD-P003 215

USAF AIRCRAFT WINDSHIELD/CANOPY BIRD STRIKES

Capt. R. C. Kull, Air Force
Engineering and Services Center

USAF AIRCRAFT WINDSHIELD/CANOPY BIRD STRIKES

BY

CAPTAIN ROBERT C. KULL JR
UNITED STATES AIR FORCE
HEADQUARTERS AIR FORCE ENGINEERING AND SERVICES CENTER
TYNDALL AIR FORCE BASE, FLORIDA

ABSTRACT

The United States Air Force loses millions of dollars due to bird strikes each year. The most serious damage to the aircraft and injury to the pilot occurs when birds penetrate the windshield/canopy system. The Air Force Bird/ Aircraft Strike Hazard (BASH) Team has recorded over 1000 bird strikes on windshields and canopies since 1975. With this extensive amount of data, trends have been found relating to the types of aircraft, phases of flight, and types of birds most vulnerable to being involved in a serious windshield/ canopy strike. This report discusses these trends, as well as the types of birds encountered and focuses on F-4 and F-16 weapon systems.

INTRODUCTION

Aircraft collisions with birds have resulted in millions of dollars of aircraft damage and the loss of both aircraft and aircrews. In response to the increasing hazards of flying in the bird's environment, the Bird/ Aircraft Strike Hazard (BASH) Team was formed to assist Air Force organizations, worldwide and to coordinate efforts in bird control, bird avoidance, and aircraft design. The BASH Team, located at Headquarters Air Force Engineering and Services Center, Tyndall Air Force Base, Florida is the office primarily responsible for collecting and maintaining all records on Air Force bird strikes. The purpose of this report is to discuss Air Force bird strikes in general, including types of birds involved, as well as to report windshield/canopy strikes on specific aircraft.

TOTAL AIR FORCE BIRD STRIKES

During the period 1 January 1980 - 31 March 1983, there were over 4,100 reported bird strikes resulting in more than $25 million of damage/loss. Unfortunately, these figures do not necessarily include all bird strikes because the Air Force reporting procedures have changed three times since 1978. However, the BASH Team is confident that the number of strikes for 1982, as shown in Table 1, is the most complete to date. Unless otherwise stated, all figures are based on the number of strikes rather than the cost of damage.

Table 1

YEAR	NUMBER OF BIRD STRIKES	TOTAL DAMAGE/LOSS
1980	1051	$5,927,376
1981	1082	$6,113,611
1982	1894	$14,088,483
1983 (Jan-May)	162*	$1,791,055

*Nondamaging bird strikes (strikes costing less than $1,000 in damage repair) were not reported at time of publication.

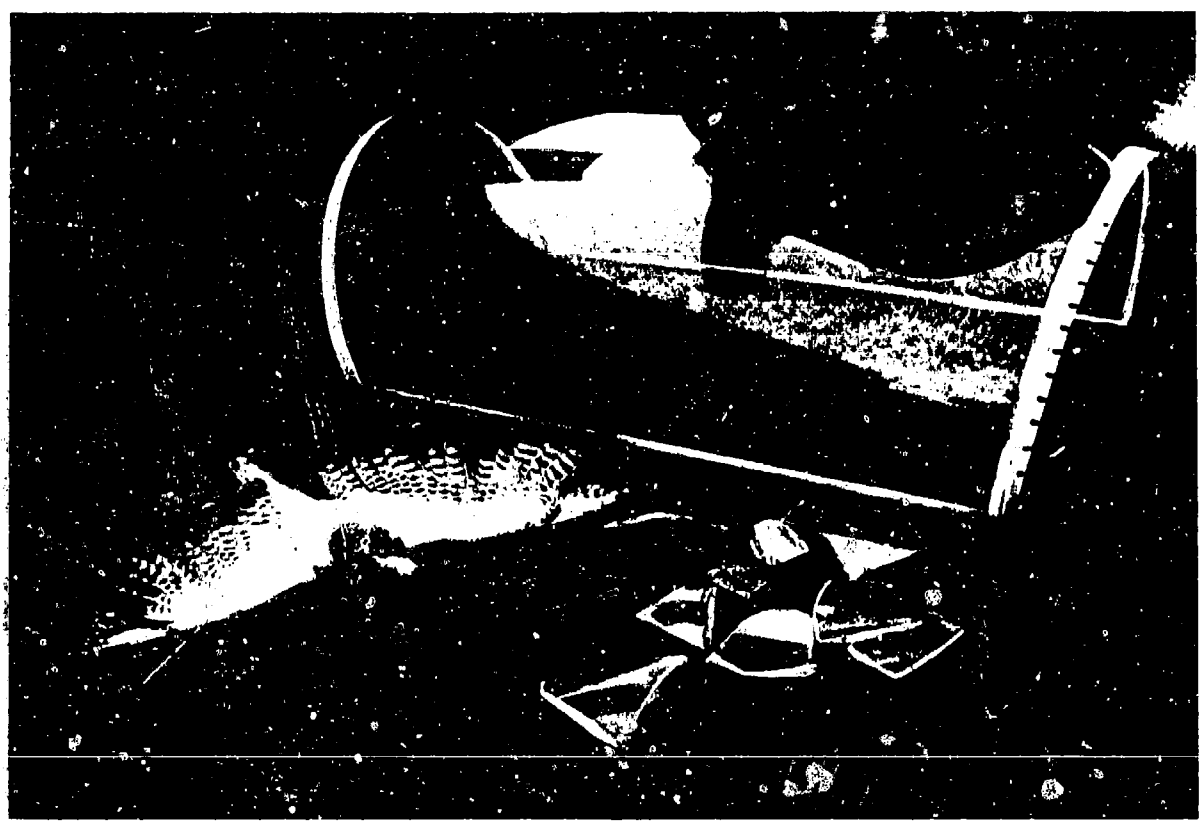

Figure 1. T-38 canopy after being struck by a 2.5Lb Swainson's Hawk. Canopy bowed in upon initial impact and exploded during a closed pull in the traffic pattern of a Texas airfield.

There are many variables involved in the total bird strike problem. Among these variables are the type of aircraft, number of flight hours, flight environment, speed, location of the base and the particular flying environment around the base. Figure 2 shows the percentage of Air Force bird strikes by aircraft group. Fighters incurred over 44% of the total number of strikes. Flight environment and speed probably account for the largest percentage of total bird strikes.

Almost all areas of an aircraft are susceptible to bird strikes. Damage to a specific impact point is related to the type of structure, as well as the weight of the bird and the speed of the aircraft. Table 2 shows engines and engine cowlings incurred the most bird strikes, while wings and windshield/canopy systems followed close behind. Almost 7% of the strikes involved multiple impact points on the aircraft caused by flocks of birds.

Table 2

BIRD STRIKES BY IMPACT POINT

IMPACT POINT	PERCENT
Engine/Engine Cowling	22.5
Wing	18.0
Windshield/Canopy	15.5
Radome/Nose	13.2
Fuselage	7.8
External Tanks/Pods/Gears	6.2
Multiple	8.0
Other	8.5

Table 3 lists major fighter weapon systems with their associated number of bird strikes, a bird strike rate per 100,000 flying hours, and the total number of windshield/canopy strikes. This shows that aircraft with a low-level flying mission incur many more strikes since they are flying in the birds' environment more often. In fact, as demonstrated in Figure 3, 25.7% of the strikes occur during low-level flying where aircraft speeds normally range from 300-500 KIAS. With the increasing number of F-4 windshield/canopy strikes/penetrations (29 penetrations from 1979-1983), I want to report specifically on F-4 bird strikes.

Table 3

AIRCRAFT	No. Strikes	Strike Rate*	Windshield/Canopy Strikes
A-10	754	95.7	93
F-111	404	65.3	71
F-16	121	61.9	25
F-4	1429	60.7	222
T-38	866	37.9	200
F-15	233	33.8	27
T-37	516	29.5	121
A-7	212	29.2	38

*Strike rate based on 100,000 flight hours

Figure 2

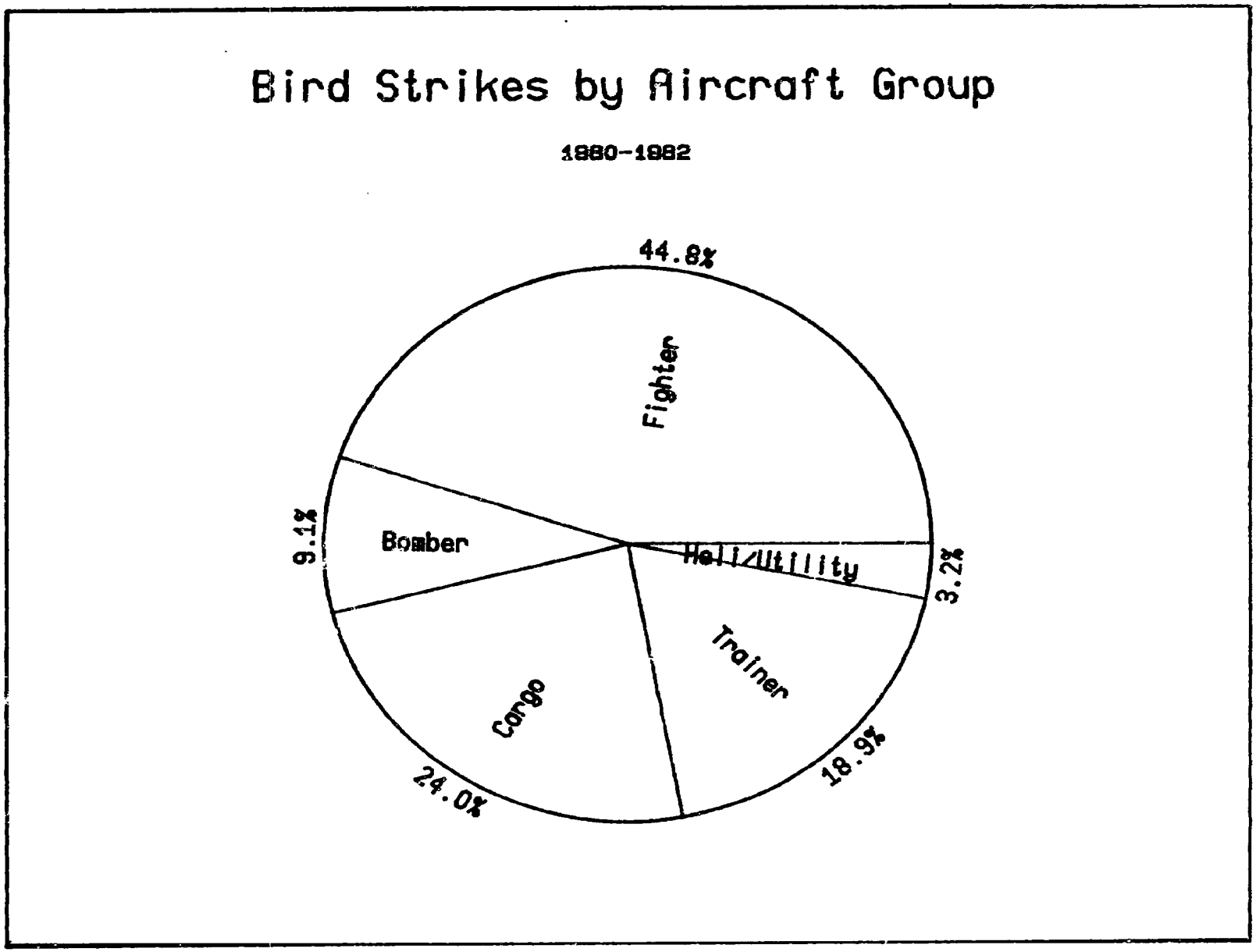
Bird Strikes by Aircraft Group
1980-1982
44.8%
Fighter
9.1%
Bomber
Heli/Utility
3.2%
Trainer
18.9%
Cargo
24.0%

Figure 3

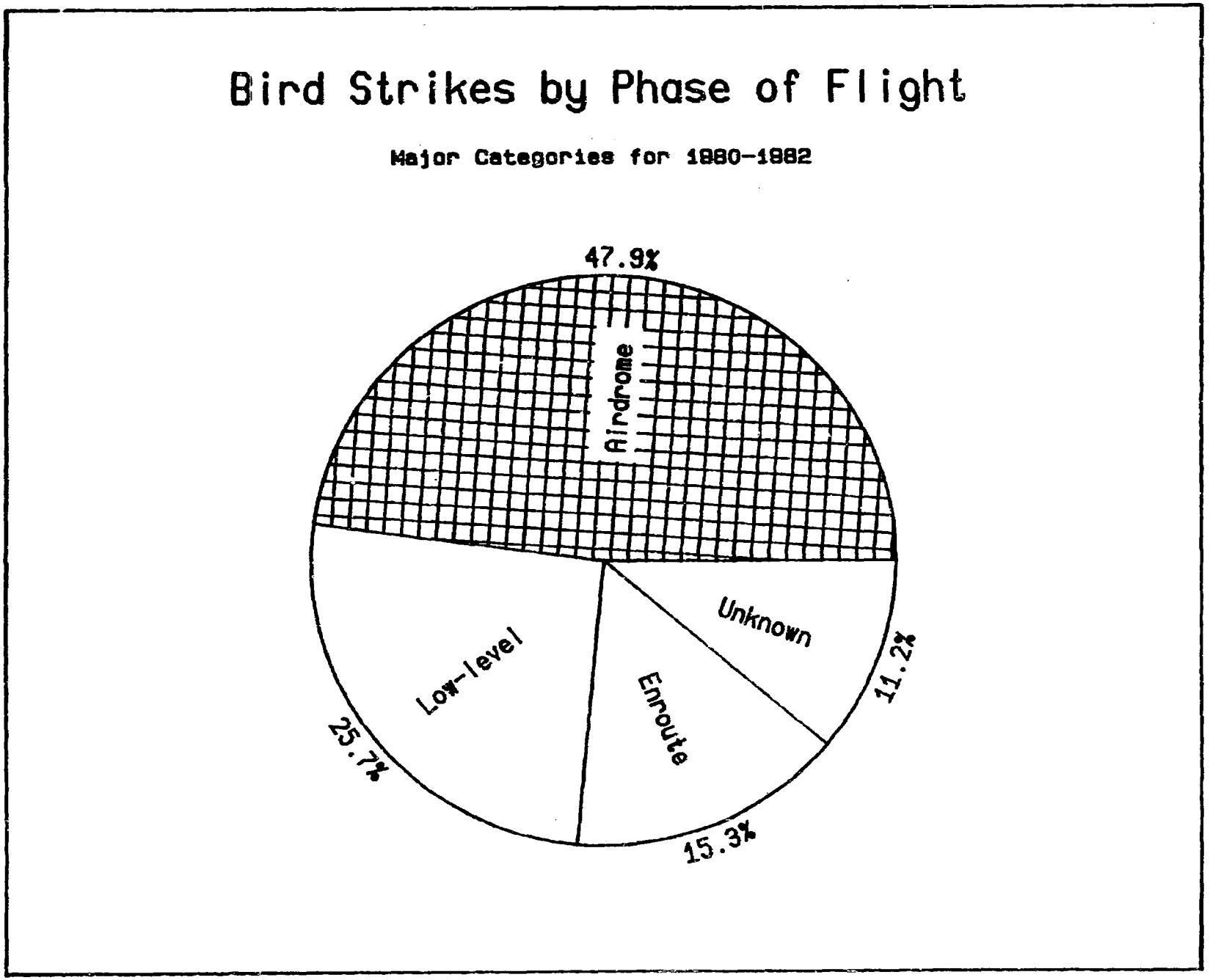
Bird Strikes by Phase of Flight
Major Categories for 1980-1982
47.9%
Airdrome
Unknown
11.2%
Enroute
15.3%
Low-level
25.7%

F-4 BIRD STRIKES

Figure 4 shows the phases of flight for F-4 bird strikes. Almost 46% of the strikes occur during low-level flying. With high speed, low altitude flying, concern for bird strikes increases due to the possibility of windshield penetrations. In fact, by examining the weight of birds involved in strikes and associated damage at various aircraft speeds, this concern is confirmed. During flying with airspeeds of 1-390 KIAS, 14% of the birds hit were one pound or greater. However, with speeds greater than 390 KIAS (typical during low-level flying), 27% of the birds were larger. This is a 13% increase in the possibility of hitting a large bird. This is not surprising since we expect a greater number of hawks, vultures, and waterfowl in these rural areas where our military low-level routes exist. The F-4 is not the only fighter aircraft where low-level flying produces increased concerns for bird strikes. Over the last three years, F-16s have had a dramatic increase in the number of bird strikes.

F-16 BIRD STRIKES

In 1981 F-16s experienced 12 bird strikes (21.3 strikes per 100,000 hours) - well within acceptable limits. However, in 1982, F-16s experienced 104 strikes (96.6 strikes per 100,000 hours). This increase may be associated with the increase in low-level flying of the F-16. Figure 5 shows the phase of flight for F-16 bird strikes. Averaged over a three year period, airdrome strikes are the most prevalent; however, associated damage is less due to relatively slow airspeed. Increased concern is for the 25 bird strikes which occurred during low-level flying in 1982 and we may see an increase in this number as the mission of the F-16 changes.

TYPES AND SIZES OF BIRDS

Identifying birds involved in bird/aircraft strikes is an important aspect of any bird strike program. For many years, the Air Force has been identifying birds from feathers and carcasses that caused reportable damage to aircraft. As I indicated earlier, the Air Force's criteria for reporting damage has changed through the years. Fortunately, the BASH Team has been able to identify many nondamaging strikes or at least put them into a category of small (less than 1Lb) or large (greater than or equal to 1Lb) bird. Of 8,386 bird strikes since 1975, 3,760 mishaps have included the relative size of the bird (Table 4). Of the 3,760 strikes, 50.7% of the birds involved were greater than one pound.

For many years the Air Force's Flight Dynamics Laboratory has used a 4Lb bird as the criteria for the structural design of windshield/canopy systems. This criteria was established based on data indicating that 92% of the birds encountered were 4Lbs or less. But from current bird strike data, how many strikes actually fall under this criteria? In an attempt to answer this question, I examined the percentage of strikes per weight of the birds. First of all, I assumed that all bird strikes not categorized as to the size of the bird were small birds (less than 1Lb). Secondly, in all cases, an average weight for each species of bird identified was computed. By multiplying the number of strikes for each species by their respective weights, I established a biomass and an average weight. That

Figure 4

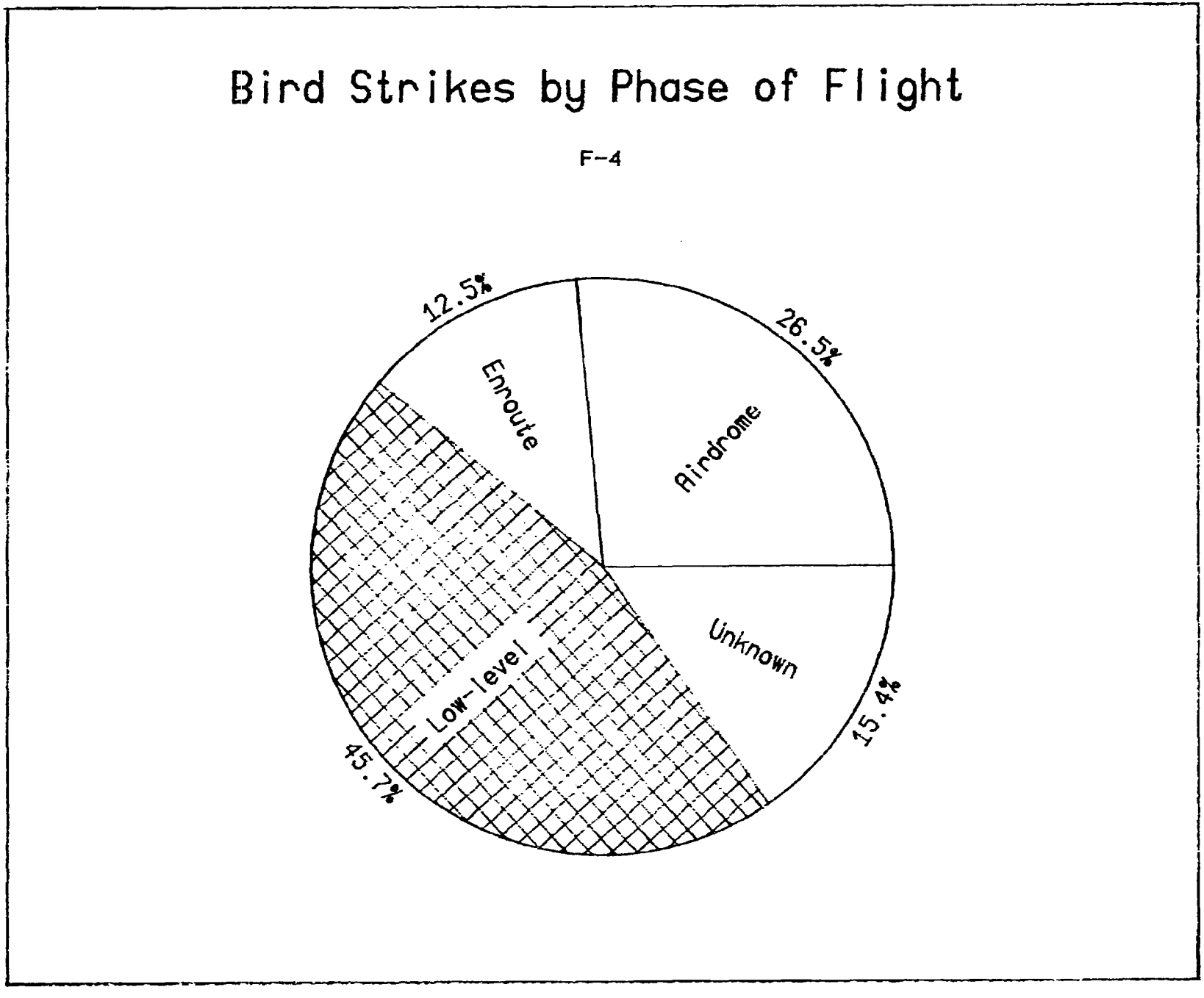
Bird Strikes by Phase of Flight
F-4
12.5%
26.5%
15.4%
45.7%
Enroute
Airdrome
Unknown
Low-level

Figure 5

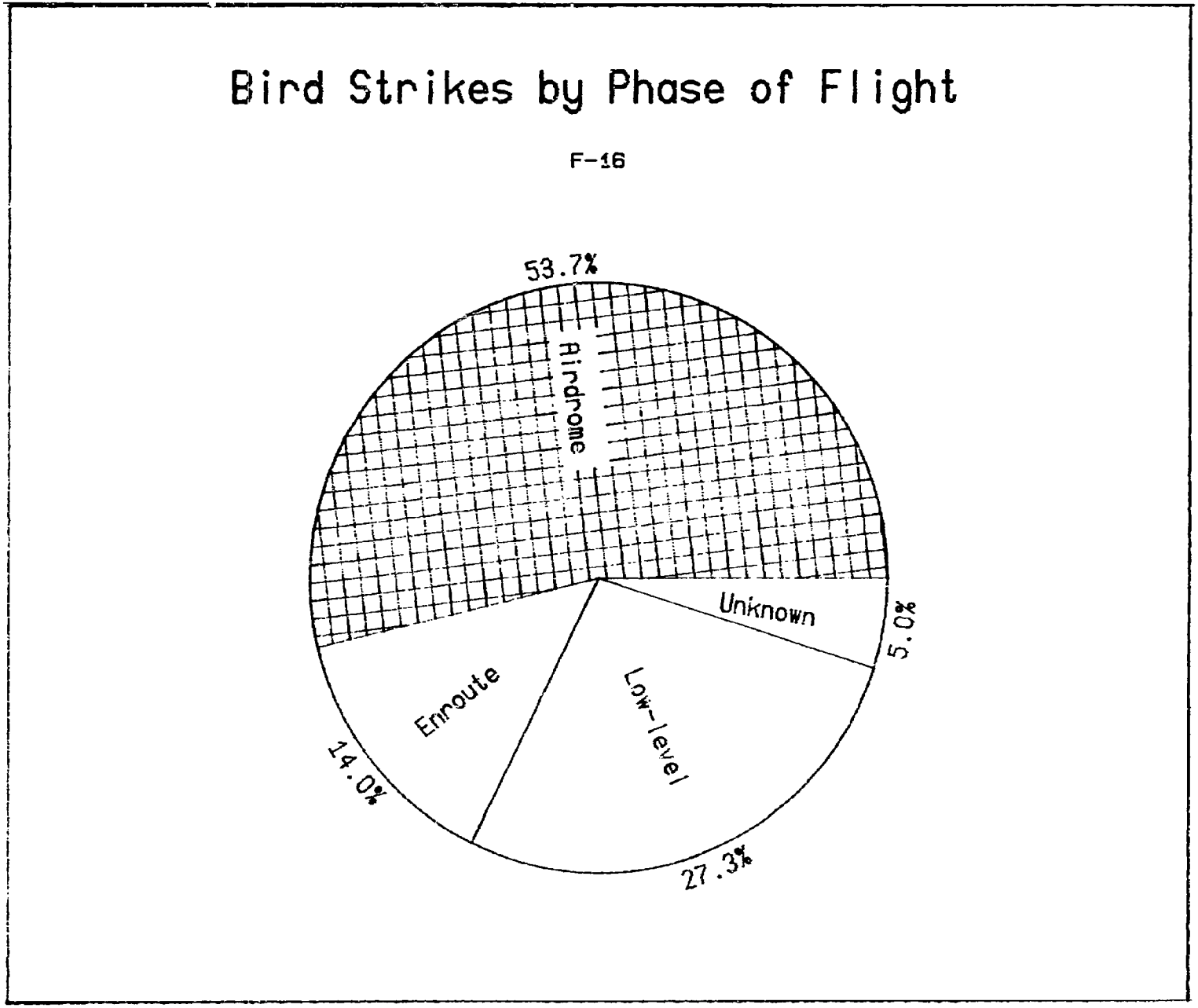
Bird Strikes by Phase of Flight
F-16
53.7%
Airdrome
Unknown
5.0%
Enroute
14.0%
Low-level
27.3%

average weight was used for a number strikes without the species identified. Figure 6 relates the cumulative percentage of strikes to the weights of the birds. In 98.5% of the strikes, birds involved were 4Lbs or less. Due to the large number of strikes with the F-4, a similar graph was possible. Figure 7 breaks down the percentages according the aircraft speed. As you can see, a greater percentage of larger birds are hit at higher speeds. As I stated earlier, 400-540 KIAS is indicative of low-level flying where more of the large birds reside. This graph also shows that even at 400 KIAS 97.6% of the birds are 4Lbs or less. In 90.2% of the bird strikes at the lower speed birds involved were two pounds or less. On the other hand, only 77.3% of the bird strikes at the higher speeds involve the same weight class. Further analysis should be done in order to produce better refined graphs.

Table 4

LIST OF BIRD STRIKES BY TYPES OF BIRDS 1975-1983

Small Birds (.05oz - 15oz)	No of Strikes	Avg Weight (in ounces)	Percent
Blackbirds	195	4	
Starlings	118	4	
Horned Larks	50	1.5	
Meadowlarks	68	4	
Shorebirds	120	10	
Doves	96	8	
Pigeons	95	12	
Other	1112		
Total	1854		49.3

Large Birds (1LB - 20+1Lbs)	No of Strikes	Avg Weight (in pounds)	Percent
Crows	33	1.0	
Egrets	50	3.0	
Gulls	583	2.0	
Ducks	250	2.5	
Hawks	376	3.0	
Vultures	185	4.0	
Geese	60	6.0	
Cranes	11	9.0	
Pelicans	7	15.0	
Albatross	23	8.0	
Cormorants	9	4.0	
Pheasants	5	2.5	
Other	314		
Total	1906		50.7

NOTE: The percentages are based strictly on the number of birds per size category. Over 55% of the strikes were not classified according to small or large. The list of actual birds is not inclusive, but a sample of the types of birds involved in collisions.

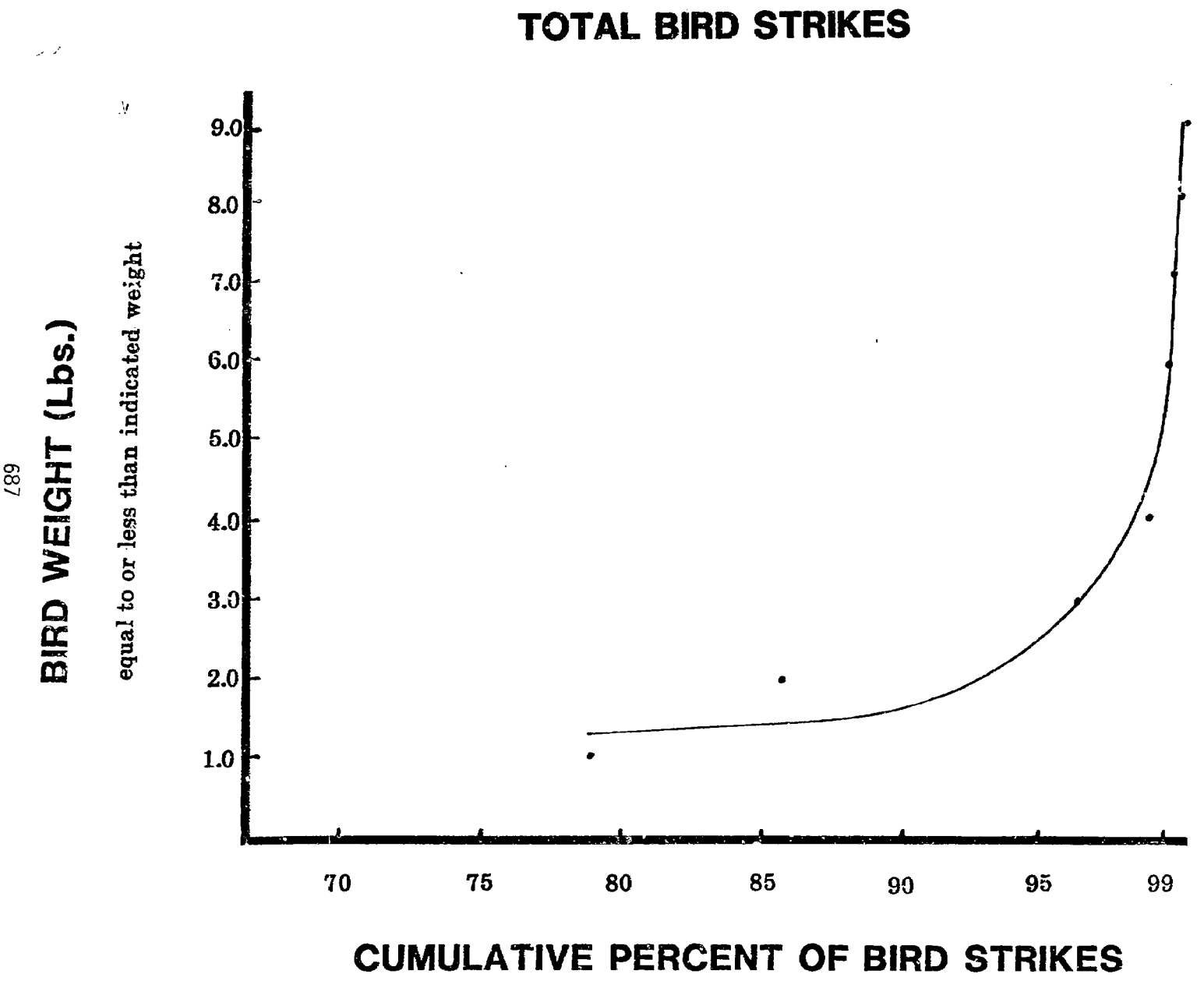
TOTAL BIRD STRIKES
BIRD WEIGHT (Lbs.)
equal to or less than indicated weight
9.0
8.0
7.0
6.0
5.0
4.0
3.0
2.0
1.0
70
75
80
85
90
95
99
CUMULATIVE PERCENT OF BIRD STRIKES

Figure 6

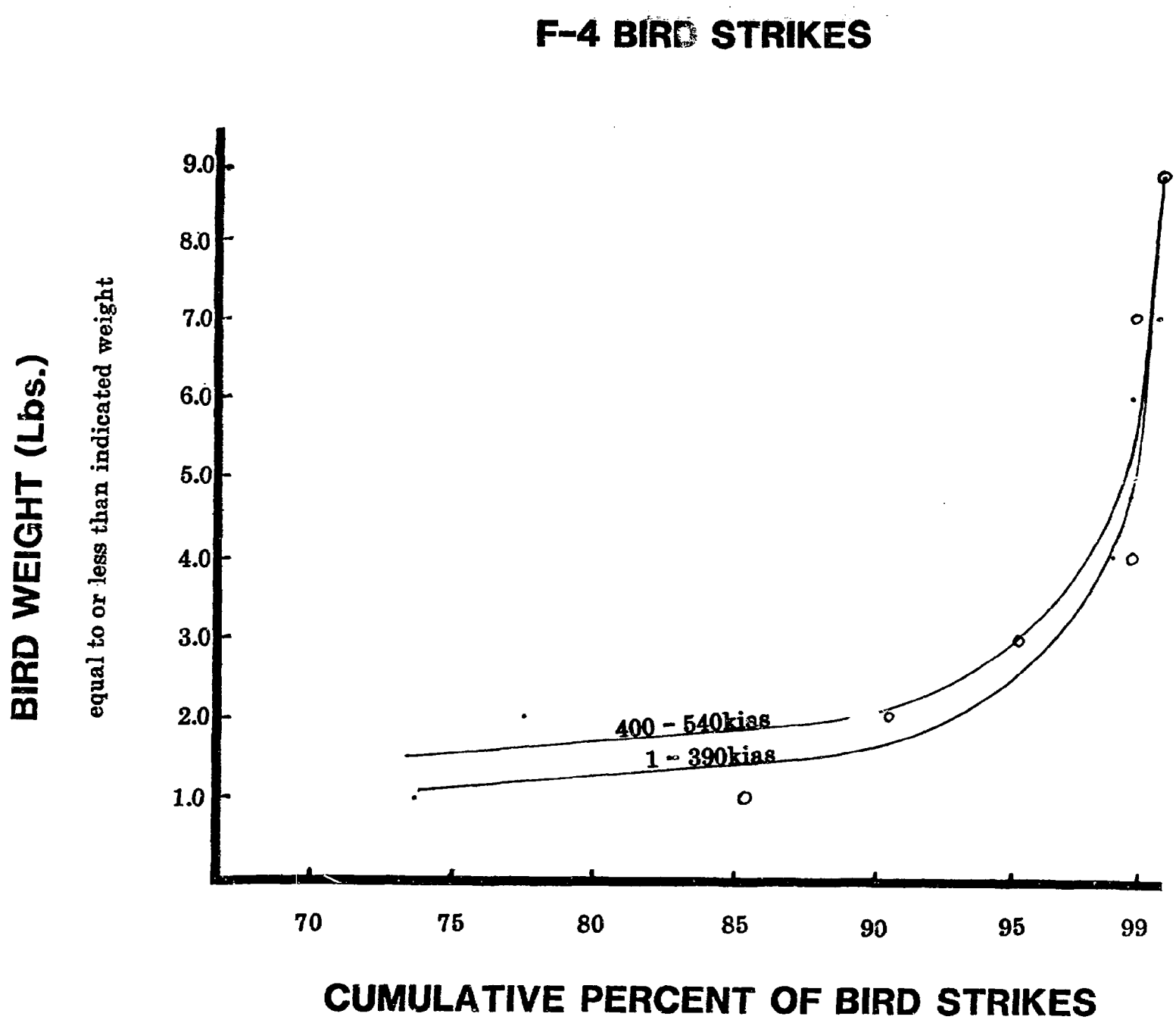
F-4 BIRD STRIKES
BIRD WEIGHT (Lbs.)
equal to or less than indicated weight
9.0
8.0
7.0
6.0
5.0
4.0
3.0
2.0
1.0
400 - 540kias
1 - 390kias
70
75
80
85
90
95
99
CUMULATIVE PERCENT OF BIRD STRIKES

Figure 7

CONCLUSIONS

These data presented shows the ever-present hazards aircraft encounter when flying in an environment where birds normally exist. Even though bird strikes occur most often around the airdrome, a great concern exists for aircrews flying low-level routes at 500 KIAS. By further examination of the types of birds encountered, as well as the improvement of windshield/ canopy systems to withstand the impacts predicted, we can ensure a safer flying environment for our pilots.

AD-P003 216

INCREASING BIRDSTRIKE RATES AND IMPROVED BIRDSTRIKE ANALYSIS OF THE ROYAL NETHERLANDS AIR FORCE

L. S. Buurman,
Royal Netherlands Air Force

Increasing birdstrike rates and improved b.. 'strike analysis of the Royal Netherlands Air Force

L. S. BUURMA

airforce ornithologist

ABSTRACT

The option of a fully birdproof jet fighter seems unrealistic. The capability of aircraft to withstand bird impact has therefore been formulated on the basic of a compromise between operational, technical and flight safety requirements. An increasing concern about the birdstrike risk did not prevent some Western European countries, like The Netherlands, from being faced with an increasing birdstrike problem.

The primary aim of the paper is to show why birdstrike statistics to a varying extent fail to produce a realistic picture of the birdstrike risk. Several type of biases will be described. The problems can be reduced by improving reporting standard and, especially, by taking microscopic examination of minuscule bird remains as a routine procedure.

The most important result is a substantial growth of data on the species- and weight distribution of birds struck "en route". In the case of high but normal jet fighter cruising speeds eighty per cent of all two-pound birds involved in birdstrikes appear to have caused damage.

After having given a specification of the birdstrike frequency in relation to the fight envelope, data of the Royal Netherlands Air Force will be used to demonstrate the effects of an increase in jet fighter cruising speeds and a decrease in minimum flight altitudes. A recent change in the training concept with respect to these aspects of flight performance caused birdstrike figures to rise dramatically.

A correct quantification of the birdstrike frequency and risks may enable the authorities to regulate operations selectively and to provide the industry with adjusted design criteria.

1. INTRODUCTION

Complete "birdproofing" of aircraft, especially jet-fighters, seems to be an unreachable ideal. The unavoidable compromise between operational, technical and flight safety requirements implies that users have to decide which level of damage and risk resulting from birdstrikes they are willing to accept. Careful documentation and analysis of the birdhazard on the basis of experiences in practice is a prime prerequisite.

Unfortunately birdstrike statistics do show big differences between countries. Birdstrikes not only can be defined, documented and analysed in many ways, but also the nature of damage and risks and the circumstances under which they occur may differ greatly. In the forthcoming analyses one fundamental discrimination should be made: whether the problems result from a particularly vulnerable aircraft (part) or from the frequency of collisions. On the basis of this separation of causes airworthiness requirements might be tightened and/or certain risks might be accepted or be avoided by flight restrictions.

Although during more than two decades birdstrike data have been pooled and analysed this did not prevent some West European air forces, including the Royal Netherlands Air Force, from being faced with an increasing birdstrike problem. Within the RNLAF this happened despite the fact that modern aircraft (parts) also show improved resistance against bird impact (e.g. the F-16 canopy). This contribution is aimed at showing how conclusions can be drawn from birdstrike experience of a small and therefore more easily studied air force. It will be explained how improvements in reporting can result in refined insight of the birdstrike problem, which might be used to judge airworthiness of different aircraft (parts) and the consequences of presently employed and future flightenvelopes.

2. TRENDS IN RNLAF BIRDSTRIKE RATES

Figure 1[a] shows the absolute numbers of birdstrikes with damage over the past 25 years. The graph includes crashed aircraft initiated by a confirmed bird collision. Taking into account a year by year decreasing number of flyings hours we consider the recent increase of birdstrikes as alarming. In the early sixties the ratio reached values up to 7 strikes per 10.000 flying hours. Afterwards, when the F-84 and T-33 jet-fighters disappeared from the scene and firstly F-104 and secondly NF-5 appeared the ratio went down to values around 2 strikes. However, during the period 1977 - 1982 a yearly average was reached of 13.1 collisions between jet-fighters and birds resulting in damage. How extremely high this figure is may appear from a comparison with American rates. According to data

from three authors (refs 1, 2, 3) USAF-jets suffer ca 350 birdstrikes with damage per year. Taking a yearly total of 1½ million flying hours for the aircraft types concerned (estimated on the basis of a flying hour table of 1982 in ref 4) this would mean a recent rate of 2, 3 damagestrikes per 10.000 flying hours per year. This figure is more than 5 times lower than the average value of the RNLAF during the past 7 years!

Since 1980 a further increase has been detected. If one considers the rates for all birdstrikes (including non-damage cases) during 1977 up to and including 1982 in figure 2 a, b, c one sees that the F-104 Starfighter as well as the newly introduced F-16 more than doubled their total-rates during the past two years. The NF-5 doesn't yet follow. There are good indications that this large increase coincides with a recent intensification of extreme low level flying. Discriminating between the Dutch F-104 squadrons according to task makes clear that it is the reconnaissance squadron that encounters more and more birds (figure 2 d, e). Especially this recce-squadron has been forced by operational reasons to practise lower flight altitudes and also higher speeds. In contrast to the preceding years more collisions with the numerous birds on short low-altitude "local" flights do occur. Formerly "en route" birdstrikes were more exclusively confined to the birdmigration seasons, when migrating birds reach higher altitudes. Clearly flying altitudes of aircraft and birds form the key of the problem. Similar trends show up in neighbouring air forces.

Apart from changes of flightenvelopes also birdstrike prevention measures will influence the trend as was most probably the case in the period 1964 - 1974. See also figure 3 and its explanation. Further, there are also geographical differences in birdstrike risk resulting from differences in bird densities. These variations can only be unravelled when reporting standards in different countries become comparable. On the follow pages we will describe and analyse how birdstrike data within the RNLAF were improved and what effects were reached.

3. IMPROVEMENTS OF BIRDSTRIKE REPORTING IN TIME

Birdstrikes have been reported within the RNLAF since 1956. Initially only damage cases were reported. However since 1965 air- and groundcrew were asked to fill in birdstrike forms for all birdstrikes irrespective of damage. It can be seen from figure 4 that after some years a ratio was reached of 3 non-damage cases against 1 birdstrike with damage. Not withstanding fluctuating attention upon the problem this ratio was maintained at a rather stable level. Notably this was even more the case during the last 7 years when interest heavily intensified especially due to the establishment of Bird Control Units at

Dutch jet-fighter bases (ref 5). For the three different types of jetaircraft the proportion of damage cases per year remained remarkably close to 25%. A simular ratio for jetfighters was found by RICHARDSON (ref 3) during a two-year reporting campaign within the USAF and by JOENSEN (ref 6) for the Danish Air Force. As table I shows, small differences may occur among aircraft types. For instance, the F-16 shows a somewhat lower figure. This doesn't necessarily mean a better construction but may also be caused by a difference in chance that the pilot will notice the bird strike (see below).While a registration of the total number of birdstrikes seems easily reached it appears much more difficult to accomplish a full documentation per case. Out of the three most important data, namely 1) type of damage 2) speed of the aircraft during the collision and 3) weight of the bird concerned,the last mentioned is especially difficult to acquire. For this reason the RNLAF initiated a two year study on the possibility of microscopic identification of feather remains. By using the micro structure of the downy barbules (see foto 1) it was possible to set-up a determination key enabling us to find the identity of birds at least at the level of the order, and in several cases down to family or even genus and species (ref 7). In most cases the outcome gives enough information to classify the bird in a certain weightclass. While formerly 50-60% of the identifications were fully unsuccesfull, now 96% of all(small) remains sent to the museum result in at least some (weight) information (see also ref 8). Consequently the other major improvement to be reached was the conviction of pilots and especially groundcrew of the value of sending even the smallest bird remains to the contracted ornithologist at the Institute of Taxonomic Zoology in Amsterdam.

4. STATISTICS WITHOUT AND WITH IMPROVED BIRD IDENTIFICATION

We compare the RNLAF statistics from the years 1964-1976 (period I) and the years 1977-1982 (period II) (see also figure 4). The birdstrike numbers from those periods are grouped in tables 2 and 3 according to speed of aircraft and weight of bird. For both parameters four classes were chosen, resulting in 16 sets of birdstrikes. Further margintotals are included. Most important, also the incompletely documented birdstrikes were grouped. We could rank them either as "speed known/weight not" (no birdremains found, or sent in, or identified, as "weight known/speed not", or as "weight and speed unknown". In order to facilitate easy comparison, all numbers (cursively printed at the bottom of each block) were also expressed as percentages from the "grand total". Between brackets the percentage of damage-cases within each category is given.

4.1. BIRDWEIGHT VERSUS AIRCRAFTSPEED ("LOCAL"VERSUS"EN ROUTE" STRIKES)

Although since 1965 reporting of birdidentity was backed up by professional ornithologists only 32.5% of all birdstrikes in period I were completely documented. In period II this figure was 48%. The big gain (from the microscopic identification method) appears in the "en route" strikes (> 300 kts): in period I we used to know the birdweight in only 25%, now this figure is 53%. The proportion of the identification of very small birds even increased five fold.

The importance of these improvements lays in the fact that only now we get a realistic picture of the distribution of birdweights involved in birdstrikes "en route"(to be correlated with the nature of damage).Up to now innumerable birdstrike analysis lumped birdstrike data from all speed categories in order to get large enough samples. As a result airport-birds biased the picture because of the bigger chance of those birds to be identified. Another type of bias follows from the fact that remains of big and white birds (gulls!) are more easily found than those of small and dark birds (Swifts !).

This effect is nicely confirmed in figure 5, where local and "en route" strikes are sorted out on the basis of aircraft speed. The percentual distribution of total numbers of strikes and of damage-cases is given for both periods. The same figure also contains the percentual distribution based only upon those birdstrikes where bird weight is known. The difference between these distributions is remarkable in period I and nearly absent in period II.

In figure 5^a (period I) we also see that <u>within</u> the group of local birdstrikes again there is a bias, towards overrepresentation of fully documented strikes in the lower speeds. This changes into underrepresentation at 240 kts and above. The explanation is that the aircraft at these speeds have left the air space above the runway so that possible remains of birds do not fall on the concrete and are therefore hard to find. Both biases would be strengthened if so called "slipstream victims"(crashed on the runway by airturbulence and not by a collision with the airplane) are included in the figures. From figure 5 we may conclude that the birdweight data of period II can be safely analysed deeper.

When we look at the distribution of birdstrikes with and without damage according to weight class in table 3 we see that small birds by far dominate the picture. Furthermore these collisions with small birds cause damage in no less than 26% of all cases. This figure reaches a staggering 82% for strikes with birds over 700 gram at speeds of 450 kts and more.

As small and medium seized birds are much more numerous than bigger ones they account for a higher absolute number of damage cases despite the smaller probability of damage per case. This effect will be even stronger when cruising speeds increase. One should realise that birds heavier than what is often seen as the critical weight (4 lbs) form only 0.1% of the total avian population. This can be seen in figure 6 showing the birdweight distribution of the breedingbird population of The Netherlands taking into account the difference in abundance per species (ref 9). Considering the shape of this weight distribution one might decide to ignore the chance of meeting such heavy birds. But if aircraft-parts, depending on aircraft speed do not withstand birds of 2 lbs or more then the density of birds with critical weight is raised with a factor 50! That military aircraft actually do suffer from hitting medium sized birds even to the point of crashing, appears from a listing of well documented crashes in table IV.

4.2. BIRDWEIGHT DISTRIBUTIONS OF BIRDSTRIKES REPORTED BY PILOT AND GROUNDCREW

Figure 6 also shows the total weight distribution of birds hit by Dutch jet-fighters. It turns out that medium weight birds are still overrepresented despite improved registration. However the further data on birdweight distributions we will discuss below may explain this finding.

From the comparison of tables 2 en 3 it follows that the biggest shift is from category "speed known/species not" to "speed and species known". This means that gathering and identifying featherremains has improved much more than the rate of detecting birdhits in flight. The last mentioned way of registration accounted for 74.1% in period I (e.g. birdhits whereby speed was known), while in period II this figure hardly increased: 77.4%. However, the proportion of birdstrikes with birdweight known increased 7 times more, namely from 41.5% towards 62%. We must conclude that usually pilots cannot registrate more birdstrikes than they already did in period I.

Apart from the pilot registrations there was a small increase in the completeness of birdstrike reporting from period I to period II. This mainly concerns small birds whose remains were discovered by groundpersonnel while the pilot did not noticed anything. This proportion grew from 9% to 14%. The way in which new birdstrikes come in into the category "weight known/speed not" while others move to the category "fully documented" (which means: pilots more willing to report) is interesting: See figure 7 a, b. This figure shows for both periods the percentual distribution of birdhits over 4 birdweightclasses for the category "speed known" and the category "speed unknown". In period I both distributions show a maximum for medium sized birds (1 lbs),

while the "speed unknown" curve includes a small second peak for the lowest weight category. This indicates that pilots have some difficulty in noting some hits of small birds. In period II both curves shift in favour of the two lowest weightclasses, whereby this is more pronounced in case of the group "speed unknown". Because the improvement with respect to bird-identification of the group reported by the pilot was 7 times better than the growth of the proportion birdhits discovered after the flight we conclude that the shift in figure 7 is caused by birds hitting aircraft parts far from the cockpit. It however remains to be seen wether this is a matter of size of the bird, and/or wether birds do only graze the aircraft or disappear unnoticed into the engine. In this connection it is important to emphasize that the share of birds smaller than 100 gram in the category "speed unknown" increased to 67% in period II. This appcaches the 71% of that this weightclass forms among all Dutch breeding birds(figure 6) !These findings indicate that we might be able to estimate accurat ly the actual total number of birdstrikes. (see 4.4.).

4.3. DIFFERENCES PER AIRCRAFT PART

Table 5 shows the percentual birdhit distribution over the various parts of the aircraft, for all cases and for strikes with damage respectively. Three types of jet-fighters were compared. It is shown clearly that canopy-strikes rank higher in the totals than in the damage-cases. With engine-strikes it is exactly the opposite case. Not only does this show that engine strikes are more problematical than canopy strikes, but it also strengthens our suspicion that many engine problems due to birdstrikes go unnoticed as such. Tabel 6 supports this supposition, by showing that in all strikes where weight was either "unknown" or "below 100 grams" canopy-strikes contain a very high proportion, while the group of small birds is under-represented in the engine-strikes. This is especially notable in the F-16.

When we suppose that the pilot will notice all birds that hit the canopy, and secondly, that all birds have the same change of leaving feather remains, then table 5 would predict that 28% of the total bird population weights 100 gram or more. This perfectly corresponds to figure 6 giving 29%.

4.4. ESTIMATE OF THE ACTUAL NUMBER OF BIRDSTRIKES

We start with the assumption that birds hitting the aircraft on other places than the canopy (or windshield) will all be noticed when they weigh over 100 grams. Furthermore we assume that birds

leave featherremains irrespective of their weight. Finally we believe that we were succeeding in period II to convince all people concerned to report all strikes and to gather even the smallest bird remains. Because, as indicated in 4.3, all canopy strikes are noticed we consider the number of expected and found birdstrikes on canopies to be the same. With the ratio < 100 gram/≥ 100 gram found in this group we calculate the actual number of strikes for the other parts of the aircraft: table 7.

Two third of all strikes appear to be registered under present reporting practices.

5. CONCLUSIONS AND DISCUSSION

From the comparison of two periods both with high reporting standard but differing in the possibility of identifying very small birdremains due to the introduction of a microscopic determination key, four major conclusions may be drawn:

a. only a few extra birdstrikes will be reported, especially small birds;

b. however, by deletion of "unknowns"the distribution of weights of birds involved in birdstrikes completely changes in favour of medium sized and especially small birds;

c. due to high cruising speeds "en route" strikes may cause damage, from 26% in case of birds weighting less than 100 grams up to over 75% in case of birds over 700 grams;

d. "local strikes" only cause damage in 12% (birds 100 gram) up to 17% (birds over 700 gram). This damage usually concerns engines even after sucking in very small birds (NF-5 as well as F-16).

We further arrived at the conclusion that on average one third of all birdstrikes will not be detected. Small birds are especially prone to be overlooked, simply because they leave few (but recognizable!) remains. This might look unimportant but when aircraft speeds further increase, and/or design criteria change in a negative sense these birdstrikes may show up as an unexpected problem. Accumulation of unnoticed bridremains (completely destructured or even burned) perhaps may consistute an as yet undiscovered factor which may urge shorter intervals between overhauls.

The fact that pilots appear to be the main information source (4.1.) may lead towards as unknown under estimation of the

proportion of crashed aircraft initiated by a birdstrike. Even if the pilot survives, his presumption that a birdstrike occurred will not always be accepted as firm proof. To illustrate this point the last 3 crashes of the RNLAF may serve as an example. The first case concerned an engine failure during take-off. The pilot was killed after the plane had crashed behind the end of the runway. It is uncertain whether the tiny bird remains(Kestrel,Falco tinnunculus 220 grams), hardly recognizable by the naked eye, would have been found if a specialist had not been sent along with the investigation committee. This simply happened because of the fact that the airfield was described in a manual as "bird dangerous". The second birdstrike occurred "en route". Here the pilot clearly saw, heard and felt a large "buzzardlike raptor" entering the air intake. However, no remains were found in the totally destroyed wreckage which was recovered several weeks later. Only the third crash was an obvious case of birdstrike in all respects. The Eider, one out a flock of nine, was observed in advance but could not be avoided. The bird was found in a hole in the wing just between an air intake and fuselage of the F-104 Starfighter, where it damaged a fuel tank. The F-104 lost fuel inflight and caught fire while rolling out the runway.

Finally, this paper has shown that canopy-strikes tend to become overrepresented. Up to now the F-16 only seldom suffered critical canopy strikes, no doubt thanks to the great concern of industries for the birdstrike threat. The change of hitting a bird heavier than 4 lbs at speeds over 350 kts is very small. Nevertheless in 1980 a Norwegian pilot was forced to bail out from his F-16-aircraft after a crane (Grus grus) (11 lbs) deformed his canopy in such a way that it cracked at the head-up display. More recently a Dutch pilot tried to avoid a Blue heron (Ardea Cinerea) (4lbs). The sudden reaction caused the F-16 aircraft to loose 350 ft in height and as a result it cut through two cables of a power-line. Luckily the pilot was able to save the aircraft.

Recent changes in the low level training program of several West-European air forces cause the birdstrike threat to increase sharply. As a result the RNLAF birdstrike rate (damage-cases) in 1982 was over 10 times as high as the average USAF-rate, while it used to be only 2 times higher. During the last years European NATO forces seem to have reached a yearly average of up to 10 crashes due to birdstrikes, for instance RNLAF 0.5, GAF 1-4 (ref 3) and RAF 2-3. A similar small decrease of flying height (e.g. from 500 ft down to 250 ft) will certainly also get USAF pilots in trouble. The fine F-16 canopy giving good panorama-vision, as well as modern terrain following devices, will probably promote such a trend.

6. REFERENCES

(1) Seaman,E.A. 1969 US Air Force problems in bird/aircraft strikes. Proc. World Conf. on Bird Hazards to Aircraft. Kingston. Canada. 87 - 92

(2) Vaughan,P. 1975 What you've always wanted to know about birdstrikes, but... Airscoop febr. 26-29

(3) Richardson,J.E. 1981 Birdstrike report. Flying Safety sept pp 14 - 16.

(4) Miholick, J.I. 1983 The Crystal Ball. Flying Safety Magazine Vol 39 no 4 pp 5 - 7.

(5) Buurma, L.S. 1977 Establishment of Bird Control Units at 6 Dutch air bases. BSCE 12 WP 27.

(6) Joensen, A.H. 1978 Bird species involved in bird strikes with military aircraft in Denmark 1968 - 1977. Issued by RDAF. 18 p.

(7) Brom, T.G. 1980 Microscopic identification of featherremains after collisions between birds and aircraft. Issued by RNLAF. 89 p.

(8) Brom, T.G. and L.S. Buurma 1979 The quality of identification: a microscopic key to the determination of feather remains. BSCE 14 WP 19.

(9) Teixeira, R.M. (ed) 1979 Atlas van de Nederlandse Broedvogels. 's Graveland, The Netherlands.

7. ACKNOWLEDGEMENT

This paper has been made possible by stimulating discussions with Col W.P.H.Bezemer, Chief Flight Safety Division RNLAF, and Mr A. Dekker, who also sorted out many data by hand. Mrs and Mr Van der Leeuw kindly corrected the english text.

Figure 1 *BIRDSTRIKES ROYAL NETHERLANDS AIR FORCE 1958 - 1982*

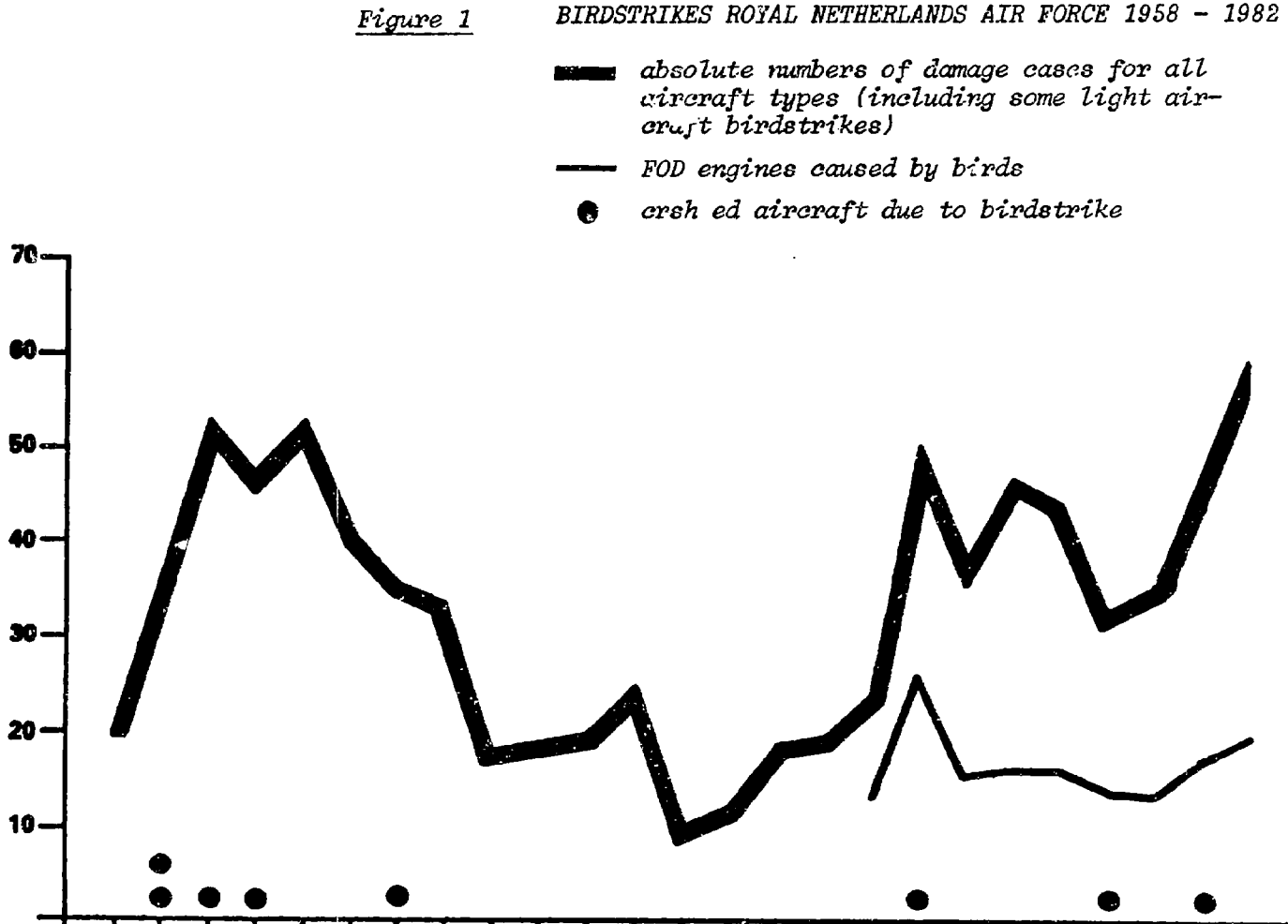

Figure 2

NUMBERS OF BIRDSTRIKES PER 1.000 FLYING HOURS
FOR THREE TYPES OF R.NL.A.F. JET FIGHTERS

total rate — — *rate of cases without damage*
— · — *rate of damage cases*

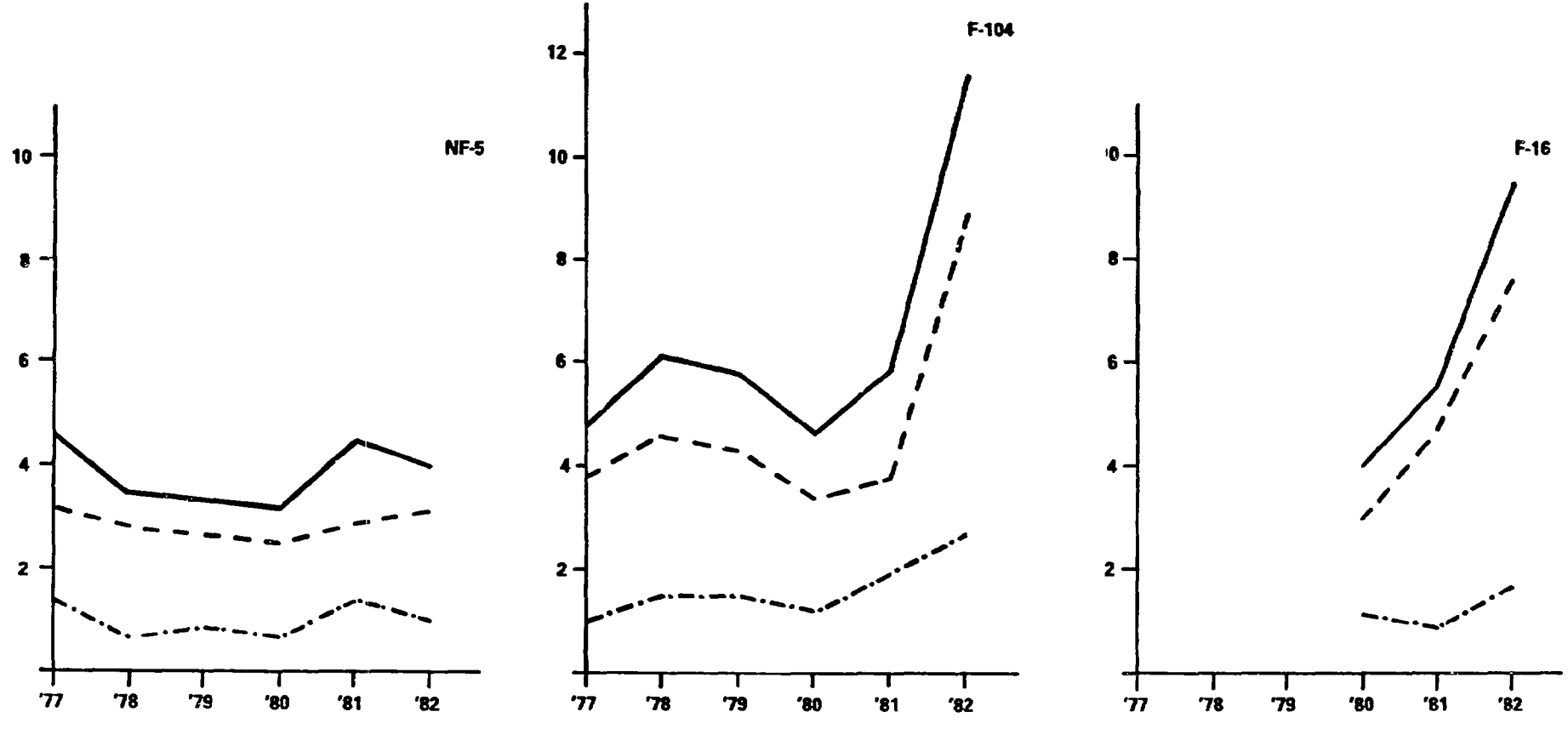

Figure 2 (cont'd)

F-104 birdstrikes per 1.000 flying hours according to task

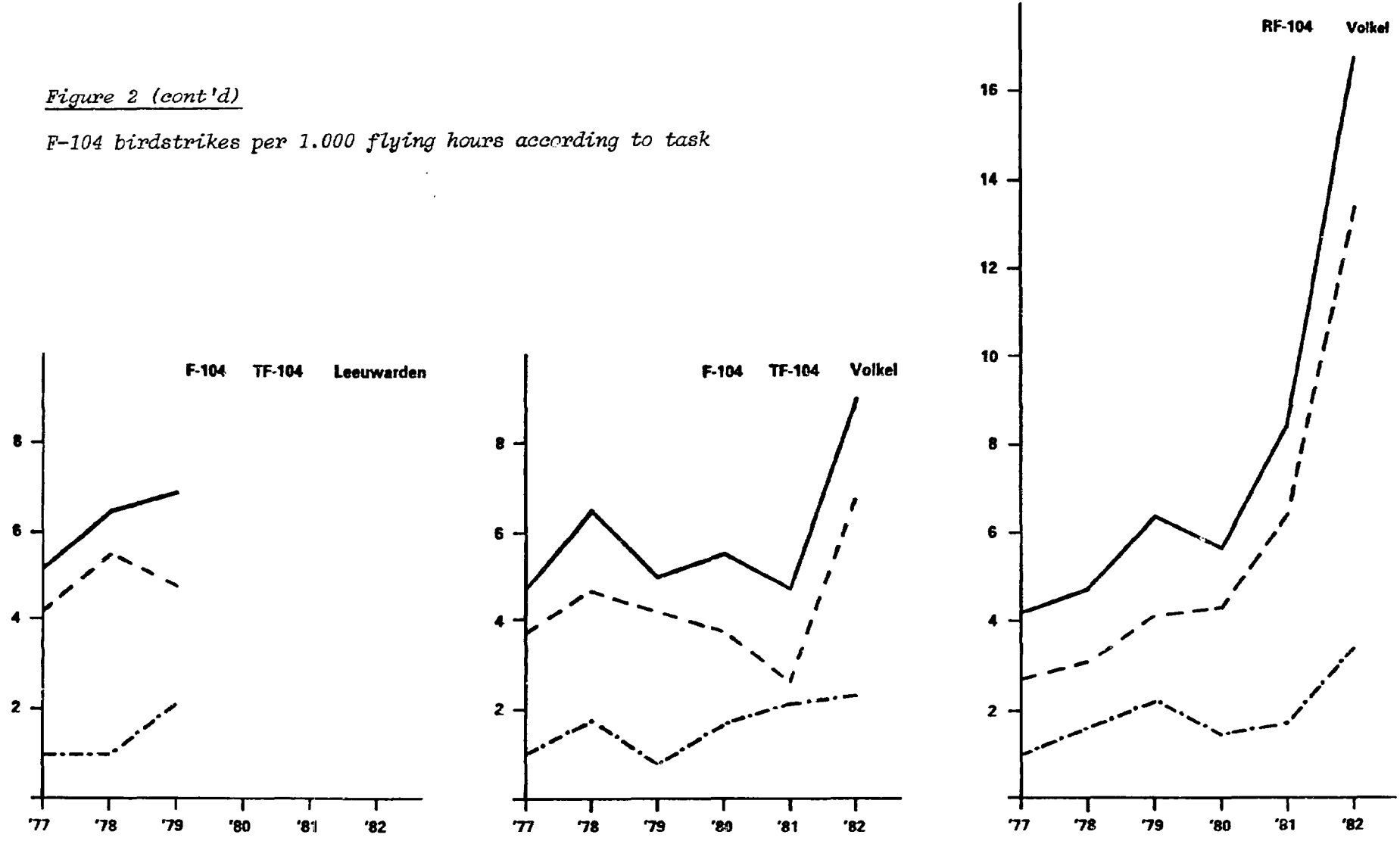

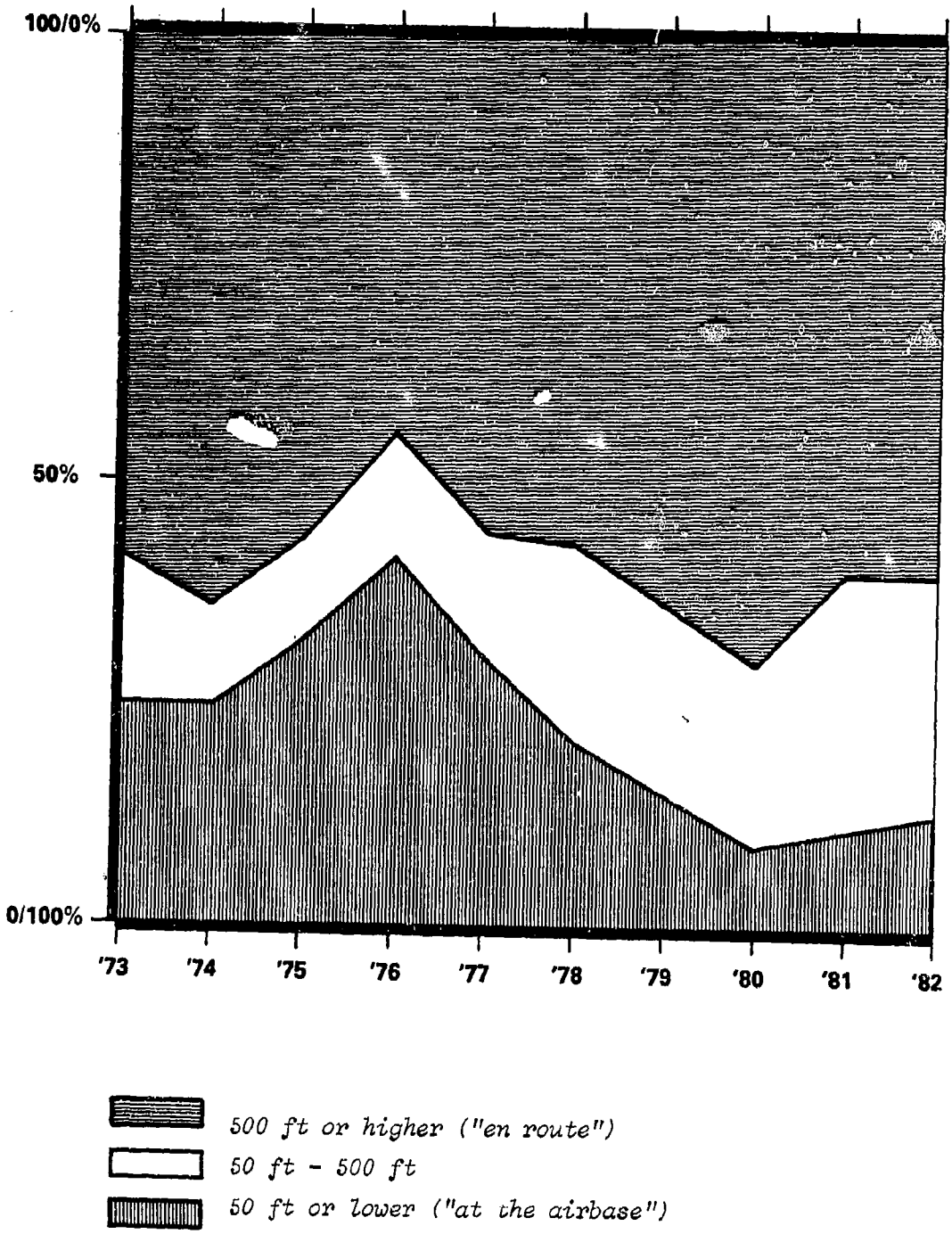

Figure 3 *Percentual proportions of birdstrikes irrespective of damage of R.NL.A.F. jet fighters for three flight altitude classes.*

Since 1974 the use of bird migration warnings was is heavily promoted. From 1976 onward bird control units were established at all Dutch jet fighter bases.

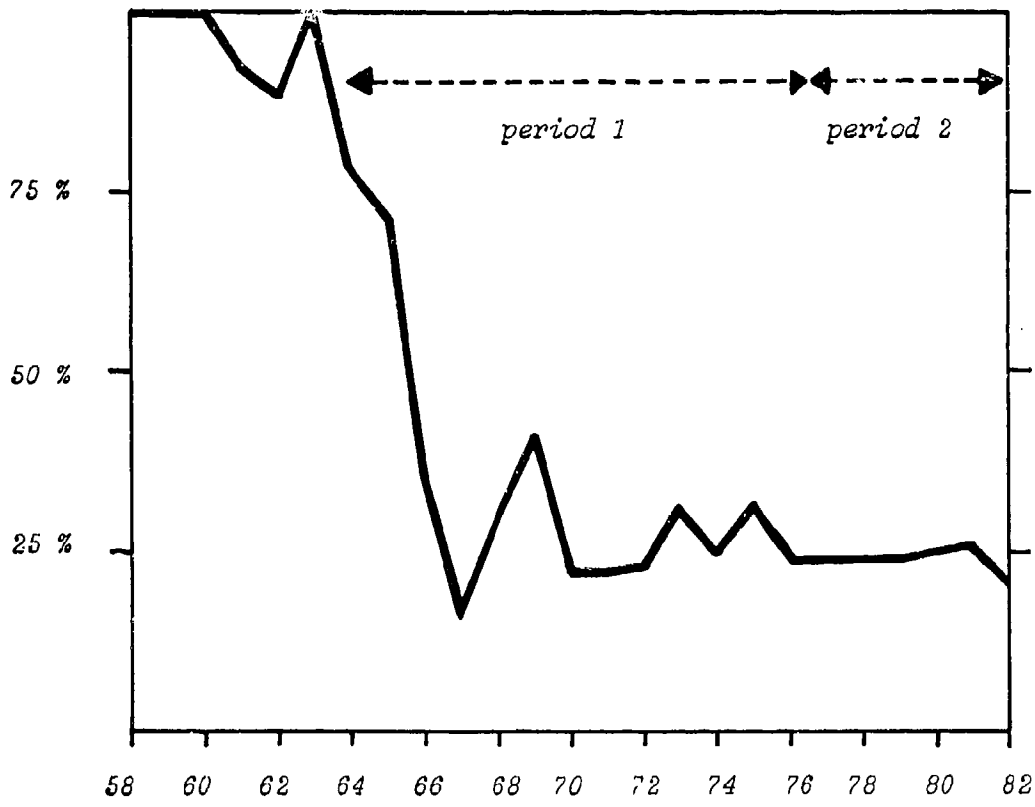

Figure 4 *Percentage of damage cases during 25 years of R.NL.A.F. birdstrike registration (formal introduction of full reporting in 1965)*

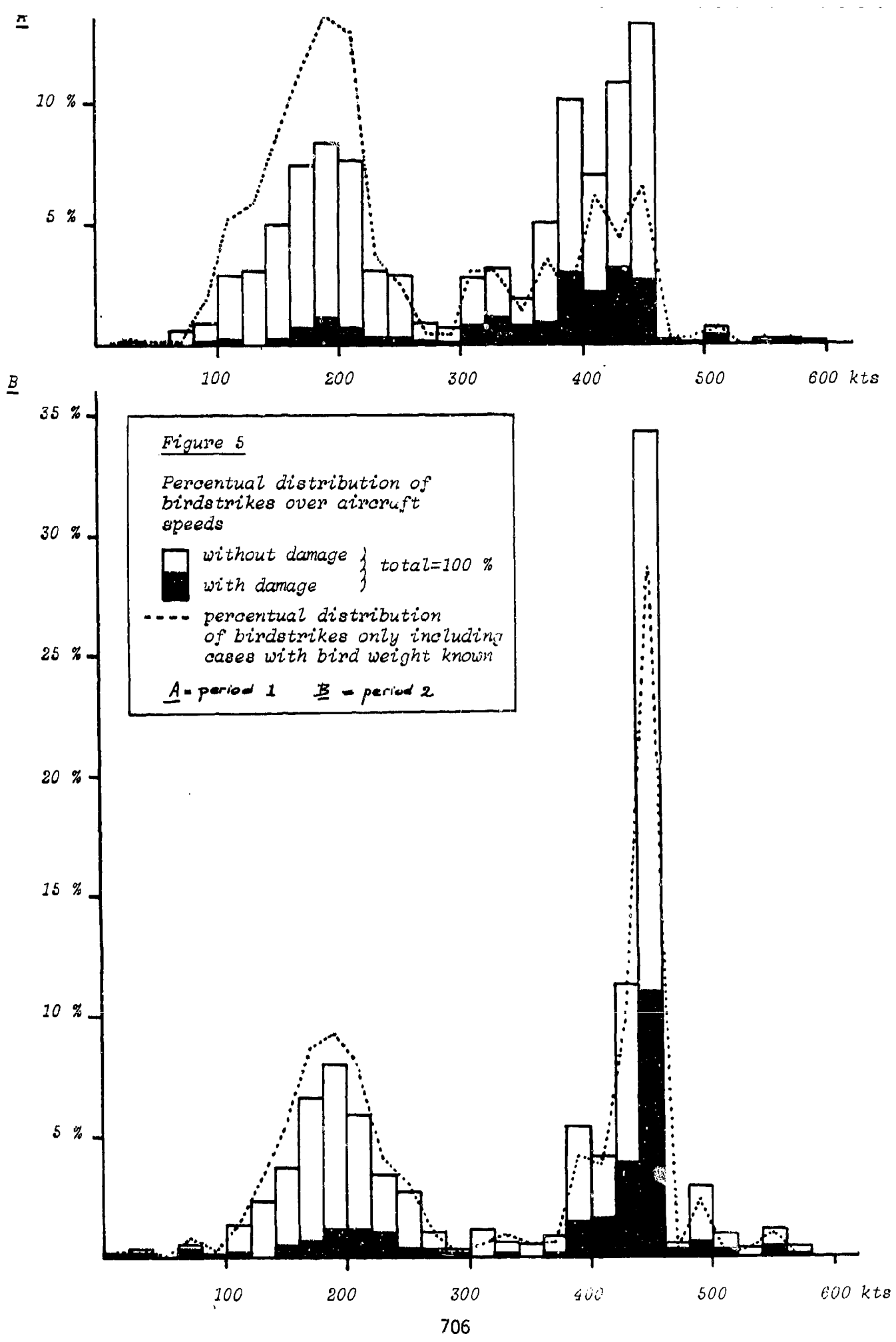
A
10 %
5 %
100
200
300
400
500
600 kts
B
35 %
30 %
25 %
20 %
15 %
10 %
5 %
100
200
300
400
500
600 kts
Figure 5
Percentual distribution of birdstrikes over aircraft speeds
without damage
with damage
total=100 %
percentual distribution of birdstrikes only including cases with bird weight known
A = period 1
B = period 2

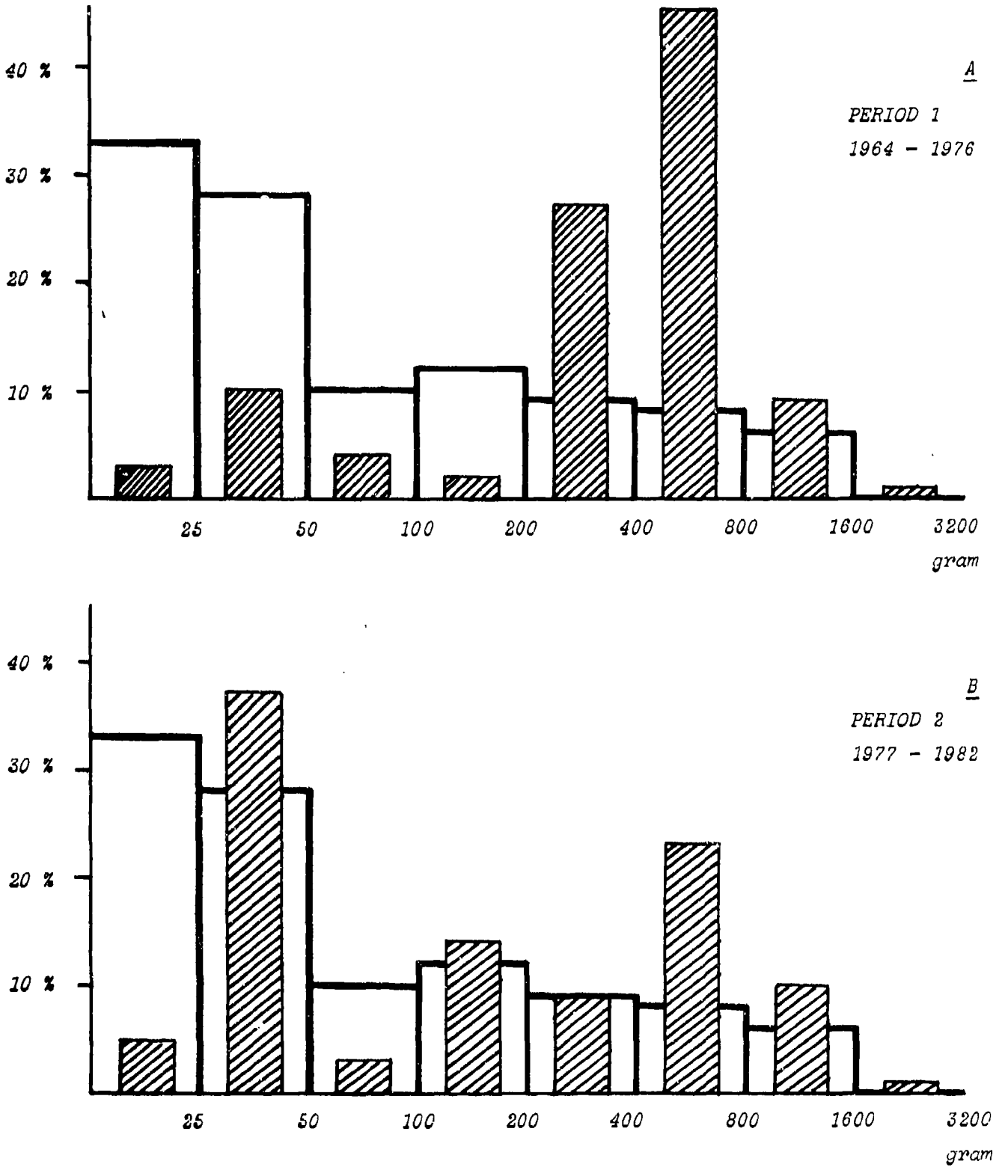

Figure 6 *Percentual distribution of birds involved in collisions with R.NL.A.F. jet fighters (shaded columns) and Dutch breeding birds (white columns) over eight weight classes Breeding bird totals per species (11 million pairs in total) taken from ref 9*

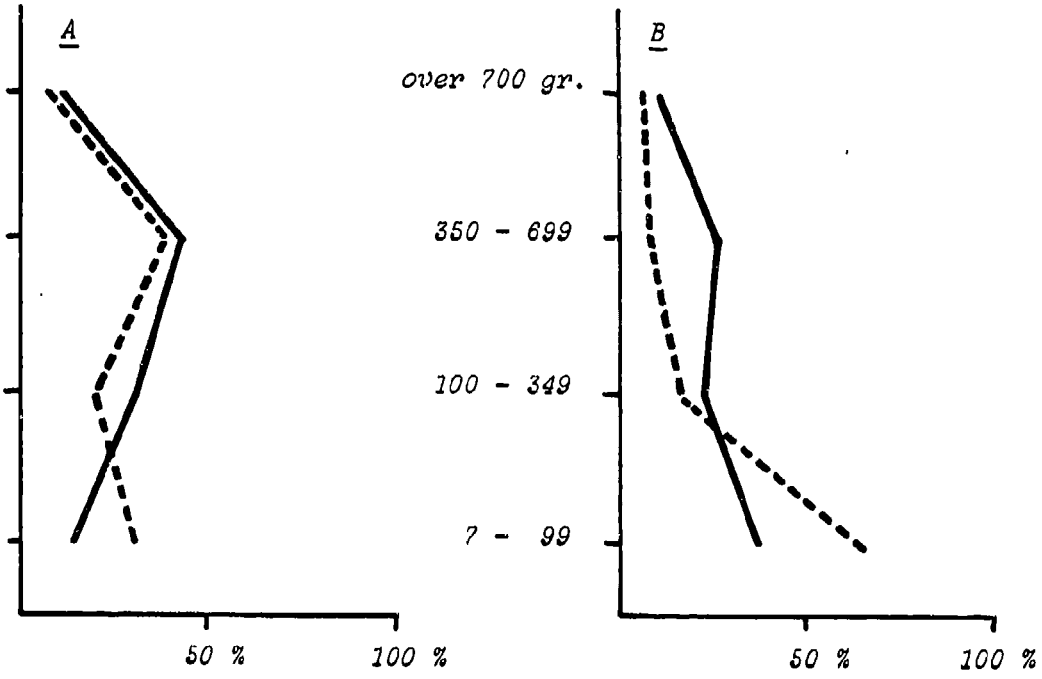

Figure 7 *Percentual distribution of birds involved in collisions with R.NL.A.F. jet fighters where aircraft speed is known (——) or unknown (- - -) for two periods*

A: 1964 - 1976 (n = 393 and 109 resp.)
B: 1977 - 1982 (n = 490 and 142 resp.)

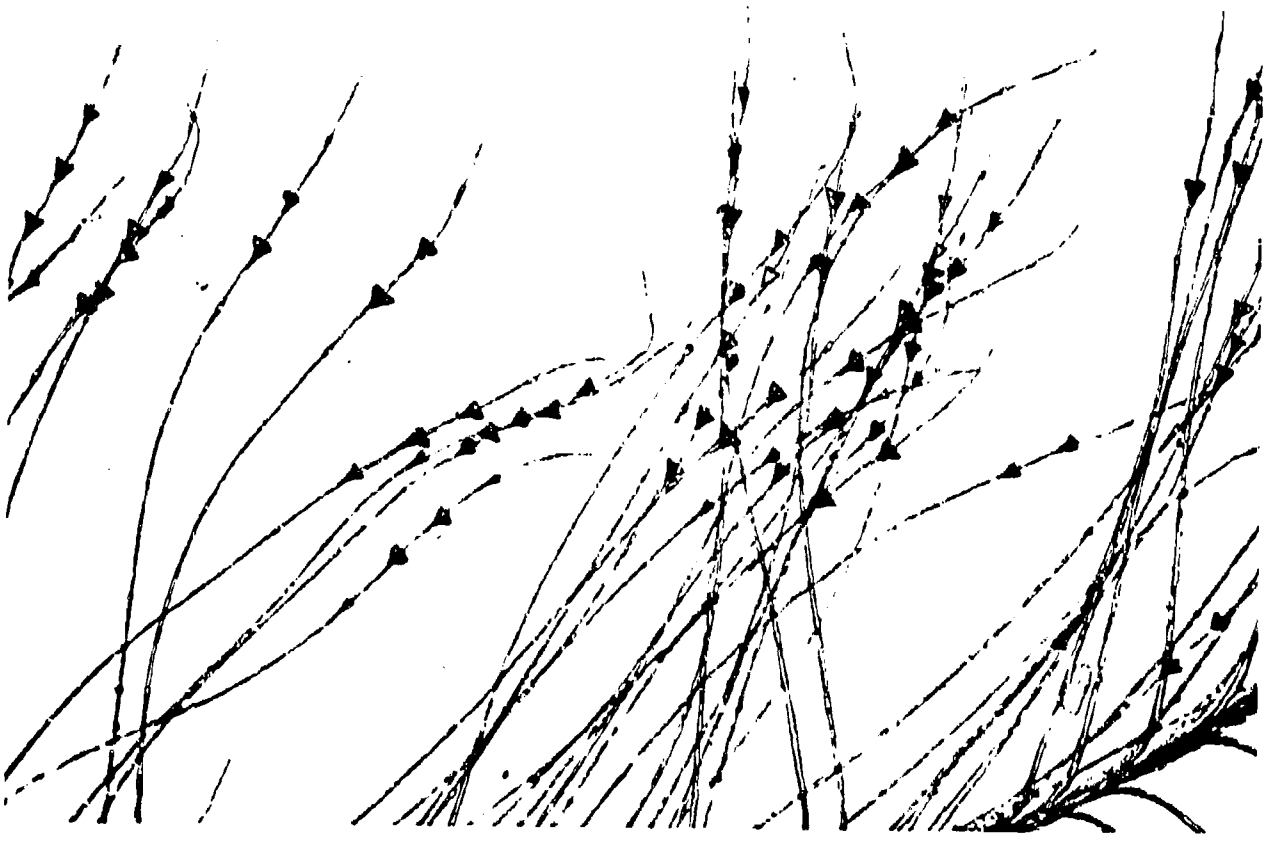

Photo: Microscopic picture of heart-shaped nodes at the distal part of the barbules of a Pochard (Aythya ferina)

F-104	26 %	(± 5 %, n = 533)
NF-5	25 %	(± 5 %, n = 362)
F-16	21 %	(± 7 %, n = 117)

Table 1 Average percentage of birdstrikes with damage per year during the period 1977 up to and including 1982

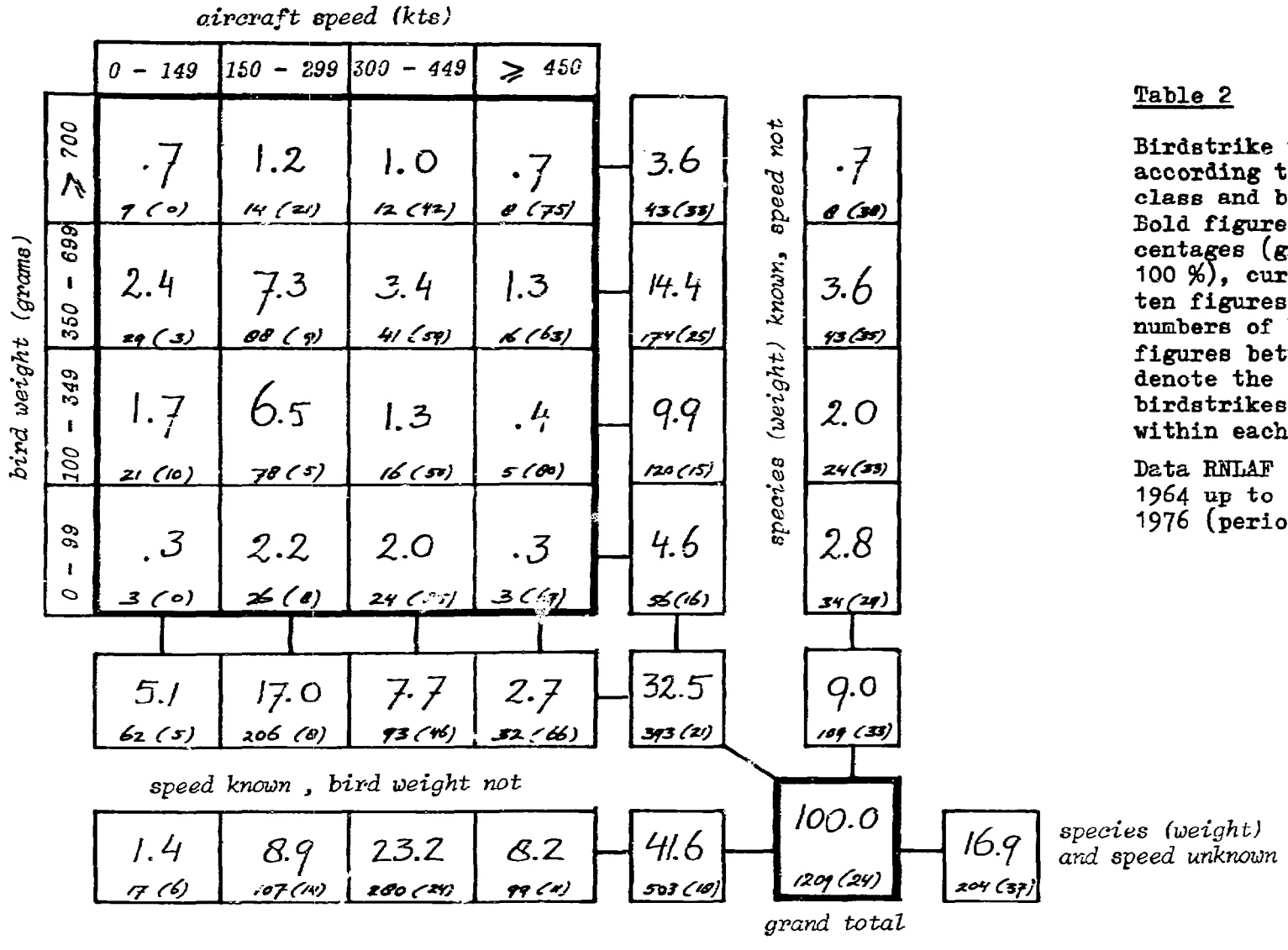

Table 2

Birdstrike numbers according to speed-class and birdweight
Bold figures are percentages (grand total 100 %), cursively written figures are absolute numbers of birdstrikes, figures between brackets denote the percentage of birdstrikes with damage within each group

Data RNLAF jet fighters 1964 up to and including 1976 (period 1)

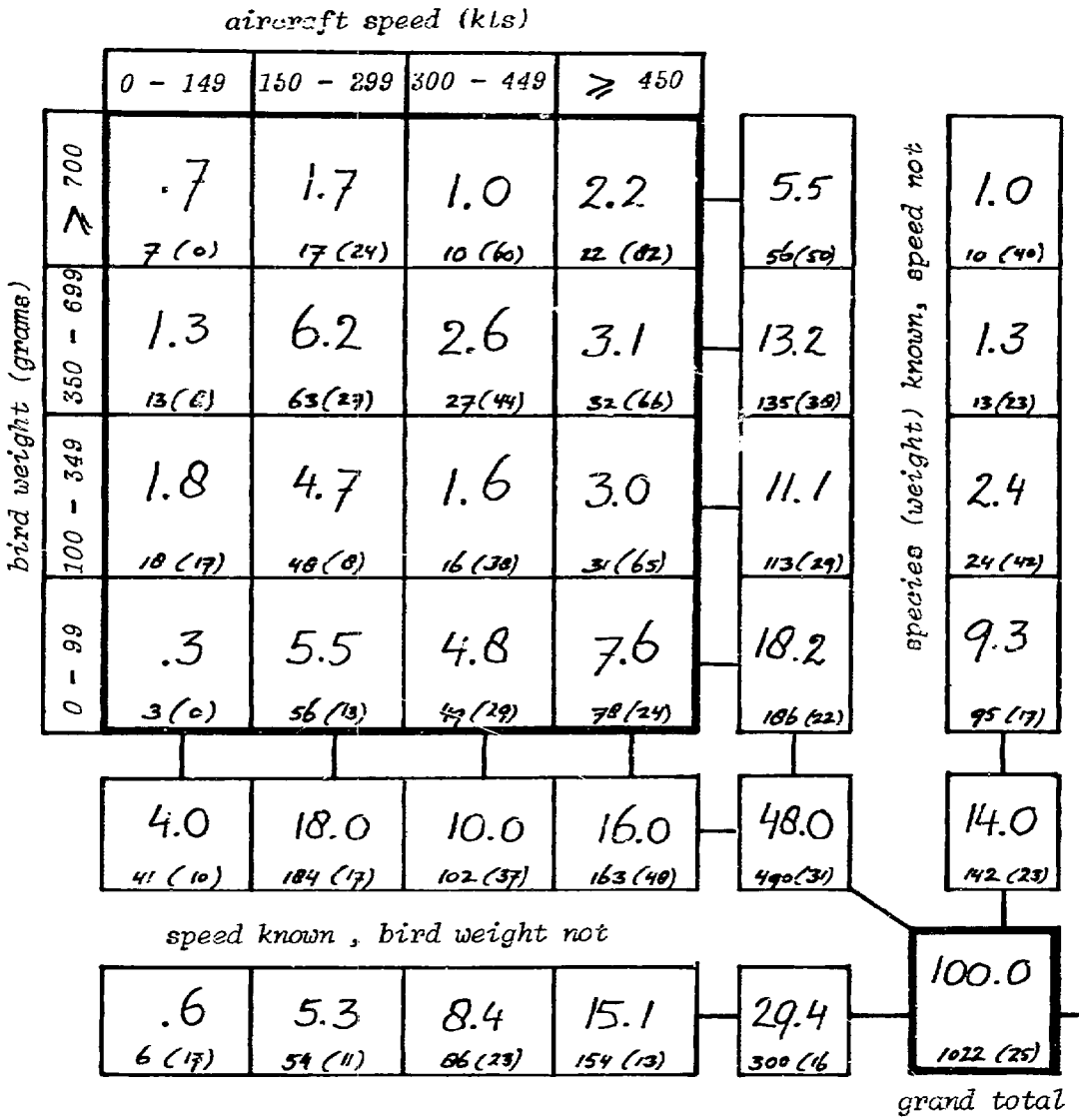

Table 3 for explanation see table 2 1977 up to and including 1982 (period 2)

air force	year	type of jet fighter	fate of pilot	part struck	bird species	weight of bird in lbs
GAF	58-70	F-84	serious	cockpit	Buzzard	1.9
GAF	58-70	G-91	2 serious/ 1 fatal	?	Doves	1.0
GAF	58-70	F-104	2 serious/ 1 fatal	?	Duck	2.0
GAF	58-70	F-104	-	cockpit	Gull	1.0
GAF	58-70	F-104	-	engine	Crow	1.0
CAF	1966	CF-104	-	?	Snow Goose	5.0
RNoAF	1971	F-5	1 fatal	windshield	Lesser Black-backed Gull	1.9
GAF	1971	G-91	-	?	Gull	1.0
GAF	1972	G-91	-	?	Rough-legged Buzzard	1.9
RAF	1975	Harrier	-	?	small bird	0.25
RNLAF	1975	NF-5	1 fatal	engine	Kestrel	0.5
GAF	1976	F-104	-	?	Barnacle Goose	4.2
GAF	1976	G-91	-	?	Buzzard	1.9
CAF	1977	F-104	-	?	Gull	1.0
GAF	1977	TF-104	-	?	Dove	1.0
RNLAF	1979	F-104	-	engine	Buzzard	1.9
RAF	1980	Jaguar	-	?	Rook	1.1
RNoAF	1981	F-16	-	canopy	Crane	11.0
RNLAF	1981	F-104	-	wing	Eider	4.0

Table 4 List of crashed jet fighters due to birdstrikes whereby the identity of the bird concerned is known (by far not complete)

	F-104				NF-5				F-16			
	total		damage		total		damage		total		damage	
Canopy	57	(20.2)	11	(15.9) $^{-}$	49	(21.5)	1	(2.0) $^{=}$	23	(16.1)	2	(8.0) $^{=}$
Engine(s)	70	(24.8)	29	(42.0) $^{+}$	39	(17.1)	29	(58.0) ‡	31	(21.7)	11	(44.0) ‡
Radome/nose section	62	(22.0)	15	(21.7)	40	(17.5)	6	(12.0) $^{-}$	20	(14.0)	5	(20.0) $^{+}$
Wing	18	(6.4)	1	(1.5) $^{=}$	30	(13.2)	1	(2.0) $^{=}$	19	(13.3)	6	(24.0) $^{+}$
Other	75	(26.6)	13	(18.8)	70	(30.7)	13	(26.0)	50	(35.0)	1	(4.0)
Total	282	(100%)	69	(100%)	228	(100%)	50	(100%)	143	(100%)	25	(100%)

Table 5 Absolute numbers and percentual distributions of birdstrikes at different parts of three R.NL.A.F. jet fighters for the years 1980, 1981 and 1982) Over- and underrepresentation of damage cases compared to total is indicated by -, $^{=}$ and +, ‡ signs.

		all jet fighters			F-16		
		?	100	100 gram	?	100	100 gram
A:	Canopy	58	51	20	12	9	2
	Engine	41	49	50	7	12	12
	Other	99	131	154	19	41	29
	Total	198	231	224	38	62	43
B:	Canopy	45.0	39.5	15.5	52	39	9
	Engine	29.3	35.0	35.7	23	39	39
	Other	25.8	34.1	40.1	21	46	33
	Total	100%	100%	100%	100%	100%	100%

Table 6 Absolute (A) numbers and percentual (B) distributions of birdstrikes over weight-class "unknown","less than 100 gram" and 100 gram or more for canopystrikes, engine strikes and others

	weight unknown		more than 100 gram		less than 100 gram			Total	Total
	expected ‖ found		expected ‖ found		expected		found	expected	found
Canopy	58	+	20	+	51	=	51	= 129	129
Engine	41	+	50	+	128	≠	49	= 219	140
Other	99	+	154	+	393	≠	131	= 646	384
								994	653

Table 7 Calculation of real number of R.NL.A.F. birdstrikes during the years 1980, 1981 and 1982

SESSION V

BIRDSTRIKES - PROBLEM DEFINITION AND REDUCTION (PART II)

Chairman: J. Thorpe
Civil Aviation Authority
Surrey, England

Co-Chairman: W. Bussard
Flight Dynamics Laboratory
Wright-Patterson
Air Force Base, Ohio

AD-P003 217

INVESTIGATIONS CONCERNING IMPROVEMENTS OF THE SAAB 37 WINDSHIELD BIRDSTRIKE RESISTANCE

B. P. Fonden and
K. I. Persson, Saab-Scandia

INVESTIGATIONS CONCERNING IMPROVEMENTS OF THE SAAB37 WINDSHIELD BIRDSTRIKE RESISTANCE

Börje P Fondén and Kurt I Persson
SAAB-SCANIA AEROSPACE DIVISION
LINKÖPING, SWEDEN

ABSTRACT

Originally a Viggen prototype windshield was birdstrike tested in 1961, before the aircraft flew for the first time.

In 1980 some tests at Holloman AFB indicated that the windshield was less resistant than previously anticipated. Further birdgun tests were therefore started in Sweden. A method for accurate measuring of windshield deflections using high speed cameras was also developed.

Beside establishing the protection level given by the serial windshield, the tests also made clear that the windshield might rupture below its "undisturbed" strength, if the bird impact made it deflect to contact with underlaying equipment. The head-up display was the main but not the only such equipment. Also birdspray entering the cockpit between the deflected windshield and the canopy was a major problem.

The study now concentrated on establishing the probabilities of aircraft losses due to birdstrikes. Calculations were performed both regarding overall loss rates and risk levels for individual aircraft versus speed. The calculations specially dealt with the improvements that could be gained by a number of proposed modifications and the safety levels thereby achieved.

Dynamic computer models were utilized to assess windshield deflections versus impact point, as reported in a separate paper. Also the present knowledge of squadron flight profile (speed versus altitude), Swedish bird weight distribution and birdstrike statistics were used.

Since also the cost for each investigated improvement measure was given, the Air Force could be presented with information about the technical and cost effectiveness for each proposed measure. It also made it possible to compare cost for bird strike improvements with other safety increasing modifications.

BACKGROUND

The SAAB 37 VIGGEN features an unconventional configuration employing a delta-shaped canard located in front of and above a delta-shaped main wing. Figures 1 and 2 show ground attack and fighter versions of the Viggen Aircraft.

The windshield of the aircraft is made of stretched acrylic 23 mm thick and has a single curvature with a radius of 400 mm.

Originally a prototype of the windshield was birdstrike tested before the aircraft flow for the first time. In combination with escape system testing at the Holloman Test Track, New Mexico, USA, during the Autumn of 1980, the serial configuration of the windshield was birdstrike tested, reference 1. These tests indicated that the windshield was less resistant than previously anticipated. For further investigation of the windshield ability to withstand a bird impact, additional birdstrike tests were performed at SAAB SCANIA, Aerospace Division.

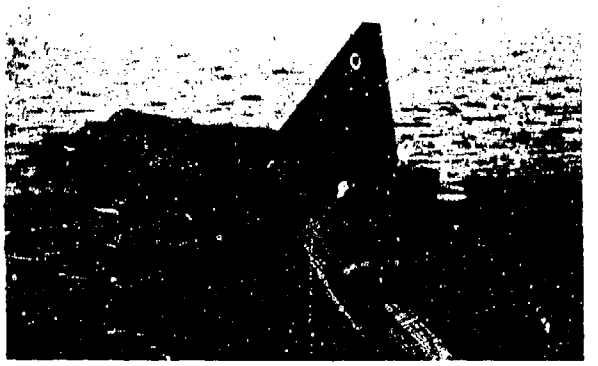

Figure 1.
GROUND ATTACK VERSION (AJ37)

Figure 2.
FIGHTER VERSION (JA37)

TEST FACILITY

The test facility at SAAB SCANIA consists of an 18 m long powder driven gun with an interior diameter of 14.2 cm.

The front part of the gun tube is made of glassfiber reinforced plastics and contains a velocity measurement system. The muzzle end is constructed as a sabot stopper.

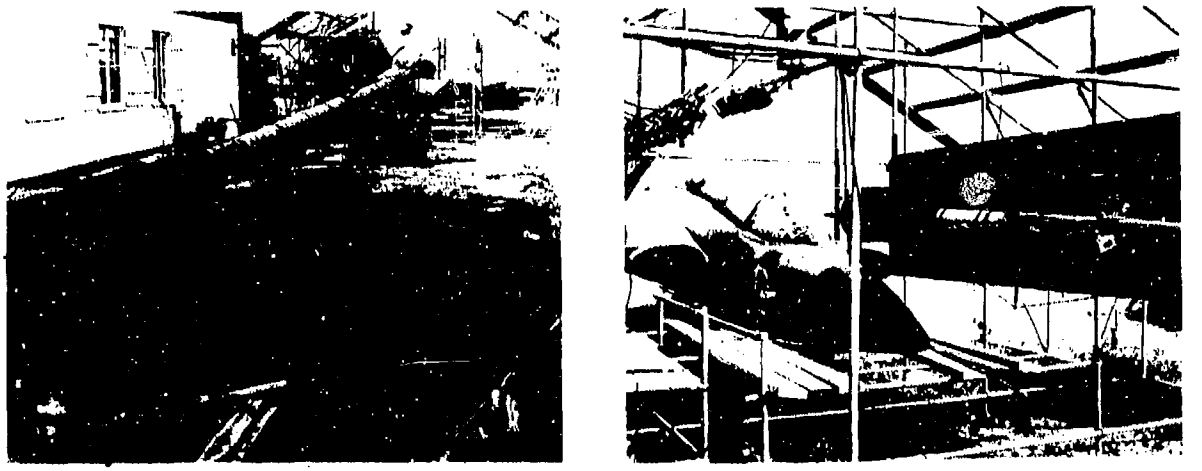

Figure 3.
BIRDGUN SETUP

DEFLECTION MEASUREMENT PROCEDURE

The windshield deflections during the impact event are important to assess the risk of rupture due to contact between windshield and HUD glass and amount of bird debris (birdspray) in the face of the pilot.

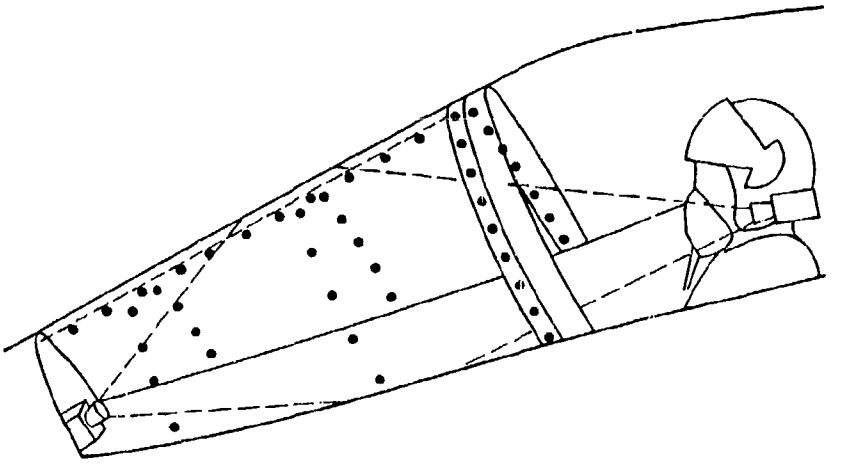

Figure 4.
CAMERA SETUP

A technique for accurately recording windshield deflections utilizing high speed cameras was developed. One forward and one aft looking camera recorded actual deflections, figure 4.

For calibration purpose, artificial vectors were mounted at actual points perpendicular to the windshield surface. Each of the vectors was 100 mm long, with clearly visible small balls at the vector ends, figure 5.

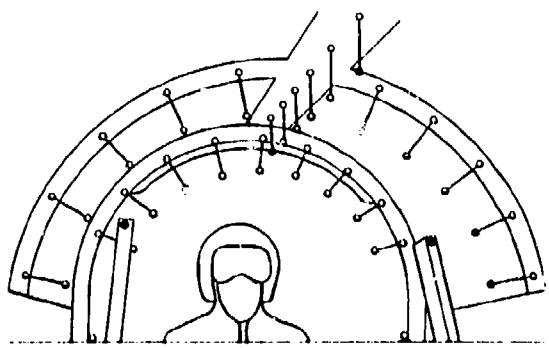

Figure 5.
CALIBRATION PICTURE FRAME

The films taken during the impact event were than laid over the calibration film. The deflections could thus be measured directly utilizing the calibration vectors as units, figure 6.

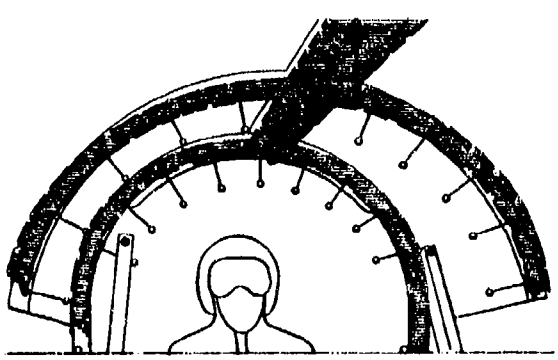

Figure 6.
MEASUREMENT PICTURE

The deflection parallel to the flight direction of the windshield surface is small compared to the deflection perpendicular to the surface. Thus, this deflection is neglected. The measurement error due to the fact that the optical axes of the cameras are not exactly parallel to the windshield surface is also neglected.

A time history of windshield deflection along an arc at the HUD glass, generated with this technique, is shown in figure 7. Figure 8 shows a time history of the windshield aft arch deflection generated at the same impact event.

The main purpose of these measurements was to assess the validity of calculated windshield deflections. The calculations were used to determine which further actions to take.

THESE DEFLECTIONS ARE IMPORTANT TO ASSESS RISK OF RUPTURE DUE TO CONTACT BETWEEN WINDSHIELD AND HUD GLASS AND AMOUNT OF BIRD DEBRIS IN THE FACE OF THE PILOT

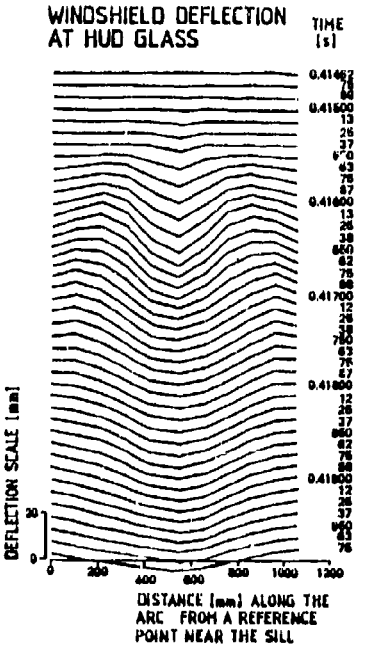

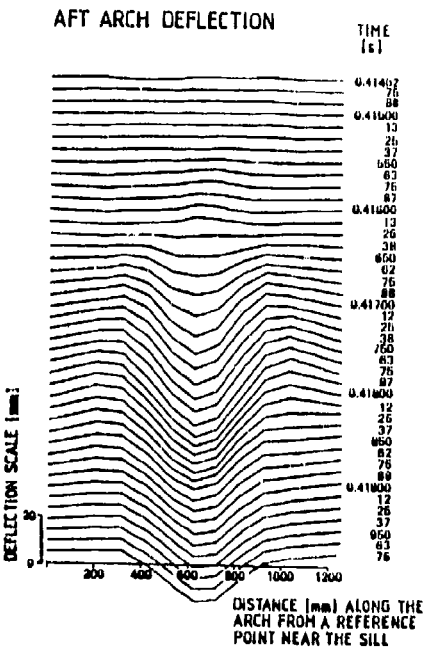

BIRDSTRIKE TEST, 717

Speed = 898 km/h

Figure 7.

Figure 8.

INVESTIGATIONS

Beside establishing the protection level given by the windshield, the test also made clear that the windshield might rupture if the bird impact made it deflect to contact with underlaying equipment. The main such equipments were the HUD glass and an illumination sensor for the gunsight recording camera, figure 9.

Also birdspray entering the cockpit between the deflected windshield and the canopy was a major problem.

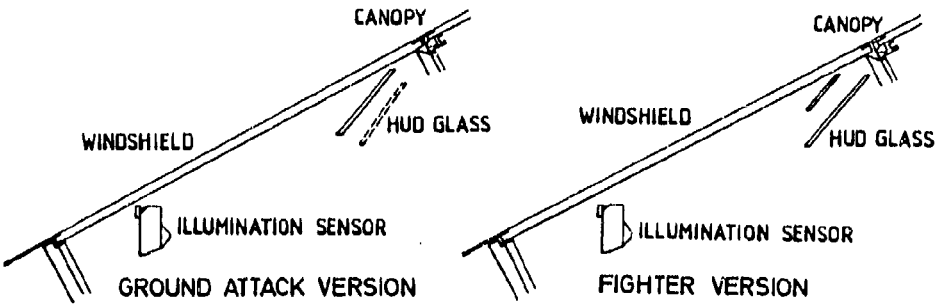

Figure 9.

CLEARANCE TO HUD GLASS AND ILLUMINATION SENSOR FOR THE VIGGEN GROUND ATTACK AND FIGHTER VERSIONS.

To find out what could and should be done to improve the windshield birdstrike resistance a number of calculations that covered the original design and quite a few proposed modifications, were performed by IFM Akustikbyrån AB, Stockholm, Sweden in close cooperation with SAAB SCANIA, reference 2. These calculations will be presented at another conference session.

Calculated locations of critical points for a 1 kg bird impact are shown in figure 10.

To establish the probabilities of aircraft losses due to birdstrikes these graphs were transformed into critical impact areas on the windshield surface versus bird velocity upon impact, figure 11.

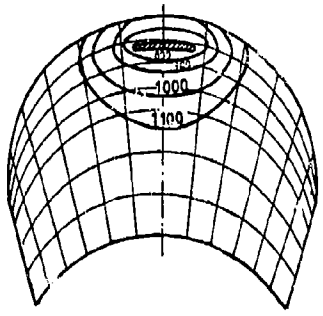

WINDSHIELD CONTACT
WITH THE HUD GLASS

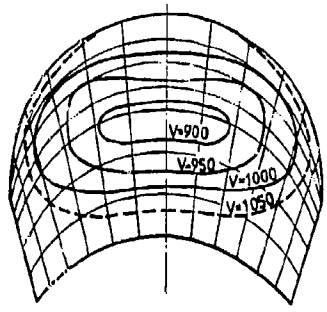

WINDSHIELD PENETRATION

V = SPEED [KM/H]

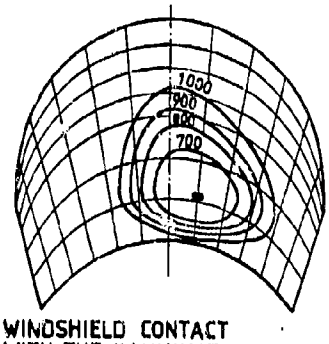

WINDSHIELD CONTACT
WITH THE ILLUMINATION SENSOR

Figure 10.

LOCATIONS OF CRITICAL IMPACT POINTS FOR 1 kg BIRD. UNMODIFIED DESIGN GROUND ATTACK VERSION.

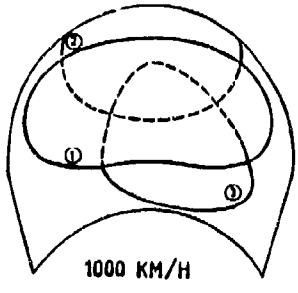

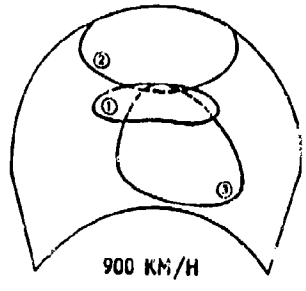

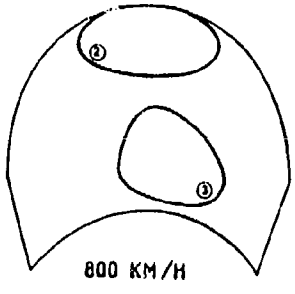

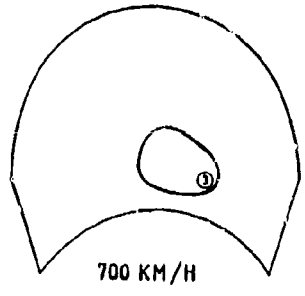

① WINDSHIELD PENETRATION
② WINDSHIELD CONTACT WITH THE HUD GLASS
③ WINDSHIELD CONTACT WITH THE ILLUMINATION SENSOR

Figure 11.

CRITICAL IMPACT AREAS vs SPEED FOR 1 kg BIRD. UNMODIFIED DESIGN GROUND ATTACK VERSION.

Assuming the bird impact points are randomly distributed over the windshield surface the percentage of critical 1 kg bird impacts was calculated for the original design, figure 12 and for some proposed modifications.

The 1 kg bird is a fictitious one and available bird statistics gave an approximate weight distribution and altitude behaviour as shown in figure 13.

In the Swedish bird population the greatest hazard to aircraft is dominated by the Herring Gull (Larus Argentatus) with an average weight of 1.1 kg.

By statistically combining the 1 kg bird risk levels with the assumed bird weight distribution the resultant risk versus speed levels for proposed modifications were obtained, figure 14.

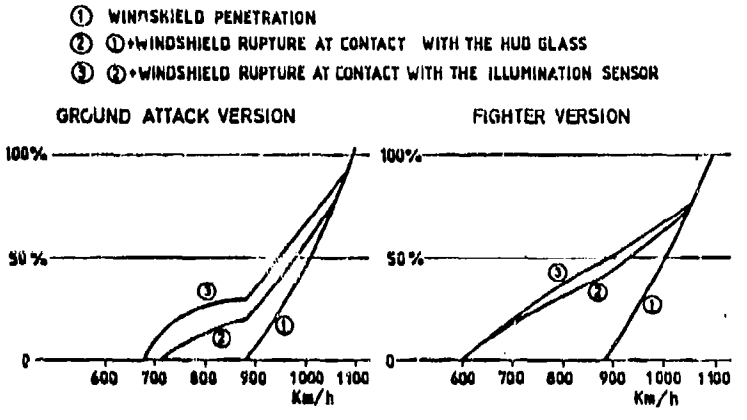

Figure 12.

PERCENTAGE OF CRITICAL IMPACTS ON THE WINDSHIELD. BIRD WEIGHT 1 kg. UNMODIFIED DESIGN.

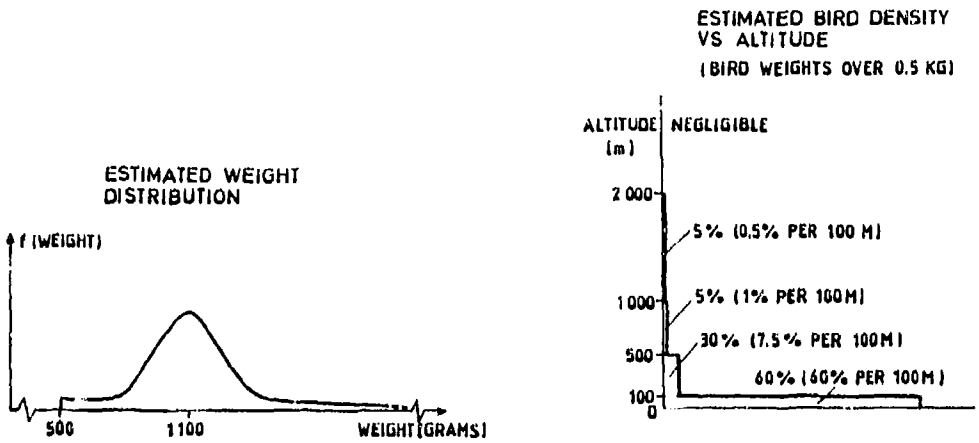

Figure 13.

ASSUMED WEIGHT DISTRIBUTION AND ALTITUDE BEHAVIOUR OF SWEDISH BIRDS.

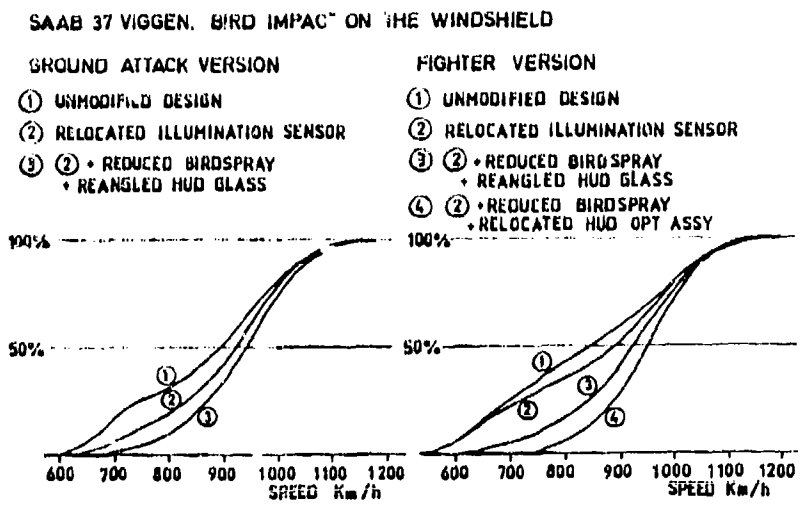

Figure 14.

PERCENTAGE OF CRITICAL IMPACTS ON THE WINDSHIELD.
SWEDISH BIRD WEIGHT DISTRIBUTION.

Before a specific flight mission the pilot may be interested to know the birdstrike risk level. This information is however not sufficient for the Air Staff to asses long term loss rates.

For this purpose information about squadron flight profiles was needed. A flight profile forecast, used for specifying life expectancy, was available for the fighter version and for the ground attack version an assumption was made,figure 15. These flight profiles are rough approximations but give results with acceptable accuracy.

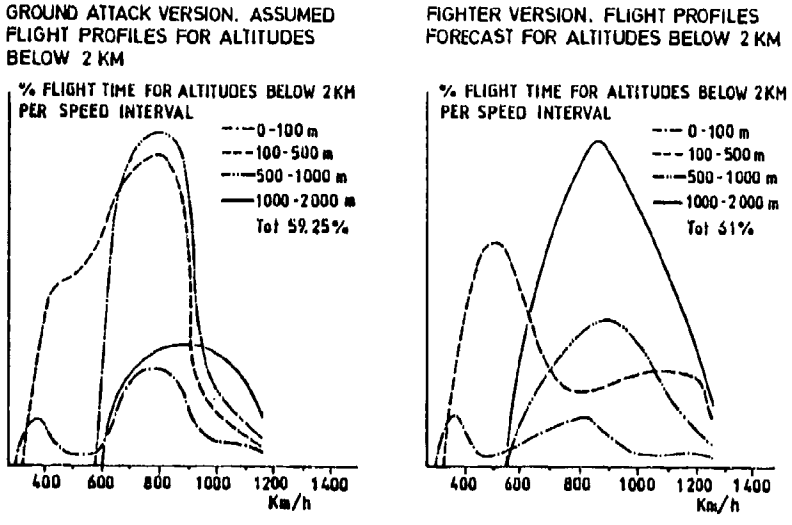

Figure 15.

APPROXIMATE FLIGHT PROFILES FOR THE SAAB 37 VIGGEN GROUND ATTACK AND FIGHTER VERSIONS.

The birdstrike rate on the windshield must also be known. Probably this is the most doubtful input as flight behaviour changes with time and type of aircraft. However, available statistics indicated that somewhere between 1 and 6 collisions per 100 000 flight hours are to be expected.

Statistical combination of the flight profiles and the probability of a bird impact on the windshield gave estimated loss rates for various modifications expressed as percentages of windshield impacts and as absolute loss rates assuming 3 impacts per 100 000 flight hours, figure 16.

ESTIMATED LOSS RATES FOR VARIOUS MODIFICATION STEPS EXPRESSED AS:

	PERCENTAGES OF WINDSHIELD IMPACTS			ABSOLUTE LOSS RATES WITH THE ASSUMPTION OF 3 IMPACTS PER 100 000 FLIGHT HOURS		
	AJ	JA	JA_{AJ}	AJ	JA	JA_{AJ}
UNMODIFIED DESIGN	39	53	48	1.2	1.6	1.4
RELOCATED ILLUMINATION SENSOR	30	50	47	0.9	1.5	1.4
MODIFIED HUD	25	40	23	0.8	1.2	0.7
REDUCED BIRDSPRAY	21	38	18	0.6	1.1	0.5
RIGID WINDSHIELD AFT ARCH	16	36	16	0.5	1.1	0.5
WINDSHIELD THAT (EXACTLY) WITHSTANDS AN IMPACT OF A 1 KG BIRD AT 1100 KM/H	7	26	7	0.2	0.8	0.2

AJ = GROUND ATTACK VERSION

JA = FIGHTER VERSION

JA_{AJ} = FIGHTER VERSION WITH FLIGHT PROFILE FOR GROUND ATTACK VERSION

Figure 16.

CONCLUDING REMARKS

The cost for each investigated improvement measure was estimated and the Air Force could be presented with information about the technical and cost effectiveness for each proposed measure. This also made it possible to compare cost for birdstrike improvements with other safety increasing modifications.

REFERENCES

1. Niss, Gösta, Bird Strike Testing of the Viggen Aircraft at the Holloman Test Track, New Mexico, USA.

Paper presented at the 15th Bird Strike Committee Europe meeting in Brussels, May 1981.

2. Samuelson, Lars-Åke, et al., Theoretical evaluation of the structural performance of Swedish fighter aircraft windshields subjected to bird impact.

Paper presented at the Conference on Aerospace Transparent Materials and Enclosures, Scottsdale, Arizona, July 1983.

AD-P003 218

BIRD IMPACT EVALUATION OF F/RF-4 TRANSPARENCY SYSTEM

G. T. Stenger, University of Dayton and
Lt. R. Simmons, Flight Dynamics Laboratory

Bird Impact Evaluation of the F/RF-4 Transparency System

Lt. Robert Simmons*
Flight Dynamics Laboratory
Wright-Patterson Air Force Base

G. J. Stenger**
University of Dayton Research Institute

ABSTRACT

Birdstrikes to the crew enclosures of USAF F/RF-4 aircraft have resulted in major aircraft damages coupled with severe/fatal pilot injuries. Analysis of operational bird impact statistical data indicates that the trend of damaging bird impacts on the F-4 is continuing to rise. Impacts to the F-4 transparency system also continue to rise resulting in a continued flight safety risk to the aircraft and the aircrew. The Air Force Wright Aeronautical Laboratory, Improved Windshield Protection Office has initiated a program to develop a transparency system for the F-4 aircraft which has four pound, 500 knot bird impact capability. The first step in this program was to experimentally determine the existing transparency system capability by bird impact testing full scale flight hardware. Eight impact locations on the windshield and forward canopy were tested to failure with four pound birds. Tests on experimental, laminated windshield side panels were also conducted to investigate the capability of the windshield frame. The baseline birdstrike test results are presented through the use of post test photographs and an impact capability diagram.

Introduction

Due to the advancement in radar detection techniques as well as the development and increased use of terrain following instrumentation, an increased amount of high-speed flight time is performed at altitudes below 10,000 feet. Many air force high-speed aircraft transparency systems were not designed to meet the increased bird impact risk associated with this phase of the flight operation. The F/RF-4, Figure 1, is but one example of an aircraft which was not designed with a transparency system capable of surviving the bird impact event. Analysis of birdstrike statistical data obtained from the Air Force Inspection and Safety Center at Norton AFB, California shows that during the period January 1971 to March 1981, 30 of the 68 reported birdstrikes against the transparency resulted in penetration into the crew compartment. Associated with these penetrations were 12 injuries (some permanently disabling) to aircrew personnel, loss of one aircraft, and one pilot fatality.

* Project Manager, Air Force Wright Aeronautical Laboratories, Vehicle Equipment Division
**Associate Research Engineer, Aerospace Mechanics Division

Recent birdstrike data continues to show an increase in the number of impacts and, without significant changes in the mission requirements that have resulted in this increasing birdstrike rate, an even larger number of damaging birdstrikes may be expected for the F/RF-4 aircraft in the future.

Background/Objective

As a result of the loss of a USAF F-4E aircraft and a pilot fatality due to a windshield birdstrike in November 1980, the Improved Windshield Protection Program Office was directed to develop an improved bird impact resistant transparency system for the F/RF-4 aircraft. The initial phase of this program included an experimental test series which was conducted to determine the baseline bird impact capability of the current F/RF-4 transparency system (Figure 2).

The primary objective of this bird impact test program, conducted during the periods August-October 1982 and February 1983 was to determine the minimum bird penetration velocity as a function of birdstrike location for the windshield and forward canopy. Secondary objectives of the test program were to: (1) collect sufficient data (photographic, strain, and accelerometer) to support the subsequent transparency system redesign effort; and (2) to investigate the capability of the windshield support structure to absorb (and transfer into the fuselage) the energies associated with the bird impact event.

Experimental Procedure

The bird impact testing of the F/RF-4 transparency system was accomplished at Range S-3 of the von Karman Gas Dynamics Facility of the Air Force System Command's Arnold Engineering Development Center. Figure 3 shows the test area arrangement. Capabilities of the S-3 Range are contained in Reference 1. The basic procedure employed in testing in the S-3 Range consists of launching bird carcasses at specified velocities (using an air-driven launcher) into predetermined impact locations on a test article. For the F-4 baseline tests, six impact locations on the windshield and forward canopy were investigated with the fuselage aligned at 0° pitch and 0° yaw relative to the launch path. Side impact tests were conducted at one location on the windshield side panel and one on the forward canopy with the fuselage yawed at 15° relative to the launch path.

Test Fixture/Test Articles

To more closely simulate the actual bird impact response of the transparency and to get realistic load transfer, an F-4 forward fuselage section was used as the test fixture (see Figure 4). All transparencies and related hardware were actual aircraft structures removed from aicraft in storage at the Military

Aircraft Storage and Disposition Center at Davis-Monthan AFB, Arizona. Test articles consisted of the forward windshield assembly (two plexiglas side panels, laminated glass center panel, and supporting structure) and the forward canopy assembly (reference Figure 2). The cross-section of each transparency component is shown in Figure 5.

The windshield frame capability was determined by utilizing laminated side panels which were designed, developed, built, and donated by Goodyear Aerospace Corporation, Litchfield Park, Arizona. The laminated panel cross-section may be seen in Figure 6. When a transparency failed in a test, it was removed from the frame, the frame was inspected, and if no structural damage had occurred, another transparency was mounted in place.

Projectiles and Sabots

Projectiles launched during this test program were nominally four-pound chicken carcasses. The birds were asphyxiated, quick-frozen, and stored at 0°F until needed. Prior to testing, the carcass was thawed in still air at room temperature (75°F) for approximately 24 hours or until the body cavity temperature was 70 ±10°F. Adjustments to the bird carcass weights were required to achieve the desired weight within ±0.1 lb. These adjustments were accomplished by clipping carcass appendages or injecting water into the body cavity. In no case did the adjustment exceed 10 percent of the bird weight.

The packaged bird was mated to the launch tube using a one-piece sabot of balsa wood construction. The sabot material density was nominally 10 lb/ft providing a sabot weight of 1.7 lb and a total launch weight of 5.7 lb. Separation of the bird and sabot after launch was accomplished with the use of the tapered and threaded cylindrical sabot stripping section attached directly to the vent section of the launch tube (Figure 3). As the launch package entered the stripper section, the sabot velocity was gradually decreased by the shearing of thin layers of sabot material, permitting the bird to exit in free-flight.

Instrumentation

Instrumentation for this series of tests was primarily designed to collect data for use with analytical transparency analysis tools. Four to five high-speed movie cameras were used to record the impact event. The cameras were situated in such a manner as to gain an overall perspective of the impact point (Figure 7). In addition to the high-speed cameras, still photographic coverage was used to record pre- and post-test conditions.

A total of 20 strain gages were monitored during each impact. These gages were located in such a manner as to record

the load characteristics of the transparency support structure during impact.

Two accelerometers were used to monitor the motion of the frame during bird impact. X-ray shadowgraphs were used to monitor the bird position and orientation prior to the impact (Figure 3). These were also used to verify the impact velocity.

Test area temperature was measured by two thermocouples positioned near the test transparencies.

Impact Location/Impact Velocities

The eight impact locations used may be seen in Figure 8. These locations were chosen through the use of an angle of incidence study and represent areas where the maximum energy could be transferred from the traveling bird to the stationary structure. At least two impact locations on each transparency system component were investigated so that a capability map could be developed for the entire system. Impacts at locations "A" through "G" were made with the fuselage section aligned at 0° pitch and 0° yaw relative to the launcher flight path. Impact locations "H" and "I" were chosen to investigate the transparency capability in the sill area. Impacts at these two locations were made with the fuselage yawed at a 15° (clockwise) angle so that sufficient bird contact could be made with the test article.

The initial impact velocity was slightly below the expected failure velocity. Failure velocities were analytically determined at each impact location by employing the prediction methods found in Reference 2. Succeeding impact velocities were increased until transparency failure at that location occurred. The failure velocity range could then be bracketed between the highest velocity at which failure had not occurred and the velocity at which failure had occurred.

TEST RESULTS

The baseline birdstrike capability for the F/RF-4 transparency system was defined with a total of 25 bird impacts at eight locations on the transparency system. The results of these tests have been summarized in a capability diagram as shown in Figure 9. This diagram presents the four-pound bird impact capability of the existing windshield system with the fuselage oriented at 0° pitch and 0° yaw. This diagram is based on the actual test data with the areas being defined after considering the recorded post-test observations, the high-speed movies, the strain data, the impact angle of incidence, and the proximity to the edge attachment. The values represent an approximate threshold-of-failure velocity (in knots) for various areas on the windshield and canopy.

Windshield Side Panel

The most critical impact location was on the forward area of the 0.38-inch thick stretched acrylic windshield side panel, impact point "A". The impact angle of incidence was 27 degrees at the target point. Impact point "A" was initially impacted with a four-pound bird at 190 knots which resulted in no damage. A subsequent shot at 200 knots resulted in about half of the four-pound bird penetrating the transparency with several pieces of spalled acrylic (see Figures 10 and 11). The transparency frame was undamaged.

The aft area of the windshield side panel was tested at location "B" and was found to have a failure threshold of 210 knots. The small increase was due to the reduced angle of incidence: 21 degrees.

Windshield Center Panel

The 1.2-inch-thick laminated glass windshield center panel demonstrated the highest capability of any part of the current transparency system. A four-pound, 300 knot shot on the forward end of the glass center panel (location "D") resulted in a substantial amount of glass spalling off the inside surface; however, no bird penetrated. A shot at 375 knots at location "D" resulted in the failure of the glass center panel. This test was classified a failure because much of the lower half of the transparency spalled into the cockpit, and the pilot would have been facing a considerable wind blast even though no bird actually penetrated (see Figure 12).

A four-pound, 375 knot shot was made on the aft end of the windshield center panel at location "C" and resulted in a small amount of the bird penetrating the windshield and canopy frames. Some glass was spalled into the cockpit; however, neither the glass nor the bird would have posed a serious threat to the pilot, and this test was classified a pass.

A 450 knot shot at location "C" resulted in a substantial amount of spalled glass. In addition, the center panel was pushed down, buckling the windshield arch supports, and the bird impacted the forward frame of the forward canopy. This failed the canopy frame and transparency, resulting in several large pieces of spalled acrylic as shown in Figure 13. This test was classified a failure because of the potential injury to the pilot.

One shot was made at 300 knots on the sheet metal panel forward of the windshield center panel. Some bird penetrated the structure and the capability was estimated to be 250 knots.

Forward Canopy

The 0.30-inch thick stretched acrylic canopy was impacted seven times at three locations ("F", "G", and "I"). The demonstrated capabilities were 240 knots at location "F", 220 knots at location "G", and 230 knots at location "I". A 300 knot area was added in the capability to reflect the decreased angle of incidence. No damage to the frame or support structure was found in any of the tests. The transparency, when failed, spalled several large pieces of acrylic (estimated at over 8 sq. in.), in addition to many small pieces. This spalled acrylic could cause serious injury to the pilot. Also, the pilot would be subject to considerable wind blast and buffeting through the large holes left in the transparency (Figures 14 and 15).

Windshield Frame

The capability of the F-4 production frame was determined by utilizing laminated panels formed in the F-4 side panel shape. The panels were mounted in the framework using aircraft grade bolts. Five impacts were made on the windshield structure with the laminated panels installed, one at location "A" and four at location "B". The impact at location A and the first impact at location "B" were performed at 450 knots with catastrophic failure of the frame occurring in both instances. The impact point "B" failure resulted in parts of the windshield arch entering the forward cockpit, posing a significant hazard to the pilot (Figures 16 and 17). For this reason, it was determined to perform additional tests at location "B". The three subsequent tests at location "B" resulted in a frame failure at a velocity of 375 knots. Failure at this velocity could have been predicted from a plot of the strain data taken at gage location GL4 (closest gage to the failure point) and the impact velocity (Figure 18). Note how rapidly the stress rises with velocity in this particular loading situation; the magnitude of the loads in the structure appear to be extremely sensitive to velocity in the 350-to-375 knot range. Frame baseline capability was accepted as 375 knots.

CONCLUSION

The F/RF-4 transparency birdstrike tests have established the existing capability of the transparency system and have generated a useful data base for designing and evaluating various bird impact resistant designs. In-field service has demonstrated the need for improved birdstrike protection and these tests confirm this need.

The data generated from these tests show that the acrylic side panels and forward canopy must be replaced with bird resistant designs which will provide the degree of protection required. Also, the tests indicated that a new or reinforced windshield frame is required.

A program currently under way will evaluate several alternative bird impact resistant transparency system designs. The result will be an affordable transparency system which will protect the F/RF-4 crew during high speed, low level flight.

REFERENCES

1. Test Facilities Handbook (Eleventh Edition), Arnold Engineering Development Center,Arnold Air Force Station, Tennessee, April 1981.

2. Lawrence, D. H., Jr., Guidelines for the Design of Aircraft Windshield/Canopy Systems, AFWAL-TR-80-3003, Air Force Wright Aeronautical Laboratories, Wright-Patterson AFB, OH, February 1980.

3. Storslee, J. H., Bird Impact Testing of Windshield and Canopy Assemblies for the F-4 Aircraft, AEDC-TSR-82-V39, Arnold Engineering Development Center, Arnold AFS, TN, December 1982.

4. Storslee, J. H., AFWAL F-4 Canopy Birdstrike Test Project, C784VJ, Arnold AFS, TN, October 1982.

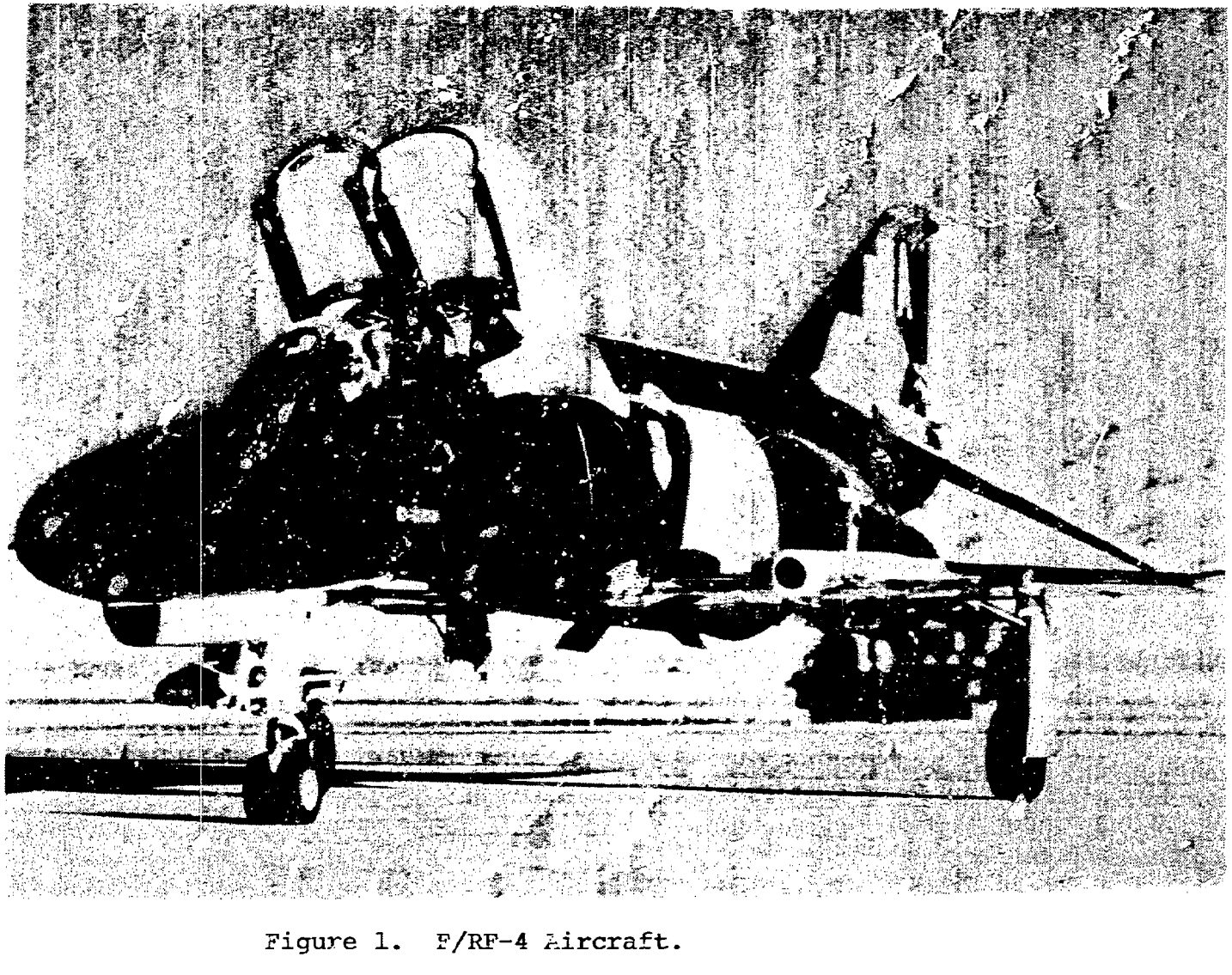

Figure 1. F/RF-4 Aircraft.

Figure 2. F/RF-4 Transparency System.

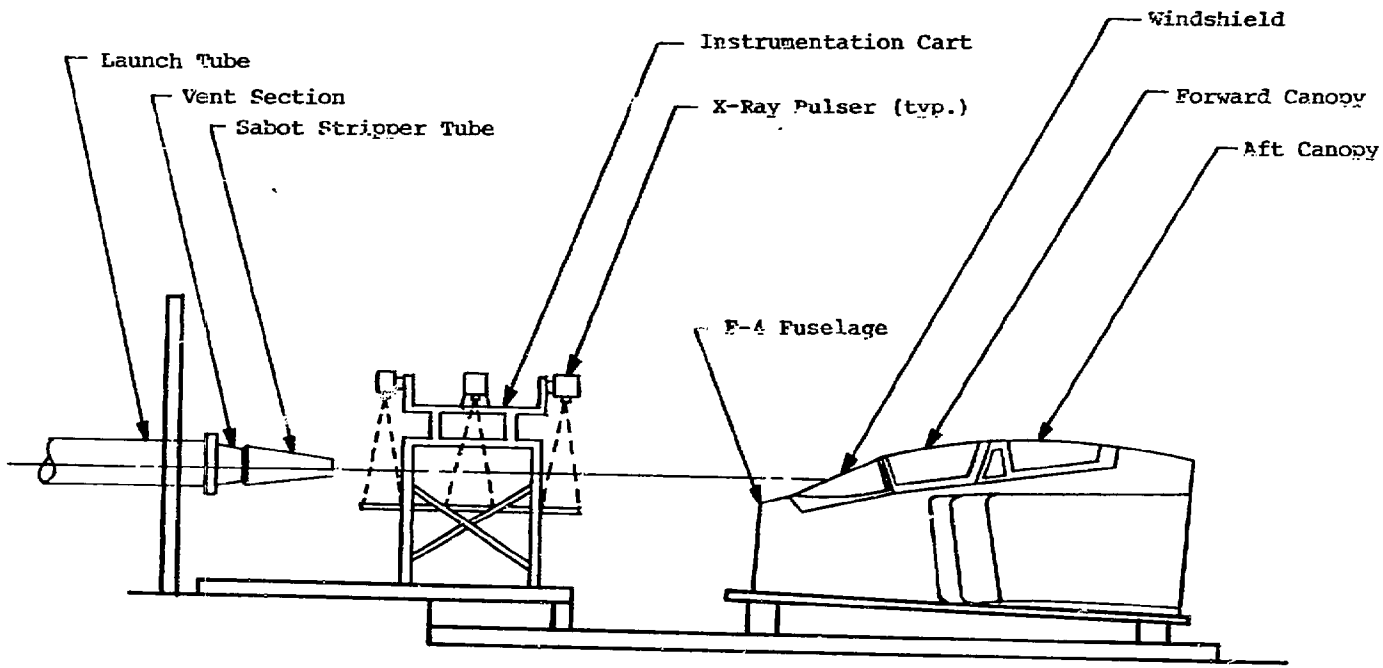

Figure 3. AEDC Test Area Arrangement.

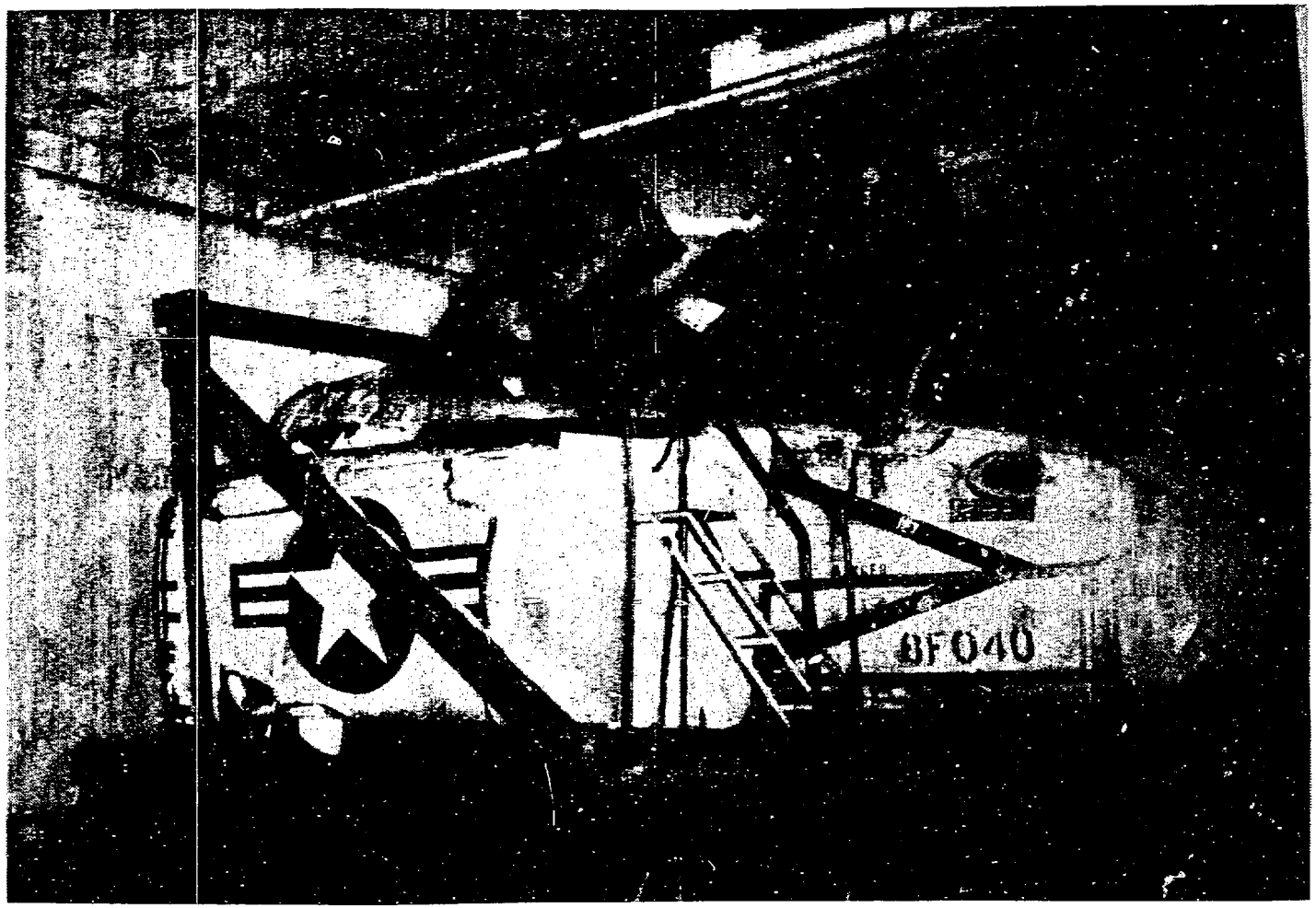

Figure 4. F-4 Forward Fuselage Section Installed in AEDC S-3 Range.

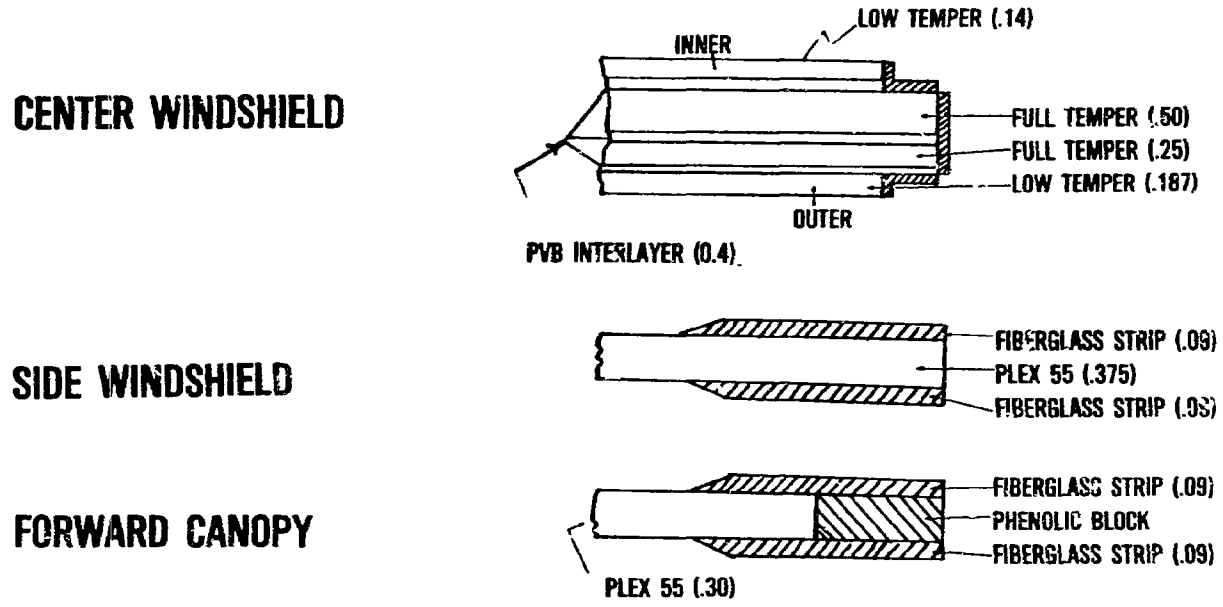

Figure 5. Cross-Sectional Properties of Production Transparency System.

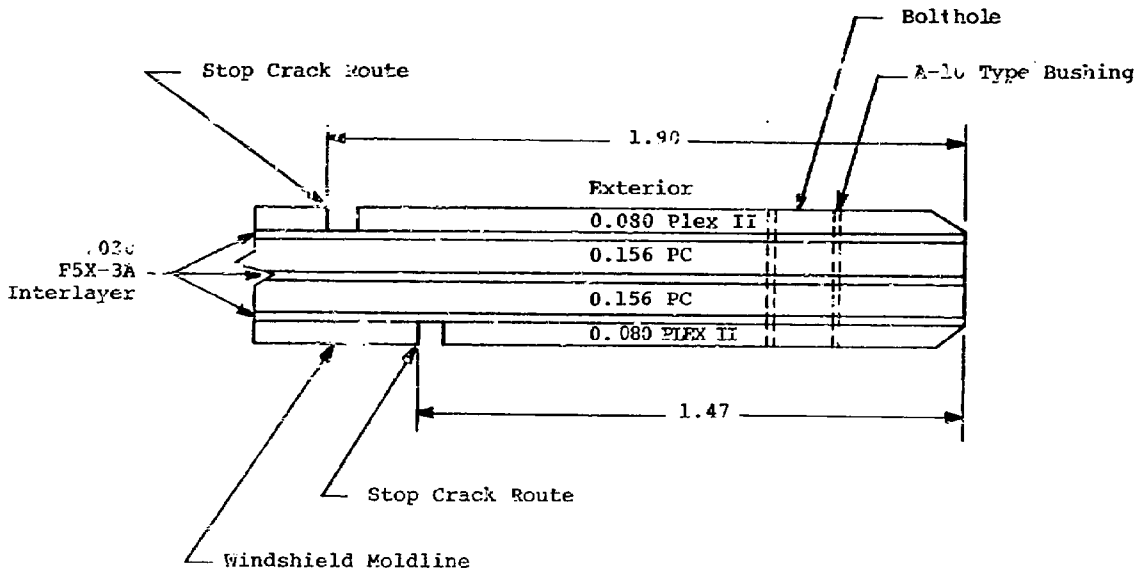

PC - Polycarbonate
Total Thickness 0.562
All dimensions in inches

Figure 6. Goodyear Laminated Side Panel Cross-Section.

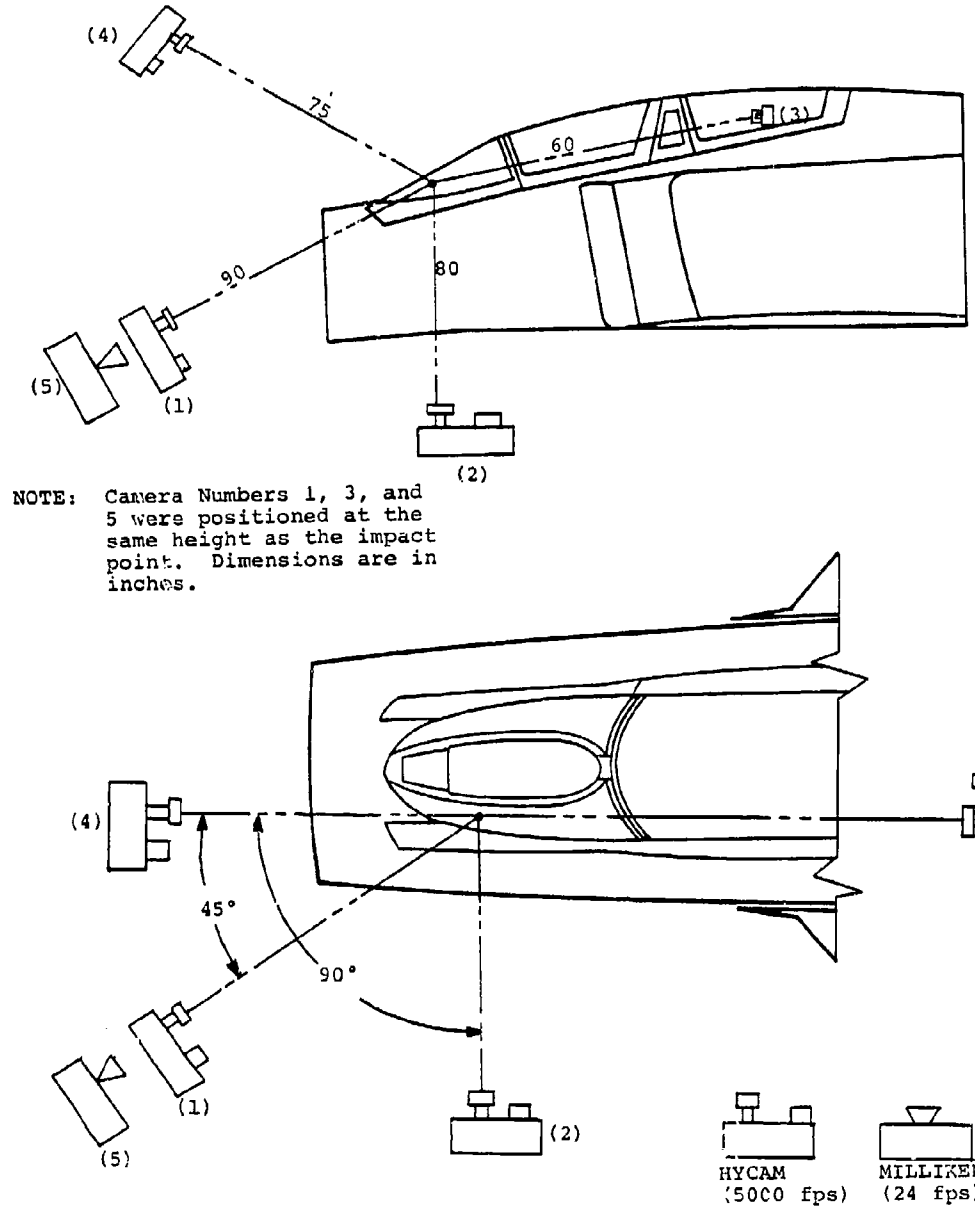

Figure 7. Location of High Speed and Real Time Motion Picture Cameras.

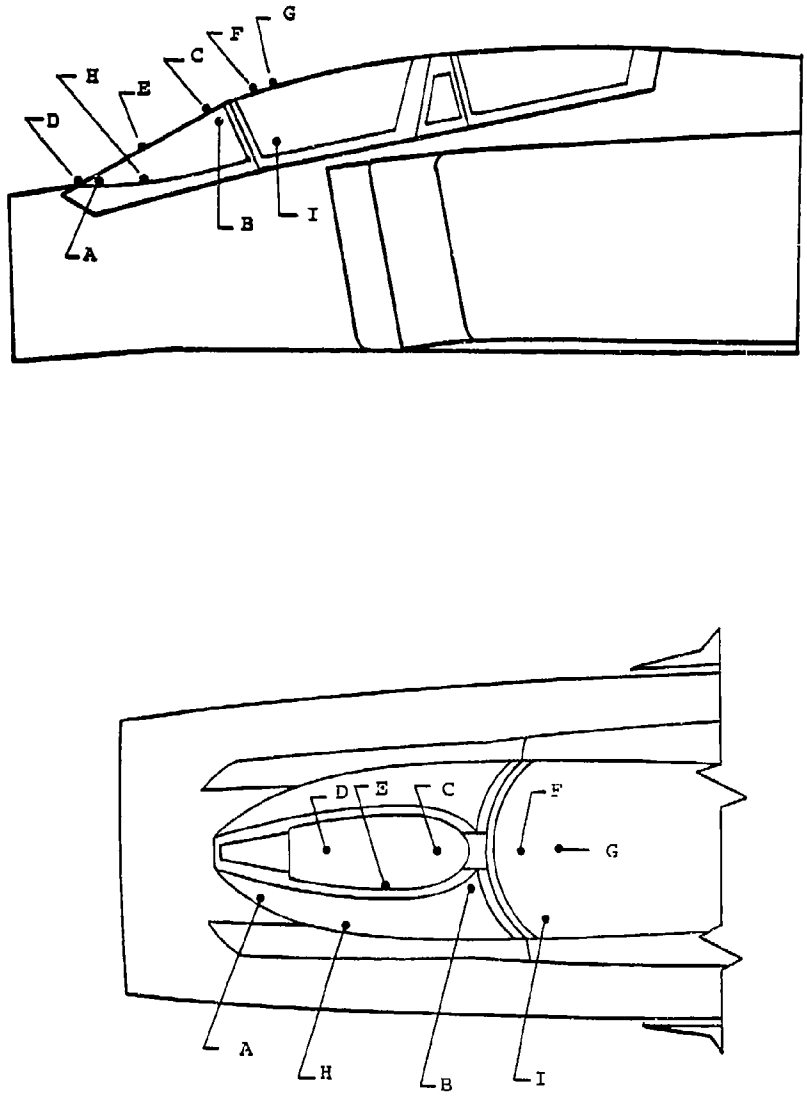

Figure 8. Impact Locations.

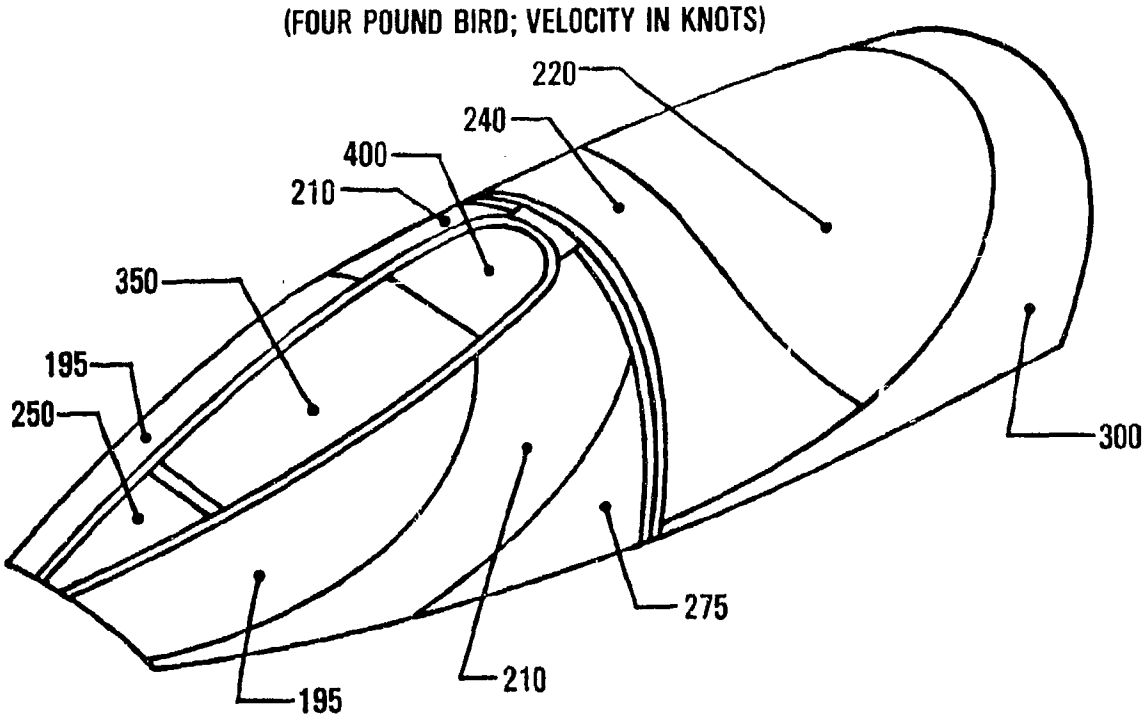

Figure 9. F/RF-4 Windshield and Forward Canopy Bird Impact Capability Diagram.

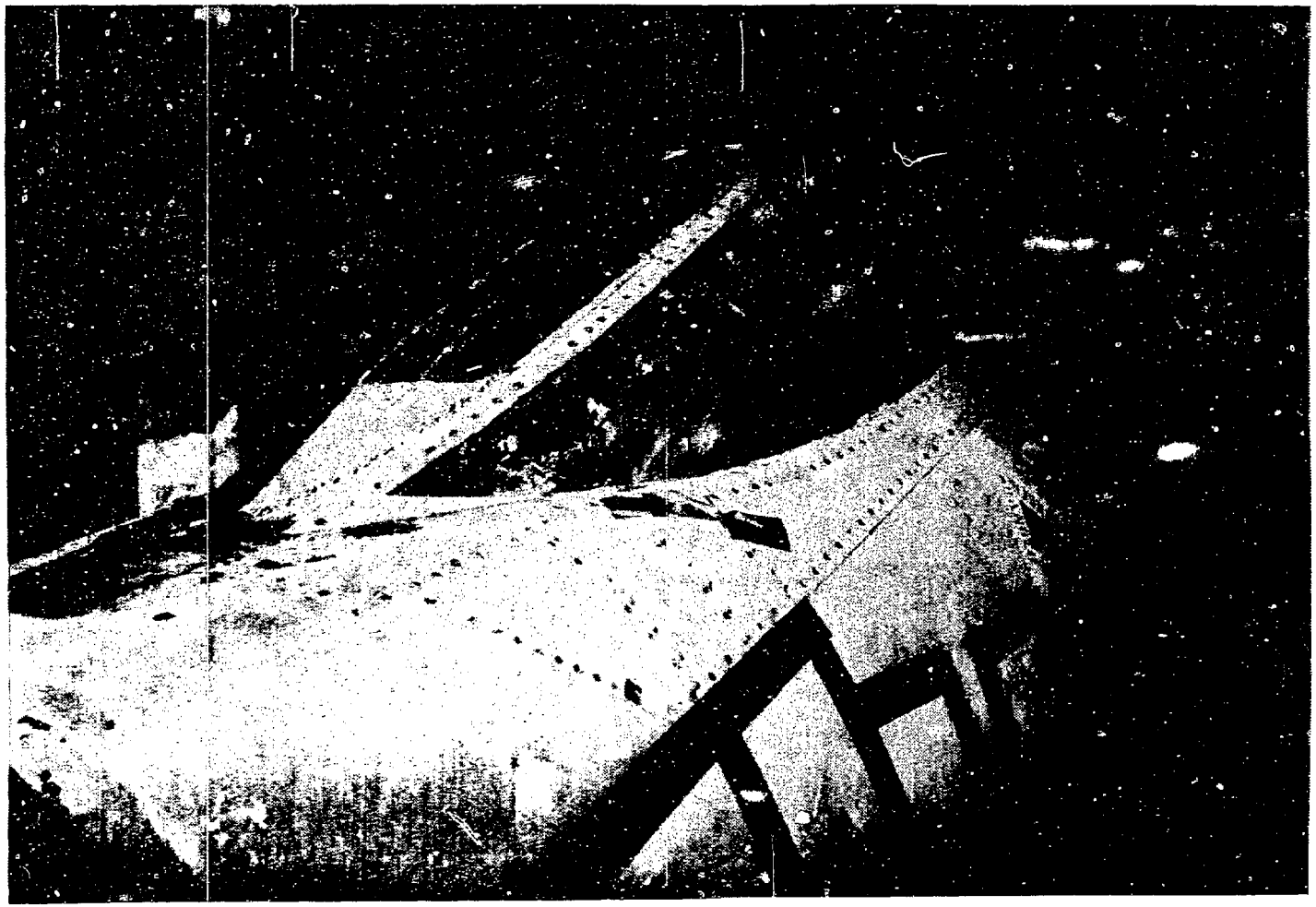

Figure 10. Post Test Damage, 200 Knot Impact on Windshield Side Panel.

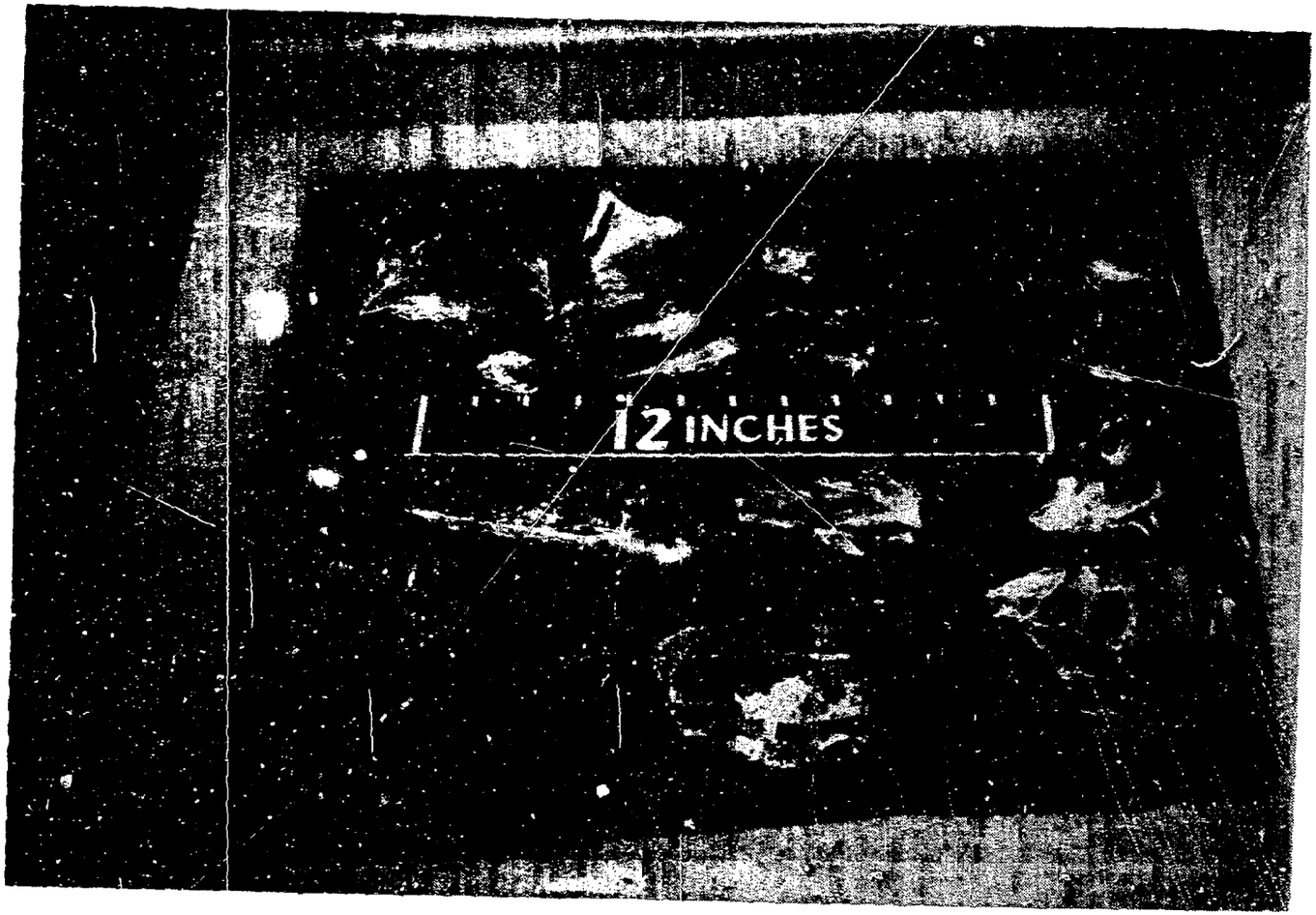

Figure 11. Typical Spalled Acrylic from Windshield Side Panel.

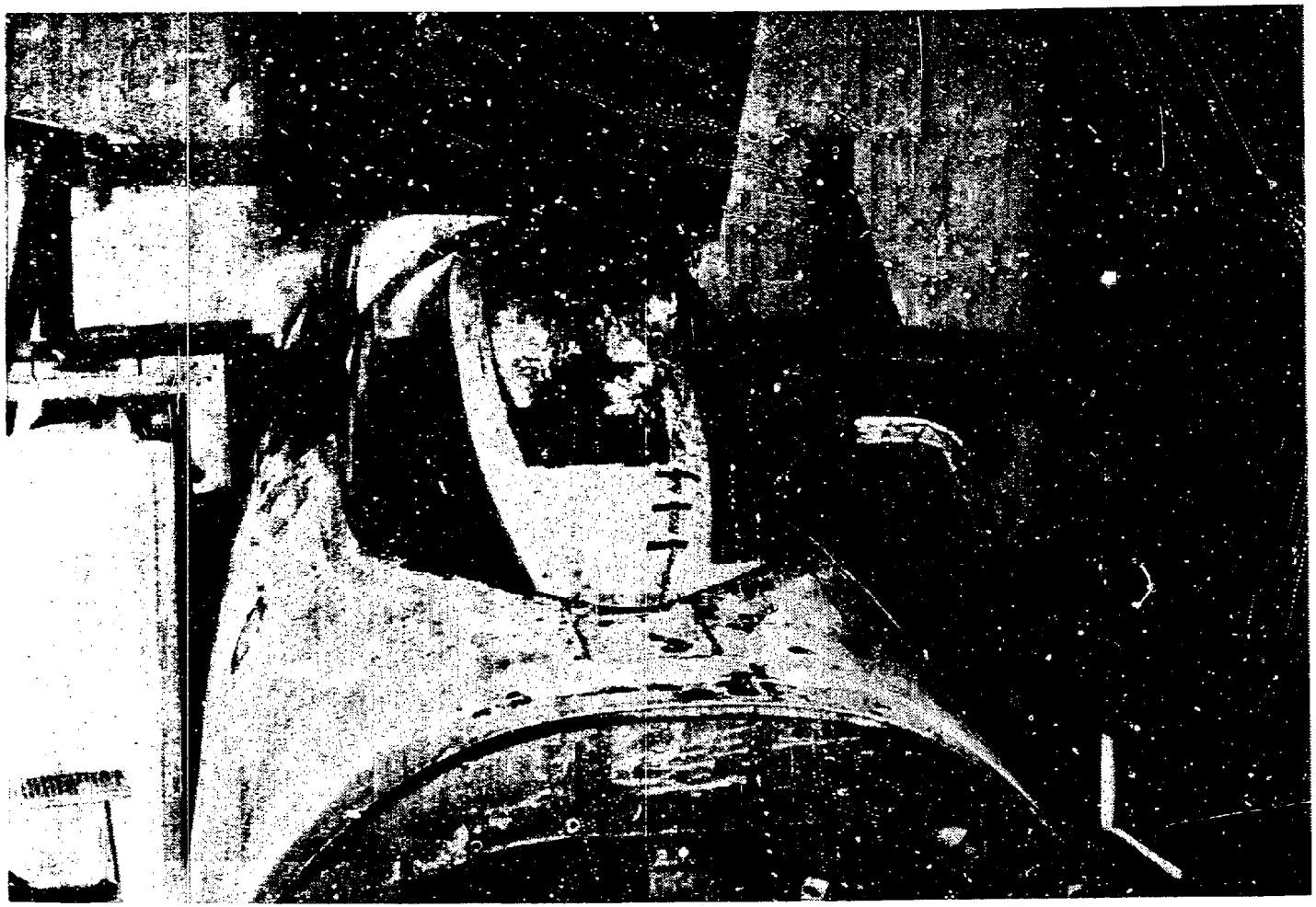

Figure 12. Result of 375-knot Impact Low on Windshield Center Panel.

Figure 13. Post Test Damage, Four Pound Bird, 450-knot Impact High on Windshield Center Panel.

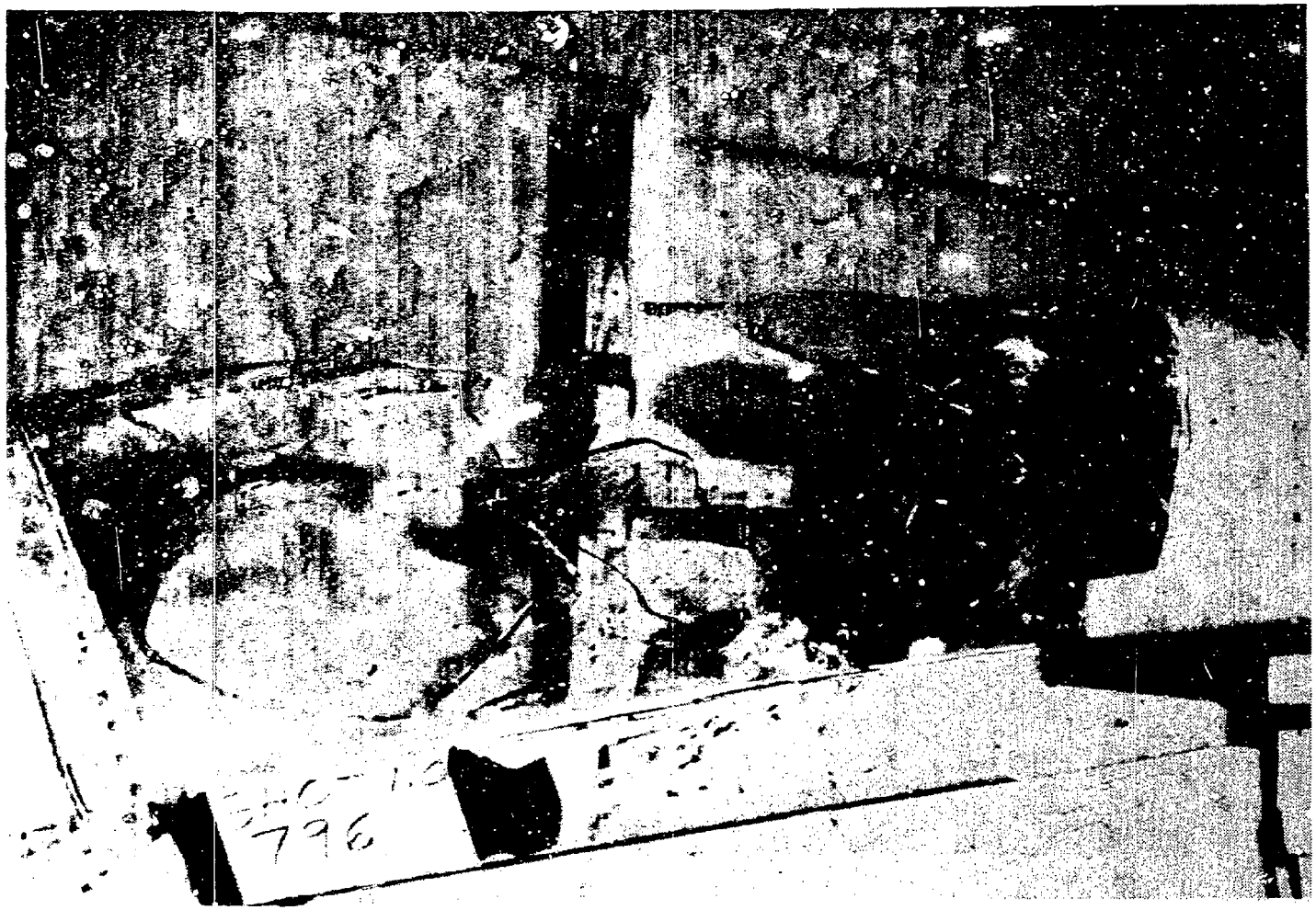

Figure 14. Result of 270-knot Impact, Centerline of Forward Canopy.

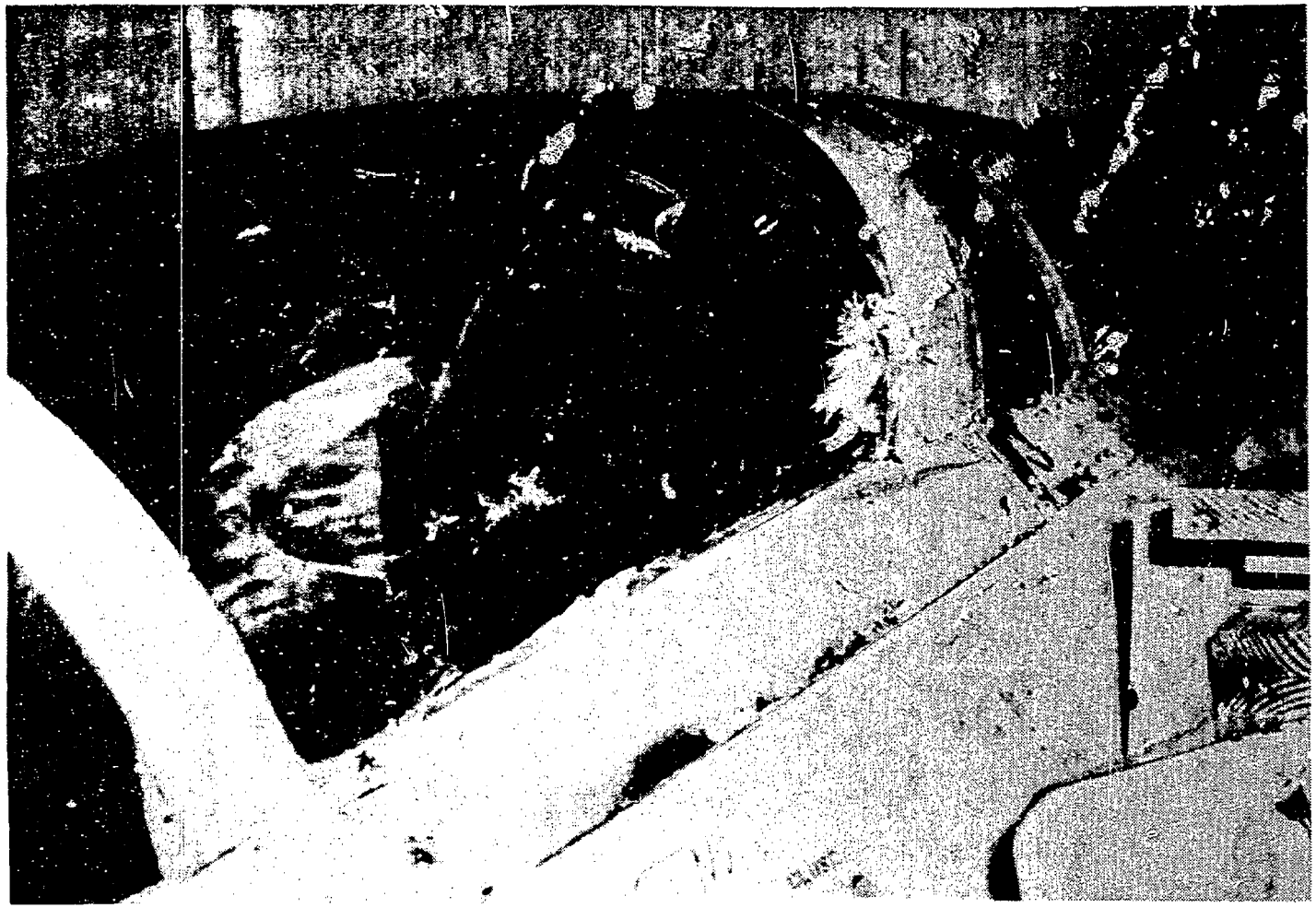

Figure 15. Result of 260-knot Impact, Canopy Sill Location, Fuselage Yawed 15°.

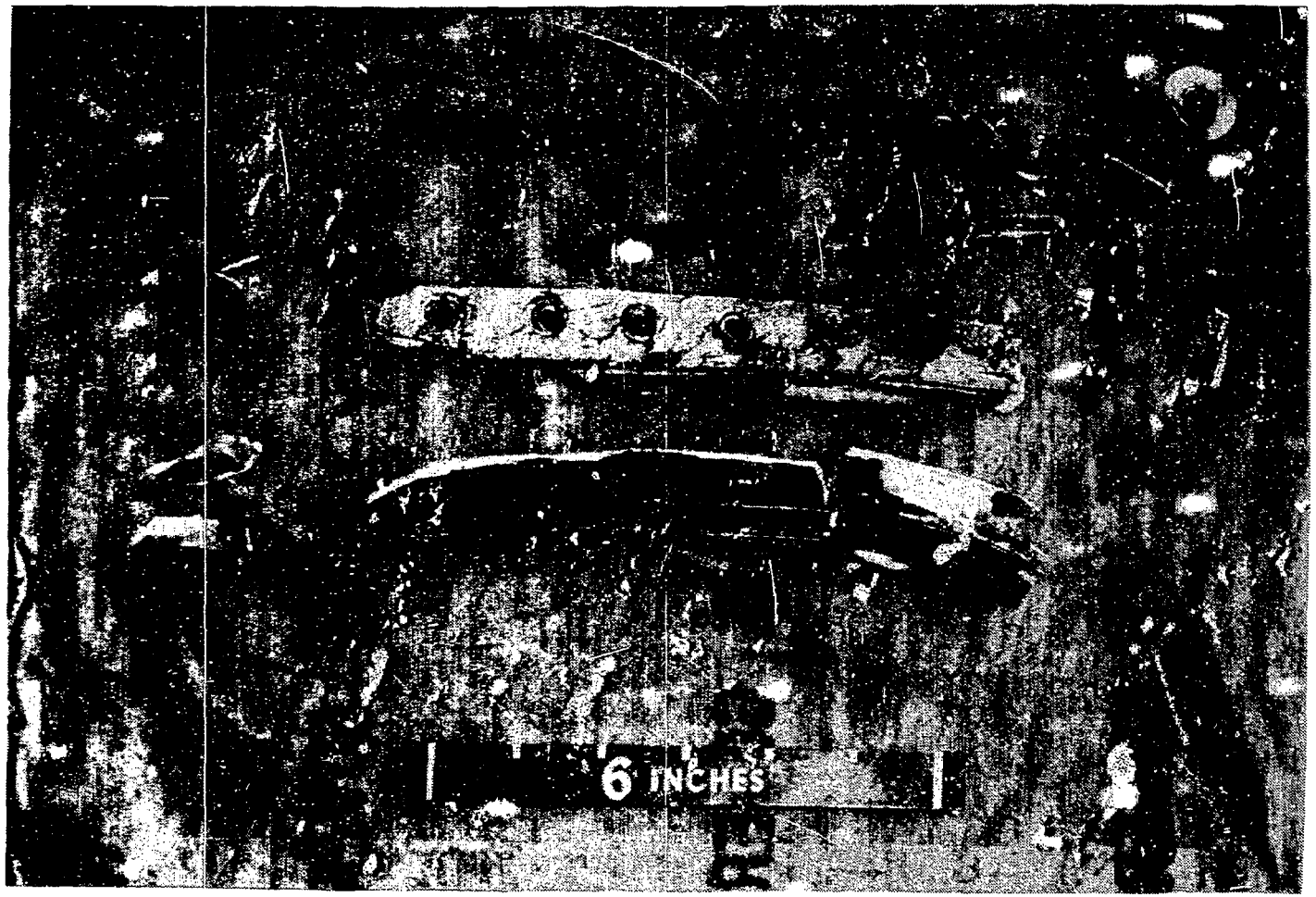

Figure 16. Failed Windshield Arch Fragments After 450-knot Side Panel Impact on Laminated Side Panel.

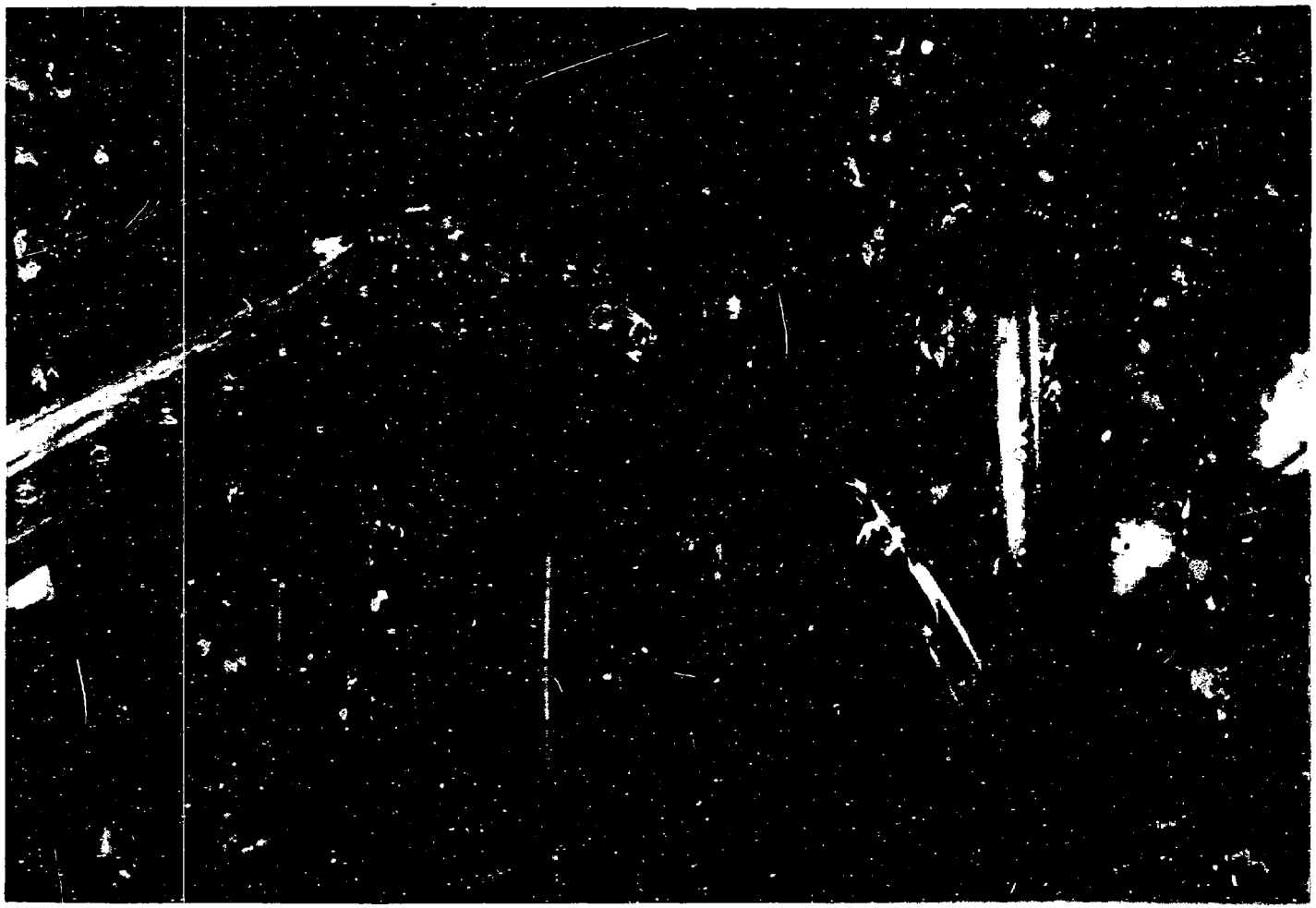

Figure 17. Failed Windshield Arch After 450-knot Impact on Laminated Side Panel.

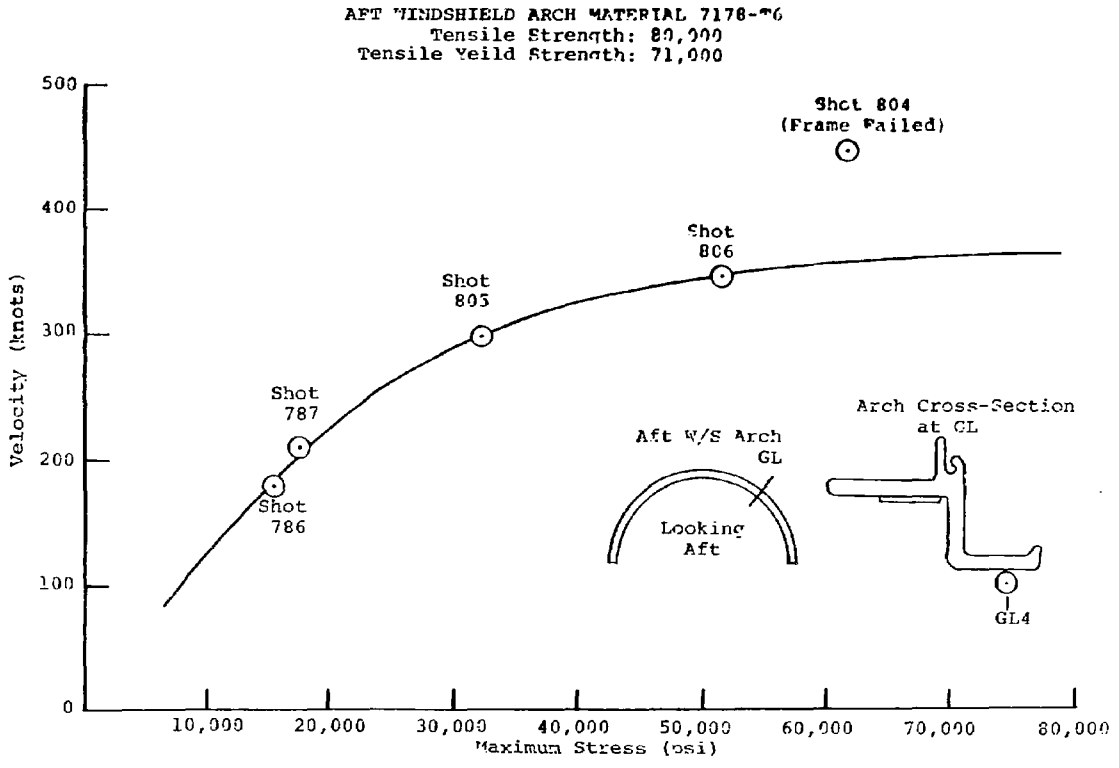

Figure 18. Maximum Measured Stress vs. Velocity for Gage Location GL4 and Bird Impacts on Location B

AD-P003 219

ALTERNATE T-38 TRANSPARENCY DEVELOPMENT

B. S. West and K. I. Clayton,
University of Dayton, and
Capt W. W. Saeger, Jr.,
Flight Dynamics Laboratory

ALTERNATE T-38 TRANSPARENCY DEVELOPMENT

Blaine S. West and Kenneth I. Clayton
University of Dayton Research Institute
Dayton, Ohio 45469

Capt. Walter W. Saeger, Jr.
Air Force Wright Aeronautical Laboratories
Wright-Patterson Air Force Base, Ohio 45433

ABSTRACT

T-38 missions at speeds above the existing crew enclosure damage threshold will result in flight safety risk to aircraft and crew. This paper summarizes the design/development of alternate T-38 transparencies having the capability of defeating the impact of a four pound bird at aircraft speeds up to 400 knots. To successfully accomplish a forward (student) windshield redesign which provides the desired improvement in birdstrike capability, four specific tasks were conducted. A preliminary design and evaluation defined the guidelines and constraints governing the modifications, defined and assessed candidate transparency configurations, and conducted a birdstrike risk assessment. Edge attachment screening tests were conducted for the most promising cross-sections to compare edge response, fracture mechanism, and energy absorption potential. A parametric finite element analysis examined the effects of transparency and support structure stiffness versus peak load and deflection. A full-scale flight hardware test program established the failure threshold for the existing T-38 forward windshield and forward canopy for a four pound birdstrike at six impact locations. Major findings from each of these four tasks were integrated into the detail design of a birdstrike resistant forward windshield panel. Forward canopy and instructor windshield concepts are also discussed. Recommendations are made for full scale hardware, fabrication, testing, and evaluation.

INTRODUCTION

The T-38 aircraft was originally designed to train Air Force pilots in the fundamentals of high speed aircraft flight at altitudes exceeding 10,000 feet above ground level. Recently, the mission usage has changed with the addition of low level navigation training flights as low as 1,500 feet above ground level at speeds approaching 400 knots. This has significantly increased the danger of sustaining birdstrikes on the aircraft since the bird population is concentrated below 10,000 feet.

This increased birdstrike potential caused concern within the using command, Air Training Command (HQ ATC) over pilot safety and aircraft survivability. Originally, the T-38 transparency system was not designed to provide birdstrike protection since no specific birdstrike requirement existed and it was

believed that aerodynamic flow would not allow damaging bird impacts with the transparencies. This assumption has proved wrong on numerous occasions, resulting in four aircraft being destroyed and three pilots killed (as the direct result of transparency birdstrike) since the T-38 became operational in 1964. The birdstrike protection level of the forward windshield was increased in 1969 but it is now considered inadequate for mission requirements. The forward canopy impact resistance was not increased due to the ATC's desire to retain through-the-canopy (TTC) ejection as a back up means of escape.

The Vehicle Equipment Division Advanced Development Program Office of the Flight Dynamics Laboratory has instituted a program to develop improved forward facing transparencies for the T-38 (reference Figure 1). Originally the program was to address only the forward windshield and forward canopy but when ATC decided in November 1979 that it could not give up the back up TTC ejection capability, the instructor windshield was included in the development effort. This was done in recognition that development of a forward canopy that provides the desired four pound 400 knot birdstrike protection requirement while retaining TTC ejection capability will require integration of diverse technologies that may take significantly longer development times than the development of a canopy that satisfies only the birdstrike requirement. By including the instructor windshield for development of increased birdstrike protection, the current forward canopy can be continued in use while the instructor pilot, who sits in the aft cockpit, is provided adequate protection from birdstrikes that penetrate the forward canopy.

As part of the Flight Dynamics Laboratory's continuing development/demonstration of the technology/methodology required for the design and verification of birdstrike resistant transparent crew enclosures, the University of Dayton Research Institute (UDRI) has applied recent advances in birdstrike technology to the design/development of alternate T-38 transparencies having the capability of defeating the impact of a four pound bird at aircraft speeds up to 400 knots. The successful design/analysis of bird resistant crew enclosure structures is a complex problem, characterized by geometric and material nonlinearities and by coupling of the bird induced load with the structural response. Therefore, the structural design/analysis approach for bird impact should be a systems analysis approach similar to that commonly applied to a primary structural system. The successful execution of the alternate T-38 transparency redesign effort to upgrade the birdstrike capability was accomplished by melding the supporting parameters of preliminary design/evaluation including risk assessment, edge member screening test results, parametric analyses, and full-scale birdstrike test results into the design development cycle.

PRELIMINARY DESIGN AND EVALUATION

The effort associated with the preliminary design and evaluation: (a) defined the guidelines and constraints governing the modifications, (b) defined and assessed candidate transparency configurations, and (c) defined the birdstrike risk assessment.

The first step to determine the feasibility of upgrading the T-38 aircraft crew enclosure forward transparencies (student windshield and student canopy) to be compatible with current and expected usage, was to evaluate preliminary and potential designs. As part of this effort, a UDRI/Swedlow team, in conjunction with the AFFDL Project Engineer, defined the guidelines and constraints that would govern the modifications, defined candidate transparency cross-sections, assessed the cost and optics performance of each candidate design concept, assessed the maintainability requirements and limitations imposed by each configuration, and conducted birdstrike probability studies to evaluate the cost effectiveness of a retrofit program.

The preliminary design guidelines are enumerated below.

(a) The student (forward) windshield and student (forward) canopy to be considered for redesign;*

(b) Present student canopy life: 4,000-5,000 hours (8-10 years);

(c) Present student windshield life: 4,000-5,000 hours (8-10 years);

(d) Through-the-canopy ejection capability not mandatory for student canopy;*

(e) Present T-38 fleet size: 1,000 aircraft;

(f) All feasibility studies based on remaining fleet life of 10 and 20 years;

(g) T-38 fleet size assumed to remain at present level for assumed fleet life spans;

(h) Today's value of fully equipped T-38 aircraft assumed at $1.5 million;

(i) Primary fuselage structure not affected by the redesign effort; and

(j) Basic transparency edge design and attachment to be adequate for upgraded transparencies.

---

*HQ-ATC later determined that it was necessary to retain through-the-canopy (TTC) ejection capability for the student canopy, at which time the aft windshield was included for study to provide interim birdstrike protection for the instructor pilot.

The preliminary design constraints are enumerated below.

(a) No decrease in maintainability with respect to existing transparencies;

(b) Optics requirements to meet to exceed current Northrop Process Specifications IT-51 and IT-33;

(c) Minimization of overall weight increase and center of gravity change;

(d) No redesign of primary structure;

(e) No major redesign of canopy operating mechanism or crew equipment;

(f) Minimization of changes to exterior moldline, fairings, and associated hardware;

(g) Minimization of transparency outer ply spall during bird impact event;

(h) Interchangeability with existing transparencies to be maintained if possible;

(i) Simplification of fleet retrofit, preferably at field level but with no more than depot level facilities required; and

(j) Capability to withstand hot powder from aircraft cannon equivalent to existing transparencies.

The governing guidelines and constraints were subdivided into "must" requirements and "want" requirements. The "must" requirements were those which must be totally satisfied, and included:

- four pound-400 knot birdstrike capability,
- producibility, and
- interchangeability.

The selected design was to satisfy the "must" requirements and consisted of a compromise among and an optimization of remaining requirements according to their relative importance. These other desired requirements were classified as "want" requirements and were in the form of performance in certain key properties, namely:

- optics,
- cost,
- edge attachment configuration, and
- weight.

In general, available test data indicates that laminated polycarbonate panels separated by low modulus ductile interlayers offer high strength/weight performance for center panel

bird impact. The opportunities to vary stiffness and strength and thus performance are almost limitless. One may depart from balanced laminates and vary the thickness of the structural plies and the thickness and material properties of the interlayers. However, there are many considerations to panel design other than center panel impact, and these may well dictate the choice of a monolithic polycarbonate panel.

Structurally, edge design is very important and may prove to be critical for birdstrikes near the panel edge. It is important to consider total system response, edge member cross-section, and the details of edge member attachment.

Optics are critical, especially when based on viewing the T-38 student's windshield (forward) and the student's canopy (forward) from the instructor's position (aft). The optics requirement is thus an important factor which affects the choice of monolithic or laminated panels and the composition of the laminated panels. As with any flightworthy components, the weight of the transparency assemblies is of concern and should be held to a minimum.

Serviceability and life of candidate windshield/canopy transparencies are also key factors in selecting a design. The present monolithic stretched acrylic transparencies offer good serviceability and life excepting the birdstrike requirement.

The use of polycarbonate would increase the birdstrike capability for a given thickness. In order to protect the surfaces of monolithic polycarbonate transparencies, protective coatings must be applied. Historically, these treatments are not as durable as stretched acrylic. With laminated polycarbonate assemblies, the outer plies can be thin stretched or as-cast acrylic layers to provide the serviceability and surface resistance equivalent to those of the present panels.

It is obvious that the best possible transparency is not desirable if it cannot be produced, or produced within the required tolerances. Hence the manufacturing trade-off becomes a key variable to be considered early in the choice of candidate design configurations. Another significant factor, or variable, which has been considered in the optimization of the design configuration is life-cycle cost of the transparency assemblies.

Baseline cross-sections of the existing T-38 student windshield and student canopy are:

(a) Windshield: 0.600 in. stretched acrylic at a nominal weight of 34 pounds;

(b) Canopy: 0.230 in. stretched acrylic at a nominal weight of 32 pounds.

Twelve preliminary candidate windshield transparency cross-sections and 11 preliminary candidate transparency cross-sections were defined to satisfy the four pound-400 knot bird-strike requirement. The minimum thickness cross-sections, considering various combinations of monolithic and laminated acrylic and/or polycarbonate were identified and configured based on the experience of UDRI, Swedlow, Inc., and the Air Force and were assessed in each of the key requirement areas.

At the conclusion of the preliminary design and evaluation study, UDRI, in concurrence with AFWAL/FIEA Project Engineer, selected five windshields (Figure 2) and three canopy (Figure 3) transparency configurations which best satisfied the evaluation criteria. The selected configurations were presented as candidates for further evaluation.

A statistical model was utilized to predict the number of damaging birdstrikes to the existing T-38 windshield and canopy during the next ten years for each of four velocity distributions. Rationale used in modeling these components were dependent on the operational density and weight distribution of birds in the aircraft environment, the forward-projected area of the hardware, transparency capability, aircraft velocity distribution in the bird environment, and total time spent in the bird environment. Total flight time was obtained from the data files on birdstrikes maintained at Norton Air Force Base. Figure 4 presents the estimated birdstrike capability, generated internally by UDRI, for the existing windshield and canopy. Table 1 presents the predicted T-38 transparency penetrations for the 10-year period.

EDGE ATTACHMENT SCREENING TESTS

Structurally, edge attachments are a primary design consideration, especially when impacts are near the edges. The generation of design trade-off data required to finalize the T-38 alternate transparency cross-section and associated edge design would be prohibitive in terms of dollars, manpower, availability of parts, and calendar time if fully obtained from the testing of full-scale flight hardware. Therefore, UDRI screened five windshield and four canopy configurations in the laboratory. A flexure beam (3-in. x 15-in.) construction simulated the candidate transparency cross-sections and the canted fuselage station 184.35 fixity shown in Figure 5. Nine configurations of three-point loaded beams were tested with simulated T-38 edge fixity at a displacement rate of 2,000 inches per minute using the University's high performance, electrohydraulic closed-loop (MTS) system. The test specimens, representative of aircraft baseline and proposed edge constructions, were manufactured in a T-38 production environment by Swedlow, Inc. For all tests, load versus displacement data was stored in the digital memory of a transient recorder and played back at reduced speed on an X-Y recorder; high speed motion picture coverage was provided by

Wright-Patterson Air Force Base personnel. Information on edge response, fracture, and energy absorption provided by these laboratory screening tests aided the definition of design deficiencies and allowed comparison of the relative merits of candidate design.

Initial tests subjected windshield beams having slotted edge attach holes to center of beam impact (13.50 inch span; 6.75 inch 1/2 span) and canopy beams having clamped edges to center of beam impact. All proposed edge designs exceeded the ultimate load capability of the baseline design. Excessive deflection resulted in edge pullout at the slotted holes, without failure, of the polycarbonate windshield candidate design. Therefore, additional off-center tests were conducted for selected four-point flexure beams (4.50 inch 1/3 span) (2,000 inches per minute) as follows:

Beam Configuration	Ultimate Load, Pounds
#1, 0.60 acrylic baseline	1000
#2, 0.90 acrylic 400 knot	1750
#3, polycarbonate 400 knot	1950 (no failure)

Since excessive deflection again resulted in edge pullout of the polycarbonate beam without failure, one additional test was conducted for the #4 beam configuration with impact at the 1/4 span points (3.375 inches from each end), resulting in an ultimate load at pullout of 2,400 pounds, again without failure.

PARAMETRIC ANALYSIS

Parametric studies, encompassing a range of design variables which affect the ability of a transparency structural system to absorb impact loading, were conducted to examine the effect of such variations in the transparency/support structure on the performance of the total system during the birdstrike event. These studies involved the application of new technology to the birdstrike problem; specifically, the application of the nonlinear finite element method to the dynamic response analysis of the T-38 structural system. The use of the finite element method in a parametric study of this type has not previously been extended to include the nonlinear response characteristics of a transparency system of this complexity. For this parametric study, concentration was focused on the range of stiffness provided by single ply transparencies, the existing 0.6 inch and candidate 0.9 inch stretched acrylic and 0.45 inch polycarbonate; the 0.45 inch polycarbonate being part of a laminated configuration.

All finite element studies were made using a geometrically and materially nonlinear analysis computer program called MAGNA. The MAGNA computer program is a large scale, general purpose finite element system intended for the nonlinear analysis of

complex engineering structures. Unlike many available nonlinear analysis software packages, MAGNA has been developed primarily for the efficient solution of three dimensional problems, involving many degrees of freedom and large bandwidth. Isoparametric modeling techniques and state-of-the-art numerical solution methods are combined in MAGNA to provide effective analytical capabilities for three dimensional structures experiencing large displacements, finite strains, arbitrary rotations, and elastic-plastic behavior.

Both static and dynamic analyses were performed, examining the effects of changes to the transparency stiffness and intensity of the applied load, both coupled and uncoupled. For the static analysis, the 0.45 inch polycarbonate and the 0.9 inch stretched acrylic showed approximately the same capabilities. For the dynamic analysis the peak stresses at the impact point were somewhat lower for the 0.9 inch stretched acrylic. However, this is not conclusive because of the known difference in the failure mode for the two materials. Furthermore, based on past experience, failure at the point of impact is an unlikely event in an uncoated polycarbonate transparency during a birdstrike test. Frame failure, or frame-induced failure in the transparency, was not evaluated because the dynamic analysis was not carried out for sufficient duration to define that portion of the response.

Significant results of the finite element analysis, including transparency deflection, peak load versus transparency stiffness, and resultant force plots along the aft arch, will be discussed in detail at tomorrow's session of this conference by Richard Nash during his presentation entitled, "Parametric Studies of the T-38 Student Windshield Using the Finite Element Code MAGNA."

EXISTING BIRDSTRIKE CAPABILITY

During Northrop Corporation's development of the 0.6-inch forward windshield, birdstrike testing was conducted on the windshield but limited to an impact point at the vertical/horizontal centerline of the windshield and parallel to the aircraft centerline. Although this gave the windshield centerline birdstrike capability, there was some question as to the adequacy of the edge attachment design should a birdstrike occur off-center so as to involve the transparency edge attachments.

The primary objective of the birdstrike testing conducted in August 1979 at the Arnold Engineering Development Center (AEDC) was to determine the baseline birdstrike protection level as a function of birdstrike location for the current production forward windshield and forward canopy in use on the T-38 fleet. The forward windshield is currently 0.6-inch monolithic stretched acrylic while the forward canopy is 0.230-inch monolithic stretched acrylic.

The baseline capability derived from the testing was used for two purposes: (1) provide design/redesign inputs to the T-38 birdstrike resistant transparency development program, and (2) provide data for use in the birdstrike risk assessment model. Risk assessment studies using the birdstrike probability model were conducted using estimated values for the critical impact energy level of the T-38 forward transparencies. The test results provided corrected data for use in the prediction model. Six impact locations on the T-38 forward transparencies were investigated. All tests at impact points along the fuselage centerline were conducted with the fuselage oriented at 0° pitch - 0° yaw attitude relative to the launch path. Transparency side tests at two locations were made with the module yawed 15° clockwise. From two to five tests on each transparency were required to determine the ballistic limit at each impact location.

Forward windshield and forward canopies representative of current production models were mounted on an F-4/T-38 forward fuselage section for testing (reference Figure 6). Four high speed movie cameras (4,000 frames/sec) were utilized to provide a photographic record of each shot. The cameras were positioned to obtain coverage of the impact location and failure modes, transparency edge attachment reactions, and transparency-support structure interactions. Since the total impact-failure sequence occurs in milliseconds, high speed film provides a means to visually examine the events as they took place. In addition to high speed movies, still color photographs were taken before and after each shot to record damage or other visual evidence which would aid in interpreting and documenting the test results.

Strain gage readings were taken just before and just after each test to evaluate the permanent deformation resulting from each test. Before and after each test, measurements were made of the canopy frame-to-windshield frame clearance to monitor structural member deformation during the tests.

The six impact locations, three on the forward windshield and three on the forward canopy (Figure 7), were chosen to minimize the number of test articles required to characterize the impact failure levels of each transparency. Impact locations 1, 2, and 3 on the forward windshield were chosen so that the failure impact energy and failure modes in these areas could be determined. Of primary concern was the strength of the transparency-edge attachment design and the method of fastening the windshield in its frame. Of a secondary concern was the strength of the frame itself but it was doubtful whether sufficient energy could be imparted to the frame in these tests to cause failure, due to the potentially low failure velocities of the transparency. No shots were conducted at an impact location at the vertical-horizontal centerline of the windshield since Northrop Corporation had conducted its series of tests in

1968 at this location, and sufficient data was available from their test report. The no-failure velocity for the horizontal-vertical centerline impact location of the current windshield design was 319 knots in the Northrop tests.

The forward canopy impact locations, 4 and 6, were also chosen to characterize the edge attachments and frame strength. Location 5 was chosen to provide data for an impact as far aft from the canopy bow frame as possible while still allowing the bird to impact fully on the canopy at a relatively large angle of incidence. The forward edge of the canopy is restrained only between a forward arch and retainer that is riveted to the arch; no fasteners pass through the transparency or its edges in this area. There was some concern that the transparency might pull out of the frame along the leading edge so impact location 4 was chosen to determine if such a tendency did exist.

The side edge attachments consist of a fiberglass overlay transitioning into a hinge node arrangement. The transparency mounted nodes interlock with alternating nodes in the canopy frame side rails. A retainer pin passes through holes in the nodes parallel to the canopy frame, locking the sides of the transparency in place. Impact location 6 was selected to determine the response of the transparency-edge attachment bond and the transparency-frame nodes to bird impact.

Impact locations 1, 2, 4, and 5 were all located along the aircraft horizontal centerline (butt line zero). Impact locations 3 and 6 required that the fuselage test fixture be yawed 15° clockwise.

The sequence in which the impact locations were tested was based on two considerations. To preserve the transparency/support structure as long as possible, those impact locations (3 and 4) which were most likely to cause damage to the frame were scheduled late in the test sequence. The sequence was also arranged to minimize the frequency of transparency change-out and test module relocation.

The initial impact velocities for each impact location were selected prior to the initiation of testing on the basis of previous testing conducted by Northrop on T-38 windshields, tests on other aircraft transparency systems, and an analysis of flat panel birdstrike test results. The initial velocities were selected so as to be below the expected failure velocities of the transparencies at the desired impact locations when utilizing a nominal four pound bird. The impact velocities for each impact location were to be increased on succeeding shots until the transparency failed. By using this step method of increasing the impact velocity until failure was achieved, the energy required to induce failure for each impact location could be established within a known range. The failure energy range would exist

between the highest velocity at which failure had not occurred and the velocity at which failure occurred. For this test program, a bird weight of 4.0 ±0.1 pound was used for all tests.

The results of the test sequence to establish the birdstrike capability of the existing T-38 forward transparencies are summarized in Table 2. The test results are presented chronologically and the significance of each test is summarized. Figure 8 presents an existing capability plot for the forward windshield and forward canopy based on the birdstrike test results.

Based on test results of the existing T-38 stretched acrylic forward transparencies, the following conclusions can be reached:

(a) The 0.6 inch stretched acrylic forward windshield can withstand nominal four pound bird impacts at velocities ranging from about 320 knots at the horizontal/vertical center of the windshield to approximately 210 knots at the aft edge of the transparency. The specific critical velocity is impact location dependent.

(b) The 0.230 inch stretched acrylic forward canopy can withstand nominal four pound bird impacts at velocities ranging from about 165 knots at the centerline leading edge of the canopy to about 125 knots at a location along the centerline 14 inches aft of the leading edge. Again, the critical velocity is impact location dependent.

(c) The existing framework for the forward windshield and forward canopy was capable of withstanding the impact forces that the transparencies were subject to without catastrophic failure. The ability of the support structure to withstand significantly higher impact velocities could not be determined from this test series.

INSTRUCTOR'S WINDSHIELD DEVELOPMENT

An experimental investigation was conducted to investigate the feasibility of upgrading the T-38 instructor's windshield to provide birdstrike protection for the instructor pilot as an interim measure until a student canopy with upgraded birdstrike protection and TTC ejection capability becomes available. Structural modifications to maximize the birdstrike capability of the existing instructor's windshield/support structure were the result of an iterative approach which combined numerical analysis and developmental testing, each building on the results of the other. The initial analytical phase identified important criteria which affect and limit the overall capability; this included a stress analysis of various components of the windshield structure. The experimental phase of the instructor's

windshield program consisted of nineteen four-pound artificial bird impact tests conducted at UDRI and designed to evaluate the birdstrike capability of the structure. High-speed movies, strain gage data, and post-test observations were used to evaluate and analyze test results and determine what changes, if any, could be made to the structure to increase its capability. The test setup and impact locations are shown in Figure 9.

Projectiles used during the test program were nominally 4.0±0.1 pound artificial birds. All tests were end-on impacts with an artificial bird (right circular cylindrical shape) having a length (8-1/2 inches) of twice the diameter. The birds were made from a commercial grade gelatin with microballoons added in to obtain the proper density (0.0347 lb/in^3). Each shot was rated as a pass or fail depending on the damage incurred. Failure was defined as any damage that would result in probable pilot injury and/or prevent the aircraft from returning to base.

Examination of the test results on the existing T-38 instructor's windshield indicated a capability of about 125 knots. This was an expected result because the windshield and support structure were designed for wind loading only. Structural modifications developed to obtain 250 knot-no penetration capability were designed to fail in an acceptable mode prior to catastrophic failure of the original production structure and with a minimum of spalled structure, so as to maximize the crew and aircraft survivability in the event of a high speed bird impact on this transparency. This capability is twice the velocity (four times the energy) of the existing system.

Listed below are the key modifications of the bird resistant instructor's windshield transparency system.

- Energy Absorbing Rear Support Rods
  - Designed to utilize the support capability of the rear canopy.
- High Strength Shroud
  - Increases the support to the lower frame.
- Reinforcing Straps Between Shroud and Lower Frame
  - Controls twisting of the lower frame.
  - Reduces stress concentrations in the lower frame.
- Reinforcing Strips on Lower Frame
  - Distributes loads in lower frame.
- Circumferentially Bolted Transparency
  - Holds polycarbonate transparency in frame.
  - Distributes the impact energy throughout the frame.
- Reinforcing Caps on Side of Frame
  - Allows motion between transparency and frame.
  - Potted in RTV to reduce stress concentrations.
  - Designed to deform and absorb energy prior to failure.

- Transparency Retainer
  - Increases effective depth of channel.
  - Reduces edge related stress concentrations.
- Top Fore and Aft Transparency Reinforcements.
  - Provides rigid support to transparency in the plane of the transparency.
  - Designed to deform prior to failure (controlled failure).
  - Allows initial flexibility normal to the transparency (cushioning effect).

The hardware tested was designed to structurally modify the instructor's windshield so as to maximize the impact resistance while providing for an acceptable failure mode and a minimum of spalled structure. It was not intended to serve as flight hardware.

CONCLUSIONS

- Low level training missions and/or operating time at speeds above the existing T-38 crew enclosure damage threshold will result in flight safety risk to aircraft and crew. A demonstrated need exists for improved birdstrike protection.
- Increased capability to defeat a four pound bird impact at 400 knots is within the state of the art.
- Implementation can be by retrofit or attrition.
- The T-38 aircraft effectiveness/survivability will be enhanced by alternate T-38 transparencies.

RECOMMENDATIONS

For the forward (student) windshield, all the supporting parameters were carefully weighed and melded into a recommendation of the following windshield cross-section for full-scale hardware fabrication, testing, and evaluation.

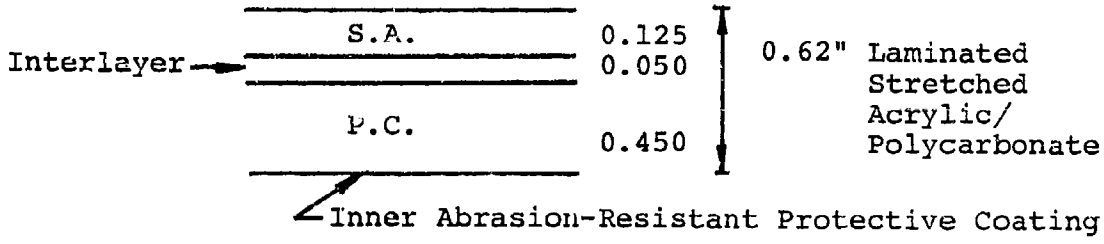

AFWAL/FIEA detail design drawing No. 19260107-01 has been prepared to support fabrication.

For the forward (student) canopy, incorporate a pyrotechnic fragmentation or comparable system into a birdstrike resistant transparency configuration to provide through-the-canopy ejection capability.

For the aft (instructor's) windshield, substitution of coated polycarbonate for the existing stretched acrylic panel and incorporation of modified support structure should be considered in combination with the improved forward windshield until development of an improved alternate forward canopy is successfully completed.

The Air Force is currently pursuing a program to further evaluate the above recommendations to determine the feasibility of a T-38 fleet retrofit.

ACKNOWLEDGEMENT

The studies described herein were performed under Contracts F33615-76-C-3103 and F33615-80-C-3401 with the Air Force Wright Aeronautical Laboratories (AFWAL/FIEA), Wright-Patterson Air Force Base, Ohio.

TABLE 1

T-38 BIRDSTRIKE PROBABILITY STUDY

VELOCITY DISTRIBUTION	BASELINE*	PREDICTED TRANSPARENCY PENETRATIONS FOR A 10 YEAR PERIOD		
		BASELINE + 3 LOW LEVEL MISSIONS/STUDENT	BASELINE + 6 LOW LEVEL MISSIONS/STUDENT	BASELINE + 9 LOW LEVEL MISSIONS/STUDENT
WINDSHIELD				
EXISTING CAPABILITY	1.6 (2.1)	2.0 (2.6)	2.5 (3.2)	3.2 (3.9)
NOMINAL 400 KT CAPABILITY	0.3	0.5	0.7	1.0
CANOPY				
EXISTING CAPABILITY	5.5 (4.6)	6.3 (5.3)	7.1 (6.0)	8.1 (6.9)
NOMINAL 300 KT CAPABILITY	0.6	0.8	1.0	1.3
NOMINAL 350 KT CAPABILITY	0.3	0.4	0.5	0.7
NOMINAL 400 KT CAPABILITY	0.1	0.2	0.3	0.4

*BASELINE FOR MODEL USES FLIGHT VELOCITY PROFILE ACTUALLY RECORDED IN 1967-72.

( ) BASED ON ACTUAL EXISTING CAPABILITY FROM FULL-SCALE BIRDSTRIKE TESTS

TABLE 2

SUMMARY OF T-38 BASELINE BIRDSTRIKE TESTING

Shot Number/ Date	Location	Velocity				Bird Weight		Kinetic Energy Ft-lb$_f$	Remarks
		Expected		Actual					
		Kts	Fps	Kts	Fps	Gms.	Lbs.		
632 6 Aug 79	1	210	355	208	351	1805	3.98	7614	First bird shot, existing W/S capability > 208 kts at shot Location 1.
633 7 Aug 79	1	250	422	236	400	1817	4.01	9963	Catastrophic failure velocity at Location 1 ≤ 236 kts.
634 9 Aug 79	5	110	186	112	189	1818	4.01	2224	First shot Location 5, no visible damage, bird orientation questionable.
635 10 Aug 79	5	145	245	146	246	1813	4.00	3759	Catastrophic failure at aft-bow frame.
636 13 Aug 79	4	85	144	84	142	1807	3.98	1246	First shot Location 4, no visible damage.
637 14 Aug 79	4	110	186	107	181	1818	4.01	2040	No visible damage except for surface abrasions.
638 15 Aug 79	4	135	228	130	220	1819	4.01	3014	Surface abrasions, no other visible damage.
639 16 Aug 79	4	155	263	154	260	1814	4.00	4199	Surface abrasion larger, failure had been expected.
640 17 Aug 79	4	180	304	178	300	1812	3.99	5576	Catastrophic failure at or near shot Location 5. Instructor's windshield cracked by bird debris.
641 22 Aug 79	2	190	321	191	322	1834	4.04	6506	First shot Location 2. Windshield bruised, gap changed.
642 23 Aug 79	2	230	388	224	378	1880	4.01	8897	Catastrophic failure, bird and windshield debris in cockpit. Module canted 15° to right for remaining shots.
643 24 Aug 79	6	110	186	105	177	1825	4.02	1956	Surface abrasions but no visible damage to angle nodes.
644 27 Aug 79	6	145	245	141	238	1818	4.01	3527	Canopy failed with cracking radiating into hinge area but no actual failure of any nodes; acrylic broken out from impact location back to frame.
645 29 Aug 79	3	200	338	200	338	1812	3.99	7078	No failure, bird remains in frame gap but not cockpit.
646 29 Aug 79	3	250	422	247	417	1811	3.99	10774	Catastrophic failure with all acrylic going inside fiberglass edge. Attachment broken as was part of ramp in area of failure.

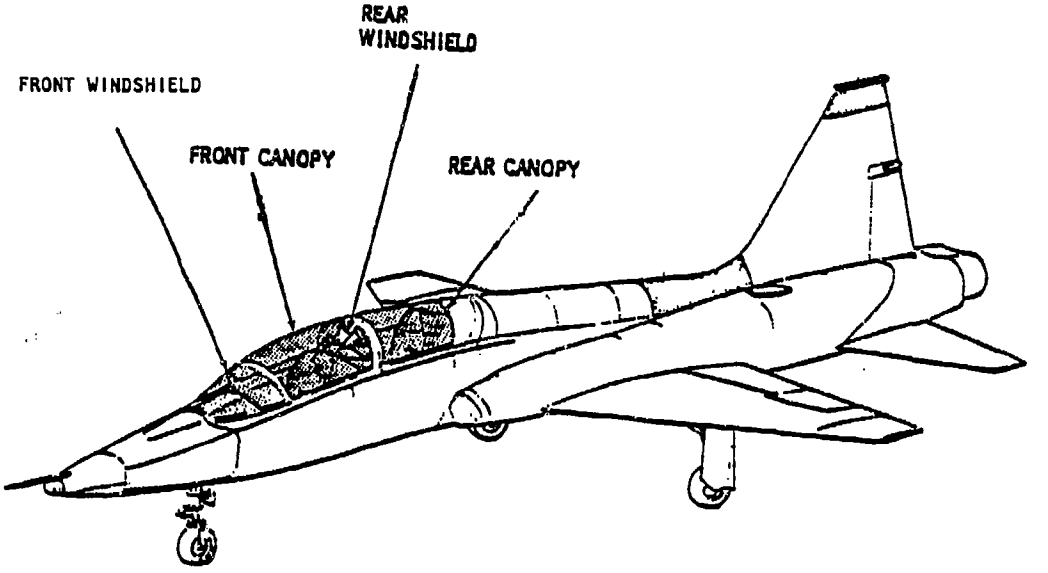

Figure 1. T-38 Crew Enclosure.

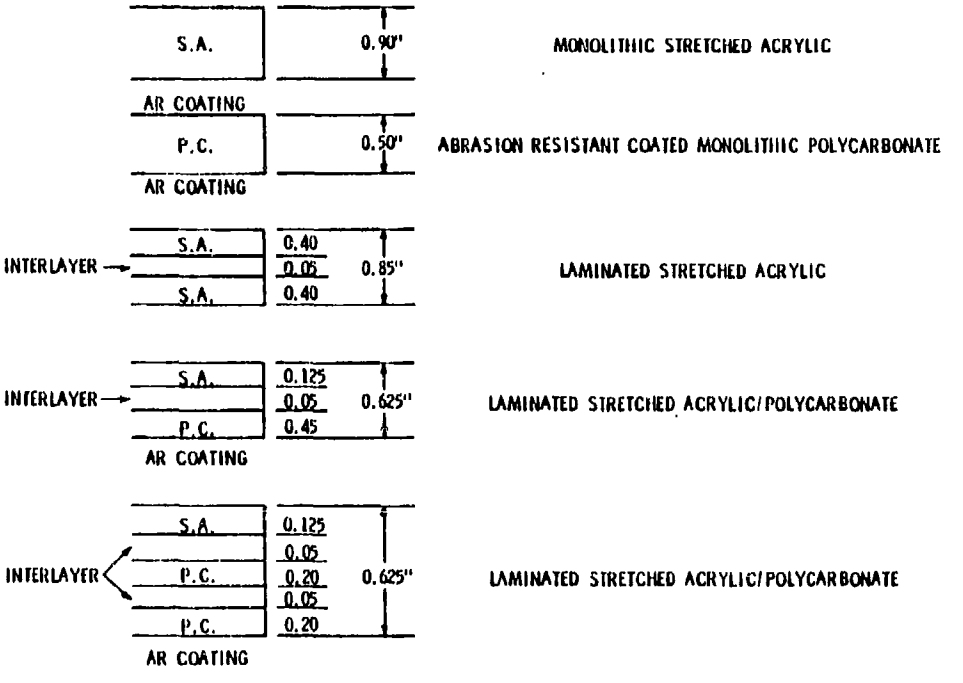

Figure 2. Selected Windshield Candidate Configurations.

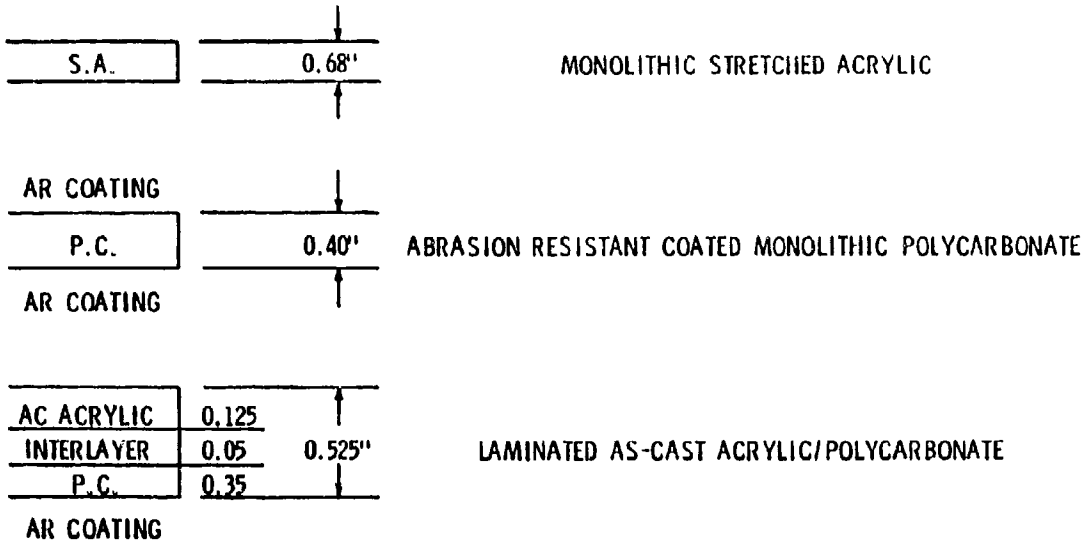

Figure 3. Selected Canopy Candidate Configurations.

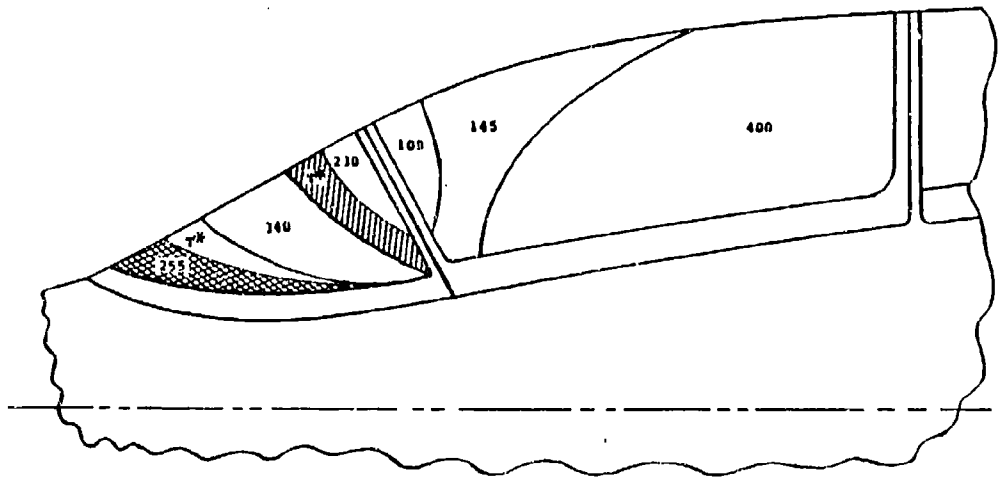

Figure 4. Estimated T-38 Existing Transparency Capability.

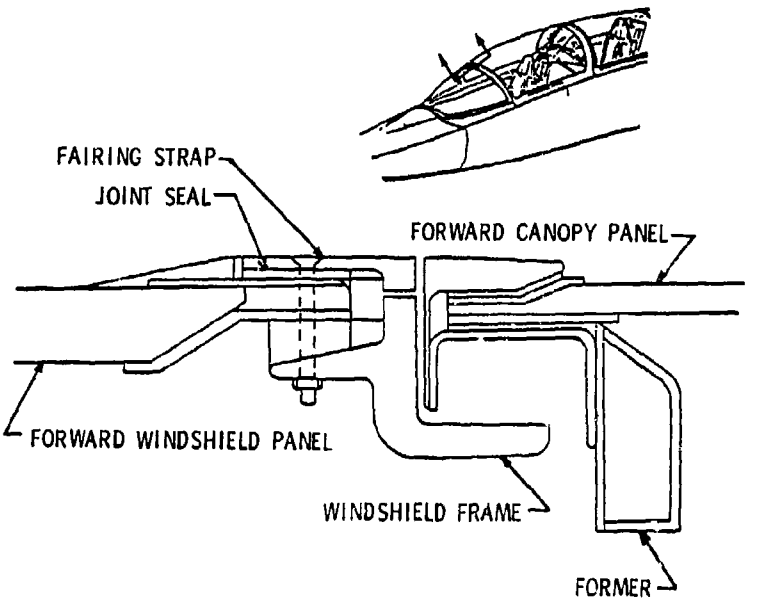

Figure 5. Canted Fuselage Station 184.35 Support Structure.

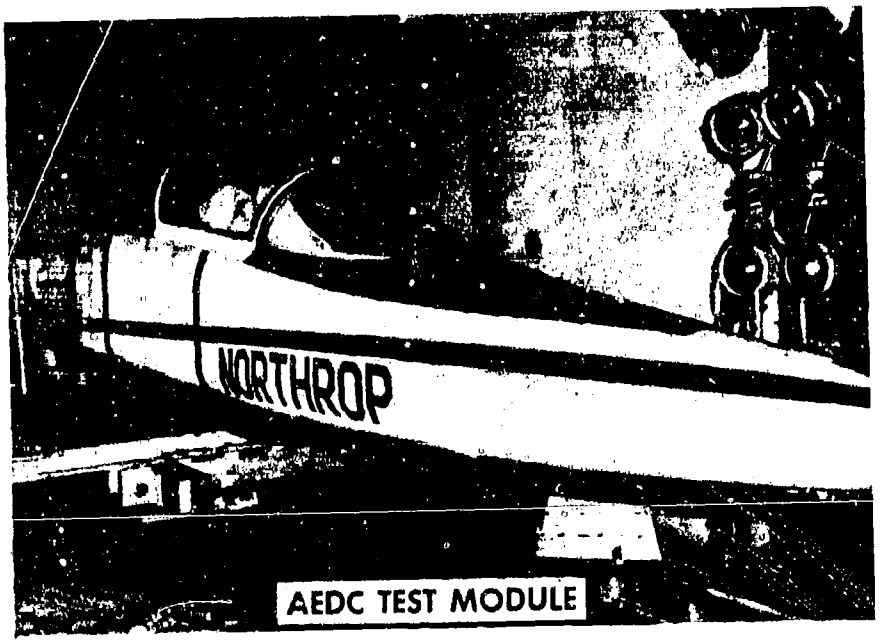

Figure 6. Test Module Installed at Arnold Engineering Development Center Test Facility.

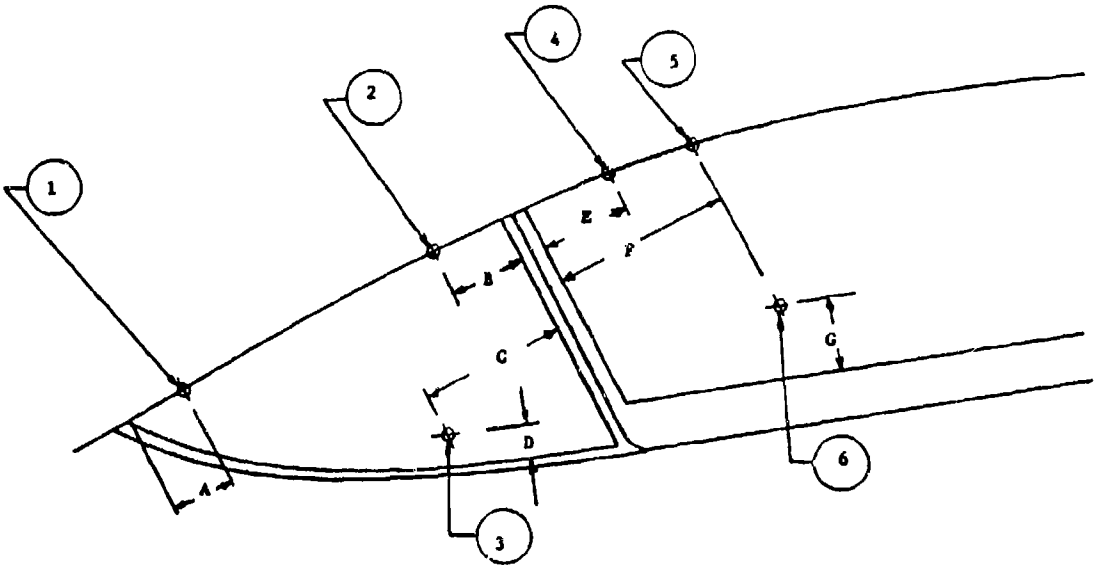

Notes: (1) Impact points 1, 2, 4, and 5 on fuselage centerline
(2) All dimensions in inches, as measured along transparency surface.

A - 6.125
B - 6.25
C - 9.875
D - 3.00
E - 7.00
F -12.55
G - 6.00

Figure 7. Bird Impact Test Locations.

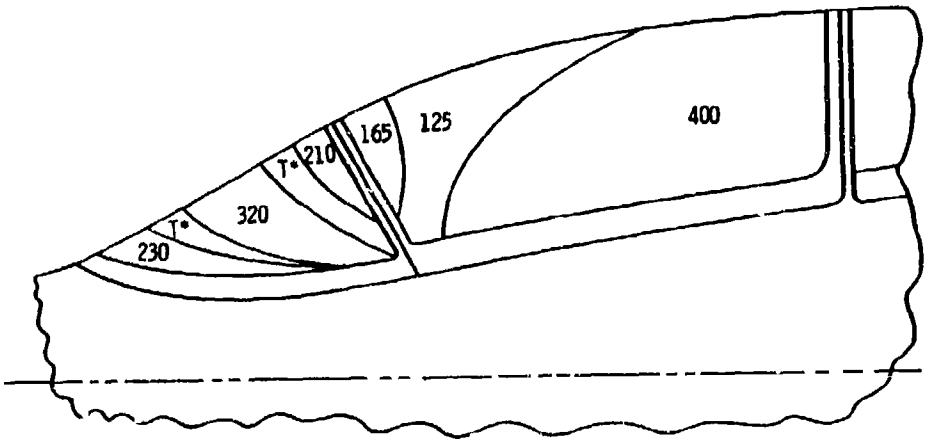

*TRANSITION ZONE

IMPACT VELOCITY IN KNOTS

Figure 8. Existing Transparency Capability.

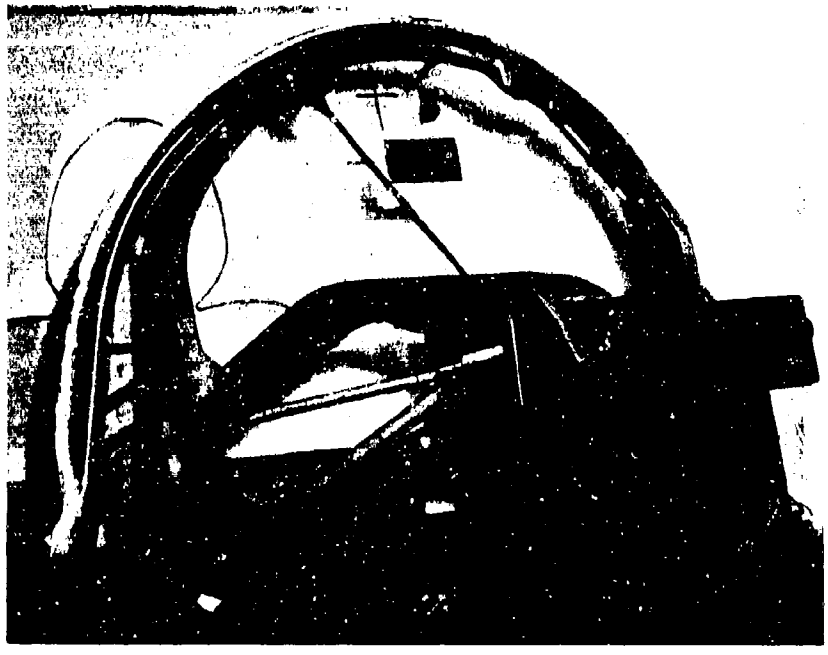

Figure 9. Instructor Windshield Frame-Tixture Test Setup.

AD-P003 220

A TRIANGULATION TECHNIQUE FOR OBTAINING DEFLECTIONS OF AIRCRAFT TRANSPARENCIES DURING BIRD IMPACT TESTING

W. R. Pinnell and 2 Lt. D. A. Crocker,
Flight Dynamics Laboratory

A TRIANGULATION TECHNIQUE FOR OBTAINING DEFLECTIONS OF AIRCRAFT TRANSPARENCIES DURING BIRD IMPACT TESTING

a paper prepared by

William R. Pinnell
and
2Lt Dale A. Crocker

Air Force Wright Aeronautical Laboratories

AFWAL/FIE

Wright-Patterson Air Force Base, Ohio 45433

for presentation at the

Conference on Aerospace Transparent Materials and Enclosures

11-14 July 1983

Phoenix, Arizona

SUMMARY

A technique for determining a time history for the displacement in space of points on the inside surface of an aircraft transparency during and after the simulated impact of a bird has been developed. This method utilizes two high speed motion picture cameras located in a three dimensional space which also contains designated points on the transparency surface. The cameras are positioned so that a common field of view contains points for which deflection history is required. Displacements of the images of given points in the film frames from each camera are used to obtain positions in a three dimensional space. All optical magnifications and changes in point to camera distances are accounted for.

In addition to obtaining deflection data for selected points, the films are also useful for describing the footprint of the bird on the transparency, an important improvement in the ability to model bird loading in computerized dynamic analysis efforts.

As an example of the application of this process, data resulting from a bird impact on a T-38 windshield is included.

BACKGROUND

An important facet of the efforts to develop bird impact resistant aircraft transparencies is bird impact testing. This testing normally includes subjecting a candidate windshield or canopy to the impact of a bird or simulated bird which has been accelerated to a predetermined speed by some catapulting device (usually a compressed gas gun). The most obvious result of such testing is "did the transparency fail." Often this "pass/fail" assessment is the entire test result. Since test items and test facilities are costly in terms of dollars, manpower, and time, the motivation to develop analytical models and performance prediction techniques exist. Development of the desired analytical tools demands measurement of quantitative data describing the performance of the test item. Among those data are time histories of stress, position of the bird relative to the transparency, and deflection.

Obtaining a time history of the deflection of points on the transparency is the subject of this paper. In analytical models, strain and deflection are meaningful parameters for comparison of test results and analytical predictions. Strain in transparency materials (specifically polycarbonate) can be difficult to measure due to large deformations and in some cases degradation of material properties by adhesives needed to install strain measuring devices.

In addition to input for development of analytical models and tools, deflection data measured during simulated bird impact testing has some direct applications. Among these are contact of the inside surface with items in the cockpit which might include HUD (head up display) or other hardware and the pilot's head. Deflection of forward transparencies with respect to adjacent down stream transparency frames and edges can be critical when preventing entry of the bird debris into the cockpit. An example of this is the T-38 forward windshield/forward canopy juncture. An impact on the windshield can cause deflection of the windshield aft arch to a low position relative to the forward canopy arch forming an entry path (scoop) for bird material. In these instances measurement of deflection during testing may produce the data upon which the successful performance of test items is determined.

Prior to development of the triangulation technique, a method for obtaining deflection histories utilizing Moire' fringes had been developed under an Air Force contract by the University of Dayton Research Institute (References 1 and 2). This Moire' fringe technique is effective only when the transparency is made opaque to the extent that the bird cannot be observed from inside the transparency. Since making the transparency opaque also prohibits good observation of the initiation of failure points and propagation of cracks, the Moire' fringe technique is limited in practicality.

DESCRIPTION OF PROBLEM

The problem of obtaining time histories for selected points on a transparency during simulated bird impact tests includes the following considerations:

Accuracy - Total deflection from initial position of a given point should be within .1 inches for a total 2 inch deflection.

Retention of View Through Transparency - Deflection measuring technique and hardware should not preclude viewing failure origins and crack propagation, and the position of the bird relative to the transparency for the duration of bird contact.

Reliability - Deflection measuring hardware and operation should be reliable without being expensive.

Hardware - The technique should not require unusual or special hardware and development time should be minimal.

Surface Contact - The vulnerability of polycarbonate transparency material to surface damage does not tolerate physical contact between the transparency surface and deflection measuring devices.

Distortion - The technique for obtaining deflection shall not depend on optical viewing through the transparency.

APPROACH

In order to avoid hardware contacting transparency surfaces, a photographic or optical approach was adopted. Location of points moving in space is commonly achieved by photo theodolite systems through geometrically solving triangles formed by the point in a three dimensional space, and location of two (or more) cameras in that space. For the desired system to produce deflections, it is necessary to mark points on the transparency which are in the field of view of two high speed motion picture cameras which run simultaneously and for which some method of synchronizing film frames is available. Positions of a specific point in projections of film frames which were simultaneously exposed must be measured. From this frame position a set of parameters which describe (in a 3 dimensional space) the line of sight from the camera reference point to the specific point on the transparency can be obtained. Parameter sets for each camera include azimuth and elevation angles as described in Figure 1. To obtain these angles from linear positions in the projected film frames, it is necessary to account for magnification due to all lens elements. Calibration of each camera/lens combination is required to obtain distance/magnification functions which can be used to account for magnification due to all optical elements in the camera, lens, and projection equipment. Using the calibration functions, the linear position of specific points in projected film frames (i.e distances from the projected frame center) and an estimated distance from the point to the camera, the azimuth and elevation angles can be calculated.

ANALTYICAL SOLUTION

The method used to obtain the desired deflection involves determining the location of specific points on the transparency in a three dimensional space at time intervals during the bird impact test. Deflections then are computed as arithmetic and vector sums of changes in space position.

To determine the position of points in space, the principles of photothedolite tracking systems commonly used on test ranges are applied. The system basically consists of two high speed motion picture cameras which view the points on the transparency simultaneously. The position of both cameras and the pre-impact position of points on the transparency must be known. From projected film frames which were exposed simultaneously by the two cameras, positions of the transparency points in the projected frames are measured. From these measurements, direction angles for the line of sight from a given camera to specific points can be calculated. These angles and the point in space for the camera location determine a line of sight for each camera to a specific point. The intersection coordinates for these two lines of sight is the position of the point for the time which corresponds to the film frames used to establish angles. Figure 1 depicts the angles, lines of sight, and a representative relative position of the cameras and a transparency point. The technique for solving for the coordinates of the transparency point utilizing the angles and known camera positions is referred to as the "triangulation" method.

3D Space - A three dimensional space must be established at the test facility within which coordinates for each of the cameras and each of the pre-impact transparency points can be measured. This has been accomplished by establishing an origin on the test facility floor with the Y axis parallel to the aircraft fuselage longitudinal axis, a right hand coordinate system would usually be used with the Z axis positive upward. Azimuth and elevation angles are then defined in this space as shown in Figure 1.

Determination of Azimuth and Elevation Angles - On the projected image of film frames exposed simultaneously, measurements from the center of the projection to the image of the transparency points are made. Figure 2 represents a typical film frame projection and shows the dimensions to be measured. Since the pre-impact coordinates for transparency points are known, the initial values for azimuth and elevation angles can be computed. The pre-impact distance from the camera reference point to points on the transparency can also be computed and is used to account for camera/lens/projection magnification as discussed below.

Magnification and Camera Calibration - In order to account for magnification of cameras, lenses, and projection equipment in processing the frame position measurements of Figure 2 for obtaining azimuth and elevation angles, it was necessary to expose a calibration film for each camera/lens combination. Calibration films include exposed frames at varying distances from a target grid board (½ inch square grid). The range of distances to the target grid board was chosen to include the distances from cameras to points on the transparency. Magnification factors as a function of distance to the target grid were determined using projection equipment to be utilized in obtaining

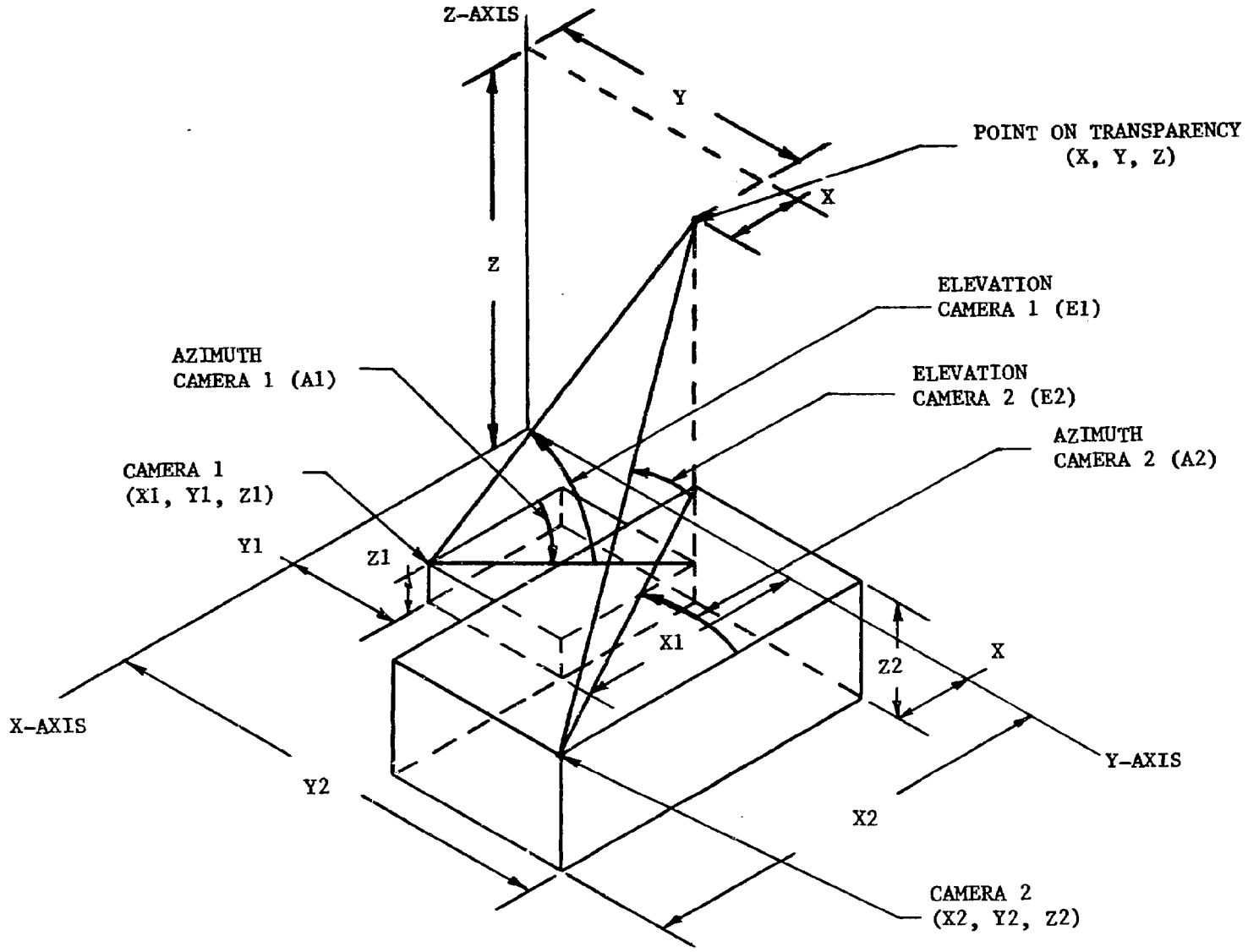

FIGURE 1 TRIANGULATION SYSTEM GEOMETRY

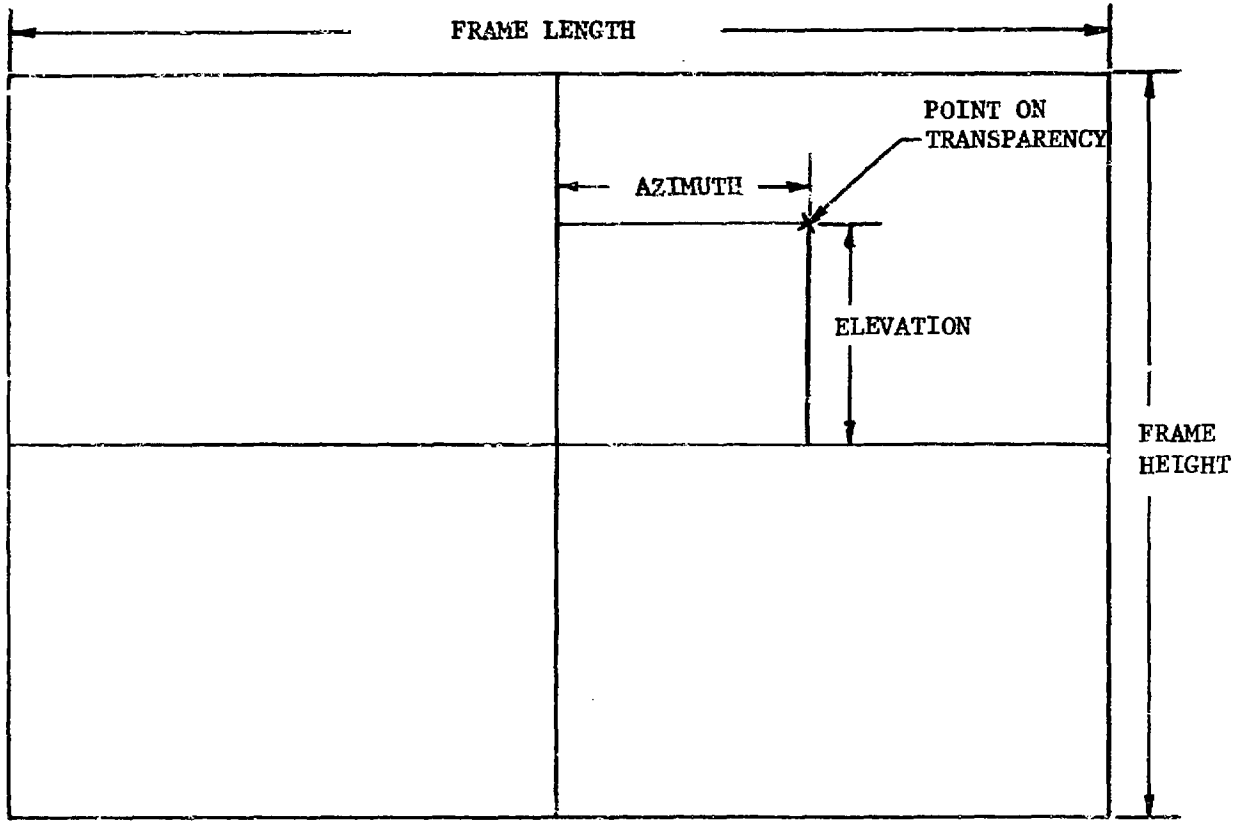

FIGURE 2: TYPICAL PROJECTED FRAME SHOWING POINT POSITION MEASUREMENTS

point frame position measurements. Projected frame size was recorded during camera calibration efforts and this frame size used for obtaining point frame position measurements. For each camera/lens combination, values of magnification factor and distances to the grid were used to fit a function for magnification factor in terms of distance. From these functions, magnification factors for point frame position measurements are calculated for distances from the cameras to transparency points. These calibration functions are usually linear.

Analytical Solution - The pre-impact geometry with known coordinates for camera reference points and points on the transparency can be utilized to calculate distances from the cameras to the points. For a given point the pre-impact distance is used to obtain the initial value of magnification factor from the proper calibration function. Raw point frame position measurements (see Figure 2) are then multiplied by this factor to obtain actual dimensions of the transparency point from the lens centerline (also the center of the projected frame). These actual dimensions are combined with the pre-impact distance (camera to point) to obtain the pre-impact azimuth and elevation angles of Figure 1. After establishing the pre-impact distances, the process progresses to the next set of simultaneous film frames. New point frame positions are measured, the pre-impact magnification factors are applied, and azimuth and elevation angles are calculated for the first post impact frame. The coordinates for points in space are then calculated using relationships discussed in the next paragraph. Algebraic differences between pre-impact point coordinates and the coordinates calculated for the first frame are three components of the deflection vector from the pre-impact to the first frame point position in space. Knowing the camera frame rates permits calculating a time relative to the initial bird contact. The process is repeated resulting in deflection vector components which are accumulated as the process marches from frame to frame with magnitude of the vector sum of accumulated components being the total deflection for given frame times.

Analytical Relationships - Simple Pythagorean relationships and known quantities are used to calculate the pre-impact distances and azimuth and elevation angles are computed from simple trig function and the geometry represented in Figure 1.

To obtain values for X, Y, and Z coordinates for a specific point and frame pair (time), relationship for the known angles in terms of known camera coordinates and coordinates of the point are as follows (refer to Figure 1).

$$TAN(A1) = \frac{Y-Y1}{X1-X} \qquad EQN(1)$$

$$TAN(E1) = \frac{Z-Z1}{\sqrt{(X1-X)^2+(Y-Y1)^2}} \qquad EQN(2)$$

$$TAN(A2) = \frac{Y2 - Y}{X2 - X} \qquad EQN(3)$$

$$TAN(E2) = \frac{Z - Z2}{\sqrt{(X2-X)^2 + (Y2-Y)^2}} \qquad EQN(4)$$

Rewriting EQN(1) and EQN(2) yields:

$$X = X1 - \frac{Y - Y1}{TAN(A1)} \qquad EQN(5)$$

and $$Z = TAN(E1)\left[\sqrt{(X1-X)^2 + (Y-Y1)^2}\right] + Z1 \qquad EQN(6)$$

Similarily for EQN(3) and EQN(4)

$$X = X2 - \frac{Y2 - Y}{TAN(A2)} \qquad EQN(7)$$

and $$Z = TAN(E2)\left[\sqrt{(X2-X)^2 + (Y2-Y)^2}\right] + Z2 \qquad EQN(8)$$

Y can now be solved for by the following sequence:

Substitute EQN(7) RHS into EQN(8) for X generating EQN(9) which is an expression for Z in terms of Y.

Substitute EQN(5) RHS into EQN(6) for X generating EQN(10) which is a second expression for Z in terms of Y.

Equate EQN(9) and EQN(10) and solve for Y in terms of known parameters (equations 9 and 10 not shown in text):

$$Y = \frac{Y2(TAN(E2))J2 + Y1(TAN(E1))J1 - Z1 + Z2}{TAN(E2)J2 + TAN(E1)J1} \quad EQN(11)$$

where

$$J1 = \left[\frac{1}{(TAN(A1))^2} + 1\right]^{1/2} \qquad J2 = \left[\frac{1}{(TAN(A2))^2} + 1\right]^{1/2}$$

After utilizing EQN(11) to calculate values for Y, these values can be substituted into EQN(5) or EQN(7) to obtain values for X and into EQN(6) or EQN(8) to obtain values for Z.

REQUIRED HARDWARE

In order to utilize the triangualtion technique the following items are required.

1. Two High Speed Cameras - Motion picture cameras equipped with timing lights which enable determination of actual frame rates are required. For bird impact speeds from 200 to 400 knots a 5,000 frames per second nominal frame rate has been used successfully. Matching of simultaneous frames can be effected best if timing lights for both cameras are triggered by a common signal, but this has been unnecessary in applications to date. When actual frame rates vary significantly, the effects of simultaneity can be obtained by developing time/frame position relationships for one of the cameras.

2. Camera Lenses - Lenses for cameras should be selected to yield the largest image compatible with the desired field of view. The lenses should be reasonably free of distortion to make calibration functions simple.

3. Lighting - Normal lighting for the film, lens, frame rate, and camera is adequate.

4. Camera Mounts - When the transparency is supported on a fuselage section and points are located on the section and inside surface, space for cameras and mounts can be limited and special camera mounts may be necessary. Fabrication of special mounts may not be necessary if viewing ports can be cut in the fuselage permitting external camera mounting.

5. Projection Equipment - When special film reading equipment is not available, a common stop frame motion picture projector is adequate. Selection of projector lenses is relatively unimportant since projection distance can easily be changed to satisfy the requirement to keep the projected frame size constant. Automated and semi-automated film reading equipment is applicable.

6. Point Marking - Point position on the projected film frames are more readily and more accurately read if the locations are marked with high contrast to background and in some cases if the marks are three dimensional. An arrangement utilizing graphics tape grids with small (1/16 to 1/8 inch diameter) styrofoam spheres (obtained by crumbling styrofoam blocks) attached to tape intersections has been used on transparency surfaces. All adhesives should be checked for detrimental effects to transparent materials.

SAMPLE RESULTS

Deflection time data has been obtained by the triangulation method for bird impact tests on F-4 and T-38 windshields. Data presented here to illustrate results of the technique are from a 200 knot impact of a four pound bird on a .6 inch monolithic polycarbonate windshield for the T-38. The six points for which deflection data were obtained are on the centerline and the inside surface of the polycarbonate transparent panel. The test set-up for this test is shown in Figure 3. The tape grid affixed to the windshield as seen in Figure 3 was chosen to match elements of a finite element analysis design tool under development at the time of the test. The points analized were located on the centerline at intersections of the tape grid as indicated in Figure 4. Point number three is the intersection of the nominal bird path and the inside transparency surface. Figure 4 shows the pre-impact and maximum deflection position of the inside surface.

An indication of the time deflection history for each of the six points can be seen in Figure 5 where lines are drawn through the deflections of points corresponding to the indicated sequential film frames (times). Frame number one was the frame where the bird first contacted the windshield and for this test frame number 20 represents the time of maximum deflection for each of the points considered. Frames subsequent to frame 20 would depict the rebound of the transparency. Table 1 is a listing of the deflections for the points shown in Figure 4. The values in Table 1 and those values plotted

FIGURE 3: T-38 WINDSHIELD BIRD IMPACT TEST ARRANGEMENT

FIGURE 4: PRE IMPACT AND MAXIMUM DEFLECTION OF T-38 W/S

(4 LB BIRD, 200 KNOT TEST OCT 82)

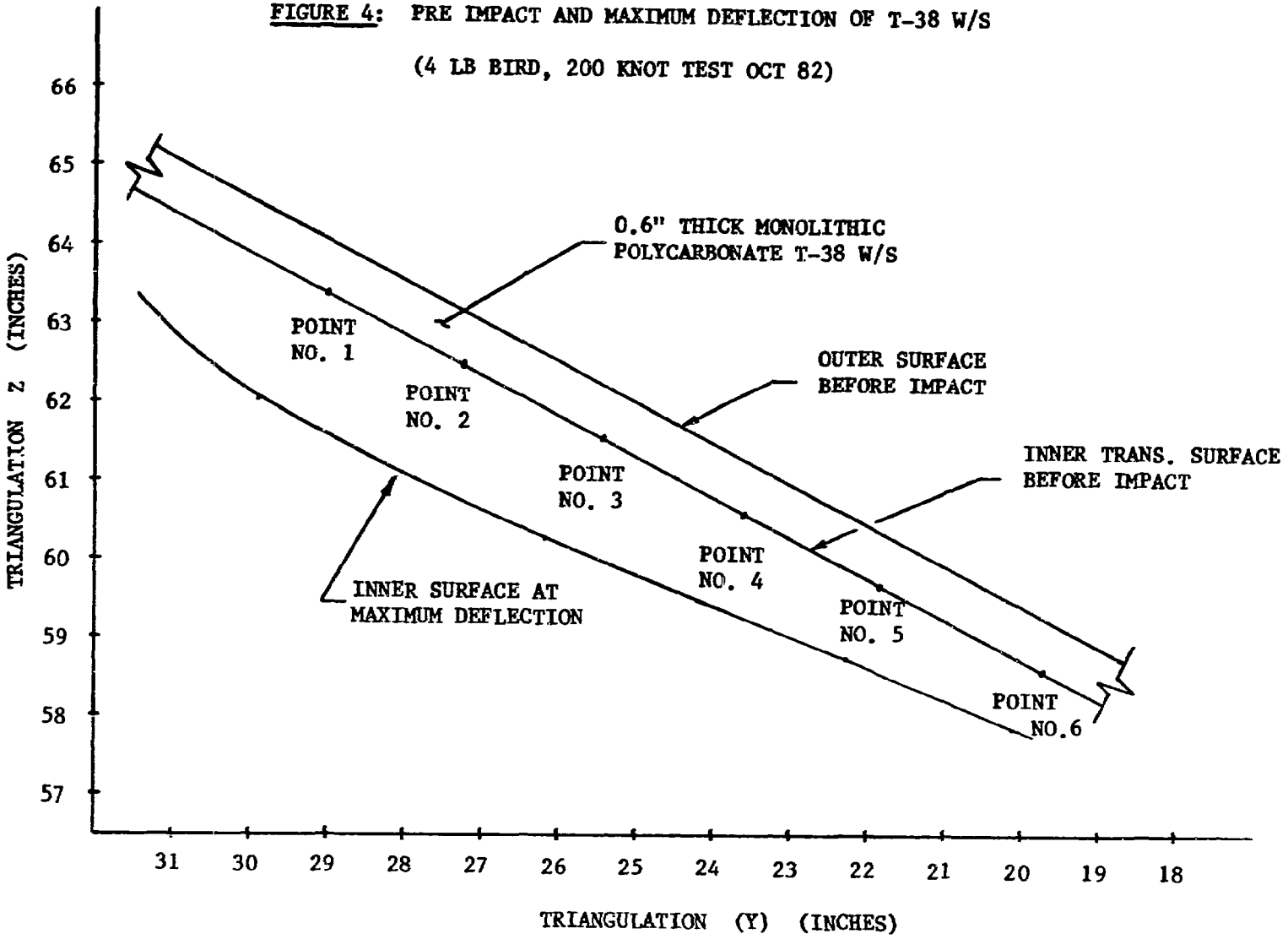

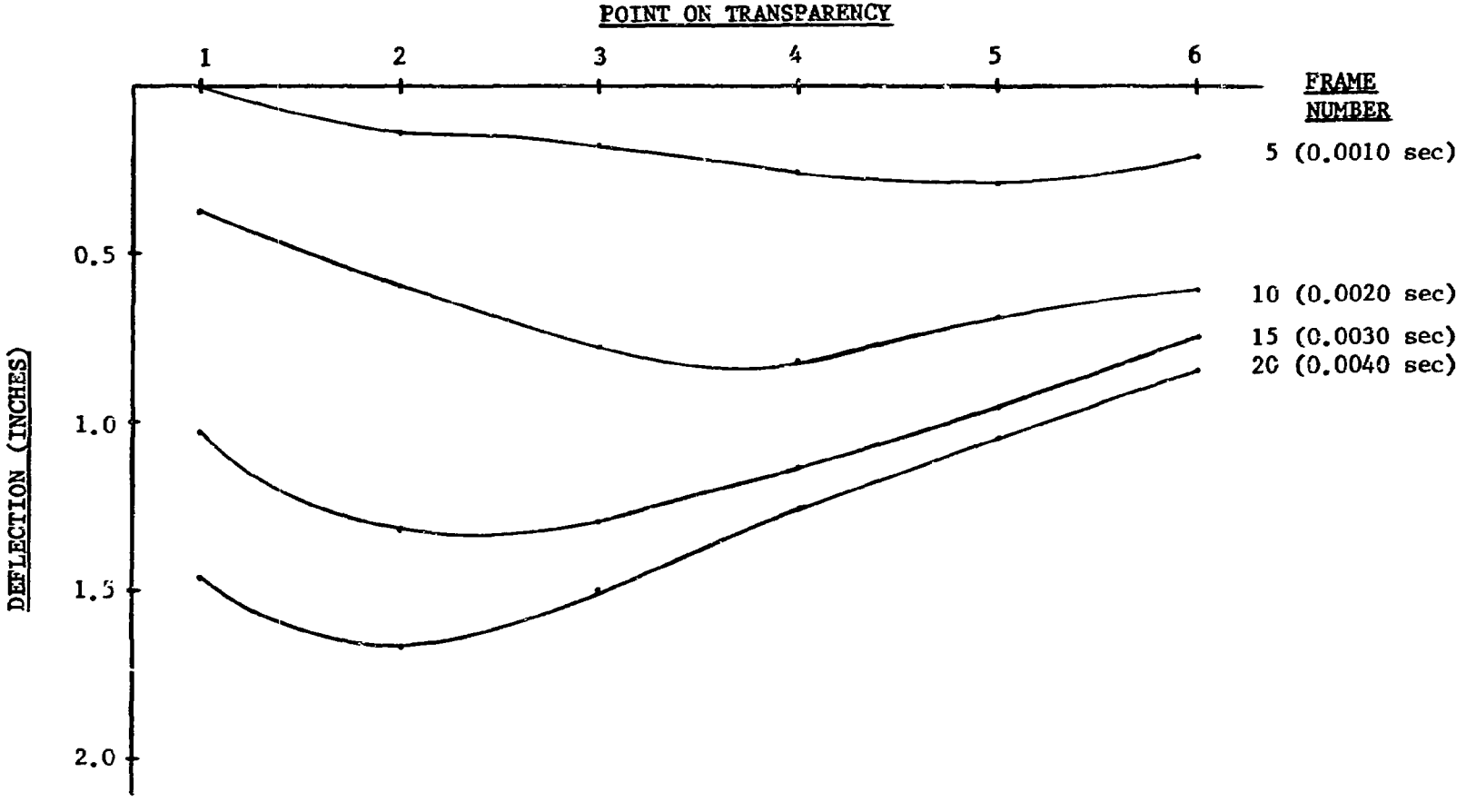

FIGURE 5: DEFLECTION TIME HISTORY FOR POINTS ON A T-38 WINDSHIELD

NOTE: DATA IS FOR 0.6" THICK MONOLITHIC POLYCARBONATE
4 lb BIRD, 200 KNOT TEST

FRAME NUMBER	POINT 1	POINT 2	POINT 3	POINT 4	POINT 5	POINT 6
1	0	0	0	0	0	0
2	0	0	0	0	0	0
3	0	0	0.004	0.054	0.050	0.039
4	0.004	0.002	0.014	0.152	0.220	0.156
5	0	0.128	0.168	0.256	0.290	0.207
6	0.051	0.153	0.295	0.396	0.451	0.332
7	0.167	0.277	0.455	0.544	0.511	0.421
8	0.200	0.352	0.539	0.641	0.565	0.465
9	0.254	0.464	0.676	0.708	0.625	0.555
10	0.370	0.593	0.779	0.811	0.692	0.601
11	0.539	0.802	0.910	0.928	0.758	0.707
12	0.716	0.966	1.047	1.046	0.860	0.738
13	0.835	1.082	1.150	1.090	0.860	0.755
14	0.918	1.162	1.200	1.107	0.916	0.722
15	1.026	1.308	1.248	1.128	0.949	0.741
16	1.154	1.403	1.367	1.138	0.971	0.787
17	1.262	1.481	1.431	1.163	0.971	0.787
18	1.337	1.551	1.440	1.192	0.978	0.777
19	1.428	1.624	1.472	1.244	1.035	0.822
20	1.461	1.655	1.499	1.258	1.044	0.832

TABLE 1: Vector Sums of Deflection of Points on a 0.6 inch Thick Polycarbonate T-38 Windshield

NOTE: Data for 4 lb Bird, 200 Knot Test
Deflections in inches

in Figure 5 are accumulations of vector sums of deflections computed from one frame to the next. Y and Z coordinates of the maximum deflection position are illustrated in Figure 4.

CONCLUSIONS AND RECOMMENDATIONS

The triangulation method can be used to obtain deflection time histories for points located on the inside surface of aircraft transparencies during bird impact testing.

Transparency behavior and the position of the bird with respect to the transparency can be observed on triangulation camera films.

It is recommended that camera installations and transparency point indicators be considered for any bird impact test where deflection is of interest. Since these films are also useful for observation of the transparency behavior, additional costs may be minimal. Post test decisions can be made concerning which tests and which points should be the subject of triangulation analysis.

In many cases the deflection (specifically maximum deflection) should be considered as a prime parameter for pass/fail determinations. When the inside surfaces are in close proximity to cockpit equipment or the pilot's head, or when deflection of a forward transparency frame creates a gap through which bird carcass material can pass, deflection may be the most important pass/fail criteria.

It is recommended that deflection time histories be utilized with measured strain data as input to and validation of design and analysis tools for transparencies and transparency frames.

REFERENCES

1. Andrew J. Piekutowski, A Device to Determine the Out-of-Plane Displacement of a Surface Using a Moire Fringe Technique, AFWAL-TR-81-3005, March 1981.

2. Andrew J. Piekutowski, Measurement of Out-of Plane Displacements, AFWAL-TR-81-3006, March 1981.

SESSION VI

UNDERSTANDING CURRENT SYSTEMS (PART I)

Chairman: G. W. Underwood
British Aerospace
Aircraft Group
Surrey, England

Co-Chairman: M. R. Pollock
Boeing Commercial
Airplane Company
Seattle, Washington

AD-P003 221

VISUAL EFFECTS OF F-16 CANOPY/HUD INTEGRATION

Lt. Col. L. V. Genco,
Air Force Aerospace
Medical Research Laboratory

VISUAL EFFECTS OF F-16 CANOPY/HUD INTEGRATION

Lt Col Louis V. Genco
Air Force Aerospace Medical Research Laboratory
Human Engineering Division
Wright-Patterson AFB, OH 45433

ABSTRACT

Future fighter aircraft will be fitted with Wide Field of View Head Up Displays (WFOV HUDs), and probably, curved windscreens. Initial flight tests with a WFOV LANTIRN HUD in an F-16 fighter resulted in test pilots complaining of several visually related problems. One of the complaints was of double vision -- either two aiming symbols or two targets were seen when the pilot kept both eyes open. Other complaints included those of blurred images and a change in depth perception when looking through the HUD-canopy combination.

This paper is a report of some of the work done by the Air Force Aerospace Medical Research Laboratory in an attempt to determine both the source of the problem and possible solutions. After a series of laboratory and field tests, some problems were found to be due to excessive retinal disparity or parallax error between the two eyes, induced by a difference in collimation or angular deviation between light from the target and light from the HUD. The angular difference between the parallel lightrays from the CRT and the divergent light rays passing through the canopy and combining glass was sufficient to "split" the images in the visual system.

Recommendations are given for the maximum parallax error tolerated by the human visual system in a WFOV HUD - canopy combination. A companion paper by H. Lee Task, Ph.D., describes more of the optical background and measurements.

INTRODUCTION

Over the last several years, aircraft avionics systems and the addition of so-called "smart" weapons have made impressive advances in the areas of accuracy and lethality. Future weapons targeting and guidance systems include automatic target designators and "fire and forget" missiles which are intended to reduce the pilot's reliance on his eyes as a detecting and sighting mechanism. However, although some targets may be acquired at extreme distances with advanced sensor technology, there are occasions in which USAF fighter pilots would prefer to release their weapons after the target is visually

identified. For this case, and for the majority of occasions when the aircraft is not equipped with "smart" weapons, the pilot's eyes serve as the tracking and sighting sensors.

Because of this reliance on the human visual system to detect and interpret data from outside the cockpit, newer aircraft are equipped with Head Up Displays (HUDs) which allow the pilot to monitor critical flight data without moving his eyes from the outside world. A HUD can be thought of as a CRT or TV tube associated with a collimating lens and a beamsplitter. Data generated by sensors and computers in the aircraft appear as alphanumerics and graphics on the face of the tube. Light from the display is then collimated. The parallel light rays from the collimator are reflected from a partially silvered mirror called a combining glass. The resultant image appears as if it came from a point located in front of the pilot's eyes at a distance corresponding to optical infinity. This is a virtual image; i.e., no light actually comes from the image -- it just appears to do so because of the optics of the system. Figure #1 shows the basic optical train of a HUD. This Figure also shows how the canopy only affects light from the target, while the combiner can affect light from both the target and the C.R.T.

The angular field of view of the HUD-generated imagery is limited by the size and distance of thecollimating optics. A common anology is a knothole in a fence. What you can see through the knothole is limited by the size of the knothole and your distance from it. What you can see at any one time without moving your head is called the "instantaneous field of view" (IFOV). If you move your head around, you can see more of what is on the other side of the fence; this is called the "total field of view" (TFOV). Since our two eyes are located a little distance apart, they each see a little different area through the knothole. Each eye has a monocular (one-eyed) field of view, and the overlapping monocular fields of view form the overlapping or binocular (two-eyed) field of view (BFOV). Figure #2 shows the knothole effect and defines the various fields of view.

The HUD instantaneous field of view (IFOV) can be enlarged considerably by introducing optical power in the combiner (as in the LANTIRN HUD using diffraction optics). As the IFOV is enlarged, so is the BFOV. This means the images generated by the CRT occupy a wider area of our normal visual field, and both eyes are used more of the time to see the images generated by the CRT.

THE PROBLEM

F-16 test pilots flying the LANTIRN HUD complained of several visual problems, including double vision, blurred images and depth perception problems. The significance of these problems was so great that both the F-16 SPO and the LANTIRN SPO independently asked AFAMRL for support in determining the cause and possible solutions to this difficulty. The complaints detrimentally impacted both near and far term plans for usage of the F-16 as an all-weather fighter, and appeared to denegate the purported advantages of the LANTIRN HUD. Similar problems were reported in 1977 with other aircraft HUDs.

Because of these and other complaints, a LANTIRN HUD Independent Review Team was organized at the reqest of Lt Gen McMullen (Commander of Aeronautical Systems Division), and Brig Gen Monahan (Commander of the F-16 SPO). The team was initiated on 17 November 1982, with Dr. J.C. Halpin (ASD/ENE) as chairman. Team members were representatives of ASD/EN, AFWAL/FI and /AA, AFAMRL, and TACSO. The team's charter was to study the technical bases of HUD operation as well as the optical and visual requirements imposed by the mission of the F-16. The ability of each of the three (LANTIRN, AFTI and standard) HUDs to meet these requirements was then to be analyzed.

BACKGROUND INFORMATION

The LANTIRN WFOV HUD presently being built for F-16 aircraft produces a 28 degree wide IFOV, and a 20 degree wide BFOV. The standard F-16 HUD has a 14 degree wide IFOV and a four degree BFOV. (See Figure #3 for a diagram of the fields of view for various F-16 HUDs). Since the IFOV and BFOV are so large in the LANTIRN HUD, minor head motion does not move the eyes out of the BFOV as happens with the standard HUD. Also, the angular size of the LANTIRN combiner is larger than that found with the standard HUD, so the pilot is unable to look around the sides of the combiner to view targets through the canopy alone. All this means that during flight, the pilot is required to look through both the LANTIRN HUD combiner and forward portion of the canopy to perform many visual tasks. Also, any problems which affect both eyes together (rather than one eye at a time) would be more noticeable with a LANTIRN HUD because of its very large instantaneous BFOV. Both eyes are in use for a much larger area or field of view in the LANTIRN HUD than in any other HUD. The small BFOVs in most other HUDs induce monocular rather than binocular vision.

There are several critical differences between monocular and binocular vision. Only one will be described here; the concept of "corresponding points." Normally, when looking at the world around us, each of our eyes sees things within a field of view roughly 60 degrees up, down, and toward the nose, and 90 degrees toward our temple. Each eye's monocular field of view overlaps with the other eye, so roughly 60 degrees of our central vision are seen with both eyes. Even though we have two eyes, and the image on each eye's retina is slightly different, we usually perceive only one "picture" of this overlapping area because our brain integrates the two retinal images.

Each retina has a tiny area where vision is the sharpest, called the "fovea". If similarly-shaped images fall on each fovea, we see only one picture because the foveas are "corresponding points" and link to the same area in the visual cortex. There are very many of these corresponding points on our retinas, so objects symmetrically displaced from our lines of sight are still seen singly. Each corresponding point also has a small area of tolerance, called "Panum's Area", which allows a little misregistration of the retinal images without causing double vision. If images are slightly misregistered laterally within Panum's area, we see them as being located at different depths. If the misregistration exceeds Panum's Area, we can see two images instead of one.

A simple demonstration: Close one eye and look at a distant object, such as a clock on the wall. Now move your right thumb into your line of sight so the clock is covered. When you open both eyes, you should see either one clock and two thumbs or one thumb and two clocks, depending on where you focus. (Figure #4 shows this relationship.) The angle between the light rays from the clock and the light rays from your thumb exceeds the tolerances allowed in Panum's Area. If you have normal binocular vision, your brain has no choice -- it sees the target at which you are not looking as double. If you look at the clock, the images of your thumb fall outside Panum's Area. If you look at your thumb, the images of the clock fall outside Panum's Area. If you alternately close one eye and then the other, you will see the target jump sideways because of the parallax error between thumb and clock.

If you had very long arms, you could move your thumb closer and closer to the clock until you saw only one thumb and one clock. The two objects would be seen singly and in depth; the clock being further away than your thumb. The light rays from each target now fall near the same corresponding point within Panum's Area, and you see the targets with stereoscopic depth, if you had normal vision. Stereopsis is one of several cues to depth perception. You may be familiar with modern stereo

cameras or the old wooden stereoptikons. Stereopsis is caused by slight angular differences in the light rays entering our eyes from different parts of each picture. Under laboratory conditions, some people are able to see depth when this parallax or retinal disparity is as little as six seconds of arc.

There has been a significant amount of study on just how little retinal disparity can cause stereopsis, but until recently, very little testing was done to determine how much disparity could be tolerated without causing double vision. The literature indicates people can tolerate somewere between two and 20 minutes of arc angular disparity before they see double, but there is little agreement as to test conditions.

When confronted with large retinal disparities, some of us might see double, but some people don't. The alternate response to diplopia or double vision is suppression, or the "turning off" of all or a part of the field of view of one eye. Diplopia is an antisurvival characteristic. If our historically distant ancestor saw two sabertooth tigers (rather than the single one which was attacking him), and swung his antelope femur at the false image rather than the real tiger, he probably didn't live long enough to bear progeny. In other words, survivors learned to ignore or suppress the secondary image. Suppression is OK for swingers of antelope femurs, but the induced parallactic error is excessive for today's fighter pilots. (The F-16 A and B canopy requirements specify a maximum angular deviation no greater than three milliradians, and an RMS value no greater than one milliradian). Neither suppression nor diplopia should be induced by the optical aiming system in today's military aircraft. Both of these visual problems significantly degrade the optimal performance of the pilot.

HUD EFFECTS

HUDs are built to produce collimated light, or parallel light rays. Light emitted from the face of the CRT passes through a collimating lens, and is reflected from a combining glass. The HUD imagery appears to be suspended in space, far in front of the aircraft. No HUD light actually reaches this point in space, but the imagery appears to be at optical infinity because it is a virtual image produced by a collimating optical system. (Recall Figure #1).

Light from potential targets also passes through the HUD combiner. Since the target is far away, its light rays are collimated or parallel. The two sets of parallel light rays enter the pilot's eyes, focus on corresponding points, and both

the target and the aiming symbol are seen to be at the same position in space. If the HUD imagery were not collimated, the aiming symbol would first appear to be at a different depth than the target, they would appear double; just as in the thumb - clock demonstration cited above. HUD manufacturers take great care to insure the light emitted by the HUD is parallel. Most HUD specifications allow tolerances of about 1 milliradian light convergence to about 2 milliradians light divergence.

CANOPY EFFECTS

Interposing the canopy in the optical path between the pilot's eyes and the target causes a problem. All F-16 canopies act as if they were weak minus lenses. This causes the image of the target to appear as if it came from some distance closer than optical infinity. Some of the "poorer" canopies we measured placed the target image between 38 and 65 feet away. Most canopies placed the image between 100 feet and 200 feet. Since all the light entering the eye at any one time is equally affected, and there are several stronger cues to depth perception (such as relative size), the pilot doesn't perceive any depth problems when he looks through the canopy alone, but optical instruments can detect the divergence of the light rays.

CANOPY + HUD EFFECTS

Now let us consider what happens when we place a HUD inside the cockpit. The HUD emits parallel light rays which appear to come from optical infinity. The canopy causes the light rays from the target to diverge as if they came from some relatively near distance. The net result is a retinal disparity or parallax error. If the disparity is small enough, the pilot will see the aiming symbol at a different depth than the outside world. Larger angular disparities cause the HUD symbology to appear blurry as the limits of Panum's Area are approached. Finally, some amount of angular disparity would cause the aiming symbol to double if the pilot concentrated on the target, or the target to double if the pilot concentrated on the pipper.

Each F-16 canopy is measured to determine its angular deviation for several points in the critical zone. After mathematical analysis, these deviation data are input into the firecontrol computer to help "correct" aiming errors induced by canopy optics. Since the firecontrol computer can only move the aiming point of the weapons, and since the HUD presents the same symbology to both eyes, the correction of diplopia cannot be accomplished with software.

This theory appeared to explain the F-16 pilots' complaints. If the angular disparity or parallax between light rays from the target and light rays from the HUD CRT were sufficient, the pilots could have depth perception problems, see blurred images, or see double. But theory alone isn't sufficient to impact a multimillion dollar avionics system. Test results, taken with HUD optics and aircrew eyeballs could be.

TEST CONDITIONS

To test our hypothesis, we constructed a HUD emulator. The device is optically similar to standard HUDs in that it has a combining glass, collimating lens and object plane. The main difference is that the aiming symbol at the object plane is not produced by a CRT, but consists of a vertical slit, behind which is a bright light. The slit can be moved closer or farther from the condensing lens with extreme accuracy, by using a computer-controlled stepper motor and optical positioning device. In other words, we can change the vergence of the light leaving the system, so the virtual image of the aiming symbol can appear at any distance from several meters in front of the device to "beyond" infinity. We also installed a shutter mechanism so the aiming symbol could be exposed to view for any amount of time from a few milliseconds up. The computer is able to convert aiming symbol position to milliradians parallax for any subject interpupillary distance.

The target for the test consisted of a vertical tower located about two miles from one of the AFAMRL Labs. We installed the HUD emulator on the third floor of Building 33, and arranged the device so the target could be seen on a distant ridgeline through a flat plate window.

Next, we looked for 50 subjects whose eye tests indicated they could pass a Flying Class II ophthalmic examination. (Flying Class II exams are required of active USAF aircrew). Many pilots were included in the group. These subjects were then tested on the HUD emulator to determine the amount of parallax or retinal disparity required to see either two aiming symbols or two targets. Several variables were tested, including two exposure times (100 msec and 3.0 sec) and two criteria of double vision ("double" and "not single"). We also determined how much disparity was required when the aiming symbol was situated either further or closer than the target. A smaller sample of subjects will be tested to determine how long they can keep things single when the disparity is close to the limits of their individual tolerances.

During this series of tests, for reasons of convenience, we varied only the apparent distance of the aiming symbol, and not the apparent distance of the target. In either case, the results of the test are equivalent because the test measures the difference in optical distance between symbol and target. The test results would then show us how much retinal disparity or parallax could be tolerated by a pilot before he saw double. At this time, we were not concerned with the operational cause of the retinal disparity -- whether it were due to canopy angular deviation or HUD parallax errors, but we were interested in ascertaining the magnitude of the disparity which first causes double vision.

SUMMARY OF RESULTS:

As of the date of writing this paper, 32 subjects were tested on the HUD emulator. Several interesting findings were discovered. First, even though all subjects apparently passed an AF Flying Class II eye exam, not all subjects were able to see double, even when they should have! In fact, more than half of the subjects would report suppression rather than diplopia as a response to extreme retinal disparities. This should not be too surprising if one recalls the "antisurvival problem" associated with double vision. Even though these pilots would not be bothered with double vision, they would still experience the aiming error induced by parallax. This is additional information suggesting why the double vision problem has been only rarely reported -- the pilot "turned off" one eye!

While looking at the ridgeline, most subjects saw double (or shifted to one-eyed vision) when the symbology was 2.8 mrad closer or 1.6 mrad further than the distant ridgeline. (If the subject looked at the symbology rather than the ridgeline, these figures would reverse). In other words, many subjects could tolerate only 1.6 mrad or less disparity between HUD symbology and target image before seeing double.

Only 10% of the subjects reported double vision or suppression when the vergence difference was 1 mrad (as measured with a 65mm IPD)

Many subjects reported depth perception effects well before the symbology split into two, but because of time limitations, we did not study the stereopsis effects.

RECOMMENDATIONS

For any wide field of view HUD, where the pilot must spend a large percentage of his time looking through the BFOV, and where the elimination or reduction of suppression or diplopia is desirable, the vergence or collimation difference between the HUD and that portion of the canopy in the FOV of the HUD should be 1.0 mrad or less. In other words, the HUD and the canopy must be considered a system since it is their interaction which affects the pilot's vision. The net disparity between the two components of this system should be no more than 1.0 mrad to prevent double vision in 90% of pilots.

Marconi Avionics (F-16 HUD manufacturers) are currently adjusting their LANTIRN HUD optics to minimize the disparity between the LANTIRN HUD and a subset of Sierracin F-16 A canopies. If future F-16 C and D canopy manufacturers (including Sierracin) deviate significantly from the existing Sierracin optical profile, the result will be an increased incidence of double vision reports. Unless the canopy manufacturers discuss their problems with the HUD manufacturer, their flexibility in both optical and structural design alternatives will be severely constrained.

Further discussion, data and research results will soon be published in an AFAMRL Technical Report. Interested parties should contact the author for copies.

REFERENCES:

1. Genco, Louis V.,Optical Interactions of Aircraft Windscreens and HUDs Producing Diplopia, NAECON 83 Mini Course Notes, Dayton, OH 17-19 May, 1983.

2. Task, Harry L., Genco Louis V., Smith, Kenneth L. and Dabbs, Albert G., System for Measuring Angular Deviation in a Transparency, US Patent #4,377,341, March 22, 1983.

3. Ogle, Kenneth N., Researches in Binocular Vision, Hafner Publishing Co., New York, 1964.

TITLE FOR FIGURES:

Figure 1: HUD Basic Optical Train

Figure 2: HUD Knothole Effect; Monocular and Binocular Fields of View

Figure 3: Fields of View for Various F-16 HUDs

Figure 4: Geometry of Diplopia

FIGURE 1

HUD BASIC OPTICAL TRAIN

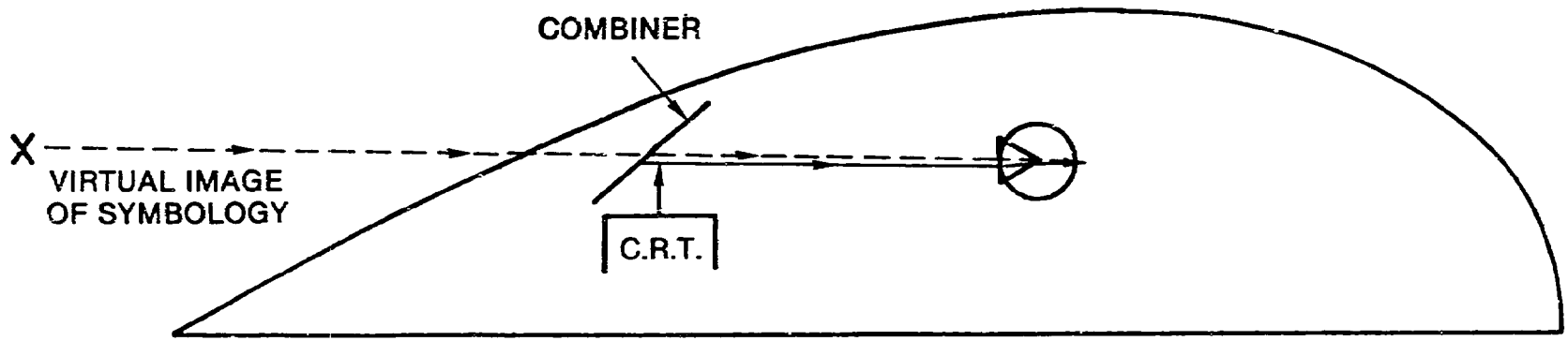

FIGURE 2

HUD KNOTHOLE EFFECT; MONOCULAR AND BINOCULAR FIELDS OF VIEW

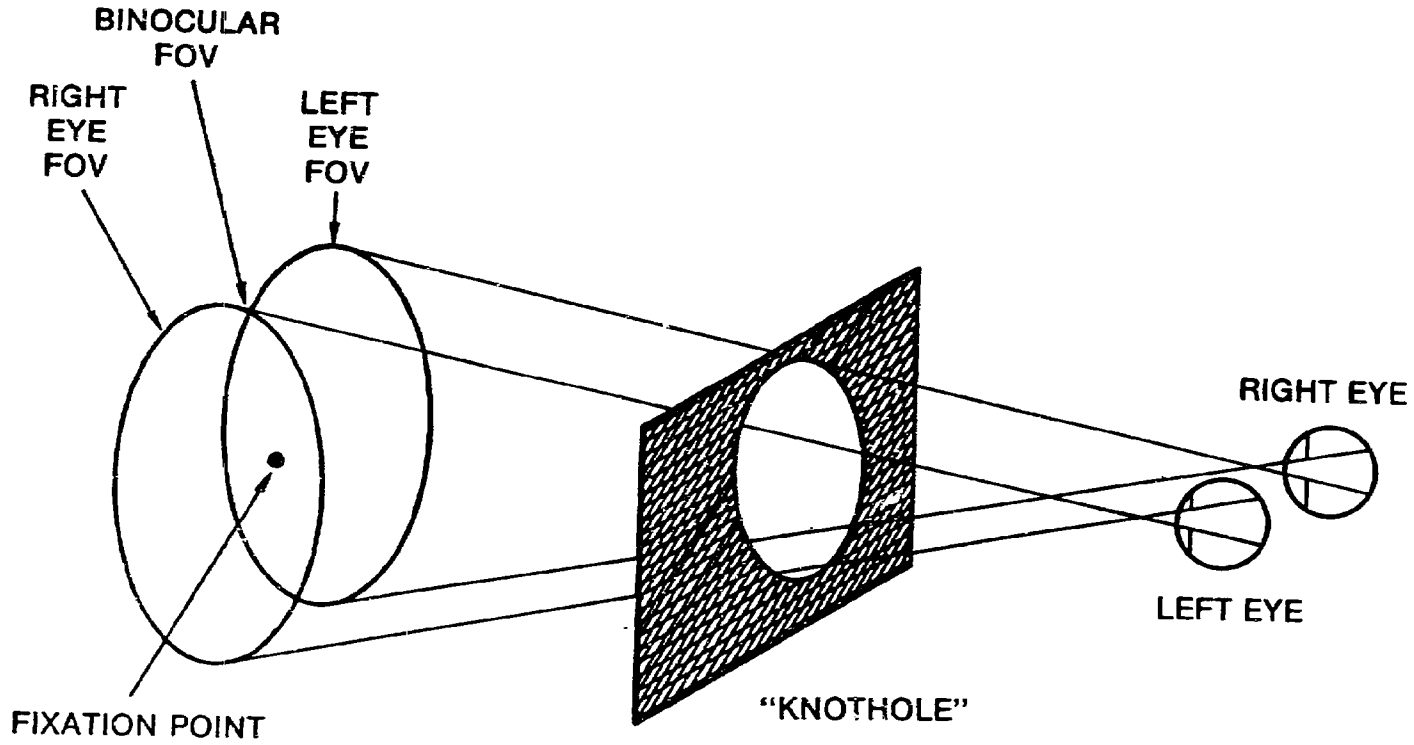

FIGIRE 3

FIELD OF VIEW FOR VARIOUS F-16 HUDs

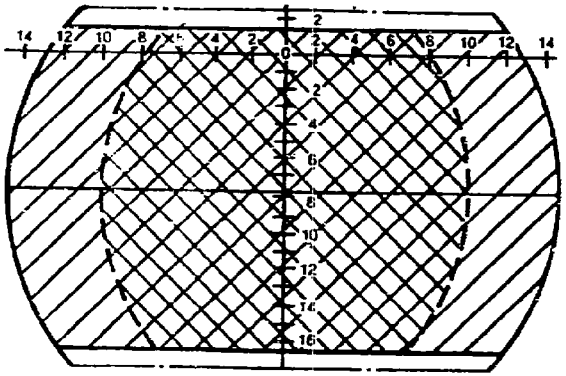

LANTIRN HUD

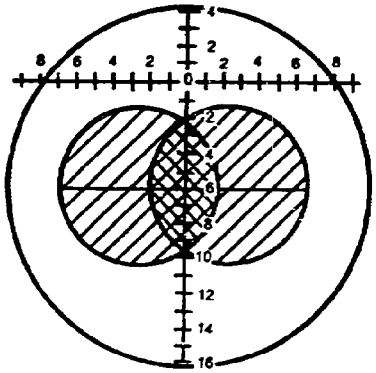

CURRENT HUD

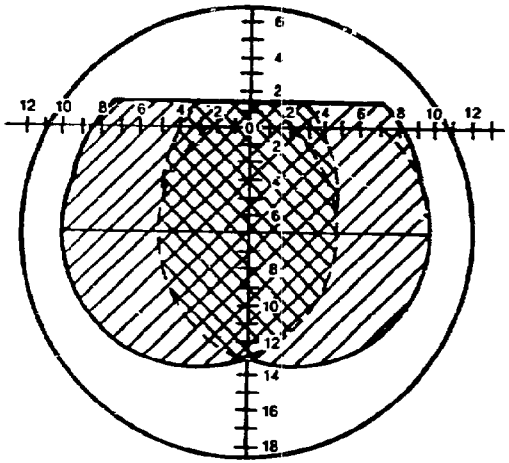

CONVENTIONAL WIDE ANGLE HUD

INSTANTANEOUS FOV

BINOCULAR OVERLAP

FIGURE 4

GEOMETRY OF DIPLOPIA

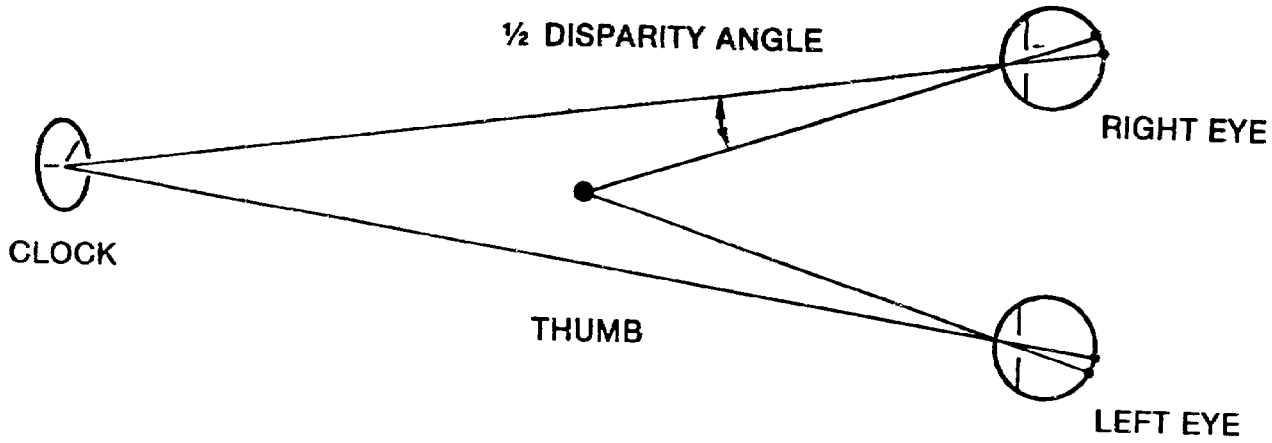

AD-P003 222

OPTICAL EFFECTS OF F-16 CANOPY AND HUD INTEGRATION

H. L. Task, Air Force Aerospace
Medical Research Laboratory

OPTICAL EFFECTS OF F-16 CANOPY-HUD INTEGRATION

H. Lee Task, Ph.D.
Air Force Aerospace Medical Research Laboratory
Wright-Patterson AFB, Ohio 45433

ABSTRACT

The F-16 heads-up display (HUD) provides the pilot with visual information in symbology form that is overlayed on the outside world scene in the forward viewing direction. This superposition of HUD symbology and outside world scene is done by using an optical combiner (beamsplitter) which is part of the HUD optical system. One of the critical items of information that is displayed on the HUD is the aiming reticle that is used for air-to-air and air-to-ground weapon aiming. In order to be effective, it is essential that the aiming reticle be accurately boresighted to the weapon system. This requires a careful integration of the optical characteristics of the HUD and the aircraft canopy. There are several optical parameters that can affect target acquisition and aiming accuracy that involve the canopy,the HUD, and interactions between the two. The primary parameter that affects aiming accuracy is angular deviation due to the windscreen and/or the HUD. This angular deviation is manifested as pointing error (prism effects), collimation errors (lens effects associated with vergence, focus, parallax problems) and distortion (higher order aberration effects).. In addition, other windscreen optical parameters may affect target acquisition, such as light transmission, and polarization. This paper describes these parameters and the techniques used to measure them.

INTRODUCTION

One of the main purposes of the F-16 heads-up display (HUD) is to provide the pilot with an accurate weapon aiming capability. To allow maximum accuracy it is absolutely essential that both the canopy and the HUD characteristics be considered and adjusted to minimize parallax error between the target and the HUD aiming symbol. If the HUD and canopy are not considered together, significant system aiming error can easily result. Recent experiences with the F-16 and the LANTIRN wide field of view HUD have made this fact very clear. The following paper discusses integration issues associated with both aiming accuracy and target acquisition.

AIMING ACCURACY

Angular Deviation in the Windscreen

The fundamental cause of aiming errors with the HUD-canopy combination is angular deviation of light rays due to the canopy. Angular deviation refers to the angular change that a light ray undergoes as it passes through a transparent material. This must be differentiated from lateral displacement which is simply a lateral shifting of the light as it passes through the material. Figure 1 shows these two effects. When measuring the windscreen it is important to differentiate between these two effects since the angular deviation causes an aiming error that linearly increases with target range whereas lateral displacement causes a fixed aiming error indpendent of range. The lateral displacement is typically less that an inch, but the aiming error caused by angular deviation can easily be several dozen yards depending on the range and degree of angular deviation.

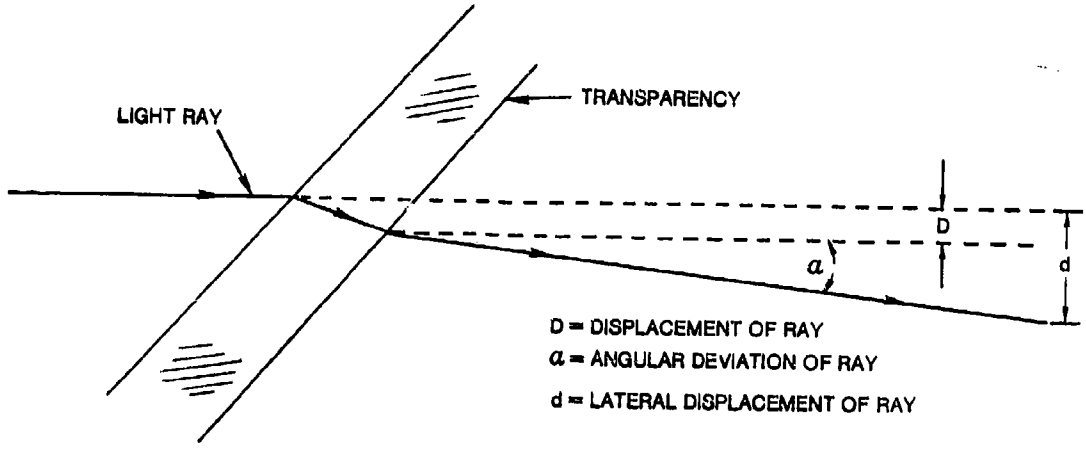

Figure 1. Angular deviation and lateral displacement of a light ray as it passes through a transparent medium.

Measurement of Angular Deviation in Windscreens

It was recognized early in the F-16 windscreen development program that the windscreen would adversely affect the weapon aiming accuracy of the HUD unless corrective measures were applied. As a result of this need, AFAMRL developed a device to measure angular deviation of aircraft windscreens that eliminated unwanted errors due to lateral displacement (Ref 1). All angular deviation measurements discussed in this paper were made using this device. Initially the windscreen was measured for angular deviation from the design eye position for azimuth and elevation angles that corresponded to the modest field of view of the HUD. It was later determined that pilots do not use the design eye position so the angular deviation was mapped for 4 eye postions (1 inch above, on, 1 and 2 inches below design eye). The resulting mass of data was then used to produce a best fit sine-wave curve to the elevation data and a linear fit to the azimuth data. The coefficients for these best fit curves were then placed on a label attached to the windscreen so that they could be input to the fire control computer of the aircraft on which the windscreen was installed. The fire control computer would then shift the aiming symbol on the HUD to compensate (on average) for the angular deviation errors introduced by the windscreen. Figures 2 and 3 show anexample of this data and the corresponding best fit curves. Table 1 is an example of the error data used to make the graphs and curve fits shown in figures 2 and 3. These corrections only work for the 4 monocular eye positions from which the data were taken.

Recently it was discovered that most pilots have two eyes, neither of which is located in the center of the pilot's head. As described in the previous paper, the two eyes work together to produce a single image in the brain under normal circumstances. In order to determine whether or not circumstances are normal it is necessary to measure the canopy angular deviation from each eye position (right and left). This has been done for several F-16 canopies from three different manufacturers and some of the initial data is shown in later figures.

Now the procedures for quantifying the windscreen have become a little more complicated: 4 eye heights and 2 eye positions (right and left); but the complication doesn't end here. With the advent of new wide field of view (WFOV) HUDs the area of the windscreen that must be measured has almost doubled. This makes it much more difficult, if not impossible, to produce a curved windscreen that will have sufficiently well behaved angular deviations to allow proper fire control computer compensation of errors. It is possible to reduce the severity of this problem by partially compensating for angular deviation in the optical system of the HUD.

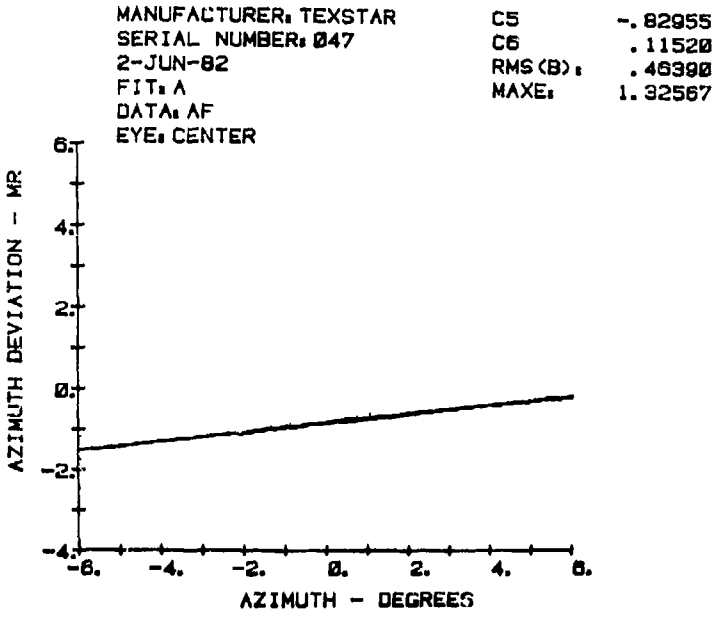

Figure 2. Standard angular deviation curve-fitting data for correcting the HUD azimuth aiming error.

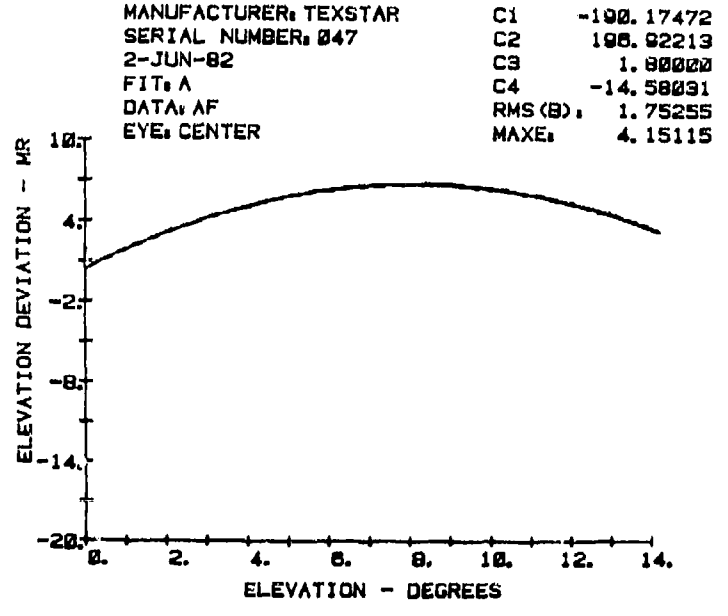

Figure 3. Standard angular deviation curve fitting data for correcting the HUD elevation aiming error.

Table 1. Error Data Used to Generate Curves 2 and 3.

OMR, DATA? (Y OR N):
Y
READ DATA FROM DISK?
Y
TYPE FILE NAME:
TO47AC

2 INCHES DOWN

			-2.	0.	2.
0.		AZ	-.7060	-.7060	-.7766
		EL	1.9062	1.9768	1.7650
2.		AZ	-.7766	-.7060	-.6648
		EL	4.0242	4.0948	3.7419
4.		AZ	-1.0590	-.6354	-.2118
		EL	5.012A	4.9420	4.7302

1 INCH DOWN

			-4.	-2.	0.	2.	4.
0.		AZ	-.4942	-.7766	-1.1294		
		EL	-.1413	-.4943	-.8472		
2.		AZ	-.6354	-.7060	-.8472		
		EL	2.4004	2.3298	2.1180		
4.		AZ	-.8472	-.7766	-.6354		
		EL	4.7302	4.6596	4.3773		
6.		AZ	-1.5532	-1.1296	-.7060	-.2824	-.0706
		EL	5.5774	5.5480	5.3454	5.2950	5.0832

DESIGN EYE

			-4.	-2.	0.	2.	4.
2.		AZ	-.4942	-.7766	-1.2708		
		EL	-.2826	-.6354	-1.1294		
4.		AZ	-.6354	-.7766	-.9178		
		EL	2.6240	2.6240	2.5414		
6.		AZ	-.9884	-.9178	-.7060	-.5648	-.7060
		EL	5.2950	5.6480	5.5774	5.2244	4.7302
8.		AZ	-1.4826	-.2824	-.6354	-.3530	-.0706
		EL	4.2128	4.2128	4.1422	4.0010	3.7892

1 INCH UP

		-6.	-4.	-2.	0.	2.	4.	6.
4.			AZ	-.4942	-.9178	-1.4826		
			EL	-.4236	-.7766	-1.4826		
6.		AZ	-.3530	-.6354	-.7060	-1.0590	-1.0414	
		EL	2.8240	3.4924	3.9660	3.1770	2.6122	
8.		AZ	-1.1296	-.9884	-.7060	-.7060	-.6354	
		EL	4.5438	4.9894	4.7774	4.4952	5.9304	
10.	AZ	-1.7650	-1.4944	-1.1296	-.5648	-.4236	-.1412	-.2118
	EL	6.9108	7.0400	7.2012	6.9188	6.7894	6.7776	6.6364
12.	AZ	-2.4710	-2.5416	-1.5296	-.2824	-.2118	-.2824	-.4236
	EL	8.7070	7.9424	8.4014	8.4720	8.0484	7.2718	6.9188
14.	AZ	-1.3002	-.7060	-.1412	-.2118	-1.4826	-1.4944	-.2824
	EL	4.7302	1.0464	-.2824	-.7766	.1412	1.7650	4.5890

HUD Imagery

Ideally the HUD is designed to produce an image of the symbology at optical infinity (i.e. a far distance away). In reality the HUD image is at some other optical distance resulting in either divergence or convergence of the light rays as they exit from the HUD optical system. In addition, the HUD

may suffer from some distortion and field curvature. These departures from ideal are usually designed to be negligibly small. However, if the F-16 windscreen is relatively uniform and moderately well behaved in its distribution of angular deviation, it is possible to redesign the HUD optics to compensate for the windscreen.

There are several degrees of freedom available to the HUD optical designer in determining the HUD image location. The simplest change is to uniformly "decollimate" the HUD image. This results in the HUD image appearing to be at some finite distance instead of optical infinity. If the windscreen acted as only a simple, weak, negative lens, then the HUD image and the image of objects viewed through the canopy could be made to appear at the same optical distance (e.g. 100 feet) from the pilot. This would entirely eliminate all aiming errors, diplopia, parallax errors and false stereo. Unfortunately, the F-16 windscreen is not a perfect negative lens.
Another variable at the disposal of the HUD optical designer is field curvature. Field curvature means that the optical distance to the HUD image varies as a function of the look angle. Thus the center of the image may appear to be at some finite distance (say 100 feet) while the edges appear to be further away. This results in some eye convergence required for viewing the center of the HUD image and a lesser degree of eye convergence required to view the edges. Roughly speaking, the F-16 canopy exhibits this type of field curvature.

The key question is how much residual error is left after the HUD is modified to "fit" the canopy as much as possible? Also, how much do the windscreens vary; both within a single manufacturer and between manufacturers? A considerable amount of data is presently being collected at AFAMRL for the F-16 SPO to answer these questions. Figures 4 through 8 show examples of the kind of binocular angular deviation data that has been collected on windscreens to date. The graphs show how much the eyes must converge (assuming a 2.5 inch distance between the eyes) or diverge (negative numbers) in order to fixate on a distant object viewed through the windscreen. All data were taken using the AFAMRL developed angular deviation measurement device (Ref 1) to first measure the canopy from the right eye position, then the left, then subtract the two. Note that these data do NOT show the absolute pointing error (which must also be measured and compensated for) but rather only show the vergence requirements to match the HUD image to the canopy image. It should be apparent from these data that there are definitely differences between canopies and between manufacturers. To achieve a successful integration of the canopy and the HUD from an aiming accuracy standpoint it is imperative that the HUD and canopy manufacturers get together to decrease the overall aiming error.

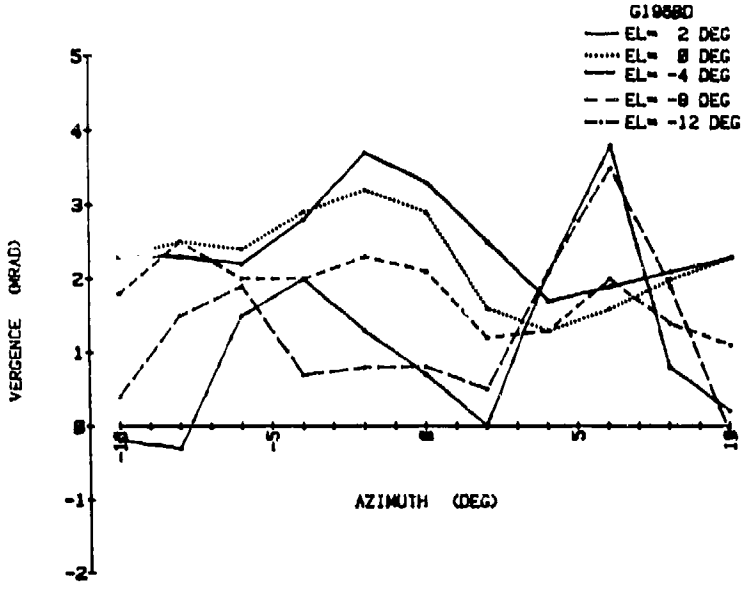

Figure 4. Binocular angular deviation vergence curves for Goodyear windscreen ser# 196.

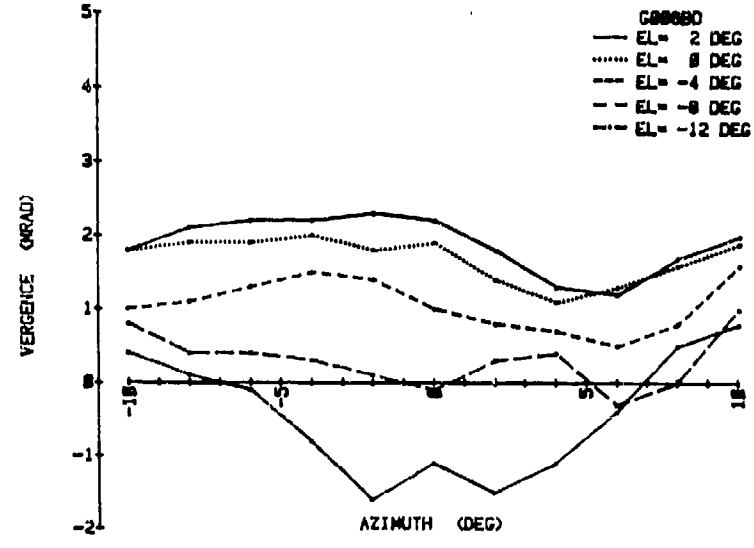

Figure 5. Binocular angular deviation vergence curves for Goodyear canopy ser# 006.

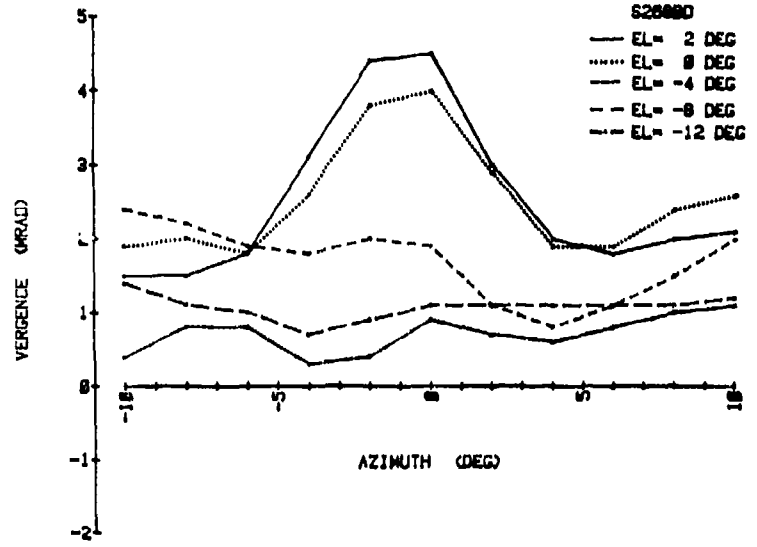

Figure 6. Binocular angular deviation vergence curves for Sierracin canopy ser# 268.

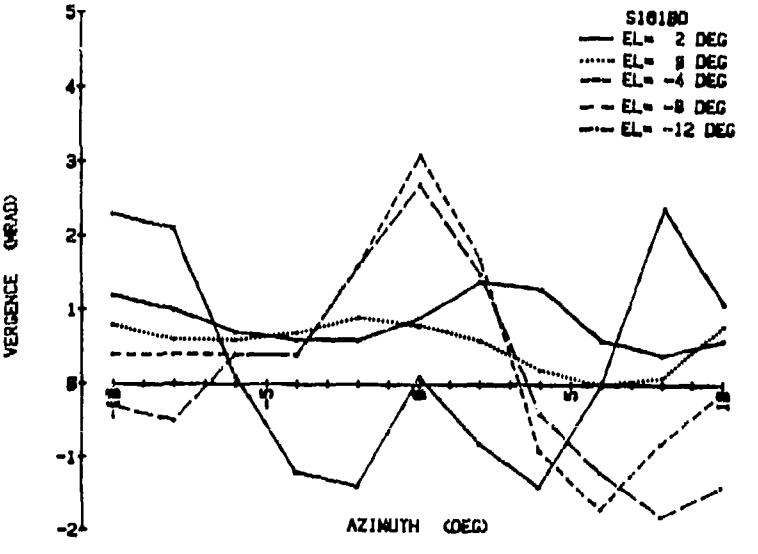

Figure 7. Binocular angular deviation vergence curves for Sierracin canopy ser# 161.

Only one Texstar canopy was available for measurement which is shown in Figure 8.

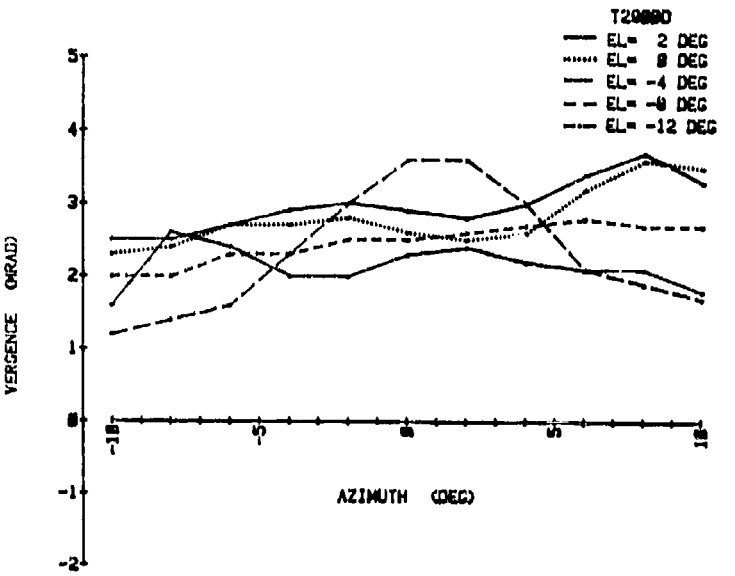

Figure 8. Binocular angular deviation vergence curves for Texstar canopy ser# 290.

HUD Combiner Angular Deviation

Another source of aiming error is caused by the HUD combining optics. Ideally the combining optics would produce no angular deviation of light rays as they pass through to the pilot. However, HUDs that use curved optical combiners and HUDs that have flat combiners that are made of cemented plates of glass may exhibit a noticeable amount of unwanted angular deviation. The LANTIRN HUD ser# 007 (a pre-production prototype) was measured using the angular deviation measurement device and the F-16 windscreen movement table (see fig. 9). The results show that this particular unit acted like a weak negative lens much as the windscreen, thus compounding the aiming accuracy problem. Table 2 shows the values of eye convergence (positive values) required as a function of elevation and azimuth look angle through the HUD.

It is apparent from the data in Table 2 that the HUD combiner contributes a sufficient amount of angular deviation to the overall system that it, too, needs to be included in designing and evaluating the HUD-canopy system. The HUD optical system must be designed to compensate as much as possible for the

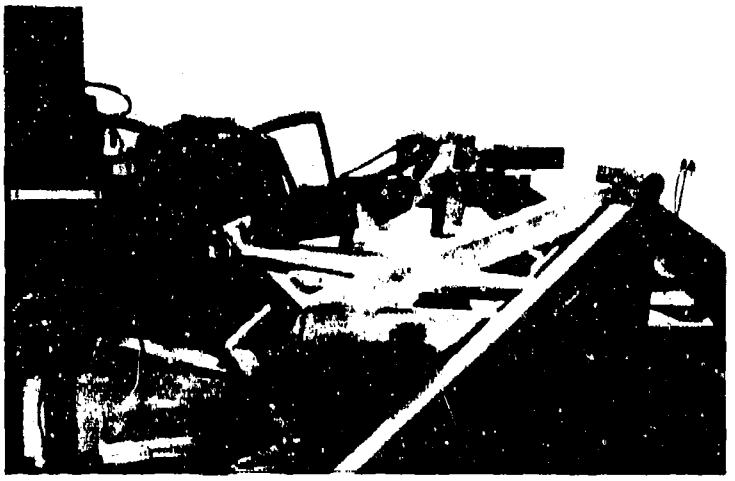

Figure 9. AFAMRL angular deviation measurement device and F-16 windscreen movement table with LANTIRN HUD

Table 2. CONVERGENCE/DIVERGENCE ERROR (AZIMUTH) AND VERTICAL ANGULAR DISPARITY (ELEVATION) THROUGH THE LANTIRN HUD SER# 007 (plus AZ values are eye convergence; negative are divergence; all error values are in milliradians)

Elev Angle (deg)		Azimuth Angle (deg)						
		6	4	2	0	-2	-4	-6
2	AZ	0.26	0.56	0.42	0.49	0.21	0.28	0.28
	EL	1.26	1.12	0.56	0.07	0.56	0.70	0.70
0	AZ	-0.07	0.98	0.84	0.77	0.56	0.56	0.21
	EL	0.21	0.28	0.28	0.14	0.21	0.07	0.07
-2	AZ	0.00	0.49	0.77	0.77	0.49	0.35	0.21
	EL	-0.07	0.00	0.00	0.14	0.21	0.49	0.21
-4	AZ	0.21	0.35	0.35	0.35	0.21	0.28	0.28
	EL	0.28	0.21	0.21	0.28	0.28	0.28	0.21
-6	AZ	0.14	0.21	0.42	0.42	0.42	0.42	0.35
	EL	0.14	0.21	0.21	0.28	0.28	0.28	0.21
-8	AZ	0.14	0.21	0.21	0.28	0.42	0.35	0.28
	EL	0.14	0.07	0.14	0.14	0.14	0.21	0.21

Note: The EL values indicate how much one eye must rotate vertically with respect to the other eye in order to view a distant object throught the HUD combiner.

angular deviations of the canopy-HUD combiner combination with the remainder of the aiming error removed in the fire control computer.

TARGET ACQUISITION (HUD-CANOPY TRANSMISSIVITY)

Many variables can affect a pilot's ability to visually acquire targets through the aircraft canopy and HUD. One parameter that is claimed to have a detrimental affect on target acquisition is transmissivity of the canopy and/or HUD. Since transmissivity does not reduce target contrast or size it is probable that it only affects target acquisition for external lighting conditions that are marginal; i.e. at dawn and dusk. In fact, pilots are provided with tinted visors (~15% transmissivity) to reduce exterior light levels for bright, daytime flights. However, there is an adverse interaction effect between the HUD and the canopy that will be described later.

Transmissivity of the HUD

The transmissivity of any transparent medium is the ratio of the light exiting the material to the light that was incident on the material. If the material is not neutral (i.e. the same for all wavelengths) then it may be necessary to measure the transmissivity as a function of wavelength across the wavelength region of interest (usually the visible wavelengths from 400 to 700 nanometers). HUDs that use holographic optical elements (HOEs) or trichroic coatings show demonstrated variations in transmissivity as a function of wavelength. In order to determine the apparent photopic transmissivity of a spectrally selective HUD combiner one must multiply the HUD transmissivity by the human photopic vision sensitivity and the object spectral distribution. This procedure and results from some objects can be found in reference 2. Table 3 shows the photopic transmissivity for several objects as calculated from data on LANTIRN HUD ser# 007 (Ref. 2).

Transmissivity of the Windscreen

Typically the aircraft windscreen is relatively neutral in its transmissivity with respect to wavelength. However, because it varies in thickness, and reflectivity increases with angle, there is some change in transmissivity as a function of angle. The transmissivity of several windscreens were measured using the simple arrangement shown in figure 10. The light source was mounted at about the design eye position of the F-16 canopy

Table 3. PHOTOPIC TRANSMISSIVITY OF SEVERAL OBJECTS FOR LANTIRN HUD SER# 007

OBJECT	UPPER HUD	LOWER HUD
LIGHT BOX	54.8%	65.1%
BLUE SKY	46.0%	57.8%
GREEN GRASS	46.8%	57.2%
HAZY HORIZON	49.1%	59.9%
ARMY TANKS	47.6%	58.6%
DISTANT TREES	47.5%	58.4%

Note: The upper HUD values were taken through the eyebrow portion of the HUD where the light must go through 3 holographic optical elements whereas the lower HUD (below the eyebrow) there are only two holographic optical elements that must be traversed.

movement table and luminance measurements of the lamp were made through the canopy as a function of azimuth and elevation. These were divided by the luminance reading of the lamp with no canopy to obtain the transmission coefficient. Canopies measured included both tinted and untinted versions. In addition, the transmissivity was measured for three conditions: no polarizer, vertical polarizer and horizontal polarizer. Since blue sky is typically highly polarized it is of interest to determine the transmissivity as a function of polarization. Figure 10 shows the location of the polarizing element. For measurements where the polarizer was used, the baseline measurement of the light source without canopy was made with the polarizer in place. Figures 11 and 12 show the transmissivity (unpolarized) as a function of azimuth for two elevation angles for tinted and untinted canopies. Figures 13 and 14 show the tremendous difference in transmissivity between the vertical and horizontal polarizations. This difference in transmissivity with polarization direction is due to the fact that the amount of light reflected from a surface depends on polarization and incidence angle. Thus light polarized in the horizontal direction is reflected to a higher degree than light polarized in the vertical direction. Since the reflected light is not transmitted, this reduces the transmitted light more for horizontally polarized light than for vertically. The effect of this is to cause a large change in apparent luminance of polarized exterior light sources (such as blue sky) as the aircraft changes its orientation with respect to the polarization.

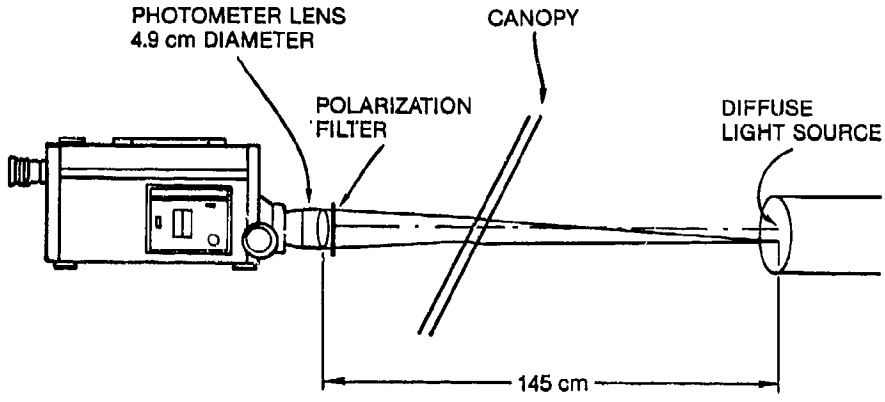

Figure 10. Optical arrangement for measuring canopy transmissivity.

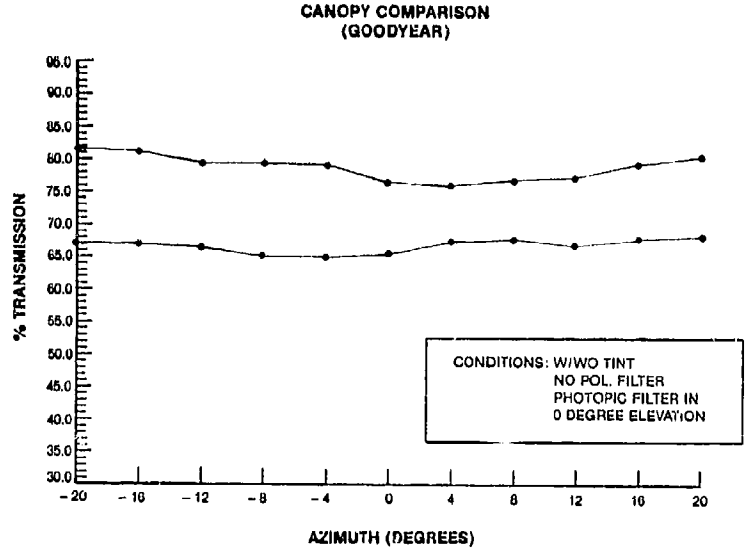

Figure 11. Photopic transmissivity of tinted (lower curve) and untinted canopy as a function of azimuth look angle for 0 degrees elevation angle (unpolarized).

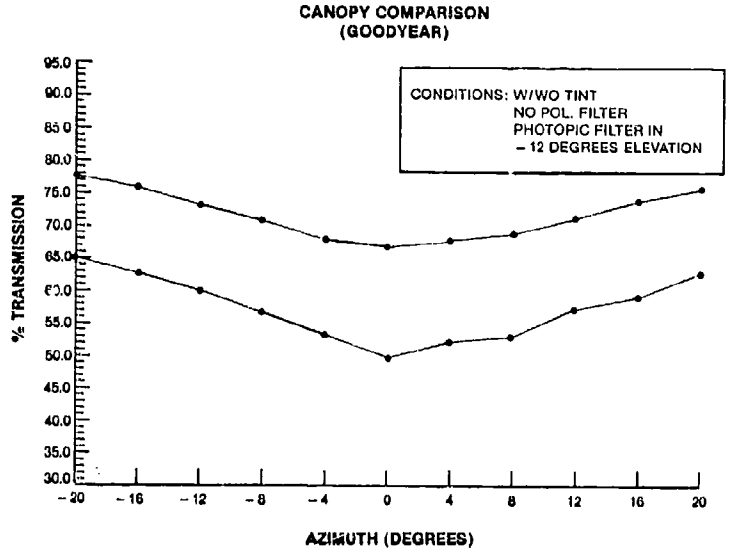

Figure 12. Photopic transmissivity of a tinted (lower curve) and untinted canopy as a function of azimuth for -12 degrees elevation (unpolarized).

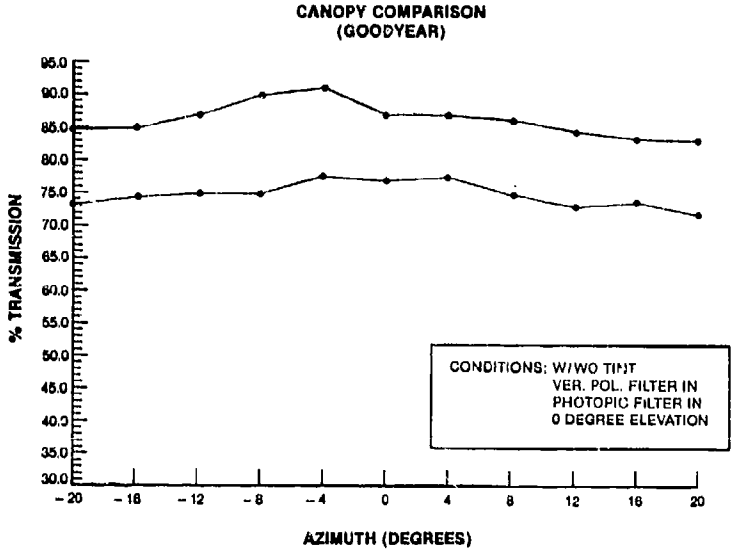

Figure 13. Photometric transmissivity of tinted (lower curve) and untinted canopy as a function of azimuth for vertically polarized light (0 degrees elevation angle).

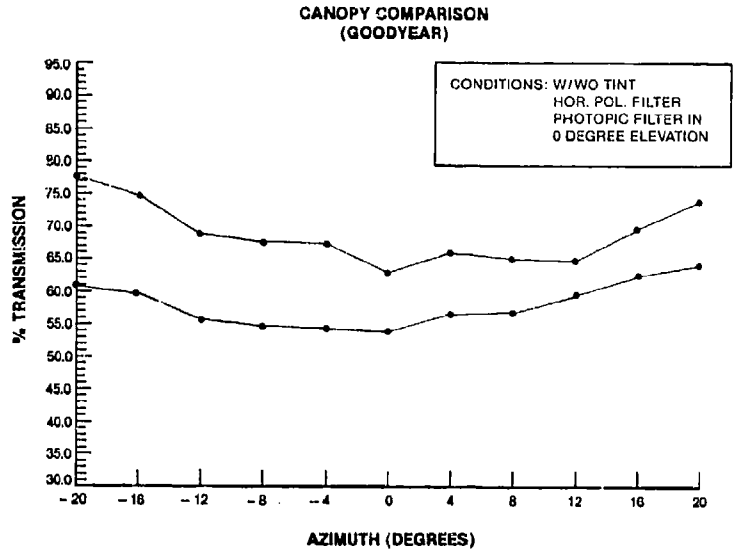

Figure 14. Photometric transmissivity of tinted (lower curve) and untinted canopy as a function of azimuth for horizontally polarized light at 0 degrees elevation; compare this to Fig. 13).

HUD-Canopy Integration: Transmissivity

As mentioned earlier, transmissivity by itself should not cause a loss of target acquistion capability except under marginal lighting conditions such as dawn and dusk. However, this assumes that the loss in transmissivity is relatively uniform. With the HUD in place, the total transmissivity in the forward direction is the product of the transmissivity of the HUD and the canopy. For the LANTIRN HUD eyebrow and untintedcanopy, the total transmissivity through the HUD is about 0.49 times 0.78 or about 0.38 (38%). The transmissivity through the area of the canopy around the HUD is about 0.80 (80%) as shown in figure 11. This means there is a greater than 2:1 difference in average luminance between looking through the HUD and looking around it. Since the eye has a relatively limited instantaneous dynamic range (the brightest and dimmest it can see at a single adaptaton level) and it adapts to the average light level available to it, it is apparent that some useful dynamic range is lost in viewing through the HUD. If one assumes the instantaneous dynamic range of the visual system for daytime viewing is about 200:1, then the HUD situation described above has reduced the dynamic range available through the HUD to (0.38/0.80)X200:1 or 95:1. It is this effect of

differential transmissivity through the HUD compared to the surround that causes a loss in target acquisition capability and is the reason the HUD combiner transmissivity should be kept as high as possible. This effect is also known as disability glare or discomfort glare (depending on the severity of the ratio). More information on this effect can be found in references 3 and 4.

CONCLUSIONS

In order to insure the target acquisition and weapon aiming accuracy are not adversely affected by the canopy and HUD it is necessary that the canopy and HUD be considered together as a single "viewing" system. The only way that unwanted binocular effects and parallax aiming errors can be significantly reduced in the F-16 with wide field of view HUDs is to design the two together to obtain an integrated system.

REFERENCES

1. Task, Harry L., Genco, Louis V., Smith, Kenneth L. and Dabbs, Albert G., SYSTEM FOR MEASURING ANGULAR DEVIATION IN A TRANSPARENCY, US Patent #4,377,341, Mar 22, 1983.

2. Task, Harry L., MEASUREMENT OF HUD OPTICAL QUALITY, NAECON 83 Mini Course Notes, Dayton, Ohio 17-19 May 1983.

3. Blackwell, H. R., Schwab, R. N. and Pritchard, B. S. , "Visibility and Illumination Variables in Roadway Visual Tasks," report of Illuminating Engingeering Research Institute, Project No. 30-G-1 (1962).

4. Fry, G. A., "A Re-Evaluation of the Scattering Theory of Glare," ILLUMINATING ENGINEERING, Vol. XLIX, No. 2, p.98 (February 1954).

AD-P003 223

VISUAL PERCEPTION THROUGH WINDSCREENS: EFFECTS OF MINOR OCCLUSIONS AND HAZE ON OPERATOR PERFORMANCE

W. N. Kama, Air Force Aerospace
Medical Research Laboratory

VISUAL PERCEPTION THROUGH WINDSCREENS: EFFECT OF MINOR OCCLUSIONS AND HAZE ON OPERATOR PERFORMANCE

William N. Kama

Air Force Aerospace Medical Research Laboratory

Abstract

Current specifications and acceptance procedures regarding the size and number of minor defects (optical occlusions) permitted on aircraft transparencies reflect a marked lack of uniformity--size requirements ranging from 0.035 to 0.25 inch and numbers allowed varying from 1 per square foot to 20 per zone. Additionally, there is, at the present time, no objective means for determining when a transparency should be replaced due to the amount of halation found in it. To address these two problems, two experiments were devised and performed in the Windscreen Facility of the Air Force Aerospace Medical Research Laboratory. The first study sought to determine the effects of size and number (density per unit area) of minor optical defects contained in an aircraft transparency on the performance of a simulated air-to-air target acquisition task while the second sought to determine what relationship, if any, existed between the amount of haze emanating from a transparency and the amount of an observer's field-of-view (FOV) or visual field that is "lost" (rendered unusable) due to the presence of the haze. Data generated from the first study can be used to relate visual performance to requirements currently specified in the various specifications and standards as well as contribute to the formation of new visual/optical specifications and standards. Data from the second study can be used in the development of an objective technique for determining when aircraft transparencies should be replaced because of haze. This paper describes the procedures used and the results obtained in these two studies.

Introduction

As aircrafts were designed to fly higher and faster, the speeds and stresses encountered made it necessary to totally enclose the cockpit in order to protect the pilot. Transparencies or windows were used to provide visual access to the outside world. The use of transparencies has led to a variety of optical and visual problems, two of which are the subject of this paper.

The first relates to the optical specifications dealing with minor defects contained in aircraft transparencies. Most of these specifications, although purporting to be based on a foundation of visual performance, are in actuality a reflection of the state-of-the-art in material availability and handling procedures. For example, several military standards and specifications state the number and size of minor defects which are allowable in various areas of aircraft transparencies. MIL-G-5485C (ref. 1) allows certain spot-like inclusions so long as they are less than 0.063 inches in diameter. MIL-G-25667B (ref. 2) specifies the allowable number of minor defects with respect to the area of daylight opening and the thickness of the part, allowing more defects in thicker samples.

Transparency industry handbooks usually include some remarks about minor defects. A common maximum limit allows defects up to 0.093 inches in maximum dimension, however defects over 0.063 inches are not allowed within two inches of each other. "The total number of optical defects for the applicable panel size and thickness shall not exceed the sum of the totals permitted by MIL-P-5425, MIL-P-8184, MIL-P-25690 or MIL-P-83310 for the individual glass or plastic plies, plus a certain number of defects for each interlayer." (ref.3).

In addition to these general standards, each aircraft has its own set of specifications which seems to be independent of both the standards and the specifications for other aircraft. For example, the F-111 (ref. 4) allows opaque inclusions of less than 0.035 square inches in area but permits no more than 12 such defects in the entire panel should these defects be between 0.035 and 0.070 square inches in size. Transparent defects up to 0.35 square inches in area are permitted "provided they do not cause a vision impairment."

Requirements for the F-16 (ref. 5) allow minor defects that cover an area that is equivalent to or less than a 0.035 inch diameter circle but limit larger defects to less than 20 per zone. Opaque particles can be no larger than 0.070 square inches in area and there will be no more than 12 particles between 0.035 and 0.070 square inches per panel.

The specification for the F-5 (ref. 6) allows no minor defects in the "supercritical" area (equivalent to the design eye), but the critical areas may have one spot per square foot as long as that spot is no larger than the area covered by a circle of 0.25 inch diameter. More than one spot of this size is permitted only if the defects are located in such positions that 2 or more cannot be encompassed in a 1 square foot area circular template.

Although many of these specifications are commendable from the visual standpoint, they seem to have little, if any, uniformity and apparently do not relate to the visual aspects of flight. The imposition of optical requirements that have little or no effect on structural integrity, aerodynamics or visual processes can only lead to a more expensive part with no performance gain on the part of the pilot.

The second problem investigated arises from the aging and the maintenance of the windscreen or transparency. As a transparency ages, and as it is repeatedly cleaned, many small scratches appear on its surface. These scratches act as light scatterers and cause the transparency (canopy) to "light up" under some conditions, especially when an aircraft is flying directly into the sun (or some other bright light source). This "lighting up" or halation condition has its prime effect on the visual system by reducing the contrast of an object or target. This reduction in contrast not only makes it impossible to detect or locate small targets but may make even large targets disappear.

Since haze is a time-dependent problem, becoming significantly worse with the age of the transparency, the question arises as to when a transparency should be replaced. Current practice tends to leave this decision to the pilots, the offending transparency being replaced when enough complaints have been directed against it. Although this is a reasonable means for arriving at such a decision, this process seems highly judgmental and not very cost effective should such a transparency be replaced before it needed to be.

A technique is required, therefore, that would provide a quantitative (objective) means for relating the amount of haze present in a transparency and its measurable effect on operator visual performance. Such a technique would involve (1) measuring the amount of haze present in a transparency; (2) determining what effect such haze had on a visual task being performed by an operator; and (3) using the obtained data (in conjunction with pilot complaints) to determine when a transparency requires replacement.

To address these two problems, i.e., the lack of uniformity in optical specifications reqarding the number and size of minor defects permitted in a transparency and the need for a quantitative technique to relate the amount of haze present in a transparency to visual performance, two experiments were planned and conducted. The purpose of the first experiment was to determine the effect of opaque optical defects of various sizes and densitites (number per unit area) on an air-to-air target acquisition task. Since target acquisition is an extremely critical task and since performance on this task is most likely to be disrupted by opaque occlusions in the windscreen, data gathered from this experiment would contribute to the formation of new visual/optical specifications for aircraft transparencies relative to minor defects.

The second experiment was designed to determine what relationship, if any, existed between the amount of haze emanating from a transparency and the amount of the observer's field-of-view (FOV) or visual field that is "lost" (rendered unusable) due to the presence of the haze. The data obtained would serve as a first step towards the development of a technique for measuring the effect of haze on visual performance.

Discussion

Experiment I - Minor Defects

Eight subjects performed a simulated air-to-air target detection task through test panels (simulated windscreens) that contained a given number (0, 11, 22, 33 or 44) of opaque defects of a given size (0.35, 0.093 or 0.032 inches in diameter). Figure 1 shows the test panel containing 44 of the 0.35 inch size defects.

The target to be detected differed in size (0.5 and 1.0 minute of arc) and contrast (80% and 10%) and appeared at random locations within a 14° FOV. The scenario used simulated an aircraft pilot performing an in-cockpit visual task followed immediately by an out-the-cockpit visual search of a segment of the sky. The visual conditions of this task were considered to be similar to those experienced by a pilot who is monitoring his radar screen and then looking out of the aircraft to obtain a visual fix. Figure 2 shows the experimental setup used in the conduct of this experiment.

Performance of each subject was evaluated in terms of the time it took to detect the target (detection time) and the accuracy of these detections (percent correct detections). Table 1 shows the data for detection time while Table 2 shows the data for percent correct detection.

With the clear (zero defects) test panel, the average time to detect the 1.0 minute, 80% contrast target was 3.2 seconds while for the 10% contrast target the average time was 11.8 seconds. For the smaller target (0.5 minutes), these average times increased to 17.2 and 20.0 seconds for the 80% and 10% contrast targets respectively.

Interposition of a panel containing defects 0.032 inches in diameter did not significantly effect performance. The average time to detect the 1.0 or the 0.5 minute high contrast target was 2.7 and 15.2 seconds respectively. When contrast was reduced to 10%, the average time to detection for these same targets increased to 12.8 and 19.4 seconds respectively. Although a defect of 0.032 inches is allowable under currently employed acceptance procedures, the number of defects per panel greatly exceeded present specifications.

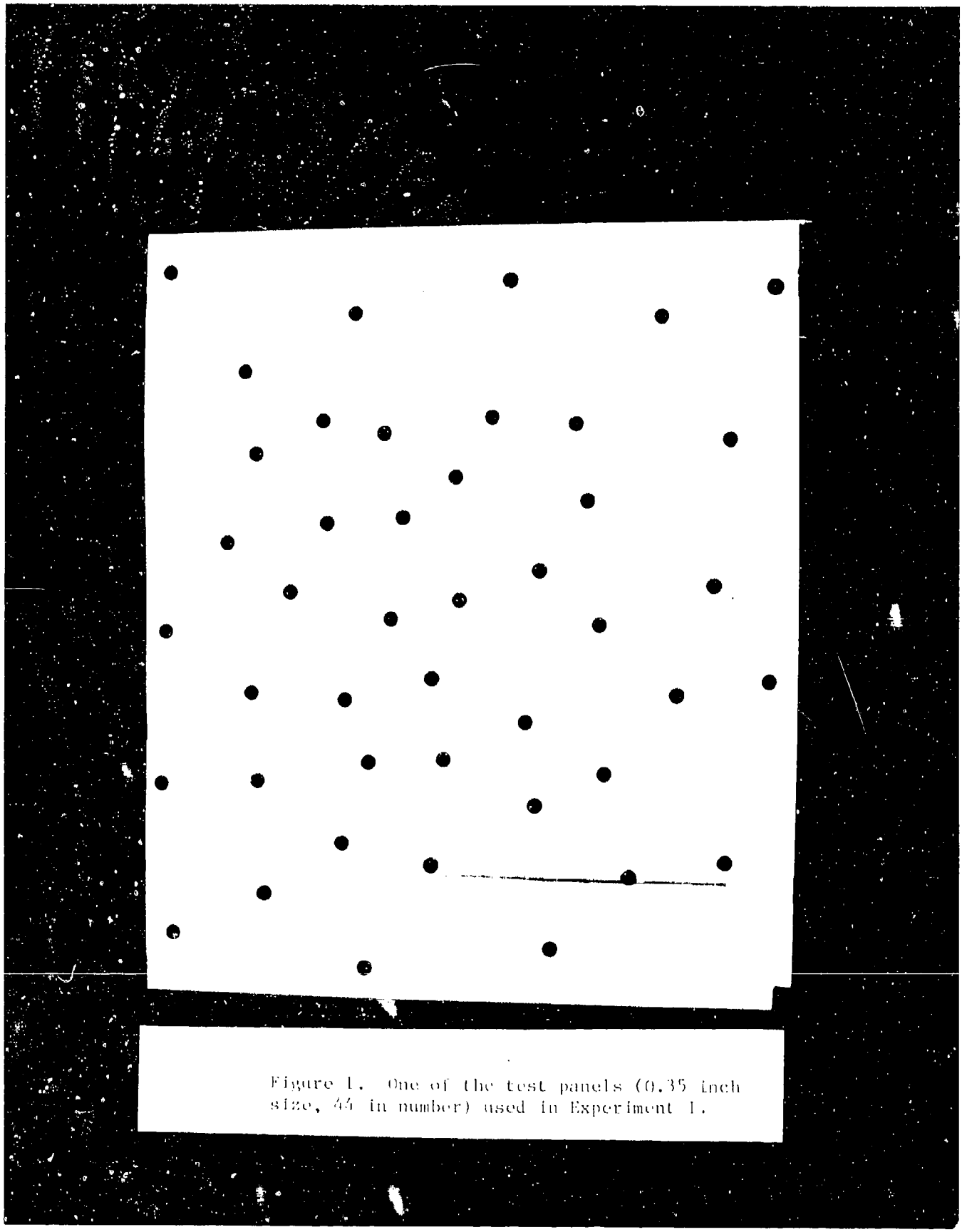

Figure 1. One of the test panels (0.35 inch size, 44 in number) used in Experiment 1.

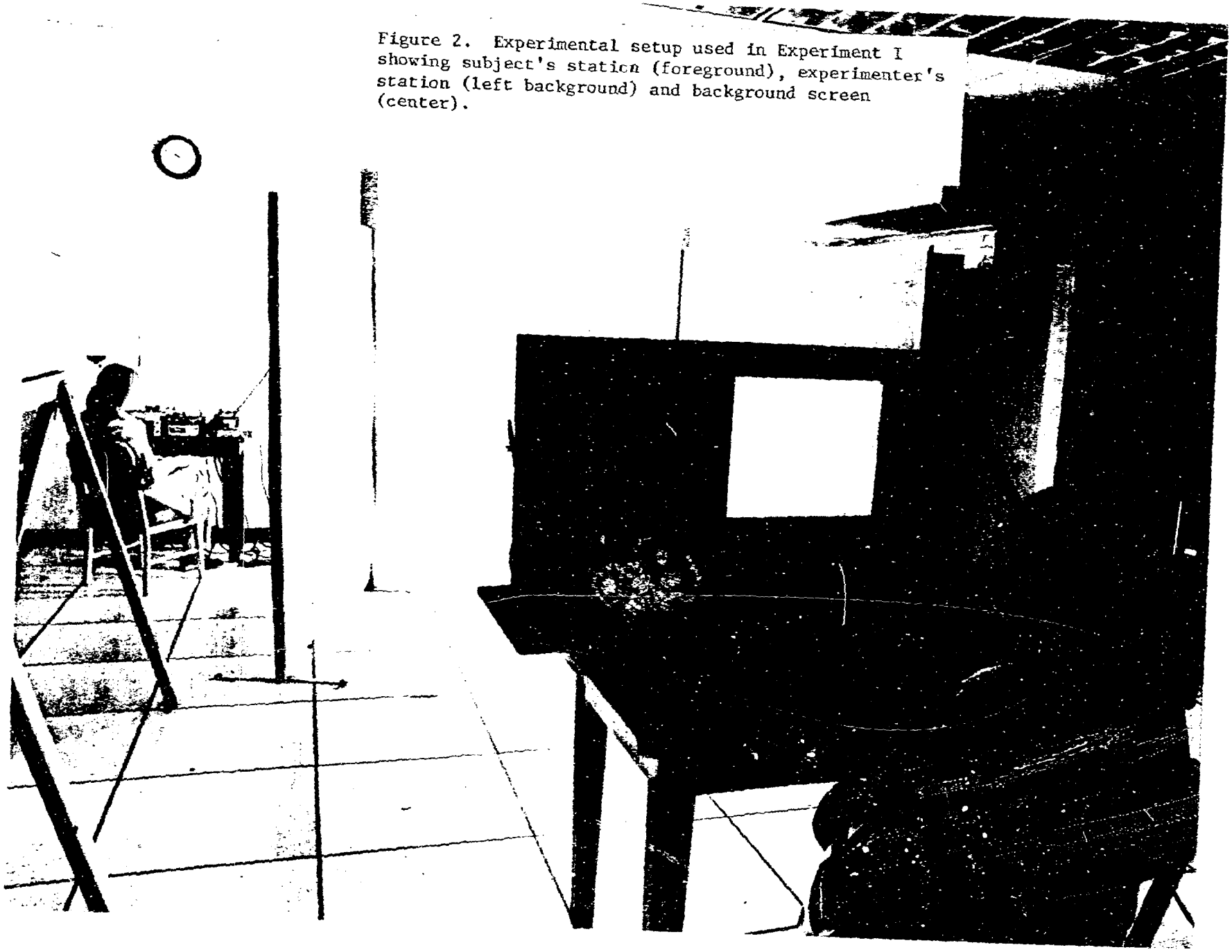

Figure 2. Experimental setup used in Experiment I showing subject's station (foreground), experimenter's station (left background) and background screen (center).

Table 1

AVERAGE TIME TO DETECTION (SECONDS)

		10% Contrast Defect Size				80% Contrast Defect Size			
	No. Defects	0.0	0.032	0.093	0.35	0.0	0.032	0.093	0.35
Tgt. Size	0	11.8	---	---	---	3.2	---	---	---
	11	---	13.1	11.7	13.2	---	2.7	2.6	2.4
	22	---	13.5	14.5	13.3	---	2.6	2.9	2.9
1.0'	33	---	11.7	14.5	12.2	---	2.4	3.0	2.9
	44	---	12.9	14.5	13.1	---	3.1	3.1	3.4
	0	20.0	---	---	---	17.2	---	---	---
	11	---	18.7	20.0	20.0	---	15.9	16.0	15.1
0.5'	22	---	21.2	24.9	21.8	---	15.5	16.6	17.1
	33	---	20.0	16.9	18.9	---	19.1	15.3	15.9
	44	---	17.8	19.7	24.0	---	13.2	14.6	23.0

Table 2

PERCENT CORRECT DETECTIONS

		10% Contrast Defect Size				80% Contrast Defect Size			
	No. Defects	0.0	0.032	0.093	0.35	0.0	0.032	0.093	0.35
Tgt. Size	0	84	---	---	---	96	---	---	---
	11	---	95	95	89	---	100	99	99
	22	---	98	88	91	---	100	100	100
1.0'	33	---	91	86	89	---	100	99	94
	44	---	89	81	89	---	95	100	96
	0	56	---	---	---	66	---	---	---
	11	---	70	71	63	---	89	83	83
0.5'	22	---	74	59	65	---	89	93	73
	33	---	74	56	56	---	85	88	81
	44	---	73	66	53	---	88	76	66

Using a panel containing defects that exceeded the acceptance standard in terms of size (0.093 inches) and specifications for number in a given area (1 to 2 per square foot), performance once again was found not to be significantly affected for the two high contrast targets. Detection times averaged 2.9 and 15.6 seconds for the 1.0 and 0.5 minute targets respectively. As was the case for the 0.032 inch defect size, these times are slightly better (faster) than those attained with the zero defect test panel. When the contrast for these same targets was reduced to 10%, detection times increased to 13.8 and 20.4 seconds repectively.

Interposition of a panel containing exceedingly large defects (0.35 inch) again resulted in little or no effect on target detection times. Detection times averaged 2.9 and 17.8 seconds for the 1.0 and 0.5 minute high contrast targets respectively. These times are again slightly faster than those obtained with the zero defect test panel. The times for these same targets at the low contrast were 13.0 and 21.2 seconds respectively.

In terms of percent correct detections, performance with the zero defect panel yielded 96% correct detections for the 1.0 minute high contrast target and 84% for the low contrast target. For the 0.5 minute target, these percentages decreased to 66% and 56% for the high and low contrasts respectively.

Interposition of test panels containing defects of 0.032, 0.093 or 0.35 inches in diameter resulted in detection performances that were superior to that obtained with the zero defect test panel irrespective of the size or contrast of the target viewed. For the 0.032 inch size defect, detection performances of 99% and 88% were obtained for the 1.0 and 0.5 minute high contrast targets respectively. For these same targets at a lower contrast, performances of 93% and 73% were achieved.

The panel containing 0.093 inch size defects yielded detection performances of 100% and 85% while the panel containing defects of 0.35 inches in size led to detection performances of 97% and 76% for the 1.0 and 0.5 minute high contrast targets respectively. When the contrast for these targets was reduced, performances of 88% and 63% were achieved with the 0.093 inch defect size and 90% and 59% were achieved with the 0.35 inch defect size.

The combination of defect size and number of defects on the test panels employed resulted in test conditions that greatly exceeded the maximum size and number of defects requirements contained in the various specifications and acceptance procedures. Therefore, the data obtained presumably can be used to determine any relationships that may exist between oeprator visual performance and the number and size of opaque optical defects found in aircraft transparencies.

The most obvious findings of this study are the superiority in performance attained due to the size (the 1.0 minute target being superior to the 0.5 minute target) or contrast (the 80% contrast target being superior to the 10% contrast target) of the target employed. In comparing the relative effects of contrast and range (size of targets) on detection time it was found that doubling the range increased target detection time by a factor of 5.7 for the high contrast target and a factor of 1.58 for the low contrast targets. Reducing the contrast of a target by a factor of 8 increased target detection time by approximately a factor of 4.41 for the large target and a factor of 1.22 for the smaller targets. This finding indicates that differences in range have a much greater impact on target detection time than do differences in contrast as long as both parameters remain above threshold. Although these findings are valid and of interest, our main concern in this experiment was to determine the effects of size and number of defects on target detection performance. A closer look at these variables will be accomplished by examining performance within a given target size and contrast level.

Looking first at performance when the 1.0 minute high contrast target was used, we find that the size of the defect or the number of defects on the test panel had no effect on performance of the required task. Detection times averaged 2.8 seconds (2.7, 2.9 and 2.9 seconds for the 0.032, 0.093 and 0.35 inch defect size respectively) irrespective of the size of the defect or the number of defects on the test panel. This was also true for detection performance, correct detections averaged 99% irrespective of the size and number of defects on the panel. These findings indicate that the size of a defect or the number of such defects has little, if any, effect on the performance of a target detection task.

When the same high contrast target, however, is reduced in size to 0.5 minutes, the variables of size and number of defects appear to effect performance. The average detection time for the largest defect size (0.35 inch) was 2 seconds longer (17.8 seconds) than the average times for the two smaller defect sizes (15.9 and 15.6 seconds for the 0.032 and 0.093 inch sizes respectively). Additionally, detection times were much more variable across number of defects for all three sizes with the worse performance (23 seconds) occurring when 44 of the 0.35 inch size defects were on the panel. Detection performance also reflect the same trends exhibited by the detection times. As defect size increased, detection performance became worse, decreasing from 88% (0.032 inch size) to 85% (0.093 inch size) to 76% (0.35 inch size). Performance is again much more variable as a function of number of defects with the worse performance (66%) occurring when 44 of the 0.35 inch size defects were on the panel.

Based on the above findings, it appears that a human observer can tolerate the presence of minor opaque defects in a far greater number and size than currently specified. Additionally, although open to conjecture, it may be that the size and number of defects permitted on a transparency may not be a valid indicator of the "goodness" or "badness" of a transparency and that perhaps some other indicator should be used.

Experiment II - Haze

Ten subjects performed a simple target detection task in which they were required to indicate when they could see a slowly moving, 1.0 minute of arc, 80% contrast target that traveled in 8 (0, 45, 90, 135, 180, 225, 270 or 315 degrees) different angular directions from the center of a background screen (see Figure 3) towards the periphery. The subjects performed the above task while looking through haze test panels (see Figure 4) mounted at 90°, 63° or 45° to their line of sight and which when illuminated by a bright light source mounted at the center of the background screen resulted in haze conditions of 2% - 3.5%, 5% - 10%, 15% - 26% or 25% - 48%. As a matter of convenience, these haze conditions will be referred to as the 2.75%, 7.50%, 20.50% or 36.50% haze conditions. A baseline condition, in which no test panel was interposed between the subject, the task and the bright light source, was also administered. A 7/8 inch annulus was positioned in the center of each panel and was used to protect the subject from having the bright light source shine directly into his eye. Figure 5 depicts the experimental setup used.

Subject performance was evaluated in terms of (1) the distance the target had traveled before being seen and (2) the number of times that it was not detected (misses). The first measure provides the data required for deriving "contour maps" of the visual area of the background FOV that is "lost" due to the amount of haze present while the second measure provides an indication of the effect of haze on visual performance.

The data obtained are presented in Tables 3 and 4. Table 3 shows the mean distances that the target traveled before being detected while Table 4 shows the number of misses that occured for each treatment condition employed. Immediately apparent from an examination of these two tables is the fact that as the percent of haze increased, the distance that the target traveled and the number of misses that occurred also increased. It is also apparent that the slope at which the panel was mounted did not effect the distance traveled measure but seem to have some effect on the number of misses that occurred.

Using the data from Table 3, contour maps of the areas "lost" as a function of the haze present are shown in Figures 6, 7 and 8 for each of the angles at which the panels were mounted. Examination of these figures shows, quite obviously, the increase in the area that is lost (occluded) as the percent of haze increases.

Although the data from Table 3 and Figures 6, 7 and 8 are helpful in showing the trends that occurred, no figure of merit can be attributed to these trends. The following technique was used, therefore, to further examine the data. The scores for each haze condition were collapsed across the variable of angular direction to obtain an average for that condition. These averages are shown in the last line of Table 3. Since the target always moved from the center of the background screen to the periphery, the assumption was made that these averages represented radii of various-sized, circular FOVs. These averages were doubled and then used to determine the FOV that each haze condition occluded. The FOVs obtained and the percent of the background FOV that it occluded are shown in Table 5. The percentages were obtained by dividing the obtained FOVs by the background FOV (26.45°) and multiplying the resultant quotient by 100.

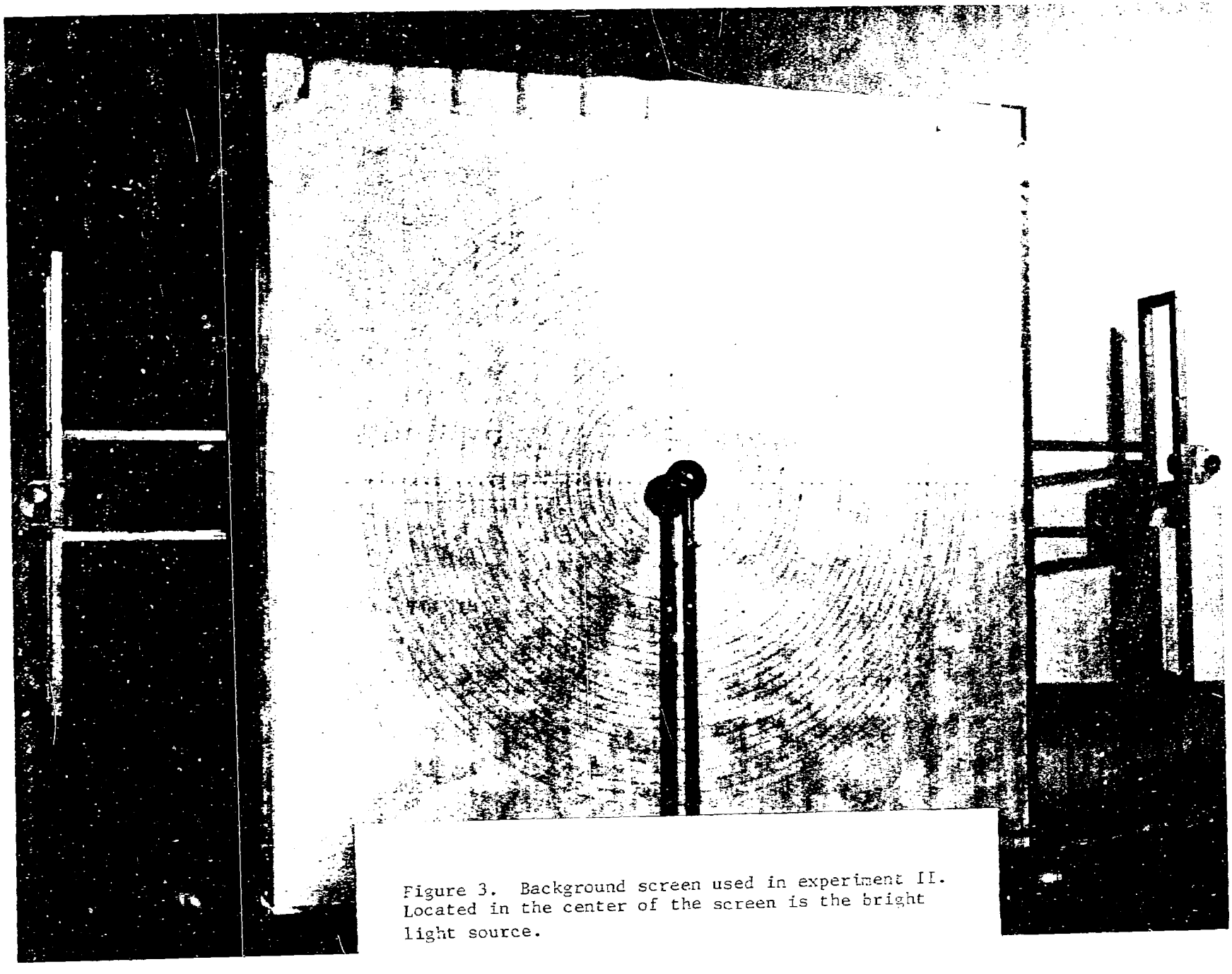

Figure 3. Background screen used in experiment II. Located in the center of the screen is the bright light source.

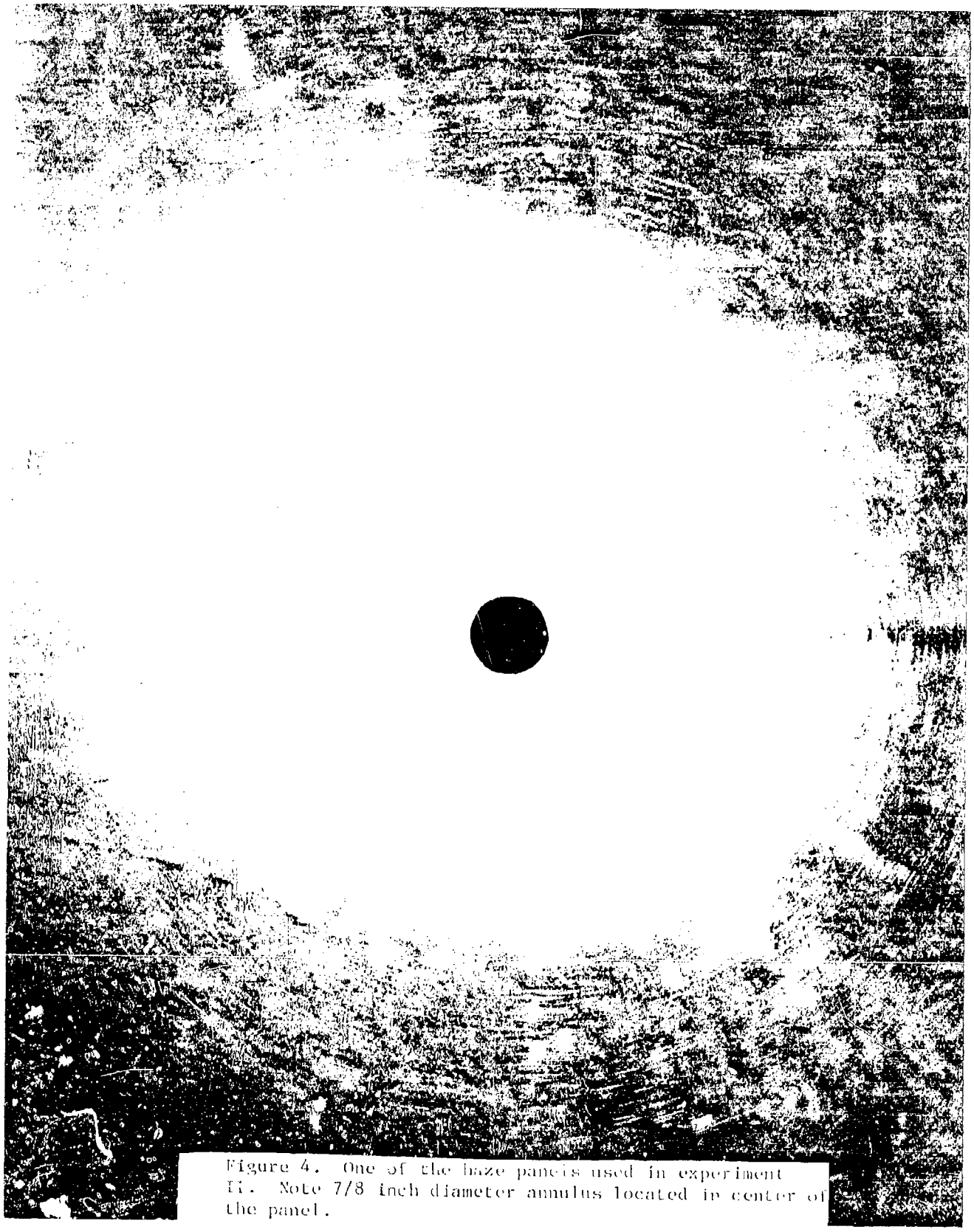

Figure 4. One of the haze panels used in experiment II. Note 7/8 inch diameter annulus located in center of the panel.

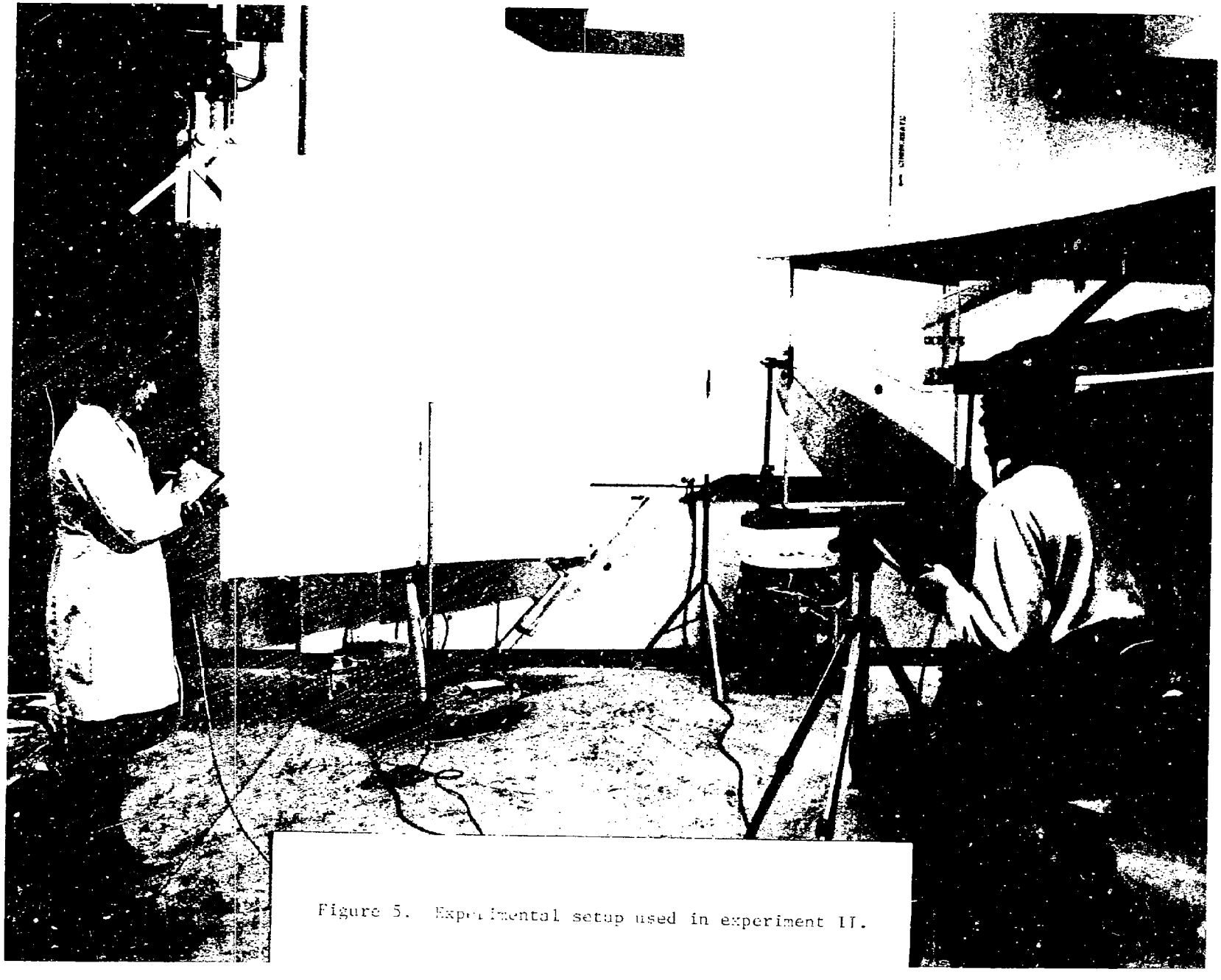

Figure 5. Experimental setup used in experiment II.

Table 3

MEAN DISTANCE TRAVELED (INCHES)

Angular Direction	Percent Haze												
	0.0	2,75			7.50			20.50			36.50		
		90°	63°	45°	90°	63°	45°	90°	63°	45°	90°	63°	45°
0	3.20	8.06	8.98	6.78	12.91	12.81	12.88	19.00	21.31	20.04	24.09	22.75	23.25
45	3.23	5.58	9.75	7.25	7.73	9.60	8.88	17.58	18.08	18.61	22.12	27.25	25.25
90	3.18	6.00	7.00	5.63	10.67	15.13	11.25	21.00	20.68	19.94	24.19	25.08	24.14
135	2.83	4.33	5.90	6.23	8.10	10.78	8.40	19.48	23.73	21.34	23.78	20.25	23.80
180	3.35	7.25	10.19	7.83	11.80	12.92	9.83	23.25	10.25	25.13	21.03	26.75	11.75
225	2.91	6.75	5.75	5.38	8.75	8.83	6.90	20.05	21.60	17.64	23.31	22.40	20.38
270	2.95	8.90	6.83	5.50	13.53	10.00	9.28	22.78	15.47	16.89	19.88	16.31	16.39
315	3.11	6.05	7.15	6.95	8.50	9.53	8.85	16.25	18.48	17.28	23.25	20.56	20.19
	3.10	6.62	7.69	6.44	10.25	11.20	9.53	19.92	18.70	19.61	22.70	22.67	20.64

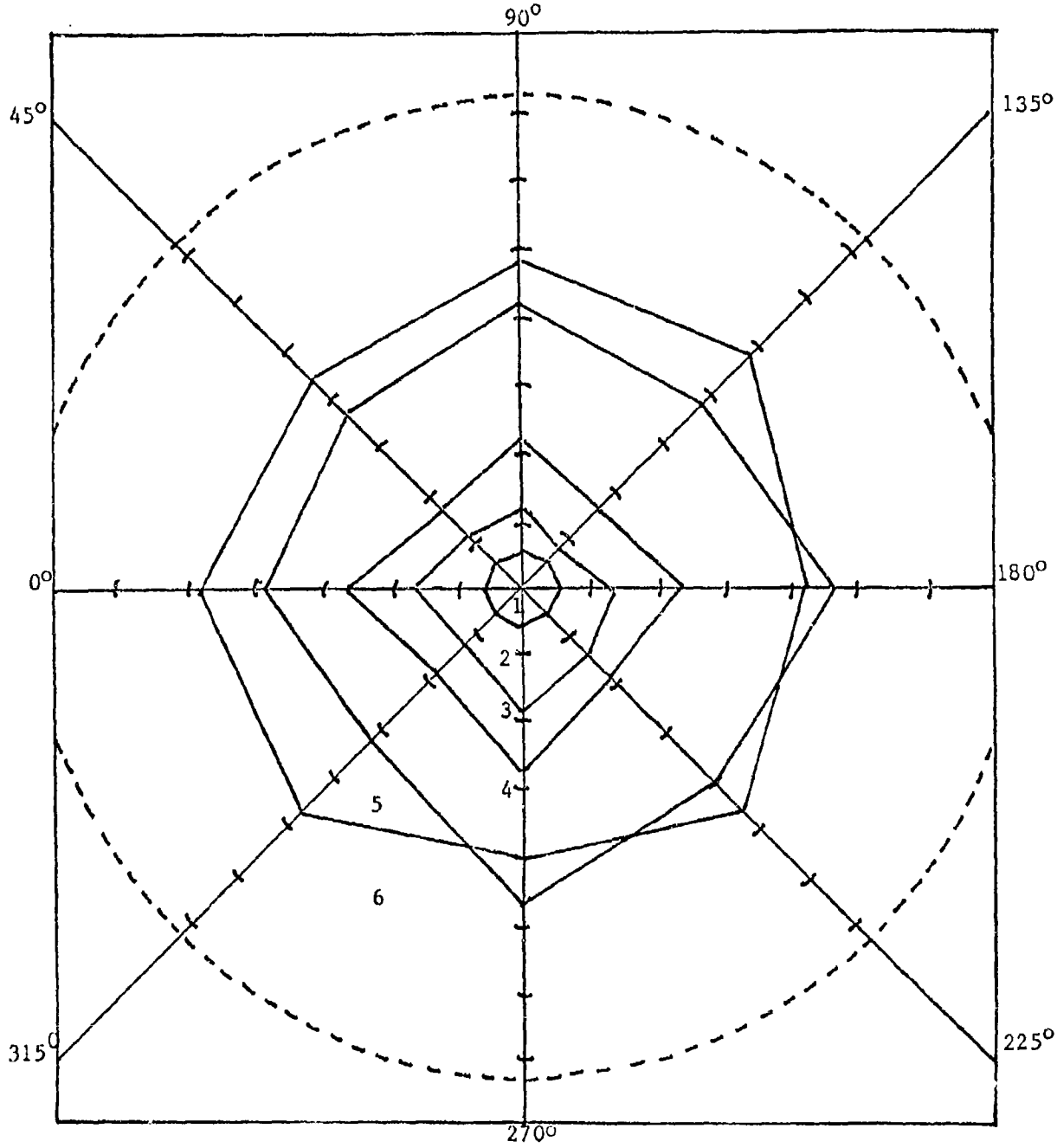

Figure 6. Regions of background FOV that is occluded as a function of percent of haze for 90° mounted panel. The Nos. 1, 2, 3, 4, 5 and 6 represent the no haze, 2.75%, 7.50%, 20.50%, 36.50% haze conditions and the background FOV respectively.

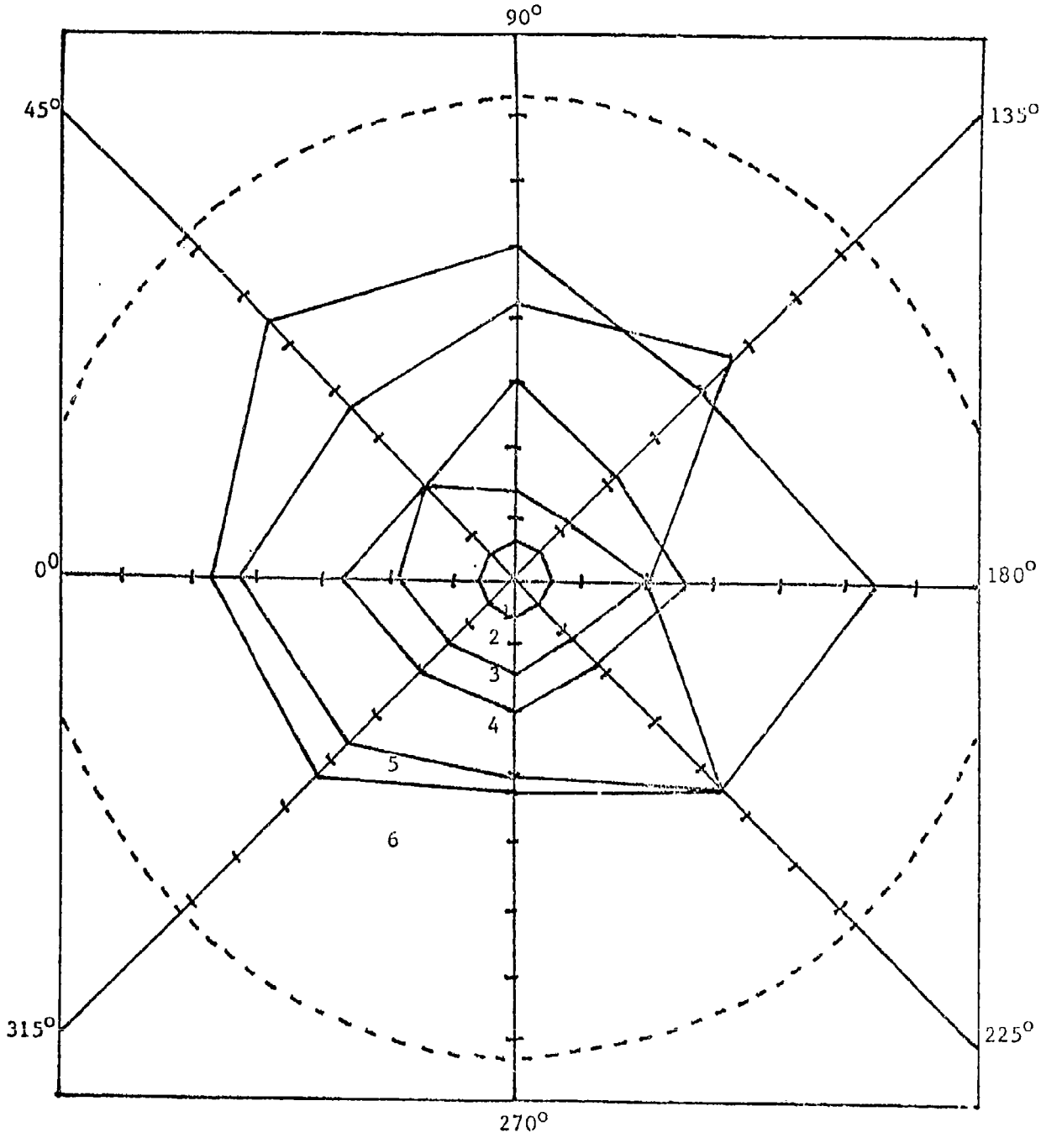

Figure 7. Regions of background FOV that is occluded as a function of percent of haze for 63° mounted panel. (See Figure 6 for explanation of Nos. 1, 2, 3, 4, 5 and 6.)

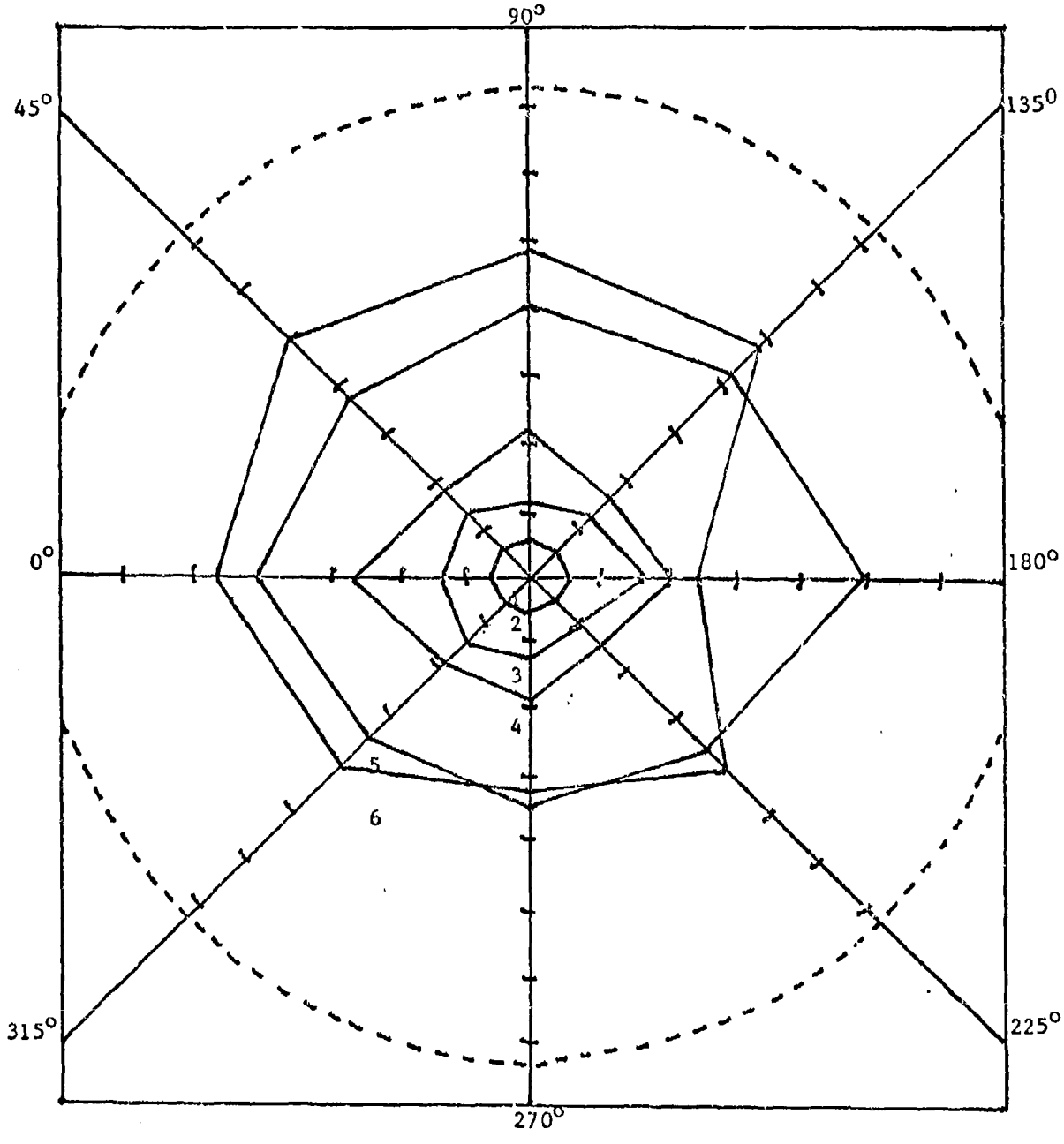

Figure 8. Regions of background FOV that is occluded as a function of percent of haze for 45° mounted panel. (See Figure 6 for explanation of Nos. 1, 2, 3, 4, 5 and 6.)

Figure 9 shows these percentages plotted as a function of the amount of haze present. Two things are immediately apparent from this figure. First, we see a rapid increase in the percent of the background FOV that is occluded as the percent of haze present increases. Secondly, the angle at which the panel was mounted to the observer's line-of-sight did not influence the amount (percent) of the area that was lost. It is of interest to point out that the percent of background FOV that is occluded increased from 9% (no haze) to 19% (2.75% haze) to 28% (7.50% haze) to 54% (20.50% haze) to 61% (36.50% haze). The loss in FOV for the no haze condition is attributed to the presence of the bright light and the 7/8 inch diameter annulus used to protect the subject.

To determine the effect of haze on the observer's visual performance, the data in Table 4 were collapsed across the variable of angular direction to obtain the total number of misses that occurred for each haze condition. These are shown in the last line of Table 4. The total number of misses for each treatment condition was then divided by 80 (the number of trials per condition) and the resultant quotient multiplied by 100 to obtain the percentage of time that the target was not detected (missed). This percentage was then subtracted from 100% to obtain the percentage of time that the target was detected. These latter percentages were then plotted as a function of percent of haze and are depicted in Figure 10.

Immediately obvious from an examination of Figure 10 is the fact that as the percent of haze present increased, detection performance decreased. Additionally, this decrease seems to be influenced by the angle at which the panel was mounted to the observer's line of sight. The decrease was greatest when the panel was mounted at 62° (100% to 49%). For the 45° mounting agle, the decrease was from 100% to 55% while for the 90° mounting angle the decrease was from 100% to 69%. This finding would seem to indicate that the angle at which the panel was mounted and the amount of haze present interacted in some manner to influence target detection performance.

Comparing the data from Figures 9 and 10, it can be noted that when 2.75% haze was present, 19% of the FOV was occluded but detection performance still was very high, 98% of the targets being detected when they emerged from behind the occluded area. When the amount of haze present was increased to 7.50%, 28% of the FOV was occluded, but again detection of the target as it emerged out of the occluded area remained high, 95% of the targets being detected. However, when the amount of haze present was increased further (20.50% and 36.50%), the percent of the FOV that was occluded became excessive (54% and 61%) and detection of the target outside of the area occluded fell off to 84% and 58% respectively. Thus, although detection performance was fairly high (95%) when 28% of the FOV was lost (haze ranging from 5% to 10%), this detection occurred only after the target emerged from behind the occluded area.

Table 4

NUMBER OF MISSES

	Percent Haze												
	0.0	2.75			7.50			20.50			36.50		
Angular Direction		90°	63°	45°	90°	63°	45°	90°	63°	45°	90°	63°	45°
0	0	1	0	2	2	2	0	1	2	3	2	6	3
45	0	0	0	1	0	0	0	0	0	1	4	8	8
90	0	0	0	0	1	0	0	0	3	1	6	4	3
135	0	0	0	0	0	0	0	0	0	2	2	8	5
180	0	0	1	0	0	4	1	4	9	8	1	9	9
225	0	0	0	0	1	1	0	0	0	1	6	3	6
270	0	0	0	0	0	0	0	2	1	1	2	2	1
315	0	0	0	0	0	0	0	0	0	0	2	1	1
	0	1	1	3	4	7	1	7	15	17	25	41	36

Table 5

PERCENT OF FOV OCCLUDED BY HAZE

	Percent Haze												
	0.0	2.75			7.50			20.50			36.50		
		90°	63°	45°	90°	63°	45°	90°	63°	45°	90°	63°	45°
FOV (°)	2.28	4.86	5.62	4.73	7.53	8.23	7.00	14.63	13.74	14.41	16.68	16.65	15.16
FOV Occluded(%)	9	18	21	18	28	31	26	55	52	54	63	63	57

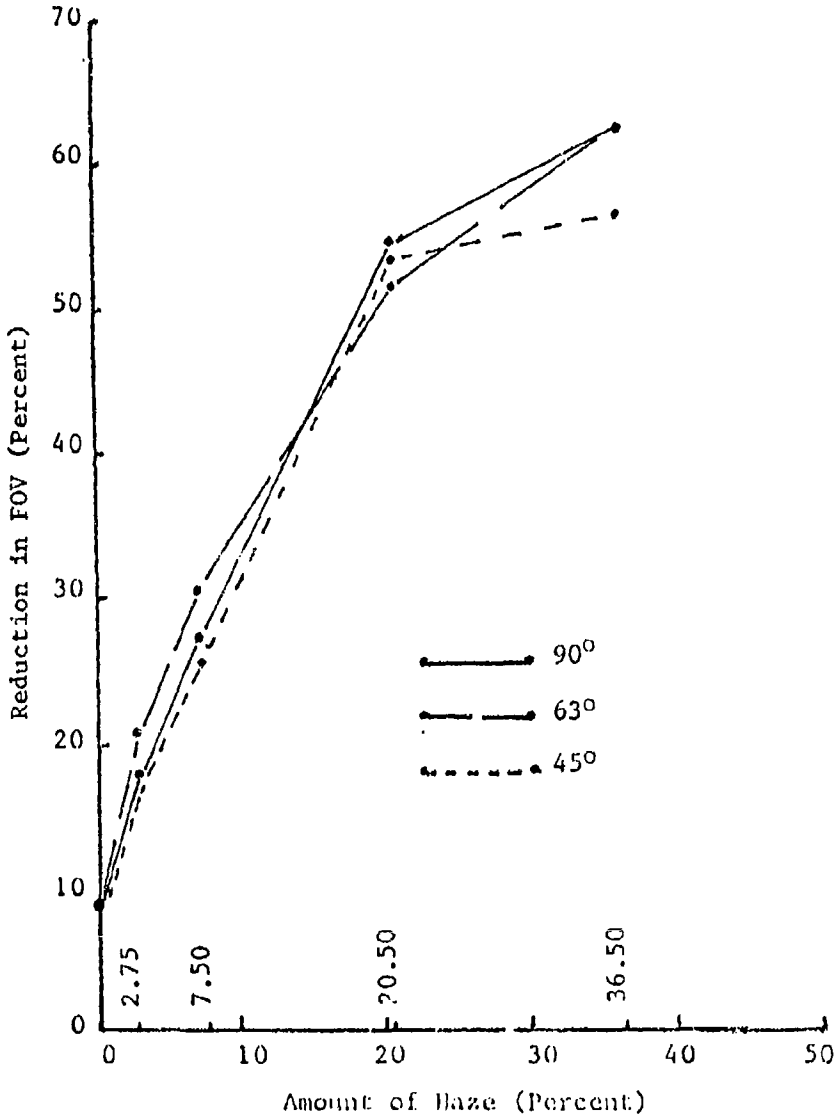

Figure 9. Reduction in FOV as a function of the amount of haze present for three panel angles.

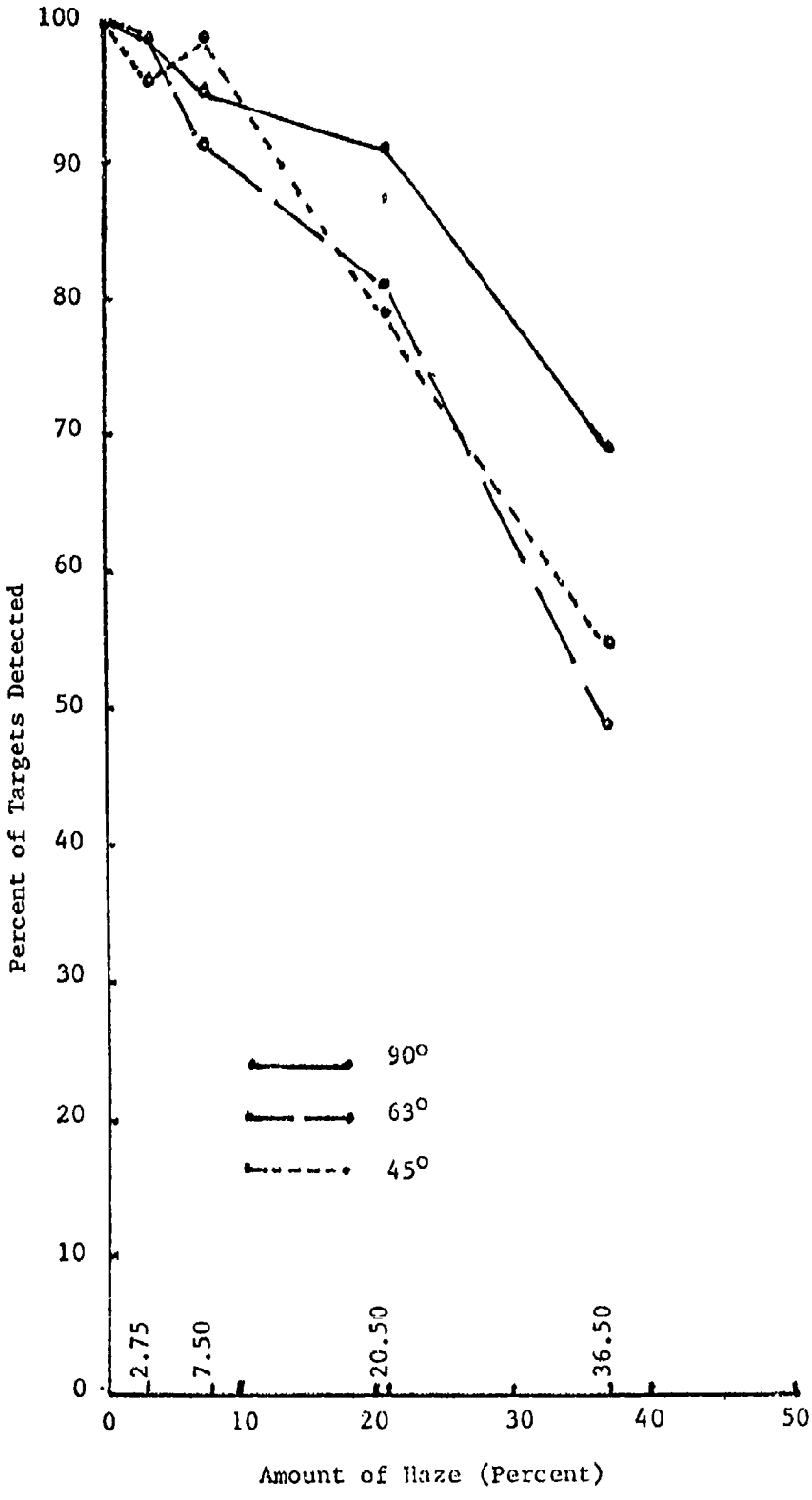

Figure 10. The percent of targets detected as a function of the amount of haze present for three panel angles.

Summary

Current specifications and acceptance standards regarding the size and number of minor defects reflect a marked lack of uniformity. Additionally, there is no objective means for determining when a transparency should be replaced due to the amount of halation found in it. To address these two problems, two experiments were performed. As a result of these experiments, it appears that (1) a human observer can tolerate the presence of minor defects in far greater number and sizes than currently specified that current specifications may be safely relaxed without impairing visual performance and (2) with a 28% FOV loss, observer's were able to detect the target at a high detection rate but only after the target emerged from the occluded area. It is suggested that perhaps another study be performed to determine not only the FOV loss but also the length of time that the target is lost from view.

Rererences

1. MIL-G-5485C, Glass, Laminated, Flat, Bullet Resistant, 23 Apr 71.

2. MIL-G-25667B, Glass, Monolithic, Aircraft, Glazing, 29 Nov 77

3. Lawrence, J. H., Jr., "Guidelines for the Design of Aircraft Windshield/Canopy Systems," Air Force Wright Aeronautical Laboratories, Wright-Patterson AFB, OH, AFWAL TR-80-3003, Feb 80.

4. Acceptance Test Procedure 601E, F-111 Windscreens and Canopies.

5. Critical Item Development Specification, F-16 Transparencies, Specification No. 16ZK002D, 21 Nov 78, General Dynamics, Ft. Worth, TX.

6. Northrop Process Specification IT-35, "Optical Requirements for F-5A, F-5E," 22 Feb 79.

AD-P003 224

THE REDUCTION OF LIFE-CYCLE COSTS THROUGH CONTINUING ACRYLIC MAINTENANCE

R. J. Stillman and H. A. Wilson,
Micro-Surface Finishing Products, Inc.

THE REDUCTION OF LIFE-CYCLE COSTS THROUGH CONTINUING ACRYLIC MAINTENANCE

Herbert A. Wilson
Robert J. Stillman

Micro-Surface Finishing Products, Inc.
April, 1983

ABSTRACT

Acrylics, with all of their shortcomings, are the preferred wearing inner and outer surfaces of most aircraft transparencies, in either laminated or solid panels. The physical properties are superior to alternate materials and the strength/weight ratio is attractive.

Acrylics do mar and craze, and the maintenance of quality surfaces was and is a challenging problem.

With the development of cushioned abrasives in 1960, a promising repair system evolved, and in 1969 and 1970 the Military introduced the RS-69 repair kit and Mil-Spec 58091-A.

Training programs at Ft. Rucker and other bases showed the way to extended life and reduced life cycle costs of aircraft transparencies. The process was adopted by all manufacturers of aircraft acrylics in the U.S. and abroad. Airlines were quick to realize the value of line maintenance to restore cabin or cockpit windows in place.

Northrup Corporation in 1978 collaborated in the design of a new kit, the NC-78-1, which may become the new Military kit, replacing the outdated RS-69. Air rework facilities are conducting seminars to upgrade the skill levels at their installations, and the aviation technical schools of the country are all teaching acrylic maintenance using cushioned abrasives.

In the future, more in place restorals will be done on civilian, Military, and airlines' aircraft. Training of personnel will be increased and transparent acrylic life cycle costs will be reduced, a promise we can all happily anticipate.

THE REDUCTION OF LIFE-CYCLE COSTS THROUGH CONTINUING ACRYLIC MAINTENANCE

When acrylics were discovered and first proposed for aircraft transparencies, proponents could not contain their enthusiasm. The material was strong, easily formed, readily cut to size and shape, and optically equal to glass. The economics of fabrication were attractive. Acrylics for aircraft transparencies swept upon the scene.

However, acrylics, while very promising, were not the answer to a "maiden's prayer". Wipers scratched the surface. Resilience was lacking. Toughness was limited. Crazing was found to be unavoidable and not tolerable; and on top of this, new demands were being continually made on aircraft transparencies to withstand impact, pressures, temperatures, and UV conditions previously unheard of. Problems abounded!

The further development of stretched acrylic increased the surface hardness and improved the physical characteristics and strength. The future looked brighter as engineers and designers responded with complex laminates combining the best of all materials, the new stretched acrylic, glass, and polycarbonates, to form our highly sophisticated aircraft transparencies of the 1970's and today.

Restoral of these acrylic and polycarbonate materials was very difficult and replacement with new units was the prevailing practice. Those pressed to extend the useful life of windscreens and canopies turned to the finest abrasives they could find: toothpaste, jeweler's rouge, and any solution of the finest abrasive powders in a slurry. The practice was to attack surface scratches by polishing them out in as small an area as possible, and distortion was always the certain result.

But what of crazing? This sub-surface defect could not be polished out and the rumor began, which is still heard today: "THERE'S NOTHING THAT CAN BE DONE ABOUT CRAZING!"

Tolerance of crazing and the black art of toothpaste and jeweler's rouge carried us through World War II and produced thousands of airplane mechanics who preached the gospel of toothpaste repairs and tolerance of crazing.

In this technological void, aircraft manufacturers' specifications were almost non-existent, polishing materials were limited, satisfactory repairs were few and far between, and replacement was the expensive corrective action. Repair shops and FEO's, having temporary custody of aircraft, instructed personnel, "For God's sake, don't touch the windshield!"

In the 1960's, cushioned abrasive products were developed, and some of these products offered promise in the maintenance of aircraft transparencies. In 1968 and 1969, Micro-Surface Finishing Products became committed to this promise and visited the aircraft companies, airlines, and military bases around the country offering a kit and instructions for not only the repair of surface damage, but the corrective repair of crazing.

Skeptics abounded at all levels. However, the powerful demonstrations could not be denied and in 1970 Mil Spec 58091-A was written, followed by the Technical Bulletin TB 55-1560-276-2411. The cushioned abrasive product was called "Polysand" at that time, but now is known as MICRO-MESH. Mr. Robert Stillman of Micro-Surface fathered the kit, the Mil Spec, and the Technical Bulletin, and in poetic justice, the Military Kit has been designated the RS-69. Robert Stillman designed that kit in 1969.

This immediately followed an extensive testing program at Ft. Rucker, in which the practicality of refinishing badly scratched HU-1 windshields was clearly demonstrated. Besides the obvious reduction in life-cycle costs, in-place restorations could be accomplished with almost no loss of effective flying time due to removal and replacement procedures. Relatively untrained personnel could easily perform this function, not only on windshields, but on other transparencies as well. The Military Technical Bulletin TB 55-1560-276-2411 was circulated at that time, followed by the full coordination of the Specification by other branches of the Military in 1971, and the issuance of NSN 1560-00-450-3622.

The ability of cushioned abrasives to reliably produce quality consistent scratch patterns reduced to a level of below one RMS, opened a whole new range of restoral possibilities to prolong the life and reduce the life cycle costs of acrylics. Crazing at depths of .003, .010, or even .035 could be effectively dealt with in appropriate windshields.

Aircraft manufacturers' response was enthusiastic; acrylic and polycarbonate materials used in manufacturing aircraft transparencies could be greatly improved, and the manufacturers of aircraft transparencies all embraced this new technology then as they do today.

Micro-Surface Finishing Products, Inc. continued its research and development program during the ensuing years in an effort to accomplish a three point goal; a more complete and effective polishing system for acrylics, procedures for the polishing of polycarbonates (heretofore an almost impossible task) and the incorporation of power tools within a system that would make possible the salvage of badly crazed transparencies.

In 1978 a refined and enlarged version of the RS-69 Military Kit was submitted to Northrup Corporation for use on F-5 aircraft canopies. After several minor modifications, this kit was designated as NC-78-1, accepted for use by Northrup, and Northrup Specification PL-1 was written around it. This kit and its specification are currently the standard at Northrup and have been accepted by other aircraft manufacturers.

Cushioned abrasives have been improved greatly over the years and earlier problems of degeneration with heat, latex bleed-out, and short shelf life have been overcome. MICRO-MESH has a guaranteed shelf life of five years.

Presently the MICRO-MESH maintenance and restoral process is specified by:

U. S. Military	Lockheed
McDonnell Douglas	Mooney
Cessna	De Haviland
Gulfstream American	Lear
Northrop	Falcon Jet
Bell	Hughes
British Aerospace	Grumman
Australian Air Force	Swearingen
Rockwell International	Fokker

At the invitation of Norfolk Naval Air Rework Facility, Norfolk, Virginia, a five day training session was initiated for their employees in February of 1981. Specific instructions were

presented in an especially prepared training manual, along with "hands-on" experience, in the removal of crazing and the repolishing of F-14 and A-6 transparencies. Teams from several USAF bases participated in this session.

The value analysis results attests to the lower life cycle costs that can be attained. These training sessions are offered to any interested military or civilian groups and several more are scheduled for 1983.

Because most of us here at this conference have had a close association with aircraft transparencies, we are much more aware of, and very concerned with, the improper handling and maintenance during day to day use. Discussions with line personnel, civilian and military alike, indicate almost complete ignorance of cleaning materials and procedures.

Realizing the lack of enlightened maintenance personnel regarding aircraft acrylics, the Association of Aviation Technical Schools (ATEC) were contacted, and at their invitation, a training manual was written for their classroom instruction of students. This manual focuses primarily on proper methods and materials for the cleaning of transparencies. Also covered in detail is the evaluation of types of defects, and other pertinent information necessary before repair can be undertaken.

Micro-Surface became a Certified FAA Repair Facility in February, 1978, for the express purpose of gaining further knowledge about the problems of acrylic maintenance and restorals, and incidentally saving many airlines thousands of dollars annually.

Our experience in the restoral of thousands of windows for all jet liners produces the following list of causes for rejection:

1. Delamination - progressing from poorly machined and vulnerable flange edges (especially prevalent in those types with a straight bevel). (See Figure 1)

2. Crazing - penetrating from flanged edges resulting in rework not allowing the L and W dimensions to be maintained. (See Figure 1)

3. Physical damage caused by personnel in removal, handling, and shipping to the repair facility.

4. Paint stripper and solvent damage which has penetrated to a depth that compromises the integrity of the transparency. Shallow damage is as easily removed as crazing.

Seldom do we see rejections due to minimal overall thickness. Our restorations remove .012 on the average and there is usually enough stock thickness above minimum manufacturer's specs to allow rework three or four times.

Our advice to airlines is to do some line maintenance in place on the airliner for light to medium scratches and haziness. Limits as to the extent of damage (time) to do restorals "in situ" are set by each airline as they deem appropriate.

Upon removal at major overhauls or due to major defects, we recommend the services of custom restorers such as Micro-Surface Finishing Products, Inc.

The future challenges all of us to achieve lower life cycle costs through better methods and procedures.

We see airlines doing more "in situ" restorals and attempting to remove deeper damage through more aggressive sanding to reduce time, thereby saving the removal and reinstallation costs, seal costs, and loss through handling damage.

Aircraft manufacturers - and aircraft acrylic manufacturers - will be challenged to reduce failures by improved machining and better surfaces to resist the formation of crazing, particularly in the flanged area, both beveled and stepped.

Military establishments must have better trained personnel capable of fast, high quality restorals.

Civilian aircraft will be seeking more in place restoration, and FBO's will actively pursue this market opportunity.

Restoration services will continue to grow and will have operators geared to handle the requirements of civilian aircraft, airlines, and the military.

Personnel to perform these services must be trained. The ATEC programs are in place to train the new generation of aviation mechanics. Training sessions for personnel at military bases have begun and are expected to increase in number.

The war on lower life cycle costs is in the early stages. The arsenal of weapons is in place. The war will be won by those who stay atop the new developments and fight the good fight, and lost by those who fail to progress. The choice is yours to make. Nothing worthwhile ever comes easy. Lower acrylic life cycle costs are no exception. However, the rewards are well worth the effort.

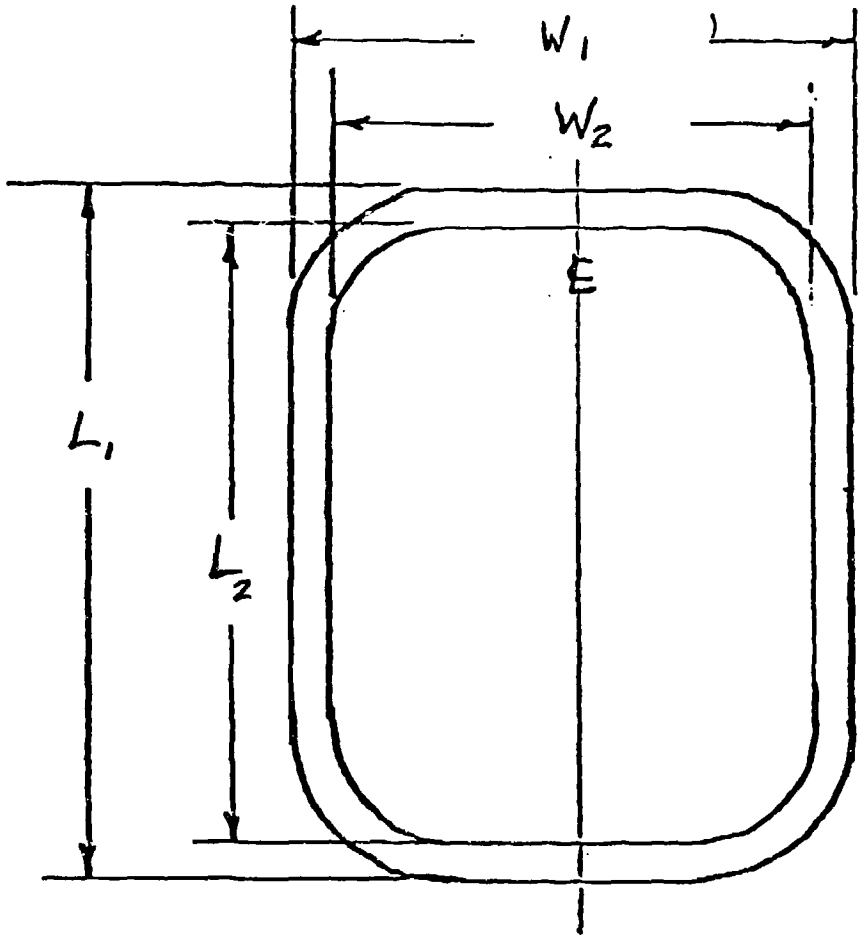

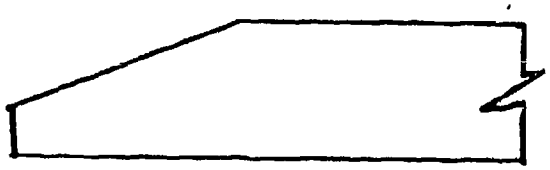

TYPICAL BEVEL EDGE

"Figure 1"

SESSION VI

UNDERSTANDING CURRENT SYSTEMS (PART II)

Chairman: M. R. Pollock
Boeing Commercial
Airplane Company
Seattle, Washington

Co-Chairman: G. W. Underwood
British Aerospace
Aircraft Group
Surrey, England

AD-P003 225

THE CERTIFICATION OF POLYCARBONATE TRANSPARENCIES - AN APPEAL FOR REASONABLE REQUIREMENTS

B. G. Hinds, Sierracin/Sylmer

"THE CERTIFICATION OF POLYCARBONATE TRANSPARENCIES - AN APPEAL FOR REASONABLE REQUIREMENTS!"

Billy G. Hinds

Sierracin/Sylmar

ABSTRACT

Aircraft design and operation conditions have changed -- so too have transparency materials. As aircraft become more fuel-efficient, glazing design must also become more fuel-efficient. New materials like polycarbonate, developed in the 1960's, make lighter weight, fuel-efficient windshields possible. The changes in aircraft and transparency design and materials must be reflected in the certification/load factor requirements imposed by the certifying authorities and in the inspection/testing necessary for quality assurance.

This paper looks at the physical properties of polycarbonate relative to glass and acrylic. It explores the current FAA/CAA certification requirements for glass and acrylic, and the ways polycarbonate can be damaged in the manufacturing processes.

In conclusion, it urges the FAA/CAA to treat polycarbonate windows as "transparent structure" and, recognizing the extent of the service life of aircraft glazings, not impose load factor requirements in excess of those required for other pressurized structure. It also urges the ASTM to develop standard procedures to evaluate as-processed polycarbonate to insure the finished product is free from induced strength or fatigue defects. Finally, it suggests the Air Force (the major user of polycarbonate in transparencies) should evaluate the effects of long-term environmental exposure on the structural characteristics of glazing materials including glass, acrylic and polycarbonate and their appropriate interlayers. The gathering of this data is long overdue.

Chief Project Engineer
Sierracin/Sylmar
Division of The Sierracin Corporation
12780 San Fernando Road
Sylmar, California 91342
© Sierracin Corporation, 1983

THE CERTIFICATION OF POLYCARBONATE TRANSPARENCIES - AN APPEAL FOR REASONABLE REQUIREMENTS

Background

The evolution of aircraft from open cockpit, slow speed flying machines to modern, high-speed commercial and business jetliners and ultra-high speed low-flying military aircraft has resulted in a dramatic change in the design of aircraft transparencies. Higher flight temperatures and pressurization levels, bird impact, anti-ice protection, and the use of transparencies to carry structural loads are all requirements that would be difficult or impossible to meet with the materials available to the early transparency designers and fabricators. Stretched acrylic and polycarbonate are two of the major material innovations developed specifically for increased aircraft performance and safety demands. But, while material developments have kept pace with aircraft changes, certification requirements do not recognize the fundamental performance differences between the most used transparency materials.

Technical Discussion

Until the early 1960's glass and as-cast acrylic were the most used materials in the manufacture of aircraft transparencies. Both materials are brittle; i.e., the percent of elongation under load is small (see Figure 1). Thus, the transparency designer could only work in the elastic range of these materials, even for ultimate loading, resulting in heavy transparencies and/or heavy structure to isolate the window from structurally induced loads. Furthermore failure of a brittle material, especially glass, is usually catastrophic.

In glass, cracks will propagate at the speed of sound because of the stored energy inherent in the tempering process. Thus for glass, and as-cast acrylic, it is necessary to keep the operating stresses very low and provide dual load paths for the entire structure.

The first significant new material development was stretched acrylic, a crack-resistant material created by physically stretching cross-linked as-cast acrylic. Stretching causes the randomly-oriented molecules of the as-cast material to re-orient in the plane of the sheet which dramatically increases the crack resistance of this otherwise brittle material (see Figure 1). The designer could substitute stretched acrylic for glass or as-cast acrylic and have a lighter, safer windshield, with improved residual vision and structural strength after ballistic or bird impact. However, two problems still existed that were related to the increase in speed of both commercial and military aircraft: a) higher flight temperatures (stretched acrylic is not usable at temperatures above 220°F); and, b) higher bird impact velocities. As a result thicker glass and/or stretched acrylic were required in designs that were already weight critical.

About this time, polycarbonate, a high temperature (280°F heat distortion point), impact-resistant glazing material, was introduced as a possible replacement for glass and stretched acrylic in high temperature and/or high velocity bird impact applications. Polycarbonate is not a brittle material. In fact, the stress-strain curve for polycarbonate (see Figure 1) is remarkable -- over ninety percent elongation, better than 6061-T6 or 2024-T3 aluminum, the most used metals in airframe manufacture, which have only 10 - 15% elongation vs. polycarbonate's 90+% at room temperature.

This ductile stress-strain curve is the basis for polycarbonate's remarkable impact resistance. Further, because of its ductility and impact resistance, polycarbonate does not fail catastrophically in contrast to glass or as-cast acrylic and, to a lesser degree, stretched acrylic.

Figure 2 compares the impact resistance of various plastics to polycarbonate. As can be seen, there is really no comparison! Even at extremely low temperatures where other thermoplastics become brittle, polycarbonate retains its elastic-plastic behavior (see Figure 3). Polycarbonate is much less temperature sensitive than stretched acrylic (only a 50% reduction for polycarbonate vs an 80% reduction for stretched acrylic) over the useful temperature range of each material (see Figure 4). Figure 5 is a summary of comparative properties of the transparent materials used in windshield manufacturing. Finally, Figure 6 shows the effects of natural weathering on unprotected polycarbonate over a period of five years. As expected, the light transmission and haze characteristics gradually degrade due to the effects of ultaviolet. However, since polycarbonate is virtually opaque to UV, this effect is limited to .001" or less at the surface, so that structural properties, especially impact resistance, are only minimally affected. And remember, those results are for unprotected polycarbonate! In a design that does not expose polycarbonate to the elements, (for example, with acrylic or glass faceplies and a UV absorbing interlayer) the effects of weathering will be negligible. Admittedly, that judgment is based on minimal data. Complete data about the long-term-service effects on structural characteristics of any aircraft glazing material is not available. We do not know the bird impact capability of glass, or acrylic, or polycarbonate windows after 3 - 5 years in service and worse, no one is gathering that data now or in the near future.

However, the data noted above clearly demonstrates the value of polycarbonate as an aircraft transparency material. Testing has shown that in bird impact, approximately one-half as much polycarbonate is needed to provide the same level of protection as stretched acrylic -- a tremendous potential weight advantage. Unfortunately, not all of that weight savings can be realized since polycarbonate has a lower modulus of elasticity resulting in higher deflections and stresses under the same pressurization loads. Designing for maximum service life can still result in a 30 - 40% weight reduction between polycarbonate and stretched acrylic and almost 50% between conventional glass and polycarbonate.

A current design problem that is an illustration of this conclusion is shown in Table 1. This is a window proposed for the next generation Boeing transport which, at the moment, shares the same flight station structure as the

757/767 windshields. The polycarbonate windshield (Design "A") would result in a fifty pound weight savings (49%) over the "strong" glass weight of the actual windshield, and forty pounds (43%) over a stretched acrylic composite. Conclusion: An optimum design polycarbonate transparency provides a significant weight reduction over a comparable glass or stretched acrylic glazing.

Optimum design are the key words. Designing a glass or acrylic window to Part 25 requirements means designing for bird impact, not pressure, because the thickness required to meet impact loads will, in most cases, automatically result in acceptably low stress levels under pressure.

Even in the fail-safe case of one broken or missing ply, the remaining ply of stretched acrylic at roughly one half the bird resistant thickness, will sustain pressure loading adequately. However, for a polycarbonate window, the minimum thickness required for bird impact will usually result in unacceptably high stress levels under flight loads. Thus, the design must be optimized relative to the flight loads for maximum service life. As can be seen from Table 2, the safety load factors applied to the flight loads vary between the the certifying authorities; yet, more importantly do not vary (with one exception) among the various materials available. However, as has been shown, transparency materials vary widely in their structural characteristics and, while arguements could be made to change the safety factors applied to other transparency materials, we specifically believe the safety factors applied to polycarbonate windows should be different.

Since windshields and side panels can be considered "transparent structure", and polycarbonate behaves, at worst, like a ductile metal, the load factors used for determining the strength of pressurized structure should be applied to polycarbonate transparencies as well. Since normal aircraft structure is only required to survive 1.33 times the relief pressure setting, we propose certifying polycarbonate windows to 1.33 times maximum operating pressure (MOP) in a failsafe (one ply out) situation which should provide more than adequate safety for the flight crew and the aircraft. In fact, with the extreme ductility of polycarbonate, the "one ply out" condition is really an unimaginable situation; thus, 1.33 times MOP is really an exceptionally conservative approach with polycarbonate. Finally, aircraft structure is certified for the service life of the aircraft; while, transparencies rarely last the life of the aircraft due to "cosmetic" abuse (scratches, cracks, etc.), or eventual electrical failure if they are antiiced. Service life is typically 2 to 5 years depending on the yearly flight hours and the severity of the operational environment. This means we currently test windows to requirements greater than the aircraft structure, which must provide service for 4 to 10 times longer than the windows! How do the current requirements impact window design? In the 7-7 example noted earlier, the current certification would be to the CAA requirements. Designing to a safety factor of four times the operating pressure means increasing the polycarbonate thickness 50% and the overall weight by 13 lbs. per window -- a 25% increase.

Conclusion

The key requirements for designing transparencies to meet Part 25 certification are bird impact and fail-safe pressure loading. For acrylic and all-glass designs, the bird impact requirement normally results in a cross-section that is over-designed for pressure, so that the load factors applied for safety do not affect the material design thickness. For polycarbonate transparencies, however, pressure safety load factors will have a significant impact on the design thickness. For fuel efficient, minimum weight "transparent structure," load factors consistent with the surrounding structure and nature of the transparent material used should be applied. That is, required certification testing should demonstrate fail-safe (one ply out) capability at 1.33 times the maximum operating pressure.

Summary

Aircraft design and operating conditions have changed, so too have transparency materials. As aircraft become more fuel-efficient, glazing design must also become more fuel-efficient. New materials like polycarbonate, developed in the 1960's, make fuel efficient windshields possible. The changes in aircraft and transparency design and materials must be reflected in the certification/load factor requirements imposed by the certifying authorities. The structural performance of the several window materials varies significantly and the certification requirements do not now accommodate the differing nature of the materials involved.

In order that the aircraft industry may take advantage of its unique aluminum-like properties, we urge the FAA and CAA to treat polycarbonate windows as "transparent structure" and, recognizing the extent of the service life of aircraft glazings, not impose load factor requirements in excess of those required for other pressurized structure. Finally, we urge the Air Force, as the largest user of transparencies of all types, to institute a program to formally evaluate the change in performance of glazing materials in-service. This information is important to the safety of all aircraft and flight personnel and necessary for the optimum design of new transparency concepts.

7-7 DESIGN COMPARISON

Configuration	Weight*	Weight Savings
o All Glass ("strong" glass)	102 lb.	0
o Glass-Faced Acrylic Composite	92 lb.	10 lb. (10%)
o "A" Glass-faced Polycarbonate Composite	52 lb.	50 lb. (49%)
o "B" Glass-faced Polycarbonate Composite	65 lb.	37 lb. (36%)

*Design condition: 41.5° impact angle, 4 lb. bird @ 360 knots

PART 25 CERTIFICATION REQUIREMENTS *

Certifying Authority	All-Glass	As-Cast Acrylic	Stretched Acrylic	Polycarbonate	Aluminum Structure
• FAA	1.33 times maximum relief pressure with one ply broken	Same as glass	Same as glass	Same as glass (estimated)	Same as (except no broken ply)
• CAA/JAR	2.0 times with one ply broken ①	4.0 times with one ply broken ①	Same as as-cast	Same as as-cast (estimated)	②

* Failsafe pressure testing requirement

① Most adverse combination of loads resulting from:

a. The maximum normal working differential pressure, and
b. The external aerodynamic pressures on the panel

② The greatest of:

a. The maximum nominal operational differential pressure multiplied by a factor of 1.3
b. The maximum relief value setting

Sierracin

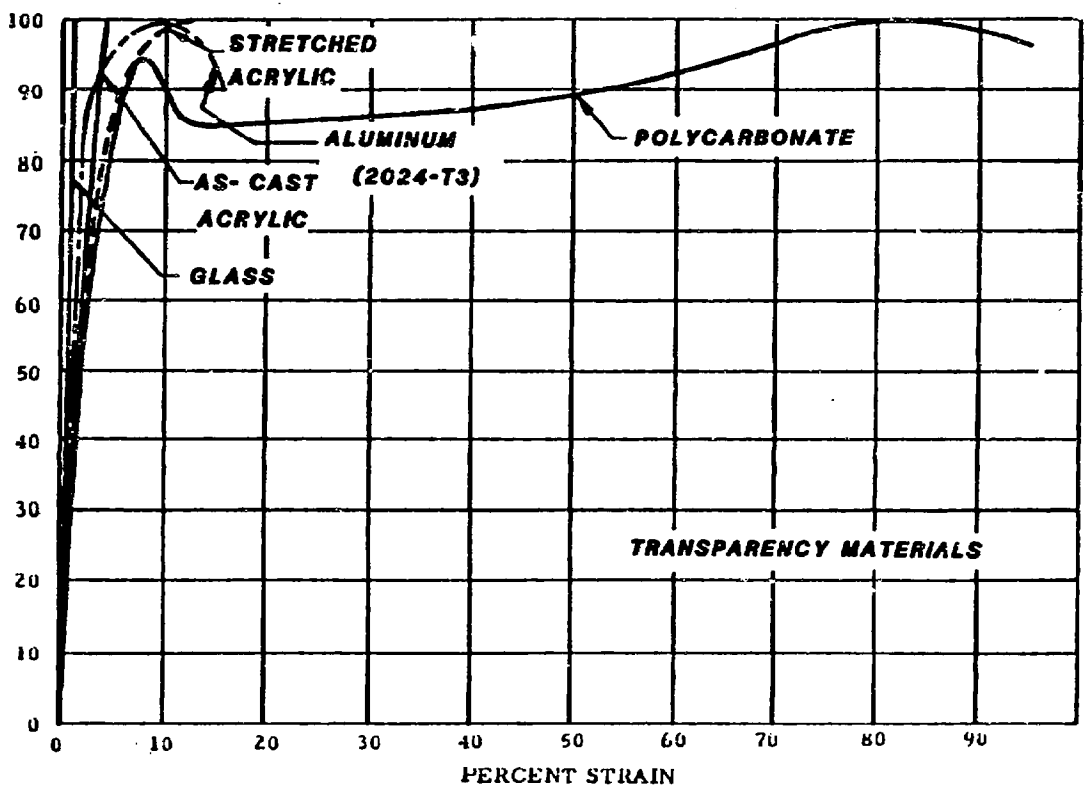

FIGURE 1

TRANSPARENCY STRUCTURAL MATERIALS
STRESS STRAIN CURVES

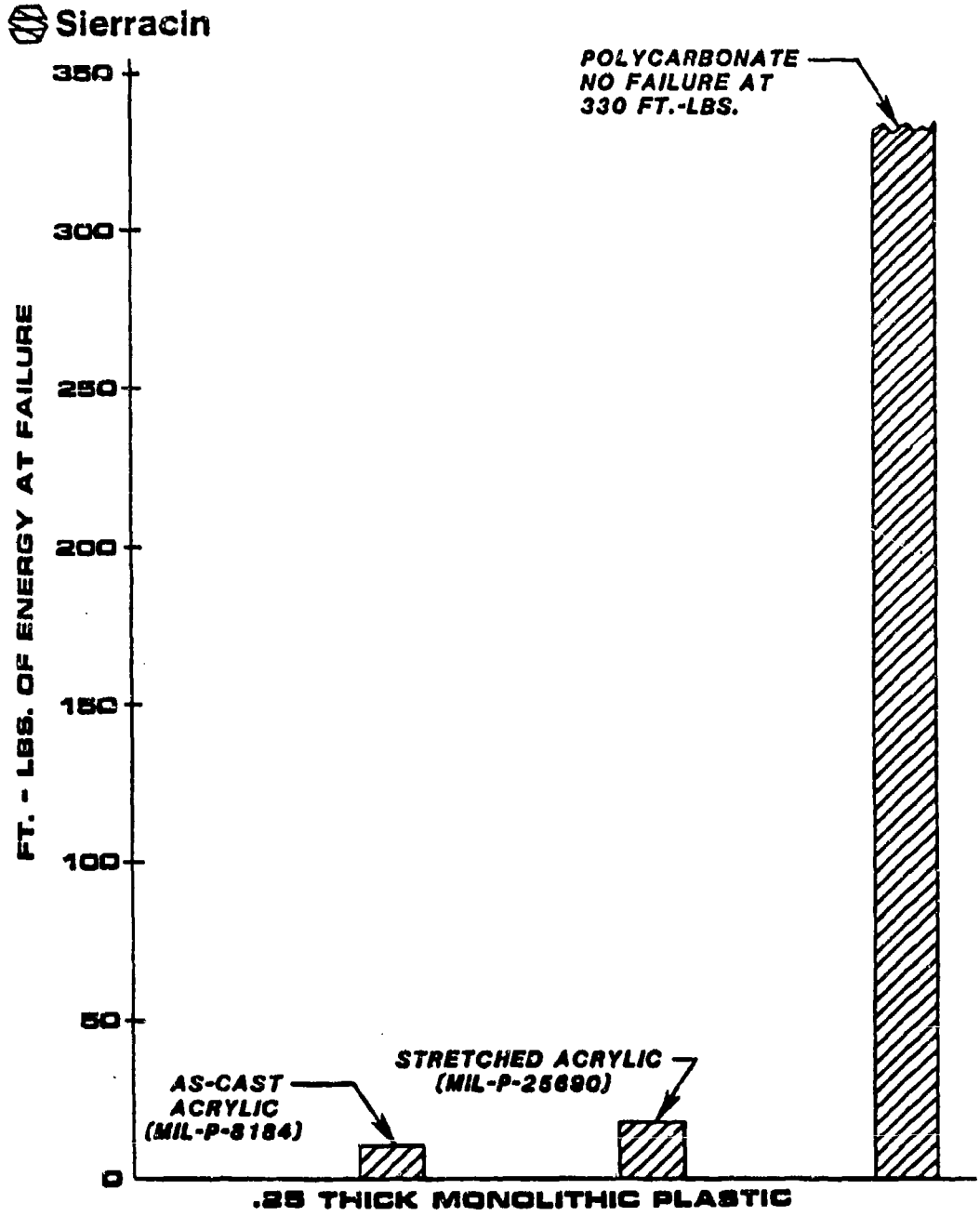

FALLING DART IMPACT STRENGTH
ROOM TEMPERATURE

FIGURE 2

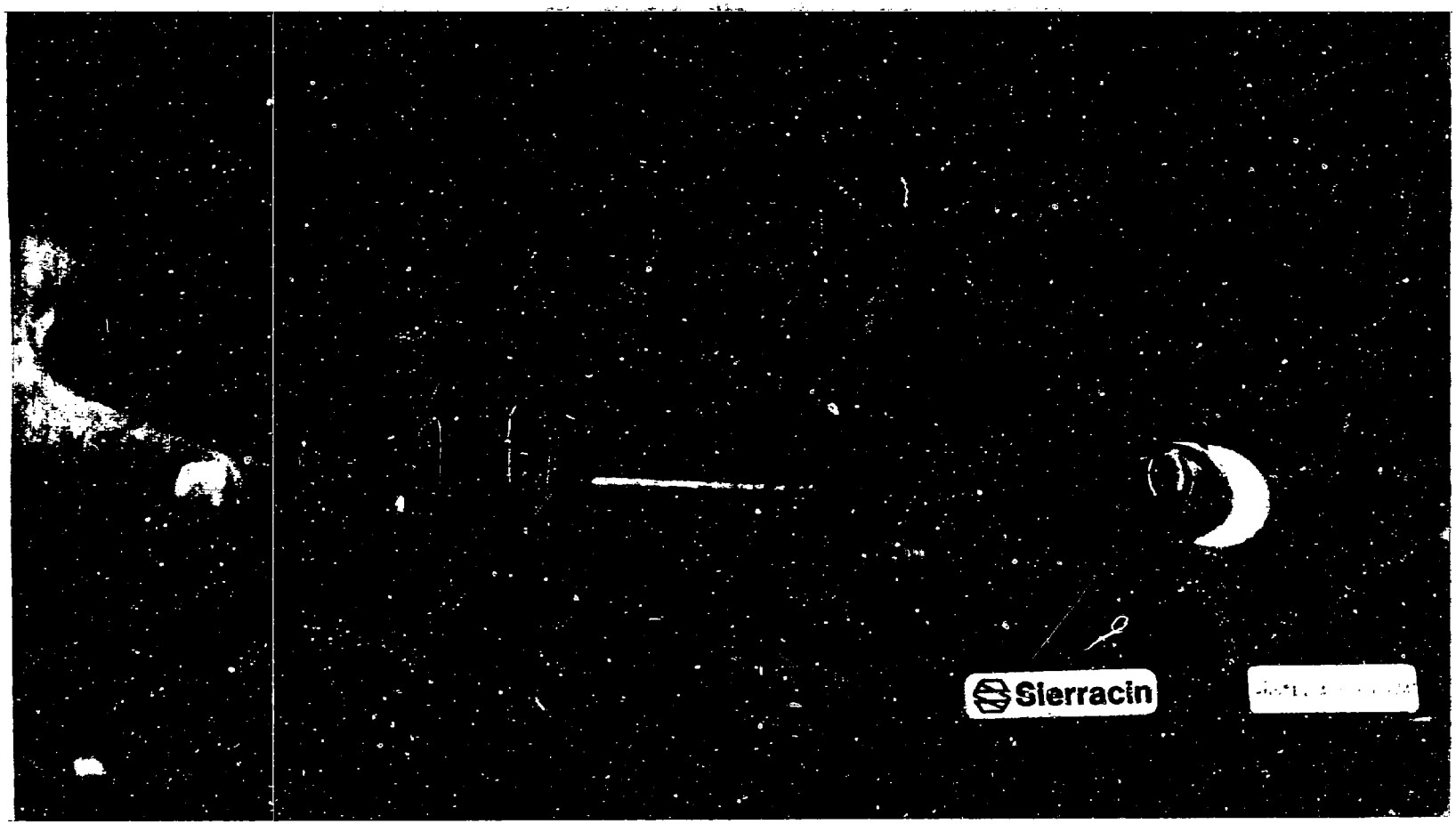

FIGURE 3

1/8" POLYCARBONATE SHEET WITHSTOOD 185 FT. LBS. IMPACT AT -65°F. NOTE THE SEVERE DIMPLE. THIS IS "COLD FORMING" AT ITS EXTREME

Sierracin

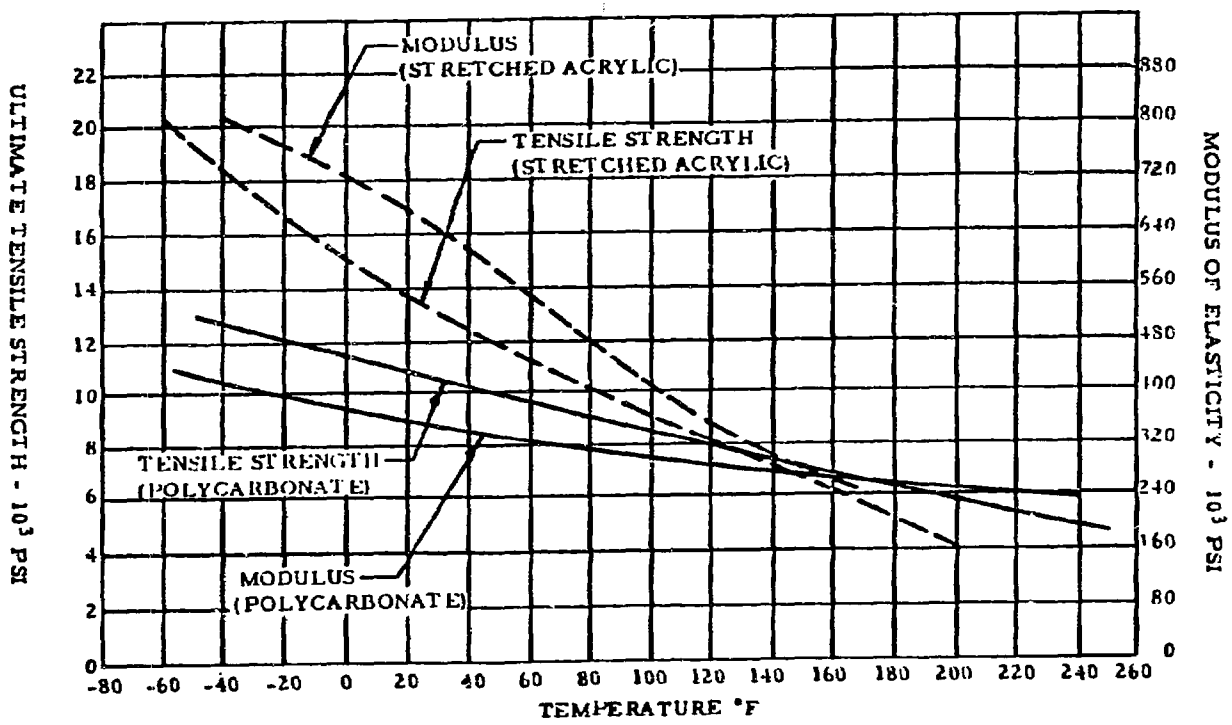

FIGURE 4

MODULUS OF ELASTICITY AND ULTIMATE TENSILE STRENGTH VS. TEMPERATURE FOR POLYCARBONATE AND STRETCHED ACRYLIC

Sierracin

FIGURE 5

TYPICAL PROPERTIES OF TRANSPARENT STRUCTURAL MATERIALS

PHYSICAL OR MECHANICAL PROPERTY	STANDARD TEST METHOD USED	SYMBOL AND/OR UNITS	POLYCARBONATE MIL-P-83310	AS-CAST ACRYLIC MIL-P-5425	AS-CAST ACRYLIC MIL-P-8184	STRETCHED ACRYLIC MIL-P-25690	SODA LIME GLASS MIL-G-25667	CHEM. STRENGTHENED GLASS MIL-G-25661-V
TENSILE STRENGTH		PSI X 10^3	9.8 - 10.5 (4)	10.0 (4)	10.5 - 11.0 (4)	11.5 - 11.9 (4)	6. - 6.5 (5) 25 - 30(6) LOF	35 - 52 (7) SIERRACIN
COMPRESSIVE STRENGTH	FTMS 406-1021 ASTM:D-694	PSI X 10^3	12.5	18.0	19.0	17.0		
MODULUS OF ELASTICITY	FTMS 406-1011 ASTM:D-747	E PSI X 10^6	3.0 - 3.5	4.5 - 4.6	4.5	4.5 - 4.9	10.0	10.5
COMPRESSIVE MODULUS	FTMS 406-1021 ASTM:D-695	G PSI X 10^5		4.5	4.5	5.0		
COEFFICIENT OF THERMAL EXPANSION	FTMS 406-2031 ASTM:D-696	IN./IN./°F x 10^3	3.47	4.1	4.1		0.46 WADCT12-53-99	0.49 SIERRACIN
SPECIFIC HEAT	ASTM:C351-54	BTU/LB/°F	0.28	0.35	0.35	0.35	0.19	0.20
DENSITY	ASTM:C177	LB/IN.^{3}	0.043	0.043	0.043	0.043	0.091	0.091
BEARING STRENGTH	LP4068-1051	PSI x 103	7.0 E/D = 1.5			15.2		
POISSON'S RATIO			0.36 AFFDL-TR-25-2	0.35	0.35	0.35	0.23	0.22
COEFFICIENT OF THERMAL CONDUCTIVITY	ASTM:C177	BTU-IN./HR/FT^2/°F	1.5 SIERRACIN	1.3 SWEDLOW	1.2 - 1.55	1.15	6.5	SIERRACIN
SHEAR MODULUS OF ELASTICITY	ASTM:D732	G/PSI	130 AFFDL-TR-25-2					
SPECIFIC GRAVITY			1.2	1.19	1.19	1.19	2.53 LOF	2.44 SIERRACIN
DESIGN STRESS		PSI X 10^3	4	1	2	3		

Sierracin/Sylmar

MATERIAL: LEXAN POLYCABONATE 103-112 RESIN

PROPERTY	NATURAL OUTDOOR WEATHERING - MONTHS							
	0	6	12	18	24	36	48	60
HAZE, %	3.6	3.7	14.4	12.2	17.0	21.2	28.3	29.9
LIGHT TRANSMISSION %	83.3	83.6	82.1	82.2	81.8	81.4	80.4	78.7
TENSILE STRENGTH, PSI								
ULTIMATE	10840	10160	8710	9100	9200	8930	8720	7980
ULTIMATE ELONGATION	118	114	93	92	100	94	95	70
IZOD IMPACT STRENGTH,								
FT-LBS/IN 1/8" THICKNESS	12.0	14.8	--	13.5	16.2	11.0	15.5	16.1

(DATA FROM GENERAL ELECTRIC)

FIGURE 6

OUTDOOR WEATHERING EFFECTS ON BARE POLYCARBONATE

Copyright 1983, Sierracin® Corporation

The information contained in this document is thought to be reliable, but the Sierracin Corporation expressly disclaims all responsibility for loss or damage caused by or resulting from the use of the information herein contained. The information is given on the express condition that the user assumes all risk.

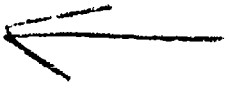

AD-P003 226

LUFTHANSA GERMAN AIRLINES EXPERIENCE WITH CABIN AND COCKPIT WINDOWS OF BOEING 707, 727, 737, 747, DOUGLAS DC10 AND AIRBUS A300

K. W. Ewald, Lufthanse German Airlines

Lufthansa German Airlines Experience with Cabin and Cockpit Windows of Boeing 707, 727, 737, 747, Douglas DC 10 and Airbus Industrie A 300

by
K. Ewald
Structures Group
Lufthansa German Airlines, Frankfurt
Germany

Abstract

This paper highlights the experience as related to the various types of windows installed on all types of aircraft operated within Lufthansa, which are 15 B747, 14 DC10, 11 A300, 7 B707, 34 B727, 42 B737.

After great improvements during 1970 to 1977 a remarkable deterioration in performance of cabin and cockpit windows is realized.

Today we are faced to more problems than ever before. Problems which have already been solved, are causing headache again. The most important problems encountered are:

Crazing, inplane cracking, deformation on acrylic windows, vinyl cracks, arcing, heating system failures, chips, cracks and distorted vision on multilayer windows, mainly glass windows.

There is nearly no chance for an operator to get an explanation for the reason of this tremendous increase of defects. Asking the manufacturers will sometimes produce more problems and even confusion, resulting in a decrease of confidence.

Up to now nearly no effort is to be seen to solve existing problems. Airlines are forced to find other ways to keep their expenses down. Therefore the experience with PMA manufactured parts and refurbished windows is also mentioned.

But manufacturers sometimes clearly show that they have the capability to produce really fantastic windows. Every test window seem to last nearly for ever. But production windows never reach the same service life.

Special attention is paid to the existing poor relations and information transfer between airlines and manufacturers to provide encouragement to the manufacturers to improve their products.

INTRODUCTION

During the Transparencies Symposium at Boeing in October 1976, J. R. Scott from American Airlines made the statement, that very significant improvements have been made in the manufacturing and operation of windshields since introduction of the jet aircraft.

But it seems, that in the meantime something has changed and this statement no longer is valid. With a very few exceptions, where really great improvements have been made, we started to step backwards. Today we are faced with more problems than ever before, as well on cabin- as on cockpit windows of all types of aircraft operated by Lufthansa.

First the problems on acrylic cabin- and cockpit windows will be presented and later the problems with cockpit glass windows.

DISCUSSION

ACRYLIC CABIN- AND COCKPIT WINDOWS

In the past - which means before 1981 - we reached considerable good average service lifes on acrylic cabin- and cockpit windows.
Besides some replacements,due to electrical problems, delamination, inplance cracking and deformation - which still is a problem on 747 cabin windows - there were only a few replacements due to crazing.

The cabin windows reached average service lifes of 30 000 FH on the DC 10, 22 000 Fh on the 747 and 16 000 Fh on 707, 727, 737.
Only on the A 300 there were some real problems. But on the A 300 we have different window design, a new material and a very, very thin window. In the meantime the material was improved and it is performing much better now.

From the beginning of 747 operations in 1970 thru end of 1978 with 10 aircraft maximum, we had to replace 12 cockpit windows no. 2 and 3 due to crazing only. Service life ranged from 10 900 to 25 700 Fh.
In 1978 8 747's were replaced by new. Now we have a fleet of 15 aircraft.
In 1979 there was one window replacement and in 1980 none.

On the DC 10, which was introduced in December 1973 these windows performed even better. Till April 1983 with 14 aircraft maximum we had to replace just 11 windows no. 2 and 3 due to crazing. Service life was up to 39 000 Fh.

But what a tremendous change.
In 1981 21 747 cockpit windows had to be replaced, in 1982 14 and till end of May 1983 already 39. All due to crazing.
In one case a new window was installed for 6 weeks only.

Since April 1983 we have to replace all DC 10 cockpit windows no. 2 and 3. But the most windows have flown more than 30 000 Fh.
The last three delivered a/c (delivered 1979 and 1981) clearly show, that something must have changed. Their windows show the same amount of crazing after just 6 000 to 10 000 Fh

On the same aircraft we received the first passenger complaints on cabin window crazing after just about 4 000 Fh!
Investigation revealed that these windows were from a different source than those on the first 10 aircraft.

On the last three delivered 747's cabin window crazing was observed in 1982/83 after 1 200 Fh - about 4 month - only. These three aircraft have windows from 4 different manufactures installed. Two of them show considerable better performance than the other two. But even these and the new A 300 material are still not satisfactory.

What has changed, that there is such a great difference compared to the past?

- Material?
- Manufacturing process?
- Enviromental conditions?
- Airline handling methods?

When we reported this tremendous increase in crazing in 1981 on cockpit windows and 1982 on cabin windows to the aircraft manufactures and asked for possible reasons, we received the simple answer: you are the first one reporting. Nothing has been changed. Look at your cleaning procedures.

Our investigation revealed, that in the past crazing mainly started at surface defects - like small scratches - and was progressing quite slowly. A faster progression was noticed on aged windows only. Now a new type of crazing is observed. It is starting as tiny starlike cracks, sometimes concentrated in some areas, close to the machined edge. But mainly spreaded uniformly on the whole outer surface. This type of crazing is progressing quite fast. Even surface defects are now causing cracks much faster.

In the meantime we received various answers from independent sources on the reason for crazing.

Three manufactures checked windows which were made by the same manufacturer, installed on the same aircraft before delivery, showing the same type and amount of crazing, and were removed on the same day after about 2600 Fh.

The answers ranged from:

First - Tested windows showed an abnormally low craze threshold - 1 250 psi - as compared to the MIL Spec standard greater than 2 000 psi (with lacquer thinner)

Second - It is not clearly visible what has caused the crazing. But we suspect that the window was overheated during polishing of the outer surface and grinding of the beveled edge. Test clearly showed, that stresses between 30 to 300 psi may be induced just due to normal final polishing and it is easy to increase these stresses.

Third - Crazing was caused by chemical attack, which does not mean that the window is being subjected to detrimental chemical attack by maintenance practices only. Different enviromental encounters in atmospheric conditions, and on the ground can be experienced by the aircraft.

If this is true, the material used, is not capable to fulfill the intended purpose.

We believe that the manner in which the windows - including rare material and stretching - are manufactured is of great importance. This is proven by the great difference in performance of the windows of different manufactures.

For an airline there is no chance to receive just the better windows, due to the fact windows are supplied through the aircraft manufacturer under one part number only.

On the A 300 a redesign is in progress and it would be a great chance to improve the windows. But again nobody is caring on airline experience and we expect the same or even more problems as in the past.

Fortunately there are some independent suppliers and they are even cheaper. But what a surprise, when you have to remove a window, totally crazed, which was installed on August 18th, 1982 and has flown till September 30rd, 1982 only. Later you have to realize that the cheaper source was the most expensive one, for this was not an isolated case.
The reason was clearly overheating the material during manufacturing.

Very seldom crazing is reaching the technical limit and most windows are reworkable. There are many companies offering their help in windows refurbishment for a reasonable price. But some seem to have not noticed the sensitivity of the material. The result is the same as mentioned before.

When we realized that crazing on new 747 windows is starting at about 1 200 Fh and on the new A 300 material at 2 700 Fh, the idea was born to test the A 300 material in correct thickness on a 747.

In the meantime this idea has grown to a greater test program. There was a remarkable response by various manufactures from Europe and the U. S. A. Since February 10th, 1983 one of our 747's is flying with 58 test windows - different materials and coatings from 6 manufacturers. 56 more windows from 5 different manufacturers will be installed during the next 4 month.

The first inspection was performed on May 3rd, 1983 after 710 Fh and 138 landings.
What a surprise. All 10 windows purchased as control windows from the aircraft manufacturer showed already crazing. On one of them the crazing could already be described as moderate. Exactly this window (and four more) was treated with an agent, which should prevent crazing.
Also some of the A 300 material windows showed very, very slight outer surface defects, which may have been caused by polishing at the manufacturer's.

At the second inspection on May 30rd, 1983 after 1 081 Fh and 200 landings the control windows were already crazed severely.
One of the A 300 material windows now showed real crazing.
Four of the coated windows of one manufacturer and 4 uncoated controll windows showed also crazing. It was clearly visibile on the coated windows and very, very difficult to detect on the uncoated windows.
Only one manufacturer's windows, which were not specially made for this test up to now showed no problems.

So, it is really time that something has to be done quickly.

Problems are often known since years. In some cases knowledge exists already to improve the product.
For example a better seal to avoid moisture penetration and deformation of the 747 cabin windows. But this seal was not designed by the aircraft manufacturer and has therefore not been introduced. Why does it always take so long before necessary modification are introduced? Is there no interest at the manufacturers? Or is it just a problem of communication between window manufacturers,aircraft manufacturers and airlines?

GLASS COCKPIT WINDOWS

At the moment it seems to be that the whole world is talking about crazing only and not too much attention is paid to the tremendous problems on glass cockpit windows.
Here a greater need for attention is required for safety is very often involved - and it is a high cost item also.

Within the last three years (01.06.80 - 01.06.83) totally 844 cockpit windows, including 198 acrylic windows had to be replaced.

Nearly everywhere a tremendous deterioration in service life is observed.
For example on the 36 new 737's we received within the last 2 years, all windows no. 2 are already replaced. Some already 2 or 3 times.
Windows no. 1, 4 and 5 are already replaced by about 60%.
The same situation exists on 727 and 707.
Nethertheless one window no. 1 of a 707 was installed for 33 000 Fh.
The average service life on DC 10 windshields decreased from about 17 000 Fh to 8 000 Fh only.

It is hard to believe. Exactly on the most difficult to make window - the 747 windshield - there is no reason to complaints.
Service life increased from 4 200 Fh in 1974 to 29 000 Fh in 1983.
A similiar situation exists on A 300 windshields, with slightly different flight hours.

The only reason why these windows are performing better and better while simple windows like on the 737, 727, 707 have a real poor performance with decreasing tendency, seems to be how the windows have to be procured.
On 747 and A 300 there is a direct competition. The manufactures have to prove their products to the users - the airlines.
Besides price for an airline service life is the most important factor, while the aircraft manufactures seem to be interested in low prices only.

Sometimes all manufactures clearly show, that they are able to produce really good products. Everytime you receive a test window for inservice evaluation, it will nearly last for ever.
Or is it just, that the pilots don't dare to complain every small defect as usual because they know it is a test window?

It is unbelievable, but problems, which already nearly had been solved in 1975 to 1978 are causing severe headache again.
Vinyl cracks, arcing, moisture penetration, vinyl bubbling and shattering or loss of outer glass ply in flight are again found in increasing numbers after very short time (even less than half a year) in service.

It seems to be, that sometimes improvements are deteriorating the situation.
For example: after improvement of the edge heaters on window no. 1 of 737, 727, 707 more vinyl cracks are found as before.

The most vinyl cracks are found in the unheated area of window no. 2. Since many years the manufacturers are talking on installation of an additional heat source - but no action could be realized up to now - knowing that safety is affected. Expecially they are aware that not every one in airline buisiness is paying the correct attention to this defect - some or many may not even know how they look like.

Here we are at a critical point of our relations - that is immediate and sufficient information of everybody involved when a new problem is realized. It takes normally much too long before the airlines are informed on a problem or they even will never be informed officially. In nearly every case there is no detail discription of the defect published.

One example: When we found chips on the outer surface of the center glass ply of 4 747 windshields, they were reported immediately. The manufacturer first stated, that we may have just delamination or vinyl cracks, which here are not critical.

After receipt of one window, the chips were confirmed and the maintenance manual revised in a very short time - stating no chips are allowed on the center glass ply.
But even everyone is aware that these defects are very difficult to realize as chips no detail information was ever published on their appearance and location.

Nobody can believe that our four cases were just isolated cases. They all happened at the same location after about the same time in service. It is a problem of a window of a certain manufacturer which affects safety.
So please do more on subjects like this in the future.

But even on just economical items a quick responce is appreciated. It is not tolerable that it takes about two years before any information was received on problems with the PSE-2-1 sensor or orange peel on a new interlayer. Especially on the orange peel the manufacturers were aware of the problem before delivery of the first window.

Now we again are faced to a problem which affects vision and again the manufacturers were aware of this before delivery of the first window. It is a type of blurred vision under heated condition only on a new type of 747 cockpit side windows from a new manufacturer. We can see absolutely no need why we should accept such a product with a significant optical quality deterioration, while the old vendors products were satisfactory.

Furthermore it is not producing confidence, when defective windows are sent back to the airlines just while the defect is not to be found with the Maintenance Manual required tests but easy detectable with other measures.

I think it is too dangerous to gamble around with safety items like windows.

The only thing I could propose is, we should work closer together. It will definitely be of benefit for everybody.

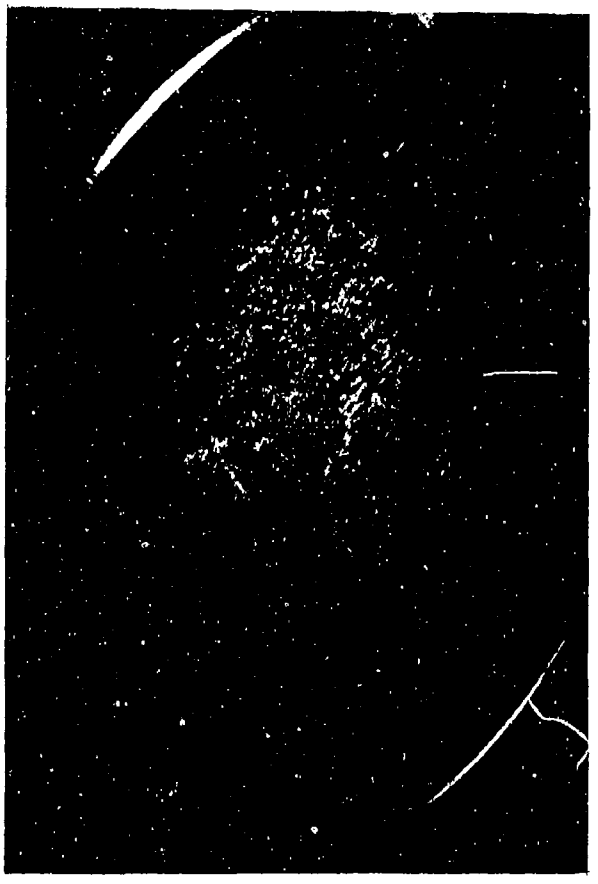

A 300 Cabin Window
Old Material Plexa 180
4000 Fh

A 300 Cabin Window
Old Material Plexa 180
4000 Fh

747 Cabin Window
Improper Rework

747 Cabin Window
Improper Rework

747 Cabin Window
Improper Rework

THIS PAGE LEFT BLANK INTENTIONALLY

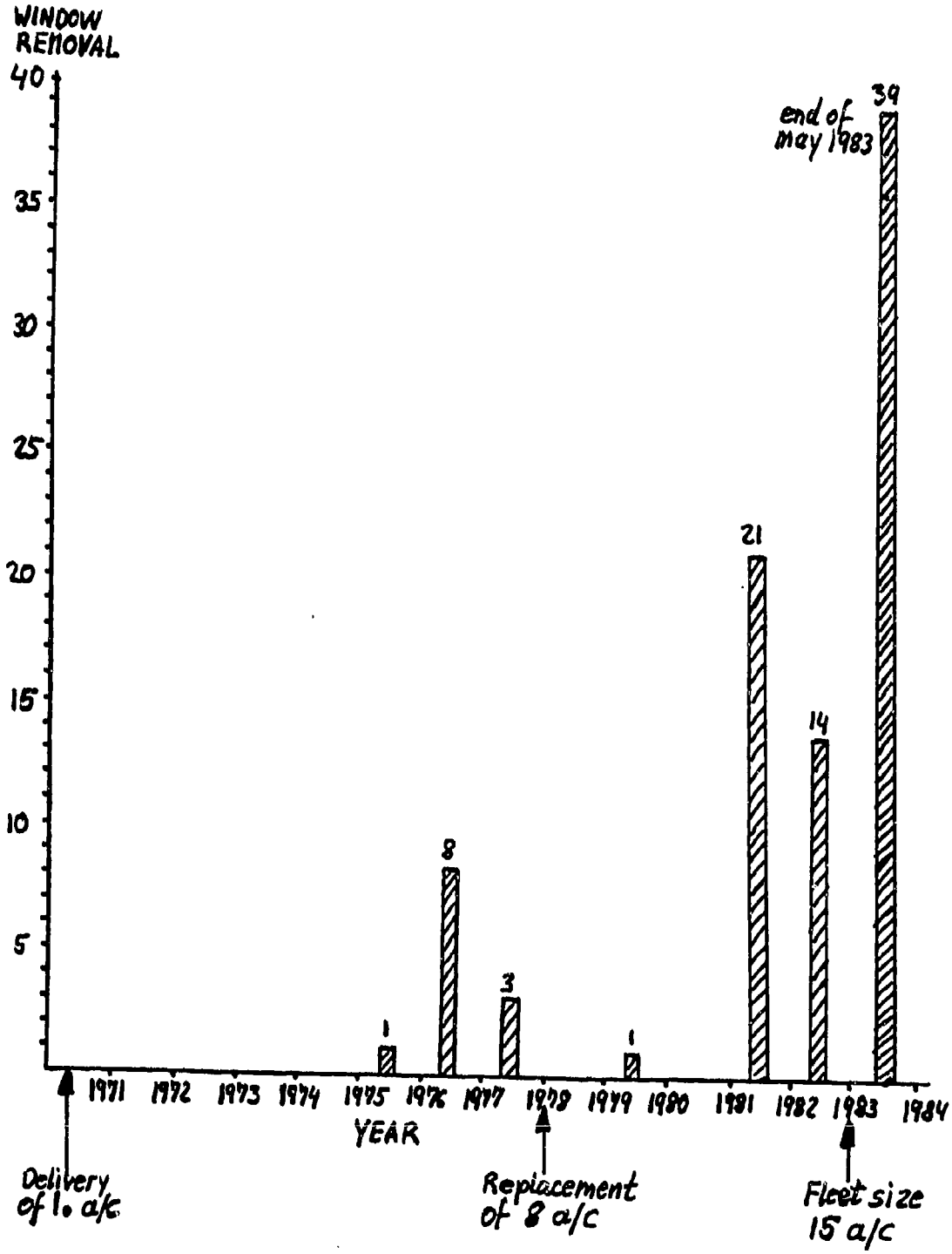

747 cockpit window no. 2 and 3 removal due to crazing

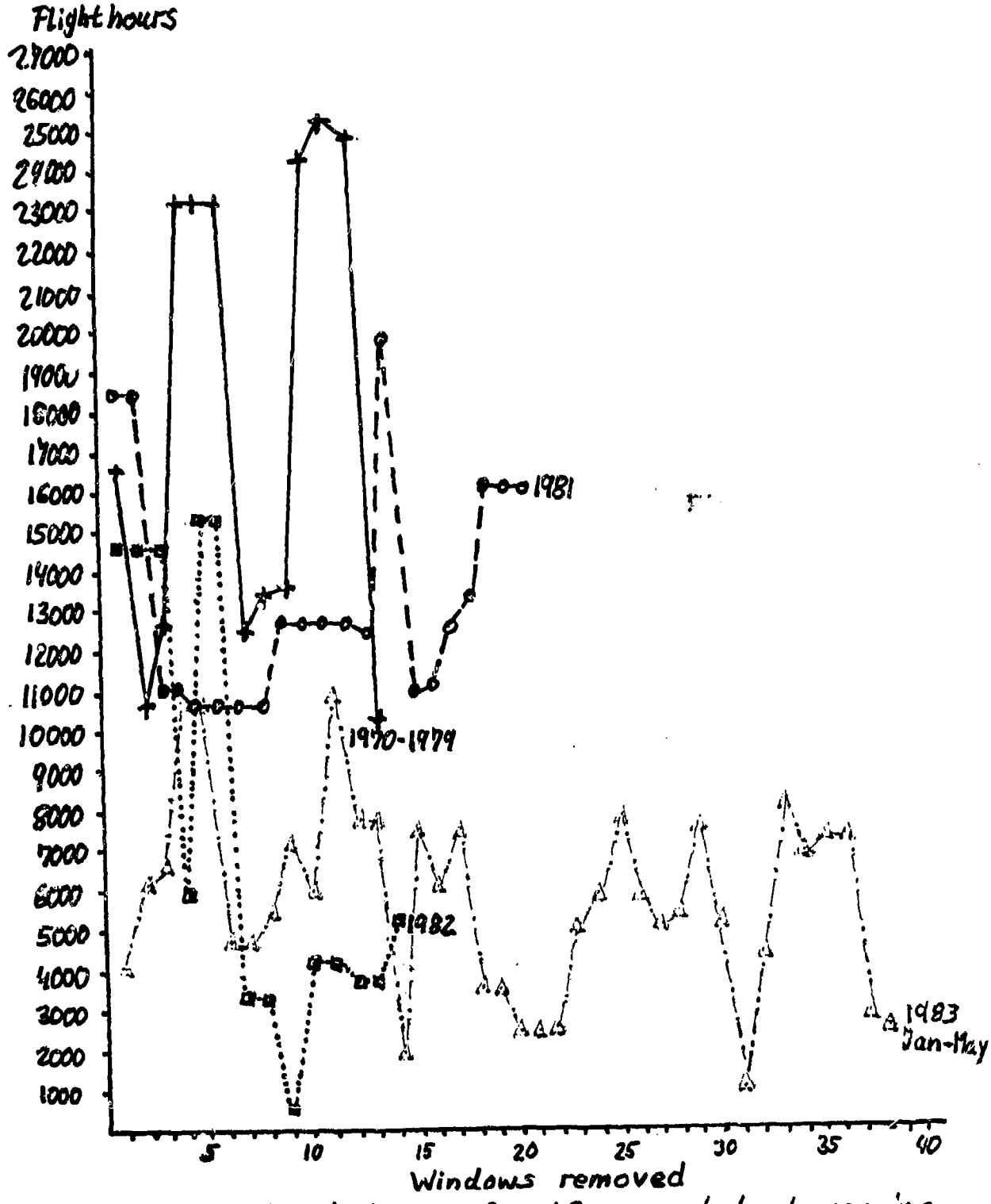

747 Cockpit windows no. 2 and 3 removal due to crazing

AD-P003 227

THE WIPER ABRASION AND RAIN EROSION RESISTANCE OF TRANSPARENT MATERIALS AND COATINGS FOR AIRCRAFT GLAZING

N. S. Corney, Royal Aircraft Establishment
and R. J. King, National Physical Laboratory

THE WIPER ABRASION AND RAIN EROSION RESISTANCE OF TRANSPARENT MATERIALS AND COATINGS FOR AIRCRAFT GLAZING

by

N. S. Corney
Royal Aircraft Establishment,
Farnborough, Hants, England

R. J. King
National Physical Laboratory,
Teddington, Middlesex, England

ABSTRACT

The requirements for improved abrasion and rain erosion resistance of transparent materials for helicopters and aircraft glazing have led to the development and application at NPL of a laboratory-scale wiper abrasion apparatus, and also to an investigation using the RAE rain erosion rig.

The NPL apparatus employs the linear motion of a short windscreen wiper blade across a 50 mm diameter specimen. The characteristics of the blade, its loading, method of mounting and speed are among the factors carefully chosen to produce even and reproducible abrasion over the rubbed area. Surface condition is assessed in detail by Nomarski interference microscopy with a quantitative estimation of abrasion damage from profilometry, light scatter and transmittance measurements.

The RAE rain erosion rig enables specimens to be exposed in a simulated rain field under conditions of known velocity and impact angle. Detailed examinations have been made of the progressive effects of rain erosion by weight loss and transmittance measurements.

The in-service degradation of glazing materials as simulated by these techniques are compared. While toughened oxide glasses are the most resistant, acrylic and polycarbonate are more easily damaged but do not show similar performance in wiper abrasion and rain erosion. The coatings for acrylic and polycarbonate materials which have been examined offer some resistance to wiper abrasion, but not to rain erosion under the very severe conditions employed.

1 INTRODUCTION

Demands for improved reliability and reduced cost of maintenance of aerospace components have led in recent years to investigations into the problem of damage by impact and abrasion of transparent plastic glazing materials, particularly for the forward facing transparencies of rotorcraft. The extent and serious nature of the problem has been reflected in the number of papers dealing with this topic in the proceedings of Transparency Conferences over the past decade, see for example Refs 1 and 2. In the UK, similar demands together with the need to assess the abrasion of infra-red transmitting windows led to the National Physical Laboratory undertaking a research programme sponsored by the Royal Aircraft Establishment, to develop testing equipment employing small windscreen wiper blades acting on the specimens under test. As part of this programme, acrylic and polycarbonate materials together with some abrasion resistant coatings were examined and the results are reported here, together with some comparative results for glass.

Additionally, as part of the long-established RAE research programme on the rain erosion resistance of aerospace materials, similar materials and coatings were examined. The rain erosion of windscreens and canopies for high speed aircraft is generally low because of the small impact angles demanded by aerodynamic considerations. However, problems are experienced from erosion of navigation and landing light covers, so an investigation of transparent plastics having abrasion resistant coatings was appropriate.

2 EXPERIMENTAL

2.1 The NPL abrasion machine

In the NPL abrasion machine sections of commercially available rubber wiper blades 20 mm in length are mounted on two reciprocating sliders driven by a variable speed motor. The surfaces under test, 50 mm in diameter, are horizontally mounted beneath the wipers and held in position by vacuum chucks. The abrasive medium is a slurry of British Standard coarse dust (as required by BS 1701:1970 and comprising mainly silica particles with a size up to 150 μm) suspended in distilled water which is continually stirred and fed to the test surfaces by means of a peristaltic pump. The wiper blades are loaded at approximately 10 g per cm length and reciprocate with a stroke of 40 mm. A general view of the abrasion machine is shown in Figure 1.

A preliminary study was made of the factors influencing the abrasion process, such as type of wiper blade, its method of mounting, degree of loading and speed across the surface; the slurry concentration and rate of flow were also varied so that optimum conditions giving the most uniform and reproducible abrasion over the rubbed area were obtained. Although the machine was designed with two arms and wiper blades primarily to reduce out-of-balance mechanical forces, this arrangement gave the further advantage that in comparing two surfaces the samples could be interchanged midway through the run, ensuring that each surface effectively received identical abrasion treatment.

2.2 Methods of assessing abrasion damage

A general assessment of the abrasion damage was obtained initially by direct visual inspection of the light scattered from the abraded surface when illuminated with a beam of light from a super-high-pressure mercury lamp. Using this intense light source the test was found to be far more sensitive than when a 4W daylight type fluorescent tube source was employed as specified by British Standard G.211:1971 paragraph 7.1.1 (reflection mode).

A quantitative measure of the light scattered from the abraded surfaces was made using a collimated beam a few millimetres in diameter of 633 nm light from a He-Ne laser directed through a small central aperture in a concave mirror. The light scattered over a cone of about 15^{o} semi-angle was collected by the mirror and focussed on to a silicon detector. The system was always adjusted to give a fixed value for an opal glass reference surface. The measurements were therefore relative ones with a scatter value from an unabraded float glass disc being typically about 5 units. Values for the scatter from abraded surfaces are quoted in the text and in Tables 1 and 2. Measurement of scattered light was found to be particularly useful for assessing the uniformity of damage over the abraded area, and the reproducibility of wear from one test run to another.

A conventional spectrophotometer and a NPL-developed photometer were used to measure sample transmittance at 550 nm, under the usual conditions prevailing in such instruments, where most of the light scattered by the sample is not collected by the photodetector.

Direct measurement of surface topography was obtained by profilometry using the RPI Talystep instrument, usually with the spherical diamond stylus (12.5 μm radius). Peak-to-valley values of roughness were measured from the Talystep traces, while roughness average values (R_A) were determined directly by means of an additional electronics unit functioning on the normal electrical output from the Talystep.

Detailed visual examination of the surfaces (usually at a magnification of ×250) was made by incident light microscopy using a Nomarski differential interference contrast system (DIC). This type of microscopy was particularly useful in detecting slight roughening of the abraded surface, while scratches, including very fine ones, were also readily visible. From the general level of surface reflectance (without DIC), it was frequently possible to see where, due to poor adhesion, the coating had been removed by the abrasion process. Detailed microscopical examination probably provided the most information of all the techniques used in this study and was particularly important in the examination of coatings on plastics, where poor surface quality often made any quantitative assessment very difficult.

2.3 The evaluation of rain erosion resistance

The rain erosion resistance of materials may be conveniently simulated by mounting coupon specimens at the extremities of a rotating arm which is arranged so that the path of these specimens lies within a simulated rainfield. In the RAE rig[3] the arm is 2.89 m long with a central drive shaft, and rotates

in a vertical plane. The rainfield is produced by pumping water on to an adjacent disc spinning co-axially with the arm, the water being flung off as drops from the periphery of the disc. By choice of the disc diameter and its speed of rotation, adjustment of the separation distance of the planes of arm and disc together with the water flow rate, the drop size and simulated rain intensity may be brought to the required conditions. Checks on these conditions are made by determining the rate of weight loss of pure aluminium or cast acrylic which have been previously established as reference materials.

The specimens of material under examination are normally flat, 25 mm square with thickness 3 mm upwards. These are retained in holders by thin stainless steel frames around the edges of the specimens; the holders may be rotated in order to permit exposure at several discrete impact angles between 30° and 90°. After exposure the specimens are inspected visually, weight loss after drying under standard conditions is determined, as well as transmittance over the range 350–700 nm at normal incidence using a Unicam SP800 spectrophotometer.

The simulated rainfall conditions in the rig, *viz.* intensity 25 mm/h with predominant drop diameter 2 mm, approximate to those of natural heavy rain likely to occur in the tropics or very occasionally in thunderstorms in Europe. The velocity of 223 m/s (500 mph) adopted for the tests is probably the maximum at which an aircraft would safely fly in conditions of such heavy rain.

3 RESULTS OF ABRASION TESTING

3.1 Types of abrasion damage

From studies on various surfaces and coatings it would seem convenient to divide abrasion damage into the following three categories:

(1) In the early stages, the surface can become scratched with grooves varying markedly in length, width and depth.

(2) Later, with increasing abrasion time, there can be a general roughening of the surface readily detectable by profilometry and DIC microscopy.

(3) Finally, poor adhesion can result in loss of areas of coating and even complete removal thereof in exceptional cases. The relative extent of these three types of damage was found to vary considerably from one coating to another.

3.2 Oxide glass and coating

The preliminary studies to determine the conditions giving most uniform and reproducible damage over the abraded area were carried out on discs approximately 3 mm thick of float glass (Pilkington Bros. plc). Typically a few scratches of varying severity were noted after 2000 strokes on the NPL abrasion machine. Further abrasion then produced more scratches and a gradual roughening of the surface so that after 10000 strokes approximately half the wiped surface exhibited some damage visible by DIC microscopy. After 20000 strokes Talystep roughness measurements on 12 discs made at various times

over a 3 year period gave R_A values between 3.7 and 5.0 nm. This may be compared with a value of 0.5 nm obtained on the corresponding unabraded glass surface. Light scatter values varied between 70 and 120 compared to 5 for unabraded glass. The relatively small spread in R_A and light scatter values obtained on abraded oxide glass specimens over 3 years is a good indication of the reproducibility of the NPL machine.

A good example illustrating the three types of abrasion damage mentioned above is shown in Figure 2 which is a DIC photomicrograph of a magnesium fluoride film (prepared by vacuum deposition on to a heated glass substrate) which had received 10000 abrasion strokes. The brighter areas are those where the coating has been removed due to poor adherence with appreciable roughness and scratching of the underlying substrate. This coating loss, confirmed by profilometry, was initially in the form of narrow scratches a few micrometres wide which, on further abrasion, gradually coalesced into broader areas. The darker regions of the photomicrograph represent intact areas of the magnesium fluoride coating and these can be seen to be almost free from any damage. This suggests that this particular coating exhibited good resistance to scratching but only moderate adhesion to the glass substrate. A multi-layer, anti-reflection coating with magnesium fluoride as the outermost layer was found to possess similar resistance to scratching and roughening as that of the single layer but also exhibited much-improved adhesion to the substrate.

3.3 Acrylic materials and coatings

Some initial tests were carried out on commercial acrylic sheet ('Perspex™' from ICI plc) approximately 6 mm thick and the results showed that this was easily abraded under the conditions used in the NPL machine. Thus after only 1000 strokes the majority of the wiped surface was badly scratched, the transmittance at 550 nm of the specimen being reduced from an initial value of 92% to 75.5%. The whole of the rubbed area had been damaged after 2000 strokes showing an R_A value of 120 nm compared with 2 nm prior to abrasion. Deterioration of image quality of an object viewed through the abraded disc was then very marked, and a very large increase in light scatter was noted, see Table 1.

An experimental abrasion-resistant coating on 'Perspex' was examined and found to provide a good degree of protection to the substrate, only a few scratches being visible after 2000 strokes. Even after 20000 strokes less than 50% of the surface had been damaged although many of the scratches were then very severe with depths about 1 μm. The light scatter and R_A value (59 nm) were less than those for the uncoated surface after 2000 strokes while the transmittance had fallen only to 86% (originally 92%). Unfortunately it was observed from an interferometric comparison of uncoated and coated samples, that the coated sample had suffered serious distortion presumably as a result of the coating process.

A sample of an alternative commercial acrylic, Plex 55™ from Rohm and Haas Inc was also examined and found to have a series of intersecting surface scratches with finer roughness visible between the scratches. After 2000 abrasion strokes the wiped surface was found to be almost completely covered

by a relatively even pattern of scratches resulting in a very marked increase in roughness, the R_A value rising from 10 nm initially to 135 nm.

A sample of a Goodyear Aerospace coating on Plex 55 substrate was available which under the DIC microscope appeared to consist of small, irregularly shaped smooth regions typically a few micrometres in size; between these regions the surface had a fine granular structure. Initial light scatter and roughness values were high and despite damage to the surface by abrasion did not increase significantly. Damage by abrasion took the form of scratches up to about 1 μm in width, increasing in number until after 10000 abrasion strokes little of the original surface was visible. A significant decrease in transmittance had then occurred, from 89 to 82.5%, with some degradation of image quality viewed through the specimen.

3.4 Polycarbonate and coatings

The surface of the polycarbonate (Lexan 3000™ from General Electric) as received displayed scratches of varying severity but with very little structure otherwise. This surface was very susceptible to abrasion; thus after 1000 strokes there was an almost complete change in surface structure the R_A value rising from the original 4.5 nm to 80 nm, and the transmittance falling from 86.5% to 70% (see Figure 3 and Table 2).

A similar specimen of polycarbonate, approximately 6 mm thick, coated with Texstar C-254 coating was initially smooth apart from a few scratches. Abrasion testing indicated that the coating provided a moderate degree of protection, see Figure 4, taken after 1000 strokes. After 2000 strokes approximately half the surface was damaged showing R_A and transmittance values of 45 nm and 70% respectively.

A further specimen of polycarbonate which had received a Texstar C-292 coating was examined and found to be much more abrasion resistant. Apart from a few coarse scratches, the surface was virtually undamaged after 2000 strokes, the R_A value being 5 nm. The appearance of the coating after 10000 strokes is shown in Figure 5; the roughness, transmittance and light scatter values were comparable to those of the C-254 coating after only 1000 strokes as shown in Table 2.

4 RESULTS OF RAIN EROSION TESTING

4.1 Oxide glasses

Early work at RAE[4] showed that annealed oxide glasses exposed at 90° impact angle at 223 m/s velocity and 25 mm/h rain intensity were severely pitted or shattered within 5 to 10 minutes. Glasses toughened by thermal or chemical treatments could, however, survive up to 100 minutes with increase in the extent of pitting before failure. More recently, a chemically toughened optical glass (Pilkington Bros. plc WX3) has been evaluated particularly with regard to degradation of transmittance by rain erosion. The results obtained from specimens approximately 6 mm thick, are shown in Figure 6; small surface pits were observed after about 10 minutes exposure and these subsequently developed and multiplied leading to a gradual decrease in transmittance due to scattering from the roughened surface. Both specimens ultimately failed by extensive cracking.

4.2 Acrylic materials

The effects of single water drop impact and rain erosion of methyl methacrylate polymers have been studied extensively and summarised recently by Adler and Hooker[5]. Little appears to have been reported, however, on the behaviour of abrasion-resistant coated acrylics and the present results supplement the earlier paper of Fischer and Harbison[6] on the properties and applications of cast acrylic coated with silica-filled polysiloxane.

Two commercial cast acrylics (ICI plc 'Perspex™' and Swedlow Inc. 'Acrivue 310™') have been tested for resistance to simulated rain and the results obtained from specimens approximately 6 mm thick, for weight loss and transmittance at 550 nm are given in Figures 7a and 7b. Figure 7c shows the results obtained on exposure of the Swedlow material which had been coated with an abrasion resistant coating (SS 6590) by the manufacturers. Under the very severe conditions of erosion prevailing in the RAE rig the two uncoated acrylics exhibited similar behaviour of weight loss and decay of transmittance with increasing exposure. The transmittance decreased rapidly in the first 2 minutes from 90% to 55-65% for a weight loss of only 0.4 mg/cm^2, demonstrating the very considerable light scattering which occurs from only lightly roughened surfaces. Thereafter the weight losses increased due to heavy pitting causing the transmittance to fall to very low values.

The coated acrylic suffered rather more rapid degradation suggesting perhaps that a mismatch of the impact properties of hard coating and substrate might hasten the surface break-up of the coated compared with uncoated substrate.

4.3 Polycarbonate materials

For many years it has been realised that polycarbonate has a rain erosion resistance considerably greater than acrylic[7] so that it was clearly of interest to examine the rain erosion resistance of hard coatings developed to improve the abrasion resistance of polycarbonate.

Figure 8 shows the effect of rain erosion at 90° impact angle on uncoated Lexan™ 9034-112 (from General Electric) and on Texstar C-254 and C-292 abrasion-resistant-coated polycarbonate specimens approximately 6 mm thick. Comparison of the results of Figure 8a with those of Figures 7a and 7b clearly shows a considerable improvement in the rain erosion resistance of polycarbonate over acrylic; transmittance, for example, is reduced to 60% in about 10 minutes for polycarbonate compared to 1.5 to 2 minutes for acrylic even though the original transmittance is higher for acrylic than polycarbonate. Interestingly however, approximately similar weight losses for the two materials correspond to similar reduction of transmittance. Comparison of Figures 8a, 8b and 8c shows almost the same reduction of transmittance with exposure for the uncoated and two coated materials, which is somewhat surprising in view of the greater weight losses for the coated compared with uncoated substrate. This suggests that the removal of coatings by rain erosion (accounting for weight losses) does not adversely affect the decay of transmittance of the substrate, contrary to that found for acrylic.

Figure 9 shows the corresponding results obtained for the uncoated and two coated polycarbonates for rain erosion at 60° impact angle. As expected, the degradation of transmittance of uncoated polycarbonate with erosion time is reduced compared with the corresponding results obtained at 90° impact angle; likewise the weight losses are also lower. For the C-254 coated material the pattern of weight loss with erosion time is similar at 60° and 90° impact angle although transmittance degrades more slowly at 60° than at 90°. This may indicate that the coating material is completely removed fairly early in the erosion process even at 60° impact angle. Figures 8c and 9c indicate that the C-292 coating is removed less rapidly at 60° impact angle than at 90°. However the differences are probably only significant where erosion has already degraded transmittance so much as to be unacceptable for satisfactory vision.

5 DISCUSSION

The NPL abrasion machine has been shown to afford a realistic means of simulating wiper abrasion under controlled conditions on conveniently small samples as is appropriate for development studies. The methods described for assessing abrasion damage fall conveniently into two categories; namely those associated with surface topography, *ie* visual examination by reflected light, differential interference contrast microscopy, surface roughness, and those more relevant to direct practical application, *ie* light scatter and transmittance. Numerical results essential for comparison of the performance of materials have been obtained from both categories and their use illustrated.

Oxide glasses are obviously much more resistant than plastics to abrasion and rain erosion, hence their extensive use in thin protective plies for thicker structural plies of acrylic in forward facing aircraft and rotorcraft transparencies. The erosion of acrylic materials exposed at high impact angle during flight through heavy rain is well known. Although it has been demonstrated here and elsewhere[6] that abrasion resistance can be afforded to acrylic by appropriate coating, the present results indicate that such coating is not likely to be effective against rain erosion.

The value of polycarbonate for aircraft glazing has been amply demonstrated in many papers in these Conferences, as has been the need to protect the exposed surface of the material[8,9]. Those abrasion resistant coatings which have been evaluated in the present work are clearly effective against wiper abrasion, the C-292 coating being considerably more efficient than the C-254 coating. These coatings do not afford sufficiently effective protection against rain erosion under the severe conditions employed. However removal of the coating by rain erosion does not appear to degrade the natural resistance of polycarbonate so that in some applications, particularly for light covers and forward facing transparencies for low speed aircraft and rotorcraft, coating could be beneficial.

Acknowledgment

The authors wish to thank Mr D.E. Putland for his work on the design and construction of the NPL abrasion machine, and to acknowledge the provision by suppliers of materials which have been evaluated during the course of this programme.

REFERENCES

1. J.H. McGarvey and B.F. Kay: "Design and development of helicopter transparent enclosures", 1975 Conference on Aerospace Transparent Materials and Enclosures, AFML-TR-76-54, 243-263

2. J.R. Plumer and W.C. McDonald: "Evaluation of scratch and spall resistant windshields", *ibid*, 196-242

3. A.A. Fyall, R.B. King and R.N.C. Strain: "Rain erosion aspects of aircraft and guided missiles", 1962, Jl. R. Aeronaut. Soc., 66 (619), 447-453

4. R.B. King, 1969, RAE Technical Report 69253

5. W.F. Adler and S.V. Hooker: "Rain erosion behaviour of polymethyl methacrylate", 1978, J. Mater. Sci., 13, 1015-1025

6. W.F. Fischer and W.C. Harbison: "Abrasion resistant coated plastic products for aircraft", 1980, SBAC Conference on Aerospace Transparencies, 185-204

7. G. Langbein: "Rain erosion of polymers", 1965 Proc. Rain Erosion Conference, Meersburg, 148-153

8. G.F. Schmitt: "Rain droplet erosion effects on transparent plastic material", SAMPE Journal, March/April 1974, 16-24

9. D.L. Voss: "Polycarbonate protection", 1975 Conference on Aerospace Transparent Materials and Enclosures, AFML-TR-76-54, 709-760

Table 1

RESULTS OF ABRASION TESTS ON ACRYLIC (ICI 'PERSPEX')
UNCOATED AND COATED

	Strokes	0	2000	20000
Uncoated 'Perspex'	Transmittance %	91	69.5	
	R_A, nm	2.5	120	
	Light scatter	20-50	2000	
Coated 'Perspex'	Transmittance %	92		86
	R_A, nm	8.5		59
	Light scatter	100-170		1150-1500

Table 2

RESULTS OF ABRASION TESTS ON POLYCARBONATE (GE 'LEXAN 3000')
UNCOATED AND WITH TEXSTAR COATINGS

	Strokes	0	1000	10000
Uncoated polycarbonate	Transmittance %	86.5	70	
	R_A, nm	4.5	80	
	Light scatter	100-150	2000	
With C-254 coating	Transmittance %	87	78	
	R_A, nm	2-4	21	
	Light scatter	100-150	1000	
With C-292 coating	Transmittance %	88.5		83
	R_A, nm	3		25
	Light scatter	60		1000

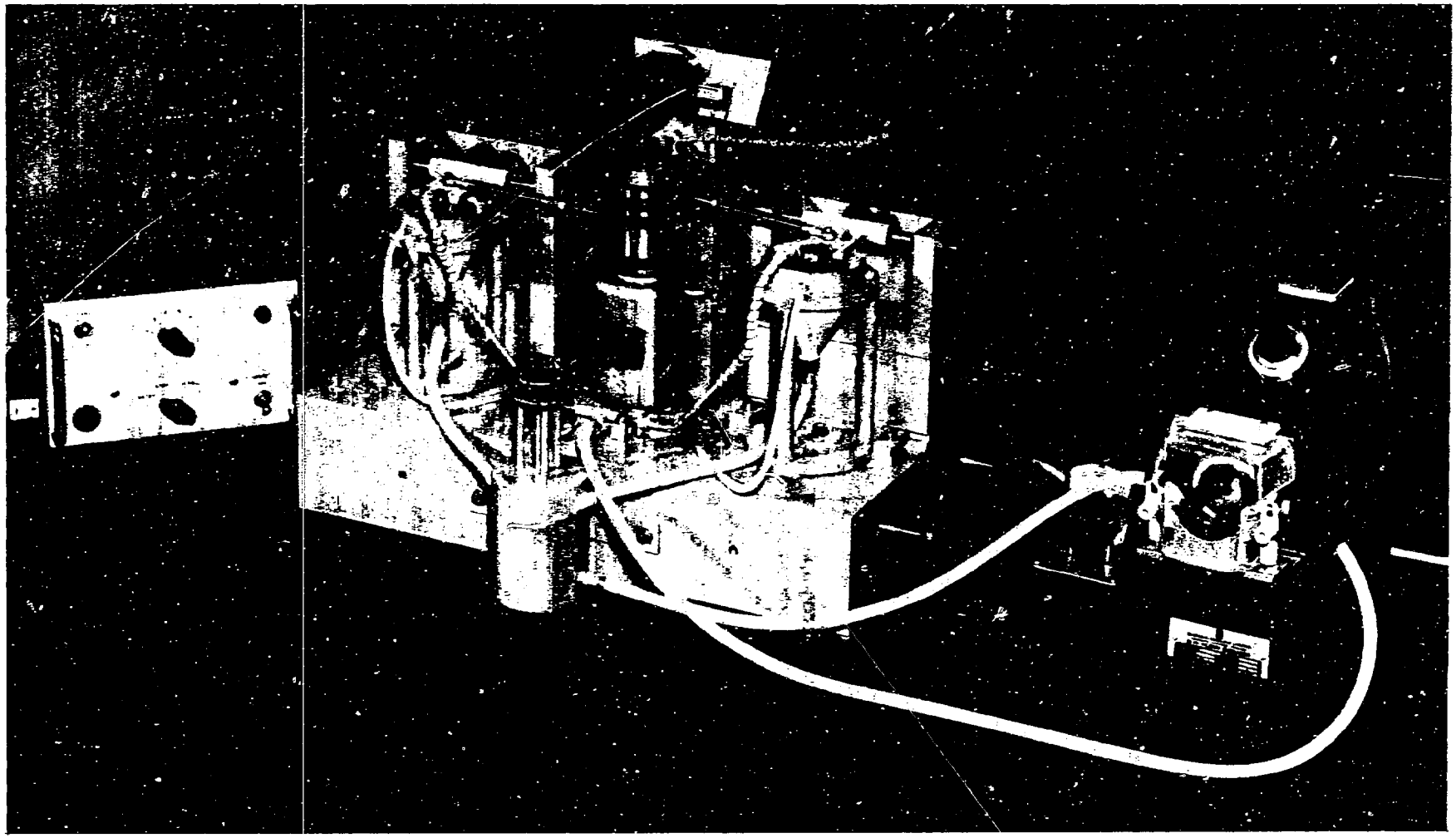

Fig 1 General view of the NPL abrasion machine

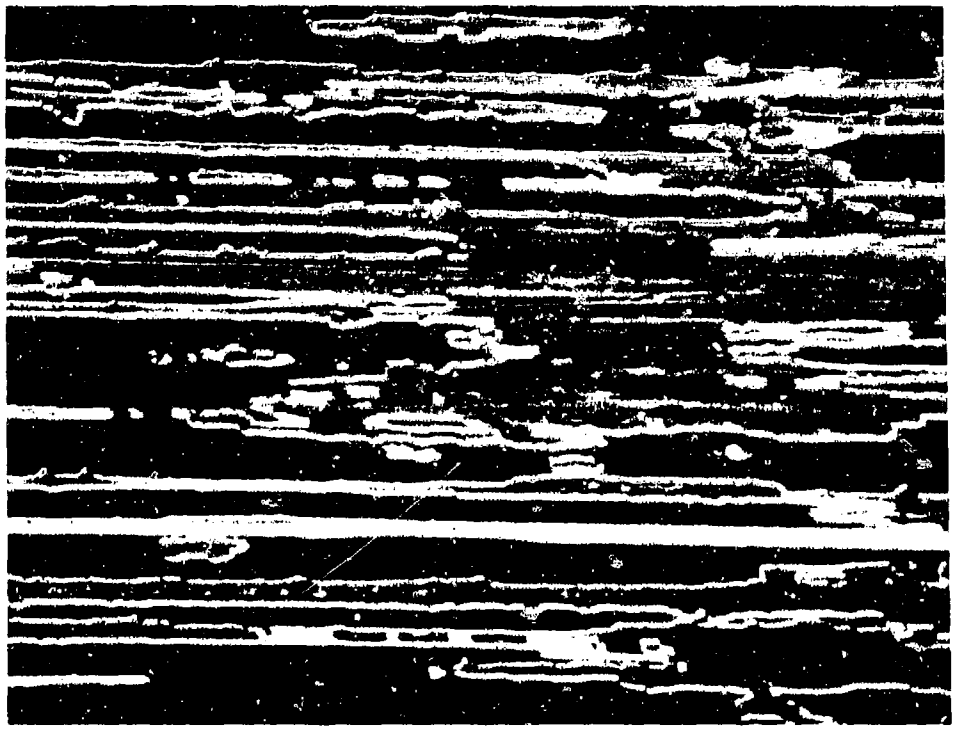

Fig 2 DIC photomicrograph of magnesium fluoride anti-reflection coating on glass after 10,000 abrasion strokes (x 500)

Fig 3 DIC photomicrograph of uncoated polycarbonate after 1,000 abrasion strokes (x 500)

Fig 4 DIC photomicrograph of polycarbonate with Texstar C-254 coating after 1,000 abrasion strokes (×500)

Fig 5 DIC photomicrograph of polycarbonate with Texstar C-292 coating after 10,000 abrasion strokes (×500)

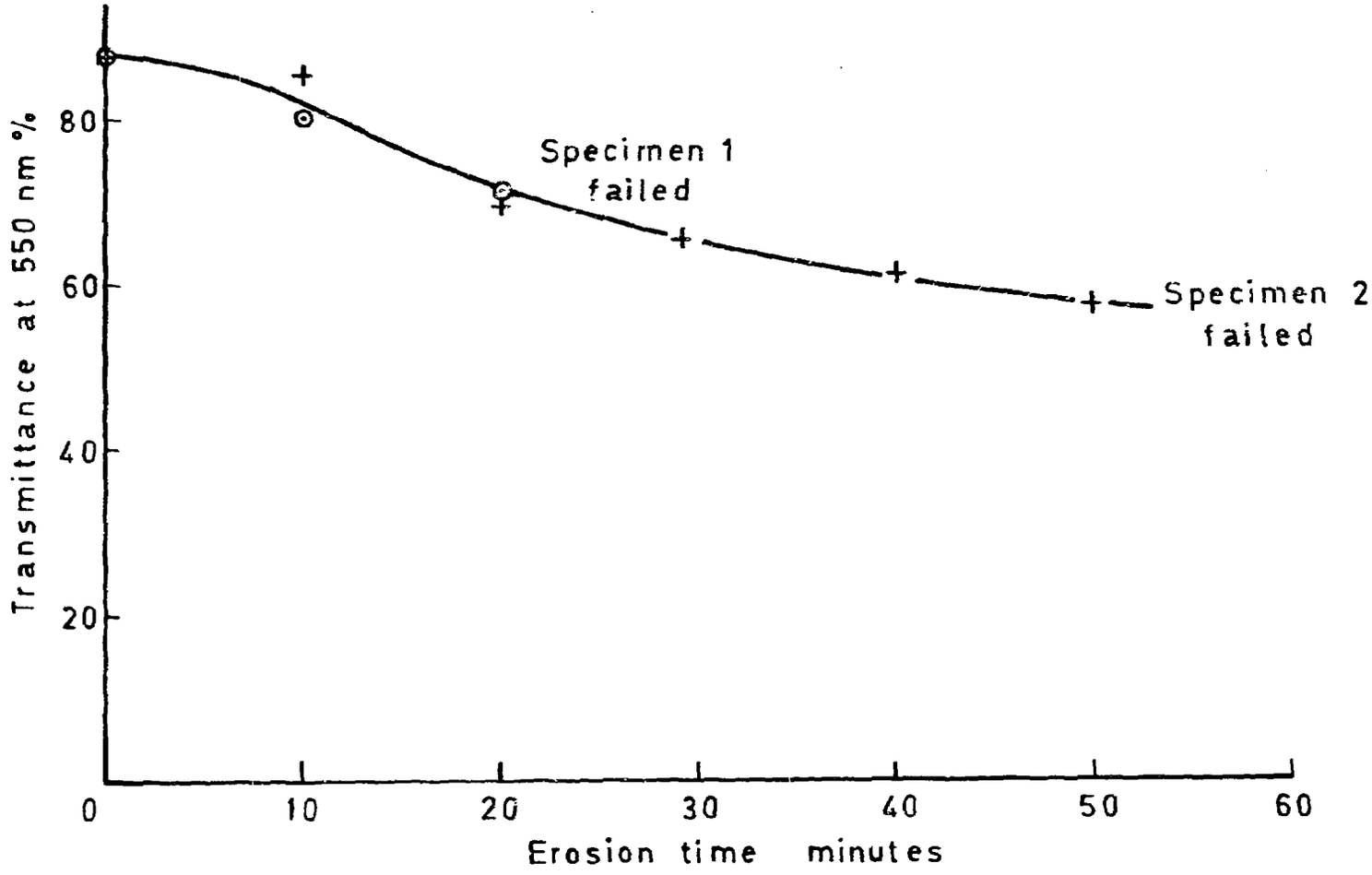

Fig 6 Rain erosion of chemically toughened glass (Pilkington WX3), velocity 223 m/s impact angle 90°

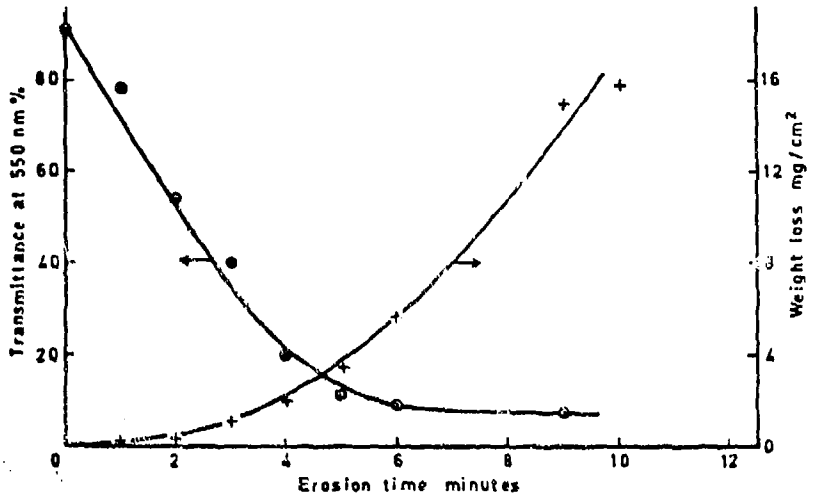

a Cast acrylic (ICI "perspex")

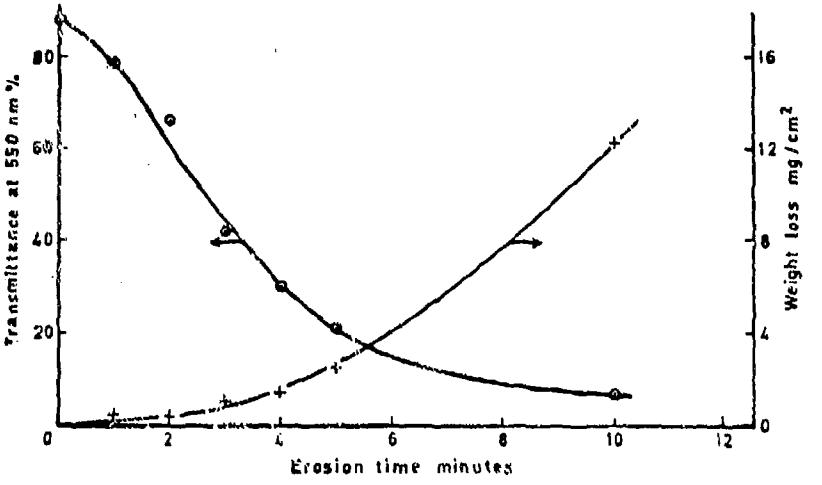

b Cast acrylic (Swedlow Inc. "Acrivue 310")

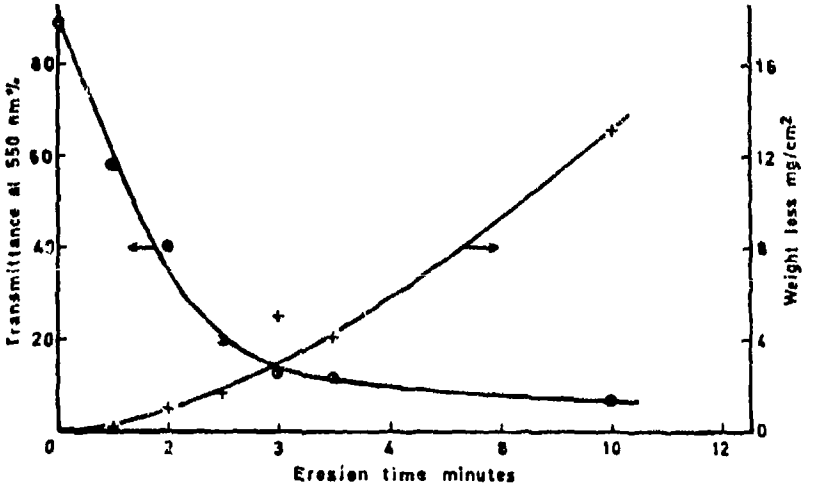

c Acrivue A – with SS-6590 abrasion resistant coating (Swedlow Inc)

Fig 7a-c Rain erosion of acrylic materials and coating; velocity 223 m/s, impact angle 90°

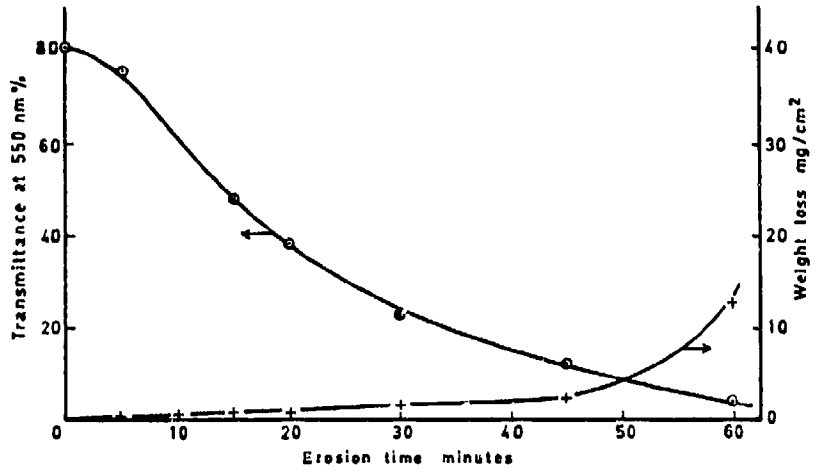

a Polycarbonate (Lexan 9034-112)

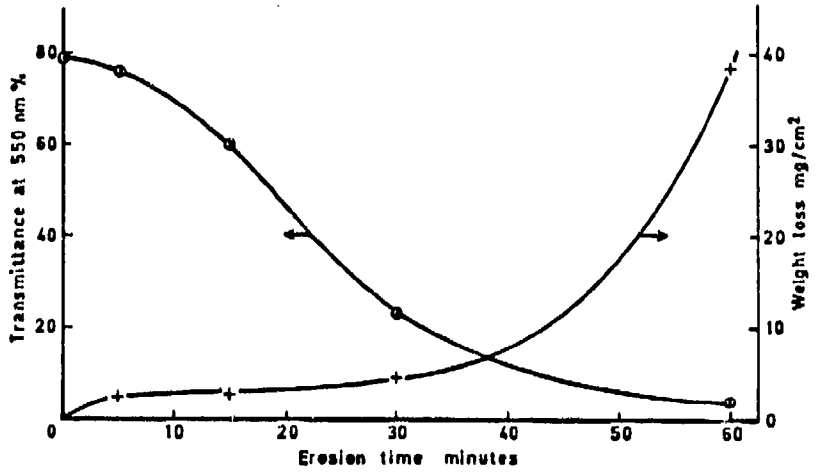

b Polycarbonate with Texstar C-254 coating

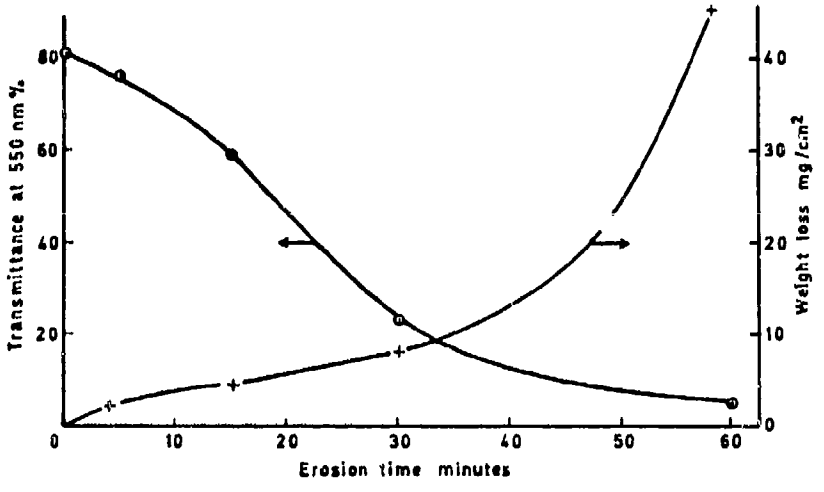

c Polycarbonate with Texstar C-292 coating

Fig 8a-c Rain erosion of polycarbonate material and coatings; velocity 223 m/s, impact angle 90°

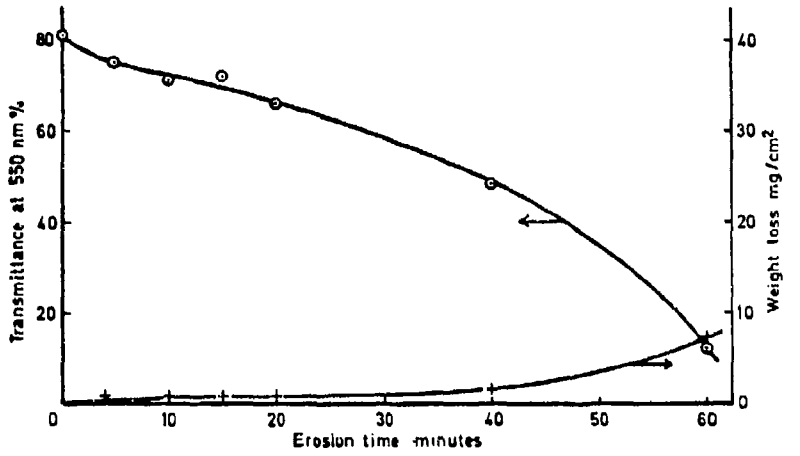

a Polycarbonate (Lexan 9034-112)

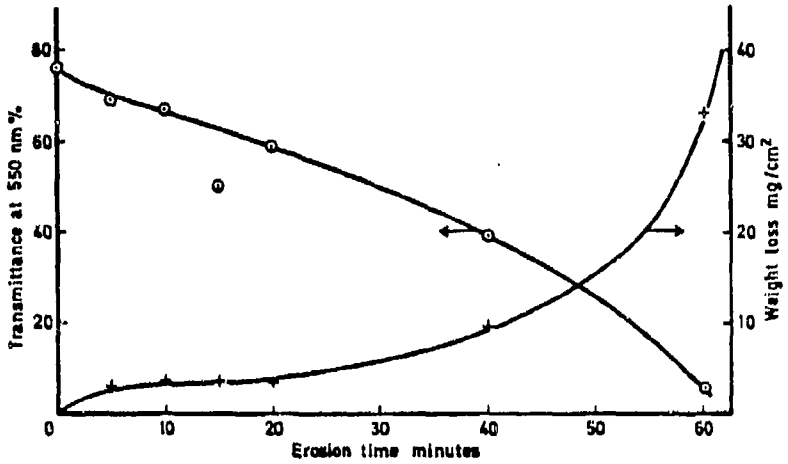

b Polycarbonate with Texstar C-254 coating

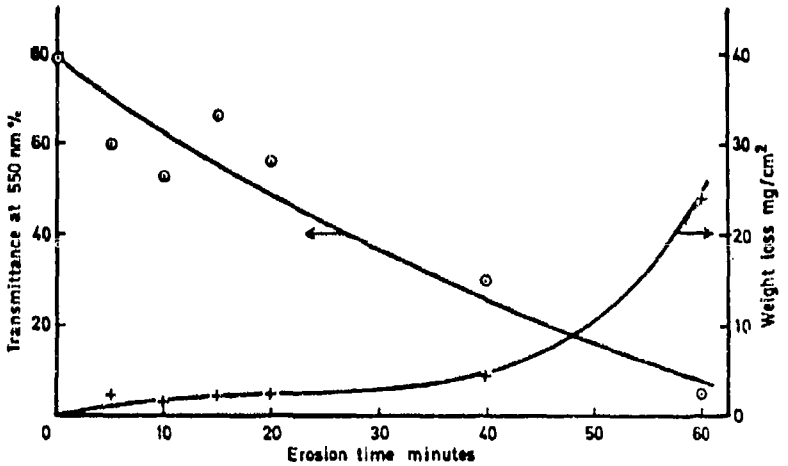

c Polycarbonate with Texstar C-292 coating

Fig 9a-c Rain erosion of polycarbonate material and coatings; velocity 223 m/s, impact angle 60°

AD-P003 228

WINDSHIELD PROBLEMS ON UK OPERATED TRANSPORT SIZED JET AIRCRAFT 1976 to 1982

J. Thorpe, Civil Aviation Authority

WINDSHIELD PROBLEMS ON UK OPERATED TRANSPORT SIZED JET AIRCRAFT - 1976 to 1982

by John Thorpe - UK Civil Aviation Authority
Safety Data and Analysis Unit

Abstract

The paper reviews windshield problems reported between 1976 and 1982 on UK operated transport sized jet aircraft. The paper shows that external causes such as hail (four cases) and birds or lightning (one case each) are outweighed by problems with the windshield itself (157 cases).

The total flying hours are 4.9 million, giving an average failure rate of one in 30,000 hours. There have been no cases of sudden loss of cabin pressure due to failure of both panes. For individual aircraft types the aircraft with the highest windshield failure rates are the Boeing 747 closely followed by Concorde and BAC1-11. By contrast there has not been a single reported problem on any of the McDonnell Douglas DC8, DC9 and DC10 aircraft or on the A300B Airbus. This is in spite of considerable flying hours on the DC10. On some aircraft types there are almost as many problems with the DV windows as with the windshield. Where the information is available it appears that on the majority of aircraft the problems are with the outer pane, however, the Boeing 707 has an above average proportion of inner pane problems. The type of failure has been divided into shattered cracked/crazed, delaminated or arcing. The Boeing 747 is most prone to shattering and delamination while the BAC1-11 and Boeing 707 are more prone to cracking/crazing. There are indications that windshield heat controllers may be a troublesome area on the Boeing 747 and Lockheed 1011.

1. Introduction

At the beginning of 1976 the UK introduced the mandatory reporting of occurrences hazarding the safety of an aircraft. Data from 1976 - 1982 has been examined in relation to windshield problems on UK operated transport sized jet aircraft. Turboprop - which are generally of older design and with lower cabin differential pressures, have been excluded, as have jet aircraft now out of service such as the Comet and the VC10.

2. Discussion of Data

(a) Problem Cause

From Table 1 it can be seen that problems within the windshield far outweigh any external causes. Hail damage accounts for any four reports, with bird and lightning damage and volcanic ash erosion accounting for one occurrence each. These outside causes have been excluded from the remainder of the Tables which concentrate on the windshield. There have been no cases at all of loss of cabin pressure or failure of both inner and outer panes. There has been one case of the whole windscreen departing from the aircraft.

(b) Aircraft Rates (Table 2)

It is surprising that there have been no reports of any windshield problems on McDonnell Douglas DC8, DC9 and DC10 aircraft, or on the A300B Airbus. This in in spite of considerable flying hours on the DC10. Of the other aircraft types the highest failure rate is on the Boeing 747 closely followed by the Concorde and BAC1-11. It could be argued that flights (i.e. cycles) should be the main criterion, however, for convenience flying hours have been used.

The data indicates that the windshield failure rate is around 30 per million flying hours. It is interesting that hail damage is about

3. Conclusions

3.1. Windshield problems are rarely a result of outside causes such as hail or birds.

3.2. From UK airline experience a windshield failure rate of about one in every 30,000 hours can be expected.

3.3. There have been no cases of windshield failure resulting in sudden de-compression.

3.4. There have been no reports at all of windshield problems on McDonnell Douglas and A300B aircraft.

3.5. The highest rate of windshield failure is on the Boeing 747, Concorde and BAC1-11 aircraft.

3.6. On most aircraft the outer pane is more likely to fail but the Boeing 707 has a higher proportion of inner pane failures.

3.7. Shattering and delamination are more prevalent on Boeing 747 aircraft while cracking/crazing are more prevalent on the BAC1-11 and Boeing 707.

3.8. There are indications that windshield heat controllers may be a troublesome area on the Boeing 747 and Lockheed 1011.

Table 1 - Problem Causes

Problem Cause	Number of cases
Windshield & Windshield Heat Problems	157
Hail Damage*	4
Bird Damage*	1
Volcanic Ash Damage*	1
Lightning Damage*	1
Crew Procedures	1

* Excluded from the remainder of the paper

Table 2 - Aircraft Rates

Aircraft Type	Transparency Manufacturer	Number of Occurrences	Flight Hours	Rate per 100,000 hours
A300B Airbus	Triplex	0	7,484	0
BAC 1-11	Nesa, Pittsburg Glass, Triplex	56	1,052,933	5.3
Boeing 707/720	NESA	29	746,172	3.8
" 727	PPG (Nesa)	5	156,746	3.2
" 737	Nesa	5	888,525	0.6
" 747	Sierracin, Triplex	42	755,580	5.5
Concorde	Triplex	2	36,909	5.4
HSA Trident	Triplex	10	641,959	1.5
Lockheed L1011	Sierracin	8	239,453	3.3
McDonnell Douglas DC8		0	47,260	0
" " DC9		0	33,774	0
" " DC10	Douglas (Pittsburg)	0	295,155	0
TOTAL	-	157	4,901,950	3.2

Table 3 - Problem Area

Aircraft Type	Part of Windshield		Windshield Layer		
	Windshield	DV Window	Outer	Inner	Unknown
BAC 1-11	54	2	18	2	36
B707/720	25	4	7	7	15
B727	3	2	2	-	3
B737	3	2	3	-	2
B747	42	-	29	1	12
Concorde	2	-	1	-	1
L1011	8	-	5	-	3
Trident	7	3	2	-	8
TOTAL	144	13	67	10	80

Table 4 - Type of Failure

Aircraft	Type of Failure				Windshield Heat Controller		
	Shattered	Cracked/ Crazed	Delam-inated	Arcing	Failed	Wiring	Switch Failure
BAC 1-11	3	44	2	8	-	2	-
B707	5	21	-	5	4	2	-
B727	1	3	-	2	2	1	-
B737	-	5	-	1	2	2	-
B747	12	10	20	6	15	-	1
Concorde	-	2	-	-	-	-	-
L1011	2	2	3	1	3	-	-
Trident	4	3	2	2	1	1	-
TOTAL	27	90	27	25	27	8	1

Table 5 - Phase of Flight

Aircraft	Ground	Climb	Cruise	Descent	Approach	Unknown
BAC 1-11	2	8	43	2	-	1
B707/720	-	2	20	2	1	4
B727	-	-	2	2	1	1
B737	-	-	4	-	-	-
B747	-	4	33	3	-	2
Concorde	1	1	-	-	-	-
L1011	2	-	5	-	1	-
Trident	1	3	4	1	1	-
TOTAL	6	18	111	10	4	8

References

1. CAA Paper 77008 Analysis of Bird Strikes Reported by European Airlines 1972-1975.

SESSION VII

COMPUTER AIDED STRUCTURAL ANALYSIS (PART I)

Chairman: R. E. McCarty
Flight Dynamics Laboratory
Wright-Patterson
Air Force Base, Ohio

AD-P003 229

VALIDATION OF THE MAGNA COMPUTER PROGRAM FOR NONLINEAR FINITE ELEMENT ANALYSIS OF AIRCRAFT TRANSPARENCY BIRD IMPACT

R. E. McCarty and 2 Lt. J. L. Hart,
Flight Dynamics Laboratory

Validation of the MAGNA Computer Program for Nonlinear Finite Element Analysis of Aircraft Transparency Bird Impact

R. E. McCarty
Lt J. L. Hart
Flight Dynamics Laboratory
Air Force Wright Aeronautical Laboratories
Wright-Patterson AFB, Ohio

Abstract

The approach taken for validation of MAGNA is based on the simulation of full scale bird impact tests followed by a comparison of the experimental data with that computed by MAGNA. To date, five of these validation studies have been accomplished and several more remain to be conducted. This paper summarizes the results of the validation studies which have been completed to date and lists the user guidelines which have been established in the process. These first validation studies may be characterized as analyses of simple structures, i.e. only single transparent panels have been analyzed as opposed to complex systems of multiple panels joined by metallic edgemember support structure. These same studies may be further characterized as involving only simple definitions of boundary conditions and a somewhat arbitrary procedure for the explicit definition of bird impact pressure loading on the surface of the structure. The cases selected for study were a flat, laminated glass windshield panel; a curved, laminated glass windshield panel; a curved, laminated plastic windshield panel; a bubble-shaped monolithic plastic one-piece canopy; and a heated glass cylinder (which involved neither an aircraft transparency system per se nor bird impact loads).

Introduction

Background

The Flight Dynamics Laboratory (FDL) has been involved with the development of bird-impact-resistant aircraft transparencies since 1972. As early as 1975, interest began to grow in the application of analytical tools to the design of new transparency systems. The design methods in use at the time were empirically based and required extensive full scale fabrication and bird impact testing. It was believed that valid analytical tools would permit the level of full scale testing required for system development to be reduced significantly. It was not intended that analytical methods would supplant full scale testing, only complement it.

By 1977 the development of a linear finite element analysis computer program had been accomplished under FDL sponsorship.[1-4] This computer program was soon found to be invalid for relatively flexible transparencies because of the large displacement (geometrically nonlinear) effects involved.[1,2] By late 1978 it had been demonstrated to be invalid even for quite stiff designs such as a heavy curved glass windshield panel.[5,6] It was determined at the time that large displacement or geometrically nonlinear effects were significant even for glass designs. The only exception to this rule was thought to be a flat glass panel. Thus, the need for a nonlinear analysis tool to design aircraft transparencies became clear in late 1978.

Renewing the search for a useful transparency analysis tool, the FDL adopted in 1979 a new nonlinear finite element analysis system called MAGNA (Materially and Geometrically Nonlinear Analysis).[7] By 1980 considerable thought had gone into the role which finite element analysis might play in the overall transparency design process.[8] General requirements for a nonlinear tool which could handle the transparency bird impact problem had been defined; these compared[8] very well with the already existing capabilities of the new MAGNA system.[8] Many different uses of nonlinear finite element analysis were foreseen in the transparency design process: generation of a great variety of parametric design data, analysis of final design configurations, providing guidance for developmental and qualification testing, etc.[8] Again, nonlinear finite element analysis was seen as complementing current test methodology, not replacing it completely.

MAGNA was first tested to demonstrate its geometric nonlinearity capability for the transparency bird impact problem during 1980. Results showed that it was capable of realistically reproducing the results of even the most severely nonlinear bird impact test.[9] Doubt was cast though on its validity for use in the design of new relatively flexible transparencies.[9]

The obstacle preventing use of MAGNA as a design tool for flexible transparencies was the fact that the bird impact loading was strongly coupled to the dynamic response of the transparency. This phenomenon will be referred to as "load/response coupling." The primary loading parameters such as footprint area on the transparency surface, period of the impact event, and impulse delivered to the transparency were found to be very sensitive to the instantaneous deformed shape and rates of deformation exhibited by the

transparency itself. If the response of the transparency was sufficiently stiff, the footprint area, impact period, and impulse were similar to what they would be for a rigid target case. Since it was known how to define these parameters for the rigid target case, it was possible to realistically predict bird impact response. For flexible designs, it was not possible to define footprint area, impact period, and impulse without knowing beforehand something about the response of the structure, so accurate prediction of bird impact response was not possible.

The reason that MAGNA could be used to reproduce test results even for very flexible transparencies was that a method for "artificially coupling" the loads to the response had been developed by the FDL.[10] This method required the existence of some full scale test data, hence precluding use of the same method during the design of a new system which hadn't yet been tested. Artificial coupling of the loads required estimates of both footprint area and impact period to be made from test data such as high speed film records. The method proved quite powerful and worked well for even the most severely coupled cases.[10]

In 1980, then, the outlook for fruitful application of nonlinear finite element methods to aircraft transparency analysis was both good and bad. It looked good because MAGNA had been validated for the analysis of test results for even the most flexible transparency designs.[10] A method of artificially coupling bird impact loading to the computed response had been developed to permit this type of application.[10] At the same time the outlook was bad because it wasn't known at the time how to implicitly calculate loads which were truly coupled to the response which was being computed. This defeated the use of MAGNA as a design tool for relatively flexible transparencies.[10] The thinking at the time was that results of any test could be analyzed with MAGNA and at least some new (relatively stiff) systems could be designed.[10] More plans were laid to improve these circumstances.

Approach

Plans in 1980 for FDL activities in further developing transparency analysis tools included four primary lines of work. First was to continue to sponsor major development of the MAGNA system through calendar year 1982. New capabilities would be added and the whole package would be tailored for convenient aircraft transparency analysis.

A second line of work would be to study, given a transparency design, at what level of impact energy load/response coupling becomes significant.

The third line of work would attempt to develop a true load/response coupling capability for MAGNA. This would be handled separately from the rest of the system improvements because of its complexity.

The fourth line of work would study several transparency systems of varying overall stiffness to see for which ones load/response coupling was significant. The ground rules for this line of work included the adoption, rather arbitrarily, of the procedures which already had been developed by FDL for uncoupled and artificially coupled definitions of bird impact loading.

These loading definitions would be applied over and over again to each transparency system studied. In this way those types of systems requiring uncoupled or coupled loads respectively could be identified and cataloged accordingly.

At the time of this writing considerable progress has been made on all four of these fronts. The first line of work to accomplish major new development of the entire MAGNA package has been completed as planned.[11-14]

The second work effort to study coupling effects for a given transparency design at various bird impact energy levels has also been completed.[15] For this work an all aluminum panel design was used to eliminate a high level of uncertainty regarding mechanical properties of transparent plastic materials.

The third activity to develop a fully coupled bird impact loading capability for MAGNA is currently in progress and shows promise.[16] This work is scheduled for completion in December 1983. On the same subject, a rudimentary method for coupling loads has been developed and demonstrated by the FDL.[17] This simple approach to the problem may prove sufficient for most if not all practical cases. Trials are in progress with the T-38 aircraft student windshield, B-1A aircraft windshield panel, and the F-16A laminated canopy.[17] Validation has already been accomplished for the TF-15 aircraft canopy. This method directly couples the impulse delivered to the instantaneous deformation computed for the transparency. Two standard user-written subroutines for MAGNA are utilized. Only the impulse changes as a function of the response, not the loaded footprint area nor the period of the impact event. The fully coupled method which is in progress would couple impulse, footprint area, and impact period to the response.

Under the fourth line of work to analyze several transparency systems of varying overall stiffness, five validation studies with MAGNA have been accomplished in-house by the FDL. The purpose of this paper is to document results of these studies for use by the aircraft transparency design community. These same studies will be documented in much more detail for reference by other finite element analysts.[18]

The purpose of these studies can be seen as two-fold. The primary purpose was to validate MAGNA for the analysis of each transparency type studied. It was felt at the outset that since MAGNA could handle very flexible transparencies, it could handle any type of transparency design. This turned out not to be the case as will be discussed further on. The second purpose of the studies was, for each case where use of MAGNA was validated, to determine whether or not load/response coupling was significant. This would help clarify the usefulness of MAGNA as a design tool by identifying those cases for which design analyses would provide realistic results.

Scope

Since 1980 five FDL in-house validation studies have been conducted using MAGNA. These involved a flat laminated glass windshield panel, a curved laminated glass windshield panel, a curved laminated plastic windshield panel,

a bubble-shaped monolithic canopy, and a heated cylindrical glass bar. The glass bar case has nothing to do with bird impact. Instead it represents a simple one-dimensional thermal loads case to test that particular analysis branch of the MAGNA system.

Each of these studies may be characterized by simple finite element modelling of only the transparent panels themselves without edgemember attachments or supporting structure, by simple boundary condition specifications, and by somewhat arbitrary definitions of bird impact loading. Future validation studies are planned to include more complex models using new finite elements (such as the laminated shell[11]), newly added features in MAGNA (such as coupling and surface contact[11]), and parametric studies of a variety of bird impact loading definitions.

For the studies which have been accomplished to date, this paper will describe the manner in which each was conducted, present the results of each, and draw conclusions regarding the validity of using MAGNA and whether or not load/response coupling is significant for each. First, however, a brief description of MAGNA itself and the FDL developed procedures for defining bird impact loading will be included.

MAGNA Computer Program

The MAGNA nonlinear finite element analysis system was developed by the University of Dayton Research Institute, Dayton, Ohio and first became operational during the summer of 1978. The first edition of MAGNA for US Air Force aircraft transparency application was delivered in late 1979.

Capabilities

MAGNA was designed for the analysis of large scale problems involving three-dimensional structures. It can account for the effects of both geometric nonlinearity (large displacements and rotations) and material nonlinearity (elastic-plastic behavior). The static, dynamic, or free vibration response of a structure can be analyzed using MAGNA. Special features such as contact analysis (e.g. bird/canopy contact, or canopy/heads-up-display contact), full restart capabilities, and convenient interactive graphics make it a powerful analysis tool which is easy to use. The interactive graphics are provided in two packages: the first, a preprocessor, enables rapid finite element modelling of transparency structures; the second, a postprocessor, permits quick visualization of the results of an analysis including structural deformation, stress, and strain. The capabilities of MAGNA are documented in more detail elsewhere.[11-14,19]

Availability

A Control Data Corporation (CDC) CYBER 750 version of MAGNA is operational at Wright-Patterson Air Force Base (WPAFB), Ohio. This installation includes the complete MAGNA package and permits free access for all US Government offices and contractors doing work for the US Government.

A CRAY-1 version of MAGNA is offered by United Information Services (UIS) through their commercial time sharing network. The CRAY installation includes only the analysis portion of the MAGNA system. The interactive graphics portions of the system are installed on UIS CDC equipment.

Other operational versions of MAGNA including VAX 11/780 and IBM editions are available through lease or purchase from the University of Dayton Research Institute, Dayton, Ohio.

The period of most intensive MAGNA development for aircraft transparency analysis sponsored by the US Air Force will most probably draw to a close at the end of 1983. A fully maintained operational installation of MAGNA is planned at WPAFB well into the future.

Bird Impact Loads Definition

Theory

Many explicit definitions of bird impact loading are possible. In 1980 the primary goals for in-house work in the FDL were to first, validate MAGNA for the analysis of many types of transparency systems and second, to determine whether or not load/response coupling was significant in each case. It was not desirable to take the time to conduct sensitivity studies for a variety of loads definitions to compare results and select what seemed to be the best.

Instead of conducting parametric loads studies, a somewhat arbitrary procedure for the definition of bird impact loading was adopted. This procedure was based on an extensive experimental data base accumulated over a period of several years.[20-27] The data base was valid for the case of a rigid, flat, inclined target and comprised pressure data recorded at the surface of the target during bird impact.

The loads definition procedure is simple and straightforward to use; it has been utilized for each of the bird impact simulations reported here. The only variation of the procedure involves some simple modifications whenever artificial coupling is desired. The essential points of the theory upon which the loads definition procedure is based are as follows:

1. The bird behaves as a fluid during impact.

2. The impulse delivered to the structure is equal to the component of the bird's linear momentum which is normal to the target surface.

3. The bird may be represented as a right circular cylinder having a length to diameter ratio of 2.0.

4. The average density of the bird material is 1.86 sl/ft^3.

5. The period of the impact event is best characterized as the time required for the bird to travel its own (effective) length.

6. The pressure resulting from bird impact is relatively constant at any point on the surface of the target (quasi-steady fluid flow).

The following section briefly sketches the procedures used to define uncoupled, and artificially coupled bird impact loads.

Procedures for Bird Impact Loads Definition

An in-depth discussion of these loads definition procedures will be documented elsewhere.[18] Only the key points for each will be noted here.

a. Uncoupled Loads Definition

The first step in the uncoupled definition of bird impact loading is the calculation of the impulse delivered to the target from Equation 1.

$$I = M\ V\ \mathrm{Sin}\Theta \qquad (1)$$

I - impulse (lb sec)

M - mass (sl)

V - velocity (ft/sec)

Θ - acute angle between bird trajectory and target surface (deg)

Next is to calculate the length and diameter of the bird cylinder using equations 2 and 3.[18]

$$L = (0.085\ W)^{1/3} \qquad (2)$$

$$D = 0.5\ (0.085\ W)^{1/3} \qquad (3)$$

L - bird length (ft)

D - bird diameter (ft)

W - bird weight (lb)

Next the period of the bird impact event is calculated using equation 4.

$$T = (L + D/\mathrm{Tan}\Theta\ )\ /\ V \qquad (4)$$

T - period of impact event (sec)

Having calculated the parameters above, the locus of the bird impact pressure footprint on the surface of the transparency is estimated. Data from bird impact testing with rigid, flat, inclined targets is used to do this.[25]

When the boundary of the pressure footprint has been located on the surface, a group of finite elements from the model being used is selected which most closely approximates the area and location of the footprint. These become the elements then to which bird impact pressure is applied during the finite element solution.

After the elements representing the impact pressure footprint have been identified, a table is assembled of the times at which load rise and unloading occur for each element. A rectangular pressure vs time history is assumed for each element. The details of this process are too tedious to cover here.

When the intervals of time have been defined during which each element in the footprint is to be loaded, a sum of products is calculated. Each product is the area of an individual element multiplied by the time interval for its loading. The sum of these products is divided into the impulse defined by equation 1, to determine the value of the constant (and spatially uniform) pressure to be applied to each element in the footprint area.

This step completes the definition of uncoupled bird impact loading. The (single) value of the pressure plus the table of load rise and unloading times for each element in the footprint are sufficient to define the applied loads for MAGNA analysis.

b. Artificially Coupled Loads Definition

This procedure is identical to that for uncoupled loads definition which has just been described except at 3 points. The first point at which the artificially coupled loads procedure differs is in the calculation of the impulse which for the uncoupled case was defined by Equation 1. For the artificially coupled case, Equation 1 represents only a lower bound for the impulse. The upper bound is equal to 100 percent of the linear momentum of the bird before impact. The true impulse lies somewhere between the two. When attempting to artificially couple bird impact loading, it has become common practise in the FDL to adopt either one of these two bounding values. In this way at least some specific conclusions may be drawn; e.g. if the upper bound for the impulse had been selected for use then it could be concluded that the results of the analysis would be conservative since it is known that the actual energy (impulse) delivered to the structure was less than the value of the impulse used in the analysis. Of course, estimating the actual impulse by selecting an intermediate value is also possible.

The next point of difference between the uncoupled and coupled loading definitions involves the determination of the period of the bird impact event. Instead of calculating the period from Equations 2, 3, and 4, an estimate is made from other sources; the FDL most frequently relies on high speed film records of full scale tests to estimate impact period. The film which has been found most useful for this purpose is one with timing marks on it which has been taken from inside the transparency. From this view it is usually possible to estimate closely the time during which bird material remains in contact with the transparency surface.

The third and last point at which the two loading definition procedures differ is in the estimation of the locus of the bird impact pressure footprint. For the uncoupled case, rigid target test data is used for this purpose. For the artificially coupled case, just as in estimating the actual impact period, the FDL relies on photographic records of full scale tests to estimate the surface area of the transparency which is loaded by bird material. At times a still photo showing a smudge left by the bird impact is used, while at others high speed film taken from inside the transparency is employed. As pointed out earlier, the procedure for artificially coupled loads is only useful for the case when data from full scale tests of a transparency is available.

Both of these procedures for the definition of bird impact loading are quite simplistic. They presume a regular geometry for the bird, ignore spikes of shock pressure which occur very early in the impact event, and assume a spatially uniform distribution of pressure. Even with these shortcomings, bird impact simulation results obtained with these procedures have been found to be useful and realistic as will be shown in the next section.

Validation Studies

Introduction

As mentioned at the beginning of the loads definition section, the studies reported here had two main goals. The first was to validate the use of MAGNA for a variety of transparency types, and the second was to determine whether or not load/response coupling was significant for each type. Parametric studies regarding the best means of defining bird impact loading were postponed for the time being . It was planned instead to focus attention on those parameters relating most directly to the system design. Four primary system parameters were addressed at the outset. The first of these was structural stiffness which was the principal factor determining the significance of load response coupling and also was one of the factors determining the importance of large displacement effects in the analysis.

The second system parameter addressed was geometrical shape. The curvature of the transparency surface was also a factor (along with stiffness) in determining the importance of large displacement effects.

The third parameter treated was cross section design. The difference between monolithic and laminated design determines to a great extent the complexity of finite element analysis required for bird impact simulation.

The last of the four system parameters encompassed in these studies was temperature. By analyzing transparency systems at cold, ambient, or hot temperatures it was planned to evaluate the importance of thermal strains in the design of bird-impact-resistant transparencies.

Aircraft transparency systems were selected from among those for which full scale data was available to best show the effects of these four parameters on bird impact computer simulation results. The cases which were

selected for study were a flat laminated glass windshield panel - the British Vulcan B Mk.1 Bomber Centre Windshield, a curved laminated glass windshield panel - the 36 in. x 36 in. Prototype B-1 Aircraft Windshield, a curved laminated plastic windshield panel - the Acrylic Faced B-1A Aircraft Windshield, a bubble shaped monolithic plastic one-piece canopy - the F-16A 1/2 in. Polycarbonate Canopy, and a hot glass part - a right circular cylinder of annealed soda lime glass.

This grouping of cases was planned to provide comparative results for stiff vs flexible designs, flat versus curved geometry, monolithic versus laminated design, and hot versus ambient temperatures. During the progress of the work effort a fifth important and unforeseen system parameter was revealed - interlayer material stiffness. Numerical problems related directly to very soft interlayer materials (Young's Modulus less than or equal to 1000 psi) were encountered and will be discussed in later sections.

The conduct of and results for each case study in turn will be discussed in the following sections.

Vulcan B Mk. 1 Centre Windshield Panel

The Vulcan is one of the British V Bombers dating from the early 1950's. Figure 1 shows a photo of several of the early aircraft. Originally designed for a high altitude, high speed mission it was subsequently adapted to the role of a low altitude penetrator. As a consequence the risk of bird impact damage was incurred; this was a hazard for which the transparency system had not been designed.

The windshield transparency system for the Vulcan consists of several panels mounted together in a frame as shown in Figure 2. During testing which was done to determine the level of bird impact protection offered by the system, a 4 lb bird impact at the center of the centre panel at 211 kt resulted in failure.[28] The level of protection against a 4 lb bird at the same location was estimated to be 175 kt as shown in Figure 3. It was reported that the level of protection offered by the panel itself was probably

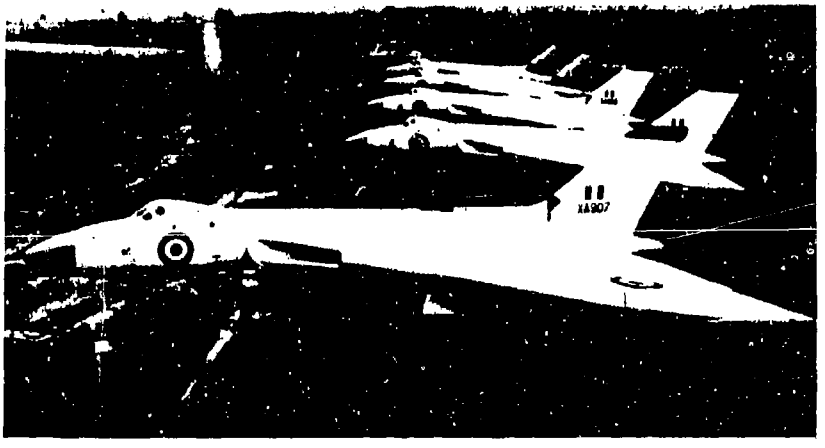

Figure 1. Vulcan B Mk. 1 Aircraft

much more than 175 kt but that the thin gauge sheet metal support for the windshield probably failed at a low energy, precipitating failure of the panel itself.[28] The cross section design and metal support for the windshield are shown in Figure 4.

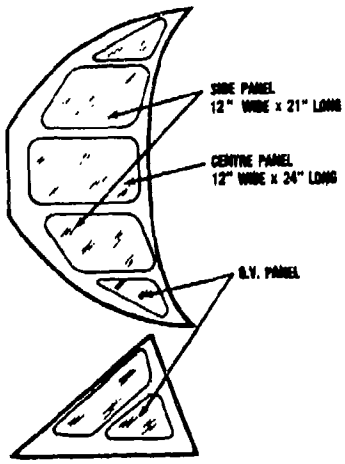

Figure 2. Vulcan B Mk. 1 Windshield Transparency System

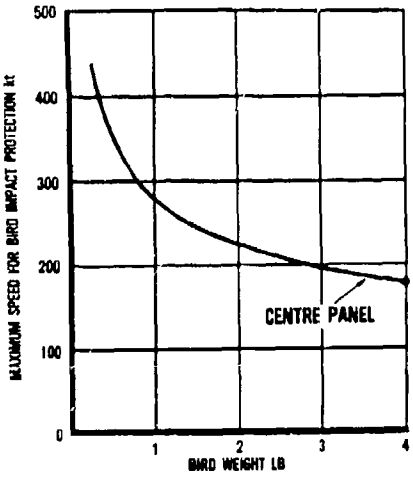

Figure 3. Centre Windshield Panel Bird Impact Protection

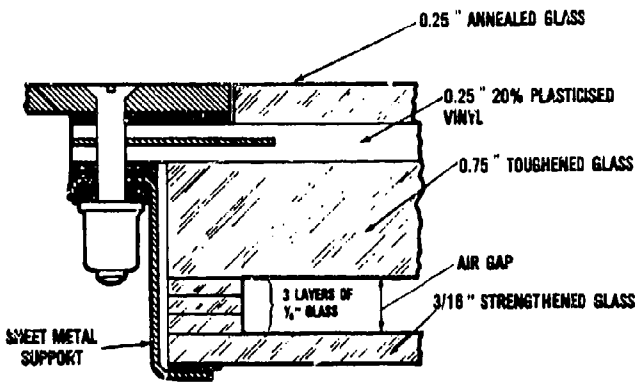

Figure 4. Centre Windshield Panel Edge Detail

The MAGNA finite element model of the centre panel included only the left half due to symmetry of the bird impact loads and the structure itself. Figure 5 illustrates the model which was generated using the CORGEN, EXPAND, and PREP modules of the MAGNA preprocessor.[12] The model only includes the outer three plies of the structure shown in Figure 4 because these must fail before any contact with the most inward ply can occur. Each ply in the structure was modelled with a separate layer of 55 solid elements for a total of 165 elements. The model contained 792 nodes - a moderate size for MAGNA nonlinear analysis. The mesh in the finite element model was designed to be finest near the site of bird impact. No supporting structure was included in the model as prescribed by the ground rules laid down for this first group of MAGNA validation studies; these ground rules were discussed in the Scope section.

The boundary conditions which were applied prevented in-plane lateral motion along the centerline of the panel. Also, out-of-plane motion was prevented all along the inner edge of the panel. Finally, all nodes lying on the inner forward edge were pinned. The number of unconstrained degrees of

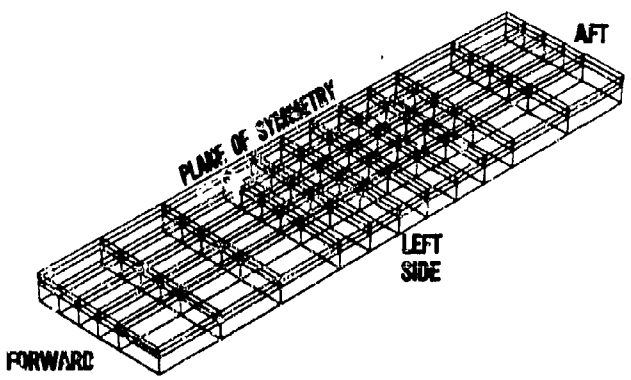

Figure 5. Centre Panel MAGNA Finite Element Model

freedom resulting with these boundary conditions was 2220. Material properties for 0 deg C were used; the values for these are tabulated in Table 1.

Table 1

Material Properties for Vulcan Centre Panel

Ply	Material	Young's Modulus (psi)	Poisson's Ratio	Rupture Stress (psi)	Mass Density ($lb\ sec^2/in^4$)
Face Ply	Annealed Glass	10.5×10^6	0.22	6,900	2.35×10^{-4}
Interlayer	PVB	14.7×10^5	0.46	3,000	1.02×10^{-4}
Main Ply	"Toughened" Glass	10.2×10^6	0.22	21,990	2.35×10^{-4}

The first MAGNA analysis with this model was to determine the first or lowest mode of free vibration for the structure. This type of analysis is normally conducted first to detect finite element modelling errors and to select a time step size for subsequent dynamic response analysis. The analysis was run at 235,000 octal words on a CDC CYBER 750 and required 132 central processor (CP) seconds. The frequency calculated was 971 Hz which is quite high indicating a very stiff transparency design. The shape of the first mode is illustrated in Figure 6. The solid lines in the figure indicate the undeformed geometry of the panel surface and the dotted lines the typical deformed shape of a first mode with the center of the panel bulging out.

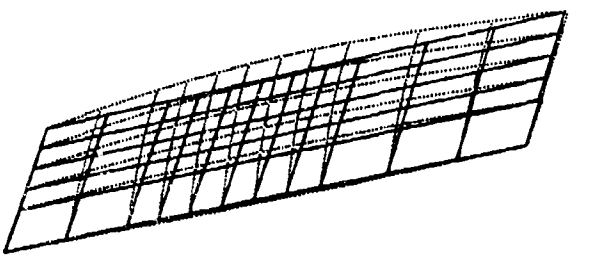

Figure 6. Deformed and Undeformed Shapes for Vulcan First Mode

The next two analyses were linear static and nonlinear static respectively to calculate the response to a concentrated 10,000 lb load applied normal to the center of the panel as shown in Figure 7. The main purpose of these jobs was to check a hypothesis made earlier about the

linearity of flat glass transparency panels.[5] This point was mentioned earlier in the background section. The hypothesis was that of all the possible structural classes of transparency systems, only flat glass designs could exhibit truly linear behavior. If the nonlinear static results were found to be the same as the linear static results for the Vulcan, this finding would support the hypothesis made.

For the linear static job linear deflection, stress and strain were calculated. This analysis was also run at 235,000 octal words and only required 122 CP sec. Displacement normal to the surface at the point of load application was computed to be -0.04163 in. This point corresponded to node 344 shown on Figure 7. The lateral component of in-plane strain at node 273, which is also shown in Figure 7, was predicted to be 0.002049 in./in. This point is on the inner surface of the panel, along the centerline, 1 element removed from the line of action of the load. The rupture strain for the toughened glass ply can be determined from Table 1 to be about 0.002200 in./in.

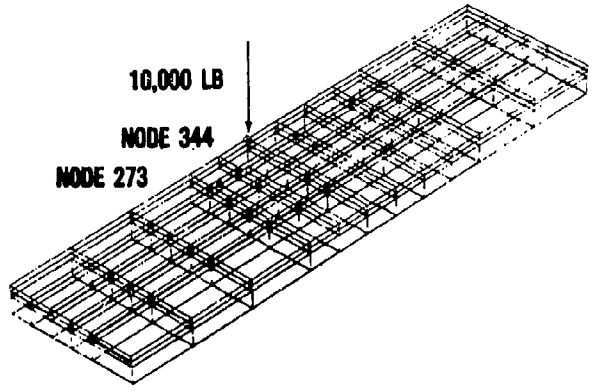

Figure 7. Load and Node Locations for Static Analysis

The next analysis conducted for the Vulcan was the nonlinear static one. It included the effects of geometric nonlinearity (large displacements and rotations) but not those of material nonlinearity. All the materials were still presumed to behave in a linear manner.

The same 10,000 lb force was assumed, acting at the same point as before. This time nonlinear deflection, stress, and strain were calculated. The load was applied incrementally in steps of either 500 or 1000 lb. The 10,000 lb load level was reached in 13 increments. The analysis was run at 350,000 octal words and took about 3300 CP sec, more than 25 times that required for linear analysis.

At the 10,000 lb load level, the normal deflection at node 344 (Figure 7) was -0.04178 in. and the lateral in-plane strain at node 273 (Figure 7) was 0.002047 in./in. Table 2 shows that these nonlinear static results are practically identical to the linear static results already obtained. This means that no significant geometric nonlinearity is exhibited by the structure

even for static loads near the rupture load. The response of flat glass panels is truly linear.

Table 2

Linear vs Nonlinear Static Results for Vulcan Windshield

Analysis Type	Normal Displacement @ Node 344 (in.)	In-Plane Lateral Strain @ Node 273 (in./in.)
Linear Static	-0.04163	0.002049
Nonlinear Static	-0.04178	0.002047

The last MAGNA analysis conducted for the Vulcan Centre Windshield panel was a simulation of a 4 lb bird impact at the center of the panel. It was a linear dynamic analysis since there was no need (based on the linear and nonlinear static results just discussed) to do a nonlinear dynamic case.

Since the edge support represented by the MAGNA finite element model of the panel was rigid, and the actual boundary condition was anything but, the 211 kt failure was not simulated.[28] Instead, other published empirical results for panels mounted in nearly rigid frames were used to estimate the true strength of the panel. The effective stiffness of the cross section was calculated using a published method.[29] This effective stiffness was then equated to a corresponding equivalent thickness using Equation 5.[30] The

$$t = 12\ (EI_{eff})^{1/3} / E \qquad (5)$$

EI_{eff} - Effective Stiffness

E - Young's Modulus (psi)

t - Equivalent Thickness (in.)

equivalent thickness of toughened glass determined for the Vulcan windshield panel (outer three plies only) in this manner was 1.18 in. Finally, an empirical relationship published for bird impact resistance of toughened glass, Equation 6, was used to estimate the ballistic limit for 1.18 in. of glass against a 4 lb bird.[31] The theoretical ballistic limit calculated in this way was 326 kt.

$$V = 400\ t/1.152\ \ W\ \cos\alpha \qquad (6)$$

α - angle between bird trajectory and surface normal (deg)

W - bird weight (lb)

t - thickness (in.)

V - ballistic limit (kt)

In view of the theoretical ballistic limit calculation just described, a 4 lb, 375 kt MAGNA bird impact simulation was conducted. It was felt that MAGNA should produce some clear indication of failure at this energy level. The uncoupled definition of bird impact loads discussed in an earlier section was used because the deformation was expected to be very small. The linear transient analysis was run at 350,000 octal words and cost 1120 CP seconds, just over 10 CP sec per increment.

Figure 8 shows the history of normal deflection at node 344 (Figure 7). The maximum displacement occurring is -0.0621 in. at 0.000480 sec. At this same time, Figure 9 shows contours of constant in-plane lateral strain for the inner surface of the main structural ply. The innermost contour, encompassing almost three elements, represents tensile strains above 0.002200 in./in. - the value of rupture strain for toughened glass. Rupture of the main toughened glass ply is clearly predicted.

Other bird impact simulations conducted for lower velocities indicated no rupture of the main glass ply.

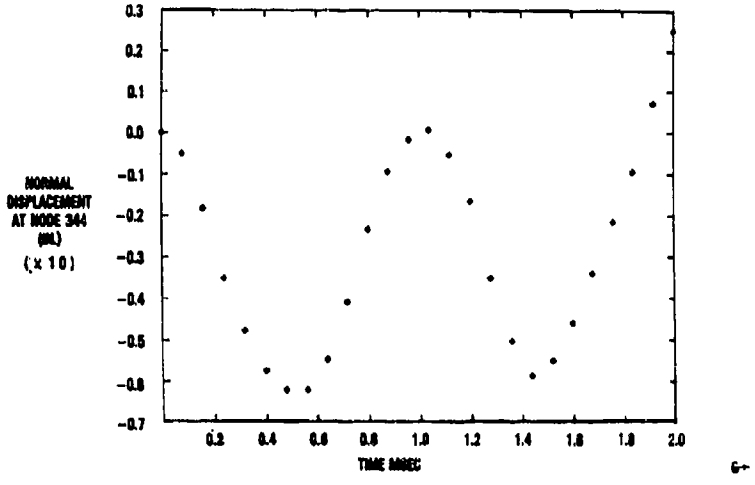

Figure 8. History of Normal Deflection at Node 344

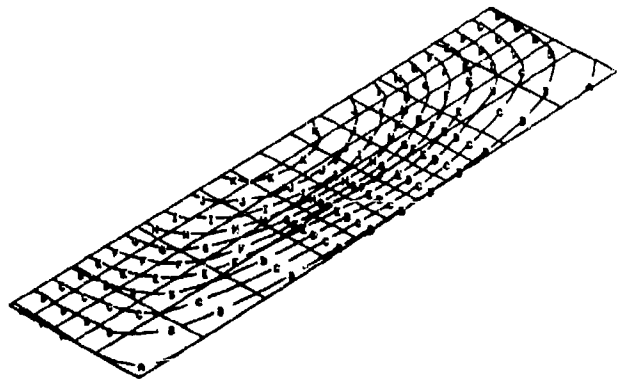

Figure 9. Contours of Constant In-Plane Lateral Strain at 0.000480 sec

Since a large area of failure is indicated, it can be concluded that linear transient MAGNA analysis using the FDL procedure for uncoupled bird impact loading is sufficient for accurate simulation of bird impact response of flat glass transparency designs similar to the Vulcan B Mk. 1 Centre Windshield. One would expect the uncoupled definition of bird impact loads to suffice because the resulting deformation (0.06 in.) is very small.

36 in. x 36 in. Prototype B-1A Windshield

In 1976 a variety of simulated B-1 aircraft windshield panel designs were subjected to full scale bird impact testing.[32,33] All of these panels were cylindrical sections and measured 36 in. by 36 in. Figure 10 illustrates the cross-sectional design for one of these panels. This particular configuration was a laminated glass design having 7 plies. It was tested (test number BM14) at a velocity of 556 kt with a 4 lb bird.[33] The impact point was near one of the corners of the panel, 8 in. measured in from either edge. Twenty

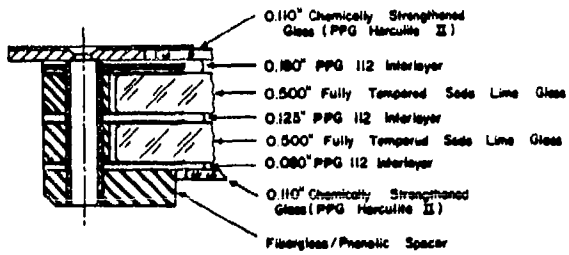

Figure 10. 36 in. by 36 in. Panel Design

channels of strain gage data were recorded from gages which had been imbedded in the panel during its fabrication. The locations of each of the strain gages is shown in Figure 11. Gages number 1, 2, 9, and 10 were mounted on the

innermost main structural ply while 3, 4 , 5, 6, 7, and 8 were mounted on the outer main ply.

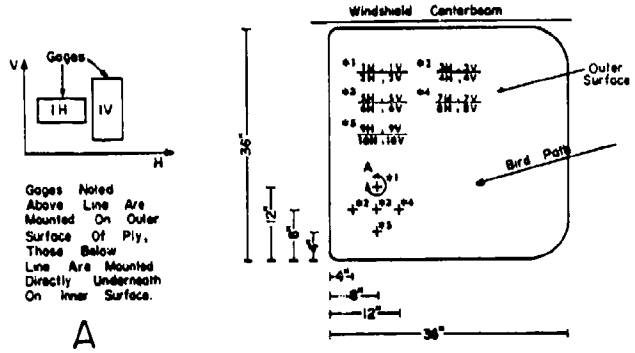

Figure 11. Strain Gage Locations

A linear dynamic analysis to simulate bird impact response for this panel was conducted previously using the (linear) IMPACT computer program.[5,6] The magnitude of strains observed during the test were found to be about twice that of the strains predicted by IMPACT.[6] At the time, this difference between experimental and computed values was attributed to the presence of significant geometric nonlinearity in the design due only to the curvature of the panel itself.[5] It was desired to test this early hypothesis using MAGNA to conduct a geometrically nonlinear bird impact simulation. If the strains predicted by MAGNA were much higher, this would confirm the presence of significant geometric nonlinearity.

The entire panel had to be modelled for MAGNA analysis because no symmetry was involved. As for the Vulcan Windshield model, the CORGEN, EXPAND,[12] and PREP modules of the MAGNA preprocessor were used in generating the model.[5] All 7 plies were included, each being represented by a layer of 36 solid elements. The total number of elements was 252 with 1064 nodes - a relatively large finite element model for nonlinear MAGNA analysis. Even though Figure 12 illustrates the completed model, only the two thickest plies can be distinguished.

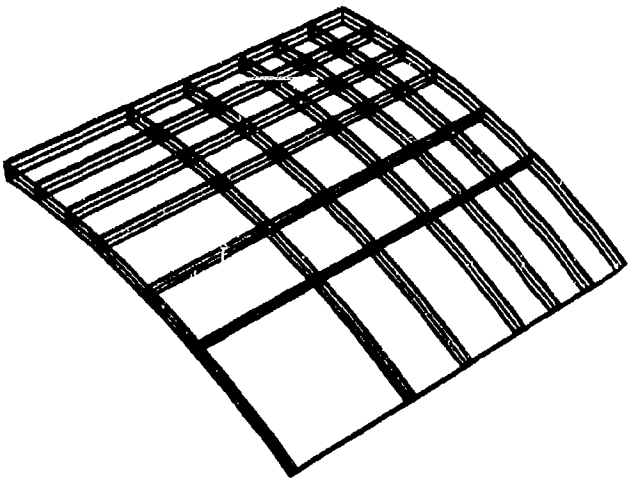

Figure 12. 36 in. by 36 in. MAGNA Model

The mesh was designed to be finest in the area of bird impact; no supporting structure was included in the model, again according to the discussion in the Scope section. The boundary conditions involved pinned nodes all along the inner edge of the panel, and were selected primarily for comparison with the earlier IMPACT results.[5] The final model had 3048 unconstrained degrees of freedom. Table 3 lists the (room temperature) material properties which were used.

The first MAGNA analysis conducted with the 36 in. by 36 in. model was a free vibration analysis to determine the first (or lowest) mode of the structure. The analysis was run at 350,000 octal words and used 542 CP sec, about 4 times what the Vulcan windshield vibration analysis cost. The frequency computed for the first mode was 245 Hz, considerably less than the 971 Hz for the Vulcan windshield as expected for the less stiff and more massive structure.

This lower natural frequency would make transient analysis less expensive than for the Vulcan windshield because the size of the finite element analysis time step is related to natural frequencies of the structure. A lower natural frequency permits the use of a larger time step in general. If the two models were the same size (which they're not) and other analysis parameters were the same, analysis of the 36 in. by 36 in. panel would be less expensive than that of the Vulcan windshield. Figure 13 shows the typical first mode shape which was predicted with the center of the panel bulging out.

Table 3

Material Properties for 36 in. x 36 in. Windshield Panel

Material	Young's Modulus (psi)	Poisson's Ratio	Rupture Stress (psi)	Mass Density ($lb\ sec^2/in^4$)
Chemically Strengthened Glass	11.0×10^6	0.22	37,000	23.5×10^{-5}
PPG 112 Interlayer	2044	0.40	5542	10.4×10^{-5}
Fully Tempered Soda Lime Glass	10.6×10^6	0.22	22,000	23.5×10^{-5}

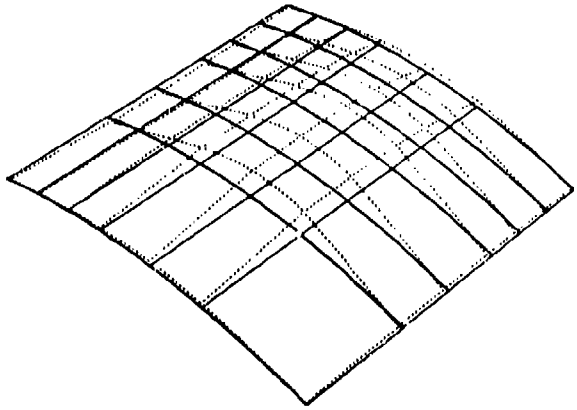

Figure 13. 36 in. by 36 in. Panel First Mode Shape

The next MAGNA analysis performed was a linear static one. A concentrated load of 10,000 lb was applied at the impact target point, node 658, as shown in Figure 14. Linear displacements, stress and strain were calculated. The analysis was run at 350,000 octal words and cost 541 CP sec, about 4 times that for the Vulcan windshield. The normal displacement calculated at node 658 was -0.114 in. The in-plane strain parallel the curved edge at node 659 was 0.000944 in./in. The location of node 659 is shown in Figure 14 and is on the inner surface of the outer main soda lime glass ply. Rupture strain for this material, as for the Vulcan windshield toughened glass, is about 0.002200 in./in.

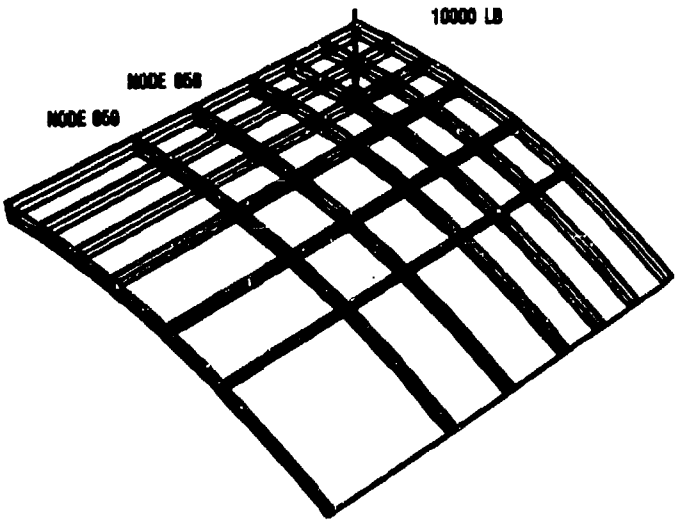

Figure 14. Load and Node Locations for Static Analysis

The next MAGNA analysis for the 36 in. x 36 in. panel was a nonlinear static one. Geometric nonlinearity was taken into account, but not so material nonlinearity. It was intended to compare the results of this analysis with those of the linear static job to define the level of geometric nonlinearity present in the structure. If significant geometric nonlinearity was indicated it would explain the poor linear bird impact correlation obtained at an earlier date.[5,6]

For the nonlinear static run, a 25,000 lb concentrated load was applied at node 658 as for the linear case. Loading was applied in steps of 5,000 lb; the 25,000 lb load level was reached in 5 solution increments. Nonlinear displacements, stress and strain were calculated. The job was run at 350,000 octal words and required 3835 CP sec, about 8 times that required for linear static analysis.

At the 25,000 lb load level, the normal displacement at node 658 (Figure 14) was -0.363 in.; scaling the linear displacement up from the previous analysis gives -0.285 in. The nonlinear in-plane strain parallel the curved edge at node 659 was 0.002842 in./in.; scaling the same piece of data up from the linear static analysis provides 0.002360 in./in. The nonlinear static deflections were about 27 percent greater than the linear static ones, and the nonlinear strains about 20 percent greater. These results are summarized in Table 4.

As hoped, the nonlinear static displacements and strains were greater than the linear ones for the 36 in. x 36 in. panel but not as much as hypothesized.[5,6] It seemed possible, however, that for the bird impact problem localized effects of geometric nonlinearity might play an even more important role than would be indicated by these static results.

The last MAGNA analysis conducted was a bird impact simulation. It was a nonlinear dynamic analysis including geometric but not material nonlinearity. A 4 lb bird impact at 556 kt was simulated using the FDL developed procedure for the uncoupled definition of bird impact loads.

Table 4

Linear vs Nonlinear Static Results for 36" x 36" in. Panel

Analysis Type	Normal Displacement @ Node 658 (in.)	In-Plane Strain (Along Arc) @ Node 659 (in./in.)
Linear Static	*-0.285	*0.002360
Nonlinear Static	-0.363	0.002842

*Scaled up from 10,000 lb load results.

During the actual test (number BM14) of the part, both soda lime glass plies fractured, but neither of the Herculite chemically strengthened glass face plies did.[33] The time of initiation for the failure was estimated from high speed film records to be about 0.001200 sec. It was felt that MAGNA should be able to reproduce similar results if it was going to be used as a transparency design analysis tool.

The bird impact simulation was run at 350,000 octal words and used 20,800 CP sec for 36 solution increments. This is about 580 CP sec per increment or nearly 60 times the cost per increment of the Vulcan windshield (linear) bird impact simulation. Fewer time steps were performed than for the Vulcan windshield but the analysis was still much more costly because the 36 in. x 36 in. panel model was larger, and primarily because the effects of geometric nonlinearity were being taken into account.

Figures 15 and 16 indicate impending rupture of both main soda lime glass plies at 0.001080 sec. Both show contours of constant value of the in-plane component of strain parallel the curved edge of the panel. The very small contour shown on the far curved edge in Figure 15 represents the value of tensile rupture strain. Because of the small size of the contour, its occurrence should be interpreted not as a clear indication of material rupture but as evidence that failure of the outer main ply is near. The somewhat

larger but innermost contour in the same location in Figure 15 represents 2/3 the value of tensile rupture strain indicating that the inner main ply is also near failure at points enclosed by this contour.

Figure 15. Inner Surface, Outer Main Ply, In-Plane Strain Contours at 0.001080 sec

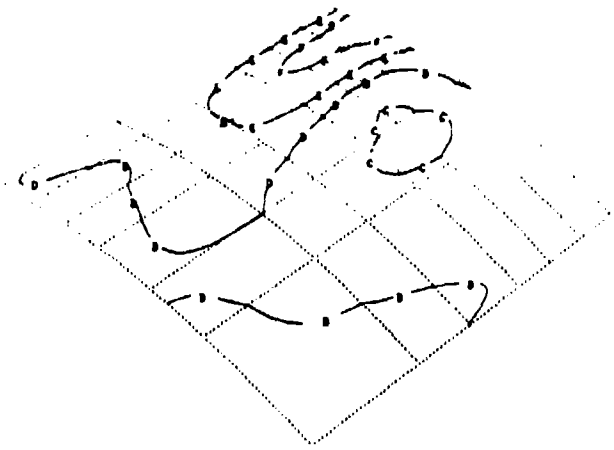

Figure 16. Inner Surface, Inner Main Ply, In-Plane Strain Contours at 0.001080 sec

Figures 17 and 18 show without question, because of the size of the innermost contour in the same location, that a short time later at 0.001280 sec both main glass plies have ruptured. The innermost contour on the far curved edge for each of these figures represents the value of tensile rupture strain for the soda lime glass. The timing of this predicted failure agrees very well with the estimate made from film records - 0.001200 sec.

No indication of either face ply rupture occurred in the computed results. The fact that both soda lime glass plies were predicted by MAGNA to fail while both Herculite face plies were predicted to survive also agrees with test results.

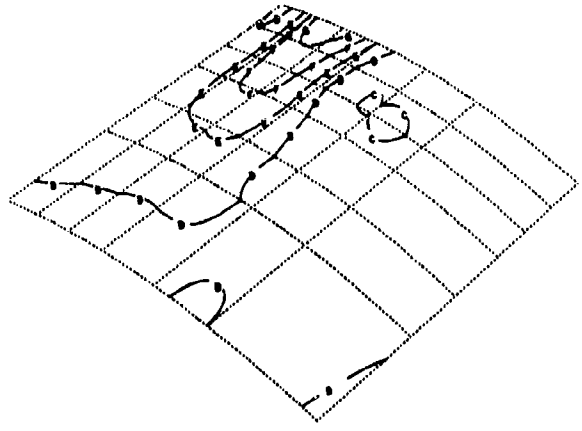

Figure 17. Inner Surface, Outer Main Ply, In-Plane Strain Contours at 0.001280 sec

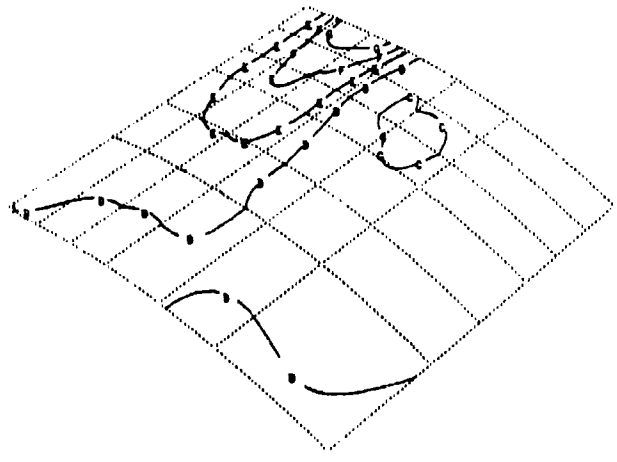

Figure 18. Inner Surface, Inner Main Ply, In-Plane Strain Contours at 0.001280 sec

Figures 19 and 20 illustrate correlation obtained for strain versus time results. Since the finite element mesh and the corresponding definition of bird impact loads was quite coarse for this analysis, very good agreement between experimental and computed strain histories should not be expected. The solid line with stars shown in the figures represents data measured during bird impact testing.[32] The dotted line with stars represents results of previous linear dynamic bird impact simulation.[5] The small open circles represent MAGNA nonlinear dynamic results. The component of strain illustrated in each case is in-plane parallel to the curved edge of the panel. Figure 11 can be used to study the locations and orientations of the strain gages involved.

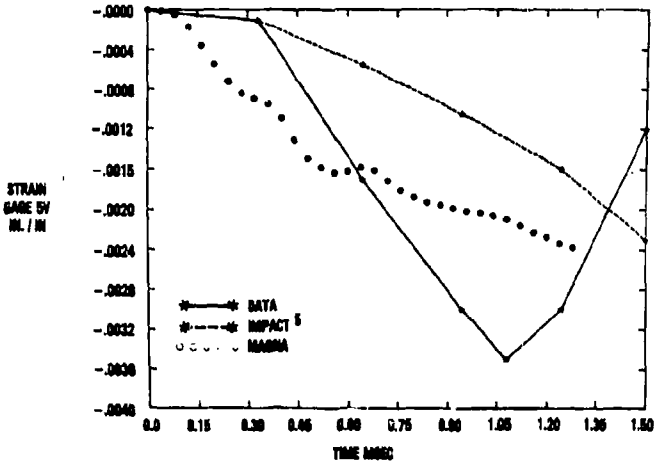

Figure 19. Outer Surface, Outer Main Ply, Strain vs Time Results for Gage 5V

While neither the IMPACT nor the MAGNA results agree very closely with the experimental data, it can be seen that the strain histories predicted by MAGNA are the more realistic of the two and that the MAGNA strain values are on the order of 100 percent greater than the IMPACT strains. For the static results discussed earlier, the nonlinear strains were only about 20 percent higher than the linear strains. This is a significant result because it means that for the case of dynamic bird impact response, slight curvature in a glass

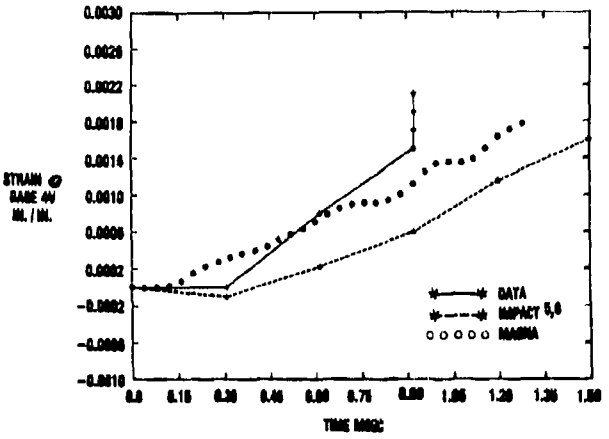

Figure 20. Inner Surface, Outer Main Ply, Strain vs Time Results for Gage 4 V

transparency structure can produce geometric nonlinearity strong enough to double the resulting strains. When analyzing bird impact response of transparencies, a geometrically nonlinear tool is clearly required whenever the geometry is curved, even if the design involves glass materials. These results support the early hypothesis made regarding the significance of geometric nonlinearity for curved glass transparencies.[5]

No indication of significant load/response coupling was indicated by the 36 in. x 36 in. panel results. This would be anticipated because the resulting displacements were still quite small, the maximum being -0.294 in. for the nonlinear dynamic bird impact simulation. This maximum displacement is almost 5 times that obtained for the Vulcan windshield panel but is still small in an absolute sense.

B-1A Windshield Panel

In 1976 an early design for the B-1A aircraft windshield panel was subjected to full scale bird impact testing.[34] The surface of this transparency is a portion of a right circular cylinder and has 5 edges. It measures about 54 in. long and 48 in. wide in surface coordinates. The windshield panels were mounted in a complete B-1A crew escape module for the bird impact tests which were conducted.

The design of the windshields tested was laminated having 5 plies with polycarbonate being used for the two structural plies and as-cast acrylic for the outer pace ply. Figure 21 illustrates the cross section.

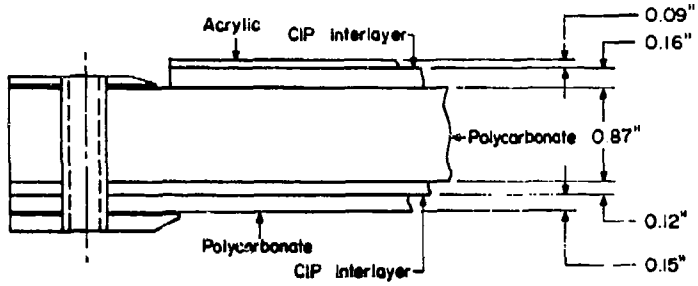

Figure 21. B-1A Windshield Cross Section

The B-1A windshield was impacted near the center with a 4 lb bird at 573 kt (Test Number BM006).[34] Deflection data was acquired from high speed film for the locations indicated in Figure 22. The deflections obtained were vertical in the aircraft coordinate system instead of normal to the surface. Static deflection was also obtained for a 2500 lb load applied normal to the surface at the bird impact target point.

The entire B-1A windshield panel was modelled for MAGNA analysis. Figure 23 illustrates the finite element model which was generated using the IJKGEN and PREP modules of the MAGNA preprocessor.[12] This path through the preprocessor required the development by the FDL of three standard MAGNA user-written subroutines (UINPUT, SURFAC, CRDTRN) to define coordinate transformations for the geometry of the structure. Even though they are not all distinguishable in Figure 23, each of the 5 plies was modelled with a layer of 54 solid elements. This resulted in a total of 270 elements and 1158 nodes, the largest solid element model used to date at WPAFB for nonlinear dynamic MAGNA analysis.

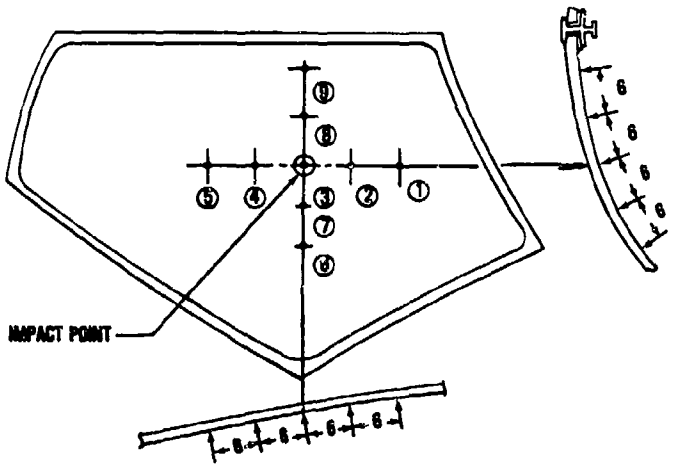

Figure 22. B-1A Windshield Deflection Measuring Points

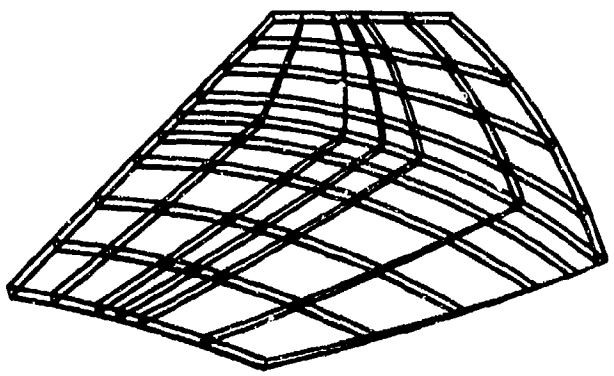

Figure 23. B-1A Windshield MAGNA Finite Element Model

The mesh was designed to be finest near the site of bird impact, and for the reasons discussed in the Scope section no support structure was included in the model. The boundary conditions prescribed were pinned joints all around the inner edge of the panel resulting in 3294 unconstrained degrees of freedom. Table 5 shows the room temperature material properties which were used.

Table 5

Material Properties for B-1A Windshield Panel

Ply	Material	Young's Modulus (psi)	Poisson's Ratio	Yield Stress (psi)	Density ($lb\ sec^2/in^4$)
Outer Face Ply	As-Cast Acrylic	450,000	0.35	10,096	1.11×10^{-4}
Interlayer	Swedlow SS-5272Y(HT)	165	0.45	580	0.96×10^{-4}
Main Ply & Inner Face Ply	Polycarbonate	324,000	0.38	9392	1.11×10^{-4}

The first B-1A MAGNA run conducted was a free vibration analysis to determine the first (or lowest) mode of the structure. The job was run at 350,000 octal words and took 431 CP sec. The frequency calculated was 86 Hz which agrees very well with the bird impact deflection data. Figure 24 shows deflection versus time data for point 3 (see Figure 22) which indicates a period of 12 msec for the initial response of the panel. This corresponds to a frequency of 83 Hz. The period of the bird impact event was on the order of 2 msec. Figure 25 shows the first mode shape obtained.

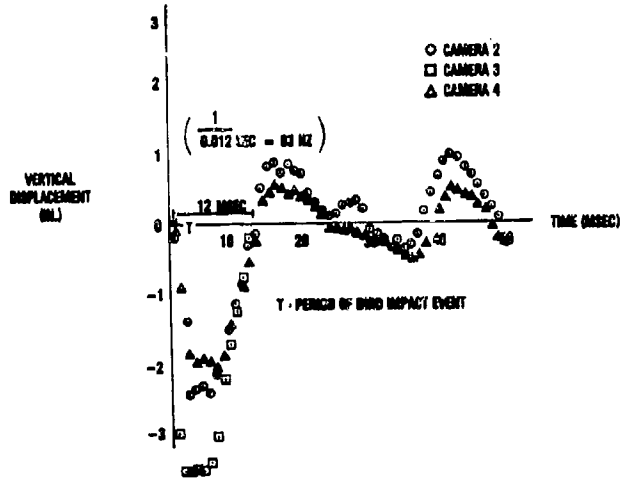

Figure 24. Deflection vs Time Data for Point 3

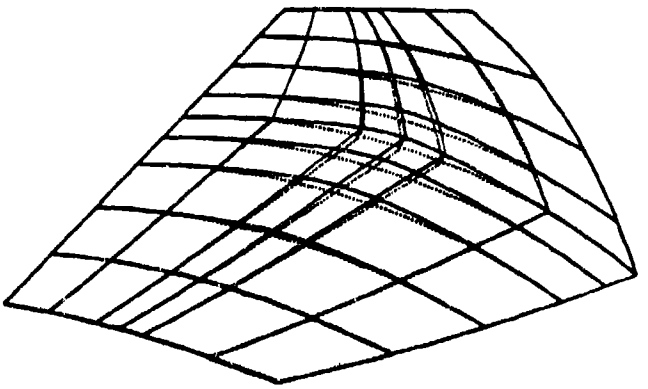

Figure 25. MAGNA First Mode for B-1A Windshield

The frequency of 86 Hz is considerably less than that obtained for the 36 in. x 36 in. glass panel (245 Hz) due primarily to the lower stiffness of the plastic materials used in the B-1A windshield. Given the same model size and the same analysis parameters, this means that bird impact simulation of plastic transparencies will in general be less expensive than that for glass transparencies.

The second MAGNA analysis conducted for the B-1A windshield was a nonlinear static one. It was known beforehand that the static response would be significantly nonlinear because the design was curved like the 36 in. x 36 in. glass panel, and the materials were plastic which would only result in greater deflections and hence stronger geometric nonlinearity. Following this line of reasoning, the time required to conduct a linear static analysis was not taken.

For the nonlinear static analysis, a 2500 lb concentrated load was applied normal to the windshield surface at the bird impact target point. The analysis included the effects of both geometric and material nonlinearity. Both the as-cast acrylic and interlayer materials were treated as behaving linearly, however, with only the two polycarbonate plies being treated as materially nonlinear. Figure 26 illustrates the polycarbonate behavior which was assumed. The polycarbonate data listed in Table 5 also pertains to the nonlinear static analysis. Load was applied in steps of 1250 lb.

This job was run at 350,000 octal words and required 1800 CP sec to reach the 2500 lb load level in 2 solution increments. At the 2500 lb load level, the normal displacement at the point of load application was -0.385 in. This was roughly the same value as that calculated for the 36 in. x 36 in. panel but at only 1/10 the applied load. This computed displacement agreed almost exactly with that measure during full scale test, -0.380 in.[33]

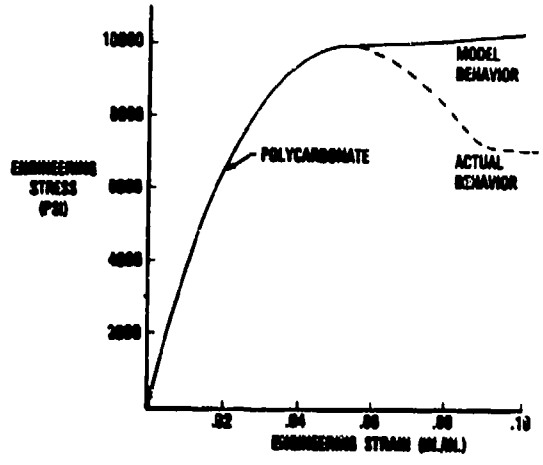

Figure 26. Polycarbonate Stress-Strain Behavior

The last B-1A MAGNA analysis conducted was a bird impact simulation. This was a nonlinear dynamic analysis including both geometric and material nonlinearity. As for the nonlinear static analysis, both the as-cast acrylic and interlayer materials were treated as being linear while only the polycarbonate structural plies were treated as being materially nonlinear. Again, both Table 5 and Figure 26 together may be used to describe the behavior of the polycarbonate material which was assumed. Treating the as-cast acrylic face ply as being materially nonlinear for either the nonlinear static or nonlinear dynamic analyses (this was attempted in both cases) would have resulted in very large incremental plastic strains being calculated in the face ply and consequent solution failure. The impact of a 4 lb bird at 573 kt was simulated.

Results of the bird impact test showed a shattered region for the as-cast acrylic face ply but no damage to either of the polycarbonate structural plies. Observed deflections were on the order of 2 to 3 in. Even though the deflections were this large, the FDL uncoupled definition of bird impact loading, which assumes rigid target behavior, was used. The thinking surrounding this decision was to do two simulations, one with uncoupled loads and a second with artificially coupled loads. In this manner the significance of load/response coupling for the B-1A windshield design could be determined by comparing results of the two analyses. As it turned out, the first simulation was never completed successfully so the second case was not run and the coupling determination could not be made.

The bird impact simulation was run at 350,000 octal words and used 5695 CP sec for 10 increments. At an average of about 570 CP sec per increment the cost was about the same as it had been for the 36 in. x 36 in. panel. Fewer time steps were required for the B-1A windshield though because of its considerably lower natural frequencies.

Technical problems brought the B-1A windshield simulation to a premature end however. Figure 27 shows that through-the-thickness compressive strain for the interlayer immediately beneath the as-cast acrylic face ply has greatly exceeded -100 percent. The figure shows an edge view of one stack of 5 elements through the thickness of the panel. Element numbers are 106 through 110 in ascending order beginning with the inner polycarbonate face ply. As can be seen from the figure, the order of elements 109 and 110 is reversed. This is due to the upper surface of (interlayer) element 109 passing completely through its lower surface, a physically impossible occurrence. This unrealistic behavior in the solution allows the as-cast acrylic face ply to penetrate or move through the main polycarbonate ply beneath it.

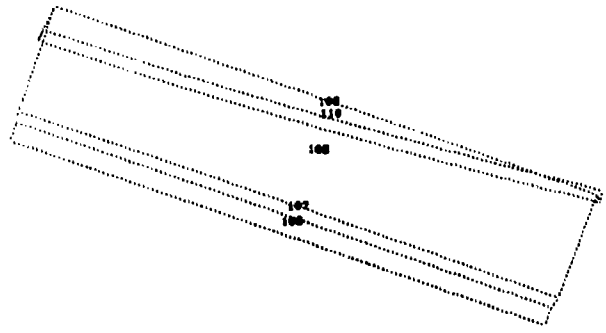

Figure 27. Face Ply Penetration of Main Ply Predicted at 0.000660 sec

The explanation for this bizarre result lies in the way the behavior of the interlayer material was described. First of all, the interlayer was assumed to behave linearly which means that strain is directly proportional to applied load. Secondly, the Young's Modulus for the interlayer had a value less than the magnitude of the bird impact pressure being applied at the outer surface of the windshield panel (165 psi vs -367 psi). For example, in a one-dimensional static case, the interlayer would have to deform (-367/165) -222 percent through its own thickness in order to be able to transmit -367 psi to the next (main) ply beneath it in the laminate. This simplistic (linear) representation of interlayer behavior produced satisfactory results when the stiffness of the material was much higher as for the Vulcan and 36 in. x 36 in. windshield panels. For the case when linear interlayer stiffness is less than the applied impact pressures, something more is required in describing interlayer behavior.

The bird impact simulation for the B-1A windshield was rerun using a standard MAGNA user-written subroutine (NELAS3) to describe a bi-linear behavior for the interlayer material. This material model is illustrated in Figure 28 and provided greater stiffness in compression than in tension for the interlayer. It was hoped that this would prevent any interpenetration of adjoining structural plies during the solution. Data for the compression behavior of the interlayer material in question was provided by the transparency vendor involved in design and fabrication of the full scale parts.[35]

It was thought that the greater stiffness in compression provided by the bi-linear interlayer model would prevent the ply penetration problem from

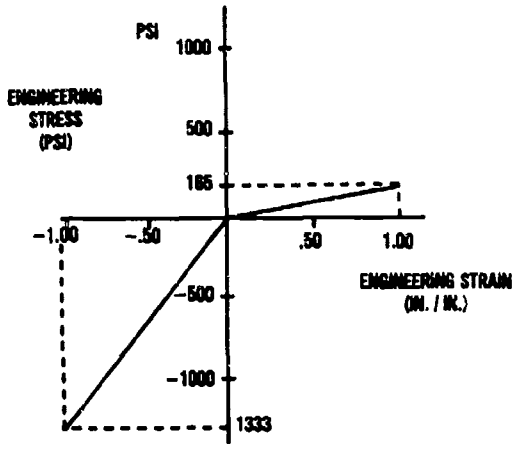

Figure 28. Bi-Linear Material Model for the B-1A Windshield Interlayer

occurring again. The second bird impact simulation was relatively successful in this respect because, at least for the number of solution increments performed, deep penetration of the face ply into the main ply did not occur.

Some problems still did occur, however. Figure 29 shows that at later times than those reached in the first attempt, some very large tensile strains are predicted in the same interlayer. In this figure, the solid lines

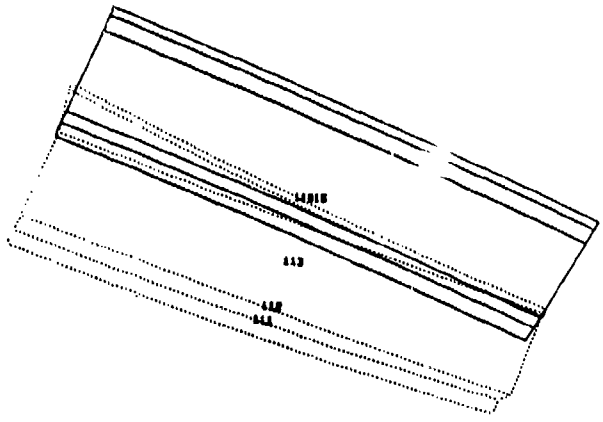

Figure 29. Windshield Deformation Predicted at 0.001430 sec

represent the undeformed geometry of a stack of 5 elements taken through the thickness of the panel as seen from an edge. The dotted lines represent the deformed geometry of the same. The left hand side indicates very large

tensile strains through the thickness of the outermost interlayer. The right hand side of the figure indicates a slight degree of face ply penetration into the main ply. Neither of these aspects of the results are physically realistic. In addition, the large incremental strains being predicted for the interlayer made obtaining convergence in the solution difficult so the analysis was suspended at 0.001430 sec, about 10 percent of the way through the primary response (Figure 24).

Possible solutions to the analysis problems which were encountered for the B-1A windshield were identified for further study. These included more realistic means for characterizing the behavior of very soft interlayer materials, and the use of the new MAGNA layered shell element which would simply circumvent the problem of calculating interlayer deformation directly.[11] Progress made on both these alternatives will be reported at a later date.

Up to the time at which the analysis was suspended, the results of the B-1A windshield bird impact simulation looked realistic. Figure 30 shows MAGNA results for deflection versus time compared to experimental data at point 3 (Figure 22). For the short period of time covered by the simulation, all looks well. It is believed that for realistic simulation at later times, an artificially coupled definition of loads would have been required because of the magnitude of the deflections involved (2-3 in.).

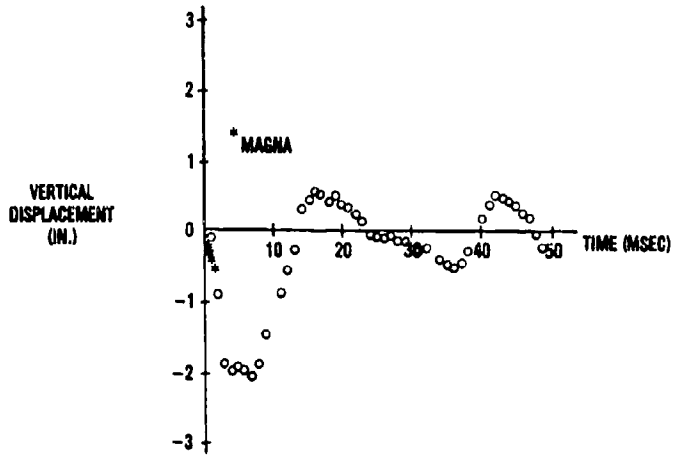

Figure 30. B-1A Windshield Deflection vs Time Correlation at Point 3

F-16A 1/2 in. Polycarbonate Canopy

One of the early designs for the canopy of the F-16A aircraft was a monolithic polycarbonate part with a nominal thickness of 1/2 in. An uncoated canopy of this design was one of several F-16A canopies subjected to bird impact testing in 1977.[36] Data acquired during testing included high speed film from which deflection data for the outer surface of the transparency was obtained. At an impact target point located on the canopy centerline at fuselage station 112.5, the uncoated canopy failed for 4 lb bird impact at 362

kt but survived a 340 kt impact with the same size bird. Deflections observed were on the order of 10.0 in., indicating a severely nonlinear structural response.

Only the left half of the canopy was modelled for MAGNA analysis due to symmetry of both the structure and bird impact loads. Because this work was accomplished before the MAGNA preprocessor had been developed, the canopy finite element model was generated using other more tedious means. Figure 31 illustrates the model which had 50 solid elements with a total of 428 nodes. The finite element grid is very coarse; the model is about as small as possible for obtaining realistic deflection results for such a highly nonlinear problem.

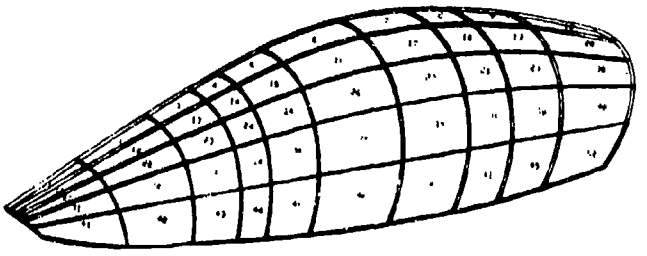

Figure 31. Coarse MAGNA Model for F-16A Canopy

A nonuniform distribution of thickness over the surface of the canopy was included in the model, the thickness data having been obtained from measurements taken on full scale parts. This feature of the model was taken to be important because of the sensitivity of bending stiffness to thickness. Bending stiffness is proportional to the third power of the thickness, so 20 percent thinning reduces local bending stiffness by 50 percent.

For the reasons discussed in the Scope section, no support structure was included in the model. Boundary conditions which were applied prevented lateral motion along the centerline and pinned all the nodes around the inner edge on the remaining three sides. The number of unconstrained degrees of freedom resulting was 1110. A bilinear representation was assumed for the behavior of the polycarbonate material as illustrated by Figure 32.

Since a free vibration analysis and both linear and nonlinear static analyses had already been conducted by others, none were accomplished by the FDL.[11] Instead, the first MAGNA analysis performed was a nonlinear dynamic bird impact simulation. The effects of both geometric and material nonlinearity were taken into account.

The simulation was for a 4 lb bird impact at 350 kt. Test results at these same conditions resulted in very large displacements in the canopy - 8.6 in. maximum. A deep pocket was formed in the canopy which grew in size and depth and traveled slowly aft over the crown area.

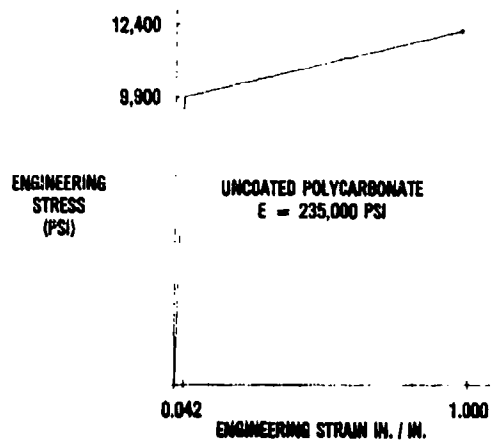

Figure 32. Stress-Strain Behavior for Polycarbonate Material

The FDL developed uncoupled definition of loads was used even though it was clearly invalid for this case because of the very large displacements involved. The thinking was to follow an uncoupled loads analysis with an artificially coupled case to define the significance of load/response coupling for the F-16A 1/2 in. uncoated polycarbonate canopy.

The bird impact analysis was run at only 156,000 octal words and required 2171 CP sec for 25 increments or about 85 CP sec per increment. This is more than 7 times less CP time per increment than that required for either the 36 in. x 36 in. panel or the B-1A windshield. This reduction in cost was due both to the lower frequency associated with the first mode of free vibration (55 Hz) and to the smaller number of elements made possible by the monolithic design of the transparency.

Figure 33 illustrates the very poor correlation with data which was obtained for this simulation. Relatively large displacements were predicted by MAGNA but the time history of the computed deformation was not realistic. At early times the MAGNA deflections were too high. Then at 10.4 msec, when the large pocket formed in the canopy was observed to grow still larger and move aft over the canopy surface, the deformation predicted by MAGNA was rapidly growing smaller and had not moved at all.

The simulation was rerun, this time using the artificially coupled definition of bird impact loading. As discussed at length in the Bird Impact Loads Definition section, this procedure requires some data from full scale bird impact testing and as a result cannot be used in the design of a new untested transparency system.

The artificially coupled simulation was also run at 156,000 octal words but for 44 increments. The computed deformation which resulted showed dramatic improvement over the uncoupled results when compared to the test data. Figure 34 shows that with artificial coupling of the loads the history

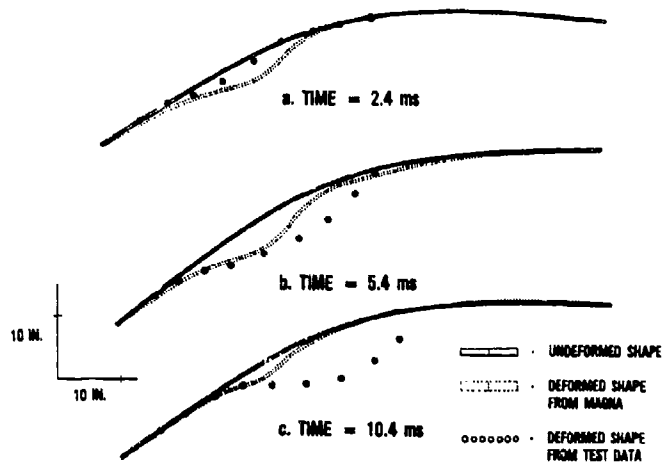

Figure 33. Deflection Correlation for Uncoupled Bird Impact Simulation

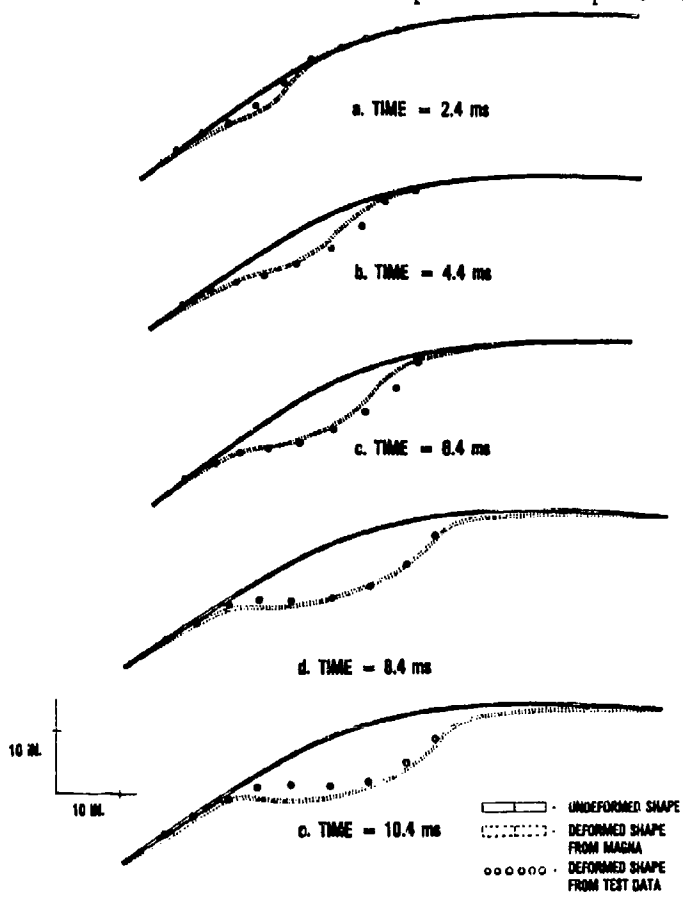

Figure 34. Deflection Correlation for Artificially Coupled Bird Impact Simulation

of the formation of the deep pocket in the canopy is quite faithfully reproduced. These results have been reported earlier in more detail but have been repeated here to emphasize again the overwhelming significance of coupling between bird impact loads and dynamic structural response in some cases.[16] For the F-16A 1/2 in. monolithic uncoated polycarbonate canopy, not taking into account the effects of load/response coupling results in completely unrealistic computed behavior (Figure 33). The more flexible the transparency structure, the more significant the load/response coupling.

These results demonstrate that MAGNA is capable of handling the most severe geometric nonlinearity resulting for the transparency bird impact problem, even when a very coarse finite element mesh is used. At the same time, however, a new problem area has been defined. As discussed in the Background section, MAGNA clearly cannot be used to design new transparencies which are as flexible as this F-16A canopy design because before full scale test results are available, the bird impact loads cannot be defined for use in MAGNA simulations. These circumstances defeat the use of MAGNA as an accurate design tool for relatively flexible transparencies. What is needed to solve this problem is an implicit scheme to calculate coupled bird impact loads during the finite element solution itself. At the time of this writing, some progress has been made in calculating coupled loads ; details of this development cannot be included here but are documented elsewhere.[17]

Having demonstrated satisfactory correlation with experimental deflection vs time data for the F-16A canopy, an attempt was also made to calculate realistic stresses for the same problem. Only the left half of the canopy was modelled as before, but this time with a finer mesh to obtain more realistic stress results. No stress (strain gage) data was available for these tests but it was known that the canopy failed at about 350 kt for 4 lb bird impact on the centerline at fuselage station 112.5. It was planned then to simulate a 350 kt test again and this time look for some indication of material rupture in the computed stress results.

To accomplish this goal another nonlinear dynamic simulation was conducted with both geometric and material nonlinearity. Figure 35 shows the model which was generated. It contains 189 solid elements and 1256 nodes

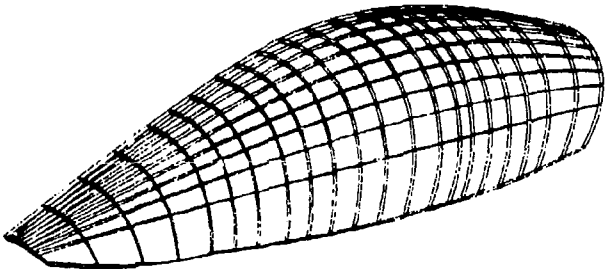

Figure 35. Fine MAGNA Model for F-16A Canopy

- a moderately sized model for nonlinear MAGNA analysis. The same non-uniform distribution of thickness and the same type of boundary conditions were used as for the coarser F-16 model. The number of unconstrained degrees of freedom resulting was 3447.

A more refined definition of the polycarbonate behavior (same as that used for the B-1A windshield) than that used for the coarse model was adopted to get the best possible stress results from MAGNA. The artificially coupled definition of bird impact loads was used again. The job was run at 245,000 octal words and required 13,000 CP sec for 100 increments. The average of 130 CP sec per increment was still far less than that required for any of the nonlinear dynamic analyses conducted with laminated transparency designs.

As for the coarse model analysis, the history of deformation predicted by MAGNA again appeared to be very realistic. The maximum deformation computed was in excess of 8 in. Figure 36 shows the deformed geometry of the canopy predicted by MAGNA at 9 msec. The contour lines appearing on the surface represent particular magnitudes of deflection. Figure 37 shows a photograph of the actual canopy at the same time. From these two figures it can be seen that the overall appearance of the computed deformation compares well with the experimentally observed deformation.

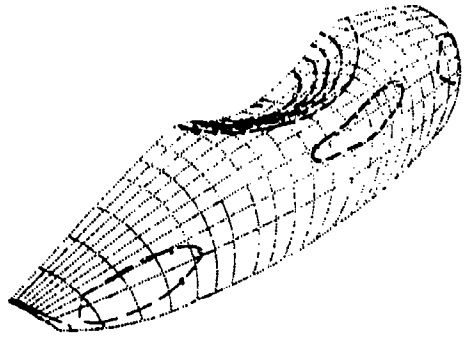

Figure 36. MAGNA F-16A Canopy Deformation at 9 msec

Figure 38 is a relief map of equivalent stress for the canopy at the same time during the solution shown in Figures 36 and 37 - 9 msec. The dotted mesh in the figure represents the undeformed geometry of the canopy, and distance between the dotted and the solid meshes represents the magnitude of equivalent stress computed at a given point on the surface of the canopy. The maximum values of stress shown in the figure are 5 percent above the yield stress for polycarbonate and occur mainly around the rim of the deep pocket where the bending stresses are highest.

As the deep pocket moved aft over the canopy, the MAGNA simulation showed that the deformation began to grow smaller, at first slowly and then much more

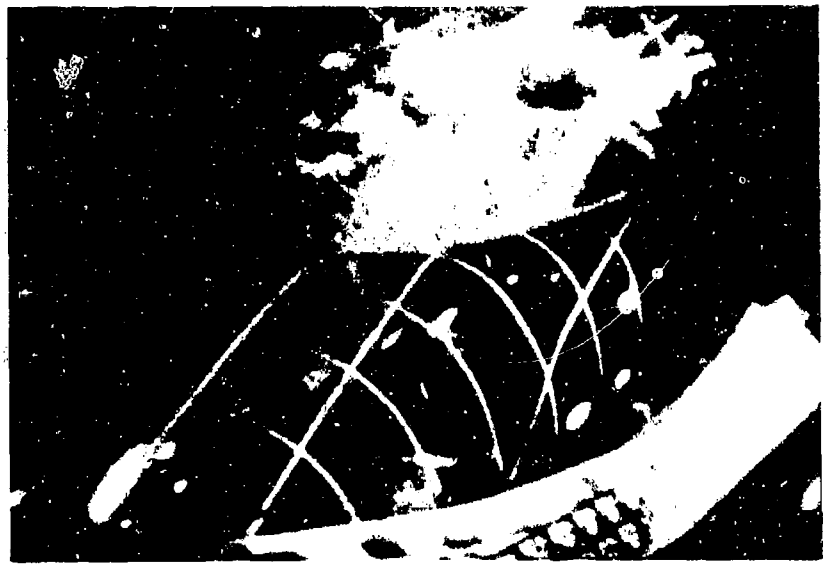

Figure 37. Experimental F-16A Canopy Deformation at 9 msec

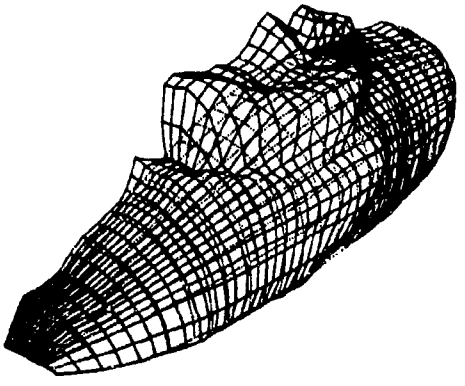

Figure 38. MAGNA F-16A Canopy Equivalent Stress at 9 msec

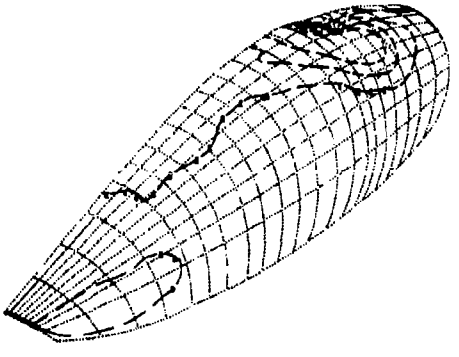

Figure 39. MAGNA F-16A Canopy Deformation at 17.2 msec

rapidly. Figure 39 shows that at 17.2 msec MAGNA predicted the presence of only a very small inward dent. This same behavior was observed in high speed films of the test. At the same time, Figure 40 shows that the equivalent stress computed by MAGNA was essentially zero everywhere on the canopy. This was a very puzzling and disappointing result because it was known that canopy rupture began near fuselage station 140 at about 18 msec after initial bird contact. The small inward dent predicted by MAGNA at 17.2 msec also was at fuselage station 140 but the stress relief map at the same time showed that no stress of any significance was predicted anywhere on the canopy.

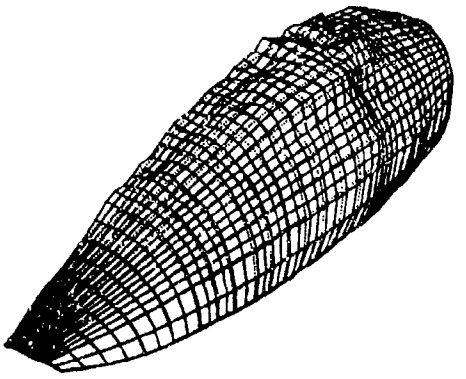

Figure 40. MAGNA F-16A Canopy Equivalent Stress at 17.2 msec

The next few increments of the MAGNA solution painted a much different picture, however, and illustrated in a graphic manner what is believed to be the mechanism of failure for the F-16A polycarbonate canopy. At 17.2 msec the rate of deformation computed for the small inward dent in the canopy was very high and was directed outward. By 17.8 msec MAGNA showed that the inward dent had "snapped through" and became a slight outward bulge less than 1 in. high. Figure 41 illustrates this deformed geometry.

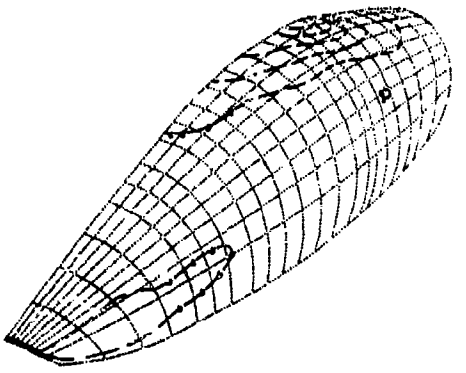

Figure 41. MAGNA F-16A Canopy Deformation at 17.8 msec

The most unexpected result was the very rapid stress rise corresponding to this "snap-through" behavior. Figure 42 shows that at 17.8 msec a stress peak on the order of the yield stress for the polycarbonate material has suddenly materialized. The magnitude of the peak stress doesn't appear quite as great as that shown in Figure 38 only because both figures present a perspective view in which line lengths are drawn shorter as they move farther from the eye.

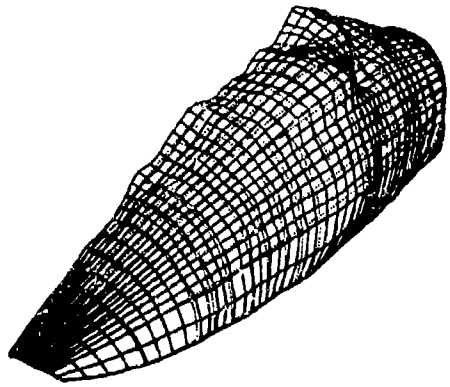

Figure 42. MAGNA F-16A Canopy Equivalent Stress at 17.8 msec

In summary, then, MAGNA bird impact simulation predicts a very rapid stress rise up to a value near the yield stress at the same time (17.8 msec) and at the same location on the canopy centerline (fuselage station 140) at which the initiation of rupture was observed during full scale testing. MAGNA illustrates an unusual phenomenon which is believed to be the mechanism for rupture: a very sharp stress spike resulting from a "snap-through" type of instability occurring during the dynamic response to bird impact. This implies that the stress history predicted by MAGNA is realistic even though no direct correlation can be made. These results have been reported in more detail elsewhere but have been summarized here briefly for completeness.[37]

Hot Soda Lime Glass Bar

One point should be clarified before discussing this heated glass bar analysis. MAGNA does not have the capability to do heat transfer analysis; i.e., it cannot be used to calculate spatial and temporal distributions of temperature as a result of convection, conduction, or radiation. What it can do is calculate material strains and stresses resulting from incremental temperatures. Given a temperature change at a node in a finite element model (at a particular time if the solution is transient) MAGNA treats the temperature change as a thermal load and computes resulting strains and stresses.

In this way, MAGNA is intended for use in accounting for the effects of heating or cooling in aircraft transparency system structures. Before attempting a transparency analysis application, however, it was planned to conduct a limited test of this MAGNA thermal loads capability.

The test selected was a one-dimensional textbook problem involving a right circular cylinder of fully annealed soda lime glass.[38] Figure 43 shows that the bar was mounted between two rigid frictionless walls.

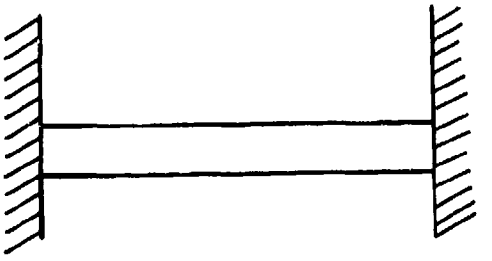

Figure 43. Heated Glass Bar Problem

For linearly elastic materials such as glass, heating the bar shown in Figure 43 will result in the longitudinal compressive stress defined by Equation 7. It was intended to generate a MAGNA finite element model of the

$$\sigma = E \alpha \Delta T \qquad (7)$$

E - Young's Modulus (psi)

α - Coefficient of thermal expansion (in./in. deg F)

ΔT - Temperature Change (deg F)

σ - Thermal Stress (psi)

glass bar, apply a uniform temperature increase, and compute the resulting stress for comparison with Equation 7.

Only half the bar was modelled due to symmetry; one quarter of the bar could have been modelled just as easily but was not. The bar had a 1 in. radius and a 10 in. length. Ten solid finite elements were used as shown in Figure 44; 82 nodes were defined. Boundary conditions prevented motion normal to the plane of symmetry and motion normal to both ends. In addition, the node at the center of each end was fixed to take out all translational rigid body modes. The number of unconstrained degrees of freedom resulting was 136.

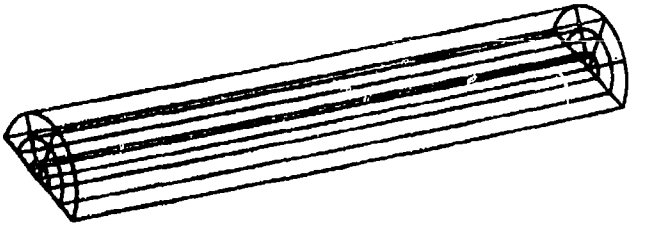

Figure 44. MAGNA Glass Bar Model

The material properties used for the annealed soda lime glass were: Young's Modulus - 10,500,000 psi, Poisson's Ratio - 0.22, density - 0.0002349 lb sec^2/in.^{4} The temperature change prescribed was +325 deg F, and the value of the coefficient of thermal expansion was taken to be 0.00000472 in./in. deg F.

A linear static analysis was run at 165,000 octal words and required 42 CP sec. Figure 45 shows the very uniform distribution of axial stress which was predicted over the end of the bar by MAGNA. The coarse mesh illustrates the end of the bar; the fine mesh represents the distribution of stress over the end of the bar; the distance between the two meshes represents the local magnitude of equivalent stress.

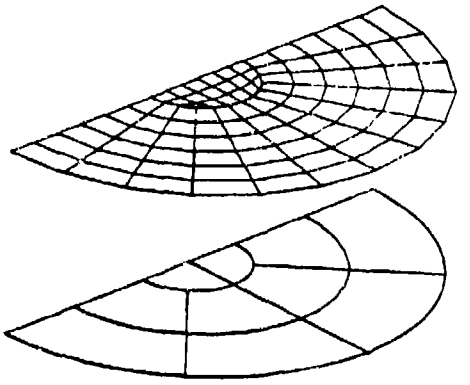

Figure 45. Equivalent Stress Relief Map for Heated Glass Bar

The value of stress predicted by MAGNA was -16,107 psi which is identically equal to the value defined by Equation 7. This simple exercise demonstrated the validity of thermal loads calculations performed by MAGNA.

Conclusions

The following can be concluded from results of the studies described above:

1. Both the (post-test) analysis of bird impact test results and the design of new transparencies using MAGNA are valid for any monolithic glass aircraft transparency design.

2. Both the (post-test) analysis of bird impact test results and the design of new transparencies using MAGNA are valid for any laminated glass aircraft transparency design if the stiffness of the interlayer material involved is not too low. When Young's Modulus for the interlayer material is not greater than the bird impact pressure being applied in the analysis, numerical problems will result when using a layer of solid finite elements to

represent the interlayer. Solution to this problem may come if the new MAGNA laminated shell element can be validated, or if a new method of characterizing soft interlayer materials is developed.[11]

3. An uncoupled (rigid target) definition of bird impact loading has been developed by the FDL which is sufficient to permit the (post-test) analysis of bird impact test results or the design of new transparencies for any glass aircraft transparency design for which MAGNA analysis is valid (see 1 and 2).[18]

4. The (post-test) analysis of bird impact test results using MAGNA is valid for any monolithic plastic aircraft transparency design.

5. The (post-test) analysis of bird impact test results using MAGNA is valid for any laminated plastic aircraft transparency design if the stiffness of the interlayer material involved is not too low. When Young's Modulus for the interlayer material is not greater than the bird impact pressure being applied in the analysis, numerical problems will result when using a layer of solid finite elements to represent the interlayer. Solution to this problem may come if the new MAGNA laminated shell element can be validated, or if a new method of characterizing soft interlayer materials is developed.[11]

6. An artificially coupled (flexible target) definition of bird impact loading has been developed by the FDL which is sufficient to permit the (post-test) analysis of bird impact test results for any plastic aircraft transparency design for which MAGNA analysis is valid (see 4 and 5).[18] This definition of bird impact loading requires some data to be obtained from previous full scale bird impact testing of the transparency involved.

7. The design of new monolithic plastic aircraft transparencies using MAGNA is valid if the maximum displacements resulting from the bird impact are not too great (less than 3 in.).

8. The design of new laminated plastic aircraft transparencies using MAGNA is valid if the maximum displacements resulting from the bird impact are not too great (less than 3 in.) and if the stiffness of the interlayer material involved is not too low. When Young's Modulus for the interlayer material is not greater than the bird impact pressure being applied in the analysis, numerical problems will result when using a layer of solid finite elements to represent the interlayer. Solution to this problem may come if the new MAGNA laminated shell element can be validated, or if a new method of characterizing soft interlayer materials is developed.[11]

9. Although not discussed in this paper, a rudimentary coupled definition of bird impact loading has been developed by the FDL which is sufficient to permit the design of new plastic aircraft transparencies for which MAGNA analysis is valid (see 7 and 8).[17] This definition of bird impact loading requires the use of two standard MAGNA user-written subroutines, ULOAD and UPRESS.

10. If the development (now in progress per the Approach section) for a fully coupled loads/response capability with MAGNA is successfully

accomplished, the design of even the most flexible plastic transparencies may become possible.

11. Other analysis parameters being the same, bird impact simulation for a glass transparency costs more than for a plastic one because the maximum time step size permitted is smaller.

12. The only type of aircraft transparency system for which linear transient bird impact simulation is valid is a flat glass design, either monolithic or laminated. All other types require geometrically nonlinear analysis; some require in addition materially nonlinear analysis. Of the three, the linear transient analysis is very much less expensive to conduct.

13. When using solid finite elements, the analysis of laminated designs becomes much more expensive than that of monolithic designs.

14. Bird impact loads/response coupling is insignificant for all glass transparencies and significant for all plastic transparencies analyzed to date.

15. The thermal loads capability provided in MAGNA has been validated.

16. MAGNA is capable of accomplishing a great variety of structural analysis applications in addition to aircraft transparency bird impact response. A number of such applications have already been accomplished or are currently in progress. Table 6 lists some of these to illustrate the breadth of use possible.

Table 6

Current MAGNA Structural Analysis Applications

Application	In-Progress	Complete	Reference
Aircraft Wing Spar Bird Impact		X	39
F-16 Acrylic Canopy Evaluation		X	37
T-38 Through-the-Canopy Escape Study		X	40
T-38 Canopy Cockpit Pressure/Thermal Loads Response		X	41
TF-15 Canopy Bird Impact		X	17
T-38 Student Windshield Bird Impact	X		
F-5E and F-20 Canopy Bird Impact	X		
Residual Strength of Battle Damaged Wings	X		
Composite Shelter Design	X		
O-Ring Response to Hydraulic Fluid Pressure		X	11
F/RF-4 Improved Transparency Design	X		42
Viggen Windshield Bird Impact		X	43
Nuclear Blast Response	X	X	18
Learjet Improved Windshield Design	X		
Vibration of Bladed Discs	X		

Table 6 (Continued)

Application	In-Progress	Complete	Reference
Fan Blade Bird Impact	X		
Radome Bird Impact	X		
T-38 Canopy Aerodynamic Pressure Loading	X		
F-16 Laminated Canopy/ HUD Contact During Bird Impact	X		

References

1. P. H. Denke and G. R. Eide, Aircraft Transparent Enclosure Bird Impact Math Model, 1978 Conference on Aerospace Transparent Materials and Enclosures, Air Force Materials Laboratory, Wright-Patterson Air Force Base, Ohio 45433.

2. P. H. Denke, Aircraft Windshield Bird Impact Model, Part 1 Theory and Application, Air Force Flight Dynamics Laboratory, Wright-Patterson Air Force Base, Ohio 45433, AFFDL-TR-77-99, Part 1, December 1977.

3. G. R. Eide, Aircraft Windshield Bird Impact Math Model - Part 2 - User's Manual, Air Force Flight Dynamics Laboratory, Wright-Patterson Air Force Base, Ohio 45433, AFFDL-TR-77-99, Part 2, December 1977.

4. R. C. Morris, Aircraft Windshield Bird Impact Math Model, Part 3: Programming Manual, Air Force Flight Dynamics Laboratory, Wright-Patterson Air Force Base, Ohio 45433, AFFDL-TR-77-99, Part 3, December 1977.

5. R. E. McCarty, Evaluation of the IMPACT Computer Program as a Linear Design Tool for Bird-Resistant Aircraft Transparencies, Air Force Flight Dynamics Laboratory, Wright-Patterson Air Force Base, Ohio 45433, AFFDL-TR-79-3103, March 1980.

6. R. E. McCarty, "Computer Analysis of Bird Resistant Aircraft Transparencies," Proceedings of the 17th Annual SAFE Symposium, December 1979, Las Vegas, Nevada.

7. R. A. Brockman, MAGNA: A Finite Element Program for the Materially and Geometrically Nonlinear Analysis of Three Dimensional Structures Subjected to Static and Transient Loading, University of Dayton Research Institute, Dayton, Ohio 45469, UDR-TR-79-45, November 1979.

8. B. S. West, "The Role of Finite Element Analysis in the Design of Birdstrike Resistant Transparencies," Conference on Aerospace Transparencies Sponsored by the Society of British Aerospace Companies, September 1980, London, England.

9. R. J. Speelman, R. H. Walker, and R. L. Peterson, "Windshield System Structural Enhancement," Conference on Aerospace Transparencies Sponsored by the Society of British Aerospace Companies, September 1980, London, England.

10. R. E. McCarty, "Aircraft Transparency Bird Impact Analysis Using the MAGNA Computer Program," Conference on Aerospace Transparencies Sponsored by the Society of British Aerospace Companies, September 1980, London, England.

11. R. A. Brockman, MAGNA (Materially and Geometrically Nonlinear Analysis) Part I - Finite Element Analysis Manual, Flight Dynamics Laboratory, Wright-Patterson Air Force Base, Ohio 45433, AFWAL-TR-82-3098 Part I, December 1982.

12. T. S. Bruner, MAGNA (Materially and Geometrically Nonlinear Analysis) Part II - Preprocessor Manual, Flight Dynamics Laboratory, Wright-Patterson Air Force Base, Ohio 45433, AFWAL-TR-82-3098 Part II, December 1982.

13. R. A. Brockman, MAGNA (Materially and Geometrically Nonlinear Analysis) Part III - Postprocessor Manual, Flight Dynamics Laboratory, Wright-Patterson Air Force Base, Ohio 45433, AFWAL-TR-82-3098 Part III, December 1982.

14. R. A. Brockman, MAGNA (Materially and Geometrically Nonlinear Analysis) Part IV - Quick Reference Manual, Flight Dynamics Laboratory, Wright-Patterson Air Force Base, Ohio 45433, AFWAL-TR-82-3098 Part IV, December 1982.

15. B. S. West and R. A. Brockman, Evaluation of Bird Load Models for Dynamic Analysis of Aircraft Transparencies, Flight Dynamics Laboratory, Wright-Patterson Air Force Base, Ohio 45433, AFWAL-TR-80-3092, August 1980.

16. R. A. Brockman, "Current Problems and Progress in Transparency Impact Analysis," 14th Conference on Aerospace Transparent Materials and Enclosures Sponsored by the Air Force Wright Aeronautical Laboratories, July 1983, Scottsdale, Arizona.

17. R. E. McCarty, "MAGNA Computer Simulation of Bird Impact on the TF-15 Aircraft Canopy," 14th Conference on Aerospace Transparent Materials and Enclosures Sponsored by the Air Force Wright Aeronautical Laboratories, July 1983, Scottsdale, Arizona.

18. R. E. McCarty, Lt J. L. Hart and R. A. Smith, Nonlinear Finite Element Analysis of Aircraft Transparency Bird Impact Using the MAGNA Computer Program, Flight Dynamics Laboratory, Wright-Patterson Air Force Base, Ohio 45433, AFWAL-TR- , pending technical report.

19. R. A. Brockman, MAGNA (Materially and Geometrically Nonlinear Analysis) General Description and Summary of Capabilities, University of Dayton Research Institute, Dayton, Ohio 45469, UDR-TM-80-27, April 1981.

20. J. P. Barber and J. S. Wilbeck, Characterization of Bird Impacts on a Rigid Plate: Part I, Air Force Flight Dynamics Laboratory, Wright-Patterson Air Force Base, Ohio 45433, AFFDL-TR-75-5, January 1975.

21. R. L. Peterson and J. P. Barber, Bird Impact Forces in Aircraft Windshield Design, Air Force Flight Dynamics Laboratory, Wright-Patterson Air Force Base, Ohio 45433, AFFDL-TR-75-150, March 1976.

22. Y. M. Ito, G. E. Carpenter, and F. W. Perry, Bird Impact Loading Model for Aircraft Windshield Design, California Research and Technology, Inc, Woodland Hills, California 91364, CRT 3090-2, July 1977.

23. J. P. Barber, J. S. Wilbeck, and H. R. Taylor, Bird Impact Forces and Pressures on Rigid and Compliant Targets, Air Force Flight Dynamics Laboratory, Wright-Patterson Air Force Base, Ohio 45433, AFFDL-TR-77-60, May 1978.

24. J. S Wilbeck, Impact Behavior of Low Strength Projectiles, Air Force Materials Laboratory, Wright-Patterson Air Force Base, Ohio 45433, AFML-TR-77-134, July 1978.

25. A. Challita and J. P. Barber, The Scaling of Bird Impact Loads, Air Force Flight Dynamics Laboratory, Wright-Patterson Air Force Base, Ohio 45433, AFFDL-TR-79-3042, March 1979.

26. J. Y. Parker, Measurement of Impact Bird Pressure on a Flat Plate, Arnold Engineering Development Center, Arnold Air Force Station, Tennessee 37389, AEDC-TR-79-14.

27. J. B. R. Heath, R. W. Gould, and G. R. Cowper, Momentum Transfer in Bird Impacts, National Aeronautical Establishment, National Research Council, Ottawa, Canada, LTR-ST-1257, April 1981.

28. I. I. McNaughtan and D. A. Perfect, Bird Impact Tests of Vulcan Aircraft Windscreens, Royal Aircraft Establishment, United Kingdom, Technical Report No. 65148, July 1965.

29. P. H. Denke and J. B. Hoffman, The Determination of Deflection and Stress Distribution for a Laminated Transparent Beam, Air Force Flight Dynamics Laboratory, Wright-Patterson Air Force Base, Ohio 45433, AFFDL-TR-76-114, November 1976.

30. J. H. Lawrence, Jr, Guidelines for the Design of Aircraft Windshield/Canopy Systems, Flight Dynamics Laboratory, Wright-Patterson Air Force Base, Ohio 45433, AFWAL-TR-80-3003, February 1980.

31. M. J. Mott, "Experimental Investigation in the Bird Impact Resistance of Flat Windscreen Panels with Clamped Edges," The Proceedings of the Symposium on Optical Transparencies, Royal Aeronautical Society, June 1971.

32. E. J. Sanders, Results of Bird Impact Testing of Prototype B-1 Windshields and Supporting Structure Design, AEDC-DR-76-100, Arnold Engineering Development Center, Arnold Air Force Station, Tennessee 37389.

33. R. H. Magnusson, High Speed Bird Impact Testing of Aircraft Transparencies, Air Force Flight Dynamics Laboratory, Wright-Patterson Air Force Base, Ohio 45433, AFFDL-TR-77-98, February 1978.

34. E. J. Sanders, Results of Further Tests to Evaluate the Bird Impact Resistance of Windshields for the B-1 Aircraft, AEDC-DR-76-43, Arnold Engineering Development Center, Arnold Air Force Station, Tennessee 37389.

35. Personal Communication, 23 June 1982, D. Holdridge and P. Lundstrom, Swedlow, Inc, Garden Grove, California 92645.

36. R. M. Watt, AFFDL F-16 Canopy Bird Impact Test: Project Number V41S-18A; Volumes 1-7, Data Package, Von Karman Gas Dynamics Facility, Arnold Engineering Development Center, Tennessee 37389, 18 February-9 May 1977.

37. R. E. McCarty, "Finite Element Analysis of a Bird-Resistant Monolithic Stretched Acrylic Canopy Design for the F-16A Aircraft," AIAA Aircraft Systems and Technology Conference, August 1981, Dayton, Ohio, AIAA Paper No. 81-1640.

38. E. F. Bruhn, Analysis and Design of Flight Vehicle Structures, Tri-State Offset, Cincinnati, Ohio, 1965.

39. R. E. McCarty and V. Venkayya, Analysis of Bird Impact on Port Wing, Air Force Wright Aeronautical Laboratories, Wright-Patterson Air Force Base, Ohio 45433, Letter Report, 24 August 1979.

40. R. E. McCarty and R. A. Smith, "Finite Element Analysis of Through the Canopy Emergency Crew Escape from the T-38 Aircraft," AIAA/ASME/ASCE/AHS 23rd Structures, Structural Dynamics, and Materials Conference, May 1982, New Orleans, Louisana, AIAA Paper No. 82-0705-CP.

41. R. E. McCarty and R. A. Smith, "Simulation of T-38 Aircraft Student Canopy Response to Cockpit Pressure and Thermal Loads Using MAGNA," AIAA/ASME/ASCE/AHS 24th Structures, Structural Dynamics, and Materials Conference, May 1983, Lake Tahoe, Nevada, AIAA Paper No. 83-0942 CP.

42. G. J. Stenger and Lt R. Simmons, "Bird Impact Evaluation of F/RF-4 Transparency System," 14th Conference on Aerospace Transparent Materials and Enclosures Sponsored by the Air Force Wright Aeronautical Laboratories, July 1983, Scottsdale, Arizona.

43. L. A. Samuelson, F. Nilsson, and L. Sornas, "Theoretical Evaluation of the Structural Performance of Swedish Fighter Aircraft Windshields Subjected to Bird Impact," 14th Conference on Aerospace Transparent Materials and Enclosures Sponsored by the Air Force Wright Aeronautical Laboratories, July 1983, Scottsdale, Arizona.

AD-P003 230

MAGNA COMPUTER SIMULATION OF BIRD IMPACT ON THE TF-15 AIRCRAFT CANOPY

R. E. McCarty, Flight Dynamics Laboratory

MAGNA Computer Simulation of Bird Impact on the TF-15 Aircraft Canopy

R. E. McCarty
Flight Dynamics Laboratory
Air Force Wright Aeronautical Laboratories
Wright-Patterson AFB, Ohio

Abstract

The F-15E aircraft is one of two evolutionary aircraft types which are currently being evaluated by the USAF for future low level, high speed, attack and interdiction missions. It is a two-place aircraft and is proposed to utilize the windshield/canopy transparency system which has been in production for some years for the TF-15 aircraft. The canopy portion of this transparency system has a high lofted shape and offers considerably more presented frontal area than the canopy for one place models of the aircraft. As a result of the lofted shape of the TF-15 canopy and the mission of the aircraft, the hazard of transparency bird impact during flight operations is significant. Some proposals to increase the level of bird impact protection for the F-15E canopy have already been aired. The availability of an analysis method which could accurately predict the dynamic structural response of such proposed canopy designs to bird impact loading would be valuable in establishing the merits of each. If the MAGNA nonlinear finite element analysis program could be validated for F-15 transparency analysis it would have significant potential for saving time and costs in the development of improved F-15E transparencies. The goal of the work effort reported in this paper was to accomplish this validation of MAGNA. The approach taken was to simulate full scale bird impact tests which have been conducted on a TF-15 aircraft canopy part. MAGNA results are presented in the form of deformed geometry plots, maximum equivalent stress versus time plots, and maximum displacement versus time plots.

Introduction

Background

The F-15E is one of two evolutionary aircraft types being evaluated by the US Air Force for a low level, high speed mission. It is a two-place aircraft and the initial design for the canopy was the same as that for the TF-15 aircraft which has a highly lofted shape and presents considerable frontal area. Current one-place F-15 aircraft models use a canopy which has much less projected frontal area. Figure 1 compares the lofted shape of both one-place and two-place F-15 transparency systems.

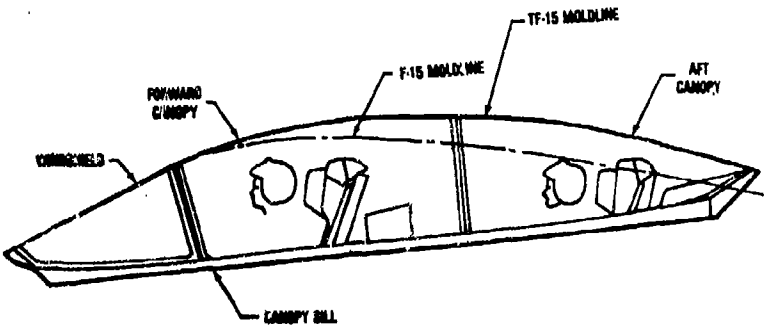

Figure 1. Profile of F/TF-15 Windshield and Canopy

As a result of the F-15E aircraft mission and the lofted shape of the TF-15 canopy, the bird impact hazard for this canopy design is high. Concern has existed for some time over the level of bird impact protection offered by the TF-15 canopy. Full scale bird impact tests which have been conducted indicate that for a 4 lb bird, only 160-180 kt protection is available.[1]

Some proposals have already been submitted[2] to improve the level of bird impact protection offered by the F-15E canopy. One of these involves a lower profile shape and another utilizes a thicker monolithic design. Analyses of the feasibility of each of these would be useful to establish their relative merit and their potential for future full scale engineering development.

A computer program which could be used for such F-15 aircraft transparency analysis has been developed by the Flight Dynamics Laboratory (FDL). It is called MAGNA (Materially and Geometrically Nonlinear Analysis) and has been designed[3-6] specifically for the analysis of aircraft transparency bird impact response. MAGNA is a complete nonlinear finite element analysis system which has already been applied[7-13] to a variety of aircraft transparency analysis problems.

MAGNA has been validated for several operational aircraft transparency systems. These include the British Vulcan bomber windshield, the B-1

aircraft windshield and the F-16A aircraft canopy.[7,9,10,13] The fact that MAGNA has been validated for these other aircraft transparency systems does not however, necessarily imply that its use is also valid for the F-15 aircraft. This is true because in general the aircraft transparency bird impact problem is a highly nonlinear one. Validation for one case does not necessarily imply validation for any other. Looking forward then to the possible application of MAGNA in the evaluation of alternate F-15E transparency designs, plans were laid to validate MAGNA for the current TF-15 canopy.

Approach

The approach taken was to simulate full scale bird impact tests conducted with TF-15 canopies.[1] During these tests the canopy survived the impact of a 4 lb bird on the center line near the forward arch at 160 kt. A subsequent test with the same size bird at the same impact location failed the canopy at 182 kt.

It was hoped that simulation of the 182 kt case would result in some indication of material fracture thus corresponding to the test results and thereby validating MAGNA for this application. This result would also mean that MAGNA was ready for use in future assessment of design alternatives for F-15E aircraft transparencies. This same approach of validating MAGNA first and then conducting follow-on system applications has been used before for the F-16A aircraft.[10]

Scope

The TF-15 canopy bird impact simulations planned with MAGNA involved two different types of analyses. The first type was a free vibration analysis intended to aid in debugging the finite element models generated as well as to select a time step size for subsequent dynamic analyses. These dynamic analyses, both linear and nonlinear, represented the second type of analysis planned and were intended to reproduce realistically the results of the full scale bird impact testing.

It was further planned to repeat this sequence of free vibration analysis and linear or nonlinear dynamic analysis for a variety of parameters related to the finite element solution. The idea behind this plan was to determine the sensitivity of the solution obtained to each one of these parameters and to define guidelines regarding each for use in other future (F-15) analyses. Hopefully in the process of accomplishing these parametric studies a recommended procedure for MAGNA TF-15 canopy bird impact simulation would be demonstrated which produces accurate results, thus validating MAGNA for future F-15 analysis.

The parameters included in these studies were nonuniform canopy thickness distribution, finite element model boundary conditions at the forward edge of the canopy, time step size for use in dynamic analysis, iteration in the nonlinear solution strategy, coupling between the bird impact loads and resulting dynamic structural response, bird impact velocity, and geometric nonlinearity inherent in the transparency structure. The question to be

answered in each case was: how important is it to address this parameter when performing MAGNA bird impact simulations? Before discussing details of the analyses which were conducted, a brief summary of the capabilities of MAGNA will be presented.

MAGNA Computer Program

The MAGNA nonlinear finite element analysis system was developed by the University of Dayton Research Institute, Dayton, Ohio and first became operational during the summer of 1978. The first edition of MAGNA for US Air Force aircraft transparency application was delivered in late 1979.

Capabilities

MAGNA was designed from the ground up for the analysis of large scale problems involving three-dimensional structures. It can account for the effects of both geometric nonlinearity (large displacements and rotations) and material nonlinearity (elastic-plastic behavior). The static, dynamic, or free vibration response of a structure can be analyzed using MAGNA. Special features such as contact analysis (e.g. bird/canopy contact, or canopy/heads-up-display contact), full restart capabilities, and convenient interactive graphics make it a powerful analysis tool which is easy to use. The interactive graphics are provided in two packages: the first, a preprocessor, enables rapid finite element modelling of transparency structures; the second, a postprocessor, permits quick visualization of the results of an analysis including structural deformation, stress, and strain. The capabilities of MAGNA are documented in more detail elsewhere.[3-6,14]

Availability

A Control Data Corporation (CDC) CYBER 750 version of MAGNA is operational at Wright-Patterson Air Force Base (WPAFB), Ohio. This installation includes the complete MAGNA package and permits free access for all US Government offices and contractors doing work for the US Government.

A CRAY-1 version of MAGNA is offered by United Information Services (UIS) through their commercial time sharing network. The CRAY installation includes only the analysis portion of the MAGNA system. The interactive graphics portions of the system are installed on UIS CDC equipment.

Other operational versions of MAGNA including VAX 11/780 and IBM editions are available through lease or purchase from the University of Dayton Research Institute, Dayton, Ohio.

The period of most intensive MAGNA development for aircraft transparency analysis sponsored by the US Air Force will most probably draw to a close at the end of 1983. A fully maintained operational installation of MAGNA is planned at WPAFB well into the future.

Structural Modelling

Geometry

The TF-15 aircraft transparency system involves the three components illustrated in Figure 1: windshield, forward canopy, and aft canopy. All three components are of monolithic stretched acrylic design. Definition of the geometry for the TF-15 aircraft transparencies exists in the form of a prime contractor drawing.[15] This drawing defines the shape of the outer moldline along the aircraft plane of symmetry - the "upper sheer line." It also defines transparency cross sections taken normal to the "upper sheer line" as being circular arcs. The radii of these circular cross sections are defined as a function of fuselage station measured along the "upper sheer line." The drawing also defines datum planes to locate the windshield arch and the canopy splice, and reference planes to locate forward and aft edges plus the sill. One unusual feature of the TF-15 transparency system is that a 0.18 ± .06 in. gap exists between the arch structures for the windshield and the forward canopy. When the canopy is closed this gap is filled with a rain seal and an inflatable pressure seal.

This definition of transparency geometry obtained from the drawing was incorporated into an FDL developed FORTRAN computer program. This computer program was used to generate the aircraft coordinates of points lying on the outer surface of the aircraft transparency system. The output of this computer program was in the format required as input for the MAGNA preprocessor, thus permitting rapid generation of TF-15 transparency finite element models.[4] Only slight modification of this computer program would be required to permit similar generation of finite element models for one-place F-15 or two-place F-15E alternate transparency designs.

The only information required in developing this FORTRAN computer program other than that obtained from the drawing was data on distribution of thickness over the transparencies. This information was provided to the FDL by the transparency vendor and included in the computer program.[16] Nonuniform thickness of the forward canopy only was taken into account since this component was the one actually impacted with a bird. Data from the vendor showed a nominal thickness of 0.335 in. and a minimum thickness in the area of bird impact of 0.302 in. (10 percent thinning).

The FORTRAN computer program was then used to prepare data for input to the MAGNA preprocessor for the complete TF-15 transparency system: windshield of uniform 0.90 in. thickness, forward canopy of nominal 0.335 in. thickness with 10 percent thinning, and an aft canopy of uniform 0.335 in. thickness. A gap of 0.18 in. was defined between adjoining edges of the windshield and forward canopy. The windshield was included in the model for visual effects only; it played no role in the analyses conducted because all the nodes in the windshield portion of the model were fixed.

Discretization

The coordinate data prepared by the FORTRAN computer program was input to the MAGNA preprocessor.[4] Since both the structure and the loads

exhibited symmetry, only the left half of the transparency system was modelled to reduce the computer resources required.

The CORGEN module of the MAGNA preprocessor was used first to generate a coarse two-dimensional grid representing the transparency system.[4] Next, the EXPAND module was used to generate a coarse three-dimensional grid.[4] This module of the preprocessor expands the two-dimensional grid in the thickness direction to obtain a three-dimensional grid.[4] Next the PREP module was used to refine the coarse mesh obtained.[4]

Figure 2 shows that the final mesh for the canopy (fore and aft components combined) was 8 by 18 elements and for the windshield was 8 by 4 elements. The total number of elements resulting was 176 - all 16 node solid type with 1212 nodes being defined. The finest region of the mesh was in the area of bird impact, on the canopy centerline near the windshield arch.

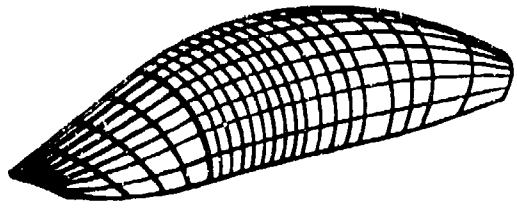

Figure 2. MAGNA Finite Element Model of TF-15 Transparency System

Time was not available during these studies to include the forward canopy arch structure itself in the finite element model. It was felt however that the canopy bird impact dynamic structural response would surely depend to some extent upon the structural characteristics of the forward canopy arch. It was decided to establish the limits of the effects of canopy arch behavior by studying the effects of a range of finite element model boundary conditions at the forward edge of the forward canopy. These boundary conditions ranged from completely fixed to completely free.

In all, four sets of boundary conditions were defined. In each case all nodes in the windshield portion of the model were fixed, and all nodes along the canopy centerline were prevented from moving laterally to account for the condition of symmetry there as shown in Figure 3. The first set of boundary conditions treated the forward canopy edge, the sill, and the aft canopy edge, as being completely fixed, or clamped as shown in Figure 4. The second set allowed rotation of the forward canopy edge, the sill, and the aft canopy edge, about the inner corner, a pinned boundary condition as shown in Figure 5. The third boundary condition permitted fore-and-aft sliding in the plane of the canopy surface at the forward canopy edge as well as rotation about its inner corner as shown in Figure 6. Canopy sill and aft edge boundary conditions remained pinned. The fourth boundary

condition permitted any motion of the forward canopy edge as shown in Figure 7, and also retained the pinned boundary conditions at the canopy sill and aft edge.

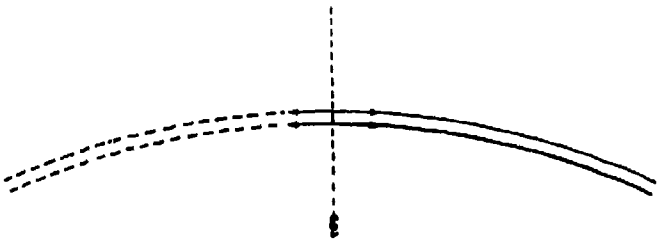

Figure 3. View from Front of Arch, Constrained Motion

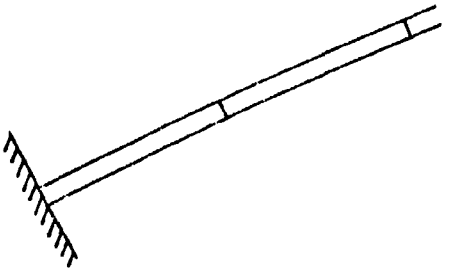

Figure 4. View from Side of Arch, Clamped Boundary Condition

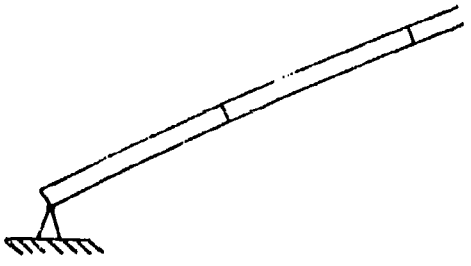

Figure 5. View from Side of Arch, Pinned Boundary Condition

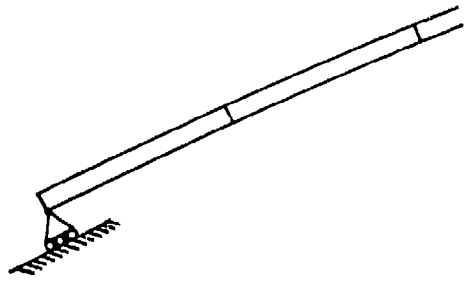

Figure 6. View from Side of Arch, Sliding Pin Boundary Condition

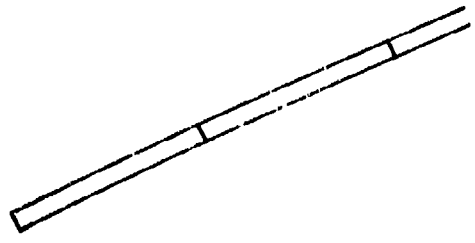

Figure 7. View from Side of Arch, Free Boundary Condition

The cross section of the actual forward canopy arch structure is shown in Figure 8. Obviously the arch structure itself would be less rigid than the clamped boundary condition, but would provide more torsional stiffness than that represented by the pinned boundary condition. Furthermore the structure of the arch would offer more in-plane (of the canopy) bending stiffness than the sliding-pin boundary condition and more out-of-plane (of

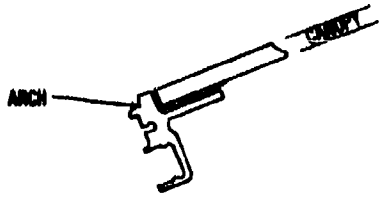

Figure 8. View from Side of Arch, Cross Section of Arch Structure

the canopy) stiffness than the free boundary condition. The action of the arch structure lies somewhere within the range of behavior included by the four boundary conditions illustrated in Figures 4-7. The number of unconstrained degrees of freedom corresponding to each set of boundary conditions used is shown in Table 1.

Material Properties

Engineering stress versus engineering strain data for the stretched acrylic material used in the TF-15 transparency system was obtained from a vendor's bulletin.[17] Figure 9 shows this behavior which was included in the model. Young's Modulus, which corresponds to the initial slope of the data shown in the figure, was taken to be 485,000 psi; Poisson's Ratio, 0.35; mass density, 0.000111 lb $sec^2/in.^4$; and (engineering) yield stress, 10,200 psi.

Having completed the definition of the structural model with this description of the mechanical properties of stretched acrylic, it was necessary to define the bird impact loading before simulation of bird impact dynamic response could be accomplished. The next section briefly describes the procedure used for the definition of bird impact loading.

Table 1

Number of Unconstrained Degrees of Freedom for Boundary Condition Cases

Boundary Condition at Forward Canopy Arch	Number of Unconstrained Degrees of Freedom
Clamped	2427
Pinned	2631
Sliding Pin (Fore - Aft)	2679
Free	2678

Bird Impact Loads Definition

Theory

A somewhat arbitrary procedure has been developed by the FDL for use with MAGNA finite element simulation of aircraft transparency bird impact dynamic response.[13] This procedure was based firmly on an extensive experimental data base accumulated over a period of several years.[18-25] The data base was valid for the case of a rigid, flat, inclined target and comprised pressure data recorded at the surface of the target during bird impact.

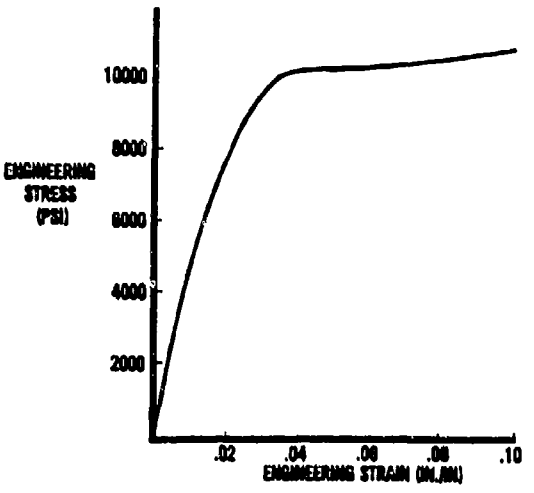

Figure 9. Stress-Strain Behavior of Stretched Acrylic Material

The loads definition procedure is simple and straightforward to use. The essential points of the theory upon which the loads definition procedure is based are as follows:

1. The bird behaves as a fluid during impact.

2. The impulse delivered to the structure is equal to the component of the bird's linear momentum which is normal to the target surface.

3. The bird may be represented as a right circular cylinder having a length to diameter ratio of 2.0.

4. The average density of the bird material is 1.86 sl/ft^3.

5. The period of the impact event is best characterized as the time required for the bird to travel its own (effective) length.

6. The pressure resulting from bird impact is relatively constant at any point on the surface of the target (quasi-steady fluid flow).

The following section briefly sketches the procedure used to define uncoupled bird impact loads. The loads are referred to here as being uncoupled because the theory upon which their definition is based assumes that the target involved is rigid, i.e. that the impact loads are uncoupled or independent from the resulting dynamic response of the target.

Procedure for Uncoupled Bird Impact Loads Definition

An in-depth discussion of this loads definition procedure will be documented elsewhere as time permits.[26] Only the key points will be noted here.

The first step in the uncoupled definition of bird impact loading is the calculation of the impulse delivered to the target from Equation 1.

$$I = MV \sin\Theta \qquad (1)$$

I - impulse (lb sec)

M - mass (sl)

V - velocity (ft/sec)

Θ - acute angle between bird trajectory and target surface (deg)

Next is to calculate the length and diameter of the bird cylinder using equations 2 and 3.[26]

$$L = (0.085\ W)^{1/3} \qquad (2)$$

$$D = 0.5\ (0.085\ W)^{1/3} \qquad (3)$$

L - bird length (ft)

D - bird diameter (ft)

W - bird weight (lb)

Next the period of the bird impact event is calculated using equation 4.

$$T = (L + D/\tan\Theta)/V \qquad (4)$$

T - period of impact event (sec)

Having calculated the parameters above, the locus of the bird impact pressure footprint on the surface of the transparency is estimated. Data from bird impact testing with rigid, flat, inclined targets is used to do this.[23]

When the boundary of the pressure footprint has been located on the surface, a group of finite elements from the model being used is selected which most closely approximates the area and location of the footprint. These become the elements then to which bird impact pressure is applied during the finite element solution.

After the elements representing the impact pressure footprint have been identified, a table is assembled of the times at which load rise and unloading occur for each element. A rectangular pressure vs time history is assumed for each element. The details of this process are too tedious to cover here.

When the intervals of time have been defined during which each element

in the footprint is to be loaded, a sum of products is calculated. Each product is the area of an individual element multiplied by the time interval for its loading. The sum of these products is divided into the impulse defined by equation 1, to determine the value of the constant (and spatially uniform) pressure to be applied to each element in the footprint area.

This step completes the definition of uncoupled bird impact loading. The (single) value of the pressure plus the table of load rise and unloading times for each element in the footprint are sufficient to define the applied loads for MAGNA analysis.

This procedure for the definition of bird impact loading is quite simplistic. It presumes a regular geometry for the bird, ignores spikes of shock pressure which occur very early in the impact event, and assumes a spatially uniform distribution of pressure. Even with these features, bird impact simulation results obtained with this procedure have been found to be useful and realistic.[13] The usefulness of uncoupled bird impact loads defined with this procedure is apparently limited, however, to glass transparency designs.[13]

Procedure for Coupled Bird Impact Loads Definition

When the target, or aircraft transparency in this case, is not actually rigid, Equation 1 represents only a lower bound for the value of the impulse delivered to the structure by the bird impact. Another limiting case which establishes the upper bound for the value of the impulse is the very flexible target which forms a pocket upon impact, completely arresting all bird material. In this case the impulse delivered is equal to 100 percent of the linear momentum of the bird before impact, or MV. For a target of intermediate flexibility or compliance, the impulse delivered to the structure lies somewhere between $MV\sin\theta$ and MV, the actual value depending upon the history of the dynamic response of the target.

The procedure for the definition of coupled bird impact loads is intended to represent this dependence of the impulse upon the resulting dynamic response of the structure. Instead of being completely defined a priori in an explicit manner, the bird impact loads are implicitly defined and as a result are continually updated or modified during the progress of the MAGNA numerical solution itself. The key points in the procedure for coupled loads definition are noted here.

The first part of the procedure is identical to that for the uncoupled definition of loads discussed above. The end results of these steps are the (constant) value of the uncoupled pressure, P_u, and the load rise and unloading times for each finite element included in the impact pressure footprint.

The next step, having P_u and the element timing, is to write two standard user-subroutines which are compatible with MAGNA. These subroutines are ULOAD and UPRESS.[3] Because the procedure for uncoupled loads definition makes the pressure, P_u, directly proportional to $\sin\theta$, the user-subroutines are used to scale P_u with the instantaneous bird impact

angle, $\Theta(t)$, as shown by Equation 5. Figure 10 shows that as local bending develops in the transparency and the slope or inclination of the surface underneath the bird material increases, so does the local instantaneous bird impact pressure. Such an increase in the instantaneous pressure results in a corresponding increase in the impulse delivered to the structure. The user-subroutines

$$P_c(t) = P_u \quad \text{Sin}\,\Theta(t)/\text{Sin}\,\Theta(0) \qquad (5)$$

$\Theta(0)$ - acute angle between bird trajectory and target surface at the beginning of the bird impact event (deg)

$\Theta(t)$ - acute angle between bird trajectory and target surface at time t (deg)

P_u - uncoupled (constant) value of bird impact pressure (psi)

$P_c(t)$ - coupled (variable) value of bird impact pressure calculated by user subroutines at time t (psi)

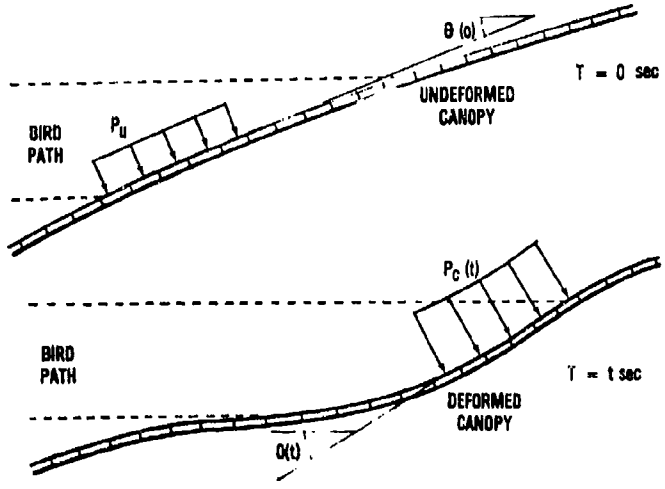

Figure 10. Bird Impact Pressure Dependence Upon Canopy Deformation

ULOAD and UPRESS use the instantaneous deformation calculated by MAGNA to modify the current value of the impact pressure.

The task of developing the user-subroutines is minimal - only 50 executable lines of FORTRAN were required for the TF-15 application. No measurable increase occurred in the computer resources required for the TF-15 analysis when these user-subroutines were used. The effect upon the computed results, however, for analysis with the user-subroutines was very significant. This will be discussed in more detail in later sections.

Analysis

As mentioned in the scope section, seven groups of analyses were conducted to determine the effects of various solution parameters upon the computed results. The parameters included were nonuniform canopy thickness distribution, finite element model boundary conditions at the forward edge of the canopy, time step size for use in dynamic analysis, iteration in the nonlinear solution strategy, coupling between the bird impact loads and resulting dynamic structural response, bird impact velocity, and geometric nonlinearity inherent in the transparency structure. The first group of analyses conducted was that to determine the effect of thinning in the forward canopy.

Canopy Thinning

The first analysis accomplished was a solution for the lowest frequency mode of free vibration for the TF-15 canopy. It was performed for the model as described above, i.e. with 10 percent thinning included in the forward canopy portion of the finite element model. The frequency obtained for the first mode was 76 Hz which is not very high, indicating a quite flexible structure. This was the first evidence suggesting that bird impact load/response coupling might be significant for the TF-15 canopy.

Figure 11 illustrates the normalized shape of the first mode obtained. Solid lines in the figure represent the shape of the deformed geometry and the dotted lines indicate the initial or undeformed geometry. As anticipated, the mode shape is typical of a first mode with the crown area moving down and the sides bulging out.

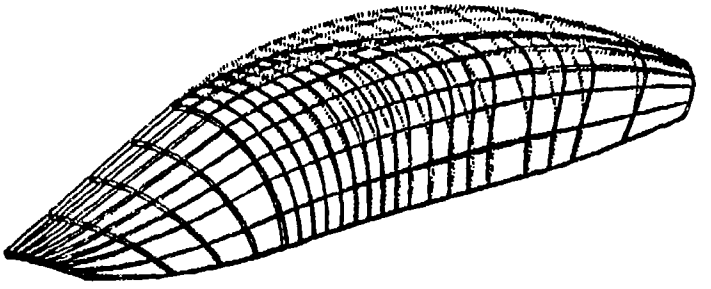

Figure 11. First Mode of Free Vibration for 10 Percent Thinning Model

This same free vibration analysis was repeated with a model having uniform thickness of 0.335 in. everywhere over the forward canopy. Essentially the same frequency and first mode shape were obtained for the uniform thickness model as for the 10 percent thinning model. Apparently no significant effect exists of thinning upon the free vibration response of the transparency system.

Next, nonlinear dynamic bird impact simulations were conducted for both of these finite element models, the 10 percent thinning model being analyzed first. Both of these analyses included the effects of material and geometric nonlinearities. The uncoupled definition of bird impact loads described earlier was used for 4 lb bird impact at 182 kt.

A time step equal to 0.000129 sec was selected for use in the 10 per cent canopy thinning analysis. This value was selected by applying a rule of thumb suggested by the developer of MAGNA.[3] The rule first requires that the frequency of the mode of free vibration judged to be primarily excited by the bird impact be obtained. The frequency for this mode is then used to establish an upper limit to the time step for use in MAGNA dynamic analysis as shown in Equation 6. For both finite element models involved the first or lowest frequency mode was obtained, and this rule of thumb required use of a time step not greater than 0.000132 sec.

$$\Delta t \leq {}^{1}/_{f} \div 100 \qquad (6)$$

f - frequency of the free vibration mode primarily excited by bird impact (Hz)

Δt - time step used in MAGNA incremental (transient) solution (sec)

After accomplishing the 10 percent thinning analysis, the uniformly thick canopy analysis was run with a time step of 0.000128 sec. Figure 12 shows the marked difference between the histories of maximum vertical deflection computed for the two cases. Table 2 gives the value of the maximum vertical deflection predicted for each case, indicating that including 10 percent thinning in the finite element model resulted in 23 percent greater vertical deflections. In either of the two cases, the deflections

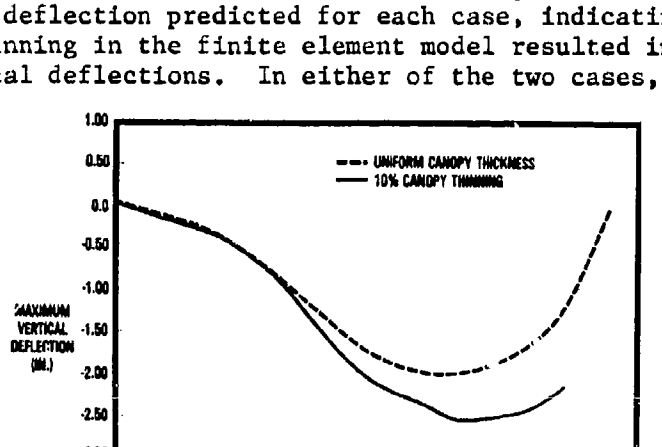

Figure 12. Maximum Vertical Deflection vs Time, Canopy Thinning Studies

predicted are high enough to indicate significant bird impact load/response coupling.

Figure 13 indicates that the sensitivity of the stresses to canopy thinning is not as great as that of the deflections. Table 3 gives the maximum equivalent stress calculated in each case, showing that 10 percent thinning resulted in less than 7 percent higher stress.

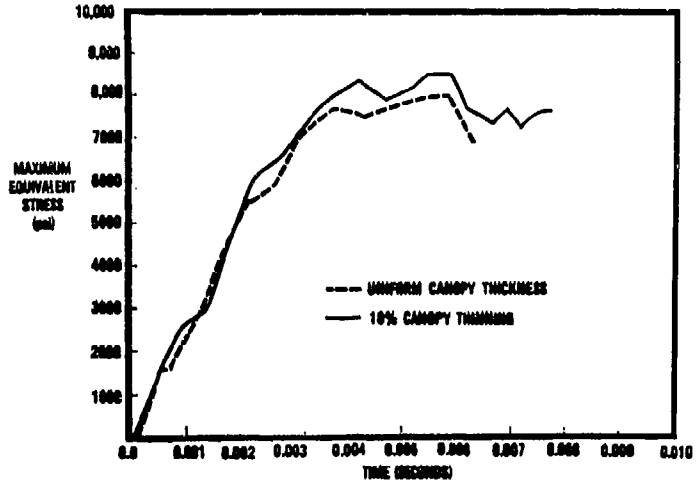

Figure 13. Maximum Equivalent Stress vs Time, Canopy Thinning Studies

It should be noted that neither one of the stress histories shown in Figure 13 indicates canopy failure. Experience to date in the FDL shows that the static yield strength of transparent plastic materials serves as a useful failure criterion when conducting MAGNA bird impact simulations. The value of the yield stress for stretched acrylic is shown in Figure 9 to be 10,200 psi.

Table 2

Effect of Canopy Thinning on Maximum Vertical Displacement

Finite Element Model	Maximum Vertical Displacement (in.)
10 % Canopy Thinning	-2.53
Uniform Thickness Canopy	-2.06

Table 3

Effect of Canopy Thinning on Maximum Equivalent Stress

Finite Element Model	Maximum Equivalent Stress (psi)
10% Canopy Thinning	8527
Uniform Thickness Canopy	7998

The value for yield stress corresponding to Figure 13 should be taken as 9808 psi, however, because the stress output by MAGNA is a theoretical one not equal to engineering stress at large values of strain. The maximum equivalent stress computed in these two analyses was 8527 psi for the 10 percent thinning case which is only 87 percent of the 9808 psi "rupture" stress.

It was concluded from these two analyses that transparency thinning should be taken into account for such studies, but more so for accurate deflections than for accurate stresses. It had been hoped that these simulations at 182 kt bird impact velocity would have predicted canopy failure as observed during full scale testing. The predicted stresses were quite high, but not high enough to indicate canopy failure. It was thought that one of the parameters remaining to be studied might turn out to be the key to more realistic computed stresses. The next group of analyses conducted examined the effects of boundary conditions applied at the forward edge of the forward canopy to represent the structural characteristics of the canopy metallic arch.

Canopy Arch Boundary Conditions

The four sets of boundary conditions already described in the Structural Modelling section were analyzed in these studies. The boundary conditions involved were clamped, pinned, sliding pin, and free at the forward edge of the forward canopy. The finite element model in each case included 10 percent thinning in the forward canopy.

A free vibration analysis was performed for each of these four models to determine the frequency of the lowest mode of free vibration. Table 4 shows the frequencies which were obtained. The shape of the first mode has already been illustrated for the clamped case in Figure 11. The mode shape obtained for both the pinned and sliding pin cases was essentially unchanged from that for the clamped case. One exception to this statement is the fact that very small displacements in the plane of the canopy were predicted at the forward canopy edge for the sliding pin case. The first mode shape obtained for the free arch case was much different than those obtained for the other

three cases. Figure 14 shows that for the free arch case, maximum displacements occurred at the arch itself rather than in the crown area of the canopy as for the other three cases.

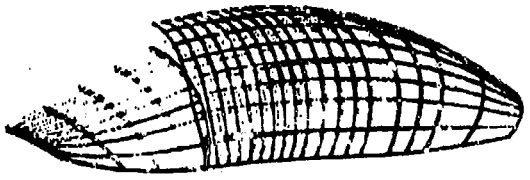

Figure 14. First Mode of Free Vibration for Free Boundary Condition at Arch

Table 4

Effect of Arch Boundary Conditions on First Mode Frequencies

Boundary Condition at Forward Canopy Arch	Frequency Computed for First Mode of Free Vibration
*Clamped	76 Hz
Pinned	74 Hz
Sliding Pin (Fore-Aft)	73 Hz
Free	18 Hz

*Accomplished previously under canopy thinning studies.

Having accomplished free vibration analyses, a nonlinear dynamic analysis was performed next for each boundary condition case. A time step of 0.000129 sec was used in each case. This value for the time step size corresponded to the rule of thumb discussed in the Canopy Thinning section in all but the free arch case. For the free arch case, the same rule of thumb would permit the use of a time step 4 times larger than 0.000129 sec (See Table 4).

Figure 15 shows the sensitivity of the history of maximum vertical deflection to boundary conditions imposed at the arch as indicated by these nonlinear dynamic analyses. Table 5 lists the maximum vertical deflection

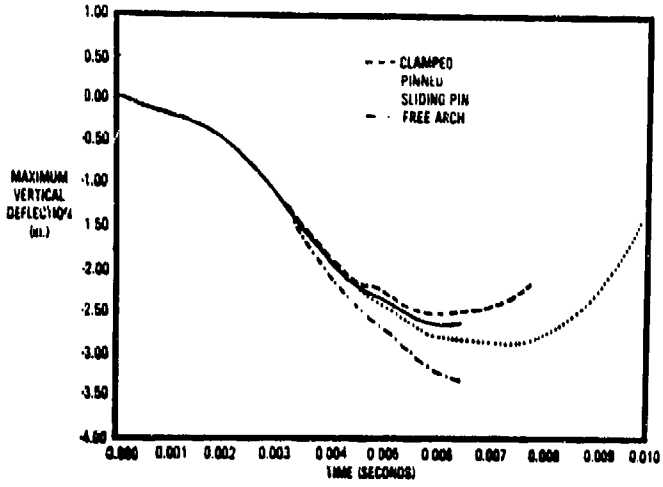

Figure 15. Maximum Vertical Deflection vs Time, Arch Boundary Condition Studies

Table 5

Effect of Arch Boundary Conditions on Maximum Vertical Displacement

Boundary Condition at Forward Canopy Arch	Maximum Computed Vertical Displacement (in.)
#Clamped	-2.53
Pinned	-2.65
Sliding Pin (Fore-Aft)	-2.86
Free	*-3.30

#Accomplished previously under canopy thinning studies.

*Displacements still increasing at time of solution termination.

calculated in each case. The trend indicated in Table 5 is clear: less constraint at the arch permits greater deformation in every case. Allowing rotation at the arch via the pinned boundary condition resulted in 5 percent greater displacement. Permitting the arch to move in the plane of the canopy surface with the sliding pin boundary condition resulted in 13 percent greater displacement (compared to the clamped case). Finally, allowing motion out of the plane of the canopy surface with the free arch boundary

condition resulted in more than 30 percent greater displacement (compared to the clamped case).

Figure 16 shows the effect of arch boundary conditions upon maximum equivalent stress predicted. Table 6 lists the maximum equivalent stress

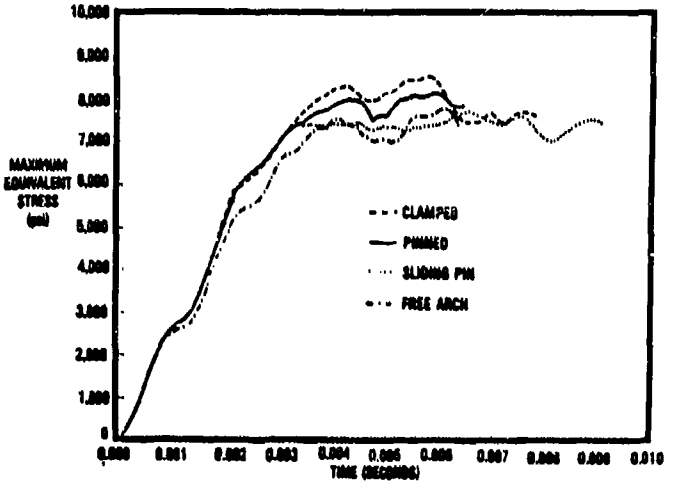

Figure 16. Maximum Equivalent Stress vs Time, Arch Boundary Condition Studies

Table 6
Effect of Arch Boundary Conditions on Maximum Equivalent Stress

Boundary Condition at Forward Canopy Arch	Maximum Equivalent Stress (psi)
#Clamped	8527
Pinned	8145
Sliding Pin (Fore-Aft)	7689
Free	7771

#Accomplished previously under canopy thinning studies.

calculated for each case. Again a general trend can be detected: less constraint at the arch results in lower maximum stress. Permitting rotation at the arch resulted in 4 percent lower stress, motion in the plane of the canopy in 10 percent lower stress, and motion out of the plane of the canopy in 9 percent lower stress.

Still, no material rupture is indicated for the 182 kt bird impact simulation. It was concluded from the boundary condition studies that to obtain conservative stress results a clamped boundary condition should be defined at the forward canopy forward edge. The maximum equivalent stress predicted thus far in the overall study was still only 8527 psi for the case with 10 percent canopy thinning and clamped arch boundary condition. The study was continued to examine each of the remaining parameters in hopes that one of them would significantly increase the stresses being predicted.

Time Step Size

The next analysis parameter considered was the size of the time step used in the dynamic analysis. This time no free vibration analyses were conducted, only additional nonlinear dynamic analyses with various values for the time step used.

The first case selected was that for 10 percent thinning with the free arch boundary condition because a nonlinear dynamic solution had already been obtained for this case using a time step 4 times smaller than that indicated by the rule of thumb (Equation 6) discussed in the Canopy Thinning section. Figures 15 and 16 illustrate the results of this free arch analysis. This previous analysis could be repeated at minimal cost using a time step 4 times larger (0.000516 sec) which corresponded directly to the rule of thumb for time step size. Such a solution was obtained and it was expected that results very similar to those shown in Figures 15 and 16 would result because the time step of 0.000516 sec did correspond to the rule of thumb. The time step of 0.000129 sec used previously should have represented overkill, being well past the (rule of thumb) point of diminishing returns for cost vs accuracy in the numerical solution. The time step of 0.000516 sec was expected to produce satisfactory results, quite similar to those obtained with the 0.000129 sec time step. (In general, more accurate results are obtained with a smaller time step).

The results from the large time step analysis came as a big surprise. The solution obtained with a 0.000516 sec time step was very poor. Figure 17 shows the effect of the larger time step upon the history of vertical deflection predicted. The displacements are a great deal smaller than they were for the 0.000129 sec time step. Figure 18 shows a similar but less significant effect upon the history of maximum equivalent stress predicted. Even though the all time maximum stress is similar for both cases, the time histories predicted differ considerably.

These results generated concern over the quality of all the other dynamic solutions obtained up to this point. A time step size corresponding to the rule of thumb had been used in each of these cases. In light of the high sensitivity of the computed results to time step size demonstrated, it seemed that a much smaller time step might be in order for the other analyses already conducted. To test this rationale, the best simulation to date - 10 percent thinning with clamped boundary condition at the arch - was repeated with a smaller time step. This simulation had already been run with a 0.000129 sec time step, and was repeated with a 0.000064 sec time step.

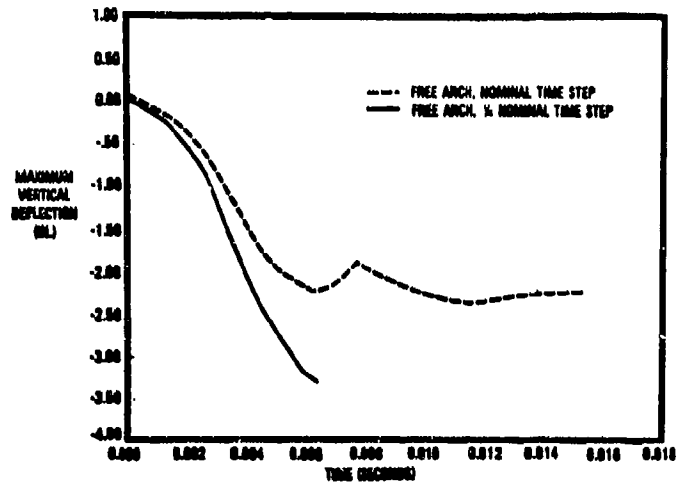

Figure 17. Maximum Vertical Deflection vs Time, Time Step Size Studies, Free Arch

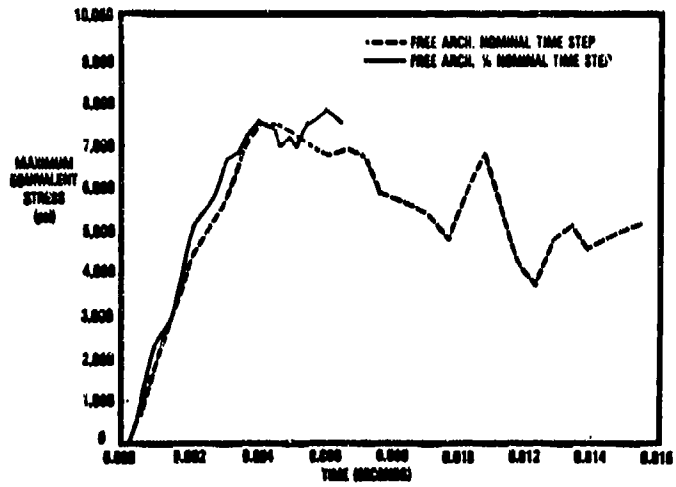

Figure 18. Maximum Equivalent Stress vs Time, Time Step Size Studies, Free Arch

Figure 19 shows the effect of a smaller time step upon the history of vertical displacements computed for the 10 percent thinning, clamped arch case. The difference between the two solutions obtained is insignificant, never exceeding 2 percent. Figure 20 also shows only insignificant differences between the two histories of maximum equivalent stress predicted, the all time maximum stresses differing by less than 1 percent.

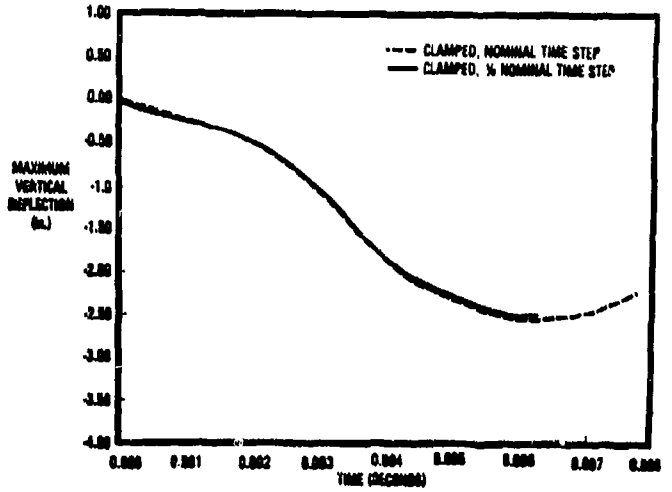

Figure 19. Maximum Vertical Deflection vs Time, Time Step Size Studies, Clamped Arch

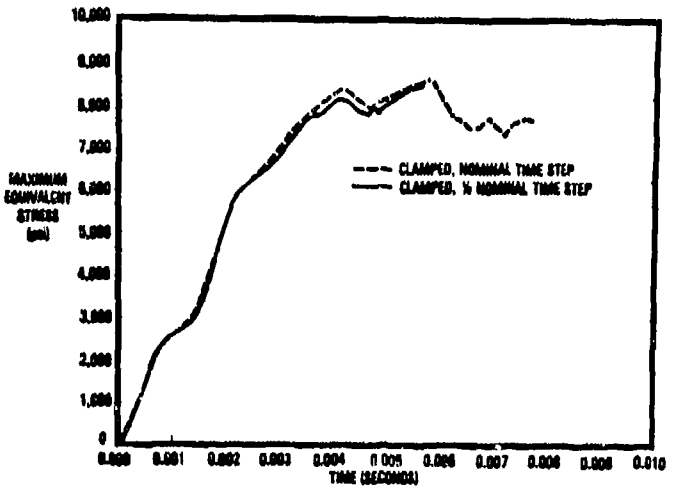

Figure 20. Maximum Equivalent Stress vs Time, Time Step Size Studies, Clamped Arch

Apparently the sensitivity of the solution to the size of the time step used is itself sensitive to the boundary conditions being applied. For the free arch boundary condition case, the rule of thumb for time step size (Equation 6) provided a value much too large for realistic results. On the other hand, for the clamped arch boundary condition case, the same rule of thumb provided highly satisfactory results. It was concluded from these results that the preferred approach for TF-15 canopy bird impact simulation thus far included 10 percent canopy thinning in the finite element model, clamped boundary conditions at the forward edge of the forward canopy, and a dynamic analysis time step of 0.000129 sec. It was further concluded that

whenever dynamic finite element analyses are being conducted, it is always necessary to check the choice made of time step size by repeating the solution obtained with a smaller time step. This is the only way to demonstrate clearly the quality of the solution obtained.

Iterative Solution

The next analysis parameter studied was iteration in the finite element solution. Nonlinear dynamic analyses performed with MAGNA may be accomplished in either an iterative or a non-iterative manner. For the non-iterative approach, a single solution step is performed at each time increment in the analysis. In the iterative case, the solution step is repeated several times, either at each or at selected time increments during the analysis. When iteration is being used, the idea is to make the solution converge to meet some previously defined criteria. The iterative approach is more expensive and, as a rule, is not utilized unless required. In general an analysis is conducted in a non-iterative fashion until it becomes apparent that non-iteration is no longer sufficient to provide realistic results; at this point the use of iteration in the solution becomes necessary.

Since the choice of an iterative solution involves judgement on the part of the MAGNA user, the question at hand was whether or not these TF-15 aircraft canopy bird impact simulations really required the extra time and cost involved in performing iterative solutions. Sixty increments of a non-iterative nonlinear dynamic solution had already been obtained for 10 percent thinning, clamped arch boundary conditions, and a time step of 0.000129 sec. Fifty of these sixty increments were repeated with iteration at each increment to determine the effects of iteration for this case.

As it turned out, a total of 255 iterations were performed during the 50 time increments in the solution for an average of just over 5 iterations per increment. The computer time required was about 2.5 times greater for the iterative case than it had been for the non-iterative case. The calendar time required also increased in about the same proportion: 17 days for the iterative analysis and only 7 days for the non-iterative one. (Both jobs were run in segments using the restart feature of MAGNA).

Figure 21 illustrates the effect that iteration in the solution had upon the history of maximum vertical deflection predicted. As for time step size, the effect of iteration is insignificant, the greatest difference between the two histories being less than 2 percent. Figure 22 shows that the same is true for the history of maximum equivalent stress, the all time maximum stress for the two cases differing less than 0.5 percent.

Obviously there is no need to perform iterative solutions for this type of MAGNA analysis. Many commercially available nonlinear finite element analysis computer programs offer only the iterative approach to nonlinear dynamic analysis. The MAGNA feature which permits a non-iterative solution to be performed can be, as in this case, a very effective time and cost saver. Non-iterative analysis has been used almost exclusively in all FDL MAGNA bird impact simulations conducted to date.[8, 9, 10, 13, 26]

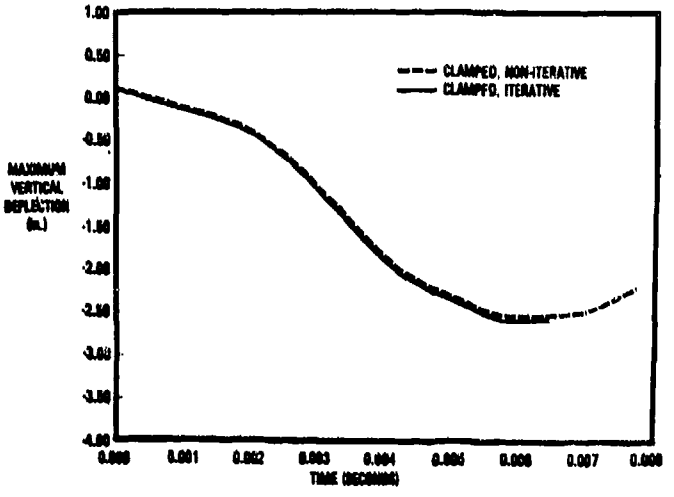

Figure 21. Maximum Vertical Deflection vs Time, Iterative Solution Studies

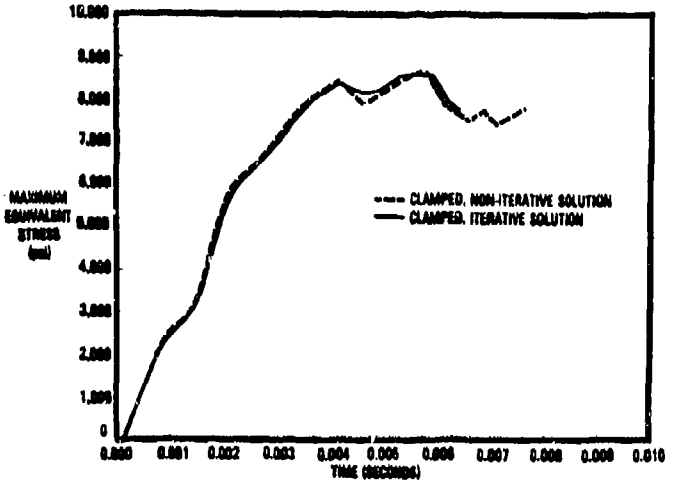

Figure 22. Maximum Equivalent Stress vs Time, Iterative Solution Studies

Load/Response Coupling

The next analysis parameter studied was coupling between the bird impact pressures and the resulting dynamic response of the transparency. None of the other parameters considered up to this point had resulted in any indication of material rupture for the 182 kt case, the highest stress predicted having been about 85 percent of the rupture stress. Some evidence that coupling might be a significant factor was seen in the magnitudes of displacements predicted in nonlinear dynamic analysis - on the order of 2.5 in. These displacements were felt to be great enough to result in significant load/response coupling.

User subroutines were written to implement coupled loads following the procedure described in the Coupled Bird Impact Loads Definition section. A coupled simulation was conducted for 4 lb bird impact at 182 kt including 10 percent canopy thinning, clamped boundary conditions at the canopy arch, a time step of 0.000129 sec, and a non-iterative solution strategy.

The results of the coupled loads simulation differed dramatically from the uncoupled results obtained earlier. Figure 23 shows how the history of coupled bird impact pressure differed from the uncoupled history applied in all other simulations up to this point. The impulse delivered to the transparency for the coupled case was 7.91 lb sec, a 29 percent increase over the value corresponding to the uncoupled case - 6.15 lb sec.

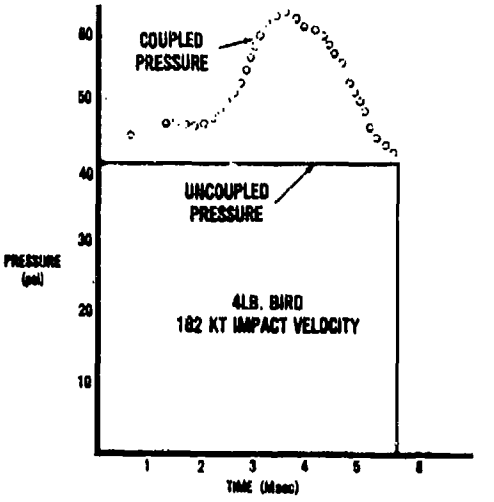

Figure 23. Coupled and Uncoupled Bird Impact Pressure Histories

Both the computed displacements and stresses turned out to be very sensitive to the load/response coupling introduced. Figure 24 shows the effect of coupling on the history of maximum vertical deflection. The all time maximum vertical deflection for uncoupled loads was -2.53 in., and for coupled loads was -3.35 in., a 32 percent increase. Figure 25 shows the effect of load/response coupling on the history of maximum equivalent stress computed. The all time maximum equivalent stress for uncoupled loads was 8527 psi and for coupled loads was 13400 psi, a 57 percent increase.

For the first time, canopy rupture is indicated as observed in testing for 4 lb 182 kt bird impact. The yield stress of 9808 psi (Figure 25) is reached at about 0.004000 sec for the coupled results after which some plastic strains occur and the stresses increase rapidly. Taking the occurence of the yield stress to indicate rupture of the stretched acrylic material, as discussed earlier in the Canopy Thinning section, the timing predicted for the initiation of rupture also corresponds well with test results. It was reported that some bird material did enter the cockpit in the 182 kt test[1]. The simulation predicts that the initiation of failure

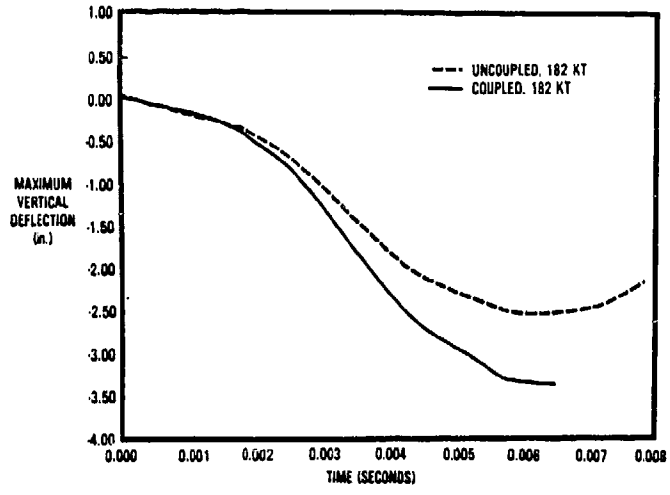

Figure 24. Maximum Vertical Deflection vs Time, Coupled Loads Studies

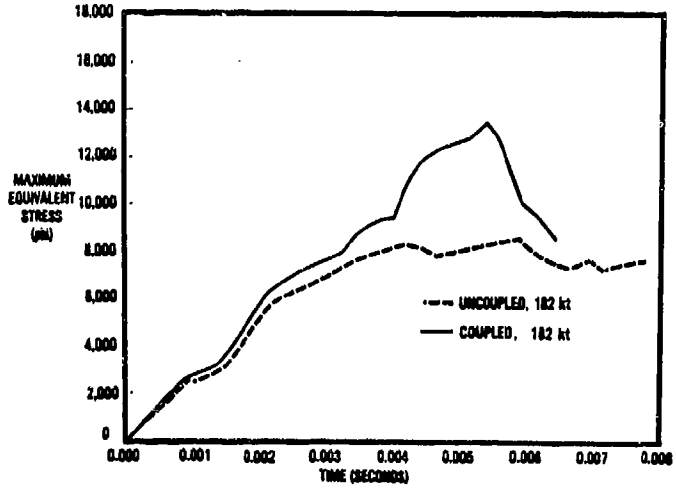

Figure 25. Maximum Equivalent Stress vs Time, Coupled Loads Studies

occurs at 0.004000 sec and the period of the bird impact event is 0.005700 sec, enough time between the two for a hole in the canopy to open and some debris to enter the cockpit.

The location of the fracture predicted by MAGNA also corresponds well with that observed during the test. Figure 26 shows the locations of the highest stresses predicted by MAGNA on both the inner and outer surfaces of the canopy. The locations of highest stress in the figure correspond surprisingly well with the edges of the fractured area resulting from the test. A hole was left through the canopy after the test which began about 6

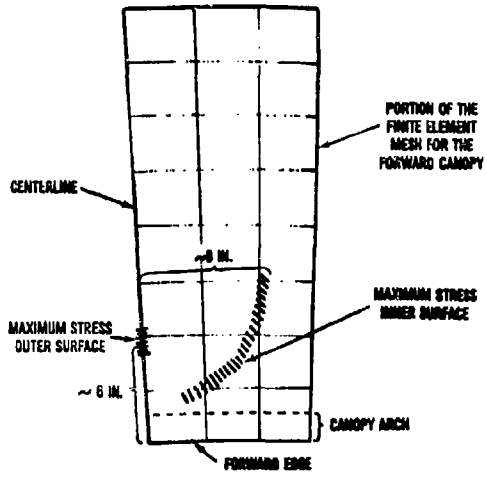

Figure 26. Regions of Highest Computed Stress

in. from the forward edge on the outer surface in the same area as that indicated in Figure 26. On the inner surface, the edge of the fractured area followed an arc very similar to that shown in Figure 26 which indicates a failed area about 16 in. wide extending all the way to the forward edge of the transparency.

Summarizing, it appears that MAGNA does predict material rupture at the same kinetic energy for which failure occurs in full scale testing. Further, MAGNA roughly predicts the time at which failure initiation occurs and even predicts realistically some of the dimensions of the area of fractured material which occurred during full scale testing.

Bird Impact Velocity

Having successfully accomplished a 4 lb 182 kt bird impact simulation, another similar analysis was conducted for 4 lb 160 kt bird impact to determine how sensitive the results were to bird impact velocity. It was known that in full scale testing no failure occurred at 160 kt. Figure 27 shows the effect of impact velocity upon the history of maximum vertical deflection predicted. Again the results are quite surprising. The all time maximum vertical deflection predicted for 182 kt was -3.35 in., but for 160 kt it was only -2.39 in., 29 percent less. The magnitude of the displacements resulting from bird impact is very sensitive to velocity.

Figure 28 shows the effect of impact velocity upon the history of the maximum equivalent stress predicted. For 182 kt the all time maximum stress was 13,400 psi; for 160 kt it was 8356 psi, 38 percent less. This result is especially encouraging because it demonstrates that the computed history of stress is very sensitive to bird impact velocity. This means that MAGNA can be used to predict the bird impact ballistic limit for aircraft transparency structures like the TF-15 canopy within narrow limits, about ±10 kt.

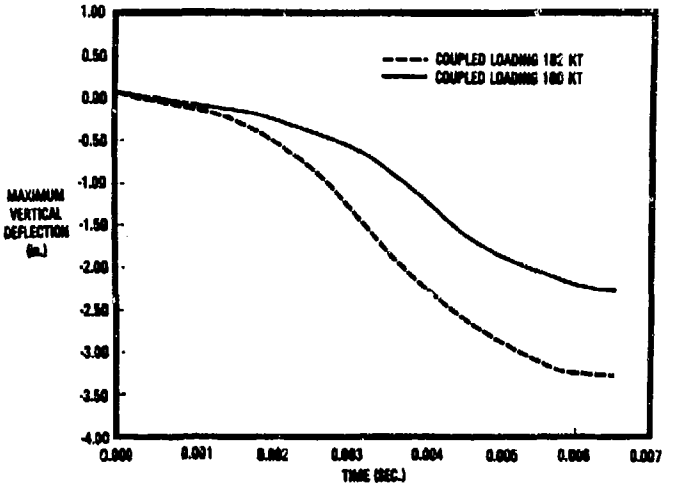

Figure 27. Maximum Vertical Deflection vs Time, Impact Velocity Studies

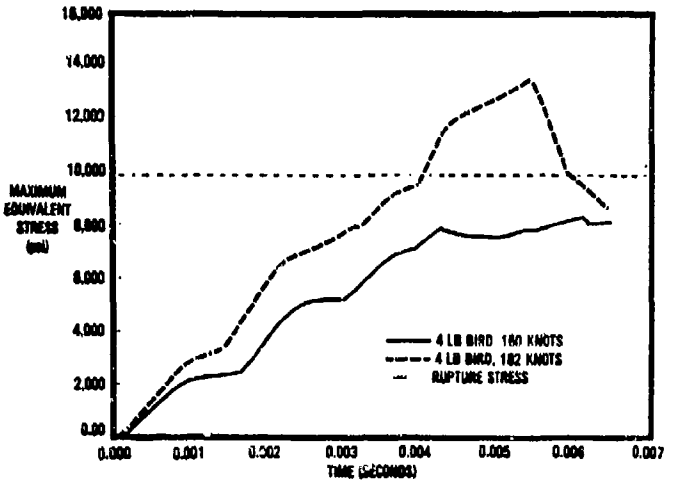

Figure 28. Maximum Equivalent Stress vs Time, Impact Velocity Studies

Linear Analysis

The only analysis parameter remaining for study was the assumption of linearity in the dynamic structural response of the transparency. To determine how significant the effects of nonlinearities were, the 182 kt simulation was repeated with coupled loads as a completely linear analysis. Neither geometric nonlinearities nor material nonlinearities were taken into account. It was desired to determine how closely the linear solution

approximated the real response of the structure. As it turned out, for the TF-15 canopy the effects of the nonlinearities present are far more significant than even load/response coupling or bird impact velocity.

Figure 29 shows the effect of the linear assumption upon the history of maximum vertical displacement predicted. No similarity exists between the two results. The all time maximum nonlinear vertical displacement was -3.35 in.; the maximum linear vertical displacement was only -0.53 in., 84 percent less than the nonlinear result. Figure 30 shows the effect of the linear assumption upon the history of maximum equivalent stress predicted. The all

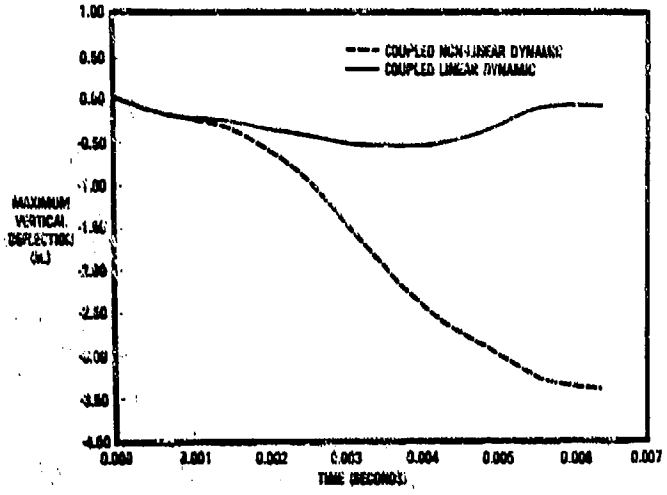

Figure 29. Maximum Vertical Deflection vs Time, Linear Analysis Studies

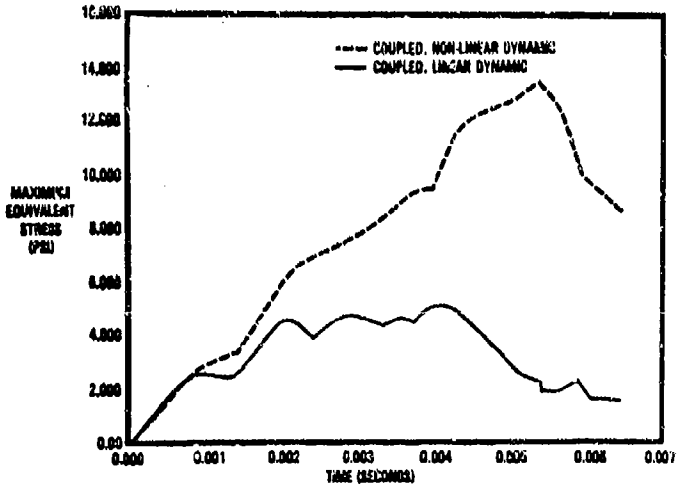

Figure 30. Maximum Equivalent Stress vs Time, Linear Analysis Studies

time maximum nonlinear stress was 13,400 psi; the maximum linear stress was 5155 psi, 62 percent less than the nonlinear result.

For deflections greater than 0.25 in. and stresses above 2000 psi, the assumption of linear behavior is totally invalid for the TF-15 canopy bird impact problem.

Conclusions

The following conclusions can be drawn from the results of the studies discussed above.

1. The use of MAGNA for accurate simulation of the dynamic response of F-15 aircraft canopy structures to bird impact loading has been validated. MAGNA can be used to predict the ballistic limit of the structure to within ±10 kt and to realistically indicate the time of initiation and location of material rupture in the canopy.

2. The use of MAGNA to evaluate the level of bird impact protection offered by proposed similar alternate F-15E aircraft canopy designs is valid. Such applications of MAGNA could save considerable time and expense if engineering development of an alternate F-15E canopy design is undertaken. Total cost of the successful 182 kt simulation reported here was $400 including computer resources plus engineering manhours. The calendar time required for the same analysis was 4 working days. All 11 simulations reported here were accomplished over a period of 60 working days.

3. Any nonuniform distribution of thickness present in an aircraft transparency should be taken into account if computer simulations of dynamic response to bird impact are conducted.

4. When conducting finite element computer analysis of bird impact near the edge of an aircraft transparency, if the supporting edge-member structure is not included in the finite element model itself, the use of a clamped boundary condition at the edge of the transparent panel is recommended for conservative results.

5. Even though rules of thumb exist for selecting the time step size for use in a transient finite element analysis, a second simulation with another (smaller) time step is always recommended to assess the quality of the solution being obtained.

6. In general, when using MAGNA to conduct nonlinear analyses of aircraft transparency bird impact response, significant time and cost can be saved by performing non-iterative type solutions.

7. For aircraft transparencies subject to bird impact loading which exhibit deformations on the order of 3 in. or more, coupling between the bird impact loading and the resulting dynamic response of the structure will be significant. Nonlinear dynamic finite element simulation of such

problems is invalid unless appropriate steps are taken to account for the effect of this coupling.

8. A rudimentary method to couple bird impact loading to dynamic structural response has been developed and briefly described (Coupled Bird Impact Loads Definition section). This method involves standard MAGNA user-written subroutines and has been shown to produce accurate results for TF-15 canopy bird impact simulation. Since this method does not modify the area on the surface of the transparency which is loaded by the impact pressures nor does it alter the (time) period of the impact event, it will probably break down and fail for cases involving deflections much greater than those exhibited by the TF-15 canopy (approximately 3 in.). Some examples involving such extreme deformation have been documented elsewhere.[8, 9, 10, 13, 26]

9. In general, the geometric nonlinearity present in the structure plays an overwhelmingly important role in determining the dynamic response of aircraft transparencies to bird impact loading. Linear transient finite element analysis produces results of very little if any practical value. The only exception to this rule which has been demonstrated is a (laminated or monolithic) flat, glass transparency.[13, 26]

References

1. L. E. Landholt, Final Report Windshield/Canopy Bird Impact Resistance, McDonnell Aircraft Company, St Louis, Missouri 63166, Report Number MDC A4888, August 1977.

2. Personal Communication, 12 August 1982, I.V. Yancey, Directorate of Engineering, Aeronautical Systems Division, Wright-Patterson Air Force Base, Ohio 45433.

3. R. A. Brockman, MAGNA (Materially and Geometrically Nonlinear Analysis) Part I - Finite Element Analysis Manual, Flight Dynamics Laboratory, Wright-Patterson Air Force Base, Ohio 45433, AFWAL-TR-82-3098 Part I, December 1982.

4. T. S. Bruner, MAGNA (Materially and Geometrically Nonlinear Analysis) Part II - Preprocessor Manual, Flight Dynamics Laboratory, Wright-Patterson Air Force Base, Ohio 45433, AFWAL-TR-82-3098 Part II, December 1982.

5. R. A. Brockman, MAGNA (Materially and Geometrically Nonlinear Analysis) Part III - Postprocessor Manual, Flight Dynamics Laboratory, Wright-Patterson Air Force Base, Ohio 45433, AFWAL-TR-82-3098 Part III, December 1982.

6. R. A. Brockman, MAGNA (Materially and Geometrically Nonlinear Analysis) Part IV - Quick Reference Manual, Flight Dynamics Laboratory, Wright-Patterson Air Force Base, Ohio 45433, AFWAL-TR-82-3098 Part IV, December 1982.

7. R. E. McCarty, "Computer Analysis of Bird Resistant Aircraft Transparencies," Proceedings of the 17th Annual SAFE Symposium, December 1979, Las Vegas, Nevada.

8. R. E. McCarty, "Finite Element Analysis of F-16 Aircraft Canopy Dynamic Response to Bird Impact Loading," 21st AIAA/ASME/ASCE/AHS Structures, Structural Dynamics, and Materials Conference, May 1980, Seattle, Washington.

9. R. E. McCarty, "Aircraft Transparency Bird Impact Analysis Using the MAGNA Computer Program," Conference on Aerospace Transparencies Sponsored by the Society of British Aerospace Companies, September 1980, London, England.

10. R. E. McCarty, "Finite Element Analysis of a Bird-Resistant Monolithic Stretched Acrylic Canopy Design for the F-16A Aircraft," AIAA Aircraft Systems and Technology Conference, August 1981, Dayton, Ohio.

11. R. E. McCarty and R. A. Smith, "Finite Element Analysis of Through the Canopy Emergency Crew Escape from the T-38 Aircraft," AIAA/ASME/ASCE/AHS 23rd Structures, Structural Dynamics, and Materials Conference, May 1982, New Orleans, Louisiana.

12. R. E. McCarty and R. A. Smith, "Simulation of T-38 Aircraft Student Canopy Response to Cockpit Pressure and Thermal Loads Using MAGNA, "AIAA/ASME/ASCE/AHS 24th Structures, Structural Dynamics, and Materials Conference, May 1983, Lake Tahoe, Nevada.

13. R. E. McCarty and Lt J. L. Hart, "Validation of the MAGNA Computer Program for Nonlinear Finite Element Analysis of Aircraft Transparency Bird Impact," 14th Conference on Aerospace Transparent Materials and Enclosures Sponsored by the Air Force Wright Aeronautical Laboratories, July 1983, Scottsdale, Arizona.

14. R. A. Brockman, MAGNA (Materially and Geometrically Nonlinear Analysis) General Description and Summary of Capabilities, University of Dayton Research Institute, Dayton, Ohio 45469, UDR-TM-80-27, April 1981.

15. McDonnell Drawing No. 68A319998, McDonnell Aircraft Company, St Louis, Missouri 63166.

16. Personal Communication, 9 December 1982, G. Nixon, Vice President-Engineering, Swedlow Inc., Garden Grove, California 92645.

17. Typical Physical Properties of Swedlow Stretched Acrylic (MIL-P-25690) Sheet - Swedlow Type 350S, Swedlow Inc., Transportation Products Division, Garden Grove, California 92645, Engineering Bulletin No. MP-3-100, 4 April 1973.

18. J. P. Barber and J. S. Wilbeck, Characterization of Bird Impacts on Rigid Plate: Part I, Air Force Flight Dynamics Laboratory, Wright-Patterson Air Force Base, Ohio 45433, AFFDL-TR-75-5, January 1975.

19. R. L. Peterson and J. P. Barber, Bird Impact Forces in Aircraft Windshield Design, Air Force Flight Dynamics Laboratory, Wright-Patterson Air Force Base, Ohio 45433, AFFDL-TR-75-150, March 1976.

20. Y. M. Ito, G. E. Carpenter, and F. W. Perry, Bird Impact Loading Model for Aircraft Windshield Design, California Research and Technology, Inc. Woodland Hills, California 91364, CRT 3090-2, July 1977.

21. J. P. Barber, J. S. Wilbeck, and H. R. Taylor, Bird Impact Forces and Pressures on Rigid and Compliant Targets, Air Force Flight Dynamics Laboratory, Wright-Patterson Air Force Base, Ohio 45433, AFFDL-TR-77-60, May 1978.

22. J. S. Wilbeck, Impact Behavior of Low Strength Projectiles, Air Force Materials Laboratory, Wright-Patterson Air Force Base, Ohio 45433, AFML-TR-77-134, July 1978.

23. A. Challita and J. P. Barber, The Scaling of Bird Impact Loads, Air Force Flight Dynamics Laboratory, Wright-Patterson Air Force Base, Ohio, 45433, AFFDL-TR-79-3042, March 1979.

24. J. Y. Parker, Measurement of Impact Bird Pressure on a Flat Plate, Arnold Engineering Development Center, Arnold Air Force Station Tennessee 37389, AEDC-TR-79-14.

25. J. B. R. Heath, R. W. Gould, and G. R. Cowper, Momentum Transfer in Bird Impacts, National Aeronautical Establishment, National Research Council, Ottawa, Canada, LTR-ST-1257, April 1981.

26. R. E. McCarty, Lt J. L. Hart and R. A. Smith, Nonlinear Finite Element Analysis of Aircraft Transparency Bird Impact Using the MAGNA Computer Program, Flight Dynamics Laboratory, Wright-Patterson Air Force Base, Ohio, 45433, AFWAL-TR- , pending technical report.

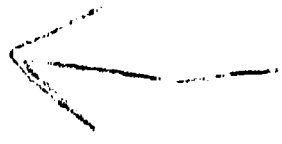

AD-P003 231

SIMULATION OF T-38 AIRCRAFT STUDENT CANOPY RESPONSE TO COCKPIT PRESSURE AND THERMAL LOADS USING MAGNA

R. E. McCarty and R. A. Smith,
Flight Dynamics Laboratory

SIMULATION OF T-38 AIRCRAFT STUDENT CANOPY RESPONSE TO COCKPIT PRESSURE AND THERMAL LOADS USING MAGNA

R. E. McCarty*
R. A. Smith*
Crew Escape and Subsystems Branch
Flight Dynamics Laboratory
Air Force Wright Aeronautical Laboratories
Wright-Patterson Air Force Base, Ohio

Abstract

The linear and nonlinear static response to cockpit pressure and (cold) thermal loads of the forward canopy for the T-38 aircraft has been predicted using the MAGNA (Materially and Geometrically Nonlinear Analysis) finite element computer program. The results obtained are compared to those of earlier analyses and full scale tests. It is concluded that the current canopy design when properly rigged can withstand more than 20 psig pressure, that thermal loads are more critical than cockpit pressure loads, and that providing more attachment fixity at both forward and aft arches would relieve stress concentrations which occur at the canopy corners.

* Aerospace Engineer
Subsystems Development Group

Introduction

In recent years, Air Force missions have involved more high speed, low altitude operations. Under these conditions, bird impacts on aircraft transparent crew enclosures pose a significant hazard and have resulted in unacceptable losses of aircraft and crewmembers. Since 1966 the original purchase cost of Air Force aircraft lost to confirmed transparency bird impact has exceeded $100 million. Replacement cost for these aircraft would of course be many times higher. Seven crewmembers lost their lives in these accidents.

The Air Force has become a worldwide leader in reducing the scope of this problem since 1972. At that time the Air Force Flight Dynamics Laboratory formed the Improved Windshield Protection Advanced Development Program Office (ADPO). Since then a second group, the Subsystems Development Group of the Crew Escape and Subsystems Branch, has also been formed and together the two offices are charged with the development, demonstration, and application of new technology for the design of improved aircraft transparent crew enclosures.

One of the current programs being conducted by the Flight Dynamics Laboratory is to develop bird resistant transparencies for the T-38 supersonic trainer aircraft. Preliminary design studies have already been conducted with various candidate designs being proposed for the student pilot windshield, student pilot canopy, and instructor pilot windshield.[1] Figure 1 illustrates the location of each of the transparencies included in the T-38 system. The instructor's canopy offers no presented frontal area in flight and so has been excluded from consideration for improved bird impact resistance.

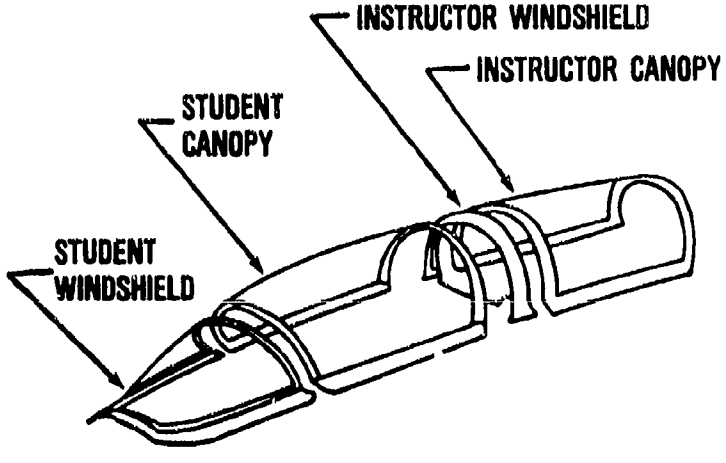

Figure 1. T-38 Transparency System

The purpose of this study is to support the work currently being conducted under contract to redesign the T-38 canopy. The approach taken was to analyze the canopy stress resulting from cockpit pressure and thermal loads. The first step taken was a linear static analysis of the canopy response to cockpit pressure. The analysis was repeated for various boundary conditions because model sensitivity to this parameter was not known. The result of these analyses provided the most appropriate set of boundary conditions for use in all subsequent analyses. Having selected appropriate boundary conditions, a nonlinear static pressure analysis was performed and the results were compared with those of the corresponding linear static pressure results. From this comparison the degree of nonlinearity in the response was characterized with respect to pressure loads. Next a linear static pressure/thermal analysis was run followed by a corresponding nonlinear analysis. The results of both these runs were compared and again the degree of nonlinearity in the response was characterized but this time with respect to thermal loads. Conclusions were drawn from the results to provide guidance to the contract redesign effort regarding both the response of the structure and the conduct of future MAGNA analysis.

A new simulation language named MAGNA (Materially and Geometrically Nonlinear Analysis) was used for this application.[2] Although this finite element code is relatively new, experience is already accumulating in using it for aircraft transparency analysis.[3-8] For this study, MAGNA was used to prepare finite element models of the T-38 student canopy and to perform the linear and nonlinear static analyses mentioned above. The capabilities of MAGNA are described in the next section.

MAGNA Capabilities

The MAGNA computer program was originally developed by the University of Dayton Research Institute, Dayton, Ohio in 1978. Since then it has been tailored under Air Force contracts for use as an aircraft transparency analysis and design tool. This special attention to one Air Force area of application does not limit the utility of MAGNA as a very efficient and effective tool for general three-dimensional nonlinear finite element analysis. Full documentation for the code has been prepared and published for unlimited distribution.[2]

MAGNA is a major system of computer programs for the static or dynamic, linear or nonlinear analysis of complex, three-dimensional structures. It includes preprocessors, a nonlinear finite element analysis package, and a variety of postprocessors. MAGNA employs isoparametric modelling as well as state-of-the-art numerical analysis and programming methods. Available elements include a three-dimensional truss element; quadrilateral plane stress, plane strain, and shear panel elements; an isoparametric eight-node thin shell element; an isoparametric layered shell element; an isoparametric solid eight-node element; an isoparametric curved beam element; an isoparametric solid variable node (up to 27) element and a variable node axisymmetric element. All elements utilize only translational degrees of freedom at boundary nodes and so are fully compatible in three-dimensional space. Time history solutions are performed using Newmark's implicit method

for direct integration of the equations of motion. Each of the available finite elements in MAGNA includes the effects of full geometrical nonlinearities using a Langrangian (fixed reference) description of motion. In shell analysis, arbitrarily large rotations can be treated. Material nonlinearities, in the form of elastic-plastic behavior, are analyzed using a subincremental strategy which minimizes the error in following the material stress-strain curve. Isotropic, kinematic, and combined strain-hardening rules are available for use in plastic analysis with MAGNA. Orthotropic elastic material behavior can also be treated. User-written subroutines can be supplied to define mesh geometry, coordinate systems, initial conditions, and incremental applied loading. Plotting utilities in both interactive and batch forms are also available for generating finite element models and illustrating the results of analyses. Deformed and undeformed geometry plotting are available as are stress, strain, and displacement contour and relief plots.

The first step in any application of the finite element method is discretization and modelling of the structure of interest. This will be described for the T-38 student canopy in the following section.

Structural Modelling

Geometry

Since for the problem of interest both the loads and the structure exhibited symmetry, only half of the structure was modelled to conserve computer resources. The starting point for the modelling task was information regarding the geometry of the structure obtained from the principal manufacturer, Northrop Corporation.[9,10]

The student canopy for the T-38 is a monolithic part fabricated from stretched acrylic 0.23 in. thick with cross sections taken in vertical planes which are circular arcs. The radius of respective cross sections is a function of aircraft fuselage station and the locus of the centers of these circular cross sections is a curved line lying in the aircraft plane of symmetry. The aft edge of the part lies on a vertical cross section but the forward edge lies on a cross section which is canted forward.

A short Fortran computer program was developed from this description of canopy geometry.[9,10] This code was designed to be run interactively and to generate coordinates for nodes lying on the outer surface of the canopy. Nodes were generated in lofting line sequences for successive cross sections. Nodes were numbered from the canopy centerline to the outer edge on each respective lofting line. The inclination of the lofting sections generated varied uniformly from the canted forward edge to the vertical aft edge. The coordinate data generated was in a format required for input to the MAGNA preprocessor.[2]

Initially, coordinates were generated for nodes in a 7 by 3 grid uniformly spaced in the longitudinal and lateral directions, respectively. The data which was generated was for the outer surface of the part.

Discretization

The nodal coordinate data generated as described above was used as input to the MAGNA preprocessor which comprises many modules.[2] First, the CORGEN module was used to generate a coarse two-dimensional grid (surface coordinates), and then the EXPAND module was used to generate through-the-thickness to get a three-dimensional model. The PREP module was used to refine the basic model. The original coarse elements were divided uniformly two or three times around the edges of the canopy. The mesh was designed to be finest at the edges because the highest stresses were anticipated there.

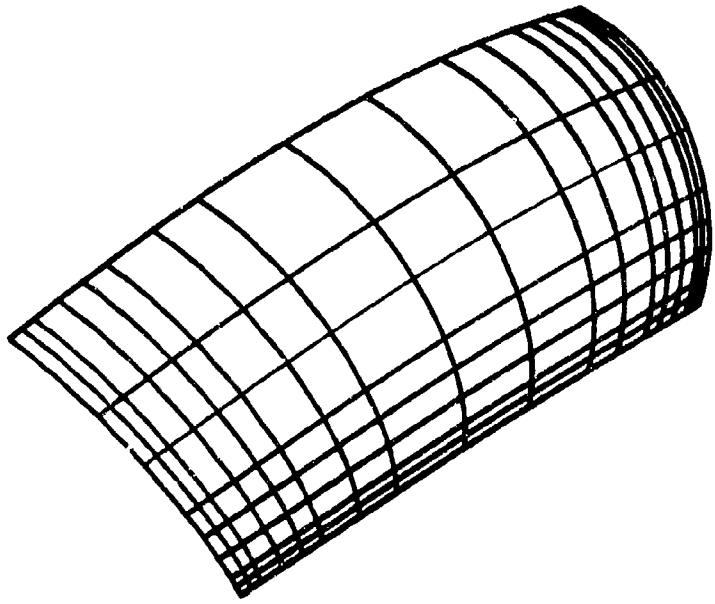

Figure 2. Finite Element Model

The resulting model, shown in Figure 2, had a 17 by 8 grid of 16 node isoparametric solid elements containing 918 nodes. The sixteen node element was chosen to equal or better the performance of a triangular shell element used in similar earlier studies.[11] Previous experience has shown that a 50 element (16 node solid) model can provide accurate displacement results and that a 189 element model (16 node solid) can provide accurate stress results.[6,7] The 136 element "T-38 student canopy" model was used in an attempt to obtain acceptable stresses while minimizing costs driven up by the extensive use of 3x3x3 point Gaussian integration. The 189 element (F-16 canopy) model run earlier used 2x2x2 point Gaussian integration everywhere.[7] The 3x3x3 point Gaussian integration was selected for use in the outer five rows of elements, because the steepest stress gradients were expected at the edges and corners. The remaining interior elements utilized 2x2x2 point Gaussian integration to minimize costs.

Six different sets of boundary conditions were defined and are listed in Table 1. This variety of boundary conditions was used to span the range

from simplistic to realistic. The intent was to determine what level of realism was really necessary for the planned study. On the actual T-38 student canopy, the sill is attached to the frame by a piano type hinge in line with the canopy inner surface. The aft edge carries slotted holes which are open to the aft edge and is clamped by bolts between the aft arch structure and a retaining strip. This clamping action is applied to a strip 1 inch wide. In-plane sliding perpendicular to the aft edge is possible. The forward edge slides into an integral retainer (channel) with no bolts through the thickness. This type of attachment method allows possible in-plane sliding of the canopy in the channel. Boundary condition 6 was intended to represent the actual attachments as closely as possible. Extensive use of linear constraints was made for boundary conditions 3-6. Boundary condition case numbers from Table 1 will be used to refer to a particular model in the remaining text.

Case Number	Boundary Conditions†	UDOF*
1.	Pinned Along the Inner Edge of the Arches	2485
2.	Clamped at the Arches	2385
3.	In-Plane Sliding Along Inner Edge on Both Arches	2581
4.	In-Plane Sliding Along Inner Edge or Forward Arch In-Plane Sliding Perpendicular to Edge Only Along Inner Edge on the Aft Arch	2581
5.	In-Plane Sliding Along Both Edges of the Forward Arch In-Plane Sliding Perpendicular to Edge Only Along Both Edges on the Aft Arch	--
6.	In-Plane Sliding for All Nodes in First Row of Elements at Forward Arch In-Plane Sliding Perpendicular to Edge Only for All Nodes in First Row of Elements at Aft Arch	2591

*UDOF - Unconstrained Degrees of Freedom
†The inner edge of the sill is pinned (see Figure 3) and the canopy centerline has lateral constraints to account for symmetry.

Table 1. Boundary Condition Cases

Material Properties

In general, the mechanical properties of the thermoset plastic materials used in the manufacture of aircraft transparencies are not as well known as those of metallic materials. Only a few handbook type reference sources are available in the literature, and remaining data is fragmented and often unpublished.[12] It is a difficult task to describe the behavior of plastics because their properties are affected strongly by many parameters such as ambient temperature and strain rate.

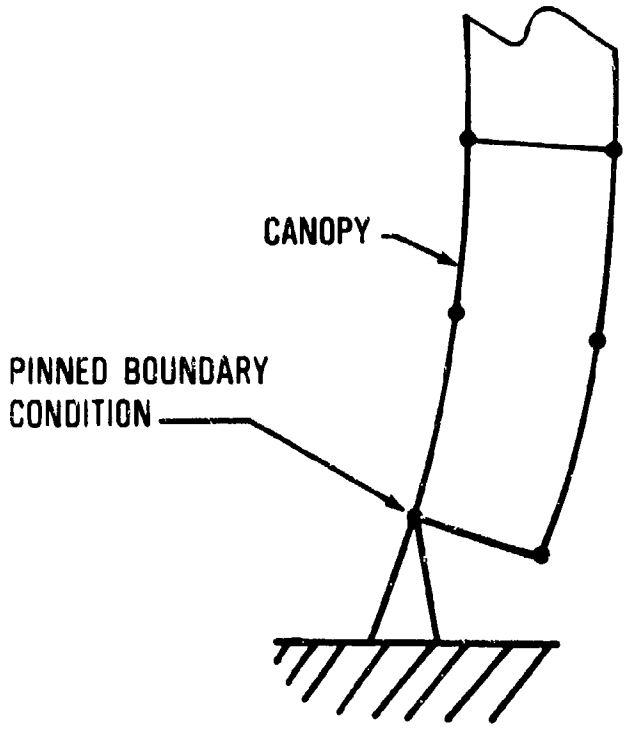

Figure 3. Pinned Boundary Condition

Engineering stress versus engineering strain data was chosen as a starting point to define the mechanical properties of stretched acrylic. (Two transformations of this data are required to change these values to those used by MAGNA: Piola-Kirchoff stress and Green St. Venant strain).[2] The data used was obtained under an ambient temperature of 72°F and a strain rate of 0.05 in./in. min.[13] Figure 4 illustrates the modelled material behavior. This description was used for the materially nonlinear analyses. The Piola-Kirchoff yield stress for stretched acrylic material was 9808 psi. For the elastic analysis, a value of 485000 psi was used for Young's modulus. For all analyses, Poisson's ratio was taken to be 0.35 and the mass density used was 0.000111 lb sec.^{2}/in.^{4}

Load Modelling

Cockpit Pressure

Two cockpit pressure values were used for these analyses. A pressure of 10.0 psig was used for two reasons: because it is the ground pressurization requirement for the T-38, and because it was used in earlier finite element analyses.[11] The second pressurization value of 6.5 psig was used because of its previous use in AFWAL pressure/thermal/fatigue tests and in Northrop pressure tests conducted in 1960.[14,15]

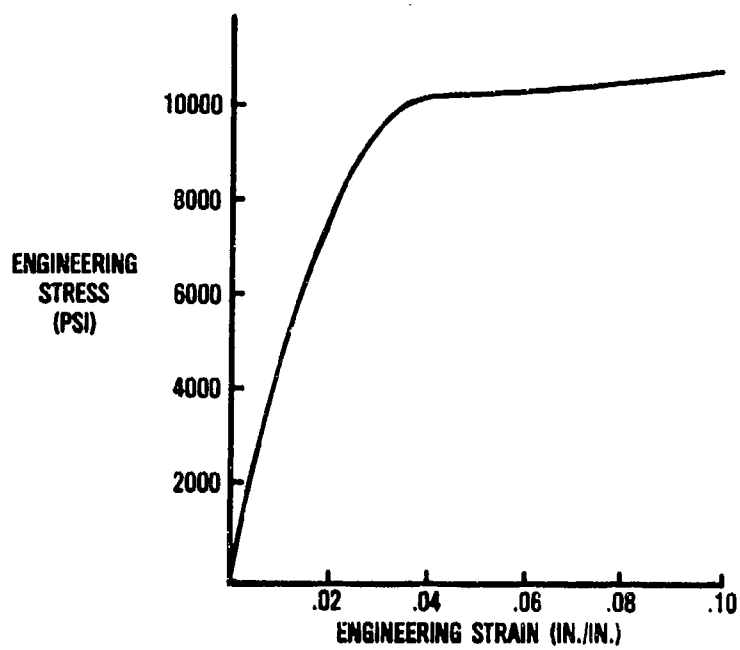

Figure 4. Stress-Strain Behavior of Stretched Acrylic

Canopy Temperatures

The purpose of specifying canopy temperatures was to study the canopy response to thermal loads. The most critical case was thought to be cold soak for which a canopy at altitude would have a steep temperature gradient through the thickness. Since no flight data was available, temperature data recorded in the AFWAL test facility Building 65, Area B, WPAFB, Ohio was used.[14] Temperatures were recorded via thermocouples located at 8 sites on the student canopy (8 on the inside, and a corresponding 8 on the outside). The locations are shown in the schematic in Figure 5. The

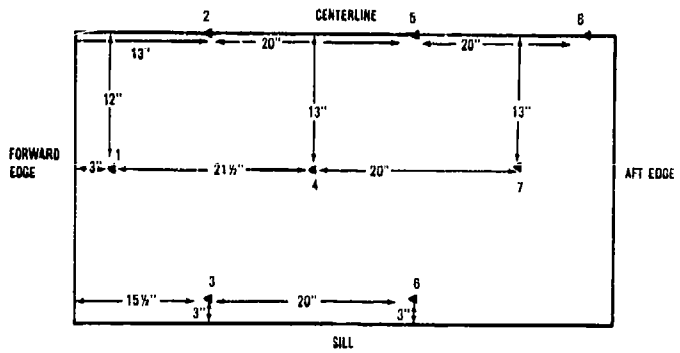

Figure 5. Thermocouple Locations

temperatures which were recorded for a (nominal) -65°F test are shown in Table 2. Over either surface, it can be seen that the distribution of temperatures was relatively non-uniform. Rather than specifying properties of stretched acrylic materials at all the temperatures indicated in Table 2, the properties already determined at 72°F were used in all of the analyses reported herein.

Gage Number	Surface	Temperature (°F)
1	Outer	-43
1	Outer	-33
2	Outer	-41
4	Outer	-36
5	Outer	-61
6	Outer	-48
7	Outer	-59
8	Outer	-81
1	Inner	+1
2	Inner	+17
3	Inner	+1
4	Inner	+10
5	Inner	-15
6	Inner	-2
7	Inner	-13
8	Inner	-40

Table 2. Canopy Surface Temperatures

A quadratic least squares fit was made to the data in Table 2; this was used to interpolate temperature everywhere on the inner and outer canopy surfaces. Figures 6 and 7 illustrate this temperature interpolation over the outer and inner surfaces, respectively. The two independent variables in these figures are distances measured on the surface of the canopy from the centerline and the forward edge respectively.

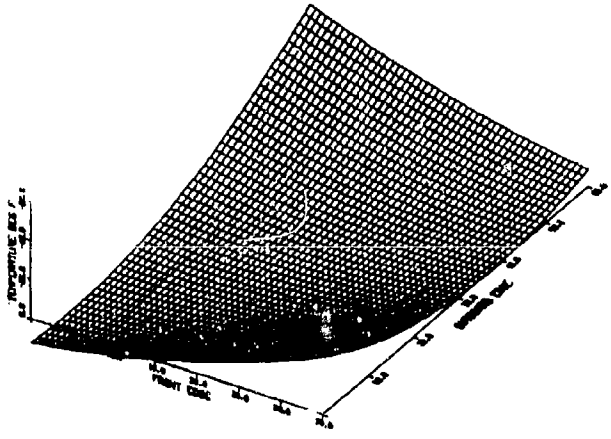

Figure 6. Outer Surface Temperature

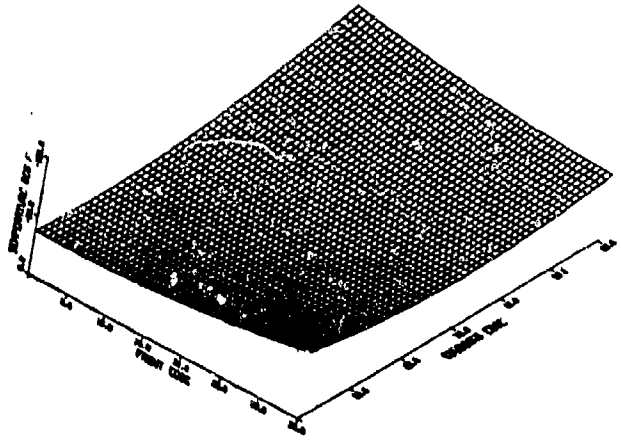

Figure 7. Inner Surface Temperature

A short Fortran code was developed to generate the nodal temperatures for the finite element model. This code computed the surface coordinates of each node in the model, interpolated the temperature at each node from the fits illustrated in Figures 6 and 7, and then placed the temperatures generated into the MAGNA finite element model.

The canopy response to the pressure and thermal loads described above was calculated in various analyses which are discussed in the next section.

Analysis

As was mentioned in the Introduction, the first six analyses conducted were linear static. These analyses applied an internal pressure load of 10.0 psig. All analyses were run with a core size of 350000 octal words on a CDC Cyber 750 at the ASD Computer Center on Wright-Patterson AFB, Ohio. All analyses also included stress averaging (extrapolating integration point values to the model nodes and averaging the values at the nodes). MAGNA uses an out-of-core, variable bandwidth (skyline) solution technique. The execution parameters of these six analyses are listed in Table 3. The execution parameters were not available for boundary condition 5.

Analyses 7 through 10 used the same boundary conditions as Analysis 6 (boundary condition case number 6). The seventh analysis was identical to the sixth analysis but with material and geometric nonlinearities taken into account. Pressure loads were applied in two steps for this nonlinear static analysis. Increment one applied 5 psig to the structure with increment two increasing the pressure to 10 psi. This analysis used the full nonlinear element stiffness formulation in conjunction with a noniterative solution option available with MAGNA (pseudo-force approach).[2] When utilizing this pseudo force approach in MAGNA nonlinear analysis, it is necessary to monitor the balance between externally applied loads and the internal

stresses being calculated. A parameter called FNORM is a measure of this force balance and is printed in the normal MAGNA output. Analysis 7 ran with an FNORM value of 1.1 which indicates an acceptable quality solution.

Analysis 8 was a linear static run with an applied pressure load of 6.5 psig and nodal temperatures as described in the Load Modelling section. Increment one applied the temperature loads and increment two applied the pressure loads along with the temperature loads.

Analysis 9 was a nonlinear static version of Analysis eight. Material and geometric nonlinearities were taken into account. Altogether, forty-eight load steps were used. The first forty increments gradually applied the temperature loads and the last eight increments were used to add on the pressure loads. The restart feature of MAGNA was used with the first five increments. A complete restart record was written after every normally completed increment.[2] There are two benefits to using restart; the first is to reduce job size permitting daily turnaround, and the second is to provide the opportunity to scrutinize the nonlinear solution at frequent intervals. This ability to examine each job permits adjustment to the solution parameters, minimizing the required computer resources. The full nonlinear element stiffness formulation was employed as for the seventh analysis but this time using full Newton-Raphson iteration. With this iteration technique, the system stiffness matrix is reformed for each iteration, making convergence as strong as possible.[2] Using this scheme, convergence (FNORM < 0.1) was obtained in about three iterations per increment. The solution hit a CP time limit and completed normally only three increments.

From the times indicated in Table 3, nonlinear analysis with pressure and thermal loads would require approximately 200 times more CP time and 100 times more IO time than linear analysis - very costly. For the case of cockpit pressure loads, the cost of the nonlinear analysis (Analysis 7) was only about twice that of the linear analysis (Analysis 6). It would appear that nonlinear analysis of thermal loads is extremely expensive for this case.

A second job was submitted for the ninth analysis, this time using the average nonlinear element stiffness formulation and the combined iteration rule. These changes were made to reduce the cost of the simulation as much as possible. The job was started at increment 3 of the previous analysis by using the restart feature. The restart was successful with the fourth (from the beginning of the two-job analysis) increment converging in three iterations. In the fifth increment, however, FNORM oscillated wildly and the solution diverged. Two remaining alternatives for accomplishing a successful solution included: returning to full nonlinear stiffness formulation and Newton-Raphson iteration, or going to even smaller loading increments. Both of these options were regarded as being non-viable due to the prohibitive cost involved. As a result the ninth analysis was stopped at this point.

Analysis Number	Applied Loads	Analysis Type	Boundary Condition Case Number	Number of Stiffness Matrix Partitions	Maximum Half Bandwidth	Average Half Bandwidth	CP Seconds	IO Seconds
1	10.0 psig Pressure	Linear	1	11	360	145	141	707
2	10.0 psig Pressure	Linear	2	10	357	140	131	667
3	10.0 psig Pressure	Linear	3	11	368	146	146	726
4	10.0 psig Pressure	Linear	4	11	368	146	146	726
5	10.0 psig Pressure	Linear	5	—	---	---	---	---
6	10.0 psig Pressure	Linear	6	11	368	146	146	716
7	10.0 psig Pressure	Fully Non-linear	6	11	368	146	344	1026
8	6.5 psig Pressure/ Thermal Loads	Linear	6	11	368	146	172	700
†9	6.5 psig Pressure/ Thermal Loads	Fully Non-linear	6	11	368	146	2000 (1675)	4307 (2659)
†10	6.5 psig Pressure/ Thermal Loads	Geometrically Nonlinear	6	11	368	146	477	1705

( ) - Second job for Analysis Number 9.
† - Not successfully completed.

Table 3. Execution Parameters

The tenth analysis was another attempt to do a nonlinear static version of Analysis eight. The difference between Analyses 9 and 10 was that with 10, only geometric nonlinearities were included. Material behavior was assumed to be linearly elastic. This was intended to determine whether the severe nonlinearities detedted in Analysis 9 were primarily material or geometrical. Temperatures were applied in 4 uniform increments and pressure loads were added in 2 subsequent increments. The restart feature was used with the first four increments. Average nonlinear element stiffness formulation and combined iteration options were used. Increment one converged, but increment two developed a rash of non-positive pivots and the solution diverged. This indicates that the nonlinearities present were primarily geometrical.

The results of each of the ten analyses conducted are discussed in the next section.

Results

One parameter which is included in the MAGNA output listing is the Von Mises equivalent stress.[2] This represents the three-dimensional state of stress at a point as an equivalent state of uniaxial tension. Figure 8 illustrates the distribution of equivalent stress over the inner surface of the canopy resulting from Analysis 1. Analysis 1 is the linear static

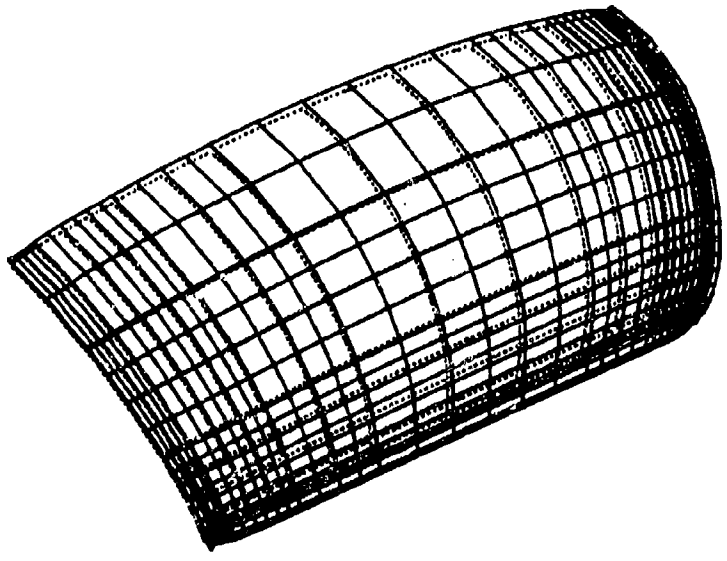

Figure 8. Equivalent Stress Relief Map Analysis 1

canopy response to 10 psig pressure for boundary condition number one. The dotted lines in the figure represent the undeformed inner surface of the canopy. The distance of the solid mesh from the dotted mesh indicates the magnitude of the equivalent stress computed at any given point. Figure 8 shows a very uniform distribution of equivalent stress over the surface except in the area of the sill where it is approximately three times greater than elsewhere (maximum 1280 psi). Plots of the outer surface (not shown) are similar except for the area along the sill where the equivalent stress is very low. Figure 9 shows a plot of the undeformed canopy geometry superimposed on the deformed geometry scaled up by a factor of 100. The dotted lines represent the deformed geometry. This figure clearly illustrates rotation about the pinned edges, bulging out of the crown area, and folding inward of the sides near the sill.

An equivalent stress relief map is shown in Figure 10 for the second analysis with clamped arches. This is an illustration for the inner surface of the canopy and shows essentially the same results as for Analysis 1. The maximum equivalent stress is equal to 1270 psi. The deformed geometry results were also very similar to those from Analysis 1 with the exception that no rotation was permitted at either arch.

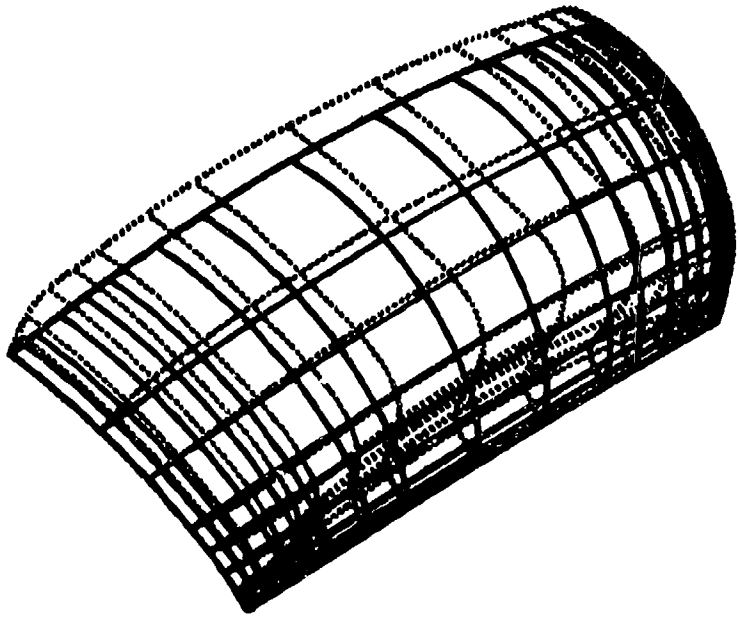

Figure 9. Deformed and Undeformed Geometry Analysis 1

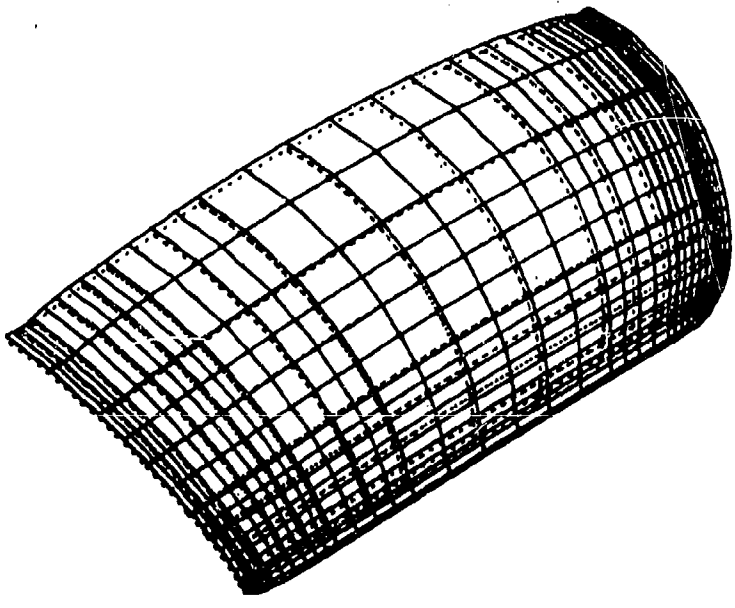

Figure 10. Equivalent Stress Relief Map Analysis 2

Analysis number 3 permitted in-plane sliding of the inner surface edges of the canopy on both forward and aft arches. Figure 11 illustrates the calculated equivalent stress on the inner surface of the canopy. These results vary significantly from those obtained for boundary conditions 1 and 2. Very high peaks of equivalent stress (maximum of 11600 psi) were indicated in both the forward and aft corners of the transparency with the forward corner being worst. Stresses along both arches were also considerably higher than for the first two cases. Apparently, stress at the canopy periphery is very sensitive to the motion of the canopy at the arches, especially so in the corners. Figure 12 shows a close-up view of the forward arch area at the centerline. The dotted lines show canopy rotation (scaled up by 100) about the inner edge under the action of cockpit pressure and the translation of the inner edge in-plane. No lateral motion of the centerline is permitted as a result of the boundary conditions applied there to account for symmetry. Motion parallel to the forward edge was seen for other areas of the forward edge.

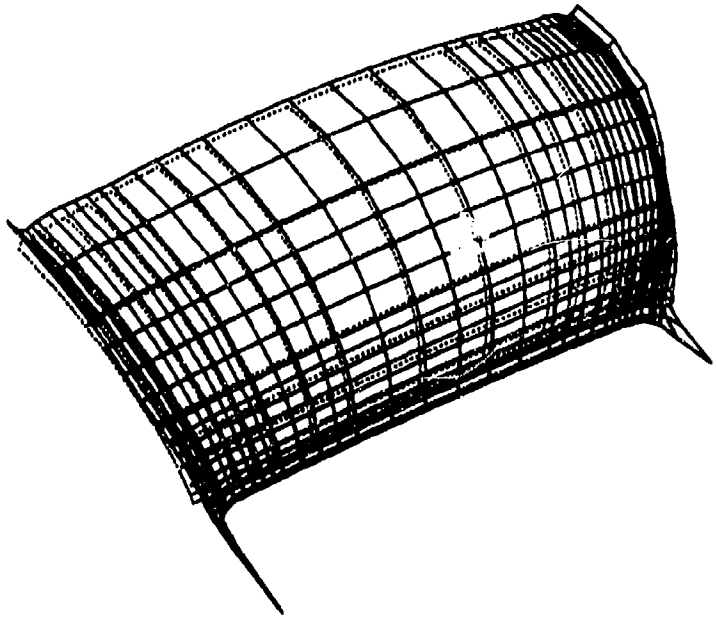

Figure 11. Equivalent Stress Relief Map Analysis 3

Analysis 4 was the same as 3 except that the nodes along the inner edge of the aft arch were only permitted to move along lines normal to the aft edge, thus corresponding to slotted holes. Figure 13 shows the equivalent stress relief map for the inner canopy surface. The stress peak which was observed in the aft corner for Analysis 3 has disappeared. The maximum equivalent stress in the forward corner is 8680 psi. This stands as additional evidence that stress in the corners is extremely sensitive to the boundary conditions which are applied to the arches. Figure 14 is a closeup view of the aft edge of the model. Rotation about the inner edge under the

action of pressure is shown along with translation of a node on the inner edge along a longitudinal grid line.

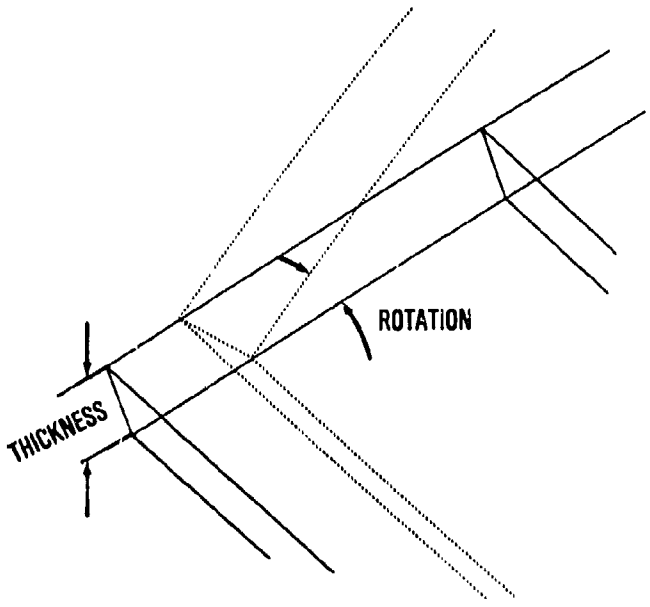

Figure 12. Deformed and Undeformed Geometry Forward Edge Analysis 3

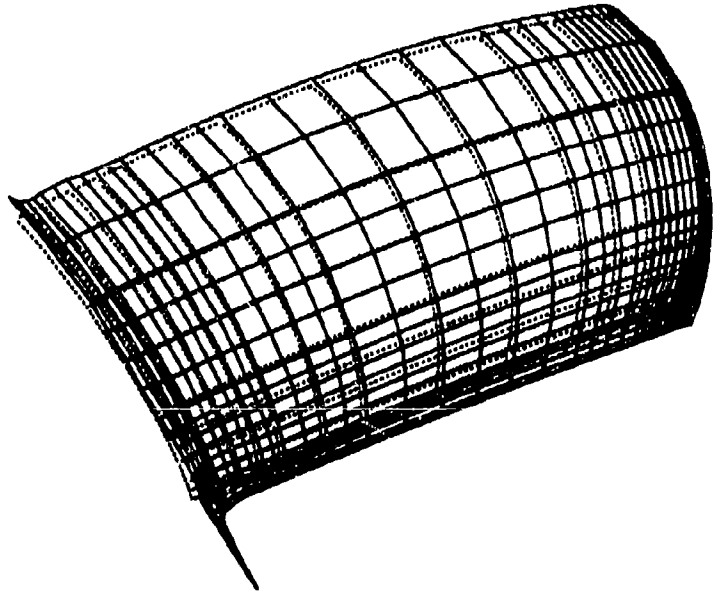

Figure 13. Equivalent Stress Relief Map Analysis 4

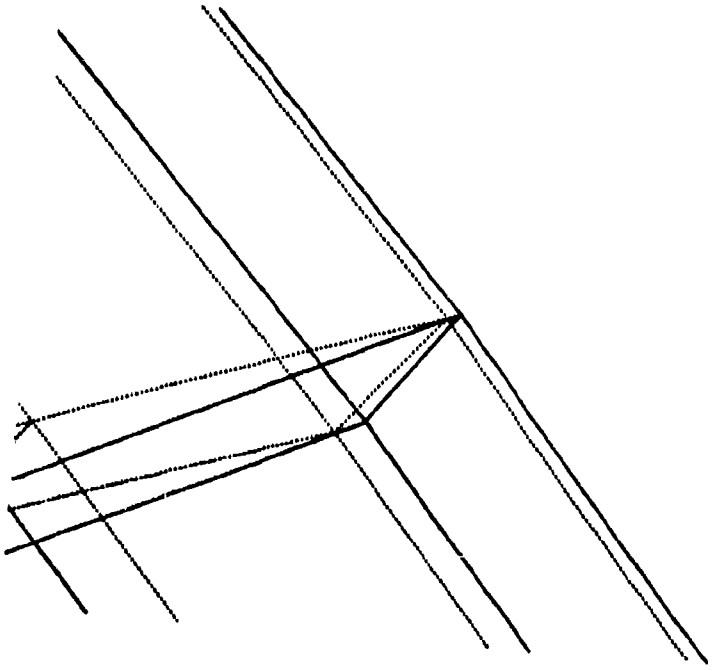

Figure 14. Deformed and Undeformed Geometry Aft Edge Analysis 4

The results of Analysis 5 are not shown because they were virtually identical to the results of Analysis 4. Adding linear constraints to permit only in-plane motion of the nodes along the outer edge of the arches had no effect because the same was already true, by definition, of the linear solution performed for Analysis 4.

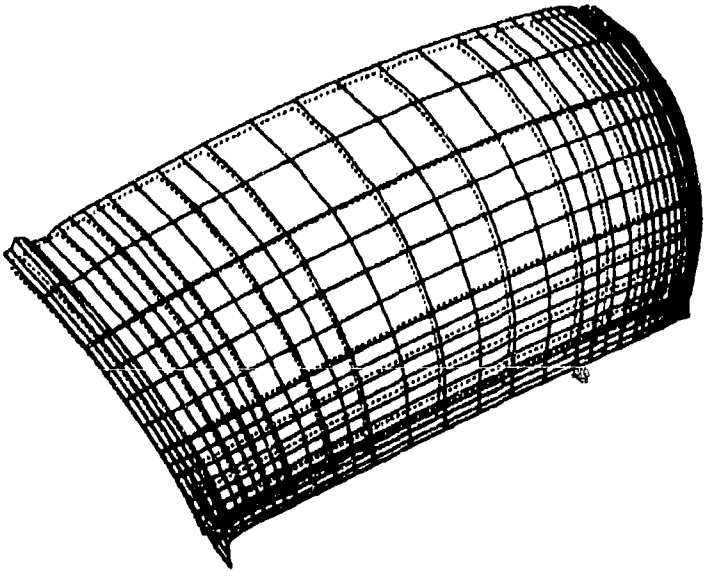

Figure 15. Equivalent Stress Relief Map Anaysis 6

The most realistic boundary conditions (boundary condition case number 6) were investigated in Analysis 6. Figure 15 shows the equivalent stress relief map of the inner canopy surface. The very sharp peaks of Figure 11 (Analysis 3) at both the forward and aft corners are absent in this figure, although a small peak remains at the forward corner. The maximum equivalent stress for the peak was 3680 psi. The sliding clamp action defined over the narrow strips of elements at the forward and aft edges was very effective in reducing high stresses in the corners. Figure 16 is a close-up of the forward edge at the centerline. The dotted lines show the canopy sliding in-plane and bending outside the first row of elements where the boundary

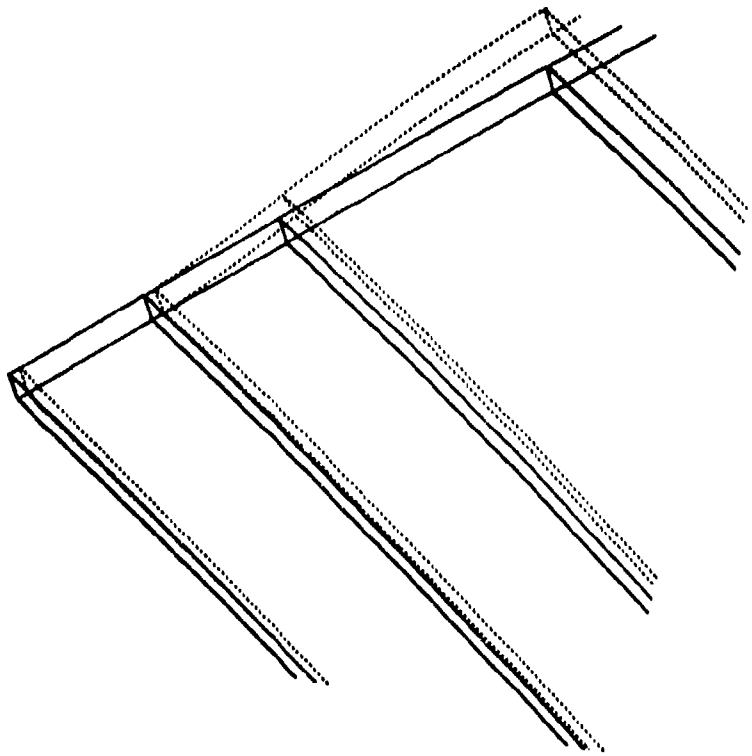

Figure 16. Deformed and Undeformed Geometry Forward Edge Analysis 6

conditions were applied. Figure 17 is a close-up of the aft edge of the canopy at the centerline. This figure illustrates deformation similar to that seen at the forward edge.

Analysis 7 was a fully nonlinear version of Analysis 6. This analysis included both material and geometrical nonlinearities, and was intended to indicate the significance of any nonlinearities present. Figure 18 shows the equivalent stress relief map for the inner canopy surface. The results shown in this figure are for increment 2 at 10 psig cockpit pressure. The results of this analysis are nearly identical to those for Analysis 6 (Figure 15). The maximum equivalent stress was 3440 psi. Apparently, any nonlinearities that are present, material or geometric, are quite insignificant. In other words the response is primarily linear and since the maximum stress resulting from 10 psig pressure was only 3440 psi, the

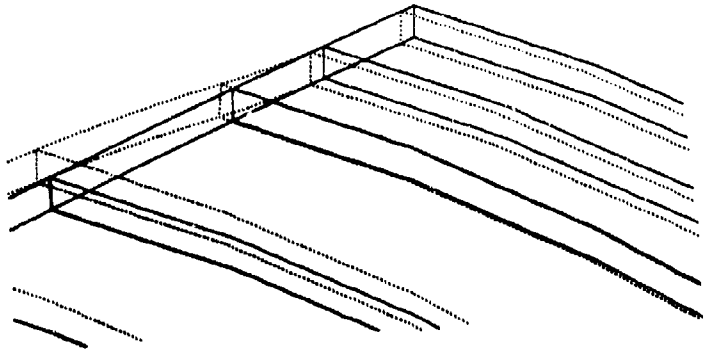

Figure 17. Deformed and Undeformed Geometry Aft Edge Analysis 6

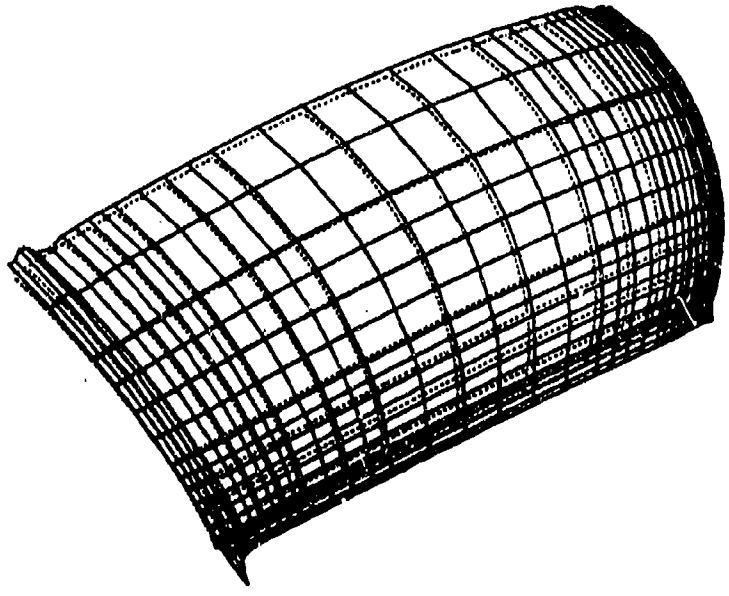

Figure 18. Equivalent Stress Relief Map Analysis 7

canopy can probably withstand more than 20 psig without rupturing (Yield strength is 10,000 psi.). Figure 19 shows a contour plot of normal displacements for the outer canopy surface. The innermost contour on the centerline represents 0.05 in. and includes the region of greatest displacements. The interval between contours is 0.005 in. The maximum normal displacement is less than 0.055 in. and occurs on the centerline in the forward portion of the canopy.

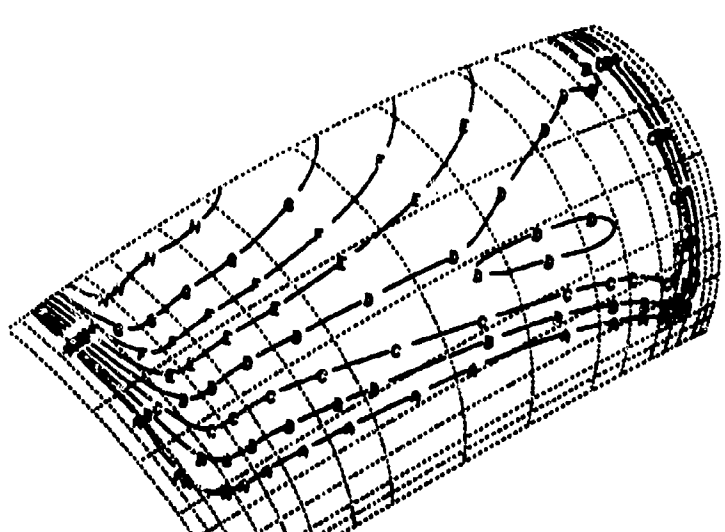

Figure 19. Normal Displacement Contour Map Analysis 7

Analysis 8 was a linear static analysis for both pressure and thermal loads. Figure 20 illustrates the equivalent stress relief map for the inner canopy surface resulting from Analysis 8. Elevated stresses are indicated all around the periphery of the canopy with the highest values occurring

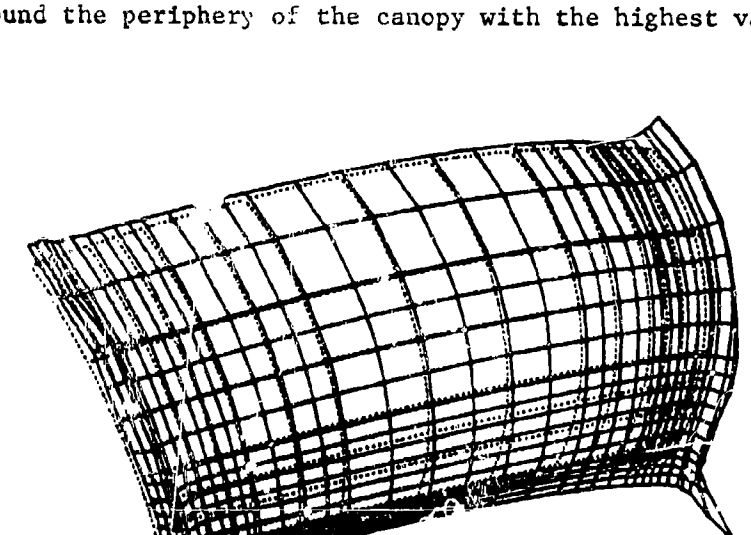

Figure 20. Equivalent Stress Relief Map Analysis 8

along the aft arch and at both corners. Maximum equivalent stress occurs at the forward corner and has a value of 10800 psi. Analysis 8 employed the same boundary conditions as Analyses 6 and 7, so Figure 20 can be compared directly with Figures 15 and 18 to measure the effect of adding thermal loads. Results for the second load case included in Analysis 8 (temperature only - no pressure) were virtually identical to those shown in Figure 20 with the maximum equivalent stress being 9120 psi. This means that the thermal loads are by far the more critical of the two load types.

No conclusions should be drawn regarding the failure of the stretched acrylic material in the canopy corners because the magnitudes of the very sharp spikes in stress are invalid. The study of stress at the corners under combined thermal and pressure loads would require additional analyses with a refined mesh at these locations.

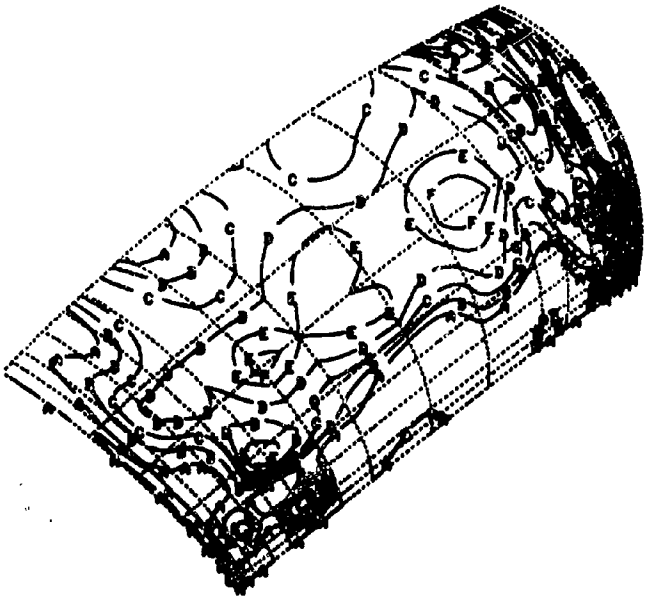

Figure 21. Normal Displacement Contour Map Analysis 9

Analyses 9 and 10 were not successful and for this reason final results can not be illustrated. Figure 21 shows a contour map of normal displacements for one of the few analysis increments which was accomplished. The contour map indicates local buckling behavior all over the part which explains the structural instability indicated by the results of the nonlinear solution. Six non-positive pivots occurred at nodes scattered over the central region of the mesh. This behavior indicates that the results are not peculiar to the unusual boundary conditions being applied but are due primarily to the presence of thermal loads and the rate at which they are being applied. If this response is typical of aircraft

transparencies subjected to in-flight or runway (non-flight) thermal loads, then the difficulty encountered in nonlinear finite element analysis with MAGNA may represent a fundamental and very general problem. Future studies planned with this and other aircraft transparency systems will answer this question.

Correlation

Originally, the intended use of MAGNA for this work effort was to accomplish a strictly theoretical investigation into the structural response of the T-38 student canopy to internal cockpit pressurization and thermal loads. As the MAGNA studies progressed, however, other analytical and experimental work efforts relevant to these MAGNA analyses became known.[11,14,15] Comparisons will be made whenever possible with the other results to establish as much confidence as possible in the results reported herein.[11,14,15]

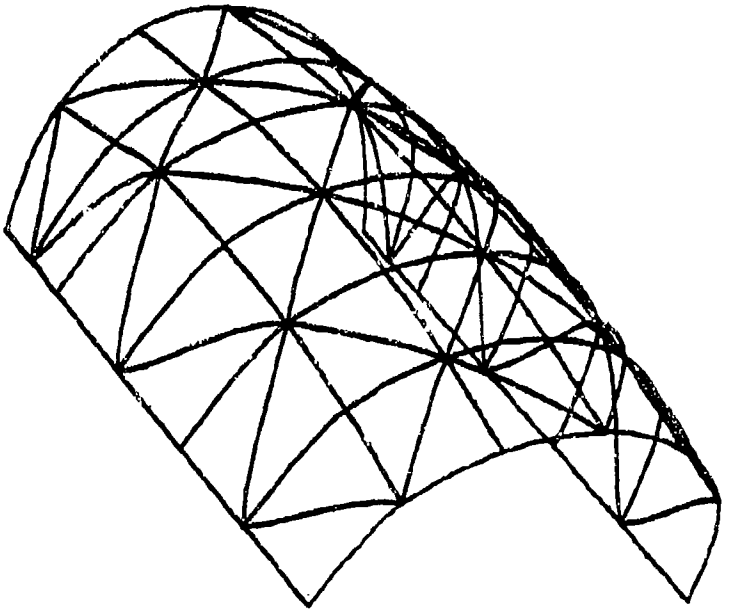

Figure 22. MARC Finite Element Model

The MARC finite element computer code has been used to analyze the pressure/thermal response of the same structure.[11] A model of the entire canopy, shown in Figure 22, was used which contained 72 isoparametric triangular shell elements with 49 nodes. The acrylic sheet was assumed to behave as an isotropic, elastic-plastic material with a load carrying capacity based on Von Mises yield criterion. A yield tensile stress of 9000 psi, modulus of elasticity of 4.25×10^5 psi and plexiglas sheet

thickness of 0.23 in. were used in all model simulations. The yield stress is the minimum specification of methylmethacrylate and the sheet thickness is typical of the T-38 student canopy. During each simulation, integration was performed in each of three layers through the thickness of the acrylic. With seven integration points per layer, the elastic-plastic analysis entailed structural analysis at twenty-one locations for each of the mesh elements. A variety of boundary conditions were applied in the MARC studies to determine appropriate condition, as for the studies reported here. The set of boundary conditions adopted for use in the MARC studies was very similar to boundary condition 6 described above.[11]

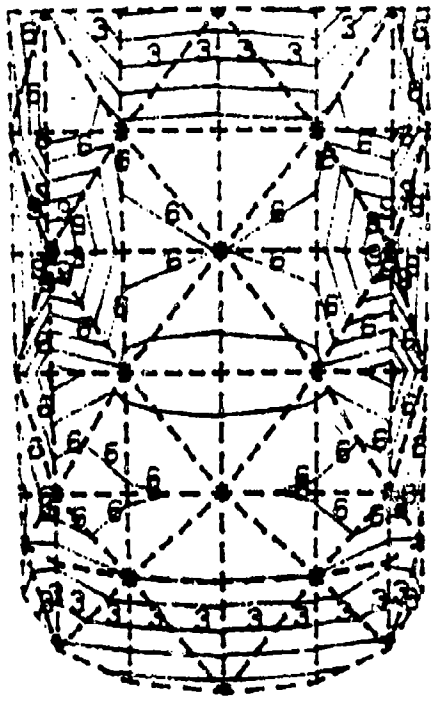

Figure 23. MARC Equivalent Stress Contour Map 10.0 PSIG Cockpit Pressure

One of the load cases treated in the MARC studies was a uniform cockpit pressure of 10.0 psig. The equivalent stress contour map of this MARC analysis is shown in Figure 23. It may be compared to Figure 18 since both represent results of similar analyses. The maximum equivalent stress in the MARC results was 3390 psi, while the MAGNA results showed 3440 psi. Both show high levels of stress along the sills with MAGNA showing a much more uniform distribution of the stress. This was expected since the MAGNA model has many more degrees-of-freedom in addition to the use of solid elements as opposed to the MARC triangular shell elements. Figure 23 seems to show areas of maximum stress at two poles a few inches above the sill, about two thirds back from the forward edge. It was reported, however, that the maximum MARC equivalent stress actually occurred in the aft corner canopy elements. Figure 18 shows the MAGNA peak stress occurring in the forward

corner. These differences may be due to the fact that the MARC results represent the central layer in the canopy while the MAGNA results are for the inner surface. These two types of results should agree over most of the canopy where the primary action is in-plane, but not along the sill and at the corners, where a three dimensional state of stress exists.

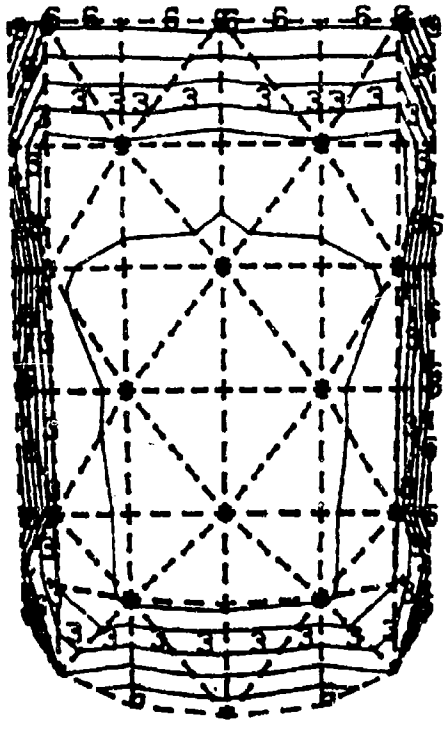

Figure 24. MARC Equivalent Stress Contour Map Thermal Loads

Another load case treated in the MARC studies was thermal loads without cockpit pressure. A uniform inner surface temperature of 140°F and a uniform outer surface temperature of 170°F were assumed. Figure 24 is a contour map of the equivalent stress resulting from this MARC analysis.[11] Figure 24 can be qualitatively compared to Figure 20 because both illustrate response to thermal loads; the MARC case - nonuniform hot, and the MAGNA case - nonuniform cold. Both show steeper gradients of stress along the sill than for pressure loads only and stress spikes in all corners. The peak MAGNA stress is 9120 psi while the peak MARC stress is only 2980 psi probably due primarily to the fact that the temperature fields assumed are so much different. Both figures indicate that stresses in the corner regions are sensitive to thermal loading.

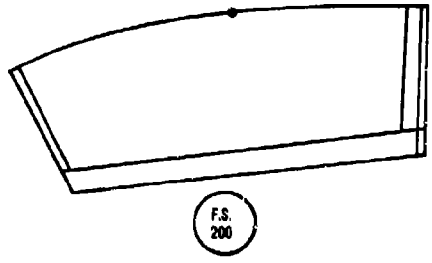

Figure 25. Point for Displacement Data

Tests have been conducted on full scale T-38 transparency systems to measure deflection due to cockpit pressurization at an ambient temperature.[15] The test setup included a complete transparency system mounted on a forward fuselage section with actual aircraft locks and hooks. One test condition was 6.5 psig cockpit pressure at a uniform temperature of 80 degrees F. One point at which normal deflection was measured is shown in Figure 25 - fuselage station 200.0 on the centerline.[15] The deflection measured at this point was 0.088 in. under 6.5 psig. Figure 19 shows the normal displacement contours predicted by MAGNA for 10.0 psig cockpit pressure. It indicates a normal displacement for the same region of the canopy of approximately 0.044 in. The experimental deflection data was expected to be greater because, in the test, the entire canopy frame would be free to deform under pressure, restrained only by its locks and hooks.

Finally, tests have been conducted on full scale T-38 transparency systems to measure transparency strains in response to combined cockpit pressure and (simulated in-flight) thermal loads.[14] In fact, Analyses 8, 9, and 10 were specifically intended to simulate one of these tests. A test was actually accomplished with the surface temperature distributions described in Table 2 and used in Analyses 8, 9, and 10 (Analyses 9 and 10 were ultimately unsuccessful). No strain data for this test was acquired, however, a second test was conducted during which canopy strains were successfully measured but the temperature distributions for this test were much different than for the first test. Table 4 lists the temperatures measured during the second test for the thermocouple locations shown in Figure 5. Unfortunately, time did not permit a repeat of Analysis 8 with the new temperature data, so only qualitative comparisons can be made. Figure 26 is a strain contour map resulting from Analysis 8 for the outer surface of the forward corner of the canopy. The component of strain illustrated is in-plane, parallel to the sill of the canopy. The contour nearest the arch has a value of -0.004 in./in., the last contour along the sill has value -0.0004 in./in., and the interval between contours is 0.0004 in./in. The location of a strain gage rosette used during testing is also indicated on the figure.[14] The contour map indicates strain values between -0.0036 and -0.0032 in./in. in the vicinity of the strain gage

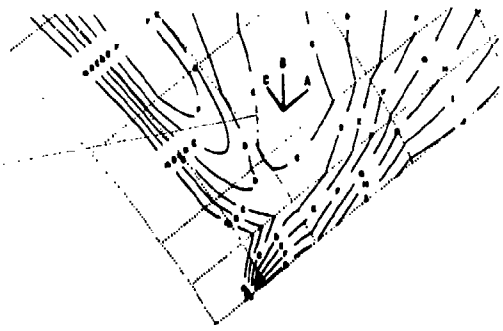

Figure 26. E_{yy} Strain Contour Map Analysis 8

rosette. The value reported for leg A of the rosette during testing was -0.0004 in./in. The sign of both the experimental and the computed strains are the same with the experimental value being smaller. This would be expected because the temperature distribution were similar in the two cases but the temperatures were less severe in the test than those represented in the MAGNA analysis. Figure 27 is the same as 26 with the exception that the component of strain illustrated is parallel to the forward arch of the canopy rather than the sill. The outermost contour has value 0.0 in./in. while the innermost has value +0.0032 in./in. with a contour interval of 0.0004 in./in. The figure indicates strain values between 0.0 an -0.0004 in./in. in the vicinity of the strain gage rosette. The value reported for leg C of the rosette during testing was 0 in./in. This close agreement would be expected even though temperatures differed in the two cases because the temperature distributions were similar. That is to say, zero strains would be expected to occur in the same locations for similar temperature distributions involving different temperature magnitudes; non-zero strains would be expected to agree in sign but not in magnitude under the same circumstances. Conclusions which were drawn from this discussion of correlation between experimental and computed data as well as from the results discussed earlier will be listed in the next section.

Figure 27. E_{zz} Strain Contour Map Analysis 8

Table 4. Canopy Surface Temperature

Gage Number	Surface	Temperature (°F)
1	Inner	-23
2	Inner	-2
3	Inner	-7
4	Inner	-3
5	Inner	-9
6	Inner	-8
7	Inner	-5
8	Inner	-2
1	Outer	-60
2	Outer	-53
3	Outer	-54
4	Outer	-42
6	Outer	-43
9	Outer	-57
7	Outer	-44
8	Outer	-39

Conclusions

The conclusions will be presented in two groups. The first group of conclusions is intended for those individuals involved in the current Flight Dynamics Laboratory program for the development of improved T-38 transparent crew enclosures. The second group of conclusions is aimed at any organization considering the use of MAGNA for similar analyses.

The following are conclusions pertaining to the Flight Dynamics Laboratory development in progress for improved transparent crew enclosures for the T-38 aircraft:

1. The current production T-38 student canopy, when properly rigged and mounted in its frame with no misalignment, can be expected to withstand more than 20 psig without rupturing. This same conclusion had been reached as a result of earlier studies with another finite element computer program.[11]

2. Thermal loads on the order of -65 degrees F are much more critical from a material strength standpoint than are cockpit pressure loads on the order of 10.0 psig. Elevated stresses occur all along the canopy periphery as a result of these thermal loads with very high stresses existing in all four corner regions. The maximum stress for the temperature distributions which were considered occurs in the canopy forward corners.

3. Consideration should be given in the development of improved T-38 aircraft transparencies to providing more fixity in mounting the student canopy transparency along the forward and aft arch structures. Increased fixity would relieve stress concentrations which occur at all four canopy corners as a result of cockpit pressure and in-flight (cold) thermal loads. Caution should be used in implementing this recommendation since the

method chosen to increase fixity at the arches might in itself generate new stress concentrations. An example might be interference between bolts and imprecisely located bolt holes; stresses resulting from such circumstances have not been treated in the MAGNA analyses reported here.

The following are conclusions pertaining to the use of MAGNA in studying the response of the T-38 stretched acrylic student canopy to cockpit pressure and (cold) thermal loads:

1. The calculated stresses in the forward and aft corner regions are extremely sensitive to the definition of boundary conditions along both the forward and aft arches.

2. The most appropriate definition of boundary conditions for the canopy along both the forward and aft arches is the sliding clamp defined as Boundary Condition 6, Table 1. A very similar boundary condition has also been suggested as the result of earlier work.[11]

3. The results of geometrically and materially nonlinear analysis are essentially the same as those of linear analysis for 10.0 psig cockpit pressure loads. In other words, linear analysis is sufficient for the study of canopy response to cockpit pressure loading; the nonlinearities involved in this case are relatively insignificant.

4. Accurate stress analysis at the canopy corners for the thermal load case will require a finite element mesh which is even finer than the one used for these studies (i.e., finer at the canopy corners).

5. It is possible that geometrically nonlinear analysis of spatially nonuniform thermal loads for any aircraft transparency system might prove very difficult technically due to the locally buckled response of the structure indicated by these MAGNA analyses. It would seem that an accurate simulation of any such structural instabilities occurring would be required in order to accomplish useful stress analysis. The cost of realistic simulation using an implicit finite element formulation such as MAGNA could be prohibitive.

6. The comparisons of MAGNA results to experimental results discussed in the Correlation Section increase confidence in the use of MAGNA for similar analytical studies in the future.

References

1. West, B. S., and Clayton, K. I., Alternate T-38 Transparency Development Part I Initial Analysis and Design, Air Force Wright Aeronautical Laboratories, Wright-Patterson Air Force Base, Ohio 45433, AFWAL-TR-80-3132, Part I, November 1980.

2. Brockman, R. A., MAGNA: (Materially and Geometrically Nonlinear Analysis) Part I, II, III and IV, Air Force Wright Aeronautical Laboratories, Wright-Patterson Air Force Base, Ohio 45433, AFWAL-TR- 82-3098, Part I, Part II, Part III, and Part IV, December 1982.

3. McCarty, R. E., and Venkayya, V., Analysis of Bird Impact on Port Wing, Air Force Wright Aeronautical Laboratories, Wright-Patterson Air Force Base, Ohio 45433, Letter Report, 24 August 1979.

4. McCarty, R. E., "Computer Analysis of Bird Resistant Aircraft Transparencies," Proceedings of the 17th Annual SAFE Symposium, December 1979, Las Vegas, Nevada.

5. McCarty, R. E., "Finite Element Analysis of F-16 Aircraft Canopy Dynamic Response to Bird Impact Loading," 21st AIAA/ASME/ASCE/AHS Structures, Sructural Dynamics, and Materials Conference, May 1980, Seattle, Washington.

6. McCarty, R. E., "Aircraft Transparency Bird Impact Analysis Using the MAGNA Computer Program," Conference on Aerospace Transparencies Sponsored by the Society of British Aerospace Companies, September 1980, London, England.

7. McCarty, R. E., "Finite Element Analysis of a Bird-Resistant Monolithic Stretched Acrylic Canopy Design for the F-16A Aircraft, "AIAA Aircraft, Systems and Tecnology Conference, August 1981, Dayton, Ohio.

8. McCarty, R. E., and Smith, R. A., "Finite Element Analysis of Through the Canopy Emergency Crew Escape from the T-38 Aircraft," 23rd AIAA/ASME/ASCE/AHS Structures, Structural Dynamics, and Materials Conference, May 1982, New Orleans, Louisiana.

9. Northrop Drawing No. 2-13005, Northrop Corporation, Aircraft Group, One Northrop Avenue, Hawthorne, California 90250.

10. Northrop Report No. 57-84, Northrop Corporation, Aircraft Group, One Northrop Avenue, Hawthorne, California 90250.

11. Labra, J. J., T-38 Forward Canopy Response to Pressure and Thermal Loads, Southwest Research Institute, San Antonio, Texas 78284, SWRI Project 03-6156-002, September 1980.

12. Military Standardization Handbook - Plastics for Aerospace Vehicles,Part II Transparent Glazing Materials, MIL-HKBK-17A, Part II, 8 June 1977.

13. Typical Physical Properties of Swedlow Stretched Acrylic (MIL-P-25690) Sheet-Swedlow Type 350S, Swedlow Inc, Transportation Products Division, Garden Grove, California 92645, Engineering Bulletin No. MP-3-100. 4 April 1973.

14. Lowndes, H. B. III, T-38 Transparency Test Strain and Temperature Data, Flight Dynamics Laboratory, Wright-Patterson AFB, Ohio 45433, Letter Report, 3 November 1982.

15. Shirreffs, W. G., Qualification Test of T-38 Cockpit Enclosure System for Structural I.D.E. Approval, Northrop Corporation, Hawthorne, California, NOR-61-235, October 1961.

AD-P003 232

PARAMETRIC STUDIES OF THE T-38 STUDENT WINDSHIELD USING THE FINITE ELEMENT OF CODE MAGNA

R. NASH, University of Dayton

PARAMETRIC STUDIES OF THE T-38 STUDENT WINDSHIELD USING THE FINITE ELEMENT CODE MAGNA

Richard Nash

University of Dayton
Research Institute

ABSTRACT

The parametric studies examine the effect of structural variations on the nonlinear dynamic response of the T-38 student windshield/support structure system to bird impact. The studies were conducted using the MAGNA (Materially And Geometrically Nonlinear Analysis) finite element computer program. Both static and dynamic analyses were performed, examining the effects of changes to the transparency stiffness and intensity of the applied load, both coupled and uncoupled. Significant results of the finite element analysis include transparency deflection, peak load versus transparency stiffness, and resultant force plots along the aft arch. A discussion of the application of the finite element method to the birdstrike problem is also presented.

INTRODUCTION

With the increased use of the T-38 aircraft in low level flight, the problem of birdstrike becomes a primary concern in regard to possible loss of life and aircraft. The present impact capability of the T-38 aircraft student windshield is 190 knots. This has been verified using a four pound bird impacted along the centerline of the T-38 student windshield[1] (Figure 1). This capability seems to be adequate during low speed landings, but for high speed, low level flight, it is not.

The purpose of this paper is to familiarize the reader with the application of the finite element technique to the design of a bird resistant T-38 student windshield. The study was performed using the finite element code MAGNA[2] (Materially And Geometrically Nonlinear Analysis). A brief discussion of the finite element method is presented along with a presentation of the T-38 student windshield parametric studies.[3] Typical results are shown for the 0.60 inch thick baseline acrylic T-38 student windshield.

FINITE ELEMENT METHOD

A finite element analysis is best suited for the comparison of the response of a structural system to structural changes within that system. For this reason, it is an ideal tool to use in evaluating the response of the T-38 student windshield to structural variations.

The finite element method is a numerical procedure used to estimate the response of a specific structure. It is the output to the finite element analysis in the form of deflections, stresses, and strains that is used in the design process. Specifically, the transparency design engineer needs to know the deflected shape, the distribution of load and its magnitude, and how additional load can be distributed throughout the structure. This information can take the form of deformed geometry plots (Figure 2), deflection/strain/stress contours (Figure 4), and stress resultants (Figure 3). Using these deformed shapes, the designer can identify any interference with the surrounding equipment, personnel, or structure. When using the deflection/strain/stress contours, critical locations can be identified. The stress resultants are used to identify the magnitude of the load and how it is distributed within the structure. The results in the form of deflected shapes and stress resultants have been used extensively in the T-38 student windshield parametric studies.

PARAMETRIC STUDIES

There is a number of variables that are candidates for iteration when conducting a parametric study, such as transparency material configuration, support structure configuration, load magnitude, and location. The T-38 parametric studies examined the effects of changes to the material configuration and load magnitude. A single load location (6.25 inches down, in the forward direction, from the aft edge of the student windshield) was used throughout the analysis.

The T-38 student windshield parametric studies were conducted to evaluate the ability of the transparency structural system to absorb impact loading effectively. Focus was concentrated on a range of stiffness provided by single ply (monolithic) transparencies. An 0.45-inch thick polycarbonate, simulating the structural ply of a laminated windshield, an 0.60-inch thick stretched acrylic transparency simulating the existing windshield, and an 0.90-inch thick alternate stretched acrylic transparency are used in the study.

Two studies were performed: one using static and the other using transient dynamic finite element analysis. Both studies used transparency stiffness and load magnitude as the independent variables. While the stiffness variables are identical for both analyses, the load distributions are not. The static finite element analysis uses uncoupled loads distributed over an elliptical area representative of the intersection of the cylindrically shaped bird and an oblique plane. The transient dynamic finite element analysis uses coupled loads (time dependence and normal loads remain normal to the deformed surface) which are distributed over a larger area, simulating the footprint of the bird as it strikes the transparency. Both analyses

use the average momentum of the bird to determine the load magnitude.

Tables 1 and 2 present the matrix of analyses performed.

RESULTS

Selected samples of the available information generated by the finite element analysis is presented herein. The deflected shapes, stress resultants, and peak loads were used to compare the response of the T-38 student windshield structural system. Figures 5 through 22 are presented following the discussion so that the static analysis can be directly compared with the transient dynamic analysis.

The deformed data, as presented, is a comparison of the centerline deflection for each of the candidate transparency configurations. For the static analysis, each transparency configuration is plotted individually (Figures 5, 6, and 7), showing the deflected shape at various load levels. For the dynamic analysis, the time dependent deflection response of each transparency configuration (Figures 8, 9, and 10) is presented for three pressure levels representing one-half, five-eighths, and full momentum transfer. Only time increment two and four are shown.

The stress resultant plots represent the normal force (Figures 11 and 12), bending moment (Figures 15 and 16), and transverse shear force (Figures 19 and 20) per unit length of transparency. They are plotted along the arch with the forces acting in the forward/aft direction. The figures presented are for the 0.60 inch thick stretched acrylic transparency configuration. The results are for a static load equivalent to a force exerted from the impact of a four pound bird and aircraft traveling at a speed of 190 knots. The transient dynamic analysis resultant force plots are also for the 0.60 inch thick stretched acrylic windshield. They represent the force distribution through the fourth time increment, approximately one-quarter through the impact event. The load magnitude represents approximately 5/8 of the total momentum transferred between a four pound bird and the T-38 aircraft student windshield at a speed of 190 knots.

Peak resultant forces are also presented (Figures 13, 14, 17, 18, 21, and 22), comparing forces transferred to the frame of each transparency configuration. The large stiffnesses correspond to the 0.90-inch thick alternate stretched acrylic transparency and the lower stiffnesses correspond to the 0.45-inch thick polycarbonate structural ply. The nonlinear material response is represented by a change from positive to negative slope at any individual curve.

CONCLUSIONS

The impact response of a birdstrike to the T-38 student windshield is a complex event. The event is over before the pilot can react. Upon slowing the event down, using high-speed photography and examining the response, the event is recognized as a transient dynamic problem. The total response of the transparency structural system depends upon both the magnitude and time duration of the loading and the design of the structural system. It is for this reason that the independent variables, transparency stiffness, and load magnitude are chosen. The time duration of the loading can be determined using high-speed motion pictures of the experimental data.

Because the event is transient and dynamic in nature, it is a reasonable assumption to conduct transient dynamic analyses during the parametric study. The advantage of using the transient dynamic analysis is the representation of the dynamic effect of the load distribution and load path. Some of the difficulties of conducting a transient dynamic analysis follow. Sufficient care must be taken in the definition of the applied load. The load distribution within the structure is both coupled to the transparency response and is highly dependent on the time history of the loading event. When conducting a transient dynamic finite element analysis, the solution should be analyzed in an iterative manner, monitoring the solution at a number of time increments, to ensure the validity of the solution. Thus, the primary disadvantage is the amount of engineering and computer time necessary to complete a transient dynamic analysis; this being dependent upon the size of the problem being analyzed and the computer system being used. Large and fast computers are available which can reduce both cost and computer time necessary to accomplish the analysis.

An alternative to the transient dynamic analysis is the use of static analyses in the performance of parametric studies. Although the dynamic effects on the load distribution cannot be identified, valuable information can be generated to compare one transparency design configuration to another. Also, it is not necessary to determine the loading generated by the bird impact since an arbitrary load which allows comparisons between design configurations would be adequate. Improved birdstrike resistance design of the F-111 aircraft was accomplished using static analyses.[4]

Clearly, both time and cost are instrumental in identifying the specifics of any finite element parametric study. Such considerations need to be addressed when implementing the finite element method to the transparency structural design process.

ACKNOWLEDGEMENT

The work described was performed under contracts F33615-76-C-3103 and F33615-80-C-3401 with the Air Force Wright Aeronautical Laboratories (AFWAL/FIEA), Wright-Patterson Air Force Base, Ohio.

REFERENCES

1. West, Blaine S., "Alternate T-38 Transparency Development, Part II, Baseline Birdstrike Testing," AFWAL-TR-80-3132, Part II, Air Force Wright Aeronautical Laboratories, Wright-Patterson Air Force Base, Ohio, December 1980.

2. Brockman, R. A., "MAGNA: A Finite Element Program for the Materially and Geometrically Nonlinear Analysis of Three-Dimensional Structures Subjected to Static and Transient Loading," AFWAL-TR-81-3181, Air Force Wright Aeronautical Laboratories, Wright-Patterson Air Force Base, Ohio, March 1982.

3. Nash, R. A. and West, Blaine S., "Alternative T-38 Transparency Development, Part IV, Parametric Studies," AFWAL-TR-80-3132, Part IV, Air Force Wright Aeronautical Laboratories, Wright-Patterson Air Force Base, Ohio, March 1982.

4. West, B. S., "Design and Testing of F-111 Bird Resistant Windshield/Support Structure, Volume I - Design and Verification Testing," AFFDL-TR-76-101, October 1976.

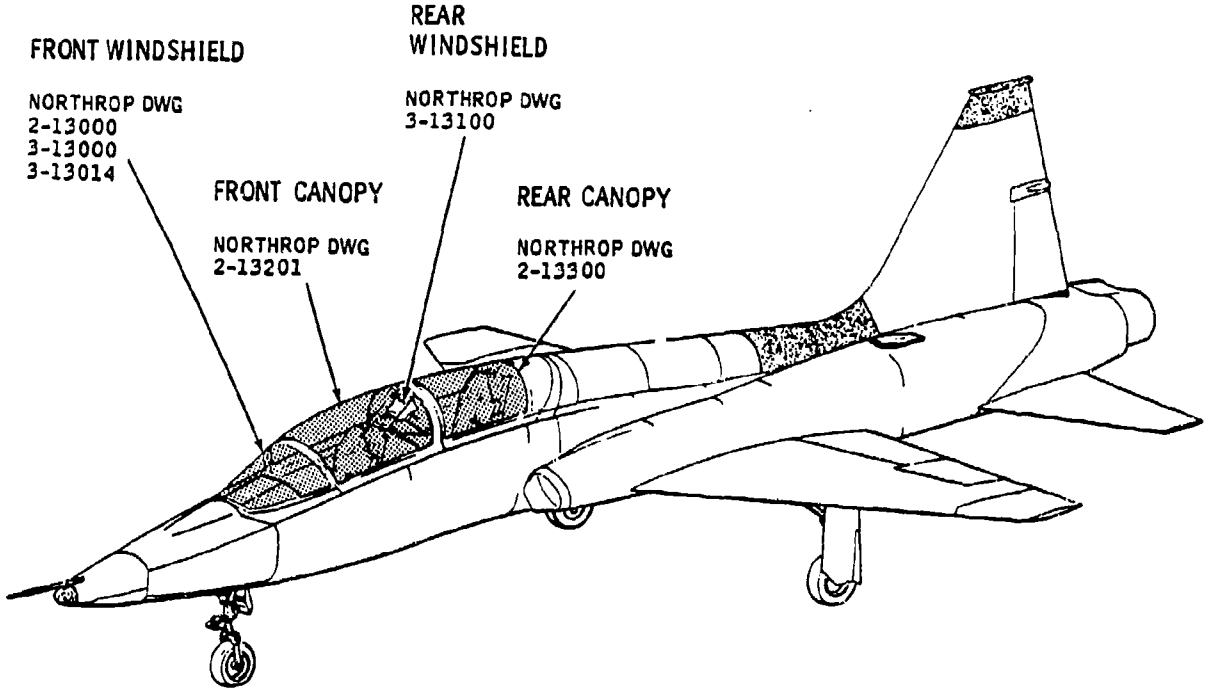

Figure 1. T-38 Aircraft.

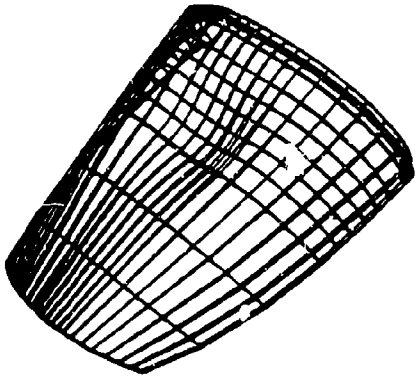

Figure 2. T-38 Deflected Shape.

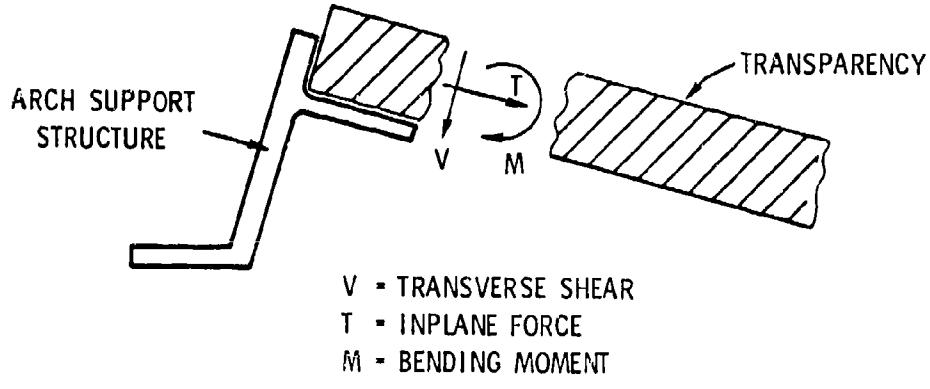

Figure 3. Stress Resultants.

(a)

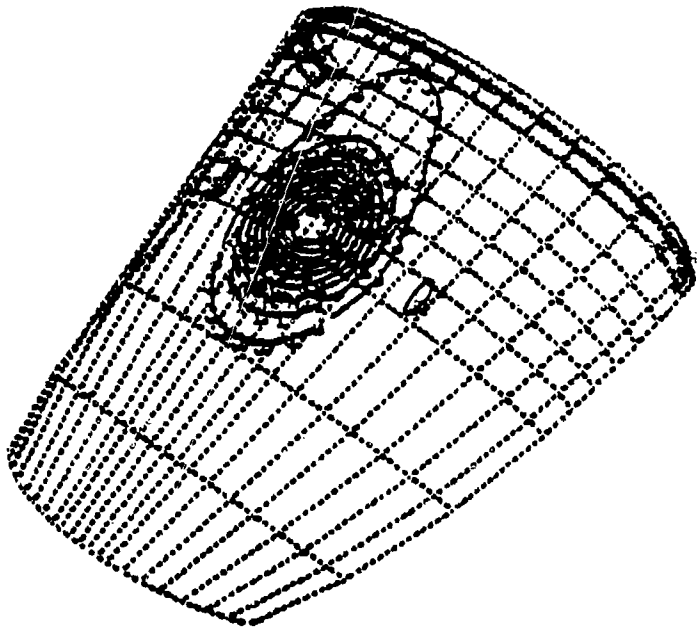

(b)

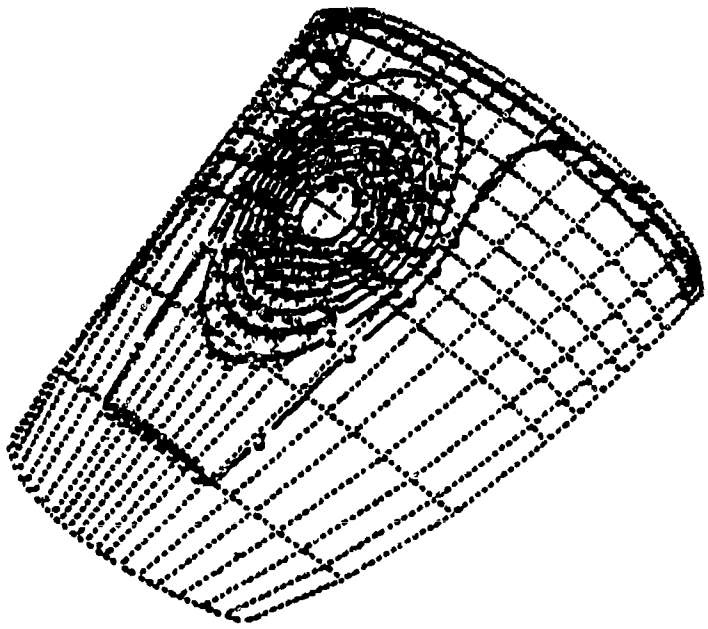

Figure 4. T-38 Z-Deflection Contours - Transient Dynamic Analysis ((a) Increment 2, (b) Increment 4).

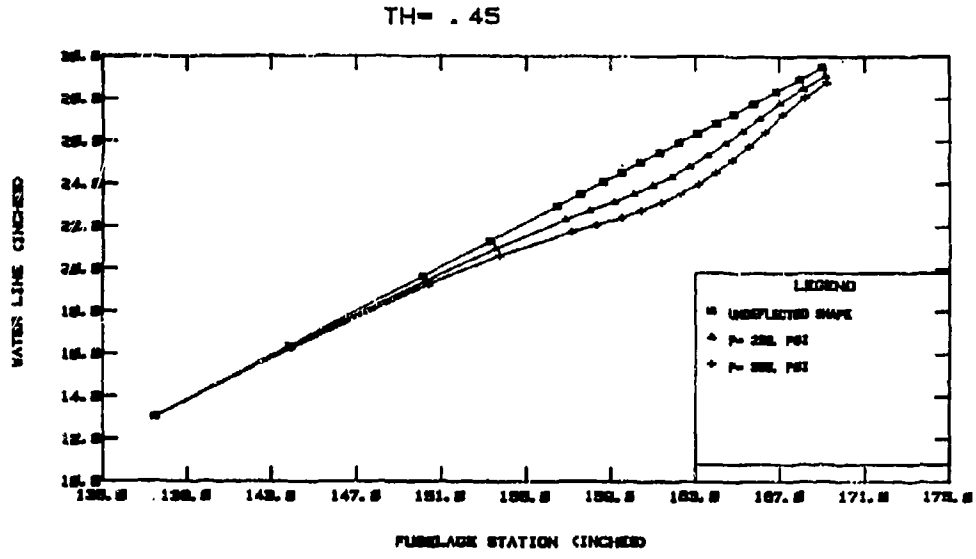

Figure 5. Centerline Deflection - Static Analysis t = .45.

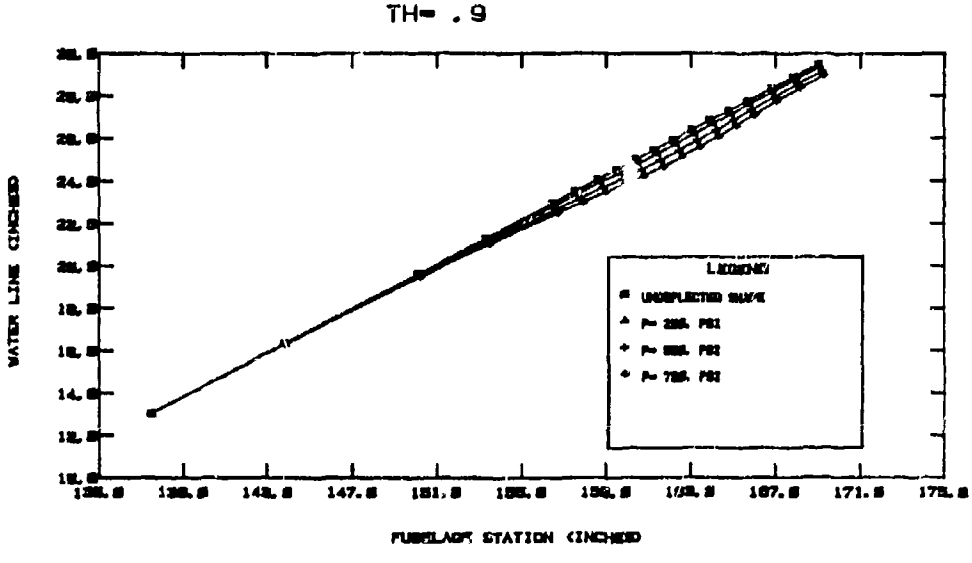

Figure 6. Centerline Deflection - Static Analysis t = .9.

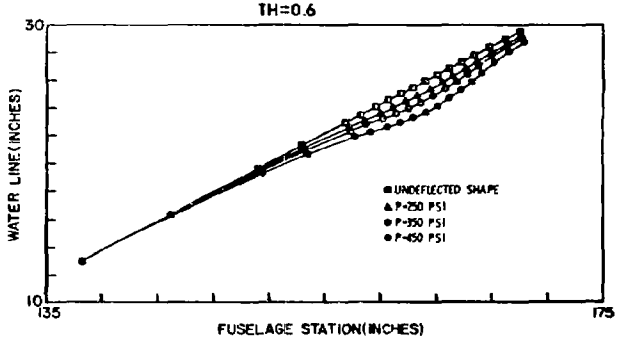

Figure 7. Centerline Deflection - Static Analysis t = .6.

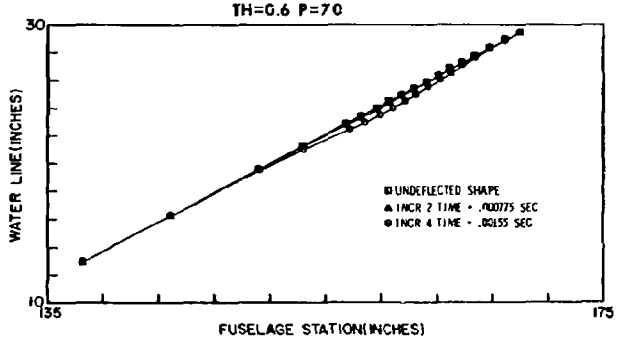

Figure 8. Centerline Deflection - Transient Dynamic Analysis 1/2 Momentum.

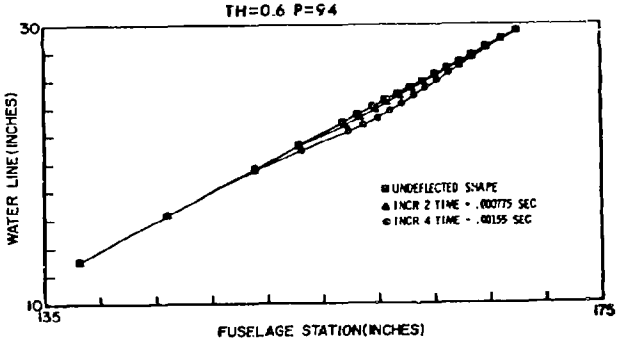

Figure 9. Centerline Deflection - Transient Dynamic Analysis 5/8 Momentum.

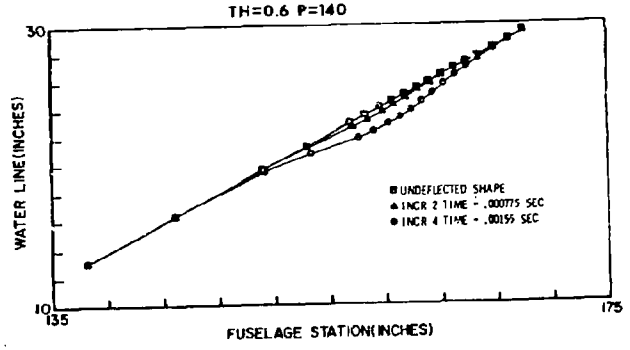

Figure 10. Centerline Deflection - Transient Dynamic Analysis Full Momentum.

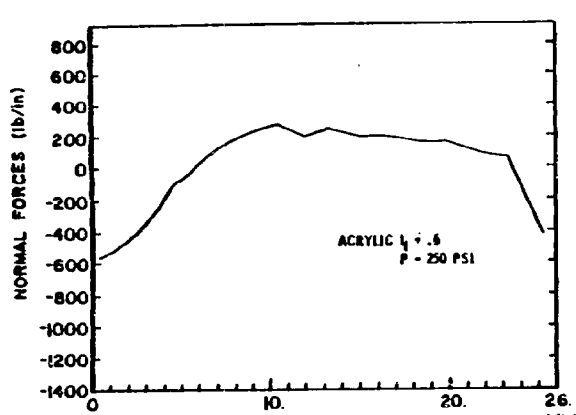

Figure 11. Normal Force Distribution - Static Analysis.

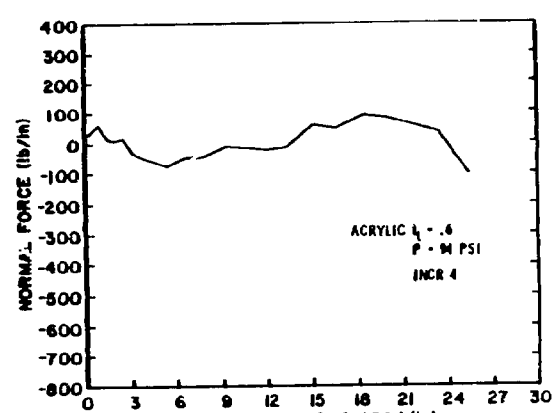

Figure 12. Normal Force Distribution - Transient Dynamic Analysis 5/8 Momentum.

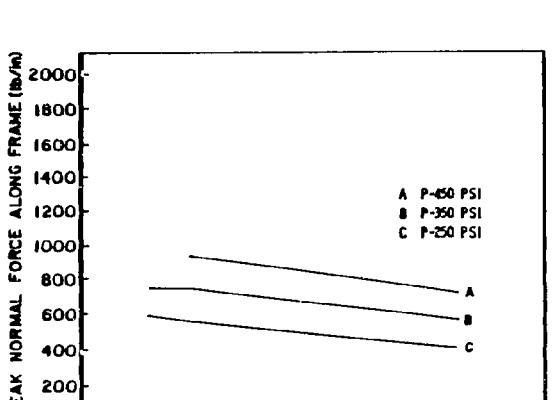

Figure 13. Peak Normal Forces Along Frame - Static Analysis.

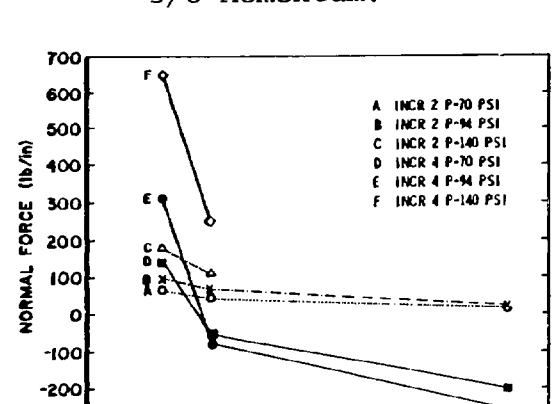

Figure 14. Peak Normal Forces Along Frame - Transient Dynamic Analysis.

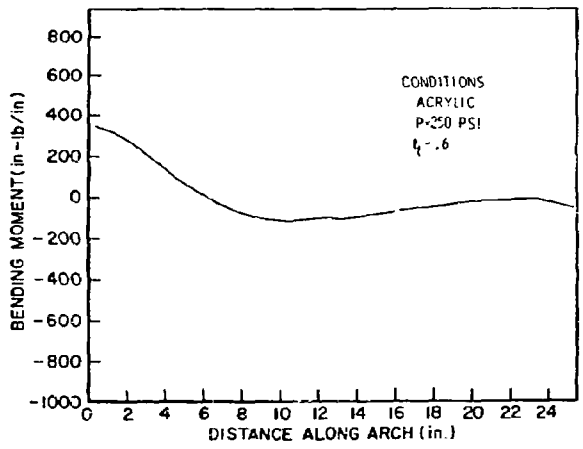

Figure 15. Bending Moment Distribution - Static Analysis.

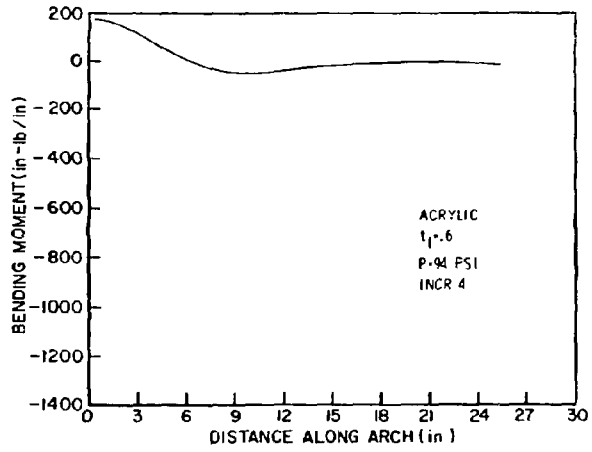

Figure 16. Bending Moment Distribution - Transient Dynamic Analysis 5/8 Momentum.

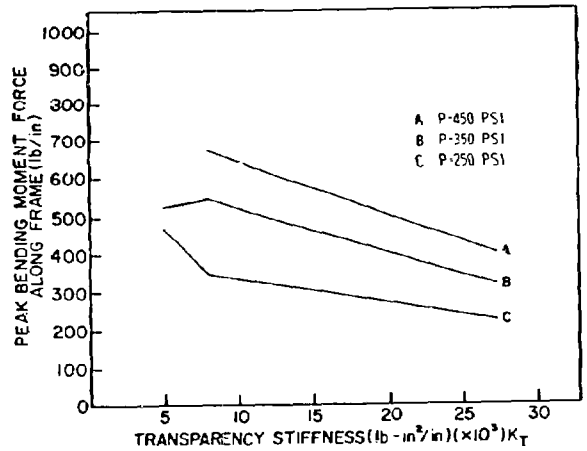

Figure 17. Bending Moment Along Frame - Static Analysis.

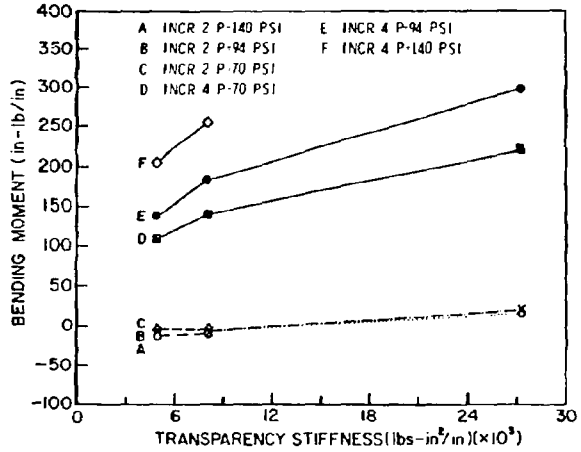

Figure 18. Bending Moment Along Frame - Transient Dynamic Analysis.

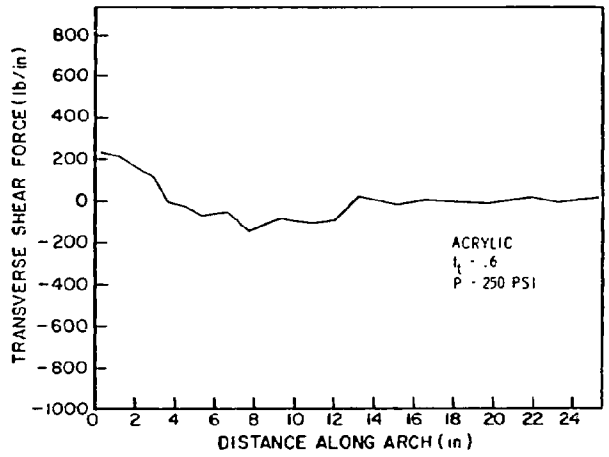

Figure 19. Transverse Shear - Static Analysis.

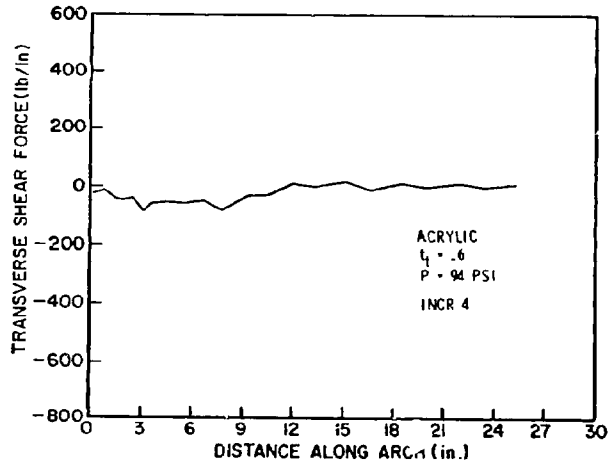

Figure 20. Transverse Shear - Transient Dynamic Analysis 5/8 Momentum.

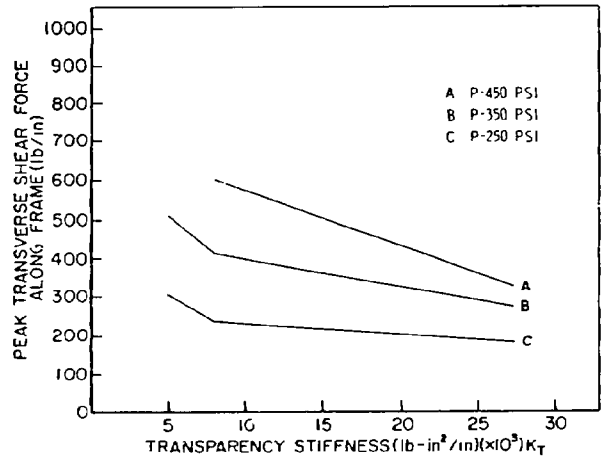

Figure 21. Transverse Shear Along Frame - Static Analysis.

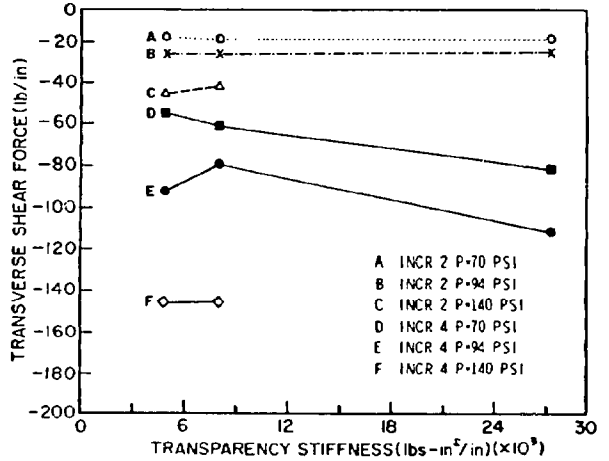

Figure 22. Transverse Shear Along Frame - Transient Dynamic Analysis.

TABLE 1

TRANSPARENCY STUDY - STATIC ANALYSIS

	TRANSPARENCY STIFFNESS LOAD AT 6-1/4 INCHES FROM FRAME				
PRESSURE (PSI)	$E_T = 1.625 \times 10^5$ $K_T = 1.233 \times 10^3$ $t_t = 0.45$	$E_T = 6.5 \times 10^5$ $K_T = 4.936 \times 10^3$ $t_t = 0.45$	$E_T = 4.5 \times 10^5$ $K_T = 8.1 \times 10^3$ $t_t = 0.60$	$E_T = 4.5 \times 10^5$ $K_T = 2.734 \times 10^4$ $t_t = 0.90$	$E_T = 1.8 \times 10^6$ $K_T = 3.24 \times 10^4$ $t_t = 0.60$
250	X	X	X	X	X
350		X	X	X	
450			X	X	
550				X	
650					
750				X	

TABLE 2

TRANSPARENCY STUDY - TRANSIENT DYNAMIC ANALYSIS

	TRANSPARENCY STIFFNESS					
	$K_T = 4.936 \times 10^3$ b $t_t = 0.45$ inch		$K_T = 8.1 \times 10^3$ b $t_t = 0.60$ inch		$K_T = 2.734 \times 10^4$ b $t_t = 0.90$ inch	
PRESSURE (PSI)	INCR 2	INCR 4	INCR 2	INCR 4	INCR 2	INCR 4
70	X	X	X	X	X	X
94	X	X	X	X	X	X
140	X	X	X	X		

SESSION VII

COMPUTER AIDED STRUCTURAL ANALYSIS (PART II)

Chairman: R. E. McCarty
Flight Dynamics Laboratory
Wright-Patterson
Air Force Base, Ohio

AD-P003 233

CURRENT PROBLEMS AND PROGRESS IN TRANSPARENCY IMPACT ANALYSIS

R. A. Brockman, University of Dayton

CURRENT PROBLEMS AND PROGRESS IN TRANSPARENCY IMPACT ANALYSIS

Robert A. Brockman
University of Dayton Research Institute
Dayton, Ohio

ABSTRACT

The design of aircraft transparencies for impact resistance poses a number of difficult problems for the structural analyst. Prominent among these are the accurate modeling of the transparency and its dynamic response, characterization of the construction materials, and evaluation of the applied loadings resulting from soft-body impact. This paper reviews current practices for mathematical modeling of transparency impacts, discusses problem areas in current analysis capabilities, and summarizes some current research on methods for impact simulation.

INTRODUCTION

The design of transparent crew enclosures for high performance aircraft is challenging, due to the many requirements which must be satisfied simultaneously. Design considerations include optical and aerodynamic performance, edge shape constraints, and structural safety under pressure, thermal and impact loading, as well as requirements for pilot ejection. These competing design requirements, together with manufacturing constraints, limit the choice of geometries, materials and support structure to be used in meeting objectives for impact resistance.

Given the three dimensional nature of transparency geometry and structural response, the specialized materials used in their construction, and uncertainty regarding the applied loads developed during soft body impact events, the evaluation of transparency impact resistance requires highly sophisticated analytical tools. Although it is generally recognized that finite element computer programs exist with which such analyses may be attempted, a number of difficulties exist which prevent the routine use of such programs for the complete simulation of transparency impacts. Most of these problem areas can be categorized as: (1) limitations in physical theory; (2) limitations in computer code capabilities; or (3) limited experience and/or training of program users.

This paper focuses on some of the more difficult aspects of transparency impact analysis, with three objectives in mind:

- to identify crucial problem areas;
- to classify them as outlined above; and
- to suggest possible means for their solution.

Current finite element solution capabilities are first reviewed, with particular emphasis on the analysis technology available in general purpose codes and on typical modeling practices. Material modeling and some related problems are discussed, and limitations are identified, both in the area of constitutive modeling and in numerical solution procedures. Finally, the problems involved in the complete simulation of soft body impacts on transparent enclosures are summarized, and recent research activities in the area are described.

FINITE ELEMENT SOLUTION CAPABILITIES

The stress analysis of transparent enclosures requires the mathematical modeling of complex, three dimensional shell forms, and possibly the surrounding support structure (Figure 1). The

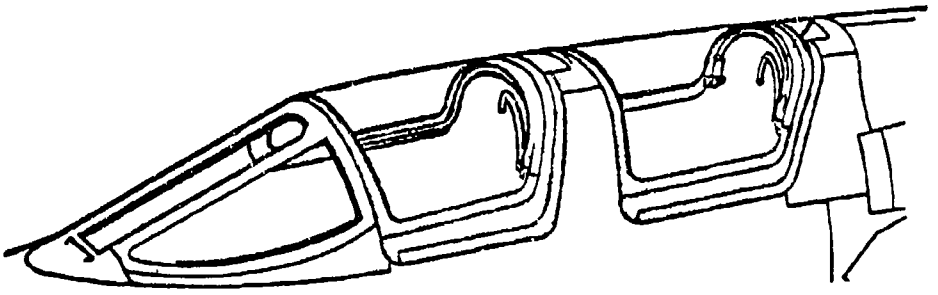

Figure 1. Typical Aircraft Transparency Geometry

quantities of interest include deflections, strains and stresses produced by static (thermal, pressurization) or dynamic (aerodynamic, free vibration, impact) forces. The utility of computer analysis methods stems from the following observations:

- the cost of analysis is usually less than the cost of a comparable full-scale test;
- detailed (although approximate) information is obtained through analysis, since results may be generated at any point in the structure;
- stress information, which is obtained routinely from an analysis, cannot be obtained directly by experiment.

While it is unrealistic to expect that numerical techniques will replace full-scale testing altogether, the value of such methods in performing conceptual studies and for assessing the effect of incremental design changes is unquestionable.

Current capabilies for transparency stress analysis are embodied in general purpose finite element programs, such as ANSYS [1], MAGNA [2], MARC [3], and NASTRAN [4]. The choice of a general purpose code is appropriate due to the wide variety of element types and analysis features which are necessary to perform transparency analyses accurately, and to the large problem sizes which often result. The disadvantages of a large analysis package may be substantial, however. The need for software developers to appeal to the widest possible audience to offset the cost of software development means that some specialized capabilities are invariably missing; meanwhile, some very common features are widely misunderstood and misused due to the complexity and idiosyncrasies of individual programs. Economic considerations favor the use of general purpose finite element programs for transparency analysis, but some care is needed to use them effectively. Several pertinent issues regarding the capabilities and usage of large-scale analysis packages are discussed in the remainder of this section.

Element Technology

Transparency modeling may involve a number of different finite element types: shells or solid elements are used to represent the shell itself, beam elements model stiffeners or support structure, and additional elements (bars, membranes, etc.) serve to represent other structural details. A general purpose structural analysis program contains the necessary variety of element types for constructing an appropriate model; however, problems often arise in selecting the proper element for a particular application, in specifying the element properties, and in properly connecting different types of elements within a single model.

Shells versus solids. Solid and shell finite elements are needed in modeling the curved surfaces of windshield transparencies; however, guidelines for choosing between the two are vague at best. Although it seems obvious that the radius to thickness ratio alone is a poor basis for choosing between shell and solid elements, this criterion is frequently used. The choice of element types depends more strongly upon the type of analysis to be performed: a shell element is rarely appropriate for modeling in the near vicinity of an impact, but is superior for most studies involving normal flight loads or internal pressurization. While most numerically integrated shell elements provide finer resolu-

tion than solids (in the form of more integration points) in the thickness direction, the absence of transverse stress in a shell element may lead to large errors in the hydrostatic stresses for impact problems, and to inaccurate yielding predictions in areas of highly localized deformation.

Shell elements. The current trend in shell elements in most general purpose codes is toward shear-flexible elements based on variants of the thick plate theory of Mindlin [5]. The principal advantages of this type of shell element are (for the user) simplicity in defining geometry and (for the developer) the use of "conventional" nodal unknowns (translations and rotations). For monolithic structures, the Mindlin type plate and shell elements can be quite effective and are simple to use.

Multilayered transparencies present difficulties which have yet to be addressed satisfactorily. Figure 2 shows a segment of

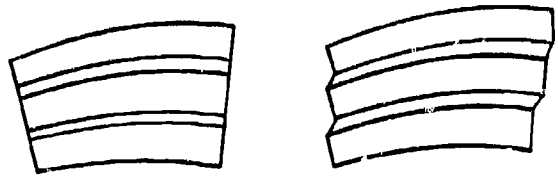

Figure 2. Undeformed and Deformed Geometries of Multilayered Shell

such a construction in the original and deformed states. Sharp discontinuities in the transverse shear strains between adjacent layers call for detailed modeling which may be prohibitively expensive in practical problems. The independent transverse shear stiffness parameters which can be defined in many shell elements are inadequate, even for linear analysis, since no theoretically sound procedures are available for computing them. An appropriate solution would appear to involve conventional (translations/rotations) variables in a single base layer, combined with "relative" degrees of freedom defining differences in the rotational motion in each successive layer from that of the base layer. The two factors which complicate such a solution are the formulation of economical elements of this type, and definition of the "relative" degrees of freedom in a form which permits inter-element compatibility and general boundary conditions to be established in an unambiguous fashion. Element economy is critical, since a special layered element must be considerably less expensive than

an assemblage of solid elements to allow the routine solution of problems of practical size; this objective is particularly difficult in nonlinear analysis, where complex kinematic assumptions typically lead to expensive elements.

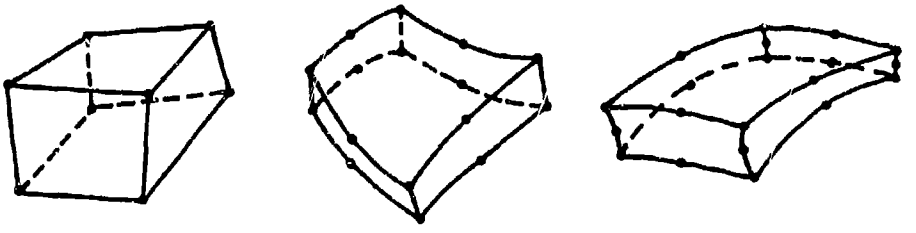

Figure 3. Typical Solid Element Configurations

Solid elements. When solid elements are used, 16-, 18- or 20-node configurations are the most common (Figure 3). Numerical integration, usually by Gaussian quadrature, is necessary due to irregular element shape, and the temptation to underintegrate is strong. A reduced (usually 2x2x2) quadrature is more economical than exact (usually 3x3x3) integration, and the computed stress results are often superior. However, the light constraints typical of windshield transparencies may permit the development of zero energy modes of deformation in the model (Figure 4). These spurious modes may contaminate the solution immediately, or may be manifested only after nonlinearities have altered the element characteristics. Non-Gaussian integration rules, such as those described by Irons [6], often yield element stiffness and stress characteristics which are competitive with underintegrated elements, without the penalty of numerical instability. In particular, the 14-point integration scheme of [6] is stable for each of the solid elements noted above, and costs approximately half

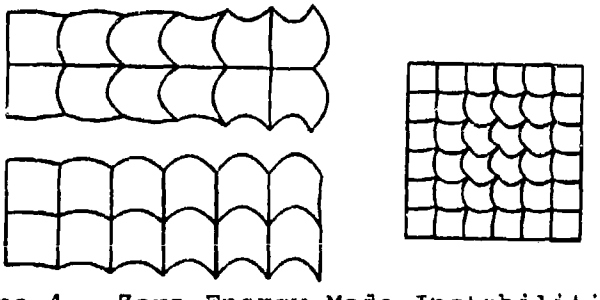

Figure 4. Zero-Energy Mode Instabilities

as much as a "safe" (3x3x3) Gaussian integration. Such nonstandard integration techniques, although effective and rather easily implemented, are rarely available in general purpose analysis packages.

Modeling Capabilities

The modeling capabilities of a finite element analysis code depend primarily upon the types of finite elements available, as well as the details of their implementation. The most serious difficulties in modeling complex practical structures arise from the need to employ several types of elements (shells, beams, and solids) in combination. Shell and beam elements usually possess both displacements and rotations as nodal variables, while solid elements use only displacement unknowns (Figure 5); furthermore,

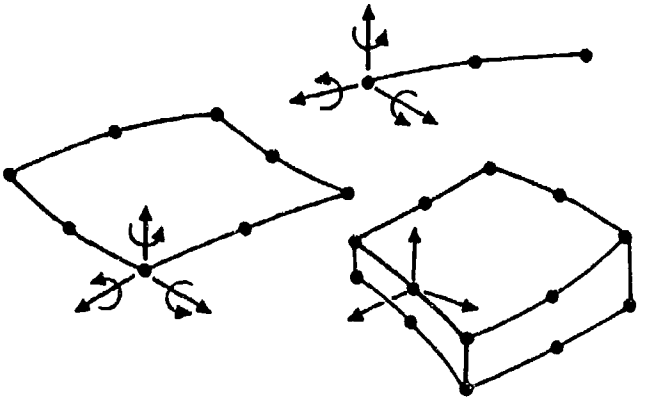

Figure 5. Nodal Variables for Beam, Shell and Solid Elements

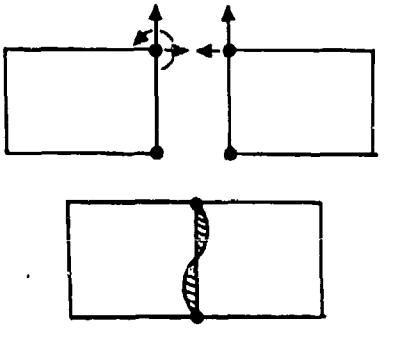

Figure 6. Incompatibility between Elements with Similar Nodes

the structural (shell, beam) elements are frequently based upon displacement functions of higher polynomial order than those of the solids. Consequently, elements having identical nodal patterns may be incompatible (Figure 6), and complex constraints are needed to couple adjacent elements properly. In nonlinear analysis these constraints are also nonlinear, and most codes do not include mechanisms for updating them continuously. Although this problem has existed for more than twenty years, little has been done to improve matters until recently [2,7,8,9].

Inherent element incompatibilities are a source of several practical problems, ranging from inability to perform the needed analysis to the generation of computed results which may be seriously in error. From the program user's viewpoint, there exist several levels of understanding regarding the problem of element incompatibilities:

(a) If the nodes of adjacent elements match, the elements behave in a compatible manner.
(b) If dissimilar elements are joined, constraints may be necessary; however, I don't know how to specify them.
(c) Dissimilar elements must be joined using constraints, which are simple to formulate; these same constraints hold for both linear and nonlinear problems.
(d) Constraints for joining dissimilar elements in linear problems can be formulated correctly, but a nonlinear analysis using this combination of element types may be impossible.

Only point of view (d) is correct, and (a) or (c) may encourage the generation of analytical results which are grossly in error. Ironically, only points of view (b) and (d) are likely to lead to further consultation with the program documentation, or with the program developers, to clarify the problem. Correct finite element modeling within the limitations of any analysis code is usually difficult and requires some measure of skepticism. Automated preprocessing, though a necessity in most practical applications, is the subject of further concern due to its ability to generate modeling errors at superhuman speed.

Solution Methodology

Transparency impact analysis normally requires a nonlinear, transient solution; linear analysis is appropriate only for the prediction of brittle failures at relatively early response time or in problems involving very mild loading levels. When ductile material behavior and/or extended-time response occur, nonlinear effects of two types may be present: material nonlinearity, due

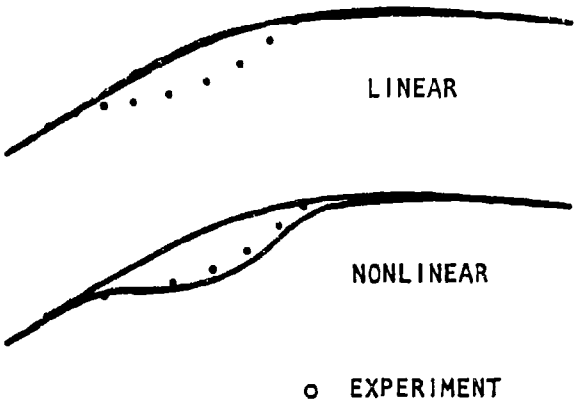

Figure 7. Linear and Nonlinear Bird Impact Solutions

to yielding or strain rate sensitivity; and geometric nonlinearity, due to large deflections and/or strain in the part. Figure 7 shows a comparison of linear and nonlinear solutions during an impact on a fighter windshield, taken from Reference [10]. Nonlinear solutions require very sophisticated numerical techniques to be cost effective, and the search for more accurate and economical solution methods is an area of much active research. The issues involved in developing and using nonlinear analysis techniques can be clarified by considering the types of errors which can occur in nonlinear finite element calculations.

Error types. In general, four primary sources of error can be identified in a nonlinear transient analysis:

- spatial discretization error,
- constitutive modeling error,
- linearization error, and
- temporal truncation error.

The first two of these are errors which are intrinsic to the finite element idealization of a structure -- they reflect differences between the mathematical idealization of a problem and the physical problem itself. The last two categories include errors incurred during the solution of the purely mathematical problem.

Modeling errors. Spatial discretization error refers to inaccuracies which can be attributed to representing the structure (or the system of partial differential equations which describe it exactly) by the finite element model. This type of error is

influenced by the choice of element type, the refinement of the mesh, the degree of approximation of the elements used, and the mathematical representations of loading and boundary conditions. The type of material model used also introduces intrinsic error, the constitutive modeling error. Some amount of each of these errors is inevitable; in fact, once they have been committed, a "substitute problem" is defined whose solution will provide some clues to the solution of the "real problem". This distinction is not purely philosophical -- too often the "real problem" and the "substitute" differ quite sharply. The discretization error and constitutive error are foremost in the mind of an analyst during the creation of a finite element model.

Solution errors. In the case of a nonlinear transient analysis, the "substitute" numerical problem consists of a system of ordinary differential equations and initial conditions which are to be integrated numerically in time. The remaining two types of errors occur during this numerical solution. Linearization error arises from nonlinearities in the system: during any time step, it is necessary to assume a path for each material particle, and this path is invariably linear over individual steps. Note that this path linearization in no way implies a linearization of the equations of motion for each step. The temporal truncation error is incurred by virtue of the particular time integration formula and time step used for the solution, since the integration formula is incapable of representing the time-dependent response exactly. In nonlinear problems, while both types of errors exist, they cannot be distinguished from one another.

Implicit solution methods (typically, those which employ a stiffness matrix) contain at least two components -- a numerical integration method for advancing the solution in time, and iteration schemes for improving the solution at particular points in time. The truncation error exhibited by the time integrator depends strongly upon the time step size and is manifested by distortion of the dynamic reponse as shown in Figure 8. Errors due to linearization amplify this effect when iteration is not used (see Figure 9). At present it is difficult to evaluate the accuracy of a nonlinear transient solution, short of repeating the calculation using a smaller step size. For this purpose, several preliminary calculations performed over short time intervals can often provide some guidance (see, for example, Reference [10]).

Prospects. For large nonlinear applications, economy and accuracy seem continually at odds, and the temptation is strong to use large time steps and forego iteration, in the interest of obtaining an inexpensive solution. The necessity for tradeoffs between accuracy and cost savings is the unfortunate result of a

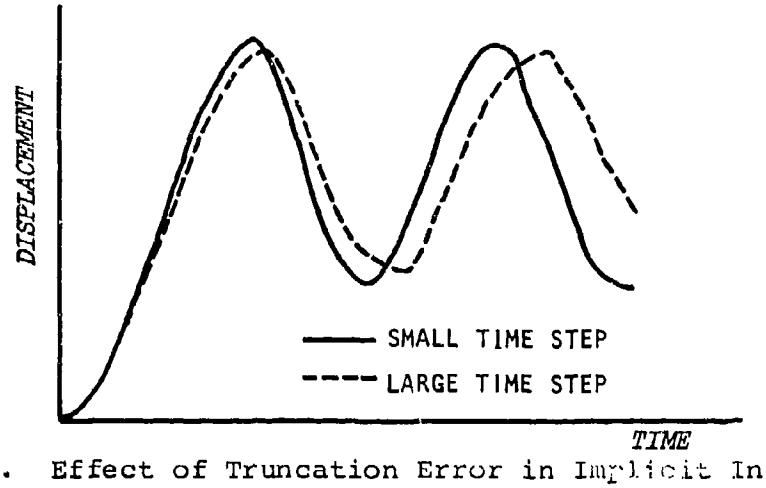

Figure 8. Effect of Truncation Error in Implicit Integration

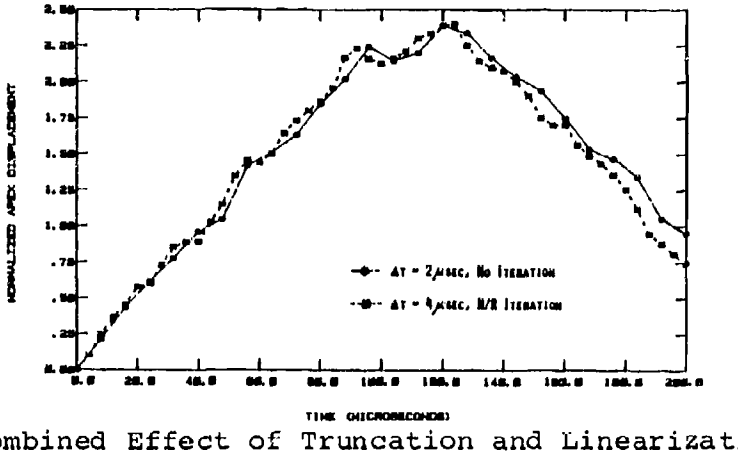

Figure 9. Combined Effect of Truncation and Linearization Error

lack of intelligence in the present generation of solution methods. Critical elements in the search for more effective solution techniques are the method of iteration, the means of monitoring errors, and strategies for controlling time steps automatically.

The most commonly used methods of iteration are based upon Newton-Raphson techniques (Figure 10); combined (full and modified Newton) iteration schemes prove to be particularly effective for dynamic problems. However, each Newton iteration requires a great deal of computational effort, and much current research is devoted to devising more streamlined iterative procedures. There is strong interest in low-rank updating techniques, such as the BFGS iteration [11];hoever, despite the high hopes expressed for such methods users have found them somewhat expensive. Without

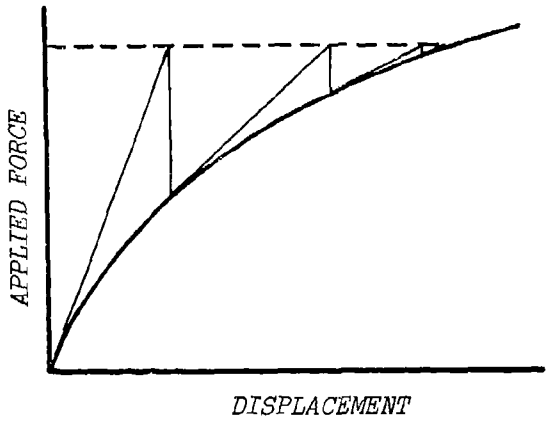

Figure 10. Newton-Raphson Solution for a One-Variable System

more convincing evidence of the superior efficiency of methods such as the BFGS update, it is likely that Newton's method will continue to provide the basis for iterative solution techniques for some time to come. Other work [12] has been directed toward improving the effectiveness of element level calculations within the Newton-Raphson framework, since element-related calculations frequently represent a substantial portion of the computing cost in implicit nonlinear solutions.

The aspect of nonlinear solution methodology which promises the most significant improvement in economy is automatic control of time increment size. One popular device is "arc length" control, as described by Crisfield [13]; however, this rather heuristic strategy appears most useful as a means of step control in static stability (postbuckling) analysis. Other research [14] is concerned with predictor corrector methods, in which the criterion for step size selection (truncation error) is more appropriate. Hibbitt [15] has recently proposed the most promising idea thus far -- once a step is complete, a solution at the middle of the step just completed is interpolated, and the residuals there are used as a criterion for step size adjustment. This technique for error estimation is important since it reflects the combined effect of linearization errors and truncation errors, in a form which can be computed quite readily.

Additional improvements to existing numerical solution procedures are on the horizon, but have not been explored in depth. One example is the notion of quantifying the degree of nonlinear behavior in individual elements or segments of a finite element model, and adjusting the element formulation and/or the solution

strategy (which may consist of a mixture of conventional and reduced-basis methods) accordingly; the theoretical foundations exist for such a scheme, but it has yet to be demonstrated. Another more distant prospect is the use of adaptive or multiple mesh techniques, which have thus far been applied only to linear problems where computable error estimates are readily available.

Typical Applications

In previous sections, several troublesome issues related to the finite element analysis of transparency structures have been discussed. Despite the number of obstacles which prevent truly routine use of finite element techniques in transparency stress analysis, current analysis technology is sufficiently developed to provide realistic and economical results for many problems of practical interest. A number of applications which demonstrate this fact convincingly have already been documented.

Engineers at the Air Force Wright Aeronautical Laboratories have performed several successful studies on relatively flexible transparencies, including impact simulation [10,16], pilot ejection studies [17], and stress analysis for internal pressurization and thermal conditions [18]. Animated film sequences, produced from geometry, contour, and stress relief plots by McCarty in connection with the above impact studies, show good agreement with experiments and have been useful in visualizing the dynamic stress fields induced by soft body impact.

Applications to several aircraft transparency systems have been performed at the University of Dayton. Most of these have focused upon the stiffness characteristics and/or load carrying capacity of canopy reinforcements and support structure [19,20] or on impact response [21]. Other studies [22] have been directed toward the study of simplified methods of evaluating applied forces which are induced during soft body impacts.

Stress analyses for pressurization and cooling conditions in flexible transparencies have also been reported [23]. Thermal stress problems in transparencies have proved particularly challenging with the present generation of analysis software; this is due in part to the physical behavior induced by cooling [18], and in part to the particular subtleties of thermal stress analysis in general.

MATERIALS CHARACTERIZATION AND RELATED PROBLEMS

Transparency stress analysis poses some rather specialized

problems related to materials characterization. Structural layers of transparent enclosures are routinely fabricated of glass, acrylic, or stiff polymeric materials (e.g., polycarbonate). The behavior of these materials is less repeatable than that of metals even when the material response is linear; in addition, they exhibit pronounced time dependence. Existing mathematical material models are strongly oriented toward metallic materials and may fail to reproduce the true behavior of typical transparency materials. Interlayer materials, which are polymeric compounds, present even more serious problems: they are simultaneously incompressible (or nearly so) and viscoelastic, a combination for which no satisfactory material model has yet been proposed. The low elastic moduli of interlayer materials in compared with that of structural glasses and plastics can lead to severe ill-conditioning in numerical solutions, which may preclude accurate predictions using the best available material models.

Material Modeling

The types of "conventional" (that is, common in finite element programs) material models which are pertinent to characterizing most transparency materials are: (1) elastic; (2) elastic-plastic; (3) viscoelastic; and (4) viscoplastic. The fundamental distinctions between these four classes of models are summarized in Table 1. An additional component of the material model is the

Table 1. Essential Features of Four Common Material Models

	Elastic	Visco-elastic	Elastic Plastic	Visco-plastic
Material Yielding	N	N	Y	Y
Creep / Relaxation	N	Y	N	Y
Strain Rate Effect	N	Y	N	Y
Incompressibility	Y	N	Y	Y
Thermal Effects	Y	Y	Y	Y
Large Strains	Y	Y	Y	Y

criterion for failure, which depends both upon the type of material model used and upon the physical behavior of the material being analyzed. Issues related to the characterization of structural and interlayer materials are discussed separately below.

Structural materials. The glass, acrylic and polycarbonate materials used in structural and/or exterior transparency layers

exhibit a wide range of behavior, from higher-modulus, brittle material to ductile materials with lower stiffness. Elastic and elastic-plastic material models, which do not reflect the actual strain rate dependence of the substance, have been used successfully in characterizing structural plies under impact conditions [10]. Often, aa acceptable representation can be obtained simply by specifying material properties which are representative of the range of strain rates expected in the simulation. When this simplification applies, the specification of material properties collected from formed specimens is most appropriate. If significant inelastic deformation is present, however, the problem becomes more difficult -- specifying the yield stress for the rate dependent material is left to conjecture, and the error which is introduced as a result of this choice is poorly understood. Both strain hardening and softening have been observel in polycarbonates, and the rate dependence of these properties at high strain levels is not yet clearly defined [24].

For the mathematical characterization of these properties, rate sensitive nonlinear material models exist [25,26] which may be capable of a reasonable representation of common transparency materials; most of these have been developed for the prediction of the behavior of metals, but are sufficiently general in form to reproduce the important features of nonmetallic material response. A primary limitation in the application of these existing theories is the lack of experimental data for moderate to large strains and strain rates. Time dependent data are available primarily for creep tests, involving rather small strain levels and very low strain rates. For polycarbonate materials, properties may vary widely between the virgin material and samples machined from preformed parts; some effort toward analyzing the state of prestress induced by forming and the resulting effect upon mechanical properties is necessary for the truly reliable simulation of transparency material behavior.

Interlayer materials. Difficulties in characterizing most interlayer materials are more fundamental in nature. The low moduli characteristic of soft interlayer material permit the development of extremely large strains, even under relatively mild loading, so that nonlinear behavior is the rule rather than the exception. Interlayer material behavior is very similar to that of some rubber compounds, which exhibit both viscous and nearly-incompressible behavior. The nonlinear nature of the incompressible response is shown in Figure 11. Despite much research on the characterization of rubber and elastomeric materials, models which encompass both of these effects have yet to be developed. The phenomenon of incompressibility is most often treated using models based upon total strain energy, such a treatment is pre-

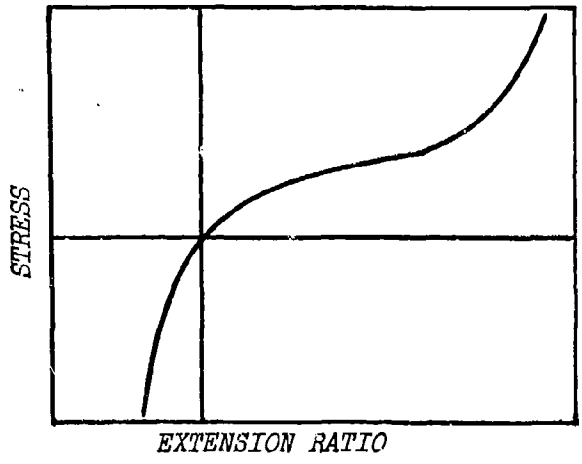

Figure 11. Incompressible Stress-Strain Behavior

cluded by the presence of the dissipative (viscoelastic) forces. Neither effect appears to predominate: impact tests on multilayered transparencies have shown conclusively that the dissipative effect of the interlayers is both pronounced and beneficial, and extremely stiff bulk behavior is certainly necessary to transmit the high forces imparted during such an impact.

Research of a basic nature will be required to provide adequate models of material exhibiting incompressible, viscoelastic response. For the transparency design community such investigation has particular importance, since the effects of interlayer behavior are of central interest in the development of improved impact resistant transparent structures. A similar interest exists on the part of engineers involved in the design of elastomeric seals for use at extreme temperatures, where viscoelastic behavior is pronounced.

For the present, several approaches are possible for modeling of interlayer material behavior with current analysis tools. One reasonable approximation is to use the incompressible theory (such as the Mooney-Rivlin [27] or Blatz-Ko [28] models) to represent the detailed behavior of the interlayer, and to introduce dissipative effects through element or system damping. The use of an incompressible idealization permits realistic transmission of forces between the interlayers and surrounding plies, thereby capturing the basic load path and deformation patterns with relatively little error. Viscoelastic damping can be introduced by the definition of (approximate) structural damping coefficients, either at the element or system level. It should be noted, however, that damping factors introduced in this fashion will norm-

ally require additional material testing, either for the interlayer material alone or on the actual laminate to be analyzed.

Numerical Ill-Conditioning

Beyond the theoretical difficulties which exist in modeling some transparency materials, the particular combinations of materials used in layered transparencies may lead to numerical conditioning problems in some analyses. The differences in elastic moduli between structural layers and interlayers may be as large as a factor of 100,000; since current element technology is such that layers with grossly different properties should be modeled separately, stiffness coefficients for adjacent layers differ in the extreme and loss of significance is inevitable.

Disparities in material properties are least troublesome in linear analyses, in which "exact" matrix operations lead directly to a solution. In linear static or transient analysis, errors due to roundoff predominate, and the loss of five digits of accuracy due to differences in material coefficients may be acceptable. It is necessary to keep in mind that conditioning problems may be aggravated by other factors, such as large element aspect ratios.

Nonlinear and natural frequency solutions are performed by iterative methods, in which numerical ill-conditioning problems are more troublesome. In a natural frequency analysis by vector iteration, successive estimates of the system eigenvectors pass through some variant of the governing equation

$$[K]\{x\} = \omega^2 [M]\{x\}$$

Convergence is measured by energy- or frequency-related criteria with tolerances placed upon variations in successive iterations. If, for example, the modal strain amplitude in a structural ply is 10%, and an energy criterion is used to measure convergence with a tolerance of 0.1%, the strain amplitude in an interlayer whose modulus is 100,000 times smaller may be as much as 1,000% (and grossly in error) without affecting convergence. Experience shows that frequencies can be computed relatively accurately in such situations, while predicted strain and stress amplitudes in softer layers may be quite seriously in error.

Convergence of a nonlinear solution is measured by the degree of force imbalance and the change in energy and/or displacements between successive iterates. In this case, large changes in the displacement or strain state of a softer layer have quite a small effect on the equilibrium between internal and external

forces, so that overall motions of the structural layers can be computed with high accuracy; however, stress data for the softer layers is likely to be inaccurate. Although this situation often does not represent a problem, the accurate prediction of damping effects in the viscoelastic interlayers may be quite difficult.

Some specialized solution procedures have been proposed for use in problems involving widely disparate stiffnesses [29,30], but these are suited primarily for use in linear analysis. Most techniques for dealing with such conditioning problems are based either upon the partitioning of degrees of freedom into "stiff" and "soft" groups (in which case iteration is necessary even for a "direct" solution), or upon a re-definition of strategic degrees of freedom in terms of relative, rather than absolute, displacements. As an example of the latter approach, consider the linear system

$$\begin{bmatrix} 1001.5 & -1000.0 \\ -1000.0 & 1001.5 \end{bmatrix} \begin{bmatrix} u \\ v \end{bmatrix} = \begin{bmatrix} 0. \\ 1. \end{bmatrix}$$

which involves stiffness coefficients which differ by only three orders of magnitude. Notice that problems arise not because of vast differences in the matrix coefficients, but rather because the effect of some contributions to the stiffness are small compared with others. In the above example, taken from a frame analysis, the bending stiffnesses of order 1.5 are small compared with the axial stiffness of the members. Defining the relative degree of freedom r=(v-u) leads to the new system

$$\begin{bmatrix} 3.0 & 1.5 \\ 1.5 & 1000.5 \end{bmatrix} \begin{bmatrix} u \\ r \end{bmatrix} = \begin{bmatrix} 1. \\ 1. \end{bmatrix}$$

which can be solved with minimal loss of precision.

In nonlinear problems, it is unlikely that the use of relative degrees of freedom will lead to significant improvements in stress results for softer layers, due to the predominance of the stiffer layers in checks on force imbalances and energy changes. One potential solution lies in the use of separate energy checks for each layer or material in the model, with tolerance levels based upon the relative magnitude of material moduli to provide a measure of scale. The merits of such a technique are open to speculation; however, its foundations are sound: the intent is to eliminate extreme changes in the strain energy of soft materials as the mechanism for correcting force imbalances in stiffer portions of the model.

MODELING OF SOFT-BODY IMPACT LOADING

The most troublesome aspect of transparency impact simulation involves the determination of dynamic loads imparted to the structure during the impact. For soft-body impacts the response of the impactor and the structure may be highly coupled, so that virtually all important parameters of the loading (spatial distribution, time-dependence and duration) are unknown. Thus far, applications to flexible transparencies have been restricted to those for which experimental data (e.g., high speed film) exist, and to studies of the effects of minor design changes upon these particular configurations. Approximate loadings based upon estimates of momentum transfer and simplified potential flow models [31,32] have been used, but cannot be applied with confidence to new situations without experimental verification.

Problem Description

During soft-body impact at the velocities of interest, the impactor, though composed of solid material, behaves hydrodynamically. That is, pressures are developed which are several times as great as the material strength, and the material behaves essentially as a fluid. The soft-body impact therefore presents a problem in fluid-structure interaction, in which the response of the fluid and structure must be analyzed simultaneously in time. The structure geometry and the desire to predict post-impact dynamic response dictate that an implicit, Lagrangian procedure be used to treat the structural motions; however, the extreme distortions of the impactor preclude the use of this type of analysis. Analytical methods which are presently used in computational fluid dynamics, while suitable for tracking arbitrarily large distortions, typically employ a fixed (Eulerian) mesh which is incapable of an accurate accounting of the free surfaces and the moving structure boundaries. Both of these boundary conditions must be considered in the soft-body impact problem, and existing methods of analyzing them are either inaccurate or prohibitively expensive.

Current Research

Accurate modeling of soft body impact forces is the subject of current research at the University of Dayton, under the sponsorship of the Air Force Wright Aeronautical Laboratories. New analysis techniques, capable of treating both large distortions and the difficult boundary conditions encountered in such impact problems, are being developed, and will be coupled with existing structural analysis software. A brief description of this work, which is scheduled for completion in December, 1983, is given in the following paragraphs.

Fluid Dynamics. Simulation of the fluid-dynamic behavior of the impacting body is accomplished using numerical techniques typical of hydrodynamics codes. Simple (eight-node solid) elements are used to minimize problems with mesh distortion, and the time integration is performed with explicit (central difference) extrapolation followed by a pressure iteration [33] stage, to relieve stability-related time step limitations. One unique aspect of the fluid dynamics analysis procedure is the use of a Lagrangian mesh, which follows the material and permits accurate tracking of free surfaces, and of motions at moving boundaries. Automatic rezoning is used whenever necessary to restore regular element geometry. A simple example of this component of the analysis technique is shown in Figure 12.

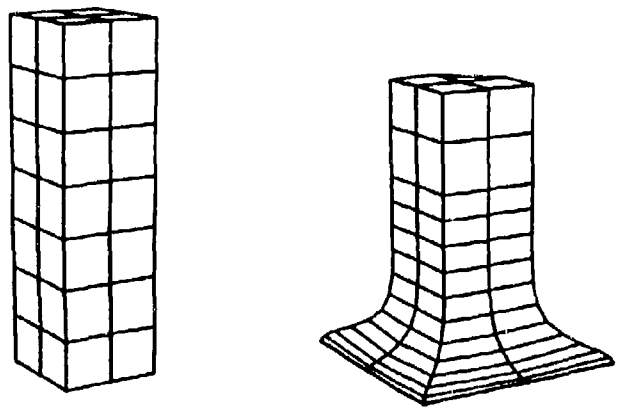

Figure 12. Impact Modeled using Lagrangian Mesh with Rezoning

Structural Analysis. Computation of the structural dynamic motion is performed using an existing finite element code, MAGNA [2]. This code has been used widely for transparency analysis, and contains a provision for three dimensional contact analysis (Figure 13), which lends itself well to the fully coupled impact problem. The dynamic structural analysis is performed in MAGNA using implicit methods based upon Newmark's time integration operator [34], in conjunction with various types of Newton-Raphson iteration.

Fluid-Structure Coupling. Interactions between the fluid and structural response are enforced through the use of the contact analysis feature in MAGNA, which detects contact conditions as they occur, applies the proper displacement constraints, and adjusts normal velocities at the impact surface to conserve momentum. For the structural model, which uses a consistent (full) mass matrix, masses can be lumped at the impact surfaces for the

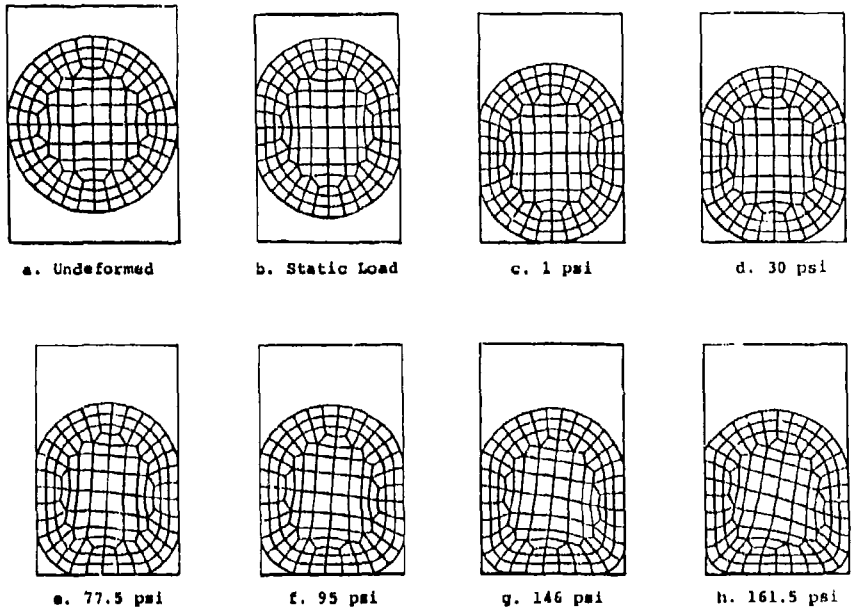

Figure 13. Example of Contact Analysis Performed with MAGNA

purpose of computing post-impact velocity and acceleration. Once the initial contact is established, velocities computed for the structure on the contact surface are treated as imposed velocity conditions during the fluid dynamic solution. Time integration for the fluid and structure meshes is performed using different step sizes, with interpolations [35] performed as needed to synchronize the two solutions.

SUMMARY AND RECOMMENDATIONS

Computerized structural analysis of transparent enclosures offers an economical means for producing better and safer equipment. The transparency design community has begun to employ this emerging technology, with varying degrees of success. This paper attempts to identify several existing problem areas in transparency structural analysis, and to classify them as limitations in physical theories, computer code capabilities, or user training and experience. Three major subject areas are reviewed: finite element analysis capabilities, material modeling, and soft-body impact modeling.

The most serious shortcomings in current finite element analysis capabilities include the lack of effective elements for

modeling multilayered shells, and solution costs which are higher than necessary due to algorithmic shortcomings. Solutions to some of these problems exist but have yet to be implemented completely. Practical difficulties may also arise in the choice of element types and in the proper use of multiple element types in a single problems; here user experience is the key to constructing an appropriate model within the limitations of a particular analysis code.

Material characterization remains a relatively unexplored area for those involved with transparent materials, and much experimental and analytical work is required to resolve existing problems. A primary shortcoming is the lack of experimental data concerning inelastic behavior and rate dependence of stiff polymers such as polycarbonate. The characterization of interlayer materials suffers from basic theoretical deficiencies, and presents some challenging problems in numerical analysis as well.

The prediction of soft-body impact loading, a central issue in many transparency simulations, is the subject of current research which is intended to eliminate the need for gross simplifications and approximations in the study of impact response. Further efforts in this area are desirable to develop guidelines for selecting "worst cases" to be analyzed for survivability under impact conditions.

REFERENCES

1. G. J. DeSalvo and J. A. Swanson, "ANSYS Users Manual", Swanson Analysis Systems, Inc., Houston, Pennsylvania.

2. R. A. Brockman, "MAGNA (Materially And Geometrically Nonlinear Analysis) Part I: Finite Element Analysis Manual," UDR-TR-82-111, University of Dayton Research Institute (1982)

3. _____, "MARC User Information Manual", Volumes A-G, MARC Analysis Research Corporation, Palo Alto, California.

4. R. H. MacNeal (editor), "MSC/NASTRAN Users Manual," MacNeal-Schwendler Corporation, Los Angeles, CA.

5. R. D. Mindlin, "Influence of Rotatory Inertia and Shear on Flexural Motions of Isotropic Elastic Plates," Trans. ASME, Journal of Applied Mechanics, Vol. 18, pp. 31-38 (1951)

6. B. M. Irons, "Quadrature Rules for Brick-Based Finite Elements," International Journal for Numerical Methods in Engineering, Vol. 3, pp. 293-294 (1972)

7. K. J. Bathe and S. Bolourchi, "A Geometric and Material Nonlinear Plate and Shell Element," Journal of Computers and Structures, Vol. 11, pp. 23-48 (1980)

8. K. S. Surana, "Transition Finite Elements for Three Dimensional Stress Analysis," International Journal for Numerical Methods in Engineering, Vol. 15, pp. 991-1020 (1980)

9. R. A. Brockman and F. K. Bogner, "An Efficient Three Dimensional Shell Element for Highly Nonlinear Problems," in A. Seirig (editor), Advances in Computer Technology -- 1980, Vol. 2, pp. 219-226, ASME, New York (1980)

10. R. E. McCarty, "Finite Element Analysis of F-16 Aircraft Canopy Dynamic Response to Bird Impact Loading," Proceedings of the AIAA/ASME/ASCE/AHS 21st Structures, Structural Dynamics and Materials Conference, Vol. 2, pp. 841-852 (1980)

11. H. Matthies and G. Strang, "The Solution of Nonlinear Finite Element Equations," International Journal for Numerical Methods in Engineering, Vol. 14, pp. 1613-1626, (1979)

12. R. A. Brockman, "Economical Stiffness Formulations for Nonlinear Finite Elements," Journal of Computers and Structures (preprint)

13. M. A. Crisfield, "A Fast Incremental/Iterative Solution Procedure that Handles 'Snap-Through'", Journal of Computers and Structures, Vol. 13, pp. 55-62 (1981)

14. J. Padovan, "Self-Adaptive Predictor-Corrector Algorithm for Static Nonlinear Structural Analysis," NASA-CR-165410, Department of Mechanical Engineering, University of Akron, Ohio (1981)

15. H. D. Hibbitt and B. I. Karlsson, "Analysis of Pipe Whip," ASME Paper 79-PVP-122, ASME, New York (1979)

16. R. E. McCarty, "Aircraft Transparency Bird Impact Analysis with the MAGNA Computer Program," Proceedings, British Aerospace Companies Conference on Aircraft Transparencies, British Aerospace Companies, London, pp. 297-313 (1980)

17. R. E. McCarty and R. A. Smith, "Finite Element Analysis of Through-the-Canopy Emergency Crew Escape from the T-38 Aircraft," AIAA 8th Annual Mini-Symposium on Aerospace Science and Technology, Air Force Institute of Technology, Wright-Patterson Air Force Base, Ohio (1982)

18. R. E. McCarty and R. A. Smith, "Simulation of T-38 Aircraft Student Canopy Response to Cockpit Pressure and Thermal Loads using MAGNA," Proceedings of the AIAA/ASME/ASCE/AHS 24th Structures, Structural Dynamics and Materials Conference, Part 1, pp. 423-444 (1983)

19. R. A. Nash and B. S. West, "Alternate T-38 Transparency Development, Part IV: Parametric Studies," AFWAL-TR-80-3132, Part IV, Air Force Wright Aeronautical Laboratories, Wright-Patterson Air Force Base, Ohio (1983)

20. B. S. West, "Design and Testing of F-111 Bird-Resistant Windshield / Support Structure, Volume 1: Design and Verification Testing," AFFDL-TR-76-101, Vol. 1, Flight Dynamics Laboratory, Wright-Patterson Air Force Base, Ohio (1976)

21. B. S. West, "The Role of Finite Element Analysis in the Design of Birdstrike Resistant Transparencies," Proceedings, British Aerospace Companies Conference on Air-

craft Transparencies, British Aerospace Companies, London, pp. 273-295 (1980)

22. B. S. West and R. A. Brockman, "Evaluation of Bird Loading Models for Dynamic Analysis of Aircraft Transparencies," AFWAL-TR-80-3092, Air Force Wright Aeronautical Laboratories, Wright-Patterson Air Force Base, Ohio (1980)

23. J. J. Labra, "Finite Element Modeling of a Fighter Aircraft Canopy Acrylic Panel," AIAA Paper 82-4152, Journal of Aircraft, Vol. 19, pp. 480-484 (1982)

24. H. F. Brinson and A. DasGupta, "The Strain-Rate Behavior of Ductile Polymers," Experimental Mechanics, No. 12, pp. 458-463 (1975)

25. M. A. Eisenberg and C. F. Yen, "A Theory of Multiaxial Anisotropic Viscoplasticity," Trans. ASME, Journal of Applied Mechanics, Vol. 48, pp. 276-284 (1981)

26. S. R. Bodner, I. Partom, and Y. Partom, "Uniaxial Cyclic Loading of Elastic-Viscoplastic Materials," Trans. ASME, Journal of Applied Mechanics, Vol. 46, pp. 805-810 (1979)

27. R. S. Rivlin, "Large Elastic Deformations," in F. R. Eirich (editor), Rheology, Vol. 1, Academic Press, New York (1956)

28. P. J. Blatz and W. L. Ko, "Application of Finite Elastic Theory to the Deformation of Rubbery Materials," Transactions of the Society of Rheology, Vol. 6, pp. 223-251 (1962)

29. J. W. Wissmann, "A Rigid-Body Transformation Algorithm for Structures with Large Stiffness Variations, with Application to Incompressible Elements," in K. J. Bathe, J. T. Oden, and W. Wunderlich (editors), Formulations and Computational Algorithms in Finite Element Analysis, M.I.T. Press (1977)

30. E. L. Wilson, "Special Numerical and Computer Techniques for the Analysis of Finite Element Systems," in K. J. Bathe, J. T. Oden, and W. Wunderlich (editors), Formulations and Computational Algorithms in Finite Element Analysis, M.I.T. Press (1977)

31. J. P. Barber, H. R. Taylor, and J. S. Wilbeck, "Bird Impact Forces and Pressures on Rigid and Compliant Targets," AFFDL-TR-77-60, Air Force Flight Dynamics Laboratory, Wright-Patterson Air Force Base, Ohio (1978)

32. A. Challita and J. P. Barber, "The Scaling of Bird Impact Loads," AFFDL-TR-79-3042, Flight Dynamics Laboratory, Wright-Patterson Air Force Base, Ohio (1979)

33. C. W. Hirt, B. D. Nichols, and N. C. Romero, "SOLA -- A Numerical Solution Algorithm for Transient Fluid Flows," Report UC-34, Los Alamos Scientific Laboratory, New Mexico (1975)

34. N. M. Newmark, "A Method of Computation for Structural Dynamics," Proc. ASCE, Journal of the Engineering Mechanics Division, Vol. 85, pp. 67-94 (1959)

35. T. Belytschko and R. Mullen, "Stability of Explicit-Implicit Mesh Partitions in Time Integration," International Journal for Numerical Methods in Engineering, Vol. 12, pp. 1575-1586, 1978.

AD-P003 234

NASTRAN ANALYSIS OF NUCLEAR EFFECTS ON HELICOPTER TRANSPARENCIES

P. T. Lin and J. S. Jorgenson,
Goodyear Aerospace Corporation

NASTRAN ANALYSIS OF NUCLEAR EFFECTS ON HELICOPTER TRANSPARENCIES

P.T. Lin, Ph.D.
Engineer Specialist
and
J.S. Jorgenson, P.E.
Engineer Specialist, Sr.
Goodyear Aerospace Corporation
Litchfield Park, Arizona

ABSTRACT

This paper deals with the linear and geometric nonlinear analysis of the gunner's window on the AH-1S Cobra helicopter in response to a nuclear overpressure environment. The work was sponsored by the Applied Technology Laboratory, U.S. Army Research and Technology Laboratories (AVRADCOM), Fort Eustis, Virginia. Both monolithic stretched acrylic and multilayered transparency configurations are considered in this report. Comparison analyses using both the NASTRAN finite element program and classical Timoshenko plate theory show good agreement.

Comparison of the analytical results with experimental observations made by other sources indicates that the geometric nonlinear mathematical models, rather than the linear models, are the more realistic and appropriate representation of transparency response to nuclear overpressure loading in the range considered. It is shown that the classical analysis of a simplified equivalent configuration serves as a useful checkpoint, while finite element programs, such as MSC/NASTRAN, are the necessary analytical tools to examine the complicated configurations and loading conditions.

INTRODUCTION

Aircraft operating in an area of sky under nuclear barrage attack are subjected to a variety of potentially disabling effects. The minimum safe distance between an aircraft and a nuclear burst depends on the weapon yield, the height of the aircraft, the height of the burst, the aircraft speed, the orientation of the aircraft with respect to the burst, and the aircraft hardness. Taking these variables into account, a lethal volume around the aircraft can be defined (by the conventional spherical method or by the constant-area-balancing (CAB) method) within which a burst can be expected to destroy the aircraft by the effects of overpressure, gusts, and thermal radiation.

This report deals specifically with the structural analysis (stress and deflection) of helicopter transparencies in response to nuclear overpressure. In order to calculate the effect of overpressure loads on transparencies using the analysis of linearly elastic structures, several assumptions are made. First, deflections and strains developed in the structure are small. Physically, this means that during the loading process, the geometry of the structure remains basically unchanged, so that the infinitesimal, first-order linear strain-deflection relations may be used, and the equations of equilibrium written for the undeformed structure remain valid. Second, stress/strain relationships for the material are linear. This assumption can be thought of as following from the first, since the stress/strain relationships for most engineering materials can be considered linear when the stresses are below the elastic limit and the deflections are small.

In many instances, even though the actual strains and deflections may be small and the elastic limits of the structural material are not exceeded, the assumptions fail. For example, stresses due to membrane action, usually neglected in plate bending, may cause a considerable decrease in actual deflection when compared to the linear solution, even though deflections are small. An accurate determination of stresses and deflections in a transparency may require the consideration of nonlinear effects.

The two basic types of nonlinear effects that occur in structural problems are material nonlinearities and geometric nonlinearities. Material nonlinearity is a result of nonlinear elastic or plastic behavior of the structural material. Geometric nonlinearity occurs when loads applied to a structure produce large deflections (relative to material thickness) and thereby change the geometry of the structure. The equations of equilibrium must then be formulated for the change in structural geometry.

Monolithic stretched acrylic and multilayered transparency configurations were analyzed for both linear and geometric nonlinear analysis using classical Timoshenko plate theory (Ref. 1) and NASTRAN finite element method of analysis (Ref. 2, 3). The results of the analyses indicate that the geometric nonlinear mathematical models produce representations of transparency response to nuclear overpressure which are more realistic than the representations produced by linear mathematical models.

DEFINITIONS OF PRESSURE

The four pressure terms are defined as follows:

1. P_{so} (peak incident overpressure) = free field nuclear overpressure in the traveling shock wave.

2. P_{ro} (peak reflected overpressure) = pressure loading dynamically applied to the transparency including both wave reflection and dynamic pressure effects (Ref. 4).

3. P_{to} (total equivalent pressure) = pressure applied statically which results in an equivalent structural response.

4. P_o = atmospheric pressure.

The four pressure terms are related as described by the following equations and some tabulated values (psi units) below.

$$P_{ro} = 2\,P_{so}\,\frac{7\,P_o + 4\,P_{so}}{7\,P_o + P_{so}} \tag{1}$$

$$P_{to} = 2.0\,P_{ro} \tag{2}$$

P_{so}	0.5	0.75	0.8	0.9	1.0	1.25	1.5
P_{ro}	1.01	1.53	1.64	1.85	2.06	2.59	3.13
P_{to}	2.02	3.06	3.28	3.70	4.12	5.18	6.26

In the following discussion, any reference to pressure denotes total equivalent pressure (P_{to}).

TRANSPARENCIES

The gunner's window of the AH-1S Cobra helicopter was the subject of the mathematical analyses described in this report. The two configurations of the gunner's window that were analyzed are a monolithic stretched acrylic transparency (configuration 1) and a multilayered transparency (configuration 2).

ANALYSIS ASSUMPTIONS

The following assumptions were made during analyses:

1. Fixed-edge boundary constraints were applied for all of the analyses. Differences, if any, between the assumed fixed edge boundary constraints and actual boundary constraints were ignored. Actual transparency geometry was used for the NASTRAN analysis of the configuration 1 transparency. Beam element approximations were used for the NASTRAN analysis of the configuration 2 transparency. An equivalent rectangular plate was used for the classical Timoshenko plate analyses.

2. For the nonlinear analyses, material stress/strain relationships were assumed to be linear, and consequently, all nonlinear effects were assumed to be due to geometric nonlinearities.

3. Flat-plate transparencies were assumed for the analyses.

ANALYSIS AND DISCUSSION

The transparencies were analyzed using classical Timoshenko plate theory and NASTRAN finite element analysis. Both linear and nonlinear conditions were applied to each of the two analysis methods.

The monolithic acrylic transparency (configuration 1) was analyzed for maximum deflection (inches) and maximum stress (psi) under 0.5-, 1.0-, 1.5-, 2.0-, and 3.0-psi pressure using classical Timoshenko plate theory, and under 2.0- and 3.0-psi pressures using NASTRAN finite element analysis.

Figures 1 and 2 depict, respectively, the grid points and the plate elements used for the NASTRAN finite element analysis model for the configuration 1 transparency.

Figure 3 (maximum deflection versus pressure) and Figure 4 (maximum stress versus pressure) describe the results of the analyses of the configuration 1 transparency. Reference to the plots for maximum deflection versus total equivalent pressure (Figure 3) reveals close agreement between the classical Timoshenko plate theory and the NASTRAN finite element analyses for both the linear theory and the geometric nonlinear theory. Reference to the maximum stress versus total equivalent pressure plots (Figure 4) reveals some variation between the classical Timoshenko plate theory and the NASTRAN finite element analyses for both the linear and the geometric nonlinear theories. The observed variation is due in part to the different assumptions (see "Analysis Assumptions," item 1) employed when the analyses were made.

A significant difference exists for maximum deflection and for maximum stress plots between linear theory results and geometric nonlinear theory results for both classical Timoshenko plate and NASTRAN analyses. For example, the classical Timoshenko plate

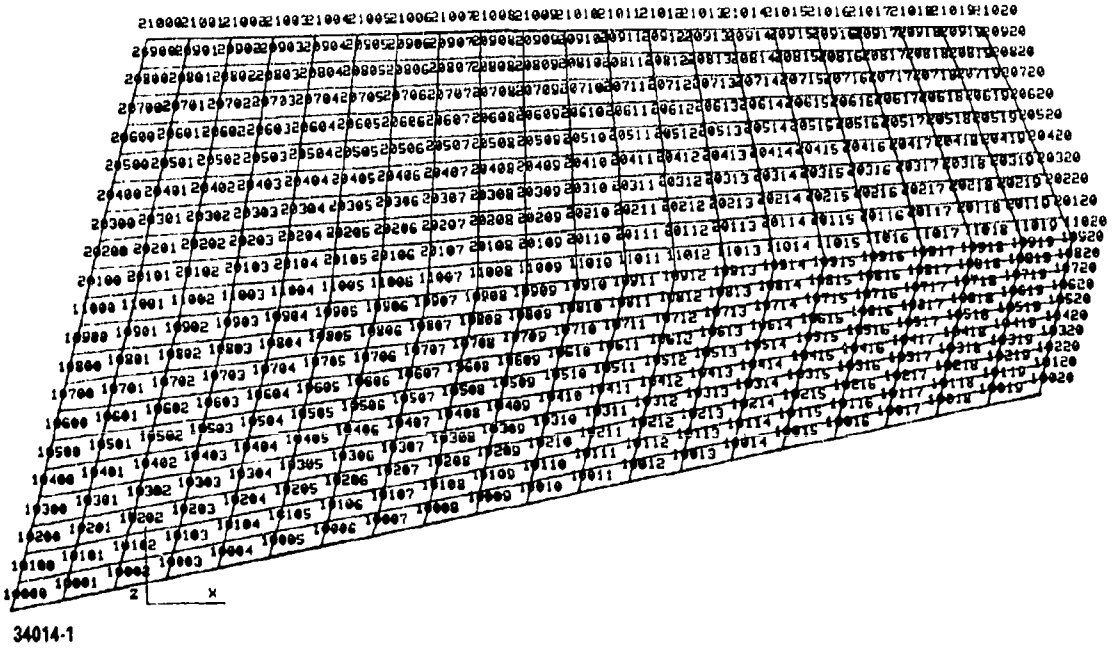

Figure 1. NASTRAN Transparency Finite Element Model Grid Points

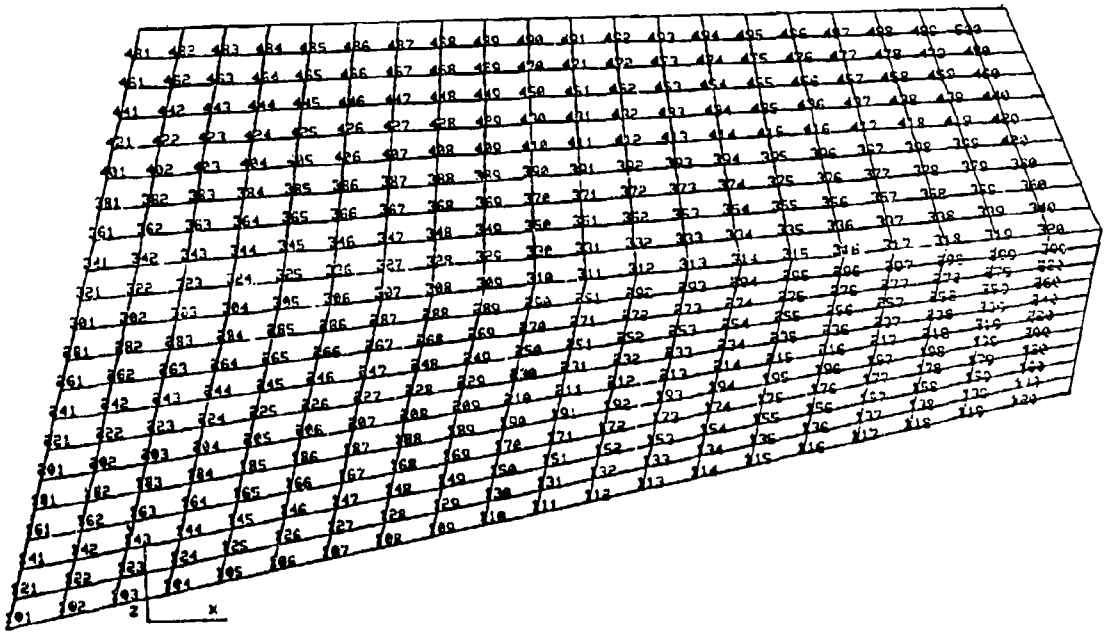

34014-2

Figure 2. NASTRAN Transparency Finite Element Model Plate Elements

analysis results for the configuration 1 transparency under 1.0-psi pressure load are as follows:

	Maximum stress (psi)	Maximum deflection (in.)
Geometric nonlinear theory	3347	0.52
Linear theory	8228	3.39

The ratios of the results of the linear theory and the geometric nonlinear theory are as follows:

	Maximum stress (ratio)	Maximum deflection (ratio)
Geometric nonlinear theory	1.00	1.00
Linear theory	2.46	6.52

Since the results given by the two theories are significantly different, a question exists as to which one or if either of the results approximates the actual value. Reference to a report (Ref. 5) containing the results of an actual test conducted on a laminated glass windshield sheds some light on the situation. A NASTRAN finite element analysis (linear

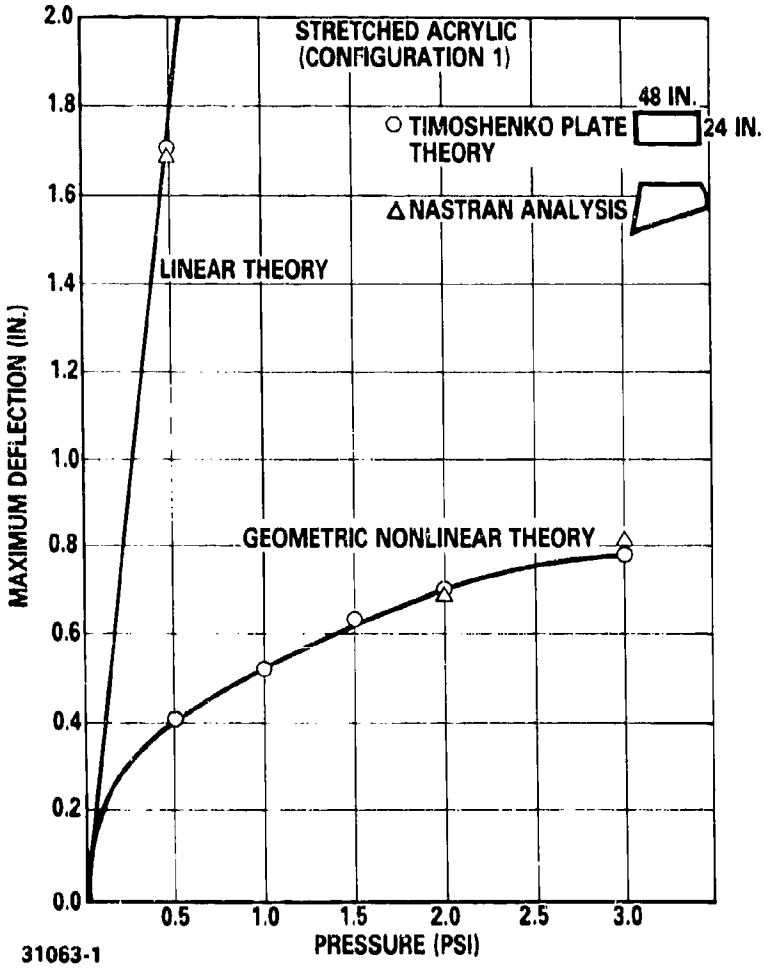

Figure 3. Configuration 1, Maximum Deflection Versus Pressure, Linear and Nonlinear Theory

theory) was also carried out on the same laminated glass windshield (Ref. 5, pp. 104-106).

The test results and the analysis results at 1.0-psi pressure load are as follows:

	Maximum stress (psi)	Maximum deflection (in.)
Test	2300	0.098
NASTRAN (linear)	6843	0.623

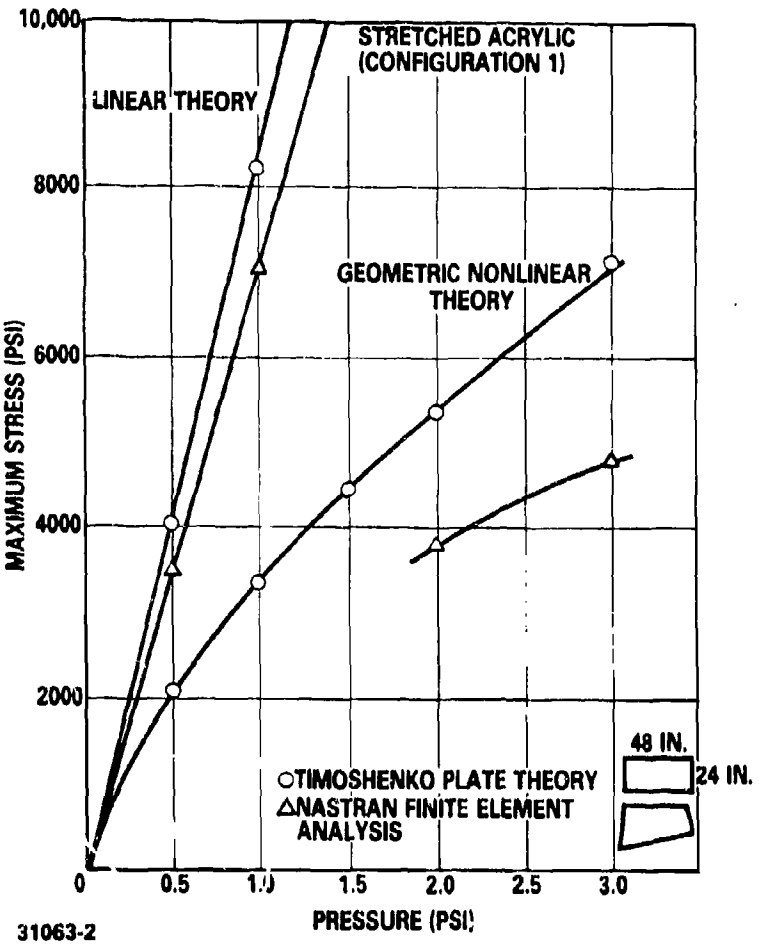

Figure 4. Configuration 1, Maximum Stress Versus Pressure, Linear and Nonlinear Theory

The ratios of the test results and the NASTRAN linear analysis results are as follows:

	Maximum stress (ratio)	Maximum deflection (ratio)
Test	1.0	1.0
NASTRAN (linear)	2.98	3.38

The test results indicated much lower stress and deflection, compared with those of NASTRAN linear anlaysis (NASTRAN geometry nonlinear analysis feature was not available until 1978). This signifies the importance of geometric nonlinear effects due to membrane stresses. Comparison of the preceding ratios leads to the conclusion that the

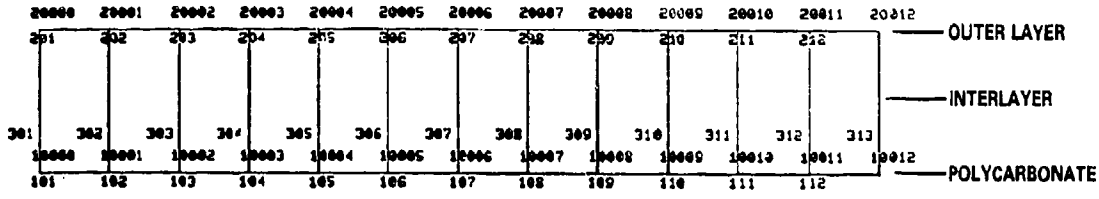

ELEMENT NUMBER	NASTRAN ELEMENT	LAYER
201-212	C-BEAM	OUTER LAYER
301-313	CONROD	INTERLAYER
101-112	C-BEAM	POLYCARBONATE

34014-3

Figure 5. Configuration 2, Multilayered Transparency G2 Structural Variation, NASTRAN Finite Element Model

NONLINEAR

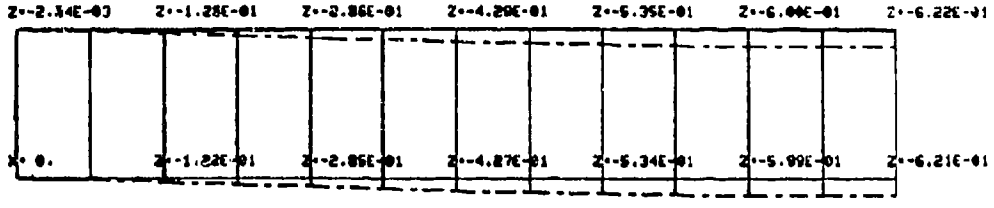

LINEAR

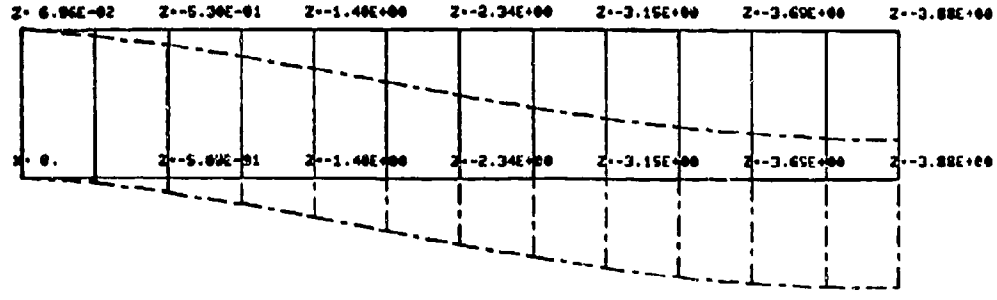

34014-4

Figure 6. Configuration 2, Multilayered Transparency G2 Structural Variation, Deformed Geometry

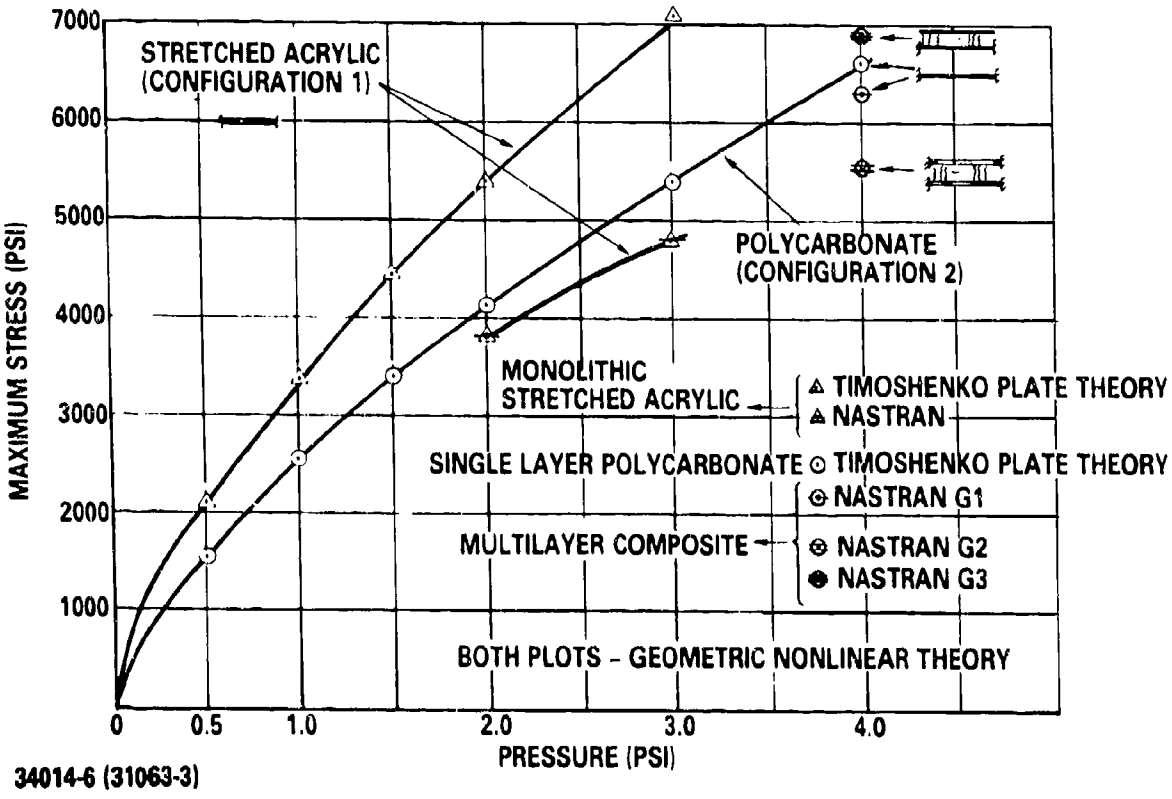

Figure 7. Configurations 1 and 2, Maximum Stress Versus Pressure, Geometric Nonlinear Theory

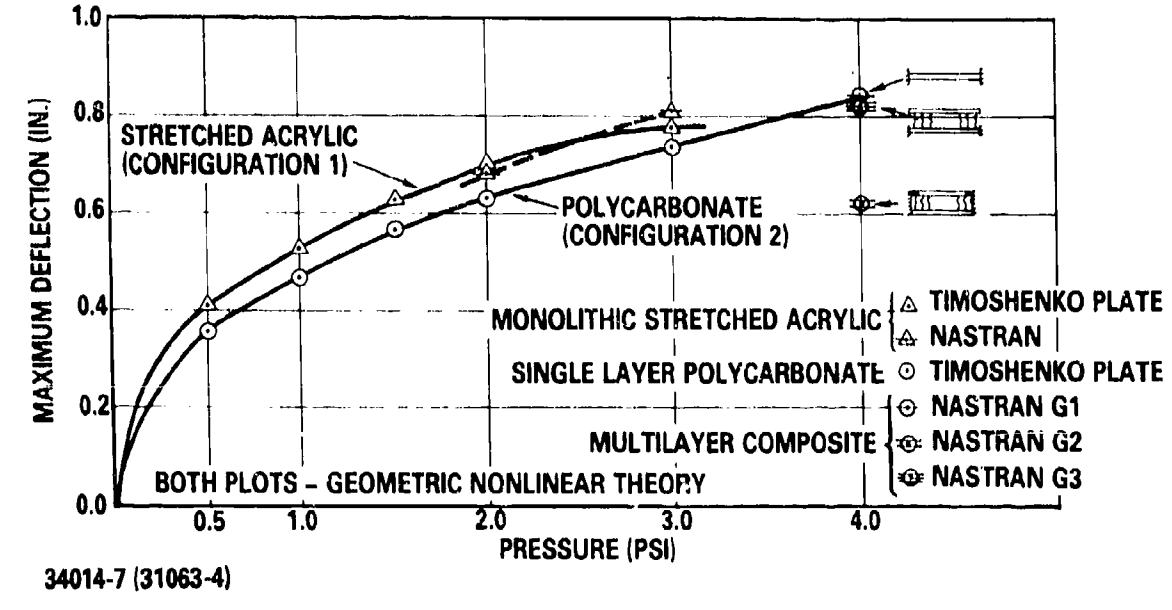

Figure 8. Configurations 1 and 2, Maximum Deflection Versus Pressure, Geometric Nonlinear Theory

geometric nonlinear mathematical models are more realistic and appropriate representations of the transparency response to nuclear overpressure loading.

The configuration 2 transparency was analyzed in three different structural variations using NASTRAN finite element analysis. The first variation (G1 on Table 1) was single-layer polycarbonate. The second variation (G2 on Table 1), which was chosen to simulate the edge construction, was a multilayer configuration consisting of an outer layer with vertical roller supports, an interlayer, and a polycarbonate structural ply with fixed edges. The third variation (G3 on Table 1), was identical to the G2 variation except that the outer layer was free to move. Only single-layer polycarbonate (G1) was analyzed using classical theory.

The NASTRAN finite element model and the deformed geometries for the NASTRAN finite element analyses of the G2 structural variation due to pressure load for both the linear and geometric nonlinear theories are illustrated in Figures 5 and 6, respectively.

Table 1. Configuration 2, Summary

	TIMOSHENKO THEORY		NASTRAN ANALYSIS					
			G1		G2		G3	
	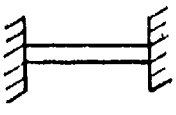				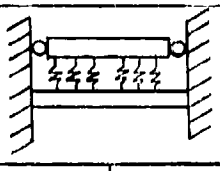		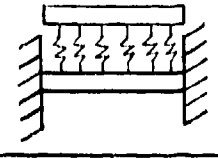	
	L	NL	L	NL	L	NL	L	NL
DEFLECTION (IN.)	7.60	0.844	7.60	0.843	3.877	0.621	3.877	0.824
MEMBRANE STRESS (PSI)	0	1098	0	1078	0	584	0	1015
BENDING STRESS (PSI)	18641	5529	18141	5224	17026	4950	17026	5893
COMBINED STRESS (PSI)	18641	6628	18141	6302	17026	5534	17026	6908

34014-5

Table 1 summarizes the linear (L) and the geometric nonlinear (NL) theory results for both the classical Timoshenko plate and the NASTRAN finite element analyses of the configuration 2 transparency. The NASTRAN-calculated response of the G1 configuration to a load pressure is very close to the response to the same load pressure calculated by the classical Timoshenko plate analysis (Table 1). As would be expected, the G2 configuration, which is the more rigid version of the two edge-band construction approximations, has the lowest calculated response (both maximum stress and maximum deflection) to the pressure load. The calculated response of the G3 configuration to a pressure load is very close to the response to the same pressure load calculated by the classical Timoshenko plate analysis. The maximum stress versus overpressure and the maximum deflection versus overpressure for the configuration 2 transparency are plotted in Figures 7 and 8, respectively. Geometric nonlinear theory results for both the classical Timoshenko plate and the NASTRAN finite element analyses of the configuration 1 transparency were plotted with the configuration 2 transparency plots for reference.

CONCLUSIONS

The following conclusions can be drawn based upon the analysis results of this paper:

1. Comparison of the analytical results with experimental observation (Ref. 5) clearly indicates that the geometric nonlinear models, rather than the linear models, are the more realistic and appropriate representations of transparency response to nuclear overpressure loading in the range considered.

2. Classical analysis of a simplified equivalent configuration serves as a useful checkpoint, while the finite element programs, such as NASTRAN, are the necessary analytical tools to examine the complicated configurations and loading conditions.

3. The MSC/NASTRAN has been shown to be a creditable analytical tool in its geometric nonlinear analysis capability.

The mathematical modeling approach employed can be used to analyze a wide variety of other transparency construction configurations and geometries for response to nuclear overpressure.

REFERENCES

1. Theory of Plates and Shells; S. Timoshenko and S. Woinowsky-Krieger; McGraw-Hill, New York, NY, 1959.

2. MSC/NASTRAN, Application Manual, Volume 1; MacNeal-Schewendler Corp., Los Angeles, CA, 1982.

3. MSC/NASTRAN, User's Manual, Volumes 1 and 2; MacNeal-Schwendler Corp., Los Angeles, CA, 1982.

4. Structural Design for Dynamic Loads; C.H. Norris, R.J. Hansen, R.J. Holley, Jr., J.M. Biggs, S. Namyet, and J.K. Minami; McGraw-Hill, New York, NY, 1959.

5. USARTL-TR-78-26; Design, Test, and Acceptance Criteria for Helicopter Transparent Enclosures; Applied Technology Laboratory, U.S. Army Research and Technology Laboratories (AVRADCOM), Fort Eustis, VA, 1978.

AD-P003 235

THEORETICAL EVALUATION OF THE STRUCTURAL PERFORMANCE OF SWEDISH FIGHTER AIRCRAFT WINDSHIELD SUBJECTED TO IMPACT

L. A. Samuelson, F. Nilsson,
and L. Sornas, Stockholm, Sweden

Theoretical Evaluation of the Structural Performance of Swedish Fighter Aircraft Windshields Subjected to Bird Impact.

Lars Åke Samuelson
Fred Nilsson
Lennart Sörnäs

IFM Akustikbyrån AB, Stockholm, Sweden

Abstract

High velocity bird impact characteristics were studied theoretically and the critical velocity, windshield deflection, "birdraulics" and associated phenomena in Swedish fighter aircraft were predicted. The investigation was carried out for the Swedish Air Force in close cooperation with the Saab Scania Aerospace Co and the results were used to optimize the test program and to propose design improvements for existing crew enclosures.

1. INTRODUCTION

The bird collision hazard has been considered in the design of Swedish fighter aircraft in the past and the design goals were verified to a certain degree of confidence through bird gun testing. A recent test series with F35 Dragon windshields showed, however, that the material of the transparancy undergoes a degradation in strength with time. Also, tests with the F37 Viggen windshield revealed that the design goals were not compeltely fullfilled and the need for a comprehensive study of the bird collision characteristics was noted.

Powerful tools for numerical analysis of various types of structural problems have been developed in recent years and the possibility to improve the efficiency of the bird impact investigations through a combined experimental and theoretical effort was recognized by the Swedish Air Force. The analysis described in the present report was carried out in close cooperation with the Saab Scania Aerospace Co with the specific objectives to

- Develop and evaluate methods of analysis for bird strike problems
- "Calibrate" the analysis against test results
- Assist in the planning of the test program
- Predict deflections and stresses as functions of bird weight, impact speed and impact point
- Predict critical collision velocities for the windshield especially due to contact forces from underlying structures such as the head up display (HUD)
- Produce "maps" of deflections and critical velocities to be used in a failure risk analysis.

2. DISCUSSION AND CONCLUSIONS

The investigation showed that theoretical evaluation of the windshield characteristics may be carried out efficiently by use of comparatively simple methods provided certain conditions are fulfilled. The results may be summarized as

- Linear modal analysis is adequate for determination of windshield deflections and stresses provided the number of eigenmodes is related to the bird size (10 modes for a 1 kg (2 lb) bird) and the maximum deflection is of the order of the windshield thickness.

- Small bird impact at high velocities is preferably analyzed by use of a direct integration method as provided in for instance MAGNA, Ref /1/.

- Linear analysis results should be checked by use of a non-linear analysis.

- Comparisons with test results showed acceptable agreement. However, the dynamic strength of the acrylic appeared to be approximately 50 per cent higher than the static values given by the manufacturer. Use of the higher value gave very close agreement between predicted penetration velocities and test results.

- Mapping of deflections and stresses due to bird impact is conveniently done by use of a linear modal analysis at very low computer costs.

- Contact between the deflected windshield and the head-up display (HUD) glass was found to be a major cause of windshield failure. Various models for solution of the problem were analyzed in order to propose modifications. Early contact through a pressure pad placed on top of the HUD glass was proposed as a practical measure. It could be shown, however, that the strength of the HUD glass was inadequate to allow the accelerations involved and it was necessary to propose an increased clearance between the HUD glass and the windshield.

- The "birdraulics" effect on the front arch of the canopy was estimated and it was shown that it was the primary cause of canopy failures observed in the test series.

3. THEORETICAL BACKGROUND

Current methods of structural analysis, such as the Finite Element Method (FEM) are well known and do not require further presentation. The bird impact problem, however, involves features like large deflections and standard linear theories may not be sufficient. When the present investigation was initiated, little experience was available on large deflection dynamic analyses. Therefore, analyses were carried out with various degrees of accuracy in order to establish and recommend requirements for bird strike analysis methods.

3.1 Dynamic analysis by modal superposition

Small deflection vibrations of a linear structure are characterized by the eigenmodes and eigenfrequencies. Transient vibrations are conveniently handled by use of modal analysis and efficient routines are available in most general purpose FEM-programs. In the present investigation the modal characteristics of the windshields were evaluated by use of the BASIS FEM-program, Ref /2/. Special purpose programs were developed for the calculation of the transient deflections and stresses. A brief summary of the theoretical base for the modal analysis is given below:

Assume that the eigenvalue problem for the windshield has been solved yielding the generalized coordinates $\bar{q}_k$ and the eigenfrequency $\bar{\omega}_k = \omega_k (1 + i\eta)$, $k = 1, 2, \ldots n$. Then a linear system of equations for the dynamic problem is given by

$$\ddot{\bar{q}}_k + \bar{\omega}_k^2 \bar{q}_k = B_{zk} F_z(t) \qquad (1)$$

where B_{zk} is the component of the eigen vector corresponding to a z-displacement at the impact point according to Figure 2. $F_z(t)$ is the force acting at point k.

The displacement at the impact point is given by

$$u_z = R_e [\Sigma B_{zk} q_k] \quad \text{and} \qquad (2)$$

the velocity by

$$v_z = R_e [\Sigma B_{zk} \dot{q}_k] \qquad (3)$$

Eqs (1-3) are sufficient for the solution of the dynamic response problem and they were solved by use of a finite difference scheme.

The force $F(t)$ is in general a fairly complex function of time and the coordinates of the windshield. The simplified model recommended in Ref /3/ was used, Figure 3, with the extension that the deflection velocity of the windshield is considered in the evaluation of the force magnitude. The distribution of the force over the surface was neglected since the use of the eigenmodes for description of the deflections leads to an "averaging effect". Tests with a distributed force showed differences of the order of a few per cent. Finally the bird slides along the surface on impact and the force moves towards the rear. This effect was neglected in the analysis. The results will be discussed below.

A tremendous advantage with the linear modal analysis, whenever applicable, is the fact that a response analysis is carried out in the reduced generalized coordinate system. Complete mapping of the deflections and stresses is therefore a matter of minutes of computer time.

3.2 Nonlinear analysis

The deflections of the windshield are of the order of the wall thickness 25 mm (= 1") during bird impact. At that level of deformation the linear shell theory may provide a poor approximation to the true behavior of the structure and a nonlinear theory may have to be used. Compare Refs /4-5/. In order to check the accuracy of the linear modal analysis, the MAGNA code, Ref /1/ was utilized in a number of sample cases for both the Dragon and the Viggen Aircraft.

A few typical results are shown in Figure 4, where the deflections at the point of impact are plotted as functions of time. It was, in general, noted that the differences in deflections and stresses between the linear (modal analysis and MAGNA linear) and the nonlinear theory were marginal for the "standard" 1 kg (2 lb) bird. For smaller birds, the linear modal analysis failed to yield acceptable results for the stresses. This is primarily due to the fact that the number of eigenmodes retained in the analysis, 10, was insufficient.

3.3 Contact problems

In the experimental investigation it was found that windshield failure was obtained at impact velocities well below that of the windshield itself due to contact with the head up display glass. One objective of the theoretical work was to estimate the forces during contact and to propose possible modifications. Different models were utilized in the work in order to study the behavior of the windshield and head up display. Figure 5a shows a simple mass-spring system for the HUD glass. The system was coupled with the deflections of the windshield in order to estimate the effect of the contact on the windshield velocity.

A second model, Figure 5 b, was used to evaluate an idea that "early gentle" contact might be used to avoid premature failure of the windshield. The concept was based on placing a crushable pad on top of the head up display providing a constant force during the contact phase. The beam model dynamic response was evaluated by use of a direct integration procedure.

Finally, the accuracy of the beam model was checked by use of a MAGNA analysis, Figure 5c.

4. EXPERIMENTAL VALIDATION

The comparisons with test data formed an important part of the investigation and the results were used as a basis for recommendations on analysis procedures in the future. Brief descriptions of the various parameters studied are given below.

4.1 Eigenmodes, eigenfrequencies

The eigenfrequencies were measured for the Dragon and Viggen windshields and complete experimental modal analyses were carried out. Typical results for the fundamental frequency are given in Figure 6. In the analysis the 10 lowest (symmetric) frequencies were extracted, the fundamental mode shapes included in Figure 6. Comparisons between measured and computed frequencies are given in Table 1.

The correlation between the theoretical and the experimental value of the fundamental frequency of the Dragon windshield is excellent, whereas a certain difference is noted for the Viggen windshield.

There is some doubt, however, about the validity of the experimental value of the fundamental frequency as illustrated in Figure 7. The windshield was tapped with a hammer at point B and the acceleration response was measured at the same point. The theoretical curve included in Figure 7 shows the transfer function at the same point (note that the scales are not comparable). The curves show that only some of the eigenmodes are active in the response to a force applied at point B. Excellent agreement is noted for the eigenmodes which participate in the dynamic response.

4.2 Deflections and stresses

The transient response analysis of the windshield subjected to a forcing function as shown in Figure 3 may be represented by the deflection along the line of symmetry as shown in Figure 8. The force F(t) is applied at node No 93 and does not move along the surface. The deflections at a number of times are given together with the envelope.Included in Figure 8 is the maximum deflection pattern measured during test no "706". It is clear that the analysis yields an acceptable result with regard to the deflection amplitude. The distribution along the windshield symmetry line is, however, shifted downstream in the tests due to the fact that the bird slides along the surface on impact. (Compare for instance Ref /4/). The difference was accepted for the analyses but there is no difficulty in

inclusion of the effect in future analyses.

Typical results for maximum deflections at various points on the windshield surface are shown in Figure 9. Considering the scatter in measured quantities usually observed in the tests the agreement is acceptable.

Stresses were measured by use of strain gauges on the inside of the windshield at the impact point. Typical response curves are given in Figure 10 where theoretical peak values are included for comparison. Moreover, measured and calculated values for various impact velocities and two different target points on the windshield are given in Figure 11. The analysis showed that higher stresses could be anticipated if the point of impact was moved to 1/3 from the forward edge. Based on these results a few tests were carried out with a forward target point. These clearly confirmed the theoretical prediction.

The stress analysis for the Dragon windshield showed that the highest stress levels sometimes occured at a point close to the lower rear corner, see Figure 12, which implies that failure might occur at a location different from the impact point. A series of high speed movie frames taken at the Saab Scania test series, Figure 13 shows the appearance of a crack at the location of high stresses indicated in Figure 12 at about 2 ms after impact as predicted by the analysis.

4.3 Critical velocity - material properties

The material properties provided by the manufacturer indicate a (uniaxial) failure stress of 80 N/mm^2 (80 MPa) for stretched acrylic. It is not clear what criterion to use for prediction of the critical windshield stress. In the analyses presented herein the maximum tensile principal stress was used as a reference for determination of the critical stress level. Some results are shown in Figure 14 for the Viggen windshield. The maximum stress is plotted as a function of the impact velocity for the two different target prints A and B according to Figure 7. The experimental critical speed was approximately 1050 km/h (1 kg birds) and the aft target point, which indicates an ultimate stress level of 110 N/mm^2. This value was used throughout the investigation.

4.4 Comments

Most of the analyses were carried out for a 1 kg bird and the model used for modal analysis was adapted to these problems. In the tests carried out at Holloman Air Force base, NM, penetration of the windshield occurred at 1100 km/h with a 0.3 kg bird. The transient analysis by modal analysis, Figure 4, with the 10 modes model showed an underestimation of the deflections and stresses. Therefore a nonlinear response analysis was carried out by use of the MAGNA code, Ref /1/. The deflections of the windshield are shown in Figure 15 at two different times after impact. It is evident that the deflections are localized during the first moments of the impact and the description of the initial phase by use of the modal characteristics would require a larger number of modes than were used in the present analyses.

5. CONTACT PROBLEMS

As indicated previously contact between the windshield and underlying structural hard points such as the HUD, could lead to failure of the windshield. Whenever possible the hard points were removed. Relocation of the HUD, however, poses considerable problems and different approaches were tried in order to find an acceptable solution.

The simplified model of Figure 5a was used in order to estimate the magnitude of the contact force between the HUD mirror and the windshield. The results, shown in Figure 16 indicate forces of the order of 10 000 N. It might be possible to arrange the contact surface in such a way that an acceptable average pressure would result. However, studies showed that nonsymmetric bird impact, for instance, would lead to problems as indicated in Figure 16. An important result of the investigation was that the HUD did not seem to have a noticable influence on the velocity of the windshield. The velocity could thus be used as a driving parameter in the response analysis of the HUD mirror.

An idea developed during the analysis that a soft cushion placed on top of the HUD mirror would make an early contact with the windshield during a bird impact and the mirror would be pushed gently away from the windshield. The arrangement is shown in Figure 17. It was assumed that the cushion was made of a crushable material and would produce a constant force during the event. The mirror was analyzed dynamically by use of a simple beam model according to Figure 5b. Typical results depending on the stiffness of the pressure pad are shown in Figure 18.

The results obtained for the HUD mirror were verified by use of the MAGNA model shown in Figure 5c. However, the stresses in the HUD mirror reach unacceptable levels even at low contact forces as given in Figure 19 leading to failure of the mirror.

6. MAPPING OF DEFLECTIONS AND STRESSES

In order to produce the failure risk analysis reported in Ref / 6 / it was necessary to map the critical velocities for different locations on the windshield. Therefore, response analyses were carried out for 9 different target points on the windshield according to Figure 20. In each analysis the maximum stress was evaluated and the deflections at points where a limited clearance to internal hard points was available. The results were transformed into maps included in Figure 20. The curves show the locus of target points for which the critical parameter is reached for a 1 kg bird at a given velocity. Impact inside the curve is assumed to lead to failure at velocities below the value indicated for the curve. A summary of the result is given in Figure 21 for an impact velocity of V = 1000 km/h. The information was used in Ref / 6 / to evaluate the risk of failure as a function of impact velocity and bird size.

7. MISCELLANEOUS

In the early tests carried out by Saab Scania secondary failures of the canopy frequently occured at impact velocities well below the critical speed for the windshield.

The original design of the canopy front arch is shown in Figure 22. During a bird strike, the windshield deflections may be of the order of 20 mm and the fairing of the canopy scoops up a major part of the bird. The pressure that builds up in the cavity between the windshield and the canopy induces a high torsional moment acting on the arch. A simple dynamic model was studied according to Figure 23 which was used to estimate the torsional deflections during bird impact. Only the torsional stiffness of the arch was considered in the analysis; The bending stiffness of the transparency was shown to yield a marginal effect on the effective arch stiffness. The result as shown in Figure 23, indicates that the risk of canopy failure is very large with the original design. Modifications to the design were introduced according to Figure 23. Stress raisers in the fairing cause an early fairing failure and together with a 45° chamfering of the front edge of the canopy the bird ingestion is reduced significantly.

References

/1/ Brockman, R A: MAGNA (Materially and Geometrically Nonlinear Analysis). Computer Program User's Manual, University of Dayton Research Institute, Dayton, Ohio. UDR-TR-80-107, 1980

/2/ Kjellberg, S, Stehlin, P, Palmberg, B, Merazzi, S: BASIS - Finite Element Structural Analysis - User's Manual, The Aeronautical Research Institute of Sweden, Stockholm Febr 1979

/3/ West, B S, Brockman, R A: Evaluation of Bird Load Models for Dynamic Analysis of Aircraft Transparencies, AFWAL-TR-80-3092, Aug 1980

/4/ McCarty, R E: Finite Element Analysis of F-16 Aircraft Canopy Dynamic Response to Bird Impact Loading. Proceedings of the AIAA/ASME/ASCE/AHS 21st Structures, Structural Dynamics and Materials Conference, Seattle, Wash., May 12-14 1980.

/5/ McCarty, R E: Aircraft Transparency Bird Impact Analysis Using the MAGNA Computer Program. Proceedings of the Conference on Aerospace Transparencies London 8-10 Sept 1980

/6/ Fondén, B P, Persson, K I: Investigations Concerning Improvements of the Saab 37 Windshield Birdstrike Resistance. Proceedings of the Conference on Aerospace Transparent Materials and Enclosures, Scottsdale, Ariz. 11-14 July 1983

/7/ Nilsson, F, Sörnäs, L, Samuelson, L Å: Aircraft Windshield Bird Impact Analyses. IFM Akustikbyrån TR 5.200.01-04 (in Swedish).

Eigenfreq. No	Dragon windshield		Viggen windshield	
	Theory	Exp	Theory	Exp
1	243	247	158	190
2	346	317	266	250
3	389	393	336	(300)
4	449	495	368	(345)
5	480		406	410
6	551		456	435
7	627	603	497	485
8	672		535	(510)
9	703		555	610
10	716		570	630

Table 1. Calculated and measured eigenfrequencies of the Dragon and Viggen windshields prior to bird impact testing.

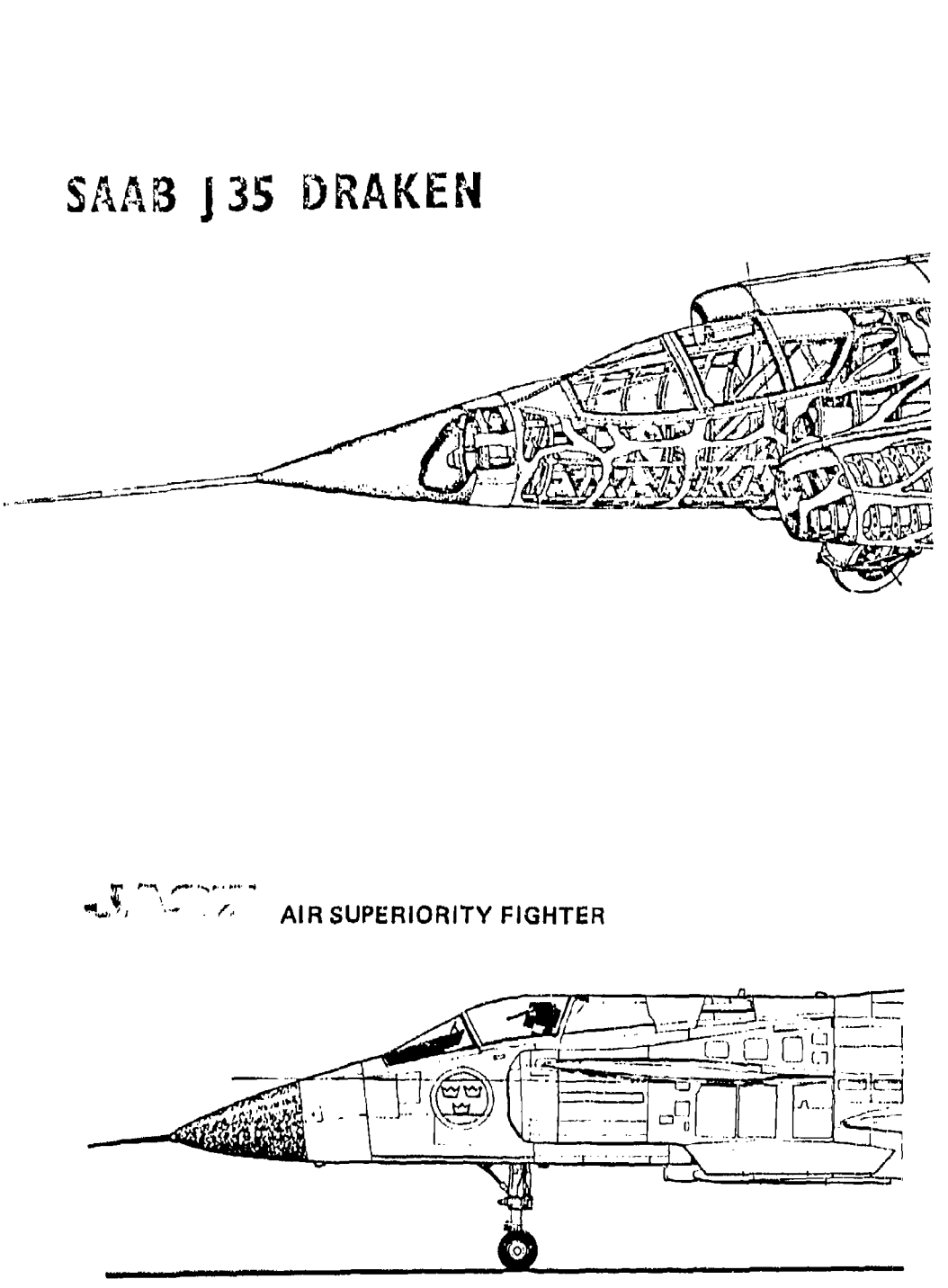

Figure 1 Windshield configuration of the Swedish 35 Dragon and 37 Viggen fighter aircraft

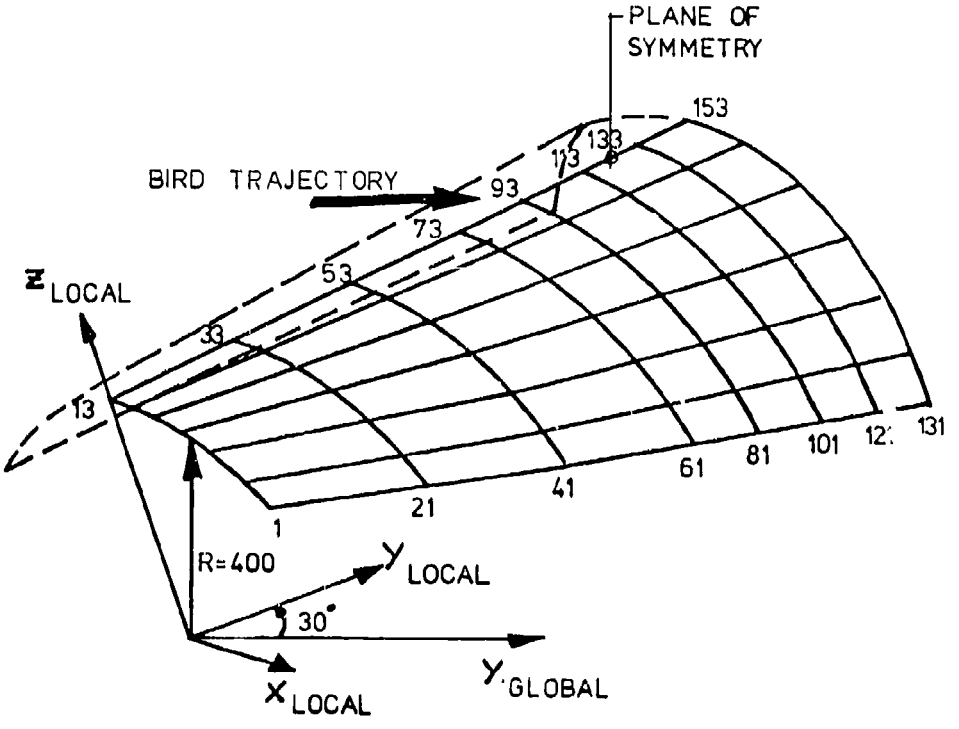

FINITE ELEMENT MODEL OF THE VIGGEN WINDSHIELD

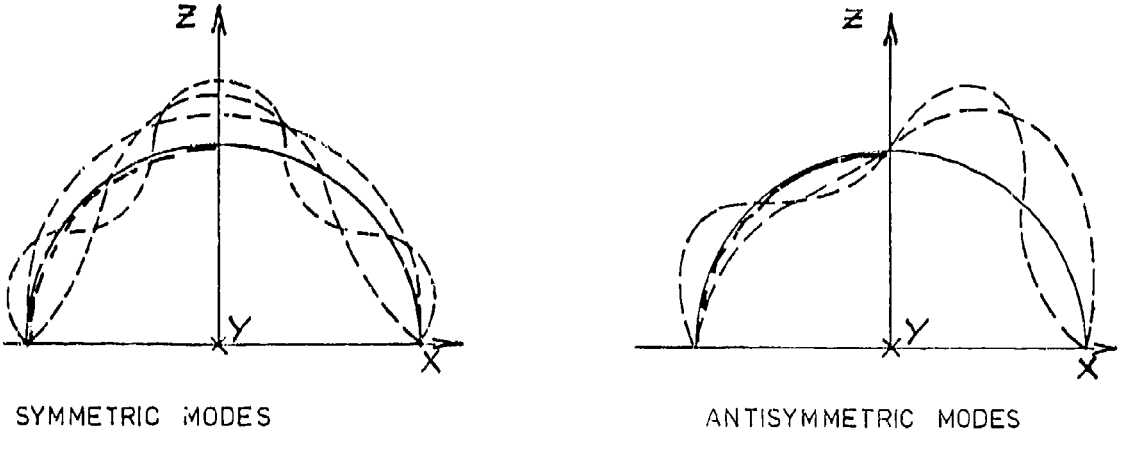

SYMMETRIC MODES

ANTISYMMETRIC MODES

Figure 2 FEM model for the Viggen windshield. 10 symmetric and 10 antisymmetric modes were retained in the analysis.

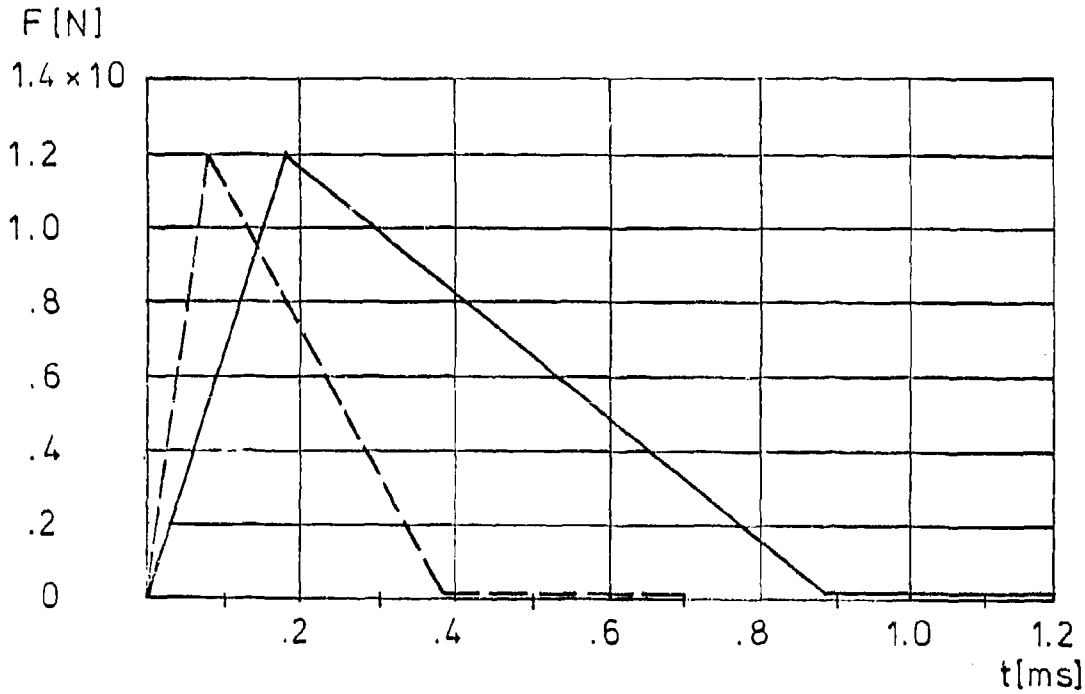

Figure 3 Typical impact force histories.

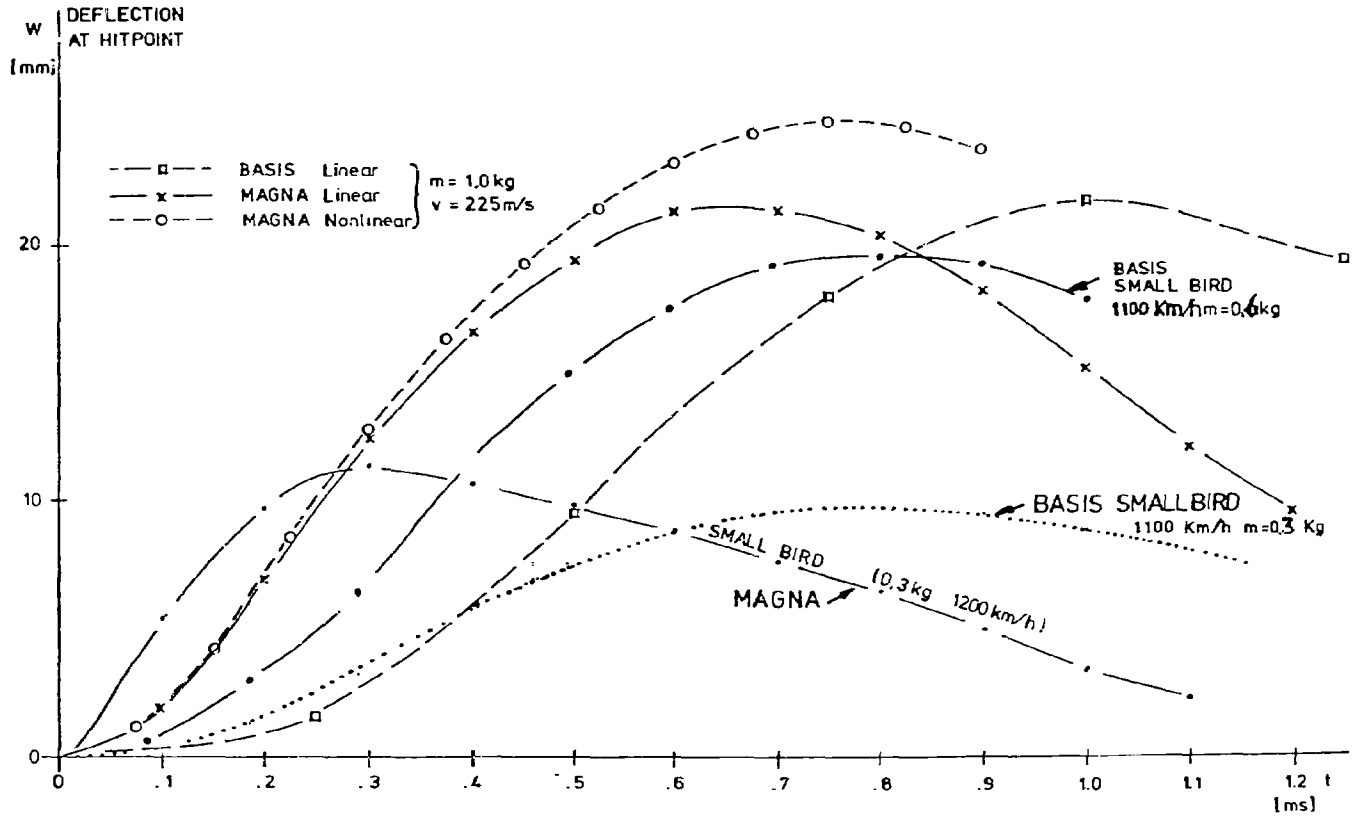

Figure 4 Deflections at the impact point evaluated by use of modal superposition and by use of MAGNA linear/nonlinear analyses.

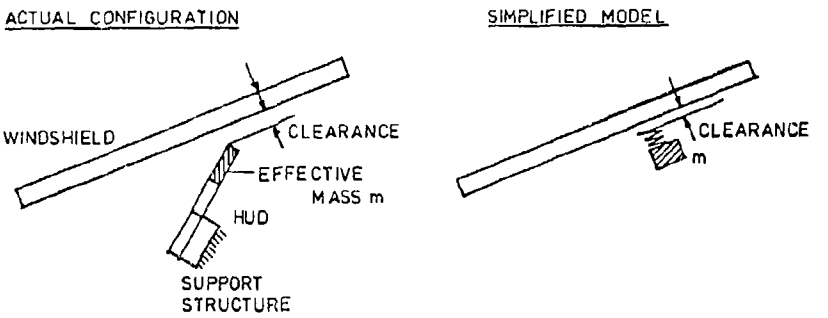

Figure 5a Simplified spring-mass model.

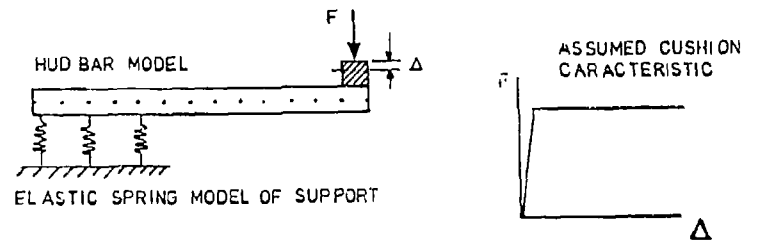

Figure 5b Bar model of HUD mirror with a constant force cushion.

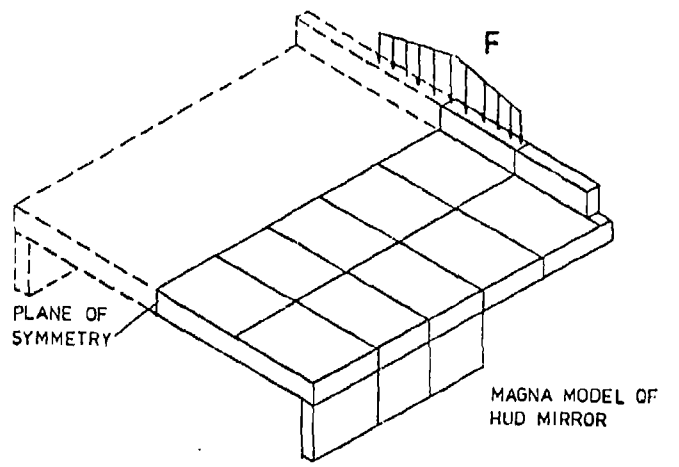

Figure 5c MAGNA model for verification of the bar model results.

Figure 5 Models for the analysis of the problem of contact between the windshield and the HUD mirror glass.

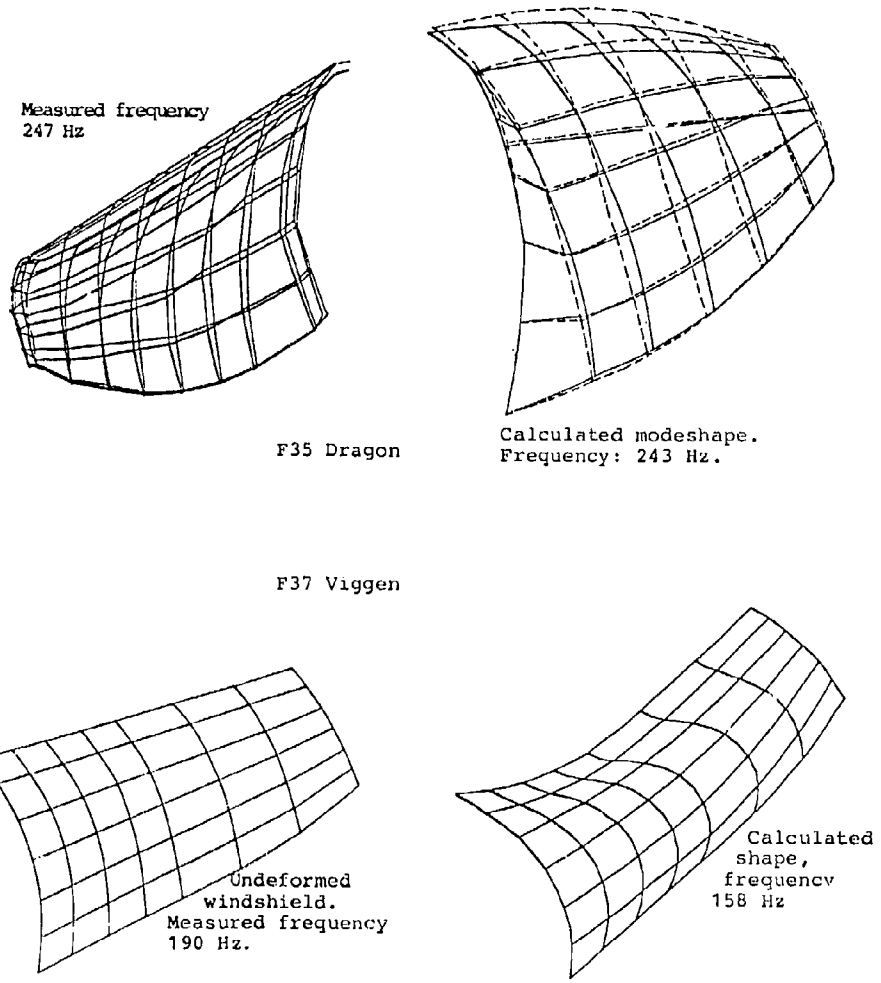

Figure 6 Measured and calculated first mode shapes for the Dragon and Viggen windshields.

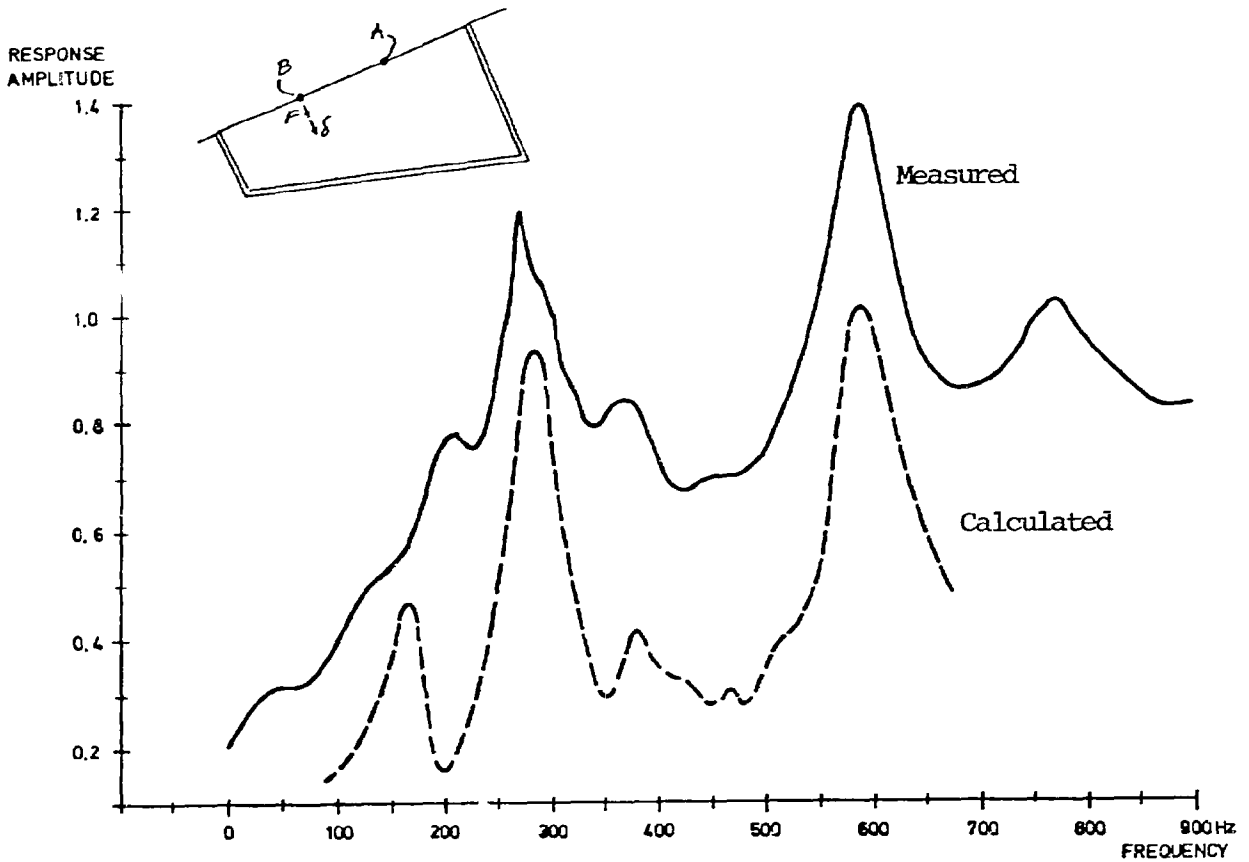

Figure 7 Measured and calculated response spectrum for the Viggen windshield.
Note: The two curves are not drawn to scale !

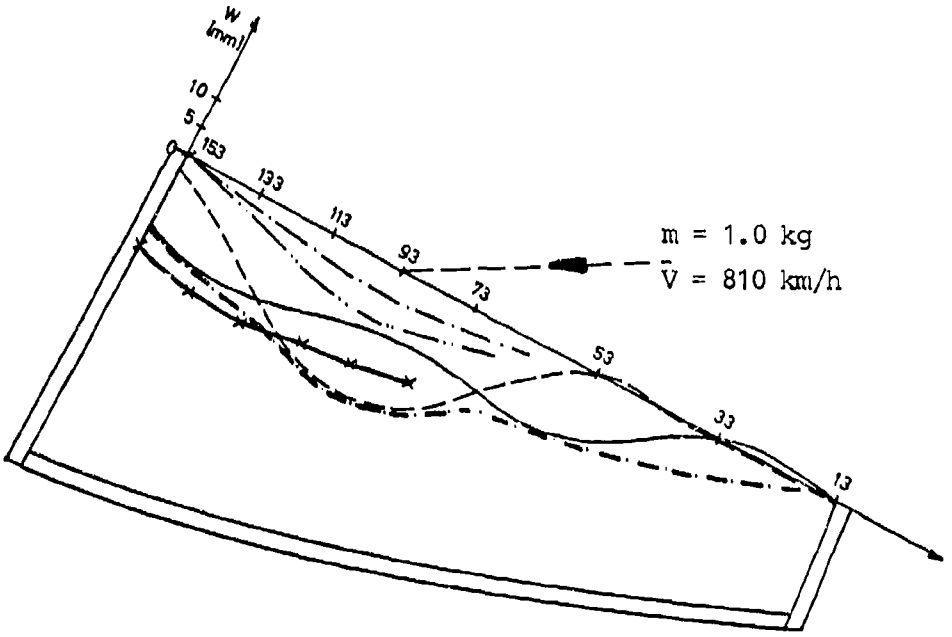

DEFLECTIONS

CALCULATED	MEASURED
t = 0,50 ms	
t = 0,75 ms	
t = 1,00 ms	
t = 1,75 ms	
ENVELOPP	

Figure 8 Response at the windshield symmetry line due to impact of a 1 kg bird at 810 km/h. Measured maximum response is included for comparison.

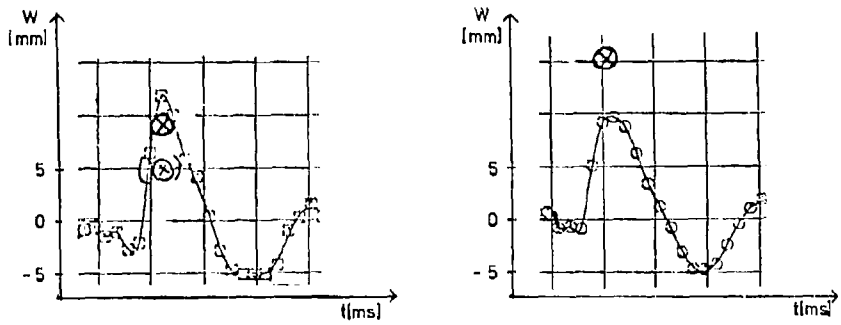

⊗ Calculated maximum deflection

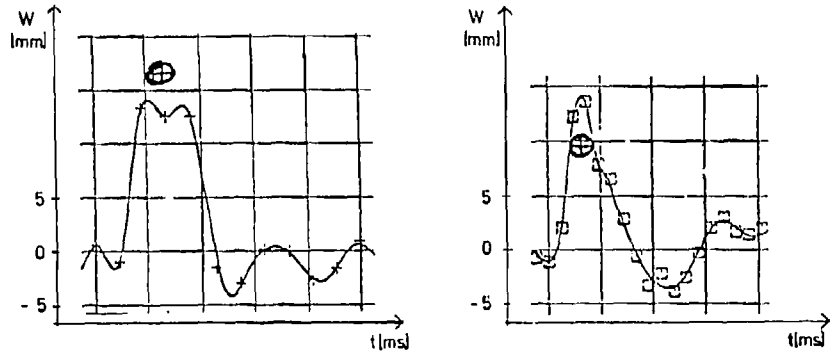

Figure 9 Typical correspondence between measured and calculated deflections.

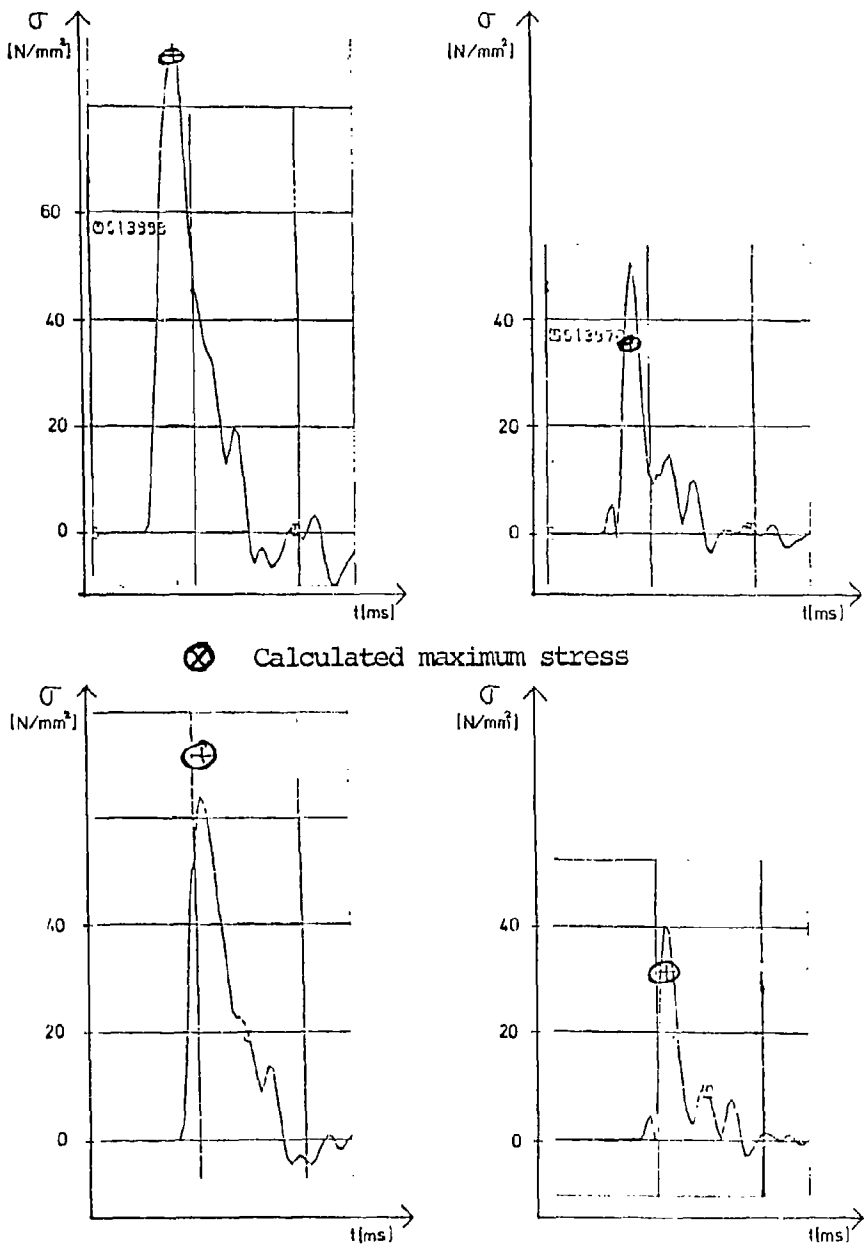

Figure 10 Typical correspondence between measured and calculated stresses in the windshield at the point of impact.

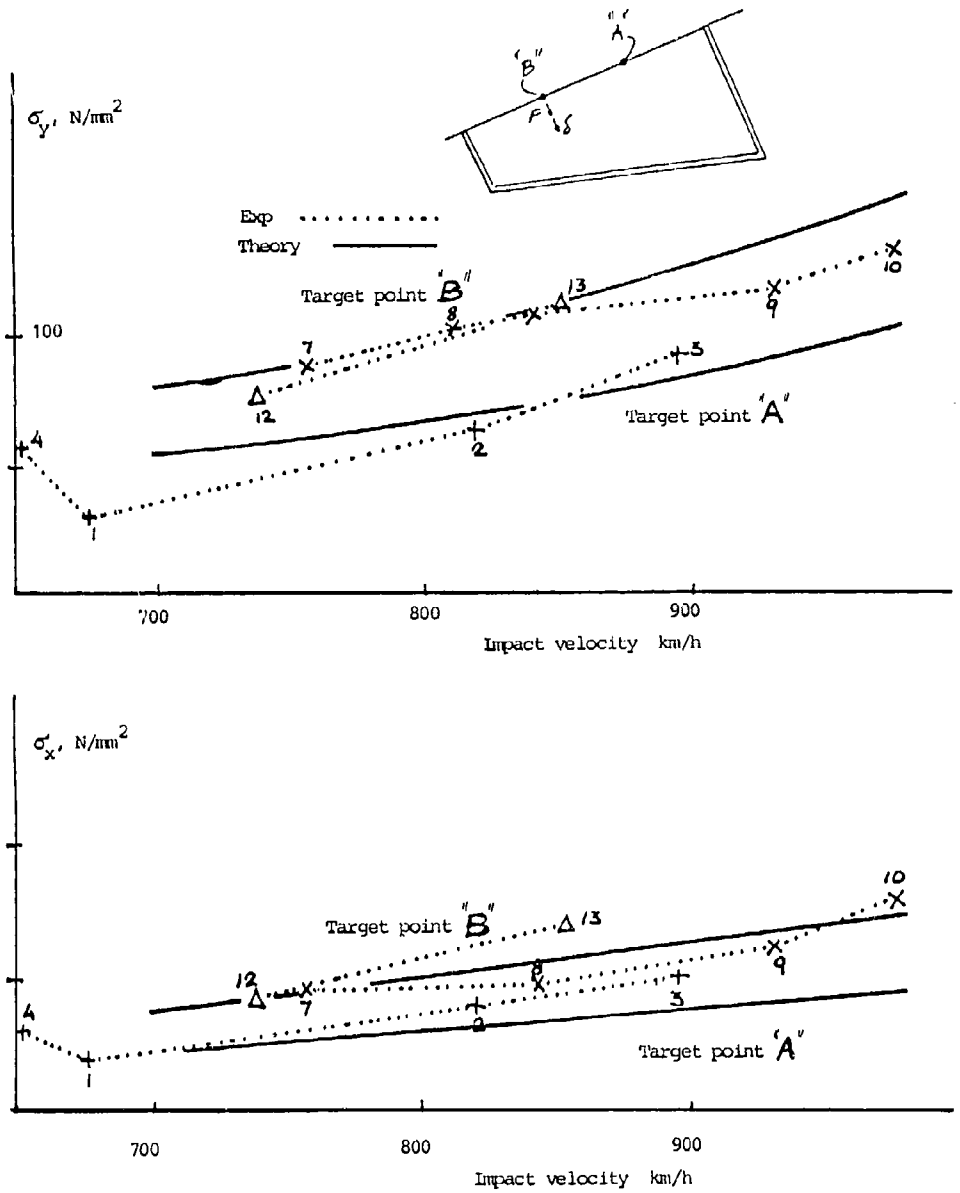

Figure 11 Measured stresses at a number of tests with target points A and B according to Figure 7 and comparison with theory.

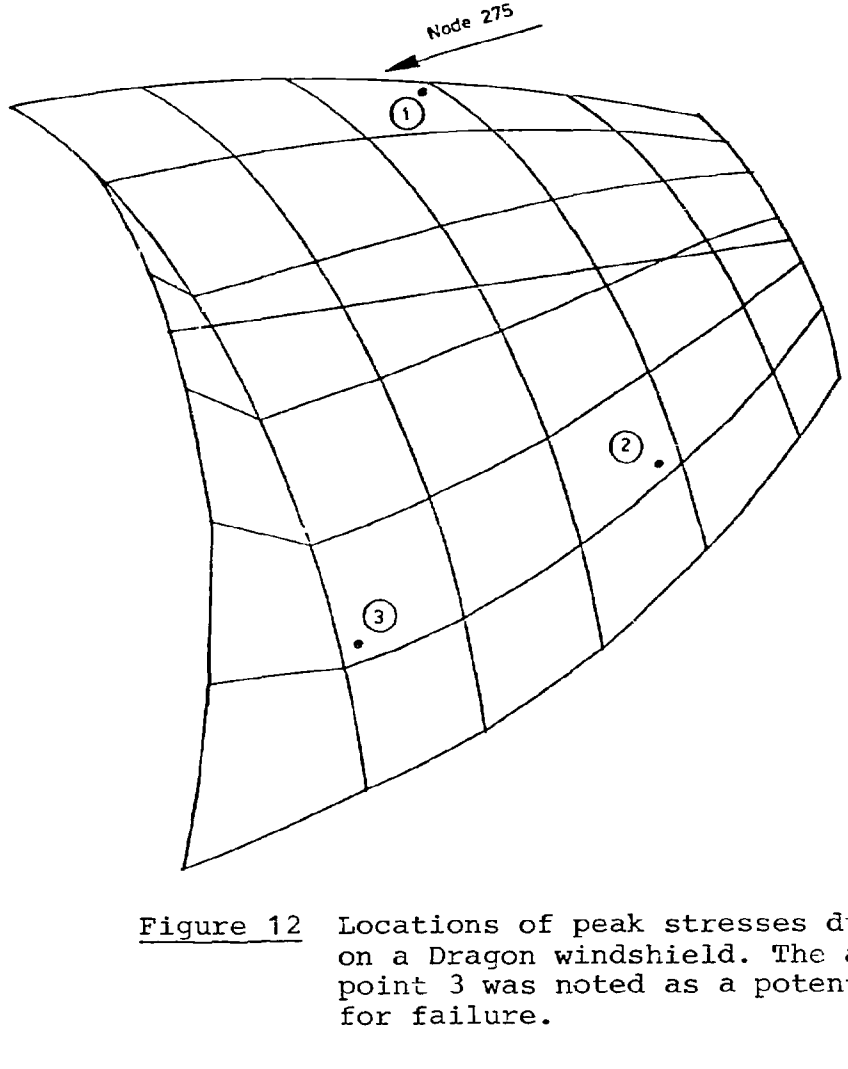

POINT (nr)	TIME (ms)	σ_{max} N/mm^2
1	1,0	75.
2	1,6	65.
3	2,2	98.

Figure 12 Locations of peak stresses due to bird impact on a Dragon windshield. The area around point 3 was noted as a potential risk zone for failure.

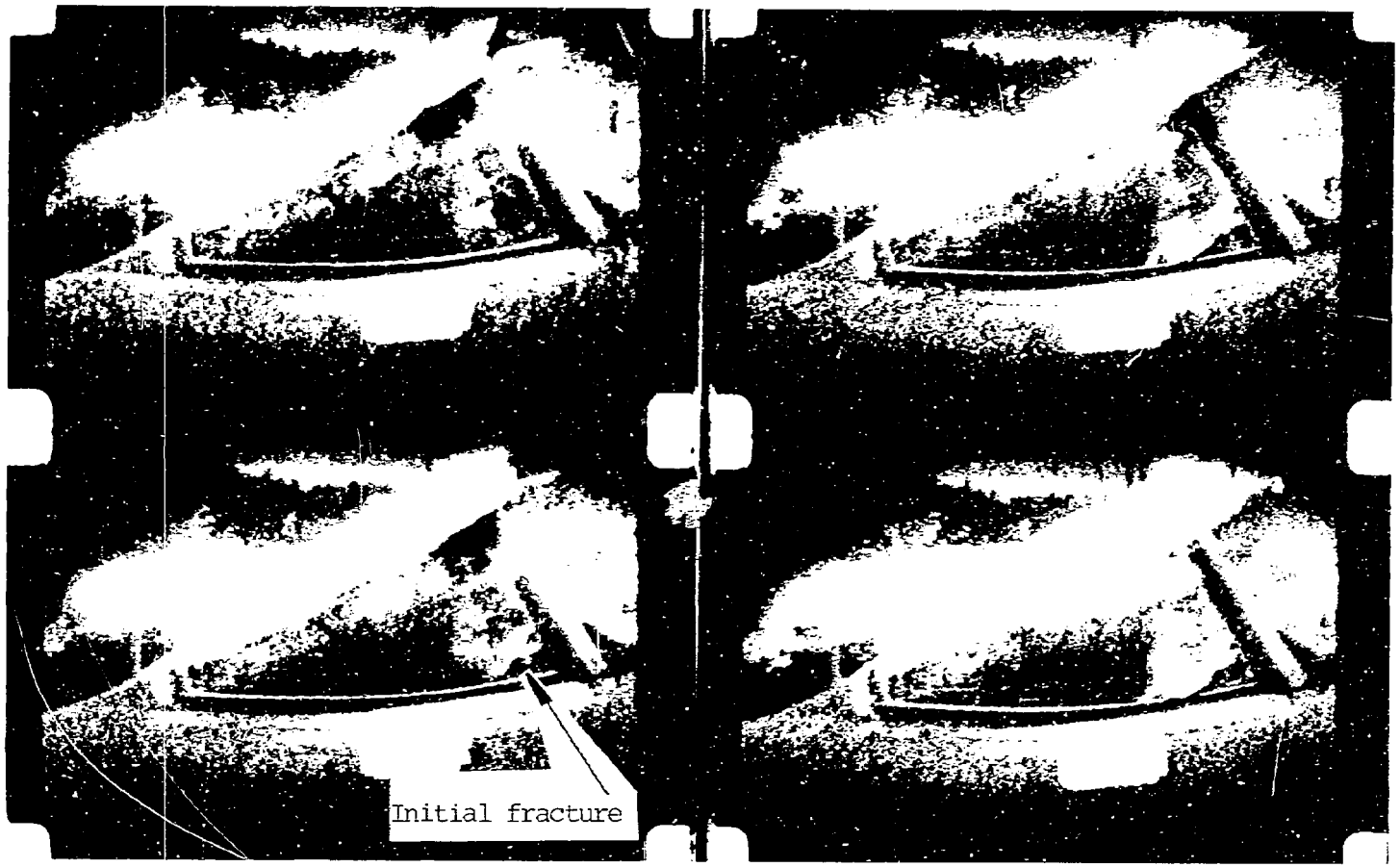

Figure 13 Series of movie frames taken during bird strike testing on a Dragon windshield. Fracture occured in the area indicated in Figure 12.

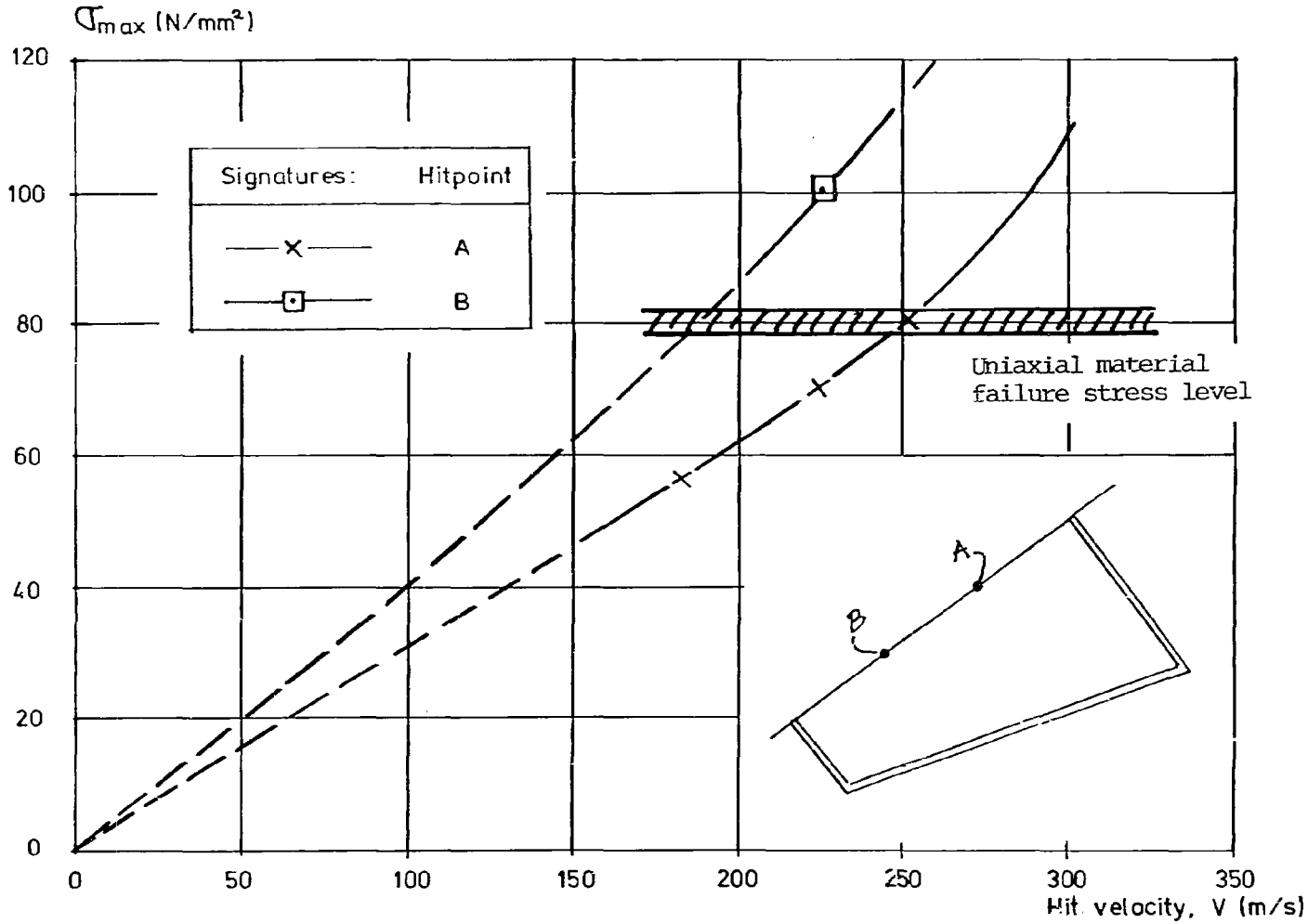

Figure 14 Maximum stresses in the Viggen windshield as a function of impact velocity.

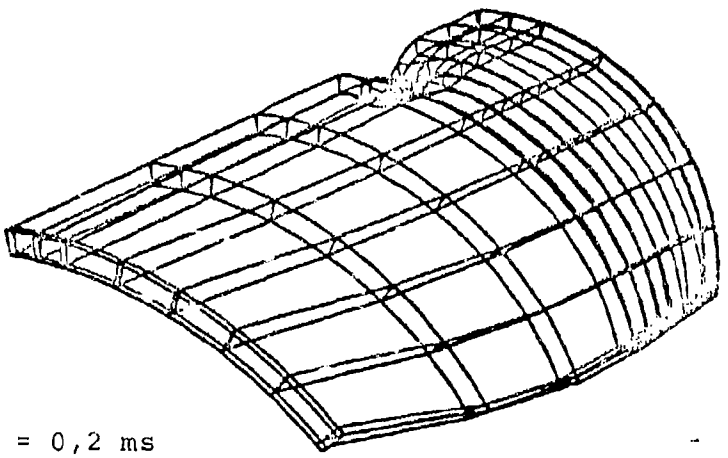

t = 0,2 ms

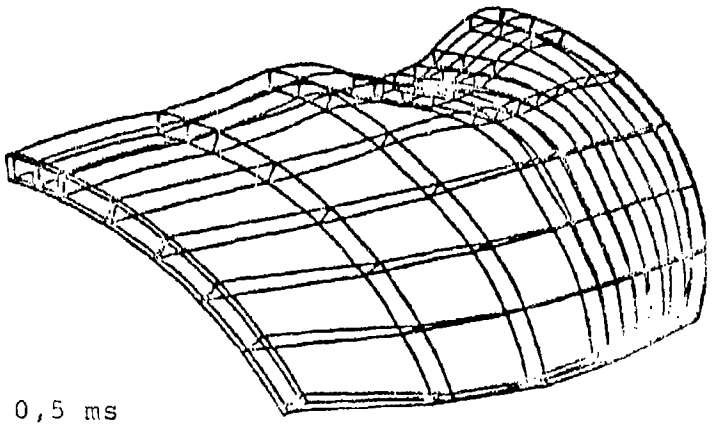

t = 0,5 ms

Figure 15 Viggen windshield response to a small bird impact (m = 0,3 kg) at high velocity (V = 1200 km/h).

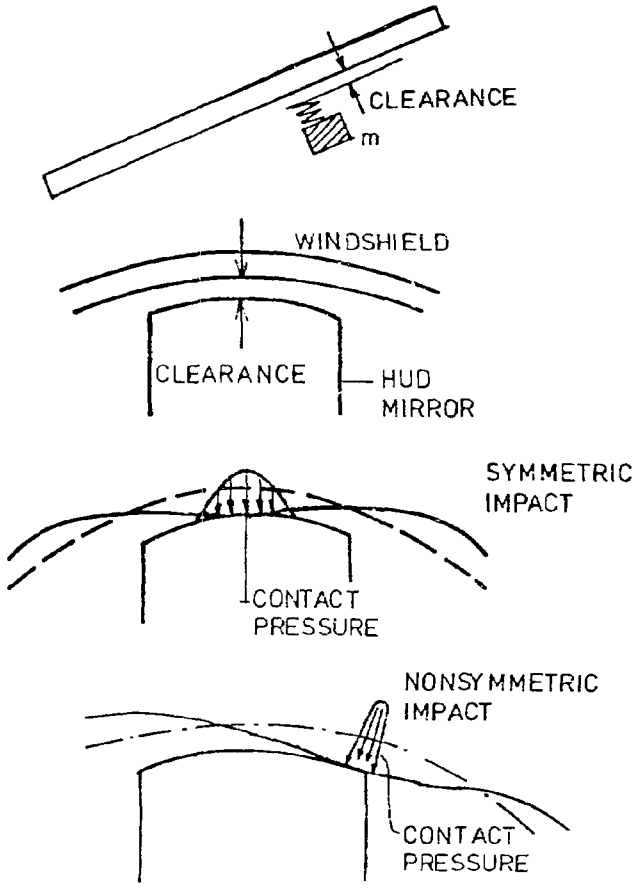

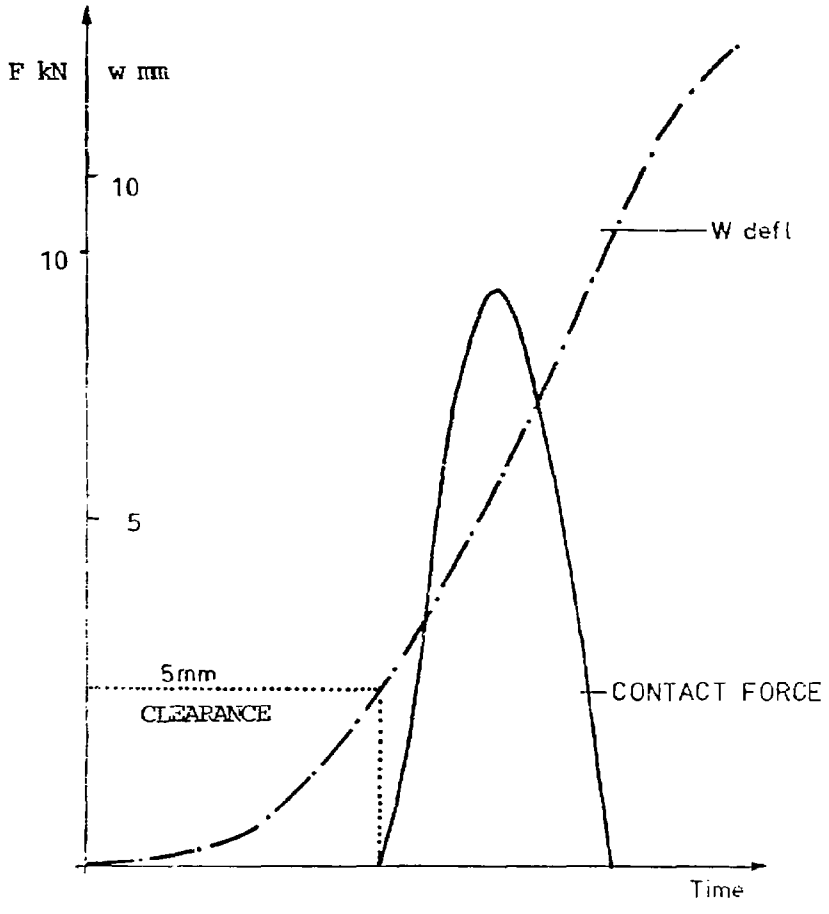

Figure 16 Rough estimate of the forces during contact between the windshield and the HUD mirror.

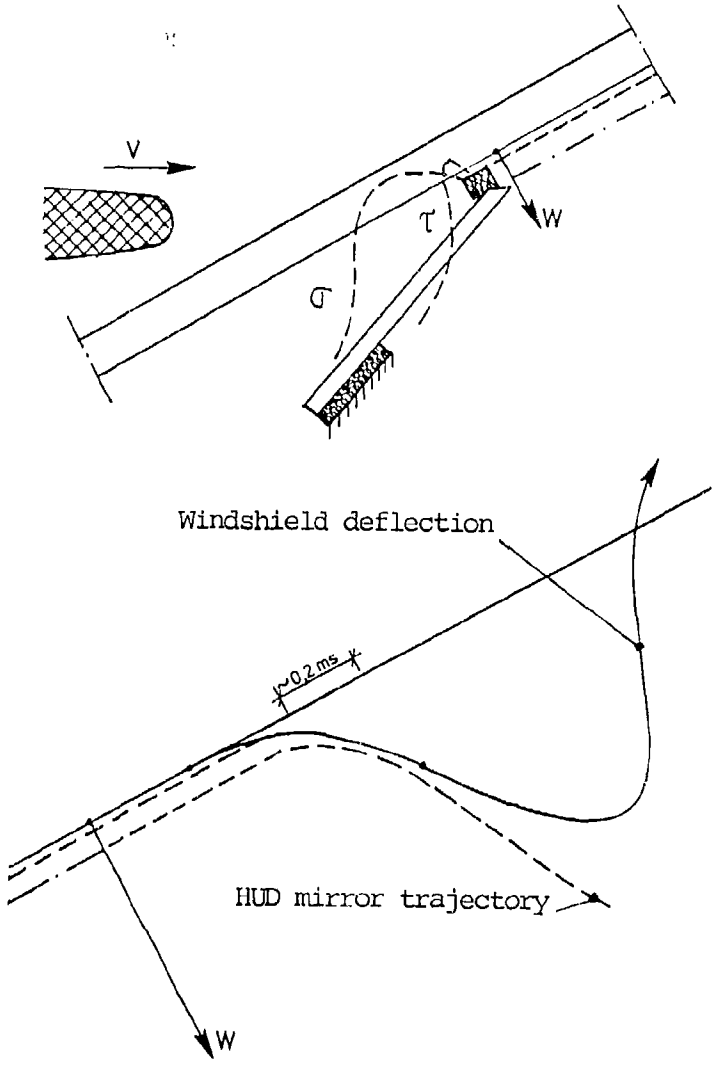

Figure 17 Early "gentle" contact windshield - HUD mirror through a cushion placed on top of the mirror.

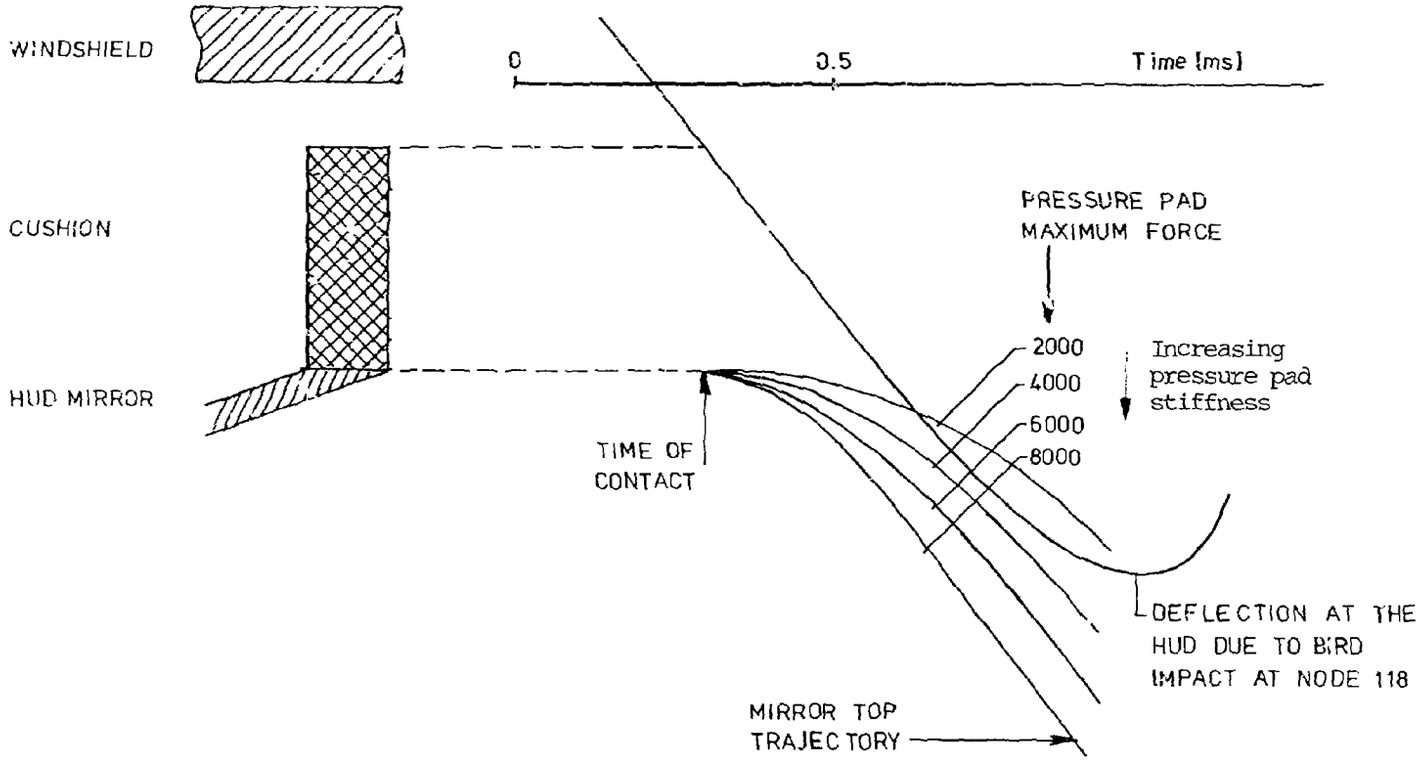

Figure 18 Evaluation of pressure pad requirements in order to avoid hard contact between windshield and HUD mirror.

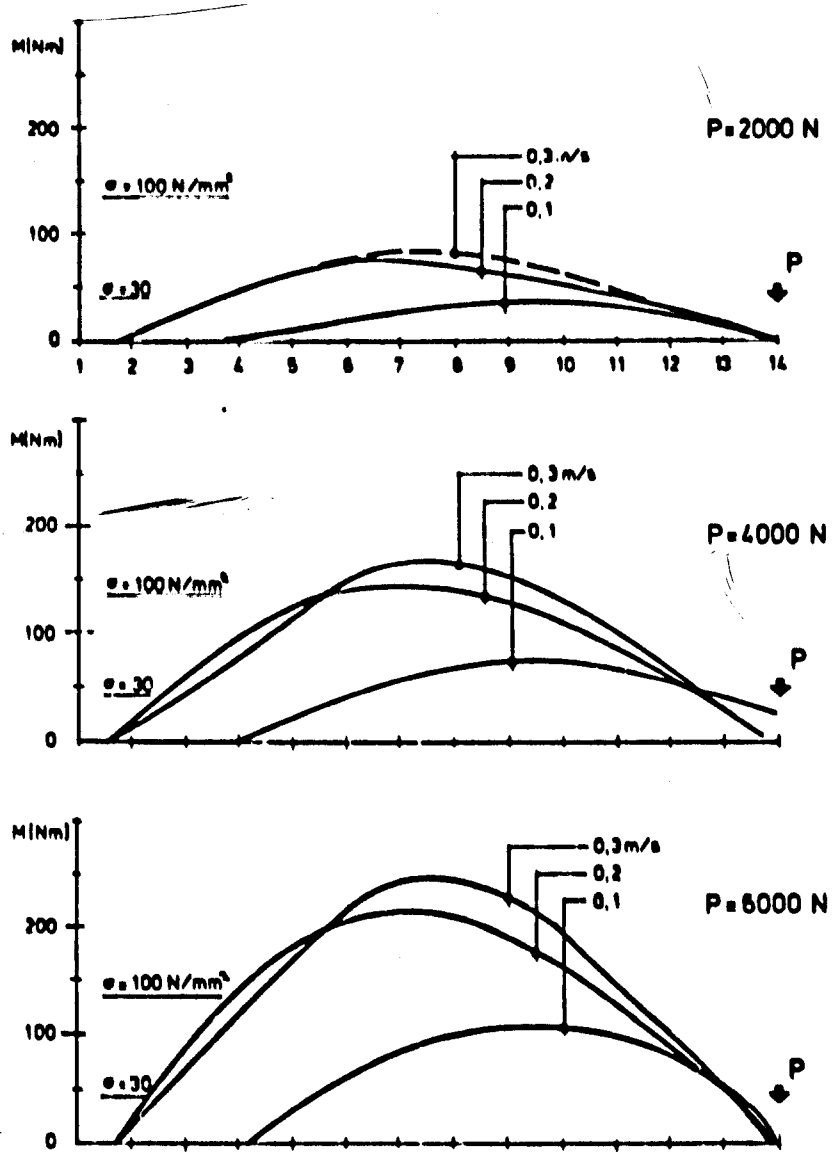

Figure 19 Stress levels in the HUD mirror glass as functions of time for various levels of the contact force P. The ultimate stress of the glass is of the order of 50 N/mm^2.

Preceding Page Blank

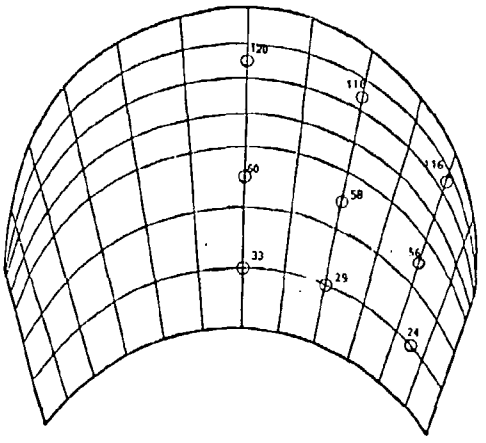

Target points used in the analysis

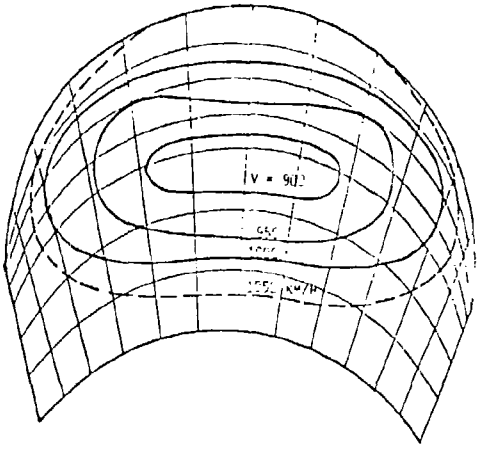

Critical velocities for windshield failure

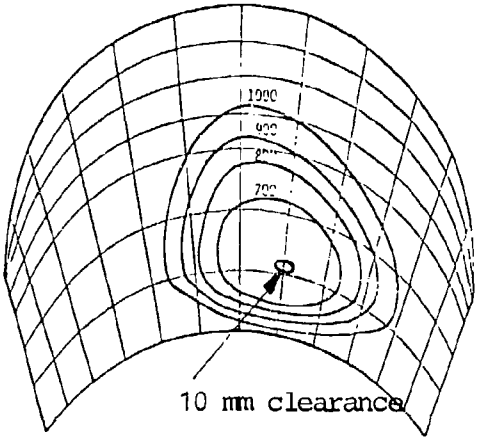

Critical deflection at exposure meter

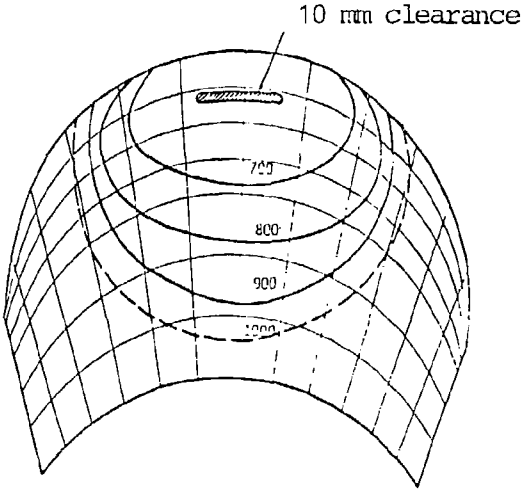

Critical deflection at head up display

Figure 20 Critical velocity maps of the Viggen windshield.

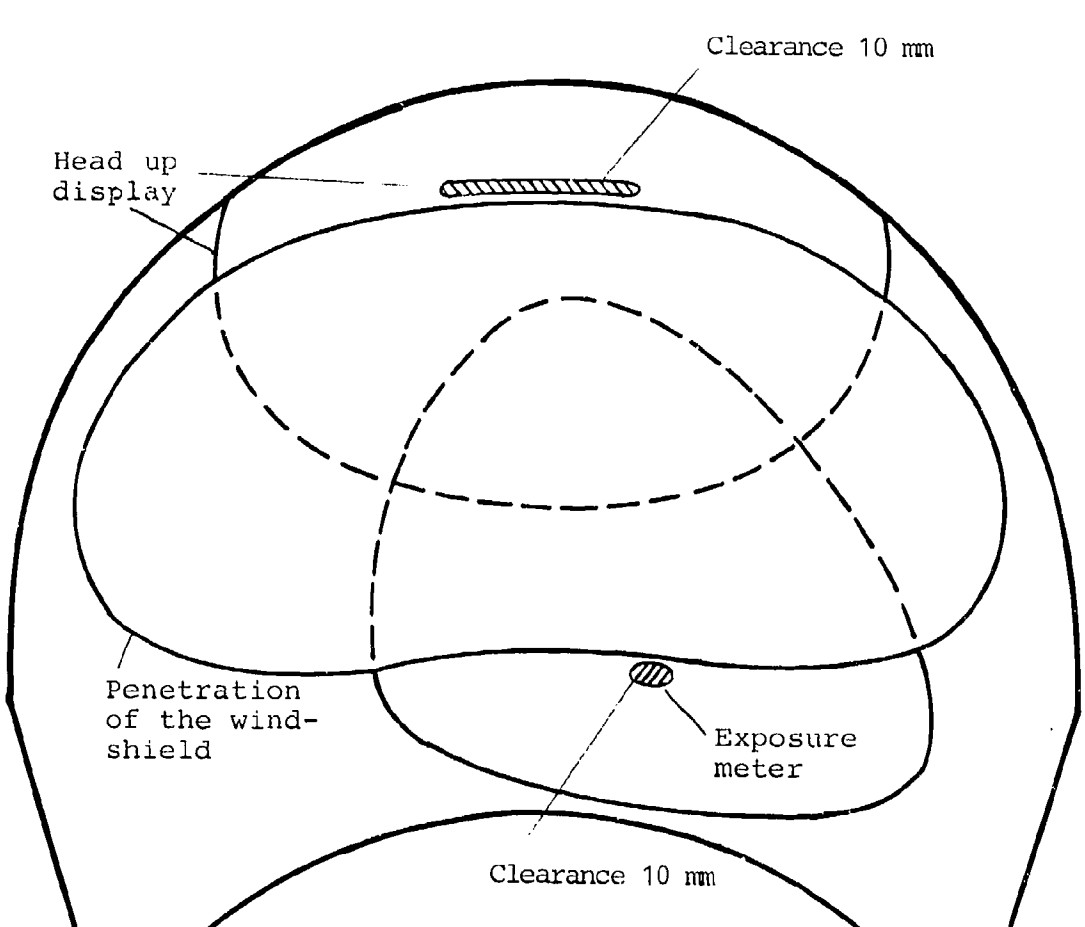

Figure 21 "Risk zones" for the Viggen aircraft during collision with a 1 kg bird at a velocity of 1000 km/h.

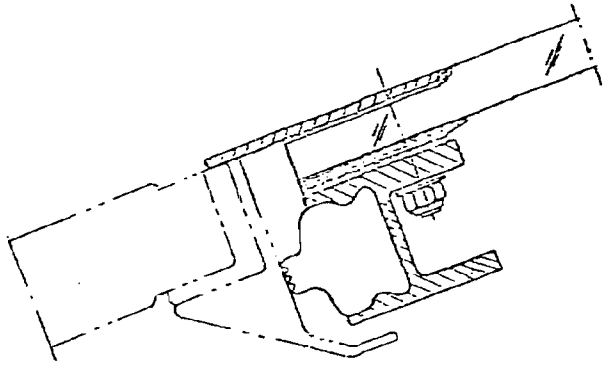

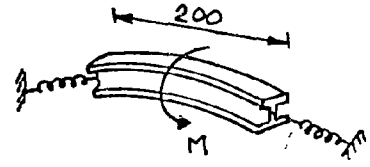

Simple beam-spring model of canopy front arch

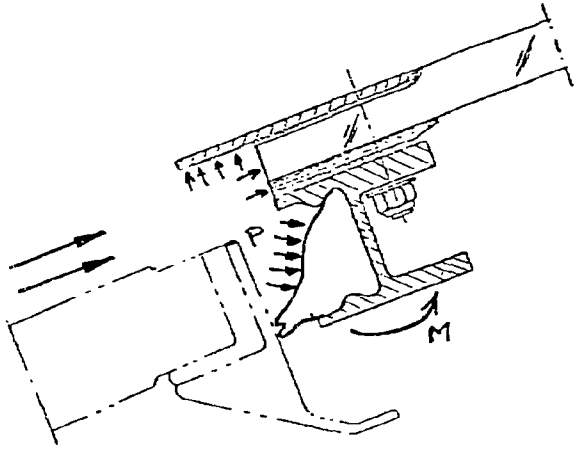

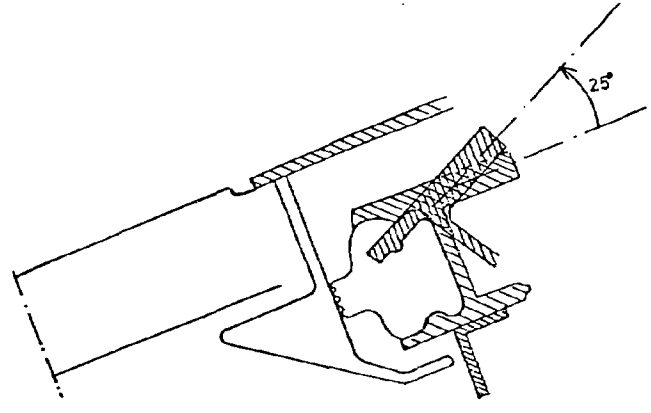

Estimated arch rotation due to birdraulics

Figure 22 The "birdraulics" effect on the front arch of the canopy. Simplified model for analysis of arch rotation.

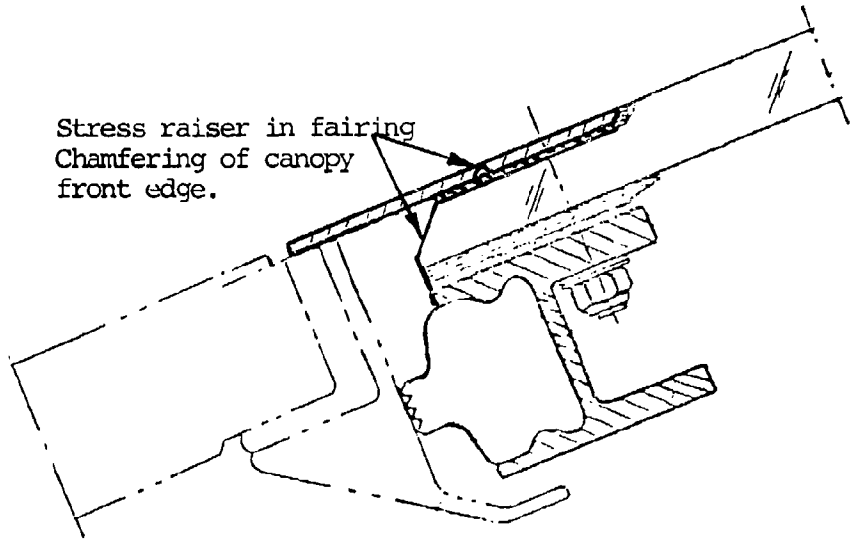

Figure 23 Modifications to the canopy.

AD-P003 236

STATUS OF NEW AEROTHERMODYNAMIC ANALYSIS TOOL FOR HIGH-TEMPERATURE RESISTANT TRANSPARENCIES

M. O. Varner, Sverdrup Technology, Inc.
and C. A. Babish, III,
Flight Dynamics Laboratory

STATUS OF A NEW AEROTHERMODYNAMIC ANALYSIS TOOL FOR HIGH-TEMPERATURE RESISTANT TRANSPARENCIES*

by

M. O. Varner**, C. A. Babish, III***

This paper summarizes the status of the definition, selection, modification, and development of a Specific Thermal Analyzer Program for Aircraft Transparencies (STAPAT). The code developed will merge state-of-the-art technology, code accuracy requirements, and the definition of code function requirements resulting in an aerothermodynamic analytical technique that is specifically applicable and limited to the study of high-temperature resistant transparencies for high-speed aircraft. The aerothermodynamic methodologies required for the definition of the convective heat-load requirements of the STAPAT are described. These include the identification of inviscid methodologies covering the subsonic-to-supersonic-speed flight regime and complex three-dimensional configurations consisting of real canopy geometries. The external forced convection methodology is described which includes complex three-dimensional effects resulting from the circumferential and streamwise variation of the local heating loads, the forced convection heat transfer as influenced by wall-temperature effects and transition location, and variable-edge entropy effects. Internal forced convection methodologies are discussed which describe cabin cooling, de-icing, and de-fogging systems as modeled for the STAPAT code. Radiation effects on the thermal environment within the transparency are described consisting of solar radiation, surface-to-surface radiation, and radiation emanating from cabin contents. The finite-element conduction code is described which is based on an 8-node brick element incorporating a skyline, blocked, out-of-core solver with an optimizer routine for efficient solution of complex nodal networks. Pre- and post-processing capabilities are described which provide for the efficient construction of finite-element transparency networks and the post-processing of the thermal environment within the transparency using an extensive graphics package. The resulting STAPAT described in this paper will be a user-oriented code which will be capable of providing not only the canopy designer, but also the researcher, with a valuable tool for the analysis of the thermal environment within complex canopies on current and future high-performance aircraft.

---

*The work reported herein was performed by Sverdrup Technology, Inc., and sponsored by the Wright Aeronautical Laboratories, Wright-Patterson Air Force Base, Ohio 45433 under Contract F33615-81-C-3412.

**Supervisor, Computational Applications Section, Computer Services Division, Sverdrup Technology, Inc., Tullahoma, Tennessee 37388.

***Aerospace Engineer, Flight Dynamics Laboratory, AFWAL/FIER, Wright-Patterson Air Force Base, Ohio 45433.

NOMENCLATURE

A_1 A_1	Surface Areas
C_p	Pressure Coefficient
F_{12} F_{21}	Configuration Factors
h	Heat-Transfer Coefficient
$h_{.8}$	h evaluated at $T_w/T_{0_\infty} = 0.8$
$h_{1.1}$	h evaluated at $T_w/T_{0_\infty} = 1.1$
N	Node number
q	Heat-Transfer Rate
r	Radial Distance
S, S1	Surface, axial or body distance
S_t	Stanton Number
T	Temperature
t	Thickness
x,y,z	Cartesian Coordinates
ψ	Local Body Slope
ϕ_1, ϕ_2	Included Angles Defined in Figure 9
τ	Transmissivity
θ, ϕ	Circumferential Angle

Subscripts

aw	Adiabatic Wall
max	Maximum
o_∞	Free-Stream Stagnation
w	Wall
∞	Free Stream

1.0 INTRODUCTION

Air Force aircraft operate at speeds where aerodynamic heating significantly affects the design and performance characteristics of their transparent windshields and canopy systems. These transparency systems must not only withstand high temperatures, but must also resist surface abrasion, bird impact, and flight pressure loads, and provide a large field-of-view with good optics at low viewing angles. In addition, they should be low in weight and cost and easily maintainable and replaceable. Current lightweight transparency systems (using acrylic and polycarbonate structural materials) are temperature limited below 300°F and therefore are restricted to short times at maximum Mach number operation. These same lightweight systems have been shown to be susceptible to surface abrasion and ultraviolet radiation degradation. Current transparency systems which provide high-temperature capabilities (using glasses) are relatively heavy and severely limit the field-of-view.

Thus, a critical aspect of current and future transparency systems is their thermal performance as influenced by the external environment in which the design is operating and its geometric and material property makeup. Aerothermodynamic analytical calculation techniques are available in the open literature for the thermal performance prediction of aircraft structures. However, these techniques are either (1) so general that their accuracy may not be sufficient for the study of a small portion of the total aircraft, (2) very accurate but very costly to operate in terms of computer resources, or (3) so limited in applicability to other aerospace heating problems that they are not useful to the study of aircraft transparency systems. What is needed, therefore, is a calculation technique that is dedicated to evaluation of the aerothermodynamic performance characteristics of proposed new high-temperature transparency system designs and the determination of the time-at-temperature limitations of current transparency systems. Based on these requirements, an aerothermodynamic analytical technique is under development that is specifically applicable and limited to the study of high-temperature resistant transparencies for high-speed aircraft (STAPAT).

The analytical technique described in this paper, will be used in the design and analysis of advanced high-temperature resistant transparency systems to improve the mission effectiveness of Air Force aircraft that operate at high speeds during tactical warfare, air-to-surface, strategic defense, and reconnaissance missions. Specifically, the technique will be used to (1) evaluate the thermal performance characteristics of current transparency systems, (2) aid in the design process of new systems, and (3) investigate design options for reducing life-cycle costs.

An application of this analytical technique could be to determine temperature distributions throughout the transparency systems of current aircraft as functions of time for actual missions flown. These temperature-time histories would show the temperatures of the transparent materials when in the bird-impact environment and would also

be used in existing analytical techniques to determine the strength degradation due to time-at-temperature. Secondly, in the design of a new transparency system proceeds, the new analytical techniques could be used in conjunction with the structural analysis methods to determine transparent material temperatures in the case thermal mission to ensure that the design allowables are not to be maintained below the [illegible].

Finally, these two analytical techniques could be combined for use in reliability/life cycle cost trade studies of transparency systems. During the design of new high performance systems for future aircraft, trades can be made between material temperature limits and the number and type of transparency plies required for the transparency systems, allowing the experienced designer to optimize the system. Thicker systems, which have a higher temperature capability, will have lower initial costs and less adverse effect on aircraft performance because of lower weight. These thicker systems may have lower life cycle costs than the longer life, thinner transparency systems. This new aerothermodynamic analytical technique would be used to determine the transparent material temperatures required for this type of life-cycle cost-trade study.

The following sections describe the capabilities that are now being incorporated in the STAPAT to provide the designer and researcher with state-of-the-art tools to predict the thermal response of transparency systems in simulated real-flight environments. Aerothermodynamic methodologies are presented which provide accurate three-dimensional external heating environments over the canopy surface. Internal forced and free convection, as well as, solar and surface-to-surface radiation environment models are described. The conduction code methodology utilized in the STAPAT is presented with a discussion of pre-processor and post-processor capabilities that will enhance the user friendliness of the technique.

2.1 STAPAT Aerothermodynamic Methodology

STAPAT must be capable of handling a variety of forcing functions which contribute to the temperature distributions on the surface of, and within, a canopy for typical missions. A number of important properties will contribute to the definition of these forcing functions, including the inviscid flow field over the canopy and forebody surfaces of the configuration and the atmospheric regime. The atmospheric regimes that STAPAT will address include both flight-type regimes which encompass the flows from subsonic to supersonic flight speeds (up to Mach 3.5) and wind tunnel test environments that simulate the flight regimes. Acceptable configurations will include typical current fighter configurations and future low-radar cross-section (RCS) configurations. In addition, typical wind tunnel models that are used in thermal transparency performance studies must also be acceptable inputs for STAPAT.

Sensitivity study results (Reference 1) have shown significant three-dimensional heat-transfer effects on the canopy due to streamline spreading over the canopy surface for supersonic Mach numbers. These

three-dimensional Mach number effects were shown to be especially pronounced for high-supersonic flight regimes where variable-edge entropy plays an important role in determining local edge Mach number properties. Comparisons with Euler code solutions for a typical fighter forebody configuration have verified the importance of this variable-edge entropy property at supersonic Mach numbers, and also the three-dimensional flow-field-induced effects on the circumferential and streamwise heat-transfer and canopy surface temperature distributions.

2.1.1 Inviscid Methodology

In order to define the heating load distribution over the fuselage and canopy surfaces, inviscid flow field values are required from subsonic to supersonic flight conditions. The inviscid values must be obtained in an efficient manner and, at the same time, reflect important trends in magnitudes of the surface flow field variables in high-gradient regions. In addition, the inviscid calculation technique must be numerically stable and require minimal core storage for execution.

The most basic approach to satisfy the constraints as defined in the preceding paragraph is the utilization of the modified Newtonian theory. The modified Newtonian theory is based on a particle impact concept. Here the pressure coefficient, C_p, is given as a function only of the local impact angle of a typical particle relative to the free stream as it impacts a body surface. The classic Newtonian theory is given in Equation 1 below

$$C_p = 2 \cos^2\psi \qquad (1)$$

where C_p is the pressure coefficient based on free-stream conditions and ψ is the angle between the free-stream direction and the normal to the body surface.

It has been shown that more accurate pressure coefficient distributions can be obtained for super- and hypersonic flow field conditions if the two in the above equation is replaced by the maximum pressure coefficient for supersonic flow. Here the maximum pressure coefficient for supersonic conditions is that pressure coefficient corresponding to the stagnation pressure behind a normal shock. Equation 2 gives the so-called modified Newtonian relationship.

$$C_p = C_{pmax} \cos^2\psi \qquad (2)$$

Here C_{pmax} is the stagnation pressure coefficient behind a normal shock for a given free-stream Mach number condition, and C_p is defined as zero in the shadow region of the body. (Shadow region modifications, using Prandtl-Meyer expansion, are being considered.)

Based on the results of the sensitivity analysis, the modified Newtonian theory is being utilized to predict the inviscid flow field over specific canopy and forebody surfaces for subsonic, transonic, and supersonic flows. Some typical comparisons for a representative fighter configuration forebody are given in Figure 1. Here, the pressure

coefficient, C_p, is plotted versus body length, S, and circumferential angle, ϕ, for Euler code (Reference 2) and modified Newtonian theory calculations. Comparisons were also made for transonic and subsonic free-stream flows yielding similar quality results.

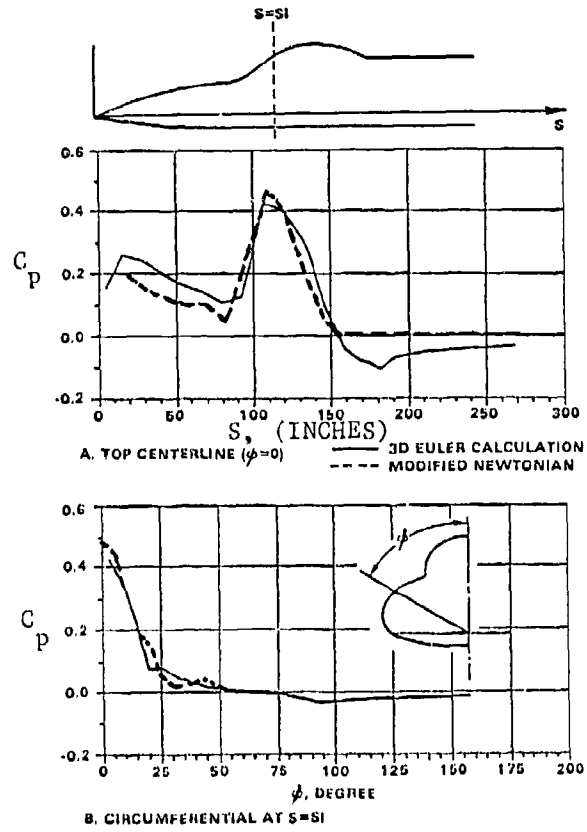

FIGURE 1. SURFACE PRESSURE COEFFICIENT DISTRIBUTION FOR A TYPICAL FOREBODY CONFIGURATION AT MACH 2.5, ZERO ANGLE OF ATTACK

Subsonic and transonic calculations (Mach Number 1 and below) are obtained in the STAPAT methodology from the modified Newtonian theory by assuming that the stagnation shock properties are equal to the stagnation pressure of the free stream. The modified Newtonian approach to be utilized in the inviscid methodology is based on the approach as presented by DeJarnette in References 3 through 5.

2.1.3 External Forced Convection Methodology

The sensitivity study reported in Reference 1 clearly showed that three-dimensional effects on the heat-transfer distribution over the canopy surface for typical fighter-type configurations is very important,

especially for high Mach number flows where the variable-edge entropy condition becomes pronounced. The sensitivity study also assessed the importance of wall temperature, pressure gradient, and number of captured streamlines on the local Stanton number distribution. In addition, the effect of transition on the local heating level over the canopy surface was examined and found to be very important.

As a result of the sensitivity study, the STAPAT heat-transfer methodology is based on the DeJarnette heating code as described in References 3 through 5, including variable-edge entropy for high Mach number flows. Real gas effects are included as an option for typical wind tunnel testing under high Mach number conditions. Based on the sensitivity study, multiple streamlines (on the order of 5) will be used to define the circumferential heating distribution over the transparency to provide the three-dimensional effects. Two-dimensional heat-transfer calculations which may be required in wind tunnel test applications will be available using the DeJarnette heating code methodology. Transition will be fixed in the nose region of the body or input in terms of a local transition momentum thickness Reynolds number.

Heat-transfer rates along the body surface in the DeJarnette code are calculated by the application of an integral boundary-layer method applied along inviscid streamlines on an equivalent body of revolution. The distance along each streamline is equivalent to the distance along the equivalent axisymmetric body of revolution. The radius of the equivalent body is a measure of the divergence of adjacent streamlines. A modified form of the Reshotko and Tucker integral boundary-layer method is used to define the momentum thickness distribution along each streamline. Correlations such as the van Driest methodology, Eckert reference enthalpy, or Spalding Chi are utilized to relate the local momentum thickness Reynolds number to the skin-friction coefficient. The skin-friction coefficient is then related through the von Karman form of the Reynolds analogy to the local Stanton number from which local heating values are obtained.

Figures 2 and 3 provide example heat-transfer calculations utilizing the STAPAT methodology for a fighter forebody configuration. Figure 2 gives a comparison of the adiabatic wall Stanton number versus axial distance measured from the nose for the STAPAT methodology and the Eckert flat plate calculations. The importance of entropy layer swallowing is evident in the forward fuselage region where the Eckert flat plate Stanton number predictions are normally 40 percent low. The effect of the strong adverse pressure gradient on the Stanton number in the canopy region accentuates the entropy layer swallowing effect appearing in the forward fuselage region. As can be seen, if flat plate heating had been used in the canopy region rather than the more precise STAPAT heating methodology, predicted heating levels could have been nominally 60 percent low. This difference is further exagerated as the Mach number is increased.

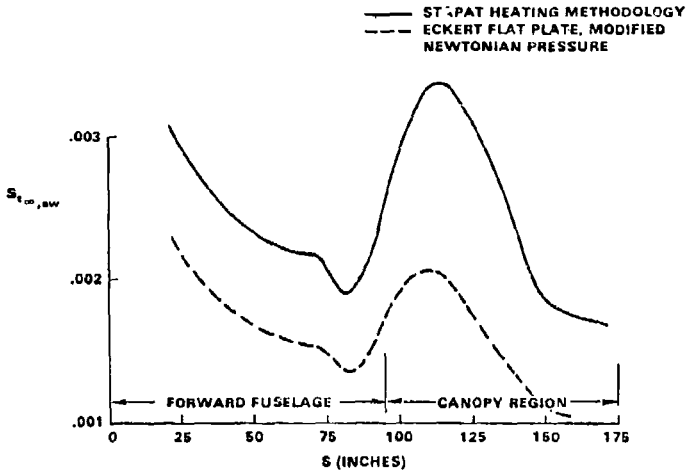

FIGURE 2. WIND RAY STANTON NUMBER DISTRIBUTION FOR A TYPICAL FOREBODY CONFIGURATION AT MACH 2.5, T_w/T_o=0.8 AND 75,000 FT. ALTITUDE

Circumferential Stanton number distributions are given in Figure 3 where results are shown for the STAPAT methodology at Mach 2.5 and 3.5. As can be seen, there is a significant circumferential gradient in the Stanton number, especially at the higher Mach number and in the peak heating region on the canopy.

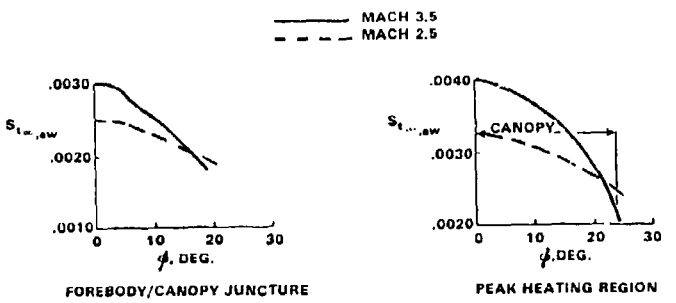

FIGURE 3. CIRCUMFERENTIAL STANTON NUMBER DISTRIBUTION FOR A TYPICAL FOREBODY CONFIGURATION AT T_w/T_o=0.8, AND 75,000 FT. ALTITUDE

The DeJarnette code in its present form can only handle blunt configurations. This is being modified in the STAPAT methodology to include sharp bodies. Current fighter configurations have nominal sharp noses and thus this option is highly desirable. It is anticipated that including this capability in the STAPAT heating module will result in savings of approximately 30 percent in computer time required to calculate the heating levels along a defined streamline.

2.1.4 Heating Code Application in STAPAT

The modified DeJarnette code, as previously discussed, is being integrated into the thermal analyzer program so that the heating calculations can be developed prior to a transparency thermal analysis. Mission profile inputs defined by Mach number and altitude will be used to define the calculation points required from the heating code. Only those conditions where the Mach number and altitude remain constant for some fixed-time interval will be used as a basis for heating code calculations. These will be obtained directly from the user input mission profile for STAPAT. The user will also have the capability of specifying the number of streamlines for which the heating calculations will be performed. The streamlines selected by the code will be defined in such a way as to capture only the area covering the canopy surface. Therefore, only heating data over the canopy surface will be stored and available for the thermal analyzer program contained within STAPAT. A block diagram showing the relationship of the heating module to the STAPAT control module is shown in Figure 4.

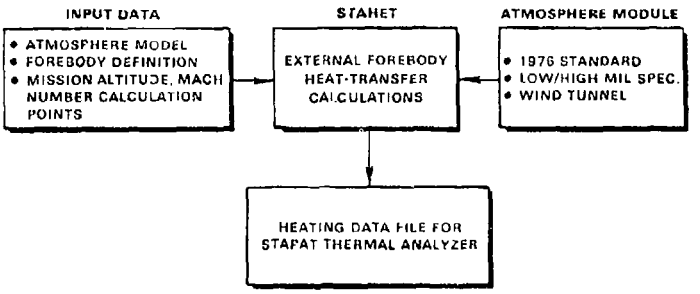

FIGURE 4. STAPAT HEATING MODULE BLOCK DIAGRAM

The three-dimensional forebody shape for the heating code (STAHET) is input through axial and radial distance and circumferential angle coordinates as shown in Figure 5. These coordinates need not be the same as the coordinates used in defining the canopy element nodes. The only requirements are that the forebody input provide axial distance and angle values which are compatible with those resulting from the canopy node definition and that the canopy nodal coordinate system must be in the same system as the forebody coordinate system as used in the heating code.

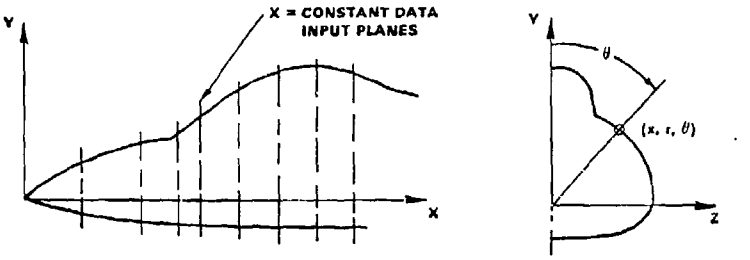

FIGURE 5. STAPAT HEATING MODULE FOREBODY GEOMETRY INPUT

Based on the results of the sensitivity study, it was shown that by evaluating heat-transfer results at wall-to-total-temperature ratios of .8 and 1.1, linear variations of the heating rate versus the difference in wall and adiabatic wall temperature could be used to define accurate local heating levels on the canopy surface. It was also shown that the heat transfer coefficient, h, is different for wall-to-adiabatic temperature ratios below and above 1. This heat-transfer rate behavior is illustrated in Figure 6 where segmented linear fits are compared to wall temperature calculations indicating excellent agreement. Thus, both wall temperature data above and below the adiabatic wall value are stored and utilized in determining the appropriate heating value. These relationships are given below in Equation 3.

$$q = h_{.8}(T_{aw} - T_w)$$
$$q = h_{1.1}(T_{aw} - T_w) \qquad (3)$$

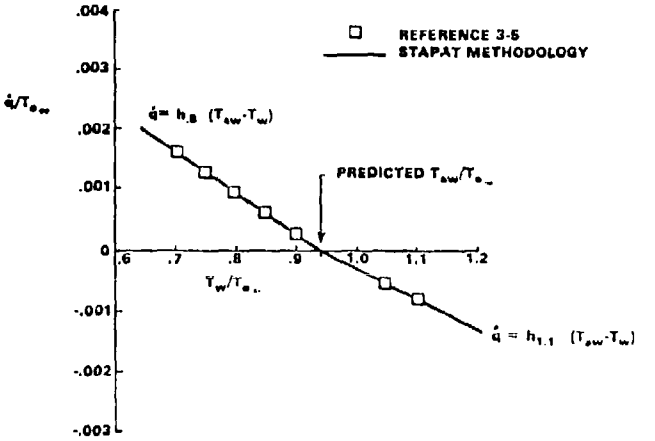

FIGURE 6. VARIATION OF HEAT-TRANSFER RATE WITH WALL TEMPERATURE FOR A TYPICAL FOREBODY SURFACE LOCATION

Once a series of streamlines are calculated by the STAPAT heating module, local values of the edge Stanton numbers (based on edge conditions), edge Mach number and temperature, and local recovery factor are written on a heating data file. These data provide the necessary information to calculate local values of the adiabatic-wall temperature and heat-transfer rate for any point on the canopy surface at the calculation point altitude and Mach number condition for a specified atmospheric model. Intermediate points between the calculation Mach number and altitude points are defined based on a linear interpolation between these known solutions using a flat plate, compressible turbulent boundary-layer correlation, Reference 6.

The data for each calculation point in a mission profile are stored in terms of axial distance along the fuselage and circumferential angle. No radial variation is included in the input data definition. This data input approach provides for the decoupling of the canopy thermal geometry model and the fuselage model for the heating code calculations. This provides a significant amount of latitude in the modeling of the heat-transfer characteristics and in the modeling of the thermal nodal grid.

2.1.5 Other STAPAT Convection Methodology

In addition to the forced external convection as described in the preceding section, there are many other convective heat-transfer mechanisms on current high-performance aircraft. These range from defogging to cabin environmental cooling capabilities. As shown in the sensitivity analyses of References 1 and 7, these mechanisms must be properly accounted for in order to accurately define the thermal environment within transparency systems. Lawrence, Reference 8, and Wilson, Reference 7, provide descriptions of current forced- and free-convection mechanisms utilized to heat or cool canopy systems. The STAPAT heating methodology utilizes these heat-transfer mechanisms.

The internal forced convection methodology required for STAPAT was examined in the sensitivity analysis for active cabin cooling. The effect of active cabin cooling on the temperature of the inner surface of the transparency was shown to be very important, especially for high Mach number missions. Based on the sensitivity results, the STAPAT methodology includes the capability of cabin cooling. The model implemented in STAPAT consists of a free and forced convection model similar to the one used in Wilson (Reference 7). This boundary condition is implemented in such a way as to allow the user to locate the cabin cooling at any surface location on the inside of the canopy, and to turn the cooling on or off at any point in the mission profile.

Lawrence (Reference 8) considers different types of forced convection models that are used in current aircraft and that may be used in future aircraft for anti-icing and defogging purposes. For anti-icing purposes there are primarily four types of mechanisms that are currently in use. One approach is an external jet blast which is used to control anti-icing on the outer ply of the canopy. A hot-air blast can also be used between double pane windshields to provide an effective anti-icing capability. This technique, as indicated, utilizes a hot gas which passes between the panes to provide an effective heat-transfer mechanism.

Other techniques that have been used more extensively are fluid de-icing and electrical-resistance heating techniques. The fluid de-icing technique uses a freezing-point depressant sprayed onto the windshield to dissolve or retard the formation of an ice layer. Electrical techniques rely on the transfer of heat through a conductive coating to provide a temperature increase of the transparent layer structure.

The external heating due to rain and hot-air blast is implemented in STAPAT based on the correlations presented by Lawrence (Reference 8). Lawrence relates the heat-transfer to the surface from a rain cloud through the latent heat of vaporization of the water, and the rate of water impingement on the canopy. The external hot-air blast system is used to remove ice from the exterior windshield surface and is based on the local external convection coefficient and the difference in wall and local slot air temperature.

The hot-air gap system is modeled as a forced convection heat-transfer process. The heat-transfer rate is defined as proportional to a heat-transfer coefficient times the difference in entry air and backside transparency surface temperature. The heat-transfer coefficient is based on laminar or turbulent flow correlations for air flow between parallel flat plates. The defogging system which uses slot-injected air at the base of the windshield is modeled as a local heat-transfer coefficient times the difference in local wall and the local bulk slot air temperature. The heat-transfer coefficient for the defogging system is related to the slot geometric characteristics, the distance from the slot, the mass flow through the slot, and the temperature of the slot air at the specific point of interest on the canopy surface.

Boundary conditions as required by STAPAT are supplied to implement the hot-air gap, defog, and external hot-air blast system. These are composed of the specification of the air-gap air temperature, mass flow rates, and geometric details where required, and the location in terms of the coordinates x, y, z, which define the reference point from which the air gas exits. In addition, each element surface is identified that receives this heat contribution. The user also has the option to turn the systems on or off individually at any point in a mission.

The electrical heating technique for de-icing or defogging purposes is available in the STAPAT heating methodology by defining the power or heat load input to a specific surface. In this way, the heat source can be placed at any position within the transparency surface. In addition, the ability to turn the electrical heating on or off at any point in the mission is also available to the user as an option.

A summary of the available STAPAT convective and electrical heating options as described in this section is given in Figure 7.

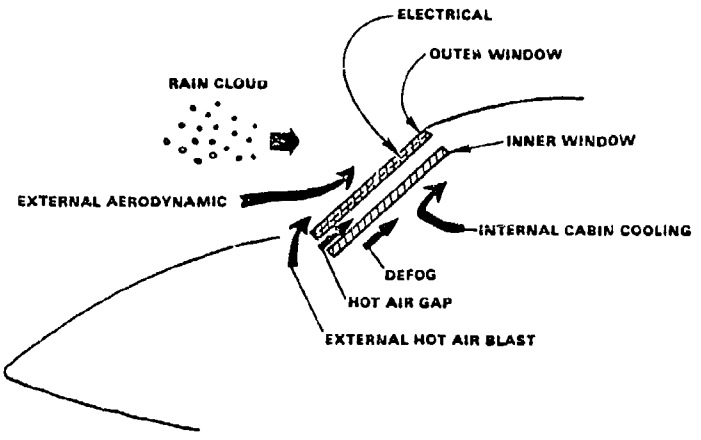

FIGURE 7. STAPAT CONVECTIVE AND ELECTRICAL HEATING OPTIONS

2.1.6 Radiation Methodology

The results of the sensitivity study revealed that solar radiation is not a critical heat source except for low altitudes in flight missions and for aircraft parked on the ground. It was determined that the external solar radiation is strongly influenced by cloud cover, precipitation, and solar altitude. In addition, it was shown that the manner in which the solar radiation heat input was included in the heat conduction calculations within the transparency was important, i.e., the layer variation of the absorbed heat from solar sources. It was also indicated that for typical transparent layers only approximately 10 to 40 percent of the direct solar radiation was absorbed within the transparency.

Based on the results of the sensitivity analysis, the solar radiation is modeled in STAPAT as a heat-transfer rate versus altitude, which includes both the direct and diffuse components. No angle deviation effects on the direct solar radiation are included since these are dependent on the atmospheric condition, solar altitude, and physical location of the mission on the earth's surface.

In order to properly handle the heat transfer absorbed by the transparent layer, a heat balance should be performed on each ply giving both the absorption, transmission, and reflection characteristics of the solar radiation as it passes from one ply to the next. Based on the importance of the solar radiation heat contribution as determined in the sensitivity analysis, the STAPAT heat- transfer methodology does not incorporate detailed interlayer calculations of the absorbed direct and diffuse radiation.

The solar radiation absorbed within a transparent layer structure is assumed to be absorbed uniformly through the layer thickness, the amount of which will be equivalent to the heat absorbed in a single transparent layer. Transmissivity characteristics of acrylic/polycarbonate/glass layer structures were examined to define a correlation describing the absorption behavior as a function of total thickness. Figure 8 gives experimental transmissivity data for typical transparencies and the curve fit utilized in the STAPAT methodology.

Modeling the absorbed radiation in this format will yield correct trends and magnitudes for typical transparency configurations. Absorbed radiation due to an electrical conductive (EC) coating will be modeled as a constant fraction of the total solar incident radiation. This will result in a net absorbed heat from direct and diffuse radiation available at a given altitude.

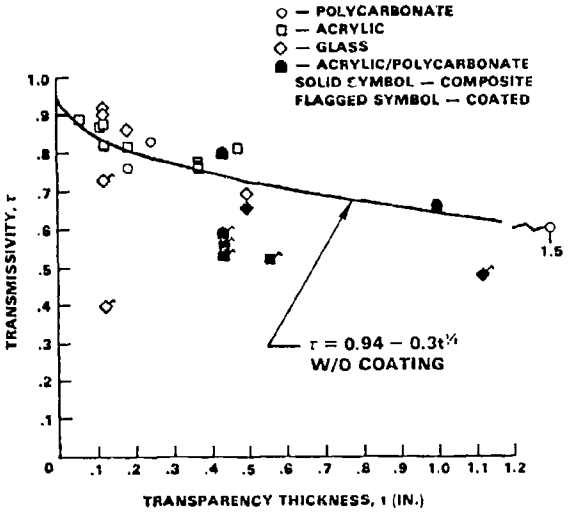

FIGURE 8. TRANSMISSIVITY CHARACTERISTICS OF TRANSPARENT LAYERED STRUCTURES

The altitude dependence of the direct and diffuse solar radiation is modeled based on the results given in Wilson (Reference 7), the calculations made by Nikolskiy (Reference 9), and results obtained from the ASHRAE for solar radiation on the earth (Reference 10). For opaque layer materials such as metallics, the absorbed solar radiation is based on the product of the local available direct and diffuse solar radiation times the absorptivity of the particular layer in question.

Another important consideration in defining the radiation environment is the local sky temperature. The sensitivity analysis examined the influence of the sky temperature on the thermal environment within the canopy for Mach 2.5 missions which covered altitudes up to 60,000 ft. It was shown that the actual value of the sky temperature was not critical to the thermal environment within the canopy except on or near ground level. It was also shown that there was a large effect of cloud cover on the sky temperature. As shown by Wilson (Reference 7), the sky temperature for clear-sky nights in Tucson, Arizona, can be quite low. However, Duffy and Beckman (Reference 11) point out that for clear-sky days the sky temperature is proportional to the local ambient temperature. A correlation was derived in Reference 11, giving the relationship between the local sky temperature and ambient temperature at ground level.

The STAPAT methodology models the effect of radiation to the sky from the outer layer canopy surface by defining the sky temperature as a function of the ambient temperature as given by Duffy and Beckman (Reference 11) with an exponential merging to a clear-sky night temperature above 100,000 foot altitudes. This relationship will be assumed to

hold for various altitudes and atmospheric models.. The configuration factor as shown by Wilson will be the emissivity of the outer ply surface that radiates to the sky, modeled as a blackbody radiation source.

Surface-to-surface radiation, an example of which is the two window system, is also implemented into the STAPAT radiation methodology. This is an important heat-transfer mechanism for high Mach number, sustained altitude missions where the backside temperature of the outer glass surface can reach relatively high temperatures and can cause a significant amount of heat transfer due to surface-to-surface radiation to the secondary window system. It is assumed that the medium separating the two window systems is a nonparticipating gas and that all surface-to-surface radiation is diffuse.

The configuration factor defining the geometrical view relationship of one surface element on one window system to another on another system is based on an approximate evaluation of the shape factor integral. The shape factor integral involves the distance between the two element surfaces, the angle between the normal to the element surfaces, and the radius vector connecting the surface elements. If it is assumed that the two element surfaces are small in comparison to the magnitude of the radius vector connecting the centroids of the two element surfaces, the integral can be replaced by Equation 4. Gray surface absorptivities and emissivities will be used for irradiated and radiating surface elements. Equation 4 gives the approximate shape factor expression that is implemented in STAPAT. A sketch showing the relevant surface to surface geometry is shown in Figure 9.

$$\frac{F_{21}}{A_1} = \frac{F_{12}}{A_2} = \frac{\cos\phi_1 \cos\phi_2}{\pi r^2} \qquad (4)$$

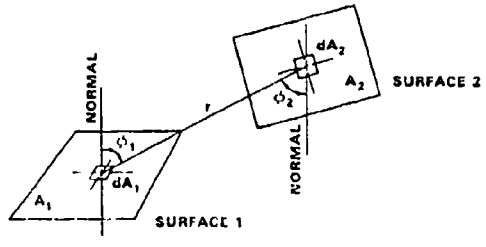

FIGURE 9. SURFACE-TO-SURFACE CONFIGURATION FACTOR DEFINITION

The sensitivity analysis also revealed that cabin contents radiation to the backside surface of the transparency can also be a significant heat input in reducing backside temperatures and internal temperatures of the canopy system, especially under ground conditions. As a result,

cabin radiation effects are included in the STAPAT methodology. From a practical standpoint the cabin surface temperatures that radiate to the backside of the canopy are, at best, difficult to determine since they are influenced to a large degree by the overall heat-transfer characteristics of the entire aircraft, by the individual configuration factors that can involve complex geometries, and by the variability of internal cabin masses which are a function of the specific aircraft being studied. Thus, the STAPAT implements the backside surface cabin radiation contribution by assuming that the cabin surfaces are at the local cabin temperature, act as blackbodies, and radiate to the back surface as a point source.

A summary of available STAPAT radiation heating options as described in this section is given in Figure 10.

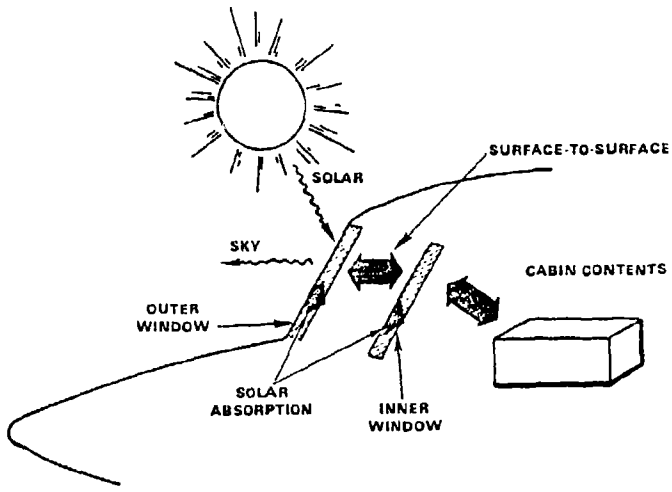

FIGURE 10. STAPAT RADIATION HEATING OPTIONS

2.1.7 Conduction Code Methodology

The sensitivity analysis showed that available three-dimensional finite-element conduction codes can handle the complex three-dimensional geometry of typical multilayer transparencies for high-performance aircraft configurations. The STAPAT capability utilizes finite-element methodology as the basis for its solution scheme. A state-of-the-art skyline solver is employed to invert the system of equations defining the temperature of each node point. This skyline approach yields minimum blocking and minimizes core requirements for large finite-element models requiring a large number of nodes to accurately define thermal behavior. Using the skyline approach also affords the user a significant latitude in the nodal numbering scheme since sparseness of the stiffness matrix is reduced by basing the solution algorithm on the skyline of the stiffness matrix rather than on the maximum bandwidth. An optimizer is also provided in STAPAT to afford an optimum rearrangement of the nodal structure that is user transparent and that will yield the most efficient solution of the stiffness matrix.

The integration algorithm used in the STAPAT is an implicit first-order-in-time algorithm. Utilization of this approach affords accurate solutions with no time stability constraints imposed on the time step. The sensitivity results indicated that nominally five steps per ramp in the mission profile are required to yield accurate thermal behavior for complex nodal structures. In order to avoid the requirement for iteration at each load step or time step in the solution process, the specific heat, conductivity, convection coefficient, and adiabatic wall-temperature conditions are evaluated at the previous time steps. This results in, as indicated, no iterations during a time step and yields fast solutions for complex input conditions.

In order to provide the greatest flexibility in application to large and small problems involving various complexities of transparency configurations, both in-core and out-of-core solution techniques are available in the STAPAT program. These are user transparent in that the program will determine when an out-of-core technique is required based on maximum core limitations and problem size constraints. Using this approach, both small and large node number problems can be executed efficiently.

The element used in the STAPAT program is an 8-node brick element. This has been shown to be an accurate heat-transfer conduction model for finite-element-type applications. It affords efficient network construction of nodes and connectivities but at the same time, can yield poor resolution in wedge-shaped regions. In order to circumvent this problem, a lower Gaussian integration order can be applied which results in the use of effective average center temperatures for wedge regions. In order to handle fixtures properly, a one-dimensional element, consisting of 2 nodes, is used to model bolts within complex fixtures and joints.

The element definitions as indicated have been applied in the sensitivity analysis (Reference 1) to coarse structure grids. These coarse structure grids are defined as the multilayer configurations over typical canopies without stiffeners, edge supports, or fixtures. In order to properly determine the thermal environment within canopies and regions where thermal gradients or temperatures are of interest, a fine-structure capability is required.

A fine-structure capability is available in STAPAT to handle fixtures and joints which occur in the region of edge attachments and is shown schematically in Figure 11. This fine structure is implemented in the STAPAT program by initially calculating the thermal environment in the multilayer coarse grid canopy for a specific mission profile and heating load constraints. Using this multilayer solution for a specific mission as an input, the fine-structure grid can be computed which contains joints, fixtures, and fine-structure details. The boundary conditions on the edge of the fine structure are imposed through temperature boundary conditions which are obtained from the layer boundaries of the coarse-grid, multilayer solution file run previously.

The fine-structure nodal network and connectivity are developed in a local coordinate system. A reference orientation is used to define the relationship between the local fine-grid coordinate system and the coarse-grid coordinate system. This allows the transfer of information from the coarse-grid solution data file to the fine-structure grid data file for the definition of the fine-structure edge boundary conditions.

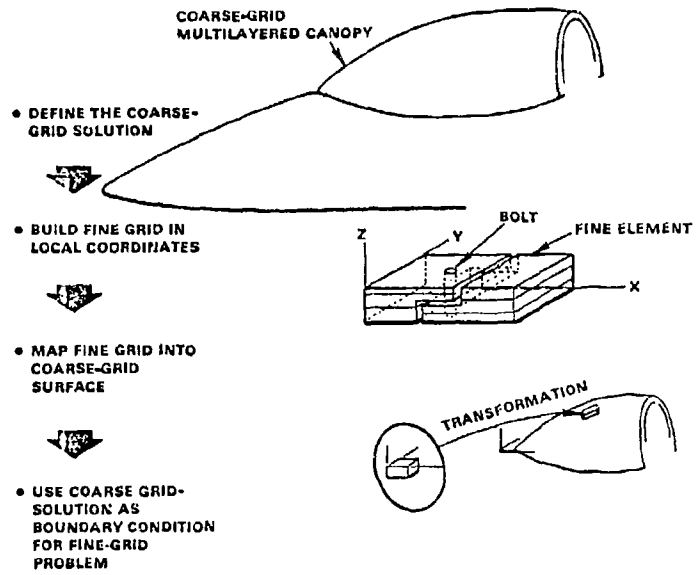

FIGURE 11. FINE GRID SOLUTION PROCEDURE

In order to satisfactorily implement this type of approach, a sufficient amount of transparent layer length must be positioned on the fixture or joint to adequately diffuse any temperature gradients that are caused by the presence of the fixture or joint on the canopy surface. This results in a model which locally can handle thermal gradients caused specifically by the presence of joints and fixtures located anywhere on the canopy structure.

There are many advantages in approaching the fine-structure problem for the thermal environment within canopies in the area of joints and fixtures in this manner. Since the fine structure would normally contain fewer nodes and elements than the coarse-grid structure, a very fast, efficient fine-structure solution can be obtained utilizing this STAPAT methodology. In addition, since the fine-structure is developed in a local coordinate system and a user-defined reference orientation is used to relate the local fine-structure coordinate system to the coarse-grid coordinate system, the fine structure can be located in any position on the canopy with a minimum amount of effort. In the local coordinate system, the fine-structure node network can be developed much more easily since coordinates can be aligned in such a way as to make nodal coordinate definitions a function of essentially two independent coordinates. Utilizing this approach also eliminates any complex matching of the fine-structure and coarse-structure grids that would occur if substructuring were used to compute the fine-structure thermal environment around joints and fixtures. In addition, this approach to fine structures

will result in a minimum user input to modify the fine structure or to move the fine structure to other parts of the canopy to assess the effect of thermal gradients caused by the fixture or joint in other regions of varying heat-transfer rate.

2.2 STAPAT Capabilities

2.2.1 STAPAT Preprocessor

A preprocessor program, called STABLD, is provided which utilizes a command interpreter to build the multilayer canopy structure consisting of the nodal coordinates and connectivities. The command interpreter provides for the use of alphabetic words or abbreviations to assist in data input. The outer surface nodal coordinates on the selected canopy surface are supplied in a sequential, formatted file in addition to their connectivity. The command interpreter is utilized to fill the multilayer transparency in depth along the outer surface normals which are determined from the user-supplied outer surface nodal coordinates.

Input variables available to the user to build this layer structure are variable number of layers per ply surface, variable thickness of each ply, variable number of plies, and variable material properties within each ply. The connectivity of the multilayer structure is defined by the preprocessor program as well as the incrementing of nodes in each layer by a specified increment.

In order to provide the highest degree of code flexibility and capability, the nodal numbering scheme is established in such a way that the node numbers, as well as element numbers, can be used to define the surfaces on which boundary conditions are applied, such as external forced convection and cabin cooling. This is implemented by requiring that the outer surface nodal numbers be between 1 and N_{max}. All other layers below the outer surface layer that make up the multilayer canopy are then numbered in increments greater than N_{max}.

In addition, the capability to delete or add nodes interactively is available to the user. Thus the capability to build a fine-structure describing fixtures or joints by entering nodal coordinates and connectivities of frames, edges, and fixtures interactively are available in STABLD. Simple commands are also available to increase nodal points and elements on the outer surface to provide a higher resolution in regions of anticipated high temperatures or thermal gradients.

Graphics capabilities are incorporated into STABLD to provide the capability of displaying elements that have been constructed using the preprocessor. Perspective plots are obtained by specifying the normalized Cartesian coordinate location of an observer looking at the grid structure. A zoom capability is also available to enlarge views using the crosshairs on a Tektronix 4014 CRT. All graphics capabilities supplied in the preprocessor are provided in Plot 10 software. The user can view node numbers in the graphics mode during the construction of coarse- and fine-structure grids.

2.2.2 Material and Atmospheric Properties

Material properties are input to the STAPAT code through a material property file. This file is organized in a sequential, formatted manner and thus is easily modified or added to as new materials become available or are defined. This material property file contains specific heat, conductivity, density, emissivity, and absorptivity versus temperature for all materials of interest, both transparent and metallic, and also insulation-type materials. Material property variations with temperature were shown in the sensitivity analysis to be of secondary importance. However, if temperature variable data is available, this can be easily input into the STAPAT code with no additional increase in complexity or code execution efficiency. The STAPAT uses a linear interpolation algorithm to define material properties at a specific material temperature.

Property definitions for each property utilized in the canopy or fixture structure is specified using the command interpreter through a material number, a material name, and an override capability to input temporary material property values for those not listed in the material property file. This provides a great deal of flexibility in that it gives the user constructing the input data file for STAPAT a visual indication of what materials are actually being used in the construction of the specific canopy or fixture.

The atmospheric model is also input through a command interpreter. The atmospheric models available are for either flight- or wind tunnel-type applications. For flight-type applications the 1976 atmospheric model, and a high- and low-MIL specification atmospheric model are available. This atmospheric model data is included in common blocks within the STAPAT structure as subroutines which can be easily modified or added to as new atmospheric models become available. For wind tunnel test application, the atmospheric definition utilizes pressure and temperature versus time as input to specify the atmospheric model condition.

2.2.3 Boundary Condition Definition

Convection boundary conditions are implemented through the command interpreter by defining, for each type of convection boundary condition, the specific nodal region over which the heating load is applied. For external convection loading, the command interpreter is used to select the forced convection heating file generated from the modified DeJarnette code. For other types of convective heat loads, the command interpreter is used to identify loads such as cabin cooling, de-icing, defogging, or hot-air gap system. Appropriate input parameters and the nodal region for each system are identified in addition to the capability to turn the systems on or off at any time in the mission profile. Electrical heating capabilities are also identified through the command interpreter where the heat-transfer rate on a nodal region is supplied by the user, including the on-off time during the mission.

Radiation boundary conditions are also implemented into STAPAT through the command interpreter. Each radiation boundary condition for specific nodal regions are specified in a manner similar to convection boundary conditions. Surface-to-surface radiation is also available through the command interpreter. STAPAT calculates the required configuration factor for the radiation, irradiation process based on the methodology as presented earlier.

Source radiation is also specified through the command interpreter for specific nodal surface distributions. Radiation to the sky is accommodated through the source radiation definition. The sky temperature, as indicated earlier, is determined as a function of ambient temperature which is a function of the atmospheric model and altitude conditions. Cabin source temperatures are utilized to define radiation from the cabin contents to the inner window surfaces. For wind tunnel missions, the user must specify the appropriate source temperature, which is equivalent to the wind tunnel wall temperature for high Mach number test environments.

Temperature boundary conditions are implemented through the command interpreter. These boundary conditions are required for the fine-structure analysis, as discussed earlier, for the solution of fixtures and joints. Here the temperature boundary condition will be implemented for a specified nodal region. The temperature boundary condition will define a specific file from which appropriate temperature data from the coarse-structure grid solution file, as discussed in preceding sections, is obtained. The cabin environment is input through the command interpreter by specifying a cabin temperature which will be assumed constant over the entire mission profile. This cabin temperature is utilized to define the backside-source blackbody radiation between the cabin contents and the back surface of the transparency.

The mission profile is also input through the command interpreter. Both flight and wind tunnel-type profiles are available for user implementation. For flight-type applications, the altitude and Mach number versus time are required. For wind tunnel applications, the Mach number as well as the stagnation temperature and pressure versus time are input.

Other operational parameters which are required to exercise the STAPAT code are implemented through the command interpreter. The user is required to specify the number of time steps, the element type, the Gaussian integration order, and the print interval. Defaults for operational parameters consist of a five time steps per mission point increment for the number of time steps, an 8-node brick element, and a print option every time step.

2.2.4 STAPAT Modular Structure

The STAPAT code discussed in the preceding sections makes extensive use of temporary scratch files to transfer data from one module to another in an efficient and effective manner. This creates a program with a minimum core storage requirement that can be run on computers

with severe core storage restrictions. A general schematic of the modular STAPAT code structure and supporting pre- and post-processor modules is shown in Figure 12. In addition, the solver routine as discussed earlier, provides a blocking capability for out-of-core solutions which results in a very efficient utilization of working core storage. Utilizing this approach, only two variables must be set within the STAPAT program to change the working area program size. This results in a code that can be implemented on a wide variety of machines and that can be easily modified to tailor the code for a particular computer configuration.

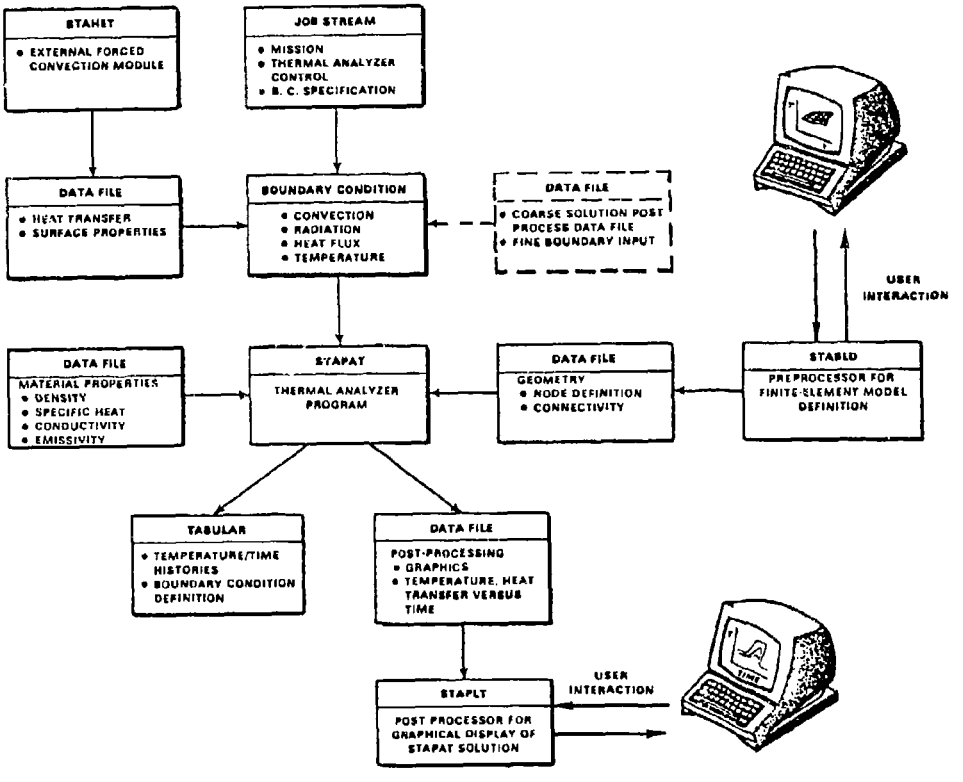

FIGURE 12. STAPAT MODULAR SOFTWARE DEFINITION

The forced external convection calculations which are provided by a modified form of the DeJarnette code are decoupled from the finite-element solution technique in STAPAT. This is provided through the methodology as discussed earlier and results in a very efficient definition of convective heat loading over the canopy surface for any point in the mission, at any point on the canopy surface. Thermal calculations within the fine- or coarse-structure utilize a data file which is generated by the STAPAT heating module. This data file must only be calculated once for a specific forebody shape and mission in terms of Mach number and altitude.

In order to display the information generated by the STAPAT code, a graphics package is utilized to assimilate the post-processing data file generated by STAPAT (called STAPLT). This graphics package is a stand alone package. In addition to its use to generate graphics output from STAPAT, it is also used to generate forebody geometry shapes and heating load distributions from the STAPAT heating module. The graphics package is configured in Plot 10 and specifically written around the Tektronix 4014 graphics terminal. The graphics package, in addition, is interactive; the user is provided a menu of available options from which he may execute.

Options available to the user consist of atmospheric property, temperature, heat transfer, and surface contours. The atmospheric properties option yields the mission pressure, temperature, dynamic pressure, Mach number, and altitude as a function of time. Temperature versus time plots are also available. Heat-transfer variables available for graphical display are the heat-transfer coefficients, the actual heating rates, and surface temperatures at the centroid of selected elements. Temperature versus time plots, used in the heat-transfer calculations such as the adiabatic wall temperature, are available as graphics options by specifying an element and face number. An important area to examine in the multilayer canopy configuration is the temperature versus depth profile through the layer thickness at a specific time in the mission and a specific point on the canopy surface. This plot option is available to the user who can specify up to nine temperature distributions for a specific surface node per plot.

Surface isotherm plots are also available for the viewing of constant temperature lines on specific layers for either a coarse- or a fine-structure grid. Here the user has to define the layer on which surface isotherms are desired. Perspective plots are presented where the user must either define the maximum and minimum temperature values and number of lines between those temperatures to be displayed, or select the default value which will produce the existing maximum and minimum value with ten lines of constant temperature equally spaced between the maximum and minimum temperatures on that surface.

The user also has the option of viewing a specific layer within the canopy with its associated surface elements and corresponding nodes shown for either a fine or coarse structure. Options are available to the user to either specify a perspective view or to select a specific orientation of the surface.

STAPLT also has the capability of plotting the fuselage grid as used in the STAPAT heating calculations to define the heating load distribution on the canopy surface. Options available to the user are a perspective view and a user-specified general orientation of the surface. Surface contours are also available for plotting from the heating file which will be utilized as input for the STAPAT code. Contour plots are available for plotting the edge pressure, edge temperature, edge Mach number, and Stanton number as a function of the axial coordinate and circumferential angle on the fuselage. The user is required to specify the Mach number, altitude and wall temperature ratio for which a plot is desired.

A sample surface isotherm plot from the STAPLT graphics package is presented in Figure 13.

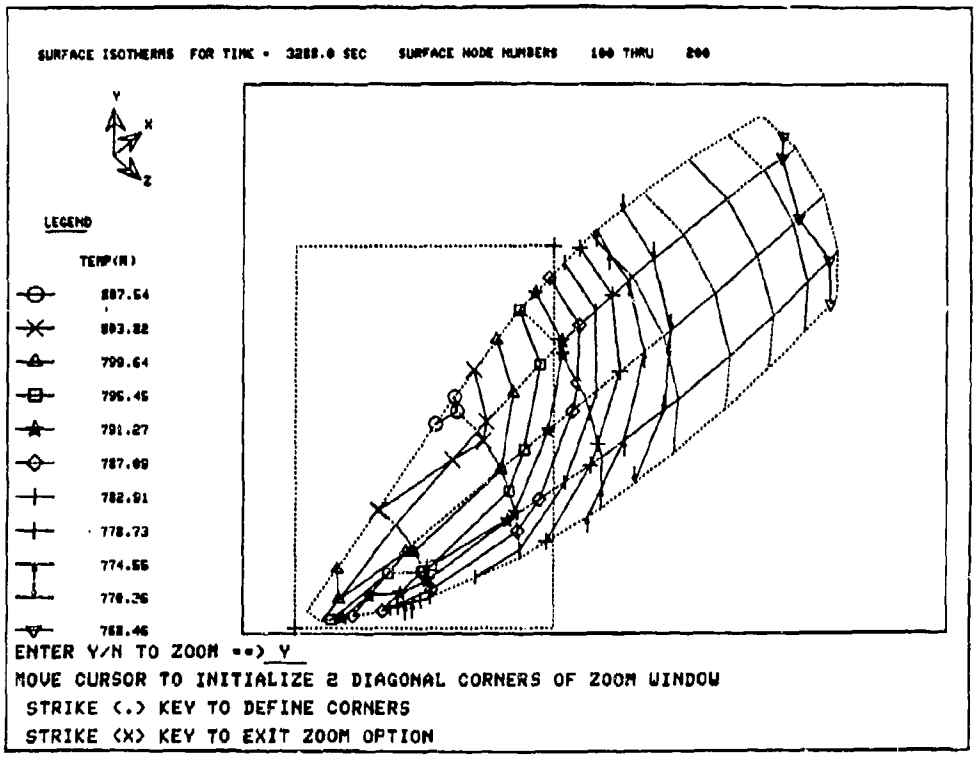

FIGURE 13. TYPICAL PERSPECTIVE PLOT FROM STAPLT

3.0 SUMMARY

The preceding sections have given an overview of the methodology and capabilities that are available in STAPAT. These methods and capabilities are a result of the sensitivity analysis and the careful interlacing of code efficiency, ease of operation, and capabilities. The resulting STAPAT is a user-oriented code which will be capable of providing, not only the canopy designer, but also the researcher, with a valuable tool for the analysis of the thermal environment within complex canopies on current and future high-performance aircraft.

REFERENCES

1. Varner, M. O., "Analysis and Definition of STAPAT Requirements - Task I Final Report for Advanced High Temperature Resistant Transparencies for High Speed Aircraft," Sverdrup Technology, Inc., Contractor Report, AFWAL Reference F33615-81-C-3412.

2. Jacocks, J. L., and Kneile, K. R., "Computations of Three-Dimensional Time Dependent Flow Using the Euler Equations," AEDC-TR-80-49, July 1981.

3. DeJarnette, F. R., "Calculation of Inviscid Surface Streamlines and Heat Transfer on Shuttle Type Configurations, Part I - Description of Basic Method," NASA CR-111921, August 1971.

4. DeJarnette, F. R., and Jones, M. H., "Calculation of Inviscid Surface Streamlines and Heat Transfer on Shuttle Type Configurations, Part II - Description of Computer Program," NASA CR-111922, August 1971.

5. DeJarnette, F. R., "Calculation of Heat Transfer in Shuttle-Type Configurations Including the Effects of Variable Edge Entropy at Boundary Layer Edge," NASA CR-112180, October 1972.

6. White, Frank M., Viscous Fluid Flow, McGraw-Hill, Inc., 1974.

7. Wilson, V. E., "Design Analysis of High Temperature Transparent Windshields for High Performance Aircraft," AFWAL TR-81-3126, November 1981.

8. Lawrence, H. J., Jr., "Guidelines for the Design of Aircraft Windshield/Canopy Systems," AFWAL-TR-80-3003, February 1980.

9. Nikolskiy, G. A., and Prokonenko, Y. V., "Attenuation of Direct Solar Radiation in the Atmosphere," IMIS AST-18201-76, November 1976.

10. Anon. ASHRAE Handbook and Product Directory, 1977 Fundamentals, Published by ASHRAE, 1977, Chapter 26.

11. Diffie, J. A., and Beckman, W. A., Solar Energy Thermal Processes, John Wiley and Sons, Inc., 1974.